



**DEVELOPMENTS IN  
PETROLEUM SCIENCE**

**40B**

# **ASPHALTENES AND ASPHALTS, 2**

**T.F. Yen**

**G.V. Chilingarian**  
editors

**ELSEVIER**



DEVELOPMENTS IN  
PETROLEUM SCIENCE

**40 B**

# **ASPHALTENES AND ASPHALTS, 2**



## DEVELOPMENTS IN PETROLEUM SCIENCE

Volumes 1-5, 7, 10-14, 16, 17, 21-29, 31 and 35 are out of print.

- 6** *Fundamentals of Numerical Reservoir Simulation*
- 8** *Fundamentals of Reservoir Engineering*
- 9** *Compaction and Fluid Migration*
- 15a** *Fundamentals of Well-log Interpretation, 1. The acquisition of logging data*
- 15b** *Fundamentals of Well-log Interpretation, 2. The interpretation of logging data*
- 18a** *Production and Transport of Oil and Gas, A. Flow mechanics and production*
- 18b** *Production and Transport of Oil and Gas, B. Gathering and Transport*
- 19a** *Surface Operations in Petroleum Production, I*
- 19b** *Surface Operations in Petroleum Production, II*
- 20** *Geology in Petroleum Production*
- 30** *Carbonate Reservoir Characterization: A Geologic-Engineering Analysis, Part I*
- 32** *Fluid Mechanics for Petroleum Engineers*
- 33** *Petroleum Related Rock Mechanics*
- 34** *A Practical Companion to Reservoir Stimulation*
- 36** *The Practice of Reservoir Engineering*
- 37** *Thermal Properties and Temperature related Behavior of Rock/fluid Systems*
- 38** *Studies in Abnormal Pressures*
- 39** *Microbial Enhancement of Oil Recovery – Recent Advances*  
*– Proceedings of the 1992 International Conference on Microbial Enhanced Oil Recovery*
- 40a** *Asphaltenes and Asphalts, I*
- 40b** *Asphaltenes and Asphalts, 2*
- 41** *Subsidence due to Fluid Withdrawal*
- 42** *Casing Design – Theory and Practice*
- 43** *Tracers in the Oil Field*
- 44** *Carbonate Reservoir Characterization: A Geologic-Engineering Analysis, Part II*
- 45** *Thermal Modeling of Petroleum Generation: Theory and Applications*
- 46** *Hydrocarbon Exploration and Production*
- 47** *PVT and Phase Behaviour of Petroleum Reservoir Fluids*
- 48** *Applied Geothermics for Petroleum Engineers*



DEVELOPMENTS IN  
PETROLEUM SCIENCE

40 B

# ASPHALTENES AND ASPHALTS, 2

*Edited by*

**Teh Fu YEN**

**George V. CHILINGARIAN**

*School of Engineering*

*University of Southern California*

*Los Angeles, CA 90089-2531*

*USA*



2000

ELSEVIER

Amsterdam – Lausanne – New York – Oxford – Shannon – Singapore – Tokyo





ELSEVIER SCIENCE B.V.  
Sara Burgerhartstraat 25  
P.O. Box 211, 1000 AE Amsterdam, The Netherlands

© 2000 Elsevier Science B.V. All rights reserved.

This work is protected under copyright by Elsevier Science, and the following terms and conditions apply to its use:

#### *Photocopying*

Single photocopies of single chapters may be made for personal use as allowed by national copyright laws. Permission of the Publisher and payment of a fee is required for all other photocopying, including multiple or systematic copying, copying for advertising or promotional purposes, resale, and all forms of document delivery. Special rates are available for educational institutions that wish to make photocopies for non profit educational classroom use.

Permissions may be sought directly from Elsevier Science Rights & Permissions Department, PO Box 800, Oxford OX5 1DX, UK; phone: (+44) 1865 843830, fax: (+44) 1865 853333, e-mail: [permissions@elsevier.co.uk](mailto:permissions@elsevier.co.uk). You may also contact Rights & Permissions directly through Elsevier's home page (<http://www.elsevier.nl>), selecting first 'Customer Support', then 'General Information', then 'Permissions Query Form'.

In the USA, users may clear permissions and make payments through the Copyright Clearance Center, Inc., 222 Rosewood Drive, Danvers, MA 01923, USA; phone: (978) 7508400, fax: (978) 7504744, and in the UK through the Copyright Licensing Agency Rapid Clearance Service (CLARCS), 90 Tottenham Court Road, London W1P 0LP, UK; phone: (+44) 171 631 5555; fax: (+44) 171 631 5500. Other countries may have a local reprographic rights agency for payments.

#### *Derivative Works*

Tables of contents may be reproduced for internal circulation, but permission of Elsevier Science is required for external resale or distribution of such material.

Permission of the Publisher is required for all other derivative works, including compilations and translations.

#### *Electronic Storage or Usage*

Permission of the Publisher is required to store or use electronically any material contained in this work, including any chapter or part of a chapter.

Except as outlined above, no part of this work may be reproduced, stored in a retrieval system or transmitted in any form or by any means, electronic, mechanical, photocopying, recording or otherwise, without prior written permission of the Publisher.

Address permissions requests to: Elsevier Science Rights & Permissions Department, at the mail, fax and e-mail addresses noted above.

#### *Notice*

No responsibility is assumed by the Publisher for any injury and/or damage to persons or property as a matter of products liability, negligence or otherwise, or from any use or operation of any methods, products, instructions or ideas contained in the material herein. Because of rapid advances in the medical sciences, in particular, independent verification of diagnoses and drug dosages should be made.

First edition 2000

Library of Congress Catalog Card Number: 94-3116

ISBN: 0 444 50324 2

© The paper used in this publication meets the requirements of ANSI/NISO Z39.48-1992 (Permanence of Paper).  
Printed in The Netherlands.

## **IN MEMORY OF OUR MOTHERS**

Ren-Chen Liu Yen,  
Woman Christian Preacher

Klavdia Gorchakova Chilingarian,  
Musician and Community Worker

Dedicated to

Dr. Rudolf W. Gunnerman

for his farsightedness and efforts in developing clean fuels

This page intentionally left blank

## PREFACE

This is the second volume in the series of *Asphaltenes and Asphalts*. Since the publication of the first volume in 1994, there has been a significant advancement in our knowledge. The editors would like to express their gratitude to all the contributors for their patience and revision of their manuscripts. The period of preparation has not been easy for the contributors, editors and the publisher. We believe, however, that this final product will become a useful reference in this specialized field.

Knowledge of both asphaltenes and asphalts is needed by several disciplines, and often the progress is dictated by interdisciplinary sciences and technology. This includes material sciences, fuel sciences, chemical engineering, civil engineering, environmental engineering, polymer sciences, transportation engineering, petroleum engineering, chemistry, geological sciences, physics, geochemistry, rheology, biological sciences, tribology, soil sciences, petroleum science. The development in this field is not based on our knowledge of chemistry or petroleum engineering alone, as many chemists and petroleum engineers believe. In this volume, therefore, we have included significant contributions made in different disciplines.

The monumental progress in this specialized field was achieved in large measure by the recent significant international conferences, such as the 1991 International Conference on Chemistry of Bitumens in Rome, Italy, the 1995 International Conference on Asphaltene and Wax Deposit for Oil Production in Rio de Janeiro, Brazil, and the 1997 Fifth Chemical Congress of North America in Cancun, Mexico. Some chapters in this volume contain representative papers from all three conferences. Therefore, let us join, with many international colleagues in this field, to welcome the appearance of this current volume. The editors would also like to thank Rochelle Wong for her invaluable help in the preparation of this volume.

TEH FU YEN and GEORGE V. CHILINGARIAN

This page intentionally left blank

## LIST OF CONTRIBUTORS

- T. CAGIN *California Institute of Technology, Pasadena, CA, USA*
- L. CARBOGANANI *INTEVEP, S.A., Centro de Investigación y Apoyo Tecnológico, Filial de Petróleos de Venezuela, S.A., Edif. Sede Central, Sector El Tambor, Los Teques Edo, Miranda, Venezuela*
- N.F. CARNAHAN *George R. Brown School of Engineering, Rice University, P.O. Box 1892, Houston, TX 77251-1892, USA*
- A. CHAKMA *Faculty of Engineering, University of Regina, Regina, Saskatchewan, S4S 0A2, Canada*
- H.-L. CHANG *Department of Civil and Environmental Engineering, University of Southern California, Los Angeles, CA 90089-2531, USA*
- Y.-Z. CHEN *Department of Chemical Engineering, University of Petroleum, Dongying, Shandong, 257062, People's Republic of China*
- G.V. CHILINGARIAN *Civil and Petroleum Engineering, University of Southern California, Los Angeles, CA 90089-2531, USA*
- M.S. DIALLO *Department of Civil Engineering, Howard University, 2300 6th NW, Washington DC 20015, USA*
- G.-J. DING *Heavy Oil Research Institute, University of Petroleum, Dongying, Shandong, 257062, People's Republic of China*
- K. DUNN *Department of Civil and Environmental Engineering, University of Southern California, Los Angeles, CA 90089-2531, USA*
- J. ESPIDEL *INTEVEP, S.A., Centro de Investigación y Apoyo Tecnológico, Filial de Petróleos de Venezuela, S.A., Edif. Sede Central, Sector El Tambor, Los Teques Edo, Miranda, Venezuela*
- Y.-H. FAN *Heavy Oil Research Institute, University of Petroleum, Dongying, Shandong, 257062, People's Republic of China*
- J.L. FAULON *Computational Materials Science Department, Sandia National Laboratories, Albuquerque, NM, USA*
- J.-M. FU *State Key Laboratory of Organic Geochemistry, Guangzhou Institute of Geochemistry, Chinese Academy of Sciences, Wushan, Guangzhou, 510640, People's Republic of China*
- I. GAWEL *Institute of Chemistry and Technology of Petroleum and Coal, Technical University of Wrocław, Gdanska 7/9, 50-344 Wrocław, Poland*
- W.A. GODDARD III *California Institute of Technology, Pasadena, CA, USA*
- L.M. GOKHMAN *79 Chaussée of Enthusiasts, 143900, Balashikha-6, Tzumzudnia str 42, room 44, Moscow, Russia*

- A. IZQUIERDO *INTEVEP, S.A., Centro de Investigación y Apoyo Tecnológico, Filial de Petróleos de Venezuela, S.A., Edf. Sede Central, Sector El Tambor, Los Teques Edo, Miranda, Venezuela*
- M.T. KLEIN *College of Engineering, Rutgers, The State University of New Jersey, Picataway, NJ 08854-8058, USA*
- H. LIAN *Department of Civil and Environmental Engineering, University of Southern California, Los Angeles, CA 90089-2531, USA*
- W.-J. LIANG *Department of Chemical Engineering, University of Petroleum, Dongying, Shandong, 257062, People's Republic of China*
- J.-R. LIN *Department of Civil and Environmental Engineering, University of Southern California, Los Angeles, CA 90089-2531, USA*
- C. LIRA-GALEANA *Mexican Institute of Petroleum, Eje Central Lazaro Cardenas No. 152, Apartado Postal 14-805, 07730 Mexico D.F., Mexico*
- C.-G. LIU *Department of Chemical Engineering, University of Petroleum, Dongying, Shandong, 257062, People's Republic of China*
- D.-H. LIU *State Key Laboratory of Organic Geochemistry, Guangzhou Institute of Geochemistry, Chinese Academy of Sciences, Wushan, Guangzhou, 510640, People's Republic of China*
- A. HAMMAMI *D.B. Robinson Research, Ltd., Edmonton, Alberta, Canada*
- M. NEUROCK *Department of Chemical Engineering, University of Delaware, Newark, Delaware 19716-3110, USA*
- J.C. PETERSEN *Western Research Institute, Laramie, WY, USA*
- G.-H. QUE *Department of Chemical Engineering, University of Petroleum, Dongying, Shandong, 257062, People's Republic of China*
- J.G. REYNOLDS *Lawrence Livermore National Laboratory, University of California, P.O. Box 808, L-369, Livermore, CA 94551, USA*
- G.-Y. SHENG *State Key Laboratory of Organic Geochemistry, Guangzhou Institute of Geochemistry, Chinese Academy of Sciences, Wushan, Guangzhou, 510640, People's Republic of China*
- R.B. SOLARI *INTEVEP, S.A., Centro de Investigación y Apoyo Tecnológico, Filial de Petróleos de Venezuela, S.A., Edf. Sede Central, Sector El Tambor, Los Teques Edo. Miranda, Venezuela*
- D. SVETAL *Highways Institute, Belgrade, Yugoslavia*
- F. THYRJON *Université Catholique de Louvain, Unité des Procèdes, Voie Minckeler, 1-1348 Louvain-la-Neuve, Belgium*
- A. VERHASSELT *Belgium Road Research Centre, 42 Bd. De la Woluwe, B-1200 Brussels, Belgium*
- D. VITOROVIĆ *Department of Chemistry, University of Belgrade, P.O. Box 550, 11001 Belgrade, and Institute of Organic Chemistry, Biochemistry and Analysis, Belgrade, Yugoslavia*
- Y.-Y. WANG *Department of Civil and Environmental Engineering, University of Southern California, Los Angeles, CA 90089-2531, USA*
- G. WONG *Department of Civil and Environmental Engineering, University of Southern California, Los Angeles, CA 90089-2531, USA*

- Z.-J. WU      *State Key Laboratory of Organic Geochemistry, Guangzhou Institute of Geochemistry, Chinese Academy of Sciences, Wushan, Guangzhou, 510640, People's Republic of China*
- T.F. YEN      *Department of Civil and Environmental Engineering, University of Southern California, Los Angeles, CA 90089-2531, USA*
- C.-X. ZHANG      *Heavy Oil Research Institute, University of Petroleum, Dongying, Shandong, 257062, People's Republic of China*
- Y.-Z. ZHANG      *Heavy Oil Research Institute, University of Petroleum, Dongying, Shandong, 257062, People's Republic of China*



This page intentionally left blank

# CONTENTS

Preface . . . . .	vii
List of Contributors . . . . .	ix
 <i>Chapter 1</i> INTRODUCTION TO ASPHALTENES AND ASPHALTS, VOLUME 2 G.V. Chilingarian and T.F. Yen . . . . .	 1
References . . . . .	4
 <i>Chapter 2</i> THE REALMS AND DEFINITIONS OF ASPHALTENES T.F. Yen . . . . .	 7
Historical review of bitumen, asphalt and asphaltene . . . . .	7
Natural and artificial asphalts and allied substances . . . . .	11
A simple scientific definition of asphaltene . . . . .	15
Generality versus uniqueness — a case study . . . . .	20
A continuum theory of carbonaceous systems . . . . .	23
Acknowledgements . . . . .	27
References . . . . .	27
 <i>Chapter 3</i> UNDERSTANDING METALS IN FOSSIL FUELS: A PERSPECTIVE OF CONTRIBUTIONS BY T.F. YEN J.G. Reynolds . . . . .	 29
Introduction . . . . .	29
Research summaries . . . . .	29
Metals in the asphaltene . . . . .	29
Metals classifications . . . . .	31
Mass spectrometry of petroporphyrins . . . . .	32
Nature of porphyrins in kerogen — evidence for trapped etio-type porphyrins . . . . .	38
Model compounds — highly substituted porphyrins . . . . .	39
Synthesis and characterization of non-porphyrin model compounds . . . . .	42
Structure of vanadium in asphaltenes . . . . .	49
Conclusions . . . . .	54
Acknowledgements . . . . .	55
References . . . . .	55
 <i>Chapter 4</i> MONTE CARLO SIMULATION OF ASPHALTENE STRUCTURE, REACTIVITY AND REACTION PATHWAYS M. Neurock and M.T. Klein . . . . .	 59
Introduction . . . . .	59
Modeling asphaltene structure . . . . .	61
Characterization and development of probability distribution functions . . . . .	63
Computational implementation: sampling probability distribution functions . . . . .	67
Modeling the thermal reactivity of asphaltene . . . . .	73
Monte Carlo simulation of asphaltene reaction . . . . .	76
General principles and techniques . . . . .	76
Application of the variable-time step monte carlo simulation to asphaltene pyrolysis . . . . .	81

Monte Carlo simulation of asphaltene structure, reactivity, and reaction: results . . . . .	82
Molecular products and characteristics . . . . .	85
Molecular weight distribution . . . . .	91
Hydrogen to carbon ratio (H/C) . . . . .	92
Average molecular attributes and average analytical results . . . . .	92
Global reaction products . . . . .	95
Solid–liquid–vapor equilibria-based global product results . . . . .	97
Bond breaking chemistry only . . . . .	97
Effect of hydrogen transfer . . . . .	98
Empirical global product determination . . . . .	99
Conclusions . . . . .	99
Acknowledgements . . . . .	101
References . . . . .	101
 <i>Chapter 5</i> THERMODYNAMIC PROPERTIES OF ASPHALTENES: A PREDICTIVE APPROACH BASED ON COMPUTER ASSISTED STRUCTURE ELUCIDATION AND ATOMISTIC SIMULATIONS M.S. Diallo, T. Cagin, J.L. Faulon and W.A. Goddard III . . . . .	103
Introduction . . . . .	103
Computer assisted structure elucidation of petroleum geomacromolecules . . . . .	105
Conventional approach . . . . .	106
Deterministic approach . . . . .	106
Stochastic approach . . . . .	107
Estimation of thermodynamic properties of condensed phase systems from atomistic simulations . . . . .	108
Computer assisted structure elucidation of arab berri asphaltenes . . . . .	111
Structural input data . . . . .	111
Model generation . . . . .	112
Volumetric and thermal properties of arab berri asphaltenes from molecular dynamic simulations . . . . .	118
Molar volume, density, cohesive energy and solubility parameter at 0 K . . . . .	118
Effects of temperature and pressure on molar volume, solubility parameters and enthalpy . . . . .	119
Summary and conclusions . . . . .	123
Acknowledgements . . . . .	124
References . . . . .	124
 <i>Chapter 6</i> KINETICS AND MECHANISMS OF ASPHALTENE CRACKING DURING PETROLEUM RECOVERY AND PROCESSING OPERATIONS A. Chakma . . . . .	129
Introduction . . . . .	129
Kinetics . . . . .	130
Asphaltene . . . . .	131
Model H1 . . . . .	133
Model H2 . . . . .	133
Model H3 . . . . .	134
Model H4 . . . . .	135
Model P1 . . . . .	135
Model P2 . . . . .	136
Model KP1 . . . . .	138
Coal-derived asphaltenes . . . . .	139
Model component studies . . . . .	141
In situ combustion . . . . .	144
Conclusions . . . . .	146
References . . . . .	146

<b>Chapter 7</b>	<b>ASPHALTENE HYDROCONVERSION</b>	
	R.B. Solari	149
Introduction		149
Asphaltene hydroconversion processes		150
Coil and soaker hydrovisbreaking reactor		150
Fixed-bed reactors		152
Mobile fixed-bed reactor		155
Ebullating-bed reactor		156
Slurry reactors		159
Catalysts		163
Asphaltene reactivity		167
Conclusions		169
References		169
 <b>Chapter 8</b>	 <b>THEORETICAL PRINCIPLES OF THE BITUMEN STRUCTURE AND THE ROLE OF ASPHALTENES (BASED ON RHEOLOGICAL METHOD)</b>	
	L.M. Gokhman	173
Introduction		173
Theoretical premises — concepts		173
The common criterion of disperse structures of bitumens and other organic binders; asphaltene complex		174
General curve of structure formation for bitumens and other organic binders; critical concentrations of structure formation: $C_v^*$ , $C_v^{**}$ , $C_v^{max}$		175
Mono-, bi-, and poly-dispersed nuclei of the dispersed-phase particles, poly-extreme curve of the structure formation		177
Complex of parameters characterizing the spatial disperse structure of binders		177
Experimental confirmation of theoretical concepts		179
Multivariate analysis of the influence of asphaltene complex quality on the properties of model bitumens; substantiation of $C_v$ as the main criterion of the binder structure		179
Multivariate analysis of influence of factors characterizing properties of asphaltenes and asphaltene complexes on the rheological and physical-mechanical properties of bitumens		187
Multivariate analysis of the influence of asphaltene chemical composition on properties of bitumens		191
Multivariate analysis of the influence of parameters characterizing an ability of asphaltenes to interact with the dispersion medium on rheological and physical-mechanical properties of bitumens		192
Multivariate analysis of the influence of parameters characterizing the properties of an asphaltene complex on rheological and physical-mechanical properties of bitumens		193
Influence of the volume of asphaltene complexes on properties of commercial bitumens; substantiation of values of the first and second critical concentrations of structure formation		194
Influence of the volume of asphaltene complexes on rheological, thixotropic and physical-mechanical properties of bitumens		195
Effect of the volume of asphaltene complexes on bitumen aging		203
Structure formation at increasing the content of the nuclei of dispersed-phase particles in the system with the formation of mono-, bi- and polydisperse nuclei; poly-extreme curve of structure formation		206
Influence of the properties of asphaltenes on parameters of the bitumen disperse structure		216
Gluing ability of binders — influence of asphaltene properties and asphaltene complexes on the strength of asphalt concretes		221
Acknowledgements		226
References		226

<i>Chapter 9</i>	<b>ELECTRON SPIN RESONANCE STUDY OF BITUMINOUS SUBSTANCES AND ASPHALTENES</b>	
	H.-L. Chang, G.K. Wong, J.-R. Lin and T.F. Yen . . . . .	229
Introduction . . . . .		229
Basic principles . . . . .		230
Mathematical representation . . . . .		231
ESR parameters . . . . .		231
Spin concentration . . . . .		231
Landé g-value . . . . .		232
Linewidth . . . . .		233
Lineshape . . . . .		233
Free radical concept of bituminous substances . . . . .		235
Origin and nature of radicals in coal and bitumen . . . . .		237
The role of radicals in fuel processing . . . . .		238
Correlation of ESR parameters . . . . .		239
Spin concentration and aromaticity of petroleum asphaltenes . . . . .		239
ESR adsorption and coal rank . . . . .		243
Lineshape and linewidth of coals . . . . .		248
g-values and heteroatom content . . . . .		252
Kerogen maturation and paleotemperature . . . . .		257
Heat treatment and ESR characteristics . . . . .		259
Temperature effects on ESR absorption . . . . .		261
Pyrolysis of carbonaceous products . . . . .		262
ESR of refinery and processed products . . . . .		265
Analytical fractions from coal liquids . . . . .		267
Process products from coal liquefaction . . . . .		271
Conclusions . . . . .		272
Uniqueness of the ESR approach . . . . .		272
Weakness of the ESR approach . . . . .		273
Future trends . . . . .		274
List of symbols . . . . .		275
Acknowledgements . . . . .		276
References . . . . .		276
<i>Chapter 10</i>	<b>CHEMICAL COMPOSITION AND CHARACTERISTICS OF RESIDUES OF CHINESE CRUDE OILS</b>	
	W.-J. Liang, G.-H. Que, Y.-Z. Chen and C.-G. Liu . . . . .	281
Introduction . . . . .		281
Experimental results . . . . .		281
Samples . . . . .		281
Separation methods . . . . .		282
Elemental analyses . . . . .		284
Average molecular weight . . . . .		284
Nuclear magnetic resonance spectroscopy . . . . .		284
Infrared spectroscopy . . . . .		284
X-ray diffraction . . . . .		285
Method of calculation of structural parameters . . . . .		285
Structural parameters by the modified Brown-Ladner method . . . . .		285
Average side chain length ( $L$ ) based on IR . . . . .		287
Results and discussion . . . . .		288
Elemental composition of residues . . . . .		288
SARA composition . . . . .		289
Average structural parameters of vacuum residues and their fractions . . . . .		291
Residues . . . . .		291

Saturates . . . . .	292
Aromatics . . . . .	293
Resins . . . . .	293
Asphaltenes . . . . .	295
Waxes . . . . .	299
Distribution of nitrogen, nickel and carbon residue of vacuum residues . . . . .	299
Nitrogen . . . . .	299
Nickel . . . . .	302
Carbon residue . . . . .	302
Conclusions . . . . .	303
Acknowledgements . . . . .	303
References . . . . .	303

#### *Chapter 11*      ANALYSIS OF ASPHALT AND ITS COMPONENTS BY THIN-LAYER CHROMATOGRAPHY

K. Dunn, G.V. Chilingarian, H. Lian, Y.Y. Wang and T.F. Yen . . . . .	305
Introduction . . . . .	305
Thin-layer chromatography in asphalt analysis . . . . .	306
TLC . . . . .	306
Chromatotron . . . . .	310
TLC-FID . . . . .	312
Quantitative aspects of TLC developed . . . . .	315
TLC . . . . .	315
Chromatotron . . . . .	315
TLC-FID . . . . .	315
Conclusion . . . . .	316
References . . . . .	316

#### *Chapter 12*      PRECIPITATION OF ASPHALTENES IN HEAVY OIL AND TAR SANDS

N.F. Carnahan . . . . .	319
Introduction . . . . .	319
Definition of terms . . . . .	319
Mechanisms . . . . .	320
Solid-fluid phase equilibrium . . . . .	321
Solubility theory and asphaltenes . . . . .	321
Solubility of resins and asphaltenes . . . . .	321
Macroscopic point of view . . . . .	322
Microscopic point of view . . . . .	322
Characterization of the petroleum heavy fraction . . . . .	323
Calculation method — macroscopic model . . . . .	323
Apparent solubility parameter for asphaltenes . . . . .	324
Solubility parameters of petroleum fluids . . . . .	325
Solubilization of asphaltenes (microscopic viewpoint) . . . . .	326
Microscopic vs. macroscopic models . . . . .	327
Ionic and/or electrochemically induced asphaltene precipitation . . . . .	328
Mechanical shear-induced asphaltenes precipitation . . . . .	329
Discussion . . . . .	329
What is the principal mechanism of asphaltenes precipitation? . . . . .	329
Other mechanisms which influence precipitation of asphaltenes . . . . .	330
Summary and conclusions . . . . .	331
References . . . . .	332

<b>Chapter 13</b>	<b>CHARACTERIZATION OF ASPHALTENIC DEPOSITS FROM OIL PRODUCTION AND TRANSPORTATION OPERATIONS</b>	
	L. Carbognani, J. Espidel and A. Izquierdo	335
Introduction		335
Deposit characterization and classification		338
SARA fractions characterization. Identification of possible causes for crude oil instability		340
Preliminary insights into the composition of insoluble organic materials		347
Deposits characterization as a guideline for cleaning operations		356
Conclusions		358
Acknowledgements		358
References		359
<b>Chapter 14</b>	<b>CHEMICAL COMPOSITION OF ASPHALT AS RELATED TO ASPHALT DURABILITY</b>	
	J.C. Petersen	363
Introduction		363
Preliminary consideration of factors affecting asphalt durability		364
Chemical composition of asphalt		364
Elemental and molecular composition		364
Asphalt composition as defined by fractionation		366
Interactions among asphalt component fractions and relationships with durability		371
Changes in chemical composition on aging		373
Molecular interactions — a fundamental approach to chemical factors affecting asphalt durability		378
Fundamentals of molecular interactions and effects of molecular interactions on flow properties		379
Major chemical functional group types affecting asphalt properties		382
Effects on asphalt performance of polar functional groups formed on oxidation		383
Effects of polar asphalt components on viscosity and aging characteristics		386
Composition and component compatibility		388
Importance of molecular structuring to the flow properties of asphalt		390
Summary and concluding concepts		393
Acknowledgements		395
References		395
<b>Chapter 15</b>	<b>BITUMEN ASSOCIATED WITH PETROLEUM FORMATION, EVOLUTION AND ALTERATION — REVIEW AND CASE STUDIES IN CHINA</b>	
	Z.-J. Wu, P. Peng, J.-M. Fu, G.-Y. Sheng and D.-H. Liu	401
Introduction		401
Genetic types of bitumen and their distribution		401
Primary authigenic bitumen		402
Secondary reservoir bitumen		403
Weathered or degraded supergene bitumen		403
Magmatic thermal alteration bitumen		404
Occurrence, classification and nomenclature of bitumens during petroleum evolution processes		404
Parameters for evaluating bitumen maturity and application		404
Classification of bitumen maturity		410
Occurrence of bitumen and its origin		412
Biological markers in bitumens		418
Methods of analyzing biomarkers in bitumens		418
Application of biomarkers in studying the origin and thermal maturity of bitumen		422
Case studies		424
High-sulfur immature bitumen in the Zhujiashuang Sulfur Deposit, Shandong Province, East China		424
Silurian bituminous sandstone in the Tarim Basin, northwestern China		427
Bitumen vein deposit in Ghost City, Jungger Basin, northwestern China		435

Bitumen in highly mature carbonate rocks, southern China . . . . .	437
References . . . . .	442
 <i>Chapter 16</i> <b>ASPHALT OXIDATION</b>	
F.C. Thyron . . . . .	445
Introduction . . . . .	445
Asphalt, resins and asphaltenes . . . . .	445
Definition . . . . .	445
Structure . . . . .	447
Molecular characterization of asphalt and its constituents . . . . .	448
Asphalt and heavy oils . . . . .	448
Asphaltenes . . . . .	450
Metals in heavy fractions . . . . .	451
Main features of oxidation of organic substances . . . . .	451
Kinetics of autoxidation . . . . .	452
Initiation . . . . .	453
Propagation . . . . .	454
Decomposition of peroxides . . . . .	454
Heteroatomic organic molecules as antioxidants . . . . .	455
Sulfur containing molecules as peroxide decomposers . . . . .	456
Phenol and amine as radical chain-breaking antioxidants . . . . .	456
The electron releasing and electron acceptor mechanisms . . . . .	458
Oxidative degradation via a non-peroxyl radical chain pathway (ETIO) . . . . .	459
Oxidation of asphalts and asphalts constituents . . . . .	459
Asphaltenes and maltenes . . . . .	459
Oxidation of asphalts . . . . .	462
Nature of the products and mechanisms . . . . .	462
Inhibitors and prooxidants in asphalt oxidation . . . . .	465
Kinetics and factors influencing asphalt oxidation . . . . .	467
Conclusions . . . . .	470
References . . . . .	471
 <i>Chapter 17</i> <b>A KINETIC APPROACH TO THE AGING OF BITUMENS</b>	
A.F. Verhasselt . . . . .	475
Introduction . . . . .	475
The aging of a bituminous binder in service . . . . .	476
Kinetic development . . . . .	476
Review of some concepts in chemical reaction kinetics . . . . .	476
Application to bitumen aging . . . . .	477
Theoretical approach . . . . .	477
Generalization of this theoretical approach . . . . .	478
Choice of indicators . . . . .	479
Procedure . . . . .	480
Evaluation of activation energy . . . . .	481
From the laboratory to the field . . . . .	481
Factors to be considered . . . . .	481
Aging in construction . . . . .	482
Kinetic mean temperature on site . . . . .	483
Experimental approach . . . . .	485
Description of the accelerated test device RCAT (Rotating Cylinder Aging Test) . . . . .	485
Bitumens investigated . . . . .	487
Test results and interpretation . . . . .	487
Extrapolation to field conditions . . . . .	492
Discussion of a few results reported in the literature . . . . .	493



Laboratory/field comparison . . . . .	494
Conclusions . . . . .	495
References . . . . .	497
 <i>Chapter 18</i> OIL SHALES IN ASPHALT MIXES	
D. Vitorović and D. Svetel . . . . .	499
Introduction . . . . .	499
Oil shales as filler . . . . .	500
Investigations of oil shale fillers . . . . .	505
Properties required of oil shale fillers . . . . .	505
Granulometric composition of the oil shale filler . . . . .	506
Investigations of oil shale filler related to the spatial designing of asphaltic mixtures . . . . .	507
Spatial design of asphaltic mixtures with oil shale filler . . . . .	508
Potential use of oil shale as a filler in special asphaltic mixtures and bituminous aggregates . . . . .	511
References . . . . .	512
 <i>Chapter 19</i> SULPHUR-MODIFIED ASPHALTS	
I. Gawel . . . . .	515
Introduction . . . . .	515
Sulphur–asphalt interaction . . . . .	515
Chemically bonded sulphur . . . . .	516
Dissolved sulphur . . . . .	518
Crystalline sulphur . . . . .	518
Preparation of sulphur–asphalt mixtures . . . . .	520
Technological processes . . . . .	521
Effect of sulphur upon the properties of asphalt . . . . .	523
Environmental and safety aspects . . . . .	528
Applications . . . . .	530
Economic aspects . . . . .	531
References . . . . .	533
 <i>Chapter 20</i> PRODUCTION AND RESEARCH DEVELOPMENT OF ASPHALTS IN CHINA	
Y.-H. Fan, C.-X. Zhang, G.-J. Ding and Y.-Z. Zhang . . . . .	537
Introduction . . . . .	537
Development of chemical composition research . . . . .	540
Investigation of asphalt aging . . . . .	546
Asphalt aging in TFOT . . . . .	546
Durability of paving asphalts by absorption of oxygen . . . . .	548
Effect of absorbing oxygen on the physico-chemical properties of asphalts and their constituents . . . . .	549
Advances in manufacture of asphalts . . . . .	550
Continuous asphalt blowing . . . . .	550
Supercritical solvent extraction of petroleum residue . . . . .	551
References . . . . .	556
 <i>Chapter 21</i> WAX PRECIPITATION FROM PETROLEUM FLUIDS: A REVIEW	
C. Lira-Galeana and A. Hammami . . . . .	557
Introduction . . . . .	557
Characterization and properties of wax components in petroleum fluids . . . . .	558
Petroleum chemistry and composition . . . . .	558
Saturates . . . . .	559
Aromatics . . . . .	559
Resins . . . . .	559
Asphaltenes . . . . .	560
Analytical methods . . . . .	561

Modified UOP 46-64 method for wax content determination . . . . .	561
UOP asphaltene content ( <i>n</i> -pentane insoluble material) . . . . .	561
Detailed PNA analysis of waxes and waxy crudes . . . . .	562
Refined PNA analysis for waxes and waxy crudes . . . . .	567
Experimental methods for wax precipitation from petroleum fluids . . . . .	569
Measurements of cloud/pour point temperatures of dead oils . . . . .	571
ASTM cloud point methods . . . . .	571
ASTM pour point method (ASTM D97) . . . . .	572
WAT using cold finger (CF) . . . . .	572
WAT using standard viscometry . . . . .	572
Cloud and pour points using complex viscometry . . . . .	573
WAT using differential scanning calorimeter (DSC) . . . . .	574
WAT using cross polarized microscopy (CPM) . . . . .	576
Cold filter . . . . .	578
Measurements of cloud/pour point temperatures of live oils . . . . .	579
WAT using light transmittance . . . . .	579
WAT using ultrasonics . . . . .	581
Bulk deposition measurements . . . . .	582
Standardized measurement techniques: WAT under flow conditions . . . . .	583
Comparisons of laboratory paraffin wax deposition data with observed field results . . . . .	584
Review of methods to model wax precipitation in petroleum fluids . . . . .	585
Thermodynamic basis of oil–wax equilibria . . . . .	586
References . . . . .	605
Subject Index . . . . .	609

This page intentionally left blank

## *Chapter 1*

# **INTRODUCTION TO ASPHALTENES AND ASPHALTS, VOLUME 2**

GEORGE V. CHILINGARIAN and TEH FU YEN

Asphaltenes are possibly the most studied and yet least understood materials in the petroleum industry. Everything about asphaltenes appears to be non-conclusive, elusive, and complex. However, asphaltenes have attracted numerous researchers with varied views and research approaches, varying from practical modeling approach to ivory tower study of asphaltene molecular structures. Many books have been published recently only to contribute to the diversity of the research ideas dealing with the asphaltene problems.

Asphaltenes are considered to be the least valuable component of the crude oil. The presence of asphaltene causes a marked increase in crude oil viscosity [19], making it difficult to transport and process. Due to their high resistance to cracking, asphaltene molecules are usually held responsible for decreasing the yield of petroleum distillates. Besides, due to the presence of heavy metal components, asphaltenes are very difficult to biodegrade, making them the most undesired compound from a petroleum waste management perspective [1]. Similar concerns persist in petroleum reservoir management. It is widely known that asphaltene precipitation can take place during miscible displacement, thermal recovery, stimulation operations, or even primary depletion, leading to wellbore plugging.

Many of the properties that make asphaltenes undesirable can also make them useful, depending on the application in question [2,3]. For instance, asphalt, a derivative of asphaltenes, is the material of choice for highway surfaces. For this application, bio-inertness, rheological toughness and adhesion are necessary properties. These same properties make asphalt an ideal candidate for protective coating applications. In the petroleum industry, asphaltene properties are desirable for use in drilling fluids (fluid-loss control) and to achieve the wellbore stability. When it comes to usefulness of asphaltenes in reservoir applications, examples are not readily available. Only recently, Islam [4] identified the contribution of asphaltic crudes in increasing the generation and retention of microbubbles that can enhance oil recovery significantly. For the same reason (charged particles), ultrasonic [5] or electromagnetic irradiation [7] can provide an attractive means to mobilize crude oil in pipelines. Further investigations show that the presence of asphaltene merits special considerations for planning an enhanced oil recovery scheme, even the emerging ones [6,7].

Despite numerous publications on the topic of asphaltene characterization [9], solubility studies [10,22], transport in pipelines [11,25] or in porous media [12], there remains a significant gap between established sciences and speculative study in asphaltene research. Today, even the impact of asphaltenes is not well understood. For instance, only recently the beneficial effects of asphaltenes, notably in reducing free gas, are coming to light [4,13]. Many scientists considered the size of asphaltene molecules to be very large, only to witness recent findings which argue that asphaltene molecules more likely are in the much shorter size range [14]. After decades of debate

over colloidal structures of asphaltene molecules, fractals are being used [15,16], only to realize that this might be a misunderstanding after all [17]. Even though it appears that engineering studies are making headway in terms of mathematical modeling, when it comes to porous medium applications, the first model, coupling irreversible thermodynamics, adsorption, mechanical entrapment, and precipitation, is yet to be perfected [8]. It is necessary to develop a reservoir simulation that captures all salient features of multi-phase, multicomponent flow while modeling asphaltene precipitation and ensuing plugging. It appears that even the phase behavior is a function of asphaltene concentration [13,18,19]. Of course, this will require the development of a new equation of state, which can also explain the time dependence of bubble release from a crude oil, especially in the presence of oppositely charged microbubbles. If one has to identify an area that needs more attention from researchers dealing with asphaltenes, it is the macroscopic description of asphaltene precipitation and propagation in porous media. The obvious complexity of the problem arises from many unknowns that are yet to be discovered from the areas of characterization of porous media as well as asphaltenes.

It is very important to mention here the research work of James G. Speight, which focused on the processability of heavy crude oil and bitumen. This research had thrown light on the chemical and physical nature of feedstock behavior during processing.

He focussed on: (1) the asphaltene structure and moved away from the conventional thought of asphaltenes as molecules that contained large polynuclear aromatic systems; (2) standard separation of asphaltenes; (3) molecular make-up of the asphaltene fraction; (4) molecular weights of asphaltenes; (5) functional types in asphaltenes; (6) thermal reactions of asphaltenes and resins, and the chemistry of coke formation; and (7) structure of petroleum [20–22]. Thus, the research work of Speight led to a better understanding of processing options [23].

Mansoori and his collaborators at the University of Illinois at Chicago [24–27] have developed a comprehensive package of computer programs and database which calculates various properties of petroleum fluids containing heavy organics. This package, which has taken over twelve years to develop and test, is based on the following principles: (1) quantum mechanics, (2) statistical mechanics, (3) neural network statistics, (4) rdf-based mixing rules and conformal solution equations of state, (5) polydisperse monomer–polymer solution theories with renormalization group theory corrections for appreciable large size differences, (6) polydisperse statistical mechanics and thermodynamics, (7) various continuous mixture phase equilibrium algorithms, (8) solid–fluid phase transition theories (variational, lattice models, dislocation theory, polymer collapse), (9) electrokinetic phenomena, (10) transport phenomena, (11) micellar and steric colloidal solution theories, and (12) fractal kinetics of aggregation and percolation theories. This package is general enough to predict the heavy organics–oil–well interaction problems wherever they may occur during oil production, transportation or processing. The emphasis of the package is on the prediction of the behavior of asphaltenes, resins, diamondoids, sulfur, organometallics and paraffin waxes, and their roles and interactions in the production and processing of natural and synthetic hydrocarbons.

This package and database can be utilized by:

(1) Reservoir and production engineers for oil recovery simulation studies and design of well completions and surface facilities.

(2) Research and process engineers for the design and performance evaluation of crude oils, bitumen, and heavy-oil-related facilities and processes.

(3) Petroleum engineers, refiners and NGL processing engineers for the design of cost-effective anti-foulants for heavy organic fouling mitigation in various processes.

As examples of its utility the package was tested for the following cases with success:

(1) Prediction of the onset, amount, size distributions, and redissolving conditions of asphaltenes, resins, and other heavy organics present in various petroleum crude oils and gas condensates due to: (a) introduction of high-pressure miscible gaseous or liquid solvents; and (b) changes of composition, pressure, temperature, and wellbore effects.

(2) Prediction of the onset and amount of heavy organic precipitation in pipeline transport, when blended with NGL at different blending ratios, temperatures, and flow conditions.

(3) Design and selection of anti-foulants to improve heavy organic dispersivity and, as a result, to prevent heavy organic fouling in processing equipment.

The kind of input data which may be used in the package are: (a) static and dynamic pour points; (b) cloud point; (c) onsets of precipitation, flocculation, and deposition data due to addition of known miscible solvents; (d) bottomhole (and/or stock-tank oil) sample(s) composition and physical property data; (e) oil aromaticity; (f) oil paraffin, resin, asphaltene, organometallics, sulfur and diamondoid contents; (g) zeta potential and refraction data; (h) characterization data for  $C_7+$  fraction of oil; and (i) NMR and chromatography (GC, LC, HPLC and GPC) data of oil fractions.

Some of the highlights of the present book are presented below.

Historical review of the terms bitumen, asphalt and asphaltene is presented by one of the editors, T.F. Yen, in Chapter 2. He also presented a simple definition of asphaltene and pointed out differences between the natural and artificial asphalts [28].

M. Neurock and M.T. Klein presented a method for the molecular modeling of asphaltene structure, reactivity, reactions, and global pyrolysis product spectrum in Chapter 4. Their stochastic modeling approach uses Monte Carlo simulation to construct and react a representative ensemble of asphaltene molecular structure, which provides a detailed molecular composition of the reacting mixture as a function of reaction time. This is a logical foundation from which to estimate the mixture properties.

The authors used the Monte Carlo method to sample quantitative probability distribution functions (pdfs) for each of the molecular attributes (e.g., length of a side chain and number of aromatic rings). These pdfs are optimized by minimizing the difference between the laboratory analytical measurements and the calculated properties (e.g., MW and H/C ratio) of the computer representation.

A. Chakma reviewed the asphaltene cracking kinetics in Chapter 6. Inasmuch as the asphaltenes constitute a complex solubility class, it is not possible to determine a comprehensive reaction mechanism based on reaction fundamentals. Kinetic models based on pseudo-component approach (reaction products are divided into a number of easily quantifiable pseudo-components) are available. Such models constitute practical tools for engineering calculations involving asphaltene cracking in petroleum recovery and processing applications.

In Chapter 11, K. Dunn et al. conclude that the thin-layer chromatography has great potential of becoming a standard method for quantification of asphaltic components.

According to N.F. Carnahan (Chapter 12), production and processing conditions favoring the asphaltene deposition are predictable using thermodynamic methods and correlations developed from experience with polymer solutions and micellar solution theories. Owing to the low mobility of asphaltene particles in heavy crude oils and tar sands, phase behavior of asphaltenes is difficult to observe experimentally.

Phase separation, aggregation, and precipitation of asphaltene in petroleum systems can be explained using (1) thermodynamics of phase equilibrium, (2) molecular theory, (3) physical chemistry of amphiphilic substances, (4) chemical principles, (5) experimental data, and (6) field observations.

In Chapter 18, D. Vitorović and D. Svetel investigate the possible use of oil shale filler instead of the standard limestone filler in asphalt mixes. Further research work is necessary to evaluate the advantages of using oil shale.

There are two reasons for considering the use of sulfur in asphalt mixes: (1) to improve the mix quality, and (2) to reduce the cost. Irena Gawel discusses sulfur-modified asphalts in Chapter 19.

Yaohua Fan, Changxiang Zhang, Guojing Ding and Yuzhen Zhang reported on the properties, characteristics and classification of asphalts in China (Chapter 20). These asphalts have a high wax content, low ductility and poor durability. The authors proposed a process of deasphalting the crude oil and manufacturing better-quality asphalts.

## REFERENCES

- [1] Al-Maghrabi, I., Bin-Aqil, A.O., Chaalal, O. and Islam, M.R., Use of thermophilic bacteria for bioremediation of petroleum contaminants. *Energy Sources*, 21 (1/2): 202–212 (1999).
- [2] Mullins, O.C., Sulfur and nitrogen molecular structures in asphaltenes and related materials quantified by Xanes spectroscopy. In: E.Y. Sheu and O.C. Mullins (Editors), *Asphaltenes — Fundamentals and Applications*. Plenum, New York, pp. 53–96 (1995).
- [3] Islam, M.R., New methods of petroleum sludge disposal and utilization. In: E.Y. Sheu and O.C. Mullins (Editors), *Asphaltenes — Fundamentals and Applications*. Plenum, New York, pp. 219–235 (1995).
- [4] Islam, M.R., Role of asphaltenes in heavy oil recovery. In: T.F. Yen and G.V. Chilingarian (Editors), *Asphaltenes and Asphalts*, I. Developments in Petroleum Science, 40, Elsevier, Amsterdam, pp. 249–295 (1994).
- [5] Islam, M.R., Potential of ultrasonic generators for use in oil wells and heavy crude oil bitumen transportation facilities. In: E.Y. Sheu and D.A. Storm (Editors), *Asphaltenes — Fundamentals and Applications*. Plenum, New York, pp. 191–218 (1995).
- [6] Islam, M.R., Abou-Kassem, J.H. and Chaalal, O., Experimental and numerical studies of electromagnetic heating of a carbonate formation. SPE Paper No. 49187, *Proc. SPE Annual Technical Conference and Exhibition*, New Orleans, LA (1998).
- [7] Gunal, O. and Islam, M.R., Alteration of asphaltic crude rheology with electromagnetic and ultrasonic irradiation. *Proc. 2nd Int. Non-Renewable Energy Sources Congr.*, 3, Tehran, pp. 42–51 (1998).
- [8] Kocabas, I. and Islam, M.R., A wellbore model for predicting asphaltene plugging. SPE Paper No. 49199, *Proc. SPE Annual Technical Conference and Exhibition*, New Orleans, LA (1998).
- [9] Bentignies, J., Christophe, C.M. and Dexpert, H., Asphaltene adsorption on kaolinite characterized by infrared and X-ray adsorption spectroscopies. *J. Pet. Sci. Eng.*, 20: 233–237 (1998).
- [10] Park, S.J. and Mansoori, G.A., Aggregation and deposition of heavy organics in petroleum crudes. *Energy Sources*, 10: 109–125 (1988).
- [11] Mansoori, G.A., Asphaltene deposition: an economic challenge in heavy petroleum crude utilization

- and processing. *OPEC Review*, pp. 103–113 (1988).
- [12] Ali, M. and Islam, M.R., The effect of asphaltene precipitation on carbonate rock permeability: An experimental and numerical approach. *SPE Production and Facilities*, pp. 178–183 (Aug. 1998).
- [13] Paddock, J. and Islam, M.R., A new equation of state for a crude oil with microbubbles. CIM Paper No. 99-43, *Proc. Pet. Soc. CIM*, Calgary (June 1999).
- [14] Sheu, E.Y. and Storm, D.A., Colloidal properties of asphaltenes in organic solvents. In: E.Y. Sheu and O.C. Mullins (Editors), *Asphaltenes — Fundamentals and Applications*. Plenum, New York, pp. 1–52 (1995).
- [15] Raghunathan, P., Evidence for fractal dimension in asphaltene polymers from electron-spin-relaxation measurements. *Chem. Phys. Lett.*, 182 (3/4): 331–338 (1991).
- [16] Sahimi, M., Rasasmdana, H. and Dabir, B., Asphalt formation and precipitation: experimental studies and theoretical modeling. *SPE J.*, 2: 157–169 (1997).
- [17] Islam, M.R., University of Regina, Canada, Personal Communication (1999).
- [18] Wu, J., Prausnitz, J.M. and Firoozabadi, A., Molecular–thermodynamic framework for asphaltene–oil equilibria. *AIChE J.*, 44 (5): 1188–1198 (1998).
- [19] Werner, A., Behar, F. and Behar, E., Viscosity and phase behaviour of petroleum fluids with high asphaltene contents. *Fluid Phase Equilibria*, 147 (1/2): 343–349 (1998).
- [20] Speight, J.G. and Long, R.B., The concept of asphaltenes revisited. *Fuel Sci. Technol. Int.*, 14: 1 (1996).
- [21] Schabron, J.F. and Speight, J.G., The solubility and three-dimensional structure of asphaltenes. *Pet. Sci. Technol.*, 16: 361 (1998).
- [22] Anderson, S.I. and Speight, J.G., Thermodynamic models for asphaltene solubility and precipitation. *J. Pet. Sci. Eng.*, 22: 53 (1999).
- [23] Speight, J.G., Chemical and physical studies of petroleum asphaltenes. In: T.F. Yen and G.V. Chilingarian (Editors), *Asphaltenes and Asphalts*, 1. Developments in Petroleum Science, 40, Elsevier, Amsterdam, pp. 7–65 (1994).
- [24] Mansoori, G.A., Modeling of asphaltene and other heavy organic depositions. *J. Pet. Sci. Eng.*, 17: 101–111 (1997).
- [25] Mansoori, G.A., Asphaltene, resin, and wax deposition from petroleum fluids. *Arabian J. Sci. Eng.*, 21 (48): 707–723 (1996).
- [26] Escobedo, J. and Mansoori, G.A., Viscometric principles of onsets of colloidal asphaltene flocculation in paraffinic oils and asphaltene micellization in aromatics. *SPE Production and Facilities*, pp. 116–122 (May 1997).
- [27] Kawanaka, S., Park, S.J. and Mansoori, G.A., Organic deposition from reservoir fluids. *SPE Reservoir Engr. J.* (May), pp. 185–192 (1991).
- [28] Yen, T.F., Asphaltenes, types and sources. In: O.C. Mullins and E.Y. Sheu (Editors), *Structures and Dynamics of Asphaltenes*. Plenum, New York, pp. 1–39 (1998).



This page intentionally left blank

## Chapter 2

# THE REALMS AND DEFINITIONS OF ASPHALTENES

T.F. YEN

## HISTORICAL REVIEW OF BITUMEN, ASPHALT AND ASPHALTENE

China was the first country in the world to discover natural gas and petroleum. In *Han File*, Ban Gu (32–92 A.D.) recorded that “the waters of the You River in Gaonu are rich enough to burn; [and that] the fat in the waters can be collected for direct use.” Consequently, petroleum was referred to as stone lacquer (190 A.D.), light water (300 A.D.) or stone fat water (600 A.D.) in the classical records of China (Table 2-1) [1].

As early as around 2250 years ago, the first recorded salt well in China was dug in Shuang Lin County of the Sichuan Province by Li Bin. This was the forerunner of drilling technology. Both salt and natural gas were recovered. The well depth recorded during the Tang Dynasty (100 A.D.) was 250 m. The name of the heavy core was given to the tall wooden structures or derricks used for drilling, well cleaning and repairing, and brine lifting. Bamboo pipelines were used for transportation. A new cable drilling method was invented in the salt wells of Zigone (ca. 1041–1048 A.D). In 1835 A.D., the first well in the world, which exceeded 1000 m, was drilled and had blow-out on completion. The daily production of 8000 m<sup>3</sup> of natural gas and 14 m<sup>3</sup> of black brine was noted [2].

Shen Kuo (1031–1095 A.D.) also cited the first petrochemical industry in his *Notes on Mengxi* during the Song Dynasty. “There is rock oil in the Yan territory generated among sands and stones with water. It burns like flax but produces dense smoke.” While in charge of the Arms Office, Shen Kuo organized the processing and storage of

TABLE 2-1

Natural gas and petroleum are discovered in China by 190 A.D.

---

石漆 (Shi Qi)	: Bitumen, 190 A.D.
弱水 (Ruo Shui)	: Petroleum emulsion, 300 A.D.
火池 (天然氣) (Huo Chi) (Tian Ran Qi)	: Methane, 650 A.D.
石液墨 (Shi Ye Mo)	: Petroleum derived carbon, 1070 A.D.

---

petroleum for warfare purposes. He also described the carbon which is derived from natural gas combustion and used in making good-quality Chinese ink. This ink was marketed as 'Yan Chuan rock liquid'.

The use of bitumen and asphalt is considered very old. As described by Abraham [3], the Sumarians, Accadians, and Babylonians had used asphalt as mortar for building stones and building blocks as early as 3800 B.C. They used it to make reservoirs, canals and bathing pools watertight. In earlier biblical quotations, Noah used asphalt in the construction of the Ark. In Genesis 6: 14: "Make thee an ark of gopher wood; rooms shalt thou make in the ark, and shalt pitch it within and without with pitch." There are many versions of cuneiforms in the culture of the Euphrates and Tigris River Basin ranging from 2500 to 1500 B.C. used to record the worldwide floods and the use of asphalt for water-proofing [4]. There are many scripture descriptions of the use of asphalt and bitumen as a binder or mortar. In Genesis 11: 3: "... And they had brick for stones, and slime they had for mortar." This sentence describes the building of the Tower of Babel which occurred at around 2000 B.C. The English version is actually equivalent to the Septuagint version in which  $\alpha\sigma\phi\alpha\lambda\omicron\varsigma$ , meaning 'asphaltos', was used. Furthermore, the bulrush basket in which Moses was placed as an infant was made waterproof through the use of bitumen, e.g., Exodus 2: 3: "And when she could no longer hide him, she took for him an ark of bulrushes and doubled it with slime and with pitch, and put the child therein; and she laid it in the flags by the river's bank." The use of asphalt as a preservative was discovered when it was noted that in the present Dead Sea asphalt region there were asphalt-pitch in which an entire army had fallen. In Genesis 14: 10: "And the vale of Siddium was full of slime pits; and the Kings of Sodom and Gomorrah fled, and fell there ...". The preservation properties of asphaltene for biomass was later adopted by the Egyptians for mummification and for embalming practices during the Roman times.

Excavations in the Indus Valley of northwestern India had found asphalastic composed of a mixture of asphalt, clay, gypsum and organic matter between two brick walls as well as on the outside of walls and beneath the floor of a bathing pool used for ritualistic cleansing. The age of the mixture dated about 3000 B.C., which is considered the prewriting period of India. This mastic was also used for inlaid decorations, as an adhesive for the application of ornaments to statues, and as a protective coating for woodwork. Seepages of liquid asphalt, as well as many rock asphalt deposits, exist today on the Basti River in Kashmir as well as near Hotien, Xinjiang, China. Without a doubt, an advanced civilization had developed in this region and the migration of ideas between East and West had taken place. The name, 'bitumen', can be traced back to Latin, which was derived from Sanskrit; and the version of all Sanskrit was based on Chinese (Table 2-2). The word, 'asphalt', can be traced back to the Assyrians and Accadians, but very close to Chinese 'Nian Tu' or 'Shi Hua Nian Tu' (Table 2-3). This is not surprising since there are a number of similarities between the New Stone Age of the Chinese culture and the Assyrians and Babylonians. An example of these similarities is that 'Gu Bei You' in Chinese is equivalent to 'Ku pur' in Assyrian. Even the Hebrew language 'zephet' for asphalt is related to the Chinese 'Yi Bei' (Table 2-4). Since asphalt and pitch have medicinal uses, especially for skin diseases, the Chinese medicine 'Yi Shi Zhi' is similar to the Sumarian 'Esirlah', and to the English 'Echthamrol' (see

TABLE 2-2

The origin of the word 'bitumen'

膠土 (Jiao Tu)	Jatu	Gwitumen	
石蠟膠土 → (Shi La Jiao Tu)	Sila-jatu →	Pixtumen →	Bitumen
石墨焦炭膠土 (Shi Mo Jiao Tan Jia Tu)	Asmajatam-jatu	Bitumen	
<u>Chinese</u>	<u>Sanskrit</u>	<u>Latin</u>	<u>French and English</u>

TABLE 2-3

The origin of the word 'asphalt'

黏土 (Nian Tu)	Iddu Ittu			
→	Ituu →	ασφαλτοζ →	Asphalte →	Asphalt
石化黏土 (Shi Hua Nian Tu)	Sippatu Asphaltu Sphallo			
<u>Chinese</u>	<u>Assyrian and Accadian</u>	<u>Greek</u>	<u>French and Latin</u>	<u>English</u>

Table 2-5). Actually, the English 'pitch' and 'tar' may also originate from Chinese (see Tables 2-6 and 2-7).

It is possible that in ancient times, about 3000–4000 B.C., there were interactions such as the trading of goods between the Near East and Far East. The transportation of culture between the two regions took a rather long time, e.g., a thousand years. In contrast, at present communication among different parts of the world requires only seconds. Nevertheless, there are many similarities in the sounds of spoken languages from Babylon, Persia, and China [5–8].

Asphaltene acquired its name more recently; in 1837 A.D., Boussingoult of France [9] gave this name to his separated product of asphalt. When asphalts are diluted with *n*-pentane, hard friable materials are precipitated. He named asphaltene for these dark materials after precipitation from *n*-pentane. In 1916, C. Richardson in England [10] gave the name carbene, meaning asphaltene which is insoluble in carbon tetrachloride,

TABLE 2-4

The origin of the word ‘zephet’ in Hebrew and ‘ghir’ in Persian

鬘柏油 (Yi Bei You)			zephet		zift zipht				
古柏油 (Gu Bei You)	→	kupur	→	kupru kukru	→	kofer kopher	→	ghir keribar	
黑柏油 (Hei Bei You)					hemar	humar houmar			
<u>Chinese</u>		<u>Assyrian</u>		<u>Babylonian</u>		<u>Hebrew</u>		<u>Arabic - Turkish</u>	<u>Persian</u>

TABLE 2-5

Medicinal ointment ‘ichthamnol’ and its origin

魚石腊 (Yu Shi La)	→	Esir	→	Ichthyoleum
		Esirlah		
魚石脂 (Yu Shi Zhi)	→	Esirea	→	Ichthamnol
		Esir-harsag		
<u>Chinese</u>		<u>Sumerian</u>		<u>English</u>

TABLE 2-6

Trace of the word ‘pitch’ to Chinese ‘Fei’

Pitch	←	Pich	←	Pic	←	Picis Pic (em) Pix	←	Pek	←	Pech	←	Pilta Pissa Pikia	←	Pi	←	Fei 肥
<u>Modern</u>		<u>ME</u>		<u>OE</u>		<u>Latin</u>		<u>Dutch</u>		<u>G</u>		<u>Greek</u>		<u>Indo- European</u>		<u>Chinese</u>

TABLE 2-7

The Chinese origin of 'tar'

tar	←	tarr (e) ter (re)	←	teru terwes	←	treow	←	teer	←	qir qhir kir	←	tjara	←	Qi 漆
<u>Modern</u>		<u>ME</u>		<u>OE</u>		<u>L</u>		<u>G</u>		<u>Arabic</u>		<u>Isl</u>		<u>Chinese</u>

but soluble in benzene and chloroform. Later, in 1931, J. Marcusson of Germany [11] classified asphalt into three fractions:

*Neutral resins* — insoluble in alkalies and acids and completely miscible with petroleum oil including the C<sub>5</sub> fraction.

*Asphaltenes* — insoluble in light gasoline and petroleum ether. Both asphaltene and neutral resins are completely soluble in benzene, chloroform and carbon disulfide.

*Carboids* — or free carbons, readily found at higher temperatures, completely insoluble in benzene.

#### NATURAL AND ARTIFICIAL ASPHALTS AND ALLIED SUBSTANCES

Although usage of the terms asphalt and bitumen are interchangeable in the United States, in Europe asphalt denotes the impure form of the generic material, whereas the bitumen, the basic mixture of heavy hydrocarbons free of inorganic impurities. The American Society for Testing and Materials has promulgated the following standard definitions [12].

(1) *Relating in general to bituminous materials.* Bitumen, a class of black or dark-colored (solid, semisolid, or viscous) cementitious substances, natural or manufactured, composed principally of high-molecular-weight hydrocarbons, of which asphalts, tars, pitches, and asphaltites are typical.

(2) *Relating specifically to petroleum asphalts.* Asphalt, a dark, brown to black cementitious material, solid or semisolid in consistency, in which the predominating constituents are bitumens that occur in nature as such, or are obtained as residua in refining petroleum.

At the Fifth World Petroleum Congress (WPC) [13] the designation naphtha bitumens was proposed for naturally-occurring organic materials soluble in carbon disulfide, such as petroleum, coal, and related products. Included are the substances commonly called asphalts, which comprise the hard native bituminous ozokerite and asphaltite. The term bitumen was suggested [14] for this family of substances and asphalt for the residual material obtained by the distillation of petroleum. The combination of the two types is sometimes referred to as asphaltic bitumen. On the other hand, the United Nation's Institute of Training and Research (UNITAR) formulated a tentative definition of asphalt which considers the origin of this material as a basis for classification [15].

Natural asphalt is normally composed of organic and mineral matter and contains variable amounts of water. The organic portion is composed of a complex mixture of hydrocarbons, asphaltenes, and resins, with significant quantities of sulfur, oxygen, and nitrogen compounds. Also present are compounds of vanadium, nickel, iron, and other metals. Asphalt is a term commonly applied to a refinery product called 'petroleum asphalt' and 'refinery asphalt'.

For convenience, asphalt can be classified into natural and artificial asphalts. Natural asphalts include bituminous materials laid down in natural deposits, such as those in the Trinidad and Bermudez lakes, and natural bitumens such as gilsonites and grahamites, which are completely soluble in carbon disulfide. Artificial asphalts, meaning man-made or synthetic, include mainly petroleum-derived asphalts and, to a lesser extent, coal tar, water-gas tars, and their pitches. A classification scheme developed in 1960 [16], and later modified [17,18], has been used for the study of asphalts and related bituminous substances (Fig. 2-1).

It should be understood that asphalt and heavy petroleum are a mixture of high-molecular-weight complex compounds; a detailed study of any crude oil reveals that thousands of compounds are contained therein. In this sense, the separation is only limited to the isolation of the main groups of molecules with similar properties. The first separation of heavy petroleum used the Hempel distillation, which is based on the average boiling point and the specific gravity of the fractions. Such a diagram can be used to classify the various types of crudes. (Correlation index is related to boiling point and specific gravity of a given fraction; see Fig. 2-2.)

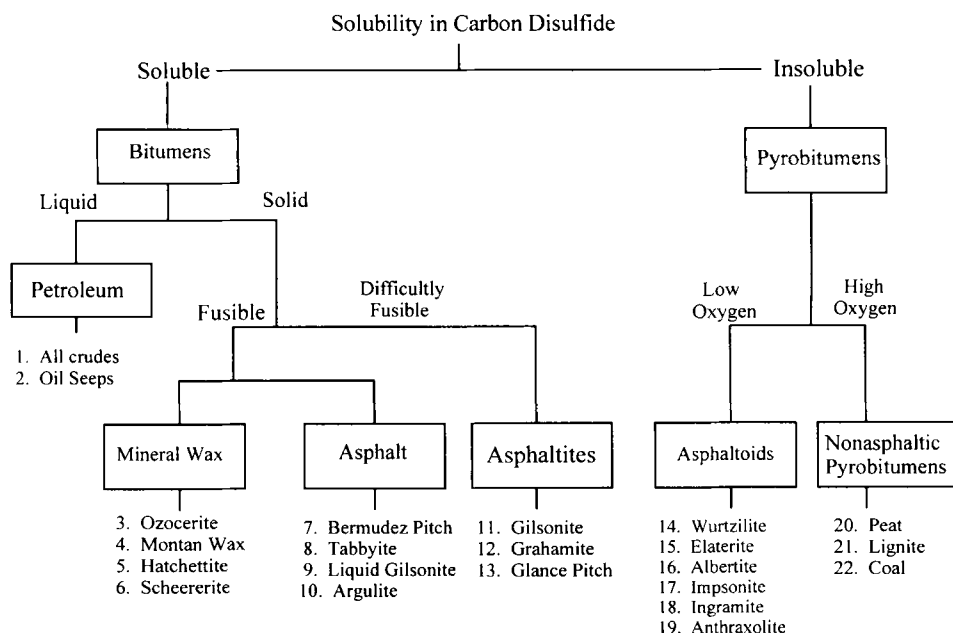


Fig. 2-1. Designation and classification of natural asphalt according to Abraham [3].

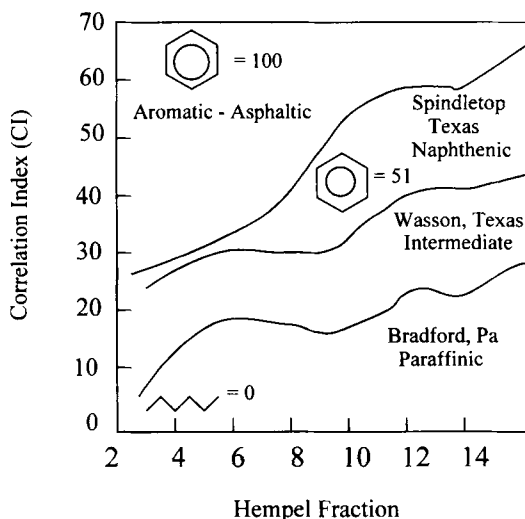


Fig. 2-2. Correlation index as a function of Hempel fractions for some U.S. crude oils.

Van Nes and Van Westen [19] proposed a ternary diagram for classification of worldwide crudes based on the  $n$ - $d$ - $M$  (refractive index, density, molecular weight) method. The ternary diagram is in the form of paraffinic, naphthenic, and aromatic carbon atoms such that:

$$C_P + C_N + C_A = 1$$

The classification by Tissot and Welte [20] is based primarily on the content of the various structural types of hydrocarbons: alkanes, cycloalkanes, aromatics, and N, S, O compounds (asphaltic non-hydrocarbons) (Fig. 2-3). The aromatic-asphaltics are by far the most important classes in terms of quantity. Then come the aromatic-naphthenic and the aromatic-intermediate. The first two comprise the enormous reserves of heavy oils and tar sands in Venezuela and Canada. The aromatic-intermediate class of crude oils is found in the large accumulations of crude oil in the Middle East.

If one refers to the ternary diagram of Fig. 2-4, thermal evolution is denoted by a diminution of aromatic and heavy constituents and an increase in paraffins. Alteration is primarily denoted by a shift away from the paraffin pole, due to biochemical degradation of alkanes.

Curiale [21] has used biological markers to correlate the extractable organic matter of asphaltites for the geochemical bitumen-bitumen correlation. This is usually achieved by using a ternary diagram showing the distribution of 5- $\alpha$ , 14- $\alpha$ , and 17- $\alpha$  of 20R stearames by carbon number of  $C_{27}$ ,  $C_{28}$ , and  $C_{29}$  (Fig. 2-5). Often, this type of ternary diagram can be used as an indicator for source input of different petroleum basins, e.g., whether the sources are from the lower aquatic organisms, from terrestrial higher plants, or represent a mixture of both.

Yen [22] used aromaticity versus the H/C atomic ratio diagram to characterize a number of carbonaceous compounds such as native petroleum asphaltics and resins,



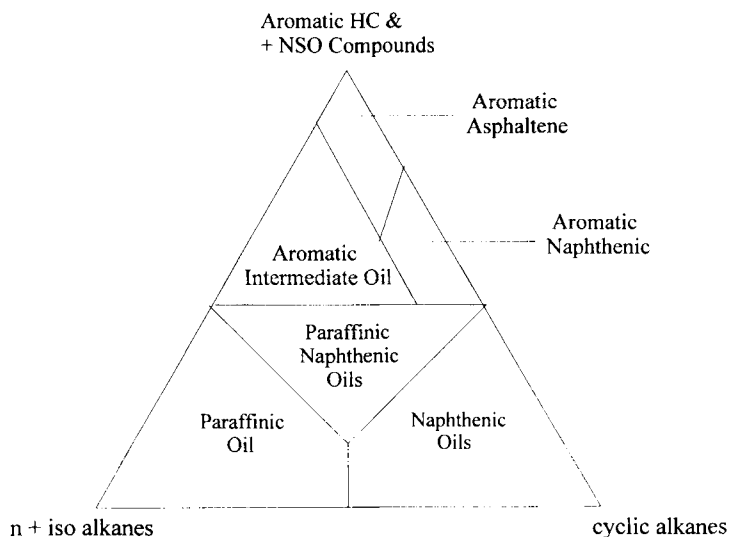


Fig. 2-3. Ternary diagram showing the composition of six classes of crude according to Tissot and Welte [20].

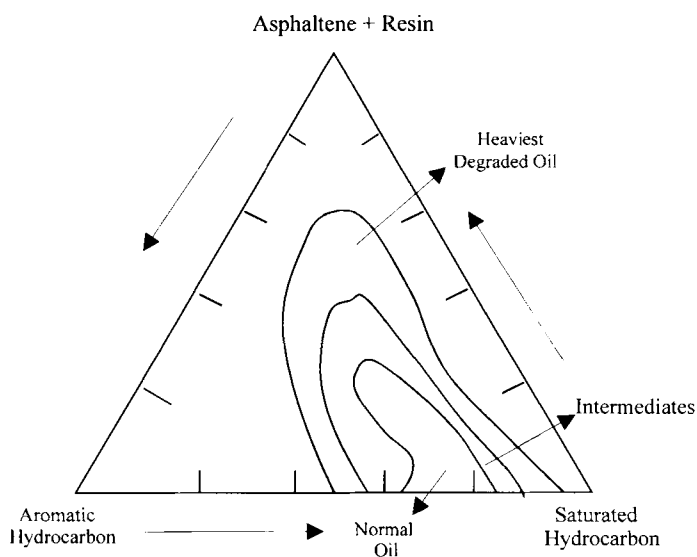


Fig. 2-4. Geochemical trend classification system according to IFP.

refined petroleum, and carbons. This diagram enables one to differentiate them. He also used [23] the ESR spin concentrations and  $g$ -tensors to differentiate between petroleum and coal-derived products. Also, the C, H, X ternary diagram can map out the carbonaceous materials distributed between petroleum and coal sources such as asphaltite, asphaltoids, etc. (Fig. 2-6). One can also obtain useful information from a simple

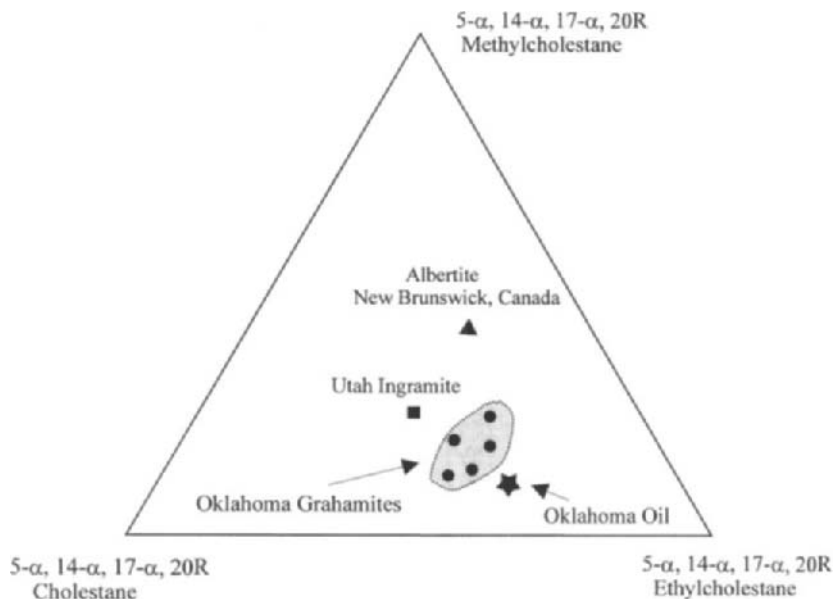


Fig. 2-5. Curiale's ternary diagram shows the distribution of 5- $\alpha$ , 14- $\alpha$ , 17- $\alpha$ , 20R stearenes by carbon number of 27, 28, and 29 (after Curiale [21]).

experimental test. For example, the unknown sample is first extracted with pentane (to obtain resin) and then with toluene (to obtain asphaltene). Subsequently, the resin and asphaltene are subtracted from the total organics to obtain the preasphaltene (Fig. 2-7).

It is quite difficult to develop a simple procedure to classify all types of heavy crudes, particularly one that is convenient for geologists and engineers to use. The use of asphaltene for the classification of oils is, therefore, proposed. The Institut Français du Pétrole (IFP) used asphaltene and resin to classify over 500 native crudes and over 1000 bitumens. The asphaltene fraction can be isolated or separated from heavy oil by a simple solvent fractionation technique, which is discussed elsewhere.

An alternative analytical procedure for the above is to determine the amount of asphaltene in a given crude oil without subjecting it to any chemical treatment. This of course can be simplified by analyzing the color intensity of the given crude oil in the visible range of 400–700 nm using a spectrophotometer.

#### A SIMPLE SCIENTIFIC DEFINITION OF ASPHALTENE

At this time, the majority of the research investigators in the asphaltene field prefer the use of an operational definition of asphaltene based on the principle of solvent fractionation. Actually, this solvent cut definition originated in 1837 by Boussingoult [9]. Since the isolation procedure from asphalt or bitumen is relatively simple, various modifications of C<sub>5</sub> to C<sub>7</sub> hydrocarbon-insoluble or the C<sub>3</sub> hydrocarbon-insoluble have been used in the literature of asphaltenes and asphalts.

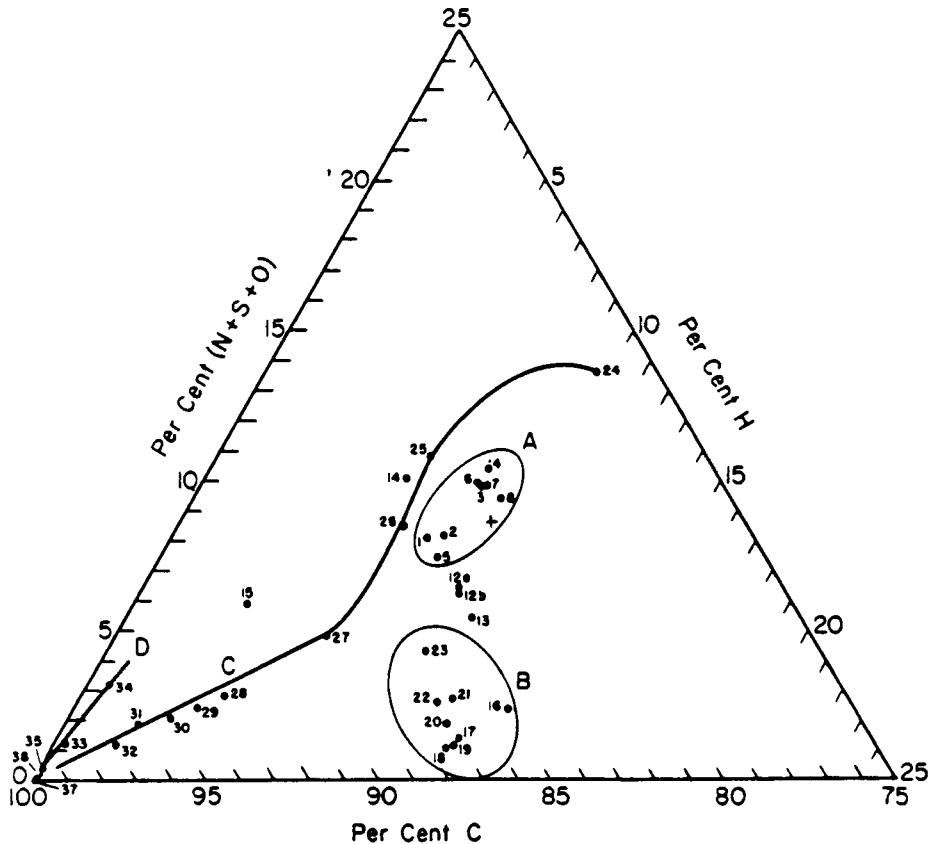


Fig. 2-6. Weight percent of C, H, and heteroatoms in four types of compounds. A = petroleum asphaltenes; B = thermal diffusion cuts from pentane-soluble fraction of 85 to 100 penetration asphalt (petrolenes); C = coal series with carbon content ranging from 77 to 97%; D = carbon blacks and graphite. The numbers identify the different samples. Data are from Yen et al. [24].

A scientific definition must make a distinction between hydrocarbons and non-hydrocarbons. Major fossil fuels (such as petroleum) contain both. The hydrocarbon moieties are much simpler; they contain paraffins or alkanes and can be classified as saturated hydrocarbon or saturates. They also contain aromatics (single-ring and fused-ring aromatic hydrocarbons) and naphthenics which are cyclic paraffins, such as cyclohexane and a great number of fused-ring saturated homologs (or per hydrogenated fused-ring aromatics). As indicated in Table 2-8, the three types of hydrocarbon — paraffins, P, aromatics, A, and naphthenics, N, and any of their combinations PA, PN, AN, PNA — form the bulk of hydrocarbons in fossil fuels. On the other hand, the non-hydrocarbons represented by X, which contain N, S, O or any metal complex and chelates in combination with the above, would represent a typical crude oil, e.g., PX, NX, AX, PAX, PNX, ANX, PNAX. In this manner, an oil from petroleum can be designated by  $P_iN_jA_kX_l$  ( $i = 0, 1 \dots n$ ).

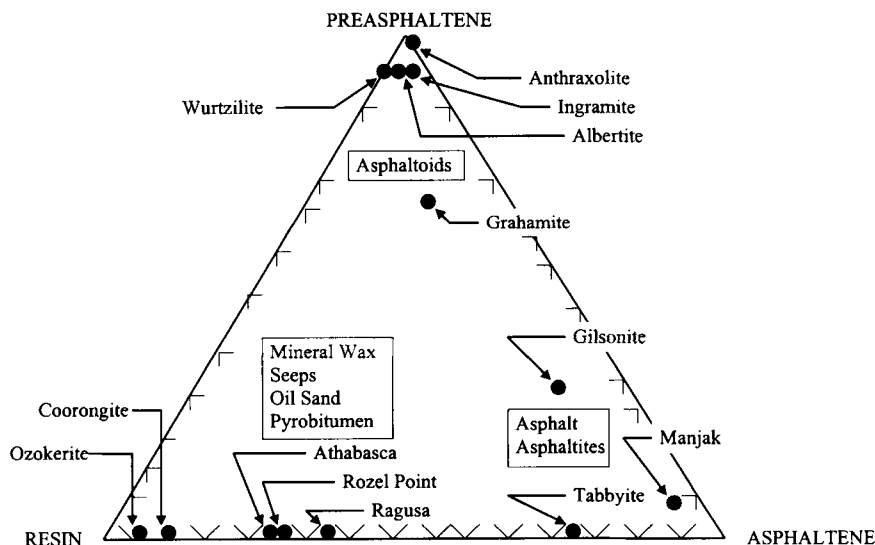


Fig. 2-7. Classification of native bitumens according to the composition of asphaltic fractions. The percent weights of asphaltene, resin, and preasphaltene are from Yen and Sprang [25]. The asphaltic fractions here are free of minerals and volatile hydrocarbons.

Because asphaltene has been considered throughout the years as a macromolecule, one must impose a polymer concept to describe the asphaltene structure. Polymers are derived from monomers which contain the repeating sequences of monomers. Usually, the polymers (high molecular weight) can be generated through a single-component compound containing the repeating sequences. Polymerization of the monomers can also yield oligomers [intermediates leading to polymers with repeating units ( $n$ ) of  $C_{30}$ – $C_{80}$ , and some low-molecular-weight polymers ( $n < 100$ )].

As can be seen from Table 2-8, the polymeric concept is useful as it identifies the realm of petroleum if one omits the first and last column from this table. Let us define the  $W$  as follows:

$$W = \sum (P, A, N, X, E)$$

According to this classification, the definition of petroleum can be expressed as  $W$ . If the monomer is expressed as  $W_1$ , the oligomer as  $W_0$ , the low-molecular-weight polymer as  $W_n$ , and the high-molecular-weight polymer as  $W_\infty$ , then petroleum can be defined as:

$$W_i = W_1 + W_0 + W_n + W_\infty$$

and

$$W_\infty > W_n > W_0 > W_1; \quad i = 1, 2, \dots, \infty, \quad n = 2, 3, \dots, \infty$$

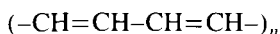
Here,  $n$  is the degree of polymerization. This definition agrees with the USGS definition that petroleum containing natural gas is a mineral. Of course most of the high-molecular-weight portion,  $W_\infty$ , has been precipitated as solids during recovery. In general, native petroleum contains very little carboids and humic substances.

TABLE 2-8

Polymer concept for petroleum components

Type	Repeating unit	Monomer (1)	Oligomer (2)	Polymer	
				low (3)	high (4)
P	(CH <sub>2</sub> ) <sub>n</sub> Linear	methylene	paraffins	wax	polyethylene
N	(CH <sub>2</sub> ) <sub>n</sub> Cyclic	cyclohexane	terpanoid (biomarkers) hydrocarbons	polymantane (adamantal derivatives and caged molecules)	diamond
N'	(CH) <sub>n</sub> Linear				
A	(CH) <sub>n</sub> Cyclic	benzene	polycyclic aromatic hydrocarbons	carbon (including fullerenes)	graphite
E	(C) <sub>n</sub> Linear	quaternary carbon radical	simple polyethyenes	retigens from meteorites	unknown
E'	(C) <sub>n</sub> Cyclic	benzyne			unknown
X	C-X <sub>m</sub> , m = 2	mono-ring heterocyclics	porphyrins	spent shale organics	humic substances (carboids or preasphaltene)

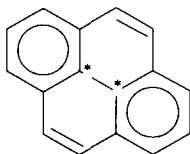
In Table 2-8, the symbol with a prime signifies that the type is rare. Each repeating unit can be either linear or cyclic (including linked- or fused-ring system). Linear conjugated polyethylene system such as the N' group



is rare due to the extensive reactivity. Cyclic polyethyenes in group E' are also not well known except for benzyne

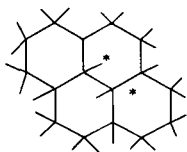


The mixed types, AE, commonly represent the pericondensed fused-ring aromatics which contain quaternary carbons.



The other two carbons marked with the symbol '\*' belong to the E type. Similarly the

class of NN' can be referred to as perhydro-peri-fused aromatics (pericondensed-naphthenics):



The symbol '\*' of the above structure indicates the N' type of bonding.

Adopting concepts from polymer science will be helpful in the explanation of the complex nature of asphalts. Polymers are defined as high-molecular-weight compounds with repeating units. A homopolymer only requires a single type of structure for the repeating units, e.g., polystyrene. A copolymer is expected to contain two different types of repeating units, e.g., polystyrene-polybutadiene which contains both phenyl groups (from styrene) and the isolated olefin function (from butadiene). A terpolymer will contain three types of repeating units and so forth. A polymer containing  $j$  types of repeating units is named multipolymer (or sometimes referred to as multimer). Mathematically, the phenol-formaldehyde resin can be expressed as:

$$W_i = [P, A], \text{ copolymer}$$

where P is methylene bridges and A is benzene. If two types of arenes (e.g., phenol and cresol) are present,

$$W_i = [P, A_2], \text{ terpolymer}$$

Here the formaldehyde linkage of methylene is still P. A multipolymer can be expressed as:

$$W_i = [P_j, A_j], \text{ multipolymer}$$

indicating  $j$  types of arenes and  $j$  types of alkane linkages and  $i$  can be any combination of the degree of polymerization. In general:

$$W_{ij} = [P_{ij}, A_{ij}, N_{ij}, X_{ij}, E_{ij}]$$

$$i = 0, 1, 2, \dots, \infty, \quad j = 0, 1, 2, \dots, \infty$$

In practice, LPG can be represented by [P]; gasoline can be represented by [P, A, PA]; wax is [P, PN]; gas oil is [AP, AN, PN], lube oil is [APN]; resin is [APNX] and asphaltene is  $[A_j P_j N_j X_j]$ .

Another polymer concept that should be imposed here is the problem of cross-linking. Usually when X are present in petroleum, the heteroatoms will form complexes with the metals from organic metallics. Under certain conditions, the sulfur will form polysulfide linkages, rendering the compounds insoluble in common organic solvents. Kerogen can be considered as a cross-linked asphaltene. To agree with the above, kerogen should belong to

$$W_{ijk} = [P_{ijk}, A_{ijk}, N_{ijk}, X_{ijk}, E_{ijk}]$$

Therefore, the definition of asphaltene is  $W_{ij}$  and kerogen is  $W_{ijk}$ . The  $k$  used here could be related to the degree of cross-linking.

## GENERALITY VERSUS UNIQUENESS — A CASE STUDY

Certain asphaltenes possess unique properties. Often, definition can be given to the general properties of a given asphaltene. A number of investigators have mistakenly used the special unique properties of a given sample, e.g., certain structural parameters or certain degradation product. Truly, the aromaticity and the degree of fusion usually change depending on the severity of the temperature to be applied on the sample. The investigators only examined one or two examples (may be the petroleum sample where the asphaltene derived was exposed to severe thermal cracking) and made a sweeping conclusion that the asphaltene structure should contain certain structural features because a given asphaltene has a certain set of parameters. In other words, they have studied some unique cases and attempted to define the general structure of asphaltene on such a basis.

A case study of a unique asphaltene is cited here. Some years ago, the writer isolated a fraction of asphaltene from Rozel Point Tar near Salt Lake City, Utah. From all indications, especially the physical properties including all the structural parameters, this asphaltene is similar to a number of typical petroleum asphaltenes. For instance, Rozel Point Tar asphaltene has a porphyrin content of 17 ppm,  $f_a = 0.18$ ,  $L_a = 12 \text{ \AA}$ ,  $L_c = 17 \text{ \AA}$ ,  $M_c = 3.87$ ,  $d_r = 4.8 \text{ \AA}$ ,  $N_g = 1.7 \times 10^{18}$ , and a  $g$  value of 2.0040. The percent carbon is 71.8; %H, 8.4; %N, 1.4; %O, 3.4; and %S, 15.3. For the above values, all structural parameters are normal for average asphaltenes of petroleum origin except the sulfur content. A second look reveals the following for the Rozel Point Tar asphaltene:

- by MS — it contains polysulfide linkages;
- by GC — positive identification of  $C_{16}$ ,  $C_{18}$ ,  $C_{20}$  fatty acids containing  $\Delta^9$  – unsaturation;
- by ESR — appears as semiquinone and hindered phenol type;
- By GC-MS — presence of an arachidonic acid.

These facts indicate that the major source material of the Rozel Point Tar is derived from biomass of bacterial origin (perhaps also from decomposition of kerogen which is known from biomass). Many of the bacteria would yield lipids of the unsaturated fatty acids with unsaturated bonds at the 14, 16, and 18 carbon chain positions (see Table 2-9). It is possible that the disulfide and polysulfide linkages originated from the salt-tolerant species of anaerobic sulfate-reducing bacteria. Therefore, a mixed source of origin is possible for Rozel Point tar.

Another striking fact is that the only major commercial application of Rozel Point tar lies in its medicinal use. It has the name ichthyoleums or ichthyol or ichthamnol. These names of Latin and Greek origin are based on Sumarian, and again the Sumarian name is very close to Chinese (see Table 2-5, maybe Chinese origin). Ichthyoleum is widely used as an ointment for skin lesions. In China, the major ingredient of a black salve or balm called 'Go Pi Gao Yo' is made from either the tar of the coastal regions or from pitch and tar, first sulfonated and neutralized with ammonia. The wide use of ichthyoleum as an anti-inflammatory medicine has a sound scientific basis, because arachidonic acid containing unsaturation at the 5, 8, 11, and 14 positions is the precursor of prostaglandins (Fig. 2-8). Furthermore, the disulfide endoperoxide is a

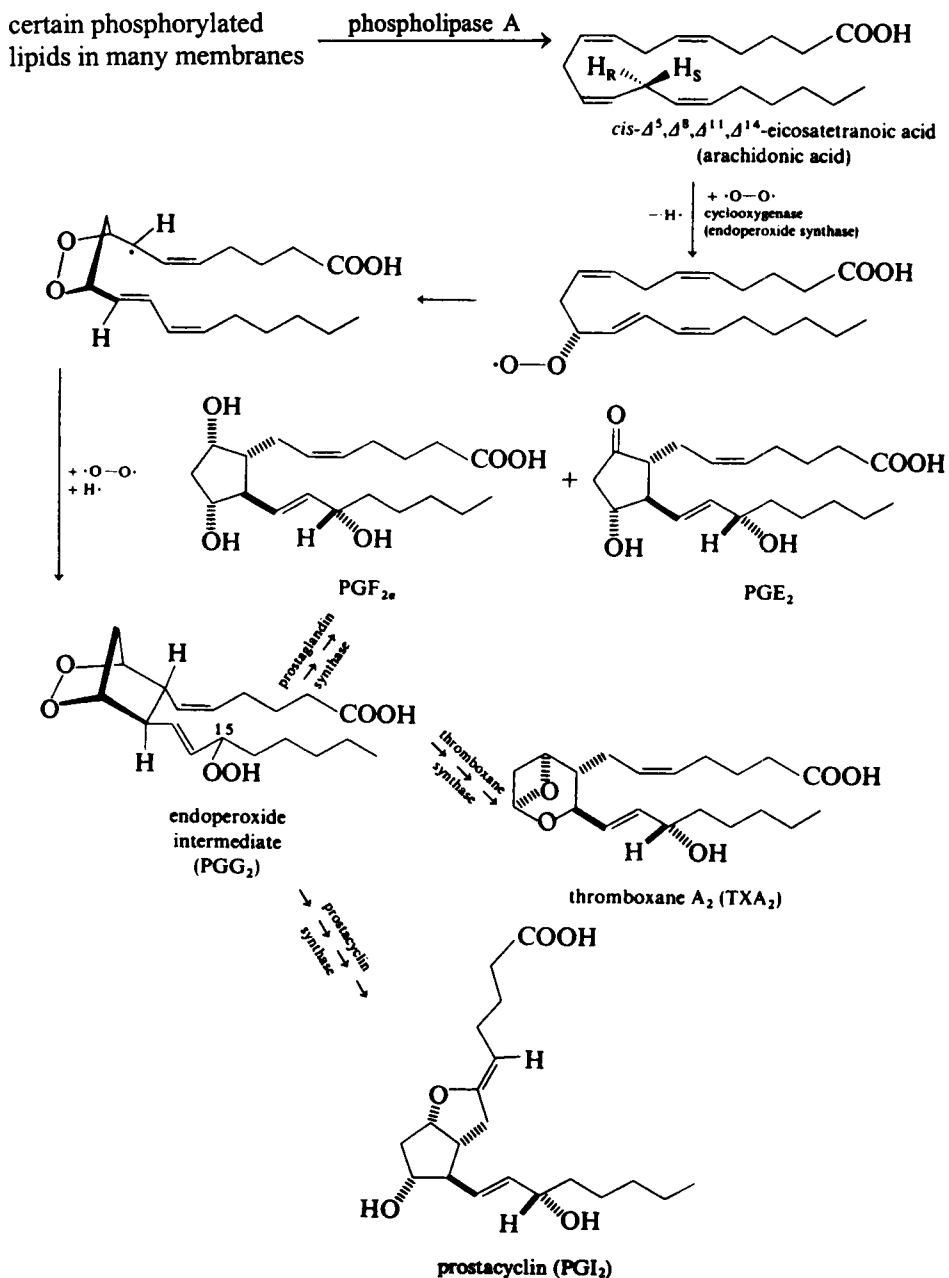


Fig. 2-8. Biosynthesis of prostaglandin and endoperoxide derivatives from arachidonic acid.



TABLE 2-9

The nature of the unsaturated acids found in some species of bacteria

Bacterial species	Number of carbon atoms in the acids		
	14	16	18
<b>Aerobic bacteria</b>			
<i>Mycobacterium phlei</i>		9 (3%)	9 (7%)
<i>Corynebacterium ovis</i>		9 (14%)	9 (6%)
<b>Anaerobic bacteria</b>			
<i>Lactobacillus arabinosus</i>		9 (4%)	11 (35%)
<i>Pseudomonas fluorescens</i>		9 (31%)	11 (12%)
<i>Rhodpseudomonas spheroides</i>			
Anaerobic culture (light)	7 (6%)	9 (3%)	11 (69%)
Anaerobic culture (dark)	7 (3%)	9 (3%)	11 (78%)
<i>Clostridium butyricum</i>	7 (0.3%)	9 (8%)	11 (2%)
<i>Clostridium pasteurianum</i>	7 (1%)	9 (3%)	11 (2%)

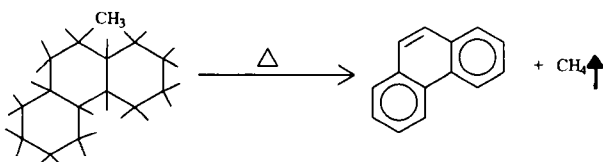
Data from Yen [26].

powerful blocker of thromboxane,  $\text{TFA}_2$  (aggregation of blood platelets) and an inducer of prostacyclin,  $\text{PGI}_2$  (dissolving platelets). Fig. 2-8 shows the prostaglandin precursor, arachidonic acid and its oxidized cyclooxygenase products,  $\text{TFA}_2$  and  $\text{PGI}_2$ . The anti-inflammatory power of ichthyoleum may come from the inhibition of cyclooxygenase, which is responsible for  $\text{TFA}_2$  formation. This is best accomplished when the medicine is used under reducing conditions where a number of sulfide and disulfide structures accompany the arachidonic acid.

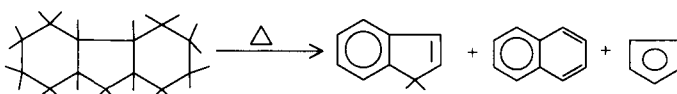
The Rozel Point Tar asphaltene is a case in point that people working in asphaltene research should remember. It is true that this asphaltene, which contains disulfide and polysulfide linkages, has properties of anti-inflammatory and therapeutic value. Can one conclude, then, that all asphaltenes that have disulfide and polysulfide structures possess therapeutic properties? A common error made by a number of researchers in asphaltenes was that they simply studied one or a few (three or four) characteristics and drew sweeping conclusions about the general structure of asphaltenes. This tendency towards generalizations really confused the public as well as the expert. Does asphaltene contain a large fused-ring system (peri-type) or a small kata-condensed system? The answer is that the meso-scaled structure is always a useful description of the general structure of asphaltenes [22]. However, the detailed chemical structure depends on the source of a given asphaltene, such as native (from wellhead) or refinery (undergo temperature treatment) or tar sand (exposed to microorganisms and degradation), or coal liquid (oxygen bonding rearrangement), or shale oil (nitrogen functions involved in polymerization). The chemical structure of asphaltene depends on the individual sources. This point will especially help those who intend to simulate molecular modeling of asphaltene structures and properties.

## A CONTINUUM THEORY OF CARBONACEOUS SYSTEMS

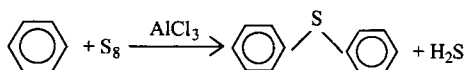
In the study of diagenesis by organic geochemistry, it is rather easy to understand that methane may be expelled from aromatization of naphthenics which bear an angular methyl group of cyclic structures, e.g.:



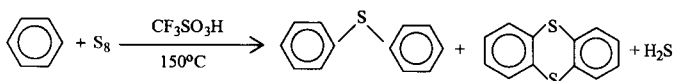
In this view, small molecules may originate from a large molecule. Another commonly occurring reaction is the expulsion of fragments during heat treatment. For example, naphthene such as perhydroflorene can be easily degraded into indene, naphthalene, cyclopentadiene and other benzene derivatives upon pyrolysis:



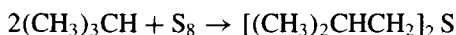
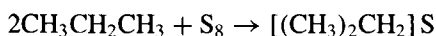
It is also feasible that heteroatoms introduced to hydrocarbon can be an addition process during diagenesis and maturation. Electrophilic functionalization of hydrocarbons for heterocyclic compounds are entirely possible. For example, an early example is the Lewis acid-catalyzed sulfur insertion into aromatic system such as:



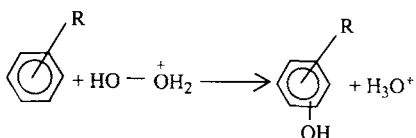
Although this reaction produces low yield in the laboratory, when hydrocarbons exposed to clay minerals (super acids related) for millions of years, conversion by sulfuration is possible, which has been demonstrated experimentally [23]:



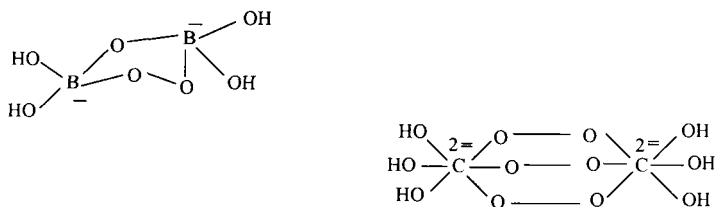
Even alkanes can be subjected to sulfuration for the sulfides formation:



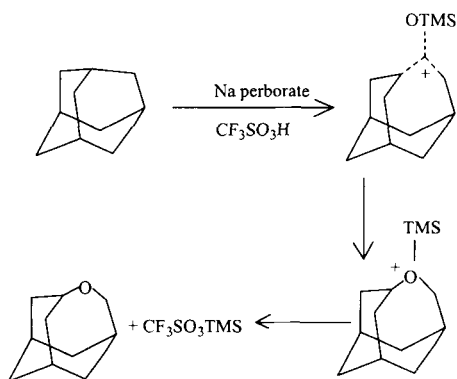
Electrophilic hydroxylation of aromatics with an incipient hydroxyl cation (e.g., protonated or complexed hydrogen peroxide) is also known:



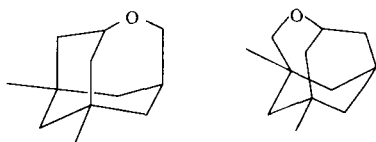
A good example is coal liquid derived asphaltene. Sodium salts of perborate or percarbonate can hydroxylate aromatics under certain conditions:



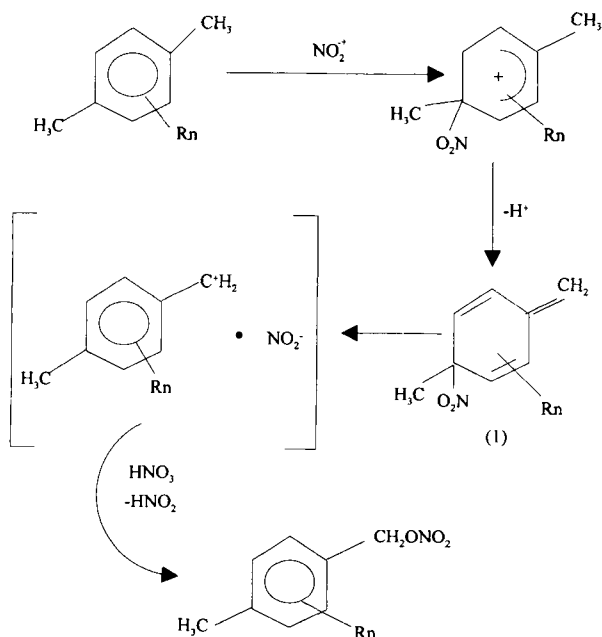
In the latter case, even caged molecules, such as adamantanes, can be inserted with an oxygen bridge (4-oxohomoadamantane):



For 1,3-dimethyl adamantane, the following products are obtained:



Nitration of the aromatics is possible from nitronium ion:



The formation of the heterocyclic system in petroleum is known to have a biogenic and an abiogenic origin. For example, porphyrin can be derived from chlorophyll, which is biogenic [27]. Equally possible is that the defect center in the aromatic sheet can also form coordination sites which behave similarly to porphyrin. Usually, a tetragonal ligand consisting of 202N, 103N, 301N, 2N2S, etc., instead of 4N (porphyrin), can be formed from weathered or pyrolyzed products from the original biomass and from later functionalization of hydrocarbons by the addition of chemical species from environment. For the biosynthesis of porphyrins, nitrogens were derived only from glycine and not from ammonia or any other amino acid. Due to the stability of the molecule, the porphyrin has been used as a good geological biomarker for petroleum.

With respect to the origin of carbonaceous materials from thermal processes with different types of biomass as precursors, a number of governing rules are known.

(1) Simultaneous polymerization and depolymerization are controlled by conditions in neighboring molecules.

(2) Weathering and aging can cause aromatization in a fused-ring pericondensation fashion [28].

(3) Distribution of hydrocarbon patterns is according to the distribution of lipids of the biomass.

(4) Jacobson rearrangement in aromatic systems is possible.

(5) Defects, including distortions, rule the structure of asphaltene, especially for dislocation and disclination of the Volterra type [29].

The different stages in which different petroleum products are isolated indicate that both polycondensation and degradation occur. In Table 2-8, using benzene as

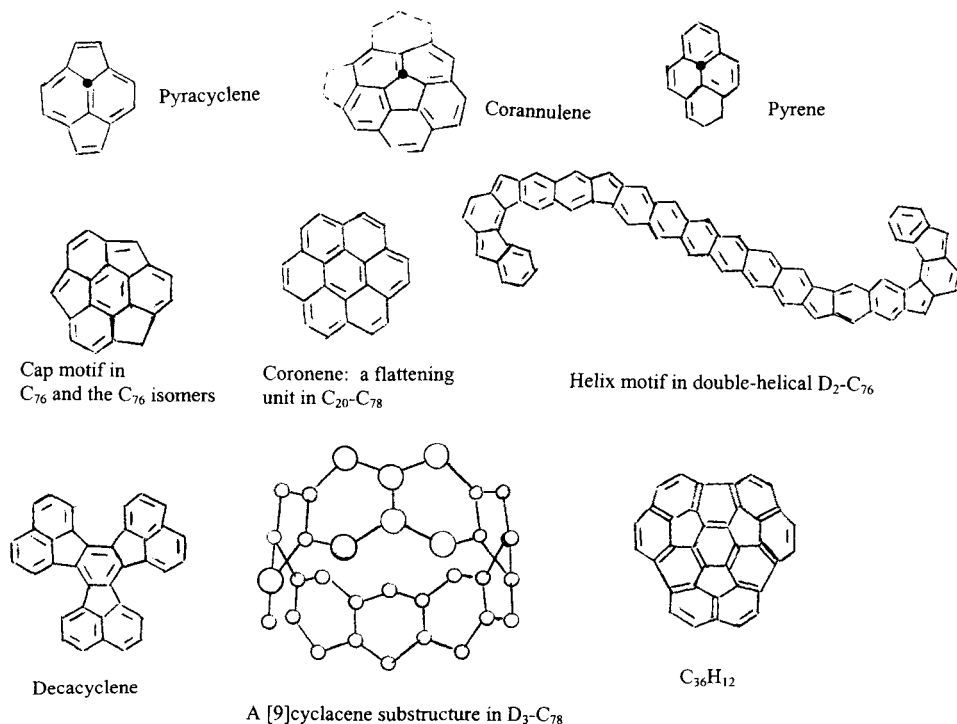
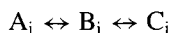


Fig. 2-9. Polydecomposition products of fullerene systems.

a monomer, the end product after polycondensation would be graphite, an infinite connection of hexagons in a two-dimensional network. The intermediate products could be polycyclic aromatic hydrocarbons (PAH) or polynuclear aromatics (PNA) and carbons with defects in the carbonization stages. The development of hexagons for infinite sheet can lead to graphite. Yet, a combination of hexagons and pentagons will lead to a sphere such as fullerenes and high-carbon homologs. It is natural for carbon to have this type of tessellation. This forms the basis of the equilibrium products from both polycondensation and depolymerization.



The decomposition (reverse) or degradation will have the structural motifs in both fullerene and graphite. For example, as listed in Fig. 2-9, all these have been shown to be present in petroleum. It is likely that the peeling off from both graphite and fullerene are possible. The first leads to PAH and the other to heterocyclics. The latter can form many of the standard motifs. Presented in Fig. 2-10 is the peeling of the spheroidal shell of fullerene. In this concept, the petroleum contains equilibrium products. An extension of this concept to other systems is listed in Table 2-8, which would explain the composition of the present-day petroleum. All the intermediates are in continuum with the simple monomers and the final polymeric form.

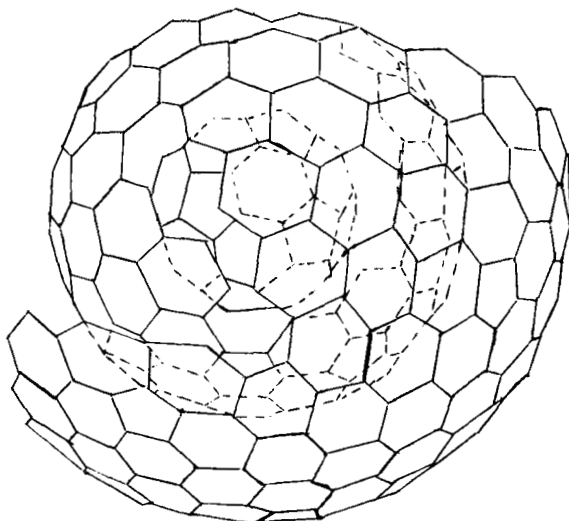


Fig. 2-10. The multishell concept of fullerene-type molecules.

#### ACKNOWLEDGEMENTS

Part of this paper is based on the 'Overall Properties of Asphaltenes as Deduced from Structure', a keynote address presented by Dr. T.F. Yen on receiving the Petroleum Chemistry Award at the 207th National American Chemical Society meeting at San Diego, CA, March, 1994 [29]. The ACS Awards in petroleum chemistry sponsored by AMOCO foundation are in recognition of T.F. Yen's pioneering efforts in developing the structure of petroleum asphaltenes. The author wants to extend his thanks to Drs. Ellis K. Field of IIT and David A. Storm of Texaco for arranging the symposium.

#### REFERENCES

- [1] Zhong, C. and Huang, J., *Drilling and Gas Recovery Technology in Ancient China*. Wictle Offset Printing, Shell Oil, Beijing (1997).
- [2] Zigon Historical Museum of Salt Industry, *Ziliujing in Ancient China*. Prepared for the 15th World Petroleum Congress, Zigong, Sichuan (1997).
- [3] Abraham, H., *Asphalts and Allied Substances*, Vol. 1. Van Nostrand, Princeton, NJ, 6th ed. (1960).
- [4] Clay, A.T., *A Hebrew Deluge Story in Cuneiform*. Yale University Press, New Haven, CT (1922).
- [5] de Lacouperie, T., *Western Origin of the Early Chinese Civilization*. Reprint, Proff and Co., Osuabrick (1966).
- [6] Staal, J.D.W., *Stars of Jade*. Mrit Press, Decatar, GA (1984).
- [7] Mallory, J.P., *The Search of the Indo-Europeans*. Thames and Hudson, London (1989).
- [8] Harper, R.F., *Assyrian and Babylonian Literature*. D. Appleton, New York (1904).
- [9] Barth, E.J., *Asphalt, Science and Technology*. Gordon and Breach, New York (1962).
- [10] Richardson, C., *J. Phys. Chem.*, 19: 241 (1915).
- [11] Marcusson, J., *Die Naturlichen and Kunstlichen Asphalte*. Engelmann, Leipzig (1931).
- [12] American Society for Testing and Materials, *Standards on Petroleum Products and Lubricants*. ASTM D8 and D4, Philadelphia (1985).

- [13] Louis, M., Eisma, E., Homsen, W.E., Jackson, C.F. and Schultze, G.R., *Proc. 5th World Petroleum Congress*, Sect. 1, Fordham University, New York, p. 1037 (1959).
- [14] Traxler, R.N., *Asphalt, Its Composition, Properties and Uses*. Reinhold, New York (1961).
- [15] Cornelius, C.D. and Omana, R., *Proceedings of Third International Conference on Heavy Crude Tar Sands*, Long Beach, CA, pp. 169–173 (1985).
- [16] Abraham, H., *Asphalts and Allied Substances*, Vol. 1. Van Nostrand, Princeton, NJ, p. 370, 6th ed. (1960).
- [17] Pfeiffer, J.P., *The Properties of Asphaltic Bitumen*. Elsevier, New York (1950).
- [18] Chilingarian, G.V. and Yen, T.F., *Bitumens, Asphalts and Tar Sands*, Vol. 7. Elsevier, Amsterdam, pp. 153–190 (1978).
- [19] Van Nes, K. and Van Westen, H.A., *Aspects of the Constitutions of Mineral Oils*. Elsevier, Amsterdam (1951).
- [20] Tissot, B.T. and Welte, D.H., *Petroleum Formation and Occurrence, A New Approach to Oil and Gas Exploration*. Springer, Berlin (1978).
- [21] Curiale, J.A., Biological markers in grahamites and pyrobitumens. In: T.F. Yen and J.M. Moldowan (Editors), *Geochemical Biomarkers*. Harwood Academic, Chur (1988).
- [22] Lian, H.J. and Yen, T.F., Classification of asphalt types by asphaltene aromaticity. In: M.K. Sharma and T.F. Yen (Editors), *Asphaltene Particles in Fossil Fuel Exploration, Recovery, Refining and Production Processes*. Plenum Press, New York, p. 63 (1994).
- [23] Wang, Q., *Studies on New Electrophilic Functionalization of Hydrocarbons*. Ph.D. Dissertation, University of Southern California (1990).
- [24] Yen, T.F., Erdman, J.G. and Saracens, A.J., *Anal. Chem.*, 24: 694 (1962).
- [25] Yen, T.F. and Sprang, S.R., *Geochim. Cosmochim. Acta*, 41: 1007 (1977).
- [26] Yen, T.F., Genesis and degradation of petroleum hydrocarbons in marine environments. In: T.M. Church (Editor), *Marine Chemistry in the Coastal Environment*. ACS Symp. Ser., 18: 231–266 (1975).
- [27] Yen, T.F., *The Role of Trace Metals in Petroleum*. Ann Arbor Science Publishers, Ann Arbor, MI (1975).
- [28] Yen, T.F., Terrestrial and extraterrestrial stable organic molecules. In: R.F. Landel and A. Rembaum (Editors), *Chemistry in Space Research*, Elsevier, New York, pp. 105–153 (1972).
- [29] Yen, T.F., American Chemical Society Award in Petroleum Chemistry. *ACS Petroleum Prepr.* 39 (2): 196 (1994).

### Chapter 3

## UNDERSTANDING METALS IN FOSSIL FUELS: A PERSPECTIVE OF CONTRIBUTIONS BY T.F. YEN

J.G. REYNOLDS

### INTRODUCTION

Professor T.F. Yen has made extensive and insightful contributions to asphaltene chemistry and petroleum chemistry in general. Receiving the American Chemical Society (ACS) Division of Petroleum Chemistry award acknowledges these outstanding contributions. Professor Yen's contributions to metal chemistry have also been extensive and important and should be acknowledged as well. Perhaps overshadowed by his interest in asphaltenes, his work in metals has impacted a wide range of areas, from fundamental synthetic inorganic chemistry to metals removal during conversion of crude oil to transportation fuels.

Presented here is a recollection of some of Professor Yen's contributions to the understanding of metals in fossil fuels. Research areas chosen are not necessarily the most important or complete, although some clearly have had a major impact on the field; they were chosen because they are a good representation of the variety of his research in this area. This is not meant to be a historically accurate (and probably is not), complete, nor chronological account of the research. It is also important to remember the state of the field at the time the research was published. Much more is now known about many of these topics, so although some concepts may seem outdated, they were cutting edge at the time.

### RESEARCH SUMMARIES

A literature search of Professor Yen's research activities over the years reveals several different research topics. Table 3-1 shows many of these important and timely topics. Most of these focus on fossil fuels and many of them utilize the asphaltene concept in an explanatory and/or exploitative role.

#### *Metals in the asphaltene*

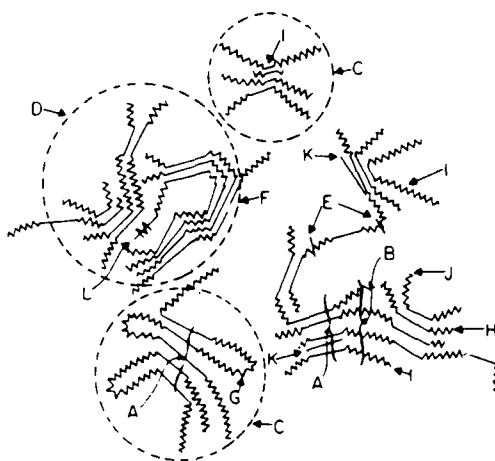
Fig. 3-1 [1] shows the overall structural model of petroleum asphaltenes. This figure, first published around 1963, is probably one of the most reproduced figures in petroleum chemistry. Various subunits are shown with their interactions to form the macrostructure of the asphaltene. The metal-containing molecules, K and L, are buried deep and on the periphery, respectively. Some researchers have speculated that K is responsible, in some part, for keeping the asphaltene macrostructure intact, and that removal of the asphaltene during processing can be achieved by attacking that site [2].



TABLE 3-1

Some research topics examined by T.F. Yen

Mesophase formation — heavy oil, coke, coals	Asphaltene peptization
Cavitation	Surfactants, tar sand recovery, generation of
Sonochemical treatment	Oil spill remediation
Enhanced oil recovery — biotech, rock porosities, permeability, well logs, drilling fluids, flooding	Asphaltenes and heavy oils — NMR, IR, utilization, ESR, fractals, metals
Micelles and vesicles	Asphalts as colloids
Asphalt and asphaltene separation — TLC, preparative, polarographic	Dechlorination by peroxide
Coal desulfurization — bacterial, biocatalytic	Kerogen oxidation
Porphyrins — in kerogen, oils, lunar rocks, MS, ESR, separation	Pyrolysis of coal
Alkanes	Oil shale — fracturing, nitrogen, characterization, transportation
Waste products — treatment, characterization	Biomarkers
Tar sand recovery, characterization	Metals — vanadium model compounds



#### Macrostructure of Asphaltics

- |                 |                   |
|-----------------|-------------------|
| A. Crystallite  | G. Intraccluster  |
| B. Chain Bundle | H. Intercluster   |
| C. Particle     | I. Resin          |
| D. Micelle      | J. Single Layer   |
| E. Weak Link    | K. Petroporphyrin |
| F. Gap and Hole | L. Metal (M)      |

Fig. 3-1. General features of the macrostructure of petroleum-derived asphaltenes and related substances [1]. Reproduced with permission.

### *Metals classifications*

Professor Yen and coworkers were some of the first to recognize that metals in petroleum appear to be grouped into two types, the petroporphyrins and the nonporphyrins [3], based on spectroscopic, reactivity, and separation properties. Fig. 3-2 shows examples of both classifications.

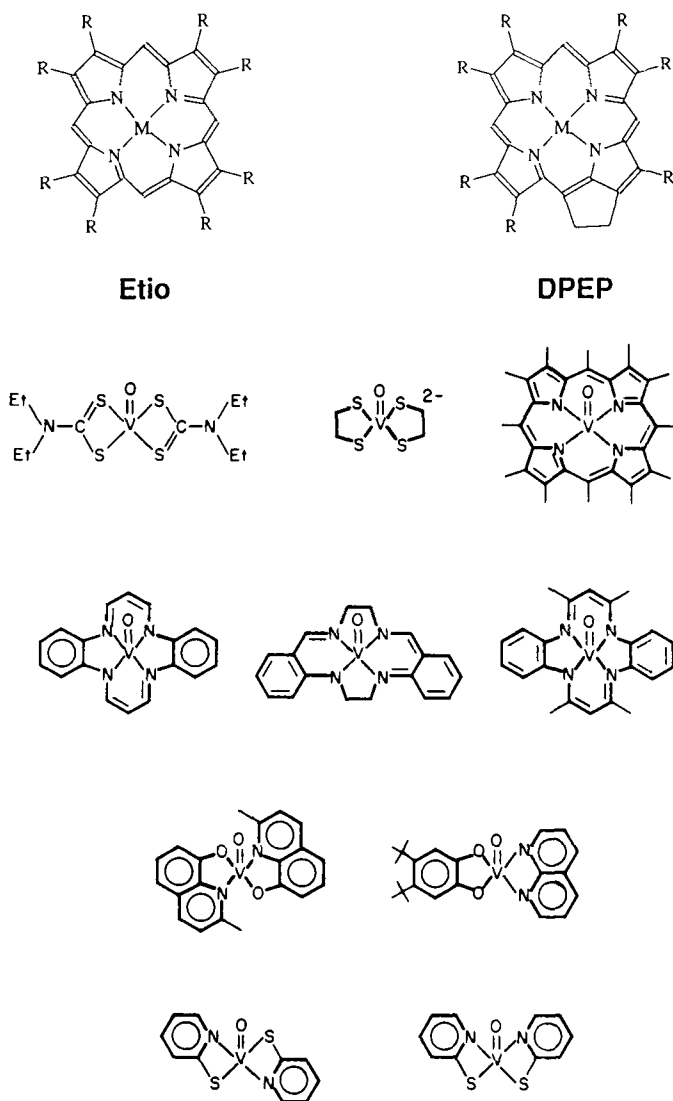


Fig. 3-2. Generalized porphyrin structures detected in crude oils and vanadium compounds synthesized to model non-porphyrin bound vanadium in crude oils.

The porphyrins are an extensively studied class of compounds. They consist primarily of a 16-annulene aromatic (conjugated) ring system with vanadium ( $V=O^{+2}$ ) or nickel ( $Ni^{+2}$ ) as the metal (M). The principal differences in the petroporphyrins are found in the substitutions on the pyrrole ring. Etio- and DPEP-type are typical examples and usually account for the majority of the petroporphyrins found in petroleum. These compounds exhibit very distinctive UV-vis properties having the very intense Soret band ( $\lambda_{max} \approx 400$  nm,  $\epsilon \approx 250,000$  mol/cm) and  $\alpha$  and  $\beta$  bands ( $\lambda_{max}$  500 to 650 nm). These bands make quantitation possible, even at levels of 1000 ppm metals or lower [4,5].

The remaining metal complexes in petroleum are defined as the nonporphyrins. These include other ring systems such as chlorophylls, chlorins and corrins (reduced porphyrins), highly substituted aromatic porphyrins, porphyrins with UV-vis properties unlike those defined above, porphyrin decomposition products and tetradentate mixed ligand complexes. Examples of models of these proposed ligand complexes are shown in Fig. 3-2.

The research examples below will discuss some efforts in the characterization and structural elucidation of both porphyrins and nonporphyrins, and the contributions to fundamental and applied petroleum chemistry resulting from those studies.

### *Mass spectrometry of petroporphyrins*

In 1935, Triebs discovered porphyrins in coal, oil shale, and natural bitumen [6]. He postulated a conversion theory of chlorophyll to DPEP and hemin to etio porphyrins during diagenesis going through the mechanisms of demetallation  $\rightarrow$  saponification  $\rightarrow$  reduction  $\rightarrow$  aromatization  $\rightarrow$  decarboxylation  $\rightarrow$  chelation. (This sequence with modifications is still used today.)

In 1966, examining extracts from asphaltenes from Wilmington crude oil, Baker [7] reported some of the first mass spectral characterizations of petroporphyrins. The results clearly indicated that the petroporphyrins were not a single compound or structure. There were several DPEP and etio homologous series (demetallated etio starts at  $m/z$   $310 + 14n$ ; demetallated DPEP starts at  $m/z$   $308 + 14n$ ,  $n$  = substituted carbons). The distributions appeared roughly Gaussian, with no obvious oxygen functionality, and chromatographic separation clearly showed etio-type, DPEP-type and unknown, porphyrins with possible aromatic substitutions. These significant findings, along with those of Morandi and Jensen [8] and others opened up an entirely new area of porphyrin analyses utilizing mass spectrometry (MS) as a detection technique.

To determine whether or not these porphyrin properties were generic to all asphaltenes and petroporphyrins, Baker et al. [9] teamed up to examine a whole suite of fossil fuels from various sources. Table 3-2 shows the types and sources of these materials varied from crude oils to bitumen and shales. The samples were extracted and isolated with methane sulfonic acid (MSA) by a patented method [10] which produced a water-soluble demetallated porphyrin dication. The extracted fraction was then neutralized and the porphyrins were isolated with  $CH_2Cl_2$ , and concentrated using silica chromatography.

Fig. 3-3 shows the low-voltage spectrum (12 eV) of the porphyrin extract of the Baxterville sample. Clearly seen is the etio series from  $n = 5$  to 15 ( $C_{27}$  to  $C_{37}$ )

TABLE 3-2

Sources and yields of petroporphyrins

Asphaltene or bitumen	Country, State	Geologic age	Concentration V in asphaltene (ppm)
Agha Jari	Iran	Lower Miocene	120
Athabasca tar sands	Canada, Alberta	Cretaceous	145
Baxterville	U.S.A., Miss.	Upper Cretaceous	28
Belridge	U.S.A., Calif.	Pliocene	3100
Boscan	Venezuela, Zulia	Cretaceous	1800
Burgan	Kuwait	Cretaceous	220
Colorado oil shale	U.S.A., Colorado	Eocene	55
Gilsonite	U.S.A., Utah	Eocene	40
Mara	Venezuela, Zulia	Cretaceous	300
Melones	Venezuela, Anzoategui	Cretaceous	300
Rozel Point	U.S.A., Utah		17
Santiago	U.S.A., Calif.	Pleistocene	38
Wilmington	U.S.A., Calif.	Miocene	570

having a broad distribution. The Rozel Point sample shows the DPEP porphyrin homologous series from  $n = 9$  to 14 ( $C_{31}$  to  $C_{36}$ ) having a narrow distribution. These results indicate very distinct differences among petroporphyrins isolated from different petroleum sources.

Table 3-3 [9] summarizes the homologous series distributions for the samples studied. Several interesting trends are seen. The average mass (arithmetic mean) of the homologous series (columns 1, 2 and 3) varied over 448 to 476 (R substitution of two  $CH_2$  groups — see Fig. 3-2). Colorado shale, Gilsonite, and Rozel Point have

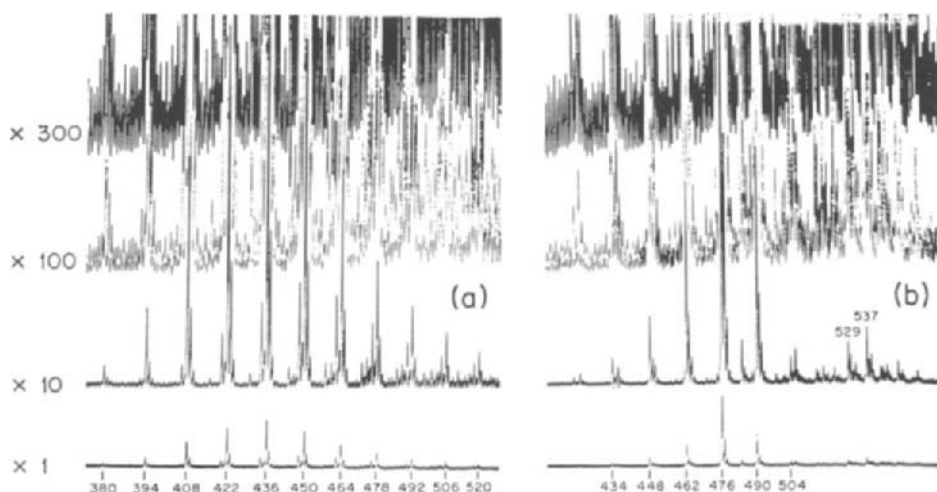


Fig. 3-3. Low voltage mass spectra of (a) Baxterville (28 ppm V in asphaltene) and (b) Rozel Point (17 ppm V in asphaltene) demetallated porphyrin fractions [9]. Reproduced with permission.

TABLE 3-3

Molecular weight distribution of petroporphyrins (average mass, mass distribution, band widths, skewness, homologous series ratios, and visible spectral type)

Sample No.	Asphaltene or bitumen	Weighted av. mass <sup>a</sup>			Band width, <sup>e</sup> $\sum$		Skewness <sup>f</sup>		8 $\frac{\sum \text{DPEP}}{\sum \text{etio}}$ <sup>d</sup>	9 Visible <sup>h</sup> spectral type
		1 DPEP <sup>b</sup> series	2 Etio <sup>c</sup> series	3 Total petroporphyrin	4 DPEP <sup>b</sup> series	5 Etio <sup>c</sup> series	6 DPEP <sup>b</sup> series	7 Etio <sup>c</sup> series		
1	Agha Jari	455	442	448	23	25	0.30	0.24	0.96	Mixed
2	Athabasca tar sands	467	457	463	24	25	0.21	0.28	1.30	Mixed
3	Baxterville	461	444	447	34	30	0.38	0.27	0.27	Etio
4	Belridge	458	448	454	20	22	-0.20	-0.73	1.90	Mixed
5	Boscan	482	469	476	27	29	0.22	0.17	1.20	Mixed
6	Burgan	473	466	469	34	34	0.32	0.47	0.70	Etio
7	Colorado oil shale	466	457	464	14	21	0.29	-0.33	5.00	DPEP
8	Gilsonite	479	469	476	13	16	0.23	0.31	1.50	Mixed
9	Mara	472	456	464	28	29	-0.14	0.21	1.10	Etio
10	Melones	468	457	462	23	32	-0.35	0.22	0.89	Mixed
11	Rozel Point	475	477	475	13	21	-0.77	- <sup>g</sup>	5.80	DPEP
12	Santiago	458	446	455	16	18	-0.25	0.17	2.90	Mixed
13	Wilmington	454	443	448	25	26	0.24	0.27	0.82	Mixed

See Ref. [9] for complete footnotes.

<sup>a</sup> From MS peak intensities.<sup>b</sup>  $\sum$  of  $m/z$   $308 \pm 14n$ .<sup>c</sup>  $\sum$  of  $m/z$   $310 \pm 14n$ .<sup>d</sup> From MS peak intensities.<sup>e</sup>  $\sigma = \sqrt{\sum (IM^2) / \sum I - (\sum IM / \sum I)^2}$  ( $M$  = mass).<sup>f</sup> Envelope asymmetry.<sup>g</sup> Not quantitative.<sup>h</sup> From  $\alpha$  and  $\beta$  bands.

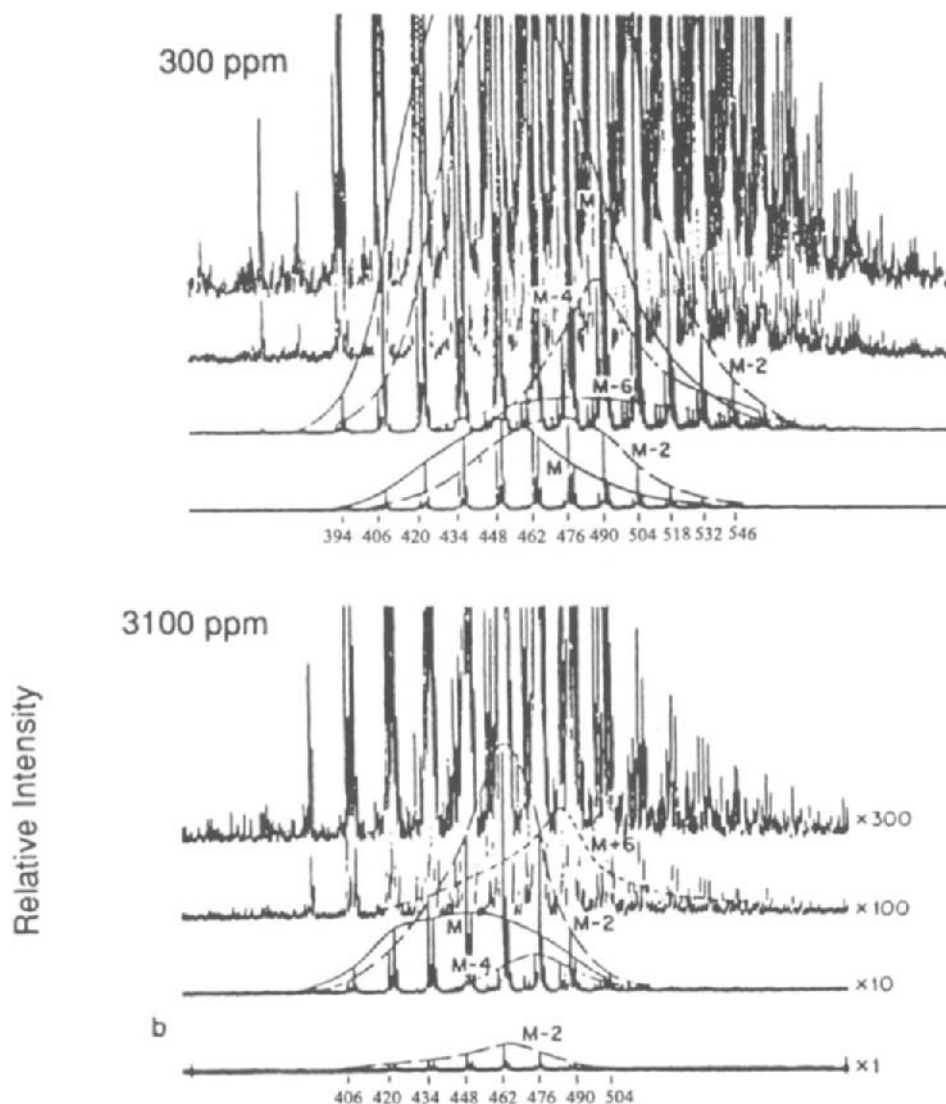


Fig. 3-4. Low-voltage mass spectra of Mara (left) and Belridge (right), demetallated porphyrin fractions [11]. Reproduced with permission.

relatively narrow distributions (columns 4 and 5). Agha Jari, Athabasca, Baxterville, Belridge, Boscan, Burgan, Mara, Melones, Santiago, and Wilmington have relatively broad distributions (columns 4 and 5). The  $\sum \text{DPEP} / \sum \text{etio}$  ratio varies from 0.27 for Baxterville to 5.8 for Rozel Point.

Fig. 3-4 shows more detailed MS examination of porphyrins isolated from other crude oil asphaltenes after using the MSA technique [11]. In addition to etio and DPEP, sev-

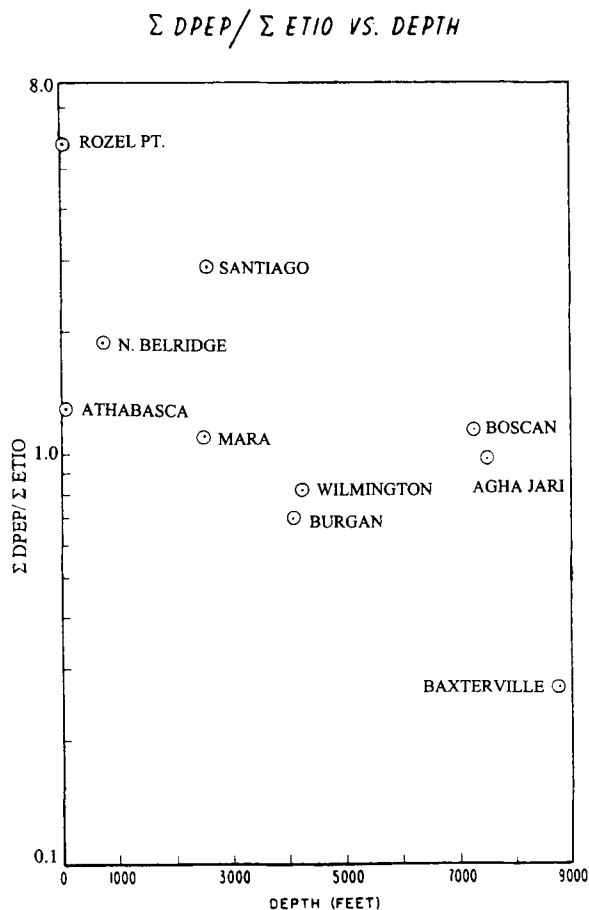


Fig. 3-5. Ratios of DPEP to etio porphyrins versus the depth of burial of a number of crude oils from which the porphyrins have been isolated [3]. Reproduced with permission.

eral other homologous series related to porphyrins with different mass relationships (for example, M-4 and M-6) were detected. These series, along with previous MS evidence and structural speculation [7,9] indicated the structural confirmation of Rhodo petroporphyrin as having a benzene ring fused to one of the pyrrole rings of the porphyrin. In all the samples studied, the Rhodo porphyrins were found at lower concentrations than etio and DPEP porphyrins. They are found in a wide variety of crude oils.

Fig. 3-5 shows the  $\Sigma \text{DPEP} / \Sigma \text{etio}$  ratio from Table 3-3 as a function of formation burial depth [3]. Although much scatter is evident, the data show that a decrease in the  $\Sigma \text{DPEP} / \Sigma \text{etio}$  ratio occurs roughly with an increase in maturity. (Maturation degree is assumed here to increase with burial depth.) This relationship indicated that DPEP was either decreasing faster, relative to etio, and/or DPEP was converting to etio with increasing maturation.

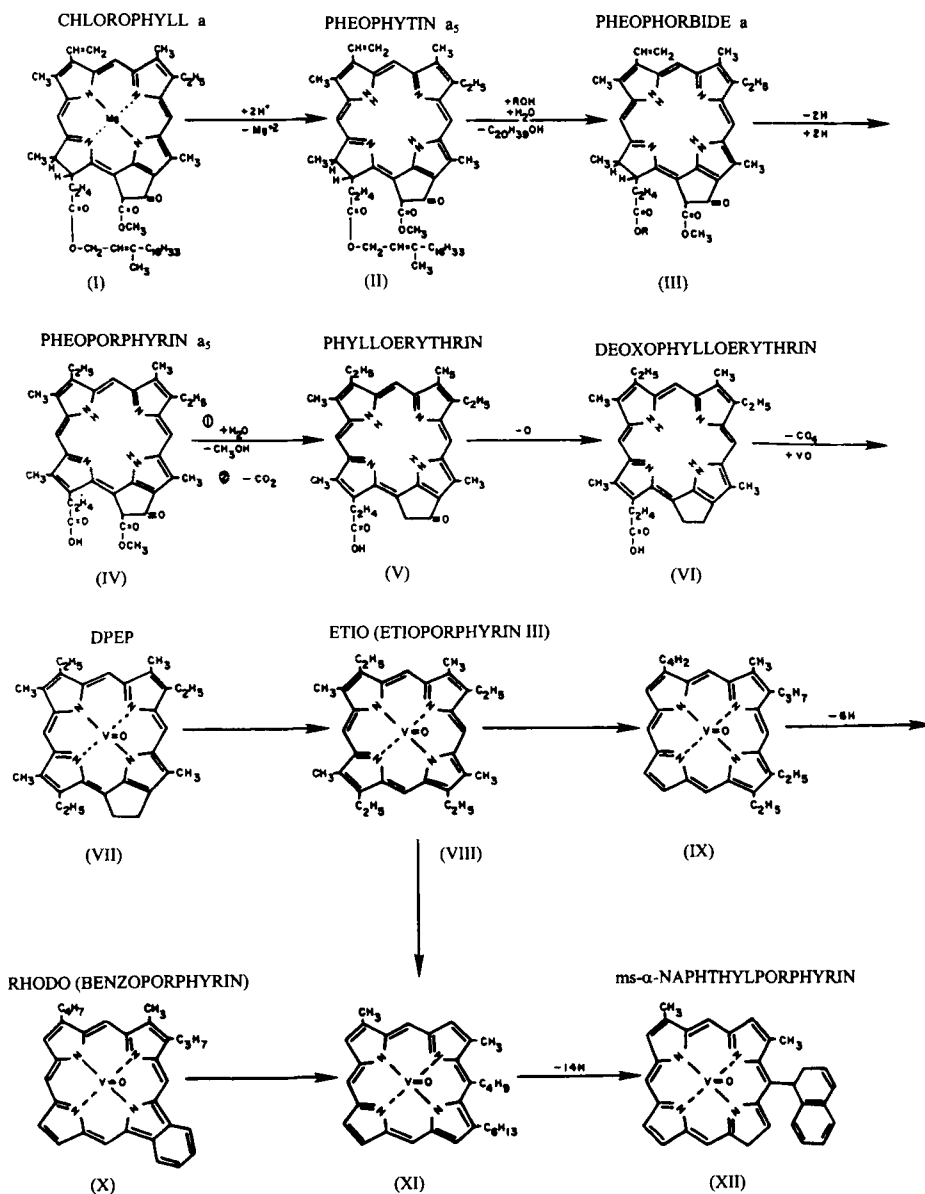


Fig. 3-6. Hypothetical scheme from DPEP to benzoporphyrin and ms- $\alpha$ -naphthyl porphyrin [3,12]. Reproduced with permission.

This newly acquired structural information correlated with geochemical properties of the samples led to the modification of/addition to the Triebs scheme, shown in Fig. 3-6 from Yen and Silverman [12] and Yen [3]. Other modifications were also made to this



scheme, including the formation of larger aromatic substituted porphyrins (see Fig. 3-6, structure XII).

*Nature of porphyrins in kerogen — evidence for trapped etio-type porphyrins*

Porphyrin complexes in crude oils, even though complicated, are generally oil-soluble, extractable species. This makes traditional spectroscopic and separation techniques useful in identification. However, whether or not these same structures are in the kerogen (thought to be the source for crude oil) is a much more difficult question to answer. Kerogen is not directly soluble in either organic or aqueous media. Thermal decomposition of kerogen produces liquid products which can contain porphyrin. However, thermal treatment is believed to alter the functionality beyond identification, as well as it does not convert all of the organic material in the kerogen.

One approach to understanding the structure of kerogen, and possibly to detecting porphyrins, has been the use of chemical oxidation to break the kerogen into smaller, more manageable (and soluble) parts for analysis. Prior to 1987, a number of agents were used to accomplish this. Refluxing chromic acid [13–15], and alkaline permanganate [16–18] were some of the most widely used methods. All had specific advantages, but were considerably severe, producing large quantities of carboxylic acids and other chemical artifacts as well as poor mass balances.

In 1987, Barakat and Yen [19] presented a new selective technique for stepwise oxidation using sodium dichromate in glacial acetic acid. The technique was not mild enough nor specific for isolation of petroporphyrins intact. However, certain degradation by-products were detected which were indicative of porphyrin structures in the kerogen.

The method was designed to remove bitumen and mineral matter before oxidation by the following steps [20]: (a) bitumen extraction ( $C_6H_6/CH_3OH$ ), (b) kerogen isolation from minerals ( $HCl/HF$ ), (c) another bitumen extraction, and (d) kerogen oxidation ( $Na_2Cr_2O_7$  in glacial acetic acid for 20 h at 20 to 40°C; repeating until kerogen is consumed). The petroporphyrin by-products from the oxidation are the alkyl-maleimides [21–23]. Because of the substitution on the porphyrin rings, etio porphyrin produces 3-ethyl-4-methyl-1H-pyrrole-2,5-dione (EMPD) and 3,4-dimethyl-1H-pyrrole-2,5-dione (DMPD) whereas DPEP produces both and 3-methyl-1H-pyrrole-2,5-dione (3-MPD).

Fig. 3-7 [24] shows the GC–MS traces of fractions isolated from the sequential extractions of kerogen oxidations for Green River and Monterey kerogens. Both EMPD (R) and DMPD (Q) are found in several of the fractions, and are most abundant in fraction #2 for both kerogens. In addition, no 3-MPD is observed in any of the traces.

Several important conclusions about porphyrins were made from these studies. Although porphyrins are not directly observed in kerogen, the kerogen oxidation method provides ample evidence through porphyrin oxidation by-products suggesting that etio porphyrins are probably the major porphyrins in the kerogens studied. The absence of 3-MPD also suggests that DPEP porphyrin is not a major species. Based on the absence of maleimides bearing  $-COOH$  or  $CH_2COOH$  (produced from oxidation) at the  $\beta$  positions, porphyrins are also probably not chemically bonded to the kerogen structure. In addition, the uneven by-product distributions (principally in fraction #2 for both kerogens) suggest that the porphyrins are not uniformly bound to the kerogen.

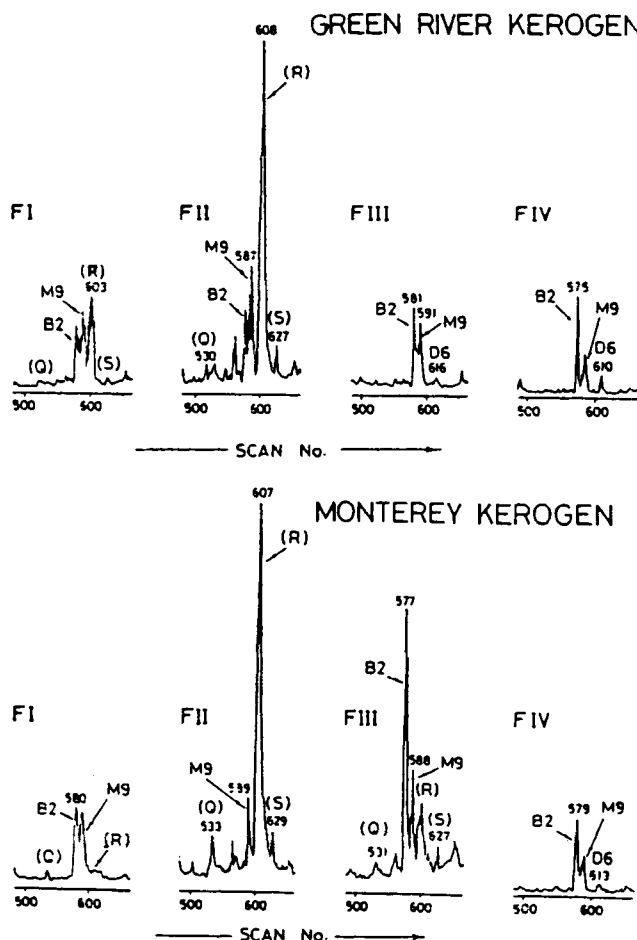


Fig. 3-7. Identical sections of reconstructed ion chromatograms illustrating the variation in the distribution of the maleimides (*R* and *Q*) isolated from stepwise oxidation of Green River and Monterey kerogens. *M9* = nonanoic acid methyl ester; *B2* = 3- or 4-methylbenzoic acid methyl ester; *D6* = hexanedioic acid dimethyl ester, *S* = 2-ethyl-3-methyl-2-butenedioic acid dimethyl ester.

### *Model compounds — highly substituted porphyrins*

By 1970, petroporphyrin chemistry was beginning to receive more attention, particularly because the work of Baker, Yen, and coworkers elucidated some interesting, but poorly understood structural properties and reactivities. In addition to the detection of etio and DPEP porphyrins, several homologous series had been detected, which indicated aromatic rings conjugated on the outside of the porphyrin ring system. Exact mass measurements also supported these as being Rhodo porphyrins. However, the nature and positioning of the ring(s) were still not elucidated.

In addition to the unanswered questions from the MS studies of petroporphyrins in

crude oils, the ESR properties of vanadium in asphaltenes were not understood. Isotropic and anisotropic parameters suggested that vanadium could be bound in a manner which was different than in a nonbonded, freely moving porphyrin. X-ray studies had also shown ordered stacking in the aromatic sheets of the asphaltene [25]. Because of the highly aromatic nature of porphyrins, it was natural to ask whether porphyrins would interact with the aromaticity of other parts of the asphaltene (see Fig. 3-1, structures K and L).

Another issue was that UV-vis spectroscopy was utilized to quantify porphyrin because of the very distinctive absorptions (see above). However, not all of the vanadium in asphaltenes could be accounted for as petroporphyrin by this method (roughly less than 50%) [26,27]. This suggested that either the vanadium is bound by some other chelation, or perhaps higher conjugation of the porphyrin ring (causing shifting of the prominent Soret band or reducing the extinction coefficient).

In an attempt to address some of these questions, in 1970, Vaughan et al. [28] synthesized porphyrins which had additional aromatic rings, and studied the spectroscopic properties. Fig. 3-8 shows the two-step synthesis for these compounds. Synthesis of porphyrins was not well developed at the time. Use of propionic acid greatly reduced the synthesis time, and yielded very clean products. In addition, there was only limited success in adding large aromatic groups to porphyrins (*meso*-substituted porphyrins are not really models for naturally-occurring porphyrins; however, no synthesis for etio or DPEP porphyrins was known at the time). Metallation occurred simply after formation of the porphyrin ring.

Fig. 3-9 shows the MS patterns of tetra-*p*-tolyl and tetra-biphenyl porphyrins. The parent ions are by far the most intense ions. Fragments are identified as porphyrins with successive loss of aryl groups, but break-up of the pyrrole is not observed. Prominent doubly charged ions are observed. This, at the time, established the MS behavior of the tetra-aryl substituted porphyrins. In comparison, etio and DPEP-type porphyrins are now known to fragment in the alkyl substituent position.

These newly synthesized porphyrins also presented the opportunity to measure some ESR properties and aromatic substitution effects. Table 3-4 shows a summary of the isotropic (free tumbling) and anisotropic properties (frozen). The transition temperature

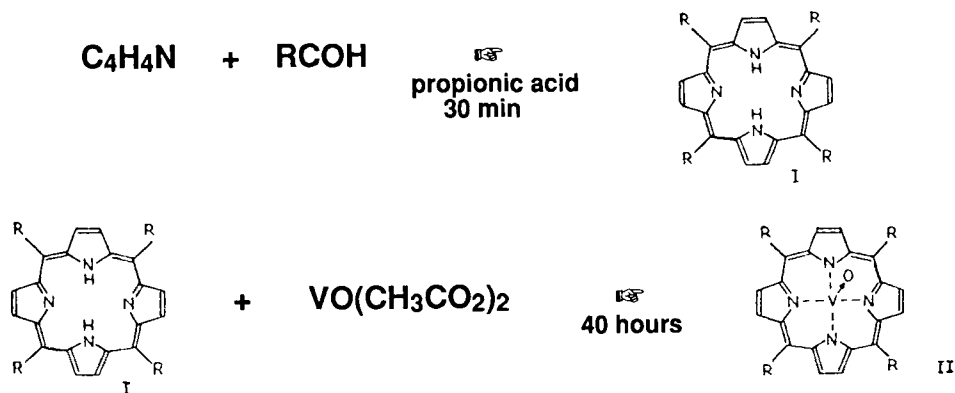


Fig. 3-8. Synthesis of tetra-arylporphyrins and corresponding vanadyl chelates [28].

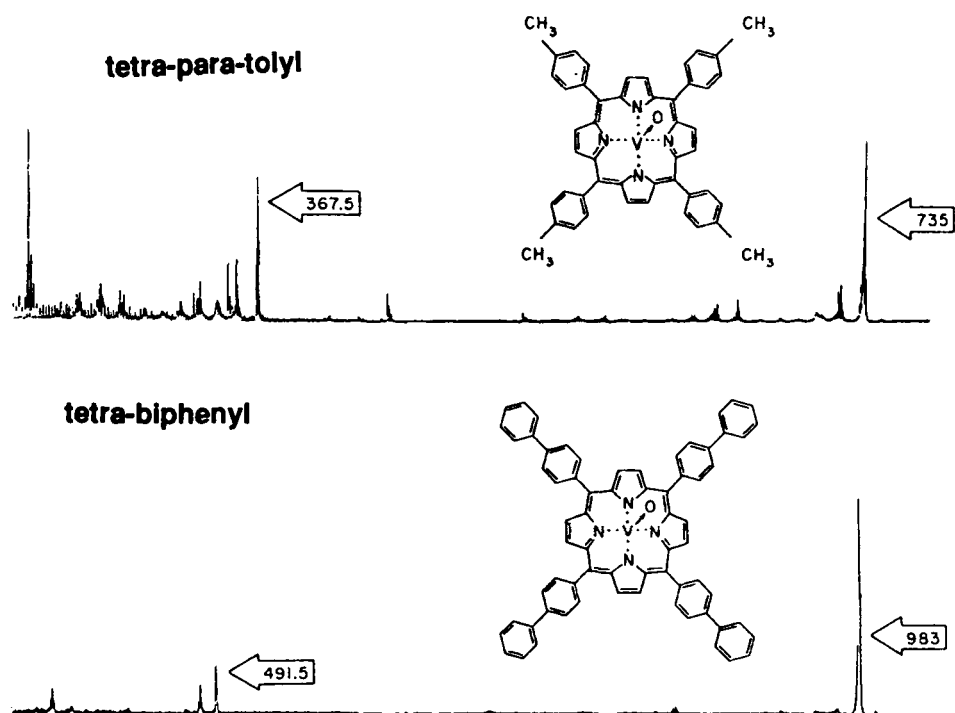


Fig. 3-9. Section of mass spectrum of vanadyl tetra-*p*-tolyl porphyrin (top) and tetra-biphenyl porphyrin (bottom) [28]. Reproduced with permission.

TABLE 3-4

ESR constants obtained from some vanadyl meso aryl porphins

Vanadyl complexes	Transition temp. (°C)	$\frac{A_0^*}{\text{gauss } g_0^{***}}$		$\frac{A_{  }^{**}}{\text{gauss } g_{  }^{***}}$		$\frac{A_{\perp}^*}{\text{gauss } g_{\perp}^{***}}$		Half width gauss	Comments
		$A_{\text{iso}}$ (gauss)*	$g_{\text{iso}}^{***}$	$A_{  }$ (gauss)**	$g_{  }^{***}$	$A_{\perp}$ (gauss)*	$g_{\perp}^{***}$		
TPP	20/110	98.5	1.979	177.3	1.962	59.1	1.998	75	very broad line
T9AP	20/157	98.3	1.981	175.2	1.968	59.7	1.987	30	LN <sub>2</sub>
T4TP	20/105	98.1	1.979	174.9	1.958	59.8	1.989	35	LN <sub>2</sub>
T4CPP	145	98.0	1.980	... (unidentified signals) ...					limited solubility
T1NP	20/118	97.5	1.980	180.7	1.958	56.0	1.991	40	LN <sub>2</sub>
T4MPP	20/110	96.8	1.981	174.7	1.961	57.4	1.989	40	LN <sub>2</sub>
T4HPP	20/145	96.7	1.981	—	—	—	—	—	aniso spectrum noisy
T2NP	20/115	96.5	1.979	176.5	1.961	56.5	1.989	40	LN <sub>2</sub>
T9PP	20/152	95.6	1.980	183.3	1.963	51.8	1.988	70	very broad lines

\* 0.5 gauss; \*\*  $\pm 1$  gauss; \*\*\*  $\pm 0.001$ .

is the temperature at which free rotation changes to highly restricted rotation. The transition temperature roughly correlates with the number and distribution of rings — the larger the ring size, the slower the motion.  $g_{iso}$  is almost the same, regardless of substitution. The biggest differences were seen in the decrease of the isotropic hyperfine coupling constant,  $A_{iso}$ , with the larger substituents, indicating delocalization of unpaired electrons.

Several other results were realized from this study: (1) a more convenient synthesis of tetra-aryl porphyrins was developed; (2) metal–nitrogen bond strength decreases with withdrawing groups on the aryl substituents as a result of inductive effects; (3) strong IR absorptions at  $\approx 1000\text{ cm}^{-1}$  may be ligand-related and not completely  $\text{V}=\text{O}$  (usually very strong in vanadyl square pyramidal complexes); (4) nuclear magnetic resonance (NMR) spectroscopy indicated that the substituent rings are not co-planar with the porphyrin ring; and (5) the stability of the porphyrin system increases with increasing aryl size.

### *Synthesis and characterization of non-porphyrin model compounds*

As discussed above, vanadium in crude oils is classified as two types, metalloporphyrins and metallo nonporphyrins, primarily because not all the vanadium in many crudes can be accounted for bound only as porphyrins. Quantifying with UV–vis spectroscopy (Soret and  $\alpha$  and  $\beta$  bands) gives only 50 to 60% of the vanadium compared to elemental analysis methods [26]. The reasons for this are still not clear. Separations (asphaltene precipitation and chromatography) indicate different types of vanadium [2,29–31], and ESR parameters and MS suggest different possible heteroatom combinations [9]. This has led some researchers to attempt to elucidate the nonporphyrin vanadium using discrete vanadium complexes other than porphyrins as models for the nonporphyrin coordination site.

In the late 1960's and early 1970's, few vanadyl square pyramidal complexes were synthesized and structurally characterized other than porphyrins ( $\text{N}_4$  coordination) and the acetylacetonates ( $\text{O}_4$  coordination). Vanadium in crude oils was known to be primarily vanadyl  $\text{V}=\text{O}^{2+}$ . The structure was thought to be roughly square pyramidal with the O of the  $\text{V}=\text{O}^{2+}$  at the apex of the pyramid, and the ligand heteroatoms at the corner of the basal plane. In most structures, the vanadium is usually  $\approx 0.2$  to  $\approx 0.7\text{ \AA}$  above the basal plane.

ESR theory for vanadyl square pyramidal complexes also had not been well developed. Structural geometry effects, as well as ligands strength and bonding (both  $\sigma$  and  $\pi$ ) effects on  $g$  and  $A$  values were not clear or systematic. Clearly, more understanding of coordination site in vanadium complexes needed to be known.

In 1968, Boucher et al. [32] reported synthesis of ligand coordination around vanadium other than  $\text{N}_4$  and  $\text{O}_4$ . Fig. 3-10 shows the general synthesis of Schiff-base complexes with  $\text{N}_2\text{O}_2$  coordination. Reactants are mixed as solids and heated to  $\approx 250^\circ\text{C}$  in vacuo for 3 h. The driving force is the acid-base reaction with the non-volatile ligand and the removal of the product acetylacetone by vacuum. Products are purified by extraction and recrystallization.

Several salicylaldehydes and  $\beta$ -ketimines were synthesized and characterized. Fig. 3-11 shows the single crystal X-ray structure of  $[\text{NN}'\text{-ethylenebis-(1-acetonylethyl)-idenimin-}$

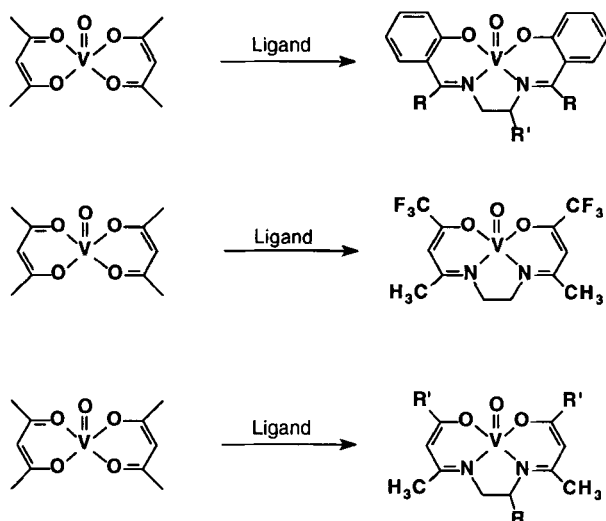


Fig. 3-10. Synthesis of vanadyl  $\beta$ -ketimines [32],  $R, R' = H, H$ ;  $H, CH_3$ ;  $CH_3, H$ ;  $CH_3, CH_3$  (top);  $CF_3$ - $\beta$ -ketimines [48] (middle); and salicylaldimines [47],  $R, R' = H, CH_3$ ;  $CH_3, CH_3$ ;  $H, C_6H_5$ ;  $CH_3, C_6H_5$  (bottom) from vanadyl acetylacetonate.

ato)-OO'NN']-oxovanadium(IV) [33,34]. The structure is very similar to  $VO(acac)_2$ , being square pyramidal with vanadyl oxygen at the apex and the N and O of the ligands at the corners of the basal plane. The vanadium is also displaced 0.58 Å above the basal plane.

This structure was extremely important at the time, being the first structure of a vanadyl compound with a coordination sphere other than  $O_4$  or  $N_4$  porphyrin. The stability of these  $N_2O_2$  complexes suggested that they might be possible models for the non-porphyrin vanadium. One possible method to access that information was through ESR spectroscopy. Vanadyl is ideal for ESR.  $^{51}V$  is  $\approx 100\%$  abundance, has a large nuclear moment, and has a nuclear spin of  $7/2$ .  $V=O^{2+}$  yields structural information because it has one unpaired electron (usually simple transitions), and has a non-cubic field, usually square pyramidal. In fossil fuels, vanadium concentrations can be reasonably high for trace elements, up to 1000 ppm in crude oils and 0.3 to 0.4 wt.% in asphaltenes; so detection is very accessible.

In 1969, Boucher et al. [35] decided to study in detail, by ESR, these  $N_2O_2$  coordinated vanadium complexes, along with those of acetylacetonates and porphyrins, to try to find a systematic behavior of the parameters which might elucidate the structure(s) of the non-porphyrin vanadium in the crude oils (at least the first coordination sphere). Fig. 3-12 shows the spectrum of  $VO(acen)$  in THF at room temperature. The complex exhibits a typical isotropic spectrum of vanadyl square pyramidal complexes — eight lines corresponding to free rotation at modest temperatures (average of the molecular asymmetric field).  $g_{iso}$  and  $A_{iso}$  are readily calculated using a second-order Zeeman correction (calculation program given in [36]).

After looking at a large number of vanadyl model compounds (those available at the time), in 1970, Yen et al. [37] summarized some relationships between ESR pa-

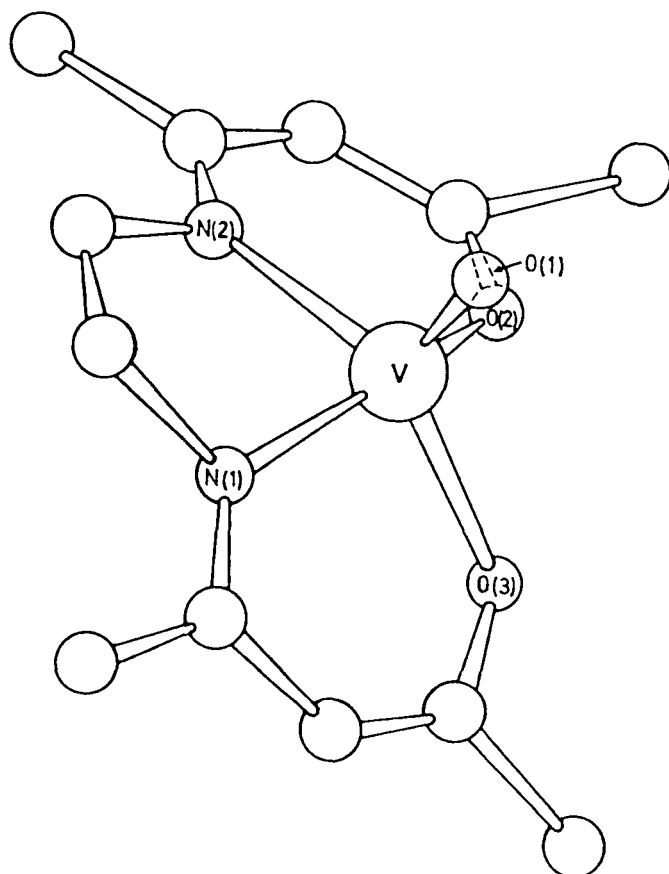


Fig. 3-11. Single crystal structure of [N,N'-ethylenebis-(1-acetonylethylideniminato)-OO'NN']-oxovanadium(IV) [33]. Reproduced with permission.

rameters and heteroatoms in the first coordination sphere around the vanadyl. Fig. 3-13 shows the relationship of the isotropic  $g$  and  $A$  values. In the left side of the figure, the known porphyrins ( $N_4$ ) are shown to have  $g_{iso}$  values around 1.980 and  $A_{iso}$  values between 93 and 100 gauss. In the right side of the figure, the acetylacetonates ( $O_4$ ) have  $g_{iso}$  values around 1.970 and  $A_{iso}$  values around 100 to 110 gauss. The  $\beta$ -ketimines ( $N_2O_2$ ) exhibit intermediate isotropic parameters of  $g_{iso}$  around 1.975 and  $A_{iso}$  around 100 gauss. The values in the figure established that an empirical relationship exist between the isotropic  $g$  and  $A$  values for a given ligand coordination around vanadyl when considering N and O. The relationship can be theoretically justified by considering dipole-dipole interactions of the electron and the nuclear moments and the amount of unpaired electron density at the nucleus. In addition, the isotropic parameters of mixed coordination spheres seem to be weighted averages of those of coordination spheres of all  $O_4$  and  $N_4$ , as seen by the values for  $N_2O_2$ .

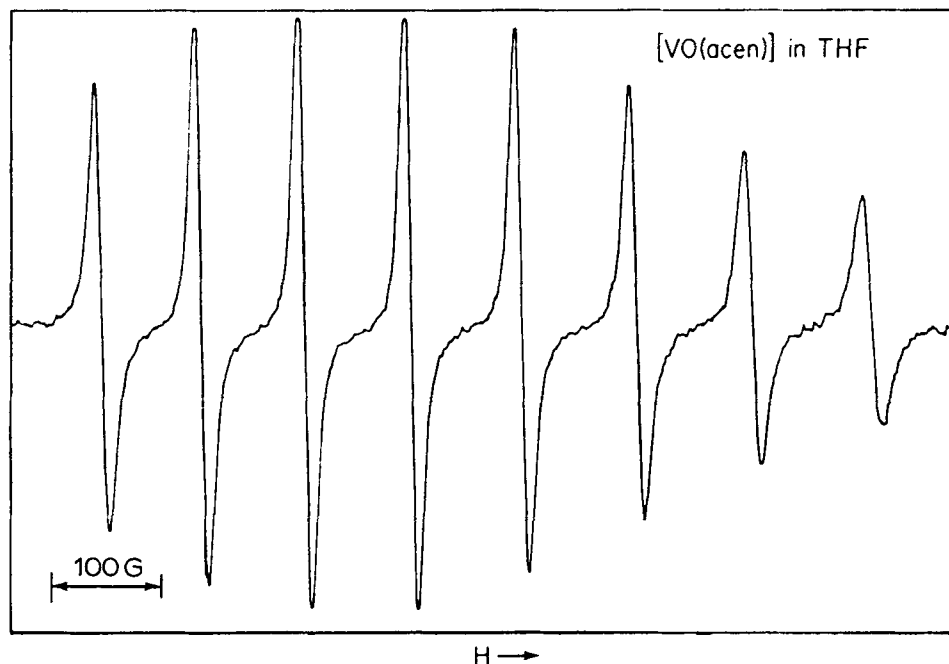


Fig. 3-12. ESR spectrum of VO(acen) (*bis*-acetylacetonethylenediimine)-oxovanadium(IV) in tetrahydrofuran at 25°C [35]. Reproduced with permission.

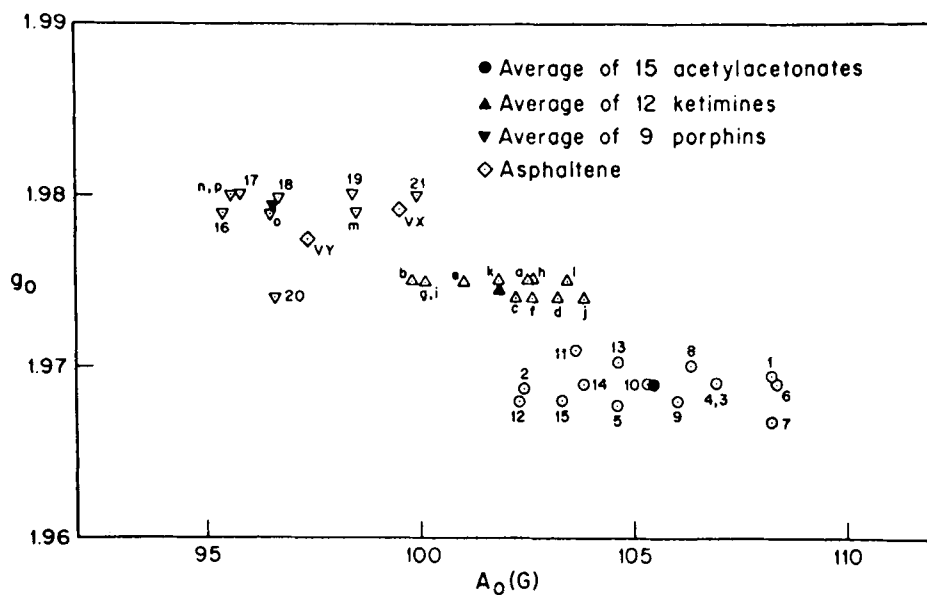


Fig. 3-13. Relationship between  $g_0$  ( $g_{iso}$ ) and  $A_0$  ( $A_{iso}$ ) for a series of vanadyl complexes [37]. Asphaltene samples, Boscan (VY) and Bachequero (VX) are also shown. Reproduced with permission.



The relationship developed in Fig. 3-13 was created to assess the first coordination sphere around the vanadium in asphaltenes isolated from Boscan (VX) and Bachequero (VY) asphaltenes. Both of these asphaltenes exhibited some of nonporphyrin bound vanadium as determined by UV-vis. From the figure, both had isotropic ESR parameters which match those of the porphyrin ( $N_4$ ) model compounds.

Since that original work was completed, several model compounds have been added to the relationship in Fig. 3-13. Fig. 3-14 [38,39] shows that the relationships between  $g_{iso}$  and  $A_{iso}$  stated above generally hold true. Compounds such as vanadyl catecholates ( $O_4$ ) [40], *mono*-thio- $\beta$ -diketonates ( $S_2O_2$ ) [46], dithiocarbamates ( $S_4$ ) [41], and dithiols ( $S_4$ ) [42] fit nicely into the correlation. However, some vanadyl complexes do not follow the pattern. Two examples are *bis*(2-methyl-8-quinolinolato)oxovanadium(IV) and pyridine-2-thiolate oxovanadium(IV).

Fig. 3-15 shows the single crystal X-ray structure of *bis*(2-methyl-8-quinolinolato)-oxovanadium(IV) [43]. Although a casual inspection of the structure would suggest that it is a standard square pyramidal vanadyl complex, more detailed analysis shows that the pyramidal structure is distorted to trigonal bipyramidal having two elongated N bonds and two compressed O bonds.

Fig. 3-16 shows the single crystal X-ray structure of pyridine-2-thiolate oxovanadium(IV) [44]. Again, the structure is not strictly square pyramidal in the solid state. In this case, there is distortion due to axial coordination of the bridging ligands formed because of the dimerization. The structure is probably not strictly square

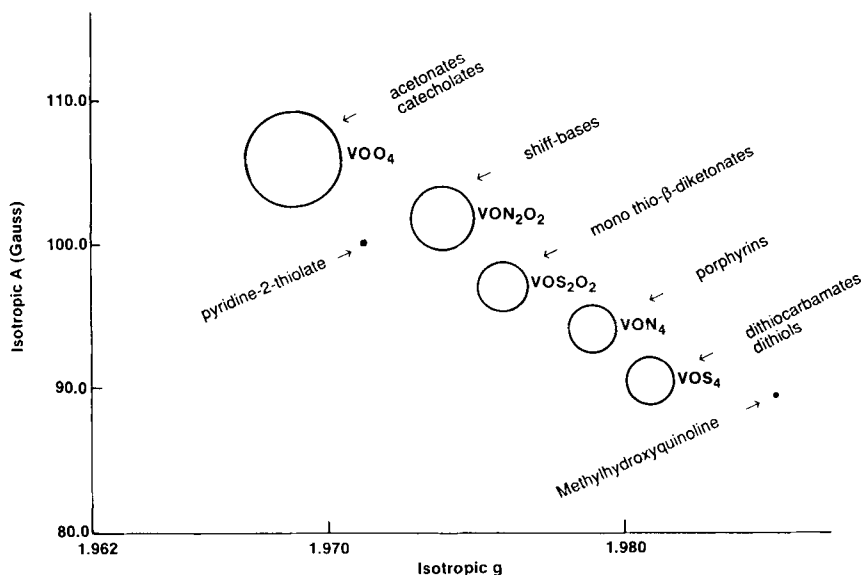


Fig. 3-14. Relationship between  $g_0$  ( $g_{iso}$ ) and  $A_0$  ( $A_{iso}$ ) for a large suite of vanadyl complexes with presumably square pyramidal structure around the vanadium. Pyridine-2-thiolate and methylhydroxyquinoline complexes show distortions from square pyramidal in the solid state.

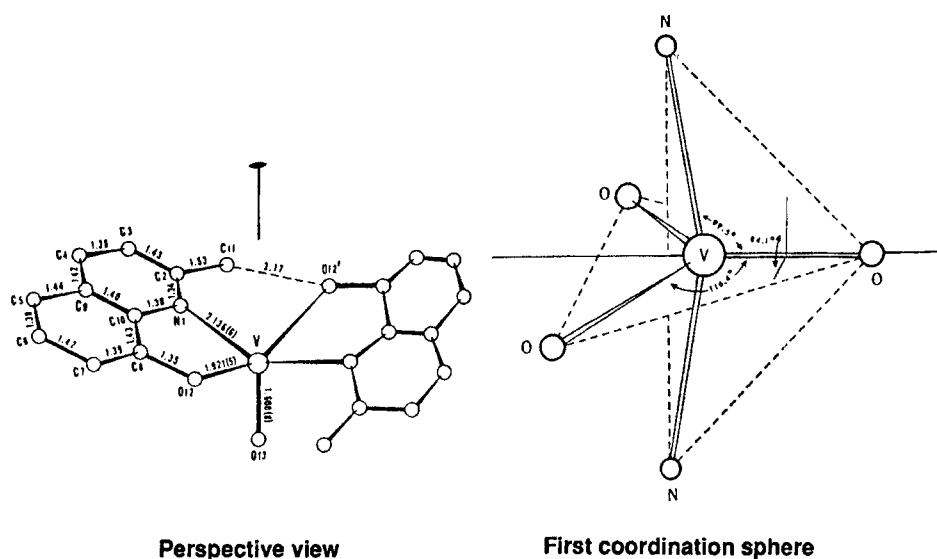


Fig. 3-15. Perspective and first coordination view of  $\text{VO}(\text{C}_{10}\text{H}_8\text{NO})_2$ . Values in parentheses (deviation in the last digit) are the estimated standard deviation of the bond distances [43]. Reproduced with permission.

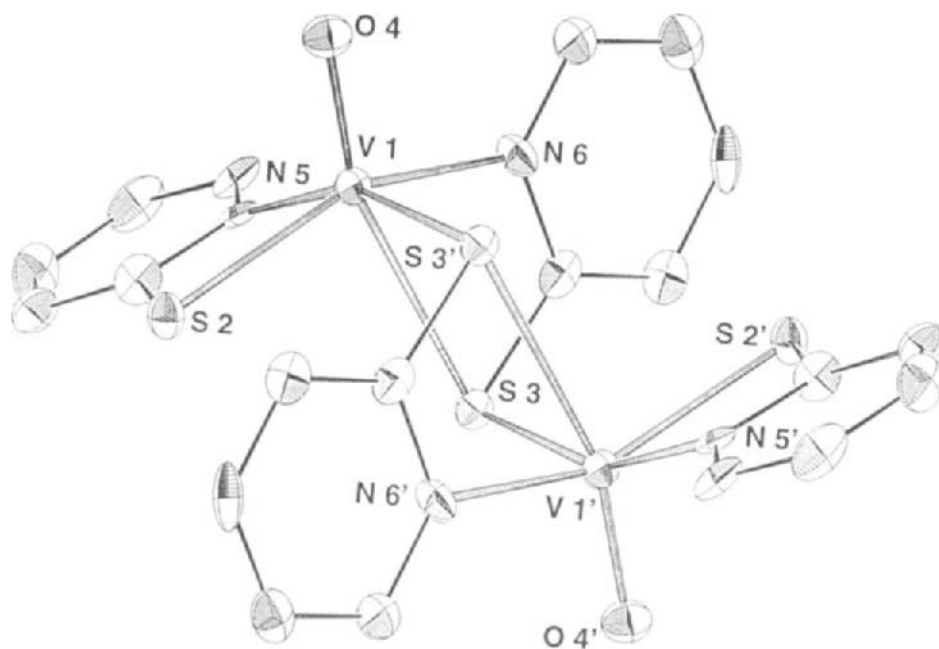


Fig. 3-16. Single crystal X-ray structure of pyridine-2-thiolate oxovanadium(IV) [44]. Reproduced with permission.

pyramidal in solution even if it does not stay a dimer because of the small ligand bite.

The relationship between  $g_{iso}$  and  $A_{iso}$  in Figs. 3-13 and 3-14 was formed on the assumption that all the compounds had similar molecular symmetry (similar crystal fields). Indeed, the relationship seems to hold true for vanadyl square pyramidal complexes. However if there is structural distortion, apparently even minor, the relationship does not hold.

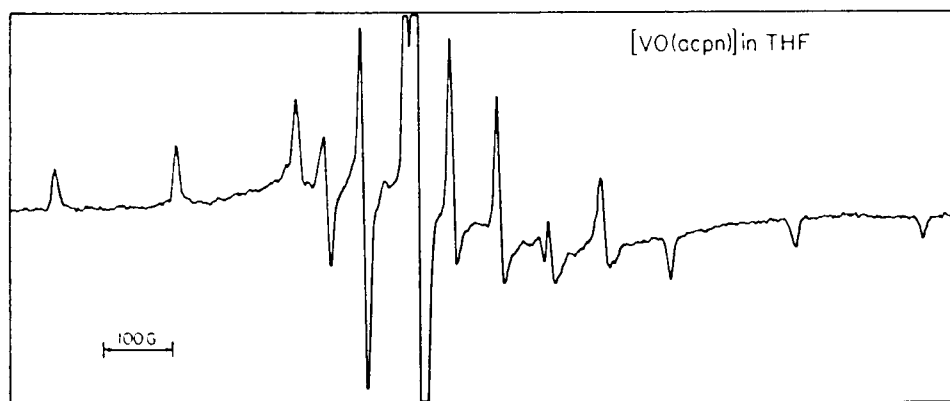


Fig. 3-17. ESR spectrum of *bis*-acetylacetonate(1,2)propylenediimineoxovanadium(IV) in tetrahydrofuran at  $-150^{\circ}\text{C}$  [35]. Reproduced with permission.

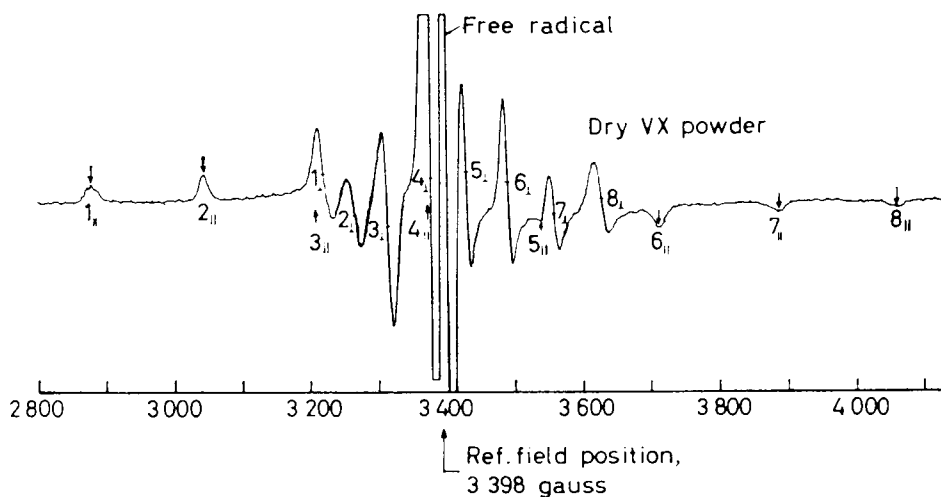


Fig. 3-18. ESR spectrum of dry Bachequero asphaltenes [45]. Reproduced with permission.

*Structure of vanadium in asphaltenes*

Fig. 3-1 shows the metals in the asphaltene model in two separate configurations. K is identified as petroporphyrins and L is identified as a non-porphyrin, buried deep in the asphaltene and possibly an essential structural link. In 1969, Boucher et al. [35] applied ESR to study, in detail, the behavior of the vanadium in Bachaquero asphaltenes to try to address this configuration of the metals.

In ESR, multiple electron–nucleus interactions can be at least partially resolved in frozen solution. Hindered rotation of molecules on the ESR time scale can allow the partial resolution of directionally dependent field gradients, if the molecule does not have spherical symmetry. For vanadyl, this can lead to a 24-line spec-

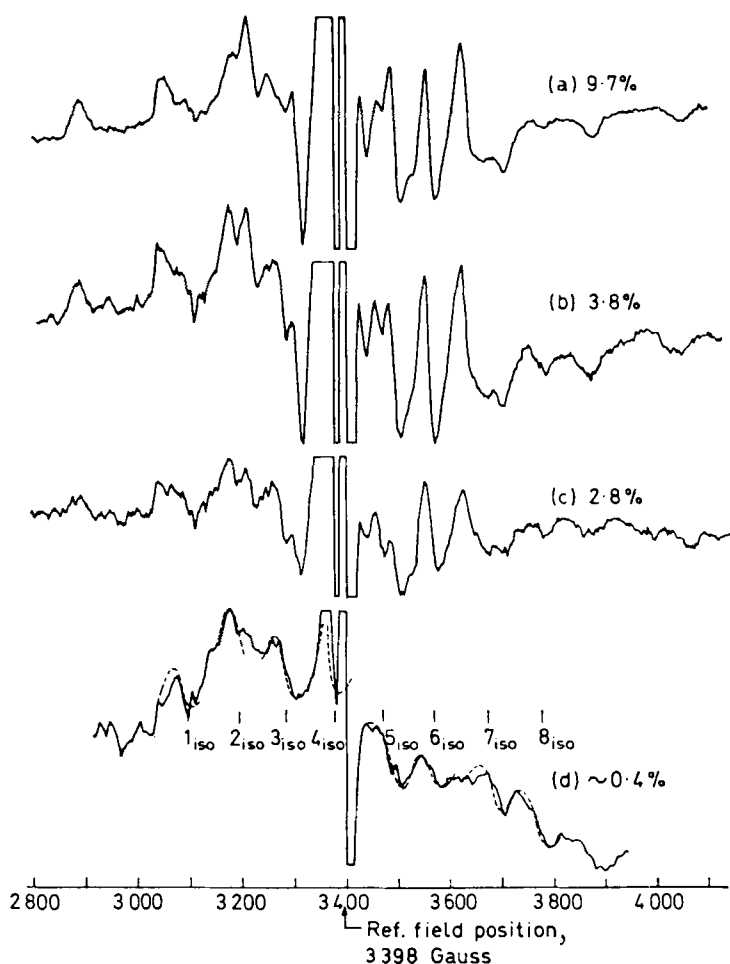


Fig. 3-19. ESR spectra of Bachaquero asphaltenes at various concentrations in tetrahydrofuran [45]. Reproduced with permission.

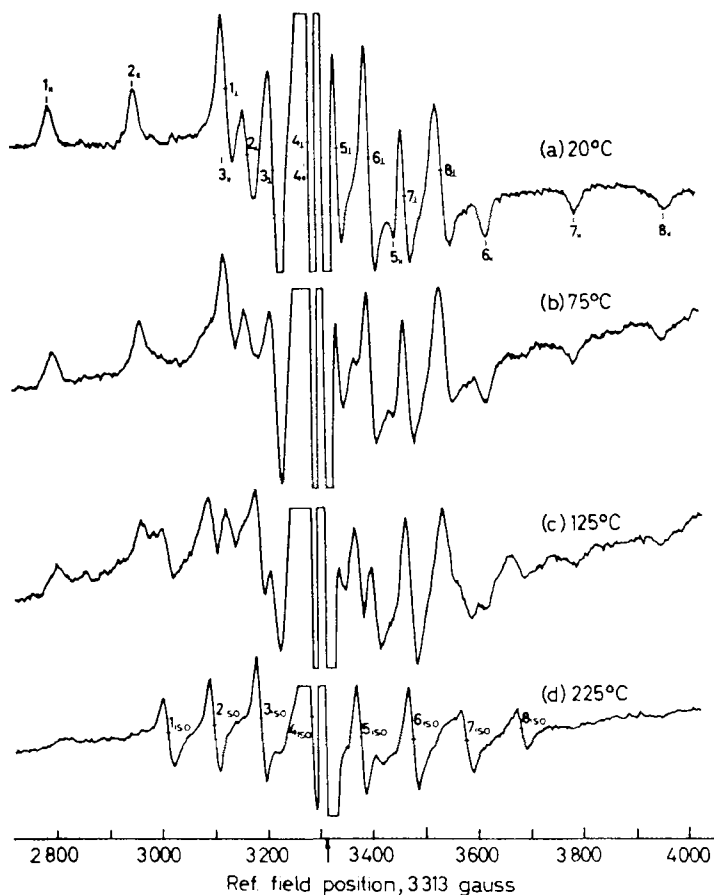


Fig. 3-20. ESR spectra of Bachequero asphaltenes at various temperatures in benzyl-*n*-butyl ether [45]. Reproduced with permission.

trum. Typically, vanadyl resolves to 16 lines, yielding  $g_{\parallel}$ ,  $A_{\parallel}$ ,  $g_{\perp}$  and  $A_{\perp}$ . Fig. 3-17 shows the frozen solution ESR spectrum of VO(acpn) at 77 K, a  $N_2O_2$   $\beta$ -ketimine complex. Most of the 16 lines are resolved in the axial spectrum (overlap prevents complete resolution). Fig. 3-18 shows the ESR spectrum of finely powdered Bachequero asphaltenes [45] at room temperature. The spectrum is also axially resolved and very similar to VO(acpn). In addition to the 16 lines due to the vanadyl, a sharp absorption at  $g = 2.0031$  is identified as a free radical, which is not directly related to the vanadium. These results suggested that the vanadium in the asphaltene behaves similarly to the vanadium model compound in frozen solution, exhibiting hindered rotation properties. Fig. 3-19 shows the ESR spectra of Bachequero asphaltenes at various concentrations in THF. The spectrum at high concentration exhibits properties which are similar to hindered rotation seen in the model compound (Fig. 3-17) and the powder spectra (Fig. 3-18). The spectrum at low concentration

exhibits the isotropic, or freely rotational ESR properties. Fig. 3-20 shows the ESR spectra of Bachequero asphaltenes at various temperatures in benzyl *n*-butyl ether. The room-temperature spectrum exhibits hindered rotation properties, having axial resolution. The high-temperature spectrum exhibits isotropic or free rotation properties.

Fig. 3-21 shows the ESR spectra of vanadyl phthalocyanine, another vanadyl  $N_4$  model compound, mixed with asphaltenes from Gilsonite dissolved in  $CHCl_3$ . Gilsonite is a vanadium-free bitumen thought to be from the Green River Formation. The asphaltene-free solution shows the isotropic or free rotation spectrum. As asphaltenes are added, even in trace amounts, the spectrum shifts to anisotropic or hindered rotation behavior. Clearly, some type of interaction between the asphaltenes and vanadium is occurring to affect the ESR spectrum.

To explain this behavior, Tynan and Yen [45] proposed that vanadium is in a bound form (ANISO) and a free form (ISO) equilibrium. If this equilibrium relationship is assumed to be first order, then  $\ln k = -E/RT + D$ . If the equilibrium constant  $K$  is assumed to be proportional to peak height, then  $K = k_1/k_2 = h_1/h_2$ .  $K$  can then be measured from selected ESR data, which span the hindered and free rotation range. Metal site symmetry reduction is ruled out because  $A_z$  and  $A_y$  are very large and would require a very large reduction in symmetry to be isotropic, as well as only high temperature or extreme dilution (Figs. 3-19 and 3-20) causes isotropic behavior, consistent with retention of site symmetry.

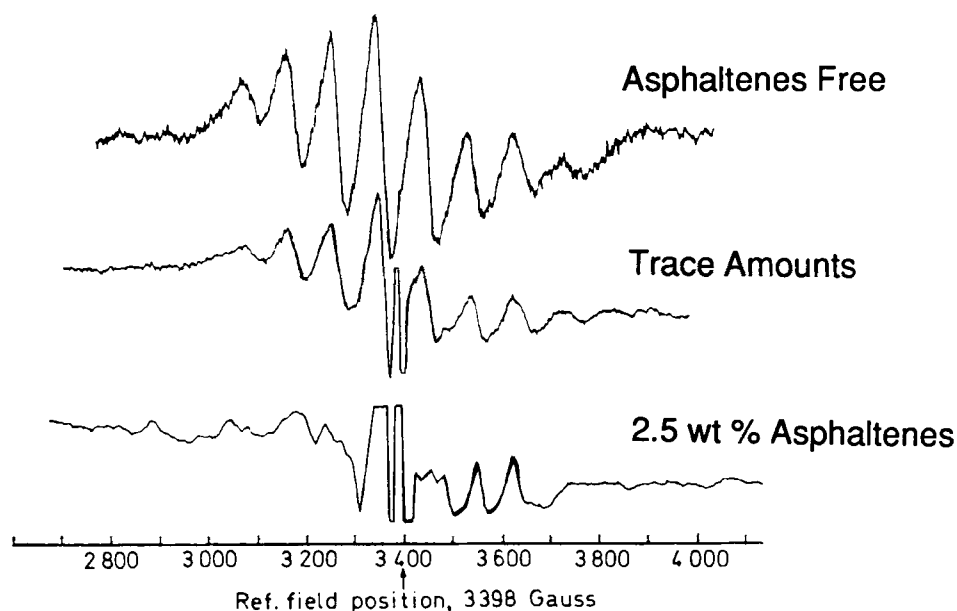


Fig. 3-21. ESR spectra of vanadyl phthalocyanine added to vanadium-free asphaltenes (gilsonite) at various concentrations in chloroform [45]. Reproduced with permission.

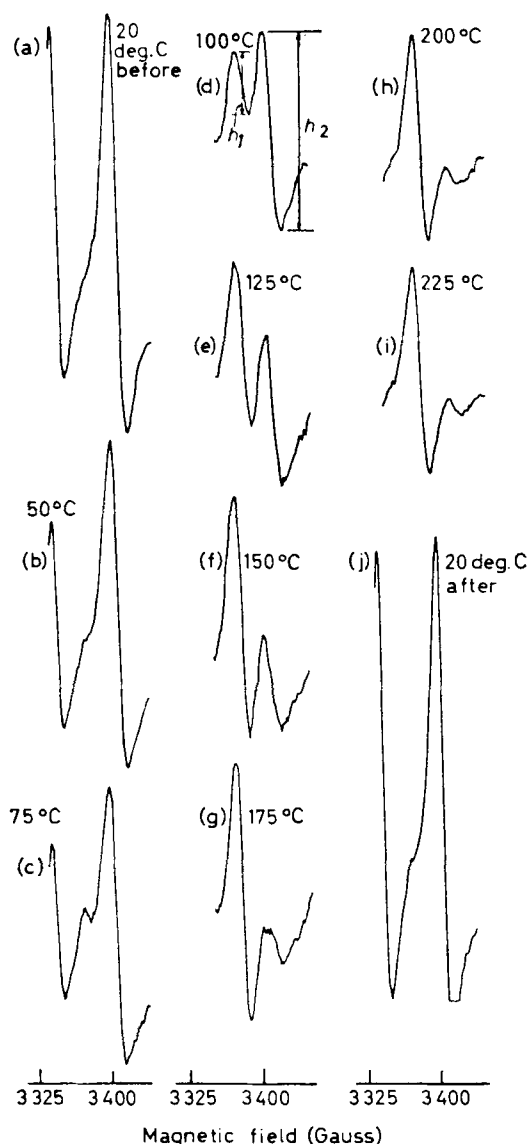


Fig. 3-22. Temperature dependence of  $5_{\text{iso}}$  and  $6_{\text{aniso}}$  peaks for Bachaquero asphaltenes (4 wt.%) in benzyl-*n*-butyl ether [45]. Reproduced with permission.

Fig. 3-22 shows the temperature-dependent behavior of the  $5_{\text{iso}}$  and  $6_{\text{aniso}}$  peaks of Bachaquero asphaltenes in benzyl-*n*-butyl ether. Other peaks were not selected because of interferences. Clearly, the  $6_{\text{aniso}}$  peak disappears with increasing temperature, while the  $5_{\text{iso}}$  peak appears. The reverse occurs when the temperature is lowered.

Fig. 3-23 shows the Arrhenius plot of the relative concentrations of  $5_{\text{iso}}/6_{\text{aniso}}$

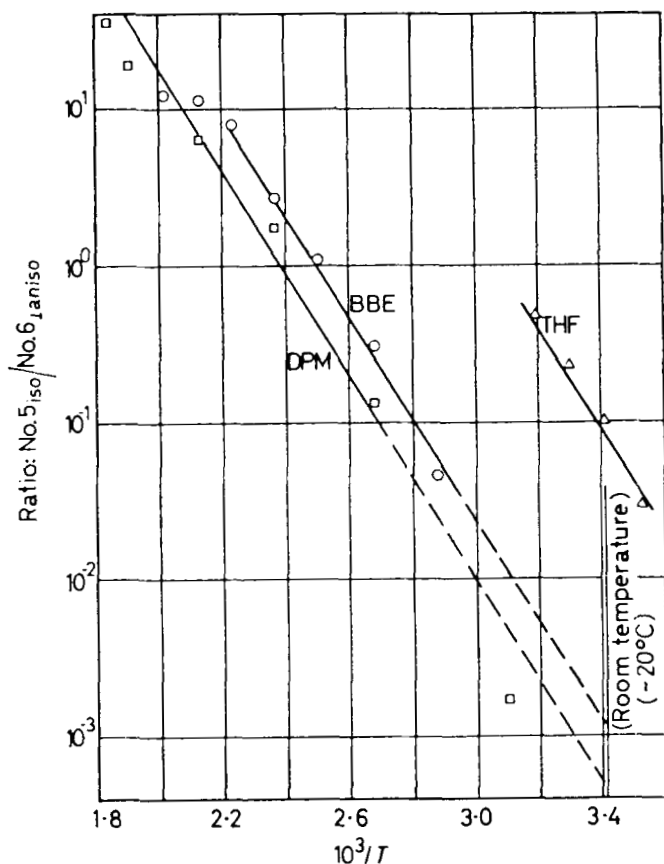


Fig. 3-23. Arrhenius plot of  $S_{150}$  and  $6_{150}$  peak ratios for Bachaquero asphaltenes [45]. Reproduced with permission.

for Bachaquero asphaltenes in different solvents. All solvents give roughly linear dependencies. The calculated activation energy is 14.3 kcal/mol.

From the results of this study, several conclusions were made about the vanadium in asphaltenes. The vanadium is attached to the asphaltene. It is associated at the edge, intercalated, or associated in the center. The vanadium is also trapped in the asphaltene. The energy necessary to free chelates from trapping from aromatic sheets is 1 kcal/mole and from hydrogen bonding is  $\approx 2$  to 8 kcal/mole. The energy needed for formation of dimerization of formic acid is  $\approx 14$  kcal/mol, tetramerization of ethanol  $\approx 23$  kcal/mol, and urea adduct is  $\approx 16$  kcal/mol. The 14.3 kcal/mol suggests oligomerization types of interactions.

Defects in the asphaltene model shown in Fig. 3-1 could be formed by incomplete graphitization of benzenoid systems due to heteroatoms like N, S, and O. Fig. 3-24 shows a molecular model exhibiting these properties.





Fig. 3-24. Molecular model indicating the metal uptake capacity of asphaltenes [3]. The left upper gap is made of sulfur, nitrogen, and oxygen atoms. Reproduced with permission.

## CONCLUSIONS

The results, concepts, and ideas elucidated in this chapter are only a few of the many which have been derived from work that Prof. Yen has been involved with. The field of metal chemistry in fossil fuels has been strongly impacted by these concepts, and will continue to be impacted in the future. The participants in the field of petroleum chemistry owe many thanks to Prof. Yen for his contributions over the years, and congratulate him on receiving the Petroleum Chemistry award.

## ACKNOWLEDGEMENTS

This work was performed under the auspices of the U.S. Department of Energy by Lawrence Livermore National Laboratory under Contract W-7405-ENG-48.

## REFERENCES

- [1] Yen, T.F., Structural differences between asphaltenes isolated from petroleum and from coal liquid. *Adv. Chem. Ser.*, 195: 39–51 (1981).
- [2] Larson, O.A. and Beuther, H., Processing aspects of vanadium and nickel in crude oils. *A.C.S. Div. Pet. Chem., Preprints*, B95–104 (1966).
- [3] Yen, T.F., Chemical aspects of metals in native petroleum. In: T.F. Yen (Ed.), *The Role of Trace Metals in Petroleum*. Ann Arbor Scientific, pp. 1–30 (1975).
- [4] Sugihara, J.M., Okada, T. and Branthaver, J.F., Reduction desulfuration on vanadium and metalloporphyrin contents of fractions from Boscan asphaltenes. *J. Chem. Eng. Data*, 10 (2): 190–194 (1965).
- [5] Lee, A.K., Murray, A.M. and Reynolds, J.G., Metallopetroporphyrins as process indicators: separation of petroporphyrins in Green River oil shale pyrolysis products. *Fuel Sci. Technol. Int.*, 13 (8): 1081–1097 (1995).
- [6] Triebs, A., Chlorophyll and hemin derivatives in organic materials. *Angew. Chem.*, 49: 682–686 (1936).
- [7] Baker, E.W., Mass spectrometric characterization of petroporphyrins. *J. Am. Chem. Soc.*, 88 (10): 2311–2315 (1966).
- [8] Morandi, J.R. and Jensen, H.B., Comparison of porphyrins from shale oil, oil shale, and petroleum by absorption and mass spectroscopy. *J. Chem. Eng. Data*, 11 (1): 81–88 (1966).
- [9] Baker, E.W., Yen, T.F., Dickie, J.P., Rhodes, R.E. and Clark, L.F., Mass spectrometry of porphyrins, II. Characterization of petroporphyrins. *J. Am. Chem. Soc.*, 89 (14): 3631–3639 (1967).
- [10] Erdman, J.G., Process for removing metals from a mineral oil with an alkyl sulfonic acid. *U.S. Patent* 3,190,829 (1965).
- [11] Yen, T.F., Boucher, L.J., Dickie, J.P., Tynan, E.C. and Vaughan, G.B., Vanadium complexes and porphyrins in asphaltenes. *J. Inst. Pet.*, 55 (542): 87–93 (1969).
- [12] Yen, T.F. and Silverman, S.R., Geochemical significance of the changes in the chemical structures of the complex heterocyclic components of petroleum. *A.C.S. Div. Pet. Chem., Preprints*, 14 (3): E32–E39 (1970).
- [13] Burlingame, A.L. and Simoneit, B.R., High resolution mass spectrometry of Green River formation kerogen oxidations. *Nature*, 222: 741–747 (1969).
- [14] Burlingame, A.L., Haug, P.A., Schnoes, H.K. and Simoneit, B.R. In: P.A. Schenck and I. Havenaar (Eds.), *Advances in Organic Geochemistry, 1968*. Pergamon Press, New York, p. 85 (1969).
- [15] Simoneit, B.R. and Burlingame, A.L., Carboxylic acids derived from Tasmanian tasmanite by extractions and kerogen oxidations. *Geochim. Cosmochim. Acta*, 37: 595–610 (1973).
- [16] Djuricic, M., Murphy, R.C., Vitorovic, D. and Biemann, K., Organic acids obtained by alkaline permanganate oxidation of kerogen from Green River (Colorado) shale. *Geochim. Cosmochim. Acta*, 35: 1201–1207 (1971).
- [17] Young, D.K. and Yen, T.F., The nature of straight-chain aliphatic structures in Green River kerogen. *Geochim. Cosmochim. Acta*, 41: 1411–1417 (1977).
- [18] Ambles, A., Djuricic, M.V., Djordjevic, L. and Vitorovic, D. In: M. Bjoroe (Ed.), *Advances in Organic Geochemistry, 1981*. Wiley, Chichester, p. 554 (1983).
- [19] Barakat, A.O. and Yen, T.F., Nature of cross-linked structures in kerogen. *A.C.S. Div. Pet. Chem. Preprints*, 32 (1): 43–47 (1987).
- [20] Barakat, A.O. and Yen, T.F., Kerogen structure by stepwise oxidation. *Fuel*, 66: 587–592 (1987).
- [21] Hodgson, G.W., Stroscher, M. and Casagrande, D.J. In: H.R. von Gaertner and H. Wehner (Eds.), *Advances in Organic Geochemistry, 1971*. Pergamon, Oxford, pp. 151–161 (1980).

- [22] Barwise, A.J.G. and Whitehead, E.V. In: J.R. Maxwell and A.G. Douglas (Eds.), *Advances in Organic Geochemistry*, 1979, Pergamon, Oxford, pp. 181–192 (1980).
- [23] Quirk, J.M.E., Shaw, G.J., Soper, P.D. and Maxwell, J.R., Petroporphyrins. II. The presence of porphyrins with extended alkyl substituents. *Tetrahedron*, 36: 3261–3267 (1980).
- [24] Barakat, A.O. and Yen, T.F., The nature of porphyrins in kerogen. Evidence of entrapped etioporphyrin species. *Energy Fuels*, 3 (5): 613–616 (1989).
- [25] Dickie, J.P. and Yen, T.F., Macrostructures of the asphaltic fractions by various instrumental methods. *Anal. Chem.*, 39 (14): 1847–1852 (1967).
- [26] Dean, R.A. and Whitehead, E.V., The composition of high boiling distillates and residues. *Proc. Sixth World Pet. Congr.*, Pap. V-9, pp. 261–279 (1963).
- [27] Yen, T.F. and Erdman, J.G., Investigation of the nature of free radicals in petroleum asphaltenes and related substances by electron spin resonance. *Anal. Chem.*, 34 (6): 694–700 (1962).
- [28] Vaughan, G.B., Tynan, E.C. and Yen, T.F., Vanadium complexes and porphyrins in asphaltene. 2. The nature of highly aromatic substituted porphyrins and their vanadyl chelates. *Chem. Geol.*, 6: 203–219 (1970).
- [29] Reynolds, J.G. and Biggs, W.R., Effects of asphaltene precipitation and a modified D 2007 separation on the molecular size of vanadium- and nickel-containing compounds in heavy residua. *Fuel Sci. Technol. Int.*, 4 (6): 749–777 (1986).
- [30] Reynolds, J.G. and Biggs, W.R., Effects of asphaltene precipitation and reprecipitation on the metal-containing compounds in heavy residua. *Fuel Sci. Technol. Int.*, 4 (6): 779–798 (1986).
- [31] Pearson, C.D. and Green, J.B., Vanadium and nickel complexes in petroleum resid acid, base, and neutral fractions. *Energy Fuels*, 7: 338–346 (1993).
- [32] Boucher, L.J., Tynan, E.C. and Yen, T.F., Spectral properties of oxovanadium(IV) complexes. I.  $\beta$ -Ketiminates. *Inorg. Chem.*, 7: 731–733 (1968).
- [33] Boucher, L.J., Bruins, D.E., Yen, T.F. and Weaver, D.L., Structure of [NN'-ethylenebis-(1-acetylacetoneiminato)-OO'NN']-oxovanadium(IV). *J. Chem. Soc., Chem. Comm.*, pp. 363–364 (1969).
- [34] Bruins, D. and Weaver, D.L., The crystal and molecular structure of N,N'-ethylene bis(acetylacetoneirminato)oxovanadium(IV). *Inorg. Chem.*, 9 (1): 130–135 (1970).
- [35] Boucher, L.J., Tynan, E.C. and Yen, T.F., Spectral properties of oxovanadium(IV) complexes. IV. Correlation of ESR spectra with ligand type. In: T.F. Yen (Ed.), *Electron Spin Resonance of Metal Complexes*. Plenum Press, New York, pp. 111–130 (1969).
- [36] Tynan, E.C. and Yen, T.F., General purpose computer program for exact ESR spectrum calculations with applications to vanadium chelates. *J. Magn. Res.*, 3: 327–335 (1970).
- [37] Yen, T.F., Tynan, E.C. and Vaughan, G.B., Electron spin resonance studies of petroleum asphaltics. In: R.A. Friedel (Ed.), *Spectrometry of Fossil Fuels*. Plenum Press, New York, pp. 187–201 (1970).
- [38] Dickson, F.E., Kunesh, C.J., McGinnis, E.L. and Petrakis, L., Use of electron spin resonance to characterize the vanadium(IV)-sulfur species in petroleum. *Anal. Chem.*, 44 (6): 978–981 (1972).
- [39] Reynolds, J.G., Gallegos, E.J., Fish, R.H. and Komlenic, J.J., Characterization of the binding sites of vanadium compounds in heavy crude petroleum extracts by electron paramagnetic resonance spectroscopy. *Energy Fuels*, 1: 36–44 (1987).
- [40] Cooper, S.R., Koh, Y.B. and Raymond, K.N., Synthetic, structural, and physical studies of bis(triethylammonium) tris(catecholato)vanadate(IV), potassium bis(catecholato)oxovanadate(IV), and potassium tris(catecholato)vanadate(III). *J. Am. Chem. Soc.*, 104: 5092–5102 (1982).
- [41] McCormick, B.J. and Belloff, E.M., On the electron spin resonance spectra of oxovanadium(IV) dithiocarbamate complexes. *Inorg. Chem.*, 9 (7): 1779–1780 (1970).
- [42] Money, J.K., Folting, K., Huffman, J.C., Temperley, J., Mabbs, F.E. and Christou, G., Isolation and structure of  $[V(OSiMe_3)(edt)_2]^-$  ( $edt^{2-}$  = Ethane-1,2-dithiolate), an intermediate in the conversion of  $[VO(edt)_2]^{2-}$  to  $[VS(edt)_2]^{2-}$  with  $(Me_3Si)_2S$ . EPR characterization of the series  $[VE(LL)_2]^{2-}$  (E = O, S,  $OSiMe_3$ , LL = edt; E = O, LL = pdt). *Inorg. Chem.*, 25: 4583–4589 (1986).
- [43] Shiro, J. and Fernando, Q., Structures of two five-coordinated metal chelates of 2-methyl-8-quinolinol. *Anal. Chem.*, 43: 10 (1971).
- [44] Reynolds, J.G., Sendlinger, S.C., Murray, A.M., Huffman, J.C. and Christou, G., *Inorg. Chem.*, 34: 5745–5752 (1995).

- [45] Tynan, E.C. and Yen, T.F., Association of vanadium chelates in petroleum asphaltenes as studied by ESR. *Fuel*, 43: 191–198 (1969).
- [46] Bozis, R.A. and McCormick, B.J., Vanadyl(IV)–Monothio- $\beta$ -diketone complexes, I. Square pyramidal compounds. *Inorg. Chem.*, 9 (6): 1541–1546 (1970).
- [47] Boucher, L.J. and Yen, T.F., Spectral properties of oxovanadium(IV) complexes, III. Salicylaldimines. *Inorg. Chem.*, 8 (3): 689–692 (1969).
- [48] Boucher, L.J. and Yen, T.F., Spectral properties of oxovanadium(IV) complexes, II. Bistrifluoro-acetyl-acetoneethylenediimine. *Inorg. Chem.*, 7 (12): 2665–2667 (1968).

This page intentionally left blank

## *Chapter 4*

# **MONTE CARLO SIMULATION OF ASPHALTENE STRUCTURE, REACTIVITY AND REACTION PATHWAYS**

MATTHEW NEUROCK and MICHAEL T. KLEIN

## **INTRODUCTION**

Environmental concerns regarding refinery emissions and acceptable gasoline product specifications coupled with tight economic processing restrictions are forcing a more stringent regulation of the molecular composition of petroleum feedstocks.  $\text{NO}_x/\text{SO}_x$  emissions, catalyst poisoning and deactivation, and heat exchanger and separation units plugging, are just a few examples of processing issues directly and indirectly tied to the nature of the molecular constituents of refinery feedstocks and products. The octane number, aromatics content, and vapor pressure all associated with the ultimate gasoline quality are inevitably tied to the molecular composition of the gasoline product fraction. Meeting these environmental challenges, maximizing product quality, and minimizing processing concerns are all forces that suggest a future where each molecule in crude oil will be identified and monitored throughout the entire refinery operation. Herein we focus specifically on the deleterious asphaltene fraction, which is highly refractory, contains the highest molecular weight components in the crude oil, has a concentrated fraction of heteroatoms, and is directly tied to many of the processing issues outlined above.

Asphaltene, strictly defined by solvent extraction protocol, is the fraction of the crude oil which is soluble in 40 volumes of an aromatic solvent, yet insoluble in 40 volumes of a paraffinic solvent. The asphaltene fraction is really a large ensemble of chemically unique oligomeric-like molecules with aromatic/naphthenic cores, terminal and bridging aliphatic side chains, and considerable levels of heteroatoms (N, S, O, Ni, V). The complex nature of this feedstock and difficulties in separating and identifying individual species have historically precluded detailed structural analysis. The chemistry of this feedstock, therefore, has been characterized at the level of global measurables, such as other solubility fractions.

Previous kinetic models illustrate the level of detail common in asphaltene experiments. Kinetic behavior is phrased in terms of interconversions of different solubility cuts. Fig. 4-1 illustrates this concept in terms of a global reaction network and its associated rate constants for the conversion of an asphaltene feedstock. Maltene and coke are defined as the paraffinic solubles and the aromatic insolubles. While this approach of measuring the lumped solubility fraction has certain merits in describing conversion kinetics for a specific asphaltene, the tight constraints in which it has been derived severely limit its range of applicability. Extrapolation beyond the ranges in which it has been derived is dangerous. Most importantly, the model provides no insight into the controlling molecular fundamentals.

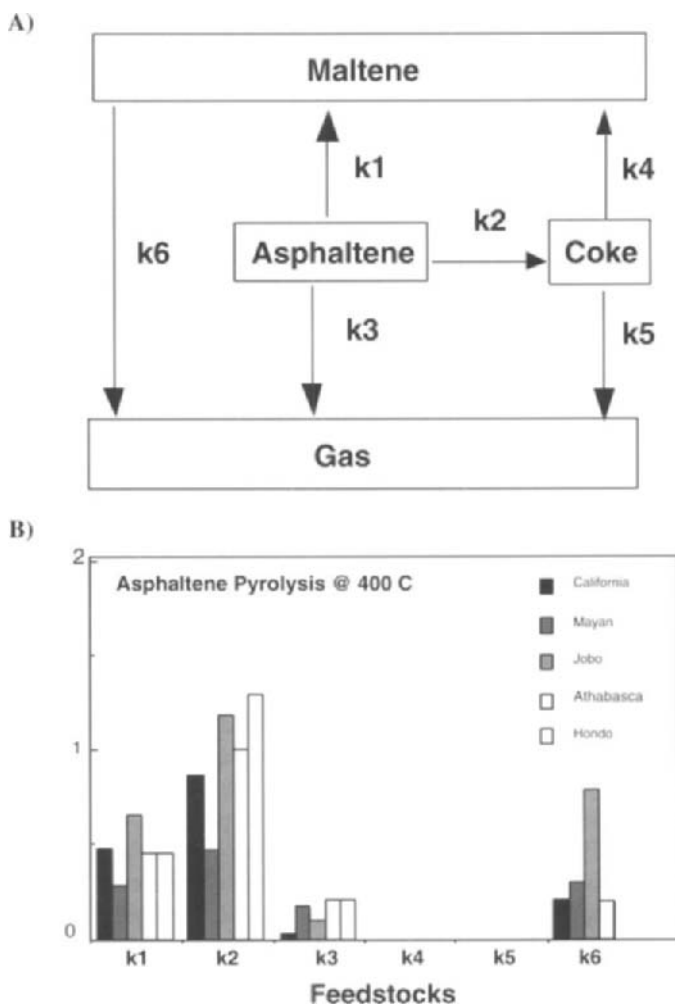


Fig. 4-1. Global reaction pathways and kinetics for asphaltene pyrolysis systems. (A) A general reaction network for asphaltene pyrolysis. (B) Effect of feedstock on kinetic parameters.

Recent developments in both characterization and separation techniques of complex heavy hydrocarbons are providing a much more detailed analysis of the structural identification of molecular species. While the molecular structure of each of the different components in a heavy residual feed or asphaltene is still beyond available techniques, more 'fine-grained' structural analysis is possible. One current limitation of the fine-grained characterization is the time associated with performing such an analysis. Thus, an approach that utilizes a small number of key analytical tests to deduce important structural attributes and structural distribution functions would be useful in the molecular representation of complex feeds.

Modeling elementary reaction pathways in heavy hydrocarbon processing has hitherto been prevented by the complexity of these feedstocks and the inability to resolve the molecules. The understanding of fundamental chemistry, on the other hand, has taken a much more progressive role due to the ease of model compound kinetic analysis. Currently, an extensive model compound literature data base exists, which can be brought together from coal, asphaltene, and resid model compound experiments. While the relevance of this information towards the processing of real systems has yet to be demonstrated, it can be combined with molecular characterization to form the basis of detailed molecular reaction models.

Herein, we report on a methodology to integrate both the extensive chemical kinetic data and explicit heavy hydrocarbon structure into a molecule-based simulation of the chemistry of asphaltene feedstocks. The basic constructs of the method allow for fine-grained molecular structure description, as well as the ability to model both the intrinsic and extrinsic kinetics of the operative elementary physicochemical processes. The complex asphaltene feedstock is represented by a large ensemble of chemically unique molecules, each of which has its complete atomic structure specified. This detailed structural basis allows for the temporal tracking of reactant, product, and intermediate species, as well as the monitoring of active centers. At this level, both molecular and mechanistic kinetics descriptions of the chemistry are readily available. In addition, explicit atomic structure permits the temporal identification of important molecular and global product properties. Monte Carlo simulation strategies provide the computational framework for capturing the time evolution of the atomic microstructure efficiently.

The main focus of this work is (1) the development of a general Monte Carlo algorithm robust enough to handle very different petroleum feedstocks at diverse processing conditions, (2) the application of this simulation to represent the structure and kinetics of an offshore California (OSC) asphaltene feedstock, and (3) the systematic evaluation of relevant molecular pathways on the simulation prediction of molecular and global product outcomes.

A schematic overview of this work is illustrated in Fig. 4-2, where the Monte Carlo simulation with its fixed intrinsic model compound kinetic data base is the heart of the molecular simulation. The only inputs to the simulation are the characterization results from a simple battery of analytical tests on the feedstock of interest. The outcomes of the simulation are a set of product molecules of  $O(10^4-10^6)$ , global product fractions, and various physical and chemical properties of both. The mechanics of the approach are mapped in Fig. 4-3. The paths in this figure serve as a rough outline for the remainder of this work.

## MODELING ASPHALTENE STRUCTURE

The defining asphaltene solubility protocol is depicted in Fig. 4-4. A heavy oil is extracted with 40 volumes of excess paraffin solvent (e.g., *n*-heptane) to produce soluble and insoluble fractions. The paraffin-soluble fraction, minus the solvent, is defined as maltenes. The insolubles are further separated by extraction with an aromatic solvent (e.g., toluene). This aromatic-soluble fraction is defined as asphaltene. The final



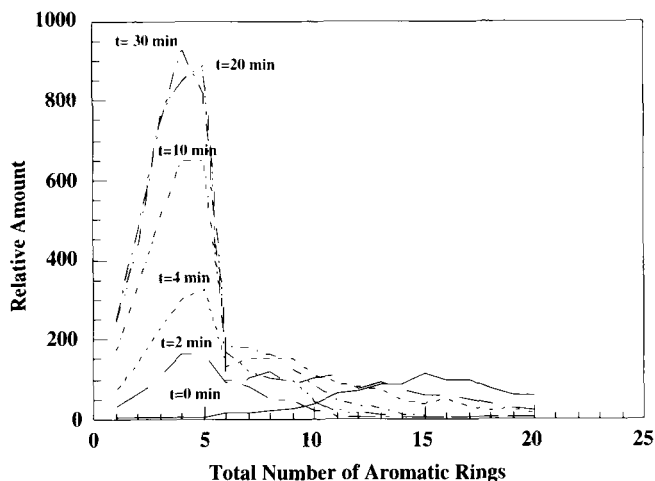


Fig. 4-2. Molecular reaction modeling overview.

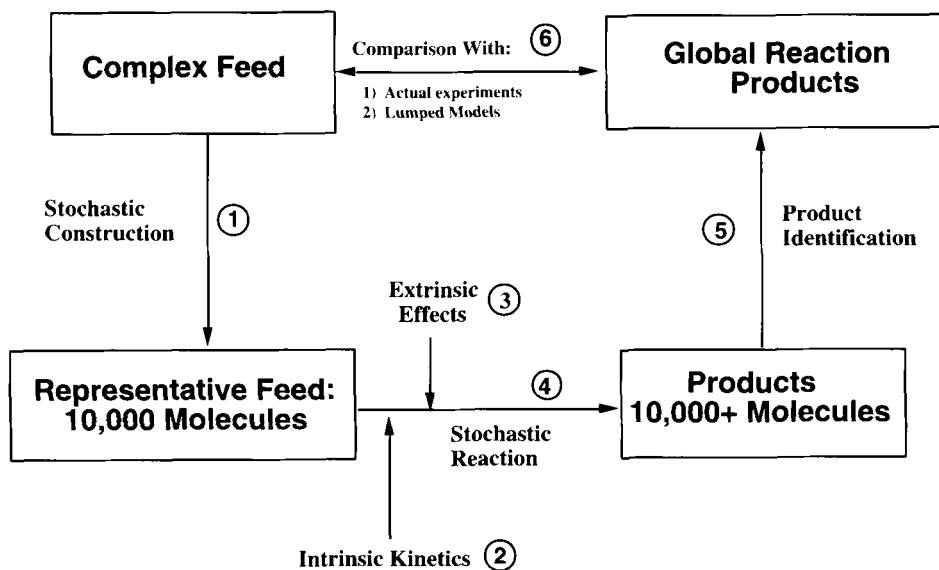


Fig. 4-3. The basic elements (modules) and their connectivity for the molecule-explicit Monte Carlo simulation reaction model.

insoluble material is defined as coke. The exact definitions for each of these solubility fractions are specific to the actual experiments performed. The amount of solvent, the atomic makeup of the solvent and the extraction conditions (time, temperature, and pressure) are all factors that can affect the relative amounts and properties of each fraction [1–3]. This combines with the ambiguity of coarse-lumped boiling-point and solubility classed pseudospecies to motivate more molecular level characterizations.

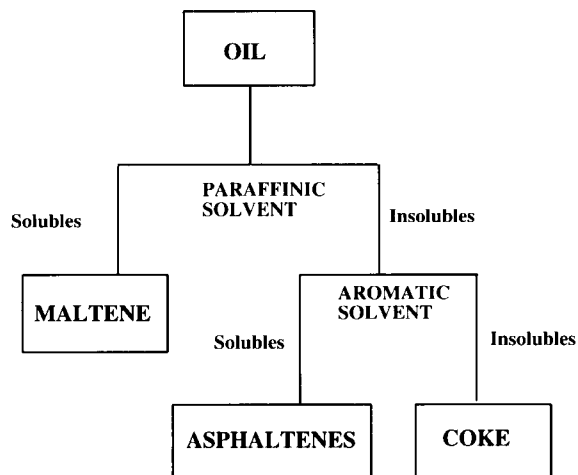


Fig. 4-4. Global solubility fractions of a petroleum heavy oil.

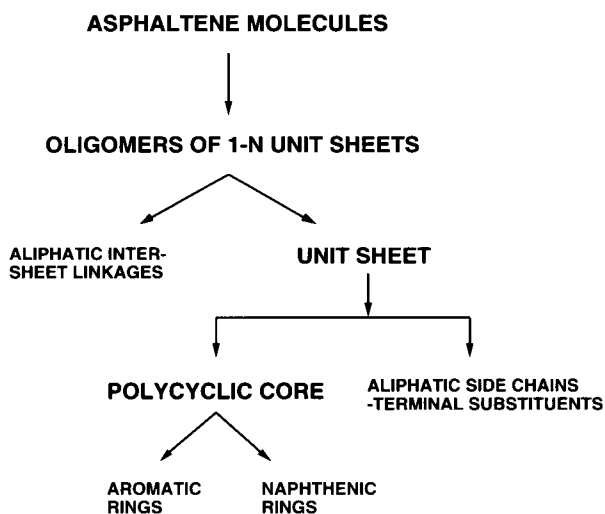


Fig. 4-5. The structural hierarchy of asphaltene as suggested by Savage and Klein [4].

#### CHARACTERIZATION AND DEVELOPMENT OF PROBABILITY DISTRIBUTION FUNCTIONS

Asphaltene, operationally defined as a solubility fraction, is nevertheless a complex collection of chemically unique molecules. Speight [2] provides an extensive review on both the macroscopic and microscopic structure of asphaltenes. Savage and Klein [4] (SK) proposed the hierarchy presented in Fig. 4-5.

In the SK hierarchy, the basic structure of each molecule is 'oligomeric', where aliphatic substituents covalently bind a sequence of different unit sheets ('monomers'). The unit sheet is composed of a polycyclic core of fused aromatic and naphthenic rings

with peripherally bonded aliphatic chains. These aliphatic substituents, which differ in chain length, are either terminal groups or serve as covalently linkages in binding different unit sheets.

The relative distribution of heteroatoms within this structural framework was also discussed in detail by Savage [3] and Speight [2]. Nitrogen, sulfur, and oxygen, are the major heteroatomic constituents and typically vary between 0.6–3.0, 0.3–10.3 and 0.3–4.9 percent by weight, respectively. Nitrogen is concentrated in the aromatic portion of the core, the sulfur in both the core (thiophenic-moieties) and within the aliphatic substituents (thioethers), and the oxygen is either bound to the core (phenolic groups) or within the aliphatic substituents (ethers). The metal-containing components are found in much smaller percentages, usually in the range of 10–100 parts per million, and are typically associated with porphyrinic or non-porphyrinic species.

From an architectural standpoint, Fig. 4-5 can be viewed as the logic diagram for constructing asphaltene molecules. Each asphaltene molecule is described by a degree of polymerization, a number of aromatic and naphthenic rings per unit sheet (monomer), a degree of substitution at the peripheral sites with aliphatic chains, and the respective length of each chain. Average values for these structural attributes can be obtained by a series of simple analytical characterizations and chemical logic [2,5]. The analytical characterizations include  $^1\text{H}$  NMR, vapor phase osmometry (VPO) for the number average molecular weight, and elemental analysis. Two variations of essentially the same chemical logic will be detailed via a specific offshore California derived asphaltene.

The analytical results for this feedstock are shown in Table 4-1. The elemental analysis provided the relative amount of each atomic constituent and  $^1\text{H}$  NMR established the relative types of each proton. VPO molecular weight was used to quantify the actual amounts. The relative fraction for each proton ( $\text{H}_{\text{Me}}$ ,  $\text{H}_{\text{My}}$ ,  $\text{H}_{\text{N}}$ ,  $\text{H}_{\alpha}$ , and  $\text{H}_{\text{A}}$ ) was determined by integrating the area under the  $^1\text{H}$  NMR spectrum in the range associated with each characteristic peak. The distinction between naphthenic ( $\text{H}_{\text{N}}$ ) and methylene ( $\text{H}_{\text{My}}$ ) hydrogens is typically difficult to determine. This was estimated graphically [6] for the present purposes. A more accurate method for providing this split has recently been suggested by Gallacher et al. [7]. In either case, these results are combined with chemical logic to generate structural attributes as follows:

TABLE 4-1

Analytical characterization data for an offshore California-derived asphaltene feedstock

Elemental	Wt. %	$^1\text{H}$ NMR	Wt. %	MW (VPO)
Carbon	80.03	$\text{H}_{\alpha}$	0.150	2683
Hydrogen	8.20	$\text{H}_{\text{A}}$	0.133	
Sulfur	7.94	$\text{H}_{\text{N}}$	0.211	
Oxygen	1.89	$\text{H}_{\text{Me}}$	0.180	
Nitrogen	1.70	$\text{H}_{\text{My}}$	0.348	
Vanadium	0.11	$\text{H}_{\text{My}} + \text{N}$	0.559	
Nickel	0.038			

TABLE 4-2

Speight's analytical characterization balance equations for describing the structural attributes of hydrocarbon feedstocks

H/C	Hydrogen to carbon	From elemental analysis
$C_T$	Total carbon	$= MW/(H/C + 12)$
$H_T$	Total hydrogen	$= MW - 12 \times C_T$
$C_S$	Saturated carbon	$= H_T(H_a/2 + H_{Me}/3 + H_{My}/2 + H_N/2)$
$C_{SA}$	Saturated carbon $\alpha$ to aromatic	$= H_T(H_a/2)$
$C_A$	Aromatic carbon	$= C_T - C_S$
$C_P$	Peripheral aromatic carbon	$= H_T(H_A + H_a/2)$
$C_I$	Internal aromatic carbon	$= C_A - C_P$
$C_{My}$	Methylene and methyl carbon	$= H_T(H_{My}/2 + H_{Me}/3)$
$C_N$	Naphthenic carbon	$= C_S - (C_{SA} + C_{My})$
$R_A$	Aromatic rings	$= (C_I + 2)/2$
$C_{SA}/C_P$		The average degree of substitution of the aromatic core.
$C_S/C_{SA}$		The average number of carbon atoms attached to a position on the edge of an aromatic sheet.
$C_P/C_A$		The average shape factor for the aromatic core.
$(C_S - C_{Me})/C_{Me}$		A measure of the degree of branching.
$fa$		The fraction of aromatic carbon atoms.

The first method of deriving average structural attributes was described in detail by Speight [2,8]. This has been used widely in various different forms to estimate the structural attributes of numerous petroleum oils, coal liquids, shale oils, tar sands and other complex materials. The method will be distinguished in the remainder of this chapter as M1. The equations used in M1 are summarized in Table 4-2. The total amounts of carbon and hydrogen are determined by the elemental H/C analysis and the average molecular weight. The abundance of each type of carbon is established from both the total carbon and hydrogen and the relative amounts of the different hydrogen types. For example, the total amount of saturated carbon is determined by all hydrogens ( $H_a$ ,  $H_{My}$ ,  $H_{Me}$ ,  $H_N$ ) with the exception of aromatic hydrogen ( $H_A$ ). The evaluation of each carbon type is subsequently used to compute the relevant functional groups specified in Table 4-2, i.e., the number of aromatic rings, the degree of substitution from an aromatic ring, the degree of substitution from a naphthenic ring, the length of aliphatic substituent chains, the shape factor, the degree of branching, and the fraction of aromatic carbons.

A second method for computing structural attributes from the available analytical data was developed by Hirsch and Altgelt (HA) [5]. Their method is similar to that of M1 in that a series of important balance equations are formulated from chemical logic. The essential difference between the two approaches is that the HA method provides a series of checks to validate the consistency of the results. Whereas the M1 method uses a set of 'up front' approximations, the HA method uses a series of four floating parameters  $\Phi$  (the ring compactness):  $a$  (fraction of peripheral aromatics bonded to benzonaphthenic carbons);  $b$  (the average number of benzonaphthenic carbons per fused ring system); and  $\eta$  (the degree of alkyl substitution from naphthenic carbon).

TABLE 4-3

Average structural attributes for the offshore California-derived asphaltene feedstock described in Table 4-2 — a comparison of both the Speight and Hirsch–Algelt methods for determining structural attributes

Structural attribute	Speight	Hirsch–Algelt
Number of unit sheets (US) per molecule	2.85	4.60
Number of aromatic rings per US	10.0	3.95
Number of naphthenic rings per US	2.2	2.92
Degree of substitution of peripheral aromatic carbons	7.30	7.30
Degree of substitution of peripheral naphthenic carbons	26.9	26.89
Alkyl chain length	13.2	13.17

Both the M1 and HA methods were used to evaluate the average structural attributes of the offshore California asphaltene feed. The results are compared in Table 4-3. Considerable differences in the number of aromatic rings per unit sheet and the number of unit sheets per molecule were obtained. The M1 method computes the number of unit sheets and the number of aromatics directly from the compactness factor (a measure of structural linearity or compactness of the aromatic core),  $C_p/C_A$ . This places considerable emphasis on the deduced value of this geometric attribute. The Hirsch–Algelt method, however, constrains the compactness factor. This minimizes the sensitivity of the number of aromatic rings and the number of unit sheets on  $C_p/C_A$ . The HA results align with molecular type characterizations that suggest smaller aromatic clusters (less than 6) for each polycyclic core.

The M1 and HA average values for each attribute were the starting point for the construction of the corresponding probability distribution functions. The approach used was to fit a reasonable function to the average data and other experimental data or approximations.

Both empirical evidence and theoretical underpinnings suggest that gamma distributions are reasonable for conveying molecular feedstock information. There are a number of cases where analytical measurements of molecular constituents in petroleum feedstocks have provided distributions which have gamma-like behavior [9]. Additionally, petroleum feedstocks can be viewed as an ensemble of reaction products formed from the degradation or depolymerization of organic macromolecules (lipids, proteins, lignin, etc.) [10]. Because of the polymeric nature of the initial structure, degradation reactions will often follow Flory-type (gamma-like) product distributions.

Nigam [11] has demonstrated the applicability of the gamma distribution in the description of a wide variety of different structural attributes (carbon number, molecular weight, sulfur distribution) of complex feedstocks, and has also devised a method for deducing gamma distributions from the average, minimum and maximum values associated with each attribute. Eq. 4-1 is the proposed gamma function:

$$f = \frac{[I - \gamma]^{\alpha-1} \exp\left[-\frac{i - \gamma}{\beta}\right]}{\beta^\alpha \Gamma(\alpha)} \quad (4-1)$$

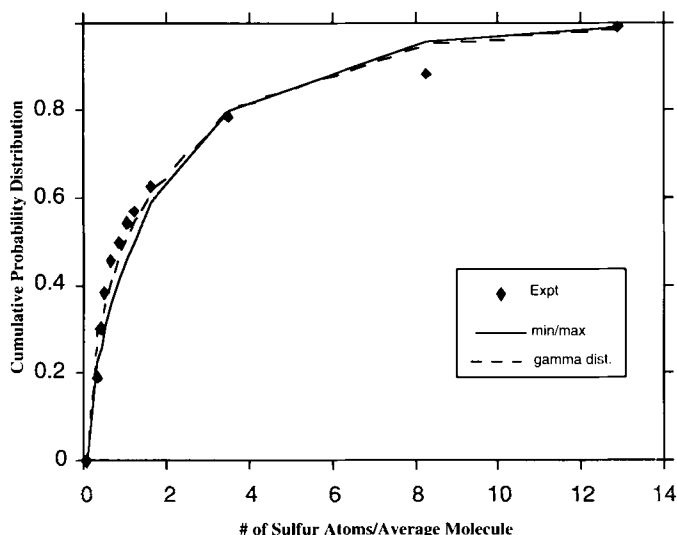


Fig. 4-6. The fit of gamma distribution functions to (1) the detailed experimental information and (2) to three simple points (min., max., and average). This illustrates the distribution of sulfur atoms in molecular petroleum mixtures as determined by the experimental analyses of Boduszynski [12,13].

where

$$\alpha = \left[ \frac{I_{\min} - I_{\text{avg}}}{I_{\max} - I_{\text{avg}}} \times f \right]^2, \quad \beta = \left[ \frac{I - I_{\text{avg}}}{\alpha} \right]$$

and  $I$ ,  $I_{\max}$ ,  $I_{\text{avg}}$ , and  $I_{\min}$  refer to the independent, maximum, average and minimum attribute values.

An example of this approach is illustrated in Fig. 4-6. The use of the entire experimental molecular sulfur distribution of Boduszynski [12,13] to correlate a gamma distribution function is shown by the dotted line. The selective use of only three simple data points (min., max. and average) to correlate the gamma distribution function is represented by the solid line. Both yield accurate fits to the detailed experimental data.

The resulting distributions for each attribute in this method are shown in Fig. 4-7.

#### COMPUTATIONAL IMPLEMENTATION: SAMPLING PROBABILITY DISTRIBUTION FUNCTIONS

The attribute distribution functions were the basis for developing a molecular representation of the asphaltene. Stochastic sampling of these distribution functions allowed assembly of the resulting structural information into representative molecules. This technique is quite general and can be applied to the assembly of molecular representations of other complex feedstocks.

The differential distributions,  $f(x)$ , discussed above were recast in terms of cumulative probability distributions by integrating  $f(x)$  over the range  $0 < x < \infty$  and renormalizing the results so that the probabilities ranged from 0 to 1. Stochastic sampling

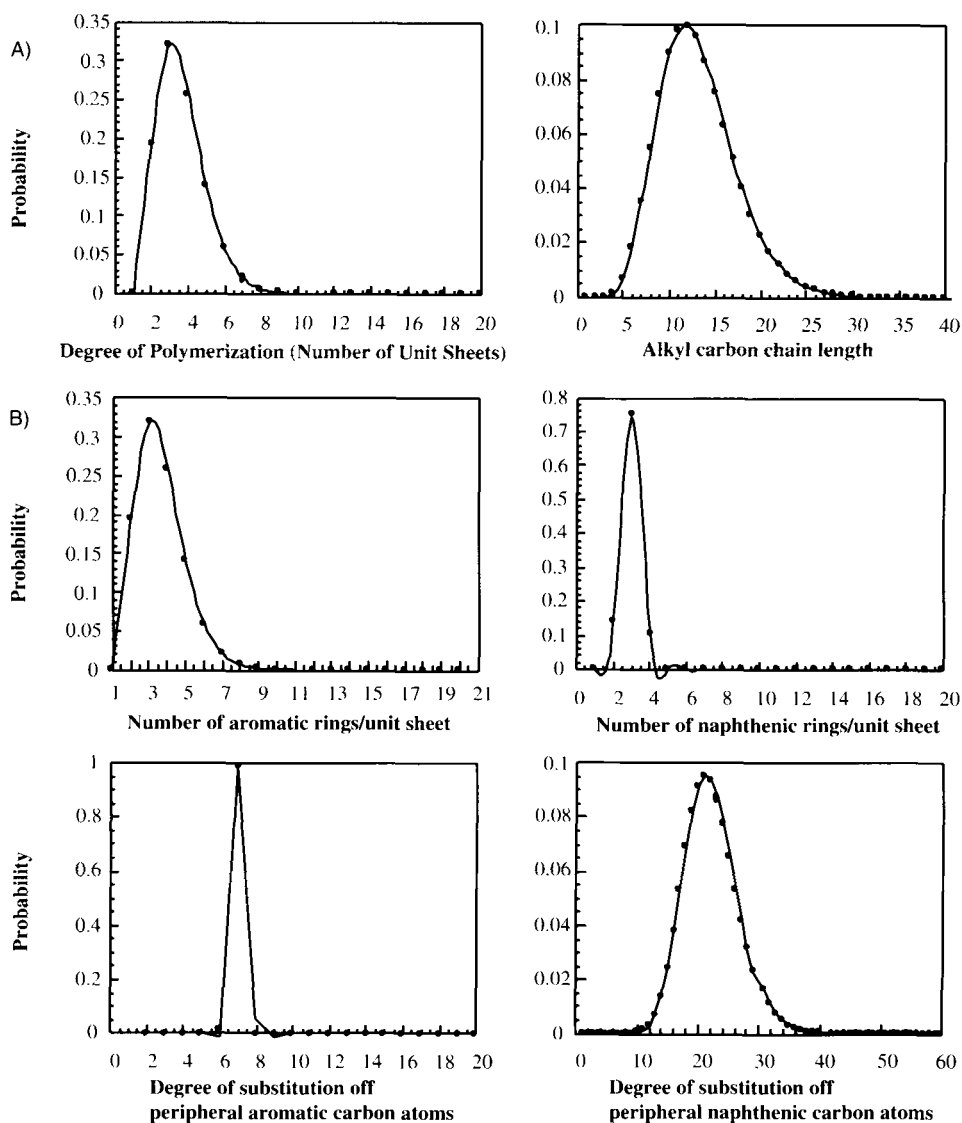


Fig. 4-7. Gamma distributions derived from analytical average results and estimates of the minimum and maximum attributes for the offshore California asphaltene feed described in Table 4-1.

involved the computational generation of a normally-distributed random value between 0 and 1, the placement of the random value on the ordinate of the cumulative probability distribution (CPD) curve, and the determination of the random variate (the value of the abscissa which corresponds to the intersection of a horizontal line through the random value on the ordinate and the CPD distribution curve). This is illustrated in Fig. 4-8 for the case where a random value of 0.6 was chosen. This resulting attribute value was 3.

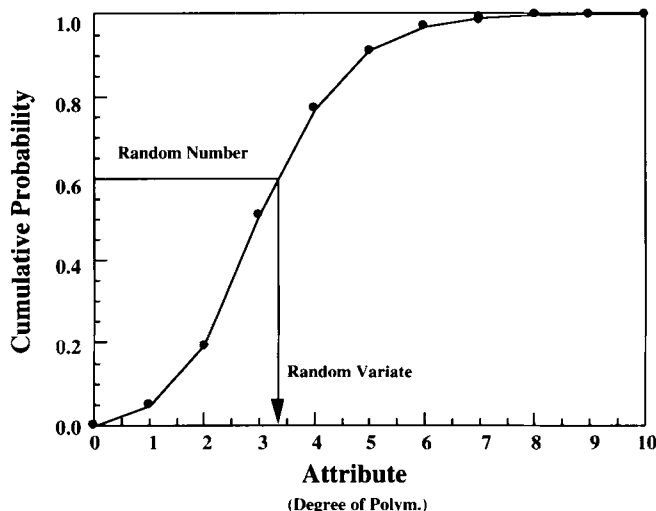


Fig. 4-8. An illustrated example of the stochastic approach of sampling attribute distribution functions.

The representation of asphaltene feedstock in terms of molecules was generated by stochastically sampling all the structural attribute distributions and building possible species through the logic of Fig. 4-5. A general schematic of this process is shown in Fig. 4-9.

The process of building an asphaltene molecule begins by determining its degree of polymerization, i.e., the number of unit sheets. In the example of Figs. 4-8 and 4-9, the resulting attribute value (3) defined the number of unit sheets of the first molecule.

The exact makeup of each of these sheets was determined by sampling the probability density functions for the possible polycyclic cores and the aliphatic substituents. The aromatic portion of this core was determined by sampling the corresponding aromatic CPD and its structural configuration CPD. The configuration of the aromatic core refers to the particular structural arrangement of rings (structural isomer). For example, three aromatic ring components can be classified as either phenanthrene or anthracene. Fig. 4-10 represents the possible structural isomers for aromatic compounds with one to five aromatic rings. The number of possible isomers increases tremendously with the increase in ring number. Specifying all conceivable ring isomers by hand was intractable; therefore, a computational algorithm which stochastically assembled aromatic ring clusters for systems with greater than five rings was developed. Resulting clusters were required to obey Hückel's rule of aromaticity, that is, only  $4n$  and  $4n + 2$   $\pi$ -electron systems, where  $n$  is the number of rings, were allowed. Little was known about the relative amount of each isomer in the feedstock; therefore, the contribution of each isomer was considered to be identical, i.e., the probability of a particular isomer was  $1/n$ , where  $n$  is the number of isomers (phenanthrene =  $1/2$  and anthracene =  $1/2$ ). In the example in Fig. 4-9B, the aromatic core of the first unit sheet was determined to be made up of five aromatic rings arranged in a benzopyrene configuration.



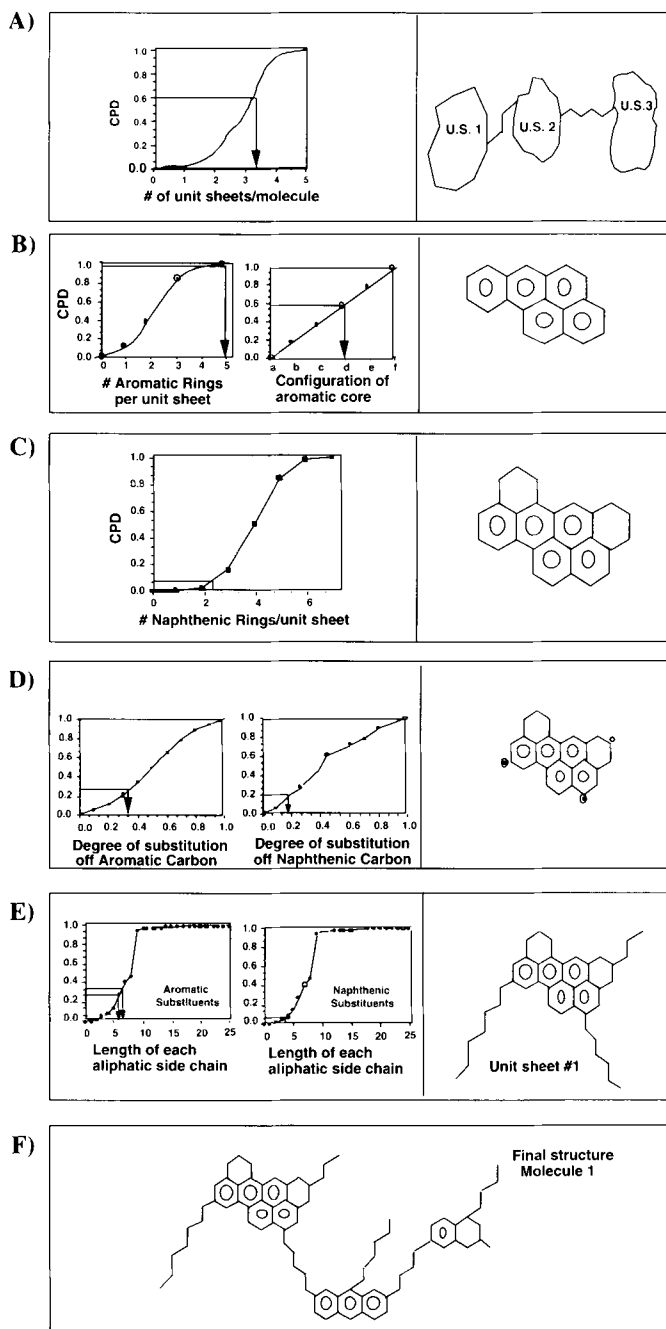


Fig. 4-9. The logic of the stochastic algorithm for assembling molecular asphaltene structures. The hierarchy of the construction process involves determining and assembling (A) of the unit sheets which make up each molecule, (B) the aromatic core of each unit sheet, (C) the naphthenic rings of the polycyclic core, (D) the number of aliphatic substituents, and (E) the length of each substituent. The final structure of the assembled molecule is illustrated in (F).

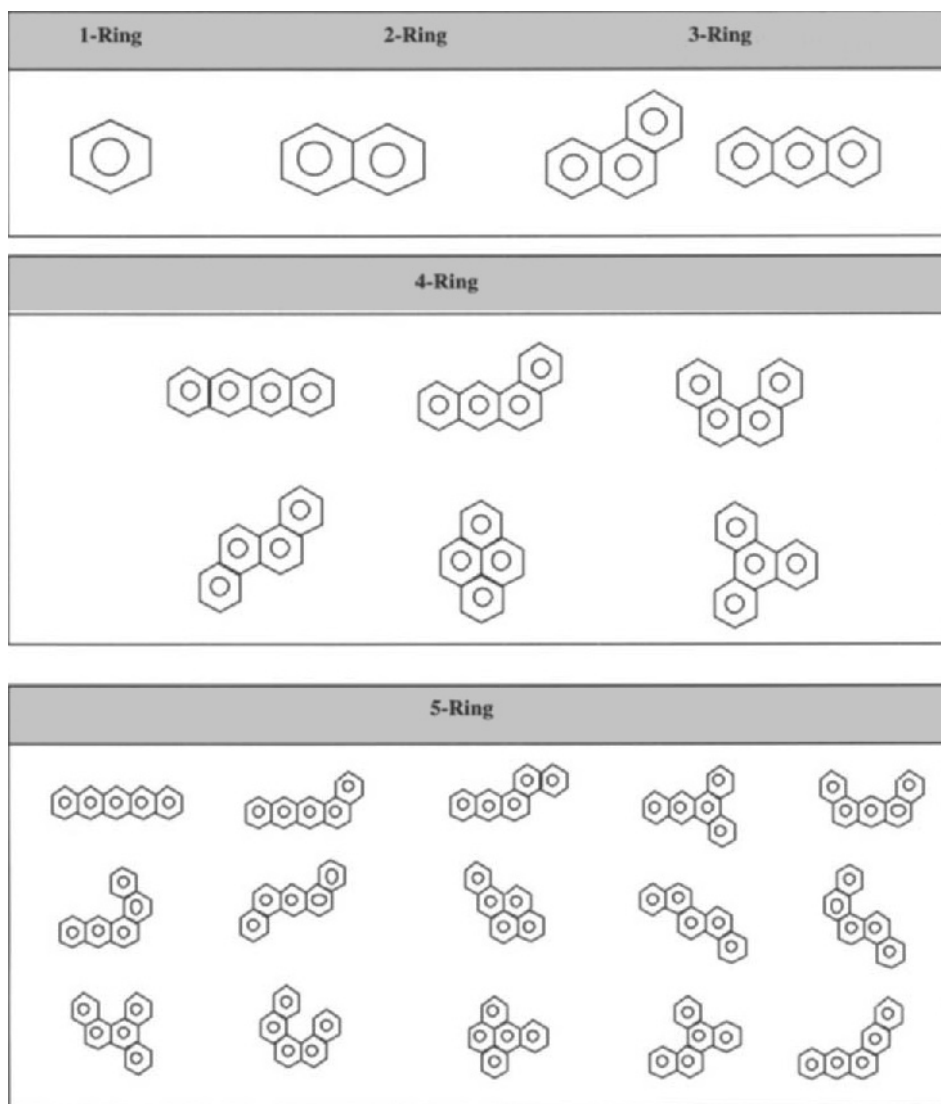
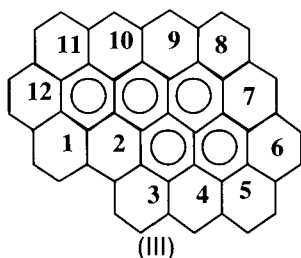


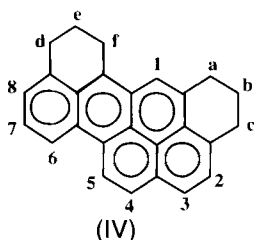
Fig. 4-10. The structural isomers of (top panel) 1-, 2-, 3-ring aromatics, (middle panel) 4-ring aromatics, and (bottom panel) 5-ring aromatics.

Continuing the example of Fig. 4-9, the number of naphthenic rings bound to this fused aromatic system was stochastically chosen from the naphthenic ring CPD. This is highlighted in Fig. 4-9C, where the example random variate was 2. The placement of these rings required computing the number of possible sites. The benzopyrene core has 12 unique sites (see III below) for the placement of naphthenic rings.



The actual sites for substitution were randomly determined with each site having an equal likelihood of occurrence. In the above example, this probability was 1/12. The sites numbered ten and seven were selected and the corresponding naphthenic rings were attached, thereby completing the polycyclic core of the first unit sheet.

The terminal and interunit sheet aliphatic substituents were chosen from two sets of two distributions. The first two distributions correspond to the degree to which the peripheral aromatic and naphthenic carbon atoms are substituted. In Fig. 4-9, two randomly selected numbers resulted in a 20 and 30% degree of substitution of the naphthenic and aromatic carbon atoms, respectively. These values were multiplied by the total number of peripheral aromatic and naphthenic atoms to determine the actual number of alkyl substituents. The example structure IV below has eight peripheral aromatic sites (1-8) and six peripheral naphthenic sites (a-f).



This results in two substituents on aromatic carbons and one on a naphthenic carbon atom. This is shown in Fig. 4-9D. The actual placement of these sites was once again random.

The second set of distributions specified the length of each of these alkylaromatic and alkyl naphthenic substituents. For example, in the above structure, the single alkyl naphthenic moiety had a chain length of three, and the two alkylaromatics groups had chain lengths of two and seven.

This sequence of random sampling completed the atomic makeup of the first unit sheet. Executing the steps outlined in Fig. 4-9B-D finished the description of the two remaining unit sheets. A single aliphatic chain off of each monomer (unit sheet) was randomly selected to be the interunit sheet linkage. The remaining chains were considered terminal substituents. The final molecular example structure is shown in Fig. 4-9F.

A large molecule sample size assured statistical precision. The entire stochastic representation of the actual asphaltene feedstock was generally the size of 1000-10,000

molecules. This repeated sampling assured that the set of computational-generated structures quantitatively matched the experimentally derived distributions. This was the Monte Carlo simulation of the asphaltene structure.

#### MODELING THE THERMAL REACTIVITY OF ASPHALTENE

The Monte Carlo simulation of structure assembles various functional groups that are susceptible to chemical reaction. This suggests that a considerable data base of hydrocarbon reaction pathways and chemistries would be required to describe these complex feedstocks. Closer examination of the Monte Carlo structural simulation results, however, revealed that these feeds contain molecules that can be organized into one of five hydrocarbon types. In general, the reactants will contain alkylaromatics, alkyltetralins, alkyl-naphthenes, paraffins, and olefins [10,11,14,15]. Some of the evident bond homolysis pathways are summarized in Fig. 4-11. This provides a succinct summary of representative reaction pathways for each one of these families. Notice that the reactions are from one molecule to another where the selectivities are provided by stoichiometric coefficients. The controlling free radical intermediates are well-known and have been modeled [15–19], but are nevertheless only implicitly contained in the pathways and kinetics as provided here.

The kinetics associated with the reactions shown in Fig. 4-11 are summarized in Table 4-4. Detailed mechanistic studies on the pyrolysis of alkylaromatics [16,17,19], alkyl-naphthenes [18], and alkyltetralins [18] model components, for example, have

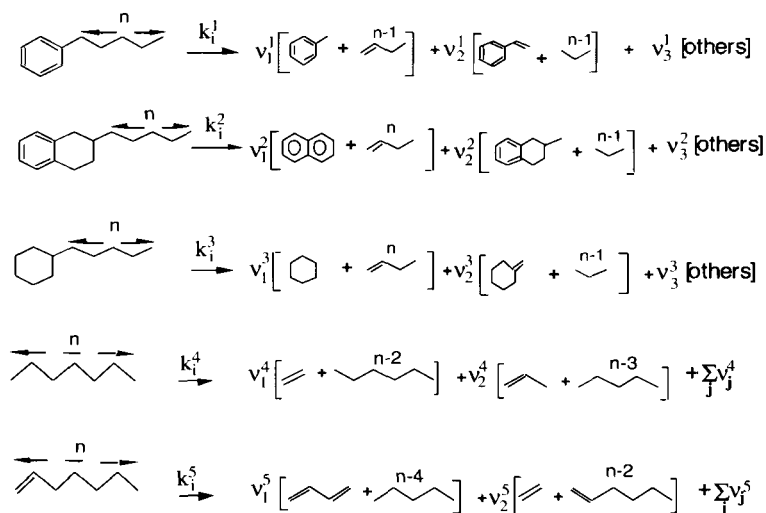


Fig. 4-11. Representative molecular reaction pathways for heavy hydrocarbon pyrolysis systems. Molecules are classified by one of five hydrocarbon types: alkylaromatics, alkyltetralins, alkyl-naphthenes, paraffins, or olefins. The kinetics are summarized by the rate constant  $k_i^j$  and the stoichiometric coefficient,  $v_j^i$ , where  $i$  refers to the alkyl carbon chain length and  $j$  to the molecule type (Table 4-4).

TABLE 4-4

Molecular model system kinetics for representative reaction pathways for hydrocarbon pyrolysis

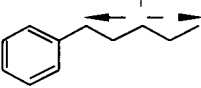
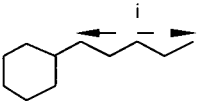
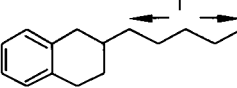
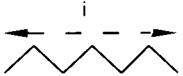

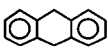
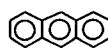
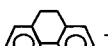
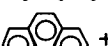


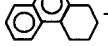
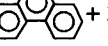
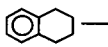
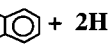
Molecular components	Expt.	$\log_{10} A$ ( $s^{-1}$ )	$E^\ddagger$ (kcal/mole)	$\nu_1$	$\nu_2$	$\nu_3$	$\nu_4$	Conditions	W	Ref.
	PDB	14.0	55.5	0.312	0.117	0.571	—	$T = 400^\circ C$	$(i/15)^{1,2}$	[16,17]
				0.454	0.117	0.429	—	$T = 425^\circ C$		
				0.510	0.108	0.382	—	$T = 450^\circ C$		
	TDC	14.9	59.4	0.08	0.07	0.85	—		$(i/13)$	[18]
	2ET	12.7	53.5				—			[18]
	$C_4-C_{20}$	12.8	56.0	0.286	0.571	0.095	0.048	$C_A = 0.001\text{ M}$		[20]
		16.7	70.2	0.286	0.571	0.095	0.048	$C_A = 1.0\text{ M}$		
	$C_4-C_{20}$	13.8	56.0							[20]
		17.8	70.2							

TABLE 4-5

Simulation pathways and kinetics for thermal dehydrogenation

Reaction path	$k$ ( $s^{-1}$ )
 $\rightarrow$  + $H_2$	$1.07 \times 10^{-3}$
 $\rightarrow$  + $H_2$	$5.44 \times 10^{-4}$
 $\rightarrow$  + $2H_2$	$3.75 \times 10^{-4}$
 $\rightarrow$  + $2H_2$	$3.75 \times 10^{-4}$
 $\rightarrow$  + $3H_2$	$8.79 \times 10^{-5}$

allowed for the formulation of the Arrhenius parameters and stoichiometric coefficients shown.

The kinetics for paraffin and olefin (asphaltene decomposition products) pyrolyses were simply extracted from the abundant literature data [20–22]. Finally, the issue of kinetic interactions have been both theoretically and experimentally addressed [23,15]. These interactions in general cause the reaction of the mixture to be different than the linear combination of the pure component rates.

Hydrogen transfer reaction paths are quite significant in pyrolysis systems. One of the most substantial routes of hydrogen transfer can be simply described by dehydrogenation. A series of important dehydrogenation pathways are illustrated in Table 4-5. Due to the lack of available kinetic information, the rate constants values fixed in Table 4-5 were estimated. These values were chosen to be somewhat greater than the values reported for tetralin reacting to naphthalene due to the added enhancement from intermolecular interactions and resonance stabilization.

Intermolecular reaction paths (i.e., kinetic coupling) can also play an important role. A previous communication reported on the general methodology for accurately handling these interactions within the Monte Carlo reaction framework [24]. A number of case studies were examined, and a specific application of the technique to model Langmuir–Hinshelwood hydrogenation kinetics for a heavy oil mixture was presented. The approach has recently been extended to treat pyrolysis kinetics for complex heavy oil feedstocks [6]. Overall, kinetic coupling enhances asphaltene conversion and results in better quantitative agreement between simulation and experiment. A more detailed description of the role of kinetic coupling and its effects on asphaltene pyrolysis are the subject of a forthcoming contribution.

In sum, the reaction pathway and kinetics information of Fig. 4-11 and Tables 4-4 and 4-5 provide the underlying reactivity information for asphaltene pyrolysis. Quantitative prediction of product composition and quality vs. reaction time thus required a modeling approach, in which attention was directed toward Monte Carlo simulation of reactions.

## MONTE CARLO SIMULATION OF ASPHALTENE REACTION

*General principles and techniques*

Monte Carlo simulation of kinetics samples the state of a molecule by comparing a randomly drawn number with a probability of reaction, in turn derived from the information of Fig. 4-11 and Tables 4-4 and 4-5. Two distinct algorithms, termed fixed-time (FT) [25] and variable-time (VT) step [26,27] approaches, have been developed in the literature.

A few basic definitions are common to both algorithms. The *system*, for example, is defined as a collection between 1 and  $N$  molecules, where  $N$  represents a statistically significant *sample size* ( $0-10^4$ ). The size of the system is insignificant for uncoupled chemical reaction systems. For reactions where intermolecular effects are important, however, the solution algorithm requires that the system represents the reaction environment. The *state* of each *system* is defined by the identity of the population of molecules defining the system at any given time. The *transformation* of the system from *state to state* as a function of time is regarded as a *Markov chain*. Finally, the averaging of  $N$  *Markovian trials* represents the *Monte Carlo* nature of the simulation.

The transition probabilities that govern the likelihood of a reaction within a particular time step make up the foundation of both methods. McDermott et al. [25] have developed the general transition probabilities for irreversible, parallel, serial, and bimolecular reaction steps. Their results are shown in Fig. 4-12. These results can be used to describe the reaction transitions of many systems.

The two Monte Carlo solution algorithms, the fixed-time (FT) and variable-time (VT) methods, differ primarily in their representation of *state space*. State space is the independent variable which defines the updating of reaction. In the FT method, *time* is defined explicitly and reaction is computed (implicit). Time, therefore, defines the state space in this approach. In the VT method, however, *reactions* (events) are followed explicitly whereby the time is now the dependent variable. This is characterized as an *event-space* algorithm.

More specific differences between the two algorithms are illustrated by the simple prototypical example of A reacting irreversibly to B, as shown schematically in Fig. 4-13. In the fixed-time algorithm, the system is defined by the single molecular component. The state of the system is the identity of the molecule, i.e., it can be either A or B. The explicit time-step allows for the calculation of the transition probability, as follows:

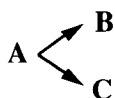
$$P_{AB} = 1 - \exp(-k_{AB} \Delta t) \quad (4-2)$$

A randomly drawn number (RN) is then compared with this transition probability to decide the fate of the molecule within the given time interval. If RN is less than the probability,  $P_{AB}$ , the reaction of A to B occurs; otherwise, the system (molecule) remains unchanged (in state A). It is clear that for large values of  $k_{AB} \Delta t$  the transition probability is close to 1, which implies a reasonable likelihood of reaction, and that for small values of  $k_{AB} \Delta t$ ,  $P_{AB}$  is closer to 0, which suggests little chance for reaction. The comparison of a randomly drawn value and the transition probability is repeated at



$$P_{AB} = 1 - \exp(-k_{AB}\Delta t)$$


---



$$P_{AR} = 1 - \exp[-(k_{AB} + k_{AC})\Delta t]$$

$$S_{AB} = \frac{k_{AB}}{k_{AB} + k_{AC}} \quad S_{AC} = 1 - S_{AB}$$


---

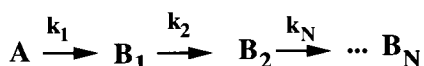


$$P_{AB} = 1 - \exp(-k_{AB}\Delta t)$$

$$P_{BC} = 1 - \exp(-k_{BC}\Delta t)$$

$$P_{AC} = -\frac{k_{BC}}{k_{AB} - k_{BC}} P_{AB} + \frac{k_{AB}}{k_{AB} - k_{BC}} P_{BC}$$


---



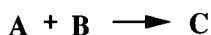
$$P_N = \sum_{i=1}^N - (1)^{N-i} \frac{\prod_{j=1}^N k_j}{k_i \prod_{j=1}^{i-1} (k_j - k_i) \prod_{j=i+1}^N (k_i - k_j)} P_{i-1,i}$$

$$P_{i-1,i} = 1 - \exp(-k_i \Delta t)$$


---



Similar to development for



$$P_A(t) = 1 - \exp(-\dot{k}_A(t)\Delta t)$$

$$\dot{k}_A(t) = [(1 - P_B(t-1))\dot{k}_A(t-1) \quad \dot{k}_A(0) = k_A 0]$$

Fig. 4-12. Stochastic transition probabilities for generic reaction paths which were taken from McDermott et al. [25].



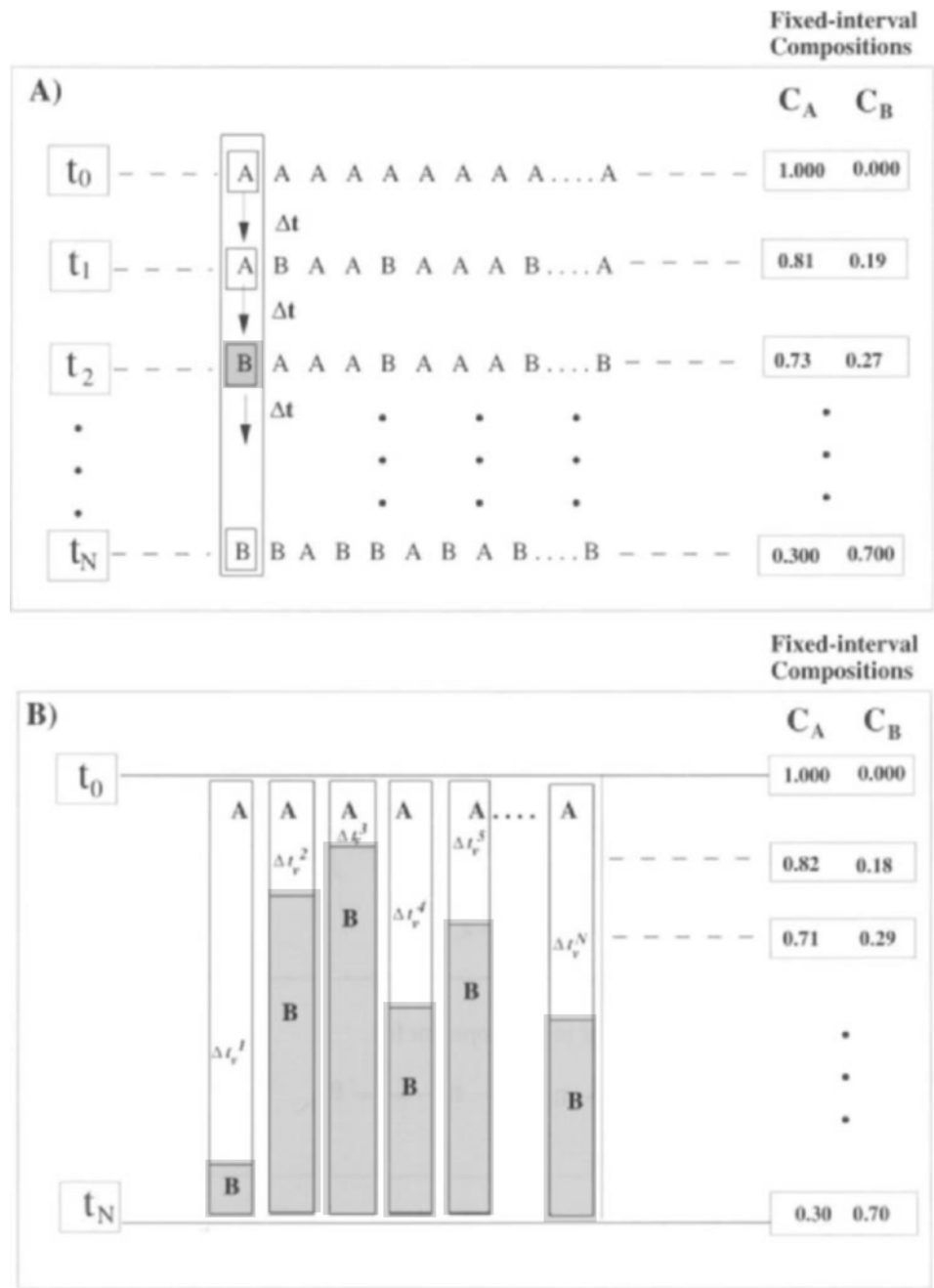


Fig. 4-13. The comparison of (A) the fixed-time and (B) variable-time step Monte Carlo simulation algorithms for the prototypical example of A reacting reversibly to B.

every time step until the final time is reached. Fixed-time steps are accumulated to give reaction time.

The foregoing procedure maps out the first of many Markov chains, as shown in the enclosed rectangle in Fig. 4-13A, which depicts the reaction of A to B as occurring between  $t_1$  and  $t_2$ . This Markov chain process is repeated for  $10^4$  molecules to describe the entire reaction system. The averaging of these results (Markov chains) at each reaction time provides the Monte Carlo solution.

Fig. 4-13B represents the variable-time algorithm for the same example. As discussed, the state space in this approach is defined by reaction events. The simulation proceeds event-by-event (reaction-by-reaction) where the time required for reaction is determined by inserting a random number (RN1) into Eq. 4-3, which is a rearranged form of Eq. 4-2.

$$\Delta t_v = \frac{\ln(1 - \text{RN})}{k_{AB}} \quad (4-3)$$

After calculation of  $\Delta t_v$ , a second random number (RN2) specifies which of the allowable events happened.

In the simple example of the irreversible reaction of A to B, only one event (reaction) per molecule can occur; in this instance, only one random variable per molecule is required. This random value determines the time at which A reacted to B. This is shown schematically in Fig. 4-13B, where the shading for each Markov chain represents the time of the system transition from state A to state B. As is the nature of random processes, the time step,  $\Delta t_v(i)$ , is different for each Markov chain. The repetitive sampling of a large number ( $\sim 10^4$ ) of Markov chains ensures, however, the precision of this approach.

A complex 'multifunctional' A molecule can react by a vector of different parallel reaction pathways,  $\mathbf{rp}^1$ . The kinetic parameters for each of these pathways are represented by the rate constant vector  $k$ . The likelihood that some reaction occurs is now governed by the overall reaction probability,  $\sum_{i=1}^{rp} k_i$ . This is inserted into Eq. 4-3 to determine  $\Delta t_v$ , as shown below:

$$\Delta t_v = - \frac{\ln(1 - \text{RN})}{\sum_{i=1}^{rp} k_i} \quad (4-4)$$

The reaction selectivity, i.e., the identity of which reaction occurs, is computed by comparing a second randomly drawn variable, RN2, with the cumulative reaction probability distribution. This is illustrated in the following equation:

$$\sum_{i=1}^{j-1} k_i < \text{RN2} \leq \sum_{i=1}^j k_i \quad (4-5)$$

where  $i$  represents an available reaction path and  $j$  is the reaction pathway which corresponds to the chosen reaction event. The remainder of the simulation proceeds as outlined above.

<sup>1</sup> In the event-based logic of the VT approach, only the primary paths of a component at time  $t$  are analyzed. Subsequent pathways are represented as primary paths of intermediate components at some later time,  $t'$ .

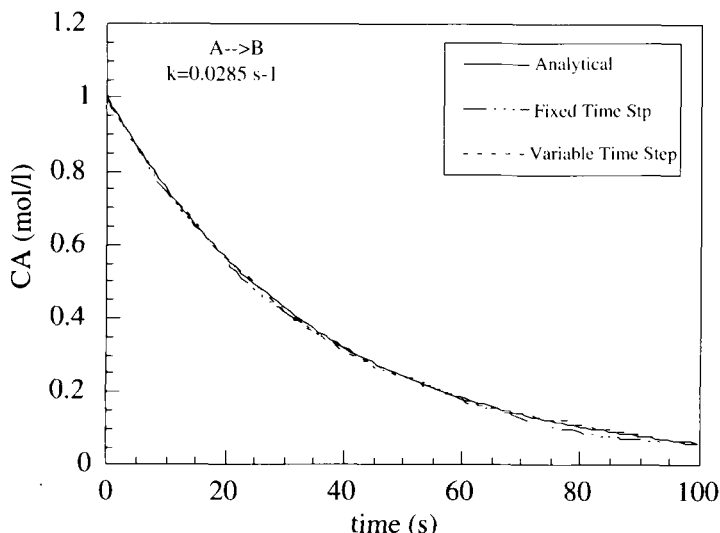


Fig. 4-14. The comparison of the fixed- and variable-time step stochastic simulation results with the analytical solution for the irreversible example reaction of A to B.

The simulation of the irreversible reaction of A to B by both the FT and VT simulation algorithms are compared with the analytical solution in Fig. 4-14. This 'method calibration' shows the accuracy of the Monte Carlo simulation in the description of chemical reaction systems to be quite high.

The rational selection of either the FT and VT Monte Carlo techniques for use in reaction modeling requires the delineation of their relative advantages and limitations. The major advantage of the fixed-time step algorithm is the ability to fix the simulation-time step interval  $\Delta t$ . This can provide considerable CPU savings, especially for 'stiff' systems, for which the long time behavior is difficult to assess due to the numerous short time events that are possible. Exploiting this feature requires attention to the number of sequential reactions possible in a given time interval, and the discrimination of the exact network of reaction paths prior to simulation.

The major advantage of the variable time approach is that the reaction paths are determined 'in situ'; only the primary reaction pathways are required. The major disadvantage of the VT approach is the inability to specify the reaction time step, because the simulation proceeds event-by-event. Processes in which many events can occur in short time intervals, therefore, will carry a considerable CPU burden. Moreover, if the transition probabilities are concentration dependent, the possibility of large  $\Delta t_v$  will add bias to the results.

This work is focused on the reactions of asphaltenes. The complex spectrum of molecular pathways was not initially available for each asphaltene component, which made the implementation of the fixed-time step approach difficult. The variable-time algorithm was, therefore, the method of choice.

## APPLICATION OF THE VARIABLE-TIME STEP MONTE CARLO SIMULATION TO ASPHALTENE PYROLYSIS

Inasmuch as the complex asphaltene molecules each comprised several reaction sites, the model compound kinetics were mapped into the asphaltene Monte Carlo simulation model on a site-by-site basis. Thus the smallest asphaltene subunits available were identified and their intrinsic chemical kinetics were taken as those of related model compounds. For example, the hypothetical structure shown in Fig. 4-15 highlights each reaction with a numerical label. This structure has nine reactive moieties: six of these are mimicked by model alkylaromatic, and three by model alkyltetralin groups.

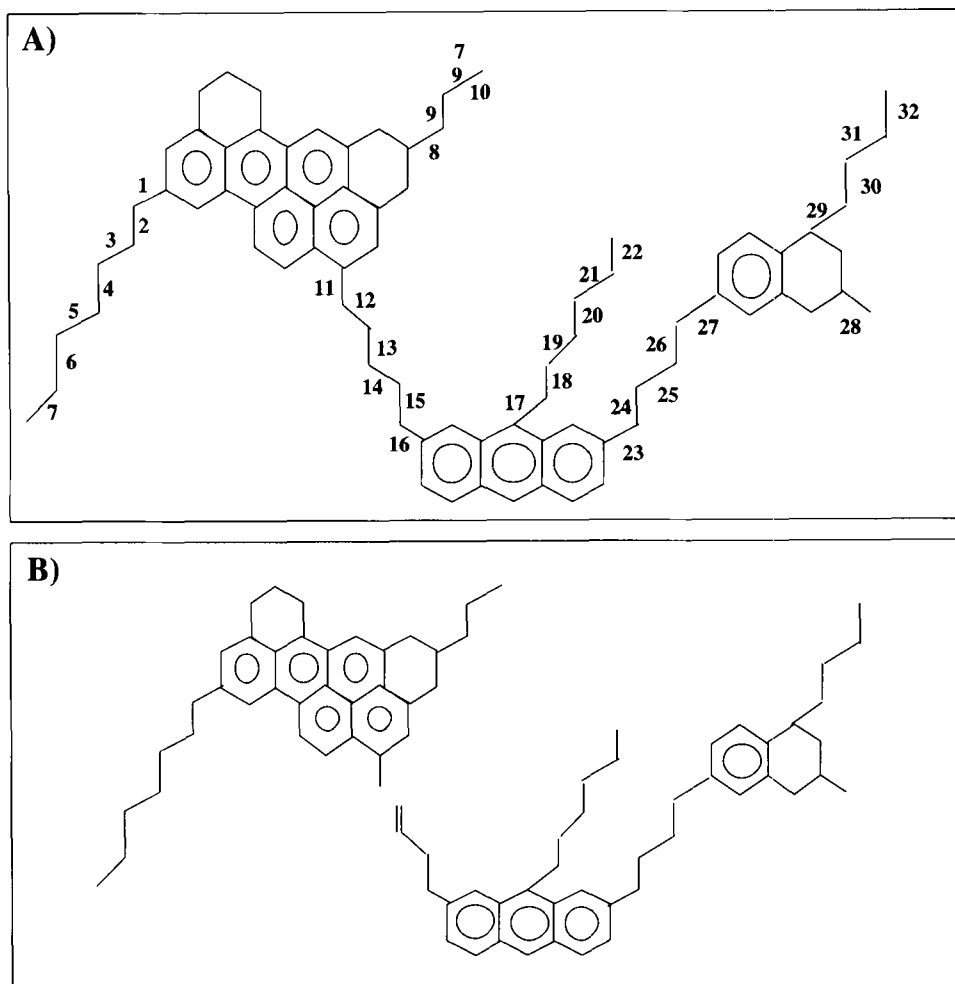


Fig. 4-15. A schematic (A) of the possible bond breaking events for a hypothetical asphaltene molecule, and (B) the result of a single reaction event.

The molecular pyrolysis chemistry was summarized earlier. In short, the kinetics of bond breaking can be described by:

$$r_{ijm} = w_{ij} v_{im} k_i C_i \quad (4-6)$$

where  $i$  identifies the reaction moiety,  $j$  is the chain length and  $m$  is an index that identifies the bond broken. The asphaltene composition is described in terms of the number of reaction moieties per unit volume in the reaction system. The term  $w_{ij}$  quantified the effect of alkyl chain length on kinetics, and the factor  $v_{im}$  represents the stoichiometric coefficient for the probability of breaking a specific bond. All of this information is summarized in Table 4-4. Their association into Eq. 4-6 and subsequent accumulation into a vector of kinetic reaction probabilities,  $\mathbf{k}$ , for the example in Fig. 4-15 is shown in the bar graph in Fig. 4-16A. This kinetic distribution was easily integrated and normalized to provide a cumulative reaction probability distribution as demonstrated in Fig. 4-16B.

The variable-time approach exploited two random numbers for each reaction step. The first (0.22 in this example) provided the time at which the molecule of Fig. 4-15 (with the kinetics of Fig. 4-16B) reacted. The elapsed reaction time was 113 s, as shown below:

$$\Delta t_v = -\frac{\ln(1 - \text{RN})}{\sum_{i=1}^{32} k_i} = 113 \text{ s} \quad (4-7)$$

The second random number (0.4 in this example) characterized the reaction. The thus-deduced reaction, corresponding to event 12, was the highly probable cleavage of the bond  $\alpha$  to an aromatic. This reaction produced two new molecular structures both susceptible to further reaction. These new molecular structures and the cumulative time are then updated. The new molecular structures provide the basis for the calculation of the new reaction probability vector,  $\mathbf{k}$ , which is subsequently used in the stochastic determination of the next reaction time and event.

This process of surveying the present structure, quantifying the probable reaction paths and their associated kinetics, stochastically determining the actual reaction events, and updating time and structure was sequentially repeated until the final reaction time was reached. Fig. 4-17 represents this Markov chain process for the randomly selected asphaltene molecule. The overall Monte Carlo simulation analysis of the asphaltene pyrolysis system entailed the stochastic generation and reaction of  $10^4$  different asphaltene molecules.

#### MONTE CARLO SIMULATION OF ASPHALTENE STRUCTURE, REACTIVITY, AND REACTION: RESULTS

The simulation results described in this section were for the batch thermolysis at 450°C of the offshore California (OSC) derived asphaltene feedstock, the characteristics of which were described in Table 4-3. The required simulation inputs were the structural PDFs of Fig. 4-7 and the intrinsic chemical kinetic data base described in Table 4-4. Ten thousand molecules were constructed, reacted and identified as described. The detailed outcome is presented in terms of molecular products and molecular analytical

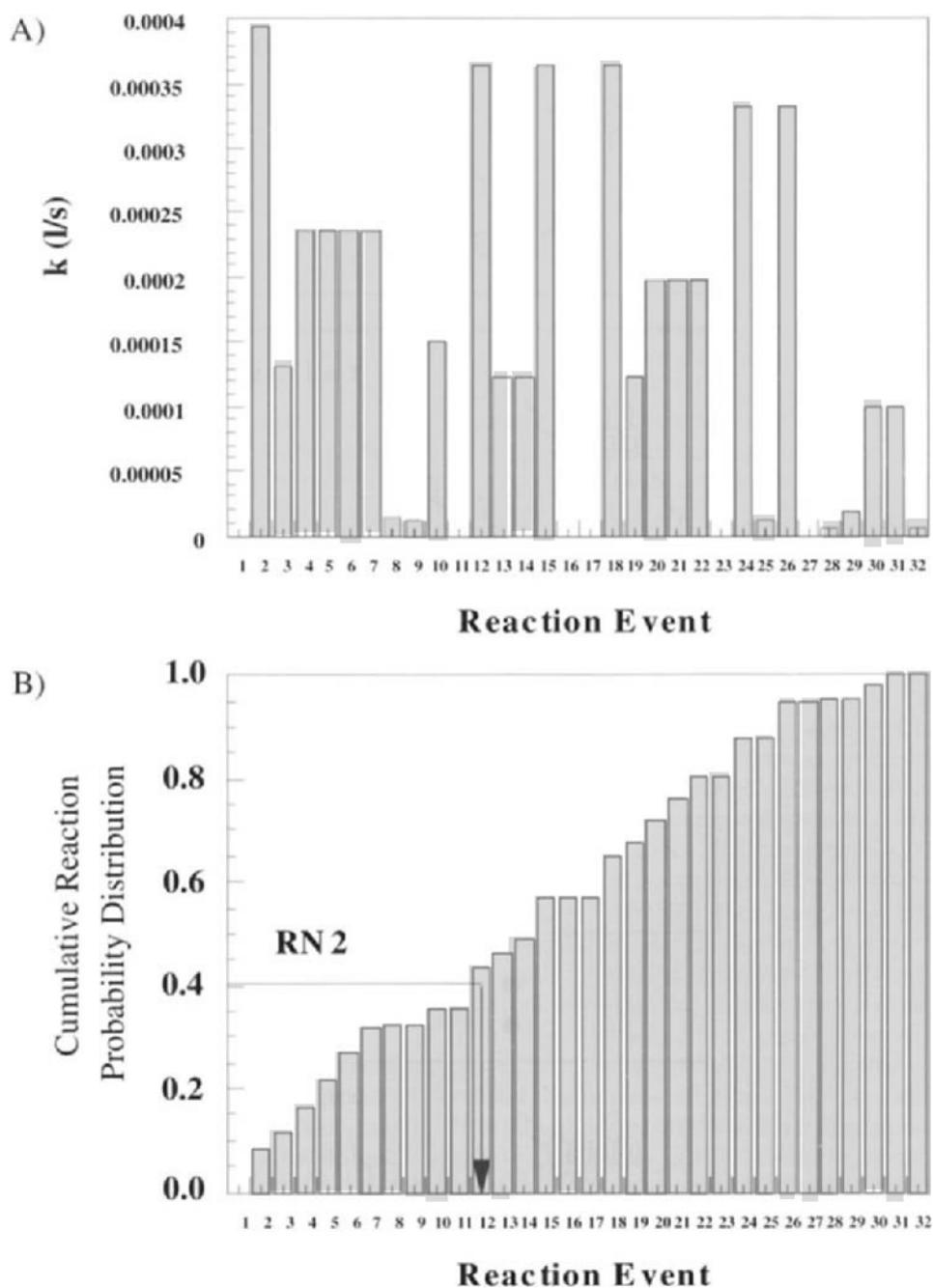


Fig. 4-16. The kinetic distributions used in the stochastic analysis of a single reaction event for the example structure in Fig. 4-4. (A) The kinetic rate constant vector,  $\mathbf{k}$ , for each event. (B) The cumulative reaction probability distribution  $\sum_{i=1}^n k_i$ .

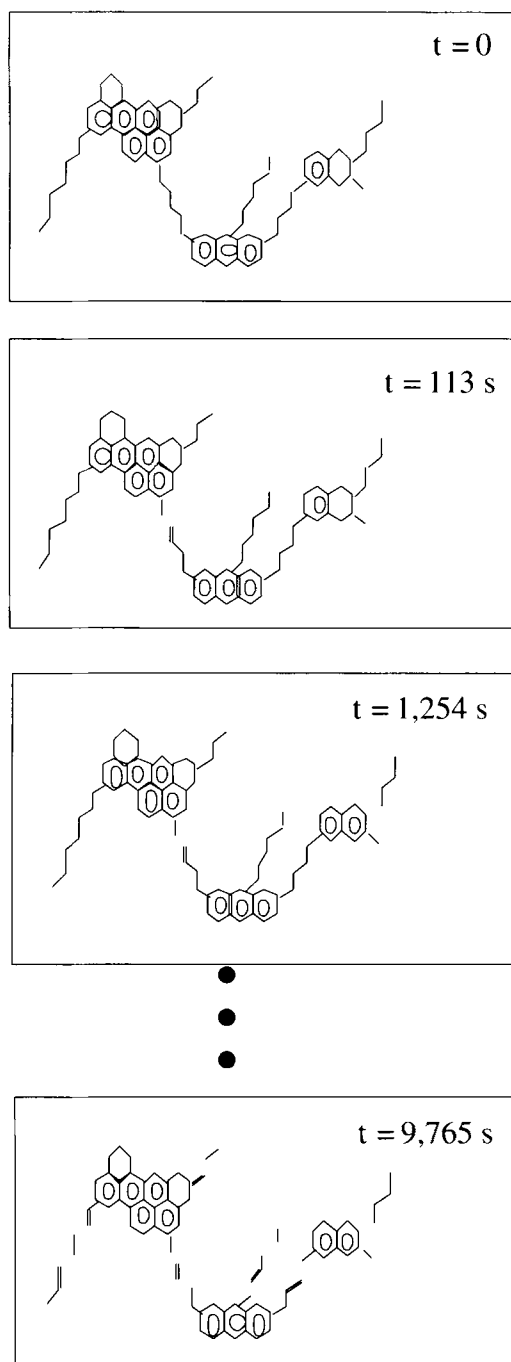


Fig. 4-17. A schematic example of the reaction trajectory for a single molecule in the asphaltene pyrolysis example. This represents a Markov chain for the single-component reaction system. Each frame demonstrates the temporal transition of the system state. Only one event per frame is updated as is characteristic of the variable-time approach.

distributions, average products and average analytical information, and global products and global product properties, as described separately above.

### *Molecular products and characteristics*

The atomic structure of each component was available throughout reaction time. This provided the temporal variation of individual molecular components. A sampling of 4 of the 10,000 computationally generated initial asphaltene structures is shown in Fig. 4-18. The complex structure of each of these components required that their molecular description be phrased in terms of detailed carbon distributions (synonymous to molecular weight) for various important structural attributes. For example, the total number of aromatic rings per molecule was used to roughly classify each molecule by type. Subsequently, the detailed carbon distribution for each type was used to represent each molecule. Fig. 4-19, for example, depicts the variation of the carbon distribution for molecules which contain a total of five aromatic rings. Initially, no five aromatic ring components were present. This was a result of the 'oligomeric' nature of the initial asphaltene feedstock. As reaction time proceeded, however, the number of 5-ring aromatic molecules increased significantly. This is illustrated by the increasing scale of the y-axis (the molar frequency) in the time-dependent distributions in Fig. 4-19. This implied that the original oligomeric components were depolymerized. Additionally, there was considerable dealkylation of these 5-ring aromatic species, as shown by the shift of the distribution to the lower carbon numbers. For example, after 2 min of reaction, the carbon numbers for these components were primarily distributed between 40 and 80; however, after 30 min of reaction, the majority of these components were bracketed between 20 and 40. At long reaction times, the relative

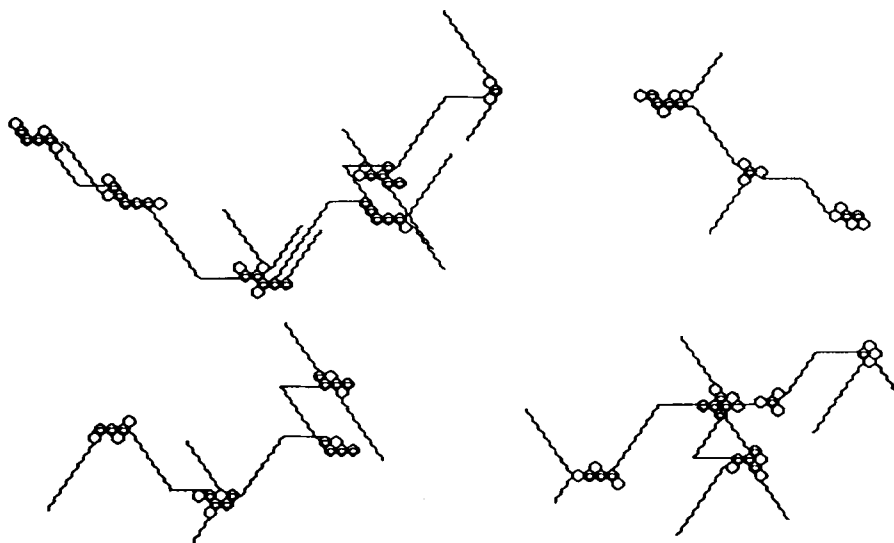


Fig. 4-18. Four stochastically generated initial asphaltene molecules.



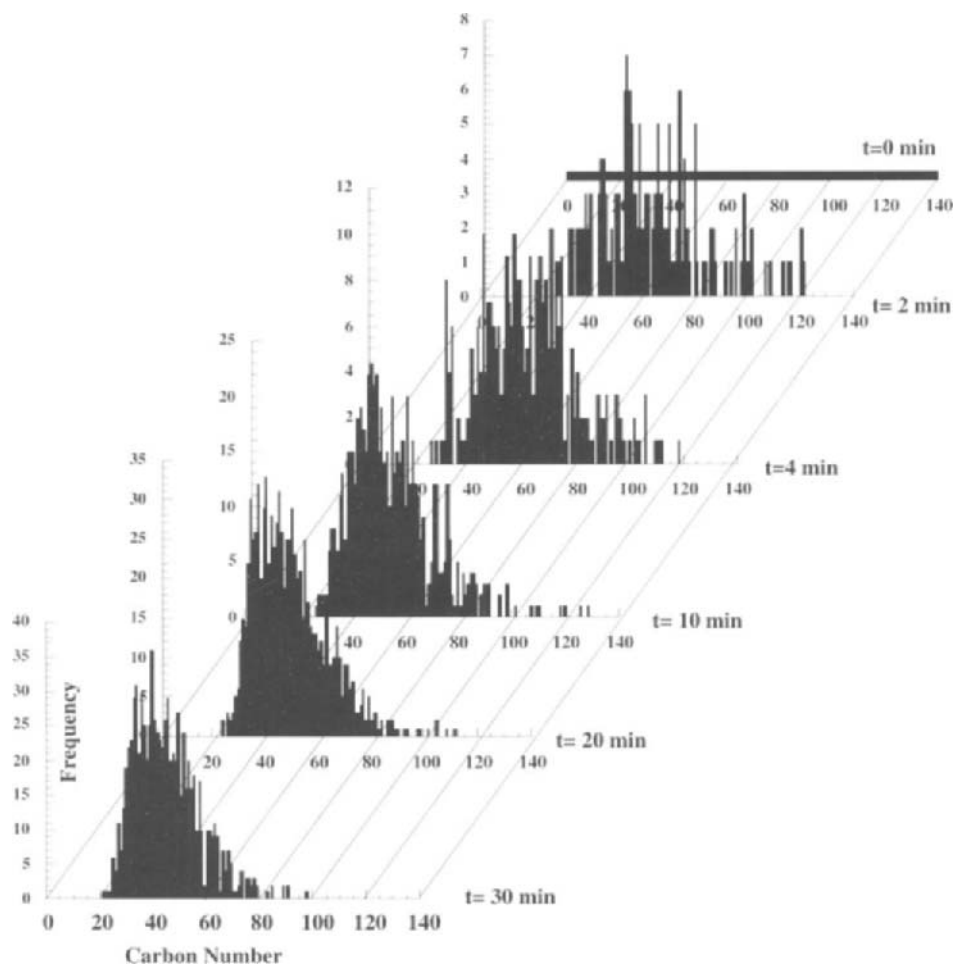


Fig. 4-19. The temporal variation of the carbon number distribution for 5-ring aromatic-containing components for the pyrolysis simulation of the offshore California asphaltene at 450°C.

changes in these distributions are very minor. The carbon distribution after 20–30 min of reaction are nearly identical. This implies that very little depolymerization or dealkylation occurs at these times and that the conversion has approached a constant level.

The temporal variation of the total aromatic ring distribution is depicted in Fig. 4-20. These results support the depolymerization ideas discussed above. The initial asphaltene was composed of a distribution of molecules which on average contained a total of fifteen aromatic rings. As reaction time proceeded, these oligomeric-like components depolymerized to yield a spectrum of different monomer units. Fig. 4-20 illustrates a relatively narrow and unchanging distribution between 20 and 30 min of reaction, where the average value is approximately four aromatic rings. This coincides with the average

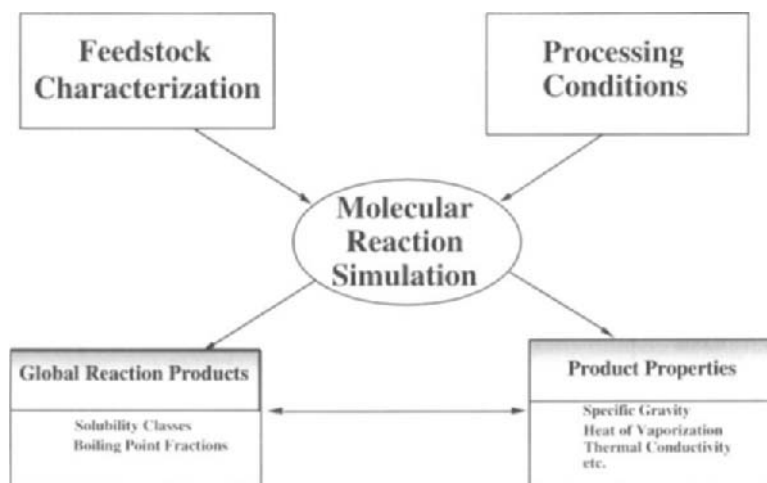


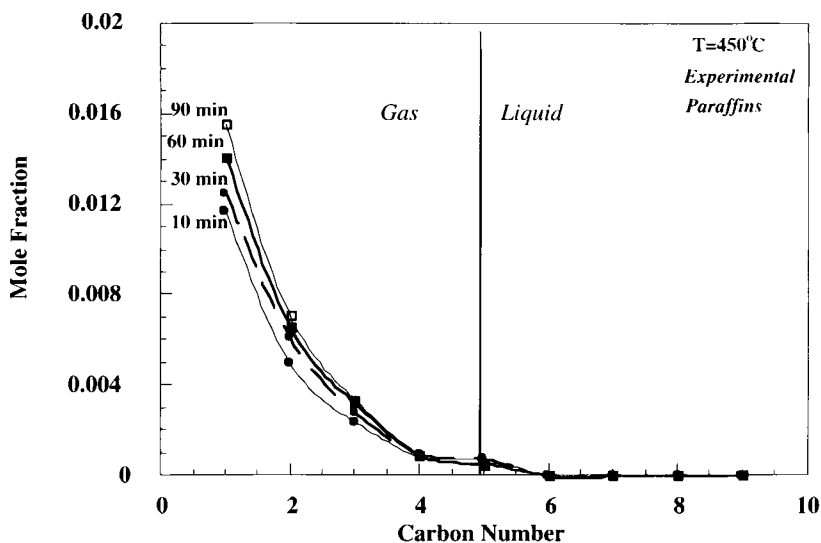
Fig. 4-20. The temporal variation of the total number of aromatic rings per molecule for the Monte Carlo pyrolysis simulation of the OSC asphaltene at 450°C.

number of aromatic rings per unit sheet of the initial feedstock ( $\approx 4$ ), and thus supports the notion of near-complete depolymerization of the original asphaltene. The detailed carbon distribution for each of the remaining total aromatic ring components was also available.

Fig. 4-21 compares the simulation and experimental paraffin distribution as a function of reaction time. The experimental values were taken from the work of Savage et al. [3,4,28] for an asphaltene feedstock derived from a nearly identical source (offshore California) and reacted under the same conditions ( $P = 1$  atm  $N_2$ ,  $T = 450^\circ\text{C}$ ). These experimental values were only reported for the gas phase species. The simulation results, however, were given for the entire distribution, regardless of phase. Initially, no paraffins were present for either simulation or experiment. As reaction time progressed, both the simulation and experiments showed an increase in the amount of methane, ethane, propane, butane and pentane that were formed. In particular, a considerable amount of methane was generated. The relative mole fraction of the  $C_1$ – $C_5$  paraffin species in both simulation and experiment appeared to follow an exponential-like distribution with respect to carbon number for each given reaction time.

The olefin products from both the simulation and experiments are shown in Fig. 4-22. As before, the experimental carbon distributions at various reaction times were only reported for gas phase components, whereas the simulation results provided the entire carbon distribution. Both results convey the increase in light olefins as reaction time is increased. The experimental results suggest that propene is the predominant olefinic product; however, the simulation results point to both ethylene and propene as the predominant species at low conversions. At higher conversions, the simulation selectivity to ethylene was much greater than that to propene. It is possible that some of the lighter products escaped the reaction vessel during the time in which the gases were allowed to equilibrate.

A)



B)

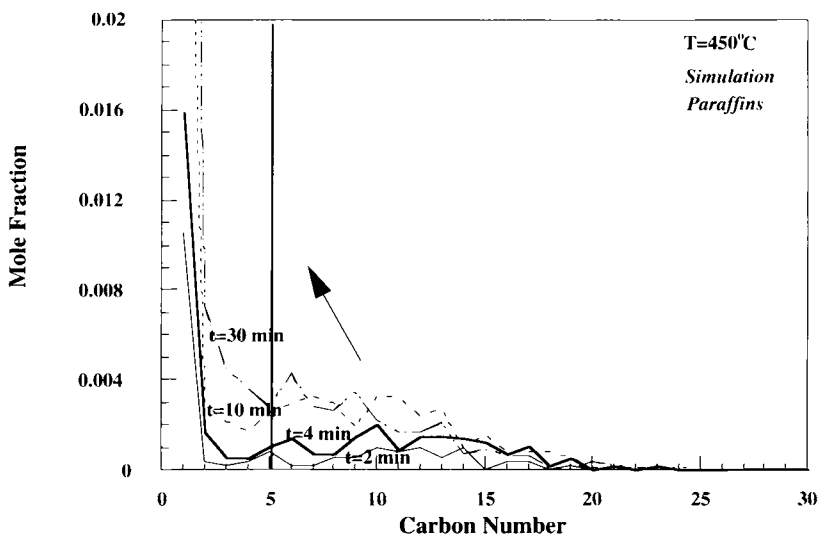


Fig. 4-21. The paraffin carbon distribution for (A) simulation (all paraffins) and (B) experimental (paraffins < C<sub>5</sub>) pyrolysis of the OSC asphaltene feedstock at 450°C.

The detailed structural accounting of each species also allowed for molecular kinetic analyses. This is shown in Fig. 4-23 for specific paraffin and olefin product molecules. In Fig. 4-23A, the yields of two relatively long paraffin products (octane and tridecane) and two smaller paraffin products (ethane and butane) are reported to illustrate the variation

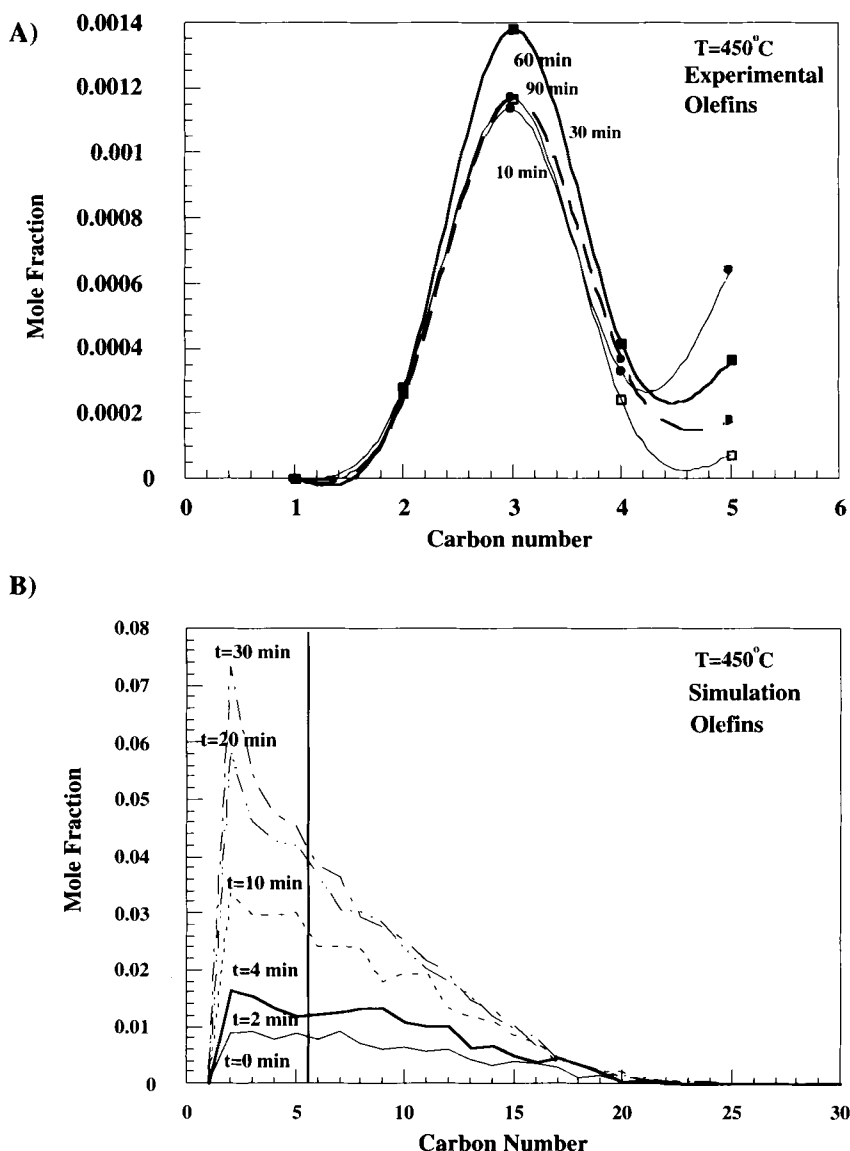


Fig. 4-22. The olefin carbon distribution for (A) simulation (all olefins) and (B) experimental (olefins < C<sub>5</sub>) pyrolysis of the OSC asphaltene feedstock at 450°C.

of kinetics with respect to chain length. The larger paraffin components, octane and 1-tridecane, both appear to be primary reaction products from the dealkylation of the aliphatic asphaltene substituents. At higher conversions, however, the composition of these larger paraffin components was somewhat diminished due to subsequent thermal cracking.

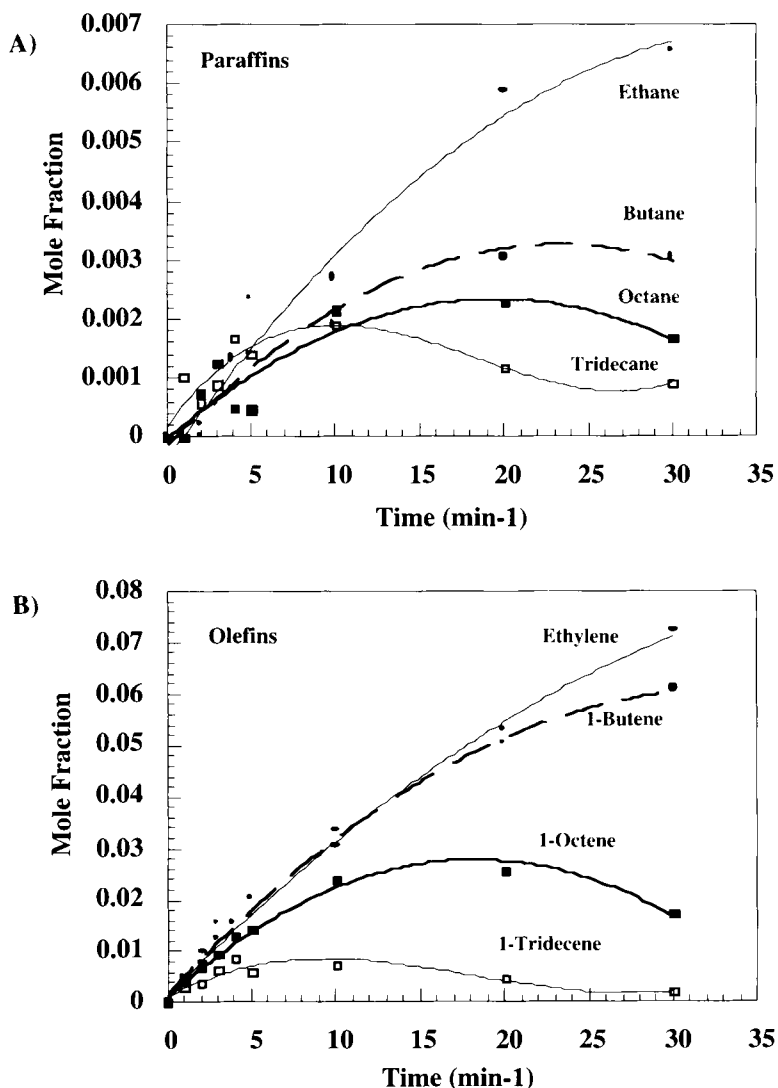


Fig. 4-23. The temporal yields of (A) paraffin and (B) olefin molecular constituents from the pyrolysis simulation of the OSC asphaltene feed at 450°C.

The molar yields for the four analogous olefin components (ethylene, 1-butane, 1-octene, and 1-tridecene) are plotted as a function of reaction time in Fig. 4-23B. These species were much more abundant than their corresponding paraffin analogs. The light components were primary products which formed very rapidly and, therefore, did not illustrate the anomalous 'secondary' characteristics that the smaller paraffins did. The larger components appeared to proceed through a maximum. Thus at high conversions the subsequent cracking of these components becomes important.

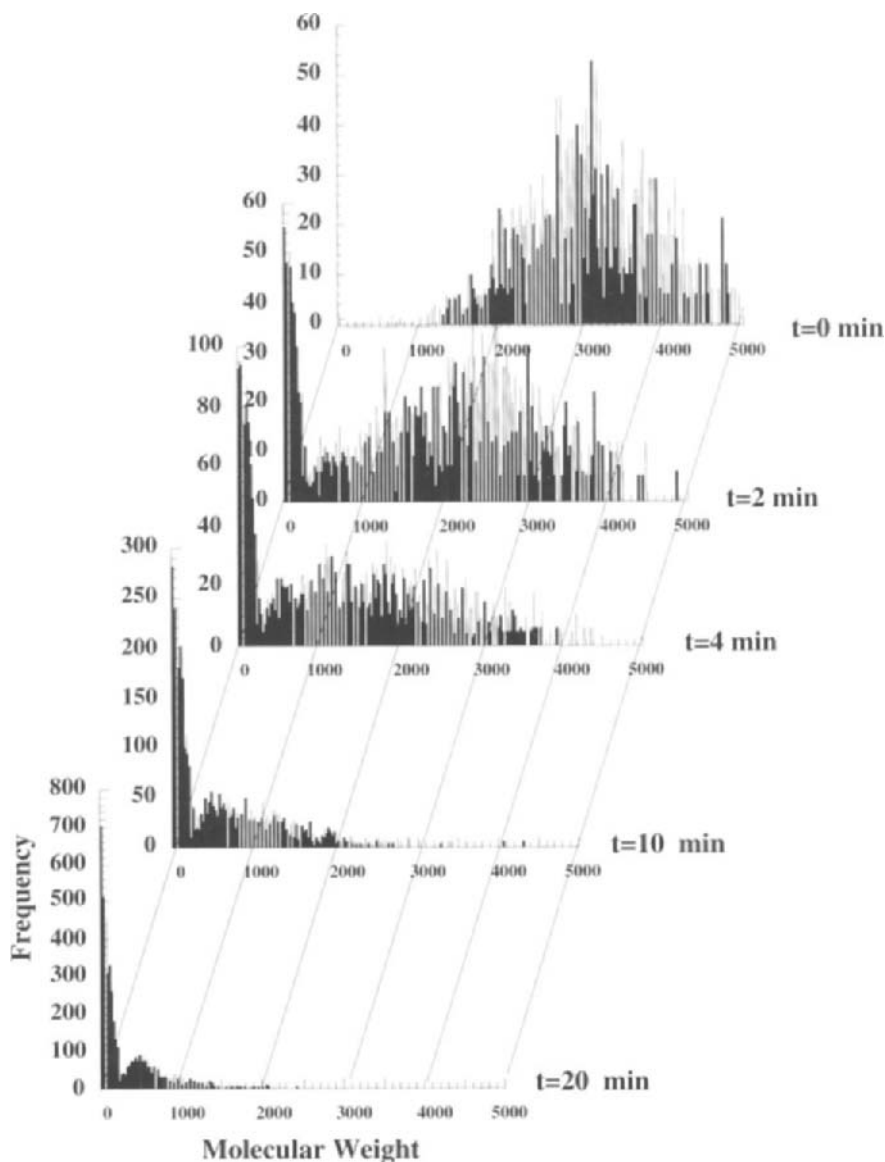


Fig. 4-24. The time-dependent variation of the overall molecular weight distribution for the pyrolysis simulation of the OSC asphaltene feed at 450°C.

#### *Molecular weight distribution*

Fig. 4-24 depicts the overall molecular weight distribution of the reaction mixture as a function of reaction time. The results illustrate a substantial change in the distribution as a function of reaction time. Initially, the molecular weight was broadly distributed between

1000 and 5000 with the average of 2773. As the reaction time progressed, however, the distribution became bimodal. The more widely dispersed high-molecular-weight peak was attributed to core aromatic–naphthenic components, whereas the intense low-molecular-weight peak was due to light olefin and paraffin product molecules.

The substantial decrease in molecular weight of the core components was the result of both dealkylation and ‘depolymerization’ reactions. Depolymerization proved to be the more dramatic of the two. As a rough estimate, the complete depolymerization of this feedstock would result in lowering the molecular weight by a factor of approximately 4.6 to the average number of unit sheets per molecule. This would produce a change in the average molecular weight from 2770 to 602. Dealkylation reactions, which enhance this reduction, are less substantial. For example, the cleavage of a 10-carbon aliphatic chain would only reduce the molecular weight by 141 amu units.

The paraffin and olefin products of dealkylation yielded the low-molecular-weight fraction (peak). Subsequent cracking of these components induces a shift to even lower molecular weights.

At long reaction times, the overall molecular weight distribution became almost constant. This suggests a near-complete depolymerization of the oligomeric structure and considerable dealkylation of the alkyl aromatic–naphthenic cores to very unreactive products. These products, which include denuded aromatic–naphthenic core components and light paraffin and olefin species, are indicative of the somewhat constant high- and low-molecular-weight peaks of the final bimodal distribution in Fig. 4-24.

#### *Hydrogen to carbon ratio (H/C)*

Fig. 4-25 summarizes the complete molecular hydrogen to carbon distribution for the aromatic–naphthenic core components as a function of reaction time. The hydrogen reduction in the core is evident in the gradual shift of the H/C ratio distributions to the right (lower H/C ratios values) as a function of reaction. Dealkylation reactions are responsible for this shift. For example, the cracking of a general saturated aliphatic substituent  $-(CH_2)_n-CH_3$ , removes  $2n + 3$  hydrogen atoms and  $n + 1$  carbon atoms. This reduces the hydrogen content of the remaining core. The removal of hydrogen from the core is balanced by the production of hydrogen-rich aliphatic products.

#### *Average molecular attributes and average analytical results*

The detailed distributions of reactant, intermediate and product molecules presented above allow for lumping into pseudo-components, components such as alkylaromatics, alkyl naphthenes, paraffins, and olefins at any particular reaction time. This provides an estimate of the average compositional yields, and also enables the molecular approach to interface with pseudo-component lumped reaction models.

Fig. 4-26A illustrates the average values for the degree of polymerization (DP), the number of aromatics per unit sheet (NAR/US) and the side chain length attached to aromatic and naphthenic rings as a function of time. The exponential decay in the average number of unit sheets with time implies the thermal depolymerization of the initial oligomeric starting components. The nearly constant average number of

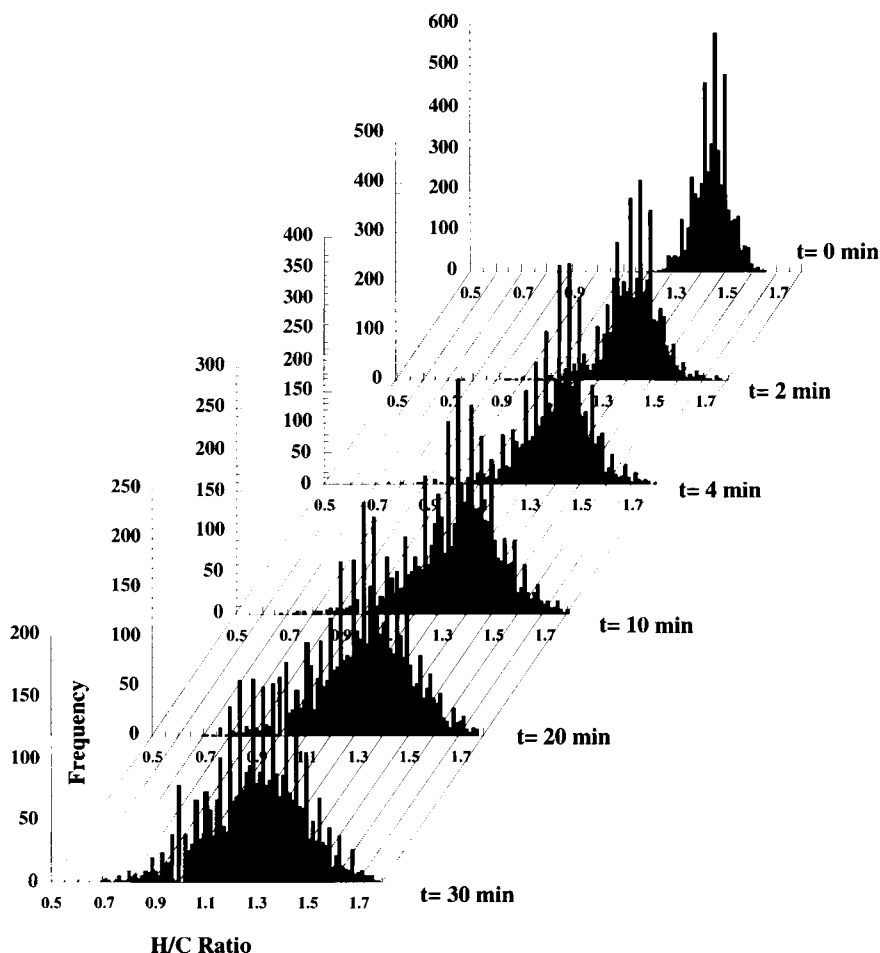


Fig. 4-25. The temporal variation of the overall atomic hydrogen to carbon distribution for the core components in the pyrolysis simulation of the OSC asphaltene feed at 450°C.

aromatic rings per unit sheet suggests that the aromatic–naphthenic core is unchanged by thermolysis. Experimental evidence from both model compound and real system studies, however, suggests that aromatization and condensation reactions can be significant and alter the makeup of the core [2,21]. This is an important issue which surfaces again in the global results section.

The last two attributes displayed in Fig. 4-26B are the average chain length of aliphatic substituents bonded from the core aromatic and naphthenic rings. Both curves in this figure illustrate the rapid dealkylation of these aliphatic substituents.

The time-dependences of average analytical properties were also computed from their detailed ensembles. For example, the temporal variation of the overall molecular weight distribution depicted earlier in Fig. 4-24 is summarized in Table 4-6 in terms



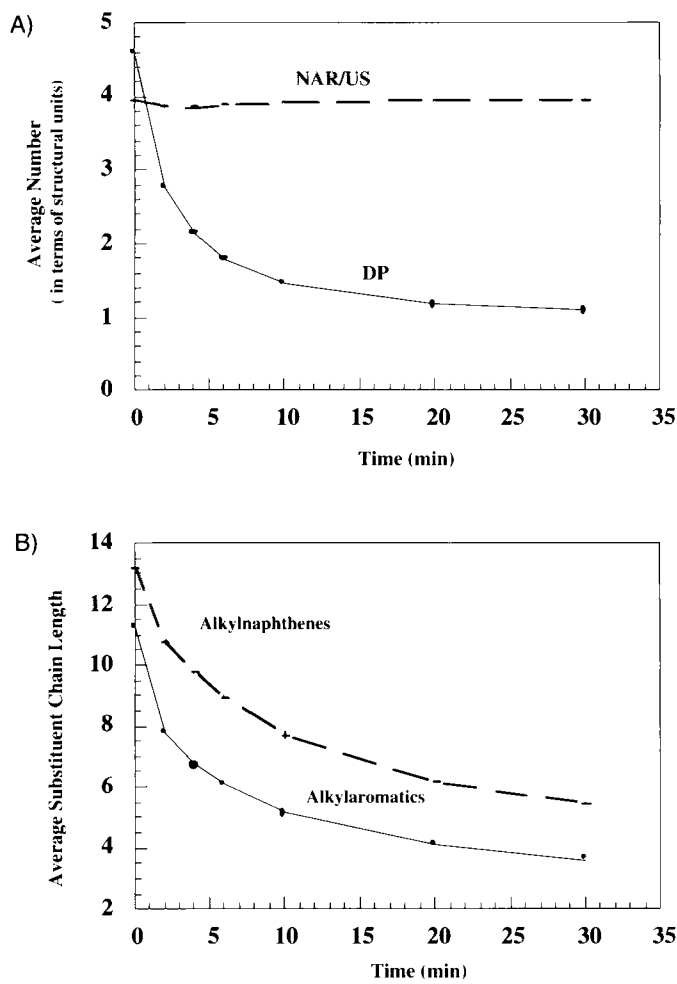


Fig. 4-26. The variation of average structural attributes with respect to reaction time for the pyrolysis simulation of the OSC asphaltene feedstock at 450°C.

TABLE 4-6

Average temporal values for the number and weight average molecular weight for the pyrolysis of the OSC asphaltene feed at 450°C

Reaction time	$M_n$	SD	$M_w$
0	2773	750	3274
2	1943	1123	2593
4	1414	1049	2192
10	678	665	1330
20	372	403	809

$M_n$  = number average molecular weight; SD = standard deviation;  $M_w$  = weight average molecular weight.

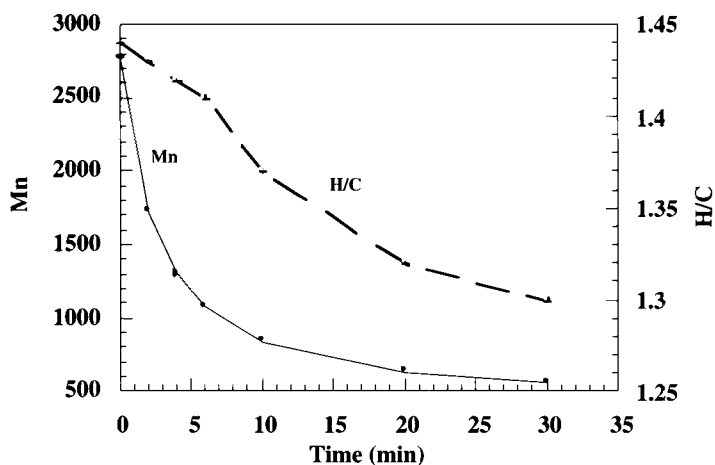


Fig. 4-27. The effect of reaction time on average analytical properties: (1) the number average molecular weight of the entire feedstock, and (2) the average H/C ratio for the aromatic-naphthenic components for the pyrolysis simulation of the OSC asphaltene feedstock at 450°C.

of the number average molecular weight, and its corresponding standard deviation, and the weight average molecular weight. Both the number and weight averaged molecular weights decline significantly over reaction time as a result of both dealkylation and depolymerization chemistry. Neither of these distributions adequately reflect the changes in the actual feedstock. The number average molecular weight overemphasizes the light components, whereas the weight average molecular weight overemphasizes the heavy constituents. Thus, the heterogeneous bimodal character of the actual distribution (Fig. 4-8) is lost upon lumping into a single average value.

The average hydrogen to carbon ratio for the aromatic-naphthenic core components is presented in Fig. 4-27. The time-dependent values of the number averaged molecular weight are also shown for comparison. This figure demonstrates that the changes in the molecular weight are quite dramatic, whereas the changes in the average H/C ratio are much less. Small changes in H/C ratios, however, can in fact severely alter the solubility and distillation characteristics of the mixture [2,28].

#### GLOBAL REACTION PRODUCTS

Fig. 4-28 provides an overall view of the entire Monte Carlo process. The last step illustrates the lumping involved in reducing the 10,000+ product molecules into global product fractions, such as asphaltene, maltene, coke and gas. This helps to stress the point that the explicit accounting of molecular detail throughout simulation provides the molecular makeup of each global fraction and thus a means for estimating the properties of each global fraction. Both solid-liquid-vapor equilibrium (SLVE) calculations and empirical correlations were used as lumping techniques to assign each of the 10,000+ product components to its respective solubility fraction.

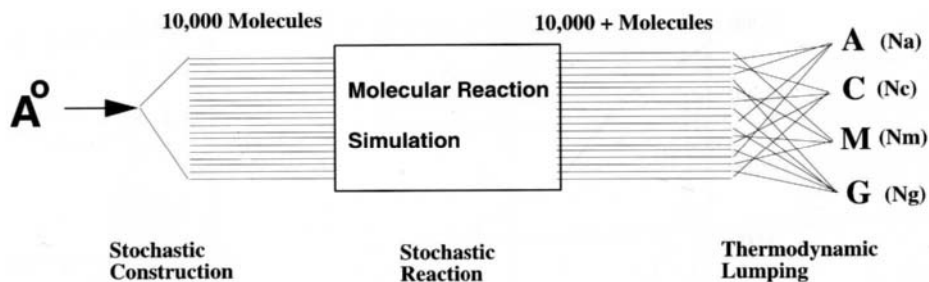


Fig. 4-28. Stochastic construction, reaction and thermodynamic lumping schematic for asphaltene pyrolysis system.  $A$  = asphaltene;  $C$  = coke;  $M$  = maltene;  $G$  = gas.

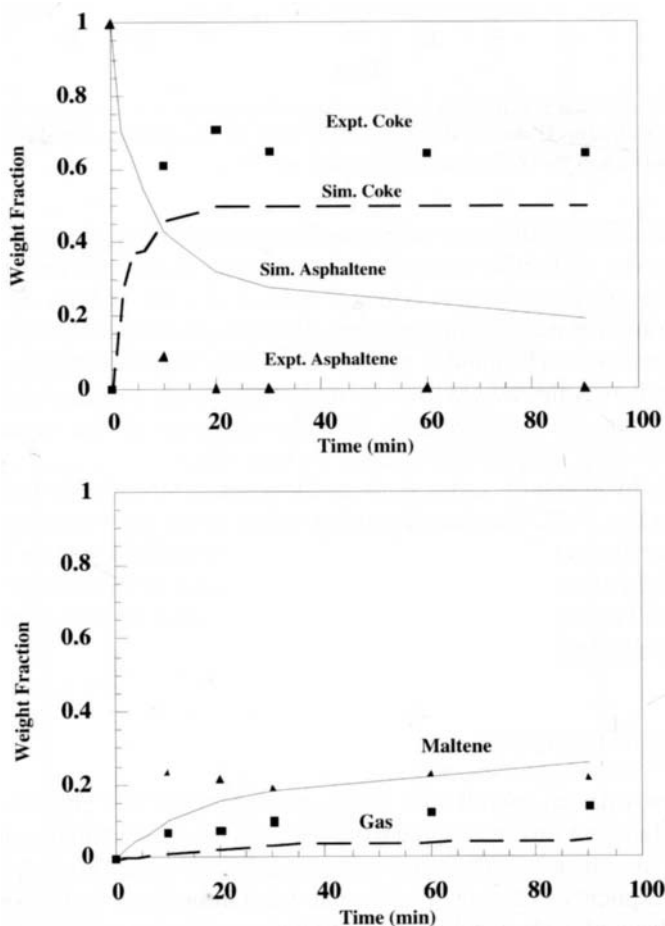


Fig. 4-29. The comparison of the temporal variation of global solubility fractions for the experimental and first-order simulation of pyrolysis of the OSC asphaltene feedstock at 450°C. The results are shown for (top panel) asphaltene and coke and (bottom panel) maltene and gas product yields.

*Solid-liquid-vapor equilibria-based global product results**Bond breaking chemistry only*

Fig. 4-29 presents experimental and simulation results, the latter being based on the chemistry presented in Table 4-4 only. This highlights the effect of bond-breaking chemistry without attendant dehydrogenation. The solubility lumps were determined through iterative SLVE calculations [6]. Both simulation and experimental results demonstrate similar qualitative features, such as the exponential conversion of asphaltene and the asymptotic approach to constant coke, maltene and gas yields. The quantitative agreement between these two, however, is quite poor. The two greatest discrepancies concern the relative values of the ultimate product yields at complete conversion and the severe underprediction of simulation kinetics of asphaltene conversion.

The asymptotic simulation yields for asphaltene, coke, maltene and gas were 0.19, 0.5, 0.22, and 0.05, respectively, while the corresponding experimental values were 0.0, 0.64, 0.22, and 0.14. The inability of the simulation results to approach complete asphaltene conversion even at very long reaction times suggests either a problem in the computational definition of coke or the absence of pathways, which can lead to coke. The latter explanation appears more reasonable. The hydrogen transfer pathways which lead to the dehydrogenation of naphthenic rings in the molecular core to aromatics and condensation (polymerization) of the dealkylated cores, were not included in the simulations that led to the construction of Fig. 4-29. This explains why the aromatic-naphthenic core of the molecular products remained unchanged with respect to reaction time as was illustrated in Fig. 4-20 and Figs. 4-25–27.

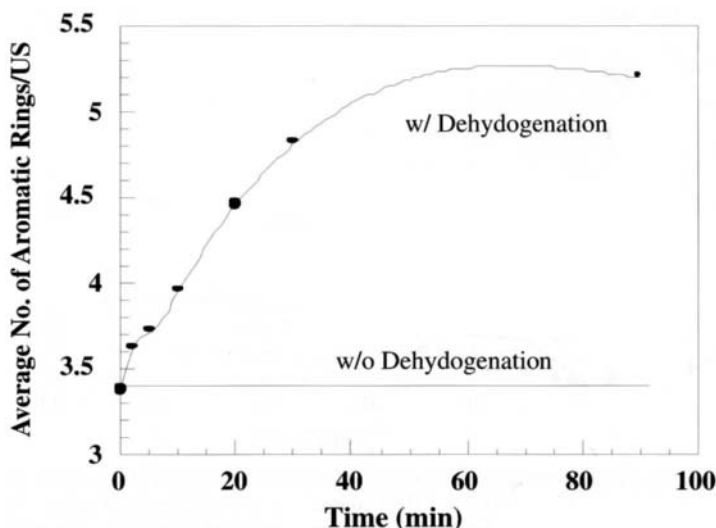


Fig. 4-30. The effect of hydrogen transfer (dehydrogenation) on the temporal variation in the number of aromatic rings per unit sheet for the OSC asphaltene pyrolysis simulation example.

### *Effect of hydrogen transfer*

The effect of dehydrogenation pathways on the simulation products was explored simply by allowing the pathways and kinetics described in both Tables 4-4 and 5 to be utilized. The molecular results for this system demonstrated the formation of highly refractive and hydrogen-poor product cores. This is illustrated in Fig. 4-30 by the increase in the number of aromatic rings per core as a function of reaction time. These data are more consistent with the experimental evidence that suggests the increase in aromaticity in thermal conversion. The effects of hydrogen transfer on the global solubility products for this system are shown in Fig. 4-31 in comparison with the previous simulation results. The addition of the hydrogen transfer pathways greatly improved the accuracy of the simulation results.

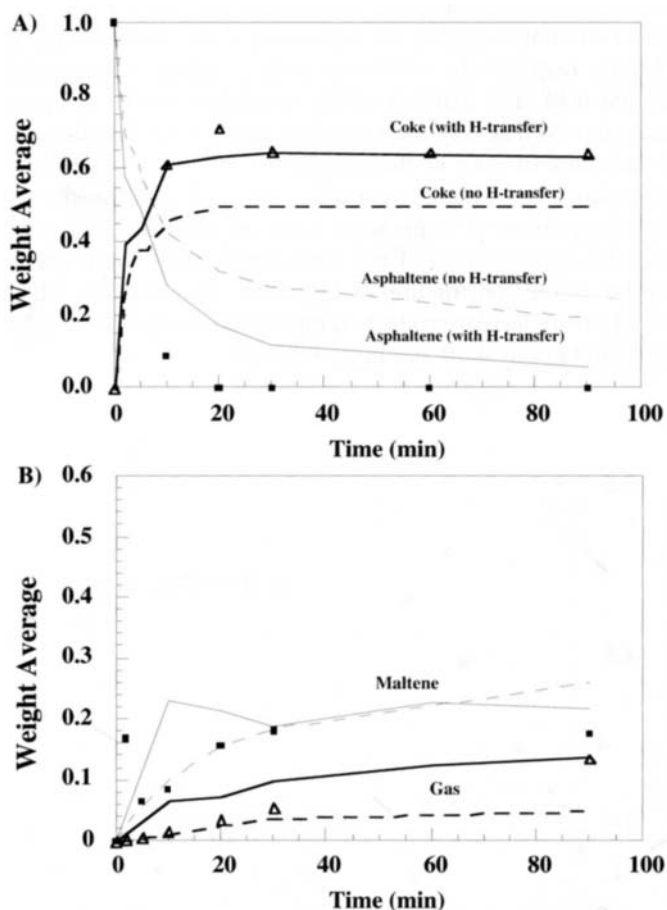


Fig. 4-31. The effects of hydrogen transfer pathways on the temporal variation of the global solubility results for the OSC pyrolysis simulation at 400°C and their comparison with experimental values. The dotted lines refer to the original simulation results, the complete lines indicate simulation results with hydrogen transfer, and the points are from actual experiments. The temporal results for (A) asphaltene and coke yields and (B) maltene and gases are shown.

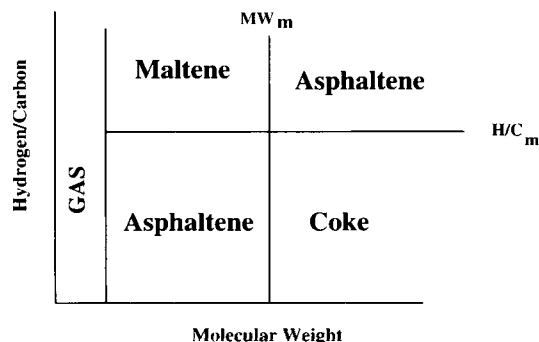


Fig. 4-32. The Savage-Klein [4] empirical model for the prediction of global reaction products. Subscript 'm' = mean value.

### *Empirical global product determination*

The empirical lumping method for the determination of global product fractions utilized empirical structure-product correlations, based on the molecular weight and the hydrogen-to-carbon ratio, to organize the 10,000+ product molecules. This lumping approach disregards molecule-molecule interactions and addresses them only superficially through the empirical parameters. This approach, however, offers a substantial reduction in the CPU burden for global product analysis.

The simulation results using the Savage-Klein (SK) [4] property correlations are shown in Fig. 4-32, with a range of  $H/C_m$  values, whereas the experimental data are shown in Fig. 4-33A,B. The experimental results are the dots and the SK correlations are the curves.

The fit between the simulation solubility cuts and the experimental data is quite good (within 5%) for  $H/C_m = 1.35$ .

## CONCLUSIONS

Monte Carlo simulation of asphaltene reaction is a flexible tool that allows accounting for the effects of feedstock structure and processing conditions (temperature, pressure, diluents) on products (molecular and global) and their properties (analytical, molecular, and global). The Monte Carlo feedstock construction algorithm permitted structural attribute information to be assembled into an ensemble of molecules which are representative of actual molecules in a particular complex heavy hydrocarbon feed. This formalism addressed the atomic structure of every component within the feedstock, thus establishing the connection between atomic, molecular and global descriptions of complex systems. Fundamental-based model compound experiments could be used to describe the intrinsic pyrolysis chemistry.

These molecular pathway models offer a unique advantage in that they permit features derived from elementary pathways to be described through composition-dependent rate expressions, while minimizing the CPU simulation requirements. The variable-time-step Monte Carlo algorithm was efficient for accounting for the time-dependent molecular

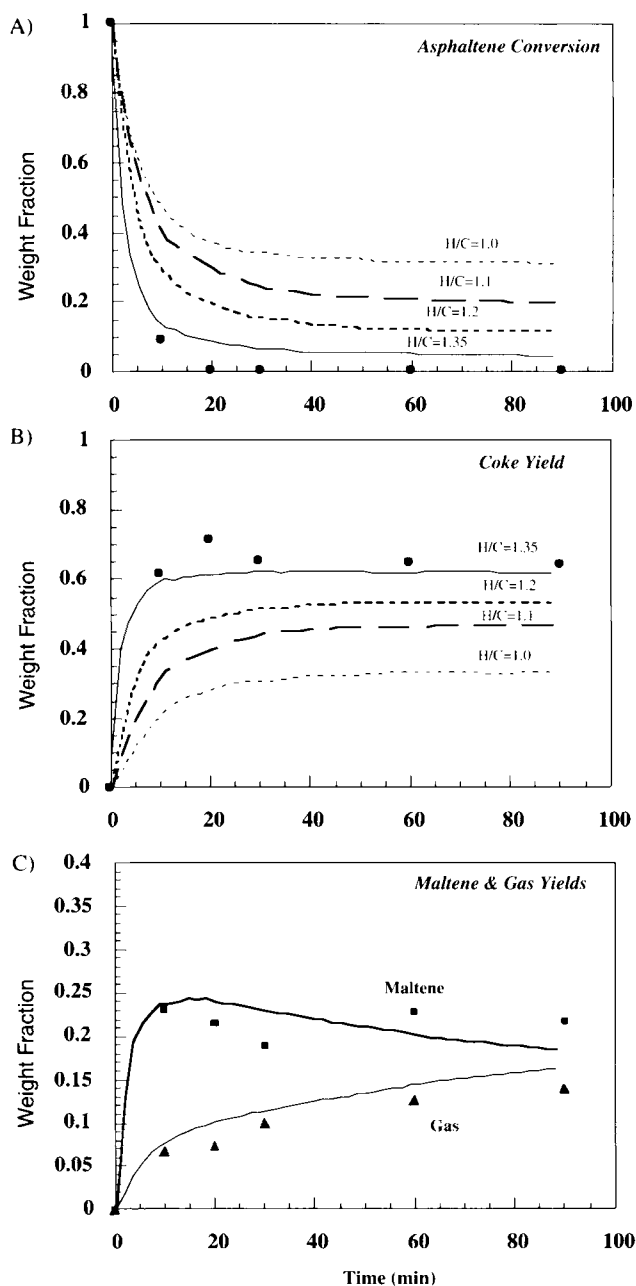


Fig. 4-33. The evaluation of the temporal variation of global solubility fraction for the simulation and experimental results parametric in the hydrogen to carbon demarcation parameter of the SK empirical lumping model. The fit of simulation and experimental results for (A) asphaltene and (B) coke weight fractions parametric in  $H/C_m$ , and (C) the final maltene and gas products.

structure. Both intrinsic and extrinsic rate factors are embodied in the stochastic transition probabilities. Thus, the elucidation of these effects can be explored.

Thermodynamic simulations and molecule/structure correlations allowed the computation of the amount of global reaction products (solubility fractions and distillate cuts) and provided property information. The former approach, which is based on rigorous simulation of the controlling SLVE phase behavior, is widely applicable. However, it is CPU intensive. The latter approach is computationally more efficient, but is only applicable to the ranges of its optimized correlation. Overall, the general intrinsic Monte Carlo reaction simulation is a useful learning tool for exploring the elements of complex chemistries.

#### ACKNOWLEDGEMENTS

The authors wish to acknowledge helpful discussions with Dr. Cristian Libanati, Dr. Abhash Nigam, and Dr. Daniel Trauth.

#### REFERENCES

- [1] Speight, J.G., Long, R.B. and Trowbridge, T.D., Factors influencing the separation of asphaltenes from heavy petroleum feedstocks. *Fuel*, 63: 616–620 (1984).
- [2] Speight, J., *The Chemistry and Technology of Petroleum*. Marcel Dekker, New York (1980).
- [3] Savage, P.E., *Chemical and Mathematical Modeling of Asphaltene Reaction Pathways*, Ph.D. Dissertation, University of Delaware, Newark (1986).
- [4] Savage, P.E. and Klein, M.T. Asphaltene reaction pathways, V., Chemical and mathematical modeling. *Chem. Eng. Sci.*, 44 (2): 393–404 (1989).
- [5] Hirsch, E. and Altgelt, K.H., Integrated structural analysis. A method for the determination of average structural parameters of petroleum heavy ends. *Anal. Chem.*, 42 (12): 1330–1339 (1970).
- [6] Neurock, M., Ph.D. Dissertation, University of Delaware, Newark (1992).
- [7] Gallacher, J., Snape, C.E., Dennison, P.R., Bales, J.R. and Holder, K.A., Elucidation of the nature of naphtheno-aromatic groups in heavy petroleum fractions by  $^{13}\text{C}$ -NMR and catalytic dehydrogenation. *Preprint Am. Chem. Soc., Div. Pet. Chem.*, Symposium on Modern Analytical Techniques for the Analysis of Petroleum, New York City Meeting, pp. 255–264 (1991).
- [8] Speight, J.G., A structural investigation of the constituents of Athabasca bitumen by proton magnetic resonance spectroscopy. *Fuel*, 49: 76–90 (1970).
- [9] Shibata, S., Sandler, S.I. and Behrens, R.L., Phase equilibrium calculations for continuous and semicontinuous mixtures. *Chem. Eng. Sci.*, 42: 8 (1989).
- [10] Speight, J.G., *Fuel Science and Technology Handbook*. Marcel Dekker, New York (1990).
- [11] Nigam, A., *Lumping Analyses of Complex Hydrocarbon Reaction Systems*. Ph.D. Dissertation, University of Delaware, Newark (1992).
- [12] Boduszynski, M.M., Characterization of 'Heavy' crude components. *Am. Chem. Soc., Div. Fuel Chem.* 365–379 (1985).
- [13] Boduszynski, M.M., Composition of heavy petroleum, 2. Molecular characterization. *Energy Fuels*, 2 (5): 597–613 (1988).
- [14] Neurock, M., Libanati, C., Nigam, A. and Klein, M.T., Monte Carlo simulation of complex reaction systems: molecular structure and reactivity in modelling of heavy oils. *Chem. Eng. Sci.*, 45 (8): 2083–2088 (1990).
- [15] Nigam, A., Neurock, M. and Klein, M.T., Reconciliation of molecular detail and lumping: an asphaltene thermolysis example. In: G. Astarita and S.I. Sandler (Editors), *Kinetic and Thermodynamic*



- Lumping of Multicomponent Mixtures*. Elsevier, Amsterdam (1991).
- [16] Savage, P.E. and Klein, M.T., Asphaltene reaction pathways, 2. Pyrolysis of n-pentadecylbenzene. *Ind. Eng. Chem. Res.*, 26 (3): 488–494 (1987).
- [17] Savage, P.E. and Klein, M.T., Discrimination between molecular and free-radical models of 1-phenyl-dodecane pyrolysis. *Ind. Eng. Chem. Res.*, 26: 374 (1987).
- [18] Savage, P.E. and Klein, M.T., Asphaltene reaction pathways, 4. Pyrolysis of tridecylcyclohexane and 2-ethyltetralin. *Ind. Eng. Chem. Res.*, 27: 1348–1356 (1988).
- [19] Savage, P.E. and Klein, M.T., Kinetics of coupled reactions: lumping pentadecylbenzene pyrolysis into three parallel chains. *Chem. Eng. Sci.*, 44 (2): 393–404 (1989).
- [20] Fabuss, B.M., Smith, J.O. and Satterfield, C.N., Thermal cracking of pure saturated hydrocarbons. *Adv. Pet. Chem. Refin.*, 9: 157 (1964).
- [21] Poutsma, M., *A Review of Thermolysis of Model Compounds Relevant to Processing of Coal*. ORNL/TM-10637, Oak Ridge National Laboratory: Chemistry Division, Oak Ridge, TN (1987).
- [22] Rebick, C., Pyrolysis of alpha-olefins — a mechanistic study. In: A.G. Oblad, H.G. Davis and R.T. Eddinger (Editors), *Thermal Hydrocarbon Chemistry*. American Chemical Society, Washington, DC, pp. 1–19 (1979).
- [23] LaMarca, C., *Kinetic Coupling in Multicomponent Pyrolysis Systems*, Ph.D. Dissertation, University of Delaware, Newark (1992).
- [24] Neurock, M., Stark, S.M. and Klein, M.T. In: E.R. Becker and C.J. Pereira (Editors), *Computed-Aided Design of Catalysts*. Marcel Dekker, New York, p. 55 (1993).
- [25] McDermott, J.B., Libanati, C., LaMarca, C. and Klein, M.T., Quantitative use of model compound information: Monte Carlo simulation of the reactions of complex macromolecules. *Ind. Eng. Chem. Res.*, 29 (1): 22–29 (1990).
- [26] Gillespie, D.T., A general method for numerically simulating the stochastic time evolution of coupled chemical reactions. *J. Comp. Phys.*, 22: 403–434 (1976).
- [27] Gillespie, D.T., Exact stochastic simulation of coupled chemical reactions. *J. Phys. Chem.*, 81 (25): 2340–2361 (1977).
- [28] Savage, P.E., Klein, M.T. and Kukes, S.G., Asphaltene reaction pathways, I. Thermolysis. *Ind. Eng. Chem., Proc. Res. Dev.*, 24: 1169 (1985).

## Chapter 5

# THERMODYNAMIC PROPERTIES OF ASPHALTENES: A PREDICTIVE APPROACH BASED ON COMPUTER ASSISTED STRUCTURE ELUCIDATION AND ATOMISTIC SIMULATIONS

M.S. DIALLO, T. CAGIN, J.L. FAULON and W.A. GODDARD III

## INTRODUCTION

Crude oil is a complex mixture of hydrocarbons and heteroatomic organic compounds of varying molecular weight and polarity [1]. A common practice in the petroleum industry is to separate crude oil into four chemically distinct fractions: saturates, aromatics, asphaltenes and resins [1–4]. Asphaltenes are operationally defined as the non-volatile and polar fraction of petroleum that is insoluble in *n*-alkanes (i.e., pentane). Conversely, resins are defined as the non-volatile and polar fraction of crude oil that is soluble in *n*-alkanes (i.e., pentane) and aromatic solvents (i.e., toluene) and insoluble in ethyl acetate. A commonly accepted view in petroleum chemistry is that asphaltenes form micelles which are stabilized by adsorbed resins kept in solution by aromatics [5,6]. Two key parameters that control the stability of asphaltene micelles in a crude oil are the ratio of aromatics to saturates and that of resins to asphaltenes. When these ratios decrease, asphaltene micelles will flocculate and form larger aggregates [7,8]. The precipitation of asphaltene aggregates can cause such severe problems as reservoir plugging and wettability reversal [9,10]. The adsorption of asphaltene aggregates at oil–water interfaces has been shown to cause the steric stabilization of (W/O) petroleum emulsions [11,12]. Consequently, the oil industry is in critical need of quantitative tools and thermodynamic data to predict asphaltene solubility and aggregation as a function of crude oil composition and reservoir temperature and pressure.

Asphaltene aggregation and solubility in crude oil have been the subject of several theoretical investigations. Hirschberg et al. [13] combined Hildebrand regular solution theory with a Flory-Huggins entropy of mixing to express asphaltene solubility in crude oil as a function of molar volume and solubility parameter. Brandt et al. [14] combined a mean field energy of mixing with a modified Flory-Huggins entropy of mixing to describe asphaltene aggregation in a given solvent. They model asphaltene molecules as flat hard discs called ‘unit sheets’ that can ‘stack’ to any arbitrary degree in the solvent. They express the volume fraction of asphaltene ‘stacks’ as a function of asphaltene concentration, asphaltene cohesive/‘stacking’ energy, asphaltene-solvent interaction energy, and asphaltene ‘unit sheet’/‘stack’ excluded volume. Victorov and Firoozabadi [15] have extended the free energy models of amphiphile micellization of Nagarajan and Ruckenstein [16] and Puvvada and Blankschtein [17] to petroleum fluids. Their new thermodynamic model combines a free energy model of micellization with the Peng–Robinson equation of state [18] and express asphaltene solubility

in a crude oil as a function of temperature, pressure, asphaltene–resin concentration, resin–asphaltene interaction energy, resin–crude oil interaction energy and a ‘molecular geometric’ parameter that accounts for resin packing constraints at the surface asphaltene micelles. Rogel [19] has carried out molecular dynamics (MD) simulations of asphaltene aggregation in *n*-heptane, toluene and their mixtures. He reported that the stability of asphaltene aggregates in the mixtures increase with the ratio of *n*-heptane to toluene. Murgich et al. [20] have carried out molecular mechanics calculations of the energies of model asphaltene and resin molecules. They reported that the interactions between the ‘aromatic planes’ of asphaltene molecules was the main driving of their aggregation.

Although these thermodynamic models have resulted in a better understanding of the phase behavior of asphaltic crude oil, the lack of accurate data are major impediments to the utilization of these models in field applications. Because of this lack of thermodynamic data, Hirschberg et al. [13] determined their model input data (solubility parameter and molar volume) by fitting the results of asphaltene solubility measurements to a thermodynamic model of asphaltene precipitation. They assumed an asphaltene molar volume of 4 m<sup>3</sup>/kmol to get “an optimal fit between calculated and experimental data” [13]. Because of the lack of a suitable structural model of asphaltene, Brandlt et al. [14] employed a “polycyclic aromatic compound with saturated substituents” to evaluate two input parameters of their thermodynamic model of asphaltene aggregation. The lack of molecular and thermodynamic data on asphaltenes and resins has also led Victorov and Firoozabadi [15] to make several simplifying assumptions including the use of ‘guessed’ values for the interaction energy of a ‘resin molecule head’ with asphaltene. Such ‘guessed’ values may increase the uncertainties in the predicted solubility of asphaltenes in crude oil.

The petroleum industry is in critical need of experimental and theoretical estimates of asphaltene thermodynamic properties. In this chapter, we describe a new methodology for predicting the thermodynamic properties of petroleum geomacromolecules (asphaltenes and resins). This methodology (Fig. 5-1) combines computer assisted structure elucidation (CASE) with atomistic simulations (molecular mechanics and molecular dynamics and statistical mechanics). To illustrate this new approach, we use quantitative and qualitative structural data as input to a CASE program (SIGNATURE) to generate a sample of ten asphaltene model structures for a Saudi crude oil (Arab Berri). We then carry out MM calculations and MD simulations to estimate selected volumetric and thermal properties of the model structures. We find that the estimated values are in good agreement with the available experimental data.

This chapter is organized as follows. In COMPUTER ASSISTED STRUCTURE ELUCIDATION OF PETROLEUM GEOMACROMOLECULES, we highlight the state-of-the art of CASE. We show that the CASE program SIGNATURE can be used to generate a sample of structural model of asphaltenes that statistically represents the entire population of all the possible structures that can be built from a given set of analytical data. In ESTIMATION OF THERMODYNAMIC PROPERTIES OF CONDENSED PHASE SYSTEMS FROM ATOMISTIC SIMULATIONS, we briefly discuss the estimation of the thermodynamic properties of condensed phase systems from Monte Carlo (MC) and molecular dynamics (MD) simulations. In COMPUTER ASSISTED STRUCTURE ELUCIDATION OF ARAB BERRI

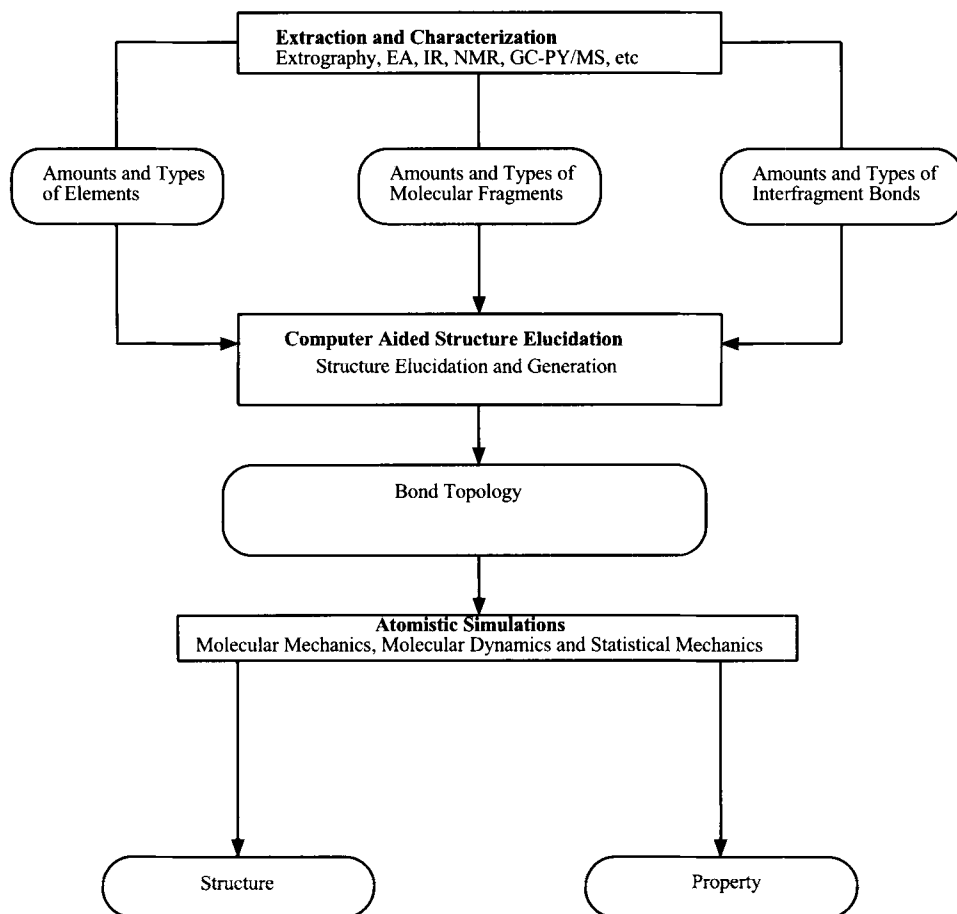


Fig. 5-1. Hierarchical approach for predicting the structures and properties of petroleum geomacromolecules.

ASPHALTENES, we input quantitative and qualitative structural data into SIGNATURE to generate a sample of ten structural models of asphaltene from a Saudi crude oil (Arab Berri). We then use molecular mechanics (MM) calculations and MD simulations to estimate the molar volume, density, cohesive energy, solubility parameter, enthalpy, thermal expansion coefficient and specific heat at constant pressure of the model asphaltene structures in VOLUMETRIC AND THERMAL PROPERTIES OF ARAB BERRI ASPHALTENES FROM MOLECULAR DYNAMIC SIMULATIONS. Finally, we summarize the main results of this work.

#### COMPUTER ASSISTED STRUCTURE ELUCIDATION OF PETROLEUM GEOMACROMOLECULES

Because petroleum geomacromolecules such as asphaltenes are operationally defined as a 'solubility class' of compounds precipitated from crude oil by addition of an excess

amount of aliphatic solvents [1], accurate structural models for these compounds are not currently available. Three approaches may be used to elucidate the structures of complex petroleum geomacromolecules: *conventional*, *deterministic* and *stochastic*.

### *Conventional approach*

The conventional approach to structure elucidation is the traditional means by which chemists infer a structural formula from a set of analytical data. This is essentially a trial-and-error process of manually matching the candidate structure with analytical data. Virtually, all the chemical structures of the compounds known to date have been elucidated using the conventional approach. There are, however, two major impediments to the systematic application of the conventional approach to petroleum geomacromolecules. First, the structure elucidation process is carried out by manual fitting. Thus, it is prohibitively time-consuming for large molecules such as asphaltenes. Second, when several isomers can be built from the same analytical data set, the conventional approach does not provide any means of selecting the 'appropriate' isomer. Consequently, it is often difficult to draw definite conclusions regarding geomacromolecules (i.e., lignin, coal and asphaltene) generated with the conventional approach because of arbitrary isomer selection [21–24].

### *Deterministic approach*

The deterministic approach is predicated upon the retrieval of all the structural models of a compound from a given set of structural data. For the past 25 years, there has been many attempts to automate the deterministic approach. Several techniques and computer programs have been proposed under the generic name *computer assisted structure elucidation* (CASE). The first CASE program capable of enumerating all the acyclic structures from a molecular formula is believed to be that of Lederberg et al. [25]. This program, which evolved out of the DENDRAL project, was the precursor of CONGEN [26] and GENOA [27], the first CASE expert systems ever published. CONGEN and GENOA can handle any structure and enumerate the isomers of a molecular formula. These can also be used to generate structures with more restrictive constraints, e.g. isomers with specified molecular fragments. However, both GENOA and CONGEN use more heuristic than systematic algorithms. Moreover, the proof of irredundancy and exhaustivity of the structure generation process was never published, and differences between the structures generated by GENOA/CONGEN and CASE programs have been reported [28]. Several CASE programs based on a more systematic structure generation protocol have been developed as alternatives to GENOA and CONGEN including the structure generators CHEMICS [29–33], ASSEMBLE [34,35] and COMBINE [36]. These programs are based on the concept of the connectivity stack, which allows an exhaustive and unique enumeration [28]. The basic building block of these programs is a set of segments (a segment is a small molecular fragment containing one, two or three atoms) representing the unknown compound. To enumerate the isomers, an exhaustive permutation of all segments is carried out. With the concept of the connectivity stack, redundancies can be avoided without cross-checking the solutions. Using this method,

exhaustivity and irredundancy of the solutions can be easily proven; in fact, all the permutations are considered and all redundant structures are rejected.

The ability of a CASE program to treat redundant information is a central issue in structure elucidation. Because chemical structural data tend to be highly redundant, the molecular fragments used as input to CASE programs generally overlap. The problem of overlapping fragments was studied by Dubois et al. [37,38]. They developed the program DARC-EPIOS [39], which can retrieve structural formulas from overlapping  $^{13}\text{C}$  NMR data. Similar techniques have also been applied with the COMBINE program, while GENOA uses a more general technique based on the determination of all possible combinations of non-overlapping molecular fragments. All the CASE programs described above generate chemical structure by assembling atoms and/or molecular fragments together. More recently, a new strategy based on structure generation by reduction has been proposed to deal with the problem of overlapping fragments [44]. Structure generation by reduction does not create bonds but removes bonds from a *hyperstructure*. Initially, the *hyperstructure* contains all the possible bonds between all the required atoms and molecular fragments. The fragments can overlap. As bonds are removed, the continued containment of each fragment is tested until a valid chemical structure is obtained. Examples of CASE programs based on the concept of structure generation by reduction include COCOA [40] and GEN [41].

Computational complexity is another critical issue in CASE. Because the treatment of overlapping fragments usually results in an exponential increase of computational time as the number of input atoms increase, current CASE programs are ill suited for large systems. In order to limit the number of combinations that generate duplicate structures, several investigators have attempted to optimize existing CASE programs [28,42–45]. The largest reported structure that has been resolved with these optimized CASE programs is a fragment of lignin ( $\text{C}_{116}\text{H}_{126}\text{O}_6$ ) that contains 122 non-hydrogen atoms [28]. Although these optimized programs can handle relatively large structures, the number of atoms or molecular fragments that can be processed by any deterministic CASE program is still limited due to the exponential complexity of the problem of structure elucidation. Consequently, the deterministic approach to structure elucidation is ill suited for large petroleum geomacromolecules such as asphaltenes and kerogen.

### *Stochastic approach*

The stochastic approach to structure elucidation is very similar in approach to the search of the conformational space of a chemical compound by Monte Carlo simulations or simulated annealing to find its lowest energy conformations. However, in the case of structure elucidation, the search space is the finite number of all possible structural isomers that can be constructed from a given set of analytical data. Faulon has shown that by using a stochastic approach [46], it is possible to: (1) generate the total number of model structures that match a given set of analytical data in a reasonable computational time; (2) generate a sample of model structures that statistically represents the entire population of all the possible structures that can be built from a given set of analytical data.

The new CASE program based on this approach, SIGNATURE (Fig. 5-2), (1) determines the best list of molecular fragments and interfragment bonds that best match the

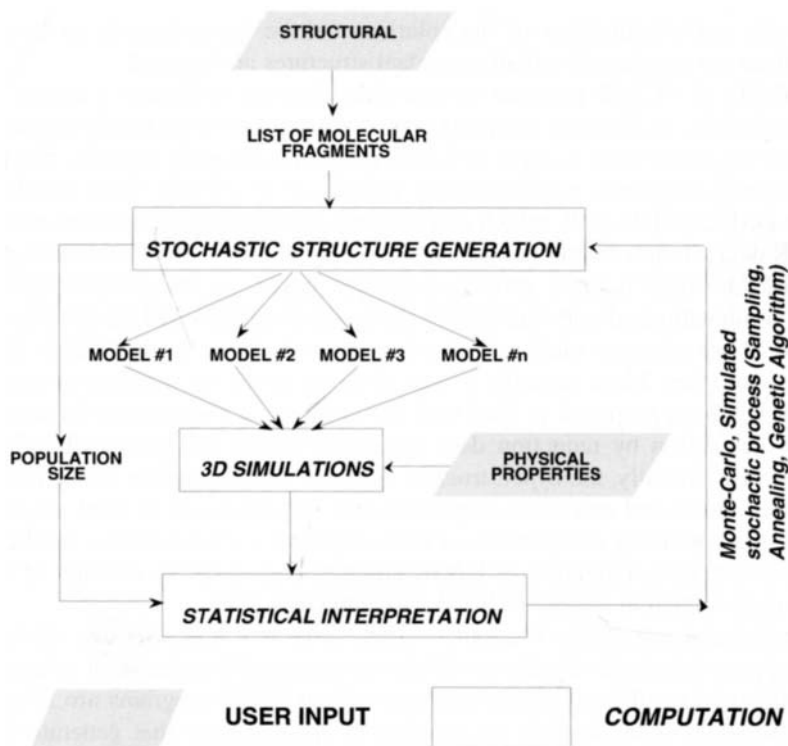


Fig. 5-2. Stochastic generator of chemical structure (SIGNATURE): general program scheme.

experimental data, (2) evaluates the total number of possible structural models that can be generated from (1), and (3) generates a sample of structural formulas that statistically represent the entire population of model structures that can be generated from (1).

SIGNATURE input data can be derived from experimental techniques as diverse as elemental analysis, UV, IR and NMR spectroscopy, GC-MS, vapor pressure osmometry and small angle X-ray/neutron scattering [46]. Thus, SIGNATURE has the inherent capability to generate molecular models of asphaltenes that take into account the properties of a specific crude oil. Kowalewski et al. [47] have recently reported the first utilization of two stochastically based CASE programs (XMOL and SIGNATURE) to generate a sample of ten model structures of asphaltenes from Boscan crude oil, a Venezuelan crude of high asphaltene content.

#### ESTIMATION OF THERMODYNAMIC PROPERTIES OF CONDENSED PHASE SYSTEMS FROM ATOMISTIC SIMULATIONS

Molecular dynamics (MD) and Monte Carlo (MC) simulations have become the most widely used theoretical methods of investigations of condensed phase systems since their inception in the late 1950's [48,49]. These two methods represent two alternatives

but equivalent approaches to the statistical mechanics of  $N$ -body systems. The original form of the Monte Carlo method was developed to model an  $N$ -body system in the canonical (NVT) ensemble. The probability distribution of states ( $\rho$ ) for this ensemble is given by:

$$\rho = \frac{e^{-E/kT}}{Z} \quad (5-1)$$

where  $E$  is the energy of the system,  $T$  is its temperature and  $k$  is the Boltzmann constant. The partition function,  $Z$ , is given by:

$$Z = \frac{1}{C} \int e^{-E/kT} d\tau \quad (5-2)$$

where  $d\tau = (dpdr)^{3N}$  is the differential element in the  $6N$  dimensional phase space of coordinates ( $r$ ) and momenta ( $p = mv$ ) of the  $N$ -body systems,  $m$  and  $v$  are the particle mass and velocity and  $C$  is a normalization constant. A microscopic variable, for instance internal pressure  $\pi(r, p)$ , may therefore be expressed in terms of phase space variables as:

$$\pi(r, p) = \frac{p^2}{mv} - W \quad (5-3)$$

where  $W = \delta U / \delta V$  is the virial, i.e. the volume ( $V$ ) derivative of the potential energy. Conversely, the macroscopic pressure is given by the ensemble average:

$$P = \frac{\int \pi(r, p) e^{-E/kT} d\tau}{\int e^{-E/kT} d\tau} \quad (5-4)$$

In actual MC simulations the kinetic degrees of freedom are not explicitly considered and the statistical mechanics is carried out in the configuration space. Thus, the full partition function is replaced by the configuration partition function and microscopic definitions for state variables are expressed only in terms of configuration variables.

In an MD simulation, a finite number of molecules are allowed to interact via prescribed intermolecular forces in a finite domain. The molecular motions caused by these force fields are deterministic; thus, the positions and energies of the molecules can be determined by solving the corresponding Newton's equations of motion. In the MD simulation methodology, a macroscopic observable  $A$  corresponding to a microscopic descriptor,  $A[p(t), r(t)]$  is given by:

$$A = \lim_{T \rightarrow \infty} = \frac{1}{T} \int_0^T A[p(t), r(t)] dt \quad (5-5)$$

Because an infinite sampling time of phase space is not feasible, current MD simulation codes implement a step-by-step strategy to solve the equations of motion for  $N$ -body systems. For a finite number of time steps  $N_t$  of duration  $\Delta\tau = T/N_t$ ,  $A$  may then be expressed as:

$$A = \frac{1}{N_t} \sum_{\tau=1}^{N_t} A(\tau) \quad (5-6)$$

where  $\tau$  is an index running over the succession of time steps.



MD simulation methodology was initially developed to model an  $N$ -body condensed phase system in the microcanonical (NVE) ensemble. Then in the early 1980s practitioners of the field, recognizing the importance of simulating physical systems under different conditions of temperature, pressure, etc., began developing extended forms of MC and MD for other ensembles (NPT, NVT, NPH, etc.). These advances have resulted in the development a number of theoretical framework for estimating the thermodynamic and structural properties of condensed phase systems from MC and MD simulations [50,51].

The connection between MC/MD simulations and equilibrium thermodynamics is made through statistical mechanics. First-order properties such as internal pressure, internal energy, density are directly obtainable by ensemble/time averaging of the corresponding microscopic quantities. Second-order properties, i.e. thermodynamic and mechanical response functions such as specific heat, isothermal compressibility, thermal expansion etc., may be obtained either using the finite difference approach or by using the appropriate statistical fluctuation formulae corresponding to these properties. To illustrate these two different approaches, consider three commonly used response functions in the isothermal isobaric ensemble (NPT): specific heat at constant pressure ( $C_p$ ), isothermal compressibility ( $K_T$ ) and volumetric thermal expansion coefficient ( $\alpha_p$ ). The finite difference method of estimation of these properties is based on their thermodynamic definitions:

$$C_p = \left( \frac{\partial H}{\partial T} \right)_p \quad (5-7)$$

$$K_T = \frac{1}{V} \left( \frac{\partial V}{\partial P} \right)_T \quad (5-8)$$

$$\alpha_p = \frac{1}{V} \left( \frac{\partial V}{\partial T} \right)_p \quad (5-9)$$

where  $H$  is the enthalpy of the system. The statistical fluctuation formulae for estimating these properties are given by [52]:

$$C_p = \frac{\langle H^2 \rangle - \langle H \rangle^2}{kT^2} \quad (5-10)$$

$$K_T = \frac{\langle V^2 \rangle - \langle V \rangle^2}{\langle V \rangle kT^2} \quad (5-11)$$

$$\alpha_p = \frac{\langle VH \rangle - \langle V \rangle \langle H \rangle}{\langle V \rangle kT^2} \quad (5-12)$$

where the angular brackets represent a time average of the corresponding system property. Eqs. 5-10–5-12 are rigorously valid in the thermodynamic limit of an infinite size system. Derivations for the finite  $N$  case have been made and the exact and thermodynamic limit formulae were compared to Eqs. 5-10–5-12; differences were found to be less significant than the other systematic and random errors for systems of size  $N$  as low as 200–300 particles [52].

## COMPUTER ASSISTED STRUCTURE ELUCIDATION OF ARAB BERRI ASPHALTENES

*Structural input data*

The starting point of any property estimation by atomistic simulations is the bond topology of the compound of interest, that is, a list of connections between all its atoms. Because asphaltenes are operationally defined as a 'solubility class' of compounds precipitated from crude oil by addition of an excess amount of aliphatic solvents [1], the assignment of a precise and definite molecular structure to asphaltenes has been a major challenge to petroleum chemists. Although a precise molecular structure of asphaltene is not currently available, elemental analysis, IR, UV and NMR spectroscopic studies have indicated that asphaltenes consist primarily of naphthenic and naphtenoaromatic rings linked by alkyl side chains [53]. The degree of condensation of the polynuclear aromatic systems of asphaltenes is still not precisely known despite several investigations [54]. However, indirect evidence from pyrolysis studies of asphaltenes indicate a small degree of condensation (less than five) of their polynuclear aromatic systems [53]. Speight [53] in his recent review of the 'molecular nature of petroleum asphaltenes' cited several studies of pyrolysis and 'transalkylation chemistry' showing that asphaltenes contain substantial amounts of alkanes. Strausz and co-workers have used the ability of Ru ion catalyzed oxidation (RICO) to remove aromatics "while leaving aliphatics and naphthenics essentially unaffected" to determine the distribution and number of carbons of *n*-alkyl groups attached to aromatic rings of asphaltenes isolated from Athabasca bitumen [54]. They reported that the alkyl side chains consisted of *n*-alkyl groups with *n* ranging from 1 to 22.

There is ample experimental evidence showing that the heteroatoms of asphaltenes consist primarily of oxygen, sulfur and nitrogen [53]. Oxygen in crude oil asphaltic fractions has been primarily found as carboxylic, phenolic and ketonic groups [53]. Sulfur, on the other hand, has been found as benzothiophenes, naphthenobenzothiophenes, alkyl-alkyl sulfides, alkyl-aryl sulfides and aryl-aryl sulfides, whereas nitrogen is found scattered at various heterocyclic positions [53]. Metals such as vanadium and nickel have also been found in crude oil asphaltic fractions [53]. However, their exact locations in the structural framework of asphaltenes remain to be determined [53]. Because asphaltenes tend to aggregate in various solvents, reported molecular weights of asphaltenes vary considerably throughout the literature [54]. However, Speight has found that the average molecular weights of crude oil asphaltic fractions "fall into a range centered around 2000 daltons" when these were measured by vapor pressure osmometry in highly polar solvents that prevent asphaltene association [53].

As stated in the Introduction, several structural models of asphaltenes have been developed and used for various purposes. Brandt et al. [14], Rogel [19] and Murgich et al. [20] used model asphaltenes in their theoretical investigations of asphaltene aggregation. Yen and co-workers [55–57] also employed a model asphaltene to describe the stacking and flocculation of asphaltenes in crude oil. Similarly, Speight has used a 'low-molecular-weight-high polarity' model asphaltene to gain insight into the chemistry of coking [53]. Although these models have led to some significant insights into the chemistry and phase behavior of asphaltenes, their ability to describe the

TABLE 5-1

SIGNATURE input parameters for Arab Berri crude oil<sup>a</sup> — atomic ratios

Element	% Weight	Atomic ratios	SIGNATURE parameters	
			minimum	maximum
H <sup>b</sup>	7.49	109.60	106.50	110.50
S <sup>b</sup>	5.15	2.35	2.14	4.14
O <sup>b</sup>	2.97	2.71	1.12	3.12
N <sup>c</sup>	0.67	0.80		
C <sup>d</sup> <sub>aromatic</sub>	50		48.00	52.00

<sup>a</sup> Elemental analysis data were taken from Mclean and Kilpatrick [58]. The molecular weight was assumed to be greater than 1224 daltons and less than 2052 daltons.

<sup>b</sup> Atomic ratios normalized per 100 C atoms.

<sup>c</sup> Because the amount of nitrogen is low (<1%), the incorporation of nitrogen in the asphaltene structural framework was not taken into account.

<sup>d</sup> <sup>13</sup>C NMR data were taken from Mclean and Kilpatrick [58].

specific asphaltene chemistry of a given crude oil remain to be established. In this work, we used SIGNATURE to generate a sample of ten structural models of asphaltenes for a Saudi crude (Arab Berri). The elemental analysis and <sup>13</sup>C NMR input data for SIGNATURE were taken from Mclean and Kilpatrick [58] and are given in Table 5-1. The conceptual framework for asphaltene model development was provided by the results of FITR studies of Arab Berri asphaltenes by Mclean and Kilpatrick [58], RICO characterization of Athabasca asphaltenes by Strausz et al. [54] and Speight's recent review of asphaltene chemistry [53]. Thus, in our development of a molecular model for Arab Berri asphaltenes, we have assumed that: (1) the degree of condensation of the naphthenic and/or naphtheno-aromatic rings is less than six; (2) the number of carbon atoms of the alkyl side chains range from four to twenty; (3) oxygen is present predominantly as carboxylic, carbonyl and phenolic groups; (4) sulfur occurs as dibenzopyrene, dibenzothiophene, sulfide and sulfoxide; (5) the molecular weight of asphaltenes is greater than 1000 daltons and less than 2500 daltons.

Because the amount of nitrogen in Arab Berri asphaltenes is relatively low, less than 1% [58], we have not accounted for the possible incorporation of nitrogen into the asphaltene molecular framework. A complete list of the molecular fragments and interfragment bonds used to generate the model asphaltenes from Arab Berri crude oil is given in Table 5-2.

### Model generation

The generation of the asphaltene models for Arab Berri crude oil consisted of two steps: (1) determination of the set of molecular fragments and interfragment bonds that best match the quantitative and qualitative data given in Tables 5-1 and 5-2; (2) generation of a sample of structural models of asphaltenes from fragments found in step (1).

The set of fragments that best match the analytical data (Tables 5-1 and 5-2) was generated by the SIGNATURE program. A simulated annealing search of five

TABLE 5-2

SIGNATURE input parameters for Arab Berri crude oil — list of molecular fragments and interfragment bonds

Linear alkanes	Aromatics	Elements and functional groups	Interfragment bonds
sl4 <sup>a</sup>	sn1 <sup>b</sup>	H	ali_ali <sup>d</sup>
sl5	sn2	O	ali_h
sl6	sn3	S	ali_o
sl7	sn4	CO	ali_s
sl8	sn5	COOH	aro_ali <sup>c</sup>
sl9	aln0 <sup>c</sup>	OH	aro_aro
sl10	aln1	SO	aro_csp2 <sup>f</sup>
sl11	aln2		aro_h
sl12	aln3		aro_h
sl13	aln4		aro_o
sl14	aln5		h_o <sup>g</sup>
sl15	a2n0		o_h
sl16	a2n1		
sl17	a2n2		
sl18	a2n3		
sl19	a3n0		
sl20	a3n1		
	a3n2		
	a4n0		
	a4n1		
	Dibenzopyrene		
	Dibenzothiophene		

<sup>a</sup> sl*i* is a saturated linear alkane containing *i* carbon atoms [59].

<sup>b</sup> sn*i* is a saturated naphthenic ring containing *i* rings [59].

<sup>c</sup> ain*j* is a naphtheno-aromatic group containing *i* aromatic rings and *j* naphthenic rings [59].

<sup>d</sup> ali\_*i* is an sp<sup>3</sup> carbon bonded to atom *i* [59].

<sup>e</sup> aro\_*i* is a resonance carbon bonded to atom *i* [59].

<sup>f</sup> csp2 is an sp<sup>2</sup> carbon [59].

<sup>g</sup> i\_*j* is an element *i* singly bonded to element *j*. [59]

annealing cycles was employed to determine this list. The initial and final annealing temperatures were respectively set equal to 10 and 1000 K. The SIGNATURE output list of molecular fragments is given in Table 5-3. It consists of two aromatics (a3n0 and a4n0), 3 naphtheno-aromatics (a2n2, a2n3 and a3n2), two aliphatic chains (sl7 and sl9), an ether oxygen (O), a carboxylic group (COOH), a sulfide sulfur (S), a heteroaromatic (dibenzothiophene) and 21 hydrogen atoms. The SIGNATURE output list of interfragment bonds is also given in Table 5-3. It consists of fifteen C–H bonds (ali\_h), six C<sub>R</sub>–H bonds (aro\_h), seven C<sub>R</sub>–C<sub>R</sub> (aro\_aro), four C–S bonds (ali\_s), four C–O bonds (ali\_o) and one C<sub>R</sub>–C<sub>sp2</sub> (aro\_csp2) bond. The combination of these molecular fragments and interfragment bonds yield a model asphaltene with a molecular formula C<sub>144</sub>H<sub>156</sub>O<sub>4</sub>S<sub>3</sub>. The average molecular weight of the corresponding model asphaltene molecule is equal to 2044 daltons (Table 5-3). This value compares very favorably with the average molecular weight of 2000 daltons reported in Speight's recent

TABLE 5-3

SIGNATURE output: best list of molecular fragments and interfragment bonds for Arab Berri <sup>a</sup>

Molecular fragments	Number of molecular fragments	Interfragment bonds	Number of interfragment bonds
a2n2	1	ali_s	4
a2n3	1	ali_o	4
a3n0	1	aro_csp2	1
a3n2	1	ali_h	15
a4n0	1	aro_h	6
sl7	2	aro_aro	7
sl9	1		
O	2		
COOH	1		
S	2		
Dibenzothiophene	1		
H	21		

<sup>a</sup> The model Arab Berri asphaltene molecule obtained from SIGNATURE's best solution has the molecular formula  $C_{144}H_{156}O_4S_3$ . Its average molecular weight is 2044 daltons.

review of the 'molecular nature of petroleum asphaltenes' [53]. However, as shown in Table 5-4, the match between the best list of molecular fragments and interfragment bonds is not perfect. For every 100 carbons of the model asphaltene molecule, 0.17 hydrogen atoms and 0.04 oxygen atoms are missing. Similarly, 1.06 sulfur atoms are missing. The average matching between the SIGNATURE solution and the data is approximately to 1.32 atoms missing or in excess for every 100 carbon atoms.

Two isomer construction modes were used to generate a sample of ten model asphaltene isomers that is statistically representative of the entire population of isomers that can be built from the set of molecular fragments and interfragment bonds given in Table 5-3. In the first mode, two samples of ten isomers were generated by directly connecting these fragments. The resulting structures were highly reticulated and thus had very high potential energies. A high degree of reticulation may be the reason why a

TABLE 5-4

SIGNATURE output atomic ratio: model predictions vs. experimental data <sup>a</sup>

Element	SIGNATURE parameters		SIGNATURE solution	Deviation
	minimum	maximum		
H <sup>b</sup>	106.50	110.50	108.33	0.17
S <sup>b</sup>	2.14	4.14	2.77	1.06
O <sup>b</sup>	1.12	3.12	2.08	0.04

<sup>a</sup> The model Arab Berri asphaltene molecule obtained from SIGNATURE's best solution has the molecular formula  $C_{144}H_{156}O_4S_3$ . Its average molecular weight is 2044 daltons. The average matching between SIGNATURE solution and quantitative/qualitative data is 1.319 atoms missing or in excess.

<sup>b</sup> Number of atoms per 100 carbon atoms.

TABLE 5-5

Molar volume, density, cohesive energy and solubility parameter of SIGNATURE model asphaltene isomers

Isomer #	$E^a$ (kcal/mol)	$E_c^b$ (kcal/mol)	$V_m^c$ (cm <sup>3</sup> /mol)	$\rho^d$ (g/cm <sup>3</sup> )	$\delta^e$ (cal <sup>1/2</sup> /cm <sup>3/2</sup> )
1	293.23	148.52	1755.83	1.16	9.20
2	445.82	178.35	1863.26	1.10	9.78
3	625.19	192.62	1730.78	1.18	10.55
4	806.70	146.99	1990.57	1.03	8.59
5	349.17	149.61	1808.77	1.13	9.09
6	350.61	195.04	1919.21	1.06	10.08
7	370.33	171.63	1741.62	1.17	9.93
8	386.01	154.84	1747.94	1.17	9.41
9	457.29	139.92	1863.93	1.10	8.66
10	597.02	149.95	1820.63	1.12	9.07
Average				1.12	9.44
Experiment				1.158 <sup>f</sup>	9.50 <sup>g</sup>

<sup>a</sup> Energy by gas phase minimization.<sup>b</sup> Cohesive energy estimated from NPT molecular dynamics simulations followed by energy minimization.<sup>c</sup> Molar volume estimated from NPT molecular dynamics simulations followed by energy minimization.<sup>d</sup> Density estimated from NPT molecular dynamics simulations followed by energy minimization.<sup>e</sup> Solubility parameter estimated from NPT molecular dynamics simulations followed by energy minimization.<sup>f</sup> Experimental density for Wafra crude oil taken from Yen et al. [65]. This crude oil originates from the Kuwait–Saudi Arabia Neutral Territory.<sup>g</sup> Experimental solubility parameter estimated by fitting asphaltene precipitation data to a thermodynamic model of asphaltene precipitation [13].

stochastically generated model of Boscan asphaltene recently developed by Kowalewski et al. [47] had a very high energy (7000 kcal/mol) even though it was annealed through a series of MD simulations for a total of 150 ps followed by energy minimizations. To reduce the degree of reticulation of the model asphaltenes, the molecular fragments and interfragment bonds from Table 5-3 were combined into segments having an average of 13 carbon atoms prior to model construction. A sample of 10 model asphaltene isomers were generated by direct linkage of these fragments. Each of the ten model isomers was then minimized (rms force of 0.1 kcal mol<sup>-1</sup> Å<sup>-1</sup>) using the Cerius2 molecular modeling software [60]. A Dreiding II force field (EXP-6 potential for the van der Waals interactions and  $\epsilon = 1$ ) were used in all calculations [61]. The charge equilibration procedure ( $Q_{eq}$ ) of Rappe and Goddard was used to determine all partial atomic charges [62]. All non-bond interactions were treated directly using a cutoff distance of 50 Å. The strain energies of the ten model asphaltene isomers are given in Table 5-5. These range from a low value of 293 kcal/mol for model asphaltene isomer #1 to a high value of 806 kcal/mol for model asphaltene isomer #4 and are approximately one order of magnitude lower than that of the most 'stable' conformation of Boscan model asphaltene of Kowalewski et al. [47]. The three dimensional structures of the ten Arab model asphaltene molecules are shown in Figs. 5-3 and 5-4.

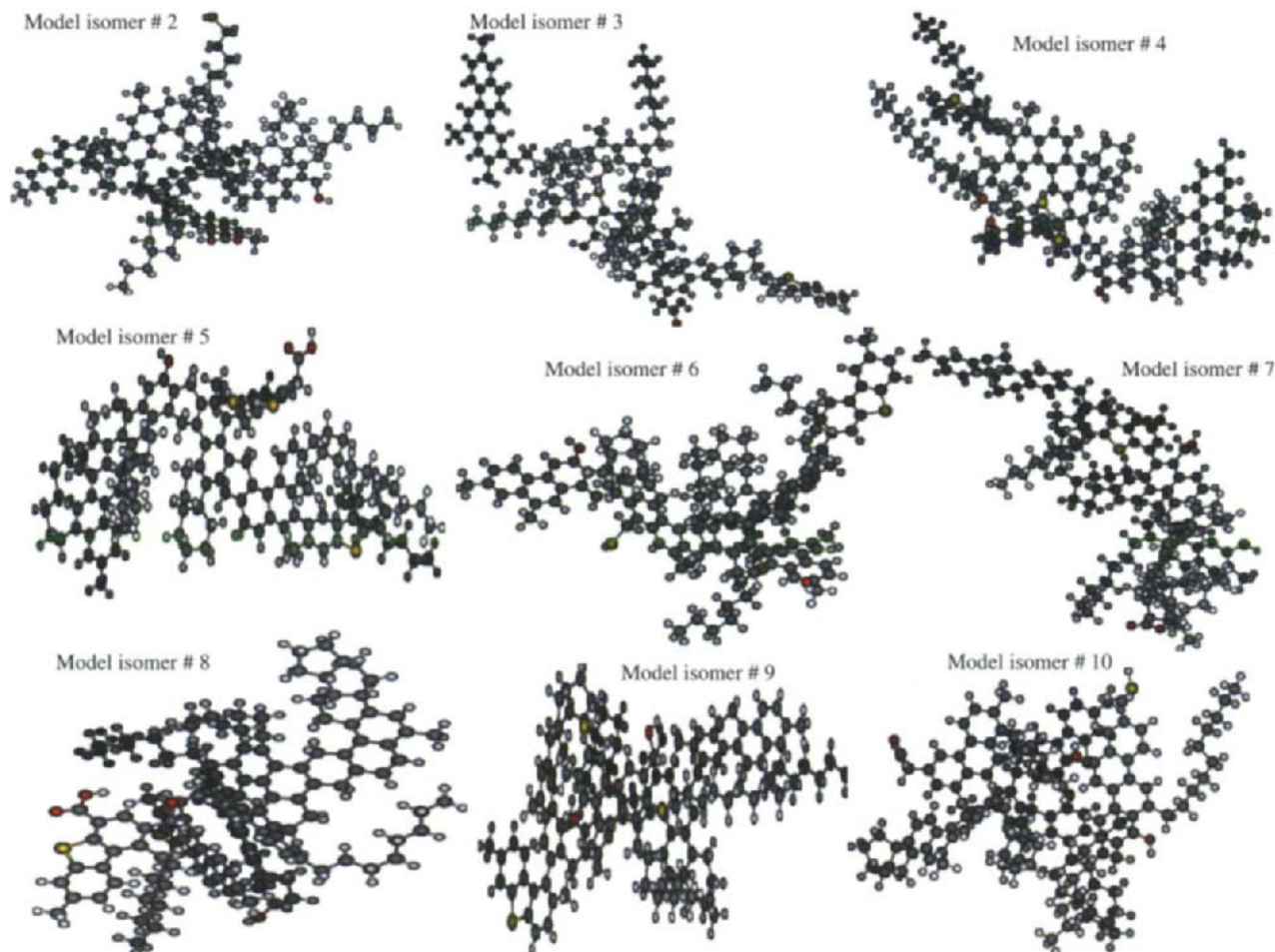


Fig. 5-3. SIGNATURE Arab Berri model asphaltenes.

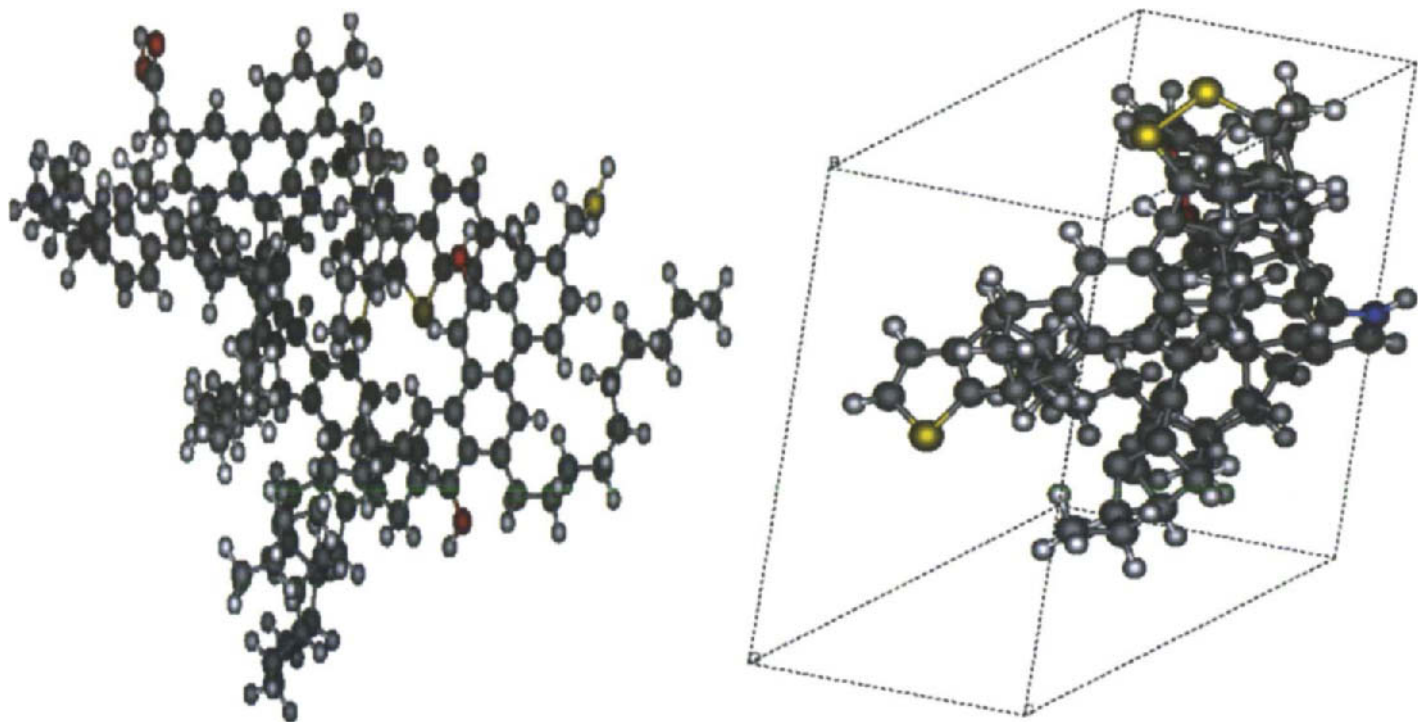


Fig. 5-4. In vacuo and periodic models for SIGNATURE Arab Barri asphaltene isomer #1.



# VOLUMETRIC AND THERMAL PROPERTIES OF ARAB BERRI ASPHALTENES FROM MOLECULAR DYNAMIC SIMULATIONS

## *Molar volume, density, cohesive energy and solubility parameter at 0 K*

Constant-pressure and constant-temperature (NPT) MD simulations followed by energy minimization were carried out to determine selected thermodynamic properties of the ten model asphaltene isomers using Cerius2 [60]. For the isolated molecules (gas phase simulations), the procedures used to treat the non-bond interactions were similar to those employed in the minimization of the ten model asphaltene isomers. For the bulk phase simulations, periodic boundary conditions were applied to each model asphaltene isomer. Ewald summation was used to calculate the long range interactions in all bulk phase MD simulations [63]. The Berendsen–Gunsteren thermal coupling method (cell mass prefactor of 0.04 and time constant of 0.1) and the Maxwell–Boltzman distribution method of assignment of initial velocities were employed in all MD simulations [60]. Each model was first minimized (rms force of  $0.1 \text{ kcal mol}^{-1} \text{ \AA}^{-1}$ ) and then placed into a 3-D cell with periodic boundary conditions. The resulting periodic structure was then minimized using Cerius2's Crystal Packer module [60]. Following this, each model was annealed by 10 ps of NPT dynamics at 300 K followed by minimization. The cell volume  $V_p$  and the strain energy  $E_p/E_{np}$  in the periodic cell/vacuum were then calculated. The molar volume ( $V_m$ ), density ( $\rho$ ) and cohesive energy ( $E_c$ ) of each model asphaltene were expressed as:

$$V_m = N_a V_p \quad (5-13)$$

$$\rho = \frac{M_w}{V_m} \quad (5-14)$$

$$E_c = -(E_p - E_{np}) \quad (5-15)$$

where  $N_a$  is Avagadro's number and  $M_w$  is the molecular weight of the SIGNATURE model asphaltene isomer estimated to 2044 daltons (Table 5-3).

Following Barton [64], the solubility parameter ( $\delta$ ) was expressed as:

$$\delta = \left( \frac{E_c}{V_m} \right)^{0.5} \quad (5-16)$$

The molar volumes, densities, cohesive energies and solubility parameters of the model asphaltene isomers at 0 K are given in Table 5-5. The densities vary from a minimum value of  $1.08 \text{ g/cm}^3$  for asphaltene model # 4 to a maximum value of  $1.18 \text{ g/cm}^3$  for asphaltene model # 3. Except for asphaltene model #4, the estimated densities compare favorably with the measured density of asphaltene ( $1.158 \text{ g/cm}^3$ ) for Wafra crude oil reported by Yen et al. [65]. This crude oil originates from a reservoir located at the Kuwait Saudi Neutral Territory. Similarly, the estimated solubility parameters, which range from a minimum value of  $8.66 \text{ cal}^{1/2}/\text{cm}^{3/2}$  for asphaltene model #4 to a maximum value of  $10.55 \text{ cal}^{1/2}/\text{cm}^{3/2}$ , compare favorably with the experimental value of  $9.50 \text{ cal}^{1/2}/\text{cm}^{3/2}$  reported by Hirschberg et al. [13].

*Effects of temperature and pressure on molar volume, solubility parameters and enthalpy*

NPT MD simulations were carried out to assess the effects of temperature and pressure on the molar volume, solubility parameter and enthalpy of model asphaltene isomer #1 (Fig. 5-4). This isomer was selected because it has the lowest energy (293 kcal/mol, see Table 5-5). The annealed and minimized 3-D periodic structure of the model asphaltene was first equilibrated for 20 ps at the specified temperatures and pressures. This was followed by 25 ps of NPT dynamics during which a trajectory frame was saved every 100 fs. The values of the cell volume ( $V_p$ ), strain energy ( $E_p$ ) in the periodic cell and enthalpy ( $H_p$ ) at each time step and those of the strain energy in vacuum ( $E_{np}$ ) at every time step of 100 fs were averaged to compute the molar volume ( $V_m$ ), solubility parameter ( $\delta$ ) and enthalpy ( $H$ ) of asphaltene model # 1. The results of these calculations are summarized in Tables 5-6 and 5-7.

TABLE 5-6

Molar volume, solubility parameter and enthalpy of SIGNATURE model asphaltene isomer #1 as a function of temperature for  $P = 100$  bar

Temperature (K)	$V_m^a$ (cm <sup>3</sup> /mol)	$\delta^b$ (cal <sup>1/2</sup> /cm <sup>3/2</sup> )	$H^c$ (kcal/mol)
200	1808.50	8.67	517.21
250	1798.45	8.66	600.52
350	1869.54	8.15	785.27
400	1863.25	8.15	877.71
500	1874.94	8.00	1092.21

<sup>a</sup> Molar volume estimated from lattice NPT molecular dynamics simulations.

<sup>b</sup> Solubility parameter estimated from lattice NPT molecular dynamics simulations.

<sup>c</sup> Enthalpy estimated from lattice NPT molecular dynamics simulations.

TABLE 5-7

Molar volume and solubility parameter of SIGNATURE model asphaltene isomer #1 as a function of pressure at  $T = 300$  K

Pressure (bar)	$V_m^a$ (cm <sup>3</sup> /mol)	$\delta^b$ (cal <sup>1/2</sup> /cm <sup>3/2</sup> )	$H^c$ (kcal/mol)
200	1886.46	8.09	699.00
400	1870.37	8.20	703.67
600	1868.24	8.22	699.41
800	1865.76	8.18	699.09
1000	1893.32	8.15	699.15

<sup>a</sup> Molar volume estimated from lattice NPT molecular dynamics simulations.

<sup>b</sup> Solubility parameter estimated from lattice NPT molecular dynamics simulations.

<sup>c</sup> Enthalpy estimated from lattice NPT molecular dynamics simulations.

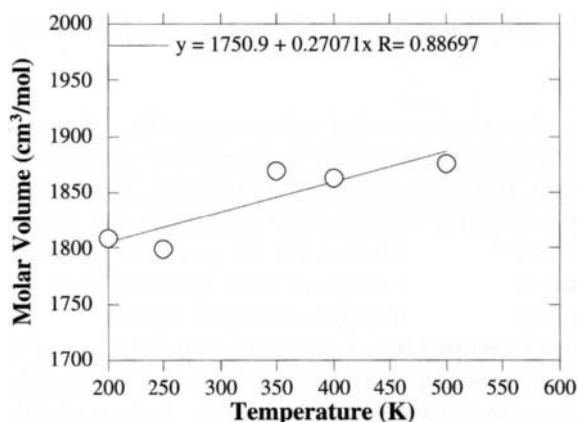


Fig. 5-5. Molar volume of asphaltene model isomer #1 as a function of temperature for  $P = 100$  bar.

TABLE 5-8

Volumetric and thermal properties of SIGNATURE asphaltene model 1 and selected hydrocarbons at  $T = 300$  K

Compounds	$\rho$ (g/cm <sup>3</sup> )	$\delta$ (cal <sup>1/2</sup> /cm <sup>3/2</sup> )	$C_p$ (J g <sup>-1</sup> K <sup>-1</sup> )	$\alpha_p$ (K <sup>-1</sup> )
Asphaltene model 1	1.12 <sup>a</sup>	8.97 <sup>a</sup>	3.71 <sup>a</sup>	$1.49 \times 10^{-4}$ <sup>a</sup>
Decane	0.72 <sup>b</sup>	7.72 <sup>c</sup>	2.20 <sup>d</sup>	$1.02 \times 10^{-3}$ <sup>d</sup>
Benzene	0.88 <sup>b</sup>	9.17 <sup>c</sup>	1.74 <sup>d</sup>	$1.14 \times 10^{-3}$ <sup>d</sup>
Toluene	0.86 <sup>b</sup>	8.88 <sup>c</sup>	1.70 <sup>d</sup>	$1.05 \times 10^{-3}$ <sup>d</sup>
Naphthalene	1.20 <sup>b</sup>	9.91 <sup>c</sup>	1.12 <sup>d</sup>	$0.28 \times 10^{-4}$ <sup>e</sup>
Anthracene	1.19 <sup>b</sup>	9.91 <sup>c</sup>	1.19 <sup>d</sup>	$1.57 \times 10^{-4}$ <sup>e</sup>
Phenanthrene	1.13 <sup>b</sup>	9.76 <sup>c</sup>	1.24 <sup>d</sup>	$2.56 \times 10^{-4}$ <sup>e</sup>

<sup>a</sup> Estimated from NPT molecular dynamics simulations at  $P = 100$  bar.

<sup>b</sup> Estimated from molar volume ( $P = 1$  bar) data taken from Ref. [64].

<sup>c</sup> Experimental solubility parameter at  $P = 1$  bar taken from Ref. [64].

<sup>d</sup> Experimental data ( $P = 1$  bar) taken from Ref. [66].

<sup>e</sup> Experimental data from Ref. [67].

The effect of temperature on the molar volume  $V_m$  of asphaltene model # 1 for a pressure  $P = 100$  bar is depicted in Fig. 5-5. The symbols represent calculated molar volumes; the solid line is a linear regression line through the data points. Fig. 5-5 clearly shows that the molar volume of asphaltene model # 1 increases linearly with temperature. From the slope of Fig. 5-5, we estimate the thermal expansion coefficient  $\alpha_p$  (Eq. 5-9) for Arab Berri model asphaltene isomer # 1 ( $T = 300$  K and  $P = 100$  bar) to be approximately equal to  $1.49 \times 10^{-4}$  K<sup>-1</sup>. This value is approximately one order of magnitude smaller than those of the liquid hydrocarbons (decane, benzene and toluene) given in Table 5-8. However, it is of the same order of magnitude as those of the polycyclic aromatic hydrocarbons (PAHs) and is approximately equal to that of anthracene ( $1.57 \times 10^{-4}$  K<sup>-1</sup>). Using the molar volume data of Table 5-6,

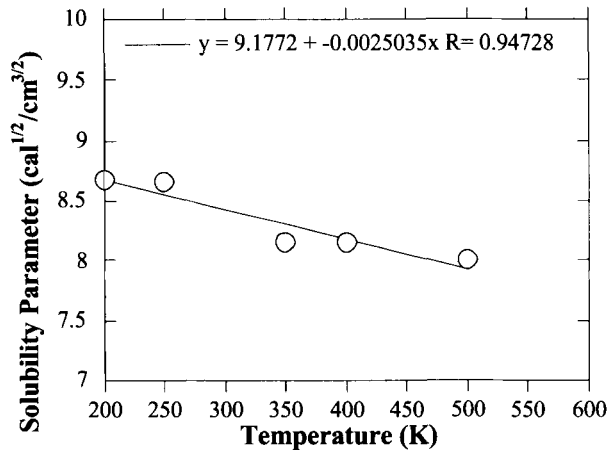


Fig. 5-6. Solubility parameter of asphaltene model isomer #1 as a function of temperature for  $P = 100$  bar.

we estimate the density of SIGNATURE model asphaltene # 1 ( $T = 300$  K,  $P = 100$  bar) to be equal to  $1.12 \text{ g/cm}^3$ . This value is substantially higher than those of decane ( $0.72 \text{ g/cm}^3$ ), benzene ( $0.88 \text{ g/cm}^3$ ) and toluene ( $0.86 \text{ g/cm}^3$ ) given in Table 5-8. It is, however, slightly lower than those of naphthalene ( $1.20 \text{ g/cm}^3$ ), and anthracene ( $1.19 \text{ g/cm}^3$ ) and approximately equal to that of phenanthrene ( $1.13 \text{ g/cm}^3$ ). This closeness between the values of the molar volume, density and thermal expansion coefficient for Arab Berri model asphaltene isomer # 1 and the PAHs is not surprising. It is consistent with the presence of aromatic rings of small degree of condensation (less than 5) in the structural framework of Arab Berri asphaltene model #1 (Fig. 5-4).

The effect of temperature on the solubility parameter of model asphaltene isomer #1 at  $P = 100$  bar is shown in Fig. 5-6. The symbols are calculated solubility parameters; the solid line represents a linear regression line through the data points. Despite the scattering of the data, Fig. 5-6 clearly indicates that the solubility parameter of model asphaltene # 1 decreases linearly with temperature. A linear decrease of the asphaltene and naphthalene solubility parameter with temperature has also been reported by Hirschberg et al. [13]. The effect of temperature on the enthalpy of model asphaltene isomer #1 for  $P = 100$  bar is shown in Fig. 5-7. The symbols are calculated enthalpies; the solid line is a linear regression curve through the data points. Fig. 5-7 indicates that the enthalpy of model asphaltene isomer #1 increases linearly with temperature. Because of this linear relationship, we can use Eq. 5-7 to express the specific heat at constant pressure ( $P = 100$  bar) as:

$$C_p = \frac{\int_{T_0}^T dH}{\int_{T_0}^T dT} = \frac{H - H_0}{T - T_0} \quad (5-17)$$

where  $T_0$  is a reference temperature. If we choose  $T_0 = 200$  K, we estimate the value of  $C_p$  to be equal to  $3.72 \text{ J g}^{-1} \text{ K}^{-1}$ . In this case, however, the estimated specific heat of the model asphaltene is closer to that of decane (Table 5-8). This

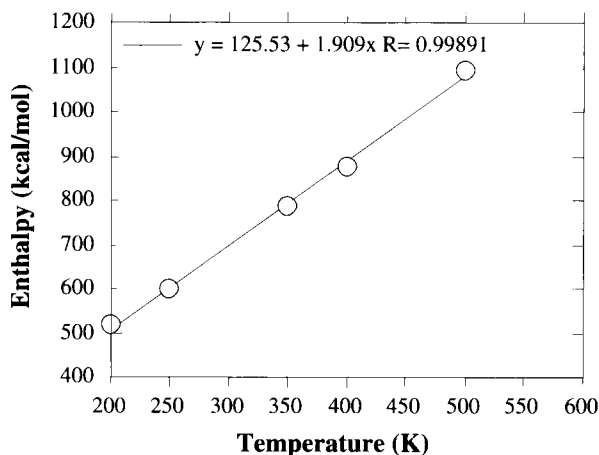


Fig. 5-7. Enthalpy of asphaltene model isomer #1 as a function of temperature for  $P = 100$  bar.

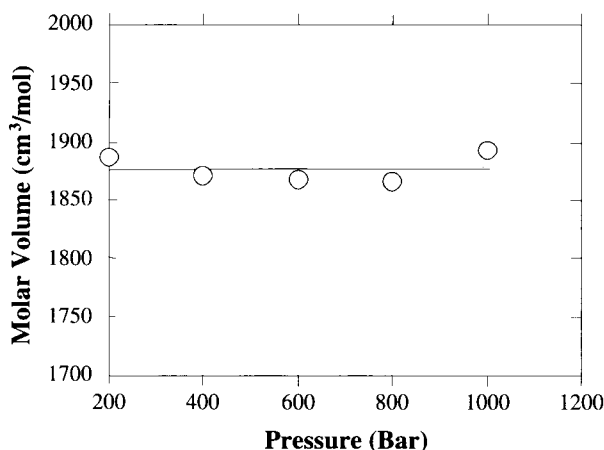


Fig. 5-8. Molar volume of asphaltene model isomer #1 as a function of pressure for  $T = 300$  K.

behavior, which sharply contrasts with those of the molar volume and thermal expansion coefficient, may be attributed for the most part to the flexibility of SIGNATURE model asphaltene isomer #1 and decane. This flexibility is expected to significantly increase the number of vibrational modes of these molecules. Consequently, heating the more flexible asphaltene model isomer #1 and decane will require more energy. Thus, the specific heat at constant pressure of Arab Berri model asphaltene isomer #1 (Fig. 5-4) is expected to be higher than those of the less flexible PAHs.

The effects of pressure on the molar volume, solubility and enthalpy of model asphaltene isomer #1 are depicted in Figs. 5-8 to 5-10. The symbols are calculated values; the solid lines are linear regression lines fitted to the data points. Not surprisingly,

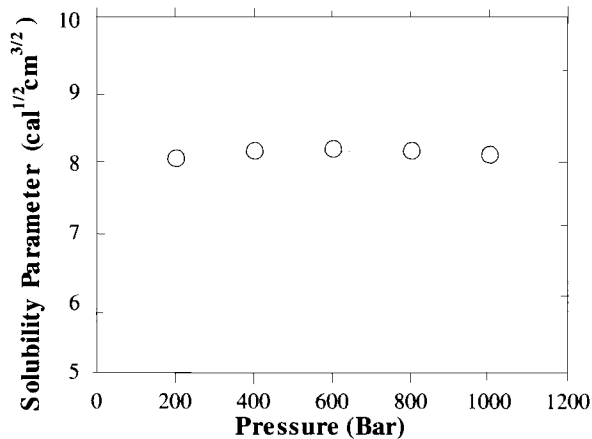


Fig. 5-9. Solubility parameter of asphaltene model isomer #1 as a function of pressure for  $T = 300$  K.

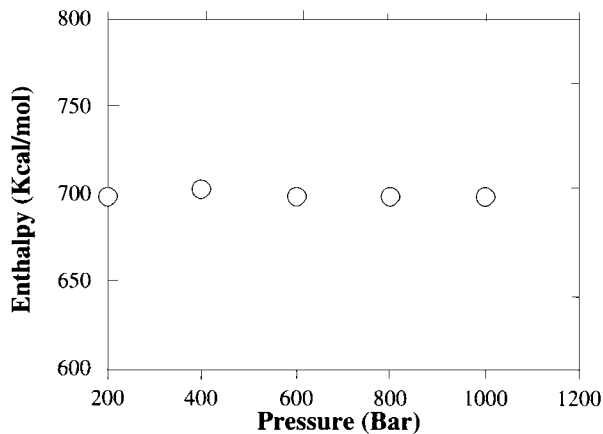


Fig. 5-10. Enthalpy of asphaltene model isomer #1 as a function of pressure for  $T = 300$  K.

Figs. 5-8 to 5-10 indicate that pressure does not very much affect the molar volume, solubility parameter and enthalpy of asphaltene model #1. These results are consistent with a number of observations showing that the molar volume, solubility parameter and enthalpy of liquids and solids are not significantly affected by changes in pressure [64].

#### SUMMARY AND CONCLUSIONS

The precipitation of asphaltene aggregates can cause such severe problems as reservoir plugging and wettability reversal. The adsorption of asphaltene aggregates at oil–water interfaces has been shown to cause the steric stabilization of (W/O) petroleum emulsions. Consequently, the oil industry is in critical need of quantitative tools and

thermodynamic data to predict asphaltene solubility and aggregation as a function of crude oil composition and reservoir temperature and pressure.

This chapter describes a new methodology used in the estimation of the thermodynamic properties of asphaltenes. This methodology combines computer assisted structure elucidation (CASE) with atomistic simulations. To illustrate this new approach, we used quantitative and qualitative structural data as input to a CASE program (SIGNATURE) to generate a sample of ten model asphaltene structures for a Saudi crude oil (Arab Berri). We then carried out molecular mechanics (MM) calculations and molecular dynamics (MD) simulations to estimate selected volumetric and thermal properties of the model structures. We found that the estimated values are in good agreement with the available experimental data. The results of this study suggest that CASE can be combined with atomistic simulations to obtain adequate estimates of the thermodynamic properties of petroleum geomacromolecules such as asphaltenes.

#### ACKNOWLEDGEMENTS

This research was funded by Saudi Aramco and NSF (CHE 95-22179 and ASC 92-17368). The facilities of the MSC are also supported by grants from DOE-BCTR, Chevron Petroleum Technology, Asahi Chemicals, Owens Corning, Chevron Chemical Co., Asahi Glass, Chevron Research and Technology Co., BP Chemical, Hercules, Avery Dennison, and Beckman Institute. We express our gratitude to Dr. Gale Hubred of Chevron Petroleum Technology and Professor Peter Kilpatrick of North Carolina State University for providing unpublished sources of references along with the elemental analysis,  $^{13}\text{C}$  NMR and IR data used to generate the model asphaltenes. MSD thanks Drs Garry Harris and Todd Shurn of the Institute for Multimedia Applications at Howard University for additional computing resources.

#### REFERENCES

- [1] Speight, J.G., *The Chemistry and Technology of Petroleum*. Marcel Dekker, New York (1991).
- [2] Speight, J.G., *Fuel Science and Technology Handbook*. Marcel Dekker, New York (1990).
- [3] Tissot, B.P. and Welte, D.H., *Petroleum Formation and Occurrence*. Springer, New York (1978).
- [4] Miller, R., Hydrocarbon class fractionation with bonded phase liquid chromatography. *Anal. Chem.*, 54: 1742 (1982).
- [5] Pfeiffer, J.P. and Saal, R.N., Asphaltic bitumen as colloid system. *J. Phys. Chem.* 139 (1940).
- [6] Sheu, E.Y., De Tar, M.M., Storm, D.A. and DeCanio, S.J., Aggregation and self-association kinetics of asphaltenes in organic solvents. *Fuel*, 71: 299 (1992).
- [7] Koots, J.A. and Speight, J.G., Relation of petroleum asphaltenes to resins. *Fuel*, 54: 179 (1975).
- [8] Anisimov, M.A., Yudin, I.K., Niktin, V., Nikolaenko, G., Chernoustan, A., Toulhoat, H. and Briolant, Y., Asphaltene aggregation in hydrocarbon solutions studied by photon correlation spectroscopy. *J. Phys. Chem.*, 99: 9576 (1995).
- [9] Leontaritis, K.J. and Mansoori, G.A., Asphaltene deposition: a survey of field experiences and reservoir approached. *J. Pet. Sci. Eng.*, 1: 229 (1988).
- [10] Collins, S.H. and Melrose, J.G., Adsorption of asphaltenes and water on reservoir rock minerals. *SPE Oilfield and Geothermal Chemistry International Symposium*, SPE Pap. 11800, Denver, CO (1983).

- [11] Mansurov, I.R., Il'yasova, E.Z. and Vygovski, V.P., Shear strength of interfacial films of asphaltenes. *Chem. Technol. Fuel Oils*, 23: 96 (1987).
- [12] Taylor, S., Resolving crude oil emulsions. *Chem. Ind.* 770 (1992).
- [13] Hirschberg, A., deJong, L.N.J., Schipper, B.A. and Meijer, J.G., Influence of temperature and pressure on asphaltene flocculation. *Soc. Pet. Eng. J.* June, p. 283 (1984).
- [14] Brandt, H.C.A., Hendriks, E.M., Michels, M.A.J. and Visser, F., Thermodynamic modeling of asphaltene stacking. *J. Phys. Chem.*, 99: 10430 (1995).
- [15] Victorov, A.I. and Firoozabadi, A., Thermodynamic micellization model of asphaltene precipitation from petroleum fluids. *AIChE J.*, 42: 1753 (1996).
- [16] Nagarajan, R. and Ruckenstein, E., Theory of surfactant self assembly. A predictive molecular thermodynamic approach. *Langmuir*, 7: 2934 (1991).
- [17] Puvvada, S. and Blankschtein, D., Molecular thermodynamic approach to predict micellization, phase-behavior and phase-separation of micellar solutions, 1. Application to nonionic surfactants. *J. Chem. Phys.*, 92: 3710 (1992).
- [18] Peng, D.Y. and Robinson, D.B., A new two constant equation of state. *Ind. Eng. Chem.*, 15: 59 (1976).
- [19] Rogel, E., Studies of asphaltene aggregation via computational chemistry. *Colloids Surf. A*, 104: 85 (1995).
- [20] Murgich, J., Rodriguez, J. and Aray, Y., Molecular recognition and molecular mechanics of micelles of some model asphaltenes and resins. *Energy Fuels*, 10: 68 (1996).
- [21] Glasser, W. and Glasser, H.R., Evaluation of lignin's structure by experimental and computer simulation techniques. *Pap. Puu*, 63: 71 (1981).
- [22] Beher, F. and Vandenbroucke, M., Chemical modeling of kerogen. *Org. Geochem.*, 11: 15 (1987).
- [23] Hatcher, P.G., Faulon, J.L., Wenzel, K.A. and Cody, G.D.A., Structural model for lignin derived vitrinite from high-volatile bituminous coal (coalified wood). *Energy Fuels*, 6: 813 (1992).
- [24] Solomon, P.R., Coal structure and thermal decomposition. *ACS Symp. Ser.*, 169: 61 (1981).
- [25] Lederberg, J., Sutherland, G.L., Buchanan, B.G., Feigenbaum, E., Robertson, A.V., Duffield, A.M. and Djerassi, C., Applications of artificial intelligence to chemical inference, I. The number of possible organic compounds acyclic structures C, H, O and N. *J. Am. Chem. Soc.*, 91: 2973 (1969).
- [26] Carhart, R.E., Smith, D.H., Brown, H. and Djerassi, C., Applications of artificial intelligence to chemical inference, XVIII. An approach to computer assisted structure elucidation of molecular structure. *J. Am. Chem. Soc.*, 97: 5755 (1975).
- [27] Smith, D.H., Gray, N.A.B., Nourse, J.G. and Crandell, C.W., The dendral project: recent advances in computer assisted structure elucidation. *Anal. Chim. Acta*, 133: 471 (1981).
- [28] Kudo, Y. and Sasaki, S., The Connectivity Stack. A new format for representation of organic chemical structures. *J. Chem. Soc.*, 14: 200 (1974).
- [29] Kudo, Y. and Sasaki, S., Principles for exhaustive enumeration of unique structure consistent with structural information. *J. Chem. Inf. Comput. Sci.*, 16: 43 (1975).
- [30] Oshima, T., Ishida, Y., Saito, K. and Sasaki, S., Chemics-UBE. A modified system of chemics. *Anal. Chim. Acta*, 122: 95 (1980).
- [31] Abe, H., Okuyama, T., Fujiwara, F. and Sasaki, A., A computer program for generation of constitutionally isomeric structural formulas. *J. Chem. Inf. Comput. Sci.*, 24: 22 (1984).
- [32] Kudo, Y. and Sasaki, S., Structure elucidation system using structural information from multisources: CHEMICS. *J. Chem. Inf. Comput. Sci.*, 25: 252 (1985).
- [33] Funatsu, K., Miyabayashi, N. and Sasaki, S., Further development of structure generation in the automated structure elucidation system. CHEMICS. *J. Chem. Inf. Comput. Sci.*, 28: 9 (1988).
- [34] Shelley, C.A., Hays, T.R., Munk, M.E. and Ramon, R.V., An approach to automated partial structure expansion. *Anal. Chim. Acta*, 103: 121 (1978).
- [35] Shelley, C.A. and Munk, M.E., CASE, a computer model of the structure elucidation process. *Anal. Chim. Acta* 133 (1981).
- [36] Lipkus, A.H. and Munk, M.E., Automated classification of candidate structures for computer assisted structure elucidation. *J. Chem. Inf. Comput. Sci.*, 28: 9 (1988).
- [37] Dubois, J.E., Carebedian, M. and Ancian, B., Automated candidate structures for computer assisted structure elucidation by Carbon-13 NMR: Darc-EPIOS method: search for a discriminant chemical structure displacement relationship. *C. R. Acad. Sci. Ser. C*, 290: 369 (1980).



- [38] Dubois, J.E., Carebedian, M. and Ancian, B., Automated candidate structures for computer assisted structure elucidation by Carbon-13 NMR: Darc-EPIOS method: description of progressive elucidation of ordered intersection of substructures. *C. R. Acad. Sci. Ser. C*, 290: 383 (1980).
- [39] Carabedian, M., Dagane, I. and Dubois, J.E., Elucidation by progressive intersection of ordered substructures from Carbon-13 nuclear magnetic resonance. *Anal. Chem.*, 60: 2186 (1998).
- [40] Christie, B.D. and Munk, M.E., Structure generation by reduction: a new strategy for computer assisted structure elucidation. *J. Chem. Inf. Comput. Sci.*, 28: 87 (1988).
- [41] Bohanec, S. and Zupon, J., Structure generation of constitutional isomers from structural fragments. *J. Chem. Inf. Comput. Sci.*, 31: 531 (1991).
- [42] Bangov, I.P., Computer assisted structure generation from a cross formula 7. Graph isomorphism. A consequence of the vertex equivalence. *J. Chem. Inf. Comput. Sci.*, 34: 277 (1994).
- [43] Contreras, M.L., Rozas, R. and Valdivias, R., Exhaustive generation of organic isomers, 3. Acyclic, cyclic and mixed compounds. *J. Chem. Inf. Comput. Sci.*, 34: 610 (1994).
- [44] Razinger, M., Balasubramanian, K. and Munk, M.E., Automorphism perception algorithms in computer enhanced structure elucidation. *J. Chem. Inf. Comput. Sci.* 197, 1993.
- [45] Faulon, J.L., On using molecular graphs equivalent classes for the structure elucidation of large molecules. *J. Chem. Inf. Comput. Sci.*, 33: 197 (1994).
- [46] Faulon, J.L., Stochastic generator of chemical structure, 1. Application to the structure elucidation of large molecules. *J. Chem. Inf. Comput. Sci.*, 34: 1204 (1994).
- [47] Kowalewski, J., Vandenbroucke, M., Huc, A.Y., Taylor, M.J. and Faulon, J., Preliminary results on molecular modeling of asphaltenes using structure elucidation programs in conjunction with molecular simulation programs. *Energy Fuels*, 10: 87 (1996).
- [48] Metropolis, N., Rosenbluth, A.W., Rosenbluth, M.N. and Teller, A.H., Equation of state calculations by fast computing machines. *J. Chem. Phys.*, 21: 1087 (1953).
- [49] Alder, B.J. and Wainwright, T.E., Phase transition for a hard sphere system. *J. Chem. Phys.*, 27: 1208 (1957).
- [50] Andersen, H.C., Molecular dynamics simulations at constant pressure and/or pressure. *J. Chem. Phys.*, 72: 2384 (1980).
- [51] Nose, S., A unified formulation of the constant temperature molecular dynamics methods. *J. Chem. Phys.*, 81: 511 (1984).
- [52] Cagin, T. and Ray, J.R., Fundamental treatment of molecular dynamics ensembles. *Phys. Rev. A*, 37: 169 (1988).
- [53] Speight, J.G., The molecular nature of petroleum asphaltenes. *Arab. J. Sci. Eng.*, 19: 337 (1994).
- [54] Strausz, O.P., Mojelsky, T.W. and Lown, E.M., The molecular structure of asphaltene — an unfolding story. *Fuel*, 71: 1355 (1992).
- [55] Dickie, J.P. and Yen, T.F., Macrostructures of the asphaltic fractions by various instrumental methods. *Anal. Chem.*, 39: 1847 (1967).
- [56] Dickie, J.P., Haller, N.M. and Yen, T.F., Electron microscopic investigations on the nature of petroleum asphaltenes. *J. Colloid Interface Sci.*, 29: 475 (1969).
- [57] Yen, T.F., Burger, J.W. and Li, N.C., Chemistry of asphaltenes. *ACS Symp. Ser.*, 195: 37 (1981).
- [58] Maclean, J.P. and Kilpatrick, P., Comparison of precipitation and extrography in the fractionation of crude oil residua. *Energy Fuels*, 11: 570 (1997).
- [59] Faulon, J.L., Vandenbroucke, M., Drapier, J.M., Behar, F and Romero, M., 3D chemical models for geological macromolecules. *Org. Geochem.*, 16: 983 (1990).
- [60] Cerius2<sup>TM</sup>. Program developed by BIOSYM/Molecular Simulations.
- [61] Mayo, S.L., Olafson, B.D. and Goddard, W.A., Dreiding: a generic force field. *J. Phys. Chem.*, 93: 7230 (1990).
- [62] Rappe, A.K. and Goddard, W.A., Charge equilibration for molecular dynamics simulations. *J. Phys. Chem.*, 95: 3358 (1985).
- [63] Karasawa, N. and Goddard, W.A., Acceleration of convergence for lattice sums. *J. Phys. Chem.*, 94: 8897 (1989).
- [64] Barton, A.F.M., *CRC Handbook of Solubility Parameters and Other Cohesion Parameters*, 2nd ed. CRC Press, Boca Raton, FL (1991).

- [65] Yen, T.F., Erdman, G. and Hanson, W.E., Reinvestigations of densimetric methods of ring analysis. *J. Chem. Eng. Data*, 6: 443 (1961).
- [66] *CRC Handbook of Chemistry and Physics*, 77th ed. CRC Press, New York (1996–1997).
- [67] Überreiter, V.K. and Orthman, H.J., Spezifische Wärme, spezifische Volumen. Temperature- und Wärmeleitfähigkeit einiger disubstituierter Benzole und polycyclischer Systeme. *Z. Naturforsch.*, 5A: 101 (1950).

This page intentionally left blank

## *Chapter 6*

# **KINETICS AND MECHANISMS OF ASPHALTENE CRACKING DURING PETROLEUM RECOVERY AND PROCESSING OPERATIONS**

A. CHAKMA

## **INTRODUCTION**

Many bitumen and heavy oils produced around the world contain asphaltenes. Asphaltenes play an important role in the recovery, transportation, processing and utilization of bitumen and heavy oil-derived products. For example, asphaltenes may precipitate during recovery and transportation of bitumens/heavy oils [1]. During the upgrading operations, the presence of bitumen may result in the formation of excessive coke in the upgrading reactor. In addition to the above-mentioned implications, asphaltenes are basically heavy-molecular-weight aromatic hydrocarbons with other impurities. Therefore, they represent certain energy values, which should be recovered. This can be achieved by cracking the complex asphaltene structure to obtain useful fuels. In petroleum recovery operations, such as in situ combustion, cracking of asphaltene not only results in lighter useful oil fractions, but the heavier components combine to form coke which serves as the fuel to sustain the in situ combustion process [2–6]. On the processing front, cracking of asphaltenes into lighter useful forms requires innovative processing of the feedstock, frequently in the presence of catalysts [7–11].

Alberta bitumens and heavy oils may be considered to be composed of macro- and micro-structures, as well as chemical constitutive molecules. The macro- and micro-structural arrangements determine the viscosity of the bitumen. Dickie and Yen [12] investigated the macro-structures of the asphaltenes and found them to be composed of polynuclear aromatic molecules with alkyl chains as attachments. These constitutive ‘asphaltene unit molecules’ are grouped in layers having several unit molecules (typically 5 or 6) surrounded or immersed into the maltene (fraction soluble in 40 volumes of *n*-pentane) fluid. The latter is composed of free saturates, mono- and di-aromatics, and resins that may be associated with the asphaltenes. This structural organization may be considered to be the micro-structure of the system. The micro-structure may form aggregates to reduce the free energy of the system. These aggregates form micellar structures that consist of several unit layers of asphaltenes surrounded by or associated with the maltenes. The micellar structures thus formed may be classified as the macro-structures of the system.

The macro-structural arrangement to a large extent depends on the size of the unit asphaltene layers. Low-molecular-weight asphaltenes (MW up to about 1000) consist of single sheets of condensed aromatic and naphthenic rings with relatively alkyl chain attachments. Larger-molecular-weight asphaltenes may consist of several sheets of condensed ring systems. Speight [13] proposed a hypothetical structure consisting

TABLE 6-1

Structural parameters for asphaltene (after Savage and Klein [26])

Atomic H/C ratio	1.09–1.29
Fraction of C atoms in aromatic rings	0.30–0.61
Fraction of C atoms in saturated rings	0.06–0.24
Fraction of H atoms in aromatic rings	0.04–0.11
Fraction of H atoms in saturated rings	0.16–0.19
Ratio of peripheral aromatic C atoms over total aromatic carbon atoms	0.31–0.55

of 12 condensed aromatic rings for Athabasca asphaltene. These individual structures may be connected together by various aliphatic, naphthenic or heteroatomic linkages [14–16]. A review on the molecular structure of asphaltenes has been provided by Speight [17]. Mojelsky et al. [18] have utilized Ru ion catalyzed oxidation reaction to determine various structural features of asphaltenes derived from different Alberta Oil Sand bitumen and heavy oils. The authors report on the determination of total number of alkyl chains, chain length and the number of carbon atoms with each chain and also on the total number and length of the bridge connecting two aromatic rings in the asphaltene molecule.

The length of the alkyl chain has been the subject of numerous studies. Spectrometric studies of asphaltene structure suggests the alkyl chains to be 3 to 6 carbon atoms long [19–22]. However, analysis of the asphaltene pyrolysis products reveal the presence of alkyl chains of up to carbon number  $C_{30}$  [13,23–25]. These alkyl chains are thought to be covalently bound to the core asphaltene unit. These bonds can be broken with activation energies of about 50 kcal/mol [26]. A summary of the structural parameters of asphaltenes is given in Table 6-1.

C–C bonds in aromatic rings are the most abundant. They are the most stable ones. However, the aliphatic C–C bonds found in alkylaromatic, alkylhydroaromatic and alkylnaphthenic positions are the most reactive ones in the temperature range of 300° to 550°C [24].

## KINETICS

Thermal cracking of hydrocarbons has generated much interest since the early days of the industrial revolution. The first systematic theory on thermal cracking was postulated by Rice in 1931 [27]. He proposed the formation of free radicals for the decomposition of the hydrocarbons.

For light hydrocarbons, the theory of Kossiakoff and Rice [28] can predict the product distributions very well. For example, product distribution arising from the cracking of *n*-nonane [29] can be predicted within 20% of the experimental data using the Kossiakoff and Rice [28] theory. Gates et al. [30] found the theory to be able to predict product distribution resulting from the thermal cracking of *n*-hexadecane well. However, the predictions for the cracking of high-molecular-weight hydrocarbons deviate considerably [31]. Blouri et al. [31] studied the cracking of *n*-hexadecane, 6-methyleicosane

and 1-phenyldodecane under relatively mild temperature (350° to 440°C) under high pressure (20 bar). They found the cracking process to follow a molecular mechanism; however, the kinetic data were similar to those of radical cracking.

## ASPHALTENE

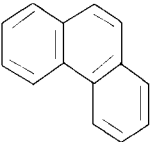
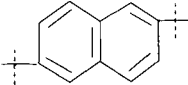
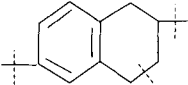
A number of studies on the cracking of asphaltenes have been reported in the literature. Most of them, however, dealt with the determination of the asphaltene structures. Moschopedis et al. [32] carried out thermal decomposition of asphaltenes in a horizontal tube reactor and analyzed the gaseous and liquid products. Ritchie et al. [23] pyrolyzed Athabasca asphaltenes and analyzed the volatile products by GC/MS.

Schucker [33] reported a thermogravimetric study of the coking kinetics of Arab heavy vacuum residuum. As a part of his investigation, he also studied the coking kinetics of the asphaltene fraction derived from the Arab heavy vacuum residuum. Inasmuch as the kinetic study was purely based on the weight loss measurement, it was not possible to analyze the reaction products. Therefore, the kinetic data obtained were for the overall disappearance of the asphaltenes. The authors found the activation energies to increase with conversion ranging from 176 kJ/mol at 20% conversion to 336.5 kJ/mol at 90% conversion. This is quite understandable. First, the lighter fractions of the asphaltenes volatilize followed by the heavier fractions. Therefore, the initial activation energies are lower, representing the lighter fractions; however, they increase when the heavier fractions are cracked.

Major constitutive asphaltene groups and their primary cracking products are listed in Table 6-2.

TABLE 6-2

Principal reaction and reaction products obtained from the cracking of major hydrocarbon groups belonging to the asphaltene molecule (adapted from Voge, [34])

Hydrocarbon class	Structure	Principal reactions	Principal products
Aromatic compounds without side chains		Negligible cracking	Coke
Aromatic compounds with side chains		Cleavage of peripheral chains	Aromatic compounds and olefins
Naphtheno-aromatic compounds		Cleavage of peripheral chains and opening of naphthenic ring	Aromatic compounds, olefins and paraffins

The groups shown in Table 6-2 are typical ring structures present in the asphaltenes. Whereas some information on asphaltene cracking characteristics may be obtained by studying the cracking mechanisms of these typical structures, it is not practical to determine reaction kinetics for asphaltene cracking from the cracking studies involving individual groups due to the complexity of the asphaltene structure and the presence of many other minor groups. As a result, kinetic studies on asphaltene cracking usually involve an easily quantifiable pseudo-component approach, where reaction products are grouped according to solubility and/or boiling point characteristics.

Hayashitani et al. [35] were the first investigators to carry out extensive kinetic experiments on the cracking of Athabasca bitumen using a pseudo-component approach. Although the focus of their study was on Athabasca bitumen, various reaction mechanisms postulated by the authors centered around asphaltenes. Hence, the kinetic models proposed can also be classified as asphaltene cracking models. These authors carried out thermal cracking of Athabasca bitumen, asphaltenes, and heavy oils (BP 400°C<sup>+</sup>) and oils (BP 200° to 400°C) fractions separated from the original bitumen, at constant temperatures in a batch reactor. The reactor was equipped with a quartz tube liner, which prevented the reactants and the reaction products from directly contacting the vessel surface. An inert atmosphere was maintained inside the reactor by pressurizing it with helium. The temperature range studied was from 303°C to 452°C. The reaction products were separated into six pseudo-components: coke, asphaltenes, heavy oils (BP 400°C<sup>+</sup>), middle oils (BP 200° to 400°C), light oils (BP 20° to 200°C) and gases.

The cracking of bitumen was found to yield all the above six pseudo-components. When asphaltenes were used as feed material, large amounts of coke and heavy oils were obtained along with small amounts of middle and light oils and gases. Cracking of the heavy oil fraction led to the formation of mainly middle and light oils and some asphaltenes. Coke formation from the heavy oil fraction was found to be negligible. Finally, the middle oil fraction yielded mostly light oils.

Based on the above observations, Hayashitani et al. [36] proposed four reaction mechanisms. They correlated the reaction rate constants for each of the reaction mechanisms by an Arrhenius type expression. The activation energies and the frequency factors are given in Tables 6-3 and 6-4.

TABLE 6-3

Frequency factors (in s<sup>-1</sup>) for the different models

	$k_1$	$k_2$	$k_3$	$k_4$	$k_5$	$k_6$
Model H1	$5.04 \times 10^{11}$	$1.17 \times 10^{18}$	$1.91 \times 10^{16}$	$4.42 \times 10^{14}$	$4.44 \times 10^{14}$	—
Model H2	$1.41 \times 10^{11}$	$1.53 \times 10^{17}$	$8.44 \times 10^{15}$	$4.50 \times 10^{14}$	$4.55 \times 10^{14}$	$1.49 \times 10^{14}$
Model H3	$2.04 \times 10^{10}$	$6.07 \times 10^{16}$	$1.18 \times 10^{15}$	$4.45 \times 10^{14}$	$8.18 \times 10^{12}$	$2.90 \times 10^{14}$
Model H4	$1.01 \times 10^{11}$	$1.40 \times 10^{16}$	$7.28 \times 10^{14}$	$1.43 \times 10^{14}$	$1.51 \times 10^{14}$	$3.00 \times 10^{14}$

TABLE 6-4

Activation energy (in kcal/mol) for the different rate models

	$k_1$	$k_2$	$k_3$	$k_4$	$k_5$	$k_6$
Model H1	48.1	67.8	64.1	57.5	59.1	—
Model H2	46.5	65.2	62.8	57.5	58.9	57.4
Model H3	44.2	65.1	60.3	57.4	53.6	55.9
Model H4	46.3	63.8	59.6	56.2	57.6	55.6

The corresponding reaction mechanisms are summarized as follows:

Model H1

In their first model, Hayashitani et al. [36] lumped middle oils, light oils and gases into a single pseudo-component, called distillable oil, and postulated the scheme shown in Fig. 6-1.

This model was able to provide reasonable predictions of the concentration versus time curves for the various pseudo-components. Addition of an additional reaction, **asphaltene** → **distillable oil**, did not improve the model's performance.

Among the major drawbacks of this model was its inability to predict (i) the initial sharp decrease in the asphaltene concentration, (ii) initial increase in the heavy oil production, and (iii) initial delay in the coke production.

Model H2

Because gases belong to a distinct group themselves, in their second model, Hayashitani et al. [36] separated gases from the distillable oil fractions. The model presented in Fig. 6-2 is the result.

This model predicted the formation of gases very well, whereas the prediction for

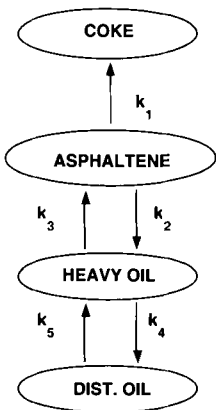


Fig. 6-1. Model H1 — asphaltene cracking model of Hayashitani et al. [36].



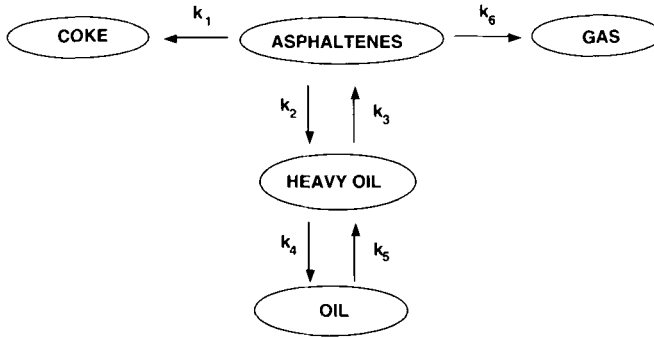


Fig. 6-2. Model H2 — asphaltene cracking model of Hayashitani et al. [35].

other pseudo-components were similar to Model H1. However, it was not able to overcome the earlier-mentioned limitations of Model H1.

### Model H3

In their third model, Hayashitani et al. [35] subdivided the asphaltene fraction into two subfractions, asphaltene-1 and asphaltene-2, in an effort to improve the model performance in describing the initial sharp decrease in asphaltene concentration. Otherwise, Model H3 was similar to Model H1. Asphaltene-1 subfraction was assumed to yield only heavy oil, whereas the asphaltene-2 subfraction was assumed to produce both heavy oil and coke upon cracking. Model H3 is summarized in Fig. 6-3.

Model H3 was able to provide a somewhat better representation of the concentration versus time curves for the asphaltene and coke fractions compared to Models H1 and H2.

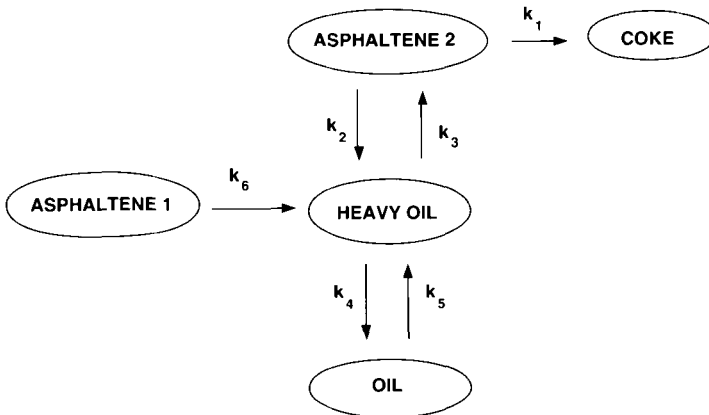


Fig. 6-3. Model H3 — asphaltene cracking model of Hayashitani et al. [35].

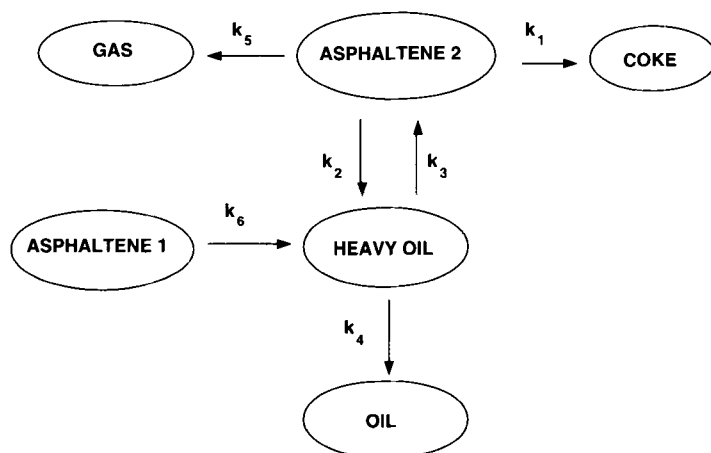


Fig. 6-4. Model H4 — asphaltene cracking model of Hayashitani et al. [36].

#### Model H4

Model H4 is a combination of Models H2 and H3 and as such incorporates all the favorable features of these two models. It is summarized in Fig. 6-4.

Savage et al. [26] pyrolyzed asphaltenes separated from offshore Californian crude oil by precipitation with 40 vol of *n*-heptane at temperatures ranging from 350° to 565°C in batch reactors to study asphaltene reaction mechanisms. They assumed an asphaltene unit to consist of condensed aromatic ring systems with heteroatomic, alkyl and naphthenic substituents. These single units were linked through linkages located along their peripheries. At low temperatures, they found that H<sub>2</sub>S and CO<sub>2</sub> are the primary products and attributed their formation to the fission of peripheral thioether and carboxylic acid moieties, respectively. Hydrocarbon gases, cycloalkanes, and paraffins were the primary products for high-temperature conditions arising from the fission of C–C bonds. Based on their experimental observations, they concluded that coke, maltenes and gas are produced from the primary reactions. Maltenes are cracked into lower-molecular-weight maltenes and additional gas is produced from the coke and lower-molecular-weight maltene fractions. The reaction scheme is shown in Fig. 6-5. However, these authors do not provide any rate constants.

Phillips et al. [37] studied the thermal cracking of Athabasca bitumen and its components in a batch reactor at temperatures ranging from 360° to 420°C in the presence of sand. They divided the products into six pseudo-components: coke, asphaltenes, heavy oils, middle oils, light oils and gases. They proposed the following two kinetic models.

#### Model P1

In the first model (Model P1), following Hayashitani's Model H1, they combined the middle oils, light oils and the gases into a single pseudo-component called distillables. They proposed the reaction mechanism shown in Fig. 6-6.

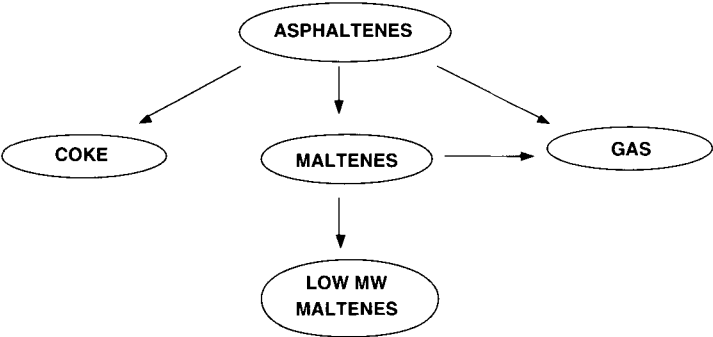


Fig. 6-5. Asphaltene cracking mechanism of Savage et al. [26].

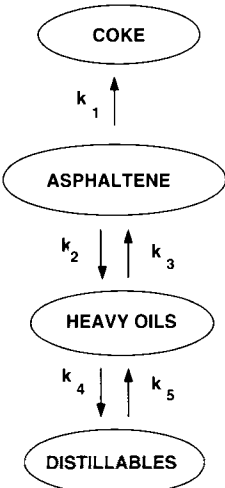


Fig. 6-6. Model P1 — asphaltene cracking mechanism of Phillips et al. [37].

They found the reaction kinetics to be of first order and to follow the Arrhenius relationship. The presence of sand was found to affect the distribution of products and resulted in the lowering of activation energies of the reactions. The authors attribute this effect to the catalytic role played by the sand matrix. Table 6-5 shows a comparison of the kinetic parameters for the model in the presence of sand with the thermal cracking data of Hayashitani et al. [36].

*Model P2*

The second model of Phillips et al. [37] included all the six pseudo-components, as shown in Fig. 6-7.

In Table 6-6, the kinetic constants for this model are compared with those obtained from thermal cracking studies of Hayashitani et al. [36].

Hayashitani et al. [36] obtained high activation energies for the reactions asphaltene

TABLE 6-5

Comparison of kinetic parameters of Model P1 with the thermal cracking data of Hayashitani et al. [36]

Rate constant	Activation energy, $E$ , with sand (kJ/mol)	Activation energy, $E$ , without sand (kJ/mol)	Frequency factor ( $s^{-1}$ )
$k_1$	174	201	$1.16 \times 10^{13}$
$k_2$	239	284	$6.37 \times 10^{18}$
$k_3$	216	268	$5.61 \times 10^{16}$
$k_4$	181	241	$5.22 \times 10^{13}$
$k_5$	181	248	$2.04 \times 10^{13}$

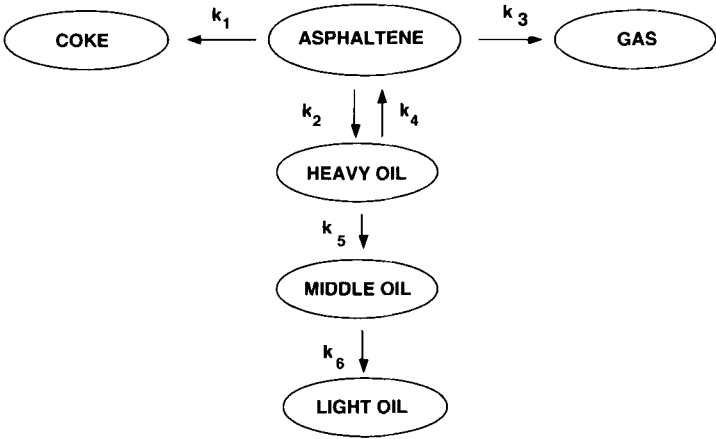


Fig. 6-7. Model P2 — asphaltene cracking mechanism presented by Phillips et al. [37].

TABLE 6-6

Kinetic constants for Model P2 with or without the presence of sand

Rate constant	Activation energy, $E$ , with sand (kJ/mol)	Activation energy, $E$ , without sand (kJ/mol)	Frequency factor ( $s^{-1}$ )
$k_1$	174	195	$1.16 \times 10^{13}$
$k_2$	250	273	$4.99 \times 10^{19}$
$k_3$	195	263	$1.41 \times 10^{14}$
$k_4$	222	241	$1.91 \times 10^{17}$
$k_5$	192	247	$4.04 \times 10^{14}$
$k_6$	230	240	$3.79 \times 10^{18}$

→ maltenes ( $224 \pm 15$  kJ/mol) and maltenes → asphaltene ( $284 \pm 28$  kJ/mol). They attributed these high levels of activation energy to the heterogeneity of the maltene fraction.

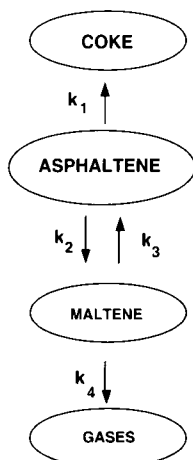


Fig. 6-8. Non-catalytic hydrocracking model of Köseoglu and Phillips [38].

### Model KPI

In a follow-up work, Köseoglu and Phillips [38] on the hydrocracking of Athabasca bitumen proposed a kinetic model for bitumen decomposition by dividing the bitumen into four pseudo-components, namely, coke, asphaltenes, maltenes and gases. They found the activation energy for the asphaltene  $\rightarrow$  coke reaction to be lower than that of the thermal cracking. They also concluded that coke formation from resins occurs via asphaltene intermediates. The model is summarized in Fig. 6-8.

The kinetic constants for the above model are listed in Table 6-7 and are compared with those obtained from thermal cracking studies of Hayashitani [36].

As can be seen from Table 6-7, the activation energies for  $k_2$  and  $k_3$  are higher than those encountered for the hydrocracking of simple hydrocarbon molecules. The authors attribute the high value of the activation energy for  $k_3$ , representing the reaction maltene  $\rightarrow$  asphaltene to the possible inhibition of polymerization and condensation reactions by excess hydrogen present. According to Belinko and Denis [39], unsaturated asphaltene molecules prefer to undergo polymerization and condensation reactions over

TABLE 6-7

Kinetic constants for Model P2 with or without the presence of sand

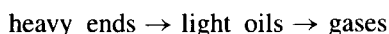
Rate constant	Thermal hydrocracking		Thermal cracking	
	Activation energy, $E$ (kJ/mol)	Frequency factor, $A$ ( $s^{-1}$ )	Activation energy, $E$ (kJ/mol)	Frequency factor, $A$ ( $s^{-1}$ )
$k_1$	142	$2.44 \times 10^6$	178	$4.53 \times 10^9$
$k_2$	224	$6.72 \times 10^{13}$	104	$2.46 \times 10^4$
$k_3$	284	$4.36 \times 10^{17}$	107	$6.78 \times 10^3$
$k_4$	186	$8.14 \times 10^9$	171	$6.31 \times 10^7$

hydrocracking reactions. Hence, the activation energies for the asphaltene  $\rightarrow$  maltene reaction ( $k_2$ ) is higher than that of asphaltene  $\rightarrow$  coke reaction ( $k_1$ ).

A comparison of the kinetic data for the thermal and hydrocracking reactions suggest that the reversible reaction asphaltene  $\rightleftharpoons$  maltene requires less activation energy in the case of thermal cracking compared to thermal hydrocracking. The reaction asphaltene  $\rightarrow$  coke, on the other hand, requires less activation energy for the thermal hydrocracking case.

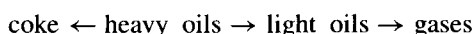
Köseoglu and Phillips [38] also proposed six kinetic models for the non-catalytic hydrocracking of Athabasca bitumen based on pseudo-components and lumped fractions.

The first model is based on three pseudo-components: heavy ends, light oils and gases and is of the following form:



The heavy ends included both coke and asphaltenes.

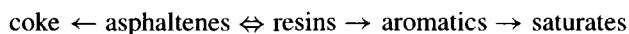
In the second model, the heavy ends of the first model was divided into coke and heavy oils. The resulting model is as follows:



The heavy oil fraction was further subdivided into asphaltenes and resins in the third model as follows:



The light oil fraction can be subdivided into aromatics and saturates. Inasmuch as all the gases produced were saturated, the saturates fraction of the light oils was lumped with the gases into a single pseudo-component called 'saturates' in the fourth model. The model thus becomes:



The lumping of liquid saturates and gases into a single pseudo-component is rather questionable and perhaps unnecessary. The model prediction in this case was not as good as that of the previous model, the general trends, however, can be reproduced.

The authors also examined the other variations of the previously described models. The final model, however, was an extension of the fourth model. The saturates were simply broken down to liquid saturates and gases. The final model (Model KP2), thus, included six pseudo-components as shown in Fig. 6-9.

All the reactions, in general, followed the Arrhenius relationship, the reaction asphaltenes  $\rightleftharpoons$  resins, however, showed some deviation from the Arrhenius behavior. The relevant kinetic parameters are given in Table 6-8.

### *Coal-derived asphaltenes*

Szczygiel and Stolarski [40] studied the hydrocracking of asphaltenes extracted from coal in the presence of a natural aluminosilicate catalyst in a batch autoclave at temperatures of 673 to 733 K and under hydrogen pressure of 9.8 to 29.4 MPa. They found coke to form mainly during the preheating period and oil to form from asphaltene. Their proposed reaction mechanism is presented in Fig. 6-10.

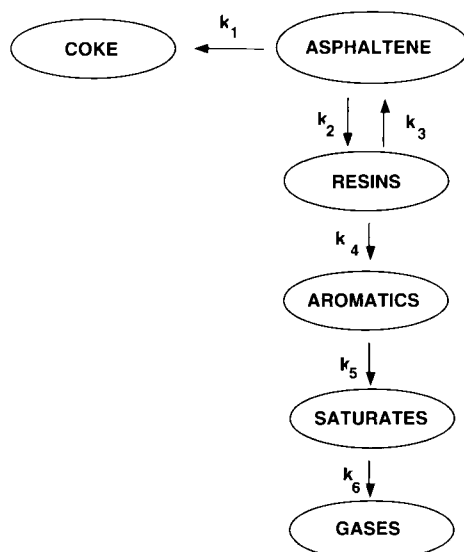


Fig. 6-9. Asphaltene cracking mechanism of Köseoglu and Phillips [38].

TABLE 6-8

Kinetic parameters of the asphaltene cracking model of Köseoglu and Phillips [38]

Rate constant	Activation energy, $E$ (kJ/mol)	Frequency factor, $\ln A$ ( $s^{-1}$ )
$k_1$	$168 \pm 17$	$27.54 \pm 2.78$
$k_2$	$103 \pm 7$	$19.34 \pm 1.39$
$k_3$	$96 \pm 9$	$17.07 \pm 1.51$
$k_4$	$85 \pm 8$	$13.57 \pm 1.27$
$k_5$	$136 \pm 12$	$24.43 \pm 2.03$
$k_6$	$175 \pm 12$	$29.90 \pm 2.10$

An analysis of the rate data that Szczygiel and Stolarski [40] provided for their model suggests Arrhenius behavior for all the reactions. Activation energies calculated from the data are shown in Table 6-9.

The lower values of activity energies indicate the effectiveness of the natural aluminosilicates as catalysts for the cracking of coal-derived asphaltenes.

Phillippopoulos and Papayannakos [41] studied the cracking and desulfurization of asphaltenes obtained from a Greek atmospheric residue in an integral trickle bed reactor using Co–Mo/ $Al_2O_3$  catalysts. They found the asphaltene cracking reaction to follow a second-order behavior with respect to the asphaltene concentration.

Schucker [33] determined coking kinetics of Arab heavy vacuum residuum and its constituent fractions, including asphaltene, by thermogravimetry. The residuum was divided into four fractions, namely: asphaltenes, polar aromatics, aromatics and saturates. The coking characteristics of the residue and its four fractions were determined.

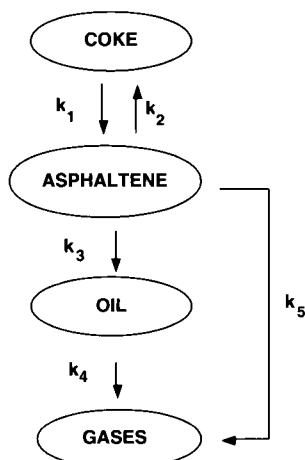


Fig. 6-10. Coal-derived asphaltene cracking mechanism.

TABLE 6-9

Kinetic parameters for the cracking of asphaltene derived from coal

Rate constant	Activation energy, $E$ (kJ/mol)
$k_1$	65
$k_2$	37
$k_3$	56
$k_4$	95
$k_5$	17

Activation energies and frequency factors were determined at various conversion levels and were found to increase with conversion level. Kinetic parameters for the asphaltene fraction are given in Table 6-10.

#### MODEL COMPONENT STUDIES

Kinetic models based on lumped solubility class or boiling point range groups are useful tools. They, however, do not provide much insight into the reaction mechanisms. Inasmuch as asphaltene is an ill-defined solubility class consisting of a number of different compounds of differing structures and chemical properties, it is not possible to study the fundamentals of the reaction mechanisms using asphaltenes directly. Model compounds, representing a given group of asphaltene constituent, are used in studies attempting to elucidate the reaction mechanism.

The major constituents of petroleum asphaltenes are variable sizes of condensed aromatic and naphthenic ring systems with alkyl side chains, sulfide linkages and bridges between the rings [7,42–44,17,45,46]. Alkylaromatic compounds can be con-



TABLE 6-10

Kinetic parameters for the cracking of asphaltene fractions derived from Arabian vacuum residuum (after Schucker [33])

Conversion (%)	Activation energy, $E$ (kJ/mol)	Frequency factor ( $s^{-1}$ )
20	176.0	$2.27 \times 10^{10}$
30	173.5	$1.47 \times 10^{10}$
40	180.6	$5.21 \times 10^{10}$
50	203.6	$2.53 \times 10^{12}$
60	213.2	$1.40 \times 10^{13}$
70	211.9	$1.22 \times 10^{13}$
80	280.9	$7.90 \times 10^{17}$
90	336.5	$3.12 \times 10^{21}$

sidered to be the key components of the asphaltene molecule. Among them, polycyclic alkylaromatic compounds are probably the most prevalent ones. Pyrolysis of singly substituted alkylcyclohexane and long-chain *n*-alkylaromatic compounds have been the subject of a number of studies. Fabuss et al. [47] studied the pyrolysis of a number of saturated hydrocarbons including cyclohexane and methyl-, ethyl-, propyl-, and *n*-butylcyclohexane and determined the activation energies for their formation. Mushrush and Hazlett [48] pyrolyzed tridecylcyclohexane at 450°C and found *n*-alkanes, 1-alkenes, alkylcyclohexanes, toluene, and benzene as the reaction products. At high-temperature and low-pressure conditions the reactions were found to follow the free-radical mechanism. The authors did not provide enough kinetic information. Trahanovsky and Swenson [49] carried out flash pyrolysis of 1-methyl- and 2-methyl-tetralin at 700–900°C under vacuum (0.1 Torr) conditions. They found naphthalene and 1,2-dihydronaphthalene to be the major reaction products indicating the ease of cleavage of the alkyl groups.

*n*-pentadecylbenzene (PDB) is a typical prototype of the alkylaromatic moiety present in asphaltene. Savage and Klein [50] studied the pyrolysis of PDB to gain insight into the reaction mechanism of the alkylaromatic constituent of the asphaltenes. The temperature was varied from 375° to 450°C. Pyrolysis resulted in the production of two major product pairs: toluene plus 1-tetradecene and styrene plus *n*-tridecene. They found the thermolysis reaction to be of free-radical type and the reaction to be of first order with an activation energy of 55.45 kcal/mol and a frequency factor of  $14.04 s^{-1}$ . They proposed the reaction mechanism shown in Fig. 6-11.

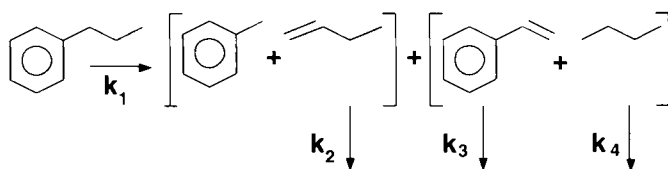


Fig. 6-11. Reaction mechanism for PDB cracking (after Savage and Klein [50]).

TABLE 6-11

Kinetic parameters for PDB cracking. (After Savage and Klein [50])

Rate constant	Activation energy, $E$ (kcal/mol)	Frequency factor, $\log A$ ( $s^{-1}$ )
$k_1$	55.5	14.0
$k_2$	47.3	12.3
$k_3$	16.6	2.5
$k_4$	18.8	53.9

The corresponding kinetic constants for the first-order rate equations are given in Table 6-11.

The rate equations based on these kinetic constants may not be directly applicable to the alkylaromatic constituent of the asphaltene due to likely diffusional limitations provided by the large asphaltene structure to the movement of free radicals generated during the decomposition.

The same authors [50] also studied the thermal decomposition of 1-phenyldodecane (PDD) and concluded that PDD thermolysis followed the free-radical mechanism, contradicting the earlier findings of Blouri et al. [51], who suggested that it was molecular a reaction.

Savage and Klein [52] also studied the reaction mechanisms of the alkylhydroaromatic and alkyl-naphthenic groups of asphaltene by pyrolyzing model compounds representing these two groups. 2-ethyl tetralin (ET) was chosen as a model compound to represent the alkylhydroaromatic group, whereas *n*-tridecylcyclohexane (TDC) was the model compound for the alkyl-naphthenic group. Pyrolysis of TDC yielded cyclohexane, methylenecyclohexane, 1-tridecene, and *n*-dodecane as major products. Cyclohexane, methylcyclohexane, *n*-tridecane, other *n*-alkanes,  $\alpha$ -olefins, alkylcyclohexane, and cyclohexylalkenes were formed as minor products. The disappearance of TDC followed first-order kinetics with an activation energy of 59.4 kcal/mol and a frequency factor of  $7.94 \times 10^{14}$ . Pyrolysis of ET-produced naphthalene, tetralin, dialin, 2-ethylnaphthalene, and 2-ethyldialins as major products. Toluene, methylindan and substituted benzenes were the minor reaction products. Like TDC, the disappearance of ET also followed first-order kinetics. The activation energy was 53.5 kcal/mol and the frequency factor was  $5.01 \times 10^{12}$ .

Savage and Klein [52] concluded that pyrolysis of TDC and ET follow the free-radical reaction mechanisms. The dominant reactions involved dealkylation near or at the ring. Ring opening reactions were considered to be minor reactions. Pyrolysis also resulted in significant dehydrogenation of the model compounds as indicated by the formation of naphthalene and toluene from ET and TDC, respectively. These observations, when applied to asphaltenes, clearly suggest that asphaltene cracking primarily involves the cleavage of the peripheral aliphatic substituents followed by aromatization of the saturated rings. As a result of thermal cracking, the remaining asphaltene will become hydrogen-deficient and more aromatic. Zou et al. [53] studied the structural changes in the Cold Lake bitumen due to in situ combustion and also found the aromaticity of the

simulated fire-flood-produced oil to be higher than that of the original feedstock due to the loss of alkyl side chains and the dehydrogenation of the alkyl ring systems.

Smith and Savage [54] pyrolyzed 1-dodecylpyrene (DDP) and found the major reactions products to be similar to those observed for alkylbenzene pyrolysis. At higher conversion levels, however, *n*-dodecane and pyrene were found to be the major reaction products, suggesting the cleavage of the strong alkyl-aryl C-C bond.

Smith and Savage [55] also pyrolyzed 1-methylpyrene and 1-ethylpyrene and found hydrogenolysis to be the dominant mechanism. Pyrene and dimethylpyrene were found to be the major reaction products due to the pyrolysis of 1-methylpyrene, whereas pyrene and methylpyrene were the major pyrolysis products of 1-ethylpyrene. The formation of these major reaction products suggested that radical hydrogen transfer was not a valid mechanism for these systems.

#### IN SITU COMBUSTION

Adegbesan et al. [3,56] have studied the reactions of Athabasca bitumen with oxygen and found the maltene fraction to oxidize to asphaltene and coke fractions, whereas the asphaltene fraction oxidized to coke fraction. They proposed a series of models describing formation of asphaltenes/coke from bitumen and its various components.

The first model, as shown below, was formulated to provide the oxygen consumption rate for the overall oxidation reaction.

##### MODEL 1



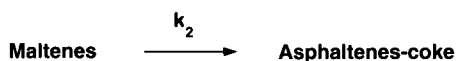
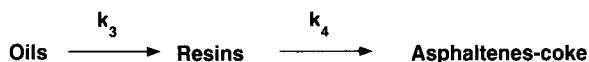
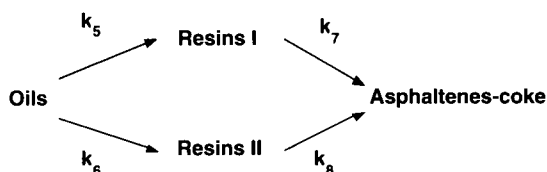
The rate constant  $k_1$  can be calculated from:

$$k_1 = 2.19 \times 10^{27} \exp \left\{ \frac{258.744}{RT} \right\}$$

where  $R$  = the universal gas constant, Pa m<sup>3</sup>/kmol K, and  $T$  = temperature, K.

The above model was able to predict the oxygen consumption rate quite well.

In addition, the authors also proposed four kinetic models for the liquid-phase reactions. They are as follows:

**MODEL 2****MODEL 3****MODEL 4****MODEL 5**

The authors found the above reactions to be of first order with respect to the pseudo-components and fractional order with respect to oxygen partial pressure. All the reactions exhibited Arrhenius behavior. Inasmuch as it was not possible to distinguish the effect of oxygen solubility, the authors calculated pseudo-activation energies in which the solubility effects were also lumped. The rate parameters for the above reactions are presented in Table 6-12.

Except for  $k_{10}$ , all the activation energies seem to be quite reasonable. The very high value of activation energy for  $k_{10}$  suggests Model 5 to be unrealistic.

TABLE 6-12

Kinetic parameters for various reactions involving asphaltene formation during in situ combustion (after Adegbesan et al. [56])

Rate constant	Pseudo-activation energy (J/mol)	Pseudo-frequency factor (h <sup>-1</sup> kPa <sup>-n</sup> )	Reaction order with respect to oxygen <i>n</i>
$k_2$	81.93	$1.00 \times 10^8$	0.41
$k_3$	77.23	$2.64 \times 10^7$	0.41
$k_4$	86.73	$7.69 \times 10^8$	0.50
$k_5$	77.75	$1.81 \times 10^7$	0.41
$k_6$	52.37	$4.64 \times 10^3$	0.50
$k_7$	89.04	$1.94 \times 10^9$	0.50
$k_8$	79.14	$4.48 \times 10^7$	0.50
$k_9$	74.92	$1.16 \times 10^7$	0.41
$k_{10}$	4877.27	$7.78 \times 10^7$	0.50
$k_{11}$	89.14	$7.78 \times 10^7$	0.50

## CONCLUSIONS

A review of asphaltene cracking kinetics has been made. Inasmuch as asphaltenes constitute a complex solubility class, it is not possible to determine a comprehensive reaction mechanism based on reaction fundamentals. Model compound studies can provide some insight into the reaction mechanisms involved in the cracking of various constituent groups of the asphaltenes. It is still not possible, however, to use kinetic data obtained from model compound studies to predict the formation of various groups due to asphaltene cracking. Kinetic models based on pseudo-component approach, in which the reaction products are divided into a number of easily quantifiable pseudo-components, are available. These models are practical tools for engineering calculations involving asphaltene cracking in petroleum recovery and processing applications.

## REFERENCES

- [1] Danesh, A., Krinis, D., Henderson, G.D. and Penden, J.M., Asphaltene deposition in miscible gas flooding of oil reservoirs. *Chem. Eng. Res. Des.*, 66: 339 (1988).
- [2] Abu-Khamsim, S.A., Brigham, W.E. and Ramey, H.J., Reaction kinetics of fuel formation for in situ combustion. *SPE Reservoir Engineering*, Nov.: 1308 (1988).
- [3] Adegbesan, K.O., Donnelly, J.K., Moore, R.G. and Bennion, D.W., Low-temperature oxidation kinetic parameters for in situ combustion: numerical simulation. *SPE Reservoir Engineering*, Nov.: 574 (1987).
- [4] Alexander, J.D., Martin, W.W. and Dews, J.N., Factors affecting fuel availability and composition during in situ combustion. *J. Pet. Technol.*, Oct.: 1154 (1962).
- [5] Bennion, D.W., Donnelly, J.K. and Moore, R.G., A laboratory investigation of wet combustion in the Athabasca oil sands. The Oil Sands of Canada-Venezuela. *Can. Inst. Min. Metall. Spec. Ed.*, 17: 554 (1977).
- [6] Jha, K.N. and Verkoczy, B., The role of thermal analysis techniques in the in situ combustion process. *SPE Reservoir Engineering*, July: 329 (1986).
- [7] Asakoa, S., Nakata, S., Shiroto, Y. and Takeuchi, C., Asphaltene cracking in catalytic hydrotreating of heavy oils, 2. Study of changes in asphaltene structure during catalytic hydroprocessing. *Ind. Eng. Chem. Process Des. Dev.*, 22: 242 (1983).
- [8] Cebolla, V.L., Diack, M., Oberson, M., Bacaud, R., Cagniant, D. and Nickel-Pepin-Donat, B., Effect of various catalysts on the chemical structure of oils and asphaltenes obtained from the hydroliquefaction of a highly volatile bituminous coal. *Fuel Process. Technol.*, 28: 183 (1991).
- [9] Chakma, A., Chornet, E., Overend, R. and Dawson, W.H., *Hydrovisbreaking of Athabasca bitumen in a high shear jet reactor*. Department of Energy, Mines and Resources, Ottawa, CANMET Report 88-58 (OP) (1988).
- [10] Nomura, M., Terao, K. and Kikkawa, S., Hydrocracking of athabasca asphaltene over  $ZnCl_2$ - $KCl$ - $NaCl$  melts with or without an additive of some transition metal chlorides. *Fuel*, 60: 699 (1981).
- [11] Takeuchi, C., Fukul, Y., Nakamura, M. and Shiroto, Y., Asphaltene cracking in catalytic hydrotreating of heavy oils, 1. Processing of heavy oils by catalytic hydroprocessing and solvent deasphalting. *Ind. Eng. Chem. Process Dev.*, 22: 236 (1983).
- [12] Dickie, J.P. and Yen, F.T., Macrostructures of the asphaltic fractions by various instrumental methods. *Anal. Chem.*, 39: 1847 (1967).
- [13] Speight, J.G., Thermal cracking of Athabasca bitumen, Athabasca asphaltenes and Athabasca de-asphalted heavy oil. *Fuel*, 49: 134 (1970).
- [14] Gould, K.A., Chemical depolymerization of petroleum asphaltenes. *Fuel*, 57: 756 (1978).
- [15] Ignasiak, T., Bimer, J., Samman, N., Montgomery, D.S. and Strausz, O.P., In: J.W. Bunger and N.C. Li (Editors), *Chemistry of Asphaltenes*. Advances in Chemistry Series 195, American Chemical Society, Washington, DC, p. 183 (1981).

- [16] Yen, F.T., Structure of petroleum asphaltene and its significance. *Energy Sources*, 1: 447 (1974).
- [17] Speight, J.G., Latest thoughts on the molecular nature of petroleum asphaltenes. *Prepr. Am. Chem. Soc., Div. Fuel Chem.*, 34 (2): 321 (1989).
- [18] Mojelsky, T.W., Ignasial, T.M., Frakman, Z., McIntyre, D.D., Lown, E.M., Montgomery, D.S. and Strausz, O.P., Structural features of Alberta oil sand bitumen and heavy oil asphaltenes. *Energy Fuels*, 6: 83 (1992).
- [19] Ali, L.H., Al-Ghannam, K.A. and Al-Rawi, J.M., Chemical structure of asphaltenes in heavy crude oils investigated by n.m.r. *Fuel*, 69: 519 (1990).
- [20] Boduszynski, M., Chada, B.R. and Szkuta-Pochopien, T., Investigations on Romashkino asphaltic bitumen, 3. Fractionation of asphaltenes using ion-exchange chromatography. *Fuel*, 56: 432 (1977).
- [21] Koots, J.A. and Speight, J.G., Relation of petroleum resins to asphaltenes. *Fuel*, 54: 179 (1975).
- [22] Speight, J.G., Structural analysis of Athabasca asphaltenes by proton magnetic resonance spectroscopy. *Fuel*, 50: 102 (1971).
- [23] Ritchie, R.G.S., Roche, R.S. and Steedman, W., Pyrolysis of Athabasca tar sands: analysis of the condensable products from asphaltene. *Fuel*, 58: 523 (1979).
- [24] Savage, P.E. and Klein, M.T., Asphaltene reaction pathways, 5. Chemical and mathematical modelling. *Chem. Eng. Sci.*, 44 (2): 393 (1989).
- [25] Simm, I. and Steedman, W., Straight-chain alkyl chain lengths in petroleum asphaltenes. *Fuel*, 59: 669 (1980).
- [26] Savage, P.E., Klein, M.T. and Kukes, S.G., Asphaltene Reaction Pathways, 1. Thermolysis. *Ind. Eng. Chem. Process Des. Dev.*, 24: 1169 (1985).
- [27] Rice, F.O., The thermal decomposition of organic compounds from the standpoint of free radicals, III. The calculation of the products formed from paraffin hydrocarbons. *J. Am. Chem. Soc.*, 55: 3035 (1933).
- [28] Kossiakoff, A. and Rice, F.O., Thermal decomposition of hydrocarbons, resonance stabilization and isomerization of free radicals. *J. Am. Chem. Soc.*, 65: 590 (1943).
- [29] Kunzru, D., Shah, Y.T. and Stuart, E.B., Thermal cracking of *n*-nonane. *Ind. Eng. Chem. Process Des. Dev.*, 11: 605 (1972).
- [30] Gates, B.C., Katzer, J.R. and Schuit, G.C., *Chemistry of Catalytic Processes*. McGraw Hill, New York, p. 10 (1979).
- [31] Blouri, B., Giraud, J., Nouri, S. and Herault, D., Steam cracking of high-molecular weight hydrocarbons. *Ind. Eng. Chem. Process Des. Dev.*, 20: 307 (1981).
- [32] Moschopedis, S.E., Prakash, S. and Speight, J., Thermal decomposition of asphaltenes. *Fuel*, 57: 431 (1978).
- [33] Schucker, R.C., Thermogravimetric determination of the coking kinetics of Arab Heavy Vacuum Residuum. *Ind. Eng. Chem. Process Des. Dev.*, 22: 615 (1983).
- [34] Voge, H.H., *Catalytic Cracking*. Catalysis, Vol. VI, Nostrand Reinhold, New York. p. 407 (1958).
- [35] Hayashitani, M., Bennion, D.W., Donnelly, J.K. and Moore, R.G., Thermal cracking models for Athabasca oil sands oil. Proc. of Oil Sands of Canada-Venezuela Symposium, *CIM Spec. Publ.* 17, 233, 1977.
- [36] Hayashitani, M., Bennion, D.W., Donnelly, J.K. and Moore, R.G., Thermal cracking models for Athabasca oil sands oil. *SPE 7549*, paper presented at the 53rd Annual Fall Technical Conference and Exhibition of the SPE, Houston, October 1-3 (1978).
- [37] Phillips, C.R., Haidar, N.I. and Poon, Y.C., Kinetic models for the thermal cracking of Athabasca bitumen — the effect of the sand matrix. *Fuel*, 64: 678 (1985).
- [38] Köseoglu, R.Ö. and Phillips, C.R., Kinetics of non-catalytic hydrocracking of Athabasca bitumen. *Fuel*, 66: 741 (1987).
- [39] Belinko, K. and Denis, J.M., *A review of some chemical aspects of the formation of coke during thermal hydrocracking of bitumen*. Department of Energy, Mines and Resources, Ottawa, CANMET Report 43 (1977).
- [40] Szczygiel, J. and Stolarski, M., Mathematical analysis of hydrogenating depolymerization of asphaltenes from coal extracts. *Fuel*, 67: 1292 (1988).
- [41] Phillippopoulos, C. and Papayannakos, N., Intraparticle diffusional effects and kinetics of desulfuriza-

- tion reactions and asphaltenes cracking during catalytic hydrotreatment of a residue. *Ind. Eng. Chem. Res.*, 27: 415 (1988).
- [42] Cyr, N., McIntyre, D.D., Toth, G. and Strausz, O.P., Hydrocarbon structural group analysis of Athabasca asphaltene and its g.p.c fractions by  $^{13}\text{C}$  n.m.r. *Fuel*, 66: 1709 (1987).
- [43] Payzant, J.D., Lown, E.M. and Strausz, O.P., Structural units of Athabasca asphaltene: the aromatics with a linear carbon framework. *Energy Fuels*, 5: 445 (1991).
- [44] Speight, J.G. and Moschopedis, S.E., In: *Chemistry of Asphaltenes*. Advances in Chemistry Series 195, American Chemical Society, Washington, DC, 1 (1983).
- [45] Takegami, Y., Watanabe, Y., Suzuki, T., Mitsudo, T. and Itoh, M., Structural investigation on column chromatographed vacuum residues of various petroleum crudes by  $^{13}\text{C}$  nuclear magnetic spectroscopy. *Fuel*, 59: 253 (1980).
- [46] Yen, T.F., Wu, W.H. and Chilingar, G.V., A study of the structure of petroleum asphaltenes and related substances by infrared spectroscopy. *Energy Sources*, 7: 203 (1984).
- [47] Fabuss, B.M., Kafesjian, R., Smith, J.O. and Satterfield, C.N., Thermal decomposition of saturated cyclic hydrocarbons. *Ind. Eng. Chem. Process Des. Dev.*, 3: 248 (1964).
- [48] Mushrush, G.W. and Hazlett, R.N., Pyrolysis of organic compounds containing long unbranched alkyl groups. *Ind. Eng. Chem. Fundam.*, 23: 288 (1984).
- [49] Trahanovsky, W.S. and Swenson, K.E., Flash vacuum pyrolysis of 2,3 dialkyltetralins. *J. Org. Chem.*, 46: 2984 (1981).
- [50] Savage, P.E. and Klein, M.T., Discrimination between molecular and free-radical models of 1-phenyl-dodecane pyrolysis. *Ind. Eng. Chem. Res.*, 26: 374 (1987).
- [51] Blouri, B., Hamdan, F. and Herault, D., Mild cracking of high molecular weight hydrocarbons. *Ind. Eng. Chem. Process Des. Dev.*, 24: 30 (1985).
- [52] Savage, P.E. and Klein, M.T., Asphaltene reaction pathways, 4. Pyrolysis of tridecylcyclohexane and 2-ethyltetralin. *Ind. Eng. Chem. Res.*, 27: 1348 (1988).
- [53] Zou, J., Gray, M.R. and Thiel, J., Structural changes in Cold Lake Bitumen due to in situ combustion. *AOSTRA J. Res.*, 5: 75 (1989).
- [54] Smith, C.M. and Savage, P.E., Reactions of polycyclic alkylaromatics, 1. Pathways, kinetics and mechanisms for 1-dodecylpyrene pyrolysis. *Ind. Eng. Chem. Res.*, 30: 331 (1991).
- [55] Smith, C.M. and Savage, P.E., Reactions of polycyclic alkylaromatics, 4. Hydrogenolysis mechanisms in 1-alkylpyrene pyrolysis. *Energy Fuels*, 6: 195 (1992).
- [56] Adegbesan, K.O., Donnelly, J.K., Moore, R.G. and Bennion, D.W., Liquid phase oxidation kinetics of oil sands bitumen: models for in situ combustion numerical simulators. *AIChE J.*, 32 (8): 1242 (1986).

## *Chapter 7*

# **ASPHALTENE HYDROCONVERSION**

RODOLFO B. SOLARI

## **INTRODUCTION**

Around 1972, when oil prices began to increase, there were high economic incentives to convert low-value asphaltenes into more valuable white products. Price differentials between diesel oil and fuel No. 6 were over US\$25 per barrel and this was the main driving force to develop technology for asphaltene hydroconversion. At that time, asphaltene conversion technology was almost limited to thermal processes such as visbreaking, delay coking, fluid coking and flexicoking. Nowadays, the driving force for new developments in this area are new environmental regulations aimed to control  $\text{SO}_x$ ,  $\text{NO}_x$  and  $\text{CO}_2$  emissions. Both in Europe and the U.S. burning asphaltenes requires significant investments to meet air pollution standards. On the other hand, asphaltene conversion using conventional coking processes is not environmentally sound considering the large amount of coke that has to be disposed of. Other technologies such as asphaltene pyrolysis, gasification or partial oxidation have also been proposed to eliminate asphaltene. Asphaltene gasification is perhaps the most promising technology providing that investment costs could be reduced and the synthesis gas could be integrated into a petrochemical complex. Power co-generation through asphaltene gasification has not yet been proven to be economically attractive, especially with the existing low-energy prices.

Asphaltene hydroconversion is an environmentally acceptable solution to transform asphaltenes with high sulfur, nitrogen and metals into clean fuels, leaving no byproducts to be disposed of. However, the existing technology is capital intensive and this has limited further applications. In the case of Venezuela, which has vast reserves of heavy oil with a high asphaltene content, there has been a permanent interest in developing new technologies that will improve asphaltene conversion. Following the world trend to develop new technologies to produce clean products, INTEVEP, S.A. (the research branch of *Petróleos de Venezuela*) has conducted intensive research in the area of asphaltene conversion for more than 10 years. This chapter summarizes some of the most important developments made by INTEVEP, S.A., as compared to some other existing or emerging technologies that are able to transform asphaltenes by hydrogen addition. This review includes an analysis of the type of technology that is available for asphaltene conversion both from the process point of view (reactor type), as well as the catalyst type, and the relationship between asphaltene reactivity and chemical composition.



## ASPHALTENE HYDROCONVERSION PROCESSES

There are many type of processes that could be applied to destroy asphaltene molecules by adding hydrogen and avoiding coke formation. All these processes operate at high pressure (70 to 300 atm) and high temperature (390 to 480°C) and they are mainly differentiated by the reactor type and catalyst used in the process. The analysis of the available technology is made according to the type of reactor used as follows:

*Coil and soaker hydrovisbreaking reactor*

Coil and soaker hydrovisbreaking reactor technology is an extension of the well known visbreaking technology that has been widely used in petroleum refinery operations for conversion of resins at low pressure without hydrogen addition. Companies have adapted this technology to operate at high pressure in the presence of hydrogen. The most advanced process is the Super Oil Cracking (SOC) developed by Asahi Chemical Industry together with Nippon Mining and Chiyoda [1]. The SOC process employs a tubular reactor without soaker, operating at 220 atm, temperature between 470 and 490°C and 1 h residence time. A dispersed catalyst is used to avoid coke formation. It is claimed to be a highly active disposable catalyst that can be disposed together with the unconverted vacuum residue which could be used as boiler fuel, in hydrogen production or as coker feed. The process can reach 90% conversion of the 520°C<sup>+</sup> fraction with 1.3% coke production. The process yields about 8% C<sub>1</sub>–C<sub>4</sub>, 64% gas oil, 28% VGO and 10% vacuum residue when processing heavy Arabian short residue.

The SOC process has been demonstrated in a 3500 BPD plant in Mizushima, Japan, that was in operation for two years. The unit was shut down in 1989 and no commercial plant has yet been built.

ASVAHL, an association of French companies comprising ELF, Total and IFP has developed the TERVAHL process [2]. In this process the residual oil and hydrogen-rich stream are heated using heat recovery techniques, fired heater and passed through the soaking drum. The gas and oil from the soaking drum effluent are mixed with recycled hydrogen and separated in a hot separator where the gas is cooled, passed through a separator and recycled to the heater and soaking drum effluent. This process has been demonstrated in a 4 t/h development plant at Lyons, France, using Boscan Venezuelan crude oil with very high metal and asphaltene contents. Conversion of the 500°C<sup>+</sup> fractions have been reported to be about 30 to 35%, while still yielding a very stable syncrude of very low viscosity (122 cSt at 50°C) that can be transported or stored. The TERVAHL technology is based on the experience gained by IFP in licensing more than twelve visbreaking plants all around the world.

From 1978 to 1982, INTEVEP also developed its own process concept on hydrovisbreaking. This process concept is called SHH [4]. The SHH process can convert heavy residues into distillate products by means of a thermal treatment in a low-residence time tubular reactor, and a second thermal stage in a bubbling column reactor (soaker) operating at the same pressure and temperature. The reaction products are separated under high pressure and temperature and the light fraction is hydrotreated to reach final product specifications. The heavy fraction is deasphalted with a heavy solvent (C<sub>5</sub>/C<sub>6</sub>)

and water. The deasphalted oil is recycled back to the second hydrovisbreaking reactor. This reactor uses up to 10% water in the feedstock and 500 to 1000 ppm molybdenum additive. This additive, as well as most of the metals, is recovered from the solid by precipitation after deasphalting. The operating temperature of the first reactor is between 400 and 460°C and the operating pressure is between 130 and 150 atm with residence times between 10 and 25 min.

The SHH process produces 13.5% gasoline, 43.6% diesel, 37.5% gas oil and 5.4% residue to be disposed. Asphaltene conversion is in the order of 90%. Two patents were issued to INTEVEP in 1986 regarding this process [3,5]; however, the process has not been scaled-up.

At this point, it is worth mentioning the HSC process developed by TOYO ENGINEERING [6]. This is a non-conventional visbreaking technology without hydrogen addition and able to reach moderate conversion higher than visbreaking, but lower than coking. In this process, thermal cracking in the heater tube is minimized and a relatively large soaking drum is used for both thermal cracking and simultaneous deepsteam stripping nearly at atmospheric pressure. The stripping steam functions also to make homogeneous enforced turbulence in the liquid phase; thus, coke-free operation of the soaking drum is achieved. Conversion of the 500°C<sup>+</sup> fraction between 40 and 50% has been reported in pilot plant work with some crude oils. A commercial plant of 14,000 BPSD has been operating successfully at the PCK refinery in Germany since 1988.

Hydrovisbreaking technology has the advantage of low investment and can be readily scaled-up based on well-known practices of visbreaking. The HSC process that requires minor scale-up investment is a good example.

The main disadvantage of the hydrovisbreaking processes operating at high conversion is the highly sophisticated control system needed to avoid runaway conditions with highly exothermic reactions. Although the technology is rather conventional, it has never been applied at a commercial scale at high level of conversion, except by the demonstration done by Asahi at Mizushima and IFP at Lyon at a rather small scale.

The coil and soaker technology, when operating at high conversion, tends to produce unstable unconverted residues that cannot be incorporated as fuel oil components. The SHH and HSC processes have solved this problem by combining the conversion step with deasphalting to get rid of the polyaromatic compounds. This solution, however, gives rise to environmental shortcomings due to the need for asphaltene disposal. This type of technology is recommended for use only when moderate asphaltene conversion is targeted (between 30 and 40%); therefore, a rather low-investment, low-risk process can be implemented to produce stable fuel oil components. If this is the case, the TERVAHL and HSC processes should be carefully considered as valuable technological options that are environmentally safe.

During 1993–98, INTEVEP developed a new hydrovisbreaking technology that uses a dual catalyst system to achieve higher conversion levels, lower asphaltene and Conradson carbon contents, and more stabilised residue than conventional visbreaking technologies [41]. Pilot plant tests by INTEVEP, S.A. and commercial tests of the new AQUACONVERSION™ process at Refinery ISLA, Curaçao S.A. Emmastad, Curaçao refinery, confirm these advantages.

In the AQUACONVERSION technology the residue is heated in the presence of

steam and a novel oil-soluble dual catalyst system. Thermal cracking occurs both in the heater and soaker drum together with mild hydrogenation of the free radicals formed. This hydrogenation is achieved by the hydrogen transfer from the water to the oil. The reaction products are separated in a fractionation column to yield naphtha, middle distillates and gas oil. The stream from the bottom of the fractionator is sent to a catalyst recovery unit to partially recover the catalyst that is reused. The process reaction sequence proceeds by the unique interaction between the non-noble metal components of the catalyst. The first catalyst component facilitates the formation of hydrogen and oxygen free radicals from water. The highly reactive hydrogen free radicals that are formed concurrently with the thermal cracking of the components of the feedstock, saturate the resulting thermal hydrocarbon free radicals. The catalyst also reduces the condensation reactions by promoting selective addition of hydrogen to the aromatic free radicals. The result is, like a typical partial steam reforming, the formation of a smaller hydrocarbon component, as well as additional hydrogen free radicals and carbon dioxide. This entire reaction sequence effectively retards and competes with the undesirable aromatic-condensation reactions so the refiner can benefit from the increased viscosity reduction associated with the higher conversion and still produce a stable converted product.

AQUACONVERSION™ is currently being offered by PDVAS–INTEVEP, UOP and Foster Wheeler as a commercial alternative both for refinery and wellhead applications. The first commercial revamp of an existing visbreaking unit is now in the basic engineering phase and is scheduled for start-up in the year 2001 at the ISLA Refinery. In addition, development programs are under-way at the three companies to extend the technology's range of feedstocks and investigate its applicability to a wide range of other refining applications. AQUACONVERSION™ has proved to be a very competitive option for the transportation of heavy crude oil in wellhead applications. Its economic advantages are due to increase in volumetric yields and low capital costs. Also, it improved the API gravity and viscosity of the crude allowing transportation without the need for additional dilution. This application is also ready to enter into the basic engineering phase in January 2000 after PDVSA's definition of a 40 TBPD production project based on AQUACONVERSION™ to produce a transportable crude oil from the Morichal area.

### *Fixed-bed reactors*

There are many commercial fixed-bed processes that are able to convert the asphaltenes contained in atmospheric or vacuum oil residues. The best known commercial processes are: CHEVRON RDS/VRDS [7], UNICRACKING/HDS [8] and EXXON RESIDFINING [9]. Other processes with less commercial experience are: HYVAHL F licensed by IFP [10], RCD UNIBON of UOP [11], R-HYC [12] from Idemitsu, and the ABC process licensed by Chiyoda [13].

All these fixed-bed, catalytic processes for the hydrotreating of residual oils have very similar process schemes. The feed and hydrogen-rich recycle gas are preheated, mixed and introduced into a guard chamber, which removes particulate matter, residual salts and a fraction of the metals from the feed. The effluent from the guard chamber flows down through the main reactors, where it contacts one or more catalysts designed

to remove metals and sulfur, to convert a substantial fraction of the 500°C<sup>+</sup> material into vacuum gas oil. The product from the reactors is cooled, separated from the hydrogen-rich recycle gas and fractionated to produce distillate fuels, upgraded vacuum gas oil and vacuum residue. Recycle gas, after hydrogen sulfide removal, is combined with makeup gas and returned to the guard chamber and main reactors.

These types of processes usually operate at 130 bar of hydrogen partial pressure. The space velocity changes according to the feedstock characteristics, but typical values are between 0.1 and 0.25 h<sup>-1</sup>. The typical start of run temperature is 365°C up to a maximum of 415°C at the end of run.

The fixed bed process can only provide up to 60% conversion of the 500°C+ fraction depending on the asphaltene content in this fraction. Degree of desulfurization (HDS) and demetallization (HDM) is within 70 and 90%. Typical yields from Arabian Heavy vacuum residue are: 5% gasoline, 10% diesel, 25% VGO and 63% of unconverted residue with lower sulfur and metal content.

Fixed-bed reactors have the advantage of being a well-proven and reliable technology. Nevertheless, its economy is extremely sensitive to feedstock properties. Most fixed-bed processes consist of two swing reactors acting as guard chambers and four main reactors as illustrated in Fig. 7-1. Despite this high equipment investment, these processes are restricted to process only feedstocks with no more than 200 ppm of metals.

For feedstocks with higher metal and very high asphaltene contents, process economy is shattered by a short life cycle and a high catalyst consumption. Recently, Idemitsu Kosan Co. [12] has reported the operation of existing resid conversion units with a feedstock containing between 9 and 11% of asphaltene. Moderate asphaltene conversion (40%) was reported with low-coke deposition using proprietary catalysts. Also, IFP [8] and Chiyoda [13] offer proprietary catalysts that can tolerate higher metal and asphaltene contents.

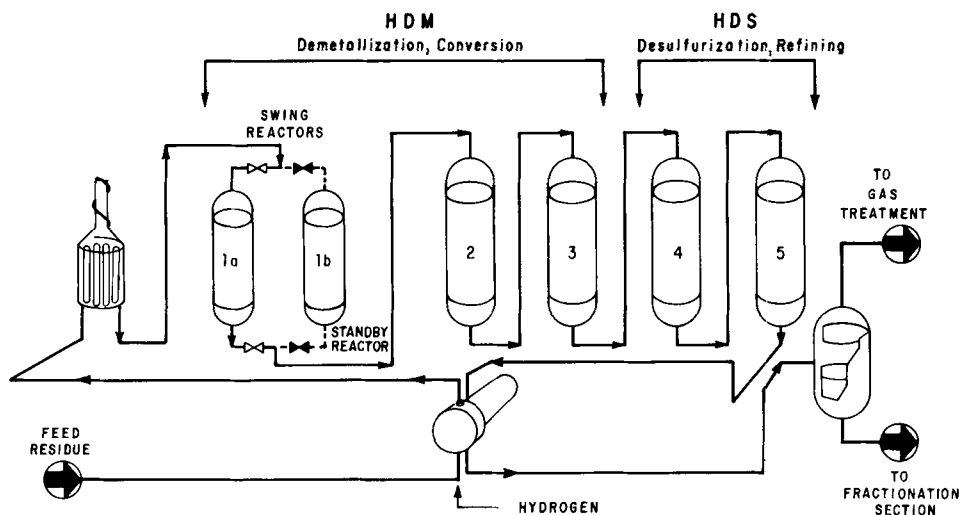


Fig. 7-1. Fixed-bed process flow scheme.

A typical value for catalyst consumption is approximately 0.5 ton for 1000 tons of feedstock containing 200 ppm of metals. This means that the metal retention capacity of the catalyst is about 40%. Some catalysts are reported to have up to 100% capacity to retain metals, but they are also affected by the asphaltene and carbon content (Conradson) in the feedstock due to coke deposition.

Recently, Chevron has introduced its Onstream Catalyst Replacement (OCR) system that provides enhanced flexibility to residue hydrotreaters [14]. The advantage of OCR is the more efficient use of catalyst and the ability to remove spent catalyst while continuing to operate. OCR is a technology that allows catalyst removal from a proprietary OCR reactor in a safe and reliable way, while the unit continues to operate. An OCR reactor differs from a normal fixed-bed reactor in that it operates with the feed upflow and contains the internals to allow addition and withdrawal of the catalysts. Fresh catalyst is added at the top of the reactor and spent catalyst is withdrawn from the bottom. The OCR reactor could be used as a guard reactor to minimize the amount of metals that contacts the downstream hydroconversion fixed-bed reactor. This could significantly increase the catalyst cycle life in the conventional fixed-bed system. The first commercial application of OCR technology went into operation on May 1992 at the Idemitsu Kosan Company's Aichi Refinery in Japan. A 50-MBPD two-train resid hydrotreater designed by Gulf Oil Co. was retrofitted with two new OCR reactors. This retrofit allows the Aichi refinery to process heavier feedstocks, while at the same time extending the run length of the existing fixed-bed from one year to two years. This technology is commercially proven, and opens new possibilities for asphaltene conversion using fixed-bed processes.

INTEVEP, S.A. has also done extensive research on fixed-bed processing of high-metal feedstocks. As a result of this effort, a deasphalting and hydrodesulfurization process was developed (DHDS) [15]. The process is based on a deep crude or residue deasphalting stage followed by hydrotreatment of the deasphalted oil. Deasphalting is done with heavy solvents ( $C_6^+$  cut) and asphaltene separation is carried out in a solid phase, with a very high yield of deasphalted oil (87%). Once the solvent is recovered, the deasphalted product obtained from the centrifugal separator is treated in two hydrotreatment stages. The first one is a hydrodemetallization stage, whereas the second stage is the hydrodesulfurization. The catalyst in the first stage is a proprietary catalyst INT-R1 developed by INTEVEP [16] and produced by KETJEN. The hydrodesulfurization stage uses a conventional catalyst. Typical yield is: 12.4% gasoline, 31.9% diesel, 28% vacuum gas oil, and 11.6% of 500°C<sup>+</sup> residues. Asphaltene yield is 13% by weight. The solid asphaltenes could be further converted using the LR coker technology that was jointly developed by Lurgi and INTEVEP [17]. This process is commercially available, but no plant has yet been installed.

A second version of the same process uses a preliminary stage of hydrovisbreaking, which improves yields and reduces the metal content in the deasphalted product [18]. The process operates at a pressure of 100 bar and temperatures between 400 and 460°C, with a residence time of several minutes. This route was jointly developed by INTEVEP and ASVAHL, and demonstration was performed in the ASVAHL's heavy oil platform pilot plant of 400 BPD capacity. No commercial plant has yet been built, but the process is commercially available from IFP.

INTEVEP, S.A. also demonstrated the advantages of the upflow reactor with the catalyst added from the top and removed from the bottom, similar to the OCR's reactor [19]. The studies done at INTEVEP, S.A. confirmed that a higher liquid hold-up in the reactor improves the hydrocarbon-catalyst contact and, therefore, increases demetallization, as compared with the traditional operation with a downstream flow. INTEVEP, S.A. has not yet commercialized this type of reactor.

Fixed-bed technology is a reliable technology for moderate conversion of asphaltenes (40 to 50%) from feedstocks with metal contents lower than 200 ppm. It is capital-intensive, however, and operating costs could skyrocket if the metal content in the feedstock increases. This technology is not recommended to convert high-metal, high-asphaltene feedstocks, but it could become an attractive alternative to process low-quality deasphalted oil or petroleum resid with a metal content less than 200 ppm. The outcome of OCR technology developed by Chevron could widen the range of application of fixed-bed reactors to convert heavier resids containing asphaltenes with higher metal concentrations. The actual potential of this innovative technology is now being evaluated and is promising.

#### *Mobile fixed-bed reactor*

The mobile fixed-bed reactor is a variation of the conventional fixed-bed reactor where the catalyst is added from the top and removed from the bottom in a periodical way. The feed and the hydrogen flow down. The best known mobile-bed process is the Shell HYCON process that went commercial three years ago at the Shell Nederland Refinery in Pernis, The Netherlands. This novel moving-bed reactor allows addition and withdrawal of the demetallization catalyst under normal operating pressure (160 bar) and high temperature (420–445°C) and is better known as the Shell bunker reactor. The special internal construction in the reactor includes screens that separate the catalyst and the process stream before these leave the reactor. A fully automated catalyst handling system, containing high-pressure slices, special rotary star valves and slurry transport loops, is used for catalyst loading and unloading. This system allows plug flow of the catalyst during the bunker operation concurrently with the process stream.

The mobile-bunker reactor makes it possible to replace the catalyst as required to maintain a high catalytic activity and avoid catalyst bed plugging. In this way, high-metal feedstocks can eventually be processed without frequent stops or guard reactor utilization.

The Pernis plant consists of two parallel trains of 12500 BPD capacity each with five reactors in series. The first three reactors of each train are bunker reactors filled with spherical silica-based hydrodemetallization catalysts. The last two reactors in the train are of the fixed-bed type filled with a standard hydroconversion catalyst. The unit was designed to operate with Maya vacuum residue containing 760 ppm of metals, but the actual start-up operation was done with Arabian Heavy vacuum residue with a significantly lower metal content. In the first cycle of operation, 7700 h were achieved, in which the longest period without interruption was 3700 h. Total conversion was 66–68% by weight with 95% of demetallization and 92% of desulfurization [20].

From the start up and during the first cycle many problems were encountered. Improperly positioned internals created catalyst sealing problems right after the start-up

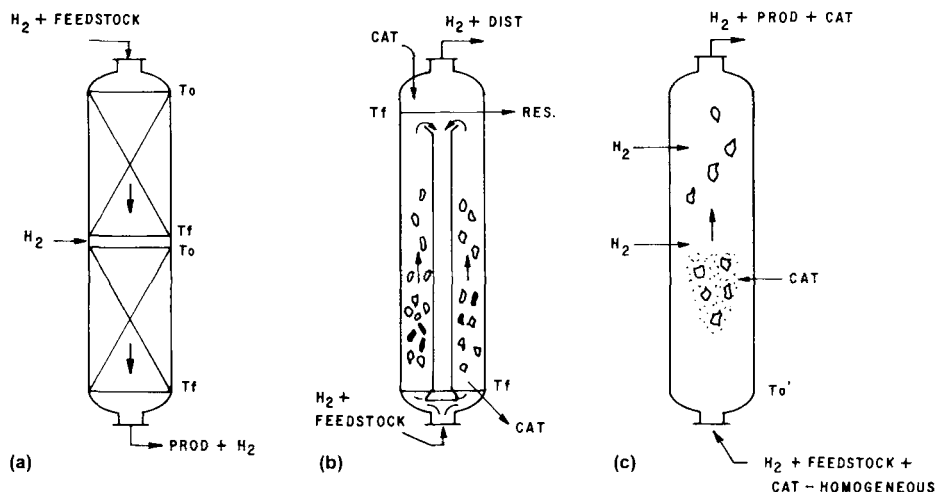


Fig. 7-2. Reactor configurations: (a) fixed bed, (b) ebullated bed and (c) slurry bed.

that required the opening of the second reactors to rectify the internals. Later on, fouling and plugging developed in the third reactor of each train. This caused serious liquid maldistribution in the catalyst bed which occasioned unscheduled shutdown. Shell has attributed the plugging to the deposition of iron particles in the catalyst bed that were introduced with the feed. After implementing the necessary modifications, the plant was restarted in November of 1992 and is currently running well.

IFP has also developed its own version of the mobile fixed-bed reactor, but no commercial application has been reported. IFP tested the periodical loading and unloading cycles in the ASHVAL platform.

Although the mobile-bunker reactor can be considered at the commercial level, its relative advantage over the existing fixed bed or ebullating bed have to be fully demonstrated in a long-term commercial run. Still there are many questions to be answered to establish a fully proven bunker technology. Process reliability and on-stream factors are still matters of concern regarding mechanical performance. From the process point of view, only a limited increase in conversion has been demonstrated as compared to the fixed-bed, and operation with high-metal feedstocks is still to be proven to be economical. Low space velocity is also detrimental to this type of technology.

### *Ebullating-bed reactor*

In the ebullating-bed reactor, the solid catalyst is suspended and perfectly agitated due to the dynamic pressure of the liquid coming from the bottom and leaving at the top of reactor. This pressure is generated by an internal or external recirculation pump. The catalyst can be removed from the bottom of the reactor and added from the top as shown in Fig. 7-2 [26]. Catalyst particle size ranges from 0.5 to 1 mm. There are two well-known commercial processes for resid hydroconversion that use this type of reactor. H-oil from HRI Inc. a subsidiary of IFC and LC-fining from ABB Lummus Crest Inc., Amoco Oil

Co. and Cities Services Co. Both processes have similar flowsheets. Oil and hydrogen are heated separately and then passed into the hydrocracking reactor in upflow, through an expanded bed of catalyst. A reactor recycle pump is used to maintain the solids suspended in the liquid, while continuously being recycled through an internal circulating channel. The mixed vapor-liquid effluent from the reaction section flows to the high-pressure, high-temperature separator. Vapor effluent from the separator after reduction in pressure goes through the condensate remover and gas purification section. The hydrogen-rich gas is recycled in the reactor and the condensates are removed as light products.

The liquid from the bottom of the hot separator is let down in pressure and stripped of light components. In both processes, the unconverted bottom can be optionally recycled back to the reactor or disposed of as a fuel oil component. In the LC-fining process, the unconverted bottom can be pumped through a coke precursor removal step to stabilize it before recycling to the reactor [21]. The H-oil process uses the patented vacuum bottoms recycle (VBR) mode of operation if recycling is needed to increase asphaltene conversion [22].

The LC-fining process has three commercial units in operation with an average capacity of 50,000 BPD, whereas H-oil has seven units of 30,000 BPD average capacity. All these units operate at a conversion level of the 520°C<sup>+</sup> fraction between 55 and 65%. Typical volumetric yields at this conversion level are: 15.5% gasoline, 22.1% diesel, 34.1% vacuum gas oil, and 32.2% of unconverted bottom which at this conversion level is stable and can be used as a fuel oil component. Operating pressure is between 130 and 160 bar and temperatures are in the range of 430 to 460°C, with a space velocity of 0.5 h<sup>-1</sup>.

Both H-oil and LC-fining claim to be able to operate at higher conversion (up to 90%), although no commercial unit is normally being operated at high conversion. HRI and Texaco have disclosed a two-month operation of the Convent unit in Louisiana [23] at 80% conversion. The unconverted bottom was fed to the Texaco gasifier to produce hydrogen. Lummus has also reported short-time commercial demonstration using the asphaltene recycle mode of operation in Amoco's Texas refinery.

Ebullating-bed reactors have several important advantages over the fixed-bed reactors. The reactor conditions are near isothermal, exhibiting little temperature gradient across the bed because the heat of reaction is absorbed immediately by the cold feed oil and the hydrogen entering the reactor due to intensive mixing regime. The catalyst in the reactor behaves like an homogeneous fluid phase, which enables it to be added to and withdrawn from the reactor onstream. Units can run for 24 to 36 months between turnarounds, depending on the type of feedstock.

The dynamic backmixing characteristic of the ebullated-bed, as opposed to the static conditions of the fixed-bed reactors, reduces the possibility of plugging or increase in pressure drop from a buildup of coke or sediment in the system. Ebullated-bed reactors allow the processing of heavy feedstocks with higher metal, sulfur and nitrogen contents. Periodical removal of spent catalyst avoid catalyst deactivation as opposed to fixed-bed operation.

The main drawback of the ebullated-bed technology is the complex system required to maintain a stable expanded bed, including the speed driver of the recirculation pump and the sophisticated proprietary internals to assure proper gas and liquid distribution.



Solid handling for the onstream catalyst addition and withdrawal requires complex control systems that have to be operated by well experienced operators. After many years of commercial operation, the technology is well established and a reliable performance can be expected. Scale-up of this type of reactor is very sensitive to the type of feedstock. Most of the new units have required intensive troubleshooting during start-up. The last LC-fining unit installed by Syncrude, Canada, for example, had some problems related to the let-down valve due to a 1% entrained solid content in the feedstock, that reduced significantly the life cycle of the same valve proven in other applications.

Another limitation of the H-oil and LC-fining processes is the high consumption of catalyst when high metal feedstocks are processed. These are synthetic catalysts with a cost of approx. 7 to 10 US\$/kg. For feedstocks with metal contents over 500 ppm, catalyst consumption most likely will have a significant impact on the process economy by increasing the operating costs. Normal catalyst consumption for a low-metal feedstock (less than 200 ppm) is 0.50 US\$/bbl of fresh feed. This cost could approach 1 US\$/bbl if the metal content is 500 ppm. In the future, there could also arise the problem of catalyst disposal due to environmental restrictions for transportation.

Although the ebullated-bed technology could increase total conversion up to 90% by recycling the unconverted bottom, this product becomes unstable and cannot be disposed of as fuel oil component. High conversion operation of these processes will require additional investment to dispose of the unstable pitch. If a gasifier or a coker is available, this could be the best way to dispose of this unstable byproduct.

To overcome some of these problems, EXXON Research and Engineering has developed the Microcat-RC (MRC) process for asphaltene conversion [24]. This is a hydroconversion process operating with a uniformly dispersed catalyst throughout an ebullating-bed reactor. The novel catalyst containing molybdenum sulfide in a carbonaceous matrix has a very small particle size ( $10^4$  Å in diameter). In this case, the catalyst flows homogeneously with the liquid phase and leaves the reactor with the unconverted bottom. Only a small amount of molybdenum is required (parts per millions (wt) over the feedstock) making it economically feasible to dispose the wasted catalyst on a once-through basis. Process conversion can be as high as 95% of the vacuum residue with 17.2% volume yield of naphtha, 63.6% of distillates, 21.9% of gas oil, and 3 to 4% by weight of unconverted bottoms. Operating conditions are in the same range as the existing ebullating-bed processes. EXXON claims that the uncovered bottom is stable and could be disposed of as a fuel oil component or as a coker feedstock.

The MRC process is still under development and has not been commercially proven. Nevertheless, EXXON has considered that the process is ready to be scaled-up to a commercial plant based on the wide experience accumulated during the demonstration of the EDS (Exxon Donor Solvent) process for coal liquefaction in a 2500-BPD demonstration unit. The MRC reactor would operate at similar hydrodynamic conditions as does the EDS reactor [25].

INTEVEP, S.A. also explored the route of the ebullating-bed reactors, but using a bauxite-based catalyst. A process concept was developed consisting of two hydrocracking stages in series. In the first step, the feedstock is hydrocracked in an ebullated bed using a MoP/bauxite catalyst, followed by a second fixed-bed hydrocracking stage using a NiMo/Al catalyst developed by INTEVEP. This process concept was tested

at bench scale at INTEVEP, S.A. and later on further tests were done in a 3-BPCD ebullating-bed pilot plant at ABB-Lummus using the INTEVEP's bauxite catalyst. The results showed conversion of the 530°C<sup>+</sup> fraction between 80 and 85%. Product slate at the lowest conversion was approximately 10% gasoline, 25% diesel, 40% vacuum gas oil, and 25% residue.

The ebullating-bed technology is an appropriate choice if moderate asphaltene conversion (less than 70%) is required to process feedstocks with no more than 500 ppm of metal content. A conversion higher than 70% tends to produce unstable unconverted bottoms that have to be further processed in a coker or a gasifier. A metal content of over 500 ppm in most cases penalizes process economy due to high catalyst consumption. Otherwise, the technology is well proven and provides an environmentally safe solution to asphaltene conversion, considering that waste catalyst can be safely disposed to metal recovery companies. Nevertheless, this type of technology requires high investments, and the process economy strongly depends on the oil price differentials.

### *Slurry reactors*

During the last twelve years, there has been significant progress in the development of slurry reactor technology to achieve high asphaltene conversion. In this type of reactor, the catalyst is in a powder form suspended in a mixture of gas and liquid that flow from the bottom to the top of reactor. The catalyst is transported through the reactor due to gas dynamic pressure generating a significant degree of mixing. The solid concentration inside the reactor can be higher than in the feedstock, but the outlet stream has the same solid inlet concentration without solid accumulation. This is usually known as a three-phase, bubbling column-type reactor.

The slurry reactor has not yet been commercially used for asphaltene conversion, except for the Bergius Pier process utilized during the Second World War for the conversion of coal operating at a pressure of 700 bar, and during the period of 1950 to 1954 for the conversion of residual oil. Veba Oel has developed a modern version of this process that can be applied to the asphaltene conversion. The process is called VCC (Veba Combi Cracking) and operates within a pressure range of 220 to 300 bar with fine particles of carbonaceous material as an additive [26].

This process integrates a liquid phase hydrogenation (LPH) slurry reactor system directly coupled with a fixed-bed gas-phase hydrogenation (GPH) reactor system. The feedstock is mixed with 1 to 3% of finely grounded additive and hydrogen before preheating. This hot mixture is fed to the LPH reactors that operate at temperatures between 465 and 480°C. The slurry from the LPH reactors is routed to a hot separator (HS), where gases and vaporized products are separated from nonconverted residue. The HS top product enters the GPH reactors that operate at a temperature between 370 and 420°C and at the same pressure as the LPH reactors and contain a fixed bed of commercial hydrotreating catalyst.

Distillates from the HS bottom product are recovered by a vacuum flash and the unconverted bottom is fed to a low-temperature carbonization unit (LTC) to produce more distillate and a small amount of coke. This is a continuous coking process patented by Veba Oel.

Typical yields from the process with Arabian Heavy vacuum residue at 95% conversion are as follows: 26.9% naphtha, 36.5% middle distillates, and 19.9% gas oil. Total hydrogen consumption is  $395 \text{ N m}^3/\text{t}$  and coke production is between 2 to 3% of the feedstock. The VCC process has a demonstration unit with a capacity of 3500 BPD in operation since 1988 at Bottrop, Germany. No commercial plant has yet been built, although the VCC process was selected to process approximately 80,000 BPD of Athabasca bitumen for the Oslo project in western Canada and 25,000 BPD for the Karlsruhe refinery of Ruhr Oel in Germany, but these plants were not built.

Petro-Canada has developed the CANMET process for oil residue and asphaltene conversion. In this process, the feedstock is mixed with a small portion of recycled hydrogen and 2 to 5% by weight of a solid additive before heating. The recycled hydrogen is heated separately. Both streams are mixed before entering the slurry reactor. The CANMET process uses only one vertical reactor where the solid additive particles are suspended in the liquid hydrocarbon phase, through which the hydrogen and product gases flow rapidly in a bubble form. [27]. The reactor exit stream is quenched with cold recycle hydrogen prior to the high-pressure separator. The heavy liquids are further reduced in pressure to a hot medium-pressure separator and from there to fractionation. The spent additive leaves with the heavy fraction and remains in the unconverted vacuum residue to be disposed of. The process uses an additive of iron sulfate, with temperatures ranging from 460 to 475°C and pressures from 140 to 170 bar. Typical yields using Cold Lake vacuum residue with 15.5% asphaltene are as follows: 19.8% naphtha, 33.5% distillates, 28.5% vacuum gas oil, and 4.5% pitch. Hydrogen consumption is 2.5% by weight of feedstock.

The CANMET process has been demonstrated in a 5000-BPD pioneer plant designed and constructed by the Partec Lavalin Inc. in the Pointe-aux-Temles refinery, Montreal, Canada. A conversion of approximately 85% was reported using only one reactor in this unit. More recently, Petro-Canada and Unocal, now UDP, have joined efforts to combine the CANMET process with UDP's technology for hydrotreating at high pressure. This combined technology is called U-CAN and integrates hydrotreating of the vapor product from the CANMET hot separator directly into the high-pressure UDP reactors. This process scheme is similar to the VCC process. However, U-CAN is said to include a proprietary design to completely avoid solid entrainment into the downstream fixed-bed hydrotreaters. This new technology will eventually be demonstrated in the 5000-BPD unit in Montreal [28].

The MRH process (Mild Resid Hydrocracking) is a three-phase reactor technology developed by Idemitsu Kosan Co. and the M.W. Kellogg [29]. In this process, a slurry consisting of heavy oil feedstock and fine powder catalyst is preheated in a furnace and fed into the reactor vessel. Hydrogen is introduced from the bottom of the reactor and flows upward through the reaction mixture, maintaining the catalyst suspended in the reaction mixture. The reactor has special internals to operate at mild pressure between 60 and 80 bar. Spent FCC catalyst could be used as powder catalyst although a proprietary catalyst is also being offered by Idemitsu. At the upper part of the reactor, vapor is disengaged from the slurry and sent to a high-pressure separator to remove light gases and hydrogen. The condensed overhead vapor is fractionated and each fraction hydrotreated separately.

From the lower section of the reactors, the bottom slurry which contains catalyst, uncracked bottom oil and a small amount of vacuum gas oil fraction are withdrawn and sent to the catalyst separation section. Here, the vacuum gas oil is recovered and the catalyst and coke are separated and fed to a catalyst regenerator. The catalyst is recycled and a purge stream is taken out of the process. Coke produced in the reactor is deposited on the catalyst and burned in the regenerator. A large amount of catalyst (approximately 20%) is mixed with the feedstock. Typical product distribution using Arabian Heavy vacuum residue as feedstock is as follows: 8.2% naphtha, 29.2% middle distillates, 31.7% vacuum gas oil, 17.5% vacuum residue, and 5.5% coke. The MRH process, due to the moderate pressure, operates in a conversion range between 70 and 80%.

INTEVEP, S.A. has done intensive research and development on heavy oil and asphaltene conversion using slurry reactors during the last ten years. The result has been the development of the HDH process (Hydrocracking, Distillation, Hydrotreatment) which is ready for commercial application [30]. The HDH process diagram is shown in Fig. 7-3. A slurry of resid and fine catalyst is prepared and heated up to the reactor inlet temperature separately from the  $H_2$  stream. This slurry of resid and catalyst is contacted with  $H_2$  in three slurry reactors in series. In these up-flow three-phase reactors, conversion and hydrogenation of the resid to lighter product take place. The reaction products are flashed in a high-pressure hot separator and the distillates recovered at the top are condensed and fractionated to be processed in separate hydrotreating units so as to meet product specifications. The slurry of spent catalyst and unconverted resid recovered at the bottom of the hot separator is fed to the catalyst separation unit. A stable and solid-free resid, which can be either recycled to the reactors or incorporated in the fuel-oil pool, is obtained. The separated spent catalyst is incinerated to enable its use in the metallurgical industry. The gases from the incinerator are desulfurized to produce a fertilizer. The HDH process is able to reach high conversion (90 to 92%) operating at moderate pressure (130 bar of  $H_2$  partial pressure) and temperatures between 465 and 475°C, under the once-through mode of operation. This conversion can be increased up to 97% in the recycle mode under similar operating conditions. Space velocity is 0.5 1/h and catalyst addition is between 2 and 4% of the feedstock. The catalyst is a cheap naturally occurring mineral that can be easily prepared through a simple grinding and classification step. The use of this low-cost but quite effective natural catalyst efficiently controls the coke and gas formation, which results in high liquid yield and moderate  $H_2$  consumption.

Typical yield of the HDH process operating with a Venezuelan oil vacuum residue (Morichal 5°API) at 92% conversion is as follows: naphtha 27.5%, middle distillates 40.4%, vacuum gas oil 27.7% and unconverted resid 5.5% by volume.

Hydrogen consumption is 258 N m<sup>3</sup>/t of feedstock. All the products obtained after hydrotreatment are of high quality and can be mixed with the main product streams from the refinery. The naphtha goes to the catalytic reformer to produce high-octane gasoline and the middle distillates are directly sent to the diesel pool. Vacuum gas oil is used as feedstock to the FCC unit to increase the gasoline and diesel production. The small amount of unconverted bottom product has very low metal (10 ppm) and sulfur contents (1.2%) and it can be incorporated in the fuel-oil pool due to its high stability generated in the catalyst separation section. This catalyst separation unit is a unique

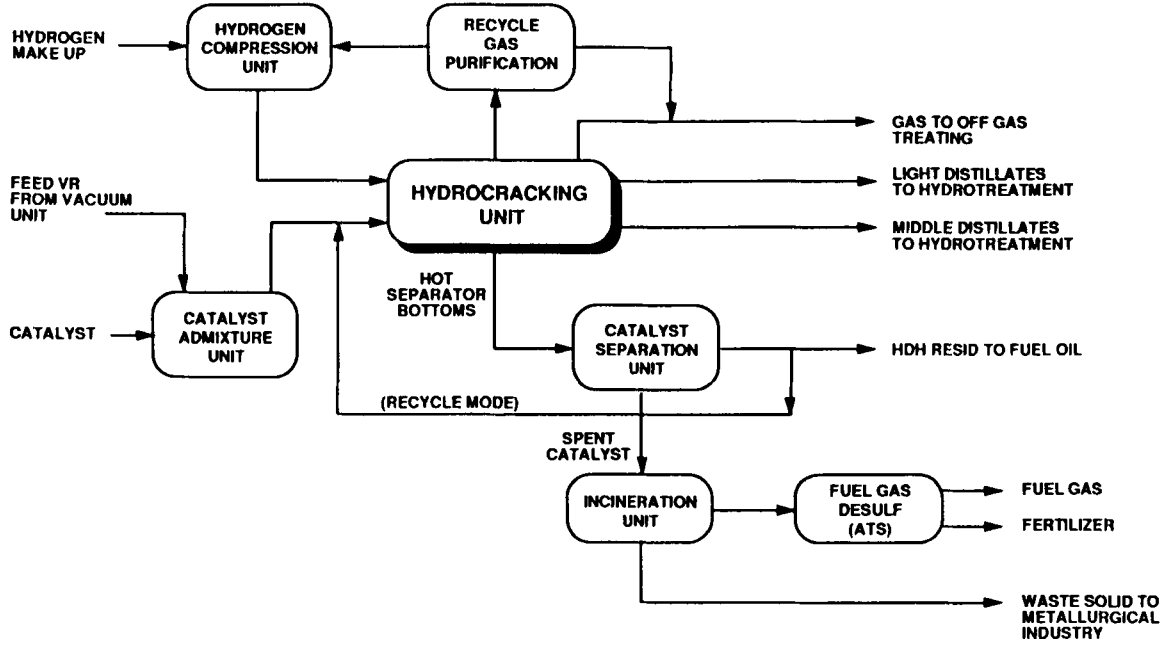


Fig. 7-3. HDH™ simplified process block diagram.

feature of the process that enables the operation of recycle mode by removal of the coke precursors from unconverted resid. If the recycle mode of operation is used, it is possible to completely eliminate the unconverted bottom stream leaving no hydrocarbon resid.

The HDH process has been successfully demonstrated in a 150-BPD pilot plant located in the Ruhr Oel refinery at Scholven, Germany. In this large pilot plant, the demonstration program accumulated over 7000 h of operation. Detail engineering design for a 15,000-BPD pioneer plant to be installed in the Cardon refinery of MARAVEN, S.A., Venezuela, was completed in 1997, but construction was deferred until the year 2001. In the last year, INTEVEP S.A. has developed an improved version of the process called HDH<sup>TM</sup> PLUS. The main changes introduced include the use of a coke-based catalyst instead of the natural catalyst and the replacement of the catalyst separation unit, the incineration unit and the fuel gas desulfurization unit by a vacuum tower and a flaker. These changes reduced significantly the investment costs [43].

It is clear that the slurry reactor is the frontier technology in asphaltene conversion. Extremely high conversion can be achieved using this type of reactor, practically eliminating production of unconverted bottom. Although this type of technology is environmentally clean, its commercial application has not yet crystallized due to the high capital investment required. Economics of the slurry-reactor technology at high conversion and with high product quality is strongly related to price differentials between middle distillates and No. 6 fuel oil. As a rule of thumb, it can be concluded that this type of process is economically attractive if this price differential is over 16 US\$/barrel. In the last years, the market has shown lower price differentials jeopardizing the possibility of installing the first commercial slurry reactor for asphaltene conversion. Future trends would tend to improve process economics due to the increasing difficulties in allocating high-sulfur resid in the fuel market. Environmental regulations will increase commercial opportunities for the high-conversion slurry process, improving its economics. Slurry reactors still have to be proven in reliable commercial operation using large-diameter reactors (over 2.5 m). Once the first commercial unit is on stream, this technology should become the preferred option for high-asphaltene conversion in a scenario where environmental concern is the primary issue. Future developments in this area shall be oriented to reducing investment costs, mainly by reducing the operating pressure and catalyst downstream processing. Otherwise, this is the technology that fits better with the future needs to transform low-value asphaltene into clean fuels without environmental impact.

## CATALYSTS

The type of hydroconversion catalysts used depends on the type of technology. Fixed-bed catalysts have a different structure from ebullated-bed and slurry-reactor catalysts. Most of the commercial catalysts used in a fixed bed or moving bed for petroleum resid hydrotreating consist of Mo on alumina with Co or Ni promoters. Their properties are also related to the type of feedstock. The high contents of asphaltenes and carbon (Conradson) with a wide distribution of molecular weights in

the feedstock require the catalyst to have a wide distribution of pore size as well as a high contribution of micropores. The macroporous structure must facilitate the diffusion of the large asphaltene molecules to the active centers. Likewise, a high hydrogenation activity will control the formation of coke, which is favored by the presence of asphaltene and a high content of carbon (Conradson). The presence of a high content of contaminants in the feedstock (sulfur, nitrogen and metals) requires catalysts to have a hydrogenolysis activity and a high capacity to store metals without detriment to their catalytic functionality.

Fan [31] has summarized the composition and properties of several hydrotreating catalysts for petroleum resids currently used in commercial applications. The catalyst bulk density ranges from 0.4 to 1 g/cm<sup>3</sup>, average pore volume from 0.2 to 0.8 cm<sup>3</sup>/g, specific surface area from 100 to over 300 m<sup>2</sup>/g, and pore size from 40 to 200 Å. It has been demonstrated that the selection of a suitable pore size distribution makes it possible to penetrate heavy molecules inside the pores, where they react at active sites, giving a good vanadium and nickel dispersion along the radius of the particle. These metals are deposited inside the particles, at active sites or nearby, decreasing the number of active sites and the effective diffusion of the reactants due to reduction of pore size. Active sites in these catalysts are provided by the acidic nature of the support and Mo–Co interactions.

Most of the fixed-bed processes use the synthetic Mo–Co catalyst on alumina. Among the newest catalysts available on the market are the catalysts developed by IFP (Procatalyse), Chevron (OCR process), IDEMITSU and the ABC catalyst from CHIYODA. IFP has developed the catalysts HMC 895 and HMC 841 with a high capacity to retain metals. IFP claims that these catalysts can retain more than 100% by weight of metal without losing activity. The IFP catalyst has been used in the Nattreff refinery in South Africa, with a live cycle of five to six months processing a feedstock with 180 ppm of vanadium. Two new units are being designed to use the IFP catalyst in Korea. Idemitsu has been successfully using a new catalyst to treat feedstocks with high asphaltene content between 8 and 10% with nine-month cycles. Chiyoda has also developed a catalyst that is able to tolerate high metal and asphaltene contents with live cycles of six months or more.

The principle behind these metal-resistant catalysts lies in the pore size distribution that allows for a smooth metal distribution in the used catalyst particle. For example, a bimodal pore size distribution allows greater access to the internal pore structure and a more complete penetration by the metal complexes. In these catalysts, the metals (Ni and V) deposit more uniformly on the pore walls.

INTEVEP's approach to hydroconversion catalyst development was two-fold. INTEVEP started the development of hydrocracking catalysts by selecting and activating natural material available in Venezuela. The route of synthetic supports impregnated with active metals, however, was also followed. Natural catalysts were developed mainly to be used in bubbling or slurry reactors, whereas synthetic catalyst development was oriented to the fixed-bed hydrodemetallization and hydroconversion.

INTEVEP developed a line of synthetic demetallization catalysts with a high metal retention capacity. Catalyst INT-R1 was developed for the demetallization of residues and deasphalted oils. This catalyst is based on a commercial alumina support impregnated with molybdenum and nickel. Distribution of pore sizes was adjusted to a

bimodal system with pore diameters ranging from 30 to 300 Å. The INT-R1 catalyst is currently being commercialized by KETJEN-AKZO [32]. Later on, a second catalyst, INT-R7, was developed. This catalyst still has a bimodal pore size distribution, but the macropores have a larger diameter to allow for the access of vanadium molecules. The metal dispersion ratios are:  $\text{Mo/Al} = 4.5$  to  $7.5$  and  $\text{Ni/Al} = 3$  to  $6$ . There is a higher number of intermediate acidity sites than in the INT-R1 catalyst. Both catalysts proved to have good stability in long-duration tests with a Venezuelan vacuum residue having high metal and asphaltene contents [32]. During these studies, it was demonstrated that basic asphaltene compounds such as porphyrins were adsorbed preferentially in the molybdenum sulfides, through the interaction of vanadium with these sulfides.

Deactivated catalysts were grinded and used again. They exhibited 50% of the initial activity, indicating that plugging of the structure in the pore throats is the cause of premature deactivation. These experiments demonstrated that highly reactive molecules tend to demetallize at the pore's entrance, whereas low-reactivity molecules need to diffuse inside the pores to react. This is the reason why most of the processes use graduated catalyst beds with different pore size distributions and activity to treat feedstocks containing asphaltene molecules with diverse chemical structure and reactivity.

INTEVEP's main objective in developing natural hydroconversion catalysts has been to produce low-cost catalysts that could be safely disposed of. The aim is to use naturally existing minerals that, upon going through a minimum pretreatment, yield cheap but active catalysts. Many iron-containing minerals were tested as catalyst sources including: ferruginous and nickel laterites, limonite, siderite, clay, bauxite, pyrite, iron monosulfate, hematite and magnetite. These natural minerals underwent thermal and/or hydrothermal pretreatment to produce catalytic materials with active surface areas ranging from 2 to 80 m<sup>2</sup>/g, pore volumes from 0.02 to 0.5 cm<sup>3</sup>/g, and average pore radii from 50 to 160 Å. Hydroconversion test results showed that some of these natural catalysts were able to convert more than 70% of asphaltene [33]. After optimization, three main catalysts were finally developed for commercial use in bubbling and slurry reactors.

A low-cost catalyst known as INT-BHC-1 was developed for hydrodemetallization and hydrocracking in an ebullated-bed process. This catalyst was prepared from bauxite with a high iron content and three types of additives: promoter, hardener, and pore developer. Phosphoric acid was used as a hardener and starch as a pore developer. The catalyst contained Fe, Mo, Al, Si, Ti and P. Surface composition is as follows:  $\text{Mo/Al} = 0.04$  to  $0.07$ ,  $\text{Fe/Al} = 0.08$  to  $0.12$ ,  $\text{Si/Al} = 0.10$  to  $0.20$ ,  $\text{Ti/Al} = 0.01$  to  $0.02$ , and  $\text{P/Al} = 0.15$  to  $0.50$ .

Surface area is between 90 and 250 m<sup>2</sup>/g and pore volume is between 0.25 and 0.55 cm<sup>3</sup>/g, 50% of the pores were larger than 200 Å and 30% were larger than 1000 Å. The pellet mechanical strength can be as high as 12 k. This catalyst was tested in the ebullated-bed pilot plant of Lummus in New Jersey, U.S.A. [34], with Cerro Negro crude as the feedstock. The results showed high conversion of asphaltene, with high demetallization and catalyst stability in a 20-day period.

In addition to bauxite-based natural catalysts, two laterite-based catalysts were developed. The INT-LHC-1 catalyst consists of nickel-containing laterite impregnated



with molybdenum and extruded with a macroporous alumina [35]. This catalyst contains 5 wt% molybdenum and 42 wt% alumina. Surface area is between 150 and 170 m<sup>2</sup>/g, pore volume, 0.60 and 0.07 cm<sup>3</sup>/g, and average pore diameter, 160 to 180 Å. The catalyst has a layered structure, high macroporosity, and an adequate substitution of magnesium for other ions to create the required acidity for asphaltene hydrocracking. Magnesium silicates with laminar-type structures, such as serpentines, provide an adequate support material for impregnation with hydrogenation metals. Both the iron and silicate particles are of vital importance for the reactions of hydrocracking of asphaltenes. A mixture of these materials yields a meso-macrosupport that allows the asphaltene molecules to diffuse into the pore system.

The INT-LHC-1 catalyst was tested in a fixed-bed pilot plant at INTEVEP, S.A., using a very refractory type of feedstock (Tia Juana short residue) at 415°C, 140 atm, and LHSV of 0.5 h<sup>-1</sup>. The catalyst exhibited a good stability for a period of 1000 h with high asphaltene conversion and vanadium removal (83%). These two natural catalysts could be used either in ebullating-bed or fixed-bed reactors. These catalysts were thoroughly analyzed after the reaction was completed. The analysis showed that 40% of the metal sulfide surface had been eliminated by coke and vanadium deposition with a 60% reduction of mesopores and practically most of the micropores. Coke was responsible for 20% of deactivation, whereas vanadium exhibited only 7 wt% loss of activity.

A third hydroconversion catalyst has been specifically developed to be used in slurry reactors. This is also an iron-based catalyst with a very wide particle size distribution. Particle size is less than 500 µm. The catalyst is prepared from a cheap iron oxide mineral with different impurities, such as aluminum (1%), silica (0.5%), and phosphorus (0.2%). Surface area is 20 m<sup>2</sup>/g and pore volume is between 0.2 and 0.6 cm<sup>3</sup>/g. Catalyst preparation is done through a very simple procedure of grinding, drying and classification yielding a low-cost catalyst [36].

The slurry-reactor catalyst, used as a fine powder, helps to achieve cracking and to provide metal sites to promote hydrogenation. Although coke formation cannot be completely avoided during asphaltene hydroconversion, it can be minimized by ensuring that there is less dependence on hydrogen transfer reactions. The INTEVEP catalyst helps to consume the hydrogen more efficiently. In the presence of this inexpensive catalyst in the reactor, the hydrogen molecules preferentially hydrogenate aromatic and polyaromatic compounds, thereby avoiding thermal dehydrogenation reactions that create condensed ring systems, unavoidably the precursors to coke formation. The INTEVEP slurry catalyst has been fully tested in the operation of the 150-BPD pilot plant. During these tests, two independent feed systems for two catalyst streams with different catalyst particle sizes were employed. One of these feed systems is employed to provide the high-activity catalyst fraction using a fine particle size, whereas the second feed stream introduces a less active catalyst with a larger particle size [37]. These demonstration tests clearly proved that larger particles are able to diminish the amount of foam inside the slurry reactors for gas velocities in use at the commercial scale, thereby increasing the liquid-phase reaction volume, which achieves the desired high conversion of the asphaltenic fraction at lower temperatures. This catalyst can also be regenerated and reused or eventually disposed of due to its low cost.

Very recently INTEVEP S.A. has developed a coke-based catalyst that is manufactured by partial oxidation of delayed coke (shot coke) to generate macroporosity. This catalyst is used as very fine particles in slurry reactors together with submicronic particles of active metals incorporated using a similar technique as in the AQUACONVERSION™ process [41,43].

#### ASPHALTENE REACTIVITY

Amerik and Hadjiev [38] have pointed out that selection of the most efficient technology for upgrading heavy residues is directly connected with the amount of available data on the physical–chemical properties of asphaltenes. These authors indicated five main characteristics related to the macromolecular nature of the asphaltenes that may influence reactivity when hydrocracked. These properties are the following:

(1) Asphaltene-analogous transformations. Like polymer-analogous transformations, the fragments, which compose asphaltene, actively enter into condensation, halogenation, nitration, sulfonation and oxidation reactions.

(2) Asphaltene molecules display the highest activity in crosslinking reactions, which are determined by the molecular weights of asphaltenes.

(3) The presence of polyconjugated structures in asphaltenes is responsible for their tendency to form coke precursors, such as carbenes and carboids. Asphaltene properties like paramagnetism, low ionization potential and high electron affinity are related to their high reactivity and their tendency towards associate formation.

(4) Asphaltenes show a high tendency to adsorb on solid surfaces. In catalytic hydrocracking, this property plays a critical role in increasing reaction rates by the presence of metallic surfaces.

(5) The mesomorphic pile-shape structure of the aromatic fragments of asphaltene molecules allows the segregation of aromatic and paraffinic–naphthenic fragments during thermal treatment.

These asphaltene properties may cause significant differences in the behavior of different type of feedstocks in a hydrocracking process. The above-mentioned parameters, however, are still too broad to enable the prediction of the performance of a given feedstock when subjected to the thermal or hydrothermal catalytic processes. In recent years, INTEVEP, S.A. has been investigating more specific correlations between feedstock properties and their reactivity. The results from these extensive research on asphaltene reactivity are summarized by Izquierdo et al. [39]. In this publication, the authors have been able to establish well-defined correlations between physical and chemical properties that can vary from one feed to another and their influence on hydrocracking processability.

Feedstock reactivity and processability depend mainly on the following parameters.

*Geologic age.* The maturity index expressed as the DPEP/ETIO porphyrin ratio is a commonly used parameter to determine the maturity of crude oils. In general, it has been observed that more mature crude oils (maturity index between 20 to 30) are less reactive than the youngest crude oils (maturity index around 50). The application of

TABLE 7-1

Structural characteristics of asphaltenes (A, B, and C) with different reactivities

Feedstock/properties		A	B	C
C	% wt	82.24	83.71	86.16
H	% wt	7.84	7.37	7.29
Sulfur	% wt	4.72	3.87	2.73
C aromatic	% wt	48.25	55.46	53.27
C saturated	% wt	51.75	44.54	46.73
C naphthenic	% wt	7.97	6.87	7.82
C paraffinic	% wt	47.79	37.67	38.91
C non-bridging	% wt	15.45	20.49	12.54
C Bridging	% wt	32.80	35.00	40.70
CI/C <sub>I</sub>	ratio	2.12	1.71	3.25

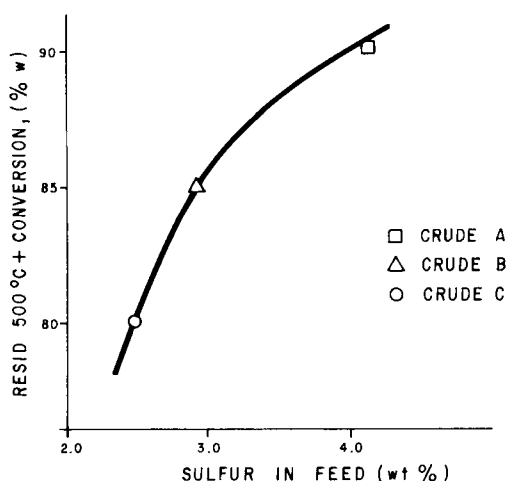


Fig. 7-4. Effect of sulfur in feedstock on asphaltene conversion at similar operating conditions.

these criteria should also take into account the origin of the crude oil and whether or not the asphaltenes have been previously submitted to pretreatment.

**Aromaticity.** Asphaltenes with high polycondensate aromatic molecules tend to produce more coke, and due to its high degree of condensation, hydrogenation becomes more difficult. Table 7-1 shows the main structural characteristics of three types of asphaltenes with different reactivity. Asphaltenes A are more reactive than asphaltenes B and C. The parameter  $CI/C_I$ , defined as the ratio of bridging or internal aromatic carbons to non-bridging or peripheral carbons, is a critical variable to predict reactivity. These values are obtained from the HNMR spectra. A high value of  $CI/C_I$  (over 3) means that the average asphaltene molecule has a more compact aromatic core and, therefore, should be more difficult to process. On the other hand, a lower value of  $CI/C_I$  (between 1.5 and 2) is characteristic of more reactive asphaltene feedstocks.

*Sulfur content.* The amount of sulfur in the feedstock is a critical parameter used to define reactivity in hydroconversion catalytic processes. Fig. 7-4 shows that as the sulfur content in the feedstock increases, a lower thermal level is required to achieve the same conversion as compared to the asphaltenes with lower sulfur content. This behavior is due to the fact that it is easier to break the sulfur-carbon bonds than the carbon-carbon bonds.

*Asphaltene polarity.* By means of SARA analysis by TLC-FID it is possible to differentiate between the polar and nonpolar asphaltenes according to the way they are retained on the silica rods. A correlation has been observed between the nonpolar/polar asphaltene ratio and the behavior of feeds during hydrocracking. Feedstocks with a higher concentration of polar asphaltenes (ratio of 0.3) have a lower reactivity than nonpolar asphaltene (ratio of 0.7). This is probably due to the higher concentration of heteroatoms and the type of polyaromatic units.

## CONCLUSIONS

Selection of the asphaltene conversion process involves many variables in addition to technological and economic issues, including: crude oil source, product specifications, environmental restrictions, secondary conversion requirements, integration with existing units, disposal of by-products, and the state of development of technology [40].

Economic comparison of different types of technologies available for resid conversion is not an easy task due to many economic factors such as: scenario of application, price of raw material, type of feedstock, scale economy, market price of final products, product quality, by-product prices, environmental investment, percent of local component, financing schemes, tax policy and data base, and the methodology. The selection of hydroconversion technology is usually limited by the amount of metals in asphaltenes. As a general rule, for metal contents higher than 300 ppm, the fixed-bed technology will not pay-out. The economy of the ebullating-bed technology is limited to 500 to 550 ppm of metals in the feedstock due to the high catalyst cost. Slurry reactor technology is not limited by the metal content in the feed, but usually requires a price differential (between No. 6 fuel oil and diesel) of over 16 US\$/bbl to yield a reasonable return on investment.

In general, it could be concluded that hydrocracking technologies are moving fast into a mature stage of development to offer an environmentally sound clean fuel production from heavy asphaltenes. New developments resulting from research activity and use of cheap catalysts and/or additives could substantially improve the economy of hydrocracking processes, balancing requirements for large capital investments.

## REFERENCES

- [1] Seko, M., Ohtabe, N., Wada, E., Kuri, K., Katos, K. and Shokji, Y., Super Oil Cracking (SOC) process for upgrading vacuum residue. *NPRA Annu. Meet.*, San Antonio, TX, March 20 (1988).
- [2] *Rarop Heavy Oil Processing Handbook*. Research Association for Residual Oil Processing, Japan, 25 pp. (1991).

- [3] Galiasso, R., Salazar, J.A., Morales, A. and Carrasquel, A., *Hydroconversion of Heavy Crudes with High Metal and Asphaltene Content in the Presence of Soluble Metallic Compound and Water*. U.S. Patent No. 4592837 (1986).
- [4] Galiasso, R., Salazar, J.A. and Huskey, D., Hydrovisbreaking of Cerro Negro crude oil. *J. Pet. Ins.*, 28 (2): 54–62 (1985).
- [5] *Process for the Conversion of Asphaltene and Resins in the Presence of Steam, Ammonia and Hydrogen*. Canadian Patent No. 1208590 (1986).
- [6] Gearhart, J.A. and Washimi, K., High severity soaker cracking. *NPRA Annu. Meet.*, Pap. AM-92-37, New Orleans, LA, March 22–24 (1992).
- [7] Reynolds, B., Johnson, D., Lasher, J. and Hung, C., *NPRA Annu. Meet.*, Pap. AM-89-16, March 19–21 (1989).
- [8] *Hydrocarbon Processing Refining Handbook*, p. 177 (1992).
- [9] *Hydrocarbon Processing Refining Handbook*, p. 184 (1992).
- [10] Billon, A., Peries, J., Couriers, D. and Speillac, M., HYVAHLF versus HYVAHLM, swing reactor or moving bed. *NPRA Annu. Meet.*, San Antonio, TX, March 17–19 (1991).
- [11] Thompson, G., *Handbook of Petroleum Refining Processes* Chapter 8.4, McGraw Hill (1996).
- [12] Yamamoto, T., Resid upgrading to produce transportation fuels. *13th World Petroleum Congress*, Buenos Aires, October (1991).
- [13] Takatsuka, T., Wada, Y., Shimizu, S., Fukui, Y. and Komatsu, S., Vis ABC process. Practical candidate to maximize residue conversion. AM-88-63. *NPRA Annu. Meet.*, March 20–22 (1988).
- [14] Reynolds, B.E., Bachtel, R.W. and Yagi, K., Chevron onstream catalyst replacement (OCR) provides enhanced flexibility to residue hydrotreaters. *NPRA Annu. Meet.*, Pap. AM-92-61, New Orleans, LA, March 24–24 (1992).
- [15] Krasuk, J., Solari, R.B., Aquino, L., Rodriguez, J.V. and Granados, A., *Solvent Deasphalting in Solid Phase*. U.S. Patent 4572781 (1986).
- [16] Morales, A., Galiasso, R., Carrasquel, A.R. and Salazar, J.A., *Catalyst for Removing Sulfur and Metal Contaminants for Heavy Crudes and Residue* U.S. Patent 4642179 (1987).
- [17] Solari, R.B., Hidalgo, R., Herbertz, H., Rammler, R. and Weiss, H., *Combined Process for the Separation and Continuous Coking of Asphaltenes*. U.S. Patent 4859284, Aug. 22 (1989).
- [18] *Evaluation of the INTEVEP's Route for Heavy Oil Upgrading*. INTEVEP-Asvahl Agreement Final Report (1986).
- [19] Galiasso, R., Belandria, J. and Caprioli, L., *Method for Withdrawing Particulate Solid from a High Pressure Vessel*. U.S. Patent 4664762 (1987).
- [20] Deelen, W.J. and Van Tilburg, T.P., The residue hydroconversion process: commercial experience and further developments for integrated refinery configurations. *13th World Petroleum Congress*, Topic 18, Pap. 6, Argentina, Oct. (1991).
- [21] Bishop, W., Smart, M., James, L.C. and McDanel, N.K., LC-fining upgrades Athabasca bitumen. *NPRA Annu. Meet.*, San Antonio, TX, Pap. AM-91-56, March 17–19 (1991).
- [22] Tasker, K.G., Wisdom, L.I., Livingston, W.B. and Sayles, S.L., Texaco H-oil unit commercial operations. *Petroleum Refining Conference*, Japan Petroleum Institute, Tokyo, October 19–21 (1988).
- [23] News Release. Questions and Answers, *NPRA Annu. Meet.*, Anaheim, CA, 14–16 Oct. (1992).
- [24] Bauma, R.F., Aldridge, C.L., Mayer, F.X. and Stuntz, G.F., Microcat-RC — a resid conversion technology contender. *Oil Sands Our Petroleum Future Conference*, Edmonton, Alta., April 4–7 (1993).
- [25] Tarmy, B.L. and Coulaloglou, C.A., Alpha-omega and beyond, industrial view of gas/liquid/solid reactor development. *Chem. Eng. Sci.*, 47 (13/14): 3231–3246 (1992).
- [26] Wenzel, F., Residual oil upgrading and waste processing in the VCC demonstration plant. *NPRA Annu. Meet.*, New Orleans, LA, March 22–24 (1992).
- [27] Upgrading of Cold Lake Heavy Oil in the CANMET hydrocracking demonstrations plant. *Unitar 4th Int. Conf. Heavy Crude Tar Sands*, Edmonton, Alta., August (1988).
- [28] Waugh, W.B., Miur, G. and Skriped, M., Advanced Hydroprocessing of Heavy Oil and Refinery Residues. *13th World Pet. Congr.*, Topic 18, Pap. 4, Buenos Aires, October (1991).
- [29] Yamamoto, T., Sue, H. and Ohno, T., Topic resid upgrading to produce transportation fuels. *13th Pet. Congr.*, Topic 18, Pap. 5, October (1991).

- [30] Solari, B., Guitian, J., Krasuk, J. and Marzin, R., HDH Hydrocracking as an alternative for high conversion of the bottom of the barrel. *NPRA Annu. Meet.* AM-90-28, March 25–27 (1990).
- [31] Fan, L.S., *Gas–Liquid–Solid Fluidization Engineering*. Butterworths, London, 653 pp. (1989).
- [32] Morales, A., Galiasso, R., Agudelo, M.M., Salazar, J.A. and Carrasquel, A.R., *Catalyst Having High Metal Retention Capacity and Good Stability*. U.S. Patent 4520128 (1985).
- [33] Agudelo, M.M., Arias, B., Garcia, J.J. and Martinez, N.P., *Rev. Tec. INTEVEP*, 10 (1): 81–91 (1990).
- [34] LC Fining of Atmospheric and Vacuum Cerro Negro Resid. Report to INTEVEP, S.A. Lummus (1982).
- [35] Garcia, J.J., Galiasso, R.E., Agudelo, M.M., Rivas, L. and Hurtado, J., *Catalyst and Method of Preparation from Naturally Occurring Material*. U.S. Patent 4701435 (1987).
- [36] Krasuk, J., Silva, F., Galiasso, R. and Souto, A., *Process for Hydroconversion and Upgrading of Heavy Crudes of High Metal and Asphaltene Content*. U.S. Patent 4591426 (1986).
- [37] Guitian, J., Krasuk, J., Marruffo, F., Krestchmar, K., Merrz, L. and Niemann, K., *Process for the Hydrogenation of Heavy and Residual Oils*. U.S. Patent 4851107 (1989).
- [38] Amerik, Y.B. and Hadjiev, S.N., Prospects of heavy petroleum residue processing: ideals and compromises. *Preprint 13th World Pet. Congr.*, Topic 18, Pap. 2, Buenos Aires, October (1991).
- [39] Izquierdo, A., Carbognani, L., Leon, V. and Parisi, A., Characterization of Venezuelan heavy oil vacuum residue. *Fuel Sci. Technol. Int.*, 7 (5–6): 561–570 (1989).
- [40] Memon, K.R. and Mink, B.N., Residue conversion options for European refineries. *Hydrocarbon Processing*, 71 (5): 100–101, May (1992).
- [41] Marzin, R., Periera, P., McGrath, M., Feintuch, H.M., Thompson, E. and Houde, E., New residue process increases conversions, produces stable residue in Curaçao refinery. *Oil Gas J.*, (Nov. 2) 79–86: (1998).
- [42] Röbschläer, K.W., Deelen, W.J. and Naber, J.E., The Shell Residue Hydroconversion Process: Development and future applications. In: *Proceedings International Symposium on Heavy Oil and Residue Upgrading and Utilization*, May 5–8, 1992, Fushun, Liaoning, China International Academic Publishers, Session II-2A, Pap. 8, pp. 249–254 (1992).
- [43] Solari, B., Faliasso, R. and Salazar, J.A., PDVSA–INTEVEP technologies for heavy and synthetic crude processing. *Vision Tecnologica*, Special Edition, pp. 63–78 (1999).

This page intentionally left blank

## *Chapter 8*

# **THEORETICAL PRINCIPLES OF THE BITUMEN STRUCTURE AND THE ROLE OF ASPHALTENES (BASED ON RHEOLOGICAL METHOD)**

LEONID M. GOKHMAN

## INTRODUCTION

The conceptual evolution of the bitumen structure began with qualitative approaches to the colloidal structures of the sol, sol–gel and gel types, proposed by Nellensteyn [1], and was later expanded by the well-known works of Hopler, Mack, Saal, and Trakslar. Bitumens were then considered as solutions of high-molecular compounds by Rudenskaya [2]. This led to the presentation of bitumens as complex dispersed systems in the work of Kolbanovskaya et al. [3]. In these works, for the first time, the composition of bitumens with various types of dispersed structures was determined quantitatively and the classification of bitumens, based on concentration and relative content of asphaltenes, resins, and hydrocarbons, was presented. Later, Fryazinov [4] suggested to take into account the component's properties, which were expressed as the coefficient of the dissolving ability of hydrocarbons. In all cases, asphaltenes are considered to be the main structure-forming component in bitumens. Fundamental investigations into the structure and property of asphaltenes conducted by Yen and co-workers were first presented in [5] and later summarized in [6].

This chapter presents a quantitative approach to the classification of bitumens based on the type of dispersion structure. Furthermore, the proposed common criterion of the dispersed structure type (the volume of a particular dispersed-phase particle,  $C_v$ ) takes properties of all components into account and makes it possible to classify all organic binding materials, including bitumens, on a common basis [7].

The main goal of this work is to improve the knowledge of the relations between the composition, structure, and properties of organic binders and asphaltic concrete. A better understanding of the structures and properties of binding materials makes it possible to predict the behavior of asphaltic concrete in the road and airfield pavements, roofing sealants, and water-proofing materials.

## THEORETICAL PREMISES — CONCEPTS

Developments in the fundamentals of the theory of bitumen structure and other organic binders should be based on these five concepts:

(1) Binder dispersed phase is a complex; in particular, it is an asphaltene complex in bitumens.

(2) Volume of binder dispersed-phase particles,  $C_v$ , is the common criterion of the type of the disperse structure of binders and their classification.



(3) Dispersed-phase particles have mono-, bi-, and poly-dispersed nuclei and their structure formation is characterized by a poly-extreme curve.

(4) Characterization of the binder dispersed structure should be based on a set of quantitative parameters obtained by rheological methods.

(5) The gluing role of binders and liquid phase in asphaltic concrete is important.

*The common criterion of disperse structures of bitumens and other organic binders; asphaltene complex*

The writer considers bitumens to be a special case of organic binders. Presently, polymer-bitumen, tar-polymer, sulphur-bitumen and other complex organic binders are made on the basis of products and residues of processed petroleum, coal, asphaltenes, polymers, and other structure-forming components. The writer considers organic binding materials as a part of dispersed systems. Based on this idea, an attempt was made to find a general approach to all organic binding materials.

As shown in Fig. 8-1, the character of the curves of the structure formation is identical for different materials. This figure shows, for example, the relation between the reduced highest Newtonian viscosity,  $\eta$ , and the weight concentration,  $C_w$ , of asphaltene or polymer (block-copolymer of butadiene and styrol of the SBS type). The curves for paints, lacquers, mastics, polymer solutions, asphalt-binding, and other dispersed systems with coagulable structures exhibit the same shape. The difference between these curves is in the values of the first, second, and third critical concentrations. From the above analysis, one may conclude that the volume of dispersed-phase particles for each critical concentration is a constant, which can be explained by physical and mechanical laws. In this analysis, the dispersed-phase particle was assumed to be a nucleus which immobilized and absorbed a part of the dispersion medium, thus forming a complicated

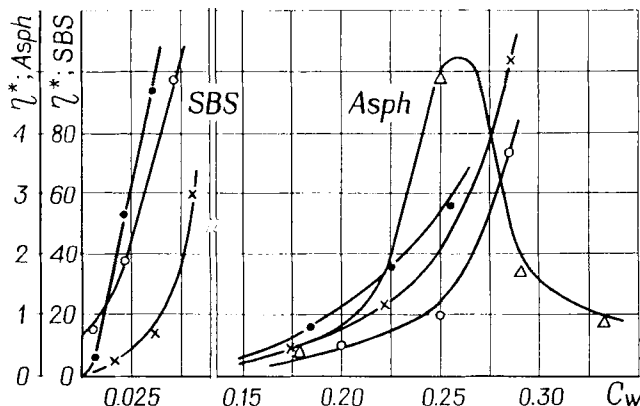


Fig. 8-1. Dependence of the reduced highest Newtonian viscosity of model bitumens on the nuclei content of dispersed-phase particles by weight [of asphaltenes (*Asph*), block copolymer-butadiene-styrene of SBS type]. ● = 51% of resins in maltenes; ○ = 32% of in maltenes; × = 23% of resins in maltenes; Δ = 0% of resins in maltenes.  $C_w$  = filler weight in the binder unit weight;  $\eta^*$  = reduced highest Newtonian viscosity;  $\eta^* = (\eta_0^* \text{ of binder})/(\eta_0^* \text{ of binder dispersion medium})$ .

complex. Any filler can play the role of nucleus, predominantly of a colloidal size (e.g., asphaltene for bitumens). That is why in bitumens, for example, the dispersed-phase particle is called the asphaltene complex. This complex behaves in a system as a whole in the processes of thermal diffusion and deformation. The writer defines the ability of nuclei to immobilize the dispersion medium as a coefficient  $\lambda$  (ratio of the volume of dispersed-phase particles to that of their nuclei). The writer has derived a simple expression for calculating  $C_v$ , using known values of weight concentration of nuclei,  $C_w$ ; coefficient  $\lambda$ ; the density of a nucleus,  $d_n$ , and of a given system  $d$ :

$$C_v = C_w \cdot \lambda \cdot d' \quad (8-1)$$

where:

$$d' = \frac{d}{d_n}$$

The difference in curves shown in Fig. 8-1 can now be explained as a result of different  $\lambda$  for different nuclei of the dispersed-phase and different materials used as a dispersion medium. Thus, the dispersed-phase particles can be considered as a complex which consists of a nucleus and a solvation shell around it. Thickness of the solvation shell depends on  $\lambda$ . The presentation of a dispersed-phase particle of a binding material as a complex compound and use of Eq. 8-1 to evaluate its volume makes the first theoretical concept.

The investigations (conducted by the writer together with E.M. Gurary) of the processes of structure formation by addition of petroleum-benzene (light) and alcohol-benzene (solid) resins into the model bitumens, led to the following suggestion: the asphaltene complexes are formed as a result of the adsorption of alcohol-benzene resins on the polar functionally active fragments of asphaltene, and of the adsorption of petroleum-benzene resins on the lyophilic aromatic portions of the surface. The shape of a complex was assumed to be quasi-spherical on the basis of the results of Yen et al. [5,6], confirmed by works of Bodan and Godun [8,9].

This approach allows one to consider the organic binders as two-phase dispersed systems with solid-like particles of quasi-spherical shape dispersed in a liquid dispersion medium. Consequently, a general curve of structure formation may exist with coordinates  $\eta^*$  and  $C_v$  for disperse systems of the type considered.

*General curve of structure formation for bitumens and other organic binders; critical concentrations of structure formation:  $C_v^*$ ,  $C_v^{**}$ ,  $C_v^{\max}$*

Fig. 8-2 shows a theoretical curve of bitumen structure formation and its relation to critical concentrations. This curve shows the relationship between the reduced highest Newtonian viscosity and the concentration of dispersed-phase particles by volume,  $C_v$ . It should be emphasized that this concentration is not the ratio of the filler concentration by weight to its density. The first critical concentration,  $C_v^*$ , is the beginning of the viscosity anomaly due to the formation of a spatial structure (Fig. 8-2). It results in a change in strength, density and elasto-viscous-plastic properties of this system.  $C_v^*$  is a point of inflection of the curve after which density of the whole system increases.

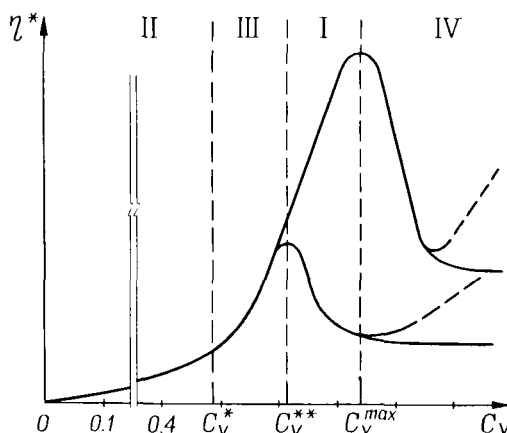


Fig. 8-2. Theoretical dependence of reduced highest Newtonian viscosity of binders on the dispersed-phase particle volume.  $C_v$  = volume of dispersed-phase particles in the binder unit volume; II, III, I, IV = types of the binder dispersed structure;  $C_v^* \approx 0.487$ ,  $C_v^{**} \approx 0.613$ ;  $C_v^{\max} \approx 0.74$ .

Thus, one may consider  $C_v^*$ , by analogy with known concepts of the structure of simple liquids, as a point of the phase-first-kind transition [10].

$C_v^*$  can be calculated using Wood's simple formula [11]. Assuming that the density of the closest regular packing of solid spheres,  $C_v^{\max}$ , is 0.7405:

$$C_v^* = \frac{C_v^{\max}}{1.525 - 1.600} = (0.625 - 0.656) C_v^{\max} = 0.463 - 0.487 \quad (8-2)$$

For further analysis,  $C_v^*$  is assumed to equal 0.487.

It is possible to assume that  $C_v^*$  is also a consequence of the emergence of the short-range order interactions in the system, which result in the thickness of dispersion-medium interlayers between dispersed-phase particles becoming less than the molecular radius (less than 10 Å). A sharp increase in the viscosity at  $0.487 < C_v < 0.613$  can be explained by the appearance of contacts between solvation shells and their involvement in a deformation process.

The second critical concentration  $C_v^{**}$  shows that the system achieved the closest packing of dispersed-phase particles. Radovsky [12] theoretically determined the density of such a packing for solid spherical particles as 0.613. The writer used this value for  $C_v^{**}$ .

It is possible to see, as viscosity increases with the aging of binders, up to  $C_v^{**}$  at  $C_v > C_v^{**}$  (see curve 2 in Fig. 8-2). This can be caused by a generation of new dispersed-phase particles in the free dispersion medium, which is due to the oxidation process until the moment when the closest packing, equal to 0.7405, is achieved. This value is assumed by the writer to be  $C_v^{\max}$ . This approach to the problem allows one to consider  $C_v$  as a common criterion which can be used for the classification of any organic binders according to the type of the dispersed structure (including bitumen), as shown in Fig. 8-2 for the four types: II, III, I and IV.

The concept of  $C_v$  as a common criterion, and usage of the first, second and third critical concentrations for the classification of any binders, is the second concept of the theoretical fundamentals of the bitumen structure.

*Mono-, bi-, and poly-dispersed nuclei of the dispersed-phase particles, poly-extreme curve of the structure formation*

At the point of  $C_v^{**}$ , the following situation is possible: interaction between the nuclei of dispersed particles may be energetically more efficient than the interaction between a nucleus and the dispersion medium. In this case, bi-dispersed or bi-molecular nuclei are formed, resulting in a decrease of the system's viscosity caused by a decrease in the volume of dispersed-phase particles (Fig. 8-3A). After a certain amount of filler is added, most nuclei become bi-disperse, and the main curve of structure formation will be repeated with further increase in  $C_w$  (Fig. 8-3B). The next maximum of this curve reflects generation of the polydispersed nuclei. The calculation shows that forming bi-, and poly-disperse nuclei leads to a decrease in  $C_v$  from 0.613 towards 0.487 due to a decrease in the surface of phase particle nuclei. This situation may repeat until the volume of the dispersion medium is not sufficient to cover all nuclei and the number of coagulable contacts in the system begins to decrease. That is why a maximum of curve 1 appears first (Fig. 8-2) and then viscosity decreases until it becomes equal to the force of friction between dry particles of the dispersed-phase with solvation shells of minimum thickness. If the nuclei are liquid-like (e.g., polymer), the viscosity of the system will increase up to the viscosity of nuclei, as shown by the dotted line.

The concept of mono-, bi-, and poly-dispersed nuclei of the dispersed-phase particles present in organic binders and corresponding poly-extreme curve of structure formation is the third concept of the theoretical fundamentals of bitumen structure.

*Complex of parameters characterizing the spatial disperse structure of binders*

The word 'structure' [13] means a combination of stable bonds of an object, which provides its integrity and identity, i.e., the conservation of basic properties at various internal and external changes. In structures of dispersed substances, including bitumens and other organic binders with the coagulable type of contacts, stable bonds are preserved due to the short-range order interaction between dispersed-phase

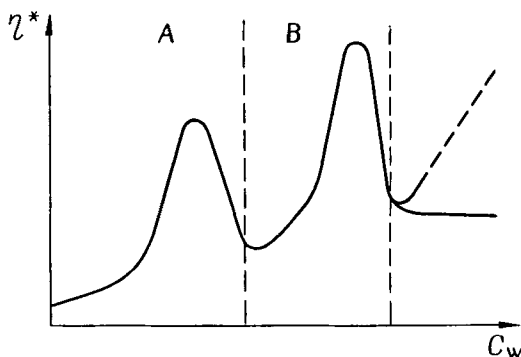


Fig. 8-3. Theoretical dependence of reduced highest Newtonian viscosity of binders on the nuclei content of dispersed-phase particles by weight. A = monodispersed or monomolecular nuclei of dispersed-phase particles; B = bi-dispersed or bimolecular nuclei of dispersed-phase particles of binders.

particles. Proceeding from the above and the assumed model of organic binders as a two-phase disperse system with quasi-spherical particles of the dispersed phase, the major parameters of the structure of such a system are as follows:

- volume of the dispersed phase  $C_v$ ;
- volumetric coefficient  $\lambda$ ;
- sizes of the dispersed-phase particles (effective hydrodynamic radius  $r_{ph}$  or diameter  $D_{ph}$ );
- number,  $n$ , of dispersed-phase particles in the unit volume of the system;
- distance between the dispersed-phase particles in the contact zone  $\delta_{ph}$  and their nuclei  $\delta_n$ ; and
- thickness of the solvation shell of the dispersed-phase particle  $\delta_{sol}$ .

The fourth concept of theoretical fundamentals of binder structures suggests using quantitative parameters for describing their dispersed structure. The writer derived several formulas to calculate these parameters.

To determine  $n$ ,  $C_v$  must be divided by the volume of a single dispersed-phase particle. Assuming that the particle is a sphere, one obtains:

$$n = \frac{6C_v}{\pi D_{ph}^3} \quad (8-3)$$

To calculate  $\delta_{ph}$ , it is necessary to determine what portion of the dispersion medium is present within the contact zones between the dispersed-phase particles.

The average thickness of the film on each particle's surface is equal to the ratio of the free dispersion-medium volume  $(1 - C_v)$  to the total surface of all particles. Thus,  $\delta_{ph}$  is equal to twice the thickness of the film. Nevertheless, it is evident that with the calculation of this kind, particularly at  $C_v > C_v^*$ , the value of  $\delta_{ph}$  will be significantly higher because a part of the dispersion medium will be outside the contact zones.

Assuming that a free dispersion medium between particles is presented by sphere particles, the density of particle packing ranges from the most probable simplest packing to the most probable closest one (the latter is assumed to be equal to 0.613). One can assume that the ratio of the regular packing to the most probable simplest packing is close or equal to the ratio of the regular packing to the most probable closest one, this ratio being equal to  $0.613 : 0.745 = 0.828$ . The most probable simplest packing will then be  $0.828 \times 0.5236 = 0.433$ . Since it is difficult to assess the kind of packing in actual systems, it was assumed to be 0.5, an approximate average between 0.613 and 0.433. Consequently, the volume of dispersion medium forming interlayers in the contact zones is equal to  $0.5(1 - C_v)$ . Thus:

$$\delta_{ph} = 2 \left[ 0.5 \frac{1 - C_v}{ns} \right] = D_{ph} \left[ \frac{1 - C_v}{6C_v} \right] \quad (8-4)$$

where  $s = \pi(D_{ph})^2$ .

The distance between the nuclei of dispersed-phase particles is equal to:

$$\delta_n = \delta_{ph} + 2\delta_{sol} \quad (8-5)$$

After simplification one obtains:

$$\delta_{sol} = \left( \frac{D_{ph}}{2} \right) (1 - \lambda^{-1/3}) \quad (8-6)$$

where:

$$\lambda = D_{ph}^3 / D_n^3 \quad (8-7)$$

Substituting Eqs. 8-4 and 8-6 into Eq. 8-5, one obtains:

$$\delta_n = D_{ph} \left[ \frac{1 + 5C_v}{6C_v} - \lambda^{-1/3} \right] \quad (8-8)$$

To obtain a formula for  $\lambda$ , the basic part of the structure formation curve was described analytically [10] in the  $0 < C_v < 0.613$  range. To do this, Moony's formula and the value of the most probable density of the random packing of the sphere particle ensemble (obtained by Radovsky [12]) were used. The Moony-Radovsky equation was thus derived:

$$\eta^* = \exp [2.5C_v(1 - 1.63C_v)]; \quad \ln \eta^* = [2.5C_v(1 - 1.63C_v)] \quad (8-9)$$

Substituting Eq. 8-1 for  $C_v$  into Eq. 8-9, the following formula for  $\lambda$  was obtained:

$$\lambda = \left( \frac{1}{C_v d} \right) \ln \eta^* (2.5 + 1.63 \ln \eta^*)^{-1} \quad (8-10)$$

Considering that a binder dispersed-phase particle is a sphere with a radius equal to the hydrodynamic radius, one obtains:

$$C_v = \frac{4}{3nW\pi r_{ph}^3}; \quad n = \frac{N\rho}{W}; \quad C_v = \frac{4N\rho r_{ph}^3}{3W} \quad (8-11)$$

where  $N$  is the Avogadro number,  $W$  is molecular weight of the dispersed-phase particle nucleus (e.g., asphaltene), and  $\rho$  is dispersed-phase weight in the unit volume of the system.

Substituting Eq. 8-9 into Eq. 8-11 for  $C_v$ , gives:

$$r_{ph}^3 = 3W \ln \eta^* \frac{(2.5 + 1.63 \ln \eta^*)^{-1}}{4\pi\rho N} \quad (8-12)$$

Thus, seven quantitative parameters were obtained to describe the binder's dispersed structure.

#### EXPERIMENTAL CONFIRMATION OF THEORETICAL CONCEPTS

The experimental confirmations of the first four theoretical concepts are presented in this section. The fifth concept is significant mostly in applications and will be explained later.

##### *Multivariate analysis of the influence of asphaltene complex quality on the properties of model bitumens; substantiation of $C_v$ as the main criterion of the binder structure*

The following was done to prove that  $C_v$  is a major criterion of the type of dispersed structure of bitumen and other organic binders and, therefore, a criterion of a set of their properties. The influence of  $C_v$  together with other parameters

on rheological properties of model bitumens (prepared and studied by Gokhman and Gurary [14,15]) was evaluated. Model bitumens contained (by weight) 30% of asphaltenes of different properties in the dispersion medium (of the same composition in each model). Asphaltenes, as a low-concentrated solution in benzol, were mixed with the dispersion medium until a homogeneous state was reached. Excessive amounts of the solvent were removed by drying to a constant weight in a vacuum cabinet.

The property of asphaltenes varied widely; it was determined by the content of asphalt-resinous components (series 1 and 4) in petroleum, depth of raw material oxidation (series 3), and procedures of bitumen preparation (series 2). Notations of asphaltene samples (in parentheses) and procedures of their preparation are listed below:

(1) Extracted from non-oxidized bitumens separated from oil of the following fields: Tuymazy (1.1), Ust-Balyk (1.2), Anastasiyevskaya (1.3), Nadlendelskaya (1.5), and from Trinidad asphalt (1.6).

(2) Extracted from bitumens separated from the Tuymazy oil by different procedures: vacuum distillation (2.1), light oxidation of heavy flux (2.2), deep oxidation of light flux (2.3), deep oxidation of the asphalt separated by deasphaltization (2.4), and thermal cracking (2.5).

(3) Extracted from bitumens separated from the Anastasiyevskaya oil by oxidation of flux to the following ring and ball temperatures: 58°C (3.2), 82°C (3.3), 96°C (3.4), 105°C (3.5), 124°C (3.6), 138°C (3.7), and extracted from residual bitumen (3.1);

(4) Extracted from bitumens, oxidized to one grade, from the oils of Tuymazy (4.1), Ust-Balyk (4.2) and Venezuela (4.3).

Samples 1.1 and 2.1, 1.3 and 3.1, 2.3 and 4.1, respectively, are identical. Thirty-six model bitumens have been studied. Each of them can be considered to represent a special case of the complex organic binders (COB). Two kinds of dispersion mediums were used: the mixture of paraffin-naphthenic and aromatic hydrocarbons in a 1 : 1 ratio with 25% of the resins by weight (medium I) and aromatic hydrocarbons with 25% of the resins by weight (medium II).

All rheological characteristics were measured in the shear-type plastometer at 20°C at constant shear stress. The highest reduced Newtonian viscosity  $\eta^*$  was determined as the ratio of  $\eta_{\text{COB}}$  to the dispersion medium viscosity  $\eta_{\text{m}}$ . Characteristics do not depend on the conditions of deformation, which was achieved by selection of the gradient of shear rate equal to about  $1 \times 10^{-6} \text{ s}^{-1}$  ( $\eta_{\text{m}}$  for the first dispersion medium was  $1.156 \times 10^4$  poises and for the second one  $8.8 \times 10^2$  poises). The molecular weight of asphaltenes was determined by cryoscopy in naphthalene. The conventional factor of lyophilicity,  $L$ , is the ratio of  $\eta_{\text{COB}}$  in the first dispersion medium to the  $\eta_{\text{COB}}$  in the second dispersion medium. Chemical and physical-chemical characteristics of asphaltenes and values of  $C_v$ ,  $D_{\text{ph}}$  and  $\lambda$  are presented in Tables 8-1 and 8-2 and rheologic characteristics of bitumens are presented in Table 8-3.

Analysis of the data (Table 8-1) showing that the sizes of asphaltene complexes (dispersed phase of bitumens under consideration) are within the  $(20-30) \times 10^{-10} \text{ m}$  range. This coincides with the experimental data of Yen et al. [5,6] and Bodan and Godun [8,9]. On the basis of the conventional lyophilicity factor,  $L$ , Gurary divides asphaltenes into three groups: at  $L$  less than 3 the size (diameter) of asphaltene particles is, as a rule, within the range of  $(20-24) \times 10^{-10} \text{ m}$ ; at  $3 \leq L \leq 10$  the asphaltene size

TABLE 8-1

Chemical and physico-chemical characteristics of asphaltenes

Sample No.	Density (g/cm <sup>3</sup> )	W	C.I.	<i>f</i> <sub>a</sub>	<i>R</i> <sub>A</sub>	<i>R</i> <sub>N</sub>	<i>C</i> <sub>r</sub> (ml)	<i>C</i> <sub>e</sub> (kat/g)	CH <sub>2</sub> /CH <sub>3</sub>	C/H	<i>L</i>
1.1	1.1742	2420	0.33	0.57	2.46	5.4	0	10.21	1.55	10.9	2.9
1.2	1.1940	2140	0.30	0.52	19.6	4.6	0	10.36	1.76	10.1	1.1
1.3	1.1066	1500	0.34	0.59	15.8	4.0	0.12	43.32	1.72	11.2	2.5
1.4	1.1813	2950	0.24	0.35	17.5	8.2	0.51	20.51	1.56	8.5	16.2
1.5	1.1692	3270	0.27	0.42	23.3	8.2	0.44	11.11	1.92	9.1	51.0
1.6	1.1315	3400	0.20	0.26	14.2	9.4	26.76	12.30	1.54	7.7	10.9
2.1	1.1742	2420	0.33	0.57	24.6	5.4	0	10.21	1.55	10.92	2.9
2.2	1.2660	3150	0.31	0.55	30.5	5.5	1.42	14.65	1.64	10.45	5.6
2.3	1.2351	3600	0.31	0.52	35.0	5.1	1.97	17.04	1.66	10.2	90.0
2.4	1.2043	4860	0.21	0.29	23.4	12.2	19.3	35.67	1.84	7.9	1.8
2.5	1.2501	1440	0.34	0.66	16.5	1.1	0.39	8.65	1.52	11.9	0.3
3.1	1.1066	1500	0.34	0.59	15.8	4.0	0.12	43.32	1.72	11.2	2.5
3.2	1.1292	1620	0.33	0.61	17.7	3.0	1.11	37.22	1.77	11.2	4.1
3.3	1.1680	1860	0.33	0.62	20.7	2.8	2.77	32.14	1.79	11.4	5.0
3.4	1.1930	1910	0.33	0.63	21.7	2.6	3.36	25.73	1.82	11.5	12.0
3.5	1.1217	2150	0.33	0.61	23.6	3.5	2.53	25.08	1.78	11.2	9.5
3.6	1.0803	2480	0.33	0.60	26.9	4.2	3.00	23.52	1.82	11.2	7.6
3.7	1.0374	2750	0.32	0.56	27.6	5.6	3.94	21.86	1.77	10.6	4.7
4.1	1.2351	3600	0.31	0.52	35.0	5.1	1.97	17.04		10.2	90.0
4.2	0.9846	2950	0.27	0.45	23.2	6.2	1.89	11.76	1.73	9.3	6.6
4.3	1.1000	4200	0.29	0.47	34.4	9.6	3.94	24.06	1.74	9.6	13.0

is  $(21-25) \times 10^{-10}$  m; and at  $L > 10$  the asphaltene size is  $(25-29) \times 10^{-10}$  m. It is important to note that the exclusion of paraffin-naphthene hydrocarbons (precipitators of the asphaltenes) from the dispersion medium results in an increase in the size of asphaltene complex by 3% to 8% and seldomly by 12% to 19%.

To simplify the rheological method of calculation of quantitative parameters of the COB structure, correlations between the asphaltene complex size, molecular weight, density and the volumetric coefficient have been obtained:

$$2r_{ph} = 15.92 + 0.0032W \quad K = 0.991 \tag{8-13}$$

$$r_{ph}^3 = -\frac{5.42 - 0.82W}{d_0} \quad K = 0.983 \tag{8-14}$$

$$\left. \begin{aligned} \lambda(I) &= 1.743213d_0 \\ \lambda(II) &= 1.79844d_0 \\ \lambda(II) &= 1.853674d_0 \end{aligned} \right\} K = 0.998 \quad \text{I, II types of medium} \tag{8-15}$$

These relations using known values of  $W$ ,  $d_0$ ,  $d_1$ , make it possible to accurately determine  $2r_{ph}$  and  $\lambda$ ,  $C_v^*$  and  $C_v^{**}$  (for a given nucleus of the phase), and also the approximate sizes of asphaltene complexes in commercial bitumens.



TABLE 8-2

Chemical characteristics of asphaltenes, parameters of asphaltene complex and bitumen structure

Sample No.	Phase volume, $C_v$		Size of asphaltene ( $\text{\AA}$ )		Voluminosity coefficients, $\lambda$		Element content				
	medium I	medium II	medium I	medium II	medium I	medium II	C	H	S	N	O <sup>a</sup>
1.1	0.501	0.520	23.36	23.90	1.950	2.110	87.28	8.02	3.22	0.86	0.70
1.2	0.496	0.571	22.30	23.94	1.950	2.330	86.67	8.56	3.13	0.88	0.76
1.3	0.515	0.527	20.22	20.64	1.910	2.040	88.48	7.93	0.75	0.93	1.91
1.4	0.533	0.530	25.36	25.70	2.070	2.145	83.69	9.92	4.51	0.98	0.90
1.5	0.529	0.517	26.30	26.48	2.050	2.090	83.23	9.13	5.62	1.00	1.02
1.6	0.536	0.534	26.28	27.20	2.020	2.110	79.70	10.31	6.04	1.92	2.03
2.1	0.534	0.542	23.36	23.90	1.950	2.110	87.28	8.02	3.22	0.86	0.70
2.2	0.541	0.530	25.70	26.30	2.200	2.320	85.95	8.26	3.67	0.99	1.13
2.3	0.543	0.551	27.20	27.40	2.180	2.250	84.70	8.32	3.72	0.97	2.29
2.4	0.525	0.563	30.20	30.70	2.145	2.265	81.45	10.32	3.06	1.21	3.96
2.5	0.513	0.524	19.80	20.60	2.130	2.380	86.03	7.23	3.78	1.08	1.88
3.1	0.530	0.538	20.22	20.64	1.910	2.040	88.48	7.93	0.75	0.93	1.91
3.2	0.535	0.536	20.72	21.16	1.940	2.060	88.44	7.86	0.67	0.95	2.08
3.3	0.537	0.536	21.80	22.20	2.045	2.170	88.50	7.78	0.61	1.01	2.10
3.4	0.538	0.538	22.00	22.18	2.100	2.190	88.50	7.70	0.63	0.98	2.19
3.5	0.538	0.545	22.40	22.76	2.015	2.090	88.46	7.88	0.58	1.09	1.99
3.6	0.523	0.530	24.20	24.60	1.960	2.050	88.36	7.92	0.55	1.07	2.10
3.7	0.510	0.560	25.20	25.64	1.905	2.050	88.04	8.30	0.55	1.03	2.08
4.1			27.20	27.44	2.180	2.250	84.70	8.32	3.72	0.97	2.29
4.2			25.64	26.10	1.790	1.880	85.91	9.24	2.70	0.93	1.22
4.3			28.40	29.22	1.890	2.075	84.85	8.82	3.53	1.08	1.08

<sup>a</sup> By difference.

TABLE 8-3

Rheological and physico-chemical characteristics of bitumens

Sample No.	Highest Newtonian viscosity ( $\eta_0 \times 10^{-6}$ Pa s)		Equilibrium elastic modulus ( $G_{m_0} \times 10^{-4}$ Pa)		Period of stress relaxation ( $\theta_{m_0} \times 10^{-3}$ s)		Elasticity index, $K$ (C/Pa)		Dynamic yield limit ( $P_{k_2} \times 10^{-2}$ Pa)	Softening point (°C)	Brittle point (°C)	Workability interval (°C)
	medium I	medium II	medium I	medium II	medium I	medium II	medium I	medium II	medium I	medium I	medium I	medium I
1.1	12.6	4.4	0.33	0.28	3.82	1.57	0.116	0.056	7.0	47.0	-15.0	62.0
1.2	8.0	7.6	0.26	0.49	3.08	1.55	0.118	0.032	11.0	47.0	-20.0	67.0
1.3	25.1	10.0	0.76	0.50	3.30	2.00	0.044	0.050	24.0	48.5	-17.0	65.5
1.4	200.0	12.4	2.50	0.70	8.00	1.77	0.032	0.025	42.0	63.5	-10.0	73.5
1.5	158.0	3.1	3.20	0.08	5.00	3.88	0.016	0.485	39.0	67.0	-16.0	83.0
1.6	398.0	36.4	4.20	0.90	9.50	3.92	0.023	0.044	46.6	78.0	-5.0	83.0
2.1	12.6	4.4	0.33	0.28	3.82	1.57	0.116	0.056	7.0	47.0	-15.0	62.0
2.2	398.0	72.0	10.00	4.10	3.98	1.76	0.004	0.004	50.0	56.0	-11.0	67.0
2.3	1260.0	14.0	6.07	0.40	20.80	3.00	0.034	0.075	88.0	77.0	-9.0	86.0
2.4	1070.0	567.0	5.00	4.80	21.40	11.80	0.043	0.025	103.0	126.0	-	126.0
2.5	83.0	220.0	1.80	6.00	4.60	4.60	0.026	0.008	29.0	45.0	-29.0	74.0
3.1	25.1	10.0	0.76	0.50	3.30	2.00	0.044	0.050	24.0	48.5	-17.0	65.5
3.2	31.6	7.7	0.75	0.30	4.20	2.56	0.056	0.086	65.0	56.0	-8.0	64.0
3.3	200.0	40.0	3.12	0.90	6.40	2.10	0.021	0.011	110.0	60.5	-7.0	67.5
3.4	500.0	42.7	6.70	0.90	7.50	4.75	0.011	0.053	156.0	67.0	-7.0	74.0
3.5	380.0	40.0	4.80	1.00	7.90	4.00	0.017	0.040	130.0	59.0	-6.0	65.0
3.6	417.0	54.8	5.63	1.96	7.40	2.12	0.013	0.011	210.0	80.0	-6.0	86.0
3.7	548.0	116.4	7.50	2.85	7.30	4.10	0.010	0.010	212.0	84.0	-4.0	88.0
4.1	1260.0	12.0	26.07	0.40	20.8	3.00	0.034	0.075	88.0	77.0	-9.0	86.0
4.2	69.3	10.5	1.33	0.57	5.2	1.83	0.039	0.039	87.5	58.0	-12.0	70.0
4.3	630.0	50.0	4.88	0.70	12.9	7.10	0.027	0.102	95.0	74.0	-14.0	88.0

It should be noted that at a high enough concentration of the dispersed phase, the size of its particles affects rheological properties of the system at higher concentrations of the dispersed phase. This is confirmed by rather high values of the coefficient of correlation,  $K$ , between the size of the asphaltene complex,  $\eta_0$ , and equilibrium elastic modulus,  $G_{m0}$ :

$$\lg \eta_0 = 3.82 + 0.43r_{ph} \quad K = 0.750 \quad (8-16)$$

$$\lg G_{m0} = -9.47 - 20.59 \left( \frac{r_{ph}^3}{W} \right) \quad K = 0.797 \quad (8-17)$$

It is evident that the rheological and performance properties of model bitumens are influenced not only by the volume,  $C_v$ , and size of the dispersed-phase particles but also by other factors. All factors were combined into three groups:

- Factors characterizing properties of asphaltenes: density, ( $d_0$ ), molecular weight ( $W$ ), condensation index (C.I.), aromaticity ( $f_a$ ), content of aromatic ( $R_A$ ) and naphthenic rings ( $R_N$ ) in the molecule.
- Factors determining the ability of asphaltenes to interact with the dispersion medium, and the contents of functional groups: carboxyl groups ( $C_r$ ), complex-ether groups ( $C_c$ ), the length of aliphatic chains being determined by the ratio  $\text{CH}_2 : \text{CH}_3$  (1), the aromaticity as approximately determined by the ratio C : H.
- Factors characterizing the quality of the asphaltene complex: volume of the dispersed phase in fractions of unit ( $C_v$ ), size of the asphaltene complex as effective hydrodynamic diameter ( $D_{ph}$ ), the conventional factor of lyophilicity ( $L$ ), and the volumetric coefficient ( $\lambda$ ).

Multivariate regression analysis has been performed using an EC-1022 computer and the multiple linear regression program 'Corre'. Linear equations (Table 8-4) as shown in Eq. 8-8 were obtained to relate rheological and performance properties of model bitumens ( $y$ ) to the parameters characterizing the properties of the dispersed-phase particles and their nuclei ( $x$ ):

$$y = a_0 + a_1x_1 + a_2x_2 + \dots + a_nx_n \quad (8-18)$$

where  $a_0$  is a free element, and  $a_1 \dots a_n$  are regression coefficients.

Regression equations for influence of parameters of all three groups together and of each group separately were obtained. It should be noted that terms insignificant by the T-criterion were not excluded from further consideration, as the properties of model bitumens are characterized by the whole set of rheological and performance characteristics.

Using the values of relative elasticity coefficients ( $\epsilon$ ) in Table 8-5, it is possible to determine which factors in the obtained equations had the greatest influence on the property being considered. The elasticity coefficient was determined as:

$$\epsilon = \frac{a_i x_i}{y_i} \quad (8-19)$$

where  $a_i$  is regression coefficient;  $x_i$  is the arithmetical average of a given factor; and  $y_i$  is the arithmetical average of a given property.

TABLE 8-4

Parameters of linear equations of regression

No.	Characteristics	Type disp. medium	Coefficient of multiple correlation	Free member $d_0$	Factors determining the quality of an asphaltene complex					
					Values of regression coefficients for factor group I					
					$d$	$W$	C.I.	$f_a$	$R_A$	$R_N$
1	$\eta_0 \times 10^{-6}$ , Pa s	I	0.978	-29435	25013	675	5487	3966	-11	-129
2		II	0.996	9651	-11501	4.67	-19238	11020	-16.5	240
3	$G_{m0} \times 10^{-4}$ , Pa	I	0.973	-58	-9.8	-8.3	-23	110	0.6	1.7
4		II	0.911	128	-146	0.058	-295.9	164.9	-0.04	3.4
5	$\theta_{m0} \times 10^{-3}$ , s	I	0.979	-419	398	18	-60	-19	-0.4	-2.7
6		II	0.985	134	-125	0.12	-371	204	0.18	4.9
7	$K$ (C/Pa)	I	0.906	-0.09	0.517	0.05	3.04	-1.9	-0.005	-0.04
8		II	0.980	-4.86	4.57	0.003	5.2	5.2	0.04	0.02
9	$P_{k_2} \times 10^{-2}$ , Pa	I	0.983	-7887	5764	-150	-3263	1830	4	16
10	$\eta_m'' \times 10^{-6}$ , Pa	I	0.951	-607	573.8	-24.9	-1735	-82	4.7	10
11		I	0.995	9981	-5064	2166.9	11370	-2863	33	-110
12	$T_s$	I	0.983	-2073	1412	8.9	484	367	-5.7	-4.9
13	$T_{br.}$	I	0.969	-207	204	51	644	-108	-3.10	-5.4
14	W.T.	I	0.988	-2279	1617	60	1128	259	-9	-10

No.	Factors determining the quality of an asphaltene complex				Values of regression coefficients for factor group III			
	Values of regression coefficients for factor group II				Values of regression coefficients for factor group III			
	$C_t$	$C_c$	$CH_2/CH_3$	C/H	$L$	$C_v$	$D_{ph}$	$\lambda$
1	18.7	11.9	-211	-436	3.6	73539	10	-18898
2	8.1	3	7605	51.7	-766	-21509	183	-70
3	0.25	0.05	-2.0	-9.0	0.02	139	0.35	6.2
4	-0.09	0.03	98.4	0.176	-14	-283	-1.43	0.26
5	0.03	0.2	-4.2	4.4	0.1	1123	-1.3	-314
6	0.05	0.02	78	-0.8	-8.1	-166	2.9	-3.2
7	-0.00067	0.00002	0.09	0.058	-0.0008	-1.4	0.02	-0.32
8	0.003	-0.006	-2.96	-0.26	0.5	6.66	0.037	0.07
9	1.9	1.4	66	-8.4	0.14	18212	49	-4606
10	-0.57	0.07	8.3	57.6	0.14	1764	-8	-455
11	56.4	1.17	-684	-406	5.8	-15841	-24.7	4139
12	0.56	0.59	18	-21	0.006	3947	23	-1069
13	0.62	-0.36	5.9	2.9	-0.08	540	-4.8	-161
14	0.06	0.23	24	-24	0.07	4487	18	-1230

TABLE 8-5

Coefficient of elasticity,  $\epsilon$ , (influence) of quality parameters of asphaltenes and asphaltene complexes on bitumen properties

Index	Medium type	group I						group II				group III			
		$d$	$W$	C.I.	$f_a$	$R_A$	$R_N$	$C_r$	$C_e$	$CH_2/CH_3$	C/H	$L$	$C_v$	$D_{ph}$	$\lambda$
$\eta_0$	I	81	5.1	4.6	5.8	0.7	2.0	0.2	0.7	-1.0	-12.6	0.14	109	0.7	-107
	II	-174	0.8	-75.6	74.7	-5.02	17.8	-0.4	0.9	214	6.9	-17.3	-152	0.8	-22.9
$G_{m0}$	I	2.9	-5.9	-1.7	14.8	3.9	2.5	0.27	0.03	-0.9	-24.5	-0.08	19	2.2	3.27
	II	-110	0.5	-58	55.8	-0.6	12.5	-0.25	0.4	138	1.2	-15.8	-100	-2.5	-4.3
$\theta_{m0}$	I	58	6.2	-2.2	-1.2	-1	-1.9	0.01	0.57	-0.9	5.7	0.15	74.8	-3.9	80
	II	-40	0.4	-30.9	29.5	1.15	7.7	0.05	0.12	46.8	-2.3	-3.9	-25	2.2	-22
$K$	I	16.5	4.2	25	-28.4	-3.7	-6.4	0.07	0.01	4.4	16.4	-0.3	-20.7	14.58	-17.9
	II	82.5	0.7	24.5	27.2	15.8	2	0.19	-2.16	-99	-42.4	13.8	56.2	1.6	28
$P_{k_2}$	I	79	-4.8	-11.6	11.2	1.15	1.08	0.09	0.36	1.36	1.03	0.02	114	14.4	-110.9
$\eta''_m$	I	81	-8.2	-63	5.2	13.3	6.9	-0.28	0.19	1.7	72.3	0.2	114	-24	-112
$\varphi$	I	-35	-2.7	20.4	-8.87	4.6	-3.7	1.38	0.15	-7	-24	0.47	-50	-3.6	50
$T_v$	I	24.5	0.36	2.2	2.8	-2	-0.4	0.03	0.19	0.47	3.2	0.001	31	3.4	-32
$T_{br.}$	I	20	11.8	16.3	-4.7	-6.4	-2.57	-0.2	0.6	0.86	-2.5	-0.09	24	-9.8	-27.57
W.T.	I	23.8	2.08	4.3	4.3	-2.6	-0.7	-0.003	0.6	0.5	-3.09	-0.01	30.2	5.6	-31
Sum	I	421.7	51.34	151.3	87.3	39.3	28.1	2.5	2.9	19.1	165.3	1.5	586.7	82.2	571.7
Sum	II	406.8	2.40	189.0	187.2	22.6	40	0.9	3.6	497.8	52.8	50.8	333.2	7.1	77.2

*Multivariate analysis of influence of factors characterizing properties of asphaltenes and asphaltene complexes on the rheological and physical-mechanical properties of bitumens*

An analysis of elasticity coefficients in Table 8-5 was carried out to determine which groups of asphaltenes and their complex characteristics have the greatest influence on bitumen properties. Results of this analysis are presented in Table 8-6, which shows the arithmetic means of  $\epsilon$  for each property index in a given group of factors.

For medium I, Table 8-6 demonstrates that the third group of factors has the greatest influence on bitumen properties. This is true for each index of properties individually and for all indices taken together.

Group 1 has less influence on bitumen properties than group 3; group 2 has less influence than group 1. The influence ratio of the factors of the third, first and second groups is 10.8:3.4:1. Model bitumens with the dispersion medium of type I have the same group chemical composition as commercial bitumens; therefore, the above conclusion may be applied to them. Comparison of the influence of all groups of factors, made by comparison of the sums of  $\epsilon$  for the most important parameters (for each index of properties in each group), leads to the same conclusions for bitumens with medium I. For medium I, the ratio of influences of the third, first and second groups is 3.6:2.7:1.

Analysis of the influence of each group of factors using sums of elasticity coefficients for each index individually and all indices taken together (Table 8-7) results in the same conclusion. The ratio of influences of groups 3, 1 and 2 is 6.5:4.06:1.

Thus, it has been proven that the group of factors (parameters) characterizing an asphaltene complex has a greater effect on the properties of model bitumens than the group of parameters characterizing the ability of asphaltenes to interact with a dispersion medium and the chemical structure of asphaltenes. Within the third group, all factors characterizing properties of asphaltenes and asphaltene complexes,  $C_v$ , have the greatest effect on bitumen properties, followed by  $\lambda$  and then by  $D_{ph}$ .

These results have proven the following:

(1)  $C_v$  is the most important parameter of the binder dispersed structure characterizing the set of properties and can be used as a common criterion (classifying criterion).

TABLE 8-6

Average absolute specific value of  $\epsilon$  for groups of factors

Medium type	Group of factors	$\eta_0$	$G_m$	$\theta_m$	$K$	$P_{k_2}$	$\eta_m''$	$\varphi$	$T_s$	$T_{br}$	W.T.	Sum
I	I	16.5	5.3	11.7	14.0	18.1	29.6	12.2	5.4	10.3	6.1	129.2
	II	2.9	5.1	1.5	4.2	0.6	14.9	6.6	0.8	0.8	0.7	38.1
	III	72.2	8.2	52.6	17.7	79.7	83.3	34.5	22.1	20.5	22.3	413.1
	Sum	91.6	18.6	65.8	35.9	98.4	127.8	53.3	28.3	31.6	29.1	580.9
II	I	58.0	39.6	19.0	25.5							142.1
	II	47.9	31.1	10.6	31.5							121.1
	III	58.6	35.6	16.4	28.3							138.9
	Sum	164.5	106.3	46.0	85.3							402.1

TABLE 8-7

Sum of elasticity coefficients,  $\epsilon$ , for three groups of factors

Indices	Medium type	Groups of factors			Sum
		I	II	III	
$\eta_0$	I	99.2	14.64	216.7	330.5
	II	347.9	239.5	175.8	763.6
$G_m$	I	31.8	25.5	24.6	81.9
	II	237.6	155.5	106.8	499.9
$\theta_{m_0}$	I	70.2	7.5	157.8	235.5
	II	114.0	53.0	49.2	216.2
$K$	I	84.0	21.0	53.1	158.1
	II	153.0	157.5	84.9	395.4
$P_{\lambda_s}$	I	108.6	3.0	239.1	350.7
$\eta_m''$	I	177.6	74.5	249.9	502.0
$\varphi$	I	73.2	33.0	103.6	209.7
$T_s$	I	32.4	4.0	66.4	102.7
$T_r$	I	61.8	4.0	61.5	127.3
W.T.	I	36.6	3.5	66.9	107.0
Sum	I	775.4	190.6	1239.5	2205.4
Sum	II	852.5	605.5	416.7	1874.7

(2) The concept that a bitumen dispersed-phase particle is an asphaltene complex consisting of the asphaltene nucleus and of a dispersion medium immobilized and adsorbed by this nucleus. Parameter  $\lambda$  characterizes the volume of the dispersion medium that is included in this complex as its part inseparable during processes of diffusion and deformation. Judging by values of  $\epsilon$ , index  $\lambda$  is the most important, after  $C_v$ , parameter influencing the structure and properties of binders. Parameter  $d$ , a representative of group 1, characterizing the properties proper of asphaltenes, has less but still noticeable influence. It should be noted that all three parameters are terms of Eq. 8-1, which confirms the concept that  $C_v$  is the most important criterion of the property of binders (bitumens in particular) and their structures.

Each of all fourteen parameters has its own unique influence on each of the bitumen properties. Not more than five parameters have the greatest influence on bitumen properties and greater values of  $\epsilon$ . These parameters are listed, for each property, by order of decreasing values of their  $\epsilon$  (Table 8-8).

Parameters  $C_v$ ,  $\lambda$  and  $d$  have the greatest influence on viscosity ( $\eta_0$ ,  $\eta_m''$ ), dynamic yield point ( $P_{\lambda_s}$ ), stress relaxation time ( $\theta_{m_0}$ ), structure distortion degree ( $\varphi$ ), temperatures of softening and brittleness ( $T_s$ ,  $T_{br.}$ ), and the range of serviceability (W.T.). Parameter  $\lambda$  has the greatest influence on performance properties in the considered range of  $C_v$  values.  $G_{m_0}$  and  $K$  are mostly affected by the aromaticity of asphaltenes ( $C/H$  and  $f_a$ ). The viscosity and strength of bitumens depend mostly on the volume and dispersity of the phase. Their elasticity also depends on the interaction between the filler and the dispersion medium. This suggestion is also confirmed by the fact that in the absence of a precipitator in the dispersion medium (medium II) all rheological properties are influenced most by the length of aliphatic chains ( $l$ ), which seems to have

TABLE 8-8

Parameters having the greatest influence on bitumen properties (medium I)

Indices	Parameters of asphaltenes and asphaltene complexes; resilience coefficients				
	$C_v$		$d$	C/H	$f_a$
$\eta_0$	109	107	81	12.6	5.8
$G_{m_0}$	C/H	$C_v$	$f_a$	$W$	$\lambda$
$\epsilon$	24.5	19	14.8	5.9	3.27
$\theta_{m_0}$	$\lambda$	$C_v$	$d$	$W$	C/H
$\epsilon$	80	74.8	58	6.2	5.7
$K$	$f_a$	C.I.	$C_v$	$d$	C/H
$\epsilon$	28.4	25	20.7	16.5	16.4
$P_{k_2}$	$C_v$	$\lambda$	$d$	$D_{ph}$	C.I.
$\epsilon$	114	110.9	79	14.4	11.6
$\eta_m''$	$C_v$	$\lambda$	$d$	C/H	C.I.
$\epsilon$	114	112	81	72.3	63
$\varphi$	$C_v$	$\lambda$	$d$	C/H	C.I.
$\epsilon$	50	50	35	24	20.4
$T_s$	$\lambda$	$C_v$	$d$	$D_{ph}$	$f_a$
$\epsilon$	32	31	24.5	3.4	2.8
$T_{br.}$	$\lambda$	$C_v$	$d$	C.I.	$W$
$\epsilon$	27.6	24	20	16.3	11.8
W.T.	$\lambda$	$C_v$	$d$	$D_{ph}$	$f_a$
$\epsilon$	31	30.2	23.8	5.6	4.3

a considerable influence on the degree of interaction between the phase and the medium.

Values of  $\epsilon$  were used to evaluate the influence of parameters of asphaltene properties on properties of model bitumens (Tables 8-5 and 8-7).

The data show that, in the absence of a precipitator in the dispersion medium of the second type, the majority of parameters determining the properties of asphaltenes (group I) mostly affect  $\eta_0$ ,  $G_{m_0}$  and  $K_{cc}$  of bitumens. This is probably caused by the predominant influence of the asphaltene properties on the interlayers of the dispersion medium.

Parameters of asphaltene complex properties were rated by their influence on the whole set of model bitumen characteristics using the arithmetical average of values for each parameter and then the sum  $\epsilon$  of values of all characteristics for each parameter (Table 8-5). Ten characteristics for the first-type medium and four characteristics for the second-type medium were used (influence of characteristics decreases from left to right and the influence of the first five is significantly greater than the rest):

First medium:

$C_v$ ;  $\lambda$ ;  $d$ ; C/H; C.I.;  $f_a$ ;  $D_{ph}$ ;  $W$ ;  $R_A$ ;  $R_N$ ;  $l$ ;  $C_\epsilon$ ;  $C_r$ ;  $L$

Second medium:

$l$ ;  $d$ ;  $C_v$ ; C.I.;  $f_a$ ;  $\lambda$ ; C/H;  $L$ ;  $R_N$ ;  $R_A$ ;  $D_{ph}$ ;  $C_\epsilon$ ;  $W$ ;  $C_r$

All bitumen characteristics were also rated by their sensitivity using data yielded by the studies of influence of the dispersed-phase properties (type II of the media is indicated with parentheses) on properties of model bitumens (Table 8-7):



$$\eta_0(\text{II}); \eta_m(\text{II}); G_{m_0}(\text{II}); K_{cc}(\text{II}); P_{k_2}; \eta_0; \theta_{m_0}; \theta_{m_0}(\text{II}); \varphi; T_{br.}; \text{W.T.}; T_s; G_{m_0}$$

The following regression equations were determined by using a step-method of multiple correlation; the method distinguishes the factors that are characterized by a close association with the argument (correlation coefficient more than 0.4) and sufficient significance ( $t$ -value corresponds to the confidence interval  $P > 0.8$ ).

$$\begin{aligned} \eta_0 &= -2000 + 892W - 262D_{ph} + 28.4R_A + 10523C_v + 19.5C_c + 4.1L; \\ K &= 0.945, \quad P > 0.85 \end{aligned} \quad (8-20)$$

$$\begin{aligned} G_{m_0} &= -29 + 37\lambda - 40d + 0.28R_A - 0.44L; \\ K &= 0.897, \quad P > 0.95 \end{aligned} \quad (8-21)$$

$$\begin{aligned} K_{cc} &= -0.1 + 1.1d - 0.7\lambda - 0.7C.I. - 0.1C_c + 0.5L; \\ K &= 0.899, \quad P > 0.95 \end{aligned} \quad (8-22)$$

$$\begin{aligned} P_{k_2} &= -1053 - 342d + 137l + 2.52R_A + 236C_v; \\ K &= 0.838, \quad P > 0.8 \end{aligned} \quad (8-23)$$

$$\begin{aligned} \varphi &= 5117 - 1014C/H + 19566C.I. - 209R_N + 61O_2 + 21R_A; \\ K &= 0.923, \quad P > 0.95 \end{aligned} \quad (8-24)$$

$$T_{br.} = 91 + 37d - 233C_v; \quad K = 0.641, \quad P > 0.95 \quad (8-25)$$

$$\text{W.T.} = 44 + 0.41C_c + 4.4R_N; \quad K = 0.727; \quad P > 0.8 \quad (8-26)$$

The above equations are suitable for practical use, but  $T_{br.}$  and W.T. are characterized by weak relations with the factors. This is the reason for conducting multivariate analysis (program developed by B. Fyne). In addition to the above factors, this analysis includes the content of heteroatoms. This program provides for the preservation of those regression members that only, by Student's test, correspond to a confidence interval greater than 0.95. The following equations with greater values of multiple correlation coefficients are obtained:

$$\begin{aligned} \eta_0 &= 627 + 70R_A - 322C/H - 322W + 352O_2 + 950\lambda; \\ K &= 0.965 \end{aligned} \quad (8-27)$$

$$G_{m_0} = -207 + 1.2C + 0.9D_{ph} + 28d + 26C_v; \quad K = 0.844 \quad (8-28)$$

$$\theta_{m_0} = 766 - 8.5C - 6.5S - 1.0W + 1.3R_A - 1.3N; \quad K = 0.925 \quad (8-29)$$

$$\begin{aligned} P_{k_2} &= 13638 - 1.77C - 200N + 146C/H + 590O_2 - 0.1W \\ &\quad - 139D_{ph} + 6.5C_c - 2.2C_e; \quad K = 0.947 \end{aligned} \quad (8-30)$$

$$\begin{aligned} \eta_m'' &= 3176 - 3435d + 1974\lambda - 2172C_v + 7.3C + 0.1W \\ &\quad - 1.8R_A - 0.8C_e; \quad K = 0.661 \end{aligned} \quad (8-31)$$

$$\varphi = 3846 - 950C/H + 19501C - 240R_N + 63K_p + 13C_e + 136S + 291R_A; \quad K = 0.975 \quad (8-32)$$

$$L = -2098 + 83O_2 + 41C - 82C/H + 54S - 0.1W + 9.4R_A; \quad K = 0.859 \quad (8-33)$$

$$\text{Ball and ring} = -56 + 15O_2 + 3.9D_{ph}; \quad K = 0.955 \quad (8-34)$$

$$T_{br.} = 791 + 1172d - 683\lambda + 767C_v - 9.3D_{ph} - 0.2W - 4.5C + 4.8C/H - 19N; \quad K = 0.939 \quad (8-35)$$

$$K_{cc} = -1.5 - 0.2S - 0.7C_v - 0.2C/H - 0.2C; \quad K = 0.883 \quad (8-36)$$

$$W.T. = 54 + 22O_2 + 4.0R_N - 0.6C_e - 23N; \quad K = 0.968 \quad (8-37)$$

It is difficult to interpret derived equations in physical terms because of the compounds that contain one or another heteroatom are unknown. The equations nevertheless, may be of practical use.

*Multivariate analysis of the influence of asphaltene chemical composition on properties of bitumens*

The data from Table 8-5 were used to rate the influence of each parameter of the asphaltene properties on the properties of bitumens (Table 8-9).

Table 8-9 reveals that asphaltene density,  $d$ , has the greatest influence on the sum of all indices of bitumen properties, which is followed by the degree of condensity C.I.

TABLE 8-9

Distribution of factors of asphaltene quality according to the degree of their influence on bitumen properties

Indices	Medium type	Factors of asphaltene quality						Sum of $\epsilon$
$\eta_0$	I	$d$	$f_a$	$W$	C.I.	$R_N$	$R_A$	99.2
$G_{m_0}$	I	$f_a$	$W$	$R_A$	$d$	$R_N$	C.I.	31.8
$\theta_{m_0}$	I	$d$	$W$	C.I.	$R_N$	$f_a$	$R_A$	70.2
$K$	I	$f_a$	C.I.	$d$	$R_N$	$W$	$R_A$	84.0
$P_{k_2}$	I	$d$	C.I.	$f_a$	$W$	$R_A$	$R_N$	108.6
$\eta'_m$	I	$d$	C.I.	$R_A$	$W$	$R_N$	$f_a$	177.6
$\varphi$	I	$d$	C.I.	$f_a$	$R_A$	$R_N$	$W$	73.2
$T_s$	I	$d$	$f_a$	C.I.	$R_A$	$R_N$	$W$	32.4
$T_{br.}$	I	$d$	C.I.	$W$	$R_A$	$f_a$	$R_N$	61.8
W.T.	I	$d$	C.I.	$f_a$	$R_A$	$W$	$R_N$	36.6
All	I	$d$	C.I.	$f_a$	$W$	$R_A$	$R_N$	775.4
$\eta_0$	II	$d$	C.I.	$f_a$	$R_N$	$R_A$	$W$	347.9
$G_{m_0}$	II	$d$	C.I.	$f_a$	$R_N$	$R_A$	$W$	237.6
$\theta_{m_0}$	II	$d$	C.I.	$f_a$	$R_N$	$R_A$	$W$	114.0
$K$	II	$d$	$f_a$	C.I.	$R_A$	$R_N$	$W$	153.0
All	II	$d$	C.I.	$f_a$	$R_N$	$R_A$	$W$	852.5

and the parameter of aromaticity,  $f_a$ . In relation to each index of bitumen properties,  $f_a$  of asphaltenes has the greatest influence on the elastic modulus and resilience index. This can be explained by the considerable influence that the properties of the dispersion medium have on these indices. It should be noted that  $d$ , C.I. and  $f_a$  of asphaltenes have the greatest effect on bitumen properties in the absence of a precipitator (medium II).

Analysis of the data also reveals that the introduction of a precipitator or decreasing amount of solvent for the nuclei of the dispersed-phase particles (here asphaltenes) reduces the influence on binder properties. Thus, the average value of  $\epsilon$  per one characteristic is 77.5 in medium I and 213.1 in medium II (Table 8-9). Using values of  $\epsilon$  (Table 8-9), it is possible to rate indices of bitumen properties by the influence that asphaltene properties have on them:

Medium I :  $\eta_m$ ;  $P_{k_2}$ ;  $\eta_0$ ;  $K_{cc}$ ;  $\varphi$ ;  $\theta_{m_0}$ ;  $T_{br}$ ; W.T.;  $T_s$ ;  $G_{Cm_0}$ .

Medium II :  $\eta_0$ ;  $G_{m_0}$ ;  $K_{cc}$ ;  $\theta_{m_0}$ .

*Multivariate analysis of the influence of parameters characterizing an ability of asphaltenes to interact with the dispersion medium on rheological and physical-mechanical properties of bitumens*

Based on the data in Table 8-5, parameters, which are referred to as the second group of factors, were rated by their influence on bitumen characteristics (Table 8-10).

The data show that the sum of all indices of bitumen properties with medium I is influenced most by the aromaticity of asphaltenes, C/H, and then by the length of aliphatic chains,  $l$ , the value of the total coefficient of elasticity for C/H being higher than for  $l$  by almost an order of magnitude. This can be explained (in the

TABLE 8-10

Distribution of factors characterizing interaction of asphaltenes with the medium according to the degree of their influence on bitumen properties

Property indices	Medium type	Factors						Sum of $\epsilon$
$\eta_0$	I	C/H	l	C	$C_r$	L		14.6
$G_{m_0}$	I	C/H	l	$C_r$	L	C		25.5
$\theta_{m_0}$	I	C/H	l	C	L	$C_r$		75.5
K	I	C/H	l	L	$C_r$	C		21.0
$P_{k_2}$	I	l	C/H	C	$C_r$	L		3.0
$\eta_m$	I	C/H	l	$C_r$	L	C		74.5
$\varphi$	I	C/H	l	$C_r$	L	C		33.0
$T_s$	I	C/H	l	C	$C_r$	L		4.0
$T_{br}$	I	C/H	l	C	$C_r$	L		4.0
W.T.	I	C/H	l	C	L	$C_r$		3.5
All	I	C/H	l	C	$C_r$	L		190.6
$\eta_0$	II	l	L	C/H	C	$C_r$		239.5
$G_{m_0}$	II	l	L	C/H	C	$C_r$		155.5
$\theta_{m_0}$	II	l	L	C/H	C	$C_r$		53.0
K	II	l	C/H	L	C	$C_r$		157.5
All	II	l	C/H	L	C	$C_r$		605.5

first approximation) by the fact that, in this dispersion medium, the affinity of plates constituting asphaltene for the dispersion medium has noticeably greater influence on bitumen characteristics than the length of aliphatic chains. At the same time, an increase in the solvent content results in some changes. For example, for bitumens without a precipitator, the length of aliphatic chains is the most significant. These chains probably straighten out, become more elongated, and form elastic structures in the interlayers of the dispersion medium. This explanation is in accordance with the fact that  $l$  of asphaltenes has the greatest influence on  $P_{k_2}$  of bitumens (medium I). This characteristic is known to define a point of transition from undisturbed structure to the beginning of its avalanche destruction with an increase in  $P$ . Therefore, this process is probably associated with the change in aliphatic chain conformation, which makes the influence of the aliphatic chain length so great.

An analysis of the data in Table 8-10 also confirms that introduction of a precipitator decreases the influence of asphaltene properties on properties of bitumens. The average value of  $\epsilon$  per one characteristic is 19.06 in medium I and 155.37 in medium II.

In Table 8-10 it appears possible to use values of  $\epsilon$  to rate indices of bitumen properties by the influence on them of the asphaltene's ability to interact with the dispersion medium:

$$\begin{aligned} \text{Medium I: } & \eta''_m; \varphi; G_{m0}; K_{cc}; \eta_0; \theta_{m0}; T_s; T_{br}; W.T.; P_{k_2}. \\ \text{Medium II: } & \eta_0; K; G_{m0}; \theta_{m0}. \end{aligned} \quad (1)$$

*Multivariate analysis of the influence of parameters characterizing the properties of an asphaltene complex on rheological and physical-mechanical properties of bitumens*

Based on the data in Table 8-5, parameters included of factor group III were rated by their influence on bitumen characteristics (Table 8-11).

The volume of the dispersed-phase particles,  $C_v$ , has the greatest influence on the sum of all indices of bitumen properties with both medium I and medium II which is followed by indices  $\lambda$  and  $D_{ph}$ . In medium I, judging by values of  $\epsilon$ , the influence of  $C_v$  is the same as that of  $\lambda$ , but the influence of  $D_{ph}$  is significantly less. In medium II,  $C_v$  has a much greater influence than  $\lambda$ . This can probably be explained by the fact that less structuralized systems are formed in medium II. This is also indicated by a significantly smaller average of  $\epsilon$  values for  $\lambda$  and  $D_{ph}$  on total characteristics: 57.1 and 8.2 in medium I, and 19.3 and 1.8 in medium II.

In contrast to the two previous groups of factors, an introduction of a precipitator, here, increases the influence of the asphaltene complex properties on properties of bitumens. For instance, the average value of  $\epsilon$  per one characteristic is 104.2 in medium II and 123.9 in medium I. This confirms the writer's main theoretical concept that it is the asphaltene complex which has a determining influence on the structure and properties of bitumens. It is, therefore, quite natural that the influence of this factor increases as the chemical composition of model bitumens resembles that of an actual bitumen.

As previously stated, indices of bitumen properties are rated by the influence that asphaltene complex properties have on them, using the data of Table 8-11:

$$\begin{aligned} \text{Medium I: } & \eta''_m; P_{k_2}; \eta_0; \theta_{m0}; \varphi; W.T.; T_s; K; G_{m0}. \\ \text{Medium II: } & \eta_0; G_{m0}; K; \theta_{m0}. \end{aligned}$$

TABLE 8-11

Distribution of factors of the quality of the asphaltene according to the degree of their influence on bitumen characteristics

Property indices	Medium type	Factors			Sum of $\epsilon$
$\eta_0$	I	$C_v$	$\lambda$	$D_{ph}$	216.7
$G_{m0}$	I	$C_v$	$\lambda$	$D_{ph}$	24.6
$\theta_{m0}$	I	$\lambda$	$C_v$	$D_{ph}$	157.8
$K$	I	$C_v$	$\lambda$	$D_{ph}$	53.1
$P_{k_2}$	I	$C_v$	$\lambda$	$D_{ph}$	239.1
$\eta''_m$	I	$C_v$	$\lambda$	$D_{ph}$	249.9
$\varphi$	I	$C_v$	$\lambda$	$D_{ph}$	103.6
$T_s$	I	$\lambda$	$C_v$	$D_{ph}$	66.4
$T_{br.}$	I	$\lambda$	$C_v$	$D_{ph}$	61.5
W.T.	I	$\lambda$	$C_v$	$D_{ph}$	66.9
All	I	$C_v$	$\lambda$	$D_{ph}$	1239.5
$\eta_0$	II	$C_v$	$\lambda$	$D_{ph}$	175.8
$G_{m0}$	II	$C_v$	$\lambda$	$D_{ph}$	106.8
$\theta_{m0}$	II	$C_v$	$\lambda$	$D_{ph}$	49.2
$K$	II	$C_v$	$\lambda$	$D_{ph}$	84.9
All	II	$C_v$	$\lambda$	$D_{ph}$	416.7

*Influence of the volume of asphaltene complexes on properties of commercial bitumens; substantiation of values of the first and second critical concentrations of structure formation*

Figs. 8-4 to 8-8 present the experimental results which confirm the writer's major theoretical concepts such as the significance of the first and second critical concentrations (Figs. 8-4, 8-6 and 8-8) and the existence of poly-extreme relations (Figs. 8-5 and 8-7). Significance of the third critical concentration has not yet been confirmed due to insufficient funding. The writer hopes that he will have an opportunity to conduct such experiments in the future.

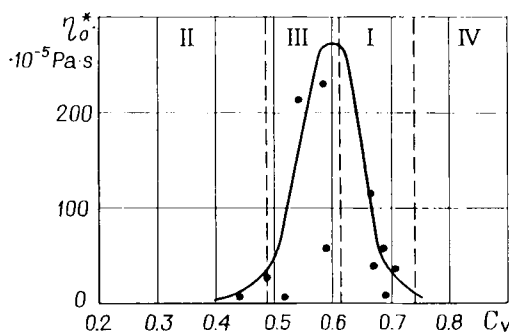


Fig. 8-4. Dependence of highest Newtonian viscosity of bitumens on the dispersed-phase particle volume (of asphaltene complexes).  $\eta_0^*$  = highest Newtonian viscosity.

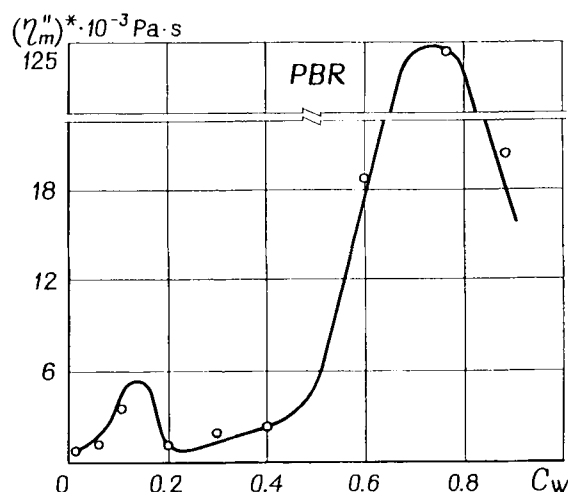


Fig. 8-5. Dependence of reduced lowest plastic viscosity of model bitumens on the content of petroleum-benzene resins by weight. PBR = petroleum-benzene resins.

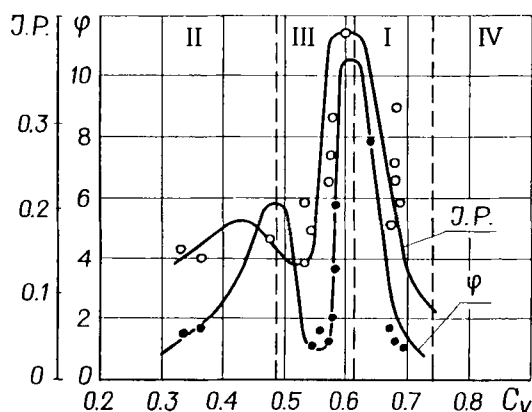


Fig. 8-6. Dependence of penetration index and the degree of bitumen structure failure on the volumetric content of dispersed-phase particles (asphaltene complexes). I.P. = penetration index;  $\varphi$  = degree of structure failure =  $\eta_0^*/\eta_m''$ .

### *Influence of the volume of asphaltene complexes on theological, thixotropic and physical-mechanical properties of bitumens*

An analysis of experimental data obtained on commercial bitumens is the most difficult, but at the same time is the most interesting. The difficulty is in calculating  $C_v$  because it is impossible to separate the bitumen into the phase and medium enough in order to determine  $\lambda$  accurately. Regrettably, a simple method to determine  $\lambda$  still does not exist. Therefore, some assumptions were made to calculate  $C_v$  for commercial bitumens.

First, since this analysis covers only viscous road bitumens (except SB), corresponding to a rather narrow range of oxidation or sampling depths, the average density of

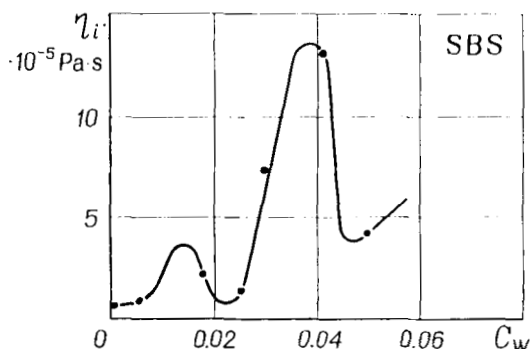


Fig. 8-7. Dependence of effective viscosity of polymer-bitumen binders on the polymer content (by weight). SBS = butadiene = styrene block copolymer of the SBS type.

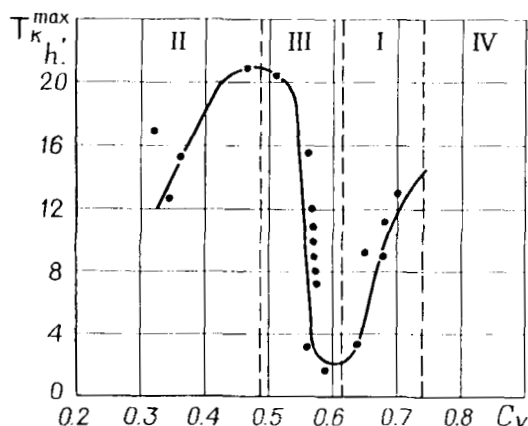


Fig. 8-8. Dependence of the bitumen aging index on the volumetric content of dispersed-phase particles (asphaltene complexes).  $T_k^{\max}$  = aging index — time of maximum cohesion achieved on bitumen heating in the 5- $\mu\text{m}$  layer and testing in the 10- $\mu\text{m}$  layer between metal plates.

asphaltenes is assumed to be  $1.15 \text{ g/cm}^3$  and the average density of dispersed-phase particles, considered to be bitumens, is  $1.0 \text{ g/cm}^3$ . Thus  $d$  is equal to 0.87.

Second, it is assumed that the main dominant nuclei of dispersed-phase particles are presented by asphaltenes which form asphaltene complexes containing almost all SBR, but SBR themselves either do not form independent SBR complexes, or their volume is negligible. Therefore,  $C_m$  is the weight content of asphaltenes (in fractions of a unit).

Third, it was assumed that:

- The nature of asphaltenes in oxidized bitumens closely corresponds to asphaltenes obtained by deep oxidation of light tars [14], for which  $\lambda$ , determined at  $C_m = 0.3$  and 0.08, is 2.18 and 6.5, respectively ([14], sample 2.3).
- In residual bitumens, French samples A, B, and C, in particular and in bitumens of grade BH, SB bitumens and low viscous bitumen BHD 200/300, the nature of asphaltenes is similar to that of asphaltenes obtained by the light oxidation of heavy

TABLE 8-12

Parameters of disperse structure of model bitumens ( $C_m = 0.08$ )

No. of samples	$\lg \eta^*$	$C_v$	$\lambda$	$D_{ph}$ (Å)	$\delta$ (Å)	$\delta_{ph}$ (Å)	$\delta$ (Å)	$n \times 10^{-18}$ (p/cm <sup>3</sup> )
2.2	1.579	0.300	4.90	33.8	27.04	13.14	6.95	14.86
2.3	3.034	0.408	6.50	39.2	27.68	9.48	9.10	12.95
2.5	1.896	0.339	5.42	27.2	20.55	8.84	5.86	32.22

tars in sample 2.2 of [14], and for these bitumens, at  $C_m = 0.3$  and 0.08,  $\lambda$  is 2.2 and 4.9, respectively.

Parameters of the disperse structures of model bitumens (at  $C_m = 0.08$ ) are presented in Table 8-12.

Fourth,  $\lambda$  was assumed to vary directly as  $C_w$  in the range of its values from 0.08 to 0.3 [14], which allowed the determination of  $\lambda$  by using the weight content of asphaltenes in bitumens (see Table 8-14). Substituting  $d = 0.87$  and  $\lambda$  from Table 8-14 into Eq. 8-1, one obtains the  $C_v$  values for bitumens.

Values of  $\lambda$  were calculated using the following formulas obtained from the equation of a straight line on a plane, and were rounded to 0.05.

For oxidized bitumens:

$$0.22\lambda = 1.77 - 4.332C_w \quad (8-38)$$

For residual bitumens:

$$0.22\lambda = 1.28 - 2.7C_w \quad (8-39)$$

Determined results of the standard indices of bitumen properties accepted in this research are presented in Table 8-13.

Bitumens group chemical compositions obtained by adsorption liquid chromatography on silica-gel grade ACK are presented in Table 8-14. Asphaltenes were preliminarily separated from maltenes by solving bitumen in benzene and precipitation by a 40-fold volume of petrol ester (narrow fraction, the starting boiling temperature = 40°C, the end boiling temperature = 70°C). Maltenes were divided into components by elution by a selecting set of solvents and then identified by the refraction coefficient in a refractometer.

As shown in Table 8-15, rheological characteristics of bitumens were determined within the regime of a simple shear between flat-parallel plates at constant shear stress. The 'plastometer' instrument was designed by the Laboratory of Polymer Rheology of the Institute of Petrochemical Synthesis of the USSR Academy of Sciences.

The minimum load at which the shear is performed is 0.001 g, the minimum gradient of shear rate is  $0.8 \times 10^{-6} \text{ s}^{-1}$ , and the least division of deformation scale is  $2.75 \times 10^3 \text{ Å}$ . Shear deformation is measured with the optical microscope grade MUC-11. The technique of determination and the physical meaning of rheological characteristics are described in [16].

Relations of concentrations of basic operating characteristics of bitumens, including rheological ones, and their dependence on  $C_v$ , are analyzed. Fig. 8-9 shows that for all



TABLE 8-13

Standard characteristics of bitumens

Bitumen grade and index	Needle penetration, 0.1 mm		Ductility (cm)		Temperature (°C)		Adhesion member		Changes after heating (°C)		$T_{br.}$ after heating (°C)	Penetration index
	0°C	25°C	0°C	25°C	brittleness	softening	marble	sand	weight %	$T, ^\circ\text{C}$		
BHD 40/60, 1088	20.0	41.0	0.6	40.0	-14.0	52.0	4	2	0.08	3.5	-13.5	-1.16
BHD 60/90, 1003	24.0	68.0	4.3	100	-15.0	50.5	4	4	0.03	3.0	-12.5	-0.33
BHD 90/130, 986	36.0	98.0	7.0	96.3	-18.0	46.0	4	3	0.03	1.5	-18.0	-0.66
BHD 60/90, 1071	26.0	67.0	3.6	50.0	-17.0	51.0	4	2	0.3	9.0	-11.0	-0.22
BHD 200/300, 1089	48.0	224.0	27.5	72.0	-20.0	35.5	3	3	0.03	3.5	-13.5	-1.71
BH 40/60, 1104	13.0	40.0	0	>100	-6.0	52.0	3	4	0.03	9.0	+4.0	-1.26
BH 200/300, 1098	34.0	201.0	>100	>100	-15.0	36.0	3	2		7.5		-2.0
BH 60/90, 1105	18.0	64.0	0	>100	-9.0	47.0	3	3		6.0		-1.4
BH 90/130, 987	24.7	103.0	0	>100	-9.0	42.0	2	2		8.0		-1.6
BHD 90/130, 1069	37.0	122.0	5.7	>100	-23.0	43.0	3	2		4.0		-0.8
BHD 90/130, 993	37.0	105.0	7.2	86.0	-21.0	46.0	3	2		8.5		-0.3
BHD 90/130, 468	10.0	116.0	9.0	>100	-20.0	47.5	4-3	2	0.01	2.0		+0.4
BHD 40/60, 1119	27	60	3.5	29	-20	52.0	2	1		10.0	-17.0	-0.2
BHD 130/200, 1120	37	107	4.1	>100	-24	43.0	2	1		7.0	-18.0	-1.2
BHD 60/90, 1329	24	74	4.7	63.7	-15	50.8	5	2		8.0		+0.1
BHD 40/60, 1358	20	53	3.9	44.7	-12.5	55.3	5	2		7.0		+0.2
Bitumen a, 1373	13	39	0	>100	-6	55.0	3-2	3	0.05	2.5	-3	-0.59
Bitumen b, 1374	15	44	0	>100	-6	52.0	3-4	2	0.08	4.0	-5	-1.04
Bitumen c, 1375	11	42	0	>100	-3	50.0	2-3	2	0	3.5	-1	-1.58
BHD 60/90, 471	24	87	-	3.5	-37	68.5						4.23
BHD 90/130, 452	15	103	5.0	23.5	-18	48.5	2-3	2				+0.4
BH 60/90, 448	18(100)	86	2.5	4.5	-28	59.5	3	1				2.46
BH 90/130, 449	20(100)	118	3.5	11.5	-30	49.5	3	1				+1.1
BH 90/130, 261	16(100)	111	16	>100	-20	45.5	3	2				-0.2
Bitumen SB	360	-	94.5	-	-28.0	26.5	2	2				

TABLE 8-14

Group chemical compositions of bitumens

Bitumen grade and index	Oils (%)				Total content of oils M (%)	Resins (%)		Total content of resins (%)	Asphaltenes A (%)	(A + SBS)/(M + PBR)	$\lambda$	$C_v/C_v''$	$T_K^{\max}$ (h)	$K_{\max}$ (MPa)
	PN	MCA	BCA	PCA		PBR	SBR							
BHD 40/60, 1088	12.0	12.8	18.0	3.5	46.3	12.3	16.4	28.7	25.0	0.71	3.15	0.685/0.559	9.5	0.61
BHD 60/90, 1003	13.2	9.4	21.4	2.7	46.7	16.9	12.2	29.1	24.2	0.58	3.30	0.695/0.564	9.0	0.51
BHD 90/130, 986	16.4	9.3	20.1	5.7	51.5	16.7	13.8	30.5	18.0	0.47	4.50	0.705/0.547	11.0	0.53
BHD 60/90, 1071	14.2	8.9	25.0	—	48.1	11.1	17.1	28.2	23.7	0.69	3.40	0.701/0.566	—	—
BHD 200/300, 1089	7.4	17.1	23.2	—	47.7	18.0	17.3	35.3	17.0	0.52	3.75	0.555	20.5	0.44
BHD 40/60, 1104	0	11.0	22.3	—	33.3	18.7	25.3	44.0	22.7	0.93	3.00	0.592	10.0	1.53
BHD 200/300, 1098	3.7	10.1	17.9	17.1	48.8	20.5	21.7	42.2	9.0	0.44	4.70	0.368	16.0	1.49
BHD 60/90, 1105	2.1	12.4	19.8	8.4	42.7	19.0	18.7	37.7	19.6	0.62	3.40	0.583	12.0	1.45
BHD 90/130, 987	4.2	12.0	23.9	6.9	47.0	28.0	16.6	44.6	8.4	0.33	4.75	0.347	13.0	1.63
BHD 90/130, 1069	14.0	8.2	28.0	—	50.2	12.2	16.8	29.0	20.8	0.60	3.95	0.714/0.564	—	—
BHD 90/130, 993	7.1	9.2	21.3	9.6	47.2	15.1	11.6	26.7	26.1	0.61	2.90	0.658/0.545	—	—
BHD 90/130, 468	14.3	13.7	18.1	1.9	48.0	14.5	16.6	31.1	20.9	0.62	3.10	0.585	11.0	0.88
BHD 40/60, 119	17.2	7.2	16.3	—	40.7	14.2	14.6	28.8	30.5	0.82	2.40	0.601	1.5	0.88
BHD 30/200, 1120	16.8	7.3	22.8	—	46.9	11.0	14.9	25.9	27.2	0.72	2.95	0.665/0.548	3.0	0.85
BHD 90/130, 468	14.3	13.7	18.1	1.9	48.0	14.5	16.6	31.1	20.9	0.62	3.10	0.585	11.0	0.880
BHD 40/60, 1119	17.2	7.2	16.3	—	40.7	14.2	14.6	28.8	30.5	0.82	2.40	0.601	4.5	0.880
BHD 30/200, 1120	16.8	7.3	22.8	—	46.9	11.0	14.9	25.9	27.2	0.72	2.95	0.665/0.548	3.0	0.850
BHD 60/90, 1329	15.9	2.5	27.0	—	45.4	14.0	14.5	28.5	25.1	0.62	2.62	0.594	4	0.670
BHD 40/60, 1358	2.5	12.7	2.5	—	17.7	29.0	37.0	66.0	16.3	1.14	3.75	0.533	3	0.640
Bitumen a, 1373	12.1	8.9	16.3	—	37.3	24.4	16.0	40.4	22.3	0.62	3.05	0.592	7.0	0.810
Bitumen b, 1374	7.5	5.9	24.9	—	38.3	30.5	13.4	43.9	17.8	0.45	3.65	0.565	16.0	0.790
Bitumen c, 1375	11.5	6.8	20.0	—	38.3	32.4	15.0	47.4	14.3	0.41	4.05	0.504	21.0	0.960
BHD 60/90, 471	17.5	26.0	10.5	4.2	57.2	6.5	10.0	16.5	27.3	0.61	2.45	0.590	9.5	0.170
BHD 90/130, 452	3.3	24.8	17.4	6.0	51.5	14.8	5.0	19.8	27.9	0.49	2.35	0.570	3.0	0.620
BHD 60/90, 448	15.7	28.5	4.6	1.7	50.5	17.7	3.6	21.3	28.5	0.47	2.30	0.570	3.0	0.480
BHD 90/130, 449	23.5	12.3	18.2	2.3	56.3	5.6	10.9	16.5	21.2	0.47	3.20	0.590	8.5	0.230
BHD 90/130, 261	18.5	13.3	11.7	2.2	45.4	7.0	26.9	33.9	21.0	0.92	3.25	0.594	25.0	0.670
SB	13.7	11.2	33.4	9.7	68.0	11.9	12.2	24.1	7.9		4.80	0.330	18.0	0.597

TABLE 8-15

Rheological characteristics of bitumens at 20°C

Binder grade and index	Highest Newtonian viscosity $(\eta_0 \times 10^{-5}, \text{Pa s})$	Equilibrium elastic modulus $(G_{m0} \times 10^{-2}, \text{Pa})$	Relaxation time $(\theta_{m0} \times 10^{-3}, \text{s})$	Elasticity coefficient $(K, \text{s/Pa})$	Bingham flow limit $(P_k, \times 10^{-2} \text{ Pa})$	Viscosity of conventionally disturbed structures $(\eta''_m \times 10^{-5} \text{ Pa s})$	Degree of structure disturbance $(\varphi)$	$C_v$
BHD 40/60, 1088	95.0	18.2	5.2	0.29	84.0	12.3	7.7	0.685
BHD 60/90, 1071	51.3	14.6	3.51	0.24	62.0	10.0	5.13	0.701
BHD 60/90, 1003	33.7	15.0	2.3	1.5	2.5	25.0	1.4	0.695
BHD 90/130, 986	3.8	6.3	0.60	0.09	2.7	2.9	1.3	0.705
BHD 200/300, 1089	0.34	0.23	1.48	6.42	0.6	0.27	1.26	0.555
BH 40/60, 1104	46.6	32.4	1.4	0.04	10.0	42.9	1.08	0.592
BH 60/90, 1105	12.1	4.8	2.52	0.52	4.0	11.0	1.06	0.583
BH 90/130, 987	2.6	0.98	2.65	2.7	0.80	1.7	1.5	0.347
BH 200/300, 1098	0.66	0.32	2.06	6.42	0.02	0.36	1.80	0.368
BHD 60/90, 1329	75.0	44.5	1.7	0.4	3.0	20.0	3.8	0.594
BHD 40/60, 1358	85.1	35.0	1.5	0.3	2.4	71.4	1.2	0.533
BHD 60/90, 1329	75.0	44.5	1.7	0.4	3.0	20.0	3.8	0.594
BHD 40/60, 1358	85.1	55.0	1.5	0.3	2.4	71.4	1.2	0.533
Bitumen a, 1373	200.0	40.7	4.9	1.21	6.0	101.0	2.0	0.592
Bitumen b, 1374	80.0	25.7	3.1	1.21	1.8	50.0	1.6	0.565
Bitumen c, 1375	23.0	19.0	1.2	0.6	9.1	3.9	5.9	0.504

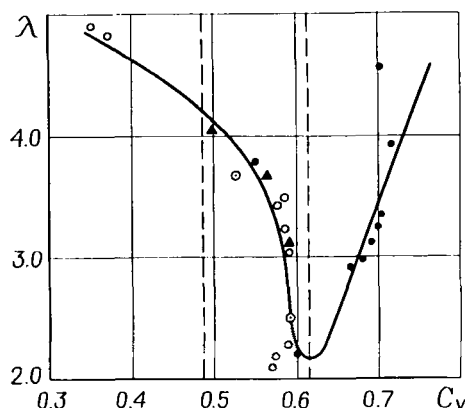


Fig. 8-9. Dependence of voluminosity coefficient of asphaltene complexes on their volumetric content in bitumens.  $\lambda$  = voluminosity coefficient, which is asphaltene complex volume/asphaltene volume.

types of bitumen dispersed structures, the changes are of the same character. Certain types of disperse structures correspond to the new classification, in which  $C_v$  serves as a main single classifying feature.

Despite the fact that the bitumens under consideration were produced from different oils, at different moments of time (during a 30-year period) and different regimes and depths of oxidation, all the data fit the same curve with small deviations. These curves have specific inflections at those theoretically obtained  $C_v$  values that separate one type of disperse structure from another. This strongly confirms that the theoretical basis of the new classification and  $C_v$  as the criterion of classification are correct.

For bitumens of the type II structure with  $C_v$  in the range  $0 < C_v \leq 0.487$ , where there is no spatial coagulative carcass,  $\lambda$  insufficiently decreases with increasing  $C_v$ , because the total surface of nuclei of dispersed-phase particles increases and the volume of components capable to be adsorbed on this surface decreases. When  $C_v$  reaches a value of 0.487 and formation of the spatial coagulation carcass becomes possible,  $\lambda$  decreases more sharply with an increase in  $C_v$ , probably because the volume of components constituting solvation shells and the diffusion layer decreases sharply.

At  $C_v = 0.613$ , the dispersed-phase particles are in direct contact with one another by their solvation shells. It is remarkable that at  $C_v$  close to 0.58, a specific inflection in the curve is observed (see Fig. 8-9). It is difficult to explain this fact unambiguously, but it is possible to suppose that at this  $C_v$ , the free dispersion medium (diffusion layer) begins to disappear from zones of contacts between the dispersed-phase particles. In other words, contacts by solvation shells begin to appear. At  $C_v = 0.613$  such contacts apparently exist throughout the system.

Following  $C_v = 0.613$ ,  $\lambda$  increases with an increase in  $C_v$ . This can be explained by the beginning of formation of bi-disperse nuclei in dispersed-phase particles. Apparently, such conditions appear in the system when the coalescence of two nuclei (asphaltenes) becomes energetically more efficient than the redistribution of the free dispersion medium upon asphaltenes newly introduced into the system. It is possible

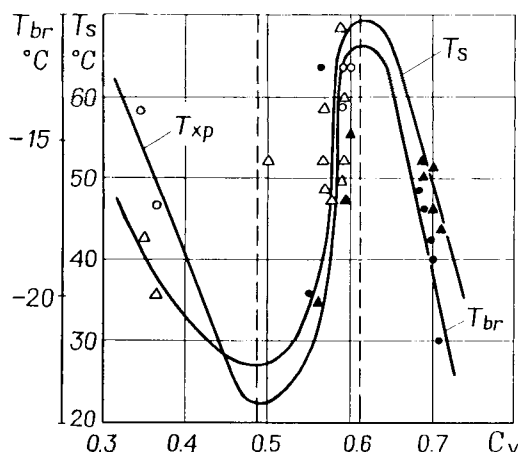


Fig. 8-10. Dependence of bitumen brittleness and softening temperature on the asphaltene complexes volume.  $T_{br}$  = Fraas brittleness temperature;  $T_s$  = softening temperature (ring and ball method).

to suppose that it is the thickening of solvation shells of the dispersed-phase particles caused by the confluence of nuclei that allows to form new dispersed-phase particles in the system, i.e., to provide the formation of a continuous solvation shell.

Two questions associated with this assumption are how strong bi-dispersed nuclei are and what is the nature of the contact bond between two coalesced nuclei. It can be supposed that if this bond is strong enough, then the molecular weight of asphaltenes must increase.

The dependence of  $\lambda$  on the ratio  $C_v/(1 - C_v)$  is analogous to the dependence of  $\lambda$  on  $C_v$ .

Analysis of the relations between concentrations of components and major operating indices of bitumen properties B temperatures of softening and brittleness (see Fig. 8-10) confirms the above suggestions about the structures of bitumens of types I, II, III and values of  $C_v^*$  and  $C_v^{**}$  and also about the decrease of dispersion medium viscosity with an increase in  $C_v$  in bitumens of type II up to  $C_v = 0.487$  and in bitumens of type I up to values greater than 0.613. This is in accordance with the suggestion that mechanisms of this phenomenon for bitumens of types II and I are different. For bitumens of type II, it is an extract of high molecular compounds (e.g., SBR) from the dispersion medium. For bitumens of type I, it is a decrease in the number of dispersed-phase particles, and therefore, in the number of contacts between them at the expense of the formation of bi-disperse nuclei.

An analysis of relations between the volume of dispersed-phase particles in bitumen and rheological characteristics  $\eta_0$ , W.T., and  $\varphi$  (Figs. 8-4 and 8-6), also confirms the numerical values of  $C_v^* \approx 0.487$  and  $C_v^{**} \approx 0.613$  obtained theoretically. As expected, the degree of structure destruction,  $\varphi$ , has extremes at  $C_v^*$  and  $C_v^{**}$ . This, apparently, is due to the fact that at these values of  $C_v$ , the dispersed structure of bitumens is in a non-equilibrium state, which corresponds to the transition from one type of structure to another. The smaller value of  $\varphi$  at  $C_v^*$  than at  $C_v^{**}$  can probably be explained by the

lower strength of the dispersed structure due to the smaller number of contacts between the dispersed-phase particles and to greater distances between them.

Relations between the concentration of components and rheological characteristics  $C_{m0}$ ,  $P_{k2}$ ,  $\theta_{m0}$  and  $K$  confirm the numerical values of  $C_v^*$  and  $C_v^{**}$  derived theoretically.

It should be noted that dispersion of the experimental data obtained for commercial bitumens is inevitable, since the assumptions made at calculating  $\lambda$  and  $C_v$  cannot take into account all nuances of the nature of petroleum raw material and the procedures of bitumen production. Further research is necessary.

#### *Effect of the volume of asphaltene complexes on bitumen aging*

One of the most important criteria of the properties of organic binders is their resistance to aging processes, i.e., their ability to maintain their properties in time. It is obvious that this aging is most rapid at the highest temperatures, i.e., during preparation, storage, and transportation of asphalt concrete mixtures to locations of use. Therefore, the aging of binders was studied by heating them in a thin layer at 160°C.

At the first stage, an attempt to assess the resistance to aging by changes in standard indices and then in cohesion kinetics was made. Efforts were made to relate changes of properties to structures of binders because only this approach can reveal the general mechanism of the intensity of the aging processes. To obtain an objective characteristic of the bitumen's resistance to aging, the aging was assessed by cohesion kinetics. In this case, heat was applied to a 5- $\mu$ m-thick layer of bitumen on a metal plate, which corresponds to the thickness of a bitumen film on mineral grains in asphalt-concrete mixtures.

The index of conventional cohesion ( $K_{cc}$ ) is more of an objective characteristic than temperature  $T_s$ , which is determined by the ball and ring method, or temperature  $T_{br.}$ , determined by the Fraas method. This is true since  $K_{cc}$  is the tension at which the binder structure fails in an avalanche way, resulting either in an anomalously rapid increase in deformation or in a brittle rupture. Shear is carried out, after gluing the plates together, at a constant rate of loading. Curves of the relations between cohesion and heating time obtained using this technique have a pronounced maximum. Thus, two characteristics of the aging process are obtained: maximum cohesion,  $K_{cc}^{max}$ , and the time needed to reach this maximum,  $T^{K^{max}}$ . Similar to relations between concentrations and standard indices of bitumen properties, derived relations of Ph/M (A + SBR/M + PBR) are ambiguous and for the same value of Ph/M there may be two or three values of  $T^{K^{max}}$  and  $K_{cc}^{max}$ . Moreover, analysis of the role of the content of asphaltenes or asphaltenes + alcohol-benzene resins shows that for one content of A or A + ABS, four values of  $T^{K^{max}}$  can exist. It was impossible to determine relations between  $K_{cc}^{max}$  and the content of A and between  $K_{cc}^{max}$  and the content of A + SBR because of a great dispersion of points.

In the writer's opinion, the indices of bitumen properties before and after aging have a non-single-value nature because the weight content of A or A + SBR or the Ph/M ratio do not determine the behavior of bitumens. The writer believes that the serviceability of bitumens and other organic binders, their physical-mechanical and rheological properties, and their resistance to aging are related to the volume of dispersed-phase particles  $C_v$ . This parameter also determines their structure type. In

other words, it is possible to conclude that both A and SBR are not particles of the bitumen dispersed phase, but are particles of their nuclei. It can be assumed that if the volume of dispersed-phase particles  $C_v$  of bitumens is determined, then single-value relations between concentrations and bitumen properties, e.g., the indices of resistance to aging, can be obtained.

As shown in Fig. 8-8, the character of changes in the most objective feature, the time of reaching maximum cohesion  $T^{K_{cc}^{max}}$  for bitumens with the dispersed structure types III and I, is similar to the character of changes of  $\lambda$ , i.e., the above-presented concepts of these bitumen structures are confirmed.

Thus, it is possible to believe that the aging time decreases with the reduction of the thickness of dispersed-phase particles solvation shells for bitumens of the type III dispersed structure ( $0.487 \leq C_v \leq 0.613$ ). It reaches its minimum value at  $C_v = 0.613$  and begins to increase at greater values of  $C_v$  in direct proportionality to the increase in  $\lambda$ . For the type II dispersed structure bitumens ( $C_v \leq 0.487$ ), the resistance to aging increases with the increase in  $C_v$  (Fig. 8-8) with some decrease in  $\lambda$  (Figs. 8-3 and 8-15). This contradiction exists because the higher-molecular components (i.e., SBR) with an increase in  $C_w$  (for bitumens of the dispersed structure of type II) are extracted from the dispersion medium and are adsorbed on newly formed asphaltenes. It results in a reduced thickness and viscosity of the dispersion medium interlayers; therefore, the aging process becomes slower. A decrease in the highest Newtonian viscosity of model bitumens caused by the introduction of asphaltenes into maltenes was demonstrated and had the same result. It is quite possible that in bitumens with the type II structure, a portion of the dispersed-phase particles is represented by SBR complexes at  $C_v < 0.4$ .

An initial structure of a binder has a determinative influence on the value of its maximum cohesion ( $K_{cc}^{max}$ ) reached in the process of aging. In the writer's opinion,  $K_{cc}^{max}$  determines the potential of binder gluing abilities. The dynamic (Bingham) yield strength,  $P_k$ , gives a more objective estimate of the binder's gluing ability and its maximum possible value.

An analysis of the relation between  $K_{cc}^{max}$  and  $C_v$  leads to the conclusion that there is an inflection at  $C_v = 0.487$  and a maximum at  $C_v = 0.613$ . The correctness of the proposed classification is confirmed and it is shown that each type of the dispersed structure follows its own law.

Based on the above data it can be assumed that bitumens with a type II dispersed structure in the aging peak, in addition to asphaltene complexes, have a significant amount of SBR complexes. In contrast to asphaltene complexes, are capable to aggregate, i.e., the distance between them may be sufficiently smaller than between asphaltene complexes, which results in greater van der Waals' forces. This can explain large values of  $K_{cc}^{max}$  for bitumens with a type II dispersed structure.

For bitumens with a type III dispersed structure, with  $C_v$  values ranging from 0.487 to 0.55–0.580,  $K_{cc}^{max}$  is significantly smaller because structuralization of the dispersion medium decreased while a greater amount of resins was included into asphaltene complexes. This resulted in the retardation of the aging process, which is confirmed by a decreased aging rate. It is possible to believe that the number of dispersed-phase particles and the number of contacts, which reaches its minimum at  $C_v = 0.55$ –0.58 at the peak of cohesion, are due to the enlarged particle sizes.

For bitumens with a type III structure and  $C_v > 0.58$ , a rapid increase in the aging process is observed which is manifested in a reduction of  $T^{K_{\max}}$  (see Fig. 8-8), rapid increase in the aging rate and an increase in  $K_{cc}^{\max}$  reaching its maximum value at  $C_v = 0.613$ . It can be assumed that beginning from  $C_v = 0.58$ , the thickness of the dispersion medium interlayers becomes so small that some dispersed-phase particles are in direct contact with their solvation shells. A calculation shows that on the average these layers are less than 0.4 nm thick.

With  $C_v$  increasing to more than 0.613, the aging rate, aging time  $T^{K_{\max}}$  (see Fig. 8-8) and the maximum cohesion  $K_{cc}^{\max}$  decrease. This may be due to the formation of bi-dispersed nuclei of the dispersed-phase particles. Associated with it is an increase in the size of the particles and a decrease in their amount, which results in the number of contacts between them.

The suggested formation of bi-dispersed nuclei of the dispersed-phase particles is inevitably associated with a decrease in  $C_v$ . This must occur because the total surface of the dispersed-phase particles should decrease. To derive a formula for calculating the volume of coalesced particles of the dispersed phase  $C_v''$  the following was assumed.

(1) Asphaltenes have the shape of a cube or a parallelepiped; when a bi-dispersed nucleus forms, they join tightly along a face. The surface of a bi-dispersed nucleus therefore is smaller than the sum of two surfaces of monodispersed nuclei. The volume,  $V_n''$ , is equal to the sum of two volumes of monodispersed nuclei:  $2V_n = V_n''$ .

(2) The thickness of the solvation shell  $\delta_s$  of the bi-dispersed nucleus does not differ from that of the solvation shell of the monodispersed nucleus, since the nature of the surface does not change. Therefore, its adsorptivity does not change and  $\delta_s'' = \delta_s$ .

(3) A portion of the solvation shell goes to the dispersion medium since the volume of the asphaltene complex with a bi-dispersed nucleus is smaller than two volumes of asphaltene complexes with monodispersed nuclei. This is due to the smaller surface of a bi-disperse nucleus in comparison to the sum of two surfaces of monodispersed nuclei.

(4) The decrease in the surface of the bidispersed nucleus is due to the presentation of the bidispersed nucleus as a sphere, the volume of which is equal to the doubled volume of a monodispersed nucleus. The diameter,  $D_n''$ , is smaller than the doubled diameter of a monodispersed nucleus,  $D_n$ .

From assumptions 1 and 4 where nuclei are considered as spheres, one obtains:

$$D_n'' = 2^{1/3} D_n \quad (8-40)$$

$$D_{ph}'' = 2^{1/3} D_n + 2\delta_s = D_n(\lambda^{1/3} + 0.259) \quad (8-41)$$

Taking into account that the number of asphaltene complexes with bi-dispersed nuclei is half the number of asphaltene complexes with monodispersed nuclei, one obtains:

$$C_v'' = (C_v/2\lambda)(\lambda^{1/3} + 0.259)^3 \quad (8-42)$$

Using the same approach, one derives an equation for the volume of the dispersed-phase particles with triple nuclei:

$$C_v'' = (C_v/3\lambda)(\lambda^{1/3} + 0.44)^3 \quad (8-43)$$

The calculated values of  $C_v''$  for asphaltene complexes with bi-dispersed nuclei are presented in Table 8-14. To check the assumption that their formation in the bitumens



is possible, values of  $T^{K_{\max}}$  for bitumens with bi-dispersed nuclei at  $C_v''$  were plotted in  $T^{K_{\max}}-C_v$  coordinates.

All points fit the descending branch of the curve, which confirms the presence of bi-dispersed nuclei in the asphaltene complexes of bitumens. The branches of the curves in Figs. 8-4, 8-6 and 8-8 at  $C_v > 0.613$  may be imaginary because the actual volume of the dispersed-phase particles in commercial bitumens is below 0.613. This is logical because at  $C_v > 0.613$  the number of coagulative contacts must decrease in the system, which in turn would have to affect the bitumen properties, for instance causing a considerable decrease in ductility, which does not occur (Table 8-13).

The writer wants to emphasize that along with the confirmation of the  $C_v^*$  and  $C_v^{**}$  values, a single relation between the bitumens' resistance to aging and their dispersed structure was derived [17] for the first time.

*Structure formation at increasing the content of the nuclei of dispersed-phase particles in the system with the formation of mono-, bi- and polydisperse nuclei; poly-extreme curve of structure formation*

To substantiate the possibility of the formation of mono-, bi-, and polydispersed nuclei in dispersed-phase particles, the writer presents results of investigations of the structure formation processes in model systems when petroleum-benzene resins (PBR) were introduced into oils [17]. Oils and PBR were separated from bitumen 1003 (Table 8-14) by adsorption liquid chromatography on silica gel. To separate PBR, bitumen was divided into all components. To separate oils, that fraction was separated from maltenes which can be washed-out by the following sequence of solvents: petroleum ether (PE), PE + 5% of benzene (B), PE + 10% of B, PE + 15% of B, PE + 20% of B, and PE + 25% B. The chemical composition of oils of the bitumen 1003 is shown in Table 8-14.

It is known that resins, distinctive from asphaltenes, can form monocrystals. Therefore, it is highly probable that bi- and polydisperse nuclei can be formed from them. The systems under consideration simulate the dispersion medium of bitumens, which influence significantly the size of asphaltene complexes and the properties of bitumens.

Rheological and physical-mechanical properties of model systems and their resistance to aging were examined (Table 8-16, Fig. 8-11). Analysis of the data indicates a complicated process of structure formation that is expressed by poly-extreme relationships and may be divided into several stages.

At the first stage, monodispersed PBR complexes form at a PBR content up to 5% ( $\text{PBR}/M = 0.5$ ). They consist of PBR themselves, swelled in aromatic hydrocarbons, which have similar natural properties. In this PBR concentration range, an increase in  $\eta_0$ ,  $K$ ,  $\theta_m$ , and  $T_s$  along with a decrease in the brittleness of the system (Table 8-16, Fig. 8-11) occur at a considerable increase in the temperature interval of serviceability (algebraic sum of softening and brittleness temperatures) of the whole system. The data obtained make it possible to determine the formation of a poorly developed coagulative structure at this stage, and to substantiate the expediency of introducing PBR (or combinations of PBR-type compounds), in the amount of 3 to 5% by weight, to prepare complex organic binders to improve properties of their dispersion medium. The formation of a poorly developed coagulative structure is confirmed by a more

TABLE 8-16

Rheological and physico-mechanical characteristics of models on PBR

PBR content in models (%)	PBR/M	Rheological characteristics							
		viscosity of undisturbed structure	equilibrium elastic modulus	relaxation period	elasticity coefficient	static limit	dynamic flow limit	viscosity of conventionally disturbed structure	degree of structure disturbance
		$\eta_0^* \times 10^{-5}$ (Pa s)	$G_{m0} \times 10^{-2}$ (Pa)	$\theta_{m0} \times 10^{-3}$ (s)	$K$ (s/Pa)	$P_{k1}$ (Pa)	$P_{k2}$ (Pa)	$\eta_m \times 10^{-3}$ (Pa s)	$\varphi \times 10^{-2}$
0	0	1.8	0.92	1.95	21.1	1.8	4.8	1.7	1.06
5	0.05	2.5	1.0	4.0	40.0	1.8	3.1	1.9	1.32
10	0.11	2.7	2.9	0.76	2.6	0.2	5.5	5.5	0.49
20	0.25	2.8	6.9	0.4	0.6	4.8	6.0	2.9	0.97
30	0.43	3.0	4.0	0.58	1.4	1.0	4.5	3.5	0.86
40	0.67	3.0	0.4	7.9	207.6	1.2	3.7	4.0	0.75
50	1.00	2.5	0.5	5.0	100.0	1.1	3.0	6.2	0.40
60	1.50	2.6	0.4	6.5	162.5	1.6	4.0	16.6	0.16
80	4.00	1.6	0.7	2.3	33.6	0.4	14.0	125.0	0.01
90	9.00								
100		1.7	0.2	7.6	345.5	—	3.5	59.5	0.03

PBR content in models (%)	Physico-mechanical properties			Time to achieve maximum cohesion $T_{max}$ (h)	Relative increment of maximum cohesion $(K_{max} - K_0)/K_0$	Maximum cohesion (MPa) $K_{max}$	Initial cohesion (MPa) $K_0$
	softening point (°C)	brittle point (°C)	temperature (°C)				
0	22.0	-43.0	65.0	110	101.6	0.1949	0.0019
5	31.5	-46.0	77.5	65	136.9	0.2620	0.0019
10	34.0	-40.0	74.0	44	111.2	0.2019	0.0018
20	29.0	-39.0	68.0	44	161.2	0.2919	0.0018
30	23.0	-36.0	59.0	42	221.2	0.3555	0.0016
40	17.5	-31.0	48.5	42	96.8	0.4499	0.0046
50	25.5	-30.0	55.5	38	76.4	0.4799	0.0062
60	24.5	-26.0	50.5	38	41.4	0.5258	0.0124
80	40	-30.0	43.0	36	7.4	2.1588	0.257
90				36	3.7	2.7072	0.576
100	37	+1.0	36.0	34	6.9	4.5583	0.577

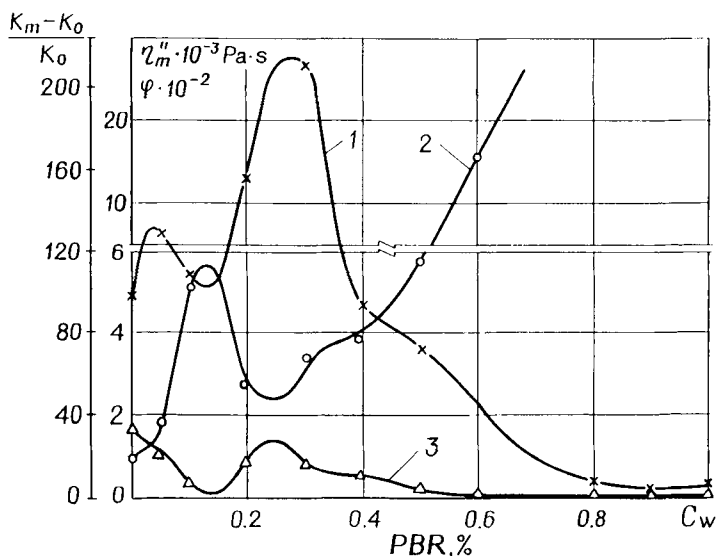


Fig. 8-11. Dependence of indices of model bitumen properties on the petroleum-benzene resin content (by weight).  $\times = K_{\max} - K_0/K_0$ ;  $\circ = \eta''_m$ ;  $\Delta = \phi$ ;  $K_m$  = maximum cohesion, MPa;  $K_0$  = initial cohesion, MPa. 1 =  $\times$ , 2 =  $\circ$ , 3 =  $\Delta$ .

rapid increase in the cohesion in the process of aging and by a greater value of  $K_{cc}^{\max}$  (Table 8-16, Fig. 8-11). The character of the cohesion kinetics curve allows one to conclude that, in this system, the dispersion medium has a determinative influence on aging, since the interlayers in contact zones between the dispersed-phase particles are large.

At the second stage of structure formation, at PBR contents of 8 to 15% ( $\text{PBR}/\text{M} = 0.09\text{--}0.17$ ), PBR appear to continue to swell and reach their maximum sizes, probably to immobilize paraffin-naphthene hydrocarbons as well as aromatic ones. This results in the thinning of interlayers between PBR complexes, an increase in the system brittleness and  $\eta''_m$ , decrease in  $K$ ,  $\theta_m$ , and  $\phi$  (i.e., decrease in serviceability of the system), and an increase in its rigidity and strength ( $P_{k_2}$ );  $\eta''_m$  reaches its maximum and  $\phi$  its minimum, i.e., the ability to have thixotropic properties decreases. In this PBR concentration range, the maximum value of softening temperature is observed. The aging process highly intensifies, which is manifested by a pronounced maximum of the cohesion kinetics curve, which confirms the thinning of the dispersion medium interlayers. In addition,  $T^{K_{\max}}$  (Table 8-16) sharply decreases and the cohesion increment rate increases (Fig. 8-11).

At the third stage, with the PBR content being increased from 15% to 25% ( $\text{PBR}/\text{M} = 0.17\text{--}0.33$ ), the free volume of the dispersed medium apparently decreases: PBR complexes can no longer exist in the form of monodispersed particles. Therefore, bi-dispersed PBR complexes begin to form at PBR contents of over 15%. As a result of monodispersed PBR complex associations in bi-dispersed complexes, the total surface of particles decreases; a portion of the dispersed medium is squeezed out from interlayers

and its free volume increases. The formation of such a structure is confirmed by a decrease in  $\eta''_m$  and  $P_{k_2}$  and by an increase in  $\varphi$  and  $K_{cc}$ . Note that at a PBR content of 25%,  $\varphi$  has its maximum,  $\eta''_m$  decreases to its minimum, and  $G_m$  reaches its maximum value. The thickness of the interlayers between bi-dispersed PBR complexes in contact zones is evidently smaller than that between mono-dispersed PBR complexes, which determines minimum pliability of the system ( $G_m$  is maximum).

The formation of such a structure in the system results in a decrease in softening temperature, and a reduction in the serviceability range, which confirms an increase in the dispersed medium free volume.

At a PBR content of 25%, the cohesion increment at the peak of aging  $(K_{cc}^{\max} - K_{cc}^{\circ})/K_{cc}^{\circ}$  has the greatest value, which confirms the concept on a system's dispersed structure at this stage.

To differentiate the influence of PBR on bitumen properties and to relate it to the data obtained on models, an analysis of group chemical compositions of bitumens of various grades and types (83 samples) was carried out. It showed that the PBR/M ratios for BHD grade bitumens lies in the 0.23 to 0.41 range (average = 0.333) and in the 0.34 to 0.84 range (average = 0.54) for BH grades. The average values of PBR/M for particular grades are as follows: 0.38 for BHD 40/60, 0.33 for BHD 60/90, 0.28 for BHD 90/130, 0.27 for BHD 130/200, 0.30 for BHD 200/300, 0.67 for BH 40/60, 0.48 for BH 60/90, 0.42 for BH 90/130, and 0.46 for BH 200/300. Thus, this stage of structure formation in model systems is typical for bitumens of BHD grades.

A further increase in the PBR content of over 25% seems to result in thinning of the interlayers in the contacts between PBR complexes and changes in their compositions — a decrease in the paraffin-naphthene hydrocarbons (PN) content, which leads to an increase in the system's  $T_{br}$ . (see Table 8-16). Evidently, phase contacts between PBR complexes also occur, which result in the formation of a rather elastic structure manifested by reduced  $G_m$  and sharply increased  $K$ . At an increase in the PBR content, the content of low-molecular components of oils in the interlayers of the dispersion medium seems to drop so much that an increase in  $\eta''_m$  and a decrease in  $\varphi$  occur. It is quite possible that this is caused by orientation of PBR complexes at greater shear stresses and by a greater value of  $\eta''_m$  (see Table 8-16). Two kinds of contacts between the dispersed phase and coagulative phase, lead to a decrease in the softening temperature (ring and ball method) since the number of phase contacts between PBR complexes does not seem to prevail. Determinative influence on the system's heat resistance therefore is due to coagulative contacts where dispersed medium interlayers have a low content of PN hydrocarbons characterized by softening temperature being highest in the oil fraction.

A decrease in  $P_{k_2}$  for this system is caused by the smaller value of  $P_{k_2}$  of the PBR themselves than that in model systems with purely coagulative contacts (at 20 and 30% of PBR in Table 8-16).

At a PBR content of 38% (PBR/M = 0.61), a phase inversion occurs, i.e., swelled bi-dispersed PBR complexes become a continuous phase, these PBR complexes being evidently jelly-like particles that do not form a strong spatial structure, which is evidenced by only slight variation in values of  $\eta_0$  and  $P_{k_2}$ . The existence of such a jelly-like structure is confirmed by  $\eta_0$  and  $\theta_{m_0}$  reaching their maximum values and by the presence of an inflection in the cohesion increment curve  $(K_{cc}^{\max} - K_{cc}^{\circ})/K_{cc}^{\circ}$ .

(see Fig. 8-11). This structure is characterized by a high elasticity, to which the high value of  $K$  testifies. However, with an increase in shear stresses or temperature, it disintegrates rapidly since the determinative influence on the system's behavior is exerted by the composition of the dispersion medium interlayers with decreased content of PN hydrocarbons. This system has a minimum softening temperature, even lower than that of oils, a higher brittle temperature, and a corresponding minimum serviceability interval, which confirms the decrease of PN hydrocarbons in the oil fraction.

Such properties of the system at  $\text{PBR}/\text{M} = 0.61$ , typical of the dispersion medium of BH grade bitumens, allows one to understand one of the causes of their lower heat resistance and crack resistance in comparison to those of BHD grade bitumens, which are characterized by a  $\text{PBR}/\text{M}$  ratio of 0.3. The data also explain the fact that for more viscous bitumens, the difference in heat resistance and crack resistance between BHD grade and BH grade bitumens is greater than such a difference for less viscous bitumens. This is due to the difference in their  $\text{PBR}/\text{M}$ 's. The systems formed at  $\text{PBR}/\text{M}$  ratios typical for BHD and BH grade bitumens have similar aging resistances,  $T^{K_{\max}}$  (Table 8-2), which makes it possible to suppose that  $C_v$  has a determinative influence on this property. A further increase in the PBR content from 38 to 48% ( $\text{PBR}/\text{M} = 0.61$  to 0.92) is followed by a reduction in oil content in the system, which results in the formation of a structure with properties approaching those of pure PBR; a portion of the PBR complexes seems to disintegrate. At a 48% content of PBR ( $\text{PBR}/\text{M} = 0.92$ ), the system still has less oil; therefore, the disintegration rate of the PBR complexes seems to grow. Nevertheless, even a small content of oil influences the values of rheological and physical-mechanical characteristics.

An increase in the PBR content of up to 50 to 80% ( $\text{PBR}/\text{M} = 1.38$  to 4.0) results in a convergence of property indices of the systems with similar indices of pure PBR. PBR is able to immobilize oils in the dispersion medium. In the case of oil excess, the aromatic fractions having a great affinity for PBR are immobilized first; then, with growing PBR content in the system, PN hydrocarbons are immobilized. Thus, the composition of the dispersion medium of systems can change depending on the ratio  $\text{PBR}/\text{M}$ .

By the analysis of the model systems behavior, it was established that an increase in PBR content in oil would lead to the formation of three types of disperse structures.

(I) At a PBR content of about 3% by weight, a dispersed phase forms at the expense of PBR complexes presented by PBR swelled in aromatic hydrocarbons. The system is characterized by a weak spatial coagulative mesh formed by monodispersed PBR complexes; interlayers of the dispersion medium are enriched with PN hydrocarbons.

(II) At a PBR content of about 25% ( $\text{PBR}/\text{M} = 0.33$ ), the structure is characterized by the presence of bi-dispersed PBR complexes that form a rigid, but thixotropic spatial structure.

(III) At a PBR content of about 38%, the structure corresponds to the phase inversion in the system and is characterized by bi-dispersed PBR complexes swelled to the maximum possible volume, interacting directly with each other and forming a continuous phase in the system. On the other hand, oils are locally distributed and play the role of the dispersed phase.

Analysis of  $\text{PBR}/\text{M}$  values for commercial bitumens and the above data make it possible to assume that PBR forms the structure of type II in the dispersion medium of

BHD grade bitumens, and the structure of type III is formed in the dispersion medium of BH grade bitumens (which in turn explains the higher heat resistance and higher crack resistance of BHD grade bitumens than those of BH grade bitumens).

The following example proves the possibility of the formation of mono-, bi- and poly-molecular nuclei of the dispersed-phase particles. In this case, the poly-extreme curve of structure formation was obtained when using polymers as nuclei, namely, the block-copolymer of butadiene and styrene of SBR type DST-30 grade. This polymer was used as a structure-forming component for obtaining new complex organic binders (COB) for highway construction [18].

COB were prepared by mechanically mixing heavy petroleum residues (bitumen raw materials) with DST at 160°C until a homogeneous mixture was obtained. Sand organomineral mixtures were then prepared on the base of COB. In COB, which are different from bitumens, major particles of the dispersed phase are not asphaltene complexes but are complexes that are formed by polymers, or DST complexes. Standard indices of COB properties and the mixtures are presented in Tables 8-17 and 8-18, respectively. The efficient viscosity,  $\eta_i$ , was calculated at the gradient of shear rate  $\dot{\epsilon} = 0.6 \text{ s}^{-1}$ , which is the minimum possible for the apparatus 'Reotest-2'. The dynamic yield strength,  $P_{k_2}$ , was also calculated. Standard parameters and water and frost resistances for mixtures were determined (Fig. 8-12). The data show that relations for COB and for mixtures on their base are very complex, yet still analogous. A common feature of all relations between concentrations and properties is the presence

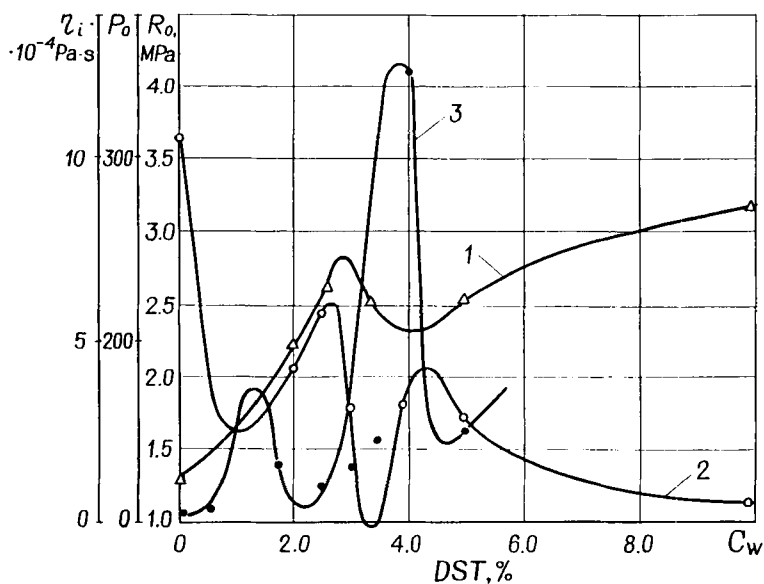


Fig. 8-12. Dependence of property indices of polymer-bitumen binders and polymer-asphalt concrete mixtures on the polymer content in the binder.  $\eta_i$  = effective viscosity at 40°C and at the shear rate gradient of  $0.6 \text{ s}^{-1}$ ;  $R_0$  = compression strength of asphalt concrete samples at 0°C;  $P_0$  = penetration at 0°C. 1 = x, 2 = o, 3 =  $\Delta$ .

TABLE 8-17

Properties of COB obtained on the basis of CB, DST

No.	COB composition (fraction of total mass of COB components, %)		Needle penetration, 0.1 mm		Ductility (cm)		Temperature			Elasticity (%)		Change of softening point after heating (°C)	Workability interval (°C)
	CB	DST	25°C	0°C	25°C	0°C	softening	brittleness	flash	25°C	0°C		
1	100	–	–	360	19.0	94.5	26.5	–28.0	190	0	0	7.0	54.5
2	98	2.0	–	181	34.0	100	41.0	–26.0	194	87.0	82.5	–1.0	67.0
3	97.4	2.6	1250 <sup>a</sup>	220	43.0	100	53.2	–30.0	200	83.5	–	0	83.2
4	97.0	3.0	925 <sup>a</sup>	160	46.5	100	59.0	–25.0	202	90.0	90.0	0.5	84.0
5	96.5	3.5	317	94	44.0	100	60.5	–25.5	182	89.0	87.0	0	86.0
6	96.0	4.0	748 <sup>a</sup>	167	49.4	100	66.5	–27.5	198	92.0	93.0	0	94.0
7	95.8	4.2	260	139	41.7	100	61.0	–21.5	–	90.0	90.0	–2.0	82.5
8	95.0	5.0	281	159	56.0	100	70.0	–30.5	204	94.0	93.0	–1.5	100.5
9	85.0	15.0	97	77	100	100	95.0	–39.0	262	95.0	94.5	–2.0	134.0
10	Bitumen a		224	48	72	27.5	35.5	–20.0	200	–	–	4	55.5
11	Bitumen b		60	24	100	4.3	50.5	–15.0	200	–	–	3	65.5

<sup>a</sup> Values obtained by recalculating the data determined for time equal to 2c, i.e., penetration determined for 2 seconds and then recalculated by multiplying by 2.5.

CB = bitumen raw material. DST = grad of copolymer of SBS type in Russia.

The quantitative indices of cohesion, determined by using the method of pigment adsorption, for COB of sample 3 and bitumen of grade BHD 60/90 are equal to, respectively, marble at 63% and 70.8%, and sand at 44.6% and 56.5%.

TABLE 8-18

Physico-mechanical properties of organoconcretes based on COB

No.	COB composition (fraction of total mass of components)		COB content in mixture (% by volume)	Porosity of aggregates (% by volume)	Residue porosity (% by volume)	Average density (g/dm <sup>3</sup> )	Compression strength (MPa)		
	CB	DST					20°C	50°C	0°C
1	100	—	7.8	21.2	4.6	2.29	0.91	0.29	1.85
2	98.0	2.0	7.4	20.8	4.6	2.29	1.0	0.50	2.92
3	97.4	2.6	7.1	20.1	4.5	2.31	1.27	0.61	2.67
4	97.0	3.0	7.2	20.1	4.5	2.31	1.28	0.55	3.13
5	96.0	4.0	7.2	20.4	4.6	2.30	1.21	0.61	2.65
6	95.8	4.2	7.4	20.7	4.6	2.30	1.32	0.57	2.90
7	95.0	5.0	7.3	20.4	4.6	2.30	1.37	0.63	3.38
8	Bitumen a		20.7	4.2	2.31	1.49	0.69	4.74	6.9
9	Bitumen b		7.3	20.4	4.5	2.31	4.26	1.20	8.06

No.	Water saturation (% by volume)				Swelling (% by volume)			Coefficients of water and frost resistance			Amount of closed voids (%)
	$R_0/R_{50}$	$W$	$W_{15}$	$W_{fzz}^{50}$	$S$	$S^{15}$	$S_{fzz}^{50}$	$K_w$	$K_w^{15}$	$K^{50}$	
1	6.4	4.9	6.6	8.1	1.2	2.1	3.8	0.73	0.62	0.38	0
2	5.8	4.1	5.4	5.5	0	0.5	1.1	0.84	1.0	0.95	10.8
3	4.4	3.0	4.8	6.0	0	0.8	2.1	1.0	0.97	0.68	33.3
4	5.7	3.7	4.8	5.4	0.1	0.5	1.4	0.91	1.0	0.90	17.8
5	4.3	3.6	4.7	4.7	0.3	0.6	1.1	0.96	1.0	0.86	21.7
6	5.1	2.7	3.9	4.6	0	0.3	1.3	1.2	1.3	0.99	41.3
7	5.4	3.6	4.0	4.9	0.1	0.3	0.8	1.1	0.99	0.88	21.7
8	6.9	3.1	4.8	7.3	0.2	0.9	4.2	1.2	1.5	1.4	26.2
9	6.7	1.9	3.0	4.6	0.14	0.4	1.6	1.1	1.0	0.96	57.8



of strongly pronounced extrema at the following concentrations of DST in COB: 32.6 to 2.7% and 4.2 to 4.3%. At 1.5 to 2.0% of DST, binders have an extremum in viscosity and penetration, but mixtures do not. An analysis of  $P_{k_2}$ , the invariant characteristic which (as distinct from all other characteristics obtained in the area of quasi-destroyed structure) makes it possible to estimate the material properties and structure in the area of undisturbed structure, shows that the spatial structure made of polymer macromolecules forms at the 1.5 to 2% content of DST in COB. It is manifested in the appearance of elasticity (over 80%) and a plateau in the  $P_{k_2}$  curve in the concentration range of 1.5 to 3.5%.

Concepts on the formation of dispersed structures in COB may be formulated on the basis of the obtained data. Formation of a polymer spatial structure in tar, beginning from low concentrations of DST (1.5 to 2%), is confirmed by a significant rise in the softening temperature of COB with values similar to viscous road bitumens, an increase of viscosity, and a gain in elasticity inherent for polymer-bitumen binders and elastomers (see Table 8-17). The dispersed phase in this system is evidently represented by monomolecular domains of polystyrene interconnected by polydivinyl macromolecules, which are present in their peripheral zone and pierce through the dispersion medium of the system. Judging by the properties of organomineral mixtures, however, this structure is not yet strong and serviceable enough (see Table 8-18).

At a DST in COB content of 2.6 to 2.7%, a sufficiently strong and serviceable structure of polymers is formed, which is indicated by a high softening temperature (similar to that of grade BHD 40/60 viscous bitumens) and a possible maximum strength at 50°C at the used COB. At the same time, one observes the maximum viscosity of COB in this content of DST, with a rather high value of  $P_0$  (over 200.01 mm) and a low brittle temperature (−30°C), which are significantly better than the characteristics of grade BHD 200/300 bitumens.

The elasticity,  $\epsilon$ , exceeds 80% at 25 and 0°C. The temperature interval of COB serviceability exceeds 80°C and the tensility at 0°C is more than 100 cm, which is better than that of BHD grade bitumens. Thus, a binder was developed that successfully combines high heat resistance, inherent for more viscous road bitumens, a higher (four to five times as high) aging resistance (experiment on cohesion kinetics was carried out by N. Amosova), a better deformability and workability than those of low-viscosity bitumens, and an elasticity inherent in polymer-bitumen binders based on DST. Mixtures made with this COB are characterized by the greatest volume of closed pores (over 60%) and by high water and frost resistances and deformability at low temperatures. The dispersed-phase particles of this COB seem to be represented by bi-molecular domains of polystyrene.

With an increase of DST content in COB to more than 2.7%, the process of structure formation begins in the dispersion medium consisting of an enlargement of the dispersed-phase volume, which is the reduction in the dissolving ability of the dispersion medium due to a decrease in the amount of hydrocarbons. This is caused by a rise in the viscosity and softening temperature of COB, a decrease in  $P_0$ , and a poorer pore structure of organoconcrete, due to the reduction in binder plasticity,  $P_{25}$  (70% decrease), and resulting in a higher compactibility of the mixture and significant reduction in the closed pore volume. Beginning with a DST content of 3.5%, the

strength of COB sharply increases with the increase in the content of DST.

At a DST content ranging from 3.5 to 4.2%, the formation of polymolecular domains seems to be more energetically efficient for macromolecules of DST, which leads to a decreased number of dispersed-phase particles in COB, a decrease in their total surface, an increase in the size of a particle, increased thicknesses of interlayers and enrichment with aromatic hydrocarbons. This is caused by a sharp reduction in COB viscosity, an increase in  $P_{25}$ ,  $P_0$  and compactibility of organomineral mixtures, with a strength of 50°C, amount of closed pores, water and frost resistances of organoconcrete.

One may believe that at a 4.2% content of DST in COB a spatial structure made of polymer macromolecules finally develops, where polymolecular domains of polystyrene are points of the lattice in contrast to bimolecular domains at a 2.6% content of DST. A comparison of properties of type I COB (2.6% of DST) and that of type II (4.2% of DST) shows that at the same  $P_0$ , COB of type II is characterized by a significantly higher softening temperature, elasticity, and aging resistance. Organoconcrete is characterized by a higher strength at 50°C, a larger volume of closed pores (80%), a higher water and frost resistances, and a better temperature resistance ( $R_0/R_{50}$ ). An increase in DST content of more than 4.5% apparently results in a phase inversion, i.e., more than 50% of the COB volume is occupied by the phase that may be visualized as large particles, consisting of polymolecular domains. These domains include more than three polystyrene blocks, which adsorbed a portion of the SBR, and asphaltenes framed with macromolecules of polydivinyl swelled in hydrocarbons.

Determined values of organoconcrete strength at 50°C are rather low. It is possible to believe that this is caused by conditions of the technique of a one-dimensional compression test: these conditions more often influence the materials with increased thixotropic properties, including COB. To estimate the shear resistance of organoconcretes  $P_{k_2}$  values were determined at 50°C [18] and compared with analogous data for asphalt concretes with the same grain size and residual porosity (2.5%). Organoconcretes based on COB, both of type I and II, are not inferior to hot asphalt concretes and essentially excel warm asphalt concretes in shear resistance despite lower values of  $R_{50}$  (Table 8-19).

By analyzing the results of these studies it may be noted that a poly-extreme curve of structure formation has a sufficiently common character for organic binders. It may be assumed that similar relations may also exist for other dispersed systems. In the writer's opinion, the existence of such relations is due to the consecutive formation of firstly monodispersed, then bi- and polydispersed or polymolecular nuclei of the dispersed-phase particles. The third theoretical concept, therefore, is confirmed experimentally.

TABLE 8-19

Dynamic flow limits  $P_{k_2}$   $10^{-3}$  Pa

Bitumens of grades					COB containing			
BHD 200/300	BHD 130/200	BHD 90/130	BHD 60/90	BHD 40/60	SB + 2.6% DST	SB + 4.0% DST	SB + 4.2% DST	SB
6.1	6.6	10.8	10.2	7.4	7.6	10.6	7.8	3.5

*Influence of the properties of asphaltenes on parameters of the bitumen disperse structure*

Multivariate analysis demonstrated that  $C_v$  had the greatest influence on bitumen properties. This index includes important parameters such as the weight content of asphaltenes in bitumen,  $C_w$ , their density,  $d$ , and volumetric coefficient,  $\lambda$ , that characterizes the ability of asphaltenes to immobilize the dispersion medium.

According to the proposed concept,  $C_v$  must define types of the disperse structures of bitumens and other organic binders; therefore, it was interesting to find out how  $C_v$  and other parameters of the disperse structure were connected with asphaltene properties. The results of the calculation of parameters of the disperse structures of model bitumens carried out using Eqs. 8.1 to 8.9 for the data of Table 8-3 are presented in Tables 8-20 and 8-21. The properties of asphaltenes were estimated using their density,  $d$ , molecular weight,  $W$ , and the conventional index of lyophilicity,  $L$ .

During the first stage of analysis, it was determined that parameters of the dispersed structure do not depend on  $C_v$  and, therefore, supplement the information. For instance, it was established, by graphical analysis, that  $C_v$  has almost no relation to  $\lambda$ ,  $D_{ph}$  and  $\delta_{ph}$  and no unambiguous relation to  $n$ .

Analyzing the influence of asphaltene properties on the complex of parameters of the dispersed structure of the model bitumen, it should be first mentioned that  $\lambda$ ,  $D_{ph}$ ,  $\delta_n$  and

TABLE 8-20

Disperse structure parameters of model bitumens (medium I)

Sample number	$C_v$	$\lambda$	$D_{ph}$ (Å)	$\delta_n$ (Å)	$\delta_{ph}$ (Å)	$\delta_s$ (Å)	$\eta \times 10^{-19}$ (1/cm <sup>3</sup> )	$P_{k_2}$ (Pa)	$-K$ (MPa · Å <sup>7</sup> )	$W/d$
1.1	0.501	1.950	23.36	8.55	3.88	2.33	75.11	700	2319	1.1742
1.2	0.497	1.950	22.30	8.22	3.76	2.23	85.69	1100	2766	1.194
1.3	0.514	1.910	20.22	7.11	3.19	1.96	118.80	2400	2204	1.1066
1.4	0.532	2.070	25.36	9.17	3.72	2.72	62.37	4200	23252	1.1813
1.5	0.529	2.050	26.30	9.49	3.90	2.80	55.63	3900	27035	1.1692
1.6	0.535	2.020	26.80	9.48	3.88	2.80	53.13	4660	31653	1.1315
2.1	0.501	1.950	23.36	8.55	3.88	2.33	75.11	700	2319	1.1742
2.2	0.534	2.200	25.70	9.68	3.74	2.97	60.14	5000	39533	1.2660
2.3	0.541	2.180	27.20	10.07	3.85	3.11	51.43	8800	93048	1.2351
2.4	0.542	2.145	30.20	11.02	4.25	3.38	37.61	10300	203286	1.2043
2.5	0.524	2.130	19.80	7.41	3.00	2.2	129.0	2900	3557	1.2501
3.1	0.514	1.910	20.22	7.11	3.19	1.96	118.98	2400	2204	1.1066
3.2	0.514	1.940	20.72	7.40	3.26	2.07	110.4	6500	7898	1.1292
3.3	0.530	2.045	21.80	7.85	3.22	2.31	97.79	11000	20206	1.168
3.4	0.535	2.100	22.00	8.01	3.19	2.41	96.05	15600	33003	1.193
3.5	0.536	2.015	22.40	7.90	3.23	2.33	91.16	13000	24965	1.1217
3.6	0.536	1.960	24.20	8.36	3.49	2.43	72.33	21000	59932	1.0803
3.7	0.537	1.905	25.20	8.49	3.62	2.43	64.13	21200	67404	1.0374
4.1	0.541	2.180	27.20	10.07	3.85	3.11	51.42	8800	93048	1.2351
4.2	0.523	1.790	25.64	8.44	3.90	2.27	59.29	8750	26541	0.9846
4.3	0.510	1.890	28.40	9.97	4.55	2.71	42.55	9500	93023	1.1000

TABLE 8-21

Disperse structure parameters of model bitumens (medium II)

Sample number	$C_v$	$\lambda$	$D_{ph}$ (Å)	$\delta_n$ (Å)	$\delta_{ph}$ (Å)	$\delta_s$ (Å)	$n \times 10^{18}$ (1/cm)	$P_{k_2}$ (Pa)	$-K$ (MPa · Å <sup>7</sup> )
1.1	0.520	2.11	23.9	8.95	3.68	2.64	72.83	100	460
1.2	0.570	2.33	23.94	8.90	3.01	2.85	79.50	180	796
1.3	0.526	2.04	20.64	7.46	3.10	2.18	114.34	900	1157
1.4	0.528	2.145	25.70	9.61	3.83	2.89	59.46	400	3028
1.5	0.517	2.09	26.48	9.90	4.12	2.89	53.24	120	1118
1.6	0.534	2.11	27.20	9.96	3.96	3.00	50.76	350	3403
2.1	0.520	2.11	23.90	8.95	3.68	2.64	72.83	100	460
2.2	0.541	2.32	26.30	10.15	3.64	3.26	56.89	—	—
2.3	0.529	2.25	27.40	10.55	4.07	3.24	49.16	—	—
2.4	0.550	3.265	30.70	11.50	4.18	3.66	36.35	—	—
2.5	0.562	2.380	20.60	8.21	2.67	2.77	122.98	—	—
3.1	0.526	2.04	20.64	7.46	3.10	2.18	144.35	900	1157
3.2	0.524	2.06	21.16	7.73	3.20	2.26	105.65	1800	2968
3.3	0.537	2.17	22.20	8.25	3.19	2.53	93.88	—	—
3.4	0.535	2.19	22.18	8.32	3.21	2.55	93.86	3250	8969
3.5	0.535	2.09	22.76	8.26	3.30	2.48	86.85	—	—
3.6	0.538	2.05	24.60	8.75	3.52	2.62	69.06	7000	27489
3.7	0.544	2.005	25.64	8.89	3.58	2.66	61.68	6000	26331
4.1	0.535	2.25	27.44	10.47	3.97	3.25	49.49	—	—
4.2	0.528	1.88	26.10	8.84	3.89	2.48	56.77	650	2742
4.3	0.560	2.075	29.22	10.13	3.83	3.15	42.91	3600	39407

$\delta_s$  are larger and  $n$  is smaller in any asphaltene series for the type II dispersion medium. This distinction is prominent with native asphaltenes (extracted from non-oxidized bitumens). It is possible, therefore, to state that their solubility decreases in the process of oxidation.

To determine the commonality for all series relations between asphaltene properties and parameters of a dispersed structure, an attempt was first made to derive the graphic relations for  $d$ . Multivariate analysis showed that, from factor group I, this factor had the greatest influence on bitumen properties. A distinct relation was found only between  $d$  and  $\lambda$  (Fig. 8-14, Eq. 8-15): an increase in  $\lambda$  with an increase in  $d$ . It is clear from Fig. 8-14 that at the same value of  $d$ ,  $\lambda$  for dispersion medium II is always greater by approximately 0.1, which is unlike the asphaltene nature. The increase in  $\lambda$  with increasing asphaltene density may be explained by the fact that denser asphaltenes have more developed aliphatic frames and, therefore, a greater ability to immobilize a portion of the dispersion medium.

The influence of molecular weight of the asphaltenes on the parameters of the dispersed structure of model bitumens was then examined. Sufficient unambiguous relations between  $W$ ,  $D_{ph}$ ,  $\delta_n$ ,  $n$ ,  $\delta_{ph}$ ,  $\lambda$  and  $d$  (Figs. 8-13 to 8-16) were established. The closest correlation (see Eq. 8-13) was found between  $W$  and  $D_{ph}$ . After a thorough examination of the plot (Fig. 8-13), nevertheless, one can notice that this dependence

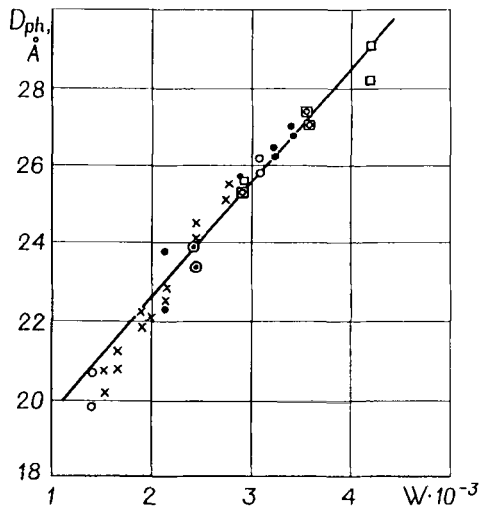


Fig. 8-13. Dependence of effective hydrodynamic diameter of asphaltene complex on the asphaltene molecular weight.  $D_{ph}$  = effective hydrodynamic diameter of asphaltene complex Å.  $W$  = asphaltene molecular weight. Asphaltene series: ● = 1, × = 2, ⊙ = 3, □ = 4.

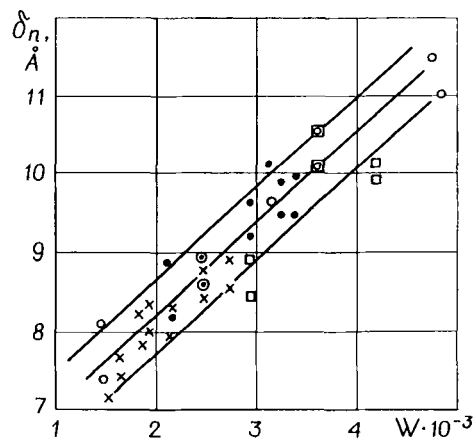


Fig. 8-14. Dependence of average distance between asphaltenes on the asphaltene molecular weight ( $W$ ).  $\delta_n$  = average distance between asphaltenes (Å).

may be presented by a broken line consisting of two straight lines, which form an angle at  $W \approx 2000$  to  $2400$ ; a stronger dependence of  $D_{ph}$  on  $W$  is observed where there are smaller molecular weights. It can be assumed that a specific change of asphaltene structures takes place with a given molecular weight. In the relation between  $\delta_n$  and  $W$  (Fig. 8-14)  $\delta_n$  is greater by approximately  $0.5 \text{ Å}$  in medium II than in medium I. The increase in  $\delta_n$  with increasing  $W$  may be explained by a significant decrease of the amount of asphaltene complexes,  $n$ , in bitumens (Fig. 8-15).

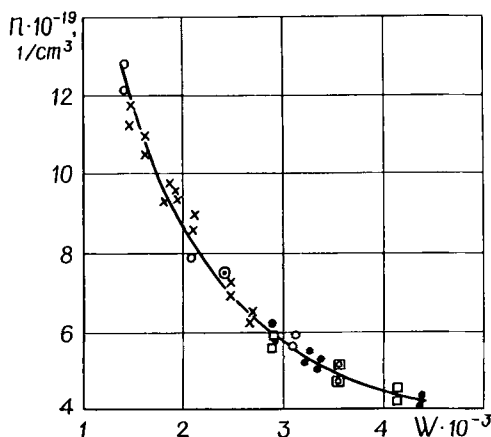


Fig. 8-15. Dependence of asphaltene complex number in 1 cm<sup>3</sup> of binder on the asphaltene molecular weight;  $n$  = asphaltene complex number in 1 cm<sup>3</sup> of binder (pieces).

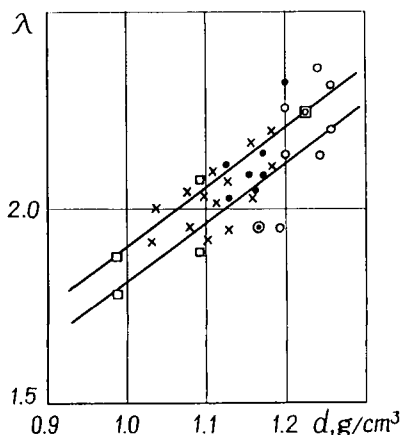


Fig. 8-16. Dependence of voluminosity coefficient of binder asphaltene complexes on the asphaltene density ( $d$ , in g/cm<sup>3</sup>).

These relations confirm that asphaltenes, contingent on the properties of asphaltenes, can be divided into three groups [14] by the lyophilicity index  $L$ . At  $L < 3$ ,  $D_{ph}$  is in the 20 to 24 Å range and for  $10 \leq L \leq 33$ ,  $25 \leq D_{ph} \leq 29$  Å. It was also shown that with an increase in  $L$  to 10, the volumetric coefficient increases but then does not change anymore. The volumetric coefficient of asphaltene complexes has a tendency to increase with increasing  $W$  of the asphaltenes. For asphaltenes of series I,  $C_v$ ,  $\lambda$ ,  $D_{ph}$ ,  $\delta_n$ ,  $\delta_{ph}$ , and  $\delta_s$  increase, and the amount of asphaltene complexes decreases with an increase in oil weight, and consequently, petroleum raw materials from which residual bitumens are obtained. In other words, larger asphaltene complexes form in bitumen, the distance between them becomes greater and their total weight decreases. Nevertheless, the strength of these bitumens,  $P_{k_2}$ , is noticeably greater. It can be assumed that unit forces

of interaction (intermolecular forces of attraction) between them are significantly greater than those of light oils. The difference in parameters of the dispersed system is most obvious when comparing bitumens with asphaltenes obtained from Anastasiyevskaya oil and from Trinidad asphalt.

In series II, the greatest volume of the dispersed-phase particles,  $C_v$ , and sizes of asphaltene complexes,  $D_{ph}$ ,  $\delta_n$ ,  $\delta_{ph}$ , and  $\delta_s$ , were determined for model bitumens made on the base of asphaltenes separated from bitumens obtained by deep oxidation of asphalts from deasphaltization. These asphaltenes are characterized by having the greatest molecular weight and molecular volume. Asphaltenes of this series were obtained from the bitumens of heavy residues of Tuymazy oil. These asphaltenes, nevertheless, have very long aliphatic chains and the greatest content of functional groups. Asphaltenes of thermal cracking by their properties are the opposite of Tuymazy asphaltenes.

Bitumens containing them are characterized by minimum  $\lambda$ ,  $D_{ph}$ ,  $\delta_n$ ,  $\delta_s$ , and a maximum  $n$ . These asphaltenes have a minimum  $m$ , a minimum length of aliphatic chains and a minimum content of functional groups. Analyzing the whole series, one may conclude that the higher the temperature of the process to which bitumen components, asphaltenes in particular, are subjected, the greater their functional activity and the more developed are the aliphatic frames; therefore, their ability to immobilize the dispersion medium and  $\lambda$ ,  $C_v$ ,  $\delta_n$ ,  $\delta_{ph}$ , and  $\delta_s$  will be greater.

The third series of asphaltenes made it possible to trace (within the same technology — oxidation) how asphaltene properties and the structure of bitumens change with oxidation depth. Bitumens produced from Anastasiyevskaya oil were used.

The above data show that when the oxidation depth of bitumens increases, the asphaltene molecular weight,  $D_{ph}$ ,  $\delta_n$ , and  $\delta_s$  increase, but  $n$  decreases.

However, beginning with the asphaltenes, separation from bitumens with a softening temperature of 105°C, decreases the density, the aromaticity factor and the volumetric coefficient of the asphaltene complex. For model bitumens based on these asphaltenes, a decrease in  $\delta_n$ ,  $\delta_{ph}$  and  $\delta_s$  (Tables 8-20 and 8-21) occurs. These factors attest that the structure and properties of asphaltenes change at the considered oxidation depth, and their ability to immobilize the dispersion medium diminishes. This complies with the results of the investigations of Kostyuk et al. [24], which showed that at a bitumen softening temperature of 96–100°C, the character of bitumen oxidation changes, which is caused by the changes in the nature of the components.

The third series of asphaltenes proves that the sizes of asphaltene complexes in model bitumens increase with increasing oxidation depth of bitumens, but at a certain moment, their ability to interact with the medium begins to deteriorate. The calculation shows that the moment shown in sample 3.35, one observes a more intensive growth of the nucleus, i.e., the asphaltene size  $D_n$  (Table 8-20), and a decrease in its density (Table 8-1). It can then be assumed that an increase in the distance between asphaltene plates and a simultaneous decrease in functional activities and chain lengths in aliphatic frames occur. It should be noted that all the above relates to asphaltenes that are separated from unusually deep oxidized bitumens (of construction grades, hard grades).

The fourth series of asphaltenes allows one to assume that the nature of raw oil materials greatly influences the properties of asphaltenes, asphaltene complexes, and model bitumens. Presented here is one that is very light with a low content of

Ust-Balykская oil resins and one that is very heavy with a high content of Venezuelan oil resins. The latter oil almost has the greatest values of  $D_{ph}$ ,  $\delta_n$ ,  $\delta_{ph}$  and  $\delta_s$  in model bitumens.

Summarizing the presented data, it is possible to conclude that the chosen complex of parameters of the dispersed structure proved to be useful for a detailed analysis of the effect of asphaltene properties on bitumen structure. Presumably, it will still be more necessary to analyze the influence of nuclei of dispersed-phase particles of different nature on the structure and properties of organic binding materials. Presented, therefore, are the results of the experimental investigation which confirm all four fundamental concepts of the theory of bitumen structures. It is important to emphasize that asphaltene properties have significant influence on both the structure and properties of bitumens. For instance, in model bitumens with the same content of asphaltenes ( $C_m = 0.3$ ), their softening temperatures change from 45°C to 126°C, from minus 29°C to minus 4°C for the Fraas brittleness temperature, change more than 100-fold for  $\eta_0$  and  $P_{k_2}$ , 10- to 30-fold for  $G_m$ , and more than 1000 times for  $\varphi$  [19].

#### GLUING ABILITY OF BINDERS — INFLUENCE OF ASPHALTENE PROPERTIES AND ASPHALTENE COMPLEXES ON THE STRENGTH OF ASPHALT CONCRETES

Organic binding materials, including bitumens, function as glues. A widespread example of this is bitumens being used as glues in asphalt concrete pavements. The fifth concept of the theoretical principles of binder structure, therefore, concerns their gluing ability. In the writer's opinion, the gluing ability depends on intermolecular forces (e.g., van der Waals' forces) acting between the nuclei of the dispersed-phase particles of organic binders [20]. To derive an equation to determine these forces, a well-known formula, which relates attraction forces between particles (molecules) and the distances between them [21], was used.

The following assumptions were made to prove this concept.

(1) The dispersed-phase particles are compound complexes (e.g., asphaltene complex in bitumens), behaving as a whole in processes of thermal diffusion and deformation. The volume of a particle in binders can be computed from Eq. 8-1.

(2) The binder's strength is the result of intermolecular interaction forces (orientation and induction forces) between the nuclei of dispersed-phase particles. This strength is equal to the Bingham yield strength,  $P_{k_2}$ , which characterizes the glue's strength and depends on the properties of nuclei of dispersed-phase particles, their volume and distances between them,  $\delta_n$ .

(3) The strength of asphalt concrete or other organomineral material depends on the strength of the organic binder itself, which increases due to a decrease in  $\delta_n$  values to the values of the molecular radius (10 Å). This decrease is a result of the following processes: (a) infiltration of a portion of binder dispersion mediums into the pores of mineral material which, having a size less than 20 Å, are inaccessible for the dispersed-phase particles; (b) consumption of a portion of the dispersion medium to coat surfaces of aggregate particles; and (c) squeezing of a portion of the dispersion medium of the binder from contact zones between mineral particles out into intergranular space.



TABLE 8-22

Disperse structure parameters of model bitumens (medium III)

Sample number	$D_{ph}$ of asphaltene (Å)	$D$ of asphaltenes (Å)	$\lambda$	$C_v$	$\delta_{ph}$ (Å)	$\delta_n$ (Å)	$n \times 10^{-19}$	$\delta$ (Å)
2.4	30.20	23.42	2.145	0.542	4.25	11.02	3.761	3.38
2.5	19.80	15.39	2.130	0.524	3.00	7.41	12.900	2.20
2.2	25.70	19.76	2.20	0.534	3.74	9.68	6.014	2.97
4.2	25.64	21.12	1.79	0.523	3.90	8.44	5.929	2.27

(4) According to the writer's belief, the particles of the binder's dispersed phase contribute most to the value of the asphalt concrete strength. Due to their colloidal sizes (from 20 to 30 Å in bitumens) and large volumes (48.7–61.3%), they provide a great number of coagulation contacts and help to realize intermolecular forces of interaction owing to the small distances between particles in contact zones that are comparable to the molecular radius (10 Å).

(5) The proposed calculations of asphalt concrete strength are rather approximate and aimed at establishing the influence of binder properties and structure on the serviceability of sand asphalt concrete, asphalt binders, mastics and other binary mixtures with a fine filler. Contributions of mineral composition, micro-roughness of the surfaces of mineral particles, their geometry and so on were not accounted for.

First of all,  $\delta_{ph}$  and  $\delta_n$  should be determined in the binders themselves. For example, the extreme values of the variation ranges are assumed as follows: sizes of asphaltene complexes ( $D_{ph}$ ) are equal to 19.8 Å (minimum) and 30.2 Å (maximum) (Table 8-20) and  $\lambda$  is equal to 1.79 (minimum) and 2.20 (maximum). Calculation results are presented in Table 8-22. As assumed  $\delta_n$  and  $n$  in the entire range of sizes of dispersed-phase particles of bitumens are such that intermolecular forces may have a determinative influence on the strength of the material. Intermolecular (van der Waals') forces, which are weak forces of attraction, are represented by orientation, induction, and dispersion forces [21]:

$$F_{str.} = -(F_{or.} + F_{ind.} + F_{disp.}) = (a \cdot \delta_n^{-7} + b \cdot \delta_n^{-7} + c \cdot \delta_n^{-7}) \\ = -(a + b + c) \delta_n^{-7} \quad (8-44)$$

Designating the sum of constants ( $a + b + c$ ) as  $K$ , which can be called a constant of interaction since it characterizes properties of the dispersed-phase particles, gives:

$$F_{str.} = -K \cdot \delta_n^{-7} \quad (8-45)$$

According to assumption 2, dynamic (Bingham) yield strength,  $P_{k_2}$ , is:

$$P_{k_2} = \sum_{l=1}^n F_{str.}$$

since  $P_{k_2}$  is just the stress above which the avalanche failure of structural bonds develops, Eq. 8-45 then becomes:

$$P_{k_2} = -K \cdot \delta_n^{-7} \quad (8-46)$$

Substituting  $\delta_n$  by its form from Eq. 8-8 into Eq. 8-46 one obtains:

$$P_{k_2} = -K \cdot D_{ph}^{-7} \left[ \frac{1 + 5C_v}{6C_v} - \frac{1}{\lambda^{1/3}} \right]^{-7} \quad (8-47)$$

A special experiment was carried out by E. Semyonova to get a preliminary estimate in the closing of the binder dispersed-phase particles due to infiltration of a portion of its dispersion medium volume into the pores of mineral materials (assumption 3). The process of structure formation at an increasing content of porous and nonporous filler (powder) in bitumen was examined. It was believed that the difference in critical volume concentrations of structure formation showed what part of the binder dispersion medium penetrated mineral material pores. To determine the infiltrated volume, mineral powder from the Obidim plant (grain sizes  $<0.025$  mm, density =  $2.73$  g/cm<sup>3</sup>) and glass powder (grain sizes  $<0.05$  mm, density =  $2.73$  g/cm<sup>3</sup>) with similar specific surfaces about  $6900$  cm<sup>2</sup>/g were used as fillers. Structure formation was estimated by changes in the softening temperature (ball and ring method).

The difference in the critical volume concentrations of structure formation was 12.6%, which supposedly is equal to the amount of the dispersion medium volume of bitumen gone into the mineral material pores. Thus, the volume of the binder dispersion medium  $(1 - C_v)$  decreased by 0.126. The values of particles closing in,  $\Delta\delta_n^{ph}$ , due to infiltration are presented in Table 8-23.

The model bitumens'  $K$  values (see Table 8-20) for each kind of asphaltenes were determined using known  $P_{k_2}$  values. Table 8-23 presents calculated values of  $P_{k_2}$  at decreasing  $\delta_n$ , owing to infiltration, and the value of  $\delta_n$  at which the  $P_{k_2}$  required for asphalt concrete is reached. This value of  $P_{k_2}$  was determined (together with D. Shemonayeva) from the correlation relation between  $P_{k_2}$  and the compression strength of sand asphalt concretes based on bitumens of various grades. For asphalt concretes with compression strength  $R = 3.0$  MPa,  $P_{k_2}$  is 0.016 MPa.

Calculation results shown in Table 8-23 reveal that the required  $P_{k_2}$  is achieved at  $\delta_n > 2\delta_s$ . Solvation shells of asphaltene complexes, therefore, will not adjoin, and in contact zones there will be a sufficient amount of free dispersion medium capable to provide required deformability (at temperatures below freezing point) and workability of asphalt concrete mixtures. These results prove that the strength of asphalt concrete may be assured by intermolecular forces of interactions between asphaltenes. However, to make sure that this conclusion is true it is necessary to prove that Eq. 8-46 is true for

TABLE 8-23

Disperse structure parameters

Sample number	$\delta_n$ at $R = 3$ MPa (Å)	Required approaching for providing $R = 3$ MPa (Å)	Approaching due to filtration (Å)	$\delta_n^{ph}$ after filtration (Å)	$P_{k_2}$ in MPa after filtration
2.4	10.32	0.70	1.19	9.83	0.023
2.5	5.79	1.62	0.75	6.66	0.006
2.2	8.17	1.51	1.04	8.64	0.011
4.2	7.72	0.72	0.99	7.45	0.021

the systems under consideration. Secondly, it is necessary to experimentally demonstrate that the nuclei of dispersed-phase particles of organic binders, if they are close enough, can be characterized by indices of strength compared to those of asphalt concrete.

Let us take a possible case of the compacting of asphalt concrete mixture with the dispersion medium of binder, which remained in it after losses to infiltration and solvation shells of asphaltene complexes that penetrated into intergranular spaces. In the zone of contacts between particles of mineral material, only asphaltenes containing only a small part of oils in clearances of 3.55 to 3.7 Å thick [22] between plates remained. Asphaltenes contain four to six plates [6,22]. Under such conditions, it is natural to expect a maximum strength of asphalt concrete. The strength of an interlayer between grains due to a minimum amount of defects (pores, irregularities in the thickness of the continuous liquid phase interlayer, contacts of components of different strengths and sizes) must be greater than that of asphalt concrete. It is possible to model such an interlayer between grains by molding samples from asphaltenes.

For this experiment, asphaltenes were separated from bitumen of grade BHD 60/90 (ind. 1003) which are obtained by deep oxidation of light tars of Tataria oils. For asphaltenes of the same nature but separated from the bitumen obtained by deep oxidation of light tar of Tuymazy oil (No. 2.3 in Table 8-20), the maximum value of  $P_{k_2}$  was determined from Eq. 8-46. To determine this,  $\delta_n$  was assumed as 3.7 Å, assuming that asphaltene particles cannot be closer than the distance between plates. It was then assumed that at such small  $\delta_n$ , the compression strength must actually be equal to  $P_{k_2}$ , since by its structure this material is close to monocrystals. For sample 2.3, at  $K = -93048 \text{ MPa} \cdot \text{Å}^7$ ,  $P_{k_2} = 9.8 \text{ MPa}$  as calculated from Eq. 8-46. The experimental value of  $P_k$  for asphaltenes was obtained by determining the dependence of the compression strength of cylindrical samples with sizes  $d = h = 1 \text{ cm}$  ( $d$  is diameter,  $h$  is height) on compacting pressure (Fig. 8-17).

It is known that in discrete materials pressure at particle contacts may exceed 10 times and even more the normal pressure applied to the mixture [22], which is evidently true for

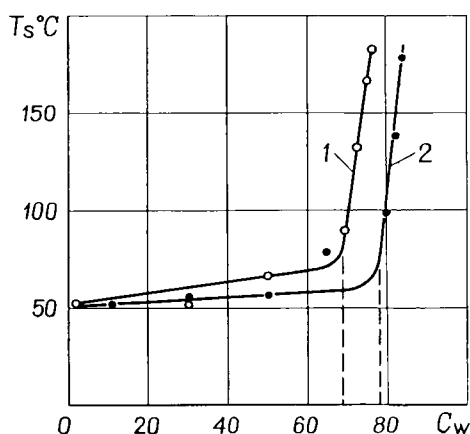


Fig. 8-17. Dependence of binary mixture softening temperature on the fine dispersion filler by weight. 1 = (○) limestone mineral powder; 2 = (●) glass powder.

asphalt concrete mixtures. The chosen range of loading, therefore, can also have a place in practice. Asphaltene samples were molded at  $20 \pm 2^\circ\text{C}$  (the experiment was carried out by I. Kapanadze). As shown in Fig. 8-17, the experimental value of the maximum strength, 9.0 to 9.5 MPa, is close to the theoretical one (9.8 MPa). To confirm the applicability of Eq. 8-46, note that the changing index of a power in Eq. 8-46 from 7 to 6 or 8 results in the strength values of 0.98 MPa and 100.38 MPa, respectively; this is unsatisfactory.

Spirit-benzene resins (SBR) also have high strengths (5.0 MPa). These data confirm the above assumption that the dispersed-phase particles of binder, including both asphaltenes and SBR [23], should also be considered as the dispersed-phase particles of asphalt concrete having more developed surfaces as compared to mineral powder and sand. These particles provide strength and serviceability of asphalt concrete by realizing intermolecular forces of attraction; the dispersion medium of binders is a continuous liquid phase. This experiment proves the applicability of Eq. 8-46 and the significant influence of asphaltenes on the strength of asphalt concrete. This, in turn, attests to the applicability of a molecular-kinetic theory for the substantiation of strength and serviceability of asphalt concrete.

In addition to and in confirmation of this conclusion, it can be noted that the specific surface of sand ( $900 \text{ cm}^2/\text{g}$ ) and mineral powder ( $5050 \text{ cm}^2/\text{g}$ ) are 4 to 6 thousand times less than the specific surface of asphaltene complexes. The numbers of particles of these materials in a unit volume of asphalt concrete have ratios of about  $1 : 10^6 : 10^{18}$ .

In standard sand asphalt concrete, the surface ( $S$ ) and volume ( $V$ ) of the dispersed-phase particles are related as follows:

	$S\%$	$V\%$
Asphaltene complexes	99.79	9.81
Mineral powder	0.12	17.82
Sand	0.09	72.37

To predict Bingham yield strength of asphalt concrete, asphalt binder, mastics and other binary mixtures using Eq. 8-46, it is necessary to know how much  $\delta_n$  will decrease due to the following processes: infiltration of a portion of the binder dispersion medium into micropores of the mineral powder ( $\delta_{ph}^{ph}$ ); distribution of the binder over the surface of mineral grains ( $\delta_{mm}$ ); and redistribution of a portion of the dispersion medium into spaces between grains in the process of mixture compaction ( $\delta_{com}$ ). In this case, Eq. 8-46 may be written as follows:

$$P_{k_2} = -K(\delta_n - \delta_{ph}^{ph} - \delta_{mm} - \delta_{com})^{-7} \quad (8-48)$$

This relation can probably also be used to estimate adhesion forces if one considers that along with the orientation effect of mineral surface, partial desorption of asphaltene solution shells is possible at high temperatures and results in a decrease in the distances between asphaltenes and mineral surface. It is possible to assume that, with a decrease in temperature, the diameter of the dispersed-phase nucleus will increase due to a faster transition of higher molecular components of the solvation shell into the glass state, which will naturally result in a decrease in  $\delta_n$ ; therefore, there is an increase in  $P_{k_2}$  of asphalt concrete and a decrease in its crack resistance.

Aging of asphalt concrete mixtures resulting in the deterioration of their workability and performance characteristics and also aging of asphalt concrete may be interpreted as a decrease in  $\delta_n$ ,  $\delta_{ph}$ , and  $\lambda$  due to the generation of new asphaltenes and SBR. The aging and crack resistance of asphalt concrete may also be estimated from Eq. 8-48.

The proposed approach to asphalt concrete made it possible to formulate some suggestions concerning the control of its properties, development of radically new materials, change in the procedures of preparation and application of asphalt concrete mixtures, and to define more precisely the area of application of bitumens with asphaltenes of different properties, with polymer additives, etc. [20].

In conclusion, the writer would like to emphasize again that: (1) the nuclei of the dispersed-phase particles have the determinative role in the structure and properties of organic binders and of composites based on them; and (2) there is another more general approach when considering structures of bitumens and other organic binding material.

#### ACKNOWLEDGEMENTS

The writer is deeply grateful to Professor T.F. Yen for his invitation to participate in this book, to Mrs. V. Polskaya and Dr. Alexander Gurevich for the translation of this article from Russian into English, and to Prof. G.V. Chilingar for editing the English text.

#### REFERENCES

- [1] Nellensteyn, F.L., *World Petroleum Congress*, 11: 615 pp. (1984).
- [2] Rudenskaya, L.M., *Petroleum Bitumens*. Rosvuzizdat, Moscow, p. 42 (1963).
- [3] Kolbanovskaya, A.S., Optimal dispersed structure of road bitumens. In: *Water Proofing and Corrosion Protection of Structures*. Leningrad, p. 18 (1967).
- [4] Fryazinov, V.V., *Investigation of the Structure of Asphaltene by X-ray Diffraction*. Ph.D. thesis, Ufa (1975).
- [5] Yen, T.F., Erdman, J.G. and Pollack, S.S., Investigation of the structure of asphaltene by X-ray diffraction. *Anal. Chem.*, 33 (11): 1587–1597 (1961).
- [6] Yen, T.F., Asphaltic materials. In: *Encyclopedia of Polymer Science and Engineering*, Index volume, 2nd ed. Wiley, New York, pp. 1–10 (1990).
- [7] Gokhman, L.M., Theoretical bases of the structure of bitumens and organic binders. In: *Petroleum Preprints, ACS Symposium, Chemistry and Characterization of Asphalts*, 35, 3: 308–313 (1990).
- [8] Bodan, A.N. and Godun, B.A., X-ray structural analysis of petroleum dispersed systems. *J. Chem. Technol. Fuels Oils*, 11: 37 (1974).
- [9] Bodan, A.N., Polyquasispherical structure of petroleum bitumens. *J. Chem. Technol. Fuels Oils*, 12: 32 (1982).
- [10] Radovsky, B.S., Gokhman, L.M., Gurary, E.M. and Dukhovnyy, B.S., Use of Mooney formula for the determination of critical concentration of structuring of dispersed systems of bitumen type. *Colloid J. Acad. Sci. USSR*, 4: 729 (1979).
- [11] Wood, V., Investigations of models of simple fluids by Monte-Carlo method. In: *Physics of Simple Fluids*. Mir Publ., Moscow, p. 275 (1973).
- [12] Radovsky, B.S., Density of random packing of spherical solid particles. *Izv. Acad. Sci. USSR, Mech. Solids*, 4: 195–198 (1977).
- [13] *Soviet Encyclopedic Dictionary*. Soviet Encyclopedia Publ., Moscow, 1291 pp. (1982).

- [14] Gokhman, L.M. and Gurary, E.M., Principles of creation and calculation methods of composition of complex organic binding materials based of petroleum residues for road coating. In: *Problems of Processing of Heavy Oils*. Nauka Publ., Alma-Ata (1980).
- [15] Gokhman, L.M. and Gurary, E.M., *Rheological Methods for Determining the Composition of Complex Organic Binders and Particle Sizes of the Dispersed Phase in Them*. Rilem, Beograd, pp. 207–222 (1983).
- [16] Gureyev, A.A., Gokhman, L.M. and Ghilyazitdinov, L.P., *Technology of Organic Binders*. The Gubkin Institute of Gas and Petroleum, Moscow (1986).
- [17] Gokhman, L.M., Gurary, E.M., Amosova, N.V. and Davydova, K.I., The influence of light bituminous resins on bitumen properties. In: *Improvements in the Efficiency of Using Materials in Constructing Asphalt Concrete and Bituminous Pavements, SoyuzDorNII Proc.* Soyuzdormii, Moscow (1989).
- [18] Gokhman, L.M., Shemonayeva, D.S., Gurary, E.M. and Davydova, K.I., Binders based on bituminous material and DST. *J. Avtomobilnye Dorogi*, 4 (1989).
- [19] Kolbanovskaya, A.S. and Gurary, E.M., Lyophilicity and structure-forming ability of asphaltenes of petroleum bitumens as dependent on their origin. *Colloid J. Acad. Sci. USSR*, 34 (4): 523–527 (1972).
- [20] Gokhman, L.M., On the role of organic binding materials in providing asphalt concrete serviceability. *J. Avtomobilnye Dorogi*, 7 (1987).
- [21] Yavotsky, B.N. and Detlaff, A.A., *Physics Reference Book*. Nauka Publ., Moscow, 136 pp. (1985).
- [22] Posadov, I.A. and Pokonova, Yu. V., *Structure of Petroleum Asphaltenes*. Leningrad Technological Institute, Leningrad (1977).
- [23] Gokhman, L.M. and Gurary, E.M., Influence of the phase/medium relation in bitumens on their properties. In: *SoyuzDorNII Proceedings*, Moscow (1981).
- [24] Kostyuk, B.L., Bodan, A.N., Voznyak, O.D., Davydova, A.P. and Lankina, P.M., Influence of chemical composition of bitumens on their structure. In: *SoyuzDorNII Proceedings*, 80: 75–80 (1975).

This page intentionally left blank

## *Chapter 9*

# **ELECTRON SPIN RESONANCE STUDY OF BITUMINOUS SUBSTANCES AND ASPHALTENES**

HUNG-LI CHANG, GARY K. WONG, JIUNN-REN LIN and TEH FU YEN

## **INTRODUCTION**

Electron spin resonance (ESR), or electron paramagnetic resonance (EPR), is an attractive technique used in identifying and studying species which contain an odd number of electrons (radicals, radical cations, radical anions, and certain transition metal species). Through the action of the magnetic field, an unpaired electron absorbs microwave radiation and undergoes transitions in energy levels. Basically, the concepts of ESR are similar to those of nuclear magnetic resonance (NMR), or proton magnetic resonance (PMR or  $^1\text{H}$  NMR). The magnetic moment of an electron is about 658 times that of a proton; this accounts for the differences in spectral regions of the two types of analytical tools, i.e., 9.5–35 GHz for ESR versus 30–100 MHz for NMR. In addition, ESR provides an advantage in that it is extremely sensitive and nondestructive. It is capable of detecting metal ion concentrations as low as a few parts per million without altering the original electronic environment of the metal complexes [1,2]. In this review, we will exclude the use of ESR for the study of metal ions in fossil fuels. The topic of ESR of trace metals in fuels and related materials can be found elsewhere (for example in Ref. [2]). In this chapter, we will restrict the discussion to ESR signals pertaining to free radicals only. In many cases, the free radical signals are interfered by, and overlapping with, the ESR features of the unpaired spin from metal ions. For example, in a number of petroleum fractions, the sixteen features of the vanadium spectrum are displayed and among these, the central features are always overlapping with the free radical signal [2–6]. Computations based on the first principle have been made to assess the net amount of the vanadium contribution and/or to separate the overlapping signals [8,9,11]. Furthermore, we will not cover the environments of the unpaired spins of the metal ions [7] and the associated super hyperfine splittings [10].

Although excellent general review articles on ESR as an analytical tool are available [12–16], only a few papers have been written on electron spin resonance of bituminous substances at the present time and there is no single book on this subject [17,46]. Yet, there are books pertaining to  $^1\text{H}$  NMR and  $^{13}\text{C}$  NMR for the study of fossil fuels [21,22]. A review of this limited field can initiate further research so that a full exploration of ESR studies on bituminous substances may give rise to new information. ESR is a unique tool for product characterization and structure elucidation. It should be brought to the attention of scientists and engineers whose interests lie in the analysis of coal and related bituminous materials.



## BASIC PRINCIPLES

The origin of the ESR experiment is based on the fact that the two possible spin states,  $+\frac{1}{2}$  and  $-\frac{1}{2}$ , of an unpaired electron have identical energies in the absence of a magnetic field. ESR spectroscopy involves the flipping of the spin between the two different energy levels under an external field, an act which is brought about by the absorption of microwave radiation. The magnitude of the spin angular momentum of a free electron  $\beta_e$ , the Bohr magneton, is  $9.273 \times 10^{-21}$  erg/gauss. In an applied magnetic field, the magnetic moment of the electron,  $\mu$ , in the direction of the field coupling spin angular momentum with the electrons' electrostatic charge can be expressed by:

$$\mu = -g\beta_e M_s \quad (9-1)$$

where  $\beta_e$  is the electronic Bohr magneton,  $M_s$  is a spin quantum number, and  $g$  is a spectroscopic splitting factor depending on the orbital and the electronic environment of the electron. If unpaired electrons are placed in a magnetic field with strength  $\mathbf{H}$ , the energy change of the electrons would be represented by the following equation:

$$E = -\mu\mathbf{H} = g\beta_e M_s \mathbf{H} = \left(\pm\frac{1}{2}\right) g\beta_e \mathbf{H} \quad (9-2)$$

The two spin states are degenerate in the absence of an applied field. The difference in energy between the two spin states related to the frequency of radiation,  $\nu$ , necessary to induce transitions between the levels is:

$$\Delta E = h\nu = g\beta_e \mathbf{H} \quad (9-3)$$

Since the spectroscopic splitting factor of a free electron  $g = g_e$ , is 2.0023, it is determined from Eq. 9-3 that an operating microwave frequency  $\nu$  of 9.53 GHz is required when a typical magnetic field strength of 3400 gauss is employed.

Another influence on the ESR spectrum is the magnetic nuclei. This phenomenon, referred to as hyperfine interaction, often leads to the splitting of ESR lines into hyperfine structure. The magnitude of the splitting is referred to as hyperfine coupling constant. In general, for nucleus of spin  $I$ , the splitting is  $(2nI + 1)$  lines, where  $n$  is the number of equivalent nuclei. The line positions,  $H_K$  of an equivalent set of nuclei are given by:

$$H_K = \frac{h\nu}{g\beta_e} - a_i M_i - \frac{\alpha_i^2}{\mathbf{H}} [I(I+1) - M_i^2] \quad (9-4)$$

where  $a_i$  is equal to  $hA_i/g\beta_e$ ,  $A_i$  is the isotropic value of the hyperfine splitting constant, and  $M_i$  is the quantum number of the component of nuclear spin in the direction of the magnetic field. The relative intensity of lines for  $n$  equivalent nuclei can be expressed by the coefficients of the binomial expansion  $(a+b)^n$ . Hyperfine interactions can be classified into isotropic and anisotropic components. In the spectra of single crystal or powder samples, both the isotropic and anisotropic parts are observed. Due to the rotational freedom of molecules in solution, only the isotropic portions of the hyperfine splitting can be observed while the anisotropic part is averaged to zero.

Two other hyperfine interactions, namely, the contact and dipolar interactions, are briefly introduced. Contact or Fermi interactions depend on the presence of a finite unpaired electron density at the position of a nucleus in accordance with the following

equation:

$$A_i = \frac{8\pi}{3h} g\beta_e g_N \beta_N |\Psi(0)|^2 \quad (9-5)$$

where  $g_N$  and  $\beta_N$  are the nuclear  $g$ -factor and nuclear magneton, respectively, and  $|\Psi(0)|^2$  represents the probability of the unpaired electron at the nucleus; for all others,  $|\Psi(0)|^2 = 0$  at  $r = 0$ . However, many systems with unpaired electrons in p- or d-orbitals do exhibit isotropic splitting. In these cases, the p-orbital will polarize the inner shell electrons. Hyperfine splitting, which arises from dipolar interactions between the nucleus and the electron can only be resolved for rigid samples. Therefore, it is not as important in analytical applications as hyperfine splitting, which arises from contact interactions. The following equation governs the behavior of the dipolar interaction as a function of the orientation of the radical in the magnetic field:

$$E(\theta) = g\beta_e g_N \beta_N \frac{1 - 3 \cos^2 \theta}{\langle r^3 \rangle} \cdot S \cdot I \quad (9-6)$$

where  $r$  is the electron–nuclear separation and  $\theta$  is the angle between the applied field and the line joining the dipoles. The average  $E$  over all orientations  $\theta$  is equal to zero.

### Mathematical representation

Considering the possible interactions related to electron spin,  $S$ , nuclear spin,  $I$ , and magnetic field,  $\mathbf{H}$ , the operator can be represented by the general spin-Hamiltonian,  $\mathcal{H}$ :

$$\mathcal{H} = S \cdot g \cdot \mathbf{H} + S \cdot \mathbf{T} \cdot I + S \cdot \mathbf{D} \cdot S + I \cdot \boldsymbol{\sigma} \cdot \mathbf{H} + I \cdot \mathbf{J} \cdot I \quad (9-7)$$

ESR is concerned with the first three terms. The first term in Eq. 9-7 is the electron Zeeman splitting, while the second and third terms are the hyperfine and zero-field splitting interactions, respectively. In the electron Zeeman interaction, both  $S$  and  $\mathbf{H}$  are vectors and the  $g$ -value is tensor, therefore, the expression becomes:

$$[S_x S_y S_z] \begin{bmatrix} g_{xx} & g_{yx} & g_{zx} \\ g_{xy} & g_{yy} & g_{zy} \\ g_{xz} & g_{yz} & g_{zz} \end{bmatrix} \begin{bmatrix} H_x \\ H_y \\ H_z \end{bmatrix} \quad (9-8)$$

The second term in Eq. 9-7 is hyperfine interaction where  $\mathbf{T}$  is a hyperfine tensor. The third term is zero-field splitting interaction. The last two terms are from NMR predominantly; the nuclear Zeeman energy term consists of the screening tensor,  $\boldsymbol{\sigma}$ , which in liquid is related to chemical shift. The spin–spin coupling term involves the anisotropic spin–spin coupling tensor which averages as a coupling constant,  $J$ .

## ESR PARAMETERS

### Spin concentration

Spin concentration is a measure of the number of unpaired electrons in a given amount of sample. The total area enclosed by the absorption curve is proportional to

the number of unpaired electrons present. The spin concentration can be estimated by taking the ratio of area of the sample to that of some standard containing a known number of radicals. High radical concentrations can be measured by using diphenylpicrylhydrazyl (DPPH) as a standard. The DPPH is completely in the free radical state and contains  $1.53 \times 10^{21}$  unpaired electrons per gram. It has been suggested that a series of substandard mixtures can be prepared by diluting a carbon black sample of known radical content with inert solid to obtain a series of mixtures varying in composition from  $10^{12}$  to  $10^{16}$  radicals per gram [23]. Since ESR spectra obtained by a high performance spectrometer are recorded as first derivatives of absorption curves, double integration is required for determination of spin concentration.

### *Landé g-value*

The Landé *g*-value is a very important ESR spectral parameter for obtaining structure and information on coals and fossil fuel-derived fuels. For a free electron, the *g*-value is 2.0023. When an electron is located in a molecule, these values shift slightly in ways which depend on the electronic state of the host molecule occupied by the unpaired electron [24,25]. Also, the presence of associated heteroatoms will lead to additional shifts of *g*-values. It has been reported that sulfur-containing radicals have considerably higher *g*-values [26]. Nitrogen-containing radicals have *g*-values similar to those containing oxygen, but usually have much broader linewidths. The *g*-values of some compound types, which are possibly found in coals and coal derived fuels, are shown in Table 9-1 [27].

Coal and other fossil fuel-derived materials are highly complex organic mixtures. The *g*-value obtained for these types of samples are those for mixtures of radicals in

TABLE 9-1

*g*-values of some possible compound-types in coal (modified from [27])

Radical type	<i>g</i> -value
Aromatic hydrocarbons, $\pi$ radicals	
1-5 rings	2.0025 (cation) 2.0026-2.0028 (anion)
7 rings (coronene)	2.0025 (cation) 2.00291 (anion)
Aliphatic hydrocarbons, $\pi$ radicals	2.0025-2.0026 (neutral)
Oxygen-containing free radicals	
$\sigma$ type	2.0008-2.0014 (neutral)
$\pi$ type	
Quinones 2-3 rings	2.00380-2.00469
Ethers	
1-ring, mono-, di-, trimethoxybenzenes	2.00350-2.00398
N-containing radicals	2.0031
S-containing radicals	2.0080-2.0081
Graphite	2.0025-2.015

the solid state; thus, they cannot be directly compared to the isotropic  $g$ -values of pure compounds. However, they do give useful information for structural characterization of the samples. The  $g$ -values lead to the conclusion that the free radical electrons in coals are delocalized over aromatic structures, with some partial localization at oxygen, sulfur and nitrogen atoms.

It has been shown that the  $g$ -value of the bitumen has a higher value than its corresponding asphaltene fraction, but lower than its petrolene fraction [28,29]. Aromatic hydrocarbon radicals exhibit  $g$ -values which are smaller than those of heteroatomic  $\pi$ -electron systems. An increase in the ring size of molecules typically lowers the  $g$ -value. Therefore, the lower molecular weight petroleums with smaller aromatic ring systems tend to support the higher  $g$ -values.

### *Linewidth*

The width of a band is inversely proportional to the lifetime of the absorbing species in its excited state. It is also a measure of the interaction between the unpaired electrons and their surroundings; the greater the interaction, the wider the band. Three mechanisms have been suggested as contributing to the deactivation of the excited state: (a) spin–lattice interaction, (b) dipolar spin–spin interaction, and (c) exchange interaction [30].

The ESR spectral linewidth of a coal sample is generally determined by measuring the distance (in gauss) between the maximum and minimum points of the first derivative curve ( $H_{pp}$ ). This corresponds to the linewidth at maximum slope of the absorption curve. In early ESR studies of coal, however, the linewidth was defined as the width of its absorption curve at half height ( $H_{1/2}$ ). Since coal is a complex mixture, the spectral linewidth is probably determined by the electron–nuclear hyperfine interaction [31].

### *Lineshape*

In general, lineshape is affected by the unresolved hyperfine structure and the anisotropic effects and is classified as either Lorentzian or Gaussian. They are distinguishable by the number of  $H_{pp}$ . Determination of the  $H_{pp}$ -value requires integration of the experimental first derivative curve. To obtain a reasonably accurate integration (5% error) of the Lorentzian line, the curve cannot be truncated at less than twenty  $H_{pp}$  [14]. Thus, it is more convenient to use a parameter obtained directly from the first derivative curve [32]. The  $H_{pp}$  has been used to directly calculate the spin intensity as well as being a representative of linewidth. However, it is not invariant with lineshape, e.g., in terms of  $1/T_2$  (where  $T_2$  is the spin–spin relaxation time);  $H_{pp}$  for the Gaussian lineshape is 70% higher than that for the Lorentzian lineshape. Using linewidth without referring to lineshape, therefore, can be very misleading. The use of a simplified formula for spin-intensity  $S = (I_{pp})(H_{pp}^2)$  gives as much as 250% error if lineshape is ignored. Thus, it is desirable to use some linewidth parameters that are independent of lineshape as well as parameters directly obtainable from the experimental curve (Table 9-2).

TABLE 9-2

Spin concentration and aromaticity values of various bituminous substances

No.	Sample	Spins per gram $N_g \times 10^{-18}$	Aromaticity $f_a$
<i>Petroleum asphaltenes</i>			
1	Baxterville	4.39	0.53
2	Lagunillas	1.81	0.41
3	Burgan	1.86	0.38
4	Wafra No. A-1	2.21	0.37
5	Mara	1.68	0.35
6	Wafra No. A-17	1.88	0.35
7	Raudhatain	1.62	0.32
8	Ragusa	2.12	0.26
9	Bachaquero	—	—
10	Boscan	—	—
11	Taparito	—	—
<i>Petroleum resins</i>			
12a	Baxterville whole fraction	0.306	0.22
12b	narrow cut	0.147	0.22
<i>Gilsonite asphaltene</i>			
13	Tabor vein	1.41	0.14
<i>Refinery asphaltene</i>			
14	Kuwait visbreaker tar	3.68	0.59
15	Petroleum asphaltene-coked Baxterville, 460°C	14.6	1.0
<i>Petrolene fractions from asphalt</i>			
16		0.0085	0.11
17		0.052	0.20
18		0.32	0.22
19		0.56	0.24
20		0.83	0.26
21		1.7	0.29
22		1.8	0.30
23		2.1	0.37
<i>Coals (ranking based on %C content)</i>			
24	77	2.5	0.69
25	83	3.6	0.75
26	85	5.3	0.76
27	89	7.2	0.81
28	93	18	0.88
29	94	25	0.91
30	95	23	0.95
31	96	15	0.98
32	97	2.2	0.99
<i>Carbons and graphites</i>			
33	Philblack A	1.00	0.95
34	Spheron 6	1.39	0.94
35	Acetylene Black	0.38	0.96
36	Graphon	0.11	0.98
37	Graphite-natural	0.0050	1.00

— = metal content is too high for a good resolution of the spin for radicals.

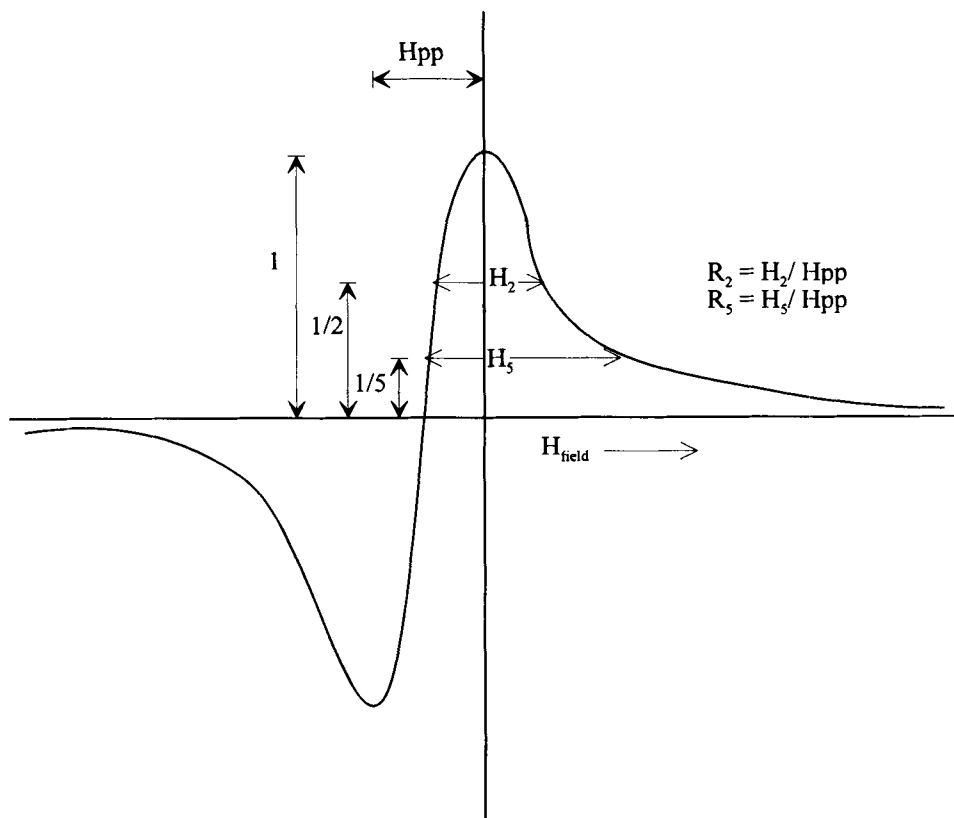


Fig. 9-1. Definition of  $H_n$  and  $R_n$ ; spectrum shown here is the first derivative format (after [32]).

It has been suggested [32] that the parameters  $H_n$  and  $R_n$  be used.  $H_n$  is the width at the position  $(1/n)$  of the peak-to-peak height of the first derivative curve, and  $R_n$  is the ratio of  $H_n$  to  $H_{pp}$  (see Fig. 9-1). The parameters of Gaussian and Lorentzian lineshape are listed in Table 9-3 [32]. The value of  $H_5$ ,  $H_{10}$  and  $R_{10}$  can be used to distinguish between these two lineshapes.

#### FREE RADICAL CONCEPT OF BITUMINOUS SUBSTANCES

Coal is believed to be nonhomogeneous. It can be treated as a mixture of chemical species associated to a three-dimensional gel structure of a cross-linked polymer. This structural system, randomly linked with multiple dissimilar units, belongs to the class of multipolymers. Maceral components are chemical species found within the coal structures. It has been shown that vitrinite, exinite, and inertinite are phyterals corresponding to particular types of substances (Table 9-4) [33]. After catagenesis (coalification) of coal, the chemical species undergo transformation to become individual 3-4-rings aromatic, hydroaromatic, or heterocyclic units, which can be linked together by either weak

TABLE 9-3

Parameters of Gaussian and Lorentzian lineshape

Item	Gaussian	Lorentzian
Absorption curve	$\left(\frac{T_2}{\sqrt{2\pi}}\right) \exp\left(-\frac{T_2^2 H_2}{2}\right)$	$\frac{T_2/\pi}{(1 + T_2^2 H_2)}$
max height	$T_2/\sqrt{2\pi}$	$T_2/\pi$
half-height line width <sup>a</sup>	2.36	2.00
integrated intensity	1.00	1.00
Derivative curve	$-\frac{T_2^3 H}{\sqrt{2\pi}} \exp\left(-\frac{T_2^2 H_2}{2}\right)$	$\frac{2T_2^3/\pi}{(1 + T_2^2 H_2)^2}$
$I_{pp}$	$0.484T_2^2$	$0.414T_2^2$
$H_{pp}$ <sup>a</sup>	2.00	1.15
$H_2$ <sup>a</sup>	1.60	1.21
$H_5$ <sup>a</sup>	2.33	2.13
$H_{10}$ <sup>a</sup>	2.71	2.86
$R_2$	0.80	1.05
$R_5$	1.17	1.85
$R_{10}$	1.36	2.50

<sup>a</sup> In units of  $1/T_2$ .

TABLE 9-4

Macerals of coals

Macerals	Phyterals	H/C ratio
<i>Vitrinite</i> ( <i>xylite</i> )	aromatic polymers	1.0–0.5
huminite (dopplerite)		
collinite		
telinite		
<i>Pseudovitrinite</i>	cellulose derivatives (?)	—
<i>Exinite</i>	lipids	1.7–1.0
resinite	wax	—
sporinite	spore	—
alginite	algin	1.8–1.2
<i>Inertinite</i>	polyamides (?)	—
fusinite		0.7–0.3
micrinite		0.4–0.5

linkage or donor–acceptor hydrogen bonding [3,4]. Occasionally, the  $\pi$ – $\pi$  association can also play an important role in this multipolymer model.

Petroleum asphaltics and related geochemical substances are macromolecules consisting of a very large number of different building blocks. From a structural standpoint, asphaltenes are considered to contain two-dimensional fabrics of condensed aromatic rings intermingled with short aliphatic chains and fused naphthenic ring systems. The

asphaltenes can be visualized as polycondensates of a multicomponent system made up of individual molecules of aromatics, paraffins, naphthenics, macrocyclics, and heterocyclics, in which the bridges or links can be cleaved under selective chemical or physical conditions. Transition metals, such as nickel and vanadium, can be located in the macrocyclic or heterocyclic system.

### *Origin and nature of radicals in coal and bitumen*

Ever since the first detection of free radicals in coal and carbonaceous products in 1954 by Ingram et al. [35] and Ubersfeld et al. [36], much research has been devoted to the study of the origin as well as the subsequent change in nature and quantity of radicals in coal. Three possible pathways have been suggested concerning the genesis and change of free radicals during the coalification process [37]:

(1) Stable free radicals were formed during diagenesis of the organic sediment having persisted throughout geological time.

(2) Radicals were formed in pyrolytic reactions during catagenesis and metamorphism. Decomposition to yield simple substances took place by homolytic splitting. A portion of the radicals remained and stabilized in the solid structure.

(3) The radicals were produced during catagenesis and metamorphism by radiation from radioactive materials in the mineral matter.

Species containing unpaired electrons are unstable; they rapidly decompose or dimerize to yield a new species in which the two odd electrons are paired. However, free radicals can be relatively stable if the unpaired electrons are delocalized over an extensive conjugated double bond system.

Yen et al. [38] proposed that during catagenesis and metamorphism, the imperfections in carbonization owing to the presence of heteroatoms such as nitrogen, sulfur and oxygen in the source material, result in gaps and holes (or defects) in the extended aromatic system. These apparently are the origin of free radicals, exemplified by structures such as perinaphthene or triangulene. The site bearing unpaired electrons is often due to structural hindrance of the complete aromatization (Fig. 9-2). Possible free spin can also be formed from macrocycles, such as porphyrin systems (Fig. 9-3).

The unpaired electrons of coal formed by homolytic bond scission are believed to be stabilized as  $\pi$ -electrons in the aromatic skeletons. The extensive aromatic clusters are separated from each other by  $\sigma$ -bonds. Free electrons are stabilized by delocalization in the aromatic clusters. Inasmuch as these aromatic clusters are close to each other, free-electron transfer among aromatic sites resulting in exchange effects is possible. In addition, free radicals are trapped inside the solid coal structure, and molecular movement necessary for dimerization is effectively prevented.

Free radicals in petroleum asphaltene are also stabilized in the extensive aromatic ring system through resonance of the delocalized  $\pi$ -electrons [38]. An ESR-temperature dependence study reveals that unpaired electrons within the bituminous aromatic sheets can exist in both doublet and singlet-triplet transition states [39]. Charge transfer interactions within and among the peri-condensed aromatic clusters of petroleum asphaltene can be attributed to excitation of diamagnetic spin couples leading to singlet to triplet transitions [39,40].



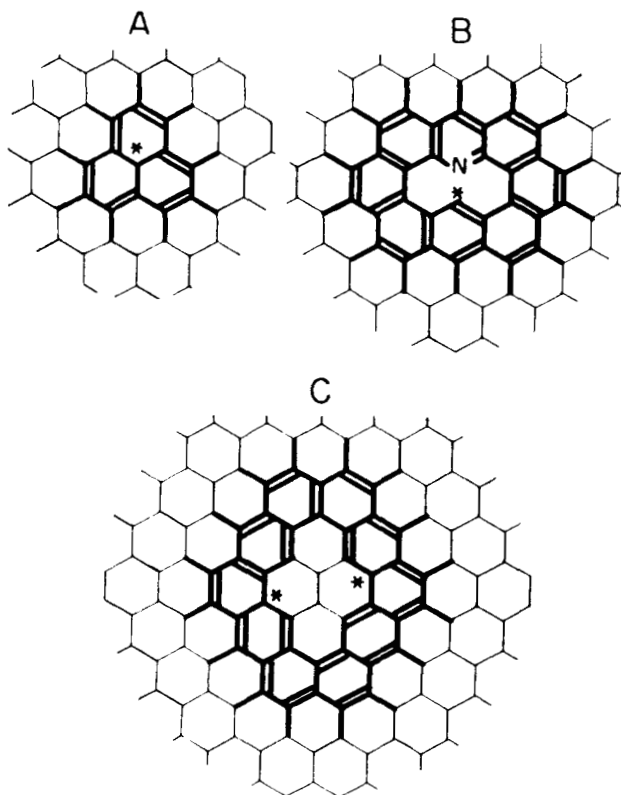


Fig. 9-2. Structures of the type which may be sites of free electrons in petroleum asphaltenes.

### *The role of radicals in fuel processing*

Coal liquefaction, bitumen coking, and heavy oil upgrading processes all involve free radical reaction mechanisms under elevated temperatures [19,41]. Homolysis of chemical bonds to produce smaller free radical fragments is the principal reaction pathway used to decompose the macromolecular structures of coal and petroleum asphaltics. Success of these operations relies on efficient delivery of hydrogen to overcome polycondensation and polymerization in the free radical termination reactions.

Transfer of hydrogen from a slurry vehicle tetralin to coal as a free radical reaction involving thermal cleavage of coal molecules has been described [42,43]. During the initial heating of coal in the liquefaction process, volatile materials within the coal network are released as coal radicals, which are formed by thermal bond scission of coal molecules. Upon further heating, coals pass through a temperature of maximum fluidity before ultimately being repolymerized and resolidified. Free radicals can be responsible for the problems encountered during coal liquefaction, such as reactor coking and poor conversion [27].

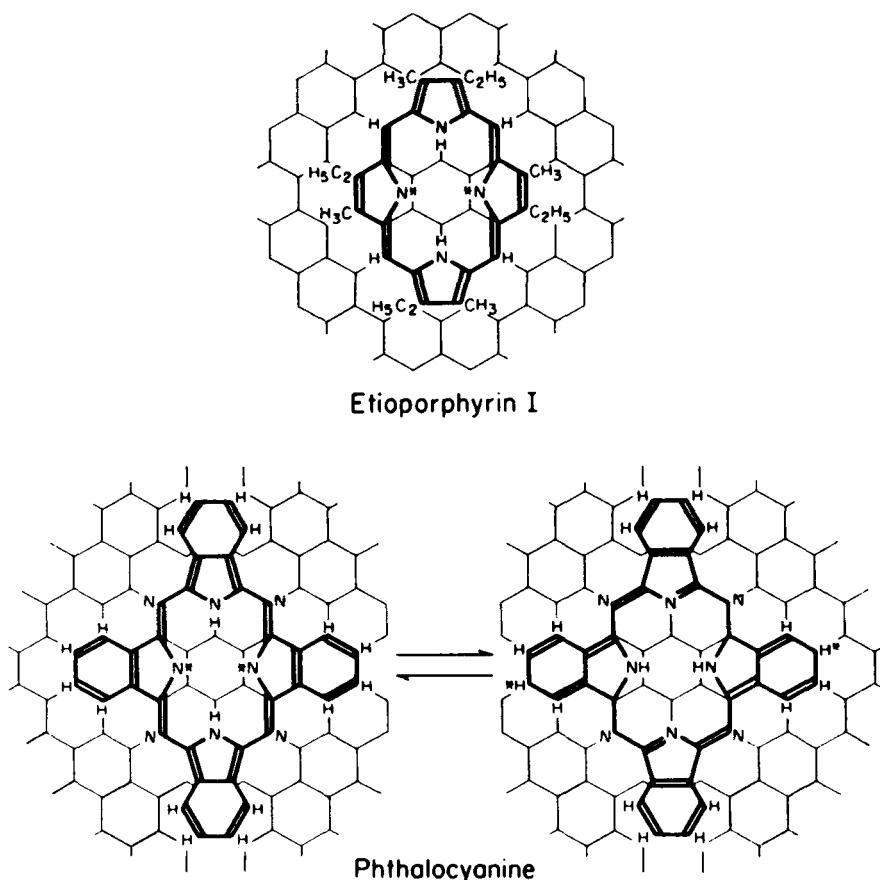


Fig. 9-3. Possible structures for etioporphyrin I and phthalocyanine which may be a source of observed ESR absorption.

As a result, study of electron spin resonance in bituminous substances and their corresponding processed products can lead to valuable information for better understanding of: (1) the transformation of carbonaceous products during maturation, and (2) the nature and roles of free radicals in fuel processing.

#### CORRELATION OF ESR PARAMETERS

##### *Spin concentration and aromaticity of petroleum asphaltenes*

Yen et al. [38,102] claimed that from a simple semilog plot of  $N_g$  versus aromaticity,  $f_a$ , asphaltenes, coals, petroleum and carbons can be differentiated. In Fig. 9-4, the A series is for petroleum asphaltene including any asphaltene which has been coked and heated. Similarly, the B series includes thermal diffusion cuts of petrolenes and resins,

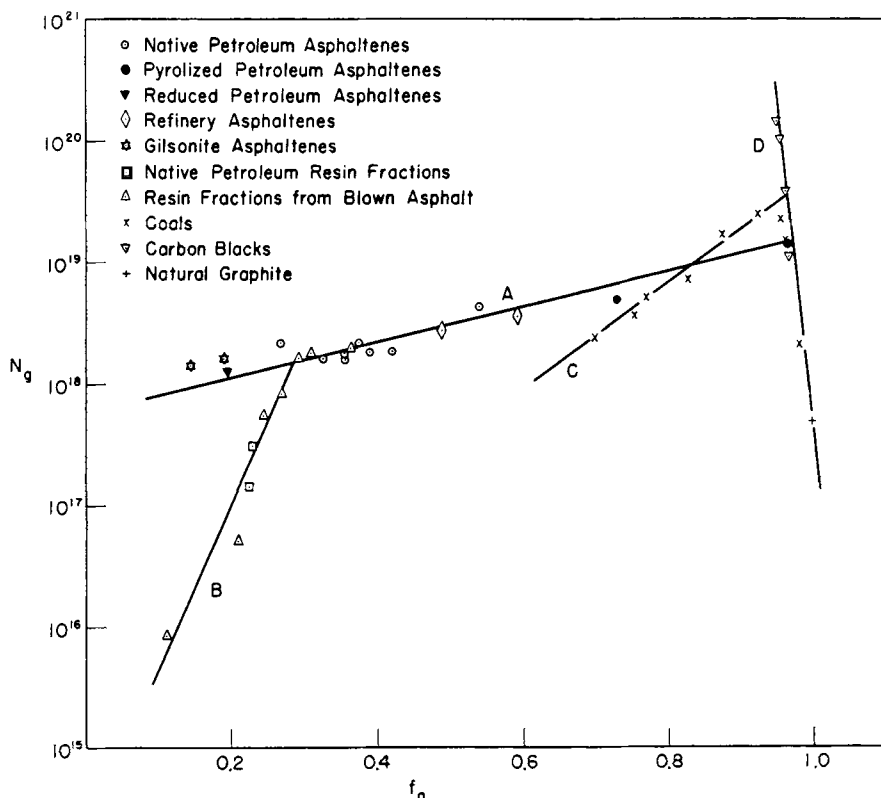


Fig. 9-4. Spin concentration versus aromaticity for coals and other related substances (after [38]).

including resins which have been pyrolyzed. All types of coal, from low C-content to high C-content, are found in the C series. Especially of interest is that line A and line C definitely intersect, whereas line B is stopped by line A. The carbons form another line, D, whereas both line A and line B terminate at line D. Actually, the correlation of %C, %H and percent heteroatoms with spin concentration can be located in a ternary graph as shown in Fig. 9-5 [88]. All samples have been identified in Table 9-2. A theory to explain Fig. 9-4 in which there is a semilog relation between  $N_g$ -values and  $f_a$  is still lacking. A plausible explanation is that the spin population is related to the total  $\pi$ -electrons as a distribution function of  $\varepsilon_\pi$ .

$$N = N_0 \exp(-C\varepsilon_\pi) \quad (9-9)$$

ESR provides two other parameters for substances containing unpaired electrons, namely, the spin-lattice relaxation time,  $T_1$ , and the spin-spin relaxation time,  $T_2$ . Structurally,  $T_1$  is a measure of the rate at which a distribution of spin systems comes into equilibrium with other degrees of freedom in a molecule. For petroleum asphaltenes, the value varied with the oxygen pressure to which the sample was exposed at the time of measurement — i.e.,  $T_1 \propto P_{O_2}$ . The  $T_1$ -values for the asphaltenes and related substances under study were all determined under normal atmospheric pressure

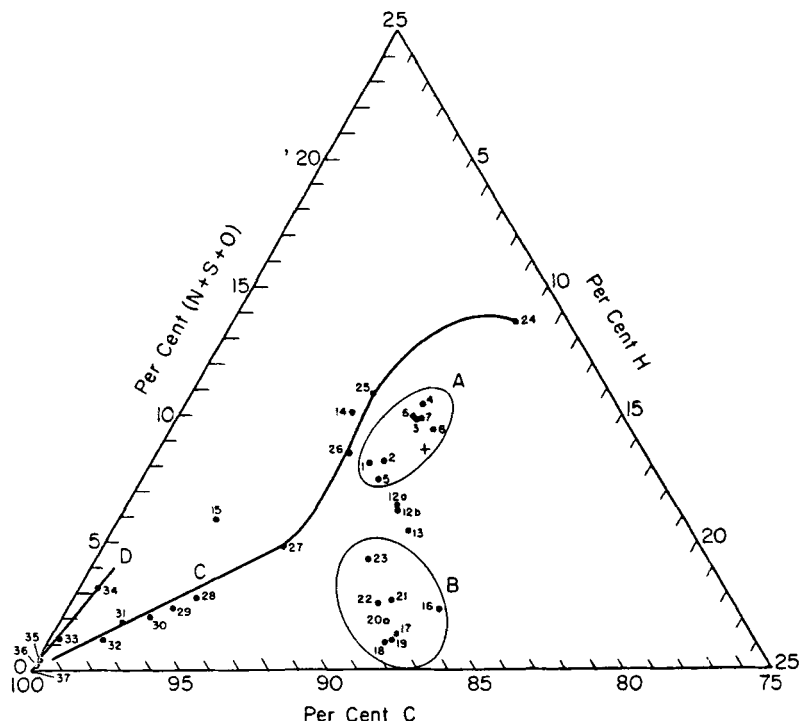


Fig. 9-5. Ternary graph of coal and other bituminous materials (after [88]).

of oxygen. The proportionality factor is assumed not to vary for these closely related substances; then,  $T_1$  might be expected to show an inverse relation to the abundance of  $\pi$  electrons. The values for  $T_1$  were plotted against the population of aromatic carbon atoms per spin,  $P_{CA}$ . These values are determined by using the following equation:

$$P_{CA} = \frac{f_a \%CN}{1200N_g} \quad (9-10)$$

where %C is the percent carbon determined by elementary analysis and  $N$  is Avogadro's number. As shown in Fig. 9-6, the values for the native petroleum asphaltene show a straight line relationship. The values for the heated petroleum asphaltene, the asphaltene fractions of gilsonite and the visbreaker tar all fall considerably to one side, while the values for resin fractions do not fall within the limits of the graph nor do they fall on an extension of the line. Therefore, it appears that the relationship,  $P_{CA}$  and  $T_1$  may provide a reasonably satisfactory method for distinguishing between native petroleum asphaltene and those modified either by heat or other refinery treatment or stemming from allied sources such as gilsonite. Further, from the empirical relationship between  $P_{CA}$  and relative values of  $T_1$ , a relation is developed whereby the aromaticity of a native petroleum asphaltene can be determined by ESR alone:

$$f_a = \frac{12N_a(1.06 - 0.112T_1)10^6}{\%CN} \quad (9-11)$$

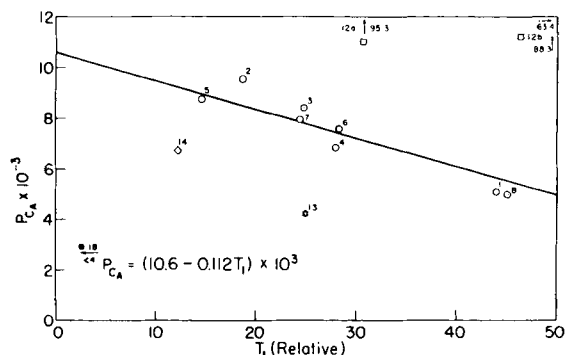


Fig. 9-6. Relation between population of aromatic carbon atoms per spin,  $P_{CA}$  and spin-lattice relaxation time,  $T_1$ . The identifying numbers correspond to those in the first column of Table 9-2.

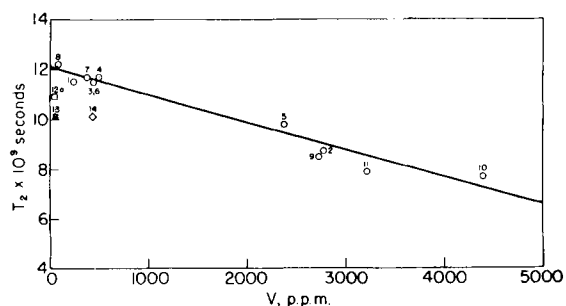


Fig. 9-7. Relation between vanadium content and spin-spin relaxation time,  $T_2$ . The identifying numbers correspond to those in the first column of Table 9-2.

An approximate value of the spin-spin relaxation time,  $T_2$ , is determined by means of the following equation:

$$T_2 = \frac{1}{\Delta H \cdot \frac{\sqrt{3}}{2} \cdot \gamma} \quad (9-12)$$

In coals and carbon blacks,  $\Delta H_{\text{air}}/\Delta H_{\text{vac}}$  may range from unity to as much as 20. For crude oils and for asphaltenes, however,  $\Delta H$  does not appear to be sensitive to the presence of oxygen. For these substances,  $T_1$  is much larger than  $T_2$ ; hence, the effect of oxygen would be primarily on  $T_1$  and the effect on  $\Delta H$  or  $T_2$  would be too small to observe. The presence of paramagnetic centers in the form of vanadium(IV) appears to affect the  $T_2$  values for the organic radicals in petroleum asphaltenes. In Fig. 9-7, vanadium content is plotted against  $T_2$ , for various substances. The petroleum asphaltenes and the resin fractions fall on a straight line, but the values for the gilsonite asphaltenes and the asphaltene from visbreaker tar deviate somewhat.

Radicals associated with mobile  $\pi$ -electron systems usually exhibit strong absorption bands at fairly long wavelengths — i.e., the radicals are colored. Accordingly, the color intensities of the petroleum asphaltenes, the resin fractions, the gilsonite asphaltene,

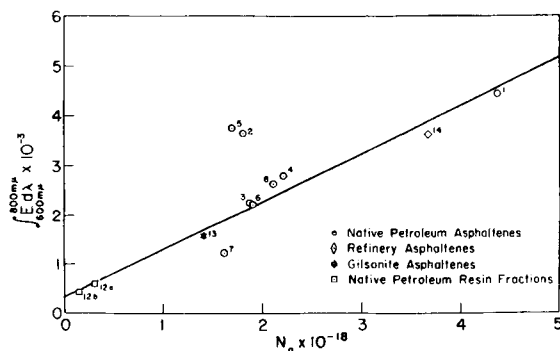


Fig. 9-8. Relation between number of spins per gram,  $N_g$ , and color intensity.

and the asphaltene from visbreaker tar were determined between 600 and 800 runs. Color intensity is defined here as the area under the curve between selected wavelength limits. Because of the insolubility of the coked asphaltene, a comparable value of color intensity for the substance could not be determined. In Fig. 9-8, these values are plotted against  $N_g$ . For the most part, regardless of origin, the substances generally fall on a straight line. Moreover, the values of  $N_g$  and color intensity vary by factors of 2.7 and 3.5, respectively. A similar variation is probable for resins. It is unlikely, therefore, that  $N_g$  and light intensity can serve as a reliable index, either for the concentration of resins-asphaltenes, or of asphaltenes without the correction for transition metals such as V(+4), Mn(+2), etc. A similar relation of color index vs.  $N_g$  has also been found, e.g., in coal liquid (Fig. 9-9).

#### *ESR adsorption and coal rank*

The ranking of coal increases with depth from subbituminous to meta-anthracites [50]. Coals are composed of polyaromatic base units, which are randomly oriented in the low-rank coals. It is believed that coalification proceeds through carbonization of coals by progressive enrichment in structural units with release of chemical groups. Therefore, carbon content can be taken as a good indicator of coal rank because of its parallel increase throughout the catagenetic stage. Relationships between ESR parameters and carbon content should then provide valuable information leading to a better understanding of the transformation of coals during coalification. Fig. 9-10 shows the variations of spin concentration,  $g$ -value, and linewidth with the carbon content which are constructed from various coal sources and coal ranks [26,51,52]. All these ESR parameters vary smoothly with the carbon content, with the only exception of meta-anthracite, which is known to be more electrically conductive than the other members of the coal series [52]. Similar results have also been reported for the trend of  $g$ -value and linewidth along with the carbon content [25].

Fig. 9-10a represents the variation of spin concentration with carbon content. The concentration of unpaired electrons rises exponentially with increasing carbon content up to about 94%C, after which a large decrease is observed. For the bituminous coals

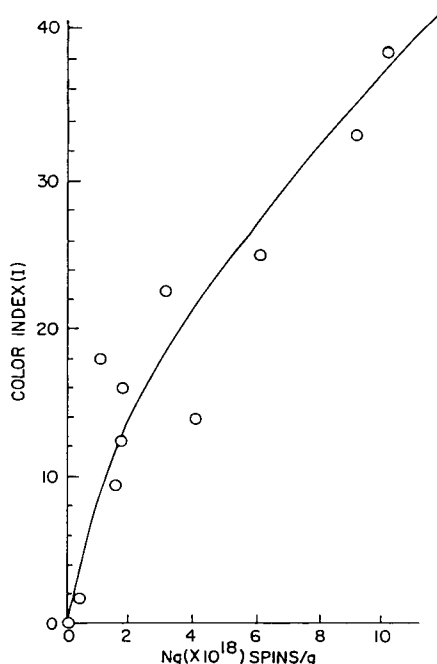


Fig. 9-9. Color index versus spin concentration for coal liquid solvent fraction (modified after [89]).

having a carbon content of less than 90%, one unpaired electron exists per 2000–3000 carbon atoms. Higher rank materials, excluding the meta-anthracite, have approximately one unpaired electron per 1000 carbon atoms. Peat sample studies by the writers found one unpaired electron per 23,000 carbon atoms. The free radical electrons are thought to be delocalized over aromatic rings and stabilized by resonance. The initial exponential increase in spin concentration of vitrains with rank is believed to be due to the formation of organic free radicals during vitrification. The decrease in spin concentration above 94% is due to the increased conductivity of the sample.

The variation of spectral linewidth with carbon content is shown in Fig. 9-10b. A gradual increase in linewidth with increasing carbon content is first observed and this trend is reversed at a carbon content of 80% [26]. Spectral linewidths for the lower rank material are between 4.1 and 8.0 gauss. The large linewidths of peats, lignites, and bituminous coals can be explained by nuclear broadening due to unresolved proton–electron hyperfine interactions. The proton line broadening hypothesis is supported by an ESR study of coals before and after catalytic dehydrogenation [31]. The relatively narrow lines of the anthracites are probably a result of less protons being present in the samples, though exchange narrowing of the ESR resonance may also occur. The very broad spectra line of meta-anthracite is possibly caused by fast spin–spin relaxation in the highly conductive graphite-like structure.

The relationship between the rank and structural characteristics of coal is often given by the typical correlation of aromaticity ( $f_a$ ) as a function of carbon content [64–67].

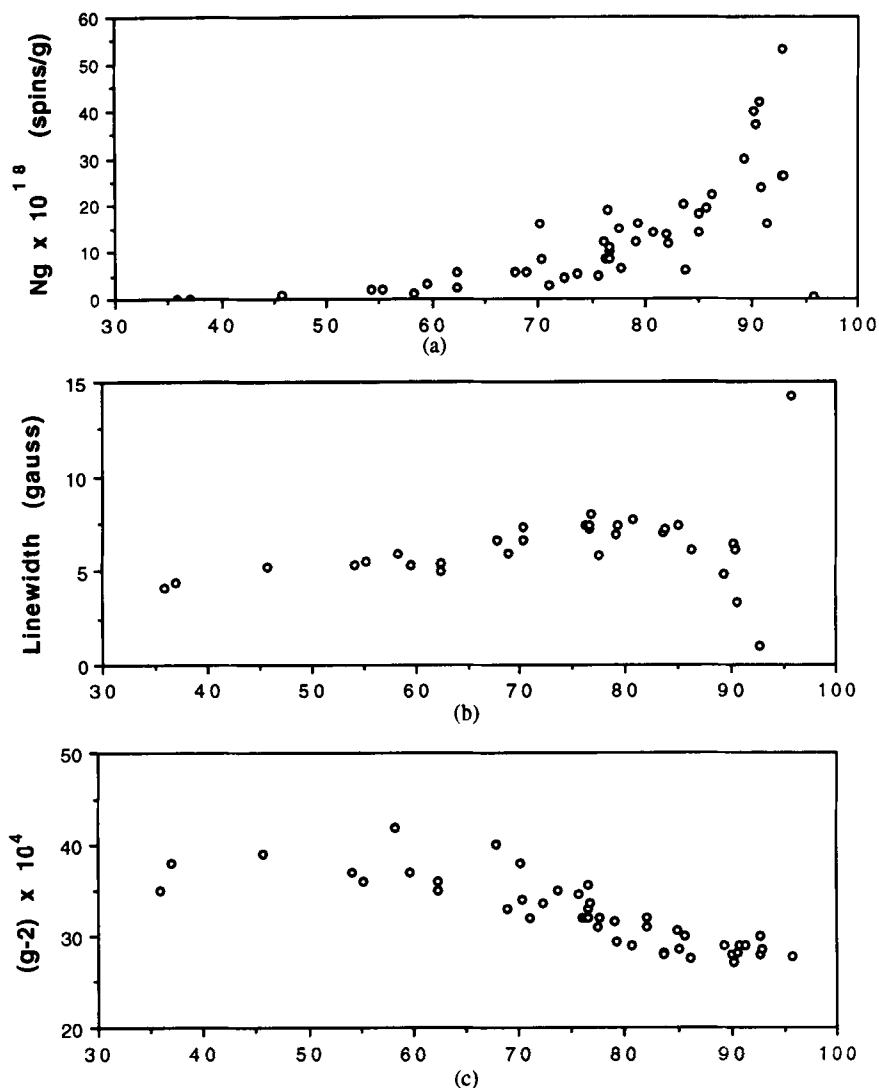


Fig. 9-10. (a) Variation of the spin concentration with carbon content. (b) Variation of the linewidth with carbon content. (c) Variation of the  $g$ -values with carbon content.

Variation of aromaticity with carbon content for a number of coals is shown in Fig. 9-11. The aromaticity follows a generally decreasing trend with reduction in carbon content, though the spread in possible  $f_a$ -values for a given carbon content is generally large. When the carbon content is less than 85%, the  $f_a$  starts to show scattering with little correlation. It has been demonstrated that  $f_a$  has a higher correlation with the percentage of volatile matter than with carbon content. Fig. 9-12 shows the variation of aromaticity with volatile matter content for various coal samples [58,68,69].



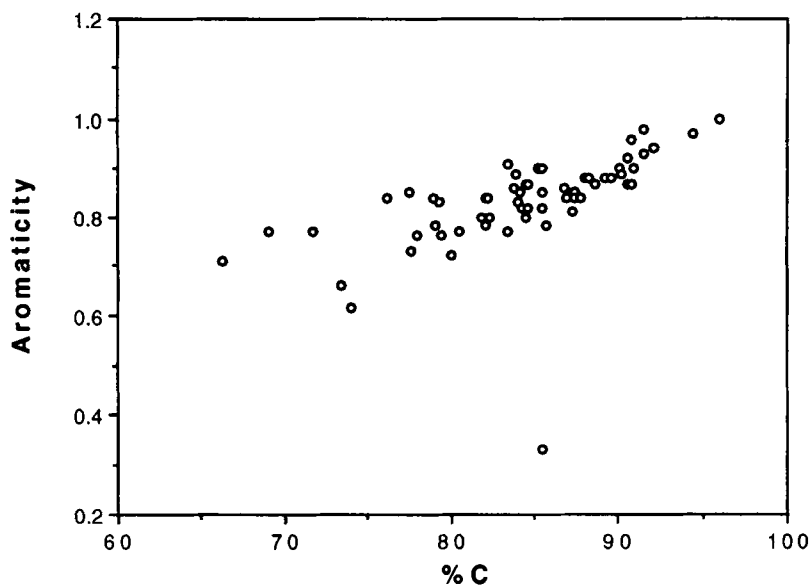


Fig. 9-11. Variation of aromaticity with carbon content.

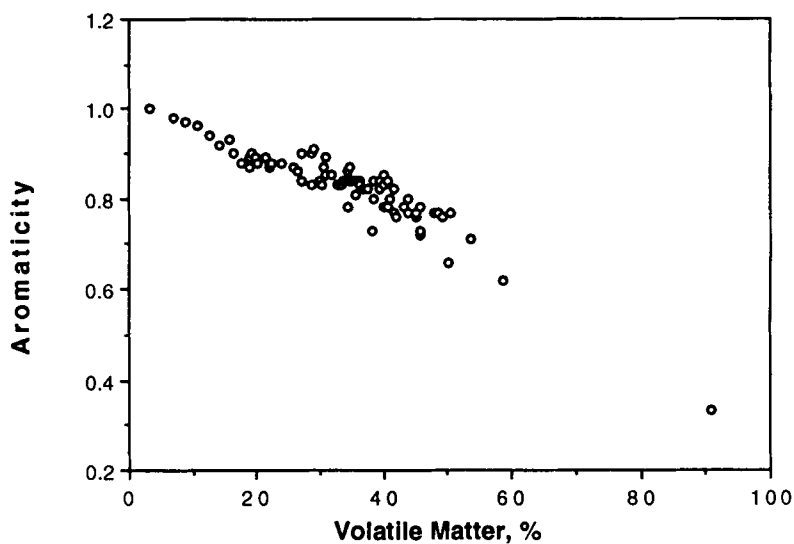


Fig. 9-12. Variation of aromaticity with volatile material content.

The  $g$ -values of coals ranging from 2.0027 to 2.0042 (Fig. 9-13) can be attributed to organic free radicals which are either localized or partially localized on atoms having high spin-orbit coupling constants. The low  $g$ -values in higher-rank coals predominantly come from those of  $\pi$ -type aromatic hydrocarbon radicals [53]. If

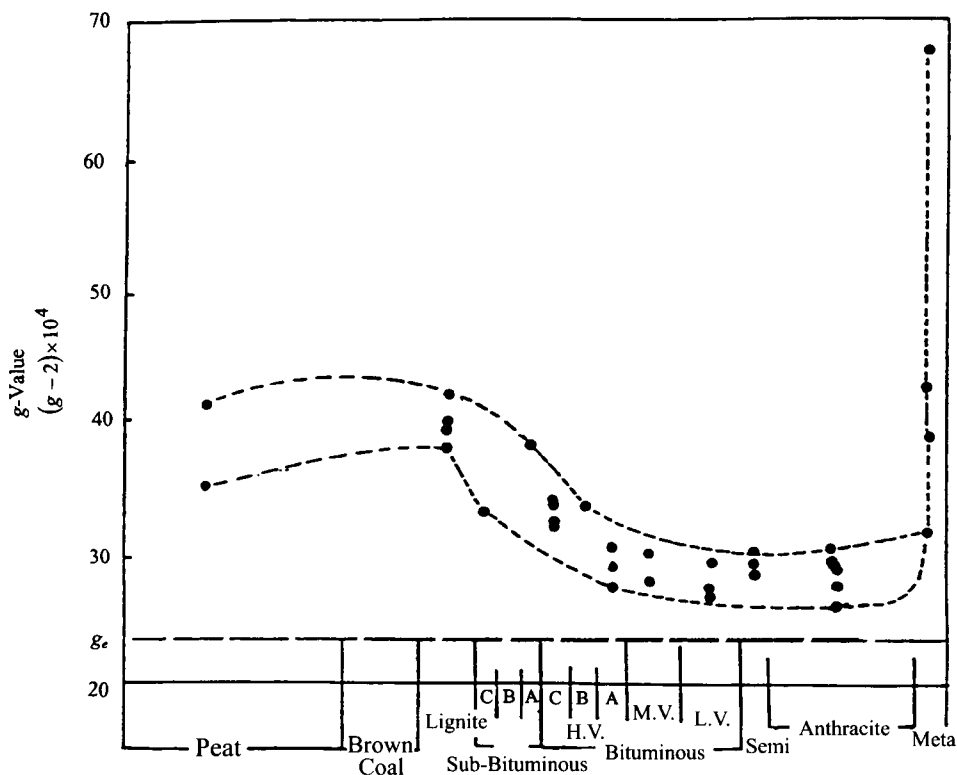


Fig. 9-13.  $g$ -value of ESR parameter of coal rank for vitrains from selected coal (modified after [54]).

present in these radicals, heteroatoms are not likely to participate in the molecular orbital of the unpaired electron to any significant degree. In low-ranking coals (peats and lignites), the high  $g$ -values can be related to aromatic radicals with some partial localization of unpaired electrons on heteroatoms, including oxygen, sulfur and nitrogen. As for lower-rank coals, the high  $g$ -values indicate that the unpaired electron has at least lower spin partially localized on atoms having spin-orbit coupling parameters which are more positive than that of carbon. Therefore, one might expect that the  $g$ -values of the coal would vary smoothly with the concentration of these atoms in the coal [26,27,52]. The decrease of  $g$ -value with coalification suggested that the radicals became more 'hydrocarbon-like'. During the final stage of coalification, the large  $g$ -value can be explained by the fusing of aromatic rings into a graphite structure.

Figs. 9-13 to 9-16 show the variation of  $g$ -value and linewidth with coal rank for vitrains and fusains [54]. The same trend is obtained for the relationship between  $g$ -value and coal rank of a coal sample. This indicates that vitrains have a larger resonance stabilization of the radicals than the fusains. This is due to the fact that vitrains from higher-rank coals contain larger polynuclear condensed aromatic ring systems [54]. The spin concentration of fusain has no discernible dependence on carbon content, which can be explained by the wide variation in thermal history experienced

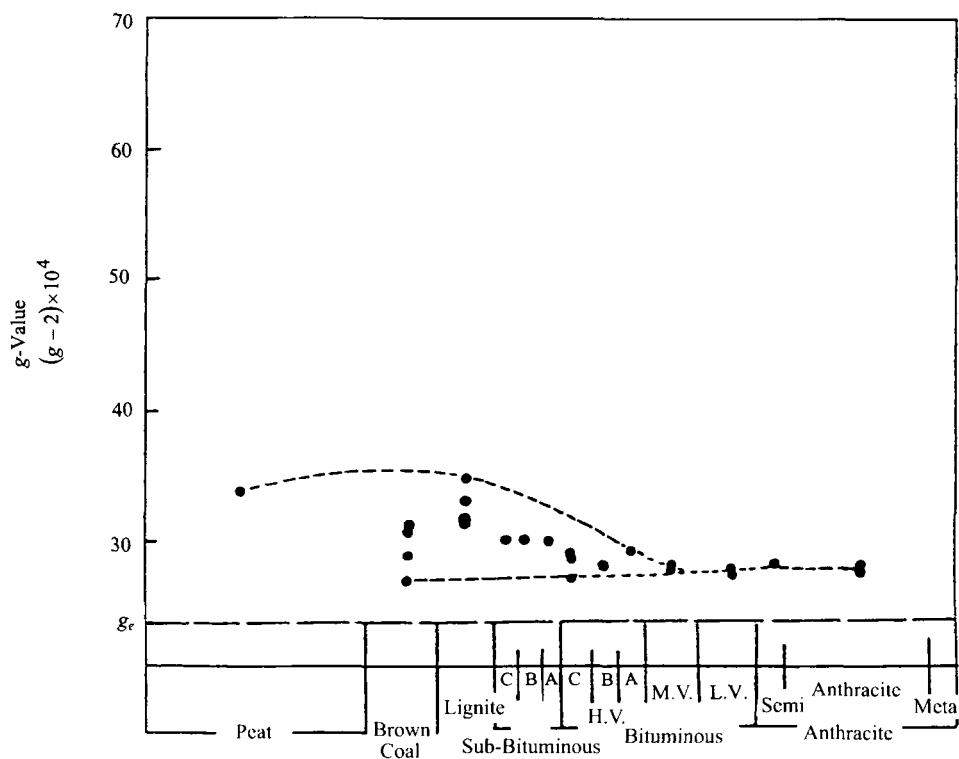


Fig. 9-14.  $g$ -value as a function of coal rank for fusains from selected coals (modified after [54]).

by fusains. The linewidths for the fusains are small, frequently less than one gauss, except for samples from the lowest-rank coals. No evidence was found for the formation of graphite structures during the latter stages of fusinization. The gradual decrease in linewidth of vitrains as coalification proceeds from the low-rank bituminous stages to the early anthracitic stage appears as a very rapid change in the fusinization plot. This is in accordance with Schopf's representation of fusinization [55].

#### *Lineshape and linewidth of coals*

Kwan and Yen [32] have suggested that ESR parameters  $H_n$  and  $R_n$  can be used for the characterization of coals, where  $H_n$  is the width at the position  $(1/n)$  of the peak to peak height of the first derivative curve, and  $R_n$  is the ratio of  $H_n$  to  $H_{pp}$ . A positive linear correlation between  $H_5$  and  $H_{10}$  versus the carbon content is shown in Figs. 9-17 and 9-18. Although the ESR lineshapes of coal samples are intermediate between Gaussian and Lorentzian,  $H_5$  and  $H_{10}$  can still be used as a representation of  $1/T_2$ , and are invariant with respect to lineshape (Gaussian or Lorentzian). The narrow linewidth (4–8 gauss) of ESR signals in coal samples suggests that exchange narrowing is dominant. Anderson and Weiss [56] pointed out that when the exchange frequency ( $W_p$ ) is represented by the spectrum content (SC) of the radical, the lineshape

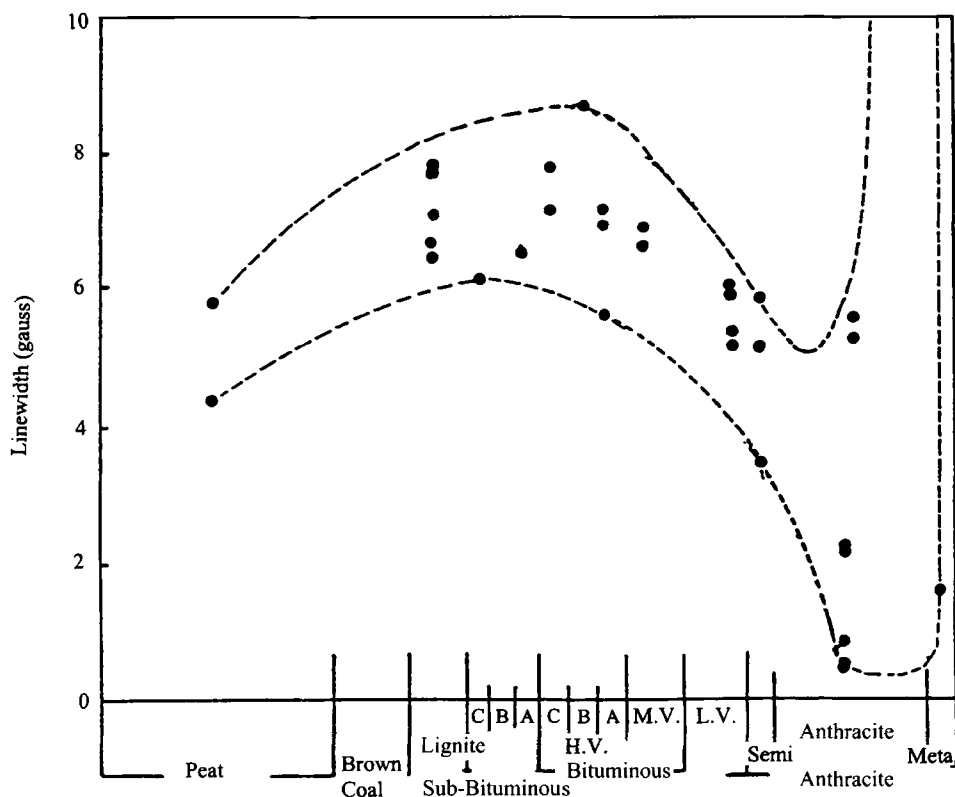


Fig. 9-15. Linewidth as a function of coal rank for vitrains from selected coals (modified after [54]).

is Lorentzian with linewidth  $1/T_2$  equal to  $W_p^2/W_e$ . Spins in higher-ranking coals are generally believed to be more delocalized than in lower-ranking coals. Exchange, therefore, is faster in higher-ranking coals. In order to obtain the positive correlation indicated in Figs. 9-17 and 9-18, it is necessary for  $W_p$  and  $W_e$  to be comparable, because they tend to compensate each other; consequently, the linewidth would be proportional to  $W_p$  and, therefore, proportional to carbon content. This is due to the fact that as the size of the paramagnetic aromatic centers increases, the spectrum content defined as the spin of the stick diagram also increases due to the larger number of peripheral hydrogen atoms. The following relationship has been suggested for hyperfine splitting constants of hydrogen atoms for aromatic systems [51]:

$$A_i = Q|\rho_i| \text{ and } SC = \sum_i A_i = \sum_i |\rho_i| \quad (9-13)$$

where  $A_i$  is hyperfine splitting constant of atom  $i$ ,  $\rho_i$  is unpaired spin density of atom  $i$ , and  $Q$  is a McConnell constant. Due to the possibility of negative spin density and larger  $Q$  for larger rings, spectrum content (SC) increases with ring size. Thus, positive correlation of linewidth can be explained by the increase of the size of the paramagnetic aromatic center as the coal becomes more mature (high-ranking coal). The positive

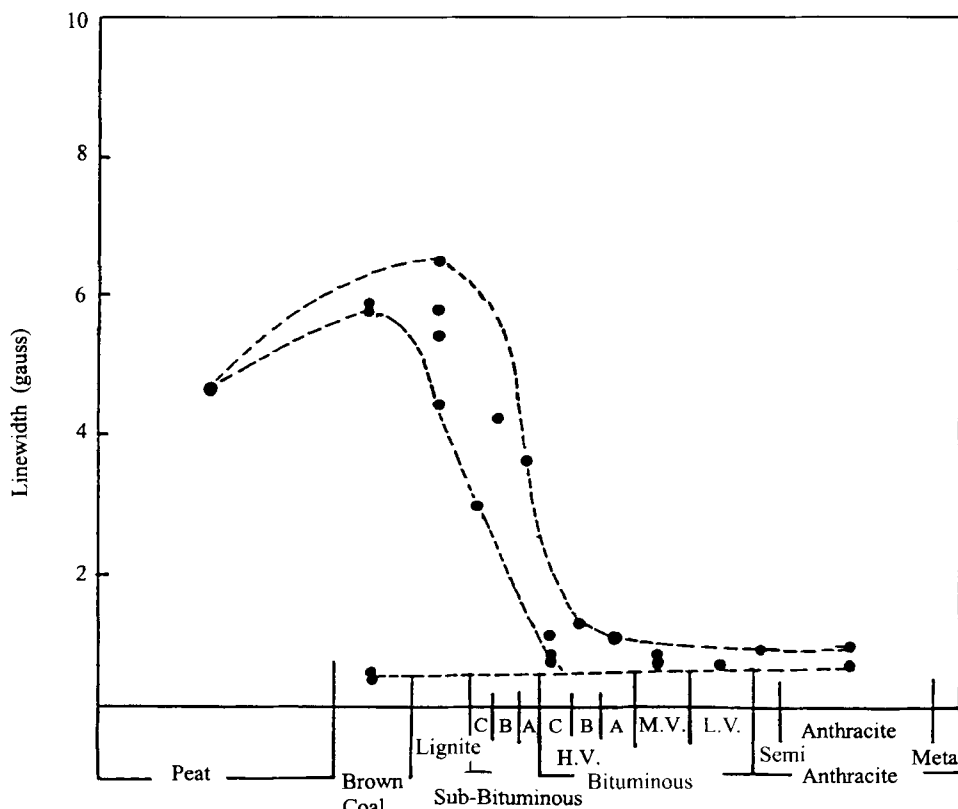
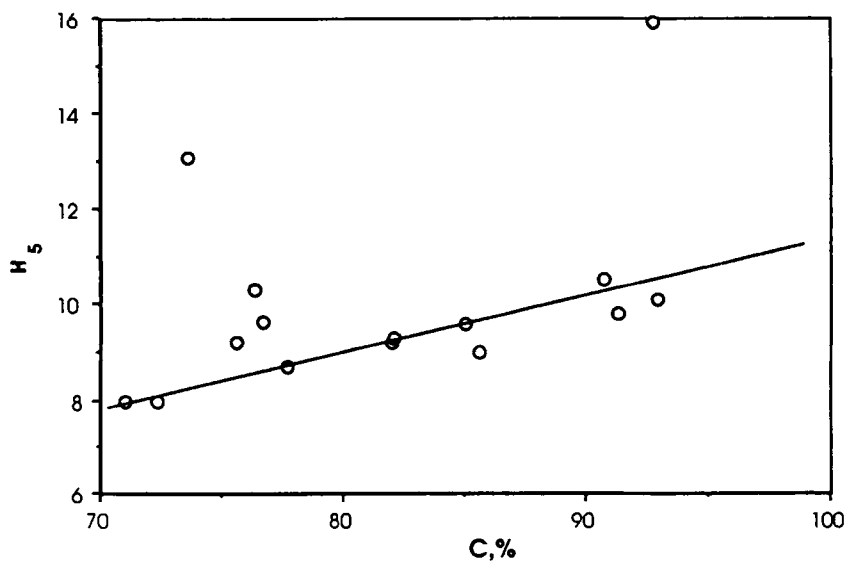
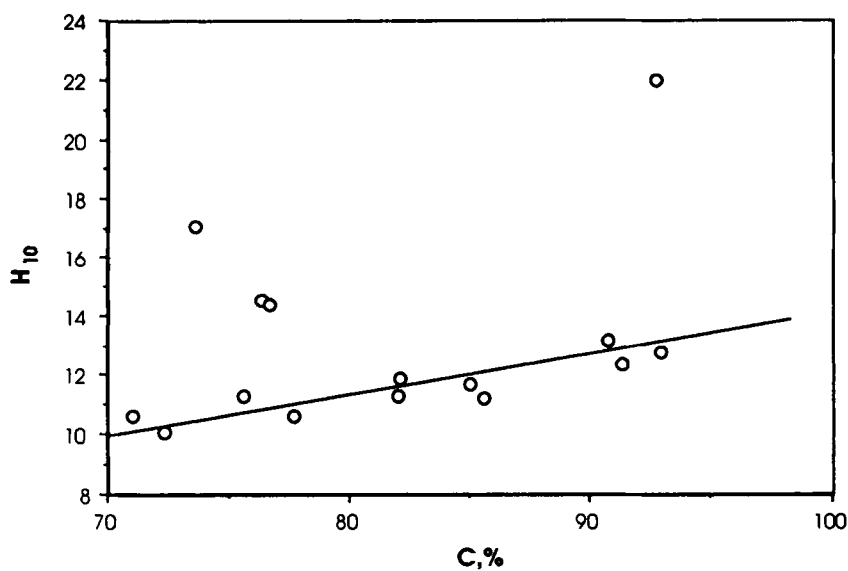


Fig. 9-16. Linewidth as a function of coal rank for fusains from selected coals (modified after [54]).

correlation of linewidth and spins per gram with coal rank is consistent with Ingram's hypothesis.

The lineshapes of coal samples are closer to Lorentzian than to Gaussian. This is consistent with the narrow linewidths which come from exchange narrowing. The plots of  $R_2$  and  $R_5$  versus carbon content and the relationship between  $R_2$  and  $R_5$  are presented in Figs. 9-19 and 9-20, respectively. Region I is occupied by low-ranking coals. These correlations suggest that lineshape parameters can be used to characterize coals. It is found that lineshapes of low-ranking coals (lignite and SB) are the same as those of high-ranking coals (LVB, MVB and Semi-An). Inasmuch as the lineshape depends on the relative magnitude of exchange frequency and spectrum content, the relative magnitude must be the same for both high-ranking and low-ranking coals.

A mechanistic view of the transformation of coals can be postulated by the observed trends of linewidth and lineshape with coal rank. As coalification proceeds from low-rank to medium-rank coal, the size of aromatic clusters grows even faster. Thus, exchange due to delocalization increases faster than the spectrum content, which corresponds directly to the size of the aromatic cluster. The process is reversed from medium-rank to high-rank coals. The number of aromatic clusters grows more slowly

Fig. 9-17.  $H_5$  as a function of carbon content (after [32]).Fig. 9-18.  $H_{10}$  as a function of carbon content.

than the size. One possible mechanism would be the fusion of two aromatic clusters to form a larger one. The increase in free radical concentration with increasing carbon content also can be explained by the high resonance stabilization of free radicals having the unpaired electrons associated with larger aromatic ring clusters.

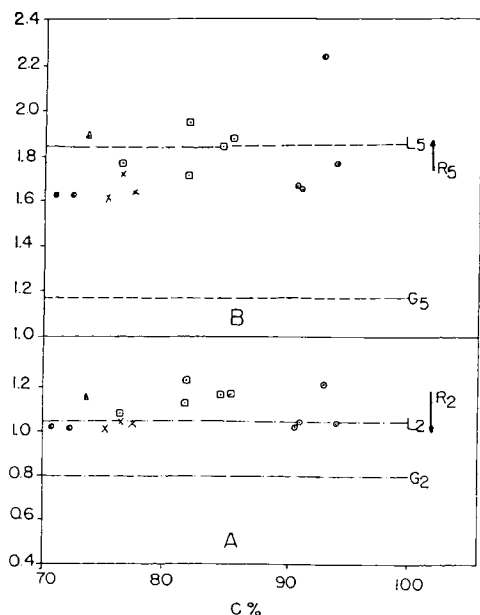


Fig. 9-19.  $R_2$  and  $R_5$  as a function of carbon content (after [32]).

#### *g-values and heteroatom content*

Most bituminous substances contain considerable quantities of sulfur, oxygen, and nitrogen. These heteroatoms all possess high spin-orbital coupling relative to carbon. It has been determined that oxygen and sulfur contents play an important role in  $g$ -values of coals. Results from linear and multilinear regression analyses of  $g$ -values have shown the importance of sulfur and oxygen containing species to the free radical structures in coals. Inclusion of the nitrogen term to oxygen-sulfur can lead to an additional 42% improvement in the statistical correlation. Although these results may be different from those reported for vitrains from some selected coals [17], one common finding from these studies is the much higher regression coefficients of sulfur as compared with those for oxygen. On the other hand, the  $g$ -values of asphaltenes derived from tar-sand bitumens and petroleum are not statistically correlated with the heteroatom content. It has been claimed that the  $g$ -value is, therefore, not a good parameter for elucidating the structure of asphaltenes derived from bituminous substances other than coals [57].

However, the ESR  $g$ -values of a variety of bituminous materials as a function of their heteroatom content:  $\sum \xi_k X_k$  (Fig. 9-21), where  $\xi_k$  is the spin-orbital coupling constant of the given heteroatom  $k$ , and  $X_k$  is its atomic fraction, has been plotted by Yen and Sprang [58]. The spin-orbital coupling constants for N, O and S are 76, 151 and 382  $\text{cm}^{-1}$ , respectively. They [58] also correlated this concept by known compounds such as halogenated semiquinones and found that they do fit straight lines as in Fig. 9-22. Thus it follows that the  $g$ -tensor is

$$|g - g_c| \cong 2 \sum \rho_k \xi_k / \Delta E_k \quad (9-14)$$

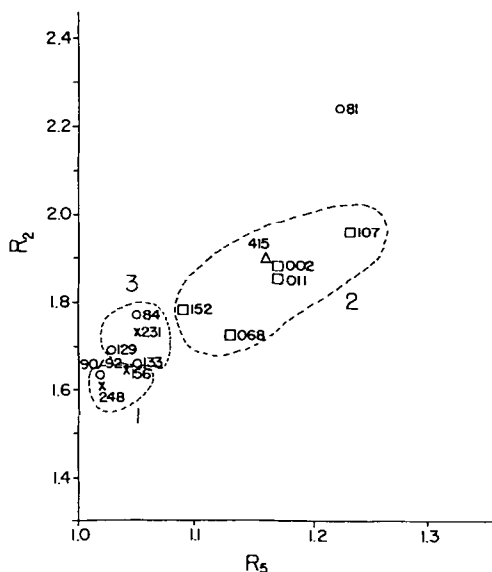


Fig. 9-20. Relationship between  $H_2$  and  $H_5$ , indicating different domains for different ranks of coal. (I) = low rank, (II) = HVB, (III) = high rank (after [32]).

where  $\rho_k$  is the electron spin density on given atoms of  $k$ , and  $\Delta E_k$  is the energy separation between the  $k$  atom from ground to excited state. Typical native coals fall into two coterminous series (Series I and II, see Fig. 9-21), whereas native petroleum asphaltenes follow only one (Series III). It is significant that the point at which the coal trend reverses itself, i.e., the intersection of Series I and II occurs at the limiting free spin  $g$ -value of 2.0023. This observation can be explained on the basis of the variations in heteroatom content and aromaticity within the coal and asphaltene series. Both petroleum asphaltenes (Series III; see Fig. 9-21) and coal samples with higher heteroatom content (Series I) tend to reflect the  $g$ -value decrease with a corresponding decrease in the percentage of heteroatoms. On the other hand, coal samples with a lower heteroatom content (Series II) show an increase in  $g$ -value with a further decrease in heteroatom content. Coal Series I with high heteroatom content is comprised of low-rank coals, which include lignite and subbituminous coal. Conversely, Series II, characterized by low heteroatom content, can be identified with high-ranking coals, such as anthracite and bituminous coal.

Certain irregularities are evident in both coal series. Both Sharigh A18 and Rasa A17 (in Fig. 9-21) are lignites which are known as abnormal [59]. These atypical coals with coking properties comparable to high-swelling bituminous coal have an unusually low heat of wetting and inherent moisture content [60]. These two lignites (A17 and A18) together with a typical North Dakota Zap lignite (A26) and a Manitowox peat sample (A25) are all outside the range of the regular coal series. In addition, two other coals, Lethridge (A21) and Yubari (A9), are found to fall into the asphaltene series. This may be explained by a possible similarity of these materials to asphaltenes, both in carbon content (A9: 86.2%; A21: 79.7%) and saturation characteristics of spin relaxation time,



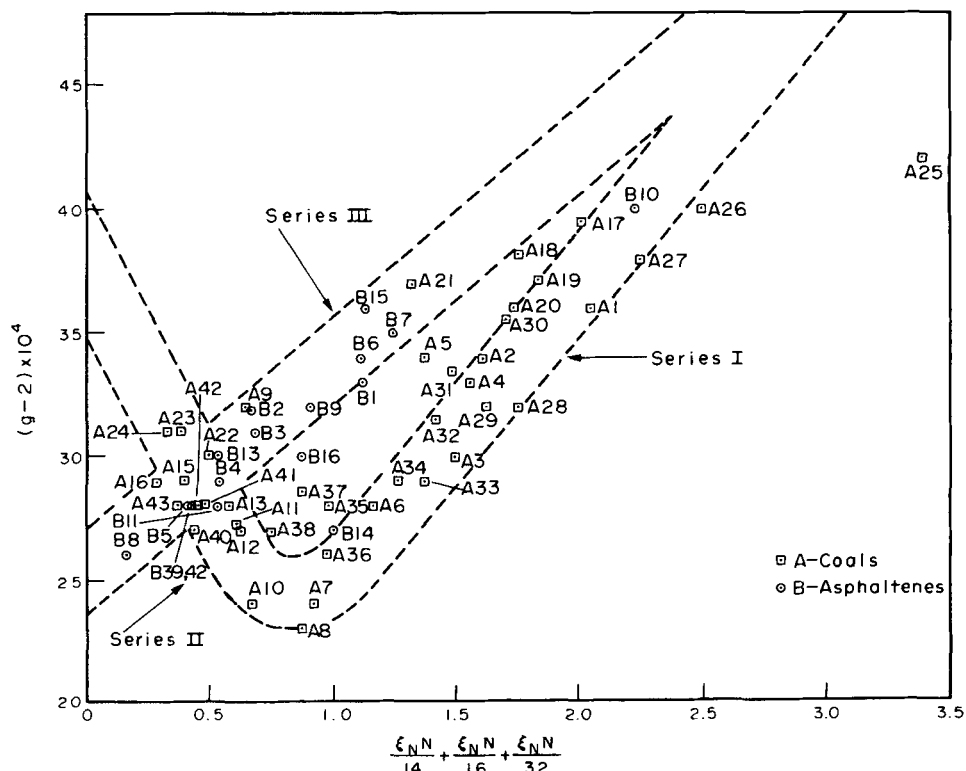


Fig. 9-21.  $g$ -values and heteroatom contribution for coals and asphaltenes. Coals from Series I and II, asphaltenes from Series III (after [58]).

$T_1$ . Yubari coal is the most easily saturated among the Japanese coals [61]. Coals in this range of carbon content usually exhibit sensitivity to oxygen absorption [62]. These observations lead to the suggestion that genetic or structural similarities may exist between these coals and asphaltenes.

Spin delocalization in samples belonging to coal Series I can be visualized as a decrease in the heteroatom content and an increase in the degree of aromatization (Fig. 9-23). The presence of free radicals predominantly of a semiquinone type in both peat and lignite leads to strong localization of unpaired electrons resulting in high  $g$ -values of the samples. Hydrocarbon radicals begin to form as aromaticity increases during coalification; these free radicals start to gain mobility to interact and delocalize until a free spin state of  $g = 2.0023$  is reached. Complete delocalization of spins in coals occurs when aromaticity reaches ca. 0.8, which represents the condensed structure consisting of large  $\pi$ -systems. This condensed aromatic system especially in meso-position is highly susceptible to reaction with trace quantities of ambient oxygen. The oxidation reaction resulting in the formation of localized system will give rise to the Series I–Series II transition. This overview explaining the transition of the coal series is supported by the structural nature of carbon after charring [70]. The low-temperature

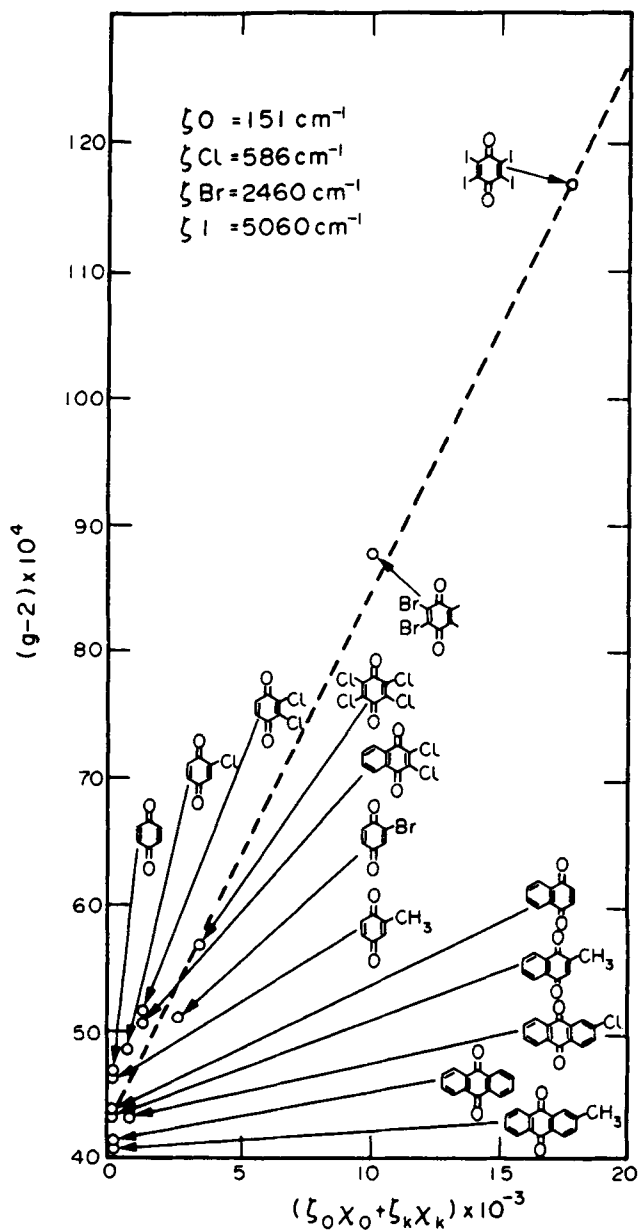


Fig. 9-22. Plot of  $g$ -values versus heteroatom contribution for a series of halogenated semiquinone radicals, rough linearity;  $K$  represents halogens; data from Blois et al. [112].

(400°C) reaction products are aromatic in nature with hydroquinone-like phenolic OH-groups (Series I), while hydrocarbons from high-temperature (800°C) reactions contain a large number of olefinic and quinonic carboxyl groups (Series II).

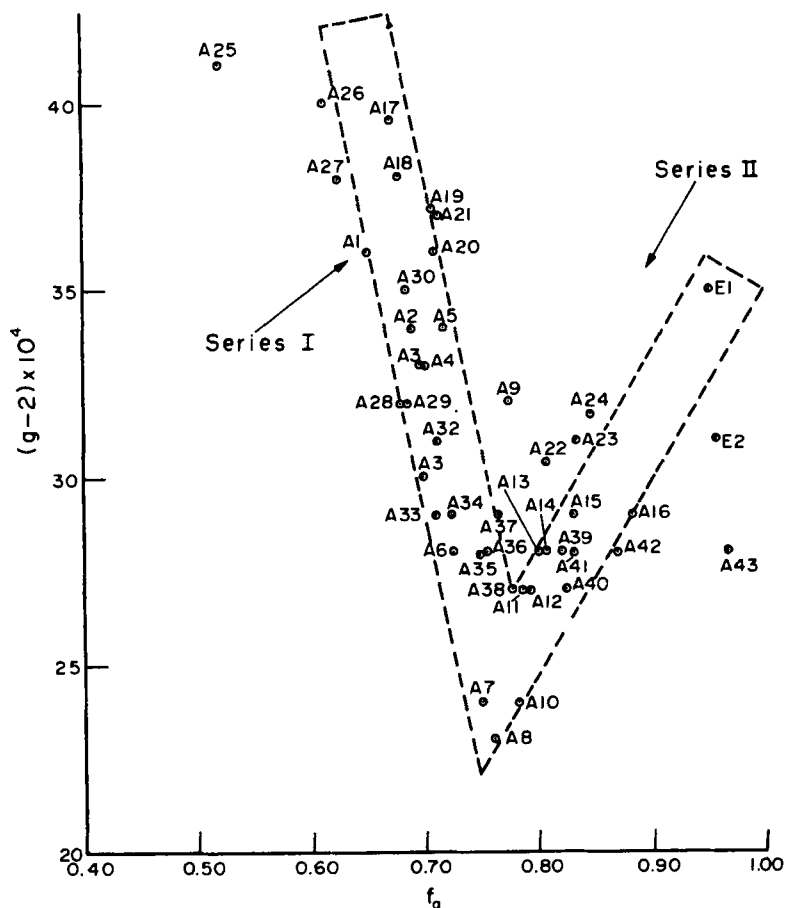


Fig. 9-23. Relationship between the  $g$ -value and aromaticity for coals, Series I and II (after [58]).

External bonding at the edge of a graphite layer can be described by four mechanisms, in which the divalent  $s^2p^2$  character of the odd boundary atoms and partially triple bonds resulting from  $sp$ -hybridization may be responsible for the reactivity of the system [71]. Localization of the spins in both high-temperature carbon products and high-ranking coals has been well documented [62,72]. Sharp and narrow lines of a composite signal of localized components have been observed for both carbons and high-ranking coals, especially fusite. Experimental verification of the above includes the oxygen sensitivity of these coals and their tendency to react with other solvent media and to initiate polymerization. Observation of the Series I–Series II transition can provide some insights into the maturation history of coals. The diagenetic and metamorphic processes probably involve an initial spin delocalization caused by aromatization of a stable and localized polyhydroxy-substituted ring system, which is followed by further localization of a delocalized system due to the formation of quinones and peroxides.

Determination of  $g$ -values requires care in such a way as not to include any overlap-

ping vanadium signal with it. Otherwise, the values can be doubtful. The same is true for spin concentration. For example, the different  $g$ -values observed in asphaltenes and resin samples indicate that bitumen ESR spectra result from superposition of different lines related to free radicals with very close  $g$ -values. The asphaltene fraction contained the highest concentration of free radicals. The asphaltene has a free radical concentration as high as  $8.9 \times 10^{18}/\text{g}$  and resins have  $1.2\text{--}2.5 \times 10^{17}/\text{g}$  [73]. After demineralization of Argonne premium coals, it is observed that the radicals concentration increases up to a factor of 3 and 3.3. Also, changes in  $g$ -value and line widths are observed. This suggests that the carbon radicals in the organic material of the coal are interacting with inorganic paramagnetic species which occur in both mineral and ionic forms [63].

### *Kerogen maturation and paleotemperature*

Kerogen is recognized as the greatest part of organic matter in sediments that is insoluble in an organic solvent. It is also regarded as the most important source of petroleum available [105]. Under thermal conditions, kerogen can be cracked to form petroleum. Cracking results in unpaired free radicals, and stable free radicals increase in the kerogen as maturation proceeds. Thus, it can be expected that the history of a kerogen diagenesis is reflected in the concentration of free radicals. Due to its heterogeneity and the presence of minerals, the determination of free radicals in the kerogen samples is generally complicated. In addition, spin measurement of kerogen to evaluate maturation of potential source rocks is further hindered by the presence of solvent-extractable organic molecules trapped within the kerogen matrices [44–46]. As a result, the suitability of ESR kerogen studies is very limited.

Nevertheless, a good correlation between free radical concentration and geothermal history can still be obtained. A regular increase of spin concentration with burial depth has been suggested for the kerogen obtained from a clay size fraction [47]. After the kerogen is treated with pyridine, it is shown that the spin concentration constantly increases with burial depth (see Fig. 9-24) in the diagenesis and catagenesis stages [48,49]. It was suggested that the deeper the sediments are buried, the higher the temperature, and therefore, the longer the duration of heating temperature to which they are subjected. Hence, the burial depth is an indication of the level of kerogen degradation. Due to the more rigid and compact structure of kerogen and the more aromatic character of the spin center, spin concentration decreases significantly in the metagenesis stage.

Earlier works used the paramagnetic susceptibility per mass,  $\chi_p$  instead of  $N_g$  as measurements. For example, for the Douala Basin, correlation of  $\chi_p$  versus the depth of burial is known (Fig. 9-25) [46]. In this case, the  $\chi_p$  value is equivalent to the  $N_g$  value. Also,  $N_g$  or  $\chi_p$  has similar relations with the vitrinite reflectance at room temperature (Fig. 9-26) [108]. Samples have been measured in  $g$ -values for kerogen types I, II, and III with the accompanying vitrinite reflectance [46]. It is difficult to use ESR as a tool for the type differentiation (Fig. 9-27).

Hwang and Pussey [18] have studied a series of kerogen samples (after removal of minerals) from the same exploration well or surface outcrops. They found that the borehole temperatures are linearly related to  $g$ -values, linewidths and spin concentration (Fig. 9-28). Inversely, the thermal history of subterranean formation of lithological

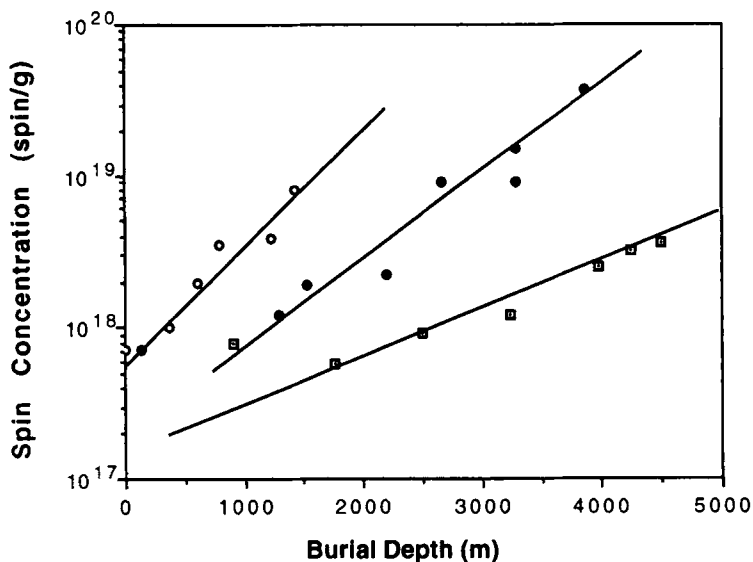


Fig. 9-24. Variation of spin concentration with burial depth of kerogen sample treated with pyridine: circle = Oashizawa kerogen; dot = MITI-Takadaheiya kerogen; square = Hamayuchi kerogen.

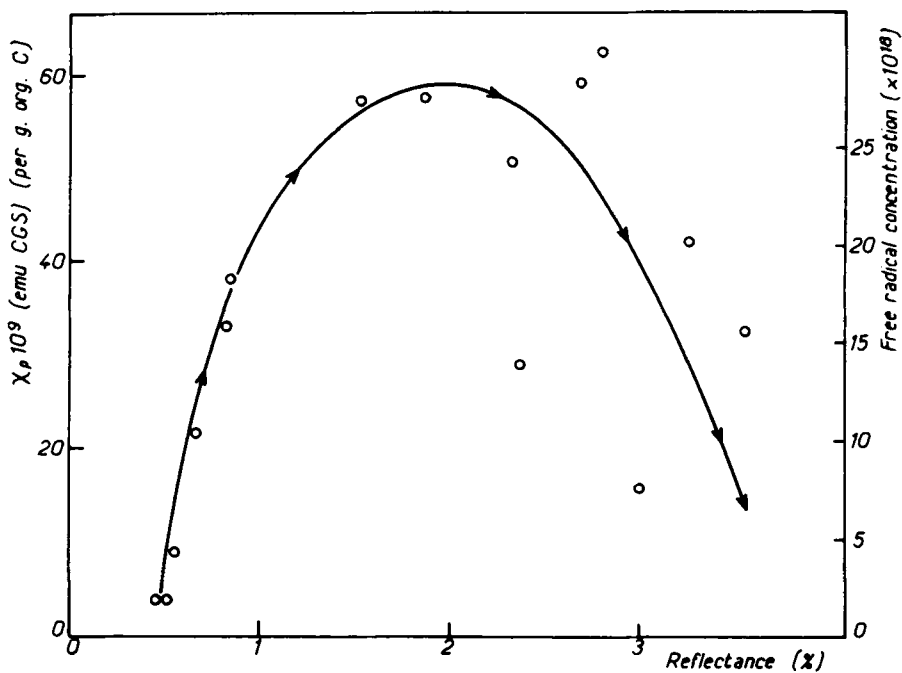


Fig. 9-25. Correlation between vitrinite reflectance and paramagnetic susceptibility  $X_p$  at room temperature (kerogen from the Douala Basin).

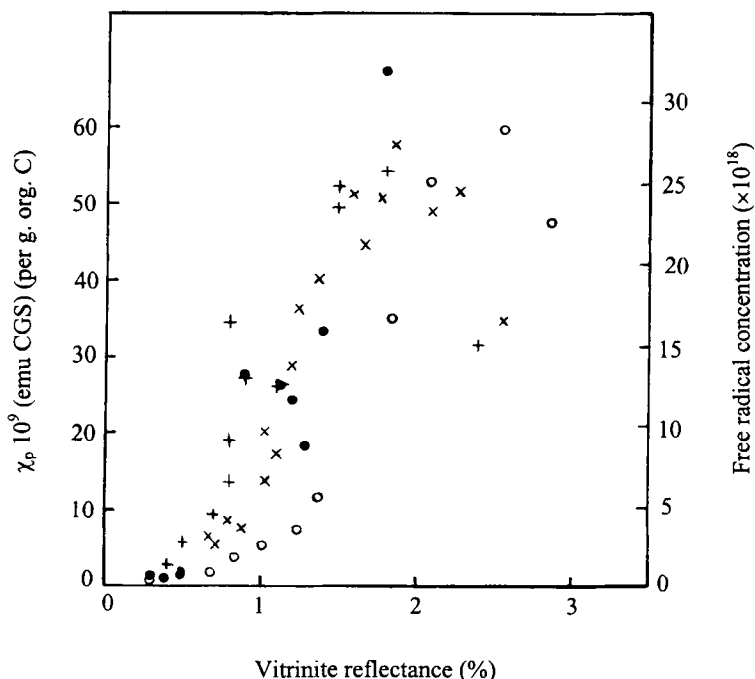


Fig. 9-26. Paramagnetic susceptibility at room temperature as a function of vitrinite reflectance. Natural kerogens of Series I (●), II (+) and artificial kerogens for Series I' (○) and II' (×) [108].

samples can be revealed if their ESR parameters are known. Using the established correlation values of maximum thermal history temperature of subterranean kerogen, the maximum thermal history gradient can be established from samples from various depths in a given location. Actually, Tissot and Welte [111] have proposed the kerogen degradation model to study the paleotemperature of the basin, which is based on free radicals of kerogen and the H/C ratio of organic matter in type III. Other geothermometers are vitrinite reflectance, apatite fission track analysis, fluid inclusion, etc. The ESR model can establish the direction of paleoheat flow in sedimentary basins [107].

One mechanism of the genesis of kerogen from biomass is via humus material. The ESR of humus material is outside the scope of the present review. However, the ESR pattern of naturally-occurring humic acid is very close to that of the Browning products [106].

#### HEAT TREATMENT AND ESR CHARACTERISTICS

The nature of unpaired electrons in bituminous substances is still not well understood despite a number of studies on free radical behavior under various external conditions, such as temperature, heating time, and heating rate [74,75]. The complexity of free radical chemistry during thermal treatment of carbonaceous materials is generally

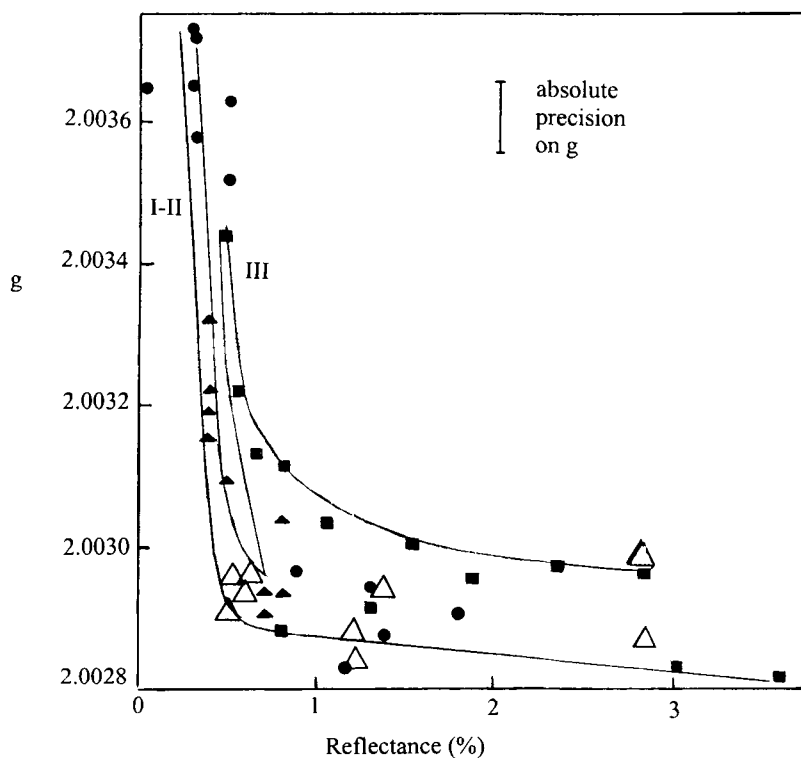


Fig. 9-27. Variation of the  $g$ -factor as a function of vitrinite reflectance: ● = Series I; ▲ = Series II (Paris Toarcian); △ = Series II (German Toarcian); ■ = Series III.

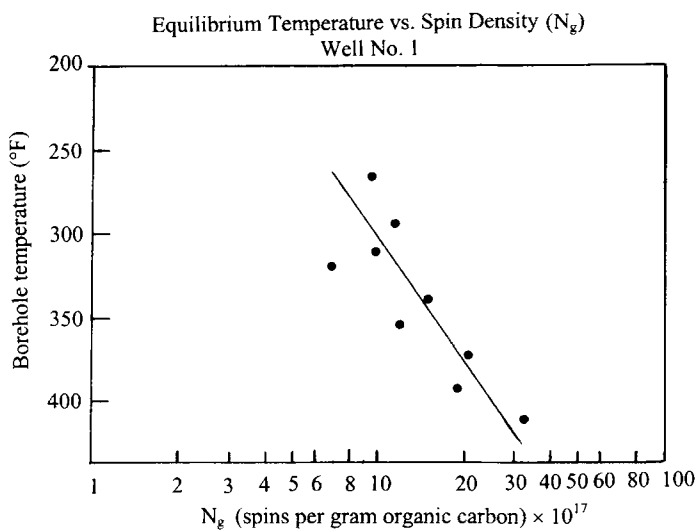


Fig. 9-28. Relationship between the borehole temperature and  $N_g$  in well No. 1 [18].

agreed upon. Reactivities of bitumens and coals are mainly governed by the forms and behavior of free radical structures evolved in the process environment. Spin–lattice and spin–spin interactions can play a key role in the stability of free radical species within the host structures. Coke formation resulting from polymerization reactions and poor hydrogen transfer is the primary cause for low conversion in thermal processing of bituminous substances.

### *Temperature effects on ESR absorption*

Spin excitation is a useful mean in identifying spin state multiplicity in bituminous substances [29,38,39,76]. Temperature dependence studies of free radicals reveal that a number of coals, as well as asphaltenes derived from petroleum, coal, and tar sand bitumen, allow for the distinction of the spin states of free radical species present [38,53,76]. When there are negligible interactions between unpaired electrons, these monoradicals (doublets) obey the Curie–Weiss law as follows:

$$I_d = x N_d \nu / 2kT \quad (9-15)$$

where  $I_d$  is the absorption intensity of doublet species,  $x$  is a constant,  $N_d$  is the number of monoradicals,  $\nu$  is the microwave quantum, and  $k$  is Boltzmann's constant. On the other hand, biradical species with significant spin–spin interactions can reside in both diamagnetic ground singlet states (spin antiparallel) and the thermally excited triplet states (spin parallel). Yen and Young [39] calculated the temperature dependence of ESR absorption intensity for these exchange spin couples as follows:

$$I_{st} = 2 \times N_{st} \nu / \{kT [\exp(J/kT) + 3]\} \quad (9-16)$$

where  $I_{st}$  is the absorption intensity of triplet species,  $J$  is the excitation energy for singlet to triplet transition, and  $N_{st}$  is the number of singlet–triplet transition. The ESR-temperature study has indicated that free radical resonance in coals is attributed to the doublets, which obey the Curie–Weiss law [53]. However, the spin behavior in asphaltenes derived from petroleum and tar sand is much more complex due to the existence of singlet–triplet species in addition to the monoradicals [29,38,76]. Charge transfer interactions in bitumen can be manifested by the singlet–triplet radicals, which are stabilized as delocalized  $\pi$ -electrons in the peri-condensed aromatic crystallites distributed randomly over the mesomorphic medium of the asphaltene fraction [38–40].

The charge transfer nature of bitumen has been investigated by examining the response of spin concentrations, linewidths, and  $g$ -values with variation in temperature. The temperature dependence of ESR parameters have been reported for a number of petroleum asphaltenes, Athabasca asphaltene, as well as the P.R. Spring tar sand bitumen and its corresponding asphaltene and petrolene fractions [29,38,76]. Unpaired electrons are present predominantly as monoradicals in the low-temperature range (10–40 K), while both doublets and singlet–triplet species exist together in thermal equilibrium at higher temperatures [29,38,76]. Thermal reversibility of spin concentration occurs after P.R. Spring Utah asphaltene has been subjected to a rapid heating and cooling cycle between 293 K and 575 K [76]. The ESR absorption line accompanied with spin increase at elevated temperature shows only a slight deviation from the Lorentzian lineshape.



Excitation and relaxation of biradical species in singlet–triplet transitions is the probable cause to the thermal reversibility of spin intensity in P.R. Spring Utah asphaltene. A small positive shift of the  $g$ -factor to higher values as temperature increases from 10 to 340 K further indicates the presence of paramagnetic effects at higher temperatures [76]. Exponential narrowing of linewidths with increasing temperature can be associated with spin delocalization and/or isotropic exchange interactions.

### *Pyrolysis of carbonaceous products*

A significant increase in spin concentration is observed during pyrolysis of Anhembi tar sand [73,77] as well as carbonization of petroleum residues as temperature is raised beyond 400°C [75]. The extent of spin increment is dependent on the inherent hydrogen donating capacities of the resids. The spin number is inversely proportional to the hydrogen donor ability of bitumen at 450°C [75]. Radical recombination reactions are dominant at the elevated temperatures [103]. Fine grain mosaics are formed in coking of petroleum residue with low hydrogen donating propensity [75]. The fine optical texture of coke products is probably the result of spin stabilization within the aromatic clusters of asphaltene followed by their agglomeration during radical recombination. The  $g$ -factor of P.R. Spring asphaltene shows a small shift toward a free electron value as the solid sample is heated to 500 K [76]. Free radical structures should be dominated by delocalized spins due to coking at elevated temperatures.

All mesophase, petroleum, and coal-tar pitch samples show a common pattern of spin increment along with linewidth narrowing above 650 K [78]. The thermally induced radicals are stabilized in the extensive aromatic systems in which the effect of exchange interactions is pronounced. The mesophase pitches having lower microwave saturation power (10 mW) as compared to other pitch samples indicate a slower spin–lattice relaxation with less effective or possibly negligible dipolar interactions. All this may explain the highly delocalized nature of free radicals in the graphite-like structure of mesophase pitches.

Free radical concentrations in coal pyrolysates are known to be a function of both pyrolysis temperature and heating rate. It has been reported that the maximum radical content decreases with an increase in the heating rate [74]. Such behavior reflects the complex nature of the underlying free radical reactions during pyrolysis. Transient free radical species are possibly present in significant concentrations during the early stages of pyrolysis [79]. Free radical content of the heat-treated Ireland Mine coal increases with time when temperature is maintained at 495°C. In a typical pyrolysis study, the radical concentrations of coals change moderately up to 400°C, with a sharp increase between 400°C and 500°C, and followed by a substantial drop upon further heating to 600°C (Figs. 9-29 to 9-31) [27]. Such temperature-dependent variation of the free radical content may be due to bond rupture starting around 400°C to 500°C, above which the increase in coal fluidity would promote recombination of the thermally induced radicals with other transient species. The end result is resolidification or polymerization of coal into char at higher temperatures.

A steady decrease in the  $g$ -value with increasing temperature in coal pyrolysis (Fig. 9-32) illustrates the change of radical structures toward those that are more hydrocarbon in nature [27]. A similar trend is also observed for the Lower Dekoven

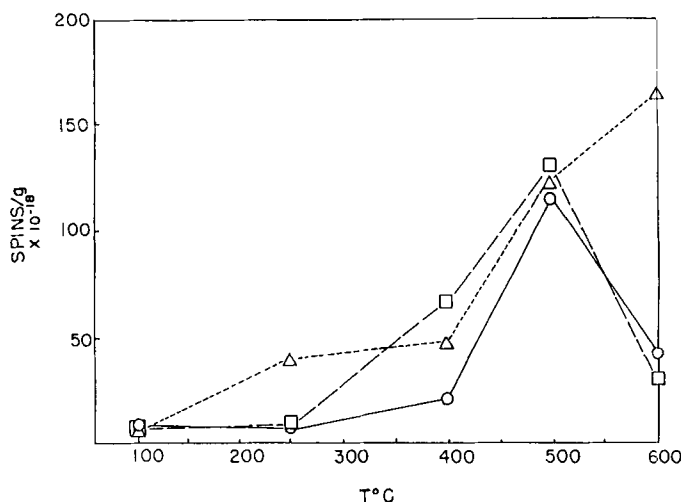


Fig. 9-29. Spin concentration versus temperature for Illinois coal #6 (modified after [27]).

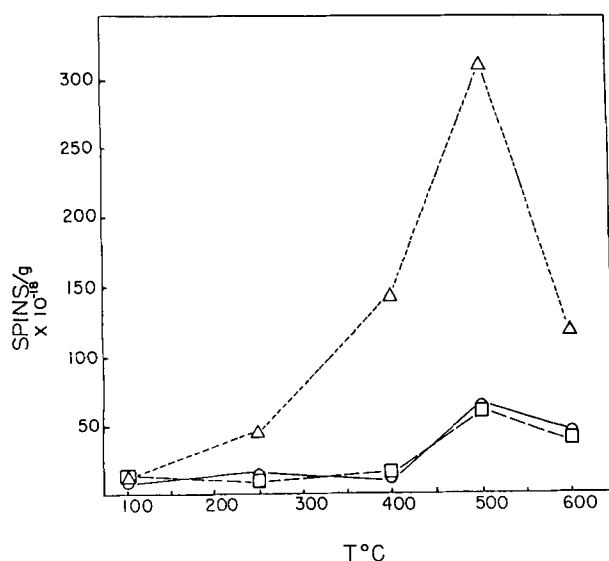


Fig. 9-30. Spin concentration versus temperature for Lower Dekoven coal (modified after [27]).

bituminous coal; the  $g$ -value decreases to an abnormal value of 2.0023 when the temperature is between 250°C and 500°C. This behavior is possibly due to molecular arrangement, some loss of oxygen as volatile material, or formation of  $\sigma$ -type radicals by bond cleavage or hydrogen abstraction. Upon heating of the Lower Dekoven coal to 600°C, recombination reactions cause a decline in free radical concentration with increase in  $g$ -value. Linear correlation of the  $g$ -value and the reciprocal of the absolute temperature were obtained for coal-derived residue [80].

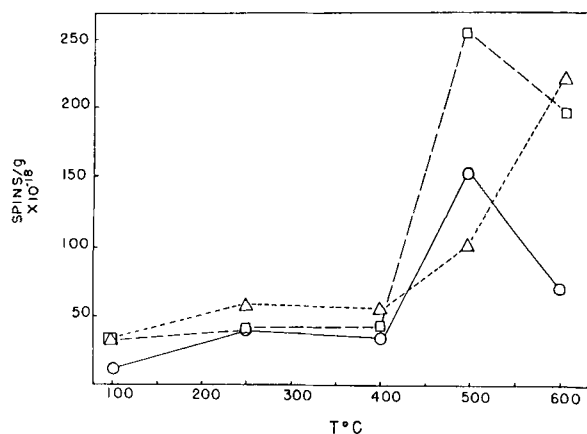


Fig. 9-31. Spin concentration versus temperature for Pochahontas #3 coal (modified after [27]).

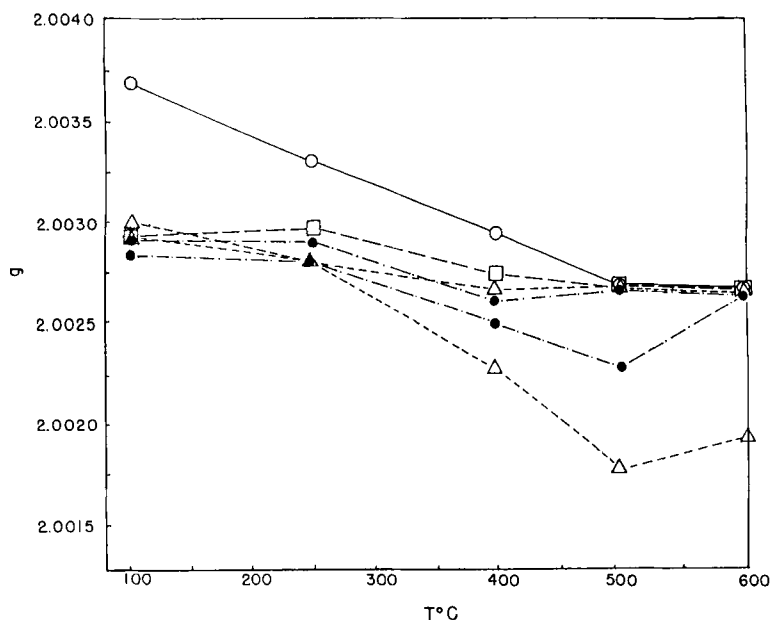


Fig. 9-32. Relationship between g-values and temperature (modified after [27]).

ESR characteristics of coal macerals during pyrolysis in nitrogen at temperatures of up to 550°C are shown in Figs. 9-33 and 9-34 [37,100]. The signals given by the vitrinite and exinite increase in both height and sharpness, whereas those given by the origins of the fusinites studied, involving exposure of woody tissue, only change very little, even at moderately high temperatures. The number of free radicals and linewidth at half height,  $H_{1/2}$ , in the temperature range of 200°C to 600°C have also been determined for several vitrains with different carbon content (Figs. 9-35 and 9-36) [81]. The variation

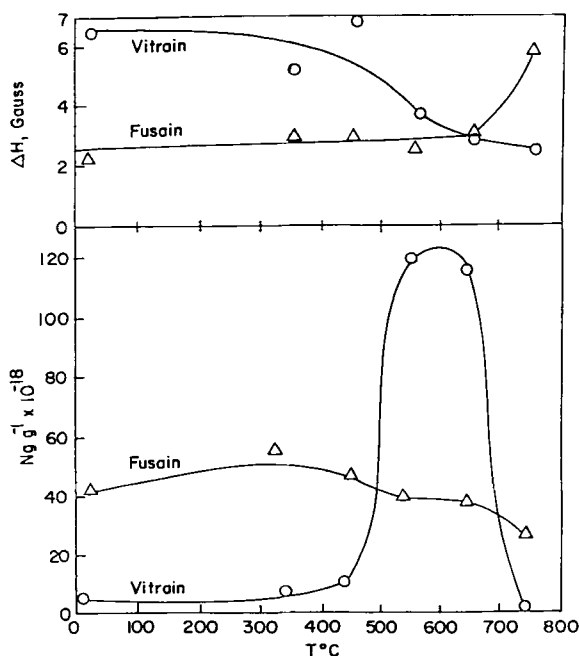


Fig. 9-33. Spin concentration and linewidth for redstone vitrain and fusain (modified after [100]).

of  $N_g$  and  $H_{1/2}$  remains constant up to about 400 $^{\circ}\text{C}$  followed by a steady decrease with a rise between 500 $^{\circ}\text{C}$  and 600 $^{\circ}\text{C}$ . The number of free radicals in non-softening vitrains hardly decreases with rising temperatures, whereas  $H_{1/2}$  increases continuously. The temperatures at which variations occur in the number of free radicals appear to be closely related to (a) the temperatures at which changes are observed in the value of  $H_{1/2}$ , and (b) characteristic temperatures of both swelling and degasification processes.

In a pyrolysis study of Rundle and Green River oil shales, the free radical densities are increased with both increasing thermal severity and increasing amount of organic matter converted [82]. A significant increase in radical intensity accompanied by a decrease in  $g$ -value is observed after prolonged pyrolysis or thermal treatment at higher severity. Thermally induced free radical generation and dealkylation due to decomposition of thermally liable heteroatom-bearing species could be important in thermal transformation of kerogen under pyrolysis conditions.

#### ESR OF REFINERY AND PROCESSED PRODUCTS

Table 9-5 lists the analytical results of various fractions obtained from Anhembi tar [73]. The asphaltene fraction contains the highest free radical concentration. Currently there are various investigations dealing with the elimination of free radical content of heavy fractions in petroleum and bitumen. A study was done by Khulbe et al. [20] to correlate the  $N_g$ -values of asphaltene in different solvents with increasing dipole

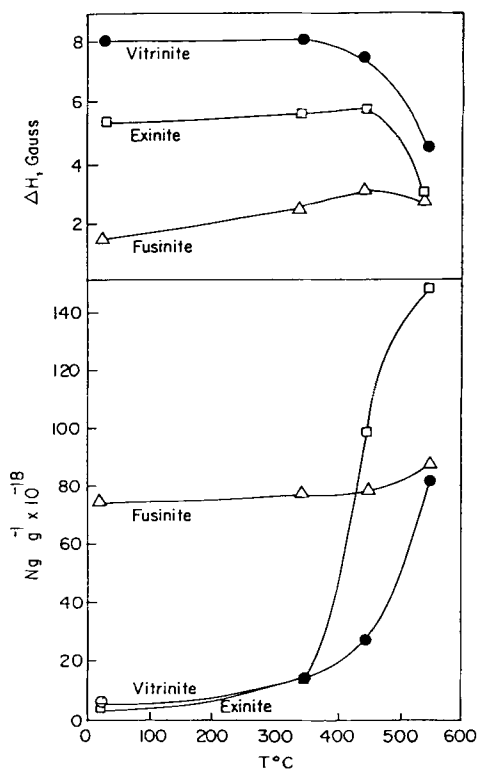


Fig. 9-34. Spin concentration and linewidth for macerals from Chislet, No. 5 coal (modified after [100]).

moment values. Often, the processing and refining of crude and coal were conducted in polar solvents in which the  $N_g$ -value decreased by 50%. Many upgrading methods are used to reduce or eliminate the stable free radicals of asphaltene and consequently to allow the active free radical to propagate cracking. For example, this includes the formation of metallocenes of asphaltene molecules by Lewis acid type catalysts before

TABLE 9-5

ESR data for carbonaceous product (modified after [73])

Sample	$g$ -value	Linewidth (gauss)	$N_g$ (spins/g)
Anhembi tar sand	2.0027	5.9	$1.8 \times 10^{18}$
Bitumen fraction <sup>a</sup>	2.0027	5.9	$1.3 \times 10^{18}$
Asphaltene <sup>b</sup>	2.0027	5.9	$8.9 \times 10^{18}$
Resin 1	2.0032	6.4	$1.2 \times 10^{18}$
Resin 2	2.0029	6.0	$2.5 \times 10^{18}$

<sup>a</sup> Derived from tar sand sample by chloroform extraction.

<sup>b</sup>  $n$ -pentane extraction residue from bitumens.

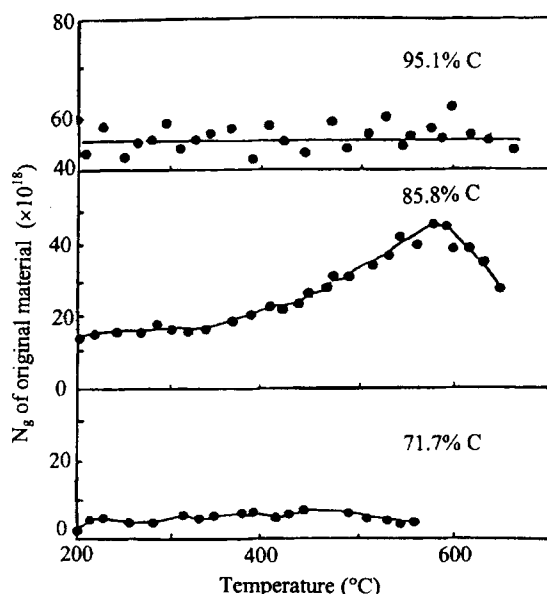


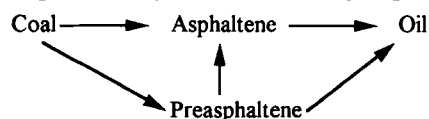
Fig. 9-35. Relationship between spin concentration of original materials and temperature for different percentages of carbon. Heating rate is 3°C per minute (modified after [81]).

oxidation by active oxygen atoms sets in. An example is blown asphalt for road paving application. The same principle has been applied to  $\text{ZnCl}_2$ -catalyzed hydrocracking of oil sand bitumen. Furthermore, a higher dipole moment medium consisting of mixed solvent (even tetralin) or additives will help. In heavy oils, a patent has been issued for using maleic anhydride ( $\mu = 3.94$  D in dioxane) in the presence of amines to prevent the flocculation of asphaltene [104].

#### *Analytical fractions from coal liquids*

Liquid products from coal liquefaction processes contain a variety of desirable and undesirable components. The desirable oil and resin fractions are composed of saturate and aromatic hydrocarbons as well as non-polar and polar non-hydrocarbons (sulfur, oxygen, nitrogen, and metal containing species). The polymerized coke-like carboids, the highly aromatic solid carbene, and asphaltenes are the undesirable materials present in coal liquids. These heavy and condensed aromatic substances containing high concentrations of heteroatoms and metal species cause many operational problems in downstream refining processes.

Under hydrogenolysis conditions, coal conversion to oil products has been suggested as progressing via the following sequence [34,83,84,109]:



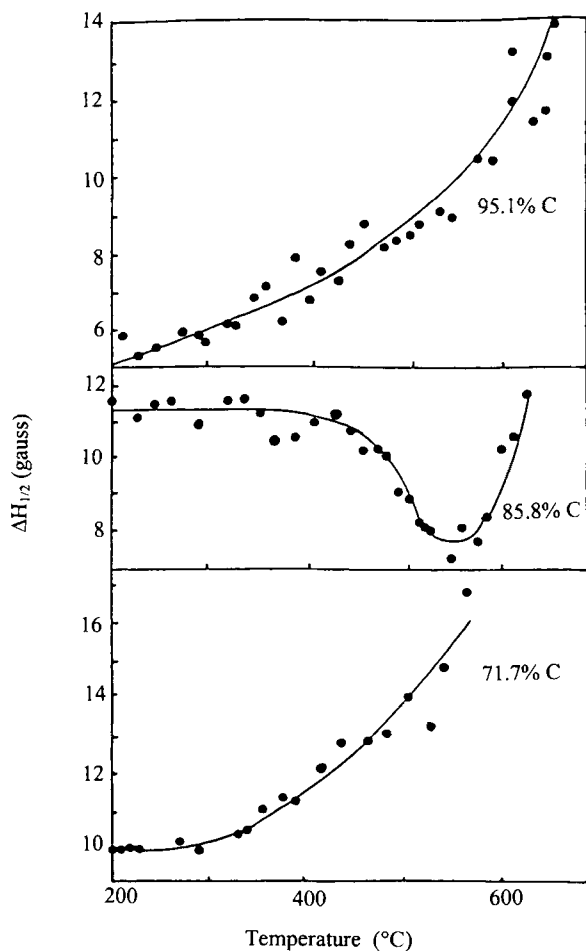


Fig. 9-36. Linewidth  $H_{1/2}$  versus temperature for different carbon percentages. Heating rate is  $3^{\circ}\text{C}$  per minute (modified after [81]).

The preasphaltenes, namely the carbene and carboid fractions, are the chemical species soluble in pyridine but insoluble in benzene. They are considered as the intermediates between coal and classical asphaltene in the liquefaction process.

Free radical reactions play a key role in liquefaction of coal. The nature of free radicals in both solid coal and its liquid products (pyridine extract, preasphaltenes, asphaltenes, and oil) have been examined by ESR (Table 9-6) [99]. The relative difference in free radical content among the samples is given as follows:

$$\text{coal} < \text{preasphaltenes} \gg \text{asphaltenes} > \text{oils}$$

Comparison of the  $g$ -values suggests the presence of hydrocarbon-like radicals with perhaps some partial localization at the heteroatoms in both asphaltene and oil fractions. The linewidths increase with increasing hydrogen content in the samples.

TABLE 9-6

MAF analyses, carbon aromaticities, and ESR data for coal and coal product <sup>a,b</sup>

MAF analysis (%)	Solid coal	Pyridine extract	Preasphaltene	Asphaltene	Oil
C	78.5	81.7	86.9	87.3	86.6
H	5.6	5.9	5.1	6.3	8.2
O	9.7	8.0	4.8	3.6	3.3
N	1.2	1.9	2.2	2.0	1.2
S	4.9	2.6	0.9	0.9	0.7
$f_a$	0.76 <sup>c</sup>	0.73 <sup>c</sup>	0.84 <sup>d</sup>	0.77 <sup>d</sup>	0.63 <sup>d</sup>
<i>ESR data</i>					
Spins/g	$1.4 \times 10^{19}$	$9.0 \times 10^{18}$	$2.0 \times 10^{19}$	$2.4 \times 10^{18}$	$9.4 \times 10^{17}$
<i>g</i> -value	2.0027	2.0031	2.0027	0.0032	2.0030
Linewidth (gauss)	5.9	5.7	6.6	7.3	8.7

<sup>a</sup> Materials produced from the liquefaction of West Virginia (Ireland Mine) hvAb coal in the Pittsburgh Energy Technology Center's 10 lb coal/h process development unit.<sup>b</sup> Modified after Retcofsky.<sup>c</sup>  $f_a$  determined by cross-polarization <sup>13</sup>C NMR.<sup>d</sup>  $f_a$  determined by high-resolution <sup>13</sup>C FT NMR.

Landé *g*-values, spin intensities, and linewidth of coal liquid solvent fractions and asphaltene-derived products are reported in Table 9-6 [89,110]. The *g*-values between 2.0028 and 2.0036 for all coal liquid-derived materials fall within the range reported previously for petroleum asphaltics, and these values are close to those observed for neutral radicals rather than radical ions or semiquinones. Spin intensities have been converted into unit concentration of free radical per molecule. The spin concentrations of both the synthoil carboid fraction and THF-eluted fraction from synthoil asphaltenes have the maximum values of about one free radical per 80 and 90 molecules, respectively. The synthoil oil fraction has the lowest value of about one free radical per 50,000 molecules. The spin intensity plotted against the color intensity of various samples (integrated intensity obtained by absorption spectrometry over the 400–750 nm range) is shown in Fig. 9-9. The spin intensity is directly related to an increase in color intensity. Inasmuch as absorption in the visible region is most likely due to the mobile electrons of the polyaromatic  $\pi$ -system, it appears that only those molecules having large delocalized aromatic  $\pi$ -systems possess free spins in solution.

The binding mechanism of asphaltene derived from coal liquid has been investigated by carrying out the ESR measurements on both synthoil asphaltene and its chromatographically separated components [85]. The weighted-average spin intensity of the benzene, diethyl ether and THF-eluted fractions is nearly identical with the free radical content of the total asphaltene before separation. This result suggests that charge transfer interactions among these synthoil asphaltene components, which could lead to spin increase via singlet excitation as observed in both petroleum and tar sand asphaltenes, may not be significant at room temperatures [37,38]. The ESR absorption curves of the synthoil asphaltene components all follow the Curie–Weiss law from



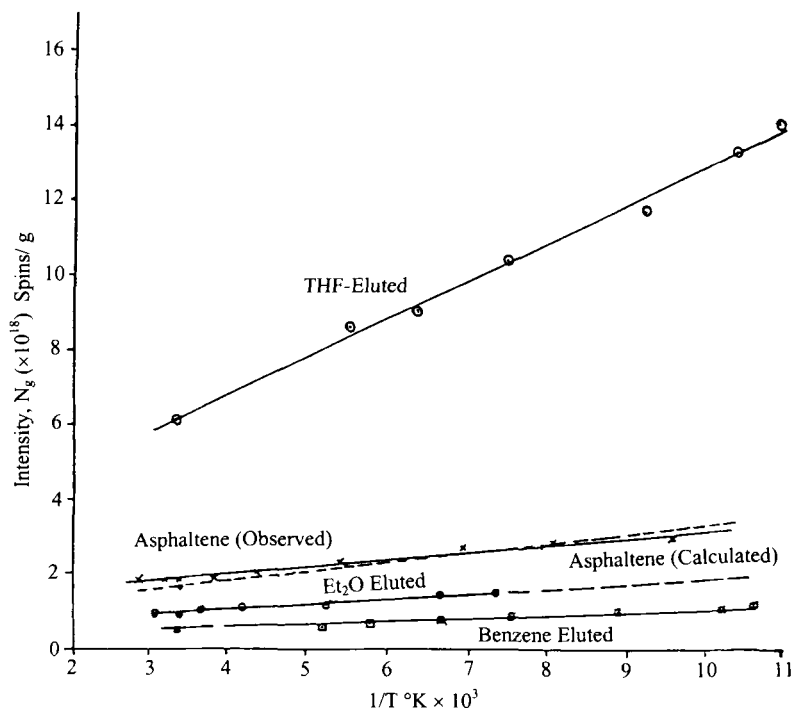


Fig. 9-37. Color index versus spin concentration for coal liquid solvent fraction (modified after [86]).

95 K to room temperature. The weighted-average temperature dependence of the three fractions reproduce the spin intensity–temperature functional relationship of the original synthoil asphaltene sample (Fig. 9-37) [89]. Similar results have been reported by other researchers [53]. Another ESR-temperature study has also been carried out at ambient to liquid nitrogen temperatures to examine the possible existence of charge transfer interactions [101]. The results for both synthoil asphaltene and its corresponding acid and base fractions are shown in Fig. 9-38. It appears that the slightly exponential dependence of temperature is probably due to the differences in processing and separation variables. In summary, the combined findings have suggested that charge transfer interactions may not be significant as binding forces between coal-derived asphaltene components; instead, they support the hydrogen-bonding model of coal asphaltene association.

The ESR spectrum of synthoil carboid fraction has been measured at high microwave power (40 mW) and modulation amplitude in order to determine whether the signals corresponding to paramagnetic metal-containing species are detectable [89]. The sample contains 9% ash with iron (400 ppm) and titanium (100 ppm) as the major transition metals present. In addition to the usual major asphaltic free radical signal at  $g = 2.00$ , the ESR spectrum (Fig. 9-39) also shows a small peak around  $g = 2.05$  and a dip around  $g = 2.08$ . A background signal is presented, which means that these signals cannot be attributed to cavity contamination. It is known that transition metals impart  $g$ -values higher than 2.00. A ferromagnetic resonance centered at  $g = 2.06 \pm 0.02$

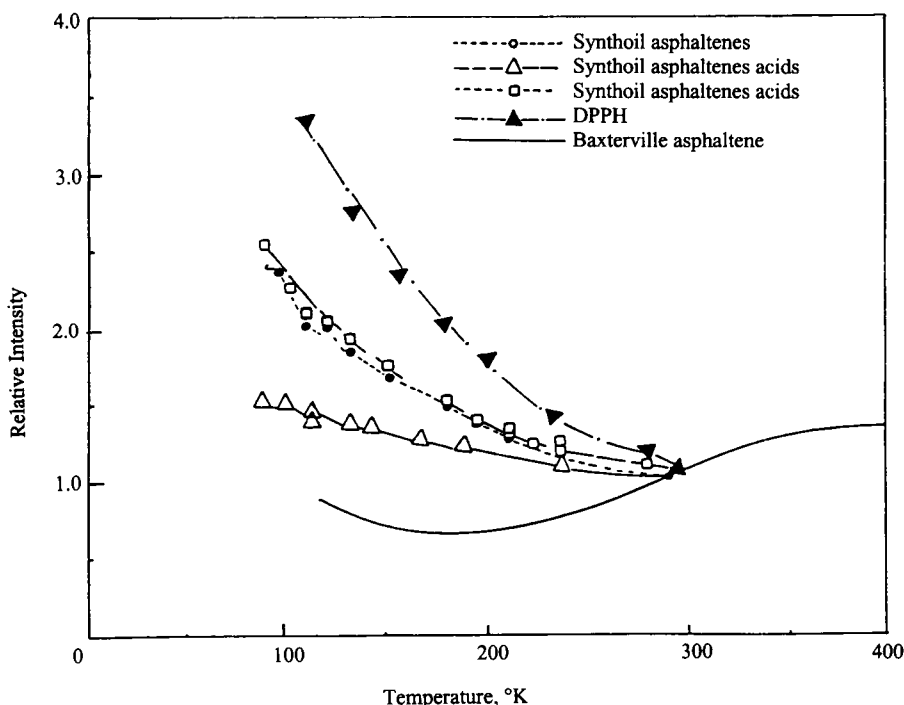


Fig. 9-38. ESR intensities as a function of temperature (after [101]).

for a colloidal suspension of pure metallic iron particles has been reported [90]. Also, low spin complexes of cobalt(II) and nickel(II) are identified with isotropic  $g$ -factors at about  $g = 2.08$ . Although the high  $g$ -value suggests the metal origin of the ESR signal, such an explanation must be considered tentative at this time. It is also interesting that the  $g = 2.00$  line shows no microwave saturation up to 60 mW at room temperature. Such fast spin relaxation can be caused by association with metal species. However, further studies will be needed to confirm this possibility (Table 9-7).

#### *Process products from coal liquefaction*

Results of ESR studies on several SRC materials are shown in Table 9-8 [91]. SRC filter cake solids have  $g$ -values typical of most aromatic hydrocarbon radicals of one to six rings. No influences due to heteroatoms are observed. Process solvent and filtrate have  $g$ -values which are at the high end of the radical center. SRC filter wash solvent has a  $g$ -value typical of many oxygen-containing radicals. All these  $g$ -values are much lower than those reported by Wooton et al. [92].

Radical concentration measurements imply that hydrogen transfer is indeed occurring. The empirical relation found between hydrogen content and linewidth for natural coals does not appear to be particularly good for the converted coal.

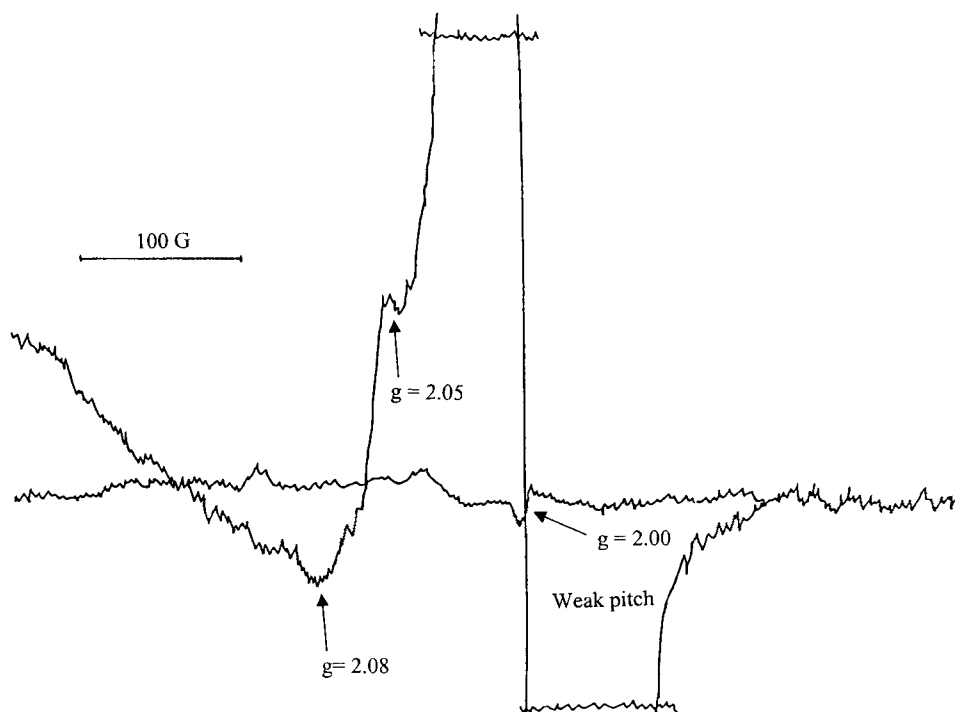


Fig. 9-39. ESR spectrum of synthoil carboid (after [89]).

## CONCLUSIONS

### *Uniqueness of the ESR approach*

ESR studies of bituminous substances can lead to useful information concerning their past thermal history and the geochemical environment during maturation. In addition, they can provide processing and engineering insights of certain bitumen or coal-based refining operations. Thus, the potential of this technique is unlimited.

ESR spectroscopy is a non-destructive technique which allows the tested samples to be further investigated by other analytical methods. ESR is highly flexible with a variety of sample matrices. Samples in the forms of single crystal, powder, glass matrix, solid mixture diluted with inert substance, solution, or colloidal suspension can all be analyzed in a typical ESR experiment.

ESR has another unique advantage in performing in-situ analyses during the course of chemical reactions. A good example is the study of coal carbonization reaction where pyrolysis is carried out in a heated cavity with temperature control. The high-temperature cavities capable of reaching carbonization temperatures have been constructed [93]. The writers have carried out elution chromatography with solvent in a quartz column using ESR as a control. The *intra muros* electrolysis built-in technique has been known for a long time and has certainly given a great amount of information

TABLE 9-7

Landé  $g$ -values, intensities and linewidth of coal liquid solvent fractions <sup>a</sup> and asphaltene-derived products

Sample	$g$ -value	Intensity, $N_g$ (spins/g)	Linewidth (gauss)	VPO (MW) <sup>b</sup>	Spin (molecules)
Synthoil asphaltene	2.0028	$4.0 \times 10^{18}$	5.6	560	300
HRI II-Coal asphaltene	2.0029	$3.0 \times 10^{18}$	5.2	502	400
FMC-COED asphaltene	2.0036	$0.4 \times 10^{18}$	5.1	350	5,000
PAMCO Inc. SRC asphaltene	2.0030	$1.7 \times 10^{18}$	5.8	480	800
Cat. Inc. SRC asphaltene	2.0030	$1.7 \times 10^{18}$	5.1	486	700
Synthoil oil	2.0034	$0.05 \times 10^{18}$	5.6	243 <sup>c</sup>	50,000
Synthoil resin	2.0032	$0.7 \times 10^{18}$	6.5	305 <sup>c</sup>	3,000
Synthoil carbene	2.0029	$6.0 \times 10^{18}$	5.2	—	—
Synthoil carboid	2.0029	$9.0 \times 10^{18}$	5.2	844 <sup>d</sup>	80
Synthoil benzene eluted	2.0029	$1.0 \times 10^{18}$	6.7	546	1,100
Synthoil ethanol-eluted	2.0030	$1.5 \times 10^{18}$	6.5	530	800
Synthoil THF-eluted	2.0030	$10 \times 10^{18}$	5.8	670 <sup>e</sup>	90
Synthoil from Sternberg-acid/neutral	2.0032	$0.4 \times 10^{18}$	6.2	466 <sup>f</sup>	3,000

<sup>a</sup> Measured in pyridine solution.<sup>b</sup> Extrapolated, infinite dilution average value in benzene and THF unless otherwise cited.<sup>c</sup> Average finite concentration value in benzene.<sup>d</sup> Average finite concentration in DMF, corrected for 8.8% ash.<sup>e</sup> Infinite dilution value in THF obtained by combining values for two THF-eluted fractions.<sup>f</sup> ESR run on neat liquid [87].

TABLE 9-8

ESR data of SRC

Sample	$g$ -value	Linewidth	$N_g$ (spins/g)
SRC filter-cake solids	2.0026	2.9	$1.8 \times 10^{18}$
Filtrate	2.0031	6.4	$0.7 \times 10^{18}$
Filter feed	2.0027	2.4	$3.5 \times 10^{18}$
Recycle or process solvent	2.0029	9.4	$0.2 \times 10^{18}$
Wash solvent	2.0037	6.8	$6 \times 10^{18}$
Wilsonville SRC solid product	2.0028	1.0	$15 \times 10^{18}$

to electrochemists. It is conceivable that ESR is a powerful tool for mechanistic studies of high-temperature coal hydrogenation, thermal decomposition, and solvent-refining of coals, as well as the catalytic effects on coal conversions.

### *Weakness of the ESR approach*

Currently, there is no other analytical technique capable of yielding information that is unique to ESR spectroscopy. This is an inherent weakness of ESR because of the difficulty of verifying results by an alternative method. Another drawback is the fact that

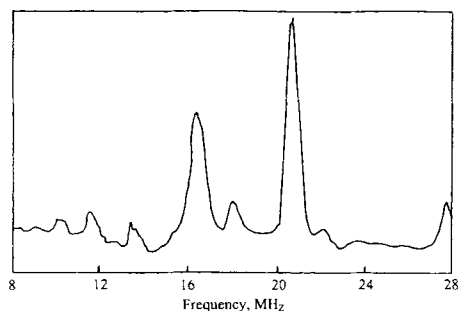


Fig. 9-40. ENDOR spectrum of vitrain-rich Pittsburgh coal (after [54]).

samples without unpaired spins cannot give any ESR signals. Therefore, spin labeling or irradiation is required in sample preparation. In addition, the concentration of reactive free radicals during coal pyrolysis is too low to be measured by ESR. Observed changes in spin concentration are due to relatively stable free radicals in the char [94].

#### *Future trends*

One of the current developing techniques is electron-nuclear double resonance (ENDOR) spectrometry. Because of its ability to resolve the hyperfine structures resulting from interactions between free radicals and their neighboring magnetic nuclear spins, ENDOR has found a number of applications in fossil fuel characterization. ENDOR has been used to investigate the dissociation behavior of asphaltene in various solvents by probing the hyperfine interactions between the unpaired electrons of the condensed aromatic clusters with the surrounding protons of solvent molecules [95,96]. By comparing the ENDOR spectra of asphaltene with those of model compounds, the porphyrin-like structure of vanadyl complexes in asphaltene has been further confirmed due to the resolved hyperfine couplings between paramagnetic vanadium and its nitrogen ligands [97]. The ENDOR study of raw coal (Pittsburgh No. 8) and the corresponding solvent-refined coal (Wilsonville, AL) has led to a conclusion that they both are similar with a single line of  $A_{\text{iso}} = 1.3$  MHz [98]. Furthermore, the ENDOR spectrum from study of a vitrain-rich Pittsburgh coal contains a number of resolvable fine structures originating from hyperfine interactions (Fig. 9-40) [54]. Actually, the hyperfine structure appears only when the system is completely free of oxygen. When using ESR, caution should be used in the sample preparation and storage, and especially in ascertaining the sources of supply. From the ENDOR spectrum the magnitude of interaction ( $< 10$  gauss) suggests that none of the radicals possess a high value of unpaired electron spin density at a particular carbon atom site.

## LIST OF SYMBOLS

$a_i$	isotropic hyperfine constant
$A_i$	hyperfine splitting constant
$\beta_e$ or $\beta$	Bohr magneton, magnitude of the magnetic moment of a free electron
$\beta_N$	nuclear magneton
$D$	spin-spin coupling tensor
$E$	energy of electron
$f_a$	aromaticity
$g$	spectroscopic splitting factor
$g_N$	nuclear $g$ -factor
$H$	proton
$\mathbf{H}$	magnetic field
$h$	Planck's constant
$\mathcal{H}$	spin-Hamiltonian
$H_K$	line position
$H_n$	width at the position $(1/n)$ of the peak-to-peak height of the first derivative curve
$H_{pp}$	peak-to-peak distance of the first derivative curve
$H_{1/2}$	linewidth at half height
$I$	nuclear spin
$D$	color index
$J$	coupling constant
$M_I$	quantum number of the component of nuclear spin in the direction of magnetic field
$M_s$	spin quantum number
$\mu$	magnetic moment
$n$	number of equivalent nuclei
$\nu$	frequency
$N$	Avogadro's number
$N_g$	spin concentration, spin per gram
$P_{CA}$	aromatic carbon atoms per spin
$\xi_k$	spin orbital coupling constant of the given heteroatom $k$
$Q$	McConnell constant
$r$	electron-nuclear separation
$\rho_i$	unpaired spin density at atom $i$
$R_n$	the ratio of $H_n$ to $H_{pp}$
$S$	electron spin
$\sigma$	screening tensor
$\mathbf{T}$	hyperfine tensor
$T$	temperature
$T_1$	spin-lattice relaxation time
$T_2$	spin-spin relaxation time
$\theta$	angle between the applied field and the line connecting the dipoles
$W_e$	exchange frequency

$W_p$	frequency of the perturbation
$X_p$	paramagnetic susceptibility per mass
$X_k$	atomic fraction of the given heteroatom $k$
$\Psi$	wave function

## ACKNOWLEDGEMENTS

Partial support by U.S. DOE ET-78-G-01-3379 is appreciated. Editing of this paper by Rochelle Wong and Amy Lin is greatly appreciated.

## REFERENCES

- [1] Graham, W.R.M., Analysis of metal species in petroleum and tar sands using the electron paramagnetic resonance and Fourier transform infrared techniques. In: R.H. Filby and J.F. Branthaver (Editors), *Metal Complexes in Fossil Fuels*, pp. 358–367 (1987).
- [2] Yen, T.F., *Electron Spin Resonance of Metal Complexes*. Plenum Pub. Corp., New York; also published by Adam Hilger Ltd., London, 204 pp. (1969).
- [3] Tynan, E.C. and Yen, T.F., Association of vanadium chelates in petroleum asphaltenes as studied by ESR. *Fuel*, 43: 191–208 (1969).
- [4] Tynan, E.C. and Yen, T.F., ESR Study of vanadium occurring in petroleum asphaltenes in solution. *ACS Div. Petroleum Chem., Preprints*, 12 (2): A89–A101 (1967).
- [5] Yen, T.F., Boucher, L.J., Dickie, J.P., Tynan, E.C. and Vaughan, G.B., Vanadium complexes and porphyrins in asphaltenes. *J. Inst. Pet.*, 55: 87–99 (1969).
- [6] Yen, T.F., Tynan, E.C., Vaughan, G.B. and Boucher, L.J., ESR studies of petroleum asphaltenes. In: R.A. Friedel (Editor), *Spectrometry of Fuels*. Plenum, New York, pp. 187–201 (1970).
- [7] Boucher, L.J., Tynan, E.C. and Yen, T.F., Spectra properties of oxovanadium(IV) Complexes, IV. Correlation of ESR spectra with ligand type. In: T.F. Yen (Editor), *Electron Spin Resonance of Metal Complexes*. Plenum, New York, pp. 111–130 (1969).
- [8] Yen, T.F. and Sprang, S., ESR  $g$ -values by bituminous materials. *ACS Div. Pet. Chem., Preprints*, 15 (3): A65–A76 (1970).
- [9] Beaseley, J.E., Anderson, P.L., Dickie, J.P., Dollish, F.R., Tynan, E.C. and Yen, T.F., ESRNMR signal enhancement with a small computer. *Spectrosc. Lett.*, 2 (5): 149–157 (1969).
- [10] Yen, T.F., Nitrogen superhyperfine splittings of vanadyl porphyrins in native asphaltenes. *Naturwissenschaften*, 233 (37): 36–37 (1971).
- [11] Tynan, E.C. and Yen, T.F., General purpose computer program for exact ESR spectrum calculations with applications to vanadium chelates. *J. Magn. Resonance*, 3: 327–335 (1970).
- [12] Bard, A.J., Electron spin resonance. In: F.J. Welcher (Editor), *Standard Methods of Chemical Analysis*. Van Nostrand, Princeton, NJ, 3: 616–635 (1966).
- [13] Beresohn, M. and Baird, J.C., *Electron Paramagnetic Resonance*. Benjamin, NJ (1966).
- [14] Wertz, J.E. and Bolton, J.R., *Electron Spin Resonance: Element Theory and Practical Applications*. McGraw-Hill, New York (1972).
- [15] Pilbrow J.R., *Transition Ion Electron Paramagnetic Resonance*. Clarendon Press, Oxford, pp. 1–61 (1990).
- [16] Atherton, N.M., *Principles of Electron Spin Resonance*. Ellis Horwood, pp. 5–128 (1993).
- [17] Sharkey, A.G., Jr. and McCartney, J.T., Physical properties of coal and its products. In: M. Elliott (Editor), *Chemistry of Coal Utilization, 2nd Supplementary Volume*. Wiley, New York, pp. 159–284 (1981).
- [18] Hwang, P.T.R. and Pussey, W.C., Process for Determining Hydrocarbon Maturity using Electron Spin Resonance. *U.S. Patent*, 3, 740, 641, June 19 (1973).

- [19] Burke, F.P., Winschel, R.A. and Brandes, S.D., *Coal Liquefaction Process Stream Characterization and Evaluation: Characterization of Coal Liquefaction Resids Employing Thermogravimetric Analysis and Electron Spin Resonance Spectroscopy, Topical Report*. DOE/PC 89883-57, October (1992).
- [20] Khulbe, K.C., Mann, R.S., Lu, B.C.Y., Lamarche, G. and Lamarche, A.M., *Fuel Process. Technol.*, 32: 133–141 (1992).
- [21] Axelsson, D.E., *Solid State Nuclear Magnetic Resonance of Fossil Fuels*. Multiscience Publishing, Ottawa, Ont. (1985).
- [22] Petrakis, L. and Allen, D.T., *NMR for Liquid Fossil Fuels*. Elsevier, Amsterdam (1987).
- [23] Ingram, D.J.E., *Free Radicals as Studied by Electron Spin Resonance*. Academic Press, New York (1958).
- [24] Petrakis, L. and Grandy, D.W., Electron spin resonance (ESR) characterization of coal and coal conversions. In: B.R. Cooper and L. Petrakis (Editors), *Chemistry and Physics of Coal Utilization — 1980*. American Institute of Physics, New York, pp. 101–120 (1981).
- [25] Silbernagel, B.G. and Gebhard, L.A., Electron spin resonance of isolated coal macerals: primary survey. In: R.E. Winans and J.C. Crelling (Editors), *Chemistry and Characterization of Coal Macerals*. American Chemical Society, Washington DC, pp. 121–136 (1984).
- [26] Korkmaz, M. and Ozbey, T., Electron spin resonance in some Turkish coals. *Fuel*, 70 (6): 789–793 (1991).
- [27] Petrakis, L. and Grandy, D.W., Electron spin resonance spectrometric study of free radicals in coals. *Anal. Chem.*, 50 (2): 303–308 (1978).
- [28] Schultz, K.F. and Selucky, M.L., ESR measurements on asphaltene and resin fractions from various separation methods. *Fuel*, 60 (10): 951–956 (1981).
- [29] Malhotra, V.M. and Graham, W.R.M., Characterization of P.R. Spring (Utah) tar sand bitumen by the EPR technique: free radicals. *Fuel*, 62 (11): 1255–1264 (1983).
- [30] Flett, M.S.C., *Physical Aids to the Organic Chemist*. Elsevier, Amsterdam (1962).
- [31] Retcofsky, H.L., Thompson, G.P., Raymond, R. and Friedel, R.A., Studies of ESR linewidths in coals and related materials. *Fuel*, 54 (2): 126–128 (1975).
- [32] Kwan, C.L. and Yen, T.F., Electron spin resonance study of coal by linewidth and lineshape analysis. *Anal. Chem.*, 51 (8): 1225–1229 (1979).
- [33] Yen, T.F. and Lee, W.C., Low temperature chemical fractionation of coal components: a novel liquefaction approach. *Proceedings, 14th Intersociety Energy Conversion Engineering Conference*, Boston, MA, pp. 832–836 (1979).
- [34] Yen, T.F., Chemistry of asphaltene in coal liquids. *Workshop on Coal Chemistry*, Stanford Research Institute, pp. 144–164 (1976).
- [35] Ingram, D.J.E., Tapley, J.G., Jackson, R., Bond, R.J. and Murnaghan, A.R., Paramagnetic resonance in carbonaceous solids. *Nature*, 174: 797–798 (1954).
- [36] Uebbersfeld, J., Etienne, A. and Combrisson, J., Paramagnetic resonance, a new property of coal-like materials. *Nature*, 174 (4430): 614 (1954).
- [37] Austen, D.E.G., Ingram, D.J.E., Given, P.H., Binder, C.R. and Hill, L.W., Electron spin resonance study of pure macerals. In: R.F. Gould (Editor), *Coal Science*. American Chemical Society, Washington DC, pp. 344–362 (1966).
- [38] Yen, T.F., Erdman, J.G. and Saraceno, A.J., Investigation of the nature of free radicals in petroleum asphaltenes and related substances by electron spin resonance. *Anal. Chem.*, 34 (6): 694–700 (1962).
- [39] Yen, T.F. and Young, D.K., Spin excitations of bitumens. *Carbon*, 11 (1): 33–41 (1973).
- [40] Yen, T.F., The charge transfer nature of bitumens. *Fuel*, 52: 93–98 (1973).
- [41] Petrakis, L., Grandy, D.W. and Jones, G.L., Free radical chemistry: key to coal liquefaction. *Chemtech*, 52–57 (1984).
- [42] Curran, G.P., Struck, R.T. and Gorin, E., Mechanism of hydrogen transfer to coal and coal extracts. *ACS, Div. Fuel Chem., Preprints*, 10 (2): C130–C148 (1966).
- [43] Curran, G.P., Struck, R.T. and Gorin, E., Mechanism of the hydrogen-transfer process to coal and coal extract. *Ind. Eng. Chem., Process Design Dev.*, 6 (2): 166–173 (1967).
- [44] Moirishima, M. and Matsubayashi, H., ESR diagrams: a method to distinguish vitrinite macerals. *Geochim. Cosmochim. Acta*, 42: 537–540 (1978).



- [45] Shibaoka, M. and Steven, J.R., Characterization of kerogen by electron spin resonance. *Fuel*, 56: 458–459 (1977).
- [46] Marchand, A. and Conard, J., Electron paramagnetic resonance in kerogen studies. In: Bernard Durand (Editor), *Kerogen: Insoluble Organic Matter from Sedimentary Rocks*. Technip, Paris, pp. 243–270 (1980).
- [47] Suzuki, N. and Taguchi, K., Characteristics and diagenesis of kerogens associated with clay fractions of mudstone. In: M. Bjoroy (Editor), *Advances in Organic Geochemistry 1981*. Wiley, New York, pp. 607–612 (1983).
- [48] Bakr, M., Akiyama, M., Sanada, Y. and Yokono, T., Radical concentration of kerogen as a maturation parameter. *Org. Geochem.*, 11 (1): 29–32 (1988).
- [49] Bakr, M.Y., Akiyama, M. and Sanada, Y., ESR assessment of kerogen maturation and its reaction with petroleum genesis. *Org. Geochem.*, 15 (6): 595–599 (1990).
- [50] Rouzaud, J.N., Guechchati, N., Kister, J. and Conard, J., Structural characterization of coalification: example of gironville borehole. *Bull. Soc. Geol. Fr.*, 162 (2): 201–209 (1991).
- [51] McConnell, H.M. and Chestnut, D.B., Theory of isotropic hyperfine interactions in  $\pi$ -electron radicals. *J. Chem. Phys.*, 28 (1): 107–117 (1958).
- [52] Retcofsky, H.L., Stark, J.M. and Friedel, R.A., Electron spin resonance in American coals. *Anal. Chem.*, 40: 1699–1704 (1968).
- [53] Duber, S. and Wieckowski, A.B., E.P.R. study of molecular phases in coal. *Fuel*, 61 (5): 433–436 (1982).
- [54] Retcofsky, H.L., Thompson, G.P., Hough, M. and Friedel, R.A., Electron spin resonance studies of coals and coal-derived asphaltenes. *ACS, Div. Fuel Chem., Preprints*, 22 (5): 90–93 (1977).
- [55] Schopf, J.M., Variable coalification: the processes involved in coal formation. *Econ. Geol. Bull. Soc. Econ. Geol.*, 43: 207–225 (1948).
- [56] Anderson, P.W. and Weiss, P.R., Exchange narrowing in paramagnetic resonance. *Rev. Mod. Phys.*, 25 (1): 269–276 (1953).
- [57] Malhotra, V.M. and Buckmaster, H.A., 9 and 34 GHz EPR study of the free radicals in various asphaltenes: statistical correlation of the g-value with heteroatom content. *Org. Geochem.*, 8 (4): 235–239 (1985).
- [58] Yen, T.F. and Sprang, S.R., Contribution of ESR analysis toward diagenetic mechanisms in bituminous deposits. *Geochim. Cosmochim. Acta*, 41: 1007–1018 (1977).
- [59] Berkowitz, N. and Schein, H.G., Some aspects of the ultrafine structure of lignites. *Fuel*, 31: 19–32 (1952).
- [60] Kreulen, D.J.W., Sulphur coal of Istria. *Fuel*, 31: 462–467 (1952).
- [61] Toyoda, S., Sugawara, S. and Honda, H., Chemical structure and properties of heated coal in the early state of carbonization v. electron spin resonance of coal. *J. Fuel Soc. Jpn.*, 45: 191–208 (1966).
- [62] Ohuchi, H., Shiotani, M. and Sohma, J., ESR studies of Virgin coals. *Fuel*, 48: 187–190 (1969).
- [63] Silbernagel, B.G., Flowers, R.A., II and Larsen, J.W., Demineralization effects on the EPR properties of Argonne premium coals. *Energy Fuels*, 5 (4): 561–568 (1991).
- [64] Zilm, K.W., Pugmire, R.J., Grant, D.M., Larter, S.R. and Allen, J., Carbon-13 CP/MAS spectroscopy of coal macerals. *Fuel*, 60 (8): 717–722 (1981).
- [65] Maciel, G.E., Bartuska, V.J. and Miknis, F.P., Characterization of organic material in coal by proton-decoupled  $^{13}\text{C}$  nuclear magnetic resonance with magic-angle spinning. *Fuel*, 58 (5): 391–394 (1979).
- [66] Khulbe, K.C., Chan, B.W., Manoogian, A. and Patmore, D.J., ESR of Alberta tar sand bitumen and thermally hydrocracked products. *Fuel*, 65 (11): 1594–1599 (1986).
- [67] Rudnick, L.R. and Audeh, C.A., Thermal chemistry of Utah tar sand: an electron spin resonance (ESR) characterization. *Ind. Eng. Chem. Res.*, 27 (8): 1366–1369 (1988).
- [68] Wind, R.A., Duijvestijn, M.J., Van der Lugt, C., Smidt, J. and Vriend, H., An investigation of coal by means of ESR, proton NMR, carbon-13 NMR and dynamic nuclear polarization. *Fuel*, 66 (7): 876–885 (1987).
- [69] Jurkiewicz, A., Wind, R.A. and Maciel, G.E., The use of magnetic resonance parameters in the characterization of premium coals and other coals of various rank. *Fuel*, 69 (7): 830–833 (1990).

- [70] Garten, V.A. and Weiss, D.E., The quinone–hydroquinone character of activated carbon and carbon black. *Aust. J. Chem.*, 8: 68–95 (1955).
- [71] Coulson, C.S., Electronic structure of the boundary atoms of a graphite layer. *Proc. 4th Conf. Carbon*, Buffalo, New York, pp. 215–219 (1961).
- [72] Yokokawa, C., A further electron spin resonance study of solvent action on coal — solvent action at higher temperatures. *Fuel*, 48: 29–40 (1969).
- [73] De Sousa, J.J.F., Vugman, N.V. and Costa, N.C., ESR of Anhembi tar sand (Brazil): investigation of organic fractions. *Bull. Magn. Resonance*, 9 (3): 96 (1987).
- [74] Yokono, T., Murakami, K. and Sanada, Y., The effect of heating rate on radical concentration during coal pyrolysis. *Fuel Process. Technol.*, 17 (1): 7–11 (1987).
- [75] Yokono, T., Obara, T. and Sanada, Y., Characterization of carbonization reaction of petroleum residues by means of high-temperature ESR and transferable hydrogen. *Carbon*, 24 (1): 29–32 (1986).
- [76] Niizuma, S., Steele, C.T., Gunning, H.E. and Strausz, O.P., Electron spin resonance study of free radicals in Athabasca asphaltene. *Fuel*, 56 (2): 249–256 (1977).
- [77] De Sousa, J.J.F., Vugman, N.V. and Mangrich, A.S., *Bull. Magn. Resonance* (1983).
- [78] Kaneko, T., Henao, L.E., Yokono, T. and Sanada, Y., Characterization of mesophase pitch by high-temperature electron spin resonance. *J. Mat. Sci. Lett.*, 9 (3): 351–352 (1990).
- [79] Sprecher, R.F. and Retcofsky, H.L., Observation of transient free radicals during coal pyrolysis. *Fuel*, 63 (4): 473–475 (1983).
- [80] Castellano, S.M., Chisholm, W.P., Sprecher, R.F. and Retcofsky, H.L., Temperature dependence of the electron spin resonance spectra of a coal-derived vacuum distillation residue and components. *Anal. Chem.*, 59 (13): 1726–1731 (1987).
- [81] Smidt, J. and Van Krevelen, D.W., Chemical structure and properties of coal — XXIII electron-spin resonance of vitrains. *Fuel*, 38: 355–368 (1959).
- [82] Silbernagel, B.G., Gebhard, L.A., Siskin, M. and Brons, G., ESR studies of kerogen conversion in shale pyrolysis. *ACS, Div. Pet. Chem., Preprints*, 32 (1): 157–160 (1987).
- [83] Weller, S., Pelipetz, M.G. and Friedman, S., Kinetics of coal hydrogenation: conversion of asphalt. *Ind. Eng. Chem.*, 43 (7): 1572–1575 (1951).
- [84] Shalabi, M.A., Baldwin, R.M., Bain, R.L., Gary, J.H. and Golden, J.O., Noncatalytical coal liquefaction in a donor solvent — rate of formation of oil, asphaltenes, and preasphaltenes. *Ind. Eng. Chem., Process Design Dev.*, 18 (3): 474–479 (1979).
- [85] Schwager, I., Lee, W.C. and Yen, T.F., Molecular weight and association of coal-derived asphaltenes. *Anal. Chem.*, 49 (14): 2363–2365 (1977).
- [86] Retcofsky, H.L. and Hough, M.R., Electron spin resonance study of coal and coal liquefaction. *Abstract, 29th Pittsburgh Conference* (1978).
- [87] Sternberg, H.W., Raymond, R. and Schweighardt, F.K., Acid-base structure of coal derived asphaltenes. *Science*, 188: 49–51 (1975).
- [88] Yen, T.F., Terrestrial and extraterrestrial stable organic molecules. In: R.F. Landel and A. Rembaum (Editors), *Chemistry in Space Research*. Elsevier, Amsterdam, pp. 105–153 (1972).
- [89] Yen, T.F., Chemistry and structure of coal-derived asphaltenes phase III. *Quarterly Progress Report*, April–June, FE-2031-12 (1978).
- [90] Baggaley, D.M.S., *Proc. R. Soc. London*, A 228: 559 (1955).
- [91] Grandy, D.W. and Petrakis, L., ESR investigation of free radicals in solvent-refined-coal materials. *Fuel*, 58 (3): 239–240 (1979).
- [92] Wooton, D.L., Dorn, H.C., Taylor, L.T. and Coleman, W.M., Inferences regarding the nature of solvent-refined coal (SRC). *Fuel*, 55 (3): 224–226 (1976).
- [93] Lewis, I.C. and Singer, L.S., Electron spin resonance and the mechanism of carbonization. In: P.L. Walker, Jr. and P.A. Thrower (Editors), *Chemistry and Physics of Carbon*. Marcel Dekker, New York, 17: 1–88 (1981).
- [94] Fowler, T.G., Bartle, K.D., Kandiyoti, R. and Snape, C.E., Pyrolysis of coals as a function of rank as studied by in situ electron spin resonance spectroscopy. *Carbon*, 27 (2): 197–208 (1989).
- [95] Schlick, S., Narayana, P.A. and Kevan, L., Matrix electron nuclear double resonance studies of the proton environment of the radical in natural and solvent-refined coal. *J. Am. Chem. Soc.*, 100 (11):

- 3322–3326 (1978).
- [96] Galtsev, V.E., Arnetov, I.M. and Grinberg, O.Y., Asphaltene association in crude oil as studied by ENDOR. *Fuel*, 74 (5): 670–673 (1995).
- [97] Atherton, N.M., Fairhurst, S.A. and Hewson, G.J., ENDOR spectra of vanadyl complexes in asphaltenes. *Magn. Resonance Chem.*, 25 (9): 829–830 (1987).
- [98] Kevan, L. and Kispett, L.K., *Electron Spin Double Resonance Spectroscopy*. Wiley, New York (1976).
- [99] Retcofsky, H.L., Hough, M.R. and Clarkson, R.B., Nature of the free radicals in coals, pyrolyzed coals, and liquefaction products. *ACS, Div. Fuel Chem., Preprints*, 24 (1): 83–89 (1979).
- [100] Binder, C.R., *Electron Spin Resonances: Its Application to the Study of Thermal and Natural Histories of Organic Sediments*. Ph.D. Thesis, Pennsylvania State University (1965).
- [101] Schwager, I., Kwan, J.T. and Yen, T.F., Charge transfer complexes of coal-derived asphaltenes. *ACS, Div. Fuel Chem., Preprints*, 23 (1): 284–289 (1978).
- [102] Yen, T.F., Erdman, J.G. and Saraceno, A.J., Die Erforschung der Natur von Freien Radicalen in Erdolasphaltenen und verwandten Verbindungen unt Itiefe der Elektronespin-Resonanz. *Bitumen, Teere, Asphalt, Peche*, 15: 141–142 (1964).
- [103] Horsfield, B., Pyrolysis studies and petroleum exploration. In: J. Brooks and D. Welte (Editors), *Advances in Petroleum Geochemistry*. Academic Press, London, Vol. 1, pp. 247–298 (1984).
- [104] Durand, J.P. and Nicholas D., Fr. *Demande FR2*, 633,935 (cl. C10L1/22) Jan. 12 (1990).
- [105] Whelan, J.K. and Thompson-Rizer C.L., Chemical methods for assessing kerogen and prokerogen types and maturity. In: M.H. Engel and S.A. Macko (Editors), *Organic Chemistry, Principles and Applications*. Plenum Press, New York (1993).
- [106] Yen, T.F. and Tang, J.I.S., Chemical aspects of marine sediments. In: T.F. Yen (Editor) *Chemistry of Marine Sediments*. Ann Arbor Science, Ann Arbor, MI, pp. 1–38 (1977).
- [107] Qiu, Nansheng, Pers. commun. University of Petroleum, Beijing (1997).
- [108] Durand, B., Marchand, A., Amiell, J. and Combaz, A. In: R. Compos and J. Gonied (Editors), *Advances in Organic Geochemistry, 1975*. Enandimsa, Madrid, pp. 753 (1977).
- [109] Lee, W.C., *Interconversion of Coal-Derived Products*. Ph.D. Thesis, University of Southern California (1980).
- [110] Schwager, I. and Yen, T.F., Chromatographic separation and characterization of coal derived asphaltenes. *Fuel*, 58: 219 (1979).
- [111] Tissot, B.P. and Welte, D.H., *Petroleum Formation and Occurrence*. Springer, New York (1978).
- [112] Blois, M.S., Brown, H.W. and Marling, J.E., *Symposium on Free Radicals in Biological Systems*. Academic Press, New York (1961).

## *Chapter 10*

# **CHEMICAL COMPOSITION AND CHARACTERISTICS OF RESIDUES OF CHINESE CRUDE OILS**

WENJIE LIANG, GUOHE QUE, YUEZHU CHEN and CHENGUANG LIU

## **INTRODUCTION**

Most of the Chinese crude oils are quite heavy, with a content of vacuum residues up to about 40–50%. The heavy crudes recently produced have vacuum residue contents as high as 60% or more. In China, because of the deficiency of petroleum, it is undesirable to burn the residue directly. A considerable market of asphalt does exist, but it accounts for only a small portion of the residue. Thus, great attention should be paid to the upgrading of residue for meeting the increasing demand of light fuels. Inasmuch as the properties and composition of various residues are quite different, it is necessary to have a thorough understanding of them.

The residue of a crude oil is the fraction that has the highest boiling point, the highest molecular weight, the highest contents of heteroatoms, and the most complex structure. In the last several decades, many authors have been working fruitfully in this area [1–8]. In this chapter, the characterization of the vacuum residues from the Chinese crude oils is reported.

For the separation of the residues, adsorption chromatography, ion-exchange chromatography, gel permeation chromatography, and solvent treatment are generally used [9–12]. The authors have used the adsorption chromatography with alumina as the main separation technique [13].

Since the publication of the methods of Brown and Ladner [1] and Williams [6], average structural parameters based on nuclear magnetic resonance (NMR) spectra have been widely used for the quantitative characterization of average residue structure. The authors have obtained a series of structural parameters of the residues and their fractions of the Chinese crude oils by the modified Brown–Ladner method with NMR spectra, elemental composition, and average molecular weight [2].

## **EXPERIMENTAL RESULTS**

### *Samples*

The vacuum residues of twelve crude oils were used. Among them, Daqing, Renqiu, and Zhongyuan crude oils are paraffinic, Shengli, Linpan, and Dagang crude oils are intermediate, Gudao, Gaosheng, Xinjiang (Region No. 9), and Jinglou crude oils are naphthenic–intermediate, and those of Shanjiasi and Huanxiling are naphthenic. Properties of these crude oils are presented in Table 10-1.

TABLE 10-1

Properties of Chinese crude oils

Name of crude	Gravity SG ( $d_4^{20}$ )	°API	S (wt%)	N (wt%)	Ni (ppm)	V (ppm)	Wax (wt%)	Fraction (wt%)			
								<200°C	200–350°C	350–500°C	>500°C
Daqing	0.8554	33.1	0.10	0.16	3.1	0.04	26.2	11.5	19.7	26.0	42.8
Renqiu	0.8792	28.7	0.31	0.38	15.0	0.73	22.8	7.3	21.1	32.4	39.2
Zhongyuan	0.8466	34.8	0.52	0.17	3.3	2.4	19.7	19.4	25.1	23.2	32.3
Shengli	0.8829	28.0	0.73	0.44	30.0	1.8	15.8	7.6	27.0	23.0	42.4
Linpan	0.9004	25.7	0.34	0.12	—	0.1	12.2	12.0	20.5	25.0	42.5
Dagang	0.8697	30.4	0.13	0.24	7.0	0.1	11.6	14.5	24.0	28.8	32.7
Gudao	0.9495	17.0	2.09	0.43	21.1	2.0	4.9	6.1	14.9	27.2	51.8
Gaosheng	0.9472	17.3	0.56	1.06	122.5	3.1	5.8	5.6	10.6	19.7	64.1
Xingjiang <sup>a</sup>	0.9273	20.5	0.15	0.35	15.4	0.7	7.4	1.7	18.3	28.7	51.3
Jinglou	0.9531	16.4	0.32	0.74	22.2	3.3	9.6	0.3	9.1	33.2	57.4
Shanjiasi	0.9731	13.8	0.82	0.72	51.3	2.5	1.9	1.7	11.5	21.2	65.6
Huanxiling	0.9434	17.9	0.26	0.41	38.4	0.5	2.3	3.7	20.6	35.4	40.3

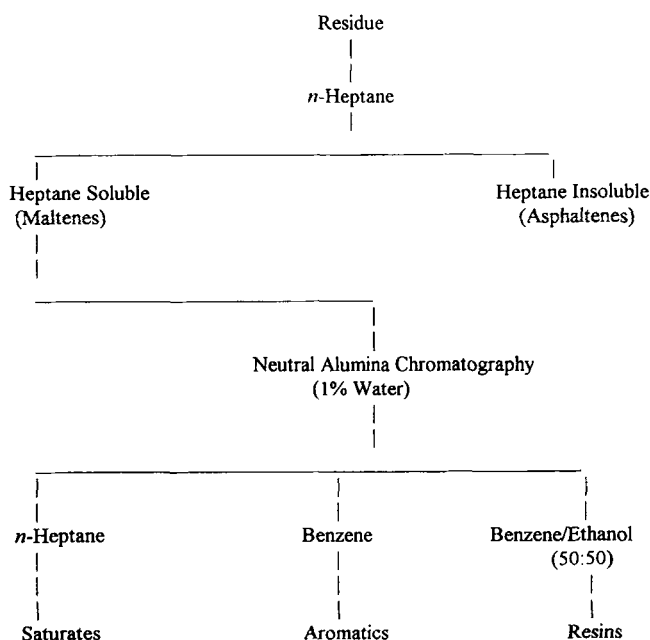
<sup>a</sup> Xingjiang, Region No. 9.

Fig. 10-1. Separation scheme for residues.

### Separation methods

**SARA method.** The asphaltenes were precipitated by *n*-heptane. The maltenes obtained were chromatographed on the alumina with 1% water. The saturated, aromatic,

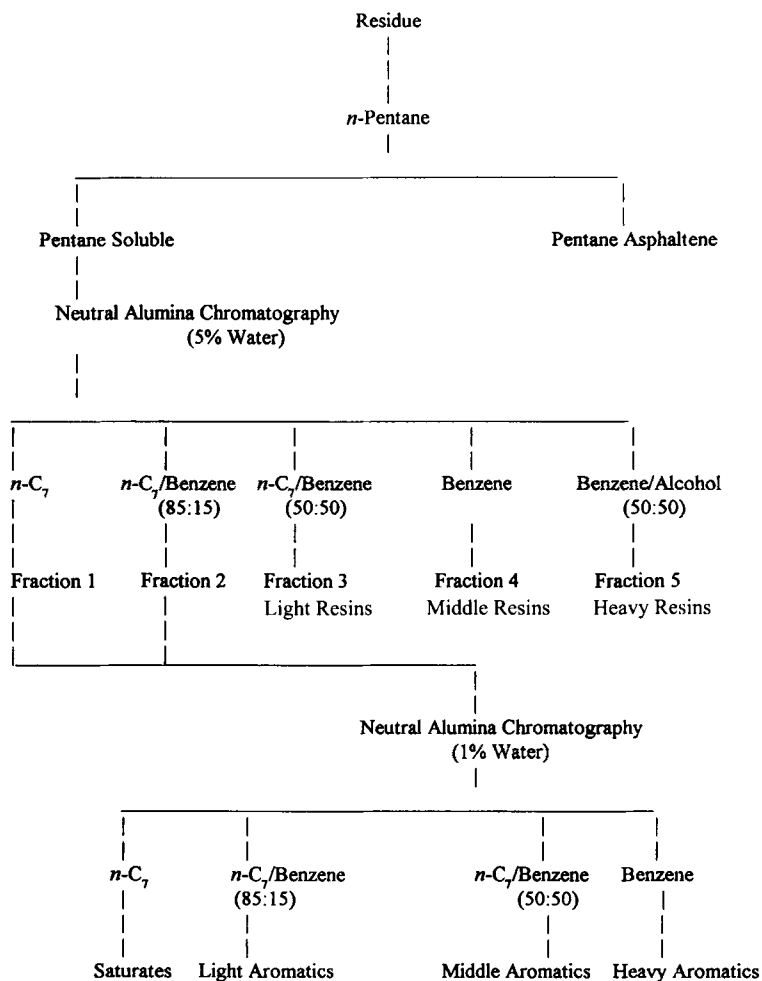


Fig. 10-2. Separation scheme of residues, aromatics and resins.

and resin fractions were eluted by *n*-heptane, benzene, and a mixture of benzene and ethanol (50/50, v/v), respectively. The separation scheme is shown in Fig. 10-1.

**Separation of aromatics.** The aromatic fractions obtained by the SARA method were further fractionated into so-called light, middle, and heavy aromatic subfractions, which roughly correspond to the mono-, di-, and polyaromatics, by gradient elution with mixed solvents, i.e., *n*-heptane/benzene (95/5, v/v), *n*-heptane/benzene (85/15, v/v), and benzene, respectively, on the alumina column with 1% water.

**Separation of resins.** The resin fractions were separated into three subfractions, i.e., light, middle, and heavy resins, by the chromatography on the alumina column with 5% water [13]. The separation scheme is shown in Fig. 10-2.

TABLE 10-2

Assignments of proton bands in the NMR spectra chemical shift

Symbol	Range (ppm, from TMS)	Assignment
$H_A$	6.0–9.0	Aromatic hydrogens
$H_\alpha$	2.0–4.0	Hydrogens in saturated groups $\alpha$ to aromatic rings
$H_\beta$	1.0–2.0	Hydrogens of methylene and methine groups $\beta$ or further to aromatic rings, and hydrogens in $\beta$ -methyl groups
$H_\gamma$	0.5–1.0	Hydrogens in methyl groups $\gamma$ or further removed from aromatic rings

*Separation of waxes.* The dewaxing of the samples was carried out with a mixture of 2-butanone and toluene (50/50, v/v) at  $-20^\circ\text{C}$ . The ratio of solvent to sample was 30 : 1 (ml/g).

*Gel permeation chromatography (GPC).* The aromatics and resins were separated into fractions according to their molecular size using a GPC column with silylated silica as packing. The eluent used was benzene with 10% methanol.

*Supercritical fluid extraction.* The Shengli residue was fractionated by supercritical fluid extraction with pentane as a solvent at constant temperature with pressure programming.

#### *Elemental analyses*

The determination of C, H, and N was carried out with a Carlo Erba microanalyzer. The nickel and vanadium contents were measured by an atomic absorption spectrometer after sample digestion.

#### *Average molecular weight*

The molecular weights were determined by a Knauer vapor phase osmometer in benzene at  $45^\circ\text{C}$ .

#### *Nuclear magnetic resonance spectroscopy*

The  $^1\text{H}$ -NMR spectra were run in  $\text{CCl}_4$  solvent with TMS as an internal standard using an RMN-250 spectrometer. The spectra were divided into four bands as described in Table 10-2, and the area under each band was determined by integration. The  $^{13}\text{C}$ -NMR spectra were obtained on a WP-80 spectrometer using inverse-gated decoupling to suppress NOE. The distortionless enhancement by polarization transfer (DEPT) pulse sequence has been applied for the measurement of  $\text{CH}_n$  group abundances in residue and its fractions.

#### *Infrared spectroscopy*

For IR, the samples were applied as films from  $\text{CHCl}_3$  solution. The spectra were compared by making the relative intensity measurements of the  $1460$  and  $1380\text{ cm}^{-1}$  bands.

*X-ray diffraction*

Powder X-ray diffraction of asphaltenes was performed on a diffractometer, equipped with a divergent 1°-slit and a receiving 0.3-mm slit. The scanning rate was 2°/s, and scanning width  $2\Theta = 5\text{--}105^\circ$ .

## METHOD OF CALCULATION OF STRUCTURAL PARAMETERS

To simplify the calculation, it was assumed that the hydrogen to carbon atom ratio of the saturated part of the average molecule of the samples equals 2 ( $x = y = 2$ ), and the aliphatic quaternary carbons are absent in the chemical structure. As shown in Table 10-3 [14], the first assumption has been confirmed by the DEPT  $^{13}\text{C}$ -NMR technique. The DEPT subspectra also show that the content of aliphatic quaternary carbon in residue is negligible. Besides, the heteroatoms have not been considered in calculation. The definitions of the symbols used in the calculations are listed in Table 10-4.

*Structural parameters by the modified Brown–Ladner method*

Based on  $^1\text{H}$ -NMR spectra ( $H_A/H_T$ ,  $H_\alpha/H_T$ ,  $H_\beta/H_T$ ,  $H_\gamma/H_T$ ), %C, %H, and average molecular weight, the average structural parameters of the residues and their fractions were calculated by the following equations:

$$f_A = \frac{C/H - (H_\alpha + H_\beta + H_\gamma)/2H_T}{C/H} \quad (10-1)$$

$$\sigma = \frac{H_\alpha/2H_T}{H_A/H_T + H_\alpha/2H_T} \quad (10-2)$$

TABLE 10-3

H/C atom ratio of the structured part ( $H_S/C_S$ ) of vacuum residues and their fractions

Name of residue	Fraction	$H_S/C_S$ by DEPT	$H_S/C_S$ by $^{13}\text{C}$ and $^1\text{H}$ -NMR
Daqing	Residue	1.97	2.03
	Aromatic	1.97	2.14
	Resin	1.94	2.03
Shengli	Residue	1.99	2.02
	Aromatic	2.01	2.04
	Resin	1.94	2.05
Gudao	Residue	2.00	1.96
	Aromatic	1.95	1.98
	Resin	1.98	2.07
Huanxiling	Residue	1.99	1.99
	Aromatic	1.97	1.99
	Resin	1.97	2.01



TABLE 10-4

Designation of symbols <sup>a</sup>

Symbol	Designation
$C_T$	Total number of carbon atoms in molecule
$H_T$	Total number of hydrogen atoms in molecule
$C_A$	Number of aromatic carbons in molecule
$C_N$	Number of naphthenic carbons in molecule
$C_P$	Number of paraffinic carbons in molecule
$C_S$	Number of saturated carbons in molecule
$C_\alpha$	Number of carbons $\alpha$ to aromatic rings
$M$	Average molecular weight
$n$	Number of unit structures in molecule
USW	Unit structure weight
$f_A$	Fraction of aromatic carbon
$f_N$	Fraction of naphthenic carbon
$f_P$	Fraction of paraffinic carbon
$R_T$	Total number of rings in molecule
$R_A$	Number of aromatic rings in molecule
$R_N$	Number of naphthenic rings in molecule
$H_{AU}/C_A$	Hydrogen to carbon atom ratio of the hypothetical unsubstituted aromatic system
$\sigma$	Degree of substitution of the aromatic ring
$L$	Average length of side chain ( $C_P/nCH_3$ )

<sup>a</sup> When symbols have an asterisk they represent the parameters for the unit structure in an average molecule.

$$\frac{H_{AU}}{C_A} = \frac{H_A/H_T + H_\alpha/2H_T}{C/H - (H_\alpha + H_\beta + H_\gamma)/2H_T} \quad (10-3)$$

$$C_A = C_T f_A \quad (10-4)$$

$$R_A = (C_A - 2)/4 \quad (\text{for catacondensed aromatic system}) \quad (10-5a)$$

$$R_A = (C_A - 4)/3 \quad (\text{for pericondensed aromatic system}) \quad (10-5b)$$

$$R_T = C_T + 1 - H_T/2 - C_A/2 \quad (10-6)$$

$$R_N = R_T - R_A \quad (10-7)$$

$$C_N = 4R_N \quad (\text{for catacondensed 6-membered ring system}) \quad (10-8a)$$

$$C_N = 3R_N \quad (\text{for pericondensed 6-membered ring system}) \quad (10-8b)$$

$$C_S = C_T - C_A \quad (10-9)$$

$$C_P = C_S - C_N \quad (10-10)$$

$$f_N = C_N/C_T \quad (10-11)$$

$$f_P = C_P/C_T \quad (10-12)$$

The aromaticity  $f_A$  can also be obtained from the H/C atom ratio using the empirical equation, obtained by the authors, without important deviation [15]:

$$f_A = 1.132 - 0.560(H/C) \quad (10-13)$$

In view of their high  $H_{AU}/C_A$  and the low molecular weight, it can be considered that there exists only one catacondensed aromatic nucleus in molecules of aromatic fractions. The molecules of the resins and the asphaltenes with large average molecular weights are assumed to be composed of more than one substituted pericondensed nucleus, i.e., there are several unit structures in each average molecule of these two heavier fractions. The number of the aromatic carbon atoms in each unit structure ( $C_A^*$ ) of the resin or the asphaltene molecule was calculated from  $H_{AU}/C_A$  by the following equation, derived by the authors, for the most compact pericondensed aromatic systems:

$$\frac{H_{AU}}{C_A} = \frac{2.503}{\sqrt{C_A^*}} \quad (10-14)$$

Then, the number of the unit structures per molecule ( $n$ ) and the unit structure weight (USW) can be obtained by the equations:

$$n = C_A/C_A^* \quad (10-15)$$

$$USW = M/n \quad (10-16)$$

In this chapter, all the structural parameters of the resin and the asphaltene fractions are given by unit structure, not by average molecule, and all the parameters of the unit structure are denoted by symbols with an asterisk.

#### *Average side chain length (L) based on IR*

With the normal paraffinic model compounds, it was found that there is a linear relationship between the relative intensities of the 1460 and 1380  $\text{cm}^{-1}$  bands ( $A_{1460}/A_{1380}$ ) and the ratio of methylene to methyl group ( $n\text{CH}_2/n\text{CH}_3$ ) in the molecule. The relationship is as follows:

$$n\text{CH}_2/n\text{CH}_3 = 2.93A_{1460}/A_{1380} - 3.70 \quad (10-17)$$

Assuming  $x = y = 2$ , the number of methyl groups in a molecule can be obtained by the equation:

$$n\text{CH}_3 = C_S/(n\text{CH}_2/n\text{CH}_3 + 2) \quad (10-18)$$

Besides, the number of the methylene and the methyl groups in an average molecule of samples have also been determined by  $^{13}\text{C}$ -NMR spectroscopy using the DEPT technique. As shown in Table 10-5 [3], it is interesting that the results obtained using these two different methods are very similar.

In this chapter, the number of side chains of the average molecule is considered to be equal to  $n\text{CH}_3$ , and the average chain length ( $L$ ) is defined as  $C_P/n\text{CH}_3$ . It appears that the parameter  $C_P/n\text{CH}_3$  would be more representative than the parameter  $C_S/C_\alpha$ , which is commonly used for the designation of the average chain length.

TABLE 10-5

*n*CH<sub>2</sub> and *n*CH<sub>3</sub> obtained by different methods

Name of residue	Fraction	DEPT method		IR method	
		<i>n</i> CH <sub>2</sub>	<i>n</i> CH <sub>3</sub>	<i>n</i> CH <sub>2</sub>	<i>n</i> CH <sub>3</sub>
Daqing	Residue	49.4	6.5	49.6	7.4
	Aromatic	55.4	7.8	57.7	7.9
	Resin	30.6	4.7	29.6	5.7
Shengli	Residue	37.6	8.0	37.0	8.4
	Aromatic	34.6	7.2	33.5	7.8
	Resin	24.1	5.6	25.0	6.1
Gudao	Residue	41.3	8.6	38.6	9.9
	Aromatic	30.0	6.0	30.2	7.2
	Resin	21.6	4.7	21.3	5.2
Huanxiling	Residue	25.8	6.8	22.1	8.2
	Aromatic	19.8	5.5	19.8	6.2
	Resin	25.2	8.4	28.5	7.3

For resins, the parameters in each unit structure are listed.

TABLE 10-6

Elemental composition and properties of vacuum residues

Name of residue	C (wt%)	H (wt%)	S (wt%)	N (wt%)	H/C atom ratio	Ni (ppm)	V (ppm)	<i>M</i> (VPO)	Carbon residue (wt%)	Average molecular formula
Daqing	87.0	12.7	0.14	0.53	1.74	8.5	0.1	1120	11.9	C <sub>81</sub> H <sub>141</sub> S <sub>0.05</sub> N <sub>0.42</sub>
Renqiu	86.2	11.6	0.76	1.08	1.60	59.0	1.2	1140	18.6	C <sub>88</sub> H <sub>144</sub> S <sub>0.27</sub> N <sub>0.88</sub>
Zhongyuan	85.6	11.6	1.18	0.60	1.61	15.0	5.7	1100	19.6	C <sub>78</sub> H <sub>127</sub> S <sub>0.40</sub> N <sub>0.47</sub>
Shengli	84.4	11.6	1.95	0.92	1.63	47.8	4.0	1080	15.4	C <sub>76</sub> H <sub>124</sub> S <sub>0.66</sub> N <sub>0.71</sub>
Linpan	87.2	11.8	0.60	0.80	1.61	36.0	—	1000	16.7	C <sub>73</sub> H <sub>117</sub> S <sub>0.19</sub> N <sub>0.57</sub>
Dagang	86.3	11.8	0.29	0.57	1.63	25.8	0.5	870	9.2	C <sub>63</sub> H <sub>102</sub> S <sub>0.08</sub> N <sub>0.35</sub>
Gudao	86.5	10.8	2.86	1.18	1.49	35.2	4.4	1030	19.2	C <sub>74</sub> H <sub>116</sub> S <sub>0.92</sub> N <sub>0.87</sub>
Gaosheng	85.8	11.4	0.77	1.19	1.58	144.8	5.0	1020	17.4	C <sub>73</sub> H <sub>115</sub> S <sub>0.24</sub> N <sub>0.87</sub>
Xingjiang <sup>a</sup>	86.9	11.7	0.45	0.79	1.61	34.3	1.3	1340	—	C <sub>97</sub> H <sub>156</sub> S <sub>0.19</sub> N <sub>0.76</sub>
Jinglou	86.5	11.6	0.65	1.18	1.60	42.3	5.1	1170	16.2	C <sub>84</sub> H <sub>135</sub> S <sub>0.24</sub> N <sub>0.99</sub>
Shanjiasi	86.0	10.8	0.87	1.42	1.50	67.7	—	960	—	C <sub>69</sub> H <sub>103</sub> S <sub>0.26</sub> N <sub>0.97</sub>
Huanxiling	86.3	10.7	0.57	0.88	1.48	120.7	4.1	1030	—	C <sub>74</sub> H <sub>106</sub> S <sub>0.18</sub> N <sub>0.65</sub>

<sup>a</sup> Xingjiang Region No. 9.

## RESULTS AND DISCUSSION

### *Elemental composition of residues*

According to Table 10-6, the carbon contents of the residues studied are in the range of 85% to 87%, and the hydrogen contents in the range of 11% to 13%. Their H/C

atom ratios are moderate, mostly in the range of 1.5 to 1.7. Most of the residues are not refractory enough to be upgraded.

Unlike the crudes in many other countries, the sulfur content of the residues of most Chinese crudes is not high, usually being below 2%, whereas their nitrogen content is relatively high, about 1%. In reference to the number of atoms in the average molecule, the number of nitrogen atoms is more than that of sulfur in most cases, and there exists about one atom of nitrogen per molecule of residue. Since most of the nitrogen is in heterocyclic structures with an aromatic character, it is more stable and more difficult to remove than sulfur during upgrading.

The contents of nickel and vanadium in Chinese residues are moderate, and without exception the nickel content is much higher than the vanadium content. Usually, the nickel content is several tens of ppm, whereas the vanadium content is only several ppm. The Ni/V ratios are higher than 10 in most cases, which is one of the peculiarities of the Chinese residues.

The average molecular weight determined by the VPO method is about 1000 for all the residues, containing 70–90 carbon atoms per molecule.

As shown by geochemists, such as Tissot and Welte [16] and Hunt [17], the metal contents in the low-sulfur crude oils are generally low, and their nickel content exceeds that of vanadium. It was also discovered that there is a good constant correlation between the sulfur content and the vanadium content. This is also true for Chinese crudes. Moreover, the low sulfur content, low metal content, and very high Ni/V ratio for most of the Chinese residues indicate that they are derived from continental organic matter.

### *SARA composition*

In Table 10-7, it is clear that the contents of saturates of residues differ widely, from 15.7% to 40.8%, but the aromatics content remains about 30% for all residues studied. It should be emphasized that for most of the Chinese residues the resin content is very high, up to 50%, and there is a low content of heptane asphaltene, usually below 1%.

The wax contents of vacuum residues, which are presented in Table 10-7, were obtained by dewaxing the saturated and aromatic fractions separately. It is shown that the contents of wax are quite different: 30.7% for Daqing and only 5.4% for Huanxiling residues. The ratios of the wax content in the saturated fraction to the wax content in the aromatic fraction are also different. As for Daqing residue, 70% of wax is present in the saturated fraction, whereas the waxes are equally distributed in the two fractions of Gudao and Huanxiling residues.

The data presented in Table 10-8 show that the contents of light, middle, and heavy aromatic subfractions range from 17.8% to 26.9%, 17.5% to 23.6%, and 53.5% to 64.7%, respectively, i.e., more than one half of the aromatics in residues are polynuclear. There are more light aromatics in the Daqing residue, while there are more heavy aromatics in the Gudao and Renqiu residues.

Inasmuch as the resins content constitutes about half of the residues, it is necessary to separate them into subfractions for further characterization. The data in Table 10-9 show the difference in the composition of the resins. In Daqing residue, there is more light resin (42.0%) and less heavy resin (34.9%), whereas there is less light resin (24.3%)

TABLE 10-7

SARA composition and wax content of vacuum residues

Name of residue	Saturate (wt%)	Aromatic (wt%)	Resin (wt%)	Heptane asphaltene (wt%)	Pentane asphaltene (wt%)	Wax content (wt%)		
						in saturate	in aromatic	total
Daqing	40.8	32.2	26.9	<0.1	0.4	21.5	9.2	30.7
Renqiu	19.5	29.2	51.1	0.2	10.1	—	—	—
Zhongyuan	23.6	31.6	44.6	0.2	15.5	—	—	—
Shengli	19.5	32.4	47.9	0.2	13.7	—	—	—
Linpan	21.2	31.7	44.0	3.1	13.8	—	—	—
Dagang	30.6	31.6	37.5	0.3	—	—	—	—
Gudao	15.7	33.0	48.5	2.8	11.3	4.2	4.1	8.3
Gaosheng	22.6	26.4	50.8	0.2	11.0	2.4	4.4	6.8
Xingjiang <sup>a</sup>	28.2	26.9	44.8	<0.1	8.5	4.4	2.7	7.1
Jinglou	14.3	34.3	51.3	0.1	5.4	2.6	10.0	12.6
Shanjiasi	17.1	27.0	53.5	2.4	17.0	0.9	2.1	3.0
Huanxiling	28.7	35.0	33.6	2.7	12.6	2.6	2.8	5.4

<sup>a</sup> Xingjiang Region No. 9.

and more heavy resin (60.8%) in Zhongyuan residue. Undoubtedly, the composition of resins will influence the processing of residues.

These separation data can be divided into eight fractions of residue (i.e., saturates; light, middle, and heavy aromatics; light, middle, and heavy resins; and asphaltene) (Table 10-10).

It is known that most of the Chinese crude oils have high wax contents (see Table 10-1), and their resin contents are high as well. Several geochemists have reviewed the probable environment of origin of some 500 high-wax crude oils worldwide and have shown their occurrence to be genetically related to continental or near-shore depositional facies. The high wax content is an inheritance from land-derived organic matter as lipids of terrestrial higher plants and of microbial organisms.

Tissot and Welte [16] and Hunt [17] have shown that there is a strong positive correlation between the sulfur content and resin-asphaltene content for more than 300

TABLE 10-8

Subfractions of aromatics of vacuum residues

Name of residue	Light aromatics (wt%)	Middle aromatics (wt%)	Heavy aromatics (wt%)
Daqing	26.9	19.5	53.6
Renqiu	18.4	17.8	63.8
Zhongyuan	22.9	23.6	53.5
Shengli	23.7	21.1	55.2
Linpan	20.1	16.6	63.3
Gudao	17.8	17.5	64.7
Huanxiling	23.2	18.3	58.5

TABLE 10-9

Subfractions of resins of vacuum residues

Name of residue	Light resins (wt%)	Middle resins (wt%)	Heavy resins (wt%)
Daqing	42.0	23.1	34.9
Renqiu	27.9	17.6	54.5
Zhongyuan	24.3	14.9	60.8
Shengli	30.0	16.3	53.7
Linpan	37.4	18.2	44.4
Gudao	34.5	17.7	47.8
Gaosheng	26.7	18.4	54.9
Xingjiang <sup>a</sup>	33.6	16.0	50.4
Jinglou	34.4	19.6	46.0
Shanjiasi	31.6	17.8	50.6
Huanxiling	38.9	20.9	40.2

<sup>a</sup> Xingjiang Region No. 9.

TABLE 10-10

Eight-fraction composition of vacuum residues

Name of residue	Saturates (wt%)	Light aromatics (wt%)	Middle aromatics (wt%)	Heavy aromatics (wt%)	Light resins (wt%)	Middle resins (wt%)	Heavy resins <sup>a</sup> (wt%)	Pentane asphaltenes (wt%)
Daqing	40.8	8.9	6.5	17.4	11.1	6.1	8.8	0.4
Renqiu	19.5	5.4	5.3	18.9	14.1	8.9	17.7	10.1
Zhongyuan	23.6	6.1	6.0	14.3	12.1	7.4	15.0	15.5
Shengli	19.5	7.8	6.9	18.3	14.2	7.7	11.9	13.7
Linpan	21.2	6.5	5.3	20.4	15.8	7.7	9.3	13.8
Gudao	15.7	6.2	6.1	22.8	16.0	8.2	13.7	11.3
Shanjiasi	17.1	6.3	4.9	15.9	16.9	9.5	12.4	17.0

<sup>a</sup> Including the heavy resins in pentane maltenes.

crude oils worldwide. This is not the case for most Chinese crudes, which have a low sulfur content and high resin content.

In addition, because most of the nitrogen in crude oils is concentrated in the resin fractions of residues, there exists a good correlation between nitrogen and resin content. Table 10-11 shows that for most of the Chinese residues, the nitrogen to resin ratios are very close, ranging from 0.018 to 0.026.

#### AVERAGE STRUCTURAL PARAMETERS OF VACUUM RESIDUES AND THEIR FRACTIONS

##### Residues

The average structural parameters of the Chinese residues are listed in Table 10-12. It is shown that for Daqing residue the aromaticity  $f_A$  is the lowest (0.16) and the paraf-

TABLE 10-11

Ratio of nitrogen content to resin content (N/R) of vacuum residues

Name of residue	Nitrogen (wt%)	Resins (wt%)	N/R $\times 100$
Daqing	0.53	26.9	1.96
Renqiu	1.08	51.1	2.11
Zhongyuan	0.60	44.6	1.35
Shengli	0.92	47.6	1.92
Linpan	0.80	44.0	1.82
Gudao	1.18	48.5	2.43
Gaosheng	1.19	50.8	2.34
Xingjiang <sup>a</sup>	0.79	44.8	1.76
Jinglou	1.18	51.3	2.30
Shanjiasi	1.42	53.5	2.65
Huanxiling	0.88	33.6	2.62

<sup>a</sup> Xingjiang Region No. 9.

TABLE 10-12

Structural parameters of vacuum residues

Name of residue	$f_A$	$f_N$	$f_P$	$R_T$	$R_A$	$R_N$	$R_A/R_N$	$H_{Al}/C_A$	$\sigma$	$L$
Daqing	0.16	0.11	0.73	5.2	3.0	2.2	1.3	0.69	0.52	6.6
Renqiu	0.23	0.18	0.59	7.8	4.2	3.6	1.2	0.57	0.29	5.1
Zhongyuan	0.23	0.16	0.61	7.1	4.0	3.1	1.3	0.62	0.44	—
Shengli	0.22	0.17	0.61	6.3	3.2	3.1	1.0	0.74	0.50	4.7
Linpan	0.23	0.18	0.59	6.7	3.5	3.2	1.1	0.70	0.55	4.3
Gudao	0.29	0.23	0.48	9.2	4.9	4.3	1.1	0.57	0.35	3.7
Xingjiang <sup>a</sup>	0.23	0.14	0.63	9.0	5.6	3.4	1.7	0.58	0.53	3.9
Huanxiling	0.30	0.22	0.48	9.2	5.1	4.1	1.2	0.67	0.45	3.7

<sup>a</sup> Xingjiang Region No. 9.

finity  $f_P$  is the highest (0.73), whereas for the Huanxiling residue the  $f_A$  is the highest (0.30) and the  $f_P$  is the lowest (0.48). The distribution of carbon atoms in different structures might reflect the average chemical nature of the residues. In their ring system, the total number of rings ( $R_T$ ) ranges from 5 to 9, the number of aromatic rings ( $R_A$ ) from 3 to 6, and the  $R_A/R_N$  ratios are slightly higher than 1. The average side chain length  $L$  is the longest for Daqing (6.6) and the shortest for Gudao and Huanxiling residues (3.7).

### Saturates

Data in Table 10-13 show that the saturates are the fractions of the lowest molecular weight (600–900) in residues, with the average number of carbon atoms about 40–60. It is clear that the average structure of saturates is also different for crude oils of different bases. For saturates of Daqing residue, the  $H/C$  ratio and  $f_P$  are the highest, while the  $f_N$ ,  $R_N$ , and  $H_\gamma/H_\beta$  are the lowest. The opposite is true for the saturates of Gudao and Huanxiling residues.

TABLE 10-13

Elemental composition and structural parameters and saturated fractions

Name of residue	C (wt%)	H (wt%)	H/C atom ratio	<i>M</i> (VPO)	<i>f<sub>N</sub></i>	<i>f<sub>P</sub></i>	<i>R<sub>N</sub></i>	Branchiness index ( <i>H<sub>V</sub></i> / <i>H<sub>P</sub></i> )	Average molecular formula
Daqing	85.5	14.4	2.01	880	0.08	0.92	0.8	0.31	C <sub>63</sub> H <sub>126</sub>
Shengli	85.7	14.2	1.98	650	0.18	0.82	1.6	0.32	C <sub>46</sub> H <sub>92</sub>
Gudao	85.6	13.9	1.94	710	0.25	0.75	2.7	0.39	C <sub>51</sub> H <sub>98</sub>
Huanxiling	85.5	13.6	1.90	580	0.35	0.65	3.1	0.41	C <sub>41</sub> H <sub>79</sub>

### Aromatics

The elementary analyses data in Table 10-14 show that the aromatic fractions obtained by SARA separation do not comprise the purely aromatic hydrocarbons, but they do contain a considerable amount of heteroatoms. This may be due to the presence of heterocyclic structures condensed with the aromatic nuclei. The average molecular weights of aromatic fractions are 700–1100, slightly higher than those of corresponding saturates. The GPC data in Table 10-15 [18] show that the molecular weight range of aromatics in the Daqing residue is 700–2400, whereas the molecular weight ranges from 500 to 1500 for the other three residues. As mentioned previously, it may be considered that the average molecule of the aromatic fractions is composed of only one unit structure. Their average structural parameters are as follows: H/C atom ratio = 1.5 to 1.7,  $f_A = 0.2$  to 0.3,  $R_T = 5$  to 6,  $R_A = 2$  to 4,  $R_N = 2$  to 3,  $R_A/R_N$  about 1, and  $L = 4$  to 7.

### Resins

Table 10-16 shows that the resin fractions constitute the main nonhydrocarbon part of residues with high contents of heteroatoms, containing on the average 1.3–2.3 atoms of nitrogen and 0.2–1.4 atoms of sulfur per molecule. The molecular weights of resins range from 1100 to 2800, and the average number of unit structures calculated per molecule is near 2 in most cases. Their structural parameters per unit structure are listed in Table 10-16. When compared to the aromatics, the resins have a higher  $f_A$ ,  $R_T^*$ ,  $R_A^*$ , and  $R_A/R_N$  ratio, and a lower H/C ratio,  $f_P$ , and  $L$ . The molecular weight distribution data of resins obtained by GPC are shown in Table 10-17. The resin subfractions with different molecular weights have been also separated from the fractions of Shengli residue obtained by supercritical fluid extraction with pentane. The properties of the resin subfractions of Shengli residue are listed in Table 10-18. As shown, the heteroatom contents of the subfractions of resin are all high without significant variation. As the molecular weight of the resin subfraction increases, the H/C ratio decreases, whereas the aromaticity  $f_A$  and nickel content increase. The heavy subfraction of resin with lower H/C ratio and higher aromaticity  $f_A$  will form more coke during processing. Data also show that in the subfractions of resin with lower molecular weight the nickel is mostly combined with porphyrin.



TABLE 10-14

Elemental composition and structural parameters of aromatic fractions

Name of residue	C (wt%)	H (wt%)	S (wt%)	N (wt%)	H/C atom ratio	<i>M</i> (VPO)	<i>f<sub>A</sub></i>	<i>f<sub>N</sub></i>	<i>f<sub>P</sub></i>	<i>R<sub>T</sub></i>	<i>R<sub>A</sub></i>	<i>R<sub>N</sub></i>	<i>R<sub>A</sub>/R<sub>N</sub></i>	<i>H<sub>Alc</sub>/C<sub>A</sub></i>	$\sigma$	<i>L</i>	Average molecular formula
Daqing	87.3	12.1	0.31	0.20	1.67	1080	0.21	0.14	0.65	6.5	3.7	2.8	1.3	0.67	0.50	7.1	C <sub>79</sub> H <sub>130</sub> N <sub>0.15</sub> S <sub>0.10</sub>
Renqiu	85.5	11.5	—	0.41	1.61	830	0.23	0.14	0.63	5.7	3.6	2.1	1.7	0.62	0.50	5.2	C <sub>59</sub> H <sub>95</sub> N <sub>0.24</sub> S <sub>X</sub>
Shengli	85.5	11.6	1.83	0.56	1.63	850	0.23	0.21	0.56	5.6	2.4	3.2	0.8	0.80	0.57	5.3	C <sub>61</sub> H <sub>98</sub> N <sub>0.34</sub> S <sub>0.49</sub>
Dagang	87.2	11.4	—	0.55	1.56	670	0.27	0.21	0.52	5.1	2.6	2.5	1.0	0.77	0.49	4.3	C <sub>49</sub> H <sub>76</sub> N <sub>0.26</sub> S <sub>X</sub>
Gudao	84.7	11.1	3.66	0.44	1.56	760	0.26	0.23	0.51	5.9	2.8	3.1	0.9	0.75	0.59	4.6	C <sub>54</sub> H <sub>84</sub> N <sub>0.24</sub> S <sub>0.87</sub>
Huanxiling	87.4	11.0	—	0.93	1.50	640	0.32	0.21	0.47	5.2	2.8	2.5	1.1	0.76	0.44	3.5	C <sub>46</sub> H <sub>70</sub> N <sub>0.43</sub> S <sub>X</sub>

TABLE 10-15

Molecular weight distribution of aromatics in residues (by GPC)

Name of residue	GPC fraction number of aromatics	Yield (wt%)	<i>M</i> (VPO)
Daqing	1	12.8	2340
	2	8.3	1850
	3	10.9	1640
	4	13.2	1330
	5	14.3	1010
	6	14.1	850
	7	10.3	720
	8	15.6	810
Renqiu	1	10.9	1440
	2	9.4	1190
	3	13.3	990
	4	16.7	870
	5	17.4	770
	6	14.2	670
	7	18.1	480
Shengli	1	12.1	1420
	2	9.7	1130
	3	14.7	1000
	4	18.7	780
	5	18.1	690
	6	12.8	600
	7	13.9	650
Gudao	1	11.7	1400
	2	9.4	1090
	3	13.6	960
	4	17.4	810
	5	18.0	650
	6	13.4	590
	7	16.4	610

*Asphaltenes*

Asphaltenes are the fractions with the highest molecular weight and polarity of the residues. Their H/C atom ratios are the lowest (1.1–1.3), whereas their contents of heteroatoms are the highest (about 5–10%). The average molecular weight determined by the VPO method usually reaches several thousand, partly due to the association of unit structures of asphaltenes, which consist of condensed polycyclic naphthenoaromatic nuclei with chains, heteroatoms and metals. The unit structure weights of asphaltenes calculated from the NMR spectra are about 1000. As shown in Table 10-19, the unit structure of asphaltenes has the highest  $f_A$  (0.4–0.5),  $R_T$  (11–18),  $R_A$  (7–14), and  $R_A/R_N$  (2–3), and the lowest  $f_P$  (0.35–0.45),  $H_{AU}/C_A$  (0.4–0.5), and  $L$  (3–4) in the residues. Besides, the crystallite parameters of pentane asphaltenes of Gudao, Shanjiasi

TABLE 10-16

Elemental composition and structural parameters of resin fraction

Name residue	C (wt%)	H (wt%)	S (wt%)	N (wt%)	H/C atom ratio	<i>M</i> (VPO)	<i>n</i>	USW	<i>f<sub>A</sub></i>	<i>f<sub>N</sub></i>	<i>f<sub>P</sub></i>	<i>R<sub>T</sub><sup>*</sup></i>	<i>R<sub>A</sub><sup>*</sup></i>	<i>R<sub>N</sub><sup>*</sup></i>	<i>R<sub>A</sub>/R<sub>N</sub></i>	<i>H<sub>AU</sub>/C<sub>A</sub></i>	<i>σ</i>	<i>L</i>	Average molecular formula
Daqing	86.7	10.6	0.31	0.99	1.47	1780	2.1	850	0.31	0.15	0.54	8.1	5.1	3.0	1.7	0.58	0.54	5.2	C <sub>125</sub> H <sub>181</sub> N <sub>1.3</sub> S <sub>0.17</sub>
Renqiu	86.3	10.4	—	1.42	1.44	2260	1.9	1190	0.32	0.13	0.55	9.6	6.5	3.1	2.0	0.53	0.53	3.8	C <sub>162</sub> H <sub>233</sub> N <sub>2.3</sub> S <sub>X</sub>
Zhongyuan	85.4	10.0	—	1.07	1.39	2780	3.0	930	0.35	0.13	0.52	9.1	6.3	2.8	2.3	0.53	—	—	C <sub>198</sub> H <sub>276</sub> N <sub>2.1</sub> S <sub>X</sub>
Shengli	84.3	10.2	1.61	1.44	1.45	1730	2.1	820	0.32	0.15	0.53	7.9	4.9	3.0	1.6	0.59	0.53	4.6	C <sub>121</sub> H <sub>175</sub> N <sub>1.8</sub> S <sub>0.87</sub>
Linpan	86.9	10.4	—	1.40	1.43	1760	2.2	800	0.34	0.14	0.52	7.6	5.1	2.5	1.9	0.61	0.46	4.1	C <sub>121</sub> H <sub>182</sub> N <sub>1.8</sub> S <sub>X</sub>
Dagang	86.3	10.4	—	1.47	1.44	1470	1.7	860	0.32	0.16	0.52	8.5	5.3	3.2	1.7	0.57	0.55	4.1	C <sub>106</sub> H <sub>152</sub> N <sub>1.5</sub> S <sub>X</sub>
Gudao	85.8	10.0	3.31	1.49	1.40	1380	1.9	730	0.36	0.17	0.47	7.8	4.8	3.0	1.6	0.59	0.53	4.1	C <sub>99</sub> H <sub>137</sub> N <sub>1.5</sub> S <sub>1.43</sub>
Xingjiang <sup>a</sup>	87.0	10.1	—	1.22	1.38	1810	2.8	650	0.36	0.16	0.48	7.2	4.6	2.6	1.8	0.60	0.49	3.5	C <sub>131</sub> H <sub>181</sub> N <sub>1.6</sub> S <sub>X</sub>
Huanxiling	85.9	9.7	—	1.74	1.35	1070	1.1	970	0.37	0.14	0.49	10.6	7.4	3.2	2.3	0.50	0.52	3.8	C <sub>77</sub> H <sub>103</sub> N <sub>1.3</sub> S <sub>X</sub>

<sup>a</sup> Xingjiang Region No. 9.

TABLE 10-17

Molecular weight distribution of resins in residues (by GPC)

Name of residue	GPC fraction number of resins	Yield (wt%)	<i>M</i> (VPO)
Daqing	1	5.4	7460
	2	12.5	5180
	3	15.6	2840
	4	17.6	1740
	5	18.8	1160
	6	17.4	1110
	7	12.7	860
Renqiu	1	12.8	4630
	2	14.1	2770
	3	11.0	2030
	4	10.8	1680
	5	10.8	1470
	6	12.0	1200
	7	22.0	1160
	8	6.5	1080
Shengli	1	5.6	4320
	2	11.4	2890
	3	13.0	1940
	4	13.4	1620
	5	17.0	1330
	6	10.6	1200
	7	15.0	1120
	8	14.0	1050
Gudao	1	9.2	3310
	2	10.0	2340
	3	13.7	1550
	4	19.6	1350
	5	14.4	1290
	6	12.2	1070
	7	21.0	1020

TABLE 10-18

Properties of resin subfraction of Shengli residue (by supercritical fluid extraction)

No. of subfraction	Resin yield (wt%)	<i>M</i> (VPO)	H/C	S (wt%)	N (wt%)	Basic nitrogen (wt%)	Ni (ppm)	Porphyrin Ni (ppm)	<i>f<sub>A</sub></i>
I	9.05	850	1.54	2.82	1.39	0.44	54.5	54.5	0.27
II	12.24	910	1.52	3.28	1.36	0.39	62.3	58.1	0.28
III	8.09	1400	1.50	2.99	1.43	0.32	84.1	77.2	0.30
IV	5.84	2000	1.46	2.35	1.49	0.31	98.6	81.9	0.32
V	6.51	2880	1.44	2.74	1.48	0.28	89.1	50.5	0.33
VI	58.27	3550	1.30	2.24	1.76	0.28	112.4	9.4	0.40

TABLE 10-19  
Elemental composition and structural parameters of heptane asphaltenes

Name of residue	C (wt%)	H (wt%)	S (wt%)	N (wt%)	H/C atom ratio	<i>M</i> (VPO)	<i>n</i>	USW	<i>f</i> <sub>A</sub>	<i>f</i> <sub>N</sub>	<i>f</i> <sub>P</sub>	<i>R</i> <sub>T</sub> <sup>*</sup>	<i>R</i> <sub>A</sub> <sup>*</sup>	<i>R</i> <sub>N</sub> <sup>*</sup>	<i>R</i> <sub>A</sub> / <i>R</i> <sub>N</sub>	<i>H</i> <sub>Al</sub> / <i>C</i> <sub>A</sub>	<i>σ</i>	<i>L</i>	Average molecular formula
Shengli	84.1	9.0	2.27	1.73	1.28	3410	3.9	870	0.41	0.17	0.42	10.5	7.1	3.4	2.1	0.51	0.54	4.3	C <sub>239</sub> H <sub>304</sub> S <sub>2.4</sub> N <sub>4.2</sub>
Gudao	81.0	7.8	7.37	1.36	1.16	5620	5.8	980	0.47	0.18	0.35	13.5	9.5	4.0	2.4	0.46	0.57	3.4	C <sub>379</sub> H <sub>435</sub> S <sub>12.9</sub> N <sub>5.5</sub>
Shanjiasi	85.1	9.0	1.53	1.86	1.27	9730	10.5	930	0.42	0.16	0.42	11.3	7.9	3.4	2.3	0.48	0.46	2.9	C <sub>689</sub> H <sub>869</sub> S <sub>4.7</sub> N <sub>12.9</sub>
Huanxiling	87.4	8.2	—	1.90	1.11	6660	5.3	1260	0.50	0.12	0.38	18.5	14.0	4.5	3.1	0.37	0.45	4.0	C <sub>485</sub> H <sub>542</sub> S <sub>X</sub> N <sub>9.0</sub>

TABLE 10-20

Crystallite parameters of pentane asphaltenes (by XRD)

Sample	$d_M$ (Å)	$L_c$ (Å)	$L_a$ (Å)	$M_c$
C <sub>5</sub> -asphaltene of Gudao residue	3.56	20.8	11.9	5.8
C <sub>5</sub> -asphaltene of Shanjiashi residue	3.56	19.1	13.7	5.4
C <sub>5</sub> -asphaltene of Xingjiang gilsonite	3.56	18.4	15.4	5.2

residues and Xinjiang gilsonite have been obtained based on XRD spectra using Yen's method [19]. Table 10-20 [20] shows that the interlayer distance ( $d_M$ ) of the asphaltene crystallite is 3.56 Å. The average size of the aromatic cluster perpendicular to the plane of the sheets ( $L_c$ ) is about 20 Å; the average diameter of the aromatic sheets ( $L_a$ ) ranges from 11.9 to 15.4 Å, and the effective number of aromatic sheets associated in a stacked cluster ( $M_c$ ) is 5–6.

### Waxes

The structural parameters and other properties of the waxes from the saturate and aromatic fractions of Daqing and Gudao residues are presented in Table 10-21 [23]. Data show that the waxes from aromatics have a higher molecular weight, refractive index, number of rings, and aromaticity, but a lower H/C ratio than that of saturates. Moreover, the size of the crystallites of waxes in saturates is larger and the crystallinity is higher. This is the reason why the waxes in saturates have a more negative effect on the low-temperature performance of the paving asphalt than those in aromatics [21,22]. It is interesting that although the Daqing and Gudao residues are quite different in composition, the structural parameters of their waxes in saturates or aromatics are very close to each other.

In Table 10-22, the structural parameters of different fractions of residues are summarized. The structural parameters of each fraction lie within definite ranges. From saturate to aromatic to resin to asphaltene fractions, the parameters  $M$ ,  $n$ ,  $f_A$ ,  $R_T$ ,  $R_A$ , and the  $R_A/R_N$  ratio increase, whereas the H/C ratio,  $f_P$ , and  $L$  decrease systematically. The decrease in the  $H_{AU}/C_A$  ratio indicates an increase in the compactness of condensation of the aromatic nuclei from aromatic to asphaltene fractions. Table 10-22 also shows that the unit structure weights are about the same (1000) for all the fractions of all the residues.

## DISTRIBUTION OF NITROGEN, NICKEL AND CARBON RESIDUE OF VACUUM RESIDUES

### Nitrogen

The distribution of nitrogen among the six fractions of the residues, obtained according to the separation scheme shown in Fig. 10-1, are presented in Table 10-23. Data show that the nitrogen content of Fract. 1 is very low. From Fract. 1 to C<sub>5</sub>-asphaltene, the nitrogen content does not increase continuously with the maximum

TABLE 10-21  
Properties and structural parameters of waxes

Name of residue	Sample	<i>M</i> (VPO)	<i>n</i> <sub>D</sub> <sup>80</sup>	H/C	N (wt%)	<i>f</i> <sub>A</sub>	<i>f</i> <sub>N</sub>	<i>f</i> <sub>P</sub>	<i>R</i> <sub>T</sub>	<i>R</i> <sub>A</sub>	<i>R</i> <sub>N</sub>	Dimension of crystallite (nm)		Crystallinity (%)
												<i>L</i> <sub>200</sub>	<i>L</i> <sub>110</sub>	
Daqing	Wax in saturates	1070	1.4545	1.98	0	0	0.11	0.89	1.50	0	1.50	45.7	40.4	25.0
	Wax in aromatics	2060	1.4910	1.80	0.25	0.08	0.20	0.72	9.86	2.45	7.41	21.6	19.4	17.5
Gudao	Wax in saturates	860	1.4547	1.99	0	0	0.12	0.88	1.30	0	1.30	55.5	47.2	36.3
	Wax in aromatics	1550	1.5021	1.75	0.40	0.11	0.23	0.66	8.70	2.50	6.20	14.6	16.2	13.6

TABLE 10-22

Comparison of structural parameters of various fractions of vacuum residues

Parameters	Saturated	Aromatic	Resin	Heptane asphaltene
H/C	1.9–2.0	1.5–1.7	1.4–1.5	1.1–1.3
$M$ (VPO)	600–900	700–1100	1400–2800	3500–10000
$n$	–	1	1–3	4–6
USW	–	700–1100	800–1200	800–1200
$f_A$	0	0.2–0.3	0.3–0.4	0.4–0.5
$f_P$	0.7–0.9	0.5–0.7	0.45–0.55	0.35–0.45
$R_T^*$	1–3	5–6	7–10	11–18
$R_A^*$	0	2–4	5–7	7–14
$R_N^*$	1–3	2–3	2.5–3.5	3.5–4.5
$R_A/R_N$	–	0.8–1.3	1.6–2.3	2–3
$H_{AU}/C_A$	–	0.6–0.8	0.5–0.6	0.4–0.5
$L(C_P/nCH_3)$	–	4–7	4–5	3–4

TABLE 10-23

Distribution of nitrogen in vacuum residues

Name of residue		Fract. 1	Fract. 2	Fract. 3 light resins	Fract. 4 middle resins	Fract. 5 heavy resins	Pentane asphaltenes
Daqing	N (wt%)	0.30	0.69	1.23	1.03	1.20	–
N/total	N (%)	7.9	15.7	31.8	14.6	24.6	–
Renqiu	N (wt%)	0.30	1.20	1.50	1.49	1.32	0.95
N/total	N (%)	11.9	11.7	17.0	11.1	21.5	9.4
Zhongyuan	N (wt%)	0.25	0.61	0.88	1.01	1.22	1.09
N/total	N (%)	16.7	10.2	17.7	12.5	30.5	20.2
Shengli	N (wt%)	0.15	0.82	1.31	1.52	1.63	1.70
N/total	N (%)	6.0	11.1	22.1	13.5	24.5	25.1
Gudao	N (wt%)	0.55	1.15	1.50	1.66	1.75	1.62
N/total	N (%)	17.6	12.7	20.9	11.5	20.3	15.5
Xingjiang <sup>a</sup>	N (wt%)	0	0.51	1.22	1.04	1.21	1.38
N/total	N (%)	0	6.3	23.0	9.4	21.1	14.8
Jinglou	N (wt%)	0.36	1.14	1.56	1.89	2.13	2.07
N/total	N (%)	10.8	13.1	23.1	16.0	32.7	9.5
Huanxiling	N (wt%)	0.26	1.24	1.56	1.48	1.68	1.78
N/total	N (%)	16.6	14.2	21.5	10.9	12.1	18.0

<sup>a</sup> Xingjiang Region No. 9.

content in Fract. 3, 4, 5 or  $C_5$ -asphaltene. About 70–80% nitrogen is present in the resin-asphaltene fraction. Thus, there is a good correlation between nitrogen and resin contents (Table 10-11).



TABLE 10-24

Distribution of nickel in vacuum residues

Name of residue		Fract. 1	Fract. 2	Fract. 3	Fract. 4	Fract. 5	Pentane asphaltene
Daqing	Ni (ppm)	0.0	3.0	15.0	20.0	37.0	—
Ni/total	Ni (%)	0.0	3.5	19.6	14.4	38.1	—
Renqiu	Ni (ppm)	0.9	3.5	44.2	51.1	83.3	101.6
Ni/total	Ni (%)	0.9	1.1	16.7	12.2	39.5	27.5
Zhongyuan	Ni (ppm)	0.3	1.7	16.5	27.7	22.0	34.6
Ni/total	Ni (%)	0.7	1.2	13.3	13.7	22.0	35.8
Shengli	Ni (ppm)	0.0	7.1	87.4	75.1	64.7	127.5
Ni/total	Ni (%)	0.0	1.8	25.8	12.1	16.0	36.6
Gudao	Ni (ppm)	0.7	6.3	34.3	55.1	46.0	115.4
Ni/total	Ni (%)	0.8	2.3	15.6	12.8	17.9	37.0
Gaosheng	Ni (ppm)	0.3	41.5	467.5	120.2	150.2	375.5
Ni/total	Ni (%)	0.1	3.2	42.9	7.6	17.2	28.5
Xingjiang <sup>a</sup>	Ni (ppm)	0.0	10.8	19.5	35.5	80.4	171.6
Ni/total	Ni (%)	0.0	3.2	8.5	7.3	32.4	42.6
Jinglou	Ni (ppm)	0.1	7.0	54.7	35.9	85.0	176.1
Ni/total	Ni (%)	0.1	2.3	22.6	8.5	36.3	22.5
Shanjiashi	Ni (ppm)	0.5	48.5	140.4	59.4	80.5	206.5
Ni/total	Ni (%)	0.3	8.0	27.8	6.4	10.0	46.7
Huanxiling	Ni (ppm)	0.4	52.7	154.1	109.7	153.6	486.7
Ni/total	Ni (%)	0.3	6.3	22.0	8.4	11.4	51.2

<sup>a</sup> Xingjiang Region No. 9.

### Nickel

The distribution of nickel in the six fractions of vacuum residues is presented in Table 10-24. There is only a very small content of nickel in Fract. 1 (below 1 ppm), and the nickel content of Fract. 2 is relatively low. More than 95% nickel is present in the resin-asphaltene fraction. The content of nickel in the pentane-asphaltene fraction is the highest. As in the case of the nitrogen content, the nickel content does not increase continuously from Fract. 1 to pentane asphaltene, and the nickel content of Fract. 3 (light resin) ranks second in some cases. It appears that nickel in the lighter subfraction of resin is more difficult to remove by deasphalting because of its higher solubility in solvent.

### Carbon residue

Table 10-25 shows that the values of carbon residue of Fract. 1 are very low (about 1–2%), and they increase systematically from Fract. 1 to pentane asphaltene. The carbon residues of middle and heavy resins and pentane asphaltenes are quite high (about 30–50%), which means that they will tend to form more coke during processing.

TABLE 10-25

Carbon residues of fraction of vacuum residues

Name of residue	Carbon residue (wt%)					
	Fract. 1	Fract. 2	Fract. 3 light resins	Fract. 4 middle resins	Fract. 5 heavy resins	Pentane asphaltene
Renqiu	1.7	12.8	21.2	31.1	40.1	41.1
Zhongyuan	1.1	15.7	27.4	33.1	34.6	43.9
Shengli	1.1	12.8	20.5	24.8	28.7	34.7
Gudao	2.4	16.2	21.9	27.0	29.5	48.8

## CONCLUSIONS

Most of the vacuum residues of the twelve Chinese crude oils tested have high nitrogen, nickel, wax, and resin contents, and low sulfur, vanadium and asphaltene contents. This constitutes a convincing proof that they are of continental origin.

The structural parameters that were calculated using the NMR spectra with the modified Brown–Ladner method might reflect the average molecular structure of various residues from the crude oils of different types and the chemical nature of their fractions. The structural parameters of each fraction lie within definite ranges and vary systematically in the following order: saturates, aromatics, resins, and asphaltenes.

The resins, which are the main components of the Chinese residues and contain most of the nitrogen and nickel, have a high propensity for coke formation during processing.

## ACKNOWLEDGEMENTS

This work was funded by the Commission of Science Foundation of China. The authors acknowledge the assistance of Prof. Lao Yongxin, Mr. Yang Jiamo, Mrs. Zhang Yanfang, and Mrs. Wang Hong. The help extended by Professors George V. Chilingarian and T.F. Yen is also greatly appreciated by the authors.

## REFERENCES

- [1] Brown, J.K. and Ladner, W.R., A study of H distribution in coal-like materials by NMR. *Fuel*, 39: 87 (1960).
- [2] Liang, W., Que, G. and Chen, Y., Study on chemical structure of vacuum residues by  $^1\text{H-NMR}$ . *Pet. Process.*, 4: 40 (1982).
- [3] Liang, W., Que, G. and Chen, Y., Chemical composition and characteristics of residues of Chinese crude oils. *Energy Sources*, 13 (2): 251 (1991).
- [4] Lu, W. and Zhang, S., Peculiarities of chemical composition of Chinese crude oils. *Pet. Process.*, 7: 1 (1979).
- [5] Qian, S., Chen, F. and Li, C., Structural analysis of some domestic petroleum heavy residues by combined  $^1\text{H-NMR-IR}$  spectroscopy. *J. Fuel Chem. Technol.*, 10 (10): 353 (1982).

- [6] William, R.B., *Symposium on Composition of Petroleum Oils*. ASTM, Spec. Tech. Publ. 224 (1958).
- [7] Yen, T.F. and Erdman, T.G., Investigation of the structure of petroleum asphaltenes and related substances by infrared analysis. *Am. Chem. Soc., Div. Pet. Chem., Preprints*, 7 (1): 5 (1962).
- [8] Zhang, S., Yue, S., Shen, J. and Qiao, C., Composition studies of vacuum residues from Daqing, Shengli, and Renqiu crudes. *Pet. Process.*, 1: 24 (1982).
- [9] Snyder, L.R. and Saunders, D.L., Adsorption and partition chromatography. In: K.H. Altgelt and T.H. Gouw (Eds.), *Chromatography in Petroleum Analysis*. Marcel Dekker, New York, NY, pp. 215–272 (1979).
- [10] Corbett, L.W., Composition of asphalt based on generic fractionation, using solvent deasphalting, elution-adsorption chromatography, and densimetric characterization. *Anal. Chem.*, 41 (4): 576 (1969).
- [11] McKay, J.F., Amend, P.J., Harnsberger, P.M., Cogswell, T.E. and Latham, D.R., Composition of petroleum heavy ends. *Fuel*, 60 (1): 14 (1981).
- [12] Selucky, M.L., Chu, Y., Ruo, T.C.S. and Strausz, O.P., Chemical composition of Athabasca bitumen. *Fuel*, 56 (4): 369 (1977).
- [13] Liu, C., Que, G., Chen, Y. and Liang, W., Characterization of vacuum residues by adsorption chromatography and  $^1\text{H}$ -NMR spectroscopy. *Fuel Sci. Technol. Int.*, 6 (1): 449 (1988).
- [14] Liang, W., Li, X. and Xiang, T., Study of the average structure of residues by DEPT  $^{13}\text{C}$ -NMR. *J. Fuel Chem. Technol.*, 19 (3): 245 (1991).
- [15] Liu, C., Que, G., Chen, Y. and Liang, W., Empirical equations for calculation of aromaticity  $f_A$  of vacuum residue. *Pet. Process.*, 12: 53 (1987).
- [16] Tissot, B.P. and Welte, D.H., *Petroleum Formation and Occurrence*, 2nd ed. Springer, Berlin (1984).
- [17] Hunt, J.M., *Petroleum Geochemistry and Geology*. Freeman, San Francisco, CA (1979).
- [18] Que, G., Chen, Y. and Liang, W., Study of aromatics in vacuum residues by GPC and  $^1\text{H}$ -NMR. *Pet. Process.*, 11: 45 (1983).
- [19] Yen, T.F., Erdman, J.G. and Pollack, S.S., Investigation of the structure of petroleum asphaltenes by X-ray diffraction. *Anal. Chem.*, 33 (11): 1587 (1961).
- [20] Zhang, Y., Liu, C. and Liang, W., Study of asphaltenes in two Chinese asphalts by X-ray diffraction. *Fuel Sci. Technol. Int.*, 7 (7): 919 (1989).
- [21] Que, G., Chen, Y. and Liang, W., Relationship between chemical composition and performance of paving asphalt, Part I. *Pet. Process.*, 10: 12 (1985).
- [22] Que, G., Liu, C., Chen, Y. and Liang, W., Relationship between chemical composition and performance of paving asphalt, Part II. *Pet. Process.*, 6: 32 (1987).
- [23] Lao, Y. and Liang, W., A study on composition and structure of waxes of Daqing and Gudao vacuum residues. *J. Univ. Pet., China*, 13 (4): 59 (1989).

## *Chapter 11*

# **ANALYSIS OF ASPHALT AND ITS COMPONENTS BY THIN-LAYER CHROMATOGRAPHY**

K. DUNN, G.V. CHILINGARIAN, H. LIAN, Y.Y. WANG and T.F. YEN

## **INTRODUCTION**

Petroleum asphalt is a dark brown to black cementitious material, which belongs to a class of extremely complex organic macromolecules. Its predominant constituents are bitumens that either occur in nature or are obtained as residue from the refining of petroleum. In the United States, a stylized barrel of crude oil yields approximately 45% gasoline, 5% kerosene, 34% light and heavy distillates, and 4% asphalt [1]. Due to economic and energy resource demands, compounds which have lower molecular weights are removed during the refinery process. Hence, the average molecular weight of asphalt is now higher than before, making it difficult to separate and analyze it properly. Since the early 1900s, most asphalts have been produced from the refining of petroleum and applied primarily to paving and roofing. Currently, some research has focused on the reconstitution of asphalt with special properties. These include paving asphalts having an extended lifetime, and asphalts that are suitable for the coating of metals and fixation of hazardous wastes.

Asphalt is a colloidal system similar to petroleum, but with the lighter molecules removed [2]. In general, asphalt can be fractionated into four major components: saturates, aromatics, resins and asphaltenes, by either the SARA [3] method or the ASTM D4124 [4] procedure. The fractionated part of saturates and aromatics is generally considered to be gas oil. The polarity of these four fractions can be arranged in the following order: saturates < aromatics < resins < asphaltenes [5]. In the colloidal asphalt system, asphaltene can exist in fine or coarse dispersions, depending on their resin content. These micelles can be dispersed in gas oil with resins as peptizing agents. The minor constituents are organometallics (such as porphyrins), metals and polar molecules (such as amphiphiles) [6].

The chemical composition of asphalt is very complex. Present characterization techniques include: computerized capillary gas chromatography (GC), GC-mass spectrometry (GC-MS), Fourier transform infrared spectrometry (FT-IR), GC/FT-IR, high performance liquid chromatography (HPLC), field ionization mass spectroscopy (FI-MS), supercritical fluid chromatography (SFC) and  $^1\text{H}$  and  $^{13}\text{C}$  nuclear magnetic resonance spectrometry (NMR). For details please refer back elsewhere, i.e., Vol. 1 of this book. The fractional techniques of heavy oil involving solution and precipitation, and chromatography on columns, glass plates or rods, have been most widely used owing to their effectiveness and the low cost in comparison with other methods.

Hydrocarbon-type fractions from bitumens, heavy crude and distillation residues

were separated by thin-layer chromatography (TLC). This is a rapid, effective and inexpensive method with the potential of becoming a major tool for use in the semi-quantitative analysis of heavy hydrocarbon mixtures (e.g., asphalt and heavy oil). TLC, first introduced in 1983 by Izmailov and Shraiber [7], has been widely adopted for use in many different analyses, including that of amino acids from food protein, hallucinogenic alkaloids from plants, steroids from the urine of newborn infants, morphine in the blood of overdose victims, pesticides in soil, pharmaceuticals, etc. [8]. The use of TLC for the separation of polycyclic aromatic hydrocarbon alone has been reviewed by many authors, and other uses have also been identified: Killer and Amos [9] successfully applied the technique to petroleum products in 1966, Mathews [10] used TLC to identify petroleum and coal tar oils and residues, Poirier and George [11,12] used it to determine the asphaltene content in crude oil and bitumens, and Coates [13] separated lubricating oils and their additives by this method. Wang and Yen [14] have also used TLC to identify jet fuel.

This paper describes several analytical methods such as thin-layer chromatography (TLC), Chromatotron, and TLC-FID based on the principle of thin-layer chromatography for the identification of heavy hydrocarbon compositions. Each method provides specific advantages. For example, the rapid thin-layer chromatography (TLC) method can characterize and differentiate between heavy and residue fractions of petroleum, coal liquids, tar sands, bitumens, and asphaltenes. Using appropriate adsorbents, solvent systems, and stepwise development, it is possible to separate and detect aliphatics, mono-, di-, tri-, and polycyclic aromatics, resins and asphaltenes. Using preparative TLC plates, the separated fractions may be collected for further identification by other techniques [14]. The preparative method — centrifugal TLC using the Chromatotron — is suitable not only for the quantification of asphalt, but also for collection of fractions. The collected fractions could be used for the reconstitution of asphalt. TLC-FID can achieve quantitative analysis quickly and simply. It involves separation of asphalt of solvent-extractable organics on silica-coated rods into four fractions, combined with semi-quantitative detection by automated FID. The main attraction of the TLC methods is that they are very rapid compared to the time-consuming preparative column fractionation technique.

#### THIN-LAYER CHROMATOGRAPHY IN ASPHALT ANALYSIS

##### *TLC*

TLC is a very effective tool for the characterization of saturates, aromatics, resins and asphaltenes from asphalt without the use of supplementary techniques. When separating asphalt into four fractions by TLC, the primary prerequisites for a support material to hold the chromatographic solvents are the following: mechanical strength, chemical resistance to solvents and developer reagents, ability to withstand temperatures needed for reaction on the plate, uniformity of thickness and low cost. Glass plates meet these requirements best. It is important to employ high-quality plates of uniform thickness — either commercially precoated plates or home-made thin-layer plates.

Before chromatographic analysis, one must decide which solvent should be used to thoroughly dissolve the sample. The process of applying the sample to the TLC plate is one of the most important steps to ensure success of the separation. Proper preparation of the sample is required prior to its application. Generally speaking, polar compounds will not dissolve in nonpolar solvents and vice versa. For proper application of the sample to the layers, the solvent used should be highly volatile and as nonpolar as possible, because solvents with high boiling points or high polarity are difficult to remove from the adsorbent during application. Moreover, moisture from the air will also influence the activity of adsorbents during this period. If a small amount of solvent is retained in the adsorbent after application of the sample, it will adversely affect the separation due to spreading of the sample in the matrix. Fig. 11-1 shows the step-by-step TLC process generally used in asphalt separation.

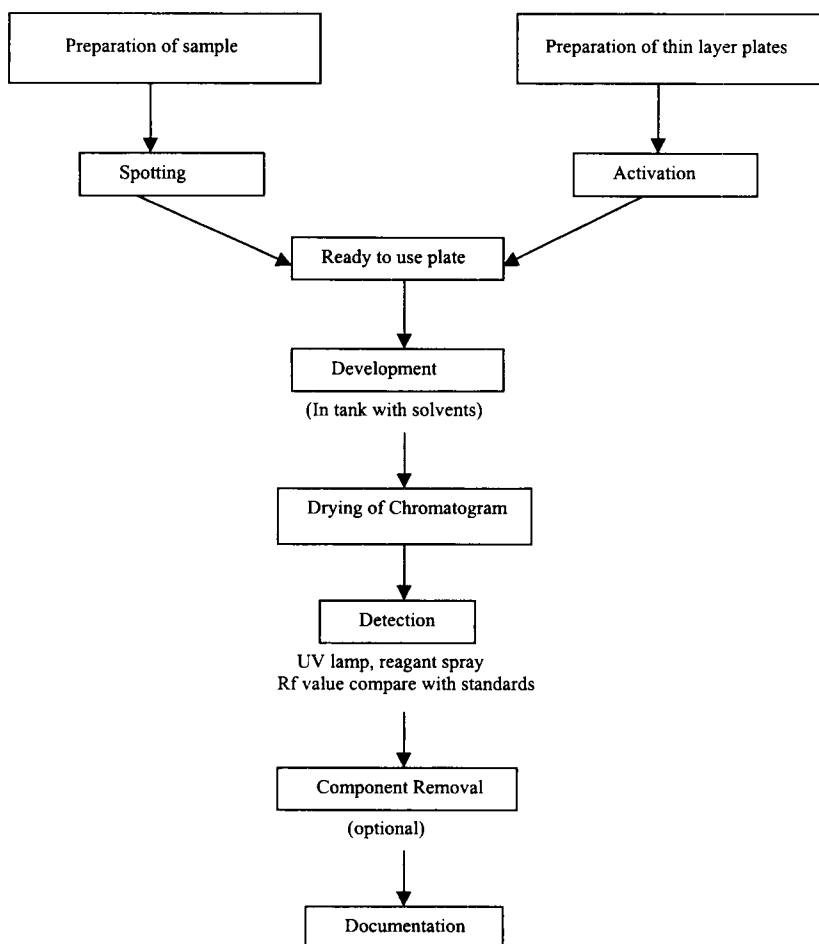


Fig. 11-1. The protocol procedures for thin-layer chromatography.

TABLE 11-1

 $R_f$  values of asphalt fractions

Asphalt fractions	$R_f$ value
Saturates	0.90–0.92
Aromatics:	
Mono-	0.81–0.83
Di-	0.77–0.79
Poly-	0.68–0.74
Resins	0.45–0.47
Asphaltenes	0.20–0.21

Samples should be applied at suitable concentration solution in the least polar solvent in which they are soluble. The diameter of spots must be as small as possible. The load applied is critical as it affects the shape and position of the zone after development. If the amount of the sample is not enough, a fuzzy spot rather than a sharply defined one appears, or spots may not appear at all. Spots that are too highly concentrated will give poor separation because the mobile phase solvent tends to flow through the point of least resistance and will travel around the spots. This will result in spots that are poorly separated and unsymmetrical after development.

The  $R_f$  is an important property used in qualitative analysis and is defined as follows:

$$R_f = \frac{\text{distance moved from point of application by solute}}{\text{distance moved from point of application by mobile phase}} \quad (11-1)$$

The  $R_f$  value of all the adsorbed solutes is less than 1.00. There are many factors that can affect the measurement of  $R_f$ ; consequently, reproducibility varies from laboratory to laboratory. These factors include the chemical nature, surface area, particle size and activity of stationary phase, layer thickness, purity of mobile phase (one of the most important), position of starting point in relation to depth of mobile phase in developing tank, developing distance and sample size. The  $R_f$  supplies information on the shapes and sizes of the spots. Using the  $R_f$  values in two different mobile phases will characterize a sample. Table 11-1 lists the approximate  $R_f$  values of four fractions of asphalt. If the samples and a series of standard solutions are chromatographed together on the same plate, visual comparison of the spot size and intensities can give a semi-quantitative indication of the amount present with an accuracy of about 20%; if quantified by densitometry, the error is within 5%.

The asphalt samples on the plate are eluted at 18–25°C in an unsaturated developing tank, which are separated into different fractions. The solvent selection and elution sequences are important steps essential to the success of separation. The elution solvent system of asphalt analysis is listed in Table 11-2. The solvent elution sequences are petroleum ether, 10% diethyl ether in pentane, 10% ethyl alcohol in benzene for isolating saturates, aromatics and resins individually [14]. TLC is performed in three stages. First, elution with petroleum ether (30–60°C) yields the separation of the major classes of nonpolar hydrocarbons (aliphatics, and aromatics by ring number). In the second step, all aromatics migrate further. Some nonpolar or low-polarity heterocyclic

TABLE 11-2

Elution solvent system of asphalt analysis

	TLC	Chromatotron	TLC-FID
Saturates	petroleum ether	petroleum ether	hexane
Aromatics	pentane-diethyl ether (90: 10, v/v)	petroleum ether-ether (80: 20, v/v)	toluene
Resins	benzene-ethyl alcohol (90: 10, v/v)	ethyl acetate	dichloromethane-methanol (95: 5, v/v)
Asphaltene		tetrahydrofuran (THF)	

compounds, such as benzothiophene and dibenzothiophene, if present, have  $R_f$  values similar to those of aromatics having the same number of rings. The third solvent is applied to the separation of polar compounds like asphaltene, which is insoluble in light  $n$ -paraffinic hydrocarbon but soluble in toluene. In this solvent system, the resin fraction can be developed and moved near the solvent front. Preasphaltene, the most polar material, remains at the origin, and asphaltene develops between the resin and preasphaltene spots. Fig. 11-2 shows the separation and characterization of asphalt by TLC.

For the identification of different aromatics, plates can be examined by irradiation with UV light ( $\lambda = 254\text{ nm}$ ) when spots having the following colors are observed: monocyclic aromatics, gray-yellow; dicyclic aromatics, dark gray; tricyclic aromatics, purple; and polycyclic aromatics, dark; all against a light green background. Spots can also be visualized by using freshly prepared sulfuric acid-formaldehyde solution (98 + 2%, v/v) The following colors can then be obtained: saturated compounds,

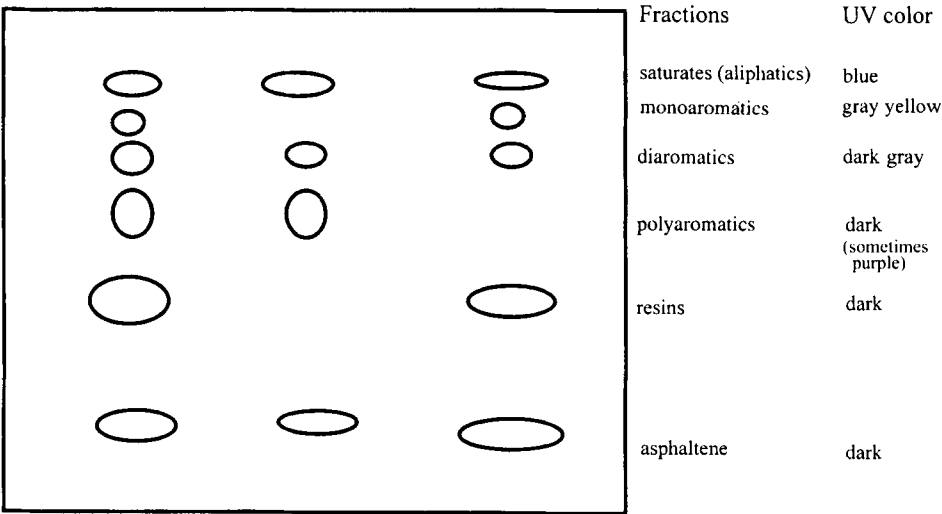


Fig. 11-2. Thin-layer chromatogram of asphalt separation and identification of major hydrocarbon types.



no color; monocyclic aromatics, reddish brown; and dicyclic aromatics and different polycyclic aromatics, dark green. All aromatics can be observed at the ppm level [5].

### *Chromatotron*

A relatively inexpensive chromatography equipment — centrifugal, high performance, radial, preparative, gradient developed, thin-layer chromatography — can be used for the analysis of constituents of fossil hydrocarbons, and, especially, for the determination of asphalt composition. Basically speaking, the Chromatotron is a type of thin-layer chromatographer which performs chromatography through a rotor coated with a thin layer of adsorbent. The mobile phase and solutions of compounds are introduced to the adsorbent by an inlet, which delivers them close to the center of the rotor. A motor drives the rotor at a constant speed to establish radial elution of solvents and samples, forming concentric bands of separated substances that move through its edge and which are channeled by an output tube for collection. Detection of UV absorbing bands is accomplished through the UV light transparent Chromatotron Teflon lid. The schematic diagram of a Chromatotron, Harrison Model 7924T, is illustrated in Fig. 11-3. The silica gel 60 HF254 + 366 can be used as an adsorbent with the addition of a binder coated manually on the rotor as a thin layer.

The intermolecular forces between the solutes present in asphalt include electrostatic, Van der Waals, London, hydrogen bonding and chemical bonding. Therefore, it is very important to select the appropriate solvents for the separation of asphalt into four fractions. Following the solubility principle “like dissolves like” [15], each fraction can be dissolved in a solvent which can overcome the pertinent intermolecular forces. The likelihood that a solvent can dissolve a given solute can be estimated from the solubility parameter,  $\delta$ , of the former. Fig. 11-4 shows the solubility parameters of a number of common solvents in relation to those required to dissolve the various asphalt fractions [2]. Solvent mixtures are also used for the separation of asphalt: solubility parameters of such mixtures can be calculated from the following formula [16]:

$$\delta_m = \Phi_1 \delta_1 + \Phi_2 \delta_2 \quad (11-2)$$

where  $\delta_1$  and  $\delta_2$  are the solubility parameters of solvents, and  $\Phi_1$  and  $\Phi_2$  are their volume fractions.

Nonpolar solvents are preferred for the separation, because of the longer time taken to eliminate polar solvents adsorbed on the thick adsorbent layer. Sample injection is performed by means of a pump operated at a low flow rate. This enables a large volume of sample to be applied to the rotor, forming a narrow initial band which greatly enhances resolution. The solvent system for the separation of petroleum is transferred from conventional analytical TLC as illustrated in Table 11-2. Table 11-3 lists the solubility parameters of the four solvents selected to perform the separation of eluted fractions. The solubility parameters of the selected mobile phases should be higher than required for each of the asphalt fractions in order to overcome the adsorptive strength of the silica gel. The details of the four-step development procedures are discussed as follows [5].

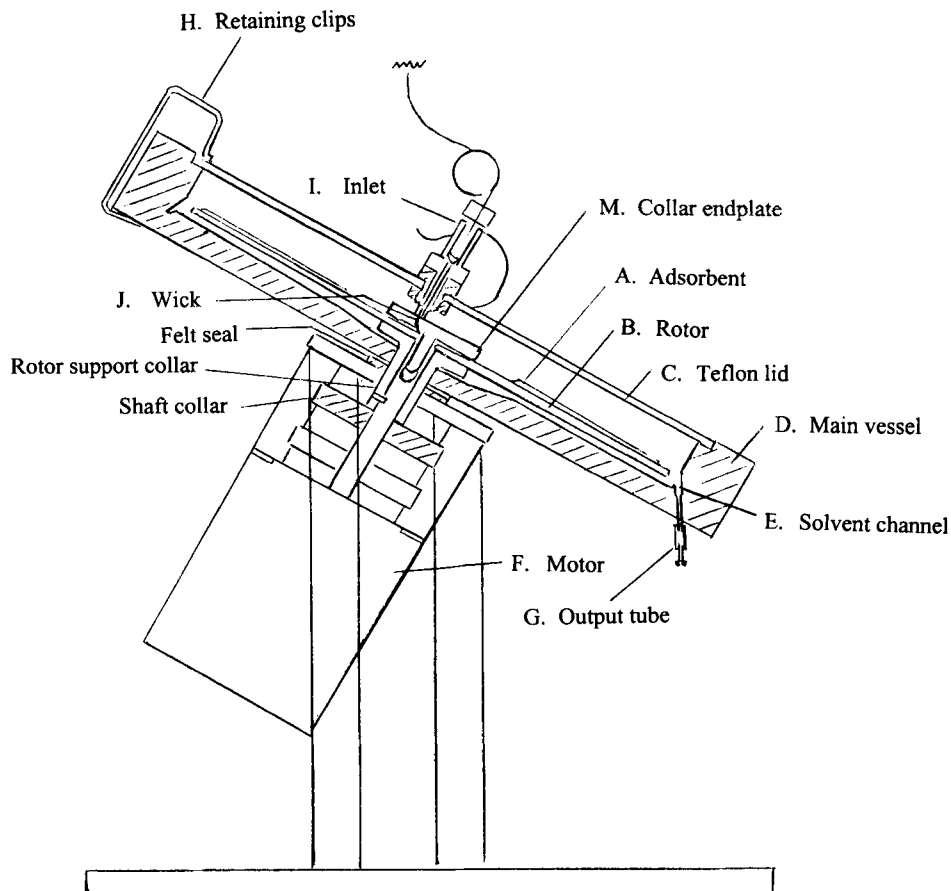


Fig. 11-3. Schematic diagram of the Chromatotron [17].

(i) Petroleum ether is used to elute saturated compounds and mono- and diaromatic compounds.

(ii) Polyaromatic compounds and resin-1 can be eluted with petroleum ether–ether (80 : 20, v/v), a mixture found most suitable for ensuring that the aromatic compounds form a concentric band.

(iii) Ethyl acetate is used to elute resin-2.

(iv) Tetrahydrofuran is used to elute the asphaltene.

It is very important to select the cut-off point for the separation process in order to collect fractions of high purity. There are two methods which can be used to identify the different fractions for the cut-off point.

(1) *UV examination.* This previously discussed method is useful for the estimation of the cut-off point of saturates and aromatics.

(2) *Spot test.* A spot test with formaldehyde–sulfuric acid solution can be used to identify the cut-off points of saturates, aromatics and resins.

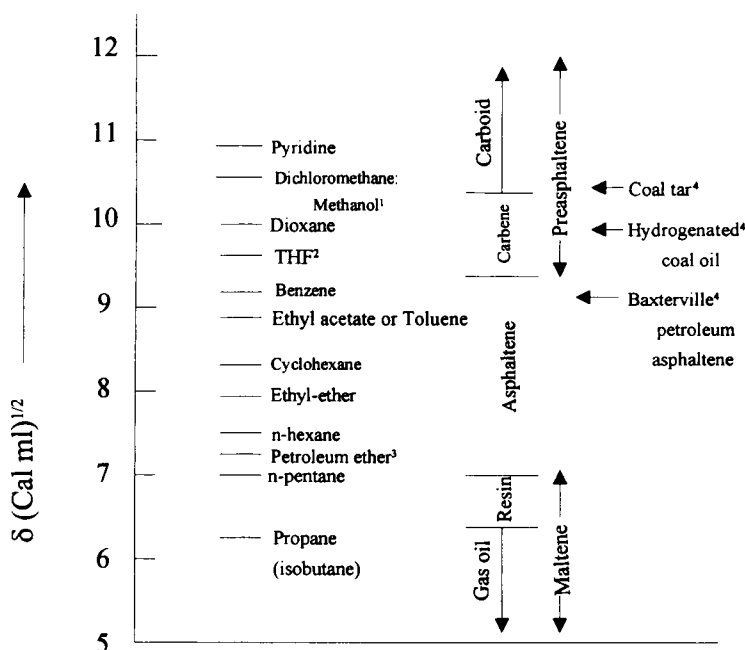


Fig. 11-4. Solubility parameters of common solvents in relation to the values required for the dissolution of asphalt fractions. 1 = 95 : 5 (v/v); 2 = tetrahydrofuran; 3 = estimated, mixture; 4 = calculated value.

TABLE 11-3

Solubility parameters of solvents and solvent mixtures

Solvent	Solubility parameter
Petroleum ether	7.2
Petroleum ether-diethyl ether (80 : 20, v/v)	7.3
Ethyl acetate	8.9-9.1
Tetrahydrofuran (THF)	9.6

This analytical method can be used to establish both quantitative and preparative procedures; the complete process is summarized in Fig. 11-5. The fractions could be used for the manufacture of synthetic asphalt, e.g., paving asphalts with extended lifetimes, effective coatings for metals, and materials for encapsulation of hazardous wastes.

### TLC-FID

The fingerprinting of asphalt and its components can be done by thin-layer chromatography with flame ionization detection (TLC-FID) much more rapidly and simply than by the classical column chromatography and preparative TLC method. The analysis is undertaken with a full understanding of the characteristics of thin-layer

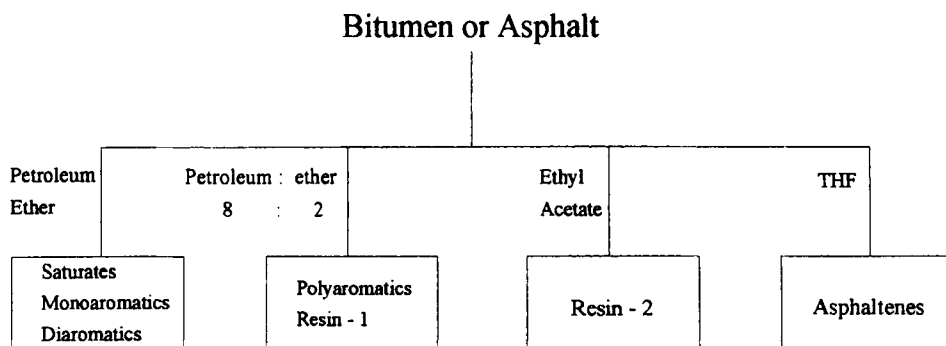


Fig. 11-5. Characterization of asphalt by preparative Chromatotron.

chromatography and flame ionization detection [18]. TLC-FID involves separation of solvent-extractable organics on silica-coated quartz rods, called Chromarods, into saturates, aromatics and polar components combined with semi-quantitative detection by automated FID [18,22-24].

The working principle of a commercially available instrument, Iatroscan TH-10, designed to scan the adsorbent-coated Chromarods, is illustrated in Fig. 11-6. A set of up to 10 coated rods are mounted on rod holders that are used for both chromatography and subsequent scanning. The samples to be analyzed are dissolved in a solvent and applied near one end of the coated rods, which are then developed using suitable solvents as in conventional TLC. The developing solvent is removed by evaporation and, finally, the coated rods are scanned in the FID device. The fractions resolved on each of the Chromarods are then successively vaporized/pyrolyzed, and the ionizable carbon is converted to ions that are detected in the collector electrode. The FID signals from each fraction are amplified and recorded as separate peaks [17-20].

Inasmuch as asphalt comprises a complex mixture of various substances, which are impossible to isolate, a compositional analysis technique is generally used whereby a sample is separated into its groups by performing multi-stage development with several eluting solvents of varying polarities. Therefore, it is very difficult to separate the asphalt without any impurities in each component. The TLC separation is based on the solubility of the component types to be analyzed. The component-types are defined as follows: gas oil — propane soluble; resin — propane insoluble, *n*-pentane soluble; asphaltene — *n*-pentane insoluble, benzene soluble [2]. In order to overcome the pertinent intermolecular forces, the appropriate solvents must have slightly higher solubility parameters than that of eluted components. The solvent elution sequences of separating asphalt are *n*-hexane, toluene, dichloromethane: methanol (95:5, v/v) for isolating saturates, aromatics and resins individually. The approximate  $R_f$  ratio of each eluted component on the rods is: saturates = 0.7; aromatics = 0.4; and resins = 0.2. Asphaltenes remain on the original spots of rods.

TLC-FID is a fast, multiple-analysis method which can be performed simultaneously, and all sample components are amenable to measurement. The total elapsed time for the analysis of a set of 10 samples simultaneously by the TLC-FID method is less than 2 h

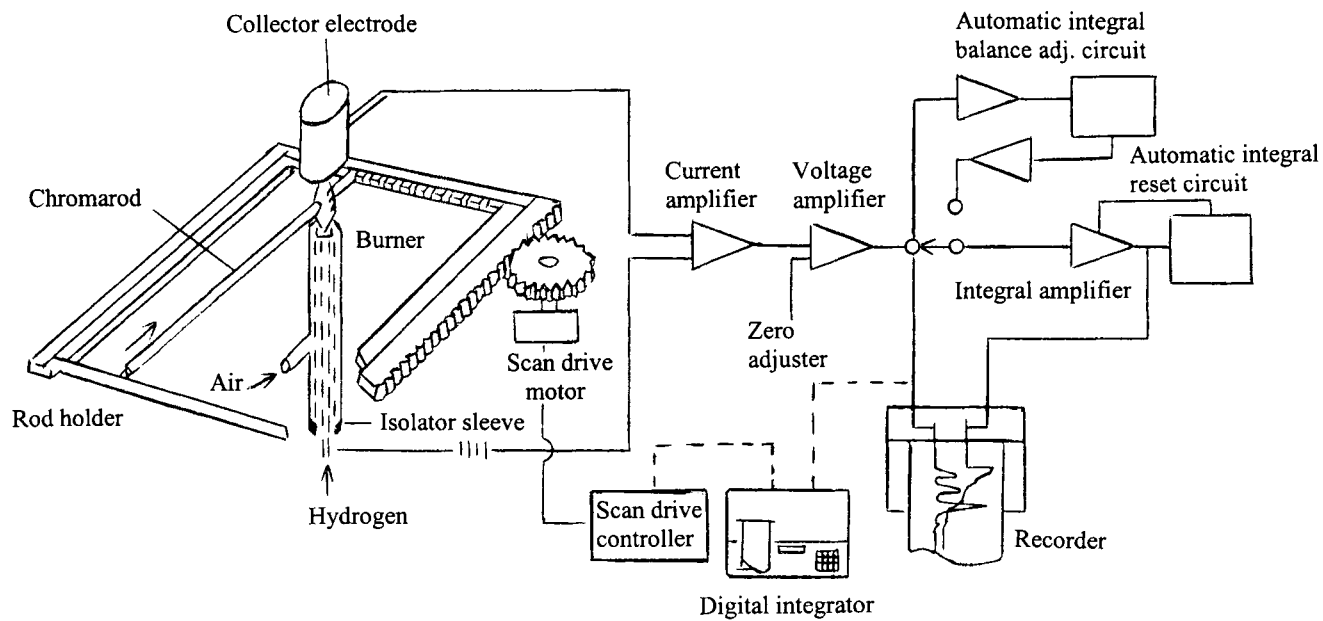


Fig. 11-6. Construction of a coated-rod TLC scanner, Iatroscan TH-10 MkIII [17].

compared to about 2 days per sample by the routine SARA procedure [23]. Therefore, the destructive TLC–FID has been adopted in order to overcome the deficiency of the more time-consuming procedure.

Linearity of the response with the concentration is important in quantification [21]. The sample size, the flow rate of hydrogen fed to the FID, and the speed of scanning have considerable effect on the linearity of response by the FID, baseline stability of the FID signal, and reproducibility of response factors, respectively. Thus, the proper operation of both chromatography and scanning are crucial for satisfactory sensitivity of detection and reproducibility in quantitative analysis by TLC–FID technique.

#### QUANTITATIVE ASPECTS OF TLC DEVELOPED

##### *TLC*

TLC is suitable for qualitative identification of asphalt, but not for the quantitative analysis. For quantification, the zone elution method can be used to determine the fractionated components of asphalt. The zones are scraped and transferred carefully to a suitable container. The fractionated component is eluted from the sorbent using a proper solvent that provides complete, or at least reproducible, recovery. The quantitative recovery of the material from conventional TLC is difficult. The recovery rate can reach only about 90% for the light fraction, because of the loss of light boiling material during the solvent removal step. Therefore, the semi-quantitative analysis can be accomplished by conventional TLC method.

##### *Chromatotron*

Chromatotron is an effective method for separating and collecting fractionated components of asphalt. By selecting the right cut-off point for changing the collecting container, the fractionated components can be separated and preserved with good purity in the containers. This technique is superior to the column chromatography, because it saves adsorbent, solvent and sample. Chromatotron is also a more time-saving method. By evaporating the light fraction away, TLC can clearly reveal the residual fractions of higher molecular weights. Unfortunately, this preparative chromatotron method still takes about 3 to 6 h to completely evaporate the solvent from each sample fraction.

##### *TLC–FID*

TLC–FID method has the potential to become a major tool for determination (quantitative analysis) of the composition of heavy hydrocarbon mixtures, because it is fast, simple, effective, and inexpensive. FID quantitative results can be obtained by integrating the peak area corresponding to each fraction. Calibration can be done by accumulating sufficient materials from a TLC plate or Chromatotron, and performing a TLC–FID measurement. Linearity of the FID response with the concentration is important in quantification.

The matrix method also can accomplish the quantification of TLC–FID analysis. The TLC–FID matrix created by synthetic asphalt (a combination of four fractions) can be used to replace the calibration curve (internal standard) for asphalt analysis and overcome the difficulty of impure sample for calibration [28].

In this step, the following matrix and formula were used to compute sixteen coefficients for calibrating each fraction's chemical contents in the asphalt system from the ratio of the area to the weight percentage ( $WT_j$ ):

$$\begin{bmatrix} C_{si} \\ C_{ai} \\ C_{ri} \\ C_{ni} \end{bmatrix} = \begin{bmatrix} F_{s1} & F_{s2} & F_{s3} & F_{s4} \\ F_{a1} & F_{a2} & F_{a3} & F_{a4} \\ F_{r1} & F_{r2} & F_{r3} & F_{r4} \\ F_{n1} & F_{n2} & F_{n3} & F_{n4} \end{bmatrix} \times \begin{bmatrix} A_{si} \\ A_{ai} \\ A_{ri} \\ A_{ni} \end{bmatrix} \quad (11-3)$$

where  $C$  is the concentration,  $F$  is the coefficient, and  $A$  is the area. The subscripts are: 's', saturates; 'a', aromatics; 'r', resins; and 'n', asphaltenes.

$$WT_j (\%) = C_{ji} \times 100 / (C_{si} + C_{ai} + C_{ri} + C_{ni}) \quad (11-4)$$

$i = 1, 2, 3, 4, \quad j = s, a, r, n$

Data obtained from the integrator were used to calculate sixteen coefficients on the matrix by using the Gauss–Jordan elimination method modified by Pascal [25–27]. The matrix obtained from the normal order was called the normal matrix, and the one from the inverse order was called the inverse matrix. Actually, four mixed sample solutions can produce one matrix as above, so that five matrices can be obtained for five mixtures.

## CONCLUSION

Thin-layer chromatography has great potential of becoming a standard method for quantification of asphaltic components. Compared with ASTM D4124 and SARA methods, it is rapid, accurate, needs only a small amount of sample, and does not involve complicated instrumentation. Preparative TLC as well as centrifugal high performance TLC (Chromatotron) are capable of isolating material in amounts required for further identification by other instrumental techniques. TLC interfaced with FID (TLC–FID) is a destructive method operating quickly and easily, using a simple solvent elution procedure. The time-consuming process of fractionation with solvents can, thus, be avoided.

## REFERENCES

- [1] Izatt, J., Asphalt. In: J.J. McKett (Editor), *Encyclopedia of Chemical Processing and Design*, 3. Marcel Dekker, New York, p. 421 (1986).
- [2] Yen, T.F., Asphaltic materials. In: H.F. Mark et al. (Editors), *Encyclopedia of Polymer Science and Engineering* (2nd ed.). Wiley, New York (1990).
- [3] Altgelt, K.H., Jewell, D.M., Latham, D.R. and Selucky, M.L., *Chromatography and Petroleum Analysis*. Marcel Dekker, New York, pp. 194–196 (1976).
- [4] *ASTM D4124, Standard Test Method for Separation of Asphalt into Four Fractions*. American Society for Testing and Materials, Philadelphia, PA (1988).

- [5] Lian, H., Lee, C.Z.H., Wang, Y.Y. and Yen, T.F., Characterization of asphalt with the preparative chromatotron. *J. Planar Chromatogr.*, 5: 263–266 (1992).
- [6] Yen, T.F., The colloidal aspect of a macrostructure of petroleum asphalt. *Fuel Sci. Technol. Int.*, 10 (4–6): 723–733 (1992).
- [7] Izmailov, N.A. and Shraiber, M.F., *Farmatsiya*, 3: 1–7 (1938).
- [8] Touchstone, J.C. and Dobbins, M.F., *Practice of Thin-Layer Chromatography*. Wiley, Chichester, Chapter 1 (1977).
- [9] Killer, F.L.A. and Amos, R., *J. Inst. Petrol.*, 52: 315–328 (1966).
- [10] Mathews, P.J., Thin-layer chromatography for identification of petroleum and coal-tar oil and residues. *J. Appl. Chem.*, 20: 87–92 (1970).
- [11] Poirier, M.A. and George, A.E., A rapid method for hydrocarbon-type analysis of heavy oils and synthetic fuels by pyrolysis thin-layer chromatography. *Energy Sources*, 7 (2): 151–164 (1983).
- [12] Poirier, M.A. and George, A.E., Thin-layer chromatographic method for determination of asphaltene content in crude oils and bitumens. *Energy Sources*, 7 (2): 165–175 (1983).
- [13] Coates, J.P., The analysis of lubricating oils and oil additives by thin-layer chromatography. *J. Inst. Petrol.*, 57: 209–217 (1971).
- [14] Wang, Y.Y. and Yen, T.F., Rapid separation and characterization of fossil fuels by thin-layer chromatography. *J. Planar Chromatogr.*, 3: 376–380 (1990).
- [15] Masterton, W.L., Slowinski, E.J. and Stanitski, C.L., *Chemical Principles*. CBS College Publishing, Philadelphia, PA, p. 356 (1986).
- [16] Weast, R.C. (Editor), *Handbook of Chemistry and Physics* (66th ed.). CRC Press, Boca Raton, FL, pp. 676–678 (1985).
- [17] *Iatroscan TH-10, Instrument application*. Iatron Laboratories, Tokyo (1982).
- [18] Sharma, J. and Fried, B., *Handbook of Thin-Layer Chromatography*. Chromatographic Science Series, 55. Marcel Dekker, New York (1991).
- [19] Selucky, M.L., Quantitative analysis of coal-derived liquids by thin-layer chromatography with flame ionization detection. *Anal. Chem.*, 55: 141–143 (1983).
- [20] Poirier, M.A. and George, A.E., Rapid method for the determination of malthene and asphaltene content in bitumen, heavy oils, and synthetic fuels by pyrolysis TLC. *J. Chromatogr. Sci.*, 21: 331–333 (1983).
- [21] Poirier, M.A., Rahimi, P. and Ahmed, S.M., Quantitative analysis of coal-derived liquids residues by TLC with flame ionization detection. *J. Chromatogr. Sci.*, 22: 331–333 (1984).
- [22] Behar, F. and Pelet, R., Characterization of asphaltenes by pyrolysis and chromatography. *J. Anal. Appl. Pyrolysis*, 7: 121–135 (1984).
- [23] Fuhr, B.J., Holloway, L.R. and Reichert, C., Rapid analytical characterization of residues from heavy oil and bitumen upgrading processes. *J. Can. Pet. Technol.*, Sept.–Oct.: 28–32 (1986).
- [24] Pollard, S.J., Hrudehy, S.E., Fuhr, B.J., Alex, R.F., Holloway, L.R. and Tosto, F., Hydrocarbon wastes at petroleum- and creosote-contaminated sites: rapid characterization of component classes by thin-layer chromatography with flame ionization detection. *Environ. Sci. Technol.*, 26: 2528–2534 (1992).
- [25] Jenson, K., *Pascal User Manual and Report: ISO Pascal Standard* (4th ed.). Springer-Verlag, New York (1991).
- [26] Koffman, E.B., *Pascal, a Problem Solving Approach*. Addison-Wesley, Reading, MA (1982).
- [27] Dodes, I.A., *Numerical Analysis for Computer Science*. North-Holland, New York (1978).
- [28] Lian, H., Dunn, K. and Yen, T.F., Unpublished results (1992).



This page intentionally left blank

## Chapter 12

# PRECIPITATION OF ASPHALTENES IN HEAVY OIL AND TAR SANDS

NORMAN F. CARNAHAN

## INTRODUCTION

Asphaltenes precipitate from petroleum mixtures as a result of complex phenomena involving at least three categories of mechanisms, individually and in various combinations: (1) classical solid–fluid and fluid–fluid equilibrium, including nucleation, agglomeration, precipitation, and interfacial phenomena; (2) ionic and/or electrochemically induced agglomeration; and (3) mechanical shear-induced agglomeration.

Each of these precipitation mechanisms for asphaltenes can be described in terms of fundamental physical and thermodynamic principles. The present work shall attempt to summarize some of the principles involved in asphaltenes separation from crude petroleum mixtures. First, it is necessary to define some terms that will be discussed.

### *Definition of terms*

*Asphaltenes* are herein defined as those petroleum components, that are residues, determined using industry-accepted analytical laboratory procedures, typically using *n*-heptane or *n*-pentane as the precipitation-inducing fluid. Asphaltenes are essentially polynuclear aromatic components of the  $C_7^+$  fraction, which contain very few alkyl groups per aromatic ring. Asphaltene structures also contain sulfur, nitrogen, oxygen, and certain metals (nickel, vanadium, etc.). They are lipophobic [1] polar macromolecules, having average carbon numbers in the range of about 40 to 80. They are very solubilizable in toluene, but exhibit very limited solubility or solubilizability in low carbon number normal alkanes. In crude oil, asphaltenes commonly exist as aggregates of 2 to 100 individual macromolecular asphaltenes ‘adhesive particles’ or platelets. Other polar constituents of the heavy fraction are resins and aromatics<sup>1</sup>.

*Petroleum resins* exhibit structural similarities to asphaltenes. They are polynuclear aromatic structures; however, resins contain more alkyl attached groups (side-chains) per aromatic ring. They contain fewer nonhydrocarbon atoms per molecule. The effect of the alkyl groups is such that the resins exhibit lipophilic behavior [1] and have average molecular weight values lower than those of asphaltenes. Petroleum resins appear to form a nonadhesive skin or peptide coating of the asphaltenes aggregates.

Aggregates of lipophobic asphaltenes physically combine with lipophilic resins to form a reverse micelle, which is dispersed in the asphaltenes-free petroleum fluid, apparently as a colloidal system in crude oil.

<sup>1</sup> One must exercise caution in reading the literature on asphaltenes, paying special attention to which solvent is used for obtaining the material referred to as ‘asphaltenes’.

## MECHANISMS

Fig. 12-1 describes an idealized spherical micellar configuration of an asphaltene-resins amphiphilic complex. Aggregated asphaltenes are depicted as the dark central sphere. Resins are depicted as an idealized concentric film or zone that surrounds the core of asphaltenes. The outermost portion of the resinous film is in contact with the continuous hydrocarbon or crude oil phase, whereas the innermost portion of the resinous film is in contact with the asphaltene core material. At equilibrium, micelles composed of asphaltenes and resins are assumed to be dispersed in the continuous hydrocarbon fluid.

Phase separation, aggregation, and precipitation of asphaltenes from heavy oils and tar sands depend upon the composition, thermal and mechanical conditions, which existed at the time of formation of the original mixture. The phenomenon also depends upon the composition, thermal and mechanical histories of the system until the time that conditions change sufficiently to result in nucleation, agglomeration, phase separation and/or precipitation of asphaltenes as solids or pseudo-solids. After phase separation occurs, the precipitation and/or deposition mechanisms are governed by viscosity and diffusion characteristics of the asphaltene-free petroleum fluid. In lighter petroleum liquids, aggregated asphaltenes can precipitate and deposit with relative ease; however, in heavy crudes and tar sands, even though phase separation and agglomeration of asphaltenes occur, transport mechanisms (e.g., convection and diffusion) proceed at a slower rate and inhibit the precipitation process.

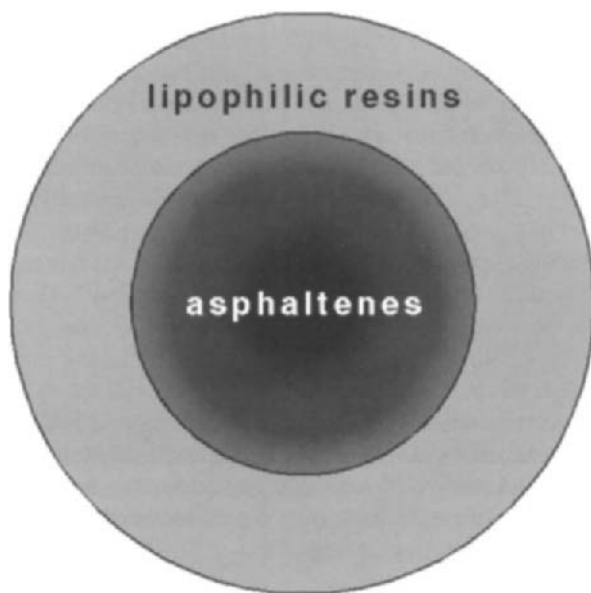


Fig. 12-1. Model of asphaltenes + resins micelle. Resins act as an amphiphilic agent between the continuous hydrocarbon fluid phase and the asphaltene aggregate complex.

### *Solid–fluid and fluid–fluid phase equilibrium*

In petroleum reservoir fluids, asphaltenes can exist in at least two distinct forms: (1) as dissolved asphaltenes monomers and low-order ‘enmers’, and (2) as solubilized amphiphilic structures, such as reverse micelles, composed of resins and asphaltenes, for example. The latter is the more commonly encountered form.

A distinction must be made between the concepts of *solubility* and *solubilization*, as the terms are used herein. In the case of *solubility*, a substance is truly in solution (i.e., dissolved) in a continuous fluid solvent. The dissolved substance is usually very compatible with the solvent phase. In the case of *solubilization*, a substance may exist in a dispersed or colloidal state suspended (solubilized) in a continuous fluid medium. The solubilized substance can be solid, an immiscible liquid phase, or micellar complexes, etc.

Macroscopically, especially in the case of microemulsions and colloidal suspensions in obscure fluids, many outward appearances and behaviors of solutions and solubilized systems appear to be the same.

### *Solubility theory and asphaltenes*

A number of studies have successfully used a macroscopic approach to correlate apparent asphaltenes precipitation behavior, assuming that asphaltenes are soluble in crude oil; however, using the classical solution theory in that manner is not in accord with experimental evidence obtained on the microscopic scale. Solution theory methods are indeed applicable on the macroscopic and microscopic scale; however, in that case, the ‘solute’ is resinous material, naphthenates, and other substances that act as natural amphiphiles and peptize asphaltenes agglomerates, inhibiting their aggregation and precipitation from the petroleum system.

The following review outlines the basis for application, on the macroscopic scale, of the classical solution theory to this phenomenon and presents an alternate interpretation of the physical evidence, using a point of view that is consistent with experimental results obtained on the microscopic scale. For reasons of simplicity, a hypothetical 3-component system composed of asphaltenes, resins and asphaltenes-free oil will be considered.

### *Solubility of resins and asphaltenes*

Solution theory predicts that high molecular weight, relatively nonvolatile hydrocarbon components, such as macromolecular paraffins, resins and, perhaps, some low molecular weight asphaltenes, are of limited solubility in lower molecular weight solvents, such as paraffinic and aromatic lighter ends of naturally-occurring petroleum reservoir fluids. In terms of chemical structure, asphaltenes are complex polynuclear aromatic, high molecular weight petroleum components, which include hydrocarbon, and nonhydrocarbon groups, such as nitrogen, oxygen, sulfur, vanadium, nickel, etc.

A minor amount of asphaltenes may be truly dissolved in lighter ends, especially in highly aromatic reservoir fluids. When conditions change, such that the solubilizing capacity of the lighter ends decreases, the system becomes effectively supersaturated.

From the supersaturated system, nucleation, agglomeration and precipitation of the excess amount of solubilized components (e.g., asphaltenes, resins, and/or macromolecular paraffins) will result, in accordance with principles of macroscopic phase behavior.

A change in the solubilizing capacity of the continuous external phase (e.g., the asphaltenes-free fluid), can result from: (1) variation of the temperature of the solution; (2) addition of components which compete with asphaltenes for the solvent, or which affect the solubilizing power of the solvent such that the characteristic solubility parameters of the solvent and the solute become increasingly similar or dissimilar; and/or (3) variation of the pressure of the system, such that the density of the solvent phase varies sufficiently to affect the solubilizing power of the continuous fluid phase.

#### *Macroscopic point of view*

Hirschberg and Hermans [2] and others have presented macroscopic models for calculation of solid-liquid phase equilibrium, assuming that asphaltenes are indeed soluble in crude oil and that precipitation is thermodynamically reversible. Fussel [3] describes solid-liquid equilibrium for asphaltenes in terms of vapor-liquid and liquid-liquid phase behavior. Others have described the phenomenon in terms of Flory-Huggins and/or regular solution concepts developed for polymer solutions. Labout [4], Mitchell and Speight [5], Rogacheva et al. [6], Waxman et al. [7], Burke et al. [8], Thawer et al. [9] and Kawanaka et al. [10] describe asphaltene precipitation mechanism(s) in terms of solubility parameter variations between solubilized asphaltenes and the solvent portion of several crudes. Hirschberg and Hermans [2] applied such a model to describe asphaltenes precipitation from an Iranian crude oil and a North Sea crude oil. Using the macroscopic point of view, one can examine the applicability and consequences of using the classical solution theory to correlate experimental results for apparent solubility of asphaltenes in crude oils and liquid hydrocarbons. Solubility is consistent with reversible solid-liquid phase behavior. In the absence of complex formation in the precipitate, solubility would mean that the precipitate could be redissolved in the liquid by restoring the system to the initial conditions.

#### *Microscopic point of view*

As early as 1923, Nellensteyn [11] defended the point of view that asphaltenes are not in solution in crude oil; rather, they exist in the form of a colloidal suspension in crude oil. If true, then classical solution theory should not apply to the phase equilibrium for asphaltenes precipitation from crude oil. Yet, solution theory might be useful to describe the phase equilibrium between amphiphilic resins and crude oil. The interfacial phenomenon requires simultaneous consideration of Langmuir-type adsorption equilibrium between amphiphilic resins and 'crude oil insoluble' material(s), including asphaltenes. Thus, one needs to solve interfacial adsorption equilibrium equations for the resins + asphaltenes system simultaneously with solubility phase equilibrium equations for the resins + oil system. Solubilization is consistent with irreversible solid separation from the liquid phase.

*Characterization of the petroleum heavy fraction*

Regardless of which point of view one adopts, the complex nature of the petroleum system, in the case of crude oils and tar sands, requires careful characterization in terms of the components and/or pseudo-components contained therein. Traditionally, crude oils have been characterized on the basis of a distillation curve. More recently, it is becoming well recognized that detailed analysis of many narrow boiling cuts is necessary for proper phase equilibrium and thermodynamic calculations. For the oils considered by Hirschberg and Hermans [2], extended composition analyses, derived from regression of mole percents vs. carbon number, result in the following correlation formulas:

$$\text{Iran: Mol.\%} = 10.29 \times [10^{(-0.106 \text{ CN})}]$$

$$\text{North Sea: Mol.\%} = 8.75 \times [10^{(-0.107 \text{ CN})}]$$

The exponents indicate that the slopes of the composition correlations for these two crude oils, on a semi-logarithmic graph, are very similar. The major difference is the magnitude of the pre-exponential coefficient, which relates to the intercept on the vertical axis of a semi-logarithmic graph. Although the oils in the examples used by Hirschberg and Hermans [2] are inherently different, their estimated distribution of higher carbon number components appears to be semi-logarithmic. The semi-logarithmic distribution of macromolecules in petroleum fluids was empirically observed by Whitson [12] and has been justified on theoretical grounds by Levelt-Sengers and de Swaan-Arons [13]. Correlation of extended composition of the high carbon number components in this manner supports the applicability of polymer solution theory for macroscopic description of these phenomena.

*Calculation method — macroscopic model*

Hirschberg summarizes, from a macroscopic point of view, the apparent effects of temperature, pressure and composition on the deposition of asphaltenes from liquid petroleum.

Hirschberg [14] used the Soave equation of state for VLE calculations, assuming a negligible amount of solid asphaltenes-rich phase, based on a 22-component representation of the crude oil. Light ends, methane through hexanes, including nitrogen and carbon dioxide, were determined by PVT analysis. The  $C_7^+$  fraction was subdivided into six paraffin pseudocomponents and six aromatic pseudocomponents. Alternatively, one can characterize the  $C_7^+$  fraction as a continuous mixture, using semi-logarithmic correlations (as previously described), and subportions (e.g., boiling point cuts) of the semi-continuous mixture can be characterized according to their paraffin/naphthene/aromatic (PNA) distributions, as pointed out by Mansoori and Jiang [15]. The PNA ratio for various petroleum fractions can be defined experimentally or estimated in terms of exhibited PVT properties, using such correlations as presented by Yarborough [16]. No matter how the  $C_7^+$  fraction is characterized, it is necessary to properly define the amount of resins and asphaltenes in the heavy end fractions.

Solid–fluid phase equilibrium can be approximated using rigorous thermodynamic criteria for phase equilibrium. The presence of a solid phase or an immiscible liquid phase has a similar mathematical definition in terms of phase equilibrium calculations.

Consider the following analysis:

$$\mu_i^A = \mu_i^{CO} \quad (12-1)$$

Subscript  $i$  pertains to the  $i$ -th component and superscripts 'CO' and 'A' pertain to the 'crude oil-rich phase' and the 'asphaltenes-rich phase', respectively.

Considering size-related entropy effects, it is proposed that:

$$\frac{\mu_i - \mu_i^o}{RT} = \ln \phi + 1 - \frac{V_i}{\langle V \rangle} + \chi_i \quad (12-2)$$

where:  $\mu_i^o$  = chemical potential of pure-component  $i$  as a liquid;  $\phi_i$  = volume fraction of component  $i$  in the liquid mixture [ $x_i V_i / \langle V \rangle$ ];  $V_i$  = molar volume of pure-component  $i$  as a liquid;  $x_i$  = mole fraction of component  $i$  in the liquid phase,

$$\langle V \rangle = \sum_i x_i V_i \quad (12-3)$$

and

$$\chi_i = \frac{V_i}{RT} [\langle \delta \rangle - \delta_i]^2 \quad (12-4)$$

where

$$\langle \delta \rangle = \sum \phi_i \delta_i \quad (12-5)$$

$$\delta_i^2 = \frac{\Delta U_{\text{vap}}^o}{V_i} \quad (12-6)$$

$\Delta U_{\text{vap}}^o$  = molar internal energy difference due to isothermal vaporization between the liquid state and the ideal gas state.

It is assumed, in this method, that the 'asphaltenes-rich phase' is 100% asphaltenes; therefore,

$$\mu_A^A = \mu_A = \mu_A^{CO} \quad (12-7)$$

Hirschberg [14] and Kawanaka et al. [10] present an estimation of the maximum volume fraction of asphaltenes in solution with degassed crude oil, i.e.,

$$(\phi_A)_{\text{max}} = \exp \left\{ \frac{V_A}{V_{CO}} \left[ 1 - \frac{V_{CO}}{V_A} - \frac{V_{CO}}{RT} (\delta_A - \delta_{CO})^2 \right] \right\} \quad (12-8)$$

The composition of degassed crude oil remains practically invariant above the bubble point. The numerical value of the solubility parameter of the crude oil is inversely proportional to the molar volume of the liquid, which normally decreases with increasing pressure. Therefore, the apparent solubility parameter of live crude oil usually increases with increasing pressure. Likewise, the apparent solubility parameter of live crude oil usually decreases as pressure decreases.

#### *Apparent solubility parameter for asphaltenes*

The apparent solubility parameter of asphaltenes, determined via correlation of macroscopic thermodynamic data using a regular solution theory model, is approximately 10 hildebrands [1 hildebrand =  $0.1 (\text{cal/cm}^3)^{0.5}$ ]. Hirschberg et al. [19] report the apparent solubility parameter of asphaltenes in crude oil to be about 9.8 hildebrands ( $20 \text{ MPa}^{0.5}$ ). Burke et al. [8] found the apparent solubility parameter of 'asphaltenes sludge' to be about 10.0 hildebrands ( $20.5 \text{ MPa}^{0.5}$ ).

*Solubility parameters of petroleum fluids*

Solubility parameter values for light crude components depend on composition, and are often in the range of about 6–8 hildebrands. Lower molecular weight alkanes exhibit solubility parameters of lower numerical value, relative to those of higher molecular weight hydrocarbons. Hirschberg and Hermans [2], Burke et al. [8], Thawer et al. [9], and Kawanaka et al. [10] have noted the relationship between the composition (*or molecular weight*) of the continuous fluid, and the ability of crude oil to maintain asphaltenes in apparent solution. Solubility parameter values for medium and heavy oils are greater than those for light oils. Only a limited amount of reliable experimental data has been reported, although none for asphaltenes phase behavior in heavy oils and tar sands. The expected value of the solubility parameter of such heavy petroleum fluids is about 8–10 hildebrands.

Table 12-1 shows the general effect reported by Wuithier [35] which demonstrates the significant role of molecular weight (*hence the solubility parameter*) on hydrocarbon fluid compatibility with asphaltenes. Table 12-2 lists solubility parameters for several hydrocarbons, showing that the solubility parameter characteristically increases with molecular weight and/or carbon number for alkanes. Aromatic substances exhibit solubility parameters similar to the apparent solubility parameter for asphaltenes.

TABLE 12-1

Amount of asphaltenes precipitated vs. solvent molecular weight at 323.15 K (122°F) [35]

Solvent (mol wt.)	Asphaltenes precipitated (mass percent)
30 ( <i>n</i> -C <sub>2</sub> )	90.0
44 ( <i>n</i> -C <sub>3</sub> )	22.5
58 ( <i>n</i> -C <sub>4</sub> )	10.0
72 ( <i>n</i> -C <sub>5</sub> )	4.0
86 ( <i>n</i> -C <sub>6</sub> )	1.0
100 ( <i>n</i> -C <sub>7</sub> )	less than (1.0)

TABLE 12-2

Solubility parameters of various alkane and aromatic hydrocarbons

Component	$\delta$ (hildebrands)	Component	$\delta$ (hildebrands)
Propane	6.0	<i>n</i> -Heptane	7.45
<i>n</i> -Butane	6.7	<i>n</i> -Octane	7.55
<i>i</i> -Butane	6.25	<i>n</i> -Nonane	7.65
<i>n</i> -Pentane	7.05	<i>n</i> -Hexadecane	8.00
<i>i</i> -Pentane	6.75	Benzene	9.15
neo-Pentane	6.25	Toluene	8.90
<i>n</i> -Hexane	7.30	Naphthalene	9.90



Alkanes typically exhibit lower solubility parameter values than aromatic hydrocarbons, which macroscopically appear to be more compatible with heavy crude oils and asphaltenes. The linear mixing rule, according to their volume fractions in the mixture, enables blending of solvent mixtures to obtain a desired value of the effective solubility parameter. Such blending of solvents was used by Burke et al. [8], who reported experimental results of asphaltenes deposition from simulated field crude oil mixtures.

#### *Solubilization of asphaltenes (microscopic viewpoint)*

Although Hirschberg and Hermans [2] and Burke et al. [8] were able to correlate observed macroscopic effects of asphaltenes precipitation from crude oils and hydrocarbon fluids, the concept of asphaltenes solubility in crude oils may have been over-extended and/or obscured in the cause-and-effect relationship assumed in the correlation model. There is no doubt that asphaltenes can precipitate as a result of changing the composition of the fluid. Such change in the composition is the basis for the well-established laboratory method for determining the asphaltenes content of petroleum fluids, e.g., addition of *n*-pentane or *n*-heptane to a sample of petroleum fluid. Asphaltenes precipitate as a result of such changes in the composition of crude oil. It does not necessarily follow, however, that asphaltenes precipitate from petroleum fluid due to a decrease in their solubility in the petroleum fluid, as a result of the addition of lower molecular weight alkanes. The key question is: are asphaltenes soluble in crude oil or do asphaltenes exist in a colloidal state in crude oil? A preponderance of experimental evidence and field observations indicate that asphaltenes exist in a colloidal state in crude petroleum.

It is, indeed, tempting to conclude that precipitation of asphaltenes results from a significant difference between the solubility parameter of the fluid mixture and the solubility parameter of the asphaltenes. On the macroscopic scale, one can certainly develop such an argument. However, such a conclusion appears at odds with considerable evidence indicating the colloidal nature of asphaltenes in petroleum fluids [21–23]. Waxman et al. [7] and Hotier [24] indicate that asphaltenes precipitation may not be fully reversible.

From the microscopic point of view, however, asphaltenes are assumed to have little or no solubility in crude oil. Asphaltenes are assumed to be an insoluble or immiscible material that is solubilized in the crude oil in the form of colloidal particles or similar amphiphilic structures, with the help of naturally-occurring resins and similar amphiphilic components of the crude oil.

Using a microscopic model, it is obvious that a key factor in the stability of asphaltenes in petroleum fluids is the integrity of the protective film of the amphiphilic material that surrounds the core of asphaltenes. Anything that damages or removes the amphiphilic film allows the aggregation of asphaltene particles that can result in precipitation or deposition. Likewise, anything which enhances the amphiphilic film would stabilize the system. Experiments have shown that addition of resins or amphiphiles can increase the stability of asphaltenes in certain crude oils [36,38–42]. According to established models of phase behavior involving reverse micelles (*so called, because the oil is on the outside and the 'non-oil' is on the inside of the micelle*), it is acceptable to characterize the phase behavior of asphaltenes using classical solubility theory. However, in this case, the solute is the amphiphilic substance(s) and the solvent

is the asphaltenes-free petroleum fluid. Asphaltenes are assumed to be, for all practical purposes, totally immiscible and/or insoluble in the asphaltenes-free petroleum fluid.

As a consequence of the microscopic model, then, existing precipitation data for asphaltenes suggest that the mutual compatibility of resins and petroleum fluid increases as the average molecular weight of the petroleum fluid decreases. Thus, the effective solubility parameter value for amphiphilic resins must be similar to that of the lower carbon number alkanes, i.e., about 5–6 hildebrands.

The microscopic point of view also indicates that asphaltenes are not soluble in the higher molecular weight petroleum fluids, but remain suspended in them, as stable colloidal particles. Likewise, asphaltenes precipitate when low carbon number alkanes are added to petroleum fluid, due to the destabilization of the colloidal particles, with resultant coalescence, agglomeration and precipitation. This viewpoint is quite the opposite of that which Hirschberg [14] and Burke et al. [8] assumed. The experimental picture, on the macroscopic scale, is indefinite with regard to the true mechanism leading to precipitation of asphaltenes. Evidence from the microscopic scale must be used to distinguish among competing mechanisms, only two very simplified versions of which are presented here.

One also has to include in such a microscopic model a definition of the interfacial adsorption effects, between the resins and the asphaltenes. There is a competition between the asphaltenes and the asphaltenes-free petroleum for the resins and other naturally occurring amphiphiles. When temperature, pressure or composition changes such that the asphaltenes-free petroleum fluid exhibits greater compatibility with the resins, a certain amount of the resins are solvated away from their protective role surrounding the reverse micelles. As a result, some micelles become unstable, coalesce or agglomerate to form larger micelles, and may precipitate from the fluid or deposit on solid surfaces.

The previously described entropy-modified regular solution theory model for the fluid phase can be combined with a suitable model of adsorption of amphiphilic substances, such as resins, at the asphaltenes–petroleum fluid interface. The resulting model, including fluid–fluid equilibrium and fluid–nonfluid interfacial effects, indicates that simultaneous solution of both types of equilibrium equations is necessary in order to correlate and/or predict the phase behavior of systems such as oil + resins + asphaltenes.

#### *Microscopic vs. macroscopic models*

Interestingly, phase equilibrium of asphaltenes in crude oil can be correlated with reasonable success using either the macroscopic or the microscopic point of view. The fundamental picture strongly favors the microscopic model as a true representation of the physical phenomenon. From the macroscopic viewpoint, one observes an apparent inverse relationship between precipitation of asphaltenes and the effective solubility parameter of the crude oil. Asphaltenes appear to have a solubility parameter of about 10 hildebrands and tend to precipitate in increasing amounts as the effective solubility parameter of the petroleum fluid decreases below approximately 9 hildebrands. This observation is based upon, among other factors, the assumed relationship between solubility of asphaltenes and the magnitude of the difference in solubility parameters of the solvent and the asphaltenes, i.e.,  $(\delta_A - \delta_{CO})^2$ .

On the microscopic scale, the solubility relation between resins and petroleum fluid is assumed to be modeled by similar physics, e.g.,  $(\delta_R - \delta_{CO})^2$ .

In this scenario, however, resins appear to be increasingly soluble in the petroleum fluid as the solubility parameter of the petroleum fluid decreases from about 9–10 hildebrands toward about 5–6 hildebrands. Thus, one is led to observe that the apparent solubility parameter of petroleum resins is in the range of about 5–6 hildebrands. Asphaltenes are assumed to be negligibly soluble in petroleum fluid. Interfacial adsorption effects, between resins and asphaltenes can be described in terms of Langmuir-type models using parameter values determined from experiments.

### *Ionic and/or electrochemically induced asphaltene precipitation*

Changes in the ionic and/or electrochemical environment of asphaltenes in crude oil can cause flocculation of microscopic asphaltenes particles in the crude oil. Reports of asphaltenes deposition following acidizing procedures are common. The nature of asphaltenes particles in crude oil is such that they exhibit polarity and/or induced polarity. Although a resinous skin usually protects and stabilizes asphaltenes aggregates, the polar resins can be affected by changes in pH and/or mineral ion environment. Contact with acids and with mineral ions favor flocculation and deposition of asphaltenic solids.

Consider resins to have a net charge that is electrically opposite to that of asphaltenes, such that the resins are attracted to the asphaltenes globule and tend to render the resins + asphaltenes particle electrically neutral. Indeed, this is a possible mechanism whereby resins can be attracted to the asphaltenes–resins interface. Upon contact with a strong solution of acid and/or ionic solution of minerals, especially iron, calcium and magnesium, the resins may be attracted away from the asphaltenes, such that unprotected asphaltenes particles agglomerate and precipitate as a sludge, together with coagulated resins and minerals.

Asphaltene deposits are frequently encountered following acidizing procedures downhole, even when asphaltene deposits had not been a problem before the acidizing procedure. Such deposition seems to result from interaction between ions and the polar asphaltenes globules, resembling a process of coagulation or flocculation. Chemical analysis of such deposits commonly shows the presence of minerals such as iron, calcium and magnesium.

Models for correlating and predicting this ion-related mechanism for asphaltenes deposition need to account for the association effect between the ‘monomers’ and the ‘monomer complexes’. Heidemann and Prausnitz [18], Jackson et al. [20], and Suresh and Elliott [25] present models useful for describing phase equilibrium, chemical equilibrium and PVT behavior of associating substances. For example, consider the reversible interaction



If ‘A’ represents an individual asphaltene particle or globule, such that two such globules associate to form a ‘2A’ dimer, then the computation of equilibrium composition of coexisting phases must also involve the simultaneous solution of the association

equilibrium, which can be viewed either as a chemical reaction or a physical combination. In nature, the combination mechanism of asphaltenes particles is quite complex, involving a distribution of particles and groups of particles. The general problem of particle association is well suited to statistical mechanical analysis, and has been studied by Wertheim [26], Chapman et al. [27], and others.

Empirical methods for predicting and correlating the association of asphaltenes particles and their precipitation due to ionic effects involve application of equations of state for associating substances. To date, researchers using these methods have not extensively studied the problem of asphaltenes. This area of research should be of interest to companies that experience costly production problems due to asphaltenes.

### *Mechanical shear-induced asphaltenes precipitation*

The concept of asphaltenes as adhesive colloidal particles encased in a thin non-adhesive resinous skin, well dispersed in crude oil, lends itself to the interpretation of shear-induced deposition of asphaltenes solids. Damage or rupture of the resinous skin, by mechanical shear effects and/or solvent action, can result in agglomeration of asphaltenes and precipitation of solids from crude oil.

Shear effects occur when the fluid is subjected to high-energy shear fields, such as in turbulent flow through porous media, perforations and screens, sudden acceleration in production tubing, surface and downhole pumps and chokes. Such effects may also result from injection of gas into crude oil, as in gas lift production systems.

The literature contains very little reliable experimental data pertaining to mechanical shear-induced deposition of asphaltenes, although numerous studies of shear-induced alteration of similar colloidal systems have been described. Field experience indicates that such deposition may occur; however, reported data are insufficient for development of useful correlations and/or predictive methods.

## DISCUSSION

### *What is the principal mechanism of asphaltenes precipitation?*

The principal mechanism of asphaltenes deposition seems to be desolubilization, nucleation, agglomeration and precipitation of solid material due to changes in solvent power of crude oil and dissolved light ends. Such phenomenon may result from physical changes in the environment to which crude oil is subjected, such as reduction in pressure from an initially high reservoir pressure toward bubble point pressure of the system. Such phenomenon may also result from the admixture of light ends with a heavy crude. McHugh and Krukoni [28] discuss nucleation phenomena. Andersen and Birdi [29] and Sheu et al. [30] report critical micelle concentrations (CMCs) of asphaltenes. Such studies support the concept of colloidal nature of asphaltene complexes in petroleum fluids.

The apparent solubility parameter for asphaltenes seems to be about 9.54–10.00 hildebrands. The basic principle of solvent action is that 'like dissolves like'. Hildebrand and Scott [31] discuss the regular solution theory, which describes the compatibility

TABLE 12-3

Effect of solvent carbon number on solubility of asphaltenes in tank oil [14]

Solvent	Asphaltenes deposited (wt.%)	$\delta_{CO}$	$(\delta_A - \delta_{CO})^2$
<i>n</i> -C <sub>5</sub>	3.61	7.05	8.7
<i>n</i> -C <sub>7</sub>	1.82	7.45	6.5
<i>n</i> -C <sub>10</sub>	1.45	7.75	5.0

between solute and solvent via a functional relation between their respective solubility parameters, i.e.,

$$\text{Solvent power of crude oil} \propto (\delta_A - \delta_{CO})^2 \quad (12-10)$$

Burke et al. [8] found that the solubility parameter of crude oil, including the effect of dissolved light ends, changes with pressure and temperature, such that  $|\delta_A - \delta_{CO}|$  reaches a maximum. Hirschberg [14] reports asphaltenes solubility in relation to the effective solubility parameter of *n*-alkane solvents. Table 12-3 shows a qualitative forecast of the expected solubility of asphaltenes in three solvents, in terms of the similarity or dissimilarity of their solubility parameters. Agreement between measured and predicted solubility is qualitatively correct, although such measurements are very difficult, often nonrepeatable, and may be of questionable statistical accuracy.

Hirschberg [14,17], Burke et al. [8], and others have found that asphaltenes precipitation can be predicted using a modified version of the regular solution theory, together with established principles of solubility. Mansoori and Jiang [15] and Kawanaka et al. [10] present a method based on the Scott and Magat [32] theory of polymer solutions, using a polydisperse mixture concept of the asphaltenes fraction.

Sufficient evidence shows that precipitation and deposition of asphaltenes can be correlated and predicted using solution theory models such as a Flory-Huggins Modified Regular Solution Theory. Using a macroscopic approach, one can correlate asphaltenes phase separation in terms of the solubility parameter of the solvent. However, a more fundamentally correct approach should account for effects observed on the microscopic scale, i.e., solubility of naturally-occurring amphiphilic resins in the solvent phase, and to model the aggregation of asphaltenes resulting from distribution of resins between the continuous solvent phase and the asphaltenes-rich phase. In order to develop such models and to test theories of solution for asphaltenes, additional reliable experimental data need to be available to theoreticians. Data reported in the literature are useful, although very limited at this time.

#### *Other mechanisms which influence precipitation of asphaltenes*

Solution theory, as reviewed herein, accounts for a very substantial portion of asphaltenes problems experienced in industry. Other mechanisms can also have an effect on solubility of asphaltenes in reservoirs and in deep wells.

Supercritical fluids, such as methane, ethane and propane, act as supercritical solvents at typical reservoir pressures and temperatures, but lose some of their solvent capability

when pressures are reduced. In deep reservoirs in which the reservoir fluid contains a substantial amount of light ends and dissolved gases, supercritical effects can be significant in terms of deposition of asphaltenes and other heavy substances dissolved in or suspended in reservoir fluids. Several mechanisms of supercritical solution phenomena in reservoir fluids have been previously reported [33,34,37].

## SUMMARY AND CONCLUSIONS

This review of fundamentals of the oil + resins + asphaltenes phenomenon in heavy oils and tar sands presents a rational framework for reservoir engineers to use in evaluating the benefits and consequences of proposed production methods and/or operations involving asphaltenic crudes.

(1) Asphaltenes phase behavior is predictable using classical solution theory models of solid-liquid and liquid-liquid phase equilibrium, together with appropriate adsorption equilibrium models for interactions between asphaltenes and resins. Development of improved models requires additional reliable experimental data, including measurements of asphaltenes nucleation, agglomeration and precipitation, and additional phase equilibrium data for well-defined compositions. Precipitation and deposition of asphaltenes in heavy crudes and tar sands is inhibited by transport processes, but may be significant in high-temperature reservoirs. Reliable experimental data for such systems in the literature are very limited at the present time.

(2) Asphaltenes precipitation due to electrochemical effects is not yet well defined. Equations of state for associating fluids have appeared in the literature, but have found few applications relating to asphaltenes precipitation phenomena. Such applications are certainly warranted. Experimental measurements are needed, in order to provide necessary data for development of models for the interaction between asphaltenes and ionic species, and for modeling the behavior of asphaltenes in contact with ionic solutions.

(3) Asphaltenes precipitation and deposition data due to mechanical shear effects have not been reported in the literature; however, the phenomenon is herein described in terms of field experiences. This mechanism should be experimentally investigated in order to define its importance, related to field-experienced problems and problems which may occur in-situ during production of asphaltenic hydrocarbon fluids.

In summary, the state of our knowledge of asphaltenes deposition mechanisms is certainly improved from a decade ago; however, the development of fundamentally correct solution models of asphaltenes behavior is just beginning. With additional reliable experimental data, theoreticians should be able to accurately define the mechanisms and establish interaction parameters between components of the fluid-fluid and fluid-solid systems. Electrochemical effects and mechanical shear effects are not yet sufficiently well defined. Accurate and precise experimental data are needed in order to determine these mechanisms and their practical importance.

In heavy oils and tar sands, although phase separation can be predicted according to rigorous thermodynamic phase equilibrium principles, transport mechanisms interfere with aggregation, precipitation and deposition of asphaltenes from the petroleum fluid. In viscous fluids that experience a quantitative imbalance between asphaltenes and their

associated resins, mechanisms of micelle destabilization, aggregation and precipitation operate on a much slower time scale than for less viscous fluids. Thus, the physical properties of heavy oils and tar sands can ameliorate the problem of asphaltenes drop out, by maintaining such particles in suspension within the fluid phase. Furthermore, due to the dissimilarity between the solubility parameter values for resins and for heavy crudes, resins + asphaltenes micelles tend to remain relatively stable in heavy crudes and tar sands.

## REFERENCES

- [1] Speight, J.G., *The Chemistry and Technology of Petroleum*. Marcel Dekker, New York, pp. 192–194 (1980).
- [2] Hirschberg, A. and Hermans, L., *Asphaltene Phase Behavior: A Molecular Thermodynamic Model*, Publication 676 (Feb., 1984); Koninklijke/Shell E and P Laboratorium, Rijswijk; *Proc. of International Symposium on the Characterization of Heavy Crude Oils and Petroleum Residues*, Lyon (June 1984).
- [3] Fussell, L.T., A technique for calculating multiphase equilibria. *Soc. Pet. Eng. J.*, pp. 203–208 (1979).
- [4] Labout, J.W.A., Constitution of asphaltic bitumen. In: J. Pfeiffer (Editor), *The Properties of Asphaltic Bitumen*. Elsevier, Amsterdam (1950).
- [5] Mitchell, D.L. and Speight, J.G., The solubility of asphaltenes in hydrocarbon solvents. *Fuel*, 52: 149–152 (1973).
- [6] Rogacheva, O.V., Rimaev, R.N., Gubaidullin, V.Z. and Khakimov, D.K., Investigation of the surface activity of the asphaltenes of petroleum residues. *Colloid J.*, 42: 490–493 (1980).
- [7] Waxman, M.H., Deeds, C.T. and Closmann, P.J., Thermal alterations of asphaltenes in Peace River tars. *55th Annu. Tech. Conf. SPE, SPE Pap. 9510*, Dallas, TX (Sept. 1980).
- [8] Burke, N.E., Hobbs, R.E. and Kashou, S.F., Measurement and modeling of asphaltene precipitation. *Proc. SPE Fall Meeting, SPE Pap. 18273*, Houston, TX (Oct. 1988). *J. Pet. Technol.*, pp. 1440–1446 (1990).
- [9] Thawer, R., Nicoll, D.C.A. and Dick, G., Asphaltene deposition in production facilities. *SPE Prod. Eng.*, 5 (4): 475–480 (1990).
- [10] Kawanaka, S., Park, S.J. and Mansoori, G.A., Organic deposition from reservoir fluids: a thermodynamic predictive technique. *SPE Pap. 17376. SPE Reservoir Eng.*, 6 (2): 185–192 (1991).
- [11] Nellensteyn, F.J., *Bereiding en Constitutie van Asphalt*. Ph.D. Dissertation, Technische Hoogeschool, Delft (1923).
- [12] Whitson, C.H., Characterizing hydrocarbon plus fractions. *1980 European Offshore Petroleum Conference, EUR Pap. 183. Soc. Pet. Eng. J.*, 275: 683–694 (1983).
- [13] Levelt-Sengers, J.M.H. and de Swaan-Arons, H., manuscript privately communicated by the authors (1989).
- [14] Hirschberg, A., Asphalt in reservoir oil: its structure and influence on viscosity. *Shell Laboratory Report RKRS 84.07*, The Hague (1984).
- [15] Mansoori, G.A. and Jiang, T.S., Asphaltene deposition and its role in EOR miscible gas flooding. *Proc., 3rd European Meeting on Improved Oil Recovery, Rome* (April 1985).
- [16] Yarborough, L., Application of a generalized equation of state to petroleum reservoir fluids. In: K.C. Chao and R.L. Robinson (Editors), *Equations of State in Engineering and Research*. Advances in Chemistry Series 182, American Chemical Society, Washington, DC, pp. 385–439 (1979).
- [17] Hirschberg, A., The role of asphaltenes in compositional grading of a reservoir's fluid column. *59th Annu. Tech. Conf. SPE, SPE Pap. 13171*, Houston, TX (Sept. 1984).
- [18] Heidemann, R.A. and Prausnitz, J.M., A van der Waals-type equation of state for fluids with associating molecules. *Proc. Natl. Acad. Sci.*, 73: 1773 (1976).
- [19] Hirschberg, A., de Jong, L.N.J., Schipper, B.A. and Meijers, J.G., Influence of temperature and pressure on asphaltene flocculation. *SPE Pap. 11202, Soc. Pet. Eng. J.*, pp. 283–293 (June 1984).

- [20] Jackson, G., Chapman, W.G. and Gubbins, K.E., Phase equilibria of associating fluids: chain molecules with multiple bonding sites. *Mol. Phys.*, 65 (5): 1057–1079 (1988).
- [21] Nellensteyn, F.J., *J. Inst. Pet. Technol.*, 10: 311 (1924).
- [22] Pfeiffer, J.P. and Saal, R.N.J., Asphaltic bitumen as colloid system. *J. Phys. Chem.*, 44 (2): 139–149 (1940).
- [23] Leontaritis, K.J., Asphaltenes deposition: a comprehensive description of problem manifestations and modeling approaches. *Proc., SPE Production Operations Symposium, Oklahoma City, OK*. Society of Petroleum Engineers, Richardson, TX (1989).
- [24] Hotier, G., *A Study of the Solutions and Suspensions of Asphaltenes in Heavy Fuel Oils and Heavy Crude Oils*. Technip, Paris (1983).
- [25] Suresh, S.J. and Elliott Jr., J.R., Applications of a generalized equation of state for associating mixtures. *Ind. Eng. Chem. Res.*, 30: 524–532 (1991).
- [26] Wertheim, M.S., Thermodynamic perturbation theory of polymerization. *J. Statist. Phys.*, 87: 7323–7331 (1987).
- [27] Chapman, W.G., Gubbins, K.E., Joslin, C.G. and Gray, C.G., Mixtures of polar and associating molecules. *J. Pure Appl. Chem.*, 59: 53–60 (1987).
- [28] McHugh, M.A. and Krukonis, V.J., *Supercritical Fluid Extraction*. Butterworths, Boston, MA (1986).
- [29] Andersen, S.I. and Birdi, K.S., Aggregation of asphaltenes as determined by calorimetry. *J. Colloid Interface Sci.*, 142 (2): 497–502 (1991).
- [30] Sheu, E.Y., De Tar, M.M., Storm, D.A. and DeCanio, S.J., Aggregation and kinetics of asphaltenes in organic solvents. *Fuel*, 71: 299–302 (1992).
- [31] Hildebrand, J.H. and Scott, R.L., *The Solubility of Nonelectrolytes*, 3rd ed., Dover Publications, New York (1964).
- [32] Scott, R.L. and Magat, M., The thermodynamics of high-polymer solutions, I. The free energy of mixing of solvents and polymers of heterogeneous distribution. *J. Chem. Phys.*, 13 (5): 172–177 (1945).
- [33] Carnahan, N.F., Asphaltenes in Venezuelan petroleum production, Plenary Lecture. *Proc. CEPET Conf Asphaltenes, August 2, Maracaibo* (1991).
- [34] Carnahan, N.F., Fundamentals of asphaltenes deposition. *5th UNITAR/UNDP Int. Conf. Heavy Crude and Tar Sands, August 4–9, 1991, Caracas* (to be published).
- [35] Wuithier, P., *Petrole-Raffinage GE V2* (1972).
- [36] Carnahan, N.F., Salager, J.-L., Anton, R. and Davila, A., Properties of resins extracted from Boscan crude oil and their effect on the stability of asphaltenes in Boscan and Hamaca crude oils. *Energy Fuels*, 13 (2): 309–331 (1999).
- [37] Carnahan, N.F., Quintero, L., Pfund, D.M., Fulton, J.L., Smith, R.D., Capel, M. and Leontaritis, K., A small angle X-ray scattering study of the effect of pressure on the aggregation of asphaltene fractions in petroleum fluids under near-critical solvent conditions. *Langmuir*, 9 (8): 2035–2044 (1993).
- [38] Carnahan, N.F. and Quintero, L., HLB and CMC Influence in Asphaltenes, Maltene Resins, and Natural Amphiphiles, *1993 Spring National Meeting of the American Institute of Chemical Engineers, Symposium of Solids Deposition, Fuels and Petrochemicals Division, March 28–April 1, 1993, Houston, TX*.
- [39] Gonzalez, G. and Middea, A., Peptization of asphaltene by various oil soluble amphiphiles. *Colloids Surf.*, 52: 207–217 (1991).
- [40] Chang, C.L. and Fogler, H.S., Stabilization of asphaltenes in aliphatic solvents using alkyl benzene derived amphiphiles, part I. Effect of chemical structure of amphiphiles on asphaltene stabilization. *Langmuir*, 10 (6): 1749–1757 (1994).
- [41] Chang, C.L. and Fogler, H.S., Stabilization of asphaltenes in aliphatic solvents using alkyl benzene derived amphiphiles, part II. Study of asphaltene–amphiphile interactions and structures using FTIR spectroscopy and SAXS techniques. *Langmuir*, 10 (6): 1758–1766 (1994).
- [42] Fogler, H.S., Permsukarone, P. and Chang, C., A kinetic study of asphaltene dissolution in amphiphile/alkane solutions. *Ind. Eng. Chem. Res.*, 36 (9): 3960 (1997).
- [43] Chang, C. and Fogler, H.S., Peptization and coagulation of asphaltenes in apolar media using oil-soluble polymers. *Fuel Sci. Technol. Int. J.*, 14: 75 (1996).



This page intentionally left blank

## *Chapter 13*

# **CHARACTERIZATION OF ASPHALTENIC DEPOSITS FROM OIL PRODUCTION AND TRANSPORTATION OPERATIONS**

L. CARBOGNANI, J. ESPIDEL and A. IZQUIERDO

## **INTRODUCTION**

Asphaltenes as a solubility fraction separated from hydrocarbon mixtures, is a term coined by Boussingault in 1837 [1]. It refers to a mixture of molecules comprising the most polar and/or higher-molecular-weight components of oil [2]. Their significance really came into the scene after the development of the Dubbs thermal cracking process. Their generation during fuel production via this process, hampered the storage, transportation and burning properties of the combustibles. From this starting point, refining upgrading operations have been continuously plagued by their influence [3]. The problem was further engrossed by the increased processing of heavier feedstocks, for which coke generation is always of concern [4–7].

Colloidal existence of asphaltenes in oil was first proposed by Nellensteyn [8], and Pfeiffer and Saal [9], suggesting that micellization was favored by the resin constituents, i.e., the polar heteroatomic compounds. Since then, many authors have adopted such model [10,11], but lack of definitive proof has been the cause for continuous discussion of this topic. Recently, evidence has been published showing micellization of asphaltenes in their natural matrix, i.e., a vacuum residue [12]. However, over this same period studies pointed out an opposite view, suggesting that the vacuum residue can be modeled like a continuous single phase ‘microstructural’ mixture of polar and nonpolar molecules [13].

In Venezuela, such components were, to the best of our knowledge, first reported to affect oil well production during the 1970s, thanks to the compilation work done by Nierode on Cretaceous wells located on Maracaibo Lake [14]. At this early stage, suggested procedures to minimize or try to avoid their deposition were based on the judicious choice of production conditions, being low wellhead pressures recommended as the best option [15].

Problems caused by asphaltene deposition have been reported in different oil-fields worldwide. Among these occurrences are the Hassi Messaoud field in Algeria [16], different oil fields in Venezuela [15,17,18], Campeche, Tecoaminoacan and Jujo fields in Mexico [19], and the Ventura field in California, USA [20]. The topic has been reviewed by Kokal and Sayegh from the points of view of reservoir and processing [21]. Several control mechanisms are currently used to eliminate solid depositions. One way is by judiciously adjusting of production parameters, such as well flow, as mentioned at the end of the previous paragraph [15]. The most commonly used practices are based on periodical cleaning of the tubings, using mechanical means [22],

aromatic solvent treatments [23–27], use of tailor-designed solvent mixtures [23,28,29], and very often, combinations of the above treatments. All these procedures have very costly effects on revenue, because they imply stops in production or use of expensive chemicals.

Recently, new strategies have been introduced, which involve the injection of chemical dispersants as inhibitors directly into the well, to minimize the growing process of the deposit. Natural petroleum-derived resins have been proposed for asphaltene deposition inhibition [30]. Among injected chemicals, dispersant additives have found widespread acceptance to inhibit asphaltene deposition. Two classes of compounds are commonly described in recent publications: (1) polymeric dispersants [31,32]; and (2) oil-soluble amphiphiles [22,33–38]. Other recent strategies to avoid deposit formation are currently under evaluation. Tubing coating with different polymers is one of the suggested approaches [22]. Magnetic fields have been cited to minimize asphaltene deposition [39], but their effect has only been unequivocally demonstrated for carbonate-scale inhibition [40].

The mechanism of asphaltene deposit formation is not clearly understood. This is partly because despite the 50-year-long research effort on asphaltene characterization, there is no clear picture of their composition. Asphaltenes cannot be classified as a hydrocarbon family, since they are mixtures of big nonpolar and small polar molecules, grouped on a solubility basis [2]. Nobody has published definitive results on the real molecular weights (MW) they typically span. Several orders of magnitude can be referred to, depending on the technique employed and the particular conditions adopted, as thoroughly described in a review by Speight et al. [41]. Vapor-pressure osmometry (VPO) is widely used to determine MW due to its simplicity. The lower values measured by this technique are currently considered as the most reliable [41]. However, even with this approach and taking all the precautions into consideration, errors due to aggregation still persist [42]. Thanks to the studies carried out using FIMS (field ionization mass spectrometry) [43,44], the picture arising during the past decade is that asphaltenes are mixtures of relatively small components (<2000 daltons). Their intermolecular aggregation has been attributed to aromatic moieties interaction [10], H-bonding [45], and dipole–dipole charge transfer [46]. The complexity of this issue can be visualized in Fig. 13-1 [47]. It shows two ‘average molecular representation’ extremes of the same asphaltene. These structures, better described as graphic representations of average molecular parameters, are strongly affected by the estimated MW. When the determined MW is small, a combination of multiple structures is required to account for fractionary elemental contents and functional groups. Extended aromatic condensed structures were shown, imposed by the high aromaticity and polyaromatic condensed structures obtained when Nuclear Magnetic Resonance (NMR) is used for the average molecular parameters determination. Such structures have been often found in the literature from past decades. Recent studies reporting on asphaltenes [48,49] have not been able to identify such extensive aromatic networks, leaving an open field for debate on these topics.

Further difficulties in the understanding of deposit formation arise from the effects exerted by pressure and temperature changes during oil production [33]. Some of these influences have been recently discussed by Angulo et al. [50]. One of the most important findings cited in their work is the reversibility of asphaltene precipitation. Also, they

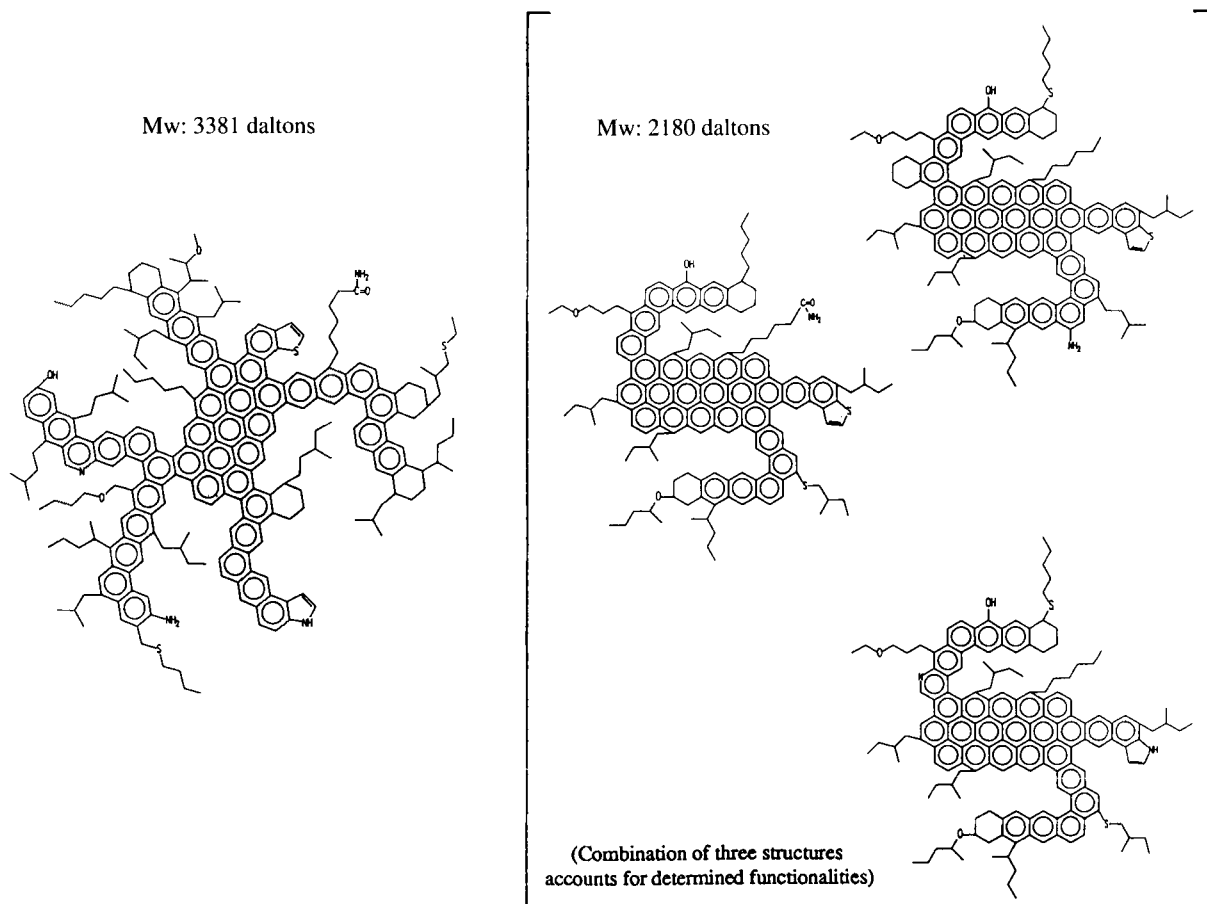


Fig. 13-1. Graphic representation of average molecular parameters for a single crude asphaltene sample, as a function of its average molecular weight.

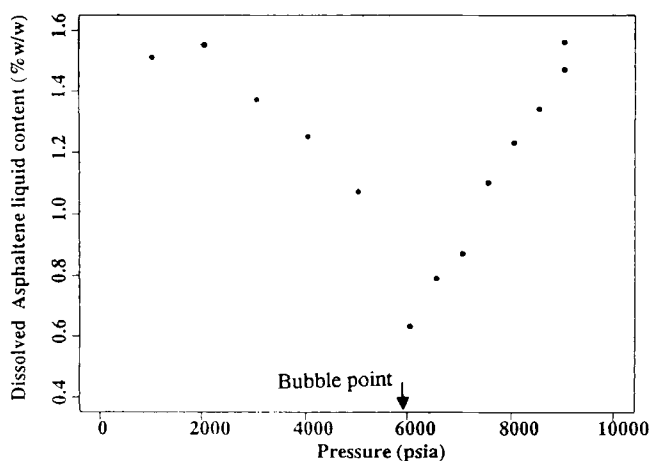


Fig. 13-2. Content of heptane asphaltenes for NM26C live crude oil, as a function of pressure (after Angulo et al. [50]).

found that this process is pressure and temperature dependent. Their experiences indicate that maximum asphaltene precipitation occurs around the bubble point (BP), although the phenomenon is a continuous process that starts well before BP is reached (Fig. 13-2). Other authors have recently proposed a model to describe this precipitation [51]. Furthermore, it can also be seen from the figure that redissolution of asphaltenes occurs after the BP, as the pressure goes down.

Prediction of organic deposition has been attempted by means of thermodynamic or colloidal models [52]. The first types of models are generally known as thermodynamic-molecular, and imply reversible processes which can be described through state equations [33,51,53–55]. Most of the thermodynamic models consider equilibrium between two liquid phases. On the other hand, colloidal models consider the equilibrium established between a liquid and a solid or dispersed phase [56]. A recent model developed by Rivas et al. [55] considers equilibria between three phases (vapor–liquid–solid), where the solid phase can be considered as a mixture of different hydrocarbon group-types. Detailed chemical composition is required as an input for the model.

Recent studies on detailed deposit characterization [19,27,39,57] have introduced a new set of parameters that increase the difficulty of understanding asphaltenic deposit formation in real production and transportation facilities. It appears that complex interactions between organic-soluble, organic-insoluble and inorganic materials are playing a role for deposit formation. A better understanding of these types of interactions is important for the prevention and/or removal of deposits.

#### DEPOSIT CHARACTERIZATION AND CLASSIFICATION

Over the past four years, solid deposits from two different sedimentary basins located in Venezuela have been studied, i.e., northern Monagas and Maracaibo Lake. The

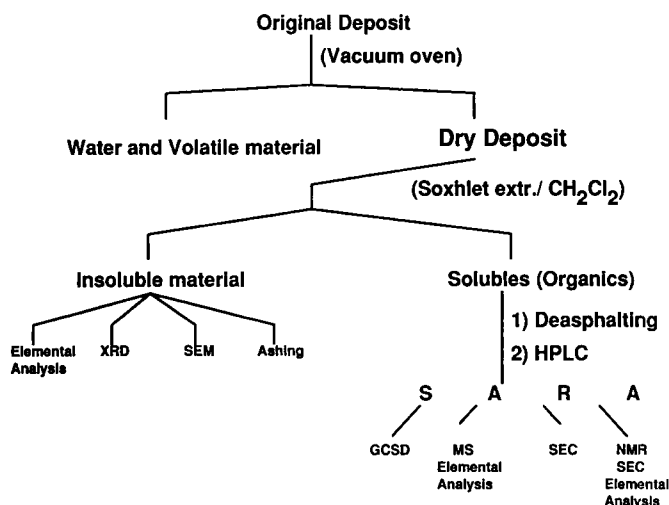


Fig. 13-3. Separation and analysis scheme for deposits.

majority of the solids were sampled from well tubings, although some came from surface transportation or storage facilities. For the present work, a notation was adopted to identify deposits from these basins, respectively, as NMx or MLx. Related crudes will be distinguished by adding a C (NMxC, MLxC), and deposits from surface installations will be differentiated by addition of an S (NMxS, MLxS). Some extra heavy crudes from the Orinoco oil belt located in eastern Venezuela have been included in the study and were identified with the key OBxC. The samples have been studied according to a specific scheme developed for this purpose (Fig. 13-3). Experimental details have been previously published [57]. The scheme involves the separation of volatile, organic, and insoluble materials. The organic fraction is separated by SARA group-type analysis (saturates, aromatics, resins and asphaltenes). The insolubles are differentiated or, eventually in some cases, separated into organic and inorganic materials. Water and volatile component (naphtha-kero fractions) variations were detected in all the studied samples. However, they were not considered in the following discussion because it is thought that their contribution to solid formation is not relevant. SARA separations and fraction characterization were performed on some of the crudes related to the deposits, as well as on stable crudes from other production units, in order to shed some light on the problem. These results will be discussed later in this work.

The gross composition of the studied deposits is shown in Fig. 13-4. All SARA group-types were found to contribute to solids formation. Minerals were ascertained to be present in nearly all samples analyzed, but insoluble organic materials were found in one third of the samples. The results in Fig. 13-4 suggested that deposits can be classified into three categories, namely: (I) predominantly organic, (II) predominantly inorganic, and (III) mixed composition. The boundaries between these categories were arbitrarily defined as the ratios of 70/30 wt% organics/minerals for type I, 30/70 wt% organics/minerals for type II and in-between these values for the mixed or composite

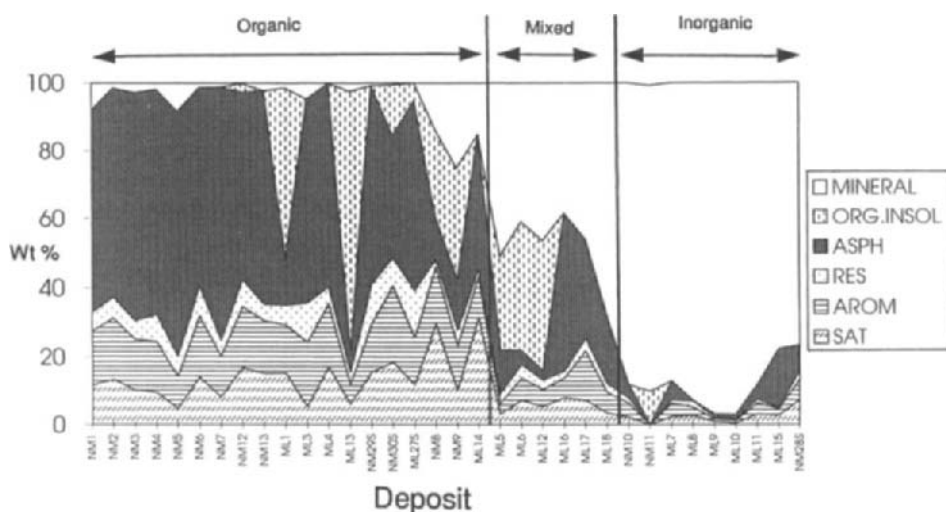


Fig. 13-4. Overall deposits composition.

types. Predominantly inorganic deposits (category II), which comprise approximately one third of the data, will not be discussed in this work because they fall outside the scope.

#### SARA FRACTIONS CHARACTERIZATION. IDENTIFICATION OF POSSIBLE CAUSES FOR CRUDE OIL INSTABILITY

Separated hydrocarbon group-types (SARA) from organic deposits were characterized to relative high levels of complexity. Saturate distributions were studied by simulated distillation (SimDist) and the results are presented in Fig. 13-5. Since a gas-oil methodology was adopted for these analyses [58], components with boiling points above 538°C were generally undetected. Preponderance of paraffins greater than  $nC_{26}$  was determined for the deposits when compared with atmospheric distillation residua of crudes (>220°C) from related reservoirs. However, these analytical results are not easily observed in the corresponding chromatograms (Fig. 13-5). The use of high temperature SimDist could overcome this detection problem, allowing the proper detection of large paraffins, approximately  $C_{100}$ – $C_{120}$ . Prediction can then be made so that the picture will probably be more dramatic, i.e., the amounts of measured high-molecular-weight components will increase. Additional results were obtained from the saturate fractions separated from some deposits. These were analyzed by inclusion of linear paraffins in 5 Å molecular sieves. The results are presented in Table 13-1. They show a high proportion of iso- and cyclo-paraffins (non-included fractions), as well as a low contribution of  $n$ -paraffins.

ASTM mass spectrometry method D-3239 routinely used in our laboratories is not suited to handle non-volatile vacuum residue molecules [59]. Nevertheless, an

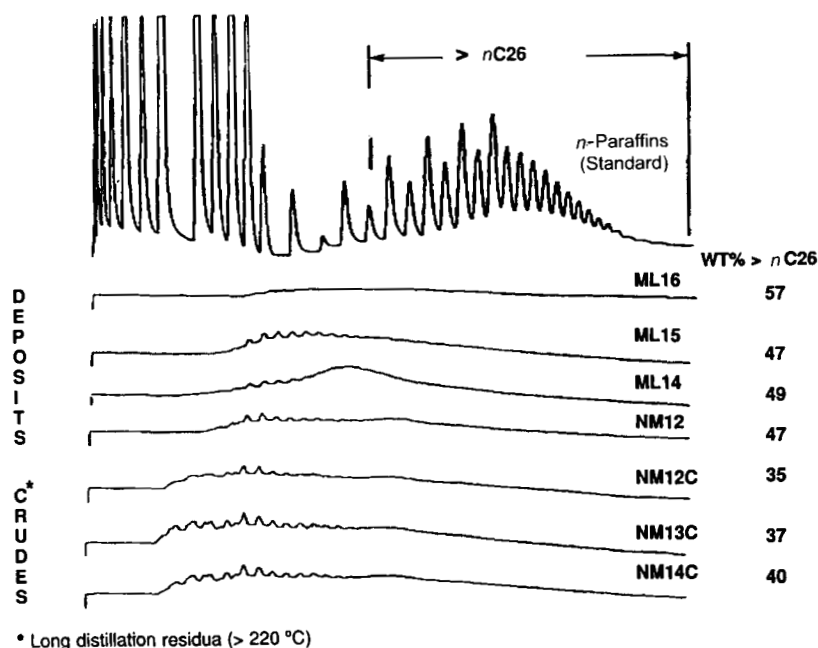


Fig. 13-5. Saturates distributions by GC simulated distillation.

TABLE 13-1

*n*-Paraffins contents in some of the deposits <sup>a</sup>

Deposit	wt% saturates	wt% <i>n</i> -paraffins
NM12	15.8	3.4
ML14	27.8	1.8
ML16	7.6	0.5

<sup>a</sup> Results expressed on whole deposit basis.

attempt was made to get an idea of the relative aromatic group-type distributions of the volatilizable compounds from whole aromatic fractions, which have been separated from crudes and deposits. The results showed a monotonous behavior for deposits and evaluated crudes. The relative distribution obtained for the different types of aromatic rings was Monoaromatics > Di > Tiophenics > Tri > Tetra > Pentaromatics. This does not give any valuable information related to the stability or precipitation tendencies of crudes.

It has generally been stated that a high ratio of resins to asphaltenes is indicative of enhanced stability for colloidal particles, and consequently, of lower asphaltene precipitation risks [11,41]. From the present study, it has been found that even with a high ratio between these two fractions, crude instability is noticeable (Fig. 13-6). These findings indicate that not only a high ratio of resins to asphaltenes plays a role in



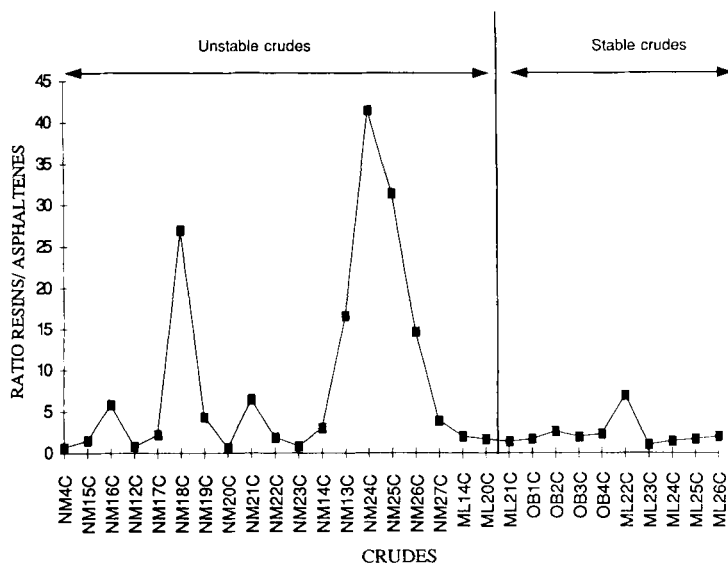


Fig. 13-6. Ratios wt% resins/wt% asphaltenes for studied crude oils.

asphaltene stabilization but other factors, like (i) chemical functionalities, (ii) apparent molecular size or (iii) steric recognition between the molecules from the two fractions, may also be important. Factor (ii) has been investigated by means of size exclusion liquid chromatography (SEC). The results suggest that the high-molecular-weight compounds (HMW) from the asphaltenes have to be matched with a corresponding HMW from the resins fraction, in order to stabilize asphaltene dispersions (Fig. 13-7).

The ratio of HMW resins to HMW asphaltenes was plotted against wt% HMW asphaltenes, which is shown in Fig. 13-8 for the different crudes and deposits studied. It is possible to group the data into three distinct regions, where the one for the stable crudes is the one that shows an almost equal concentration of HMW resins and asphaltenes. This clearly supports what was previously stated on the requirements to have almost equal percentages of both HMW asphaltenes and resins in order to have stable crudes.

Asphaltene from crudes and deposits were further characterized by nuclear magnetic resonance spectroscopy (NMR) and elemental analysis. Information generated with these techniques was fed as input for a program to calculate average molecular parameters [60]. This allowed the determination of two useful parameters, namely, aromaticity and aromatics condensation index. Aromaticity ( $f_a$ ), is widely used [51, 61, 62], and represents the percentage of aromatic carbons over the total carbon atoms for the sample. Aromatics condensation index ( $CI/C_1$ ) is a measure of the number of internal or bridging carbon atoms in fused aromatic rings, divided by the number of external or peripheral carbon atoms in such moieties [62]. Fig. 13-9, prepared by using aromatic molecules typically found in crudes, illustrates these concepts.

A plot of  $f_a$  vs.  $CI/C_1$  for asphaltene is shown in Fig. 13-10. The plot can be divided into three regions. Going from left to right in the  $f_a$  axis they are grouped as: (i) stable crudes, (ii) unstable crudes, and (iii) deposits. Two important features are evident from

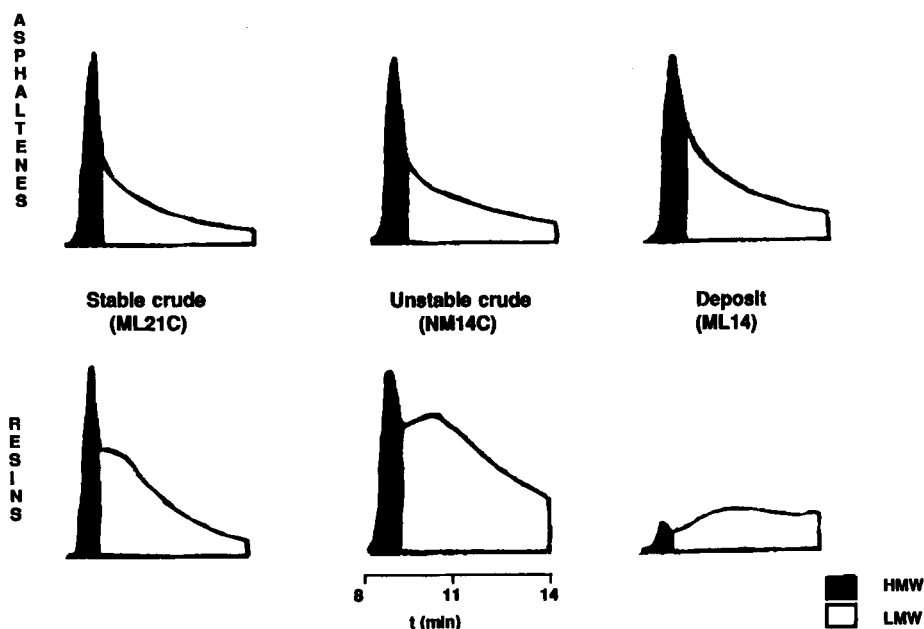


Fig. 13-7. Molecular weight distribution (SEC) of resins and asphaltenes.

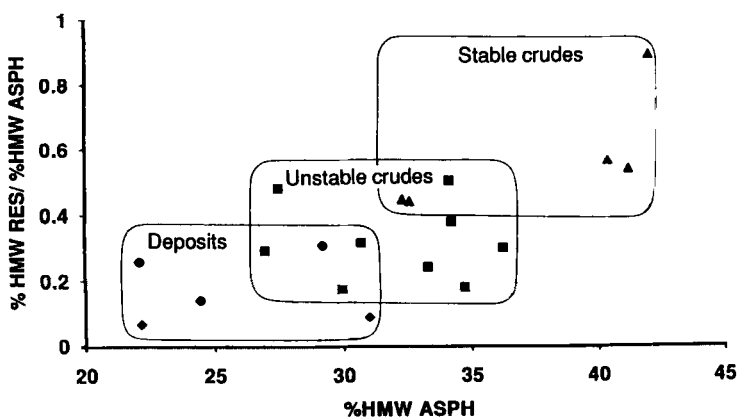


Fig. 13-8. Relative abundance of HMW resins and asphaltenes in crudes and deposits.

this graph. The first is the fact that asphaltenes from deposits and crudes produced from reservoirs where precipitation is common show a tendency to have higher aromaticities than corresponding asphaltenes from stable crudes. This result suggests smaller amounts of solubilizing side-chains in asphaltenes from unstable crudes. This suggestion is supported by the content of aliphatic chains in this type of asphaltenes, obtained by infrared spectroscopy (Fig. 13-11).

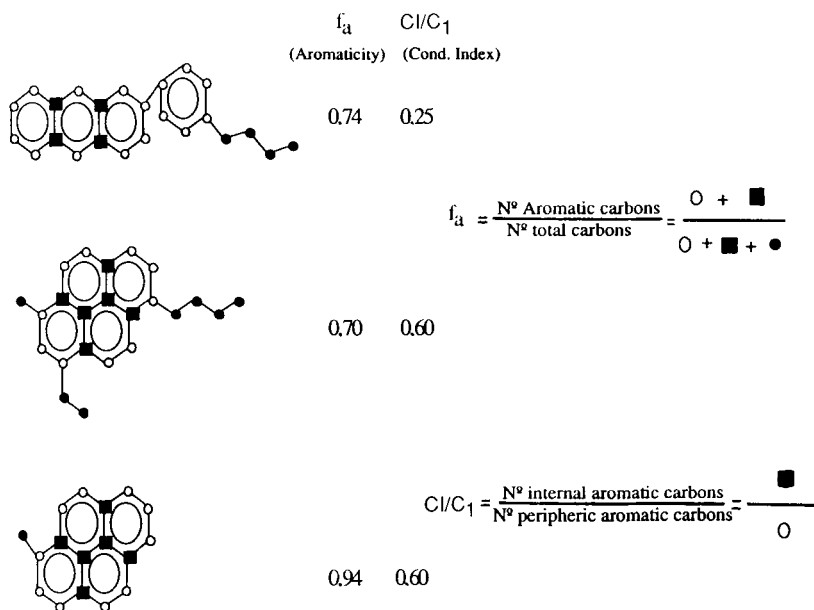


Fig. 13-9. Aromaticity and aromatic condensation indexes for aromatic molecules.

The second feature from Fig. 13-10 is less obvious, and it is related to the aromatics condensation indexes obtained from deposits and unstable crude asphaltenes, when compared with the asphaltenes from stable crudes. The picture arising from this finding is that deposit and unstable crude asphaltenes, in many of the cases, have extended aromatic nuclei (greater value of  $CI/C_1$ ) when compared with stable ones, which have smaller aromatic cores. This is an important fact from a solubility point of view, since extended aromatic cores require better solvation properties of the solubilizing media (the oils), in order to remain in solution and/or dispersion. Better solvation avoids the direct interaction of aromatic moieties, also known as aromatic stacking in carbon-rich fossil fuels [63,64].

Keeping the ensuing discussion on the topic of solubility, a survey of SARA fractions abundance was performed, and a comparison was established between the obtained distributions for unstable crudes with those determined from the stable ones. The aim of such comparison was to identify differences that besides the previous findings can give some clues on the causes of precipitation in unstable crudes.

The determined SARA distributions are shown in Fig. 13-12. They are grouped according to the geographical origin of the studied crudes. The most striking difference found between unstable crudes and stable ones is their saturates and aromatics contents. In unstable crudes, saturates represent about half of the crudes, whereas in the stable ones it is approximately one fifth. At the same time, aromatics represent the major fraction for stable crudes (ca. half of the crude).

These findings are considered of great significance. Unstable crudes appear as intrinsically prone to precipitation because their contents of saturates are high, and at the

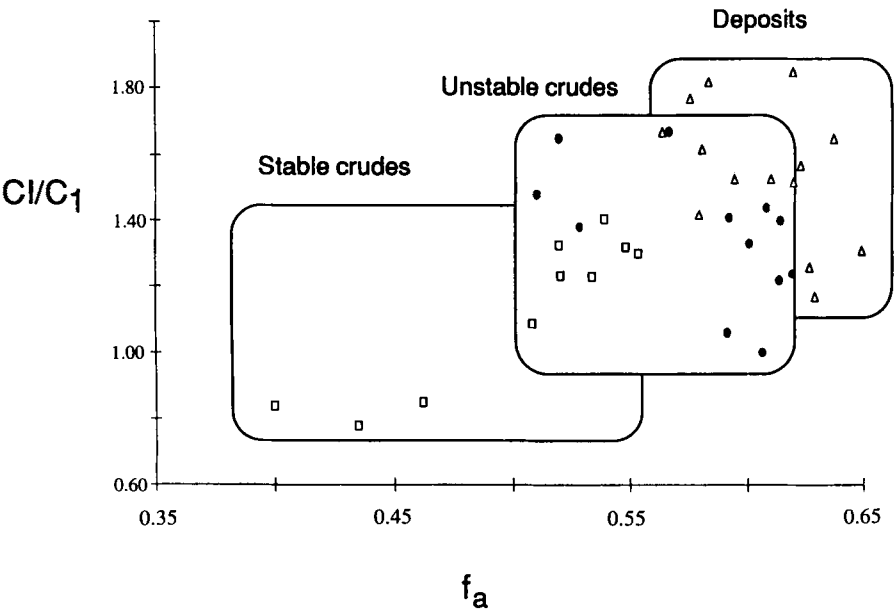


Fig. 13-10. Aromaticity and aromatic condensation index for asphaltenes separated from crudes and deposits.

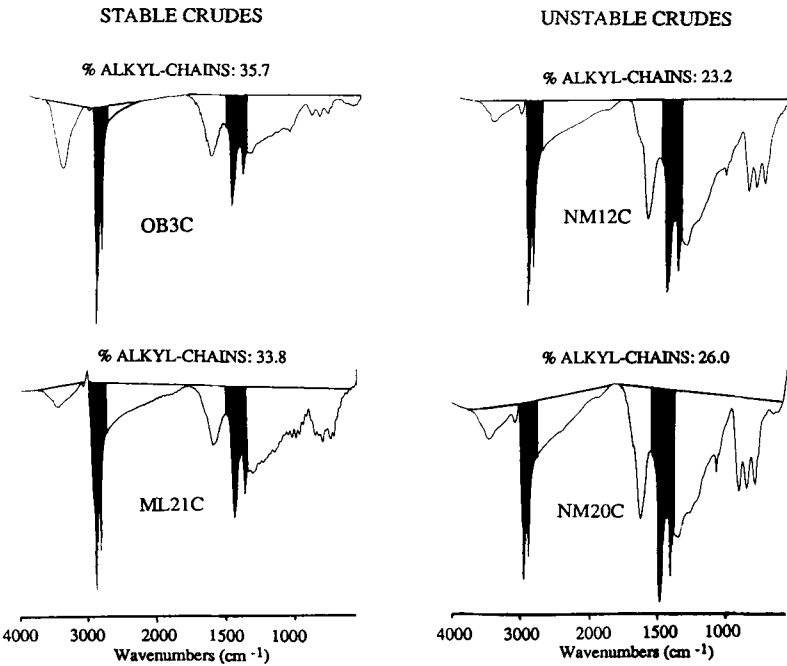


Fig. 13-11. Infrared spectra for asphaltenes separated from crude oils.

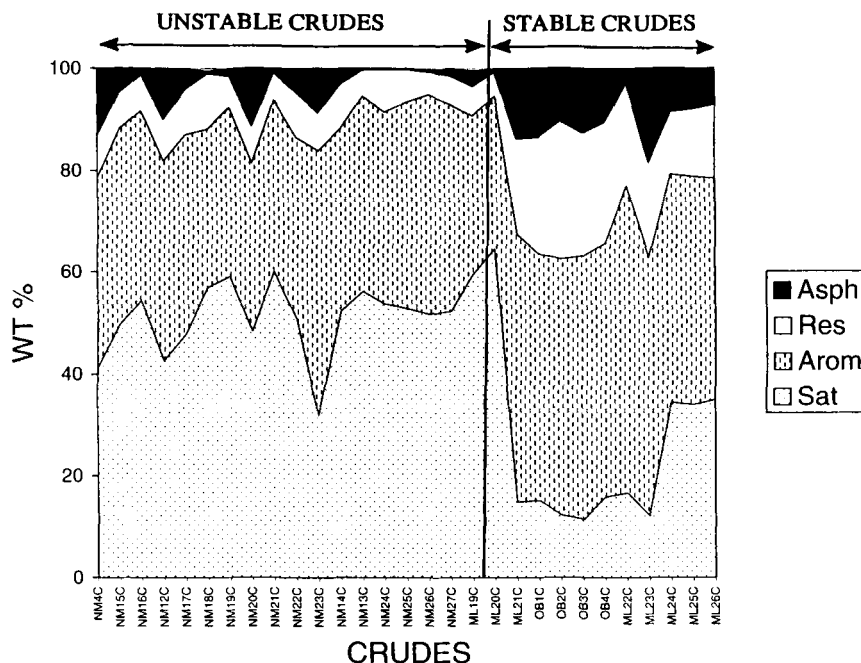


Fig. 13-12. Group-type SARA distributions for crude oils.

same time, their respective asphaltenes are more aromatic and condensed. The behavior of stable crudes is presumably due to better solvent properties of their aromatic-rich oils, as well as the properties of their asphaltenes, which are less aromatic, and less condensed. This can be further supported by a function defined as the ratio of the aromatics content of the oil divided by the aromaticity of the respective asphaltene ( $\text{wt\% arom.}/\text{asph. } f_a$ ). The values of this function, plotted against behavior of the crudes, can be observed in Fig. 13-13. Values for unstable crudes are centered around 70, while stable ones are upset at higher values centered on 100. Different indexes of oil fraction stability have been proposed, like the Shell  $P$ -value [65], Exxon toluene index, and a xylene index [66], which has been automatized by British Petroleum researchers [67]. It was not surprising to find that the two parameters involved in the proposed ratio ( $\text{wt\% arom.}/\text{asph. } f_a$ ) strongly affect the stability of whole crudes. All the mentioned indexes are simply different versions of two fundamental properties governing solubility and stability of oil fractions, namely, solvent power availability of the oil (in the present case: available aromatics), and intrinsic aromaticity of the dispersed or solubilized phase (asphaltene aromaticity). It is important to emphasize that a difference of 30 in the ratio ( $\text{wt\% arom.}/\text{asph. } f_a$ ) is very significant for the differentiation between stable and unstable crudes. When a comparison is established with  $P$  values, the difference between unstable and stable samples is more critical.  $P$  values less than 100 indicate unstable samples, those equal to 100 represent borderline samples, and those greater than 100 represent stable samples.

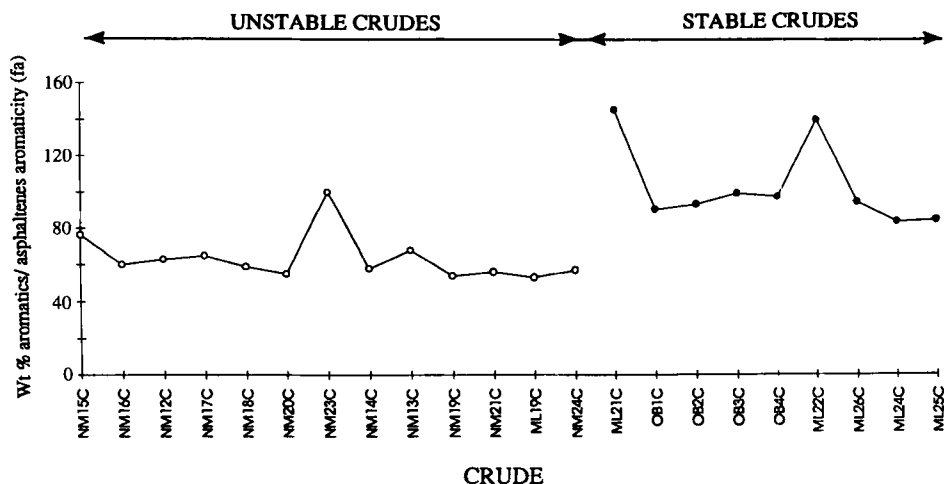


Fig. 13-13. Ratio wt% aromatics/asphaltene aromaticity for crude oils.

Other indexes involving more complicated combinations of chemical constituents have been described [68,69].

#### PRELIMINARY INSIGHTS INTO THE COMPOSITION OF INSOLUBLE ORGANIC MATERIALS

It has been indicated in the literature that a proper separation scheme for maltenes, asphaltenes, and pre-asphaltenes is a sequence of benzene extraction followed by *n*-heptane precipitation of the extract [70]. Having said that, a decision was made to use methylene chloride instead of benzene to obtain organic extracts from deposits, based on health reasons and due to its common use by geochemists for the extraction of bitumen from core samples. The use of the solvent sequence methylene chloride–*n*-heptane afforded preparative separations of asphaltenes from insoluble fractions. The latter were further differentiated into inorganic and insoluble organic fractions. The results from this scheme are those previously presented in Fig. 13-4. Let us now concentrate the discussion on asphaltenes and insoluble organics.

To assess if the separated asphaltenes were representative according to a common definition (benzene solubles), a cross-validation of extraction and separation with different solvents was performed with one of the available deposits (NM12). The solvent sequence employed, fraction identification keys, and yields of the different fractions are presented in Fig. 13-14 and the following conclusions can be drawn from this study. First, the maltenes or oil fractions are the same regardless of the path taken (DSHS  $\approx$  BSHS  $\approx$  HS). Second, the efficiency of the different solvents employed to extract organic soluble materials increase in the order  $B < X < D$ . Third, the three possible fractions that can be identified as asphaltenes vary widely in abundance depending on the separation path chosen (HIDS  $<$  BSHI  $<$  DSHI). DSHI is the fraction considered as asphaltenes in this work, and these are the values reported in Fig. 13-4.

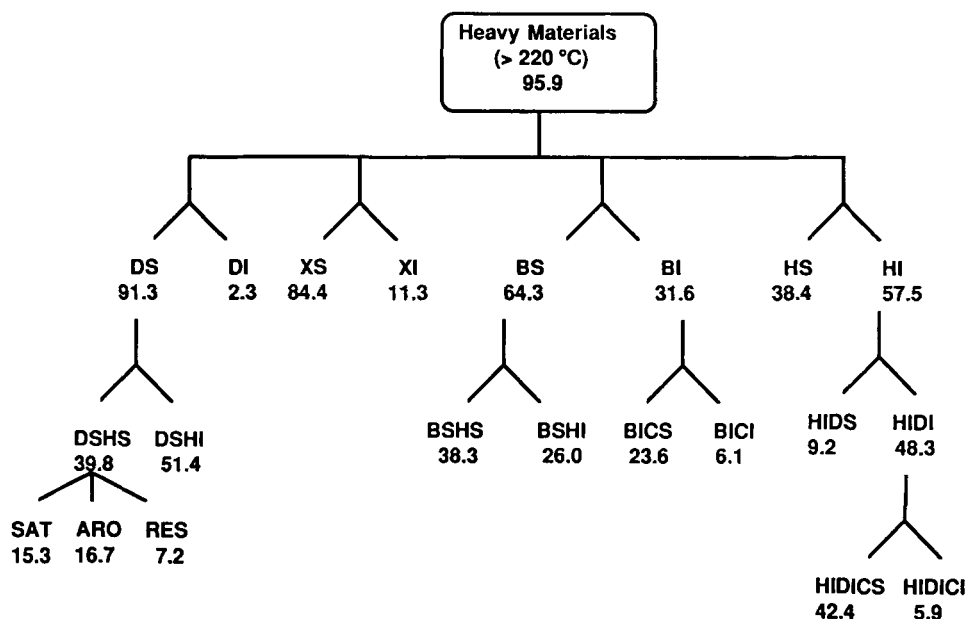


Fig. 13-14. Solubility fractionation scheme applied to deposit NM12. Numbers refer to wt% of original deposit. *X* = xylene; *D* = methylene chloride; *B* = benzene; *H* = *n*-heptane; *C* = carbon disulphide; *S* = soluble; *I* = insoluble.

According to Speight [70], asphaltene should be the fraction identified as BSHI. Therefore, asphaltene contents reported in Fig. 13-4 are higher than those obtained by the Speight definition. In this way, some of the pre-asphaltenes are included in the group defined as asphaltenes during this work. This result can explain the higher aromaticity and condensation indexes reported in Fig. 13-10. The separation scheme presented in Fig. 13-14, allows differentiation between asphaltenes (BSHI), carbenes (BICS, HIDICS), and carboids (BICI, HIDICI). The solubility differences among these groups can be rationalized on the basis of their respective increases in hydrogen deficiency, aromaticity and aromatic condensation indexes, as shown in Table 13-2.

A study of solubility fractions from another deposit was undertaken in order to elucidate if the same identified reasons, which explained the differences in solubility for NM12 deposit, also apply to asphaltenes and insoluble organics. Hydrogen deficiencies were determined by C,H elemental analysis. Alkyl chain abundances were measured by the ratio of their characteristic absorption bands, divided by the total absorbance of the sample in the IR region of the spectrum. The assignment of the different bands was based on previous reports [45,71-78]. The results presented in Fig. 13-15 suggest that the deficiency of hydrogen strongly affects the solubility of organic materials. IR spectra gave some clues on the nature of the moieties where this hydrogen is missing from insoluble organic materials. The low concentration of hydrogen was found to be related to smaller contents of alkyl chains for these types of materials. In most cases, it appears that alkyl chain contents below approximately 28% correlate with the insolubility of

TABLE 13-2

Dehydrogenation, aromaticity and aromatic condensation index for solubility fractions separated from deposit NM12

Fraction <sup>a</sup>	H/C	$f_a$	CI/C <sub>1</sub>
DI	0.99	0.60	1.48
DSHI	0.96	0.62	1.40
BShI	1.07	0.55	0.99
BICS	0.95	0.63	1.41
HIDICS	0.94	0.62	1.65
HIDS	1.00	0.60	1.30

<sup>a</sup> X = xylene; D = methylene chloride; B = benzene; H = *n*-heptane; C = carbon disulfide; S = soluble; I = insoluble.

TABLE 13-3

Composition of selected solid deposits from oil production and storage facilities

Sample	Content (wt%)							Identified elements (MEB)	Main minerals (DRX)
	humidity and volatiles	minerals <sup>a</sup>	insoluble organics <sup>a</sup>	S <sup>b</sup>	A <sup>b</sup>	R <sup>b</sup>	A <sup>b</sup>		
NM12	4.1	≈0.2	2.3	15.8	16.7	7.2	51.4	ND	ND
NM30S	12.7	0.5	13.0	16.2	19.2	7.1	31.3	ND	quartz; iron oxides <sup>c</sup>
ML1	14.0	≈1.3	43.2	13.1	12.2	4.9	11.3	S <sup>d</sup>	ND
ML5	22.4	≈39.6	≈20.8	2.4	2.4	2.4	10.2	S <sup>d</sup> , Al, P, Si, Ba, Fe	BaSO <sub>4</sub> <sup>d</sup> , CaCO <sub>3</sub>
ML6	21.8	≈32	≈29	5.6	5.3	3.1	3.2	S <sup>d</sup> , Fe <sup>d</sup> , Ca	FeCO <sub>3</sub> <sup>d</sup> , CaSO <sub>4</sub>

ND = not determined.

<sup>a</sup> Fractions obtained as total insolubles. Analysis of an aliquot allows to differentiate between minerals and insoluble organics.

<sup>b</sup> Saturates, aromatics, resins and asphaltenes ( $\pi C_7$ ).

<sup>c</sup> Observed by optical microscopy, after ashing the insoluble organics.

<sup>d</sup> Element and/or predominant component.

organic materials. This does not apply for the case of deposit ML1, where the soluble asphaltene has a chain content of 23.7%. It has to be noticed that in this case the H/C value for the insoluble material is the lowest. This suggests that other mechanisms apart from dehydrogenation play an important role in insolubility. One of these can be the presence of minerals.

In addition to the previous findings, investigation of the composition of mixed deposits was attempted in order to try to understand the role of the combined effects from organic and inorganic materials. Details on the fraction distributions of studied mixed-deposits is presented in Table 13-3 (also see Fig. 13-4). Relative proportions between insoluble organics and inorganics do not follow any recognizable pattern, and range between ca. 1/1 and 40/1. The increase of insoluble organics seems to be at the expense of the asphaltene contents. However, the reason for this behavior is not understood.



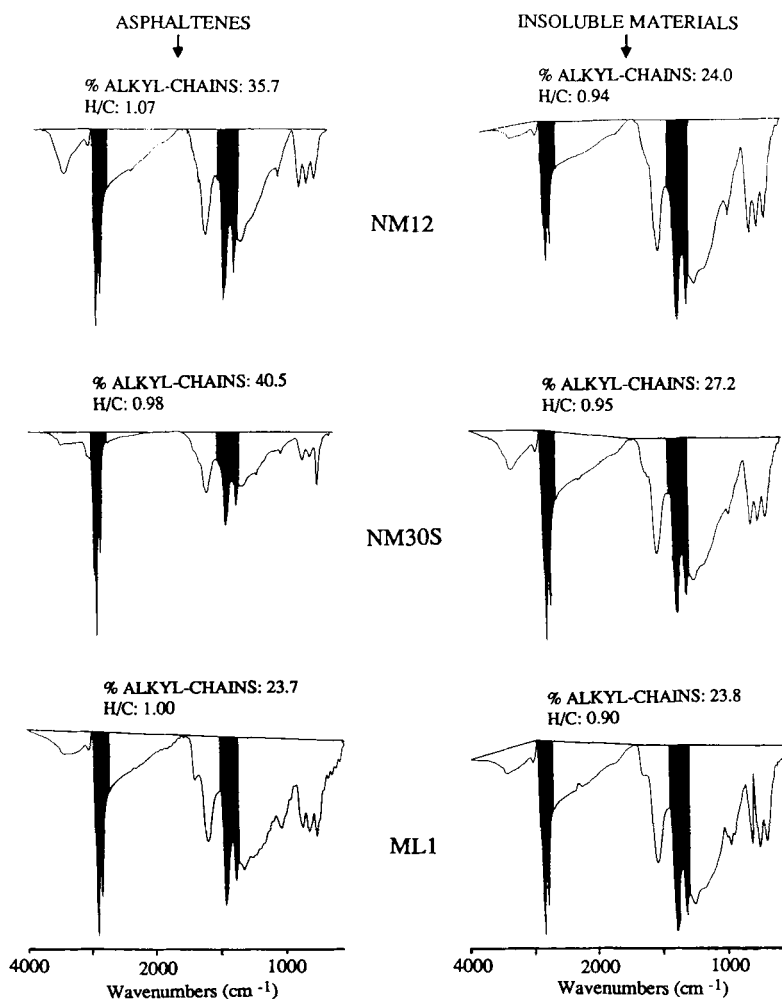


Fig. 13-15. Infrared spectra and atomic H/C ratios for asphaltenes and insoluble materials separated from deposits.

It is interesting to note that iron was detected in ca. 80% of the studied deposits. A detailed composition for five of these deposits has been included in Table 13-3, where it can be observed that forms of this element are present in three of the samples. Suggestions have been made regarding the important role played by iron compounds on the complexation between insoluble organic materials and the mineral part of oil sands [79–83]. Fig. 13-16 shows physical evidence for the presence of magnetite, iron oxide, and steel spheres in ashes from deposit NM30S (organic type). The origin of these materials cannot be traced and for the particular case described is probably related to steel-made production and storage facilities. The presence of iron species in the majority of the studied deposits points towards their possible role in the insolubilization

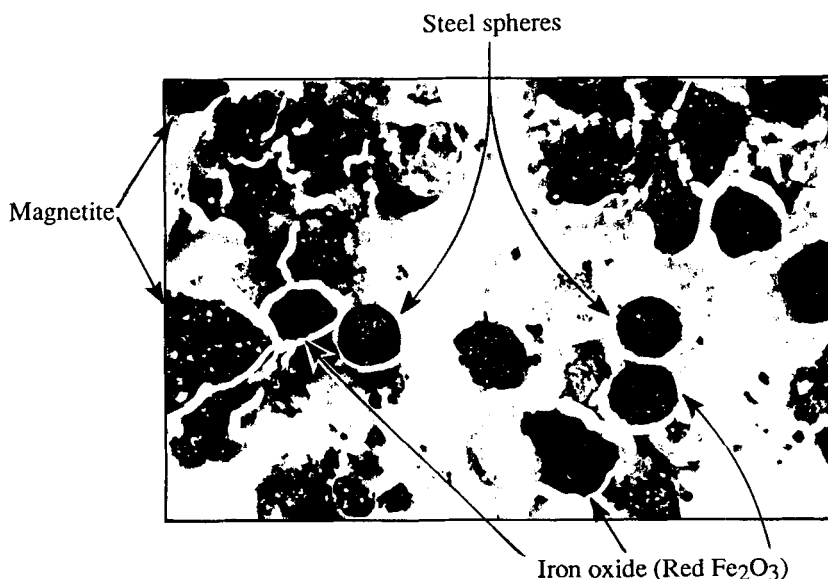


Fig. 13-16. Microphotograph of ashes from deposit NM30S.

or aggregation of organic materials. Further support for this idea is given by the fact that for a long time ferric salts have been known to be selective in the adsorption of oil polar compounds, when dispersed on clays [84–87].

Iron sulfides and iron oxides are commonly reported as the most common Fe compounds present in oil reservoirs. Two of them, pyrite and ferric oxide, were used to perform some experiments in order to test their effect on the asphaltenes when they are physically mixed. The changes were monitored by IR spectroscopy. Pyrite proved to be inert, whereas the oxide produced dramatic changes in the IR spectrum, and they are presented in Fig. 13-17. Noticeable increase in the signal intensity below  $1800\text{ cm}^{-1}$  is observed for the sample mixed with the iron oxide. Other important changes were noted on the OH (ca.  $3100\text{--}3600\text{ cm}^{-1}$ ) and bridged-H related to carboxylic structures (ca.  $1900\text{--}2900\text{ cm}^{-1}$ ). The bridged-H effect has also been found for other studied asphaltenes and the results are presented in Fig. 13-18 as the ratios of alkyl chains content to carboxylic hydrogen bridging. Another important finding is the fact that the effect prevailed after the iron compound has been physically removed by filtration (OB3C filtered, Fig. 13-18). The same relation is presented in Fig. 13-19 for a wide variety of samples. It is interesting to note that insoluble fractions and aged asphaltenes (stored for ca. 3 years under ambient conditions) have the same ratio as those treated with ferric oxide. The fact that the insolubles showed the lowest ratios, i.e., higher bridged-H contribution, could suggest that bridged-H on carboxylic derivatives is an important mechanism for insolubility.

The presence of minerals was ascertained in nearly all the studied deposits in this work (Fig. 13-4). The importance of inorganic particles for the aggregation of organic materials had been suggested by Strausz et al. some years ago [88]. They reported that

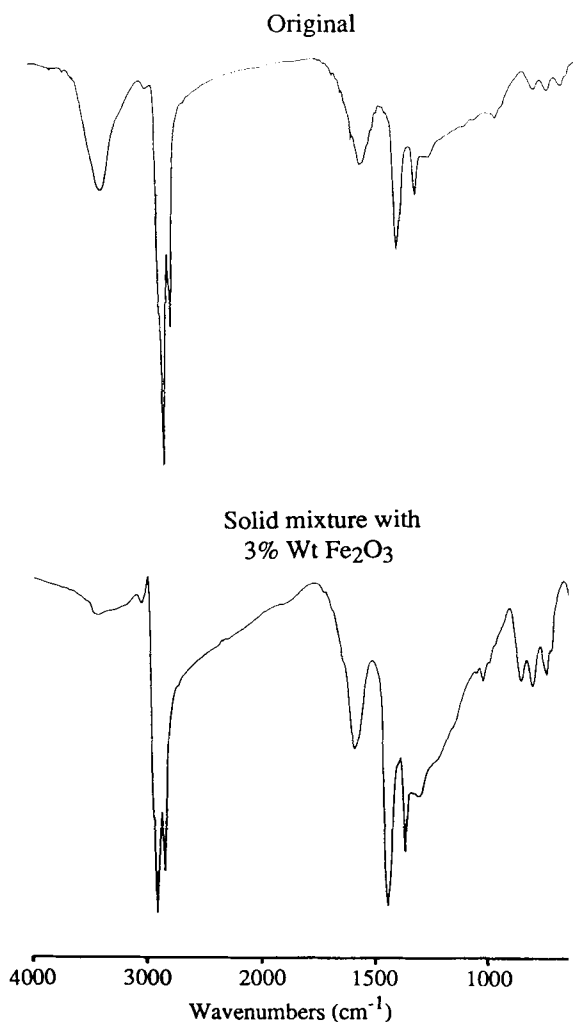


Fig. 13-17. Infrared spectra of OB3C asphaltenes before and after addition of Fe<sub>2</sub>O<sub>3</sub>.

the amount of high-molecular-weight components in Athabasca asphaltene correlated with the ash contents being determined by sample calcination. In the present work, mineral contents  $\approx 3$  wt% were measured for type I deposits (organics). These were determined by ashing, and are shown in Table 13-4. These results are in agreement with those published by Strausz. However, further investigation has to be undertaken in order to understand the effects of minerals upon deposit formation.

Investigations carried out in Canada suggest that carbonyl compounds from the bitumen can associate selectively with inorganic materials present in tar-sands [80–83,88–93]. This has also been observed for some of the deposits studied in the present work. Particularly, this has been the case for deposits from reservoirs containing

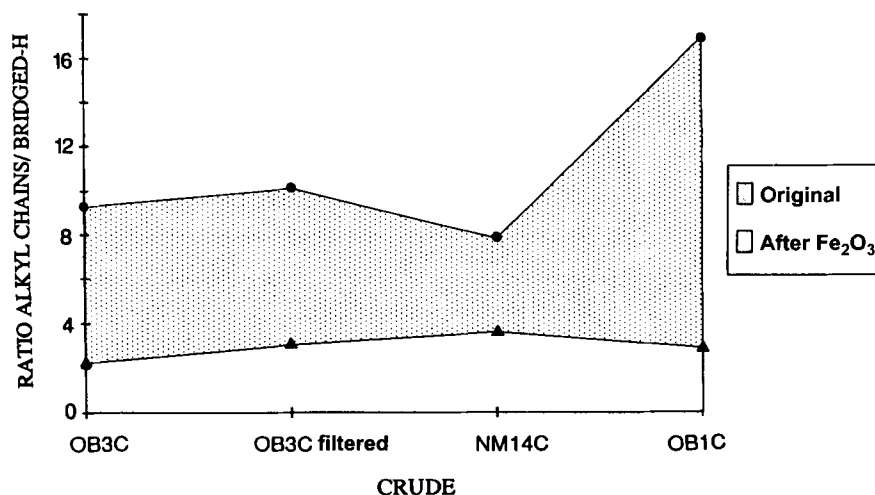


Fig. 13-18. Infrared measured ratio of alkyl-chains/bridged-H for crude oil asphaltenes before and after addition of Fe<sub>2</sub>O<sub>3</sub>.

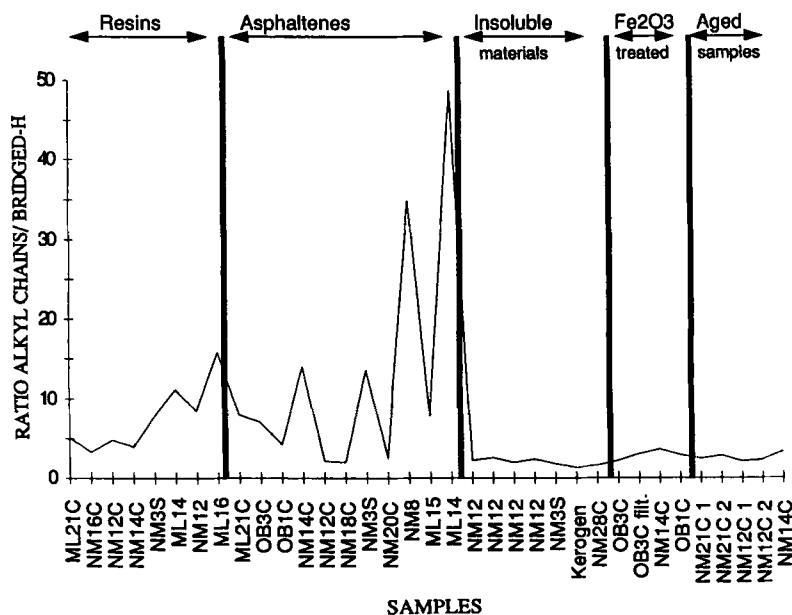


Fig. 13-19. Infrared measured ratio of alkyl-chains/bridged-H for different types of samples.

carbonates. There are cases where the IR spectrum taken from the asphaltene fraction separated from deposits showed a significant carbonyl band, whereas in other cases this band is weak (Fig. 13-20). The difference observed between the two sets of

TABLE 13-4

Minerals contents on organic type deposits

Deposit	wt% minerals
NM12	0.20
NM13	2.30
ML3	4.70
ML4	0.12
NM1	8.06
NM2	1.54
NM1	2.86
NM4	1.90
NM5	8.49
NM6	1.38
NM7	1.23
ML1	1.50
NM29S	0.81
NM30S	0.60
ML27S	0.00

samples was the presence or absence of carbonates in the oil reservoirs. Deposits formed in production wells drilled in carbonate rocks showed increased contents of carbonylic compounds. This evidence suggests that carbonates can act as selective substrates for retention (generation?) of carbonyl compounds. Similar findings have been published for stable organic residues separated from limestone and phosphatic rocks [94].

Preliminary investigation was carried out for the identification of the main chemical functionalities present on the insoluble organic fraction from a mixed deposit, using ML6 as target (see Figs. 13-4 and 13-20). The scheme used for this purpose is presented in Fig. 13-21. Initially, attempts were made to separate the organics from the minerals based on a flotation method using sodium pyrophosphate, previously described by Canadian researchers [79,81,83]. The amount of floating organic material recovered following this procedure was 27 wt% (see fraction B in Fig. 13-21). The IR spectrum of fraction B is presented in Fig. 13-22B. A comparison between this spectrum and that corresponding to the original material (Fig. 13-22A) shows better definitions of the alkyl stretching bands ( $2900\text{--}3000\text{ cm}^{-1}$ ), and the carbonyl and aromatics signals ( $1700\text{--}1600\text{ cm}^{-1}$ ). The improved detection of these signals points toward a certain level of organic matter purification. However, strong signals of carbonates ( $\approx 1442$  and  $736\text{--}605\text{ cm}^{-1}$ ) and silicates ( $\approx 1200\text{ cm}^{-1}$ ) suggest that purification has been largely precluded.

In order to recover the remaining organic materials, the dense fraction was then treated with a sequence of two digestions performed with HCl–HF. These acid treatments were adopted, since they have been used for a long time to get rid of minerals from kerogen samples [91,95,96] (recently, a proposition has been made to substitute the former procedure with a milder treatment with HF–BF<sub>3</sub> [97]). Disappearance of the carbonate signals was obvious after HCl treatment (see fraction C in Fig. 13-22). The

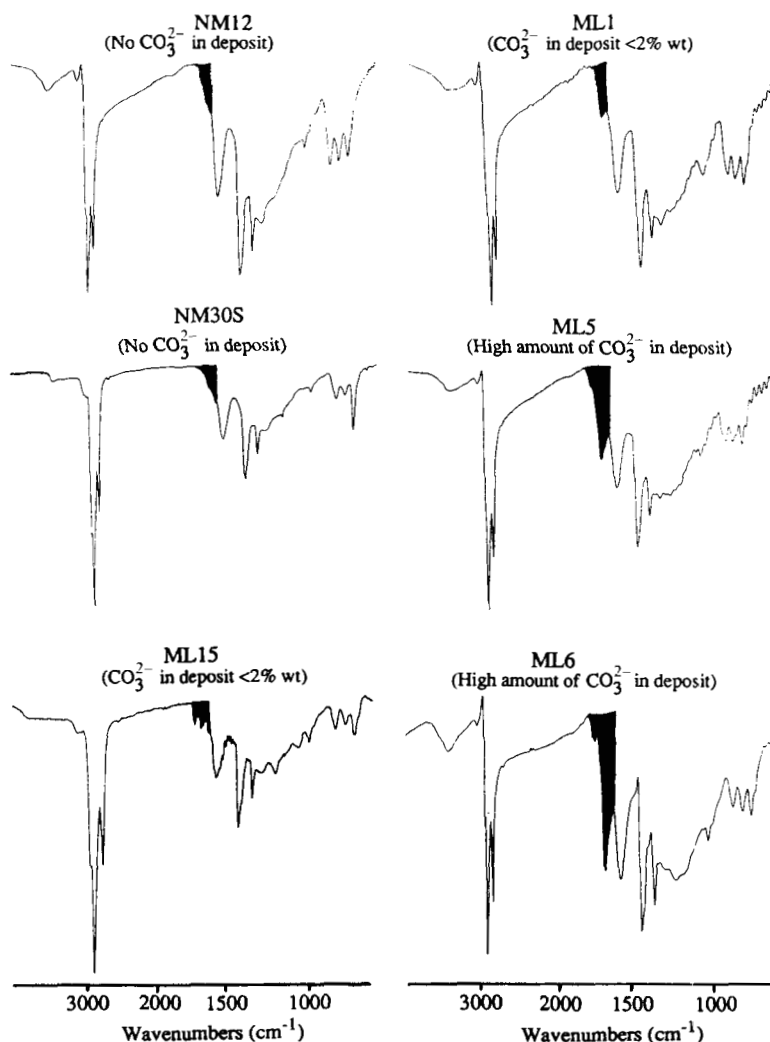


Fig. 13-20. Infrared spectra for asphaltenes separated from solid deposits.

same can be said regarding the silicate signals, after the HF digestion was performed (see fraction D in Fig. 13-22). With this procedure, 73 wt% of insoluble organics were recovered. An attempt was made to shed some light on the nature of the carboxylic components whose presence was fairly obvious at this stage (fraction D in Fig. 13-22).

Detailed characterization schemes for the determination of oxygen functionalities in asphaltenes have been previously described [76,77]. However, a simpler approach was followed in this work using basic hydrolysis followed by neutralization. The reaction sequence was monitored by IR spectroscopy, as indicated in Fig. 13-22. After alkaline

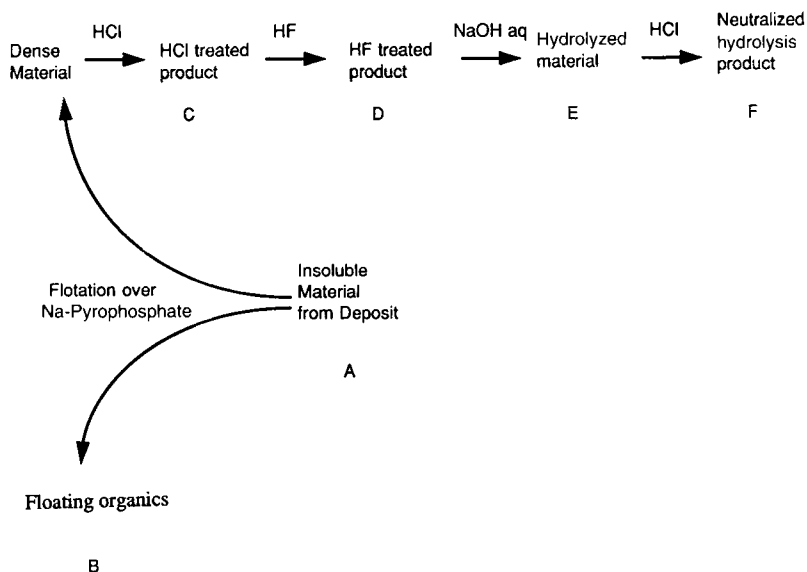


Fig. 13-21. Schematic for the preparative separation of insoluble organics and their subsequent basic hydrolysis.

hydrolysis was carried out, an increased absorption of the C–O–C region was observed ( $\approx 1200\text{ cm}^{-1}$ ), but no changes were apparent on the carbonyl band ( $1688\text{ cm}^{-1}$ ) (compare Fig. 13-22D and Fig. 13-22E). After the hydrolysis product was neutralized, dramatic changes were observed in the IR spectrum (Fig. 13-22F). The C–O–C band was clearly differentiated ( $1273\text{ cm}^{-1}$ ) and, what is more significant, the carbonyl band was split into two signals ( $1720$  and  $1697\text{ cm}^{-1}$ ). The presence of the  $1720\text{ cm}^{-1}$  band is unequivocal proof that carboxylic acid derivatives of the type  $\text{RCOOR}'$  were initially present in the insoluble organics. The persistence of the other carbonyl signal is indicative of the presence of other types of base-unreactive compounds, probably ketones, like those described by other authors studying insoluble organics [80,82,91,93]. Eventually, compounds protected against the basic hydrolysis can be also present as previously suggested for kerogen samples [98].

#### DEPOSITS CHARACTERIZATION AS A GUIDELINE FOR CLEANING OPERATIONS

The experience gained during this work provided the basis for proposing two different types of characterization schemes, so that possible causes for deposition can be identified. These schemes are identified as short and long. The short one is illustrated in Fig. 13-23. Its purpose is to give a quick answer to production engineers. It provides the tool to decide whether the deposit removal will be accomplished with the aid of organic and/or inorganic treatments. Usually, the decision is reached in 24 hours after the sample has been received in the analytical laboratory.

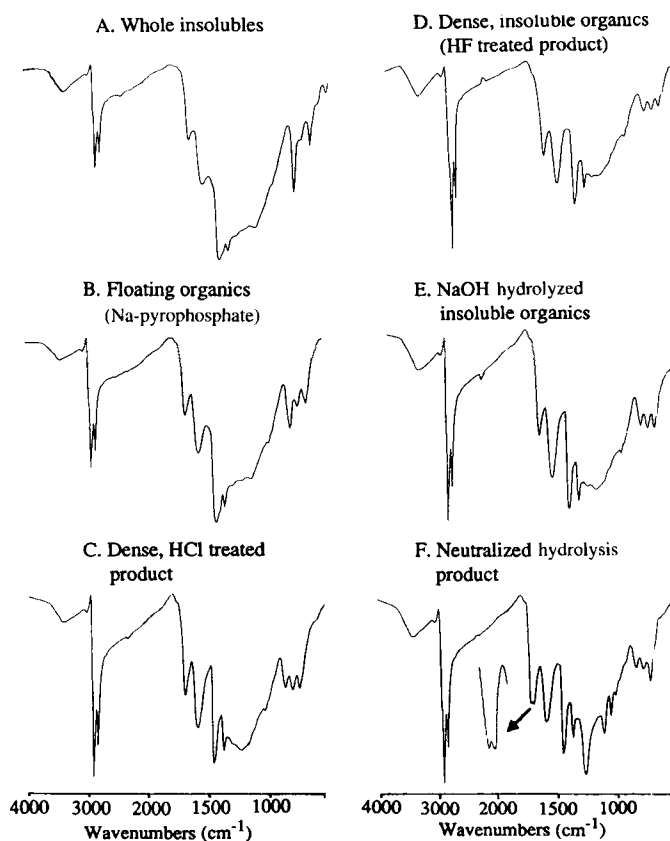


Fig. 13-22. Infrared monitoring of inorganics removal and basic hydrolysis of separated insoluble organics from ML6 deposit. For identification of fractions see Fig. 13-21.

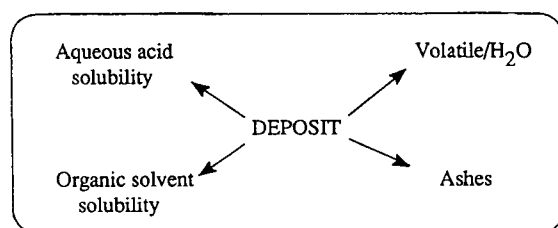


Fig. 13-23. Deposits short characterization scheme.

The long or detailed scheme is the one which has been described and followed in this work (Fig. 13-3). Two to four weeks are needed to complete the characterization through this path. It provides a more detailed information and understanding of the different factors influencing deposit formation. The preparative nature of this procedure is one of its strengths. Another is the possibility to generalize the causes of precipitation for



the whole reservoir with few studied points. This aspect is really important, and it can be evidenced when Fig. 13-4 is reexamined, i.e., most of the studied northern Monagas deposits proved to be predominantly organic (type I deposits), whereas the majority of the Maracaibo Lake deposits were of type II (inorganic).

## CONCLUSIONS

Deposits commonly found in oil production and transportation facilities are very complex mixtures, having soluble and insoluble organic components which interact with varying amounts of inorganic materials. Three main classes can be defined depending on the relative proportion of their components: (I) predominantly organics, (II) predominantly inorganics, (III) mixed composition.

The main characteristic of asphaltenic deposits is their high content of highly aromatic and condensed asphaltenes. Lower contents of high-molecular-weight paraffins, low-molecular-weight resins, and minerals are usually found in this type of solids. Influence of mineral matter on mixed-type deposit formation was ascertained for carbonates. Studied cases showed selectivity towards retention of carbonyl and carboxyl derivatives.

Investigation into the possible causes of crude oil stability showed that stable crudes present high contents of neutral aromatic compounds and, at the same time, asphaltenes with low aromaticities. Unstable crudes, on the contrary, are rich in paraffins and at the same time have highly aromatic and condensed asphaltenes. The relative amount of resins and asphaltenes does not correlate with stability of crudes, but apparent molecular size distribution of such components was found to influence crude stability.

The insolubility of organic materials was found to be strongly dependent on their hydrogen content and, in particular, on the low H/C ratios due to the lack of aliphatic chains. Gathered evidence from this and other works points toward the possible role of iron compounds on the complexation with organic components to form insoluble ones.

Finally, deposit characterization can be a guide for actions to be taken on reservoirs related to the studied samples.

## ACKNOWLEDGEMENTS

Funding by Intevep, S.A., and the operating affiliates of Petróleos de Venezuela, S.A., Corpoven, Lagoven and Maraven, made this study possible. The work was carried out under the research projects 'Asphaltenes deposition', 'Inhibition of solids deposition' and 'Characterization of bitumens, crudes, oil fractions and heavy products'. Helpful discussions held with the asphaltene team, particularly with O. Rivas, are greatly appreciated. The help extended by M. Orea and M. Fonseca of Intevep in analyzing the deposits is greatly appreciated. Analytical support given by the Analysis and Evaluation Department of Intevep is very much appreciated.

## REFERENCES

- [1] Boussingault, M., Mémoire sur la composition des bitumens. *Ann. Chem. Phys.*, 64: 141 (1837).
- [2] Long, R.B., The concept of asphaltenes. *Prepr. Am. Chem. Soc., Div. Pet. Chem.*, 24 (4): 891–900 (1979).
- [3] Batts, B.D. and Zuhdan, F.A., A literature review of fuel stability with particular emphasis on diesel oil. *Energy Fuels*, 5: 2–21 (1991).
- [4] Barbier, J., Deactivation of reforming catalysts by coking — a review. *Appl. Catal.*, 23: 225–243 (1986).
- [5] Izquierdo, A., Carbognani, L., Leon, V. and Parisi, A., Characterization of Venezuelan heavy oil vacuum residua. *Fuel Sci. Technol. Int.*, 7 (5–6): 561–570 (1989).
- [6] Belinko, K., Nandi, B.N. and Denis, J.M., The distribution of coke precursors in the reactor during thermal hydrocracking of Athabasca bitumen. *Proc. Oil Sands*, pp. 189–196 (1977).
- [7] Speight, J.G., Upgrading heavy oils and residua: the nature of the problem. In: S. Kaliaguine and A. Mahay (Editors), *Catalysis on the Energy Scene*. Elsevier, Amsterdam, pp. 515–527 (1984).
- [8] Nellensteyn, F.J., The colloidal structure of bitumens. In: A.E. Dunston (Editor), *The Science of Petroleum*, 4. Oxford Univ. Press, Oxford, pp. 2760–2764 (1938).
- [9] Pfeiffer, J.P. and Saal, R.N.J., Asphaltic bitumens as a colloidal system. *J. Phys. Chem.*, 49: 139–149 (1940).
- [10] Yen, T.F., Chemistry of asphaltenes. In: J.W. Bunger (Editor), *ACS Symposium Series 195*. American Chemical Society, Division of Petroleum Chemistry, Washington, DC, pp. 39–51 (1981).
- [11] Koots, J.A. and Speight, J.G., Relation of petroleum resins to asphaltenes. *Fuel*, 54: 179–184 (1975).
- [12] Storm, D.A., Barresi, R.J. and Sheu, E.Y., Asphaltene molecules in vacuum residue. *Prepr. Am. Chem. Soc., Div. Pet. Chem.*, 40 (4): 776–779 (1995).
- [13] Youtcheff, J.S. and Jones, D.R. IV, Guideline for asphalt refiners and suppliers. Strategic Highway Research Program – NRC. *Report SHRP-A-689*. Washington, DC (1994).
- [14] Cassani, F.C., *Personal communication*. Intevep, S.A. Miranda (1992).
- [15] von Albretch, C., Diaz, B., Salathiel, W.M. and Nierode, D.E., Stimulation of asphaltic deep wells and shallow wells in Lake Maracaibo, Venezuela. *Proc. 10th Pet. Congr.*, 3: 55–62 (1980).
- [16] Hasket, C.E. and Tartera, M.A., Practical solution to the problem of asphaltene deposits, Hassi Messaoud field, Algeria. *J. Pet. Technol.*, 17: 387–391 (1965).
- [17] Lichaa, P.M., Asphaltene deposition problem in Venezuela crudes — usage of asphaltene in emulsion stability. In: *CIM Conference on the Oil Sands of Canada and Venezuela, June 1977*. *Can. Inst. Min. Metall. Spec.*, 17: 609–624 (1977).
- [18] Lichaa, P.M. and Herrera, L., Electrical and other effects related to prevention of asphaltene deposition. *SPE AIME Pap. 5304, Soc. Pet. Eng.* (1975).
- [19] Escobedo, J. and Mansoori, G.A., Heavy organic deposition and plugging of wells (analysis of Mexico's experience). *Soc. Pet. Eng. Pap.*, 23696: 1–14 (1994).
- [20] Tuttle, R.N., High pour point and asphaltenic crude oils and condensates. *J. Pet. Technol.*, 35 (4): 1192–1196 (1983).
- [21] Kokal, S.L. and Sayegh, S.G., Asphaltene deposition: a literature review. *Pet. Recovery Inst. (Canada)*, Rep. 1990-5, pp. 1–80 (1990).
- [22] Akbar, S.H. and Saleh, A.A., A comprehensive approach to solve asphaltene deposition problem in some deep wells. *Soc. Pet. Eng. Pap.*, 17965: 377–384 (1989).
- [23] Thaver, R., Nicoll, D.C. and Graeme, D., Asphaltene deposition in production facilities. *Soc. Pet. Eng. Pap.*, 18473: 137–146 (1989).
- [24] Thomas, D.C., Becker, H.L. and Del Real Soria, R.A., Controlling asphaltene deposition in oil wells. *Soc. Pet. Eng. Pap.*, 25483: 679–687 (1993).
- [25] Barberis Canonico, L., Del Bianco, A., Piro, G., Stroppa, F., Carniani, C. and Mazzolini, E.I., A comprehensive approach for the evaluation of chemicals for asphaltene deposit removal. In: P.H. Ogden (Editor), *Recent Advances in Oilfield Chemistry*. The Royal Society of Chemistry, London, pp. 220–233 (1994).
- [26] Broadbush, G., Well- and formation-damage removal with nonacid fluids. *J. Pet. Technol.*, 40 (6): 685–687 (1988).

- [27] Carbognani, L., Espidel, J. and Izquierdo, A., Characterization of solid deposits sampled in Venezuelan oil production and transportation facilities. *Proc. IS COP'95, 1st Int. Symp. Colloid Chem. Oil Prod.*, Rio, pp. 40–43 (1995).
- [28] DelBianco, A., Stroppa, F. and Bertero, L., Tailoring hydrocarbon streams for asphaltene removal. *Soc. Pet. Eng. Pap.*, 28992: 493–498 (1995).
- [29] Trbovich, M.G. and King, G.E., Asphaltene deposit removal: long-lasting treatment with a cosolvent. *Soc. Pet. Eng. Pap.*, 21038: 393–400 (1991).
- [30] Acosta, A., *Efecto de las Resinas en la Deposición de Asfaltenos*. Trabajo especial de grado. Escuela de Ingeniería y Ciencias Aplicadas. Univ. de Oriente (1981).
- [31] Schantz, S.S. and Stephenson, W.K., Asphaltene deposition: development and application of polymeric asphaltene dispersants. *Soc. Pet. Eng. Pap.*, 22783: 243–249 (1991).
- [32] Stephenson, W.K., Producing asphaltene crude oils: problems and solutions. *Pet. Eng. Int.*, 62 (6): 24–31 (1990).
- [33] DeBoer, R.B., Leerloyer, K., Eigner, M.R.P. and VanBergen, A.R.D., Screening of crude oils for asphalt precipitation. Theory, practice, and selection of inhibitors. *Soc. Pet. Eng. Pap.*, 24987: 259–270 (1992).
- [34] Chang, C.L. and Fogler, H.S., Asphaltene stabilization in alkyl solvents using oil-soluble amphiphiles. *Soc. Pet. Eng. Pap.*, 25185: 339–349 (1993).
- [35] Chang, C.L. and Fogler, H.S., Stabilization of asphaltenes in organic solvents using alkylbenzene-derived amphiphiles, 1. Effect of the chemical structure of amphiphiles on asphaltene stabilization. *Langmuir*, 10: 1749–1757 (1994).
- [36] Chang, C.L. and Fogler, H.S., Stabilization of asphaltenes in organic solvents using alkylbenzene-derived amphiphiles, 2. Study of the asphaltene–amphiphile interactions and structures using Fourier transform infrared spectroscopy and small-angle X-ray scattering techniques. *Langmuir*, 10: 1758–1766 (1994).
- [37] Gonzalez, G. and Middea, A., Peptization of asphaltene by various oil-soluble amphiphiles. *Colloids Surface*, 52 (3–4): 207–217 (1991).
- [38] Samuelson, M.L., Alternatives to aromatics for solvency of organic deposits. *Soc. Pet. Eng. Pap.*, 23816: 447–454 (1992).
- [39] Carbognani, L. and Espidel, J., Characterization of solid deposits from production facilities. Identification of possible causes of deposits formation. *Visión Tecnol.*, 3 (1): 35–42 (1995).
- [40] Sohnel, O. and Chianese, A., Scaling in the chemical industry. *Chim. Ind.*, 72 (3): Q2–Q8 (1990).
- [41] Speight, J.G., Wernick, D.L., Gould, K.A., Overfield, R.E., Rao, B.M.L. and Savage, D.W., Molecular weight and association of asphaltenes: a critical review. *Rev. Inst. Fr. Pet.*, 40 (1): 51–61 (1985).
- [42] Green, J.B., Diehl, B.H. and Shay, J.Y., Effects of composition and boiling range on the accuracy of average molecular weight of petroleum fractions determined by vapor pressure osmometry. *Proc. UNITAR 5th Int. Conf. Heavy Crude and Tar Sands*, 4, pp. 133–142 (1991).
- [43] Boduszynski, M.M., McKay, J.F. and Latham, D.R., Composition of heavy ends of a Russian petroleum. *Prepr. Am. Chem. Soc., Div. Pet. Chem.*, 26 (4): 865–881 (1981).
- [44] Altgelt, K.H. and Boduszynski, M.M., Properties of heavy petroleum fractions. In: *Composition and Analysis of Heavy Petroleum Fractions*. Marcell Dekker, New York, pp. 75–128 (1994).
- [45] Moschopedis, S.E. and Speight, J.G., Investigation of hydrogen bonding by oxygen functions in Athabasca bitumen. *Fuel*, 55 (7): 187–192 (1976).
- [46] Sheu, E.Y. and Storm, D., Colloidal properties of asphaltenes in organic solvents. In: E.Y. Sheu and O. Mullins (Editors), *Asphaltenes. Fundamentals and Applications*. Plenum Press, London, pp. 1–52 (1995).
- [47] From Ref. 12 cited in: Rivas, O., Desarrollo de una metodología sistemática para el control de la precipitación de asfaltenos. *Visión Tecnol.* 2 (2): 4–17 (1995).
- [48] Strausz, O.P., Mojelsky, T.W. and Lown, E.M., The molecular structure of asphaltene: an unfolding story. *Fuel*, 71: 1355–1363 (1992).
- [49] Speight, J.G., Polynuclear aromatic systems in petroleum. *Prepr. Am. Chem. Soc., Div. Pet. Chem.*, 31 (3–4): 818–825 (1986).
- [50] Angulo, R., Borges, A., Fonseca, M. and Gil, C., Experimental asphaltene precipitation study.

- Phenomenological behavior of Venezuelan live oils. *Proc. ISCO'95 1st Int. Symp. Colloid Chem. Oil Prod.*, Rio, pp. 109–110 (1995).
- [51] Cimino, R., Corraera, S., DelBianco, A. and Lockhardt, T.P., Solubility and phase behavior of asphaltenes in hydrocarbon media. In: E.Y. Sheu and O. Mullins (Editors), *Asphaltenes: Fundamentals and Applications*. Plenum Press, London, pp. 97–130 (1995).
- [52] Leontaritis, K.J., Kawanaka, S. and Mansoori, G.A., Descriptive account of thermodynamic and colloidal models of asphaltene flocculation. *Prepr. Am. Chem. Soc., Div. Pet. Chem.*, 33 (1): 196–204 (1988).
- [53] Hirschberg, A., Dejong, L.N.J., Schipper, B.A. and Meyer, J.G., Influence of temperature and pressure on asphaltene flocculation. *Soc. Pet. Eng. Pap.*, 18273: 283–293 (1988).
- [54] Kawanaka, S., Park, S.J. and Mansoori, G.A., Organic deposition from reservoir fluids: a thermodynamic predictive technique. *Soc. Pet. Eng. Reserv. Eng.*, 6 (2): 185–192 (1991).
- [55] Rivas, O., Desarrollo de un método sistemático para el control de la precipitación de asfaltenos. *Visión Technol.*, 2 (2): 4–17 (1995).
- [56] Leontaritis, K.J. and Mansoori, G.A., Asphaltene flocculation during oil production and processing: a thermodynamic colloidal model. *Soc. Pet. Eng. Pap.*, 16258: 149–158 (1987).
- [57] Carbognani, L. and Espidel, J., A comparison study of SARA fractions from conventional and heavy oils in relation to their deposition tendency in production pipelines. *Proc. UNITAR 6th Int. Conf. Heavy Oil and Tar Sands*, 2, pp. 551–560 (1995).
- [58] ASTM-D-2787, Standard-test method for boiling range distribution of petroleum fraction by gas chromatography. *Ann. Book ASTM Standards. Pet. Prod. and Lub. (II)*, 05-02, pp. 483–490 (1989).
- [59] ASTM-D-3239, Standard-test method for aromatic types-analysis of gas-oil aromatic fractions by high ionizing voltage mass spectrometry. *Ann. Book ASTM Standards. Pet. Prod. and Lub. (II)*, 05-02, pp. 643–655 (1989).
- [60] Leon, V., Average molecular weight of oil fractions by nuclear magnetic resonance. *Fuel*, 66 (10): 1445–1446 (1987).
- [61] Petrakis, L. and Allen, D., *NMR for Liquid Fossil Fuels*. Elsevier, Amsterdam (1986).
- [62] Waller, P.R., Williams, A. and Bartle, K.D., The structural nature and solubility of residual fuel oil fractions. *Fuel*, 68 (4): 520–526 (1989).
- [63] Quinga, E.M. and Larsen, J.W., Noncovalent interactions in high rank coals. *Energy Fuels*, 1: 300–304 (1987).
- [64] Mallya, N. and Stock, L.M., The alkylation of high rank coals. Non-covalent bonding interactions. *Fuel*, 65 (5): 736–738 (1986).
- [65] SMS 2526-78, Flocculation ratio and peptizing power of oils containing asphaltenes. *Shell Method Series* (1978).
- [66] Zerlia, T., Valutazione della stabilita e della compatibilita di oli residui, II. Compatibilita. *Riv. Combust.*, 48 (5): 207–213 (1994).
- [67] Lambert, D.C. and Holder, K.A., IR analyzer for stability measurement of residual oils. *Proc. UNITAR 4th Int. Conf. Heavy Crude and Tar Sand*, 2, pp. 449–455 (1988).
- [68] Gaestel, Ch., Smadia, R. and Lamminan, K.A., Contribution a la connaissance des proprietes des bitumes routiers. *Rev. Gen. Routes Aerod.*, 466: 95–98 (1971).
- [69] Leni Figuereido, M.L., Caracterizacão química dos cimentos asfálticos. *B. Tecn. Petrobrás*, 33 (1): 31–37 (1990).
- [70] Speight, J.G., *The Chemistry and Technology of Petroleum*. Marcell Dekker, New York, 2nd ed. (1991).
- [71] Avram, M. and Mateescu, Gh.D., *Spectroscopie Infrarouge, Application en Chimie Organique*. Dunod, Paris (1970).
- [72] Dyer, J.R., *Applications of Absorption Spectroscopy of Organic Compounds*. Prentice-Hall, Englewood Cliffs, N.J. (1965).
- [73] Ignasiak, T., Strausz, O.P. and Montgomery, D.S., Oxygen distribution and hydrogen bonding in Athabasca asphaltene. *Fuel*, 56 (10): 359–365 (1977).
- [74] Petersen, J.C., An infra-red study of hydrogen bonding in asphalt. *Fuel*, 46: 295–305 (1967).
- [75] Moschopedis, S.E. and Speight, J.G., Oxygen functions in asphaltenes. *Fuel*, 55 (10): 334–336 (1976).
- [76] Speight, J.G. and Moschopedis, S.E., Anomalous effects in the character of the carbonyl absorption

- (ca.  $1700\text{ cm}^{-1}$ ) in the infrared spectra of petroleum resins and asphaltenes. *Prepr. Am. Chem. Soc., Div. Pet. Chem.*, 26 (4): 907–911 (1981).
- [77] Moschopedis, S.E., Fryer, J.F. and Speight, J.G., Investigations of the carbonyl functions in a resin fraction from Athabasca bitumen. *Fuel*, 55 (7): 184–186 (1976).
- [78] Frakman, Z., Ignasiak, T.M., Lown, E.M. and Strausz, O.P., Oxygen compounds in Athabasca asphaltene. *Energy Fuels*, 4: 263–270 (1990).
- [79] Sengupta, S., Hall, E.E. and Tollefson, E.L., Isolation and characterization of non bituminous organic materials which may interfere with recovery of bitumen from oil sands. *Proc. UNITAR 4th Int. Conf. Heavy Oil and Tar Sand*, 1, Pap. 103 (1988).
- [80] Mikula, R.J., Axelson, D.E. and Sheeran, D., Mineral matter and clay-organic complexes in oil sands extraction processes. *Fuel Sci. Technol. Int.*, 11 (12): 1695–1729 (1993).
- [81] Kotlyar, L.S., Ripmeester, J.A., Sparks, B.D. and Kodama, H., Comparative study of organic-rich solids present in Utah and Athabasca oil sands. *Proc. UNITAR 4th Int. Conf. Heavy Crude and Tar Sand*, 1, Pap. 16 (1988).
- [82] Kotlyar, L.S., Ripmeester, J.A., Sparks, B.D. and Woods, J.R., Characterization of strongly bound organic matter present in Athabasca oil sands using a combination of alkaline and supercritical fluid extraction. *Proc. UNITAR 5th Int. Conf. Heavy Crude and Tar Sand*, 1, pp. 97–102 (1991).
- [83] Kotlyar, L.S., Sparks, B.D., Kodama, H. and Gratam-Bellew, P.E., Isolation and characterization of organic-rich solids present in Utah oil sand. *Energy Fuels*, 2: 589–593 (1988).
- [84] Coleman, H.J., Dooley, J.E., Hirsch, D.E. and Thompson, C.J., Compositional studies of a high boiling  $370\text{--}535^\circ\text{C}$  distillate from Prudhoe Bay, Alaska, crude oil. *Anal. Chem.*, 45 (9): 1724–1737 (1973).
- [85] Latham, D.R. and Haines, W.E., Chromatographic techniques used in the characterization of high boiling petroleum distillates. *Prepr. Am. Chem. Soc., Div. Pet. Chem.*, 18 (3): 567–571 (1973).
- [86] Jewell, D.M., Albaugh, E.W., Davis, B.E. and Ruberto, R.G., Integration of chromatographic and spectroscopic techniques for the characterization of residual oils. *Ind. Eng. Chem. Fundam.*, 13 (3): 278–282 (1974).
- [87] Galya, L.G. and Suatoni, J.C., Rapid SARA separations by high performance liquid chromatography. *J. Liq. Chrom.*, 3 (2): 229–242 (1980).
- [88] Ignasiak, T., Kotlyar, L., Sanman, N., Montgomery, D.S. and Strausz, O.P., Preparative gel permeation chromatography of Athabasca asphaltene and the relative polymer forming propensity of the fractions. *Fuel*, 63 (3): 363–369 (1983).
- [89] Kotlyar, L.S. and Ripmesster, J.A., Application of solid state silicon-29 and carbon-13 nuclear magnetic resonance spectroscopy to the characterization of inorganic matter–humic complexes in Athabasca oil sands. *Prepr. Am. Chem. Soc., Div. Pet. Chem.*, 33 (2): 253–256 (1988).
- [90] Kotlyar, L.S., Ripmeester, J.A., Sparks, B.D. and Woods, J.R., Comparative study of organic matter derived from Utah and Athabasca oil sands. *Fuel*, 67 (11): 1529–1535 (1988).
- [91] Majid, A., Sparks, B.D. and Ripmesster, J.A., Characterization of solvent insoluble organic matter associated with mineral matter from oil sands. *Fuel Sci. Technol. Int.*, 11 (2): 279–292 (1993).
- [92] Kotlyar, L.S., Ripmesster, J.A., Sparks, B.D. and Montgomery, D.S., Characterization of oil sands solids closely associated with Athabasca bitumen. *Fuel*, 67 (6): 808–814 (1988).
- [93] Axelson, D.E., Mikula, R.J. and Potoczny, Z.M., Characterization of oil sands mineral components and clay–organic complexes. *Fuel Sci. Technol. Int.*, 7 (5–6): 659–673 (1989).
- [94] Benalioulhaj, S. and Trichet, J., Comparative study by infrared spectroscopy of the organic matter of phosphate-rich (Oulad Abdoun basin) and black shale (Timahdit basin) series (Morocco). *Org. Geochem.*, 16 (4–6): 829–852 (1990).
- [95] Tissot, B.P. and Welte, D.H., Kerogen: composition and classification. In: *Petroleum Formation and Occurrence*. Springer, Berlin, pp. 123–147 (1978).
- [96] Barakat, A.O. and Rullkotter, J., Extractable and bound fatty acids in core sediments from the Nordlinger Ries, southern Germany. *Fuel*, 74 (3): 416–425 (1995).
- [97] Robl, T.L. and Davis, B.H., Comparison of the  $\text{HF-HCl}$  and  $\text{HF-BF}_3$  maceration techniques and the chemistry of the resultant organic concentrates. *Org. Geochem.*, 20 (2): 249–255 (1993).
- [98] Rullkotter, J. and Michaelis, W., The structure of kerogen and related materials. A review of recent progress and future trends. *Org. Geochem.*, 16 (4–6): 829–852 (1990).

## *Chapter 14*

# **CHEMICAL COMPOSITION OF ASPHALT AS RELATED TO ASPHALT DURABILITY**

J. CLAINE PETERSEN

## **INTRODUCTION**

Two major chemical factors affecting asphalt durability are the compatibility of the interacting components of asphalt and the resistance of the asphalt to change from oxidative aging. Historically, studies of the chemical components of asphalt have been facilitated by separation of asphalt into component fractions, sometimes called generic fractions. These fractions, however, are still complex mixtures, which can vary significantly among asphalts of different sources. The reaction of asphalt with atmospheric oxygen is a major factor leading to the hardening and embrittlement of asphalt. The hardening phenomenon is primarily a result of the formation of polar oxygen-containing functional groups in asphalt, which increase asphalt consistency through strong molecular interaction forces. The characterization of the chemical functional types (that are normally present in asphalt or formed by oxidative aging) gives a fundamental approach to the relationships between asphalt composition and asphalt properties and the performance of asphalts and asphalt–aggregate mixtures. In addition to the polar chemical functional groups formed by oxidation, asphalt properties can also be significantly altered by molecular structuring, which is sometimes called steric hardening. This potentially reversible phenomenon, although highly elusive and difficult to quantify in asphalt pavement mixtures, may be a major factor contributing to pavement embrittlement.

Differences in the quality of asphalts depend on their crude oil sources because different crude oils have different chemical compositions. Relationships between composition and performance properties have long been recognized, as shown by the many publications on the subject, a few of which are cited [1–13]. Asphalts with the same specifications often produce pavements with widely differing performance and serviceability. Factors such as aggregate characteristics, design, construction variables, and environment play major roles in determining pavement performance. However, studies such as the well-known Zaca-Wigmore Experimental Road Test [4–9], in which construction variables were carefully controlled and asphalt sources were intentionally varied, clearly demonstrate the importance of asphalt chemical composition on pavement durability.

For the purposes of this review, a durable asphalt is defined as one that (a) possesses the physical properties necessary to produce the desired initial product performance properties, and (b) is resistant to changes in physical properties during long-term, in-service environmental aging. Although design and construction variables are major factors in pavement durability, more durable asphalts will produce more durable pavements.

The importance of chemical composition to asphalt durability, although not well understood, cannot be disputed. Durability is determined by the physical properties of

the asphalt, which are determined directly by chemical composition. An understanding of the chemical factors affecting physical properties is thus fundamental in order to understand the factors which control asphalt durability.

The purpose of this chapter is to examine the literature dealing with the chemical composition of asphalt and changes in composition during environmental aging that affect durability-related properties. Past and recent research are considered. Due to the extreme breadth of the subject and the voluminous literature related to durability, a complete bibliography will not be attempted, but sufficient references will be cited to allow the serious researcher to find additional literature. An approach to the fundamental chemical factors affecting asphalt properties and durability will also be presented.

#### PRELIMINARY CONSIDERATION OF FACTORS AFFECTING ASPHALT DURABILITY

To provide a background for the documented discussions that follow, the major composition-related factors affecting durability are briefly outlined. The most important aspect of a durable asphalt, assuming that it meets initial performance requirements, is its resistance to change while in service. The dominant physical change leading to reduced asphalt durability is a change in flow properties related to excessive stiffening or hardening of the asphalt. Three fundamental composition-related factors govern the changes that could cause hardening of asphalts in pavements: (1) loss of the oily components of asphalt by volatility or absorption by porous aggregates; (2) changes in the chemical composition of asphalt molecules from reaction with atmospheric oxygen; and (3) molecular structuring that produces thixotropic effects (steric hardening).

With current specifications and construction practices, volatility loss is probably not a significant contribution to pavement hardening. Reaction with atmospheric oxygen is probably the major and best understood cause. Molecular structuring, although elusive and difficult to quantify, may also be a significant contributor.

Irreversible adsorption of polar asphalt components by mineral aggregate surfaces, although not a factor that might be expected to harden asphalt, will produce compositional changes in the asphalt that may significantly affect asphalt properties and aging characteristics. It is also recognized that environmental factors which affect the properties of the asphalt-aggregate bond, water in particular, can seriously affect the performance and durability of asphalt pavements. However, even though moisture-induced damage may be related to asphalt composition and adsorption of asphalt components on aggregate surfaces, it is primarily an interfacial phenomenon and beyond the scope of this paper.

#### CHEMICAL COMPOSITION OF ASPHALT

##### *Elemental and molecular composition*

Before an attempt is made to discuss the relationship between chemical composition and asphalt properties affecting durability, the chemical composition of asphalt will be reviewed. Asphalt is not composed of a single chemical species, but is rather a complex

TABLE 14-1

Elemental analyses of representative petroleum asphalts [14]

Element	Asphalt <sup>a</sup>			
	B-2959 (Mexican)	B-3036 (Ark.-La.)	B-3051 (Boscan)	B-3602 (Californian)
Carbon (%)	83.77	85.78	82.90	86.77
Hydrogen (%)	9.91	10.19	10.45	10.94
Nitrogen (%)	0.28	0.26	0.78	1.10
Sulfur (%)	5.25	3.41	5.43	0.99
Oxygen <sup>b</sup> (%)	0.77	0.36	0.29	0.20
Vanadium (ppm)	180	7	1380	4
Nickel (ppm)	22	0.4	109	6

<sup>a</sup> From study by Welborn et al. [15].<sup>b</sup> By difference.

mixture of organic molecules that vary widely in composition from nonpolar saturated hydrocarbons to highly polar, highly condensed aromatic ring systems. Elemental analyses of several representative petroleum asphalts are presented in Table 14-1. Although asphalt molecules are composed predominantly of carbon and hydrogen, most molecules contain one or more of the so-called heteroatoms (nitrogen, sulfur, and oxygen) together with trace amounts of metals, principally vanadium and nickel. As seen in Table 14-1, the heteroatoms, although a minor component compared to the hydrocarbon moiety, can vary in concentration over a wide range, depending on the source of the asphalt. Inasmuch as heteroatoms often impart functionality and polarity to the molecules, their presence may make a disproportionately large contribution to the differences in chemical and physical properties among asphalts from different sources.

Elemental analyses are average values and reveal little information about how the atoms are incorporated into the molecules or what type of molecular structures are present. Molecular type and structure information is necessary for a fundamental understanding of how composition affects physical properties and chemical reactivity. The molecular structures in asphalt will be discussed in more detail in subsequent sections; however, an overview is important at this point.

Inasmuch as the asphalt is undoubtedly produced from living organic matter by maturation in the earth for millions of years, the molecular structures of the compounds present are highly diverse. Carbon in aromatic ring systems is estimated by correlations based on carbon-hydrogen analyses and densities [16,17] and directly by nuclear magnetic resonance (NMR) [18]. Concentrations of aromatic carbon determined by NMR typically range from 25 to 35% for petroleum asphalts. The aromatic carbon is incorporated in condensed aromatic ring systems, which contain 1 to 10 rings per aromatic moiety [18]. These ring systems may be associated with saturated naphthenic (cycloalkyl) ring systems. Both the aromatic and naphthenic ring systems may have attachments composed of a variety of types of normal or branched hydrocarbon side chains. Concentrations of carbon associated with naphthenic ring systems in asphalts, as determined using NMR [18], are typically in the range of 15 to 30%. Normal



and branched chain hydrocarbons are present either as individual molecules or as the previously mentioned moieties associated with naphthenic or aromatic rings. The nonaromatic and nonnaphthenic carbon content of asphalt would typically range from 35 to 60%. It should be noted that examples outside these ranges may be found and the variety of possible combinations of molecular structures in an asphalt is astronomically large and may vary widely from one crude source to another. The hydrocarbon molecular structures are further complicated by the heteroatoms, sulfur, nitrogen, and oxygen, which are often present in sufficient combined amounts so that, on the average, one or more heteroatom(s) per molecule may be present. These may be incorporated within the ring or non-ring components or in more discrete chemical functional groups attached to these components.

The heteroatoms, particularly nitrogen and oxygen, and the aromatic ring systems contribute considerable polarity or polarizability to the molecules that produce the major association forces affecting physical properties. This will be discussed in more detail in a later section.

Inasmuch as there are a large number of molecules in asphalt with different chemical structures and reactivities, chemists have not seriously considered attempts to separate and identify them. Considerable progress, however, has been made in the study of asphalt composition by separation or characterization of asphalt based on the reactivity or polarity or both of the various molecular types present. The molecules in asphalt can be conveniently separated or grouped into classes of molecular types or fractions based on their chemical functionality. This separation and classification of molecular types has been useful to provide simpler component fractions that permit further characterization and has aided in determining how different molecular types affect the physical and chemical properties of the whole asphalt.

#### *Asphalt composition as defined by fractionation*

A variety of procedures have been employed in attempts to fractionate asphalt into less complex and more homogeneous fractions. Some procedures are simple [19], while others are more complex [20,21]. Many are specialized for a given research endeavor in which they were used to prepare fractions for further characterization. Several, however, have found a more general use to characterize and classify asphalts. These classical separation schemes used extensively in the past can be classified into three general types based on the procedure used: (a) partitioning with partial solvents [22–24], (b) selective adsorption–desorption [10,19,25], and (c) chemical precipitation [5,6]. Size exclusion chromatography (SEC), also called gel permeation chromatography (GPC), is also an important separation method; however, it has been used primarily in the past as an analytical method on very small samples to characterize the molecular size distribution of asphalt molecules or molecular agglomerates [26–30] rather than as a method to separate asphalt components for further analysis. More recently SEC was applied as a preparative method in the Strategic Highway Research Program (SHRP) to prepare gram-sized quantities of separated asphalt components for further analysis [31,32]. Also during SHRP another preparative separation technique called ion exchange chromatography was applied to asphalt [32–34]. This technique separates

asphalt molecules on the basis of their acidic and basic properties. Both SEC and IEC were used extensively during the research of the SHRP to study relationships between asphalt chemical composition and physical properties. These techniques will be discussed later on in more detail.

Schematic diagrams illustrating the three classical types of component fractionation schemes are shown in Fig. 14-1. Partitioning with selective solvents (Scheme 1-A) has not been widely used. Although it avoids contact with adsorbents and chemicals that might irreversibly adsorb or alter asphalt components, the fractions obtained are usually not as distinctively different as with the other separation types. In general, one sequentially treats the asphalt with increasingly polar solvents, which precipitate a series of fractions with decreasing polarity.

Selective adsorption-desorption chromatography is the most widely used separation technique. This technique is typified by Scheme 1-B in Fig. 14-1. The asphaltenes are first separated based on their insolubility in a nonpolar paraffinic solvent. This removes the most polar and least soluble asphalt components and generally facilitates further separation. The remaining petrolene (maltene) fraction, which is dissolved in the paraffinic solvent, is then adsorbed on a chromatographic column and sequentially desorbed with solvents of increasing polarity. By proper selection of the adsorbant and desorption solvents, a series of fractions with increasing polarity is obtained. The fractions obtained will be described in some detail to provide background for discussion in later sections of this chapter.

The saturate fraction, because it lacks polar chemical functional groups, is not adsorbed on the column and emerges first. (It is important to note that although the names of component fractions were often intended to describe the predominant chemical types, component fractions are still complex mixtures and do not represent clear-cut compound-type separations.) The saturate fraction may contain saturated normal and branched-chain hydrocarbons, saturated cyclic hydrocarbons (sometimes called naphthenic hydrocarbons), and possibly a small amount of mono-ring aromatic hydrocarbons; however, those molecules containing ring systems are dominated by attached saturated hydrocarbon side chains. Sulfur is often found to be incorporated in molecules of the saturate fraction. Addition to the chromatographic column of a more polar aromatic solvent, such as benzene (now usually replaced by toluene), which competes for the polar sites on the adsorbants, displaces the more weakly adsorbed asphalt molecules. These molecules usually contain condensed nonaromatic and aromatic ring systems, and in addition to sulfur, the heteroatoms, oxygen and nitrogen, may also be part of the molecule. In Scheme 1-B, this fraction has been called the naphthene-aromatic fraction.

Finally, a highly polar solvent, such as an alcohol, is added to the benzene to displace most of the strongly adsorbed and most polar components of the petrolene fraction. The alcohol debonds these components, which are held strongly to the adsorbant by highly polar functional groups, and the benzene provides solubility for these components as they elute from the column. This fraction, called polar aromatics, contains highly condensed aromatic ring systems and functional groups containing heteroatoms. It should be noted here, and will be important later when durability and oxidation susceptibility are discussed, that all fractions contain, to a greater or lesser degree,

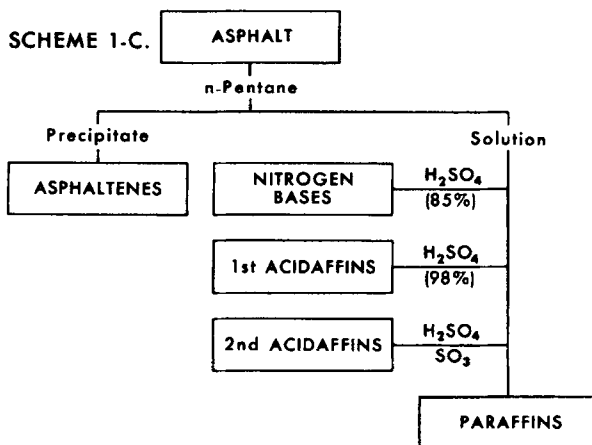
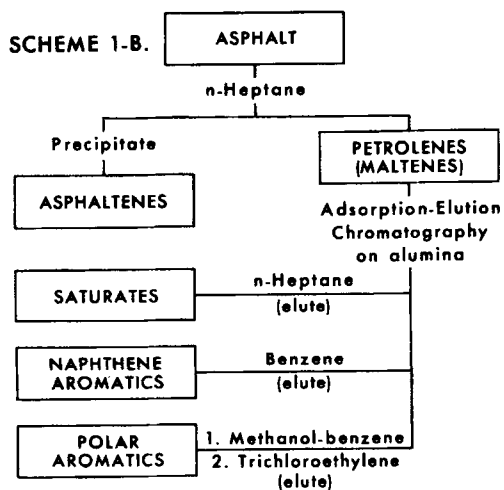
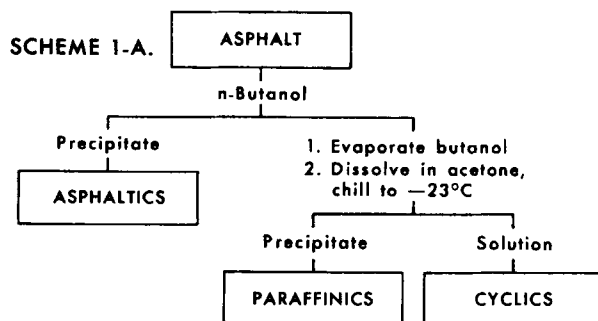


Fig. 14-1. Schematic diagrams illustrating three types of asphalt fractionation schemes. (Scheme 1-A, Partitioning of partial solvents [25]; Scheme 1-B, Selective adsorption-desorption [10]; Scheme 1-C, Chemical precipitation [6].)

cyclic and noncyclic saturated hydrocarbon fragments either as individual molecules in the saturate fraction or as moieties attached to the aromatic ring fragments in the more polar fractions. Sulfur is usually found in a large percentage of the individual asphalt molecules; but in unoxidized asphalt, it is rather nonpolar and is found distributed among all the component fractions. The so-called asphaltene fraction is chemically similar to the more resinous or polar components of the petrolene fraction [35]. Although the asphaltene fraction may contain small amounts of occluded or insoluble saturate-type material such as waxes, the significant differentiating feature of this fraction is the preponderance of molecules with highly condensed planar and polarizable aromatic ring systems together with a high concentration of polar, heteroatom-containing functional groups. Due to these features, molecules of this fraction are strongly attracted to each other, strongly associated, and difficult to disperse, even in polar solvents.

The third classical fractionation scheme to be considered is that of chemical precipitation (Scheme 1-C in Fig. 14-1). This scheme and its modifications are based on a fractionation procedure developed by Rostler and Sternberg [36] and later applied to asphalts [5,6]. It may not be exactly correct to call this fractionation procedure a separation scheme because it is really a method of analysis. Some of the steps are destructive and the method does not require the recovery of the altered fractions for further analysis. After separation of the asphaltenes, the remaining components are sequentially separated into fractions based on their reactivity with sulfuric acid of increasing acid strengths (decreasing degree of hydration). In practice, the sulfuric acid phase is added to a nonpolar hydrocarbon solution of the components to be separated, thus forming a second polar acid phase containing those components reactive with the sulfuric acid phase. In the first step, an 85% sulfuric acid solution is used to remove the most polar components, including most of the basic and nonbasic nitrogen compounds and many of the oxygenated molecules. This fraction is called nitrogen bases. Because the nitrogen in asphalt is usually associated with condensed aromatic ring systems, the so-called nitrogen-base fraction is quite aromatic. Concentrated sulfuric acid (98%) is used next to precipitate the first acidaffin fraction, which has been reported to contain unsaturated hydrocarbons [5]. The use of the term 'unsaturated' is unfortunate because the term is usually reserved for the designation of double and triple carbon-carbon bonds in nonaromatic ring structures (olefinic and acetylenic types), which have not been found in significant amounts, if at all, in petroleum residues. The first acidaffin fraction is quite aromatic and low in nitrogen content. The most likely reaction leading to the separation of this fraction is sulfonation or complex formation involving the aromatic ring systems. Sulfuric acid containing 30%  $\text{SO}_3$ , which is a powerful sulfonating and complexing agent, is used to precipitate those components with less reactive or polarizable aromatic ring systems. Analysis of this fraction, called second acidaffins, indicates that it is considerably less aromatic than the nitrogen bases or first acidaffins [5]. The final remaining fraction is called paraffins. This fraction is the oily component of asphalt and is composed primarily of molecules embodying straight-chain, branched and cyclic alkanes.

Although any of the discussed fractionation schemes separate asphalt into less complex and more homogeneous fractions, the generic fractions obtained are in themselves still complex mixtures and not well-defined chemical species. In all the separation meth-

ods, equilibria are involved. This may be solid–liquid equilibria in the chromatographic separation or liquid–liquid partitioning in the chemical precipitation method. The same generic fraction can vary considerably in composition and properties from one asphalt source to another; however, the separations are often sufficiently definitive to provide useful information in studies relating chemical composition with physical properties.

As previously mentioned, during the Strategic Highway Research Program (SHRP) two new preparative separation methods, size exclusion chromatography (SEC) and ion exchange chromatography (IEC), were extensively utilized. An important change was made in the SEC procedure over that used in the routine analytical method. This was to replace the solvent tetrahydrofuran (THF) with the solvent toluene. Since the object of the preparative SEC work was to identify those asphalt molecules that are strongly associated, toluene was chosen as the solvent because its solubility parameter is near that of the solvating components of asphalt. The use of the classical SEC solvent, THF, was deemed undesirable because its strong Lewis base characteristics tend to break up the association of asphalt molecules.

In the preparative SEC method [31,32], the first fraction to elute from the column was found to consist of agglomerates of highly associated asphalt molecules. These molecules contain highly polar chemical functionality and are the primary viscosity building components of asphalt. This fraction corresponds roughly to the dispersed phase in asphalt, or the asphaltene-like components. The amount of this associated fraction varies widely with asphalt source, and the relative amount of this component in an asphalt correlates quite well with the relative elasticity or gel-like properties of the asphalt.

The preparative IEC technique used in the SHRP [32–34] is shown schematically in Fig. 14-2. It should be noted that this method is performed in the absence of water, and thus the asphalt molecules are separated based on their relative Lewis acid or base characteristics rather than ion exchange properties as is typical of aqueous ion exchange chromatography. Five fractions based on chemical types were obtained: strong acids, strong bases, weak acids, weak bases, and neutrals. The neutrals fraction, which generally comprises about half of the asphalt, was least polar, and had viscosities at least two orders of magnitude lower than the parent asphalts in the SHRP studies. Of the fractions, the polar fraction designated as strong acids is the most aromatic, and contains the largest concentration of polar chemical functional groups. Because this fraction is separated first, it also contains the amphoteric molecules which could contain several other functional groups, both acidic and basic, on the same molecule. Since amphoteric molecules are polyfunctional they can form polymeric networks through association. They have been shown to be major contributors to molecular agglomeration in asphalts, and have a large influence on asphalt viscosity and viscoelastic properties [34]. Chemical functionalities that dominate in the acid fraction are carboxylic acids, phenolics and 2-quinolone-types. Pyrrolids are a major component of the weak acids fraction, and ketones and sulfoxides (which are oxidation artifacts formed during the separation) are found in the weak bases fraction. The combined strong acids and strong bases fractions obtained by IEC correspond roughly to the strongly associating fraction obtained in SEC separation. These polar components comprise the so-called ‘micellar’ or dispersed components of the asphalt.

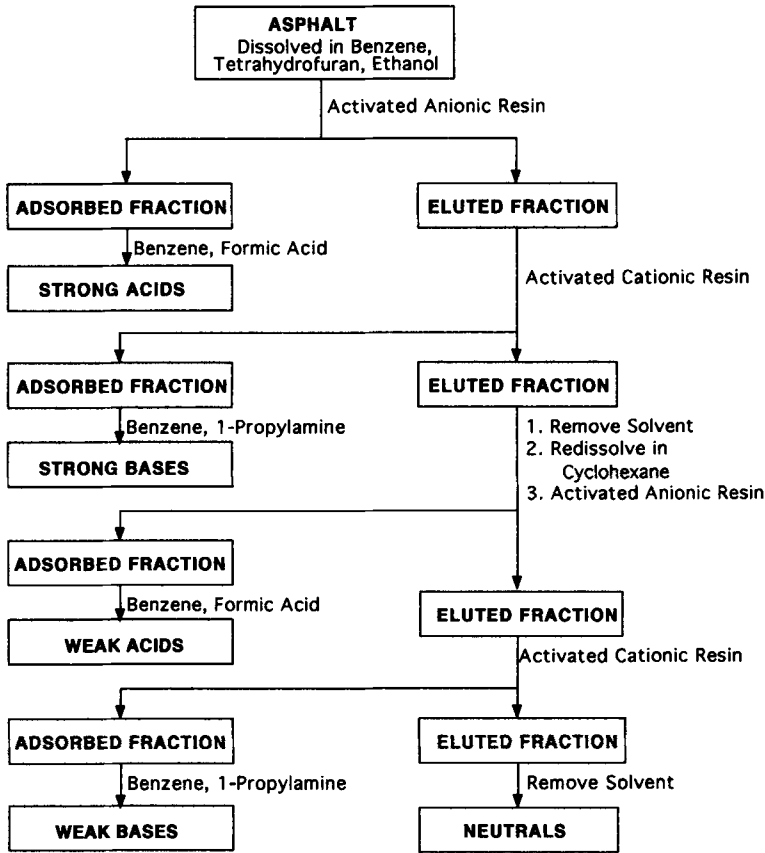


Fig. 14-2. Separation scheme for fractionation of asphalts into five fractions using anion and cation resins.

INTERACTIONS AMONG ASPHALT COMPONENT FRACTIONS AND RELATIONSHIPS WITH DURABILITY

As shown from the results of component fractionation, a wide spectrum of molecular types is present in asphalt. The most nonpolar or oily fraction, in the absence of the resinous components, is so unlike the asphaltene fraction that the two fractions are not mutually soluble. Yet, these extremes in molecular types must coexist in neat asphalt as a microscopically homogeneous mixture. This is made possible by the interaction of various components of asphalt with each other to form a balanced or compatible system. It is this balance of components that gives asphalt its unique viscoelastic properties that are so important to its application as a pavement binder. Lack of compatibility or balance, as sometimes manifested by component phase separation, leads to undesirable properties. The role of the various component fractions in contributing to asphalt component compatibility and, thus, durability, will be considered next.

It has long been recognized that asphalt exhibits properties that deviate from those of a true solution. The colloidal nature of asphalt was first recognized by Nellenstyn

[37,38], who considered asphalt a dispersion of micelles in an oily medium. The asphaltene fraction was early associated with the dispersed or micelle phase [39]. It was also recognized that the inability of the resinous components to keep these highly associated asphaltene components dispersed in the oily phase largely determined the gel or non-Newtonian flow characteristics of the asphalt [40,41]. Rostler and White [5] described the asphaltene fraction as the component of asphalt primarily responsible for asphalt viscosity and colloidal behavior, because of its limited solubility in the remaining components. They concluded that the asphaltenes are kept dispersed by the peptizing ability of the nitrogen bases. The peptized asphaltenes are in turn solvated by the resinous acidaffin fractions and gelled by the paraffins. Corbett [42] described the effects on the physical properties of the four fractions separated by his procedure: the asphaltenes function as solution thickeners; fluidity is imparted by the saturate and naphthene aromatic fractions, which plasticize the solid polar aromatic and asphaltene fractions; the polar aromatic fraction imparts ductility to the asphalt; and the saturates and naphthene-aromatics in combination with asphaltenes produce complex flow properties in the asphalt. In summary, they concluded that "each fraction or combination of fractions perform separate functions in respect to physical properties, and it is logical to assume that the overall physical properties of one asphalt are thus dependent upon the combined effect of these fractions and the proportions in which they are present."

For purposes of comparison, the polar aromatic fraction from the Corbett separation [10] (Scheme 1-B in Fig. 14-1) may be considered to contain many of the components found in the Rostler nitrogen base fraction and possibly part of the first acidaffin fraction. The Corbett naphthene aromatic fraction may be roughly compared with the Rostler second acidaffin fraction and some components found also in the Rostler first acidaffin fraction. The saturate and paraffin fractions from the two schemes might also be somewhat comparable.

It has been widely recognized [6,7,12,43–47] that a proper balance of chemical components is necessary in a durable asphalt. Not only may too much or too little of a given generic type as defined by the fractionation schemes be detrimental to the compatibility of the system, but also variations in chemical composition within the same generic type classification may be detrimental. For example, the presence of waxes in the oily fraction, which tend to crystallize and cause phase separation, can be detrimental [43]. Asphaltenes that are not properly dispersed, either because of their inherent solubility properties or because of the solvent properties or dispersing power of the resinous components of the petroleums, will reduce compatibility with the oily fraction and thus reduce asphalt durability [5,46]. Exudation of oil may occur and undesirable gel characteristics may be imparted.

Rostler et al. [6,47,48] showed that the balance of the component fractions, as indicated by the ratio of the most reactive fractions (nitrogen bases and first acidaffins) to the least reactive fractions (paraffins and second acidaffins), was important to the resistance of pellets of asphalt and Ottawa sand to abrasion loss in laboratory testing. Although the Rostler fractionation scheme has been used by many laboratories and correlations with field performance have been attempted [49,50], it has not been accepted as an accurate predictor of field performance. Lack of consideration of the asphaltene fraction, which contributes so significantly to flow properties, in the Rostler

durability parameter may be unfortunate and a serious omission. In field tests conducted in California [50], the Heithaus parameter ( $P$ ) (state of peptization), which is an attempt to measure the internal compatibility of an asphalt by evaluating the peptizability of the asphaltenes and the dispersing power of the petrolenes [46], was found to correlate better with pavement field hardening than the Rostler durability parameter. Using six asphalts of widely differing composition, Traxler [51] found a correlation between his coefficient of dispersion (resins and cyclics divided by asphaltenes and saturates) and the rate of hardening during laboratory oxidative aging. Better-dispersed asphalts hardened more slowly. He further suggested that the degree of dispersion of the asphalt components is inversely related to the complex (non-Newtonian) flow properties of the asphalt and is indicative of the asphalt's colloidal characteristics.

#### CHANGES IN CHEMICAL COMPOSITION ON AGING

The discussion thus far has addressed chemical compositional factors which determine the physical properties of asphalts. Without question, a durable asphalt must possess acceptable physical properties to produce a pavement with initially acceptable performance properties. The companion requirement of a durable asphalt is that these initial properties be resistant to change during environmental aging in field service. Asphalt composition, however, changes with time when the asphalt is exposed to atmospheric oxygen in the pavement. Asphalt reacts with atmospheric oxygen, which stiffens or hardens the asphalt. Atmospheric oxidation is the major factor responsible for the irreversible hardening of asphalts [2] and is the reason why pavement void content (which allows access to atmospheric oxygen) correlates so strongly with asphalt pavement hardening [52,53]. Hardening from loss of volatile components, the physical factor that might affect the correlation of hardening and void content, is not considered a significant factor when asphalts which meet current specifications are used. The potentially volatile components would be part of the saturate fraction; Corbett and Merz showed that the amount of this fraction remained virtually constant during 18 years of service in the well-known Michigan Road Test [54]. Thus, in dealing with asphalt durability, a major factor that must be addressed is the change that takes place in asphalt composition from oxidative aging.

The change in the amounts of fractional components of asphalt generally seen on oxidative aging is a movement of components from the more nonpolar to the more polar fractions. The saturates in the Corbett analysis [54] and the paraffins in the Rostler [6] analysis show the least change on oxidation. There is usually some loss of the Rostler second acidaffins and a greater loss of the more reactive first acidaffins and these losses are offset by a significant increase in the asphaltene fraction. Similarly, the Corbett naphthene aromatics and the polar aromatics decrease as asphaltene content increases.

King and Corbett [55] using thin films at 150°C and Knotnerus [11] using dilute toluene solutions showed that the saturate fraction is relatively inert to reaction with oxygen as measured by oxygen uptake. The naphthene aromatic (King and Corbett) and aromatic (Knotnerus) fractions showed slight and no reactivity, respectively. The Corbett polar aromatic fraction and the Knotnerus resin with asphaltene fractions, however,



were highly reactive with oxygen. Corbett's asphaltene fraction showed intermediate reactivity. Direct measurement of the formation of oxygen-containing functional groups by Petersen et al. [56] ranks the relative reactivity with atmospheric oxygen of the saturate, aromatic, polar aromatic and asphaltene fractions as 1 : 7 : 32 : 40, respectively, for a Wilmington (California) asphalt when the fractions were oxidized separately at 130°C. Evidence, however, was found that in neat asphalt, components of the more polar fractions may promote more oxidation of components of the less polar fractions than when they are oxidized separately.

The asphaltene fraction has been considered by some [5] to be chemically almost inert; however, the foregoing data indicate that asphaltenes are quite reactive with oxygen. The apparent contradiction regarding the chemical reactivity of asphaltenes might be explained by the following observations made by the author. Isolated asphaltenes are brittle solids and in this state at ambient temperatures are indeed quite unreactive with atmospheric oxygen, probably because their solid, highly structured state reduces molecular mobility, which in turn reduces reactivity with oxygen. When the asphaltenes are melted (as in the 130 and 150°C oxidations) or in solution in solvents, however, their mobility and apparent reactivity are increased. Thus, in neat asphalt, the degree to which asphaltenes are oxidized probably depends upon their degree of dispersion or solubilization in the dispersing (maltenes) components of the asphalt. The degree of dispersion of asphaltene molecular agglomerates in neat asphalt should be highly temperature dependent; therefore, oxidation of these components may be much greater in higher temperature laboratory aging tests than at ambient temperatures in pavements.

More definitive chemical studies [14,56–61] have yielded considerable information on the specific chemical changes that take place in asphalt on oxidative aging by reaction with atmospheric oxygen. The major oxygen-containing functional groups formed on aging are listed in Table 14-2 for four asphalts of different crude sources and aged under identical conditions (air, 130°C, thin film). The data [14] represent averages for the four asphalts aged on four different aggregates and the same asphalts as shown in Table 14-1. The level of oxidation has been judged to be equivalent to that typically found in asphalts after five years or more of pavement service [9]. The chemical functionality developed during laboratory oxidation at 130°C is similar to that developed during

TABLE 14-2

Chemical functional groups formed in asphalts during oxidative aging [14]

Asphalt	Concentration (mol l <sup>-1</sup> )				Average hardening index <sup>b</sup>
	Ketone	Anhydride	Carboxylic acid <sup>a</sup>	Sulfoxide	
B-2959	0.50	0.014	0.008	0.30	38.0
B-3036	0.55	0.015	0.005	0.29	27.0
B-3051	0.58	0.020	0.009	0.29	132.0
B-3602	0.77	0.043	0.005	0.18	30.0

Note: column oxidation [62], 130°C, 24 h, 15-μm film.

<sup>a</sup> Naturally occurring acids have been subtracted from reported value.

<sup>b</sup> Ratio of viscosity after oxidative aging to viscosity before oxidative aging.

TABLE 14-3

Comparison of oxidation products in column-oxidized and pavement-aged samples

Asphalt	Concentration (mol l <sup>-1</sup> )			
	Column oxidized <sup>a</sup>		Pavement aged <sup>b</sup>	
	Ketone	Anhydride	Ketone	Anhydride
60	0.76	0.024	0.53	0.018
25	0.70	0.025	0.53	0.022
30	0.64	0.027	0.64	0.038
61	0.67	0.022	0.44	0.020
67	0.43	0.013	0.32	0.010
71	0.76	0.026	0.51	0.022
72	0.82	0.033	0.68	0.029
73	0.49	0.013	0.35	0.011
74	0.72	0.027	0.43	0.017

<sup>a</sup> Thin film oxidation, 130°C, 24 h [62].<sup>b</sup> Recovered from 11- to 13-year-old pavements [15].

normal pavement aging at ambient temperatures, which is supported by data given in Table 14-3 [63]. Reasons for the lower levels of oxidation in some pavement samples compared with laboratory oxidation are discussed elsewhere [63], but they relate to the inaccessibility of some of the asphalts in the pavement to atmospheric oxygen.

Data in Table 14-2 show that ketones and sulfoxides are the major oxidation products formed during oxidative aging; anhydrides and carboxylic acids are formed in smaller amounts. In some asphalts, the summed concentrations approach 1 mole per liter. If a molecular weight of 1000 is assumed for an asphalt molecule, on the average one functional group is formed for each asphalt molecule. Of course, not all molecules of asphalt have the same reactivity. Data in Table 14-4 show that ketones are formed in the highest concentrations in the asphaltene and polar aromatic fractions; lesser amounts are formed in the aromatic fraction, and considerably less in the saturate fraction. These data are consistent with the earlier-cited oxygen uptake experiments [11,55].

TABLE 14-4

Carbonyl functional groups formed in Wilmington asphalt fractions during column oxidation [56]

Fraction	Concentration (mol l <sup>-1</sup> )		
	Ketone	Anhydride	Carboxylic acid
Saturate	0.045	0.010	trace
Aromatic	0.32	0.017	— <sup>a</sup>
Polar aromatic	1.48	0.088	— <sup>a</sup>
Asphaltene	1.82	0.080	nd <sup>b</sup>
Whole asphalt	1.02	0.052	0.007

<sup>a</sup> Some acids lost on alumina column during component fractionation.<sup>b</sup> Not determined.

The oxidation products formed are consistent and in good agreement with what is known about the hydrocarbon types in asphalt and the general chemistry of hydrocarbon oxidation. A major reaction pathway of hydrocarbon air oxidation is the formation of carbonyl compounds via the hydroperoxide intermediate [57,58]. The sensitive hydrocarbon moiety present in asphalt and associated with this reaction is the carbon atom adjacent to an aromatic ring system, commonly called a benzylic carbon. The hydrogen attached to the carbon in this position is relatively easy to displace, forming a free radical on the carbon. Branching in the attached hydrocarbon chains also increases the sensitivity of the asphalt to oxidation.

The mechanism(s) of asphalt oxidation has been highly elusive because of the molecular complexity of asphalts, and the details of proposed mechanisms are often disputed among researchers. More recently as a result of the studies of the oxidation kinetics of asphalt during the SHRP, insight was gained on asphalt oxidation to permit a mechanism to be proposed that appears to rationalize all previous, and often conflicting, proposed mechanisms. It is well recognized that asphalt has unusual oxidation kinetics for a hydrocarbon. Classical hydrocarbon oxidation shows an induction period; however, the kinetic plot for asphalt viscosity increase on oxidation is hyperbolic, with an initial rapid oxidation rate followed by a leveling off to a much slower and nearly constant rate [32,64].

It is proposed that the asphalt oxidizes by a dual mechanism [65,66]. During the initial rapid oxidation represented by the front part of the hyperbolic curve (called the oxidation spurt) it is proposed that reactions (1) and (2) shown in Fig. 14-3 dominate. Following the inflection point and leveling off of the hyperbolic kinetic plot, it is proposed

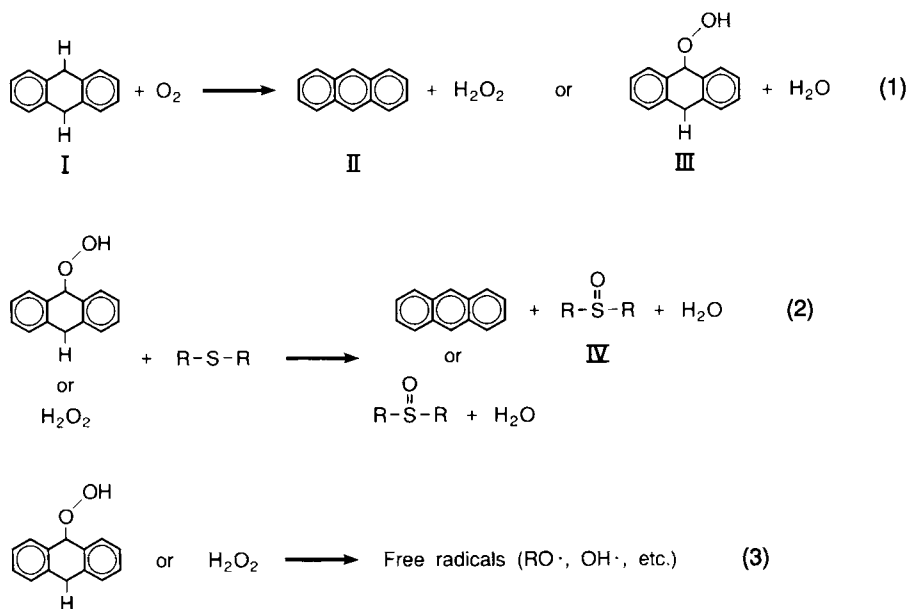


Fig. 14-3. Reaction sequences for oxidation of proposed polycyclic aromatics in asphalt during the oxidation spurt (illustrated for dihydroanthracene) [65,66].

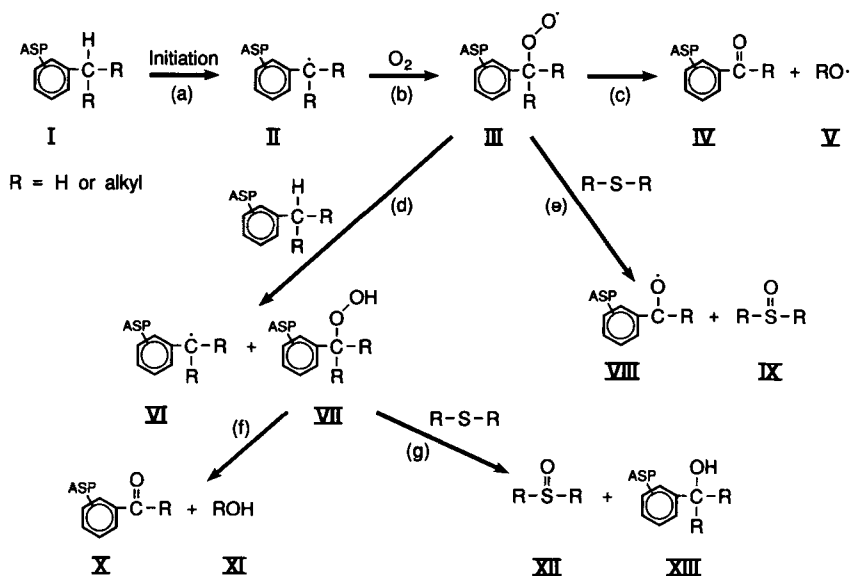


Fig. 14-4. Proposed reaction schemes for ketone and sulfoxide formation during oxidation of asphalt benzylic carbon [65,66].

that a classical free radical reaction involving the asphalt benzylic carbons dominate as represented by possible pathways in Fig. 14-4. The rapid initial reaction (1) shown in Fig. 14-3 is initiated by reaction of atmospheric oxygen with highly reactive hydrocarbons present in the asphalt, represented in the figure by the model hydrocarbon dihydroanthracene (I). Oxidation of this polycyclic hydroaromatic (which has no induction period) could produce either hydrogen peroxide ( $H_2O_2$ ) or a hydroaromatic hydroperoxide [III, reaction (1)]. Either product could then react with reactive asphalt sulfides to produce sulfoxides (IV) together with aromatization of the hydroaromatics [reaction (2)] by well known mechanisms. Note that sulfoxides (not ketones) are the only oxygen-containing asphalt oxidation products formed by this reaction. This result is consistent with observations over the years by the author and coworkers [65,66] that at low temperature oxidations (e.g.  $25^\circ C$ ), large amounts of sulfoxides are formed before significant amounts of ketones begin to form. However, as oxidation temperatures are increased, the hydroperoxide intermediates become increasingly less stable and can decompose in increasing amounts to form free radicals [reaction (3), Fig. 14-3]. These radicals can then initiate and accelerate the free radical reactions shown in Fig. 14-4 which produce ketones and sulfoxides in the asphalt. This explains the increasing ratio of ketones to sulfoxides during the oxidation spurt as oxidation temperature is increased [65,66]. These results have pragmatic implications since the amount of ketones formed in an asphalt correlates with the amount of new asphaltenes formed and viscosity increase [14,64], while the sensitivity to viscosity increase from sulfoxide formation is estimated to be at least an order of magnitude less than that from ketones [65]. The apparent absence of an induction period for the classical benzylic carbon free radical oxidation is also explained

by the dual mechanism since the induction period is masked by the rapid initial reaction of the highly reactive asphalt hydrocarbons [66], as illustrated in Fig. 14-3.

These mechanisms adequately account for the ketones which are the major hydrocarbon oxidation product in oxidized asphalt. Ketones in oxidized asphalt have been positively verified [57]. Smaller amounts of anhydrides are formed [58] through an alternate hydroperoxide decomposition route in certain asphalt molecules having stereospecific ring systems associated with the oxidizable alkyl moieties. Under certain conditions, the alkyl moiety may oxidize to the carboxylic acid; however, only small amounts of carboxylic acids (and no measurable esters [58]) have been found in laboratory- or pavement-aged asphalts. It appears that the oxidation reaction almost always stops at the ketone stage.

Due to the fact that the polar aromatics and asphaltene fractions contain the highest concentrations of aromatic ring systems, and thus benzylic carbons via the alkyl moieties attached, they have the highest content of hydrocarbon types sensitive to air oxidation. It is then not surprising that the polar aromatics and asphaltenes (Table 14-4) showed the highest ketone formation on oxidation.

The formation of sulfoxides, the other dominant oxidation product, results from oxidation of organic sulfides that are part of complex asphalt molecules [61]. These sulfides are highly reactive. Sulfoxides are formed in asphalt at a much higher rate than ketones and their formation often precedes significant ketone formation as explained previously. This is because sulfides are hydroperoxide scavengers and are converted to sulfoxides by the scavenger reaction.

The significance of the polar oxygen-containing functional groups to physical properties will be discussed in detail later in this chapter. Their influence on the hardening of the asphalt, however, is apparent from the aging indexes (ratio of viscosity after oxidation to viscosity before oxidation) of the asphalts in Table 14-2, which range from 27 to 132. It is apparent that the relative amount of hardening is not directly related to the amount of oxidation when one asphalt source is compared with another. The asphalts with the smallest and greatest aging indexes (Table 14-2) both showed about the same chemical reactivity with atmospheric oxygen. This is because all asphalts do not show the same sensitivity to the oxidation products formed. Asphalts from different sources have different compositions and, thus, their components interact differently with the oxidation products formed to increase viscosity. This varying sensitivity to oxidation products will be discussed later in more detail.

#### MOLECULAR INTERACTIONS — A FUNDAMENTAL APPROACH TO CHEMICAL FACTORS AFFECTING ASPHALT DURABILITY

In this section, a fundamental approach to relationships between asphalt chemical composition and physical properties will be addressed. The approach draws heavily on past chemical data and information from component analyses, but is based on more recent research that recognizes the fundamental chemical factors that affect asphalt properties. Parts of this section have been summarized previously [67]. Since the physical properties of asphalt are controlled by the interactions of the molecules from

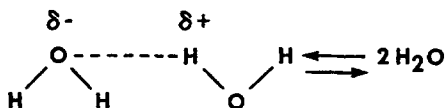
which it is composed, an understanding of these interactions should provide the basis for understanding its physical behavior and thus its durability. It is not necessary (and would be virtually impossible) to know the exact structure of each molecule for a workable understanding. It should be sufficient to identify or characterize the various types of chemical or structural features of the asphalt molecules and how these interact with each other and their environment.

Many molecules of different composition will have similar features, or functionality, that will produce similar effects on physical properties. Functionality analysis has the advantage over component fractionation by taking the multiple functionality of asphalt molecules into account. Many asphalt molecules have several types of chemical functionality on the same molecule, often of diverse types, which frustrate chemical fractionation procedures because whole molecules must be moved into a given fraction. The molecular interaction approach taken here is primarily that of the author; however, many researchers, both past and present, have recognized the importance of chemical functionality on asphalt properties.

*Fundamentals of molecular interactions and effects of molecular interactions on flow properties*

Because the chemical and physical properties of an asphalt are the result of its composition and the interactions of its individual molecules, it is essential to briefly review some fundamentals of molecular interactions. Molecules attract one another and interact through a variety of secondary bonds or association forces. These association forces are generally one to two orders of magnitude weaker than the covalent chemical bonding forces that hold the atoms together in the molecule. The association forces are significantly different from covalent bonding forces in that they form bonds that are generally reversible and are usually in dynamic equilibrium. That is, they 'make' and 'break' under forces induced by such factors as temperature and external stress and, thus, they largely determine the physical properties of the composite material.

To illustrate the principles involved, the classic example of the hydrogen bonding of water molecules is considered. An oversimplified schematic of this bonding is as follows:



The electronegative oxygen atom reduces the electron density of the hydrogen atom by attracting its electron field, thus creating a dipole-dipole interaction involving the oxygen and hydrogen of two different water molecules. In reality, additional dipole interactions involving additional water molecules produce a three-dimensional network of associated species. When water flows or is vaporized, the hydrogen bonds are the major association forces that must be overcome so that the molecules are able to move with respect to one another and are the major forces controlling the properties of water. The formation and breakdown of molecular structure via association forces are extremely rapid. In liquids, the average lifetime of a given arrangement of molecules, a structural unit, may be as short as  $10^{-13}$  s and for water is estimated at  $10^{-11}$  s.

To further illustrate the great influence of the electronegative oxygen atom on physical properties, consider replacing the oxygen in water with sulfur to yield hydrogen sulfide,  $\text{H}_2\text{S}$ . Since sulfur is less electronegative than oxygen, the strength of the hydrogen bond is greatly reduced. As a result, hydrogen sulfide, even though a heavier molecule than water, is not a liquid but rather a gas at room temperature. Its boiling point is  $162^\circ\text{C}$  lower than that of water. The effects of intermolecular forces, as illustrated by the hydrogen bond, are necessary in order to understand the effects of chemical composition on asphalt properties, because the intermolecular forces are the primary determinants of physical properties.

It should not be implied from the foregoing discussion that the hydrogen bond is the most important interaction force in asphalt. Many other reversible interaction forces are important in a material so chemically complex. These include a variety of dipole and induced dipole interactions. For simplicity in discussing molecular interactions in this chapter, all molecular structural types in asphalt that exhibit these forces are considered as chemical functionality. These functionalities include, but are not limited to, the more classical chemical functional groups.


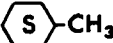
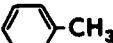
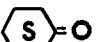
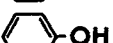
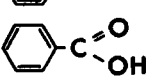



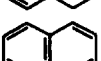
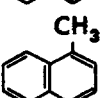
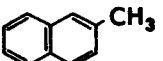
Nonpolar hydrocarbon components in asphalt, such as those dominant in the saturates or neutrals fractions, exhibit only weak interaction forces, which accounts for the rather fluid character of these fractions. On the other hand, asphalt components containing highly condensed ring systems and chemical functional groups that contain oxygen and nitrogen atoms may be highly polar or polarizable, and thus, interact strongly with each other. These strong interaction forces largely account for the fact that asphaltenes, even though they may not be significantly different in molecular weight than the saturates and neutrals [32,68], are high-melting solids.

To illustrate the potential applicability of molecular interaction theory and molecular structuring to the physical properties of asphalt, it is helpful to examine the effects of the chemical functionality of a series of model compounds on the physical properties of these compounds. A list of selected model compounds together with their structure, boiling point, and melting point are shown in Table 14-5. These chemical functionalities also represent important types found in asphalt and, thus, the reasoning developed may have direct application.

First, consider the series of compounds from *n*-heptane through benzoic acid. All were chosen from the same molecular weight range to minimize the effects of this variable and are listed in order of increasing polarity or increasing tendency of the molecules to interact. As previously mentioned, molecular interaction forces must be overcome in order to allow vaporization; thus, changes in boiling point reflect changes in the strength of the interaction forces between molecules. Note the continuously increasing boiling point with increasing polarity. The introduction of aromaticity in the molecule with toluene introduces mobile  $\pi$ -electrons, which can be polarized. Thus, its boiling point over methylcyclohexane is increased. Introducing the ketone group with cyclohexanone adds a polar oxygen-containing functional group and significantly increases the boiling point over methylcyclohexane. Phenol has both aromaticity and a polar OH group that can form strong hydrogen bonds; thus, it has an even higher boiling point. Finally, benzoic acid possesses a carboxylic acid functional group that forms strong hydrogen-bonded dimers. Note its extremely high boiling point.

TABLE 14-5

Effects of molecular interactions and molecular structuring on the physical properties of model compounds

Compound	Structure	Boiling point (°C)	Melting point (°C)
<i>n</i> -Heptane		98.4	-90.5
Methylcyclohexane		100.3	-126.4
Toluene		110.6	-95
Cyclohexanone		156.7	-45 (frz.)
Phenol		182	41
Benzoic acid		249	122
Benzene		80	5.5
Hexahydronaphthalene		205	liquid
Tetrahydronaphthalene		207.2	-30
Naphthalene		217.9	80.2
1-Methylnaphthalene		240	-22
2-Methylnaphthalene		245	35.1

Next, consider the properties of the series hexahydronaphthalene through 2-methylnaphthalene in Table 14-5. As expected, the boiling point increases in a regular fashion with increasing aromaticity and the introduction of the methyl group; however, the melting point shows no such correspondence. As shown in Table 14-5, the melting point is greatly reduced when a methyl group is introduced on benzene to form a higher-boiling toluene. The melting point, which reflects the interaction forces between molecules when in an ordered or structured configuration, is greatly influenced by the geometry of the molecule. Interfering appendages on, or structural arrangements of, the molecules that do not allow them to fit together easily in the necessary geometric pattern for effective interaction greatly reduce the melting point. Thus, molecular shape dominates the low-temperature structuring properties.

It is important to consider the molecular interaction effects previously described with regard to the flow properties of asphalts. The predictable effect of polar functionality



on the boiling point can be related to the effects of polar functionality in asphalt on its flow properties at higher temperatures in the Newtonian flow region. The polar interactions between molecules dominate in influencing the flow behavior, and the effects of molecular shape on geometry are minimized. This reasoning may explain why asphalts have different flow properties at low temperatures and more similar flow properties at higher temperatures.

At lower temperatures, however, as the kinetic energy of the system is lowered, the asphalt molecules tend to associate or agglomerate into immobilized entities with a more or less ordered or structured spatial arrangement. Although this ordered arrangement is influenced by polar functionality, it is also greatly influenced (as was the melting point of pure compounds) by the geometry of the molecules. Thus, at low temperatures the effects of differences in chemical composition of asphalt play a more significant role in determining the complex low-temperature flow properties, for example, viscosity shear and temperature susceptibilities.

Data obtained on asphalt-based systems will now be considered. To illustrate the effect of different types of molecular interactions on viscosity, consider data taken from an early paper by Griffin et al. [12] and abstracted as follows (to convert to viscosity in poise, multiply by 10):

Fraction	Apparent molecular weight	Viscosity (Pa s), 25°C
Saturate	500	10
Aromatic	500	1,000
Resin	500	100,000

Griffin et al. [12] separated asphalt into component fractions and then determined molecular weight versus viscosity profiles on the fractions. The foregoing data are taken for components of each fraction having the same molecular weight of 500.

The saturates had a viscosity of only 10 Pa s. They do not contain polar chemical functionality and molecular interactions are weak. Molecular interactions of increased intensity are exhibited by the aromatic fraction, the viscosity of which was 1000 Pa s. Finally, the resins that contain polarizable condensed-ring systems and heteroatom functionality, which causes even more intense molecular interactions, had a viscosity of 100,000 Pa s. Because the molecular weights of all fractions were the same, the differences in viscosity resulted primarily from differences in the type and strength of the molecular interactions. The association forces among asphalt molecules give asphalt many of the properties of high-molecular-weight polymers.

#### *Major chemical functional group types affecting asphalt properties*

As previously stated, asphalt molecules contain hydrocarbon structural constituents varying from saturated, paraffin-like chains to highly condensed and polarizable aromatic ring systems. From the previous discussion of model compounds, it is apparent that the relative amounts of the different structural or functional moieties of each molecule determine how molecules interact with each other. Those molecules that are most alike are most compatible and vice versa. In fact, as stated earlier, some asphalt

components, such as the saturates and asphaltenes, are not mutually soluble when separated from the whole asphalt. It is the wide spectrum of molecular types in asphalt all interacting together that gives asphalt its unique properties and makes it appear as a homogeneous material. On a molecular level, however, asphalt is undoubtedly heterogeneous, and a delicate balance exists among strongly associated or agglomerated components and dispersing or solubilizing components. It is this delicate balance, or the lack of it, that affects the performance properties of asphalts. Incompatibility and poor performance generally follow when one component type unduly dominates at the expense of others.

As discussed previously, although asphalt molecules are composed primarily of hydrocarbon constituents, heteroatoms such as nitrogen, sulfur, and oxygen may also be present as part of the molecule. Heteroatom concentrations vary widely among asphalts. In many asphalts, heteroatom concentrations are sufficient to average one or more heteroatoms for every asphalt molecule. Oxygen, nitrogen, and some forms of sulfur may introduce high polarity into the molecule, and although only minor components, they can exhibit a controlling influence on the molecular interactions that control asphalt flow properties. Thus, chemical functionality containing these atoms becomes a major consideration in understanding asphalt properties.

Much work has been done by the author and coworkers in identifying polar, strongly associating functional groups in asphalts, either naturally present or formed on oxidation, and in characterizing their association forces [9,14,56–60,63,69–76]. Structural formulas of important chemical functionality in asphalts are shown in Fig. 14-5. Nitrogen, which occurs in concentrations of 0.2 to 1%, is present in several forms from the slightly acidic pyrrole types to the more basic, strongly interacting pyridine types [76]. The nitrogen types naturally-occurring in asphalt are not known to be significantly altered by oxidation. Sulfur, in concentrations from about 1 to 5%, is present primarily as sulfides. Many of these sulfides are readily oxidized to polar sulfoxides by atmospheric oxygen during normal aging [61]. Phenolics are also usually present. Naturally occurring carboxylic acids and 2-quinolone-type functionality, although occurring in relatively small amounts in asphalts, are highly polar and associate strongly [71]. As discussed previously, asphalts are susceptible to oxidative aging by reaction with atmospheric oxygen, which is a major factor contributing to age hardening and embrittlement. The major oxygen-containing functional groups formed on oxidative aging are also included in Fig. 14-5.

#### *Effects on asphalt performance of polar functional groups formed on oxidation*

Asphalts vary considerably in their susceptibility to the effects of deteriorating oxidation. If during aging the concentration of polar functional groups becomes sufficiently high to cause molecular immobilization through increased intermolecular interaction forces (that is, the asphalt molecules or micelles are not sufficiently mobile to flow past one another under the stress applied), then fracturing or cracking of the asphalt will result.

Data in Fig. 14-6 show a relationship between the amount of strongly interacting polar groups formed in a series of asphalts during controlled laboratory oxidative aging and

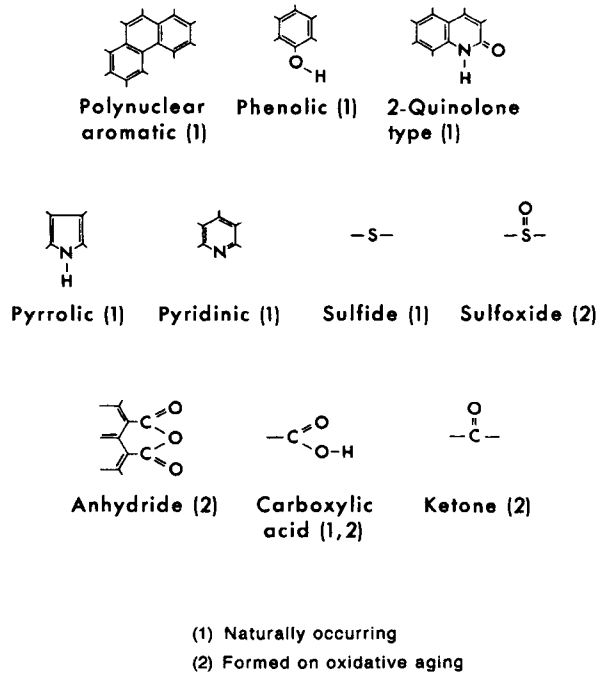


Fig. 14-5. Chemical functionality in asphalt molecules present or formed on oxidative aging.

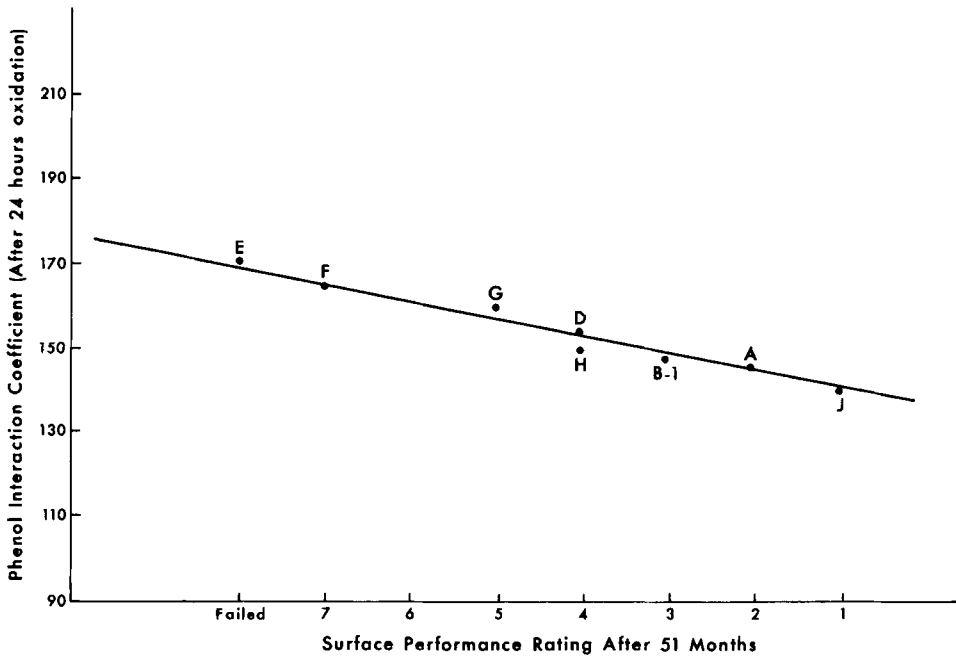


Fig. 14-6. Relationship between phenol interaction coefficient and pavement surface performance rating.

the resistance to failure from cracking in roads in which these asphalts were used. The asphalts were from the California Zaca-Wigmore Experimental Road Test mentioned previously [4,9], in which construction variables were kept as constant as possible to evaluate the effect of asphalt composition (or source) on durability. In laboratory studies [9], these asphalts were coated as thin films on inert fluorocarbon particles and were aged in a gas chromatographic (GC) column at 130°C for 24 h by passing air through the column [63]. (This procedure oxidizes the asphalt an amount equal to approximately five years or more in a road.) Following oxidative aging, a polar test compound, phenol, was passed through the GC column by using an inert gas carrier, and its interaction with the polar groups formed in the asphalt during oxidation was determined from the phenol retention time. As phenol passes through the column it is in equilibrium with the asphalt; those asphalts having a greater concentration of polar groups interact more strongly with the phenol functionality, giving a larger phenol interaction coefficient.

As seen from Fig. 14-6, an excellent correlation was found between the asphalt polarity as measured by the phenol interaction coefficient and the service performance rating after 51 months of road service. Those asphalts that developed greater amounts of strongly interacting polar groups during aging failed sooner in the road. Fig. 14-7 shows a similar correlation developed on twenty roofing asphalts, the weatherability of which was determined by resistance to cracking when aged in a carbon arc Weather-Ometer. Thus, strong evidence exists relating the development of polar functional groups in asphalts on aging with asphalt failure from embrittlement and cracking.

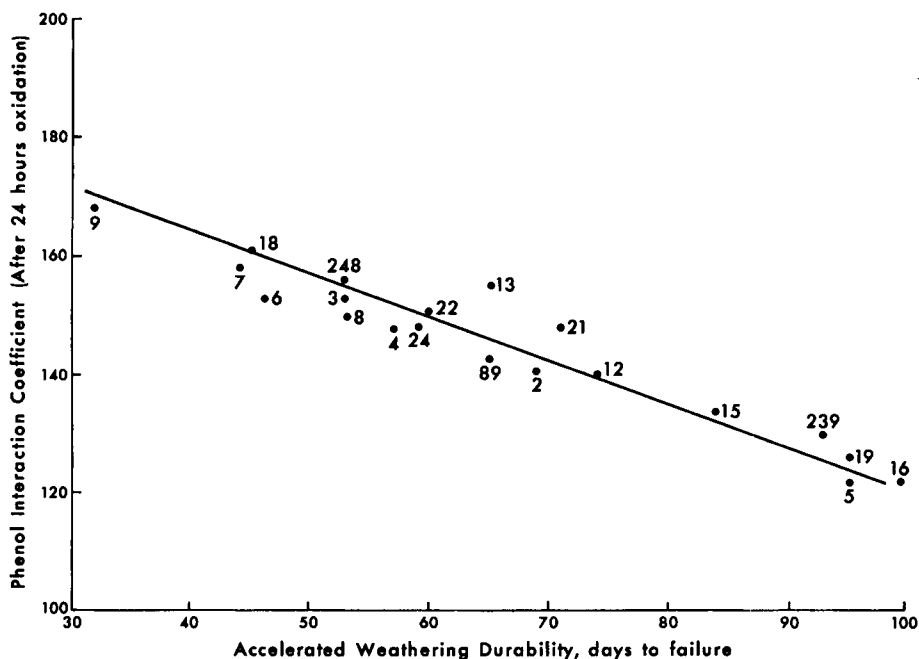


Fig. 14-7. Relationship between phenol interaction coefficient and durability of twenty roofing asphalts.

*Effects of polar asphalt components on viscosity and aging characteristics*

Data plotted in Fig. 14-8 show the important influence of polar constituents (in this case, asphaltenes) on asphalt viscosity. In the study cited [14], four asphalts (all meeting the same specifications) were oxidatively aged in the laboratory both before and after a hydrated lime treatment (the lime with adsorbed asphalt components, which was about 4% of the asphalt, was separated from the asphalt during the treatment). The asphalts were aged by different methods to achieve different levels of oxidation. Following aging, both asphaltene content and viscosity were determined at 25°C. Each data point in the figure represents a separate level of oxidation. Although each asphalt had its own unique relationship, a good correlation existed for each asphalt between asphalt viscosity and asphaltene content. Several important points can be inferred from the data in Fig. 14-8. First, the asphaltene fractions of the different asphalts are quite different from each other in composition or the petroleum fractions have widely different solubility power for the asphaltenes or both. This is a necessary condition in order for asphalts with widely varying asphaltene contents to have the same viscosity. Second, asphaltenes formed in asphalt on oxidative aging appear to have a predictable effect on viscosity increase.

The data in Table 14-6 show the effect of the lime treatment in reducing the hardening rate of the asphalts when subjected to a laboratory GC column oxidation procedure [14,63], during which the asphalts were supported as thin films on the surface

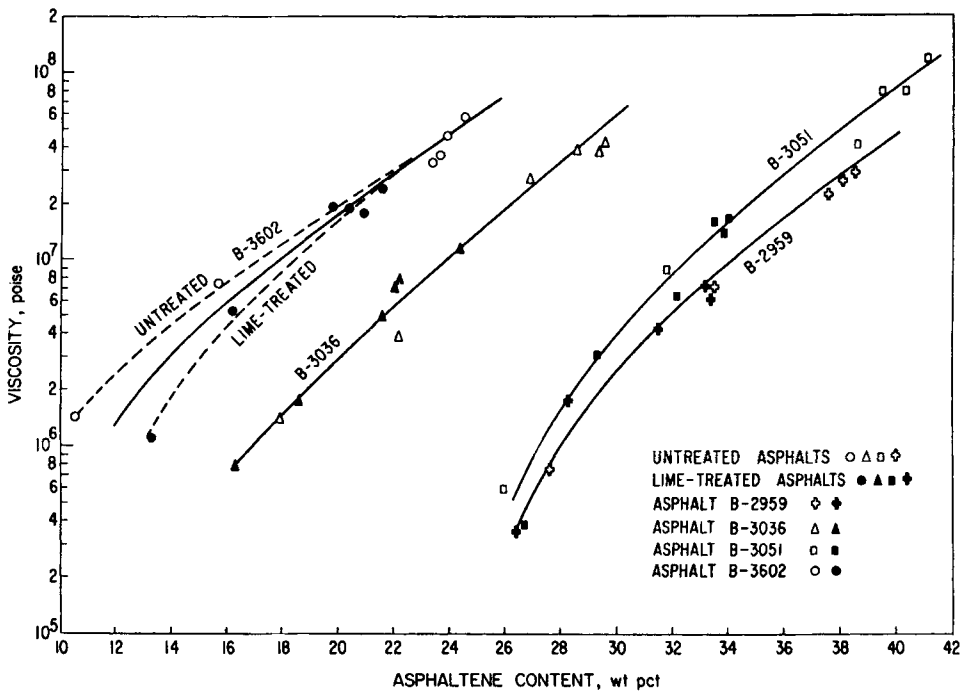


Fig. 14-8. Relationship between viscosity at 25°C and asphaltene content of untreated and lime-treated asphalts aged by different methods.

TABLE 14-6

Reduction of hardening rate of asphalt by treatment with hydrated lime [14]

Sample	Hardening index <sup>a</sup>		
	Untreated	Lime treated	Reduction (%)
<i>Asphalt</i> <sup>b</sup>			
B-2959	37	17	54
B-3036	27	10	63
B-3051	132	35	73
B-3602	29	18	39
<i>Aggregate</i> <sup>c</sup>			
Quartzite	57	22	61
Hol limestone	58	22	61
Riverton limestone	36	13	63
Granite	75	22	70

<sup>a</sup> Hardening index = viscosity after oxidative aging divided by viscosity before oxidative aging.<sup>b</sup> Averaged for aggregates.<sup>c</sup> Averaged for asphalts.

of four different aggregates. It should be noted that except for asphalt B-3602, lime treatment reduced the hardening index of the asphalts by more than 50%. Asphaltene formation on aging was also reduced by about 50% [14]. Functional group analyses, however, showed that the oxidation reaction, as measured by the formation of ketones, was reduced by only about 10% by lime treatment. What was concluded was that lime removed carboxylic acids and other highly-polar functionality that would otherwise have interacted with oxidation products to increase asphalt viscosity. Separate studies showed that the introduction of carboxylic acid functional groups into asphalt molecules greatly increases asphalt viscosity.

The reduction of asphalt viscosity by inactivating polar functionality was demonstrated [77] by adding 3 wt% hydrated lime to an asphalt (B-3051), leaving the lime in the asphalt, and measuring its viscosity versus time at 25°C. During the initial 24 h after lime addition, asphalt viscosity steadily decreased in a regular fashion from about  $5 \times 10^4$  to  $1.5 \times 10^5$  Pa s ( $5 \times 10^5$  to  $1.5 \times 10^5$  poise). This decrease was interpreted as the result of the adsorption of polar, strongly interacting groups on the lime surface, thus removing these viscosity-building components from the asphalt matrix. In some asphalt-aggregate systems, such phenomena might impart slow-setting or tenderness characteristics to a pavement mixture; however, the stiffening effect of lime as a mineral filler may offset this.

The flow properties and hardening rate of asphalt might also be significantly altered by manipulation of molecular interactions through chemical modification or the addition of modifiers that can interact with polar chemical functionality in the asphalt and alter its activity as suggested by the data on lime addition. The ability of surface-active materials, such as antistripping agents (often amines) to alter asphalt viscosity, often to an extent not expected from simple additive effects, is widely known. Because

antistripping agents have polar chemical functionality, they might be expected to affect the dispersibility of asphaltene-like components in asphalt by associating with polar functionality, thus altering the association and micelle structure within the asphalt. The ability of high-molecular-weight amines to interfere with molecular structure buildup and subsequent viscosity increase in asphalt cutbacks during storage was reported as early as 1951 by Hoiberg [78].

The effects of antistripping additives on altering the flow properties and oxidative hardening rate of asphalts have also been reported [79]. It has been suggested by J.N. Dybalski of Akzo Chemie America that cationic asphalt additives augment the peptization of the asphaltene constituent in many asphalts, thus reducing the asphalt hardening rate as reported in a trade newsletter [80]. According to the report, of 82 asphalts tested, 81% benefitted from the additives with a minimum of 15% and a maximum of 65% reduction in hardening rate during the rolling thin-film oven test (ASTM D 2872-77). The hardening rate of a recycled pavement mixture during laboratory aging was also reduced several-fold by a high float emulsifying agent used to emulsify the recycling agent before recycling of the pavement mixture [81].

### *Composition and component compatibility*

Previously reference was made to the need for a good balance among asphalt components of different polarities. Compatibility in asphalt deals with the mutual solubility of a variety of components with widely differing solubility and solvent powers. Earlier workers in the field considered compatibility in terms of the state of peptization of asphaltenes. Heithaus [46] stated that asphaltenes are the most polar and aromatic components in asphalt and are present in asphalts as rather concentrated solutions (10 to 40%). To obtain maximum solvency for the polar, strongly associating species in asphalts, the polarity of the solvent (maltenes, sometimes called petrolenes) must be matched to the materials to be dispersed (asphaltenes). For example, more polar asphaltenes require petrolenes with greater solvent power to effectively dissolve or disperse them.

A number of studies have addressed the dispersibility of asphaltenes and methods to measure dispersibility and compatibility [7,46,82–84]. Altgelt and Harle [83] clearly demonstrated that selected asphaltenes from different sources had different effects on blend viscosity (different thickening power) when added to the same petroline fraction. They further showed that petroline fractions derived from asphalts of different sources had different solubility power for asphaltenes. To illustrate the principles they developed, consider what happens when a highly polar asphaltene fraction having a strong tendency to self-associate is added to a petroline fraction having relatively poor solvent power for the asphaltenes. Intermolecular agglomeration will result, producing large, interacting, viscosity-building networks. Conversely, when an asphaltene fraction is added to a petroline fraction having relatively high solvent power for the asphaltenes, molecular agglomerates are broken up or dispersed to form smaller associated species with less interassociation; thus, the viscosity-building effect of the asphaltenes is reduced. It must be concluded that chemical composition becomes an important factor when asphalts (or crudes) are blended from different sources or when asphalt components are blended. The prin-

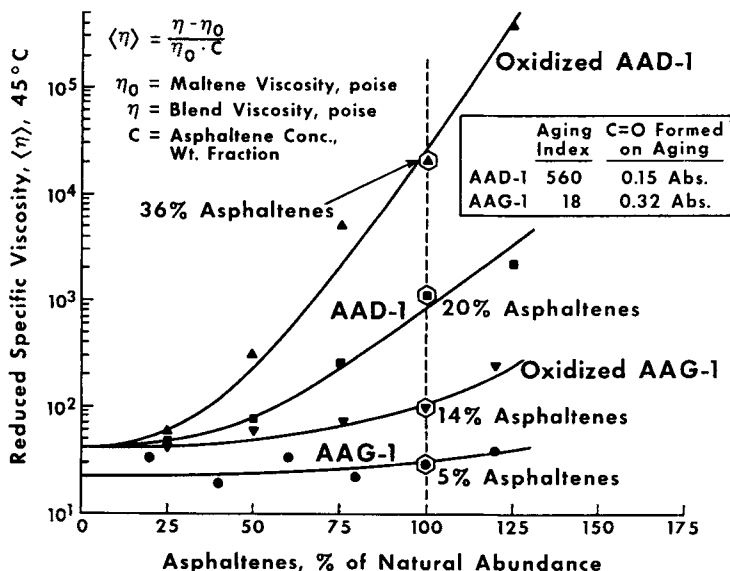


Fig. 14-9. Reduced specific viscosity measurements at 45°C for SHRP core asphalts AAD-1 and AAG-1 before and after thin film aging at 113°C, 72 h.

ciples described help explain why viscosities of asphalt mixtures of blends often show irregularities when compared with the viscosities of the original asphalts. The effects of asphalt crossblending on rheological properties have recently been studied in detail [85].

It follows that asphalt compatibility can be improved or worsened by blending and that the initial properties of blended asphalts are not necessarily additive in determining blend properties. Compatibility considerations are also important with regard to the aging characteristics of asphalt because, as already described in detail, oxidative aging greatly alters the polarity of asphalt molecules, which affects their interactions. Reduced specific viscosity measurements, as illustrated in Fig. 14-9 [64], provide information on the relative size of the agglomerates of asphaltene molecules, and the effects of asphalt component compatibility and oxidation on the relative size of these agglomerates.

Reduced specific viscosity,  $\langle \eta \rangle$ , is defined [83], as illustrated in Fig. 14-9, as the increase in the viscosity of the neat maltene fraction,  $\eta - \eta_0$ , as a function of increased asphaltene content divided by the neat maltene viscosity,  $\eta_0$ , times the asphaltene concentration,  $C$ , in g/100 g. The reduced specific viscosity is proportional to the apparent molecular weight of the asphaltene micelle and is analogous to intrinsic viscosity which is used by polymer technologists to determine molecular weights of polymers. To obtain the data in Fig. 14-9, viscosity measurements were made at 45°C on a highly compatible, well dispersed asphalt (AAG-1) and a less compatible, highly associated asphalt (AAD-1) at both below and above their natural asphaltene abundance, both before and after thin film oxidation at 113°C.

The data in Fig. 14-9 are interpreted as follows. If little or no increase occurs in the  $\langle \eta \rangle$  as asphaltene content is increased, this shows that the asphaltene agglomerate is not



increasing in apparent molecular weight (size) with increasing asphaltene content. From this it can be concluded that the asphaltene particle is solubilized or does not further inter-associate as the asphaltene concentration is increased. That is, if the asphaltenes are particulate bodies they are very well peptized and dispersed and do not significantly interact with one another. This type of asphalt has Newtonian flow properties at the temperature of the viscosity measurement, which is apparently true for asphalt AAG-1 [64,65]. On the other hand, if the  $\langle \eta \rangle$  increases with increasing asphaltene content, this shows that the asphaltene particles agglomerate into larger species and become less peptized and less dispersed as their concentration increases, thus increasing the apparent molecular weight of the asphaltene agglomerates. This is exemplified by asphalt AAD-1 in the figure. As a result, increasing asphaltene concentration has a disproportionately greater effect on increasing viscosity in asphalt AAD-1 than in asphalt AAG-1. Asphalt AAD-1 has highly non-Newtonian flow properties at the temperature of the viscosity measurements [64,65]. In asphalt AAD-1, asphaltene agglomerates are interacting with each other, which interactions must be overcome to allow flow, thus creating the non-Newtonian flow properties.

Also, it can be seen from Fig. 14-9 that oxidation, which produces oxygen-containing functional groups and increases asphaltene content, has a greater effect on the apparent molecular weight of the asphaltene agglomerates for the less compatible asphalt, AAD-1, than for the more compatible asphalt, AAG-1. It is important to note from the data in the box in Fig. 14-9 that the formation of only 0.15 absorbance units (quantitative infrared analysis, 0.16 mol/l in this case) of carbonyl (ketones) corresponds with a 540-fold increase in viscosity; this is in contrast to only an 18-fold viscosity increase for the formation of 0.32 absorbance units (0.28 mol/l) of carbonyl for the compatible asphalt AAG-1. Reduced specific viscosity data presented in Fig. 14-9 are extremely significant in that they demonstrate by an unambiguous method that the asphaltenes in a neat asphalt exist as particulate or micellar species.

The discussion, thus far, implies that a better knowledge of the chemical functionality responsible for the strong interaction forces in asphalt, and the ability to manipulate these forces, have great practical value in altering the flow and the performance properties of asphalt. Application of compatibility principles to pavement recycling, in which a recycling agent is added to restore useful properties, should also greatly benefit this rapidly emerging practice.

#### *Importance of molecular structuring to the flow properties of asphalt*

Non-oxidative molecular structuring in asphalts is probably one of the least understood physicochemical phenomena affecting physical properties. Unlike oxidative aging, which produces irreversible changes in asphalt composition, molecular structuring is a reversible phenomenon that can produce large changes in the flow properties of asphalt without altering the chemical composition of the asphalt molecules. Several factors account for its elusive nature and resistance to quantification. First, in asphalts at ambient temperatures, structuring is a slow process that may go on for days and even years; second, it is promoted by mineral aggregate surfaces (as in pavement mixtures) in an environment where it is difficult to measure its effects; and third, most

normal asphalt recovery methods using solvents or heat, or both, destroy or reverse the structuring process. Yet molecular structuring is largely responsible for the asphalt's unique physical properties. Without it, pavement mixtures would not 'set' to produce a nontender pavement with the desired structural integrity, and too much structuring can produce pavements with poor low-temperature properties and high shear susceptibility.

Although the phenomenon of structuring in asphalt is not well understood, it was recognized and received considerable study by early investigators [78,86–92] and is often called steric hardening [90]. It has been related to the thixotropic flow behavior commonly encountered in colloidal materials [87]. The early literature is extremely revealing and should be read carefully by present-day technologists, because little work has been done to build on or take advantage of the excellent past studies.

Traxler and coworkers characterized molecular structuring (which they also called age hardening, not to be confused with age hardening caused by oxidation) in a number of asphalts from a variety of sources, and related it to the degree of complex flow (sensitivity of measured viscosity to shear rate) [86–89]. Their experiments were carried out on bulk asphalt in the absence of significant oxidation. Selected data in Fig. 14-10 and in Table 14-7 document this nonoxidative, time-dependent hardening.

In Fig. 14-10, selected data on three paving asphalts show different hardening rates as a function of asphalt source. Air-blown asphalts showed a greater rate of structure hardening than unblown asphalts as illustrated by the air-blown Venezuelan asphalt in Fig. 14-10. For the air-blown asphalt, the log viscosity versus log time plot was not

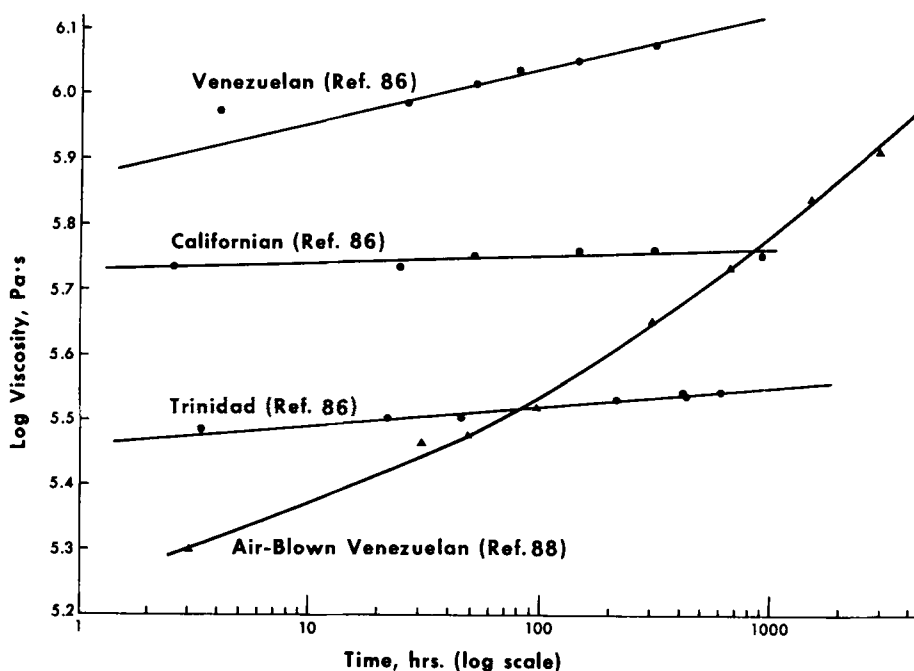


Fig. 14-10. Hardening of asphalts from reversible molecular structuring at 25°C.

TABLE 14-7

Correlation between reversible molecular structuring and degree of complex flow [89]

Asphalt	Asphalt aging index <sup>a</sup>	Complex flow <sup>b</sup>
Pressure-still	0.017	1.0
Air-blown, Californian	0.023	0.95
Air-blown, Midcontinent	0.073	0.85
Air-blown, Northeast Texas	0.183	0.50

<sup>a</sup> Slope of log-log plot of viscosity versus time in hours (nonoxidative hardening).

<sup>b</sup> Slope of log-log plot of shearing stress versus shear rate (measure of non-Newtonian flow).

linear as with the unblown asphalts, but the rate of change increased with time. Traxler and Schweyer [86] devised an expression called the asphalt aging index to quantitatively measure reversible hardening from molecular structuring. This index is the slope of the log viscosity versus log time plot. Asphalt aging indexes for eight unblown asphalts from different sources are shown as follows [86]:

Asphalt	Asphalt aging index
Californian	0.012
Californian	0.018
Trinidad	0.026
Venezuelan	0.037
Midcontinent	0.039
Mexican	0.051
Venezuelan	0.063
Venezuelan	0.071

The structuring phenomenon was found reversible and structured asphalt could be brought back to near its initial viscosity by heating it to a temperature above its softening point or by continued mechanical working [88,92].

These early researchers found a correlation between the complex flow of asphalt (non-Newtonian behavior or viscosity lowering with increasing shear rates) and its tendency to exhibit molecular structuring. This is illustrated by the data in Table 14-7, which compare the complex flow (a value of 1 indicates Newtonian flow) for a series of asphalts with the asphalt aging index resulting from nonoxidative structural hardening. Those asphalts that showed more structuring possessed a greater degree of non-Newtonian flow behavior.

The relationship between complex flow and structural hardening has considerable potential significance with regard to the hardening of pavement mixtures. It is known that as asphalts undergo oxidative aging, their flow behavior becomes more complex or non-Newtonian. The author and coworkers, while studying oxidation [63], found that two asphalts that had been previously oxidatively aged increased significantly in measured viscosity, because of reversible molecular structuring after standing for two years; the increase was from  $2.5 \times 10^4$  to  $1.2 \times 10^5$  Pa s and from  $1.1 \times 10^5$  to  $3.0 \times 10^6$  Pa s. The structural hardening was reversed on heating of the samples. The original unoxidized asphalt showed almost no increase from structural hardening

( $3.8 \times 10^2$  to  $4.2 \times 10^2$  Pa·s) on standing for the same length of time. This strongly suggests that the oxidation taking place during the natural oxidative aging of some asphalts in pavements significantly increases the rate of reversible structural hardening and that oxidative and structural hardening may be synergistic.

A problem encountered in the determination and quantification of structural hardening is that the structuring is destroyed during the solvent recovery of asphalts from aged pavements and, therefore, escapes detection during measurement of the recovered asphalt properties. Thus, the tendency for an asphalt to harden from structuring, which may be a major contributor to loss of durability and pavement failure, is being virtually ignored in pavement performance considerations by present-day pavement technologists. Brown et al. [90,91], who studied reversible molecular structuring (called by them 'steric hardening') in 1957, approximately two decades after the studies of Traxler and coworkers, noted that "this is not a new discovery, but has had relatively little emphasis." Since this statement, not much has changed in this regard but the need is still there.

More recently, studies of molecular interactions of asphalts and of asphalt-aggregate interactions have been conducted at higher temperatures (above 130°C) by microcalorimetry [73,93,94]. Reversible molecular interactions were shown to be present at temperatures as high as 250°C. Interactions at these high temperatures undoubtedly reflect the disassociation-association of the more stable micellar bodies in asphalt [95]. Aggregate surfaces have been shown to promote molecular structuring and immobilization of asphalt molecules in the vicinity of the aggregate surface, which should have considerable effect on bond properties and properties of pavement mixtures [73,94,96]. A relationship between molecular structuring and the setting characteristics of pavements was proposed by Hveem et al. [97] and a cohesiograph test was proposed to measure the setting property. A good correlation was found between the tendency for asphalts to form 'tender-mix' pavements and their lack of molecular structuring when in contact with the surface of a standard Ottawa sand aggregate [94]. Thus, the phenomenon of molecular structuring is important not only to the bulk properties of asphalt, but also to the asphalt-aggregate interaction. Both types of structuring will affect the performance and durability of asphalts in pavements. The common practice of evaluating asphalt performance in the absence of the aggregate, with which it is to be used, leaves unevaluated important criteria for pavement performance.

#### SUMMARY AND CONCLUDING CONCEPTS

Chemical composition is important in determining the physical properties and performance characteristics of asphalts. The interactions of polar or polarizable chemical functionality, either naturally present or formed by oxidative aging, play a major role in determining asphalt viscosity and related complex flow properties.

Two major factors affecting asphalt durability are (1) the compatibility of the interacting components of asphalt, and (2) the resistance to changes resulting from oxidative aging. Both factors are a function of chemical composition, which can vary widely depending on the asphalt source because of inherent differences in crude sources or from processing and blending.

Historically, the study of asphalt chemical composition has been facilitated by the separation of asphalt into component fractions based on the polarity characteristics, adsorption characteristics, or both, of the molecular components present. The component fractions, sometimes called generic fractions, are useful in classifying and characterizing asphalts and providing simplified mixtures for further study. Nevertheless, they are still complex mixtures, the composition of which is a function of asphalt source. The component fractions, however, are sufficiently unique to identify their particular contribution to the complex flow properties of asphalt. A proper balance of component types is necessary for a durable asphalt.

Because asphalt occurs as a film exposed to atmospheric oxygen in pavements, it rapidly oxidizes in service with the formation of polar, strongly interacting, oxygen-containing chemical functional groups that greatly increase viscosity and alter complex flow properties. This hardening often leads to asphalt embrittlement and ultimately asphalt pavement failure. Not only does the susceptibility to oxidation vary from one asphalt to the other, but the effect of the oxidation products formed on physical properties also varies widely with asphalt source. The sensitivity of the asphalt to the chemical functionality produced on oxidation can be significantly reduced by removing or altering the polar chemical functionality initially present that would otherwise interact with the oxidation products to increase viscosity.

The identification and characterization of the chemical functional types normally present in asphalt or formed on oxidative aging, that influence molecular interactions afford a fundamental approach to the chemical compositional factors that determine physical properties. This in turn, governs the performance properties of both asphalts and asphalt-aggregate mixtures.

The physical properties of asphalt are significantly altered not only by oxidative formation of polar chemical functional groups, but also by reversible molecular structuring (also called steric hardening). This latter phenomenon is a slow process that appears to proceed concurrently and synergistically with oxidative aging during the lifetime of the pavement and may be a major factor contributing to asphalt pavement embrittlement in the later stages of the pavement service life. Limited data indicate that the complex flow properties of asphalt and the tendency of asphalt to structure are directly related. This suggests possibilities for ways to evaluate this elusive property.

Since the chemical composition of asphalt can vary widely with asphalt source, and a variety of combinations of asphalt components with varying chemical structures in individual asphalts may produce asphalts that will provide satisfactory service, it seems unlikely that satisfactory chemical composition specifications can be devised for asphalts. Such specifications would likely exclude from use many asphalts that would otherwise perform satisfactorily. Ideally, specifications should define the performance properties desired. Chemical information would be important in producing asphalts that meet the performance criteria.

Composition information is useful in helping to provide an understanding of what makes asphalt behave as it does and what makes different asphalts behave differently. With given asphalt sources available, composition information can be used to improve the product through modification with additives, by blending, and so on, or to alter use design procedures to accommodate specific properties. Composition information

can be used to match asphalt and aggregate, provide clues as to what modifications are necessary to make an asphalt-aggregate system more serviceable under a given environment, diagnose failures, and provide information needed in taking corrective measures.

As asphalts from new sources are utilized, and as processing and design procedures change, the use of more fundamental information, both chemical and physical (particularly as related to long-term performance and durability) should provide for product improvement and reduce the number of early or unexpected failures of asphalt products.

It is hoped that this review will bring about a better understanding of the chemical compositional factors that control the properties of asphalt and will assist in providing direction to both research and application leading to improved asphalt products with better performance and durability.

#### ACKNOWLEDGEMENTS

The author is grateful to the FHWA, U.S. Department of Transportation, for partial financial support during the compilation of this review. The author is also grateful to his former employer prior to retirement, Western Research Institute, for their support during preparation of much of this manuscript. Parts of the material have been summarized in Transportation Research 999-13-30 (1984). Permission was obtained to use this material.

#### REFERENCES

- [1] Hveem, F.N., Quality tests for asphalts — a progress report. *Proc. Assoc. Asphalt Paving Technol.*, 15: 111–152 (1943).
- [2] Van Oort, W.P., Durability of asphalt. *Ind. Eng. Chem.*, 48: 1196–1201 (1956).
- [3] Blokker, P.C. and Van Hoorn, H., Durability of bitumen in theory and practice. *Proc. 5th World Petroleum Congress, Section VI*, New York, NY, pp. 417–432 (1959).
- [4] Hveem, F.N., Zube, E. and Skog, J., Progress report on the Zaca-Wigmore experimental asphalt test project. In: *Special Technical Publication 277, American Society for Testing and Materials*. Philadelphia, PA, pp. 1–45 (1959).
- [5] Rostler, F.S. and White, R.M., Influence of chemical composition of asphalts on performance, particularly durability. In: *Special Publication 277, American Society for Testing and Materials*. Philadelphia, PA, pp. 64–88 (1959).
- [6] Rostler, F.S. and White, R.M., Composition and changes in composition of highway asphalts, 85-100 penetration grade. *Proc. Assoc. Asphalt Paving Technol.*, 31: 35–89 (1962).
- [7] Greenfeld, S.H. and Wright, J.R., Four methods for predicting the durability of roofing asphalts. *Mater. Res. Stand.*, 2: 738–745 (1962).
- [8] Smith, C.D., Scheutz, C.C. and Hodgson, R.S., Relationship between chemical structures and weatherability of coating asphalts as shown by infrared adsorption spectroscopy. *Ind. Eng. Chem., Prod. Res. Dev.*, 5: 153–161 (1966).
- [9] Davis, T.C. and Petersen, J.C., An inverse GLC study of asphalts used in the Zaca-Wigmore experimental test road. *Proc. Assoc. Asphalt Paving Technol.*, 36: 1–15 (1967).
- [10] Corbett, L.W., Composition of asphalt based on generic fractionation using solvent deasphalting, elution-adsorption chromatography, and densimetric characterization. *Anal. Chem.*, 41: 576–579 (1969).

- [11] Knotnerus, J., Bitumen durability-measurement by oxygen adsorption. *Ind. Eng. Chem., Prod. Res. Dev.*, 11: 411–422 (1972).
- [12] Griffin, R.L., Simpson, W.C. and Miles, T.K., Influence of composition of paving asphalts on viscosity, viscosity-temperature susceptibility and durability. *J. Chem. Eng. Data*, 4: 349–354 (1959).
- [13] Peters, R.J., Compositional considerations of asphalt for durability improvement. In: *Transportation Research Record 544, TRB*. National Research Council, Washington, D.C., pp. 46–55 (1975).
- [14] Plancher, H., Green, E.L. and Petersen, J.C., Reduction of oxidative hardening of asphalts by treatment with hydrated lime — a mechanistic study. *Proc. Assoc. Asphalt Paving Technol.*, 45: 1–24 (1976).
- [15] Welborn, J.Y., Oglio, F.R. and Zenewitz, J.A., A study of viscosity-graded asphalt cements. *Proc. Assoc. Asphalt Paving Technol.*, 35: 19–60 (1966).
- [16] Schweyer, H.E. and Chipley, E.L., Composition studies on asphalt cements: a progress report. In: *Highway Research Record 178, HRB*. National Research Council, Washington, D.C., pp. 30–59 (1967).
- [17] Corbett, L.W., Densimetric method for characterizing asphalt. *Anal. Chem.*, 36: 1967–1971 (1967).
- [18] Ramsey, J.W., McDonald, F.R. and Petersen, J.C., Structural study of asphalts by nuclear magnetic resonance. *Ind. Eng. Chem., Prod. Res. Dev.*, 6: 231–236 (1967).
- [19] Hubbard, R.L. and Stanfield, K.E., Determination of asphaltenes, oils and resins in asphalt. *Anal. Chem.*, 20: 460–465 (1948).
- [20] O'Donnell, G., Separating asphalt into its chemical constituents. *Anal. Chem.*, 23: 11–20 (1951).
- [21] Bestougeff, M., Isomerism of petroleum constituents. *Proc. 3rd World Petroleum Congress, Section VI*, The Hague, pp. 11–20 (1951).
- [22] Hoiberg, A.J. and Garris Jr., W.E., Analytical fractionation of asphalts. *Anal. Ed., Ind. Eng. Chem.*, 16: 294–302 (1944).
- [23] Schweyer, H.E. and Traxler, R.N., Separating asphalt materials—butanol–acetone method. *Oil Gas J.*, 52: 133 (1953).
- [24] Bestougeff, M., Constitution des composés soutes cycliques du pétrole. *Proc. 5th World Petroleum Congress, Section V*, New York, NY, pp. 143–164 (1959).
- [25] Kleinshmidt, L.R., Chromatographic method for the fractionation of asphalt into distinctive groups of components. *J. Res., Natl. Bur. Stand.*, 54: 163–166 (1955).
- [26] Altgelt, K.H. and Hirsh, E., GPC separation and integrated structural analysis of petroleum heavy ends. *Sep. Sci.*, 5: 855–862 (1970).
- [27] Bynum Jr., D. and Traxler, R.N., Gel permeation chromatography data on asphalts before and after service in pavements. *Proc. Assoc. Asphalt Paving Technol.*, 39: 683–702 (1970).
- [28] Reerink, H. and Lijzenga, J., Gel permeation chromatography calibration curve for asphaltenes and bituminous resins. *Anal. Chem.*, 47: 2160–2167 (1975).
- [29] Such, C. and Brule, B., Characterization of a road asphalt by chromatographic techniques (GPC and HPLC). *J. Liq. Chromatogr.*, 2: 437–453 (1979).
- [30] Jennings, P.W., Pribanic, J.A.S., Dawson, K.R. and Bricca, C.E., Use of HPLC and NMR spectroscopy to characterize asphaltic materials. *Preprints, Div. Pet. Chem., Am. Chem. Soc.*, 26: 915–922 (1981).
- [31] Branthaver, J.F., Duvall, J.J., Petersen, J.C., Plancher, H. and Robertson, R.E., Preparative size-exclusion chromatography separation of SHRP asphalts: correlation with viscoelastic properties. *Fuel Sci. Technol. Int.*, 10 (4–6): 1003–1032 (1992).
- [32] Branthaver, J.F., Petersen, J.C., Robertson, R.E., Duvall, J.J., Kim, S.S., Harnsberger, P.M., Mill, T., Ensley, E.K., Barbour, F.A. and Schabron, J.F., SHRP-A-368, Binder Characterization and Evaluation, Vol. 2. Chemistry. *Strategic Highway Research Program, National Research Council*, Washington, D.C. (1993).
- [33] Branthaver, J.F., Catalfomo, M.W. and Petersen, J.C., Ion exchange chromatography separation of SHRP asphalts. *Fuel Sci. Technol. Int.*, 10 (4–6): 855–885 (1992).
- [34] Branthaver, J.F., Kim, S.S., Catalfomo, M.W. and Goray, D.C., Isolation and characterization of amphoteric compounds of SHRP asphalts by ion exchange chromatography. *Preprints, Div. Fuel Chem., Am. Chem. Soc.*, 37 (3): 1299–1311 (1992).
- [35] Davis, T.C. and Petersen, J.C., Inverse gas–liquid chromatographic studies of asphalt-comparison with analyses by fractionation. *Anal. Chem.*, 39: 1852–1857 (1967).

- [36] Rostler, F.S. and Sternberg, H.W., Compounding rubber with petroleum products. *Ind. Eng. Chem.*, 41: 598–608 (1949).
- [37] Nellenstyn, F.J., The constitution of asphalt. *J. Inst. Pet. Technol.*, 10: 311–325 (1924).
- [38] Nellenstyn, F.J., Relation of the micelle to the medium in asphalt. *J. Inst. Pet. Technol.*, 14: 134–138 (1928).
- [39] Mack, C.J., Colloid chemistry of asphalts. *J. Phys. Chem.*, 36: 2901–2914 (1932).
- [40] Pfeiffer, J.P. and Saal, R.N.J., Asphaltic bitumen as colloid system. *J. Phys. Chem.*, 44: 139–149 (1940).
- [41] Saal, R.N.J., Bass, P.W. and Heukelom, W., The colloidal structure of asphaltic bitumens. *J. Chim. Phys.*, 43: 235–261 (1946).
- [42] Corbett, L.C., Relationship between composition and physical properties of asphalt. *Proc. Assoc. Asphalt Paving Technol.*, 39: 481–491 (1970).
- [43] Manheimer, J., The effects of paraffins on asphalt. *Proc. 1st World Petroleum Congress*, 2 (1933) 553–556.
- [44] Oliensis, G.L., Compatibility between bitumens — exudition versus insudation. *Mat. Res. Stand.*, 1: 723–727 (1961).
- [45] Simpson, W.C., Griffin, R.L. and Miles, T.K., Relationships of asphalt properties to chemical composition. *Preprints, Div. Pet. Chem., Am. Chem. Soc.*, 5: A79–A87 (1960).
- [46] Heithaus, J.J., Measurement of significance of asphaltene peptization. *Preprints, Div. Pet. Chem., Am. Chem. Soc.*, 5: A23–A37 (1960).
- [47] White, R.M., Mitten, W.R. and Skoq, J.B., Fractional components of asphalt-compatibility and interchangeability of fractions produced from different asphalts. *Proc. Assoc. Asphalt Paving Technol.*, 39: 498–531 (1970).
- [48] Halstead, W.J., Rostler, F.S. and White, R.M., Properties of highway asphalts, Part III. Influence of chemical composition. *Proc. Assoc. Asphalt Paving Technol.*, 35: 91–138 (1966).
- [49] Zenewitz, J.A. and Welborn, J.Y., Predicting asphalt performance. *Report FHWA-RD-76-133*, FHWA, U.S. Department of Transportation (1975).
- [50] Kemp, G.R., Asphalt durability tests and their relationships to field hardening. In: *Special Technical Publication 532, American Society for Testing and Materials*, Philadelphia, PA, pp. 100–122 (1973).
- [51] Traxler, R.N., Relation between hardening and composition of asphalt. *Preprints, Div. Pet. Chem., Am. Chem. Soc.*, 5 (4): A71–A77 (1960).
- [52] Goode, J.F. and Owings, E.P., A laboratory–field study of hot asphalt concrete wearing course mixtures. *Public Roads*, 31: 221–228 (1961).
- [53] Vallegra, B.A., White, R.M. and Rostler, K.S., *Changes in Fundamental Properties of Asphalts During Service in Pavements*. Office of Research and Development, U.S. Bureau of Public Roads (January 1970).
- [54] Corbett, L.W. and Merz, R.E., Asphalt Binder hardening in the michigan test road after 18 years of service. In: *Transportation Research Record 544, TRB*. National Research Council, Washington, D.C., pp. 27–34 (1975).
- [55] King, W.H. and Corbett, L.W., Relative oxygen absorption and volatility properties of submicron films of asphalt using the quartz crystal microbalance. *Anal. Chem.*, 41: 580–583 (1969).
- [56] Petersen, J.C., Barbour, F.A. and Dorrence, S.M., Catalysis of asphalt oxidation by mineral aggregate surfaces and asphalt components. *Proc. Assoc. Asphalt Paving Technol.*, 43: 162–177 (1974).
- [57] Dorrence, S.M., Barbour, F.A. and Petersen, J.C., Direct evidence of ketones in oxidized asphalts. *Anal. Chem.*, 46: 2242–2244 (1974).
- [58] Petersen, J.C., Barbour, F.A. and Dorrence, S.M., Identification of dicarboxylic anhydrides in oxidized asphalts. *Anal. Chem.*, 47: 107–111 (1975).
- [59] Petersen, J.C., Quantitative method using differential infrared spectrometry for the determination of compound types absorbing in the carbonyl region in asphalts. *Anal. Chem.*, 47: 112–117 (1975).
- [60] Petersen, J.C. and Plancher, H., Quantitative determination of carboxylic acids and their salts and anhydrides in asphalts by selective chemical reactions and differential infrared spectrometry. *Anal. Chem.*, 53: 786–789 (1981).



- [61] Petersen, J.C., Oxidation of sulfur compounds in petroleum residues: reactivity-structural relationships. *Preprints, Div. Pet. Chem., Am. Chem. Soc.*, 26 (4): 898-906 (1981).
- [62] Davis, T.C. and Petersen, J.C., An adaptation of inverse gas-liquid chromatography to asphalt oxidation studies. *Anal. Chem.*, 38: 1938-1940 (1966).
- [63] Petersen, J.C., Plancher, H. and Miyake, G., Chemical reactivity and flow properties of asphalts modified by metal complex-induced reaction with atmospheric oxygen. *Proc. Assoc. Asphalt Paving Technol.*, 52: 32-60 (1983).
- [64] Petersen, J.C., Branthaver, J.F., Robertson, R.E., Harnsberger, P.M., Duvall, J.J. and Ensley, E.K., Effects of physicochemical factors on asphalt oxidation kinetics. *Transportation Research Record 1391, TRB*. National Research Council, Washington, D.C., pp. 1-10 (1993).
- [65] Petersen, J.C. and Harnsberger, P.M., Asphalt aging: a dual oxidation mechanism and its relationships with asphalt composition and oxidative aging. *Transportation Research Record 1638, TRB*. National Research Council, Washington, D.C., pp. 47-55 (1998).
- [66] Petersen, J.C., A dual sequential mechanism for the oxidation of petroleum asphalts. *Pet. Sci. Technol.*, 16 (9-10): 1023-1059 (1998).
- [67] Petersen, J.C., Relationships between asphalt chemical composition and performance related properties. *Proceedings of the 9th Annual Meeting of the Asphalt Emulsion Manufacturers Association*, Las Vegas, NV (March 1982), and *Meeting of the International Slurry Seal Association*, Phoenix, AZ (January 1983).
- [68] Boduszynski, M.M., McKay, J.F. and Latham, D.R., Asphaltenes, where are you?. *Proc. Assoc. Asphalt Paving Technol.*, 49: 123-143 (1980).
- [69] Petersen, J.C., An infrared study of hydrogen bondings in asphalt. *Fuel*, 46: 295-305 (1967).
- [70] Davis, T.C., Petersen, J.C. and Haines, W.E., Inverse gas-liquid chromatography. A new approach for studying petroleum asphalts. *Anal. Chem.*, 38: 241-243 (1966).
- [71] Petersen, J.C., Barbour, R.V., Dorrence, S.M., Barbour, F.A. and Helm, R.V., Molecular interactions of asphalt: tentative identification with carboxylic acids present. *Anal. Chem.*, 43: 1491-1496 (1971).
- [72] Petersen, J.C., Ensley, E.K. and Barbour, F.A., Molecular interactions of asphalt in the asphalt-aggregate interface region. In: *Transportation Research Record 515, TRB*. National Research Council, Washington, D.C., pp. 68-78 (1974).
- [73] Ensley, E.K., A study of asphalt-aggregate interactions and asphalt molecular interactions by microcalorimetric methods: postulated interaction mechanism. *J. Inst. Pet.*, 59: 279-289 (1973).
- [74] Barbour, R.V. and Petersen, J.C., Molecular interactions of asphalt: an infrared study of the hydrogen-bonding basicity of asphalt. *Anal. Chem.*, 46: 273-277 (1974).
- [75] Petersen, J.C., Ensley, E.K., Plancher, H. and Haines, W.E., Paving asphalts: asphalt-aggregate interactions and asphalt intermolecular interactions. *Report FHWA-RD-77-25*. FHWA, U.S. Department of Transportation (August 1976).
- [76] Petersen, J.C., Plancher, H., Ensley, E.K. and Miyake, G., Chemistry of the asphalt-aggregate interaction: relationship with pavement moisture damage prediction tests. In: *Transportation Research Record 483, TRB*. National Research Council, Washington, D.C., pp. 95-104 (1982).
- [77] Plancher, H., Chow, C.-K. and Petersen, J.C., Viscoelastic measurements and their relationship to bitumen properties. *Proc. Int. Symp. Progrossi Nella Tecnologia Dei Bitumi, Stazione Sperimentale per i Combustibili*, San Donato Milanese, pp. 248-262 (1981).
- [78] Hoiberg, A.J., Asphalt-solvent blends. *Ind. Eng. Chem.*, 43: 1419-1423 (1951).
- [79] Anderson, D.A., Dukatz, E.L. and Petersen, J.C., The effect of antistripping additives on the properties of asphalt cements. *Proc. Assoc. Asphalt Paving Technol.*, 51: 298-317 (1982).
- [80] *Highway Chemicals Newsletter*. Akzo Chimie America, (formerly Armak Company), McCook, IL (Fall 1979).
- [81] Khosla, N.P., Effect of emulsified modifiers on the characteristics of recycled mixtures. *Proc. Assoc. Asphalt Paving Technol.*, 51: 522-539 (1982).
- [82] Mertens, E.W., Predicting weatherability of coating-grade asphalts from asphaltene characteristics. *Bull. 250. ASTM*, Philadelphia, PA, pp. 40-44 (1960).
- [83] Altgelt, K.H. and Harle, O.L., The effect of asphaltenes on asphalt viscosity. *Ind. Eng. Chem., Prod. Res. Dev.*, 14: 240-256 (1975).

- [84] Plancher, H., Hoiberg, A.J., Suhaka, S.C. and Petersen, J.C., A settling test to evaluate the relative degree of dispersion of asphaltenes. *Proc. Assoc. Asphalt Paving Technol.*, 48: 351–374 (1979).
- [85] Branthaver, J.F. and Salmans, S.L., Rheological properties of asphalt crossblends. *Preprints, Div. Fuel Chem., Am. Chem. Soc.*, 41 (4): 1282–1288 (1996).
- [86] Traxler, R.N. and Schweyer, H.W., Increase in viscosity of asphalts with time. *Proc. Am. Soc. Testing Mater.*, 36 (II): 544–551 (1936).
- [87] Traxler, R.N. and Coombs, C.E., The colloidal nature of asphalt as shown by its flow properties. *J. Phys. Chem.*, 40: 1133–1147 (1936).
- [88] Traxler, R.N. and Coombs, C.E., Development of internal structure in asphalts with time. *Proc. Am. Soc. Testing Mater.*, 37 (II): 549–557 (1937).
- [89] Traxler, R.N., Schweyer, H.E. and Romberg, J.W., Rheological properties of asphalts. *Ind. Eng. Chem.*, 36: 823–829 (1944).
- [90] Brown, A.B., Sparks, J.W. and Smith, F.M., Steric hardening of asphalts. *Proc. Assoc. Asphalt Paving Technol.*, 26: 486–494 (1957).
- [91] Brown, A.B. and Sparks, J.W., Viscoelastic properties of a penetration grade asphalt at winter temperature. *Proc. Assoc. Asphalt Paving Technol.*, 27: 35–51 (1958).
- [92] Coombs, C.E. and Traxler, R.N., Rheological properties of asphalts, IV. Observations concerning the anomalous flow characteristics of airblown asphalts. *J. Appl. Phys.*, 8: 291–296 (1937).
- [93] Ensley, E.K. and Shulz, H.A., A study of asphalt–aggregate interactions by heats of immersion. *J. Inst. Pet.*, 58: 95–101 (1972).
- [94] Robertson, R.E., Ensley, E.K. and Petersen, J.C., Physiochemical studies of tender mix and nontender mix asphalts. *Report FHWA/RD-80/130, FHWA*, U.S. Department of Transportation (December 1980).
- [95] Ensley, E.K., A kinetic investigation of association in asphalt. *J. Colloid Interface Sci.*, 53: 452–460 (1975).
- [96] Ensley, E.K., Multilayer adsorption with molecular orientation of asphalt on mineral aggregate and other substrates. *J. Appl. Chem. Biotechnol.*, 25: 671–682 (1975).
- [97] Hveem, F.N., Zube, E. and Skog, J., Proposed new tests and specifications for paving crude asphalts. *Proc. Assoc. Asphalt Paving Technol.*, 32: 271–327 (1963).

This page intentionally left blank

## *Chapter 15*

# **BITUMEN ASSOCIATED WITH PETROLEUM FORMATION, EVOLUTION AND ALTERATION — REVIEW AND CASE STUDIES IN CHINA**

ZHIJUN WU, PINAN PENG, JIAMO FU, GUOYING SHENG and DEHAN LIU

## **INTRODUCTION**

For many years, there have been disagreements among bitumen researchers concerning the definitions and applications of bitumen, ground bitumen, asphalt, natural bitumen, etc. During early bitumen research, confusions about bitumens may have arisen due to the diverse physical properties of bitumens and their occurrence in different regions of the world. The confusions, moreover, may have been due to the differences between the academic majors of bitumen researchers. Since the 1980s, researchers have gained a better understanding of the composition, structure and origin of sedimentary organic matters, such as crude oils, bitumens, kerogens, and coals. The concept of bitumen, therefore, was revised from bitumen concepts of earlier research. Currently, bitumen is defined as a dark, brown or black oily solid organic substance of high molecular weight at normal temperature and atmospheric pressure, which is directly transformed from crude or geolipids.

The formation of bitumen may occur during petroleum processes of generation, evolution, migration, transportation, and degradation. As there are many ways for bitumen to form, it should be noted that naturally-occurring bitumens have distinct characteristics in their occurrence, distribution, and physical properties. The above-mentioned points have drawn the interest of petroleum geologists and geochemists. Previous workers [1–7] have initiated, conducted, and summarized studies about the chemical composition, molecular structures, physical properties, and genetic classifications of bitumens. These researchers have also written a bitumen-related literature that appeared in special magazines around the world. It cannot be safely said, however, that bitumen research has ceased. Indeed, it is necessary to describe bitumen formation in correlation with petroleum evolution, which is not commonly seen among publications. In addition, literature concerning some Chinese petroleum bitumens, which have typical occurrences and special origins, has not been internationally published. This chapter, therefore, is aimed at reviewing naturally-occurring bitumens in regard to the origin and evolution of petroleum. This will include a number of case studies that involve Chinese bitumens.

## **GENETIC TYPES OF BITUMEN AND THEIR DISTRIBUTION**

The formation of bitumen can occur in the purification, evolution, or degradation stages of sedimentary organic matter. The classification of the genetic types of bitumens

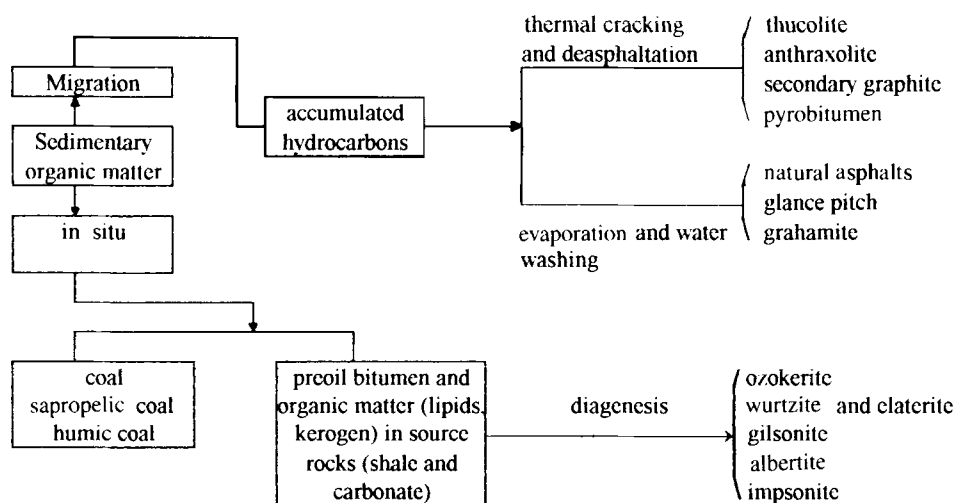


Fig. 15-1. Genetic classification of sedimentary organic matter and bitumen. After Rogers et al. [6].

is essential to bitumen research. Several bitumen classifications have been introduced. The bitumen classification by Rogers et al. [6] is relatively complete; it includes most of the naturally-occurring bitumens as shown in Fig. 15-1. Bitumen properties do not have a simple correlation with their origin because there are many processes that lead to the formation of bitumen. Bitumens that share the same properties may have undergone distinct evolutionary paths, whereas bitumens that have different characteristics share the same origin. It is difficult, therefore, to construct a detailed and clear relation between a bitumen's property and its origin. For example, when one studies concrete bitumen, it seems scientifically plausible to distinguish the bitumen genetic group first. Afterwards, the exact origin of the bitumen can be calculated by synthetic analysis. In this chapter, four macro groups of bitumen genetic types will be reviewed. They are classified by origin and evolution as follows:

- (1) *Primary authigenic bitumen* — asphalt, wurtzite, ozokerite, albertite, gilsonite, and imponsonite.
- (2) *Epigenetic reservoir bitumen* — grahamite, pyrobitumen, anthraxolite, and mezo-meta imponsonite.
- (3) *Surficial degradation bitumen* — glance pitch, grahamite, heavy oil, albertite, and bitumen clastics.
- (4) *Magnetic thermal alteration bitumen* — pyrobitumen, secondary graphite, and bitumen coke.

#### *Primary authigenic bitumen*

Primary authigenic bitumen should be distinguished from the rest of asphalt. Here, we define primary authigenic bitumen as the solid state bitumen directly transformed from sedimentary organic matter in shale or carbonaceous source rock of the same

layer. This type of bitumen is usually distributed in fissures, pores, tectonic cracks and dissolution cavities of source rocks. They do not show evident characteristics of large-scale migration. Primary authigenic bitumen, basically, is the indigenous bitumen in source rocks.

Taking the maturity of the organic matter into account, indigenous bitumen can further be identified as pre-oil bitumen and post-oil bitumen. Pre-oil bitumen occurs in immature or low-maturity carbonate and evaporite-clastic source rocks or thick organic-rich shale (oil shale), parallel to the bedding plane. For example, the bitumen in the immature Qianjiang oil shale of the Lower Tertiary System in the Jiangnan Basin and the sulphur asphalt in the Zhujiazhuang huge natural sulphur deposit in Shandong Province are typical indigenous bitumens. Post-oil bitumen predominantly occurs in carbonate source rocks. This subtype of bitumen is transformed from Asphalt C, which is released from carbonate crystals at a high-maturity stage after the oil generation peak, solely distributed in sutures, bedding planes and fossil hole spaces.

The shape and quantity of primary authigenic bitumen can reflect the hydrocarbon generation potential of source rocks, whereas the thermal maturity of source rock can be calculated by measuring the bitumen reflectance. Post-oil bitumen may be rather useful in oil-source rock relationships for high-maturity carbonate source rock. If bitumens were enriched in carbonate vugs to a certain scale, then industrial mining of bitumens could be done.

#### *Secondary reservoir bitumen*

Secondary reservoir bitumen refers to the bitumen transformed from petroleum, which has undergone large-scale secondary migration. When accumulated petroleum in sandstone or carbonate reservoirs largely loses its lighter compounds due to the tectonic destruction of pools, the heavier residual components condense and incorporate each other, leading to the formation of bitumen. Deasphaltation of this type of hydrocarbon mixture and deposition of reservoir bitumen occurs when a large quantity of natural gas from the deeper strata moves into the oil trap. As the petroleum-bearing basin continues to decrease, the reservoir oil faces increased thermal stress and liquid oil gradually cracks into gaseous hydrocarbons while its residual components condense into bitumen.

Reservoir bitumen is widely distributed and can usually be found in fractures, joints, fissures, and fault planes in sandstone reservoir beds, or in various secondary diagenetic openings of carbonates. Geochemically, the shape, state, and quantity of reservoir bitumen and its relationship with peripheral minerals can be used for studying the path, scale and time sequence of petroleum migration. Under some conditions, exposed and concentrated reservoir bitumen can be placed under the category of industrial mining. The famous giant bitumen and heavy oil deposit in Alberta, West Canada, for example, has been mined for over twenty years.

#### *Weathered or degraded supergene bitumen*

Supergene bitumen belongs to the secondary bitumen group and shares some similarities with reservoir bitumen. Supergene bitumen, however, differs from reservoir

bitumen in its distribution, occurrence, and properties due to its formation under surficial conditions. Geologically formed supergene bitumen usually occurs in the marginal zone of a compressed petroleum-bearing basin. Subsurface oil seeps to the surface through active fault planes. This oil is weathered, waterwashed and biodegraded to form tar-like bitumen or solid bitumen. An example of this can be found in the Laojunmiao Oil Field in Gansu Province, the first industrial oil field in China, which was discovered through surficial bitumen seeps.

Supergene bitumen should include the redeposited bitumen, which is currently buried in the deep subsurface beds. In past geological time, surficial bitumen was weathered into solid organic clastics and was transported and deposited with terrigenous clastics. This type of bitumen usually has good solidification and a high reflectance. It mainly occurs along the bedding planes and has a sharp boundary with adjacent minerals.

Another type of supergene bitumen is derived from oil seeps. During the production and transportation of petroleum, discharge at the drilling site and transportation, leaks left considerable amounts of oil in the natural environment, causing a severe hydrocarbon pollution problem. Leaked oil is degraded into bitumen, which has incorporated nitrogen and oxygen heteroatoms and inorganic solid materials under ground surface conditions. This bitumen, therefore, has a high resistance to degradation and high viscosity. It is not easy to remove this type of bitumen from the natural ecological system. In the future, knowledge of the research on bitumen origin will be helpful in order to effectively treat hydrocarbon contamination.

#### *Magmatic thermal alteration bitumen*

Magmatic thermal alteration bitumen has a relatively rare distribution. Oil in reservoir rocks and asphaltene in source beds, heated by high-temperature magmatic activities, are quickly 'metamorphosed' to magmatic thermal alteration bitumen. This type of bitumen has particular shapes and structures of spherulite, vesicle and poikilite, and is easy to recognize. Thermal alteration bitumen is mainly used to assess the thermal metamorphism of organic matter and metamorphic range.

### OCURRENCE, CLASSIFICATION AND NOMENCLATURE OF BITUMENS DURING PETROLEUM EVOLUTION PROCESSES

#### *Parameters for evaluating bitumen maturity and application*

Bitumen maturity can provide a vast amount of geochemical information for studying the petroleum system in a sedimentary basin. It is necessary, therefore, to make a systematic classification of bitumen maturity. Inasmuch as bitumens can be formed via many geological processes and vary sharply in physical properties and chemical compositions, a considerable number of bitumen maturity parameters have been developed. The parameters are as follows:

(1) *H/C ratio*. *H/C* ratio is one of the effective parameters for evaluating the thermal maturity of solid organic matter. Rogers et al. [6] used this ratio to systematically study

the thermal maturity sequence of reservoir bitumen in West Canada and to obtain a good correlation between H/C ratio and bitumen maturity. This method has limitations in its application because it requires a sufficient amount of available pure bitumen samples.

(2) *Bitumen solubility in CS<sub>2</sub>*. This method is only suitable for low-maturity bitumen, which has a certain amount of soluble constituent. Inasmuch as bitumen solubility can be influenced by other factors, this method is not the most suitable process for what is required. It is rarely used at the present time.

(3) *Volatile yield*. Volatile yield is defined as the yield of volatile components by heating one gram of bitumen at 900°C in vacuum for 7 min. This method gives similar results as the H/C ratio measurement and is limited in its application, because it needs a sufficient quantity of pure sample.

(4) *Bitumen reflectance*. The measuring of bitumen reflectance does not require a large sample or separation. Due to these reasons, this method has been preferred by many researchers. Fu and Shi [8] reported on the bitumen reflectance data on Sinian dolomitic of the Weiyuan Gas Field, Sichuan Province, and discussed the thermal maturity of Sinian source rock. Cook and Kantslev [5] published a research paper dealing with the determination of maturity by means of bitumen reflectance. It was also proposed that bitumen reflectance is an effective method for maturity determination in lower Paleozoic beds, which lack vitrinite. Liu [10] conducted a systematical thermal simulation experiment on the relationship between thermal evolution of organic matter and bitumen reflectance, which is shown in Table 15-1 and Fig. 15-2. The bitumen reflectance increases with increasing simulation temperature and the carbonization of bitumen increases with decreasing H/C ratio. In Fig. 15-2, the bitumen reflectance values appear offset with vitrinite reflectance at temperatures higher than 400°C ( $R_o > 2.5\%$ ). This causes difficulties in calculating the  $R_o$  value using bitumen reflectance,

TABLE 15-1

Thermal simulation experiment of vitrinite and bitumen

Sample	Experimental conditions			C (%)	H (%)	H/C atomic ratio	$R_{o,max}$ (%)	Free radical ( $10^{19}$ s/g)	Distance of carbon atomic plane ( $d_{(012)}$ , Å)
	$T$ (°C)	$P$ (atm)	$t$ (h)						
Vitrinite	Nor. temp.	Nor. pres.		71.28	5.60	0.94	0.63	1.55	3.8968
	250	1000	100				0.76		3.5047
	350	1000	100	82.28	4.68	0.68	1.39	9.06	
	400	1000	100	86.74	4.07	0.56	2.60	8.34	3.6071
	450	1000	100	88.30	3.48	0.47	2.84	15.04	
	500	1000	100	89.13	3.31	0.44	3.40	17.39	
Bitumen	Nor. temp.	Nor. pres.		77.6	7.69	1.18	0.59	1.21	3.9610
	250	1000	100				0.73		3.9515
	350	1000	100	84.1	7.46	1.06	1.12	1.96	
	400	1000	100	83.05	4.41	0.63	3.93	7.46	3.4930
	450	1000	100	78.56	3.11	0.47	6.01	4.08	
	500	1000	100	86.98	3.06	0.42	6.21	5.95	



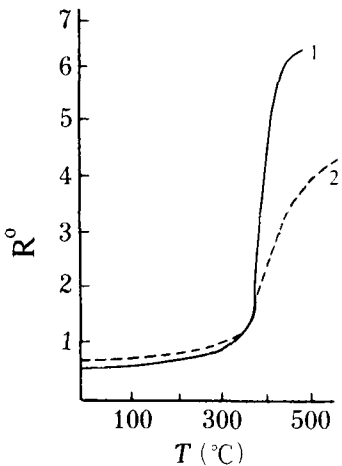


Fig. 15-2. Variation of bitumen reflectance and vitrinite reflectance in the thermal simulation experiment. 1 = bitumen, 2 = vitrinite. After Liu et al. [10].

because bitumen has a higher amount of hydrogen and lower carbon content and aromaticity.

Current research has made a new discovery in the relationship of bitumen reflectance and vitrinite reflectance. Xiao [11] reported that the thermal alteration magnitude and optical features influence bitumen reflectance. As shown in Table 15-2 and Fig. 15-3, the bitumen reflectance is lower than vitrinite reflectance at simulation temperatures lower than 350 $^\circ\text{C}$  and that there is an offset in the increasing trends of reflectance of

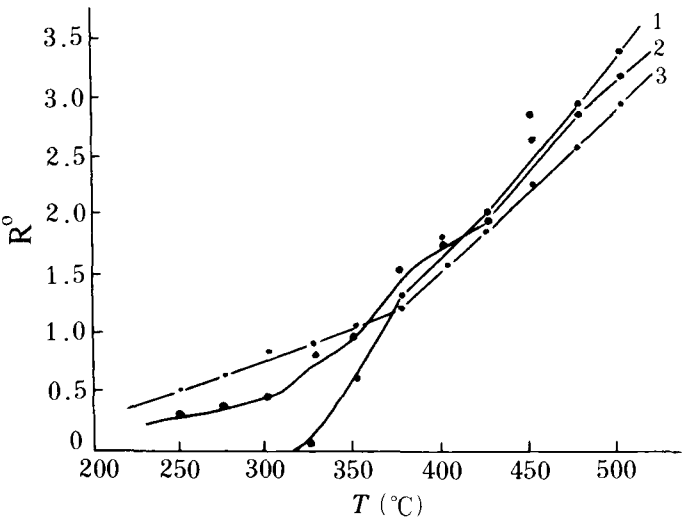


Fig. 15-3. Bitumen reflectance and vitrinite reflectance in thermal simulation experiments: 1 = Urho bitumen, heterogeneous; 2 = Guangyuan bitumen, homogeneous; 3 = vitrinite.

TABLE 15-2

Artificial thermal maturation of bitumen of different origin in China

Sample temp. (°C)	Vitrinite $R_r$ (%)	Uoho bitumen in Xingjiang, northwest China				Guangyuan bitumen in Sichuan, southwest China	
		Optical feature and texture	$R_{\max}$ (%)	$\Delta R$ (%)	$R_r$ (%)	Optical feature and texture	$R_r$ (%)
Room temp.	0.401	black, homogeneous			<0.05	black, homogeneous	0.218
250	0.521	black, homogeneous			<0.05	black, homogeneous	0.281
275	0.687	black, homogeneous			<0.05	gray, homogeneous	0.372
300	0.803	black, homogeneous			<0.05	gray, homogeneous	0.453
325	0.901	black, homogeneous			0.052	gray, homogeneous	0.801
350	1.082	gray, homogeneous			0.601	gray, homogeneous	0.990
375	1.201	gray, homogeneous			1.382	yellowish gray, homogeneous	1.541
400	1.603	grayish yellow, slightly heterogeneous	1.901	0.203	1.807	yellowish gray, homogeneous	1.762
425	1.852	yellow, poikilitic	3.109	2.612	2.093	grayish yellow, homogeneous	1.908
450	2.301	yellow, middle to coarse grain poikilitic	3.987	2.980	2.907	yellow, homogeneous	2.624
475	2.582	yellow, coarse poikilitic	3.987	2.980	2.907	yellow, homogeneous	2.624
500	2.923	yellow, schistose poikilitic in some part	5.108	4.002	3.408	yellow, homogeneous	3.232

TABLE 15-3

Correlation of vitrinite reflectance and bitumen reflectance in different maturation stages

Petroleum evolution stage	Vitrinite $R_r$ (%)	Autochthonous bitumen $R_r$ (%)
<i>Liquid hydrocarbon</i>		
Immature	<0.50	<0.05–0.10
Slightly mature	0.50–0.75	<0.05–0.10
Peak generation	0.75–1.0	>0.10, 0.40–0.90
Highly mature	1.0–1.30	0.90–1.50
<i>Gaseous hydrocarbon</i>		
Condensate and wet gas	1.30–1.8	1.50–2.20
Dry gas	>1.8	>2.20

the two bitumens. The bitumen reflectance curve is roughly parallel to that of vitrinite reflectance when the temperature is higher than 350°C. The reflectance of the optically homogeneous bitumen steadily increases with an increase in temperature, showing a good linear relationship with vitrinite reflectance (see Fig. 15-3). The random reflectance,  $R_r$ , of optically heterogeneous bitumen varies more than maximum reflectance  $R_{max}$ , and the  $R_r$  has a better linear relationship with vitrinite reflectance. As seen in Table 15-3, the correlation between the reflectance of primary authigenic bitumen and source rock maturity has been established.

(5) *Bitumen X-ray diffraction pattern.* Thermal stress causes compositional changes in bitumens and causes the aromaticity of bitumens to gradually increase. Structural changes of bitumens are revealed by X-ray diffraction patterns. As shown in Fig. 15-4, the X-ray diffraction patterns of bitumen and vitrinite vary with increasing simulation temperature, showing a regular correlation between temperature and bitumen structure. Yen et al. [1] and Wen et al. [4] made significant advances in the research of bitumen structure. They proposed a series of formulas to quantitatively determine bitumen structure as follows:

$$f_a = \frac{A_{(002)}}{A_{(002)} + A_\gamma}$$

$f_a$  = aromaticity,  $A_{(002)}$  and  $A_\gamma$  = peak areas of (002) zone and  $\gamma$  zone.

$$d_m = \frac{\lambda}{2 \sin \theta}$$

$d_m$  = distance between aromatic slices,  $\lambda$  = wavelength of X-ray,  $\theta$  = Bragg angle.

$$d_\gamma = \frac{5\lambda}{8 \sin \theta}$$

$d_\gamma$  = distance between saturated parts in bitumen structure,  $\lambda$  = wavelength of X-ray,  $\theta$  = Bragg angle.

$$L_a = \frac{1.84\lambda}{0.5\beta_{(100)}}$$

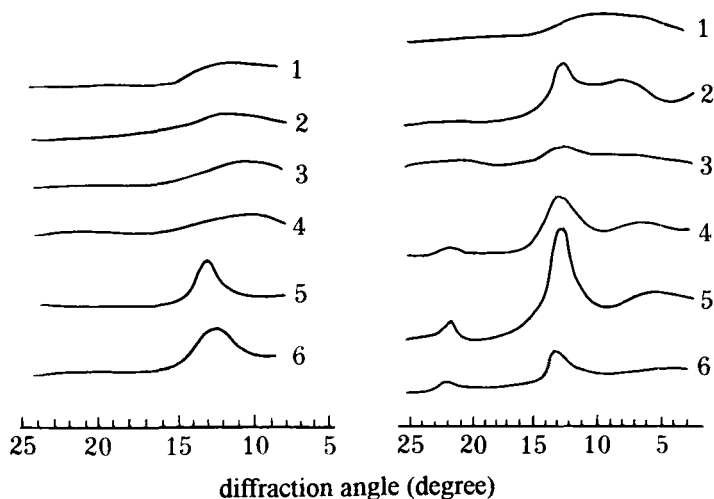


Fig. 15-4. X-ray diffraction patterns of petroleum bitumen, vitrinite (left) and naturally-occurring bitumen (right) (after Liu [12]). Left: 1, 2 = bitumen and vitrinite (normal temp. and pressure); 3, 4 = bitumen and vitrinite (250°C/1000 atm); 5, 6 = bitumen and vitrinite (400°C/1000 atm). Right: 1 = Guangyuan, Sichuan; 2 = Kaili, Guizhou; 3 = Luzhou, Sichuan; 4 = Shangling, Guangxi; 5 = Naji, Guangxi; 6 = Weiyuan, Sichuan.

$L_a$  = average diameter of aromatic slice,  $\lambda$  = wavelength of X-ray,  $\beta_{(100)}$  = radian of (100) zone.

$$L_c = \frac{0.9\lambda}{\omega \cos \theta} = \frac{0.45}{0.5\beta}$$

$L_c$  = average height of aromatic slice pile,  $\lambda$  = wavelength of X-ray,  $\beta$  = radians of (002) and (100) zone.

As bitumen maturity increases,  $f_a$ ,  $L_a$  and  $L_c$  values gradually increase, whereas  $d_y$  and  $d_m$  values decrease.

Like the H/C ratio method, the bitumen X-ray diffraction pattern method also needs a sufficient amount of pure bitumen sample.

(6) *Microwave dielectric coefficient*. The electromagnetic field of resonant cavity can be microdisturbed to different extents by placing bitumens of different maturities into the resonant cavity. In effect, the changes in bitumen composition and structure can be reflected. The formulas for dielectric coefficients are as follows:

Actual dielectric coefficient:

$$\varepsilon' = 1 + \frac{1}{2} \left( \frac{V_o}{V_s} \right) \left( \frac{f_o - f}{f} \right)$$

Virtual dielectric coefficient:

$$\varepsilon'' = \frac{1}{4} \left( \frac{V_o}{V_s} \right) \left( \frac{1}{Q} - \frac{1}{Q_o} \right)$$

$f_o$ ,  $Q_o$ ,  $V_o$  and  $f$ ,  $Q$ ,  $V_s$  represent the frequency, quality factor and volume of resonant

TABLE 15-4

Thermal alteration of Chinese bitumen

Sample Nr.	Experimental condition	Dielectric coefficients		Free radical ( $10^{19}$ s/g)	$R_{Omax}$ (%)	H/C ratio	$R_{Omax}$ (%)
		$\epsilon'$	$\epsilon''$				
K1	1 atm	3.91	0.046	1.40	1.24	1.10	0.59
K1	150°C/1000 atm	4.22	0.043	2.00	1.31		
K1	200°C/1000 atm	4.63	0.055	2.00	1.33		0.73
K1	350°C/1000 atm	5.00	0.074	2.65	1.37	1.06	1.12
K1	400°C/1000 atm	5.21	0.081	3.43	1.41	0.64	3.93
K1	450°C/1000 atm	5.75	0.080	4.45	1.46	0.47	6.01
K1	500°C/1000 atm	6.38	0.106	6.26	1.48	0.42	6.21

cavity before and after the bitumen sample is placed into the cavity. As shown in Table 15-4, the results of the bitumen thermal simulation experiment reveal that the microwave dielectric coefficient is a good parameter when compared to other bitumen maturity parameters. The dielectric coefficient is a useful maturity parameter because its values change sharply at different maturity magnitudes.

(7) *Maximum pyrolysis temperature,  $T_{max}$ , of bitumen.*  $T_{max}$  of organic matter can be useful to investigate the chemical bond type of pyrolyzable components. It can also be used to indirectly judge the internal structure of an organic matter.  $T_{max}$  increases with the increasing maturity of bitumen. Inasmuch as 599°C is the highest temperature that the pyrolysis instrument can reach, it is difficult to distinguish higher-maturity bitumens using this method. According to Liu [12],  $T_{max}$  is not useful when bitumen has an H/C ratio less than 0.4 and  $R_f$  is higher than 3%.

(8) *Free radical concentration.* Free radical concentration of solid bitumen can be measured by electric spin resonance. It can be used to determine bitumen maturity. More detailed information was presented by Yen et al. [1,2].

(9) *Morphological structure of bitumen.* Thermal evolution not only causes regular changes in the chemical composition and reflectance of bitumen, but also causes changes in its morphological structure. As bitumen maturity increases, the structure usually changes from homogeneous, heterogeneous, poikilitic, medium-grained to coarse-grained poikilitic and to a sheet structure with a more obvious double reflectance. A brief list of the relationships between bitumen reflectance and morphological structure is given in Table 15-2.

In addition to the above nine methods, there are other types of physical, chemical and spectral ways to study bitumen structure and to determine bitumen maturity. These other procedures include gravity, molecular weight, oxidation rate, nuclear magnetic resonance and infrapectra. For more detailed information, see Yen et al. [2,3,13].

#### *Classification of bitumen maturity*

Many bitumen maturity parameters have limitations in their application and are only suitable for a certain maturity range. The elemental composition and origin of bitumen,

however, influence the behavior of bitumen during thermal evolution. An international maturity classification, like coal rank, has not been established yet.

Chen et al. [14] conducted thermal simulation experiments for crude oil, naturally-occurring bitumens, and artificially oxidized bitumens in order to investigate maturity parameters for bitumens of different origins. As shown in Table 15-5, the reflectance and H/C ratio are two good parameters. Ranging from 360°C to 600°C, the  $R_{\max}$  value gradually increases steadily, whereas the H/C ratio decreases. Free radical concentration reaches a maximum value at 600°C to 650°C and drops at temperatures higher than

TABLE 15-5

Thermal simulation experiment of crude oil, thermally altered bitumen and natural bitumen

Sample Nr.	Simulation temp. (°C)	Elemental composition		Free radical ( $10^{19}$ s/g)	$R_{o\max}$ (%)	Remarks
		H/C	O/C ( $\times 100$ )			
A-1	unheated	1.69	0.8	0.20		Crude oil
A-2	360	1.14	2.2	0.75	0.23	
A-4	420	1.34	1.9	1.09	0.32	
A-5	500	0.93	1.8	2.93	0.76	
A-6	600	0.42	0.7	9.98	3.10	
A-7	650	0.38	0.9	10.06	3.05	
A-8	700	0.30	0.8	5.35	4.13	
A-9	750	0.24	1.2	4.41	5.59	
B-31	360	1.36	2.9	0.85	0.28	Artificial thermally altered bitumen under oxidized condition
B-33	420	1.39	2.0	1.06	0.36	
B-35	500			6.39	1.66	
B-36	600	0.38	0.8	13.73	2.99	
B-37	650	0.36	1.2	11.19	3.2	
B-38	700	0.27	1.2	5.04	4.16	
B-39	750	0.21	0.1	3.58	4.56	
C-40	unheated	1.79	1.4	0.20		Oxidized crude oil
C-41	360	1.39	1.9	0.78	0.59	
C-43	420	1.43	1.2	1.26	0.93	
C-44	500	0.67	0.9	3.54	1.49	
C-45	600	0.40	1.7	9.65	2.44	
C-46	650	0.34	1.3	10.56	3.12	
C-47	700	0.29	0.8	2.22	4.4	
C-48	750	0.28	3.2		5.18	
D-50	unheated	1.19	3.2	0.99	0.36	Naturally-occurring bitumen
D-51	360	1.13	3.1	1.67	0.49	
D-54	500	0.76	1.7	2.12	1.47	
D-55	600	0.41	1.1	8.49	2.1	
D-56	650	0.36	1.1	5.64	2.9	
D-57	700	0.29	1.5	2.99	5.01	
E-60	unheated	1.14	5.0	1.46	0.46	Artificial oxidized bitumen
E-61	360	1.06	4.0	2.00	0.53	
E-63	500	0.56	1.5	2.79	1.63	
E-65	600	0.35	1.4	11.98	2.16	

TABLE 15-6

Properties of natural bitumen [5]

Bitumens	$R_o$ (%)	Fluorescence	Solubility in oil	Volatile (%)
Ozokerite	<0.01–0.05	0.6–30	soluble	90–99
Wurtzite	0.02–0.15	0.02–2.0	insoluble	75–95
Albertite	0.15–0.8	<0.01–0.02	insoluble	50–75
Ground asphalt	<0.01–0.06	0.23–3.5	soluble	85–95
Gilsonite	<0.01–0.17	0.04–0.23	soluble	80–90
Glance pitch	0.17–0.4	0.01–0.07	soluble	70–80
Grahamite	0.4–0.8	4.01	slightly soluble	45–70
Epiimpsonite	0.8–0.2	4.01	insoluble	20–50
Mesoimpsonite	2.0–3.5	4.01	insoluble	10–20
Cataimpsonite	3.5–10	<0.01	insoluble	<10

650°C. It should be noted that  $R_{max}$  varies for bitumens of different origins and different H/C ratios and appears to be affected by both bitumen type and temperature.

As shown in Table 15-6, Cook and Kantslev [5] proposed a classification of bitumen thermal evolution stages based upon reflectance, fluorescence, volatile yield of bitumen, and solubility in oil. This type of classification gives detailed distinctions between low-maturity bitumens and mature bitumens, which have  $R_o$  values lower than 1.0. On the other hand, this type of classification is not reliable to distinguish mature from extremely high-maturity bitumens, being higher than impsonite in the thermal evolution stage. The disadvantage of this type of classification is that it fails to combine bitumen evolution and petroleum generation and evolution.

Using the above-recommended maturity parameters of bitumen, maturities were measured for bitumen from Sinian to Cretaceous carbonate rocks in several representative oil fields or seep zones. The results of the investigation, as shown in Table 15-7, reveal that highly evolved bitumens that are higher than impsonite are predominantly distributed. Establishment of the classification and recognition parameters and criteria for highly evolved bitumens is essential in order to determine the petroleum evolution patterns in Chinese marine carbonate regions, such as the Sichuan Basin, Tarim Basin, Ordos Basin, etc. Table 15-8 summarizes the current research on bitumen thermal evolution stages and bitumen reflectance from source rocks. The proposed classification of bitumen thermal evolution stages has found useful applications for Chinese oils.

### *Occurrence of bitumen and its origin*

The occurrence of bitumen may provide evidence on its origin and may help to describe the petroleum system. Both macrocosmic and microcosmic occurrences may be used for the above purposes.

Macrocosmic occurrences provide the most direct evidence for determining bitumen origin. In field outcrops, various dark or brown bitumens are observed in sandstone and carbonate rocks. Some bitumens are dispersed in carbonate vugs and soften under

TABLE 15-7

Maturity parameters of bitumen in Chinese carbonate rock

Location	Strata	H/C	R <sub>o</sub> (%)	Dielectric coefficient		d <sub>002</sub> (Å)	Free radical (10 <sup>19</sup> s/g)	Optical feature
				ε'	ε''			
Urho, Xingjiang	K		0.06	2.63	0.02	4.9497	0.90	weak fluorescence
Guangyuan, Sichuan	E	1.18	0.59	6.91	0.047	3.9069	1.40	minor fluorescence
Pingquan, Hebei	Z		0.95					minor fluorescence
Kaili, Guizhou	D	0.9	1.06	3.61	0.042	3.5394	2.44	minor fluorescence
Luzhou, Sichuan	T		1.27					homogeneous
Guiyang, Guizhou	P <sub>1</sub>	0.73	1.75					homogeneous
Caoning, Guangxi	T	0.68	1.80	4.86	0.120	3.5225		homogeneous
Luzhou, Sichuan	P <sub>1</sub>		1.85			3.5147		homogeneous
Ouan, Guizhou	E		2.15					weakly heterogeneous
Danzhai, Guizhou	E	0.51	5.78	4.82	0.069	3.4769		weakly heterogeneous
Duyun, Guizhou	O		2.85	4.90	0.072			weakly heterogeneous
Laibin, Guangxi	P		6.05			3.4583		heterogeneous
Tongren, Guizhou	E		3.20			3.4875		heterogeneous
Laibin, Guangxi	C	0.40	3.22	4.76	0.080	3.4452		heterogeneous
Ningming, Guangxi	P <sub>1</sub>		3.30			3.4583		heterogeneous
Chatian, Hunan	E <sub>2</sub>	0.34	3.40			3.4412		heterogeneous
Ziyun, Guizhou	D		3.97	6.25	0.033		3.13	intensively heterogeneous
Jishou, Hunan	E <sub>2</sub>	0.32	4.38	7.24	0.117		1.72	intensively heterogeneous
Fenghuang, Hunan		0.29	4.68	7.99	0.116		1.84	intensively heterogeneous
Weiyuan, Sichuan	Z	0.37	4.85	9.41	0.121	3.4434	2.03	intensively heterogeneous
Shanglin, Guangxi	D	0.27	5.56	36.6	2.13			intensively heterogeneous
Dachang, Guangxi	D	0.13	6.45	41.9	2.80		0.072	intensively heterogeneous
Naji, Guangxi	D	0.19	6.50	71.5	3.94			intensively heterogeneous
Hechi, Guangxi	D	0.19	7.61	83.0	5.54	3.4330		intensively heterogeneous



TABLE 15-8

Correlation of bitumen thermal evolution stage and petroleum generation stage

Bitumen thermal evolution stage and name	$R_r$ (%)	H/C	Volatile (%)	Dielectric coefficient, $\epsilon'$	$T_{max}$ (°C)	$d_{(0.1)}$ (Å)	Optical feature	Petroleum evolution stage
Ozokerite or wurtzite	0.05–0.10		>90					immature
Ground asphalt	<0.05		85–95					immature
Gilsonite	0.05–0.20		80–90					low mature
Glance pitch	0.20–0.40	13–1.2	70–80	2–2.5	<420	5.00–4.00	weak fluorescence	mature
Impsonite-1	0.40–0.80	1.2–1.0	45–70	2.5–3.0	420–450	4.00–3.55	micro fluorescence	peak generation
Impsonite-2	0.80–1.60	1.0–0.75		3.0–4.0	450–460	3.55–3.53	homogeneous	post generation
Pyrobitumen	1.60–2.00	0.75–0.65		4.0–4.5	450–470	3.53–3.50	weakly heterogeneous	condensate and wet gas
Anthraxolite-1	2.00–3.00	0.65–0.40		4.5–5.5	470–500	3.50–3.45	heterogeneous	dry gas
Anthraxolite-2	3.00–5.00	0.40–0.30		5.5–10.0	500–590	3.45–3.41	poikilitic	
Anthraxolite-3	>5.00	<0.30		>10.0	>590	<3.41	scale-like	dead line for generation



Fig. 15-5. Authigenic bitumen in carbonate rock.

the hot sunlight. This type of bitumen is probably either post-oil bitumen or primary authigenic bitumen (see Fig. 15-5). Other types of bitumen occur in rock fissures and fault planes, crossing the stratification. This kind of bitumen is completely solidified, is extremely hard and has a shiny black color. It belongs to the secondary reservoir bitumen formed as a result of tectonic destruction of the paleo-oil pool as shown in Fig. 15-6. Some types of bitumen are distributed in sandstones parallel to the bedding plane as thin layer bitumens or bitumen veinlets. These bitumens, as shown in Fig. 15-7, are always hard and shiny and are categorized as redeposited bitumen. Other types of bitumen are irregularly distributed on outcrop surface within a wide area, regardless of lithology. These bitumens are categorized as supergene bitumens, formed by oil seeping from the subsurface oil pools. In some modern marine coastal carbonate sediments, various bitumen lumps or particles are deposited in the sediment.

Microscopic observation is an important method when studying bitumen origin, because bitumen is widely distributed in rocks. The shape and optical features of bitumen can provide evidence for its origin. Microscopic occurrence of bitumen may be investigated from the following two aspects.

(1) *Bitumen in source rocks.* Bitumens in source rocks can provide useful information about hydrocarbon generation and source rock maturity. As shown in Fig. 15-8, exsudatinite occurred in stratified alginite in carboniferous oil shale. The occurrence of exsudatinite is controlled by stratified algae. As can be seen in Fig. 15-9, exsudatinite filled the fissures of Tertiary brown coal in Baise Basin, South China. All the above are typical primary authigenic bitumen. The exsudatinite in Fig. 15-10 is a good source rock of brown coal.



Fig. 15-6. Reservoir bitumen formed by destruction of paleo-oil pool.

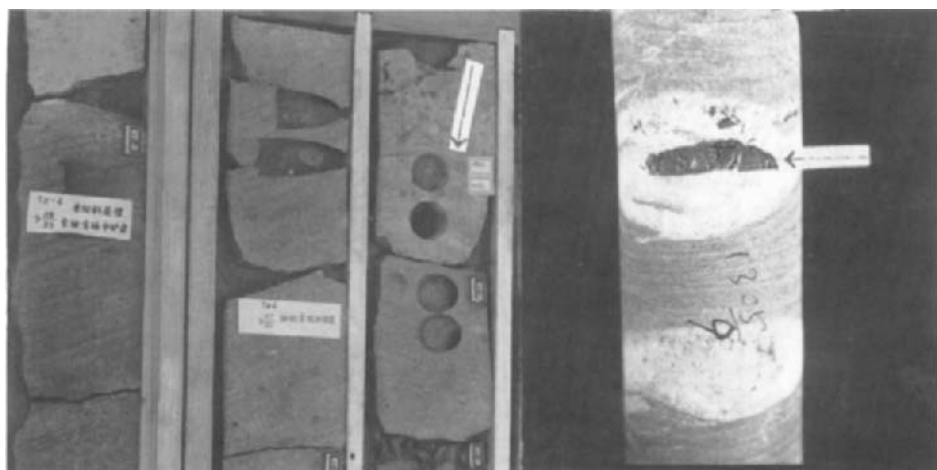


Fig. 15-7. Redeposited bitumen in drill sandstone core.

When assessing source rock maturity by bitumen reflectance, autochthonous, heterochthonous and redeposited bitumens can be distinguished from each other. The following characteristics can be used to differentiate between them.



Fig. 15-8. Microscopic photo of primary authigenic bitumen in stratified alginite.

(a) Heterochthonous bitumen is rarely found in shale (source rock). Redeposited bitumen, however, can occasionally be found in shale. Heterochthonous bitumen is usually controlled by stratification and sometimes has a higher reflectance than the host rock and oxidized ring.

(b) Redeposited bitumen occurs rarely in carbonate source rocks. Primary autochthonous and heterochthonous bitumens are found predominantly in carbonate rocks. Heterochthonous bitumen differs from autochthonous bitumen in reflectance and has many secondary migration features, such as spherical, spiral, concentrically banded and suspending structures, etc., migrating in a hydrous medium.

(2) *Bitumen in reservoir rocks.* Reservoir bitumen is the product of oil migration or is the residue of oil pool destruction. Yellow fluorescent bitumen fills the sandstone fissures with a blurred edge in Fig. 15-10. It can be concluded, therefore, that the oil probably migrated as oil phase. Bitumen reflectance is the most direct way to establish the oil migration history in a reservoir bed. Bitumens that have two or more groups of reflectance values usually indicate multistage oil migration. A detailed example, which will be discussed later, can be found in the Silurian bituminous sandstone in the Tarim Basin, China.

Bitumen in the carbonate rocks can be either (1) migrated heterochthonous bitumen or (2) primary autochthonous bitumen (pre-oil or post-oil bitumen). Inasmuch as bitumens in carbonate rocks have a rather complicated occurrence and origin, a detailed examination will be presented later in the chapter.



Fig. 15-9. Microscopic photo of primary authigenic bitumen in Tertiary brown coal.

#### BIOLOGICAL MARKERS IN BITUMENS

##### *Methods of analyzing biomarkers in bitumens*

An increase in thermal maturity will increase the condensation of the molecular structure of bitumens. The formation of bitumens always involves the loss of light components and weathering and biodegradation of liquid oil. These processes will cause a decrease in the soluble hydrocarbon extract from bitumen as well as a decrease in the percentage of the alkane fraction of the soluble extract. At normal conditions, the alkane percentage is less than 30% and is 20%–10% in most cases. In addition, biodegradation will decompose major biomarkers. This will cause difficulties in analyzing biomarkers in bitumens. Despite these difficulties, a sensitive method of gas chromatography–mass spectrometry (GC–MS) is used to detect biological markers in a microhydrogen sample. The procedure begins with Soxhlet's extraction of bitumen by chloroform or benzene and methanol (9:1) for 72 h. After asphaltene is deposited by petroleum ether, silica gel/aluminum oxide column chromatography or high-pressure liquid chromatography

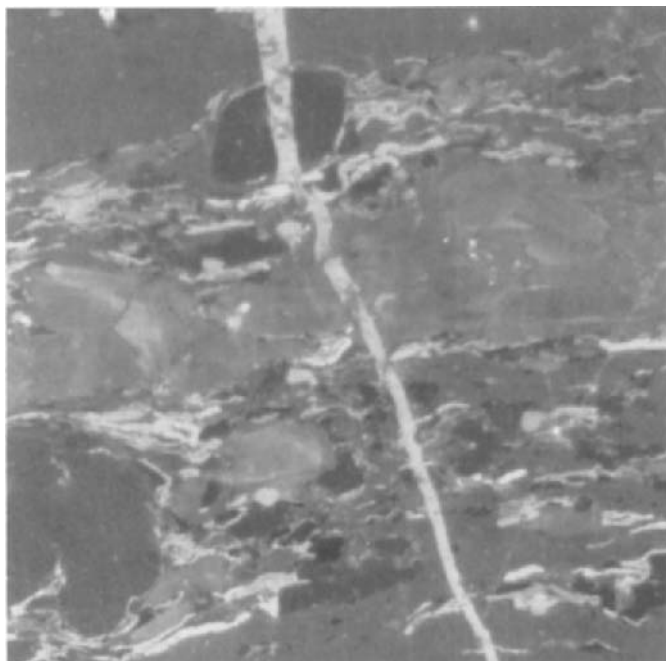


Fig. 15-10. Microscopic photo of reservoir bitumen in Triassic sandstone.

(HPLC) is used to separate the extract into three fractions, i.e., saturated, aromatic, and NSO compounds. The saturated and aromatic fractions are then sent for GC–MS analysis.

Fig. 15-11 is a schematic diagram of typical GC–MS system. This system is composed of three parts: a gas chromatograph, a mass spectrometer and a computer terminal. Fractions are separated using GC, with individual compounds injected into an ion source of a mass spectrometer by transfer line, and ionized by electric impact or chemical ionization. Compound fragments are further separated according to their mass-to-charge ratio in a mass analyzer (quadrupole rods or magnets), and detected by electron multiplier. The electric signals of fragments are amplified and are obtained using a computer. Computer systems process all the obtained fragment ion signals to reconstruct mass chromatograms of various ions and mass spectra of each individual compound. The relative abundance and structure of biomarker compounds in a sample, therefore, can be obtained by one GC–MS test.

GC–MS can operate in two modes, full scan or selected ion monitoring (SIM). In the full-scan mode, each fragment signal of every chromatographic compound is recorded. Although the SIM mode has a remarkably higher sensitivity than the full-scan mode, the latter can identify every biomarker structure. In the past twenty years, a uniform ionization condition (70 eV) has been widely used for analyzing biomarkers of sedimentary organic matter. Thus, the elution of biomarkers out of the gas chromatographic column and the distribution of biomarkers are known for many types

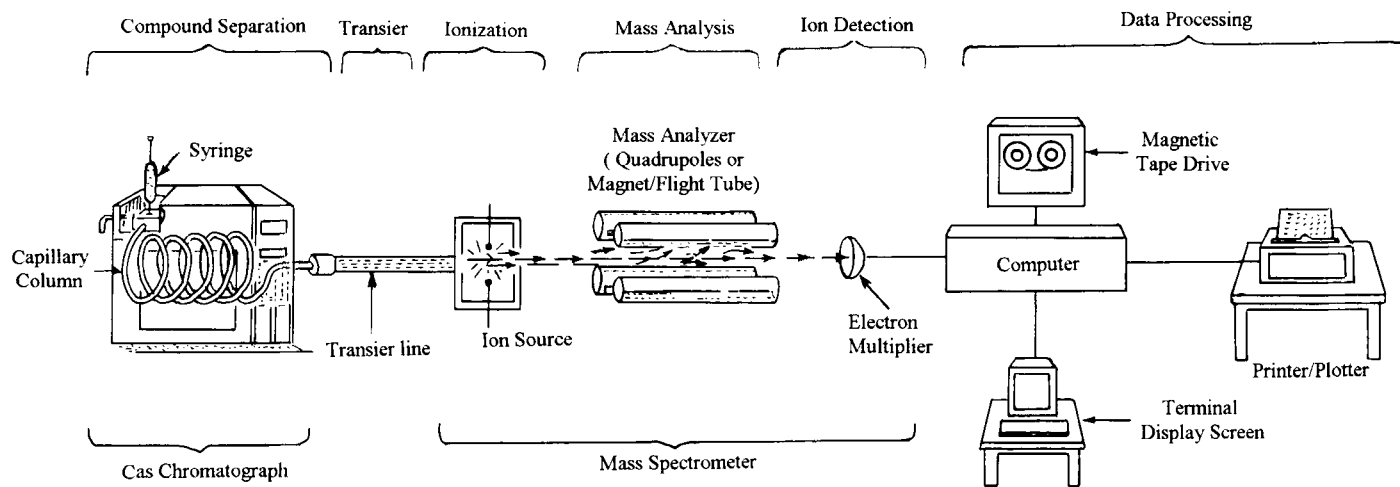


Fig. 15-11. Schematic diagram of a typical GC-MS system (after Peters and Moldovan [19]).

of sedimentary organic matter. In many cases, only several families of biomarkers need to be detected; the SIM mode is always operated for better detection sensitivity.

In many primary immature or low-maturity bitumens and heavily degraded bitumens, considerable amounts of  $\beta\alpha(R)$  configuration steranes,  $\beta\beta(R)$  and  $\beta\alpha(R)$  configuration penta-cyclic terpanes, unsaturated sterenes, hopenes, etc. exist; therefore, the biomarker composition is rather complicated. Inasmuch as this is the case, some steranes and terpanes may co-elute from the GC column. A more advanced GC-MS-MS technique, however, can solve the problem of co-elution completely. GC-MS-MS includes linked and unlinked, double focusing mass spectrometry or in tandem (e.g., triple sector quadrupole), mass spectrometry. This allows a specific parent-to-daughter relationship to be determined with little interference from other reactions and their related ions. The analytical specificity of the GC-MS-MS method will not only eliminate most of the interference created by co-eluting GC peaks, but will also determine the structures and relative amounts of co-eluting compounds. The MID-GC-MS mode does not require a large quantity of sample. It can use samples even as small as 0.1  $\mu\text{g}$  for analysis. The GC-MS-MS instrument may boost the signal-to-noise ratio to better magnitude levels than those obtained from using the conventional GC-MS SIM mode. The above analytical techniques are more than sufficient for the detection of biomarkers in bitumens.

Heavy biodegradation may cause difficulties when analyzing biomarkers in bitumens. In alkane fractions, the resistance of different compounds to biodegradation are in the following increasing order: *n*-alkane < isoprenoid hydrocarbon < regular steranes < hopanes < diasteranes < tricyclic terpanes < triaromatic steranes < norhopanes <  $\gamma$ -cerane [15,16]. Volkman [17] proposed a criterion for oil degradation, which can also be applied to bitumen, after systematically analyzing saturated and aromatic fractions of biodegraded oils in the Barrow Basin, Australia (see Table 15-9).

In many residual bitumens of paleo-oil pools, which are destroyed and moved to the ground surface by tectonic movement, heavy degradation destroys most of the biomarkers in alkane fractions. Heavy degradation, therefore, causes a problem because sufficient amounts of biomarkers are not present in order to study the origin of the

TABLE 15-9

Characteristic compounds showing the degradation of crude oil and nature bitumen [16]

Rank	Chemical composition	Extent of biodegradation
1	abundant <i>n</i> -alkanes	not biodegraded
2	light hydrocarbons removed	weakly degraded
3	90% <i>n</i> -alkanes removed	medium
4	alkyl cyclohexanes and alkyl benzenes removed	medium
5	isoprenoids and naphthalenes removed	medium
6	C <sub>14</sub> -C <sub>16</sub> bicyclicterpanes removed	strong
7	over 50% of 20R- $\alpha\alpha\alpha$ steranes removed	very strong
8	distribution of steranes and triaromatic steranes changed, abundant dimethyl hopanes	severe
9	no steranes and dimethyl hopanes dominant	extremely severe



bitumen and its oil–source correlation. It is essential that the pyrolysis technique is adopted in order to release biomarkers, which are chemically bonded in asphaltene macromolecules. The maximum pyrolytic yield can be achieved at 350°C in kerogen thermal simulation experiments. The pyrolytic temperature of bitumen, therefore, normally ranges from 350°C to 300°C (matched to the oil generation threshold at the real sediment section). Another technique that can be used is to connect pyrolysis–gas chromatography and mass spectrometer, forming the PY–GC–MS system. In the last decade, flash PY–GC–MS has been widely used in petroleum geochemistry. Flash pyrolysis is achieved by quickly heating the sample to over 600°C. Currently, the latest technique involves the microsample to be treated with magnetic reversion in a strong magnetic field. During the short time of twinkling reversion, the microsample loses its magnetism and its temperature rapidly rises to a high curie point temperature (ca. 600–700°C). The microsample can be completely pyrolyzed using this technique. Although the mass chromatograms obtained from flash PY–GC–MS normally have an increasing chromatographic line due to mutual interference of saturated and aromatic hydrocarbons, they are sufficient for conventional visual correlation and parameter calculation.

#### *Application of biomarkers in studying the origin and thermal maturity of bitumen*

The analysis of biomarkers in bitumen can be used to study the oil (bitumen)–source correlation and determine the maturity. Many publications have reported successful case studies that used the biomarker approach for bitumen–source correlations. For example, there is the biomarker research of heavy oil, bitumen and oil sand in Alberta, West Canada.

Alberta, Canada, has a length of 1200 km from north to south and a width of 600 km from east to west. From the northwest to the southeast, there is an enormous amount of oil sand bitumen and heavy oil in Lower Cretaceous sandstone and underlying Devonian limestone within an area of 600 km<sup>2</sup>. The calculated reserves are about 268 billion cubic meters. Oil sand bitumens are buried at shallow depths of 100–200 m or exposed at the surface. At deeper depths, 500–700 m, heavy oil may be produced from sandstone. Brooks et al. [18] studied 43 typical samples for the characterization of biomarker distribution. It was clearly shown that all oil sand bitumens and heavy oils were degraded above the medium level. The alkane fraction in extracts is ca. 20%, but may reach a maximum of 28.8%. The aromatic fraction content is usually higher than 30%, with a maximum of 45.7%. Resin and asphaltene fractions are higher than 40% and have a maximum of 66.5%. *n*-Alkanes are completely degraded, whereas isoprenoid alkanes are detected only in some heavy oils. Cyclic hydrocarbon compounds are dominant within saturated fractions. Biomarker distributions in Cretaceous sand oil and bitumens are quite similar. Fig. 15-12 illustrates mass chromatograms of steranes and terpanes in oil sand bitumen and heavy oils from four representative deposits. Terpane distribution in four samples is almost identical; they have complete C<sub>19</sub>–C<sub>29</sub> triterpanes (TT) with C<sub>23</sub> TT as the highest peak, complete homologues of homo-hopanes and the highest carbon number up to C<sub>35</sub> and an abundant amount of  $\gamma$ -cerane. Steranes in the four samples are also similarly distributed: they have significant contents of C<sub>21</sub> pregnane, C<sub>22</sub> homopregnane, and diasteranes. In less degraded heavy oil and bitumen

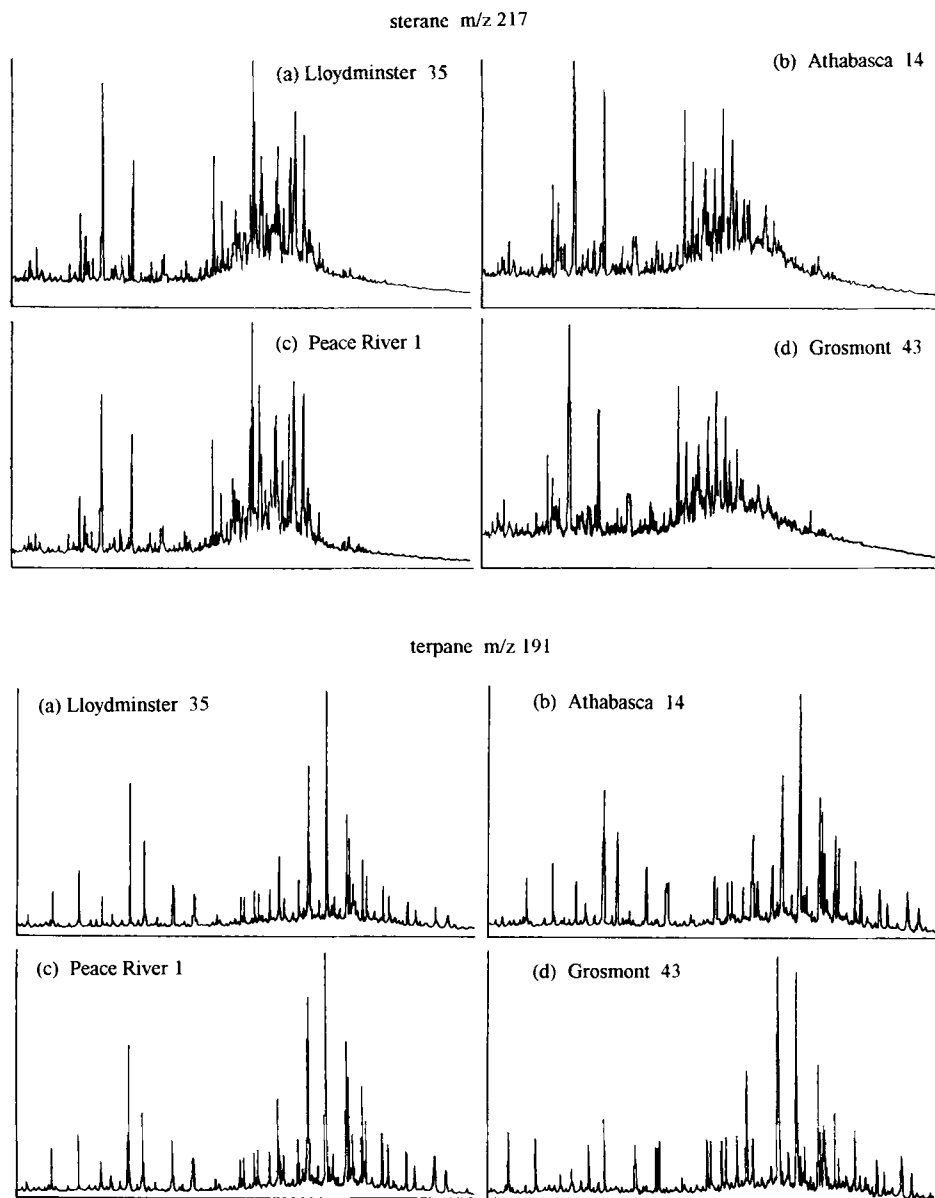


Fig. 15-12.  $M/z$  217 and  $m/z$  191 fragmentograms of four Western Canada heavy oil and oil sand bitumens (after Brooks et al. [18]).

samples (Nos. 35 and 1)  $C_{27}$  and  $C_{29}$  steranes can be detected. Fig. 15-13 illustrates a triangular diagram of  $C_{27}$ – $C_{29}$  diasteranes for all 43 samples. All sample points are closely distributed within a small area, with a 10% maximum variation between sample

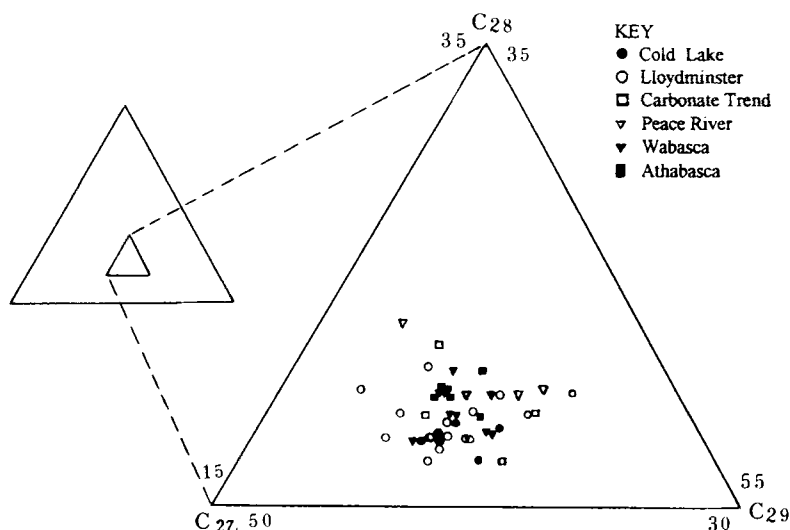


Fig. 15-13. Triangular diagram of  $C_{27}$ – $C_{29}$  diasteranes in Western Canada, oil sand bitumen and heavy oil (after Brooks et al. [18]).

points, which illustrates a common origin. Taking the geological occurrences of heavy oil and oil sand bitumen into account, it is assumed that each one of these oil sand bitumens and heavy oil originated from a common source rock mainly containing type II kerogen. These types of source rock are deposited in a marine sedimentary environment with marine biomass as a principal organic input and terrigenous organic matter as a minor input.

Biomarker maturities of the 43 samples, excluding degradation interference, have the same or similar maturity level values. Regular steranes were detected in 33 samples; their  $\alpha\alpha\alpha$   $C_{29}$   $S/(S + R)$  ratios are within the range 0.4–0.54.  $C_{30}$  hopanes  $\alpha\beta/(\alpha\beta + \beta\alpha)$  values range from 0.71 to 0.93. These values correspond to the threshold peak of oil generation. In conclusion, heavy oils and oil sand bitumens cannot come from source rocks of different geologic age.

#### CASE STUDIES

##### *High-sulfur immature bitumen in the Zhujiashuang Sulfur Deposit, Shandong Province, East China*

The Zhujiashuang Deposit is the largest natural sulfur deposit in China. Orebodies formed in the second member of the Guanzhuang Formation, Lower Tertiary Series, which was deposited in a saline lacustrine environment (see Table 15-10). There are two major ore types: marl ore (82%) and gypsum-halite ore (15%). Natural sulfur crystals are fine-grained microcrystalline (0.1–0.01 mm) or cryptocrystalline. Sulfur concentrations in ore usually range from 6% to 12%, with a maximum of 30%. In

TABLE 15-10

Core profile of drill No. SK1<sup>a</sup>: basic lithological characteristics and rock types

Top bed	Shaley marl, obvious oil stain in fractures of lower part rocks.
Ore bed	Shaley marl; well developed laminar structure; fracture and cave developed along the cross-lamination orientation; most fractures and caves were filled with sulfur, gypsum, oil and asphalt.
Bottom bed	Shaley marl and sulfur-bearing shaley marl, well developed lamination.

<sup>a</sup> Liu Yutang (1982) natural sulfur and crude, unpublished material.

TABLE 15-11

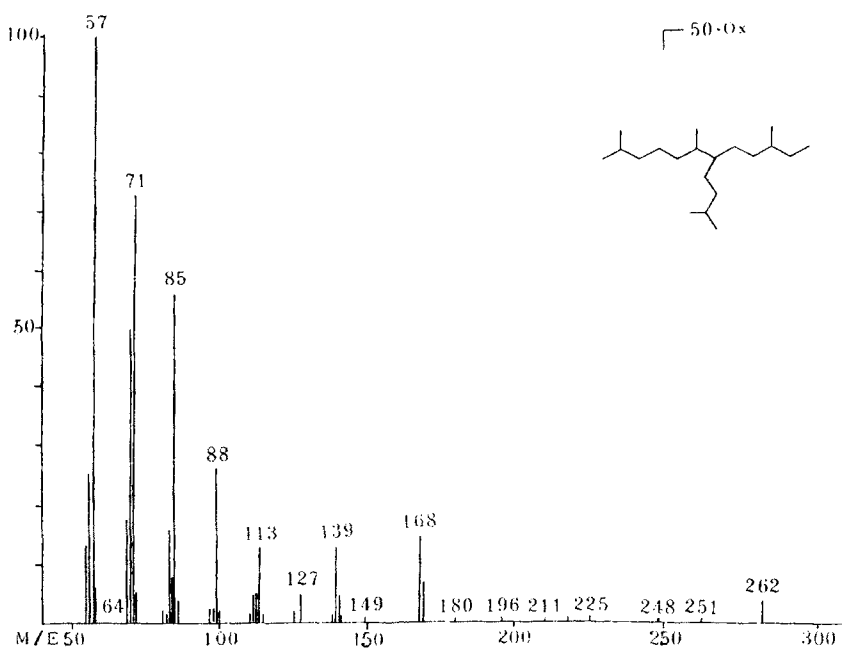
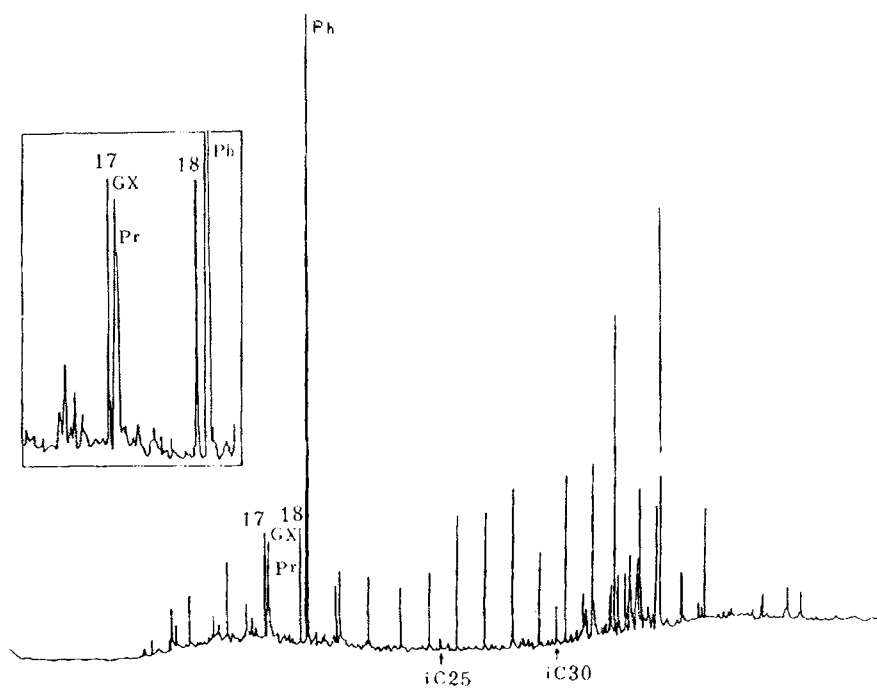
Organic molecular parameters from sulfur deposit and hypersaline lacustrine oils

Parameters	Bitumen	J <sub>18</sub> oil	Rozel point oil
Producing bed	Eg	Eq3	J
Depth (m)	340–380	610.2–658.5	Seep
Sulfur (%)	56.2	12.9	12.9
Carbon range of <i>n</i> -alkane	C <sub>14</sub> –C <sub>35</sub>	C <sub>13</sub> –C <sub>35</sub>	C <sub>14</sub> –C <sub>27</sub>
Peak <i>n</i> -alkane	C <sub>17</sub> < C <sub>29</sub>	C <sub>18</sub> < C <sub>26</sub>	
CPI	1.87	0.54	
Highest peak in alkanes	Ph	Ph	Ph
Pr/Ph		0.12	
(Gx + Pr)/Ph	0.39		0.39
( <i>m/z</i> 191)/RIC	0.036	0.033	0.026
Tricyclic terpanes	C <sub>23</sub> > C <sub>24</sub>	C <sub>21</sub> > C <sub>23</sub> > C <sub>24</sub>	C <sub>23</sub> > C <sub>24</sub> > C <sub>21</sub>
T <sub>s</sub> /T <sub>m</sub>	0.13	0.15	0–51
γ-Cerane Index	0.18	0.85	0.53
C <sub>30</sub> βα/(αβ + βα)	0.070	0.100	0.086
C <sub>32</sub> 22 S/(S + R)	0.56	0.62	0.68
Homohopanes	C <sub>35</sub> > C <sub>32</sub> > C <sub>34</sub> > C <sub>33</sub>	C <sub>35</sub> > C <sub>32</sub> > C <sub>34</sub> > C <sub>33</sub>	C <sub>35</sub> > C <sub>32</sub> > C <sub>34</sub> > C <sub>33</sub>
( <i>m/z</i> 217)/RIC	0.023	0.027	0.026
C <sub>29</sub> αα 20 S/(S + R)	0.25	0.27	0.49
C <sub>29</sub> ββ/(ββ + αα)	0.34	0.20	0.32
C <sub>27</sub> /ΣC <sub>27–29</sub> , %	34.5	48.5	31.2
C <sub>27</sub> /ΣC <sub>27–29</sub> , %	21.9	20.2	28.7
C <sub>27</sub> /ΣC <sub>27–29</sub> , %	43.6	31.3	40.1

Eg = Eogene, Eq3 = the third section of the Eogene formation, Pr = pristane, Gx = 2,6,10-trimethyl-7-(3-methylbutyl)-dodecane.

sulfur ores, significant quantities of bitumen, carbonates (calcite and dolomite), sulfates (gypsum and celestite), and mirabilite occur together.

According to biomarker studies of the bitumen, it was formed in the early diagenetic stage. This bitumen was pretreated with a chloroform extraction and column chromatographic separation. The alkane fraction was analyzed by GC and GC–MS. Fig. 15-14 shows that this bitumen has a rather low maturity in the *n*C<sub>23</sub>–*n*C<sub>33</sub> range. The content of isoprenoid hydrocarbons is extremely high; Ph has the highest peak in the alkane fraction. Also, a characteristic isoprenoid compound,



2,6,10-trimethyl-7-(3-methylbutyl)-dodecane (Gx), which has been detected only in saline lacustrine sediments and oils, was detected in this bitumen. Bitumen from sulfur deposits is also characterized by a high content of  $\gamma$ -cerane,  $C_{35}$  homophane (see Fig. 15-15),  $C_{35}$  thiophane, and  $iC_{25}$  and  $iC_{30}$  isoprenoid alkanes. All of the above biomarker distributions illustrate a saline lacustrine depositional environment and significant paleobacterial input to the sulfur ore zone. Table 15-11, alkane and biomarker distributions in typical crude oil in hypersaline facies (U.S.) are listed for comparison.

Three representative samples have similar biomarker distribution features of identical or similar origin. In bitumen from sulfur deposits, the highest Ph peak, a higher CPI value, and lower sterane and terpane maturity parameters (sterane  $\alpha\alpha\alpha C_{29} 20S/(S + R) = 0.25$ ; terpane  $C_{30} \beta\alpha/(\alpha\beta + \beta\alpha) = 0.07$ ;  $C_{32} 22S/(S + R) = 0.56$ ) indicate that the bitumen maturity is still low, probably at an early stage of 'oil window'.

Biomarker distribution of this bitumen firmly suggests that natural sulfur was formed at an immature or low-maturity early diagenetic stage. Under extreme reducing conditions of a hypersaline depositional environment, sulfates (gypsum etc.) were biochemically reduced to sulfur (elemental sulfur and  $H_2S$ ) by sulfate-reducing bacteria. Part of the reduced sulfur (probably  $H_2S$ ) was incorporated into the sedimentary lipid molecules and kerogen skeleton via active functional bonds. As natural sulfur was deposited in the early diagenetic stage, sulfur-rich kerogen and macro-lipid molecules were degraded into immature or low-maturity crude oil and bitumen, because of the weak chemical stability of the S–C bond.

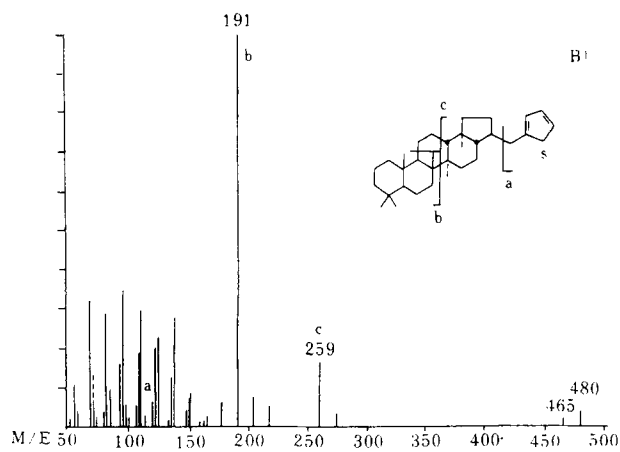
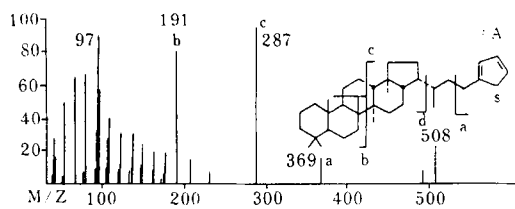
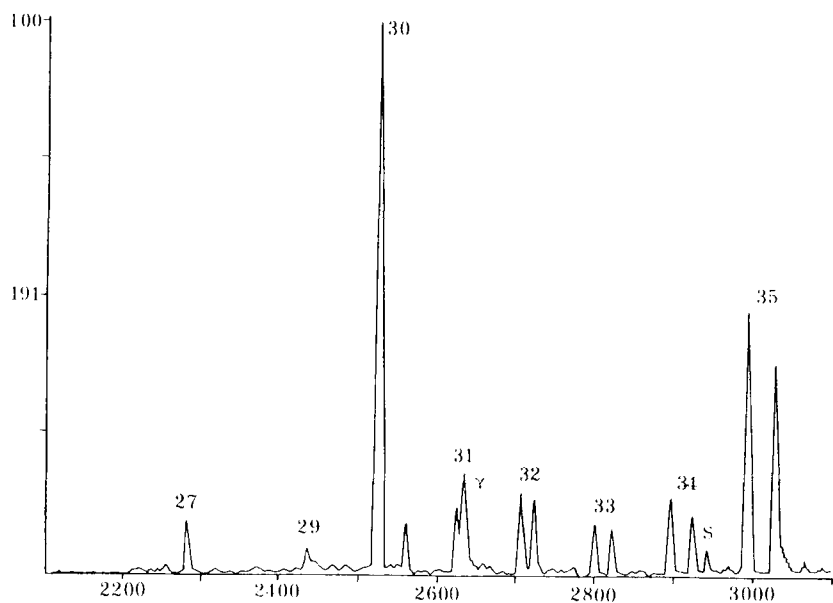
#### *Silurian bituminous sandstone in the Tarim Basin, northwestern China*

During exploration, Silurian bituminous sandstones have been drilled in many of the wells of the North Tarim Uplift and Central Tarim Uplift. Bituminous sandstones are usually several tens of meters to several hundred meters thick. In the Halahatang District of the southwestern North Tarim Uplift, an extremely thick bituminous sandstone (288.5 m in thickness) was drilled in the Middle to Upper Silurian formations (depth interval of 6050–6338.5 m in well Ha-1). The Silurian sandstone bitumen was studied using biomarker analyses, microscopic observations and thermal simulation experiments. The results are summarized as follows.

The bitumen content of the bituminous sandstones varies vertically and bitumen-rich and bitumen-poor sublayers alternate. Pure bitumen is the major occurrence in bitumen-rich layers (see Fig. 15-16), whereas in bitumen-poor layers the bitumen is disseminated in the clay matrix (see Fig. 15-17). Compared to the bitumen from the Silurian sandstone outcrop (Karpin Thrust, northwestern Tarim Basin), subsurface sandstone bitumens in the northern and central Uplifts have a lower consolidation and a higher chloroform solubility. Chloroform solubility of the bitumen from the Ha-1 well can reach 75%. It is composed of 40.2% saturates, 18.6% aromatics, and 41.2% resin and asphaltene. *n*-Alkanes are still the major hydrocarbons and  $C_{20}$  *n*-alkanes have a dominant position.

---

Fig. 15-14. GC traces and mass spectra of GX compound in bitumen of the Zhujiashuang Sulphur Deposit, Shandong Province (after Fu and Sheng [20]).



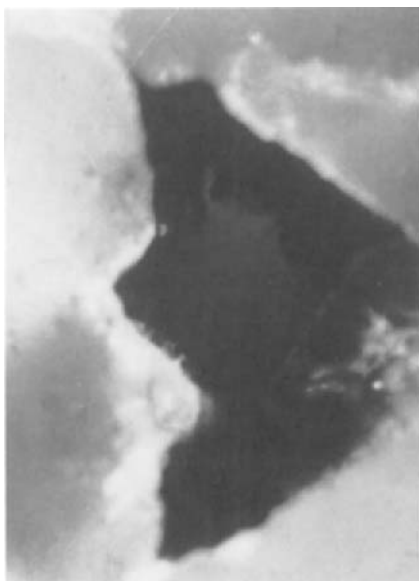


Fig. 15-16. Microscopic photo of pure bitumen in Silurian sandstone reservoir of Ha-1 well, Tarim Basin, northwestern China.

As shown in Fig. 15-18, terpane and sterane distributions of three typical sandstone bitumens (well Ha-1, well YN-1 in the north slope of the central Tarim Uplift, YGC outcrop, Karping Thrust) are presented. Terpane and sterane distributions of the three samples are quite similar. Total tricyclic terpane is represented by the highest peak in the  $m/z$  191 mass chromatograms. Among steranes,  $C_{21}$  and  $C_{22}$  pregnanes are represented by major peaks in the  $m/z$  217 mass chromatograms. Biomarker correlation indicates that the Silurian sandstone bitumen came from a common source rock. As shown in Fig. 15-19, sterane and terpane distributions of typical Paleozoic source rocks and sandstone bitumen show that the Silurian sandstone bitumen has a close correlation to Ordovician dark limestone. Carbon isotopic values of Silurian sandstone bitumen range from  $-32.32\%$  to  $-34.35\%$ , in close agreement with the  $\delta^{13}C$  values of Ordovician–Upper Cambrian source rocks. This indicates that the Silurian sandstone bitumen originates from oil of the Ordovician source rocks.

Except for the YGC outcrop bitumen, microscopic observations show that subsurface bitumens have relatively low reflectances exhibiting hydrocarbon migration phenomena (see Table 15-12). In bituminous sandstone of the Ha-1 well, yellow to yellow-green fluorescent oil fills the microfractures within and around the quartz crystal grains (see Figs. 15-20 and 15-21). Most bitumens in sandstones have a reflectance lower than 0.7%, but minor amounts of sandstone bitumen have a reflectance of up to 1.58%.

Fig. 15-15.  $M/z$  191 mass chromatogram of alkane fraction and mass spectra of thiohopane in the bitumen of the Zhujiashuang Sulphur Deposit (after Fu and Sheng [20]).



TABLE 15-12

Properties of bitumen in sandstone reservoir and carbonate rock in the Tarim Basin, northwestern China

Item	Well Ha-1	Central Tarim	Well YN1	YGC outcrop
Occurrence	at depths of 5718–6532, multilayers, total thickness of ca. 320 m	3734 m in well TZ-4 and 4871 m in well TZ-10	drilled at depth of 5964 m	surface outcrop
Bitumen filling	discontinuously filled as bands, enriched in some subbeds, 0–4% of loose sandstone, higher porosity	filling saturation varies sharply, discontinuously filled as bands and beds, loose sandstone and higher porosity	lower filling saturation, dispersed grains	very low filling saturation, low porosity and high hardness
Bitumen reflectance ( $R_b$ ) and corresponding vitrinite reflectance ( $R_v$ )	$R_b$ 0.34–0.74%; $R_v$ 0.57–0.84%	$R_b$ 0.04–0.18%; $R_v$ 0.37–0.47%		$R_b$ 1.27%; $R_v$ 1.19%
Organic enclosure	minor, fine	minor, fine		easily seen, medium size
Carbon isotopic ratio $\delta^{13}C$ , ‰	–32.32	–32.14	–31.46	–33.7

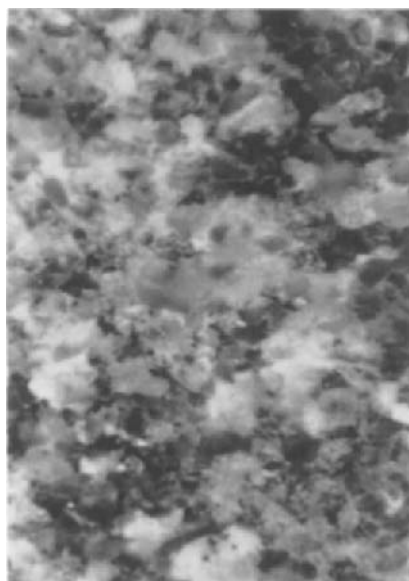


Fig. 15-17. Microscopic photo of authigenic bitumen disseminated within clay matrix in bitumen-poor Silurian sandstone of Ha-1 well, Tarim Basin, northwestern China.

The values of the higher reflectance group are within the primary range of bitumen reflectance (1.4–1.8%) in Ordovician source rocks of the North Tarim Uplift.

A thermal simulation experiment demonstrated that the subsurface Silurian sandstone bitumen has a significant hydrocarbon potential.  $S_1 + S_2$  parameter values vary between 4.82 and 8.86 mg/g; the hydrogen index value ranges from 400.85 to 508.5. A hydrogen peak occurs at a temperature range of 400–450°C. This signals the release of hydrocarbons that were formed by the thermal cracking of sandstone bitumen. The content of pyrolytic hydrocarbons can reach 40% of the total bitumen weight.

Biomarker maturity parameters of the subsurface sandstone bitumen indicate a low to medium maturity. The sterane  $\alpha\alpha\alpha$   $C_{29}$   $20S/(S + R)$  ratio has a narrow range of 0.38–0.42. The  $C_{29}$   $(S + R)$   $\beta\beta/(\beta\beta + \alpha\alpha)$  ratio is 0.60–0.70. The terpane  $T_s/T_m$  ratio ranges from 0.62 to 0.86, whereas the hopane  $C_{32}$   $S/(S + R)$  ranges from 0.59 to 0.66.

The origin of Silurian bitumen can be summarized as follows. Marine crude oil from Ordovician source rocks was generated on a large scale during the Middle Devonian and migrated into traps of Silurian sandstone. During Late Devonian time, the Caledonian Orogeny caused an uplift of a large area and erosion, leading to the distribution of paleo-oil pools in Silurian sandstone. This resulted in the formation of bitumen. In most parts of the Northern and Central Tarim Uplift, however, Silurian sandstone paleo-oil pools were not completely exposed at the surface and did not experience severe oxidation while Carboniferous sediments were deposited (see Fig. 15-22). During that time, the sandstone bitumen was a typical tectonic alteration product of soft bitumen or heavy oil, with a lower reflectance and biomarker maturity parameter. After the Cretaceous, the entire Tarim Basin began to subside quickly and the unsolidified Silurian

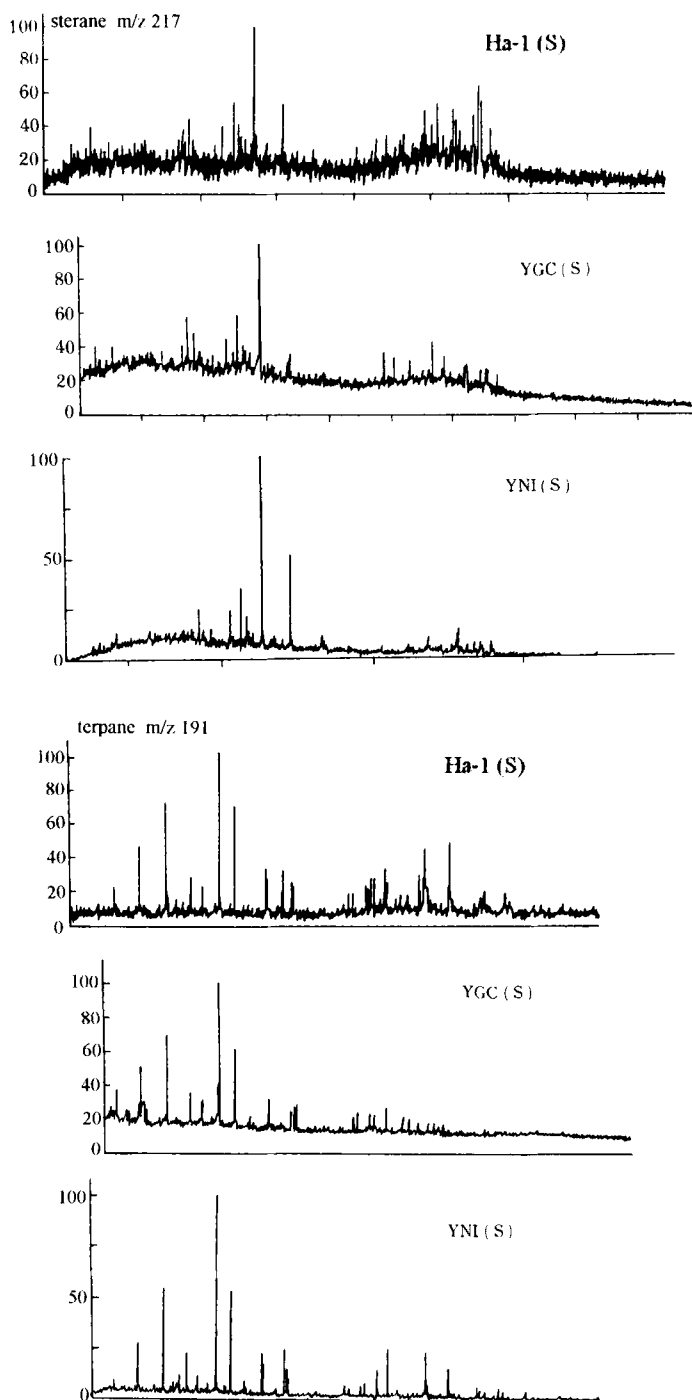


Fig. 15-18.  $M/z$  191 mass chromatogram of bitumen from Silurian sandstone in the Tarim Basin.

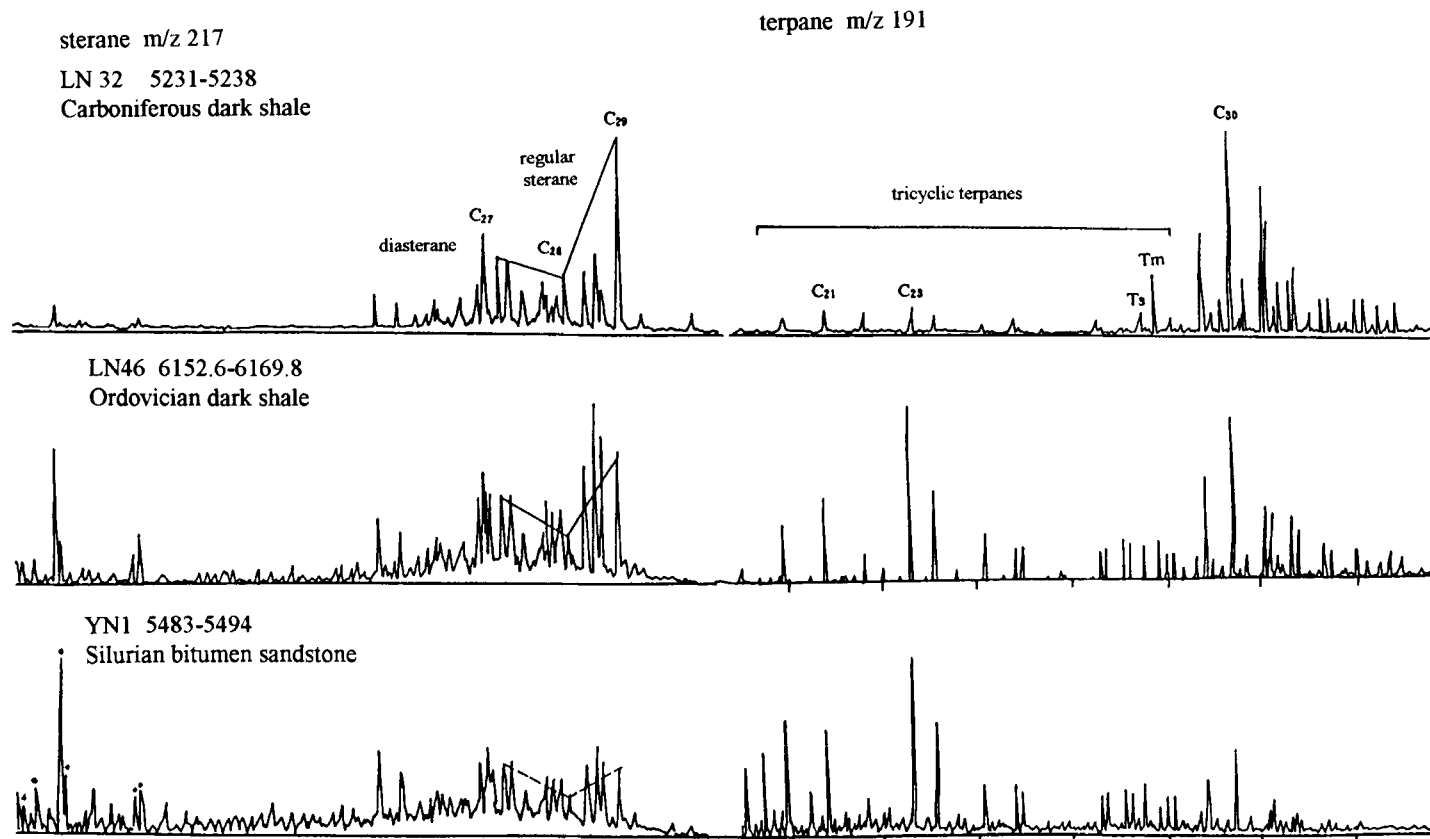


Fig. 15-19.  $M/z$  217 and  $m/z$  191 mass chromatograms of typical Paleozoic source rocks and sandstone bitumen in the Tarim Basin.

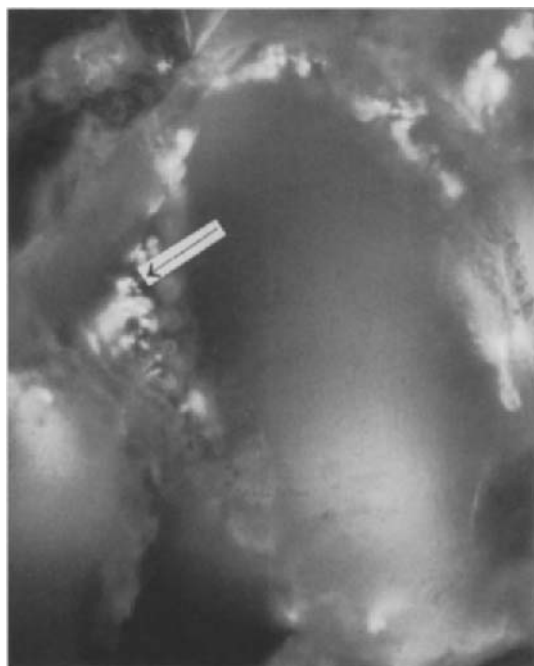


Fig. 15-20. Migrated oil (yellow to yellow-green fluorescence indicated by arrow) in Silurian sandstone of Ha-1 well, Tarim Basin, northwestern China.

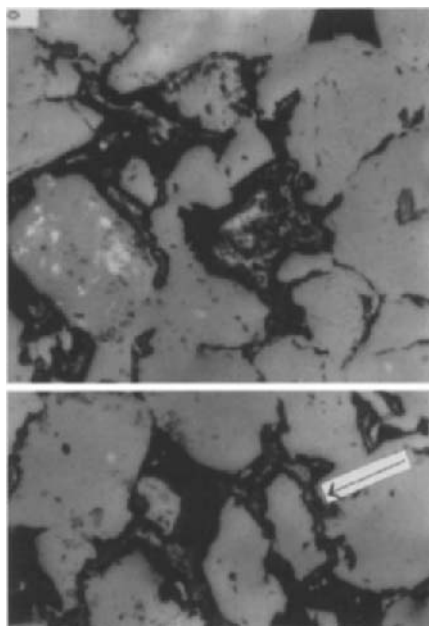


Fig. 15-21. Migrated oil (yellow to yellow-green fluorescence indicated by arrow) in Silurian sandstone of Ha-1 well, Tarim Basin, northwestern China.

sandstone bitumen was reactivated developing plastic flow and forming noticeable migration features. At the same time, a small part of the bitumen was thermally degraded in bitumen-rich layers. The bitumen residue was completely solidified and its reflectance increased considerably. Most of the sandstone bitumen, however, retained its original state with lower reflectance. This explains why sandstone bitumen in well Ha-1 has two groups of reflectance values.

*Bitumen vein deposit in Ghost City, Jungger Basin, northwestern China*

Pure bitumen veins rarely occur. The bitumen veins in Cretaceous sandstone in Ghost City, North Urho Town, in the northwest margin of the Jungger Basin are good examples of this type of occurrence. The bitumen veins stretch from the northeast to the southwest of the Jungger Basin, parallel to the regional overthrust belt line. They occur as vertical veins up to 1.2 m wide and 1100 m long. There are a total of seven veins and mining is currently concentrated on the largest one. According to an approximate estimation, the bitumen resource is over 100 tons.

The characteristics and origin of bitumen veins have been investigated by Parnell and Geng [21] and are summarized as follows.

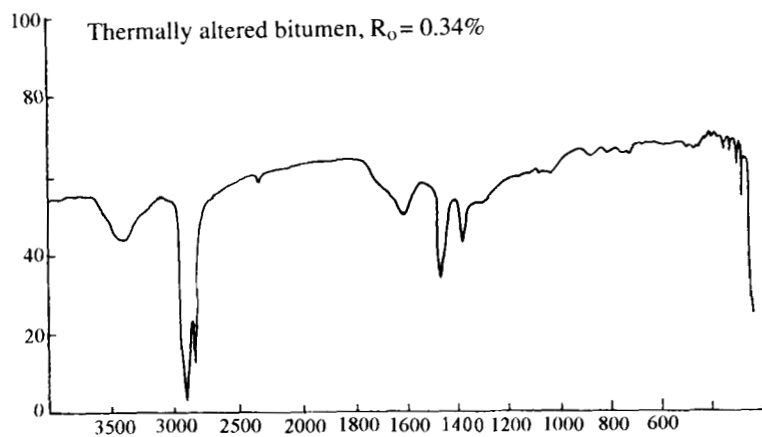
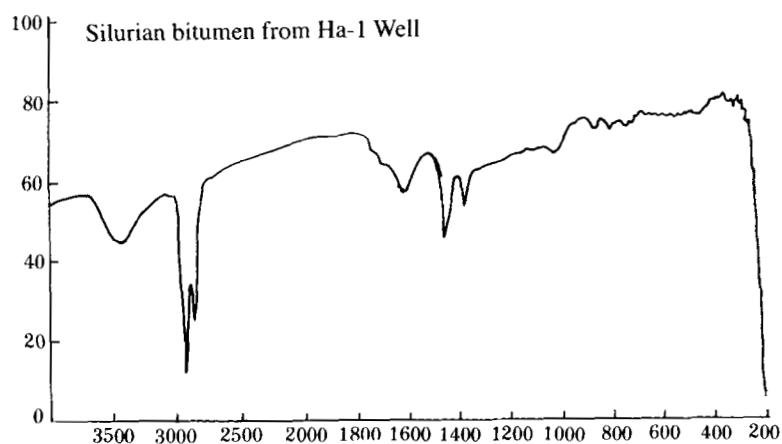
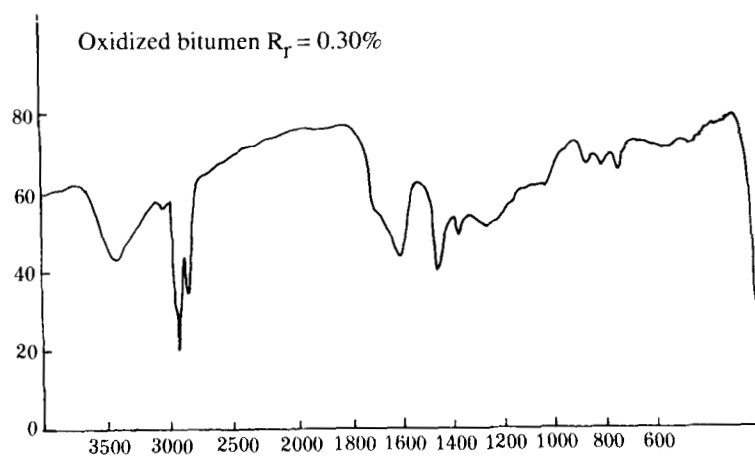
Vein bitumen has a higher H/C ratio (1.38) and a lower aromaticity (0.34). These features are rather similar to those of bitumen deposits of the Uinta Basin, U.S.A., which illustrate the thermal evolution stage of gilsonite. As shown in Fig. 15-23,  $\beta$ -carotene content is remarkably high in the saturates fraction of the bitumen vein. Although *n*-alkanes were removed by degradation, this characteristic can be compared to the source rocks of Fengchengcheng Formation of Carboniferous to Permian age and associated oils in the northwestern Jungger Basin. As shown in Table 15-13, sterane and terpane maturity parameters and  $\delta^{13}\text{C}$  values ( $-27.05$  to  $-29.30\text{‰}$ ) of bitumen and oil are very close. This suggests that bitumen veins and crude oil share a common source.

The diagenetic history of the host sandstone is summarized in Fig. 15-24. In comparison to the middle to late diagenetic stage, filling by bitumen occurred after the dissolution and recrystallization of carbonate. The burial history of the northwestern Jungger Basin demonstrates that Permian rocks were buried into the 'oil window' in the Early Jurassic, whereas the Fengchengcheng Formation (Carboniferous source rock) formed in Middle Triassic time. It can be concluded, therefore, that vein bitumen was

TABLE 15-13

Biomarker parameters and  $\delta^{13}\text{C}$  values

Sample type	Well number	Sterane $\alpha\alpha\alpha$ 20 S/(S + R)-C <sub>29</sub>	Triterpane $\alpha\beta$ 20 S/20 (S + R)-C <sub>32</sub>	$\delta^{13}\text{C}$ PDB (‰)
Bitumen		0.57	0.59	-28.14
Crude oil	Feng 3	0.51	0.58	-29.30
	Wu 135	0.49		
Source rock	Feng 6 (extracts)	0.36	0.57	
	Feng 6 (kerogen)			-27.05



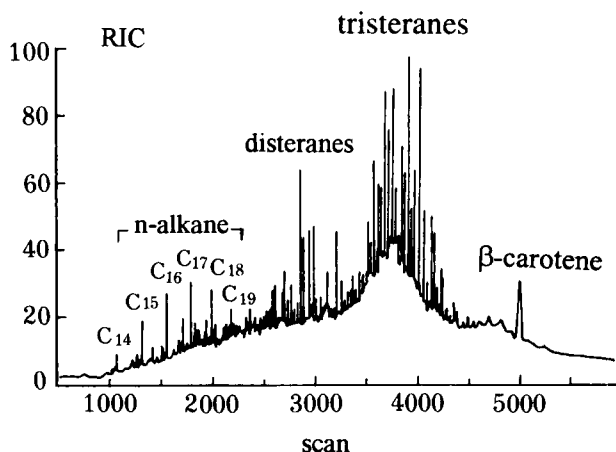


Fig. 15-23. RIC traces of bitumen from the Ghost City bitumen vein, showing high contrast of  $\beta$ -carotene (after Parnell and Geng [21]).

formed by crude oil filling the faults and fractured zone of the Cretaceous sandstone, after the deposition of Cretaceous sediments.

The above conclusion is supported by the following evidence. (a) The strike of bitumen veins (faulting zone) is parallel to the Kalamay Overthrust Belt. (b) Microfractures were completely filled by bitumen in mudrock clasts entrapped in bitumen veins. This illustrates the existence of fluid pressure when filling by crude oil occurred (see Fig. 15-25). (c) The presence of fibrous gypsum along bitumen veinlets (see Fig. 15-26) indicates that these minerals may have been deposited in an overpressured environment.

From the above evidence, it can be assumed that bitumen veins were formed by the tectonic squeezing of accumulated oil from the Permian or Triassic reservoirs into the overlying Cretaceous sandstone, with an extensive loss of lighter hydrocarbons.

#### *Bitumen in highly mature carbonate rocks, southern China*

In the Yangtze Platform of southern China (i.e., Sichan, Guzhu, Guangxi and Hunan provinces, etc.), enormous amounts of marine carbonate sediments were deposited during Sinian to Triassic time. These carbonate rocks have high to extremely high maturities due to long burial time and tectonic movements. Inasmuch as most bitumens within this type of rocks exhibit a high thermal evolution above the impsomite level, the observation of bitumen occurrence is the most effective approach for determining its origin.

Bitumens are usually formed during the evolution of organic matter in carbonate rocks. On the other hand, secondary porosity which usually formed during diagenesis

Fig. 15-22. Fourier transform infraspctra of Silurian sandstone bitumen, thermal altered bitumen and oxidized bitumen, Tarim Basin, northwestern China.



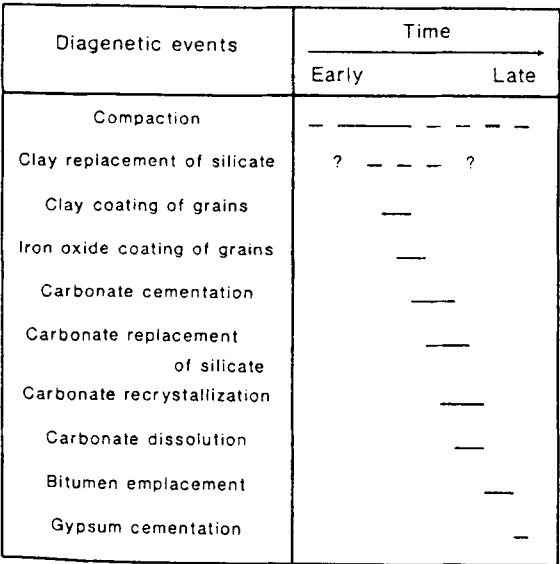


Fig. 15-24. Diagenetic history of the bitumen host sandstone.

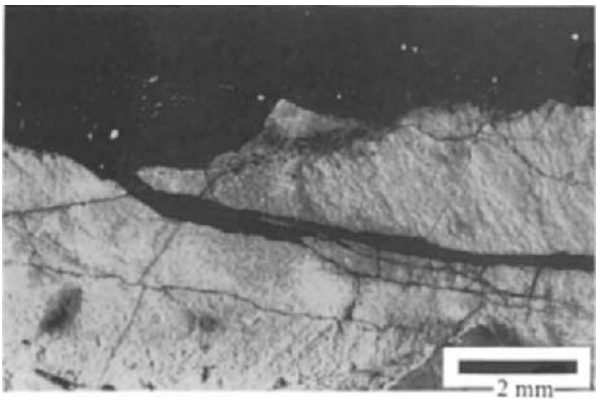


Fig. 15-25. Bitumen vein formed by crude oil filling in fractured zone of the Cretaceous sandstone, Junger Basin, northwestern China.

(i.e., dolomitization, dissolution, pressure solution, etc.), provided favorable paths for petroleum migration. Carbonate rocks not only contain primary autochthonous bitumen, but also contain migrated bitumen (reservoir bitumen). Autochthonous bitumen occurs in fossil chambers or suture lines (see Fig. 15-27). Generally, it is dispersed between recrystallized calcite or dolomite and has a blurred boundary with minerals.

Most carbonate bitumens, however, are heterochthonous reservoir bitumens. The most distinguishing feature of these bitumens is evidence of their migration and heterogeneous distribution. Reservoir bitumen can be further classified into two subtypes.

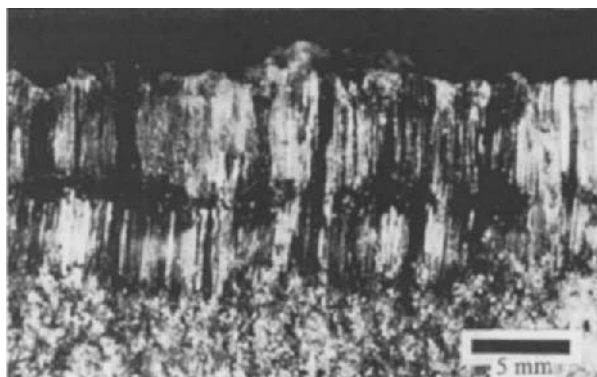


Fig. 15-26. Fibrous gypsum co-occurred along bitumen veinlets in Cretaceous sandstone, Junger Basin, northwestern China.

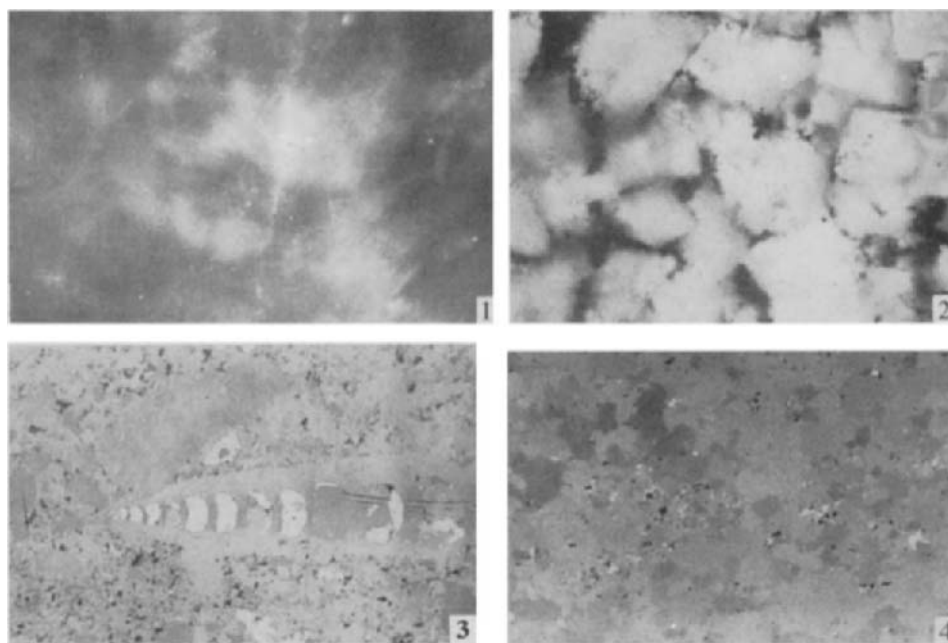


Fig. 15-27. Autochthonous bitumen of different occurrence. (1) Fluorescence ( $\times 400$ ) of dispersed autochthonous bitumen in Triassic carbonate. (2) Autochthonous bitumen between dolomite crystal (transparent light,  $\times 400$ ). (3) Autochthonous bitumen filling in fossil and mineral crystal ( $\times 200$ ). (4) Dispersed autochthonous bitumen in Permian carbonate source rock ( $\times 400$ ).

*Type A reservoir bitumen* is formed from oil, which migrates as liquid phase in the reservoir. The bitumen fills in the fractures, pores, fossil chambers, and vugs, with various xenomorphic shapes. It also has a clear boundary with the minerals (see Fig. 15-28). This type of bitumen has homogeneous properties.

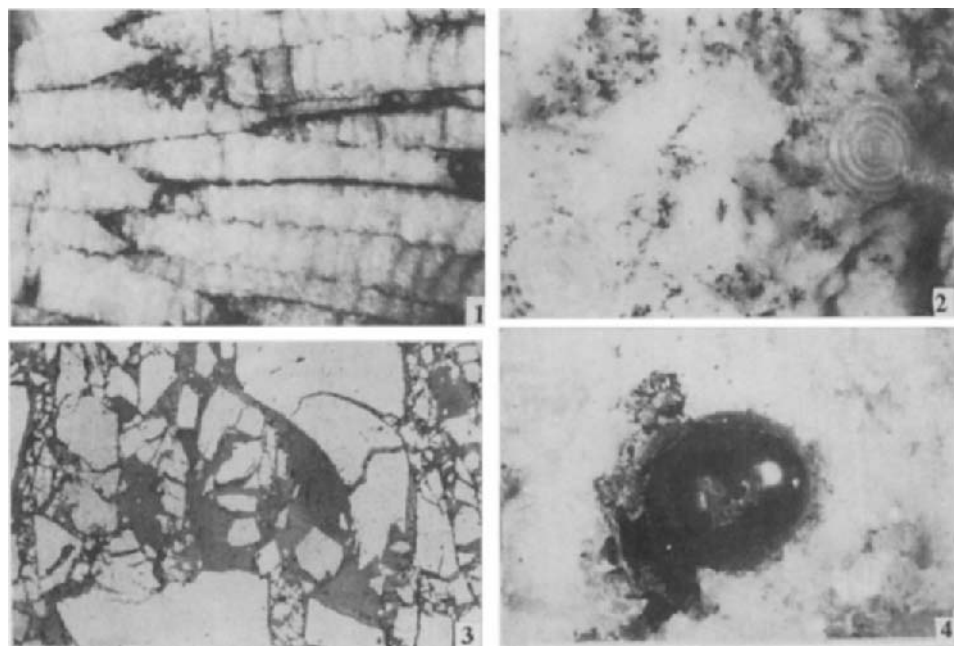


Fig. 15-28. Homogeneous reservoir bitumen (Type A). (1) Bitumen filling in coral limestone fissures ( $\times 10$ ). (2) Reservoir bitumen filling in fusulinide limestone ( $\times 80$ ). (3) Reservoir bitumen in Dachang metal ore ( $\times 160$ ). (4) Spherical reservoir bitumen in calcite vein of mercury ore ( $\times 2$ ).

*Type B reservoir bitumen* is deposited in an aqueous environment or is thermally transformed from migrated oil. Most type B reservoir bitumens have particular textures and optical features. Some typical textures of type B reservoir bitumen are presented briefly in Fig. 15-29. All of the above features reflect a higher bitumen maturity.

Reservoir bitumen can be used to determine the thermal maturity of a petroleum and the phase and timing sequence of petroleum migration. Reflectance of reservoir bitumens in limestone vugs or bitumen veinlets is an important indicator of the maturity level. In

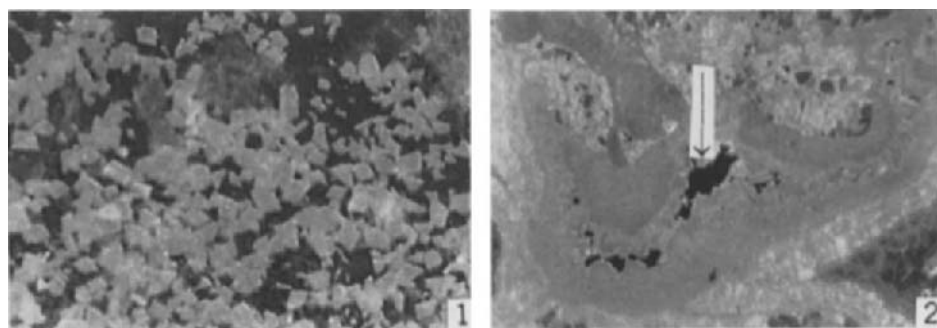


Fig. 15-29. Type B reservoir bitumen. (1) Disseminated reservoir bitumen in sandstone. (2) Reservoir bitumen in carbonate.

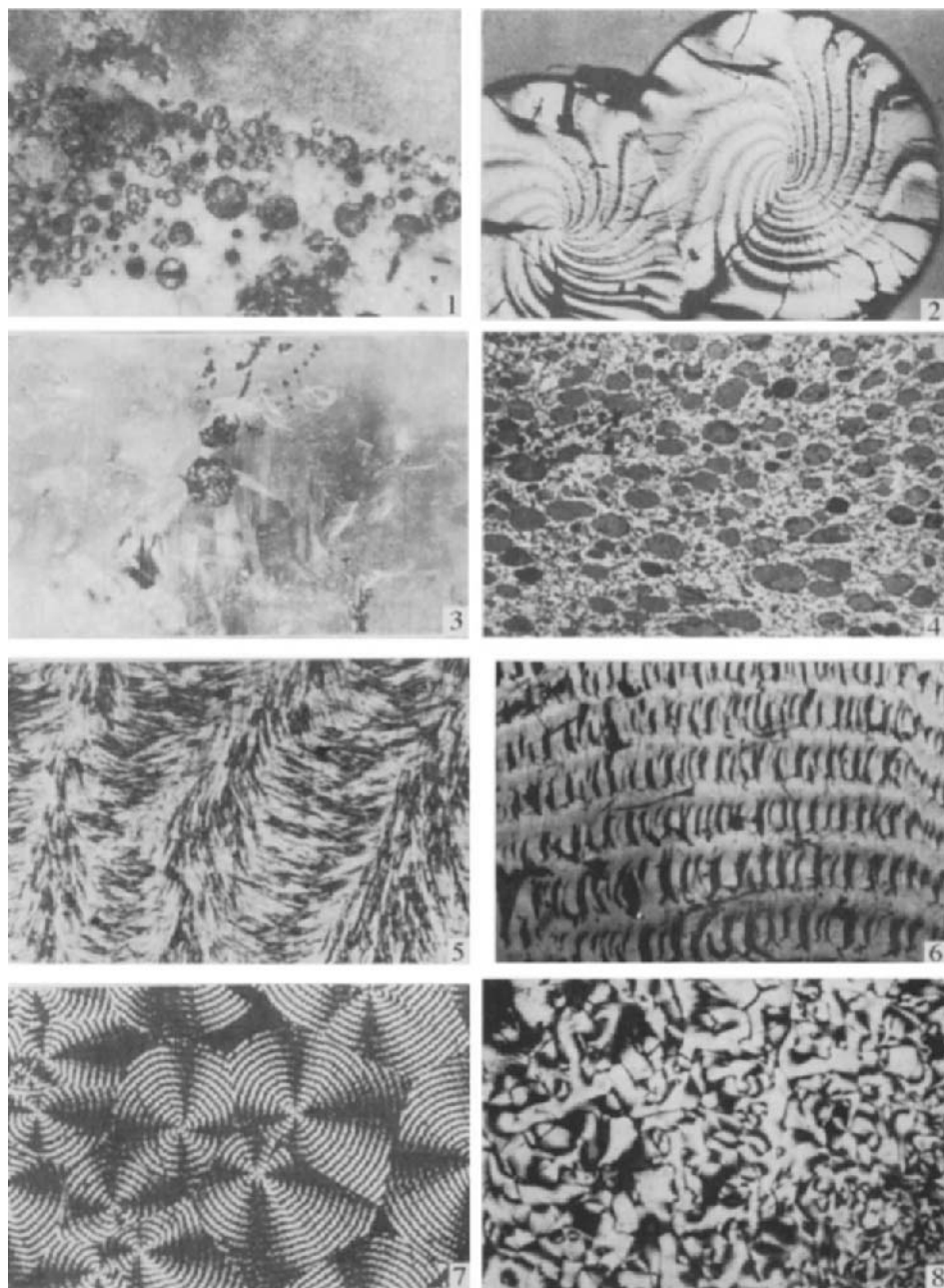


Fig. 15-30. Magenta fluorescence activated by cathode ray in Sinian dolomite in Weiyuan Gas Field, south Sichuan Province. (1) Oolitic bitumen in dolomite ( $\times 2$ ). (2) Spiral bitumen in quartz crystal ( $\times 40$ ). (3) Bitumen enclosure in quartz crystal ( $\times 2$ ). (4) Bitumen coke formed by thermal metamorphism ( $\times 80$ ). (5) Bitumen of plume texture ( $\times 400$ ). (6) Bitumen of imbricate texture ( $\times 160$ ). (7) Bitumen of concentric texture ( $\times 160$ ). (8) Coarse poikilitic bitumen ( $\times 200$ ).

Ordovician limestones of the Tarim Basin, bitumen reflectance varies in different tectonic units from east to west. In the east Tarim Basin, the bitumen reflectance of Ordovician shale is as high as 4.5%. In the Lunnan District towards the west, the reflectance ranges between 1.70 and 1.90%. The reflectance value is 1.30 to 1.56% as one proceeds westward towards the Yingmaili District. This variation of bitumen reflectance suggests that the thermal maturity of Ordovician source rocks in the Tarim Basin increases from west to east. In the Yingmaili District, Ordovician limestone reservoir contains only heavy black oil. In Lunnan, black oil or brown light oil can be found. In the east Tarim Basin, there is no significant oil discovery. This horizontal distribution of petroleum correlates with that of bitumen reflectance.

Cathodoluminescence microscopic observation can reveal the generation of carbonate minerals. It can also be used to reconstruct the time sequence of bitumen formation. For example, magenta fluorescence was used by cathode ray in Sinian dolomite of the Weiyuan Gas Field, south Sichan Province (see Fig. 15-30). Some dolomite crystals yielded four to five different color fluorescences, which reveals the recrystallization of four to five generations. Black bitumen usually has a color of bright magenta, which illustrates that the oil generation for Sinian source rock began in earlier geological time (or tectonic phase) in the Weiyuan District.

#### REFERENCES

- [1] Yen, T.F., Edman, J.G. and Pullack, S.S., Investigation of the structure of petroleum asphaltenes by X-ray diffraction. *Anal. Chem.*, 33 (11): 1587–1594 (1961).
- [2] Yen, T.F. and Sprang, S.R., Contribution of ESR analysis toward diagenetic mechanisms in bituminous deposits. *Geochim. Cosmochim. Acta* (1977).
- [3] Yen, T.F. et al., *Selected Papers of Organic Geochemistry*. In: Lanzhou Institute of Geology, Chinese Academy of Sciences, Research Institute of Petroleum Exploration and Development, China National Corporation of Oil and Gas, Lanzhou (Editors). Gansu Scientific Publishing House, pp. 208–220 (1986).
- [4] Wen, C.S., Chilingar, G.V. and Yen, T.F., Nature and structure of bitumens. In: Ghilinger, G.V. and Yen, T.F. (Editors), *Bitumens, Asphalts and Tar Sands*. Elsevier, Amsterdam, pp. 142–178 (1978).
- [5] Cook, A.G. and Kantslev, A.J., Description of the maceral groups and macerals found in coals, oil shale, and as dispersed organic matter in sediments. In: A.G. Cook (Editor), *The Origin and Petrology of Organic Matter in Coals, Oil Shale and Petroleum Source Rocks*. Elsevier, Amsterdam, pp. 36–60 (1982).
- [6] Rogers, M.A., McAlary, J.D. and Bailey, J.J., Significance of reservoir bitumens to thermal maturation studies, Western Canada Basin. *Am. Assoc. Pet. Bull.*, 58 (9): 1806–1824 (1974).
- [7] Jacob, H., Classification, structure, genesis, and practical importance of natural solid bitumen (migrated bitumen). *Int. J. Coal Geol.*, 11: 65–79 (1975).
- [8] Fu, J. and Shi, J., Theories and practices and petroleum evolution, II. Practical models and significance of petroleum evolution (in Chinese). *Geochim. Sin.*, 2: 87–104 (1977).
- [9] Yen, T.F., Edman, J.G. and Saraceno, A.J., Investigation of the nature of free radicals in petroleum asphaltenes and related substances by electron spin resonance. *Anal. Chem.*, 34: 694–700 (1962).
- [10] Liu, D., Zhou, Z., Jia, R. and Li, W., Thermal alteration of bitumens in carbonate source rocks and thermal simulation experiments of bitumens (in Chinese). *Geochim. Sin.*, 3: 237–243 (1982).
- [11] Xiao, X., *Organic Petrology and Its Applications in Assessment of Petroleum Resources*. Guangdong Scientific Publishing House, Guangdong, pp. 132–138 (1992).
- [12] Liu, D., Bitumens in carbonate source rocks and their applications in studying generation and evolution of petroleum and origin of metal ore deposits (in Chinese). In: Sedimentary and Organic Division

- of Institute of Geochemistry, Chinese Academy of Sciences (Editor), *Selected Papers of Organic Geochemistry*. Science Press, Beijing, pp. 133–138 (1986).
- [13] Yen, T.F., Structure of petroleum asphaltene and its significance. *Energy Sources*, 1 (4): 447–463 (1974).
- [14] Chen, D., Liu, G. and Peng, W., Thermal simulation experiments of artificial oil thermal alteration product and naturally occurred bitumens (in Chinese). In: *Selected Papers of Organic Geochemistry*. Science Press, Beijing, pp. 139–146 (1986).
- [15] Seifert, W.K., Moldowan, J.M. and Demaison, G.J., Source correlation of biodegraded oils. *Org. Geochem.*, 6: 633–643 (1984).
- [16] Connan, J., Biodegradation of crude oils in reservoirs. *Adv. Pet. Geochem.*, 1: 299–335 (1984).
- [17] Volkman, J.K., Biodegradation of aromatic hydrocarbons in crude oils from the Barrow Sub-basin of Western Australia. *Org. Geochem.*, 6: 619–632 (1984).
- [18] Brooks, P.W., Fowler, M.G. and Macqueen, R.W., Biological marker and conventional organic geochemistry of oil sand oils, Western Canada Basin. *Org. Geochem.*, 12 (6): 519–538 (1988).
- [19] Peters, K., Moldowan, J.M., *The Biomarker Guide: Interpreting Molecular Fossils in Petroleum and Ancient Sediments*. Prentice-Hall, Englewood Cliffs, NJ (1992).
- [20] Fu, J. and Sheng, G., Initial study on the genesis of a huge Chinese natural sulphur deposit by molecular organic geochemical approach (in Chinese). *Acta Sedimentol. Sin.*, 5 (3): 96–103 (1987).
- [21] Parnell, J., Geng, A. and Sheng, G., Geology and geochemistry of bitumen vein deposits at Ghost City, Junggar Basin, Northwest China. *Geol. Mag.*, 131 (2): 181–190 (1994).

This page intentionally left blank

## *Chapter 16*

# **ASPHALT OXIDATION**

F.C. THYRION

## **INTRODUCTION**

Petroleum asphalts are obtained during crude oil distillation as atmospheric/vacuum residues or as extracts from lubricating oil production. Here oxidation stability is one of the most important qualities of lube base stock and the presence of labile hydroaromatic compounds is known to be one of the main causes for instability.

Asphalts are also obtained as residues from thermal cracking processes. The properties of these asphaltic materials depend on the nature of the crude oil and the refinery processes employed. These asphalts do not necessarily conform with the end-product specifications of industrial grade or paving asphalts. To improve their properties, asphalts are then oxidized by air-blowing. However, slow oxidation of asphalt continues during the service life of the roadbed at a rate that appears to be partly determined by the void volume of the roadbed as well as the properties of the asphalt. The oxidation of bitumens and asphalts, whilst appearing to be a relatively facile process involving simple chemical reactions, is in fact a complicated sequence of interactions eventually resulting in the oxidized products.

Low-temperature oxidation (LTO) of heavy oil can occur during in-situ recovery processes, such as in-situ combustion, and in processes which involve the concurrent injection of steam and air.

Finally, the deterioration of petroleum products (change in physical/chemical properties upon prolonged storage under “ambient” conditions) is a complex, yet fascinating problem.

For all these reasons, it is interesting to know the conditions and reasons of the oxidizability of asphalts.

Before studying the effect of oxygen on asphalts or asphalt functions, it appears worthwhile to recall the main properties of asphalt and the characteristics of the oxidation reactions.

## **ASPHALT, RESINS AND ASPHALTENES**

### *Definition*

Petroleum is a complex mixture of hydrocarbon compounds which is complicated further by the presence of heteroatom (nitrogen, oxygen and sulfur) compounds. Most petroleum also have the organic compounds of nickel and vanadium (the porphyrins)



TABLE 16-1

Some heavy oils compositions [1]

Origin	Asphaltenes (%)	Resins (%)	Hydrocarbons		Number of samples
			Aromatics (%)	Saturated (%)	
Athabasca	23.3	28.6	32.2	15.9	15
Wabasca	21.6	30.6	32.1	15.6	7
Peace River	48.7	23.2	20.5	7.6	3
Cold Lake	20.6	28.0	30.5	20.9	7
E. Venezuela					
bitumen	22.1	37.6	26.0	14.3	9
heavy oil	12.6	32.4	36.4	18.6	5
Mean over 46 heavy oils	22.9	30.6	30.4	16.1	46
517 conventional oils	14.2		28.6	57.2	517

present in amounts varying up to several hundred ppm. In more general terms, petroleum can be considered to be a composite of four major fractions: (1) the saturates; (2) the aromatics; (3) the resins; and (4) the asphaltenes. However, it is absolutely imperative to know that the definition of any particular fraction is actually an operational aid. Depending on the origin of the crude oil, the asphaltene fraction of petroleum can be more or less important and the proportion of this fraction increases when going from normal crude oil to heavy and extra-heavy oils (tar sands).

An example of the composition of several oils is given in Table 16-1.

As already noted, the definition of petroleum asphaltenes is an operational aid and it must never be forgotten that the asphaltene fraction is actually a solubility class. A stable asphaltene yield from heavy oils and atmospheric or vacuum residues can only be obtained if certain conditions are fulfilled, i.e., the use of sufficient amounts of precipitating solvent (pentane or heptane), a contact time large enough and a reprecipitation sequence to remove any adsorbed resin material.

The deasphalted oil (maltenes) resulting from the asphaltene precipitation can undergo several types of fractionation. Many methods have been proposed for accomplishing this, each of which attempts to resolve the overall complexity of the mixture. Some of them use elution-adsorption chromatography to separate the maltene saturates, naphthene aromatics and polar aromatics (ASTM Standards) or in four fractions such as saturates and aromatics-1 (oily constituents), aromatics-2 and aromatics-3 (the last two fractions are called resins) [2]. An other method separates the heavy residues in seven fractions by combining ion exchange and adsorption chromatographies: acids, bases, neutral nitro compounds, saturates, mono-, di- and polyaromatics (USBM-API) [3].

The HPLC technique has also been used to separate maltenes into saturates, aromatics and polar aromatics [4,5].

Finally, GPC has been mainly exploited in order to determine molecular-size distributions of asphalts and their fractions [6].

### Structure

The structure of petroleum asphalts (synonymous: bitumen) is usually regarded as a suspensoid in which asphaltenes are the dispersed phase and maltenes are the dispersion medium. Some investigators regard asphalts as typical molecular colloids, considering the asphaltenes as macromolecular compounds [7,8]. Asphaltene micelles (aggregates) are assumed to be kept in solution (stabilized or peptized) by a layer of resins ('onion-skin model'). These views explain certain physical properties of asphalts but are not in full accord with their chemical composition. The chemical structure of the compounds present in asphalts varies continuously over the entire range, and this casts doubt on the possibility of existence, in asphalts, of a well-defined interface between dispersed phase and the dispersion medium.

More recently, several studies [9–12] have provided a basis for developing a molecular model for asphaltene–resin interaction.

Asphaltenes and resins are hetero-compounds and form the most polar fraction of crude oil. Recent works on asphaltene structure show that the basic asphaltene 'molecule' (asphaltene sheet [9]) has a molecular weight of the same order of magnitude as that of resins ( $5 \times 10^2$  to  $10^3$ ). Depending on 'purity' [13,10] and concentration [9] asphaltenes form aggregates with a molecular weight of the order of magnitude of  $10^3$ – $10^4$  (asphaltene 'particle' [14]). Resins have a strong tendency to associate with asphaltenes. This reduces the aggregation of asphaltenes, which determines to a large extent their solubility in crude oil [15].

Kolbanovskaja [16] has considered three fundamental types of structure for a bitumen, depending on the relative proportions of asphaltenes and resins (Table 16-2).

In the first case, the *gel* type, the asphaltenes are in large proportions and constitute a continuous network, just like a skeleton; the dispersive medium having a weak structure is localized inside it.

The second case, the *sol* type, can be considered as a dilute suspension of asphaltenes stabilized in a dispersive medium highly structured by the resins.

Finally, in the third case, micelles of asphaltenes are diluted in a fairly well structured dispersive medium (but less structured than in the *sol* type). In this state called *sol-gel*, the asphaltenes form aggregates but are unable to produce a continuous network. Most road bitumens belong to this class.

Dron et al. [17] have similarly defined several states and rheological behaviors for binary systems of maltenes and asphaltenes.

TABLE 16-2

Structure of bitumen

Bitumen type	Asphaltenes (%)	Resins (%)	Oils (%)
I: gel	>25	24	50
II: sol	<18	36	48
III: sol-gel	≈21–23	≈30–34	45–49

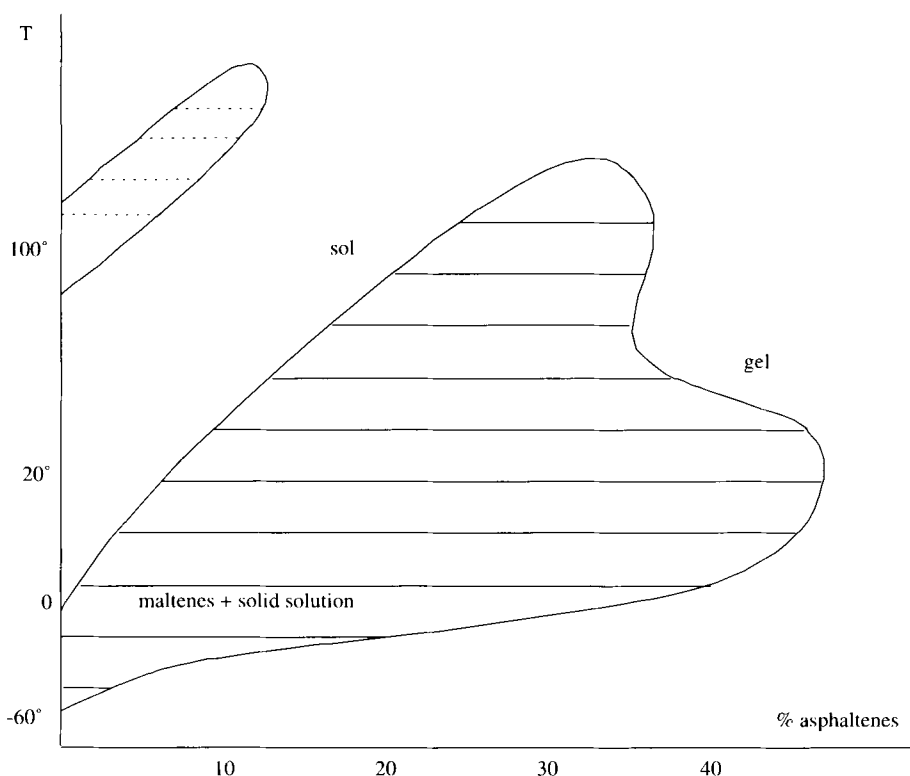


Fig. 16-1. Composition versus temperature diagram.

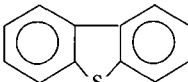
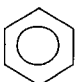
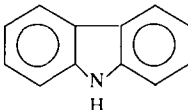
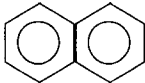
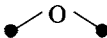
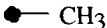

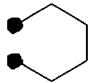
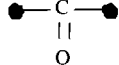
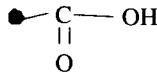
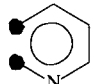
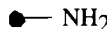
Fig. 16-1 shows the different states in a diagram composition–temperature: the sol state has a quasi-newtonian viscosity, while gel-sol has a viscoplastic and gel a plastic behavior.

Many colloidal characteristics of bitumens, such as its gel-sol conversion, temperature coefficient of viscosity, micelle stability and complex flow, etc., could be explained on the basis of a charge-transfer nature of individual aromatic systems throughout the macrostructure [18,19]. Consequently, the inter- and intra-cluster associations not only affect processing but are also relevant to problems concerning aging and chemical reaction with oxygen.



#### *Molecular characterization of asphalt and its constituents*

##### *Asphalt and heavy oils*

Many analytical procedures have been applied to the problem of characterizing the structure present in heavy oils and asphalts, but data interpretation methods rarely attempt to integrate diverse sources of data into a consistent structural characterization. Fortunately, recent works [20,21] have used the method of structural analysis to estimate the concentration of functional groups in fossil fuel fractions by performing a

1) 	0.125	9) 	0.047
2) 	0.027	10) 	0.008
3) 	0.036	11) 	0.008
4) 	0.025	12) 	0.006
5) 	0.003	13) $[\text{CH}_2]$	2.937
6) 	0.033	14) $[\text{CH}]$	0.400
7) 	0.000	15) $[\text{CH}_3]$	0.726
8) 	0.001	16) $[\text{CH}_2]$	0.073
		17) $[\text{CH}]$	0.616

**NOTATION :**

-  Bound to an aromatic ring  
 Aliphatic carbon - carbon bond

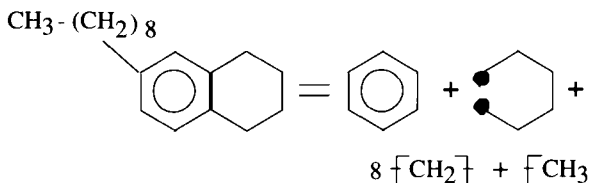
**EXAMPLE :**


Fig. 16-2. Heavy oil functional groups (after Allen et al. [20]). Functional group concentrations (moles/100 g).

least-squares minimization on analytical data from a variety of sources. This approach has been demonstrated with atmospheric tower bottoms of a Mayan crude oil. The functional groups found for this heavy oil are shown in Fig. 16-2.

The concentrations show that the degree of aromatic substitution is high and that the vast majority of aromatic rings are heteroatomic. We observed also that nitrogen and sulfur atoms are mainly or totally involved in polyaromatic structures like dibenzopyrrole or dibenzothiophene. On the other hand, the oxygen atom exists

mainly under the form of ether, hydroxyl and carboxylic functions. The fraction of aromatic carbon is 0.295 as determined by  $^{13}\text{C}$  NMR spectra. This value is similar to that found in a Safaniya vacuum residue, i.e., 0.30 and 0.31 [22]. A study [23] on the distribution of heteroatomic polyaromatic compounds (azaarenes, carbazole or thiophene derivatives) in crude oil or heavy oils having different origins has shown that in each series of varying aromaticity, a rapid decrease of relative abundance is observed with an increase in the number of carbon atoms. Moreover, with the exception of benzothiophene, unsubstituted compounds are abundant and pseudo-homologous alkyl derivatives having one or two additional carbon atoms dominate. Likewise, the distribution of carbazole derivatives is characterized by the presence of unsubstituted compounds. Tetraaromatic species (benzocarbazoles) dominate, however, whereas the triaromatic dibenzothiophenes are the major sulfur compounds.

In the same study it was shown that the distribution of azaarenes markedly differed from that of other polyaromatic compounds, because unsubstituted compounds were not observed. Unsubstituted compounds were absent and compounds having a low degree of alkyl substitution were dominating, except for the diaromatic alkyl quinoline series, which was dominated by  $\text{C}_5$ - or  $\text{C}_6$ -alkyl derivatives.

Other authors (e.g., [24]) have pointed out a strong hydrogen-bonding association between the 2-quinolones and carboxylic acids in asphalt.

### *Asphaltenes*

Petroleum asphaltenes have a varied distribution of heteroatom functionality. Unfortunately, in most studies, too little emphasis has been placed on determining the nature and location of the nitrogen, oxygen and sulfur atoms in the asphaltene structure. However, early mass spectroscopic investigations [25] of a petroleum asphaltene have allowed the identification of fragment peaks, which indicate that some of the heteroatoms exist in the ring systems. A study of the thermal decomposition of asphaltenes [25] indicated that only 1% of the nitrogen was lost during thermal treatment, whereas substantially more sulfur (23%) and almost all of the oxygen (81%) were lost as a result of this treatment. The tendency of nitrogen and sulfur to remain during thermal decomposition, as opposed to the easy elimination of oxygen, supports the concept that nitrogen and sulfur are stable because of their location in the ring system.

Thus, *nitrogen* exists as various heterocyclic types [25,26]; the more conventional aromatic amines have not been established as being present in petroleum asphaltenes. Spectroscopic investigations [10] suggest that carbazoles might be a predominant nitrogen type in asphaltenes from Athabasca bitumen, which supports the earlier mass spectroscopic evidence [25] for nitrogen types in asphaltenes. The same conclusion was derived from reactions of resins and asphaltenes with acetic anhydride and trifluoroacetic anhydride [26].

By oxidative degradation of Athabasca oil sands, asphaltenes followed by extraction and subsequent analysis by GC-MS, quinoline and a number of substituted piperidines were identified [27].

*Oxygen* has been identified in carboxylic, phenolic and ketonic locations [28,29] but is not usually regarded as being located primarily in heteroatomic ring systems. The study of oxygen distribution in the Athabasca asphaltene [30,31] has demonstrated that, on average, 75% of the oxygen is present in the form of hydroxyl group. I.R. studies in-

licated that these hydroxyl groups exist almost entirely as hydrogen-bonded complexes.

Acid–base characteristics of asphaltenes [32] brought about the nature of the groups titrated in non-aqueous solvents. The strong medium and weak acids titrated were due to the presence of carboxylic, phenolic and indolic functionality, whereas the strong bases titrated were due to pyridine groups, the medium strength bases due to pyrazines and sulfoxides and the very weak bases due to indoles and amides.

*Sulfur* occurs as benzothiophenes, dibenzothiophenes and naphthenobenzothiophenes [25,29,13]. More highly condensed thiophene types may also exist, but are precluded from identification by low volatility. Other forms of sulfur that occur in asphaltenes include the alkyl–alkyl, alkyl–aryl and aryl–aryl sulfides [14].

The reaction of Athabasca asphaltenes with tetralin [33] were interpreted in terms of thermal cleavage of sulfide bonds. The same asphaltenes as studied by radical-ion electron transfer reactions showed a sulfur polymeric framework in which the average carbon moieties, consisting of an alicyclic diaromatic structure with some alkyl substituents, were held together by sulfide linkages. If a sulfur-type polymer exists, however, it would be expected to lose much, but not necessarily all, of its sulfur by treatment with Raney nickel [34]; the particular Athabasca asphaltenes are difficult to desulfurize under these conditions. If these results, coupled with data from thermal decomposition, can be projected to all the asphaltenes, it would be indicative of sulfur existing predominantly in the heterocyclic form.

#### *Metals in heavy fractions*

The most abundant trace metals in petroleum are nickel and vanadium. The concentration of vanadium in crudes can vary from as little as 0.01 ppm to as much as 1200 ppm. Vanadium is generally more abundant than nickel. These metals and others in smaller amounts (Fe) can affect oil aging and oxidation.

Nickel and vanadium are thought to occur in petroleum in two forms: porphyrinic and non-porphyrinic [35]. Little is known about the chemical nature of the non-porphyrinic metal, but the porphyrins have been more widely studied. The concentration of vanadium and nickel as porphyrins may be estimated by silica-gel chromatography and X-ray fluorescence spectroscopy [36,37].

### MAIN FEATURES OF OXIDATION OF ORGANIC SUBSTANCES

Several reviews have appeared in the past dealing with the autoxidation of organic substances in the liquid phase with molecular oxygen [38–41]. The normal curve for oxygen uptake during autoxidation (strictly defined, autoxidation is auto-initiated oxidation by molecular oxygen) consists of an initial period when very little oxidation occurs, known as the induction period. This is followed by a rapid increase in rate due to autocatalysis by chain-branching intermediates that build up during the induction period.

The rate soon reaches a maximum value and then slowly starts to decrease. Autoxidation can be inhibited, i.e., prevented or retarded by the addition of certain compounds known as antioxidants, which lengthen the induction period or lower the maximum rate of oxygen uptake.

*Kinetics of autoxidation*

The autoxidations that are considered here involve a free-radical chain process described by the following reactions.

*Initiation:*



The radical ( $\text{R}^\circ$ ) reacts rapidly with oxygen to give an alkylperoxy radical which may either abstract an allylic hydrogen atom from another molecule or add to a double bond.

*Propagation:*



Kinetic chains are broken by removal of chain propagating radicals.

*Termination:*



From reaction 16-2

$$-\frac{d(\text{O}_2)}{dt} = k_2 [\text{R}^\circ] [\text{O}_2]$$

which for molecules giving hydroperoxides in high yields is equal to the rate of formation of hydroperoxide during the early stages of the reaction, i.e.,

$$k_2 [\text{R}^\circ] [\text{O}_2] = k_3 [\text{ROO}^\circ] [\text{RH}]$$

In contrast to reaction 16-3 and 16-3a which, except for the most readily oxidized compounds, involve appreciable activation energies, that of reaction 16-2 is very small. Consequently, at high oxygen pressures, the rate of reaction 16-2 will be so much greater than that of reaction 16-3 that  $[\text{R}^\circ]$  will be negligible in comparison with  $[\text{ROO}^\circ]$  and chain termination (whose rate is equal to the rate of chain starting,  $r_i$ ) will take place entirely by reaction 16-6, i.e.,

$$r_i = k_6 [\text{ROO}^\circ]^2$$

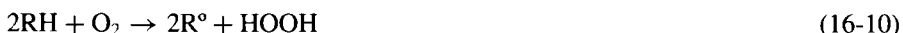
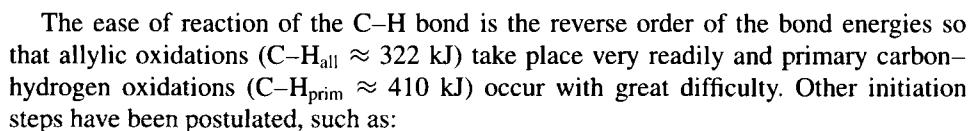
from which

$$-\frac{d[\text{O}_2]}{dt} = k_3 k_6^{-(1/2)} r_i^{1/2} [\text{RH}] \quad (16-7)$$

Eq. 16-7 describes satisfactorily the kinetics of the oxidation of a large number of hydrocarbons at pressures greater than 100 mm.

Because the rate of autoxidation can be affected by a change in the rate of any of the individual reaction steps, some comments will be given on these steps considered separately.

Reaction 1 is promoted by free radicals; therefore, compounds which can form free radicals readily, such as hydroperoxides, peroxides, diazoalkanes, etc., promote oxidation. Compounds of this type are known as initiators and are frequently used in industrial processes. In the absence of initiators, the energy required for the production of a starting radical may come from heat, light, or ionizing radiation. For a compound to serve as a useful thermal initiator, it must possess some fairly weak bond. The dissociation energies of most covalent single bonds are in excess of 290 kJ/mole, but autoxidation reactions have a unique feature over other free-radical chain reactions in that the primary products of autoxidations are themselves potential initiators. Most of the hydroperoxides like the one formed in reaction 16-3, for instance, have bond dissociation energies of the order of 138–210 kJ, that is, such that slow homolysis will occur in the temperature range 50–150°C:



An autoxidation may often be run so that a small amount of the hydroperoxide formed is decomposed homolytically, providing a continuous 'internal' source of free radicals.

$$\begin{array}{c}
 \text{H} \quad \text{O}=\text{O} \\
 | \quad \curvearrowright \\
 \text{R}-\text{C}=\text{C}-\text{R}' \\
 | \quad | \quad | \\
 \text{H} \quad \text{H} \quad \text{H}
 \end{array}
 \rightarrow
 \begin{array}{c}
 \text{H}-\text{O}-\text{O} \\
 | \quad | \\
 \text{R}-\text{C}=\text{C}-\text{C}-\text{R}' \\
 | \quad | \quad | \\
 \text{H} \quad \text{H} \quad \text{H}
 \end{array}
 \quad (16-11)$$



In a mixture of hydrocarbons such as petroleum oils, which are initially free from hydroperoxides, it may be advantageous to remove the less stable components, i.e., those with weak carbon–hydrogen bonds in order to improve stability.

### *Propagation*

Reaction 2 is extremely rapid for nearly all hydrocarbon radicals and, therefore, only peroxy radicals are of importance in chain propagation and termination except at very low partial pressures of oxygen or with very reactive organic substrates.

In any given substrate, the rate can only be reduced by providing an alternate fate for the peroxy, radical which will lower its steady-state concentration. This can be achieved by the addition of a more reactive compound such as an *inhibitor* of free radicals.

Reaction 3 is basically similar to abstraction of hydrogen by other free radicals, such as alkoxy radicals,



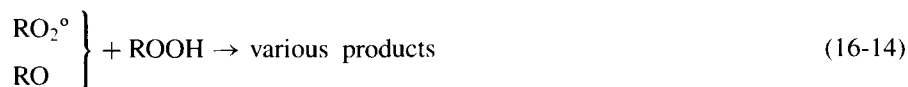
and, therefore, the relative ease of oxidation of different substrates can be correlated with the relative rates of reaction 16-12.

### *Decomposition of peroxides*

Thus far, we have considered the hydroperoxide to be a *product* of autoxidation and not in itself an agent influencing the primary free-radical chain process. Under some conditions hydroperoxides are stable reaction products. Under other conditions they may decompose by nonradical reactions:



or by reaction with radicals:



Most often, the thermal decomposition of a hydroperoxide gives some free radicals



It, therefore, leads to chain *branching* and accounts for the autocatalysis observed in many oxidations. Moreover, the solvent generally plays an important role in the decomposition of hydroperoxide. The rate of decomposition of hydroperoxide is accelerated by initiators, which provide an additional source of free radicals and is retarded to a minimum value by the addition of inhibitors of free radicals including polycyclic aromatic hydrocarbons. It is probably not possible to reduce the rate of reaction 16-15 by complexing the hydroperoxide with an additive (possible exception of sulfoxides).

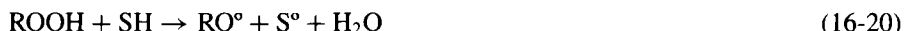
The rate of decomposition of hydroperoxide can be accelerated by many different types of compounds (*induced decomposition*). The exact reactions involved with the many different types of decomposers of peroxides recorded in the literature are not

always clear, but it seems that they can be classified as one of the following three possibilities:



where  $X$  = a heavy metal or substances like saturated hydrocarbons, alcohols, ketones, ethers, fatty acids and olefins,  $Y$  = certain sulfur compounds, and  $Z$  = a strong acid in the sense of Lewis. Inhibition results from reactions 16-18 and 16-19, and catalysis from reaction 16-17.

First, let us consider reaction 16-17 in the presence of saturated hydrocarbon solvents (SH) or olefins:



Also, a number of heavy metal ions, particularly those which possess two or more valency states with a suitable oxidation reduction potential between them (e.g., Fe, Co, Mn, Cu, etc.), can react with hydroperoxides to produce free radicals:



Certain metals (e.g., Co and Mn) can act as both oxidant and reductant and are, therefore, catalysts for the decomposition of peroxides. The complexes of metal ions and hydroperoxides are the active catalytic agents that react with more hydroperoxide as suggested by the strong catalytic effect of some metal chelates on the decomposition of hydroperoxides. The anion associated with the metal can influence its catalytic activity either by affecting its redox potential or by 'blocking' the formation of a catalyst-hydroperoxide complex: useful chelating agents are effective by virtue of their steric effect in preventing the formation of metal-ion-hydroperoxide complexes and also by modifying the redox potential of the ion so as to suppress reactions 16-22 or 16-23.

Metal ion-radical complexes are probably particularly important with aromatic substrates, because the free radicals are already largely complexed with aromatic molecules.

### *Heteroatomic organic molecules as antioxidants*

Reaction 18 involves a stoichiometric process where  $Y$  acts as a peroxide decomposer to give stable products and interrupt the autoxidation chain. On the basis of the autoxidation chain process, two mechanistically distinct classes of antioxidant can be distinguished in principle. The first one operates by a *radical chain-breaking mechanism* by removing from the medium the two important species normally involved in the chain propagating step, the alkylperoxy and alkyl radicals. The second one, the *preventive*

*mechanism*, is concerned not with the propagation reaction, but with preventing the introduction of the chain initiating radicals in the system. Because chain-breaking and preventive antioxidants interfere at different points in the autoxidation process they mutually reinforce one another, leading to an effect greater than the sum of the effects of each antioxidant alone; on the other hand, if the two classes of antioxidant frequently complement each other, the more effective peroxide decomposing antioxidants generally retain their activity at high temperatures and in the presence of metal ions.

Three families of substances will now be considered as antioxidants: sulfur-compounds, amines and phenols.

#### *Sulfur containing molecules as peroxide decomposers*

In reactions 16-24 and 16-25, the hydroperoxide is converted to the corresponding alcohol in the presence of sulfide or sulfoxide:



The sulfides are themselves converted to sulfoxides and sulfones in the process. Very often, sulfoxides have a higher order of activity than the sulfides from which they are derived.

Monosulfides which contain at least one aliphatic or cycloaliphatic group attached to the sulfur atom are more effective antioxidants than mercaptans and disulfides, whereas diaryl sulfides and sulfones are inactive.

Although many sulfides are fairly stable towards oxygen, both sulfoxides and sulfones are autoxidized rapidly; among their products are strong acids, which are probably sulfonic acids. These acids, which will almost always be produced when sulfides are used as antioxidants, are able to decompose further peroxide by a catalytic ionic rearrangement process as shown in reaction 16-19.

Careful studies have demonstrated the effects of sulfides as antioxidants in purified hydrocarbon oils and R.W. Hawkins [26] has shown that a wide variety of sulfur-containing compounds are effective heat stabilizers in polyethylene.

In conclusion, the decomposition of peroxides by sulfides is more complex than is suggested by reaction 16-24; sulfur-containing antioxidants react with hydroperoxides by a molecular process at low temperatures but perhaps by an ionic process at higher temperatures. The antioxidants are themselves oxidized to acids, which promote a concurrent catalytic decomposition. The presence of sulfur-containing compounds in a system subject to autoxidation may promote the development of resinous compounds and sludges.

#### *Phenol and amine as radical chain-breaking antioxidants*

The alkylperoxy radical is a relatively powerful electrophilic agent: it is this property which not only leads to chain propagation in the autoxidation reaction, but which is also responsible for the extremely facile electron transfer from amines or phenols leading to termination of the chain reaction.

Two possible chain-ending reactions involving the antioxidant (AH) can be considered:



followed by the termination reaction



This reaction scheme satisfactorily explains the observed inverse dependence of the rate of oxidation upon the concentration of the antioxidant in many systems.

The rates of non-inhibited oxidations are independent of oxygen pressure, except at very low pressures. In contrast, the rates of inhibited oxidations, or their induction periods, depend on oxygen pressure, so it is probable that most inhibitors react directly with oxygen:



Under some conditions, the hydroperoxide of the inhibitor is produced but under others, extensive rearrangements may occur.

Antioxidant activity is a resultant, firstly of the ability of the material to deactivate alkylperoxy radicals and, secondly, of the tendency of the antioxidant radical to continue the kinetic chain. The distinction between an *inhibitor* and a *retarder* is most conveniently made by comparing the form of the oxidation curve in the two cases. Ideally, the former gives no oxygen absorption during the inhibition period, implying high antioxidant efficiency and negligible chain transfer. The latter, however, is characterized by a measurable rate of oxygen absorption during the initial stage of the oxidation which is a consequence of effective chain transfer.

There is a good deal of information available on the relationship between the antioxidant activity of phenols and their structures. In numerous studies on 2,4,6-substituted phenols, in a variety of substrates the relative efficiencies of phenolic antioxidants were determined by the kinetic measurement of  $k_{26}$  and were shown to parallel antioxidant activity obtained from the measurement of inhibition periods. The main conclusions which emerge from these studies may be summarized as follows [41]: electron releasing groups in the ortho and para positions markedly increase the antioxidant activity, while electron attracting groups decrease activity.  $\alpha$ -Branched ortho alkyl groups considerably increase antioxidant activity of the substituted phenol just like  $\alpha$ -branched *N*-alkyl groups do in derivatives of aniline. *N*-Aryl substituents also have a powerful augmenting effect upon the antioxidant activity and some of the most important industrial antioxidants are diarylamines. Ultimately, the antioxidant activity of phenols and amines is associated with their capacity to donate electrons to alkylperoxy and alkoxy radicals.

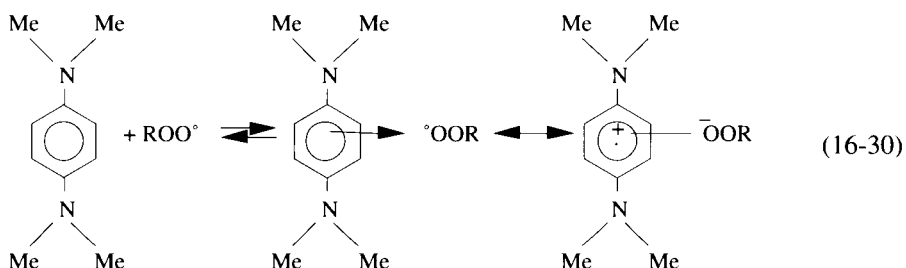
In addition to their antioxidant activity, phenols and especially amines are also suspected to act as peroxide decomposers, although they are less efficient than sulfur compounds. They generally lead to nonradical products.

*The electron releasing and electron acceptor mechanisms*

It is clear from the preceding discussion that both phenol and amine antioxidants interfere primarily by transferring either a hydrogen atom or an electron to the most abundant chain propagating species, the alkylperoxy radical.

There is strong evidence in the literature for the interaction of free radicals with the  $\pi$ -bond system of aromatic compounds and the evidence that radical complex formation is stronger for arylamine antioxidants than it is for phenols.

For instance, the antioxidant activity of aromatic amines, unlike that of phenols, is not destroyed by complete *N*-alkylation. So, tetramethyl-*p*-phenylene diamine is still a powerful antioxidant and since it has no labile hydrogen atom, the deactivating mechanism, if it is kinetic chain breaking, can only involve electron transfer from the nitrogen. There is physical evidence for the existence of the Würster radical-ion under autoxidation conditions:



Summarizing, it seems that the mechanism of amine antioxidant action is basically similar to that of phenols. As with the latter, three structural factors need to be satisfied for the highest activity. These are: (a) effective delocalization of the unpaired electron formally resident on the nitrogen; (b) high electron density on the nitrogen to facilitate electron transfer to the alkylperoxy radical; and (c) sufficient steric protection of the nitrogen atom to reduce chain transfer by the arylamino radical. In contrast to the phenols, this is better achieved by substitution on the nitrogen atom than in the ortho positions of the aromatic ring.

Up to now, we were dealing with the relatively powerful electrophilic properties of the alkylperoxy radicals and it is this property which not only leads to chain propagation in the autoxidation reaction, but which is also responsible for the extremely facile electron transfer from amines or phenols leading to termination of the chain reaction. In view of this, it would not be expected that alkylperoxy radicals should readily donate an electron by participating in reactions involving their own reduction. They do not readily add to isolated olefinic bonds unless the latter are activated. Several works pointed out, however, that autoxidation retarders are not necessarily reducing agents, and it was shown that polycyclic aromatic hydrocarbons and, particularly, substituted naphthalenes are effective retarders of autoxidation: this is a well known effect in lubricating oil. This retardation originates in the lower reactivity of the radical resulting from the reaction of the aromatic hydrocarbon with the alkylperoxy radical. The same interpretation has been given to explain the retardation observed in the highly saturated polymers, such as polyethylene, by carbon black. The latter also possesses a polycyclic nature, although

the carbon black surface is known to contain acidic (probably phenolic) groupings which might be expected to have conventional hydrogen transfer antioxidant properties.

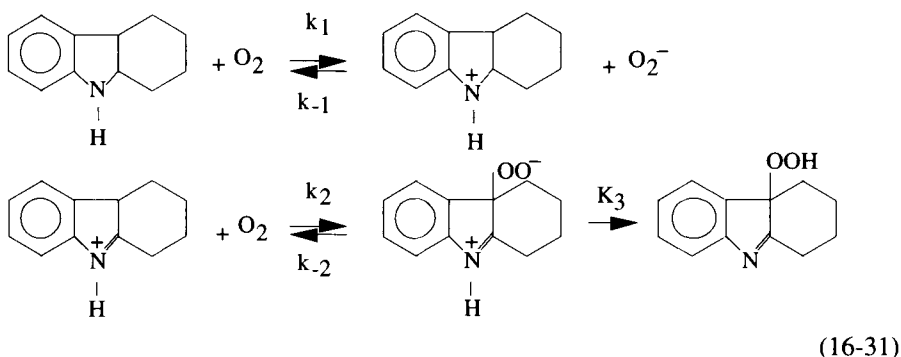
*Oxidative degradation via a non-peroxyl radical chain pathway (ETIO)*

One major weakness with proposing free-radical mechanisms for alkylpyrrole autoxidation schemes is that the presence of radical chain scavenger antioxidants has little effect on the rate of alkylpyrrole oxidation: that is the reason why Beaver and Gilmore [42] postulated the Electron Transfer Initiated Oxidation (ETIO) reaction. It is defined in the following manner: any oxidation reaction in which the rate-limiting step involves an electron transfer from the oxidation substrate to molecular oxygen.

Recently, the ETIO concept was expanded to an entire family of oxidation mechanisms in which the common feature being electron transfer as an integral part of the mechanism. For instance, the rate-limiting deprotonation in the oxidation of NH or NH compounds could enter this mechanism.

In addition, the oxidant can be either molecular oxygen or a high-valence metal complex [43].

Below is depicted the simplest possible description of an ETIO mechanism using tetrahydrocarbazole as a model substrate (case of rate-limiting electron transfer). In this reaction, the first step is the rate-limiting step with the last two steps being very fast relative to it:



The rate law from the simplest depiction of an ETIO is second-order overall (first-order in both reactants), whereas the peroxyl radical chain mechanism is first-order overall (first-order in [RH] under sufficient oxygen pressure; it is important to note that both mechanisms form the same initial oxidation product (RO<sub>2</sub>H).

The interpretation of several recently published studies, mainly in the fields of diesel fuels, supports this novel class of reaction.

## OXIDATION OF ASPHALTS AND ASPHALTS CONSTITUENTS

### *Asphaltenes and maltenes*

Asphaltenes are largely exposed to chemical degradation and oxidation due to their various functional groups and free-radical centers [44]. Asphaltenes may be of

diverse quality; their nature, among other things, depends particularly on the isolation procedure.

The proposed asphaltene structural models [45,14] raise a number of unsolved problems concerning their chemical nature and structure. Finally, one must bear in mind that the thermal decomposition of the asphaltenes in the absence of oxygen occurs readily at a variety of temperatures to yield products varying from low-molecular-weight gases on the one hand to high-molecular-weight, benzene-insoluble material on the other [46].

Asphaltenes separated with pentane or heptane from a Cerro Negro atmospheric distillation residue have been the starting point for oxidation studies at 85°C in *o*-dichloro-benzene solutions [47]: oxygen absorption curves against time showed the typical concave downwards curve for hydrocarbon oils with variable aromatics contents [41]. The maltenes resulting from the same separation were much less oxidizable. Finally, only small differences in oxygen absorption were observed with asphalts from different origins (Arabian light, Boscan, Safaniya, Cerro Negro).

The higher resistance to oxidation found with maltene is confirmed by another study which points out the higher concentration of natural antioxidants in resins [48].

Differential scanning calorimetry (DSC) and thermogravimetric analysis (TGA) have been used to study the oxidation characteristics of several asphaltenes originating from a Maya crude [49]: the DTG curve showed a bump at temperatures between 200° and 300°C and the TGA curve allowed to calculate a loss of mass of  $\approx 10\%$  up to 400°C. At temperatures higher than 400°C, there is a rapid loss of mass and the samples are completely oxidized into gaseous products. On the contrary, the maltene fraction started to lose mass at temperatures lower than 200°C. The TGA curve exhibited a profile which resembled very much the oxidation TGA for some aromatic fractions of the heavy residues.

At  $\approx 500^\circ\text{C}$ , the profile of mass loss for the residue and the asphaltene fraction was very similar but the oxidation reactions occurred at faster rates for the asphaltenes and the residue than for the maltenes. This was explained by a catalytic effect provided by the transition metals being much more concentrated in the asphaltene fraction ( $\approx 1100$  ppm) than in the maltene fraction ( $\approx 35$  ppm).

The Arrhenius plot for asphaltene oxidation under TGA conditions confirmed that the oxidation proceeds through at least two different overall mechanisms: an activation energy of  $\approx 170$  kJ/mol was attributed to the oxidation of linear or small hydrocarbon species, whereas an  $E_a$  of  $\approx 250$  kJ/mol was thought to be the result of the rupture of some highly stabilized structure.

Asphaltenes have chemical structures which are probably only exceeded in complexity by coal. Several researchers have carried out oxidative degradation in order to get some idea of their structure, the condition being that it should be sufficiently selective to leave enough recognizable structures intact that are still representative of the whole molecule.

Asphaltenes isolated from a sample of Athabasca oil sands were treated with chromic acid or sodium dichromate at room temperature during one week [27]; these agents are fairly selective in that they cleave alkyl chains from aromatic rings. The products of oxidation were separated into three classes of compounds: acids, bases and neutrals. The majority of acid products were carboxylic acids: aliphatic mono- and dicarboxylic

acids ranging up to  $C_{32}$  and aromatic acids, with most of them having no more than two rings. A small number of heterocyclic acids were present, two containing sulfur and two containing nitrogen.

The neutral aromatic compounds presented no indication of having been derived from the oxidation of a larger molecule.

The basic fraction showed the presence of piperidine, quinoline and *N*-methyl- $\alpha$ -pyridone.

When asphalt was oxidized with acidic sodium dichromate, a large number of mono- and dicarboxylic acids were formed: dicarboxylic acids were assumed to be derived from paraffinic-type materials and monocarboxylic acids from the alkyl chains on the aromatic rings [50].

Oxidation of Athabasca asphaltenes with common oxidizing agents, i.e., acidic and alkaline peroxide, acidic dichromate and alkaline permanganate, was shown to be slow with less than 10% of the product soluble in alkali after about 30 h treatment and reflux for 5 h [51].

The H/C ratios of the partially oxidized products suggest that there were two predominant oxidation routes: (1) oxidation of naphthene moieties to aromatics and active methylene groups to ketones; and (2) partial degradation of naphthene and aromatic functions to carboxylic functions with consequent diminution of aromatic moieties and an increase of the alkane ones.

The alkaline permanganate oxidation of Gudao asphaltenes gave mainly carboxylic acids (73.7%) [52] with a distribution similar to that found by Bachelor [27] with the exception of the presence of numerous polycarboxylic acids.

The progressive oxidation of asphaltenes by refluxing in concentrated nitric acid (70%) led to a massive degradation in the course of which material was steadily converted to water-soluble products. The widespread formation of carboxylic acids accounted only in part for the large oxygen uptake, whereas carbonyl and hydroxyl groups seemed the most important among the other oxygenated structures [53].

A study of the behavior of asphaltenes in an acid solution of Fe (III)-ions has been undertaken with a naphthenic-base crude oil [54]: the Fe (III)-ion in HCl solution is a relatively selective oxidizing agent [55], which generally does not break rings.

It was observed by I-R absorption that long methylene chains were present in the oxidation products and these were supposed to be originally part of the asphaltene structure. Moreover, free carboxylic groups were assumed to be very rare in the structure of the examined asphaltenes. A noticeable increase in the carbonyl content suggested that a great number of active methylene groups and hydroxyl groups should be present in the structure of the native asphaltenes. A decrease in content of aromatic hydrogen from 12 to 7% and an increase in aliphatic hydrogen from 88 to 93% indicated an enlargement of the asphaltene polycondensed nucleus in this oxidation.

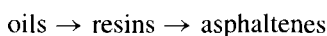
The oxidative demetallization of asphaltenes was undertaken with air at 100°C, NaOCl and peracetic acid [56]. The powerful oxidants typified by sodium hypochlorite and peroxyacetic acid exhibited high demetallization activity coupled with the ability to remove or destroy petroporphyrins. Two alternative paths for demetallization were hypothesized. In the first one, the metal atom is oxidized (e.g.,  $V^{4+} \rightarrow V^{5+}$ ), possibly leading to destabilization of the metalloporphyrin complex. The second pathway,



which was preferred, involves attack by the oxidant directly on the porphyrin, thereby destroying the ligand which binds the metal.

Oxidation of oils and resins from an Athabasca bitumen at 76–150°C in the presence of several metal salts [46] displayed the following results. The resins yielded, in the majority of cases, asphaltene-type products (max. 20 wt%) and an acceleration of oxygen uptake was noted in all the cases where the metal salts (Mn, Co, Fe, Pb, Al) were employed relative to the uncatalyzed oxidation.

The oxidation of the oils produced up to 20 wt% resins. It has been postulated that condensation was one of the essential transformations which occurred during the oxidation. The overall uptake of oxygen during this process indicated that its role was little more than that of a catalyst and the transformations which occurred may be represented by the following equation:



The criteria for the formation of resin material from the oil fraction may not only involve condensation of the components to higher-molecular-weight material, but also oxygen incorporation as hydroxyl and carbonyl groups. This would obviously alter the polarity of the reacted material to such an extent that it is then isolated as resins as dictated by the separation procedure.

It has been shown that resins are responsible for the peptization of asphaltenes in the oily medium and, hence, the stability of heavy oils, bitumens and asphalts. One of the means by which the resins peptize the asphaltenes is supposed to involve intermolecular hydrogen bonding between the two. Should this situation be disturbed as, for example, by the incorporation of polar groups into, say, the asphaltenes, it is then reasonable to assume that intramolecular hydrogen bonding will compete favorably with, and may even supersede, the intermolecular hydrogen bonding, ultimately resulting in depeptization of the asphaltenes and their deposition from the matrix.

Ruthenium (VIII)-catalyzed oxidation of asphaltene and maltene from Athabasca oil sand bitumen has suggested that in asphaltene the most prevalent side chain is that with 15 carbon atoms and in the maltene it is the one with 11 carbons. There were also bridging methylene chains present,  $-(CH_2)_n-$  where  $n$  varies from 6 to 11 [57]. These long alkyl chains have an important influence on the physical and chemical properties by increasing their solubility and increasing their capacity to form micelles in the hydrocarbon portion of the bitumen.

### *Oxidation of asphalts*

#### *Nature of the products and mechanisms*

It is generally known that asphaltenes are being formed in the process of asphalt air-blowing, but the mechanism of their formation is not well understood, although many attempts have been made to understand the mechanism [58].

Generally, it is believed that during air-blowing of an asphalt some oil components are converted into resins and the latter are converted into asphaltenes. It has been shown [59,60], however, that dehydrogenation and polymerization reactions are involved and that oxygen is not added to the asphalt product except in a very minor amount.

Boduszynski [61] has investigated the changes in the molecular size and the content of asphaltenes upon air-blowing of a SR-125 asphalt. These results show that air-blowing of the asphalt at temperatures ranging from 200° to 280°C leads not only to the increase in the asphaltene content, but also to the significant increase in the molecular size of asphaltene.

Moreover, a separation of the blown asphalt in chemically uniform groups of components such as acids, bases, saturates, aromatics-1, aromatics-2 and aromatics-3, has provided the following results. (1) There is no change in the amount or in the molecular size of saturates present in the asphalt. (2) A significant decrease (25%) is observed in the amount of the aromatics-1 fraction, but there is no change in the molecular size of components present in this fraction. (2) The amount of aromatics-2 fraction decreases upon air-blowing and the molecular size of components of this fraction increases slightly. (4) The aromatics-3 fraction increases in quantity and in molecular size.

Upon air-blowing, the amount of bases remains constant, but their molecular size increases significantly: the amount of acids present and their molecular sizes rapidly increase.

From these results, it was concluded that the formation of asphaltenes upon air-blowing was determined by two mechanisms. (1) Asphaltene formation due to the association through hydrogen bonding, resulting in the formation of aggregates of limited solubility. (2) Asphaltene formation due to chemical reactions occurring in the asphalt upon oxidation, giving high-molecular-size material of limited solubility. This lower solubility is the result of two major factors: (a) the ratio of low- to high-molecular-size components, and (b) the ratio of polar to non-polar compounds present in the treated asphalt.

Similar results were obtained by other authors on different bitumens [62–65]. All the results led to conclude that the predominant trend in the reaction with air or oxygen was the formation of more complex material of higher molecular weight and increased polarity.

Unfortunately, most of the published results were only semi-quantitative as the experimental technique gave no quantitative measure of the extent of oxidation. To fill this gap, Babu [66] confirmed that the concentration of saturates in the bitumen was not affected by the extent of oxidation, whereas the aromatic content steadily decreased with increasing extent of oxidation. The resin content decreased steadily until the extent of oxidation reached 50 mg O<sub>2</sub>/g bitumen and then increased. Beyond 75 mg O<sub>2</sub>/g bitumen, the resin content decreased again.

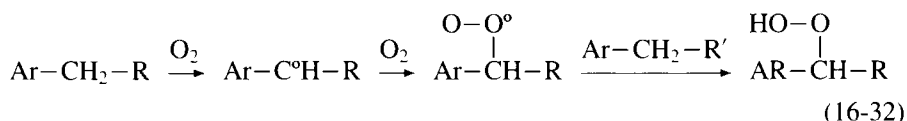
The aromatic fraction was converted to resin and then to asphaltene as the oxidation proceeded. Because of the serial nature of the oxidation process and the most readily oxidizable native resin fraction, the resin composition was observed at first to decrease, then increase and subsequently decline again as oxidation proceeded.

Lee et al. [67] have studied the effect of low-temperature oxidation on heavy oil in a rocking high-pressure reactor and have analyzed the evolution of maltenes, asphaltenes, THF solubles and coke. They found that the presence of oxygen promotes the formation of the three last classes of compounds. The asphaltenes present after oxidation contained increased amounts of sulfones, alcohols, aldehydes, ketones, phenols and carboxylic acids or esters. It was concluded that many of the oxygenated products were so polar

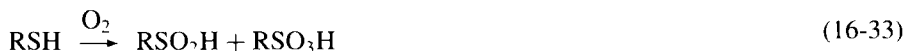
that they could not be isolated as part of the asphaltene fraction. Incorporation of oxygen increased the molecular weight and the polarity of the compounds, thus causing them to become insoluble in toluene.

Petersen et al. [68] have reported studies on the reactivity of sulfur entities in asphalts during air oxidation at 130°C on a thin film: although most of the sulfur in the asphalts appeared oxidizable to sulfones, the relative amount of easily oxidized sulfides may vary considerably with the source of the crude. The concentration of sulfoxides formed during air oxidation was found to rapidly reach a maximum value and, subsequently, remain constant on further oxidation. Model studies indicated that hydroperoxides played a role in sulfoxide formation.

The following mechanism involving a hydroperoxide was proposed by Khairudinov et al. [69] in order to explain the sulfoxide formation from sulfide at 230–290°C:



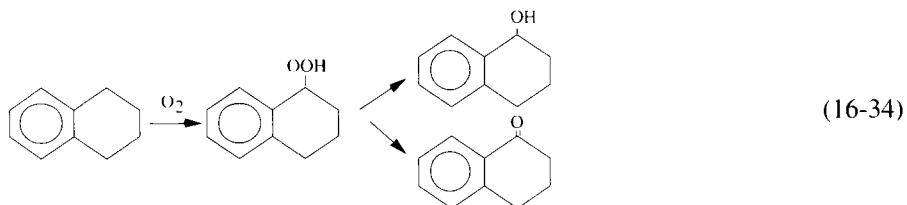
When subjecting a virgin heavy oil to analytical pyrolysis and comparing the sulfur dioxide yields to the low-temperature oxidation product (LTO), Lee et al. [67] concluded that the increase in oxygen content and acidity had to be associated with the formation of sulfinic or sulfonic acid:



This reaction as well as the reaction of sulfides to sulfoxides or sulfones has the consequence to produce molecules with sufficient polarity to cause them to be insoluble in heptane, for instance, and thus to find them in the asphaltene fraction, although they could have been in the maltene fraction before oxidation. This is consistent with the often mentioned reduction in sulfur content of the maltene fraction upon oxidation.

In a study using a thin-film accelerated aging test for evaluating asphalt oxidative aging, Petersen et al. [70] showed that the level of ketone formation could reach 0.4 mol/l at 130°C after 24 h. The increase in ketone concentration on oxidation roughly paralleled the logarithm of the increase in viscosity.

The ketone formation could be explained by a classical oxidation mechanism, such as the one proposed for cyclohexanone or tetralin oxidation by Neumann [71]:



These products will continue to react to produce a mixture of aldehydes and carboxylic acids, and finally, they will give rise to asphaltenes (and, consequently, to an increase in the mean molecular weight) by condensation reactions.

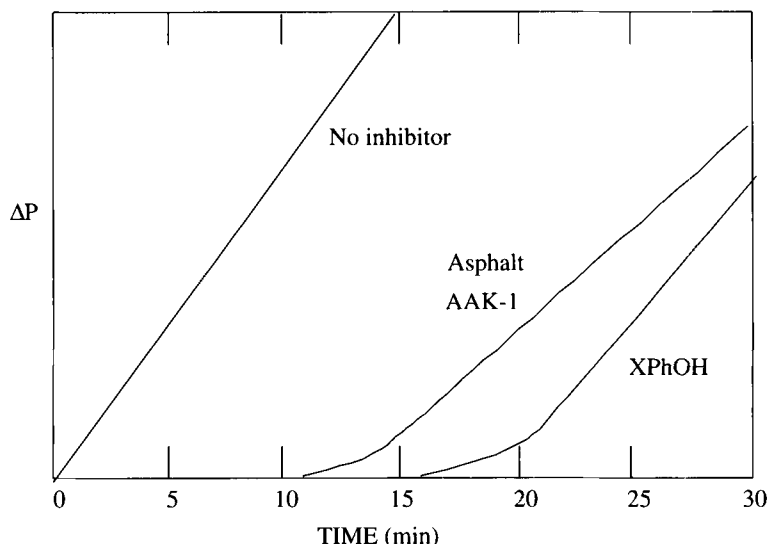


Fig. 16-3. Inhibition kinetics for cumene oxidation (50°C) (XPhOH = 2,6-di-*t*-butyl-4-methyl phenol).

#### *Inhibitors and prooxidants in asphalt oxidation*

Mill and Tse [72] have focused their efforts on understanding the mechanistic basis for slow oxidation in order to predict how rapidly an asphalt will oxidize, based on its composition, and to find better ways to inhibit the process. Two different mechanisms have been proposed for the oxidation of asphalt in the absence of light: (1) free-radical oxidation, and (2) molecular oxidation. The distinction between these two processes is important, because the first process may involve participation of free radicals which are typically inhibited by phenolic antioxidants, whereas molecular oxidation requires use of oxygen scavengers or the removal of oxygen-reactive components.

By measuring rates of oxidation of *p*-methoxyphenol by alkyl peroxy free radicals in the presence of each of six asphalts, and using an added azoinitiator, they have calculated the amount of native inhibitor present in each asphalt.

The amount of inhibitors in asphalt kinetically measured varied over a four-fold range, without apparent relationship to the amounts of asphalt phenols measured by I.R.

The same authors also measured the inhibitor content of each of the core asphalts by measuring the time required for the uptake of oxygen in cumene, oxidized at 50°C with AIBN as a source of  $\text{RO}_2^\circ$  radicals and inhibited with small amounts of the core asphalts. Fig. 16-3 shows the relation of oxygen uptake with time to concentration of the inhibitor. When there is an inhibitor, it is preferentially oxidized to a very low level; then cumene oxidation begins and this time ( $t_{\text{inh}}$ ) is related to the inhibitor concentration by the relation:

$$[\text{inh}] = t_{\text{inh}} \times r_i$$

where  $r_i$  is the rate of production of  $\text{RO}_2^\circ$  radicals.

By comparison, a core asphalt which had been methylated to remove all phenolic OH (but not amines) presented no inhibition of cumene oxidation, confirming that inhibition

is caused entirely by phenol radical chain-breaking antioxidants. It was observed that no obvious correlation existed between the inhibitor, determined by several methods, and asphaltene content.

Sidorenko et al. [73] have studied the possible application of a kinetic model for the quantitative estimation of the inhibiting ability of natural compounds in petroleum, resins and asphaltenes. As a model chain reaction, they used the initiated oxidation of cumene at 60°C for which the following integral formula could be derived:

$$\frac{[O_2]}{[RH]_0} = -\frac{k_3}{k'_3} \ln \left( t - \frac{t}{\tau} \right)$$

where  $t$  = time,  $\tau$  = the induction period,  $k_3$  ( $k_3 = 1.75 \text{ l mol}^{-1} \text{ s}^{-1}$  at 60°C) = the rate constant of chain propagation,  $k'_3$  is the rate constant for the reaction of the inhibitor with an active center,  $[O_2]$  = the concentration of absorbed oxygen, and  $[RH]_0$  is the initial cumene concentration.

They found that petroleum and its high-molecular-weight components contain several types of inhibitor groups whose activity  $k'_3$  can be estimated from the slopes of the linear section of the broken line obtained when plotting  $[O_2]/[RH]_0$  as a function of  $-\ln[t - (t/\tau)]$ .

The highest value of  $k'_3$  was found to be  $\approx 8 \times 10^5 \text{ l mol}^{-1} \text{ s}^{-1}$  in resins (West Siberian petroleum) while the largest concentration of inhibitor was calculated to be  $\approx 0.3 \text{ mol/kg}$  in the asphaltenes of the same source. The conclusion was that the antioxidative ability of natural inhibitors in petroleum equals or even surpasses the activity of known commercial stabilizers such as 2,6-di-tert-butyl-4-methylphenol. Similar studies showed that the highest concentration of antioxidants were located in the alcohol- $C_6H_6$  extract part of the resins [48].

Other authors [74] used the same method in order to evaluate the degree of catagenetic (thermal) or biodegradative (oxidative) transformation of oils from the inhibitor content in the late stages of diagenesis. Their results showed that with increasing age of oils in the course of oil methanization, the content of resins and asphaltenes capable of inhibiting radical-chain oxidation processes decreases.

On the contrary, metals tend to promote oxidation. For instance, it has been shown that vanadyl porphyrins increased asphalt oxidation, particularly as measured by the increase in ketones [75]. However, correlation of asphalt oxidation with vanadyl porphyrin concentration was observed to be linear, only when various amounts of asphalts were diluted in a light fraction of the same crude. Several reasons were proposed to explain this phenomenon.

The heat treating of the atmospheric residue at 120°C in the presence of cumene hydroperoxide (2 wt%) for 6 h, with the goal of increasing the amount of feed for catalytic cracking, has shown a three-fold decrease in metal content [76]: this lowering of metal content in heavy fractions of crude oil during their oxidation is assumed to be caused by the decomposition of metal-organic complexes and metal oxide formation, which are very stable compounds. So the hydroperoxide decomposes into free radicals, which are in turn deactivated by the asphaltene free radicals; the rest of the free radicals decomposes metal-organic complexes and activates the processes leading to the increase of molecular mass of the reaction products.

The influence of metal or metal salts has been pointed out in many publications: for instance, the oxidation of asphalt at 200°C in the presence of 2 m<sup>2</sup> of metal surface per ton of substrate showed a 5- to 8-fold increase in the reaction rate in the presence of Fe or steel, depending on the composition of the substrate [77].

The catalytic air-blowing of asphalt at 240°C has been studied in the presence of several chlorides of metal (Mn, Ni, Sn, Cr, Zn, Cu, Fe) and MnO<sub>2</sub>: the reaction velocity calculated as the average softening point change per hour increased with the salt concentration (0.3–0.6 wt%) in all cases. The rate was more than twice as high in the presence of ferric chloride compared to blank asphalt; it was the fastest in the case of ferric chloride followed by copper chloride and other salts.

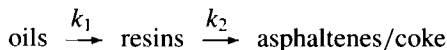
### *Kinetics and factors influencing asphalt oxidation*

Most studies reported in the literature are related to asphalt air-blowing or in-situ combustion processes. Very often, authors define two regimes depending upon temperature: a low-temperature oxidation (LTO) up to 150–250°C, and a high-temperature-oxidation above this temperature range.

Adegbesan et al. [78,79] investigated the LTO reactions of the components of bitumen and heavy oils in a laboratory-stirred semiflow batch reactor. Kinetic studies were carried out in the 333 K to 423 K temperature range and at an oxygen partial pressure of 50 to 2233 kPa. On the basis of experimental kinetic data, two main types of reaction models were proposed: (1) a non-steady-state kinetic model representing the overall rate of oxygen consumption; and (2) four non-steady-state multiresponse kinetic models representing the oxidation reactions of the liquid phase components. A typical set of curves of concentration vs. reaction time or oxygen partial pressure are presented in Figs. 16-4 and 16-5 of kinetic reactions at 408 K. These data indicate that the LTO reactions of Athabasca bitumen consist of a series of consecutive steps resulting in the formation of the asphaltene/coke component from the oils, with the resins as the intermediate components. It is interesting to note that the deviation of a single data point from the resins-I curve was reproduced at different temperatures (Resins I is issued from Soxhlet extraction with chloroform and Resins II with tetrahydrofuran). The oxygen partial pressure had a relatively strong influence on the overall rate of oxygen consumption. A second-order dependency on oxygen partial pressure was estimated for the overall rate of consumption of oxygen, whereas reaction orders between 0 and 1 were found for the bitumen lumped components.

A single reaction mechanism was found adequate for describing the overall rate of oxygen consumption. However, for the reactions of the lumped components, more than one mechanism may be assumed to take place in the temperature range considered.

The following simple model yielded excellent predictions of the LTO reactions:



with  $k_1 = 5.79 \times 10^{-4} \text{ h}^{-1} \text{ kPa}^{-0.41}$  and  $k_2 = 7.08 \times 10^{-4} \text{ h}^{-1} \text{ kPa}^{-0.5}$  at 378 K.

The Arrhenius plots for the two reaction rate coefficients were linear in the 378–423 K range and gave  $E_a$  values of 77.2 and 86.7 kJ mol<sup>-1</sup>.

A calorimetric method has been applied to the rate of oxidation of Athabasca bitumen [80]: application of a simple kinetic model for the analysis of the measurements led to

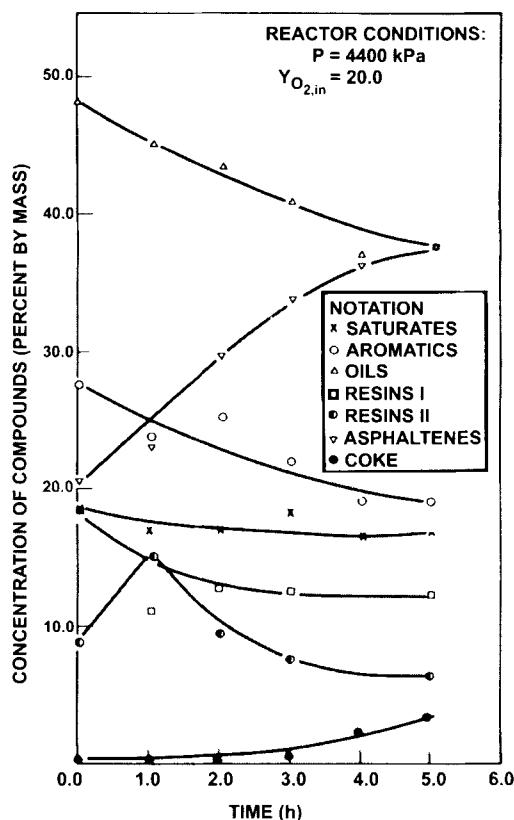


Fig. 16-4. Conversion of bitumen at 408 K.

an apparent activation energy of  $64 \pm 6 \text{ kJ mol}^{-1}$  between  $155^\circ$  and  $210^\circ\text{C}$ , which is the same as that found by Yoshiki et al. [81], using differential thermal analysis (DTA). However, the reaction order with respect to oxygen was 0.62 in the first case and 0.98 in the DTA results.

The oxidation reaction kinetics of Athabasca bitumen has also been investigated in a flow-through fixed-bed reactor at 448–573 K using gas mixtures of various compositions [82]. The oxidation was found to be first-order with respect to oxygen concentration. Two models were examined: in the first, the bitumen was considered to be a single reactant and the activation energy for the overall reaction was found to be  $80 \text{ kJ mol}^{-1}$ ; the second model assumed that the oxidation of bitumen was described by two simultaneous parallel reactions, one producing oxygenated hydrocarbons and water, the other CO and  $\text{CO}_2$ . The activation energy of the first reaction was found to be  $67 \text{ kJ mol}^{-1}$ , and for the second  $145 \text{ kJ mol}^{-1}$ .

Similar results were obtained by Barta and Hepler [83], who obtained an activation energy of  $43 \text{ kJ mol}^{-1}$  and an order with respect to oxygen of 0.55 at temperatures much lower than  $285^\circ\text{C}$ , at which the predominant reactions of oxygen with bitumen led to the deposition of coke as a result of partial oxidation. At temperatures much higher

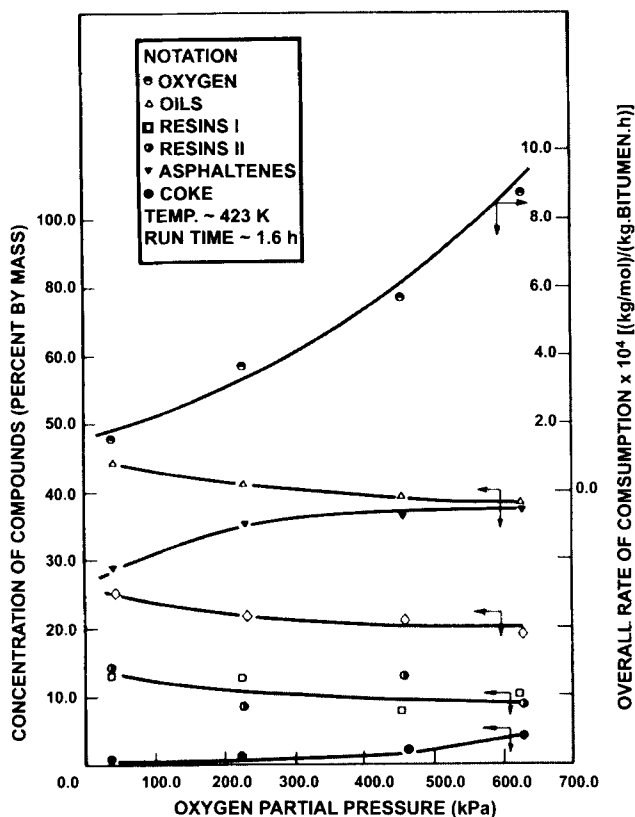


Fig. 16-5. Effect of oxygen on partial pressure and reaction rates.

than 285°C, the heavy residue is converted completely to carbon oxides and water with an activation energy of 132 kJ mol<sup>-1</sup> and a reaction order of 1.15. The rapid change in the temperature dependence of both the reaction order and rate constant at 285°C led the authors to consider two important classes of reactions as the principal contributors to the overall rate of oxidation. The first class of reactions leads to formation of coke and oxygenated bitumen, whereas the second class of reactions leads to burning of coke and other hydrocarbons. The first class of reactions is most important at low temperatures, whereas the second class of reactions becomes more important at high temperatures, with 285°C being the 'transition temperature'. Finally, the complete combustion occurred at 317°C.

Complete oxidation of sulfur to volatile products would occur between 155° and 225°C suggesting that sulfide linkages are broken and sulfur is removed as volatile product of oxidation. This result is different from that of Moschopedis and Speight [65], who found that the sulfur content remained constant at temperatures less than 250°C. These authors found that the majority of oxygen present in the original bitumen (Athabasca) and in the oxidized product occurred in the asphaltenes and resins, with



no detectable amounts of oxygen in the saturate and aromatic fractions. They proposed that, in the conversion of original resins to asphaltenes and simultaneous conversion of oils to resins, oxygen is for the most part a catalyst for condensation reactions, being incorporated initially as labile functional groups that promote these reactions and subsequently eliminated as water.

The high viscosity limitation of a stirred reactor system (see Adegbesan et al. [78,79]), imposes severe constraints on the oxidation times and temperatures. That is the reason why a plug flow reactor system packed with re-constituted Athabasca oil sands was selected by Millour et al. [84]. They also found that the oxygen uptake did not follow typical Arrhenius behavior over the temperature range investigated (22° to 275°C)

The effect of the oxygen partial pressure was very important at low temperatures, but the reaction order, with respect to oxygen partial pressure, approached zero at temperatures about 175°C. They identified three definable low-temperature oxidation reaction regions. Transitions between the regions were characterized by the rapid formation of coke and the virtual disappearance of the asphaltene fraction. In the first region, which corresponds to the total oxygen uptake of less than 0.04 g O<sub>2</sub>/g oil, essentially no coke was formed; hence, the main reaction was supposed to be maltenes converting to asphaltenes. Thus, the asphaltene yield depended on the degree of oxidation and, to a lesser extent, on the temperature and oxygen partial pressure.

The second region corresponded approximately to the total oxygen uptake between 0.04 and 0.2 g O<sub>2</sub>/g oil; the coke concentration was between 3% and 55%. Coke was formed quickly at the expense of the asphaltene and maltene fractions. However, no coke formation was reported at temperatures of 100°C and below.

In the third region, the coke concentration was greater than 55% and, in most cases, the coke was beginning to be consumed by high-temperature reactions. Asphaltenes were at a relatively low level and maltenes remaining in the coke appeared to be converting directly to coke.

## CONCLUSIONS

Oxidation of bitumens, while appearing to be relatively easy, is in fact a complicated sequence of reactions and interactions.

The main reactions are dehydrogenation, condensation, and polymerization of unsaturated species, the predominant trend being the formation of more complex material of higher molecular weight and increased polarity. Reaction variables are reported in the literature, but the difference in various asphalt types does not make it easy to compare the results. Moreover, most of the results are only semi-quantitative, because they do not give any quantitative measure of the extent of oxidation.

The complexity of oxidation studies on asphalts originates from the presence of several types of inhibitors and prooxidants in bitumen, and authors generally agree to locate the highest concentration of antioxidants in the resin fraction.

The most recognized scheme of asphalt oxidation involves the conversion of the original resins to asphaltenes and simultaneous conversion of oils to resins, with oxygen

being initially partly incorporated as labile functional group and subsequently eliminated as water.

In the kinetic study of asphalt oxidation, great care must be taken of oxygen diffusion through viscous material: a promising technique could be the thin-film oxidation.

Finally, the mechanism seems to change when increasing the temperature: a first 'transition' temperature is located around 150°C and the second one near 285°C. Above this temperature, the conversion to carbon oxides and water are favored.

## REFERENCES

- [1] Tissot, B. and Welte, D., *Petroleum Formation and Occurrence*. Springer, Berlin, 2 ed. (1984).
- [2] Corbett, L.W., Composition of asphalt based on generic fractionation using solvent deasphalting, elution-adsorption chromatography and densimetric characterization. *Anal. Chem.*, 41: 576 (1969).
- [3] Jewell, D.M., Weber, J.M., Bunger, J.W., Plancher, H. and Latham, D.R., Ion exchange, coordination and adsorption chromatographic separation of heavy-end petroleum distillates. *Anal. Chem.*, 44: 1391 (1972).
- [4] Reichert, C. and Grant, L., Liquid chromatography chemical class analysis of bitumen and heavy petroleum crudes. *Am. Chem. Soc., Div. Fuel Chem.*, 23: 72 (1978).
- [5] Suatoni, J.C. and Swab, R.E., Rapid hydrocarbon group types analysis by HPLC. *J. Chromatogr. Sci.*, 13: 361 (1975).
- [6] Brule, B., Report LPC Nr. 76, March 1978, Paris.
- [7] Nellensteyn, F.I., The colloidal structure of bitumens. In: A.E. Dunstan (Editor), *The Science of Petroleum*, Vol. IV. Oxford University Press, London (1938).
- [8] Such, C., Ramon, G. and Brule, B., The viscous behavior of bitumens related to the distribution of molecular sizes. In: *Characterization of Heavy Crude Oils and Petroleum Residues*. Technip, Paris, p. 486 (1984).
- [9] Briant, J. and Hotier, G., Etude de l'état des asphaltènes dans les mélanges d'hydrocarbures. *Rev. Inst. Fr. Pét.*, 38: 83 (1983).
- [10] Speight, J.G., Solvent effects in the molecular weights of petroleum asphaltenes. *Prepr. Am. Chem. Soc., Div. Pet. Chem.*: 825 (1981).
- [11] Speight J.G., Moschopedis S.E., On the molecular nature of petroleum asphaltenes. In: *Chemistry of Asphaltenes, Advances in Chemistry Series*, 195, American Chemical Society, Washington, DC, p. 1 (1981).
- [12] Yen, T.F., Present status of the structure of petroleum heavy ends and its significance to various technical applications. *Prepr. Am. Chem. Soc., Div. Pet. Chem.*, 17 (4): 102 (1972).
- [13] Speight, J.G., The chemical nature of petroleum asphaltenes, In: *Characterization of Heavy Crude Oils and Petroleum Residues*. Technip, Paris, p. 32 (1984).
- [14] Yen, T.F., Structure of petroleum asphaltene and its significance. *Energy Sources*, 1: 447 (1974).
- [15] Koots, J.A. and Speight, J.G., Relation of petroleum resins to asphaltenes. *Fuel*, 54: 179 (1975).
- [16] Kolbanovskaja, A.S. and Mihajlov, V.V., *Les Bitumes Routiers*. Transport, Moscow (1973).
- [17] Dron, R., Bestougeff, M.A. and Voinovitch, I.A., Rapport de recherche, LCPC, Mars, Nr. 75 (1978).
- [18] Dickie, J.P., Haller, M.N. and Yen, T.F., Electron microscopy investigations on the nature of petroleum asphaltics. *J. Colloids Interface Sci.*, 29: 475 (1969).
- [19] Yen, T.F., The charge-transfer nature of bitumens. *Fuel*, 52: 93 (1973).
- [20] Allen, D.T., Grandy, D.W. and Petrakis, L., Comparative structural profiles of heavy bitumens by a novel functional group analysis. In: *Characterization of Heavy Crude Oils and Petroleum Residues*. Technip, Paris, p. 309 (1984).
- [21] Petrakis, L., Allen, D.T., Gavalas, G.R. and Gates, B.C., Analysis of synthetic fuels for functional group determination. *Anal. Chem.*, 55: 1557 (1983).

- [22] Bouquet, M., Roussel, J.C. and Neff, B., Round Robin test for aromaticity measurement of heavy ends of petroleum by Carbon-13 Proton Magnetic Nuclear Resonance. In: *Characterization of Heavy Crude Oils and Petroleum Residues*. Technip, Paris, p. 322 (1984).
- [23] Schmitter J.M., Ignatiadis I., De Rycke G., Dorbon M., Arpino P., Distribution of polyaromatic heteroatomic nitrogen and sulfur compounds in crude petroleum. In: *Characterization of Heavy Crude Oils and Petroleum Residues*. Technip, Paris, p. 109 (1984).
- [24] Petersen, J.C., Barbour, R.V., Dorrence, S.M., Barbour, F.A. and Helm, R.V., Molecular interaction of asphalt. *Anal. Chem.*, 43: 1491 (1971).
- [25] Clerc, R.J. and O'Neal, M.J., The mass spectrometric analysis of asphalt. *Anal. Chem.*, 33: 380 (1961).
- [26] Moschopedis, S.E., Hawkins, R.W. and Speight, J.G., Identification of nitrogen functional groups in Athabasca bitumen. *Fuel*, 60: 397 (1981).
- [27] Bachelor, F.W. and Okazawa, N.E., Oxidation degradation of Athabasca oil sands asphaltenes. In: *Characterization of Heavy Crude Oils and Petroleum Residues*. Technip, Paris, p. 462 (1984).
- [28] Moschopedis, S.E. and Speight, J.G., Oxygen functions in asphaltenes. *Fuel*, 55: 334 (1976).
- [29] Nicksic, S.W. and Jeffries-Harris, M.J., Acid precipitation of crude oil asphaltenes — structural implications. *J. Inst. Pet.*, 54: 107 (1968).
- [30] Ignasiak, T., Strausz, O.P. and Montgomery, S., Oxygen distribution and hydrogen bonding in Athabasca asphaltene. *Fuel*, 56: 359 (1977).
- [31] Ignasiak, T.M., Kemp-Jones, A.V. and Strausz, O.P., The molecular structure of Athabasca asphaltene. Cleavage of the carbon-sulfur bonds by radical ion electron transfer reactions. *J. Org. Chem.*, 42: 312 (1977).
- [32] Dutta, P.K. and Holland, R.J., Acid-base characteristics of petroleum asphaltenes as studied by non-aqueous potentiometric titrations. *Fuel*, 63: 197 (1984).
- [33] Ignasiak, T.M. and Strausz, O.P., Reaction of Athabasca asphaltene with tetralin. *Fuel*, 57: 617 (1978).
- [34] Kharasch, N. and Meyers, C.Y., *The Chemistry of Organic Sulfur Compounds*, Vol. 12. Pergamon, New York (1966).
- [35] Yen, T.F., Chemical aspects of metals in native petroleum. In: *The Role of Trace Metals in Petroleum*. Ann Arbor, MI (1975).
- [36] Barwise, A.J.G. and Whitehead, F.V., Characterization of vanadium porphyrins in petroleum residues. *Prepr. Am. Chem. Soc., Div. Pet. Chem.*: 28 (1980).
- [37] Novelli J.M., Medina J.C., Lena L., Maire Y., Ruiz J.M., Vincent E.J., Vanadium in asphalts. In: *Characterization of Heavy Crude Oils and Petroleum Residues*. Technip, Paris, p. 169. (1984).
- [38] Emanuel, N.M., Denisov, E.T. and Maizus, Z.K., *Liquid Phase Oxidation of Hydrocarbons*. Plenum Press, New York (1967).
- [39] Howard, J.A., in: J.K. Kochi (Editor), *Homogeneous Liquid Phase Autoxidation*, Vol. 2. Free Radicals. (1973).
- [40] Ingold, K.U., Inhibition of the autoxidation of organic substances in the liquid phase. *Chem. Rev.*, 61: 563 (1961).
- [41] Scott, G., *Atmospheric Oxidation and Antioxidants*. Elsevier, Amsterdam (1965).
- [42] Beaver, B.D. and Gilmore, C., Oxidative degradation of petroleum products via a non-peroxyl radical chain pathway. Electron transfer initiated oxidation (ETIO) revisited. *Fuel Sci. Technol. Int.*, 9: 811 (1991).
- [43] Beaver, B.D., Hazlett, R.N., Cooney, J.V. and Watkins, S.M., A new look at the mechanisms of oxidative sediment formation in fuels. *Fuel Sci. Technol. Int.*, 6: 131 (1988).
- [44] Hunt, J.M., *Petroleum Geochemistry and Geology*. Freeman, San Francisco, CA (1979).
- [45] Hirsch, E. and Altgelt, K.H., Integrated structural analysis. A method for the determination of average structural parameters of petroleum heavy ends *Anal. Chem.*, 42: 1330 (1970).
- [46] Moschopedis, S.E., Parkash, S. and Speight, J.G., Thermal decomposition of asphaltenes. *Fuel*, 57: 431 (1978).
- [47] Ronvaux-Vankeerbergen, A. and Thyron, F.C., Oxidation of petroleum asphalts and asphaltenes. *Fuel*, 68: 793 (1989).
- [48] Zeinalov, E.B., Samedova, F.I., Velieva, K.U., Ibad-Zade, A.D. and Mir-Babaev, M.F., Oxidation inhibiting activity of asphaltenes and resins. *Azerb. Khim. Zh.*, 2: 40 (1987).

- [49] Ayala, J.A., Ringon, M.E., Alarcon, E. and Ruiz, J., The oxidation of residues and asphaltenes from heavy crude oil. In: *Characterization of Heavy Crude Oils and Petroleum Residues*. Technip, Paris, p. 467 (1984).
- [50] Al-Samarraie, M.F. and Lena, L., A structural study of asphalt by oxidation with Cr(VI) compounds. *J. Pet. Res.*, 5: 101 (1986).
- [51] Moschopedis, S.E. and Speight, J.G., Oxidative degradation of Athabasca asphaltenes. *Fuel*, 50: 211 (1971).
- [52] Fan, W. and Yang, Q., Study of the structure of Guduo asphaltenes with alkaline permanganate oxidation. *Ranliao Huaxue Xuebao*, 16: 257 (1988).
- [53] Al-Samarraie, M.F. and Steedman, W., A study of the nitric acid oxidation of petroleum asphaltenes. *Liq. Fuels Technol.*, 3: 55 (1985).
- [54] Pfendt, P.A. and Vitorovic, D., Structural changes of crude oil asphaltenes by oxidation with acid solution of Fe(III) chloride. In: *Characterization of Heavy Crude Oils and Petroleum Residues*. Technip, Paris, p. 449 (1984).
- [55] Seubert, R. and Rotermund, W., Eisen (III)-Verbindungen als Oxydationmittel. In: Houben-Weyl, *Methoden der Anorganischen Chemie*, Band 4/1b Oxydation II (E. Müller, Editor). Georg Thieme, Stuttgart (1975).
- [56] Gould, K.A., Oxidative demetallization of petroleum asphaltenes and residue. *Am. Chem. Soc., Div. Pet. Chem.*, 25: 288 (1980).
- [57] Mojelsky, T.W., Montgomery, D.S. and Strausz, O.P., Ruthenium (VIII) catalyzed oxidation of high molecular weight components of Athabasca oil sand bitumen. *Aostra J. Res.*, 2: 131 (1985).
- [58] Hoiberg, A.M., *Bituminous Materials: Asphalts, Tars and Pitches*. Vol. 2, Part I, Asphalts. Interscience, New York, p. 257 (1965).
- [59] Corbett, L.W., Reaction variables in the air blowing of asphalt. *Ind. Eng. Chem., Process Des. Dev.*, 14: 181 (1975).
- [60] Haley, G.A., Changes in chemical composition of a Kuwait short residue during air blowing. *Anal. Chem.*, 47: 2432 (1975).
- [61] Boduszynski, M.M., Asphaltenes in petroleum asphalts-composition and formation. *Prepr. Am. Chem. Soc., Div. Pet. Chem.*, 24: 935 (1979).
- [62] Ishmukhamedova, N.K. and Dyusengaliev, K.I., Oxidation of resids in the presence of high-tar petroleum. *Khim. Tekhnol. Topl. Masel*, 8: 14 (1990).
- [63] Moschopedis, S.E. and Speight, J.G., Oxidation of a bitumen. *Fuel*, 54: 210 (1975).
- [64] Moschopedis, S.E. and Speight, J.G., Influence of metal salts on bitumen oxidation. *Fuel*, 57: 235 (1978).
- [65] Moschopedis, S.E. and Speight, J.G., The effect of air blowing on the properties and constitution of a natural bitumen. *J. Mater. Sci.*, 12: 990 (1977).
- [66] Babu, D.R. and Cormack, D.E., Effect of low-temperature oxidation on the composition of Athabasca bitumen. *Fuel*, 63: 858 (1984).
- [67] Lee, D.G., Noureldin, N.A. and Mourits, F.M., The effect of low temperature oxidation on the chemical and physical properties of maltenes and asphaltenes. *Prepr. Am. Chem. Soc., Div. Pet. Chem.*, 32 (3-4): 853 (1987).
- [68] Petersen, J.C., Dorrence, S.M., Nazir, M., Plancher, H. and Barbour, F.A., Oxidation of sulfur compounds in petroleum residues: reactivity-structural relationships. *Prepr. Am. Chem. Soc., Div. Pet. Chem.*, 26: 898 (1981).
- [69] Khairudinov, I.R., Dolomatov, M.Yu., Kul'chitskaya, O.V. and Amirova, S.I., Kinetic parameter of oxidation of petroleum residues. *Khim. Tekhnol. Topl. Masel*, 12: 20 (1991).
- [70] Petersen, J.C., A thin film accelerated aging test for evaluating asphalt oxidative aging. *Asphalt Paving Technol.*, 58: 220 (1989).
- [71] Neumann, M.J., Oxidation of bitumen at normal usage conditions. *Erdoel, Erdgas, Kohle*, 103: 131 (1987).
- [72] Mill, T. and Tse, D., Oxidation and photooxidation of asphalts. *Prepr. Am. Chem. Soc., Div. Pet. Chem.*, 35: 483 (1990).
- [73] Sidorenko, A.A., Kryazhev, Yu.G., Tsepalov, V.F. and Gladyshev, G.P., Quantitative estimation of

- stabilizers in petroleum and its compounds using a model reaction. *React. Kinet. Catal. Lett.*, 6: 1 (1977).
- [74] Burkova, V.N. and Pisareva, S.I., Oxidation inhibitors occurring in bioproducts, recent sediments, ancient rocks and oils. *Org. Geochem.*, 16: 763 (1990).
- [75] Branthaver, J.F., Nazir, M., Petersen, J.C., Dorrence, S.M. and Ryan, M.J., The effect of metalloporphyrins on asphalt oxidation, II. The effect of vanadyl chelates found in petroleum. *Liq. Fuels Technol.*, 2: 67 (1984).
- [76] Bukowski, A. and Gurdzinska, E., Investigation of the influence of the cumene hydroperoxide on the decrease of the metals contents in the fractions of crude oil. *Prepr. Am. Chem. Soc., Div. Pet. Chem.*, 25: 293 (1980).
- [77] Pokonova, Yu.V. and Apostolov, S.A., Oxidative reactivity of petroleum residues. *Fuel Sci. Technol. Int.*, 9: 109 (1991).
- [78] Adegbesan, K.O., Donnelly, J.K., Moore, R.G. and Bennion, D.W., Low-temperature-oxidation kinetic parameters for in-situ combustion: numerical simulation. *Soc. Pet. Eng. Reservoir Eng.*, 2: 573 (1987).
- [79] Adegbesan, K.O., Donnelly, J.K., Moore, R.G. and Bennion, D.W., Liquid phase oxidation kinetics of oil sands bitumen: models for in-situ combustion numerical simulations. *AIChE J.*, 32: 1242 (1986).
- [80] Zhang, Z.L., Barta, L. and Hepler, L.G., Calorimetric method for measuring rates of oxidation of bitumen in a porous medium. *Austra J. Res.*, 3: 249 (1987).
- [81] Yoshiki, K.S. and Phillips, C.R., Kinetics of the thermo-oxidative and thermal cracking reactions of Athabasca bitumen. *Fuel*, 64: 1591 (1985).
- [82] Phillips, C.R. and Hsieh, I., Oxidation reaction kinetics of Athabasca bitumen. *Fuel*, 64: 985 (1985).
- [83] Barta, L. and Hepler, L.G., Kinetics and energetics of oxidation of Athabasca bitumen. *Energy Fuels*, 2: 309 (1988).
- [84] Millour, J.P., Moore, R.G., Bennion, D.W., Ursenbach, M.G. and Gie, D.N., An expanded compositional model for low-temperature oxidation of Athabasca bitumen. *J. Can. Pet. Technol.*, 26: 24 (1987).

## Chapter 17

# A KINETIC APPROACH TO THE AGING OF BITUMENS

A.F. VERHASSELT

## INTRODUCTION

The aging of bituminous binders results mainly from oxidation reactions. These affect the different functionalities on the more or less complex chains of organic molecules constituting those binders. In the most commonly used asphalt mixes, i.e., in hot-mixed materials, the bitumen or any other bituminous binder is subject, during its life, to two successive types of aging:

(1) Rapid aging in construction: this includes all the changes that occur in the bitumen during mixing (at a temperature between about 150 and 190°C), transport and laying (at  $\pm 180$  to 120°C), and cooling (from  $\pm 130^\circ\text{C}$  to ambient temperature).

(2) Slow aging in service (or 'field' aging): this comprises all the changes that occur on site in the bitumen over the years of service of the pavement layer in which it has been used.

In the laboratory, accelerated tests are used to simulate bitumen aging. The process is sped up by increasing the test (or 'exposure') temperature (130 to 180°C), by providing a flow of air or oxygen and/or by stimulating the diffusion of oxygen in the binder (mixing, thin film). The most common tests, which are being seriously considered for European standardization, are RTFOT (the rolling thin film oven test [1]) and the DIN 52016 test [2]. They simulate in-construction aging in an adequate and satisfactory way.

However, as they are conducted at too high a temperature, they are unsuitable for simulating in-service aging: the processes induced are relatively different from those observed in the field [3,4]. Test temperatures, therefore, must be lower — probably below 100°C [3–5]. Another drawback of those tests is that the quantities recovered are rather small (of the order of a few grams), which greatly reduces the number of technological and physicochemical tests that can be performed on the aged sample. Moreover, to monitor the progress of aging with time, the measurements have to be made on a different sample at each preselected age (or 'exposure time'). Increasing the quantities (thicker film) and lowering the test temperature (e.g., 60 to 100°C) would result mainly in a surface reaction with very little tendency to homogenization in the bulk of the material.

For those reasons, and to do away with most of the above-described difficulties, a new test device has been designed and tried at the Belgian Road Research Center (BRRC). The device has been named RCAT: Rotating Cylinder Aging Test. With this device and the results obtained it has been possible to develop an overall kinetic approach to bitumen aging which agrees well with findings and observations with respect to actual field aging.

## THE AGING OF A BITUMINOUS BINDER IN SERVICE

In-service aging may be influenced by a great number of factors, some of which are named and described below:

(1) The binder's intrinsic susceptibility to aging. This is obviously the most important factor, which laboratories are trying to assess from the commonly practiced accelerated tests (at temperatures above 100°C). Since this assessment is essentially relative, the greatest caution should be exercised in extrapolating to ambient temperatures (as will be shown further on).

(2) The porosity of the mix. The higher the porosity, the more the mix is pervious to air, which automatically contributes to binder aging in the bulk of the layer. A properly laid dense mix ages almost exclusively at the surface [3].

(3) Temperature. Like many chemical reactions, oxidation reactions are stimulated by an increase in temperature.

(4) Sun radiation. On account of the very high absorption coefficients of bitumens in the ultraviolet (UV) range [6], it can be stated that the influence of UV sunrays is limited to the first (one or two) micrometers of the bitumen's surface. Their contribution to aging, therefore, may be neglected, as the surface actually exposed is very small with respect to the total amount of binder in the layer. On the other hand, the influence of infrared (IR) radiation must not be neglected since its absorption leads to a rather considerable increase in mean temperature in the layer [7].

(5) The nature of the aggregates may also be of some influence. This, however, is difficult to demonstrate: in most mixes the aggregate is of a (widely) different nature according to the size fraction (filler, sand(s), rock) being considered.

(6) Other factors of which the influence is rather poorly known are rain, moisture, porosity of the aggregate (preferential adsorption of certain bitumen components), de-icing salts, etc.

When considering the above factors, it is obvious that accurate simulation of field aging in the laboratory is a utopian objective. The situation, however, can be very much simplified by starting from the (rather realistic) assumption that, all other factors remaining equal, the aging process observed in the field will depend mainly on the binder's susceptibility to oxidation. Accelerated aging tests in the laboratory, therefore, should aim at evaluating the reaction constant(s) of the asphalt concrete at service temperature, using a kinetic approach to binder aging.

## KINETIC DEVELOPMENT

*Review of some concepts in chemical reaction kinetics*

The classical kinetic theory (gaseous or liquid-state reaction) can be partly transferred to the reactions which occur in a solid or highly viscous medium. However, it has been necessary to develop appropriate kinetic models for the solid state [8]; for kinetic studies, use is generally made of measurement of the extent of reaction,  $\alpha$ , as a function of time.

In simple or simplified cases, the reaction rate is classically related to the concentration of one of the reacting substances by the following equation:

$$v = \frac{dC_A}{dt} = k \times C_A^n \quad (1)$$

where  $k$  = reaction or rate constant (at the test temperature),  $n$  = order of the reaction with respect to substance  $A$ .

The relationship between the concentration of  $A$  at time  $t$  and time  $t$  is established by integration. This relation makes it possible to estimate the constant,  $k$ , and the order,  $n$ , of the reaction from the experimental data. Knowing constant  $k$  at different exposure temperatures, it is then possible to estimate the activation energy of the reaction by applying the Arrhenius equation:

$$k_T = A \times e^{-E/R \times T} \quad (2)$$

where  $A$ ,  $E$ ,  $R$  and  $T$  represent the frequency factor, the activation energy, the perfect gas constant and the absolute temperature ( $^{\circ}\text{K}$ ), respectively.

A similar line of argument can be followed while considering the extent of reaction,  $\alpha$  ( $0 \leq \alpha \leq 1$ ). This extent can be evaluated by monitoring the increase or decrease in concentration of a product, or the development of a characteristic associated with it. In this case, however, there is often an initial value and a final value and these are not always accessible by experiment and must, therefore, be estimated.

In very general terms, the extent of reaction,  $\alpha$ , can be defined as follows:

$$\alpha = \frac{S_t - S_o}{S_f - S_o} \quad (3)$$

where  $S_o$ ,  $S_t$  and  $S_f$  represent the values of signal (or indicator)  $S$  at time  $t = 0$ ,  $t = t$  and at the end of the reaction, respectively. For example,  $S$  may be a concentration or a characteristic, depending upon the reaction. There must, however, be a linear or 'linearizable' relation between the two.

### *Application to bitumen aging*

#### *Theoretical approach*

Among the various classical kinetic models and those for solid-state reactions [8], generally that of one-dimensional diffusion (D1) [8] best applies to tests performed with the selected indicators [11]. The corresponding equation is as follows:

$$a^2 = \left[ \frac{S_t - S_o}{S_f - S_o} \right]^2 = \left( \frac{DS_t}{DS_{\infty}} \right)^2 = k \times t \quad (4)$$

As term  $DS_{\infty}$  is hardly accessible by experiment and in fact represents a constant for the bitumen being considered, this equation can be transformed into three others which are markedly more practical:

$$(S_t - S_o)^2 = DS_t^2 = K \times t \quad (5)$$

By transformation this equation becomes:

$$S_t = S_o + K^{1/2} \times t^{1/2} \quad (6)$$



or, in terms of logarithms, we find:

$$\log(DS_t) = 0.5 \log(K) + 0.5 \log(t) \quad (7)$$

where  $K = k(S_f - S_0)^2 = DS_{\infty}^2 \times k$  (= overall reaction constant).

Using Eqs. 17-5 and 17-6, it is possible to determine the overall reaction constant from experimental data as far as the tests have been conducted at an exposure temperature not higher than 100°C on an original bitumen (i.e., still virtually unaffected by oxidation) [11].

Eq. 17-7 enables mainly the validity of exponent  $\alpha$  (in principle 2, according to Eq. 17-4) to be tested. It should, however, be noted that the coefficient found by experiment is influenced very strongly by the value of  $S_0$  and by the measurements at the first exposure times, where the error in  $DS_t$  may be very large. A visual examination of the  $\log(DS_t) - \log(t)$  graphs will confirm that this coefficient is often close to 0.5. Hence, the exponent of  $\alpha$  (Eq. 17-4) and  $DS_t$  (Eq. 17-5) is probably 2 [11].

#### *Generalization of this theoretical approach*

When the test temperature exceeds 100°C [4] or the bitumen has already been subject to some aging, the results obtained no longer agree closely with Eqs. 17-5 and 17-7. As a result, it has been necessary to adapt the latter to those two situations.

*Aged bitumen.* The part of the aging process of the bitumen already completed before the beginning of the test is represented by a time of reaction,  $t_0$ , at the test temperature. Eq. 17-5 can, consequently, be rewritten as follows:

$$(S_t - S_0)^2 = DS_t^2 = K \times t_a = K(t_0 + t) = K \times t_0 + K \times t \quad (8)$$

where  $t_a$  is the actual reaction time defined as the sum of the exposure time chosen during the test and the fictitious time,  $t_0$ .

Where  $S_0$  is known, Eq. 17-8 can be applied directly to the experimental results and the value of  $t_0$  can be estimated from the ordinate at the origin ( $= K \times t_0$ ). If in addition the initial value of  $S$ , i.e.,  $S_i$ , is known, a second (generally less reliable) estimation of  $t_0$  is possible:

$$(S_i - S_0) = K \times t_0 \quad (9)$$

By transformation, Eq. 17-8 becomes:

$$S_t = S_0 + K^{1/2}(t_0 + t)^{1/2} \quad (10)$$

in which the estimated value of  $t_0$  is entered (Eq. 17-8 or Eq. 17-9) for the regression calculation.

It is also possible, by successive approximation, to find the value of  $t_0$  which leads to the best degree of correlation for Eq. 17-10 applied to the experimental results.

In practice, however, the values of  $S_0$  and  $t_0$  are generally unknown. In such cases, processing data by means of Eq. 17-10 generally results in unrealistic estimates of  $S_0$  and/or  $t_0$  and hence of  $K$ , because of experimental errors. This difficulty can be met to some degree by estimating  $S_0$  from information and specifications contained in standard tender specifications.

*Tests performed at a temperature above 100°C.* A systematic deviation from the one-dimensional diffusion model can be observed in this case, both in the tests carried out at BRRC and in the results published in the literature. Eq. 17-4 can, however, be adapted to the results obtained by changing the exponent  $\alpha$ . The general equation then becomes:

$$a^n = \left[ \frac{S_t - S_o}{S_f - S_o} \right]^n = \left( \frac{DS_t}{DS_\infty} \right)^n = k \times t \quad (11)$$

Eqs. 17-5–10 have to be changed accordingly by replacing exponent 2 with  $n$  and exponent 1/2 with  $r$  ( $= 1/n$ ). The two important equations are: Eq. 17-5  $\rightarrow$

$$DS_t^n = K \times t \quad (12)$$

and Eq. 17-6  $\rightarrow$

$$S_t = S_o + K^r \times t^r \quad (13)$$

Various cases have been examined and, generally speaking, exponent  $n$  is often close to 3/2 ( $n$  value giving the best or a very high degree of correlation). Although the physical meaning of this exponent 3/2 is not clear as far as the proposed kinetic approach is concerned, this exponent makes it possible to mathematically process results obtained at temperatures above 100°C and to represent the development of the binders' characteristics with time. This provides a basis for comparing different binders from the point of view of in-construction aging.

For certain results given in the literature (test temperature above 160°C) the determination of exponent  $n$  results in a value approaching 1. This means that from the mechanism point of view, all of the reactions can be identified with a zero-order reaction and that characteristic  $S_t$  develops linearly with time.

Extreme caution must be exercised, however, when processing data reported in the literature, as random and (not always apparent) systematic experimental errors may often lead to misinterpretation and wrong conclusions. Let us consider the example of reaction time to illustrate this. For a kinetic approach, this time must represent the actual time which the binder has been exposed to the test temperature. At the beginning of a test, it often takes some time for the test system to reach the normal operating conditions. This time will be longer if the container and the binder have not been preheated and as the test temperature is higher. On the other hand, the effect on actual reaction time decreases with the length of the test.

### *Choice of indicators*

It is well known that the oxidation (or aging) process of a bitumen is chemically reflected by an increase in asphaltenes (A7) content [3,4,9,10]. Hence this A7 content is a primary indicator of oxidation and can be substituted for  $S$  in Eq. 17-3. The major drawback of this parameter is that its determination is subject to a relative error of the order of 10%: the values generally cover a range of approx. 10–20% and the absolute error in the increase in A7 content consequently lies between  $\pm 1$  and  $\pm 2\%$ , if the initial value is assumed to be correct.

Physicochemically speaking, aging shows itself, among other things, in an increase in ring and ball (R & B) temperature, Fraass' breaking point, viscosity and certain IR

absorption bands, and in a decrease in penetration of the binder. These are secondary indicators, and some of them may also be suitable from the kinetic point of view [11]. Thus, R & B temperature, R & B, and the reciprocal of penetration,  $1/\text{pen}$ , can be substituted for  $S$  in Eq. 17-3.

However:

- the variation of penetration covers about 70 units (mm/10) for an 80/100 grade bitumen and the error in its determination is between 1 and 2 units, depending on the range of measured penetration. As the relative error becomes larger for lower penetrations,  $1/\text{pen}$  will be subject to a much greater margin of error than for higher penetrations. This may lead to distortion in the plot of experimental points;
- the variation range of, R & B, is around 50°C and the error in measurement is about 0.5°C. Because of its much smaller and constant margin of error, R & B seems to be a suitable indicator for kinetic studies of bitumen aging. This has been confirmed by the results obtained.

The IR spectrum of bitumens is a more particular case, since it develops as a whole. However, certain absorption bands are more specifically connected with bitumen oxidation, such as those at 1700 and 1030  $\text{cm}^{-1}$ . The former has also been used as an indicator [11] and the latter has a particular characteristic in which it does not develop further once a certain degree of oxidation has been reached [11]. The interpretation of IR spectra from a kinetic point of view would require a much more thorough study than has been made up to now. This could be a course to be embarked on by BRRC in the near future. That is why the processing of IR data is not discussed here.

Furthermore, an investigation of some results published in the literature has shown that the logarithm of viscosity (at 60°C and at 135°C) could be suitable as an indicator of  $S$  in Eq. 17-3.

The indicators considered further in this text are asphaltenes content (A7), R & B softening temperature (R & B) and the reciprocal of penetration ( $1/\text{pen}$ ).

As a whole, the results discussed in the experimental section show that the technological indicators considered in monitoring bitumen oxidation form a valid kinetic approach to aging without the need for specific knowledge of the reaction mechanisms. This general view has been put forward by Larsson for other reactions [18].

### *Procedure*

The procedure used to interpret the results obtained for each indicator is as follows [11]:

(1) Using Eqs. 17-12 and 17-13, the exponent which agrees best with the experimental results ( $n = 2$  or  $3/2$  and  $r = 1/2$  or  $2/3$ ) is determined. All the calculations mentioned below could be made with  $n = 2$  and with  $n = 3/2$ , but for tests below 100°C, generally exponent 2 is more suitable.

(2) Using Eq. 17-6 (calculation of the regression lines, including the bitumen before aging),  $S_0$  is evaluated for the different test temperatures. From the determined  $S_0$  values, the mean value of  $S_0$  is calculated. If this mean value is compatible with the value measured on the bitumen before aging, it is used in the subsequent calculations; if not, the value of the unaged bitumen is adopted.

(3) The overall reaction constant,  $K$ , is calculated using Eq. 17-5 on the one hand and Eq. 17-6 on the other (regression lines passing through the origin). The mean of the two constants calculated is taken as the overall reaction constant  $K_T$  for the exposure temperature and indicator being considered.

(4) The  $K_T$  constants obtained are used as real reaction constants  $k_T$  to be entered in the Arrhenius Eq. 17-2, in order to evaluate the activation energy of the reaction.

#### *Evaluation of activation energy*

The activation energy,  $E$ , of the reaction can be evaluated for each individual indicator. Although the values found are not significantly different [11], they may lead to a considerable distortion between the overall reaction constants for the different indicators when they are extrapolated to other temperatures (e.g., from 70–80°C to approx. 20°C).

Hence it is preferable, when the individual values of  $E$  are close, to consider the full set of overall reaction constants and to directly determine the common value of  $E$ . This can be done as follows (the example is given for three test temperatures):

- for each indicator, the overall reaction constants ( $K_T$ ) are normalized ( $N_T$ ), corresponding with the median temperature (i.e.,  $K_{T_1}/K_{T_2}$ ,  $K_{T_2}/K_{T_2}$  ( $= 1$ ),  $K_{T_3}/K_{T_2}$ );
- the common value of  $E$  is then calculated by regression using the linear relation of the Arrhenius Equation:

$$\ln \left( \frac{K_T}{K_{T \text{ median}}} \right) = \ln (N_T) = \ln (A') - \frac{E}{R \times T} \quad (14)$$

- the theoretical value ( $N_T^\#$ ) of the normalized constant is then calculated for the three temperatures; and
- for each indicator the theoretical values of the overall reaction constants are calculated from the theoretical normalized constants ( $K_T^\# / N_T^\# \times K_{T_2}$ ), possibly with a correction (vertical translation of the regression curve to match the points representing the  $K_T^\#$  values for the indicator being considered).

This procedure brings good consistency into the set of results and overall reaction constants calculated for other temperatures (extrapolations).

#### *From the laboratory to the field*

##### *Factors to be considered*

Various factors accelerate aging in the laboratory: temperature, mixing, oxygen instead of air, and sometimes pressure.

All these parameters must be taken into consideration when making the transition from laboratory results to in-service aging. This means that correction factors must be established, except for temperature, which is accounted for by activation energy. This is made fairly easy by the kinetic approach to data processing. The procedure is as follows:

##### *(a) Mixing (depends on the rotation rate of the container).*

(1) The overall reaction constant is determined at a given exposure temperature (e.g., 85°C) for various rotation rates (e.g., 1, 5 and  $n$  revolutions/minute):  $K_1$ ,  $K_5$  and  $K_n$ ;

(2) the ratios  $R_1 (= K_1/K_1)$ ,  $R_5 (= K_5/K_1)$  and  $R_n (= K_n/K_1)$  are calculated.  $K_1$  is taken as a reference, 1 revolution/minute being closer to reality;

(3) by extrapolating these ratios, the ratio  $R_0$ , corresponding with the actual field value of the parameter (in this case 0 revolutions/minute, since the binder is in a static state in the road) is determined; and

(4) the correction factor,  $R$ , is derived from  $R_0$ :

$$R = R_0/R_r$$

with  $r$  being the usual rotation rate of the container for the type of test conducted.

(b) *Pressure*. The procedure is similar to the above, but the extrapolation is to atmospheric pressure. The corresponding correction factor is  $P$ :

$$P = P_1/P_p$$

with  $p$  being the pressure normally used in the test.

With the system used at BRRC, correction factor  $P$  equals 1, since the tests are conducted at atmospheric pressure.

(c) *Ambient atmosphere*. The correction factor,  $G$ , is calculated from the overall reaction constants measured under air and under oxygen, all other parameters remaining equal:

$$G = K_{\text{air}}/K_{\text{oxygen}}$$

For each indicator, the overall reaction constant calculated for a given exposure temperature,  $K_{\text{extrapolated}}$ , has to be corrected for the conditions actually encountered on site (static binder and air at atmospheric pressure):

$$K_{\text{actual}} = G \times P \times R \times K_{\text{extrapolated}}$$

where  $G$  is the correction factor for the 'gas' parameter,  $P$  is the correction factor for the 'pressure' parameter, and  $R$  is the correction factor for the 'rotation rate' parameter.

### *Aging in construction*

As mentioned in the introduction, an asphalt pavement mix has already been subject to in-construction aging before its service life begins.

This aging is very variable. It depends mainly on the manufacturer and the contractor, and also on weather conditions:

(1) Observance of recommended mixing temperature and mixing time.

(2) Lapse of time between end of mixing and compaction: transport, cooling to compaction temperature, duration and effectiveness of compaction.

(3) Time required for the mix to cool to ambient temperature, which depends on weather conditions. In-depth aging of the layer during this cooling time will depend on the voids content of the mix. If the mix has been well compacted (voids content lower than 3%), only the surface of the layer will be affected.

In sum, in-construction aging is essentially dependent upon the care taken in manufacturing and laying of the asphalt mix. It corresponds to 2 to 6 hours of oxidation at 135°C, when considering the extrapolated constant  $K_{135}$  corrected as mentioned above, as well as certain data on observed field behavior [17].

*Kinetic mean temperature on site*

On site, a road pavement does not remain at constant temperature throughout the year. It is subject to variations in temperature according to the surrounding climatic conditions, the most important of which are air temperature and sun radiation [7,12,19]. Furthermore, just as for all other exposed layers on earth, temperature and its variations depend on the depth of measurement and the nature of the material [7,19]. In Belgium, the temperature of an asphalt pavement ranges from  $-10$  to  $+50^{\circ}\text{C}$  and from  $-5$  to  $+40^{\circ}\text{C}$  at the surface ( $-0.5$  cm) and at a depth of 5 cm, respectively [7,19].

Equal times of exposure to various temperatures will obviously contribute in very different ways to the aging of the binder. For example, 24 h at  $0^{\circ}\text{C}$  will have a markedly smaller aging effect than 24 h at  $40^{\circ}\text{C}$  (smaller by a factor of about 16, as it is generally admitted that the rate of aging doubles with a  $10^{\circ}\text{C}$  increase in temperature). In fact, the exact value of this factor depends on the activation energy of the aging reactions, since it is this energy which determines the value of the (overall) reaction constant and hence the reaction rate at the temperature under consideration.

Due to the variations in field temperature, the total in-service aging of a binder will be the sum of a series of partial aging processes, the contributions of which depend on the time of exposure to a given temperature. To be fully correct, the assessment of field aging must, therefore, be made by integrating these contributions on the basis of the histogram of the distribution of temperatures over the period being examined.

Another approach, which is more practical and more centered on predicting binder aging in service, consists of estimating the kinetic mean temperature of the pavement on an annual basis under the local climatic conditions in the region or country where the road is situated. This requires the availability of statistical data on temperatures at various depths in, but mainly at the surface of, asphalt pavements.

Some ground in this field has already been covered in Belgium [7,12,19]:

(1) Data on temperature at different depths (including  $-0.5$  and  $-5$  cm) in various asphalt pavements is available, as well as a set of meteorological data relating to air temperature, minimum and maximum temperature, amplitude of daily variation, sun radiation, etc. They are the result of several years of measurements by BRRC and systematic measurements by the Royal Belgian Meteorological Institute [13].

(2) From these measured data, a mean curve of temperature distribution (per  $5^{\circ}\text{C}$  interval) at different depths in asphalt concrete has been established — especially for temperatures at the surface ( $-0.5$  cm), which is the most relevant to road binder aging (Fig. 17-1, curve 1).

(3) Using the data on mean air temperature, the amplitude of variation in air temperature and total sun radiation on a horizontal surface, it has been possible to reproduce with a very good approximation the mean curve of temperature distribution at the surface of asphalt concrete [7,19]. This predictive method can be transferred to other countries and other climates [12].

To estimate the annual value of kinetic mean temperature at the surface of asphalt pavements in Belgium (more precisely in the region of Brussels), the following procedure has been used:

(a) Starting from the mean distribution curve referred to in curve 1 of Fig. 17-1, the fraction of time per year,  $f_i$ , during which the binder is exposed to temperatures between

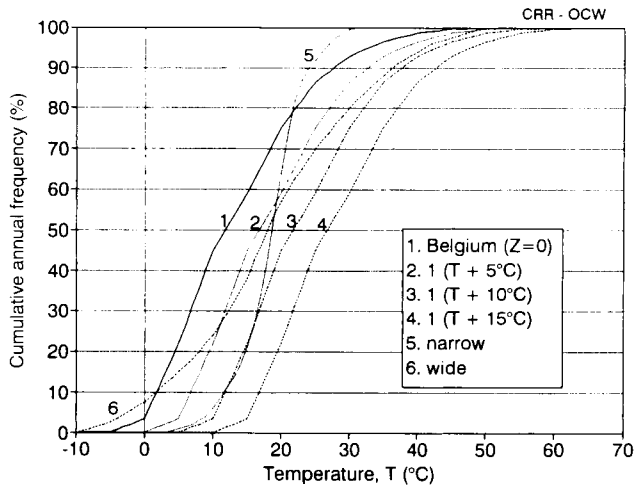


Fig. 17-1. Examples of annual distribution curves of temperature [(1) relates to the surface of asphalt pavements in the region of Brussels].

$T_{i-1}$  and  $T_i$  is determined. Since the temperature interval being used is 1°C, a linear interpolation is made for each 5°C interval on the curve between the frequency values corresponding to the limits of the 5°C temperature interval being considered.

(b) The following sum is calculated:

$$SCR = \sum f_i \times \exp \left[ -E/R \times (T_i - 0.5) \right]$$

where  $E$  is the activation energy of the reaction,  $R$  is the perfect gas constant, and  $(T_i - 0.5)$  is the absolute temperature corresponding to the middle of the temperature interval under consideration (in °K).

Given the activation energies found in the tests,  $E/R$  is determined as 9000.

(c) The value of temperature  $T$  which leads to the same SCR value is the annual kinetic mean temperature of the country or region concerned:

$$T_k \text{ (K)} = -E/R \times \ln (SCR)$$

or, in °C:

$$T_k \text{ (°C)} = T_k \text{ (K)} - 273.2$$

By way of example, Table 17-1 reviews the arithmetic mean temperatures and the annual values of kinetic mean temperature for the temperature distributions represented in Fig. 17-1, while assuming an  $E/R$  of 9000.

The divergence between arithmetic mean temperature and kinetic mean temperature increases with the width of the distribution curve (curves 5, 2 and 6) and remains more or less constant when the curve has been subjected to a simple translation (curves 1, 2, 3 and 4).

The mean temperature at the surface (13.2°C) is higher than the annual mean air temperature in Belgium, which is around 10°C. This difference is due mainly to the absorption of sun radiation by the pavement.

TABLE 17-1

Kinetic mean temperature determined from cumulative annual mean histograms of temperatures and for  $E/R = 9000$  K

Curve no.	Type of distribution curve (Fig. 17-1)	Arithmetic mean temperature (°C)	Kinetic mean temperature (°C)
1	Belgium; at -0.5 cm in asphalt course	13.2	19.55
2	5°C translation of 1	18.2	24.35
3	10°C translation of 1	23.2	29.1
4	15°C translation of 1	28.2	33.95
5	narrow	18.2	19.4
6	wide	18.2	26.25

## EXPERIMENTAL APPROACH

*Description of the accelerated test device RCAT (Rotating Cylinder Aging Test)*

A sketch is presented in Fig. 17-2. The device placed in a thermostated cabinet is shown on the photograph in Fig. 17-3.

It consists of a test cylinder (tube) in stainless steel, 124 mm in internal diameter and 300 mm in length. It is enclosed between two welded discs; the one in front has a central opening of 43 mm in diameter and, near the inner well of the cylinder, a hole of 10 mm in diameter with an internal thread for closure with a screw bolt. The binder is recovered through this hole at the end of the test. The two discs rest on two round bars which enable the test cylinder to be rotated; these bars are mounted on ball bearings and their rear ends are fitted with electrically driven pinions. In addition, two clamps have been

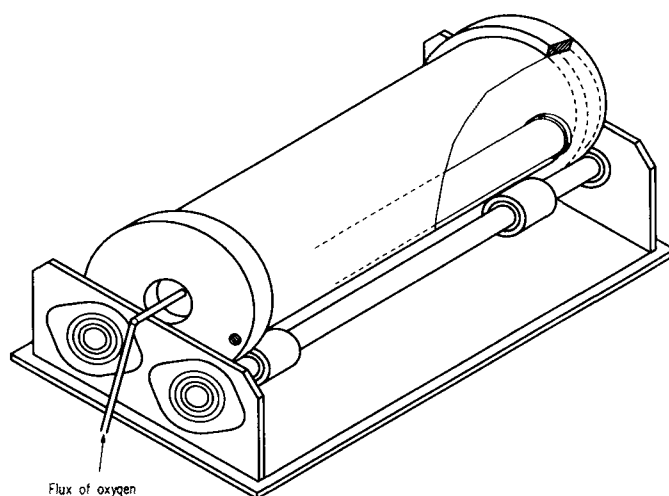


Fig. 17-2. Scheme of the RCAT device for accelerated aging of bituminous binders.



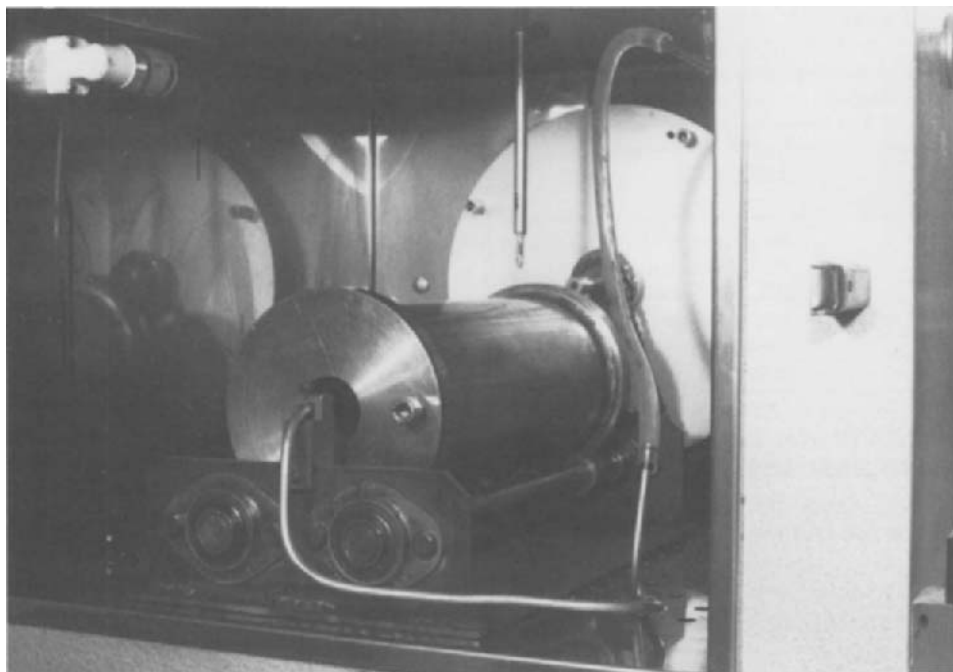


Fig. 17-3. View of the RCAT device placed in the oven.

mounted on one of the bars to prevent lateral movement of the cylinder during the test.

Inside the cylinder is a stainless steel roller 296 mm in length and 34 mm in diameter. This roller has an extra width of 3 mm at both ends, over a total length of 3 mm. By its own rotation during the test, it distributes the binder into an even film on the inner wall of the cylinder, thus homogenizing the sample.

During testing, the cylinder revolves once per minute and is fed with a constant flow of 4 to 5 l of oxygen per hour (75 ml/min), using a stainless steel tube which penetrates almost to the rear of the device. A thermocouple is fixed on this tube, with its measuring element roughly in the middle of the cylinder; this enables the temperature inside the cylinder to be monitored.

The performance potential of this new device is as follows:

(1) Temperature range: from about 70°C to 110°C. Below approx. 65°C the roller in the cylinder cannot properly rotate (uneven film and inadequate homogenization) and above 110°C, the ball bearings may be severely damaged. Temperature is kept constant to within 1°C of the set value.

(2) The thickness of the film on the inner wall is about 2 mm. Since this film is not obtained by prior dissolution nor subjected to intense attrition, this thickness permits tests on mixes in which fine particles are dispersed (polymers, slaked lime, etc.).

(3) The maximum load of binder is about 500 g. At each exposure time, a portion of about 20 g is taken for the characterization tests: ring and ball temperature, (mini) penetration (in a small tin), asphaltene content, IR spectrum, generic composition (by

TABLE 17-2

Main characteristics of the investigated bitumens

	472	481	577
<i>Technological and physicochemical characteristics</i>			
Penetration (mm/10)	92	89	87
R & B temperature (°C)	47.0	46.0	46.5
Viscosity at 135°C (Pa s)	0.308	0.336	—
Density (g/cm <sup>3</sup> )	1.012	1.019	1.020
Neutralization value (%) (Method I.P. 213/82-BS)	0.3	3.3	—
<i>Generic composition (% by mass)</i>			
Asphaltenes content	10.7	9.4	9.2
Saturates	20.8	20.2	14.4
Cyclics (nonpolar aromatics)	43.7	44.5	43.3
Resins (polar aromatics)			
R <sup>1</sup>	—	15.4	21.8
R <sup>2</sup>	—	10.3	11.4
R <sup>1</sup> + R <sup>2</sup>	24.9	25.7	33.2

HPLC chromatography), etc. Not more than seven portions should be taken, to keep conditions as similar as possible.

(4) It is thus possible, using this device, to monitor characteristics with age and to develop a kinetic approach on the aging of bituminous binders as described above. Marketing of the RCAT is now in progress.

### *Bitumens investigated*

To date, three straight-run bitumens of penetration of grade 80/100 have been subjected to aging tests at temperatures ranging from 70°C to 100°C. Their physicochemical characteristics are given in Table 17-2.

The asphaltenes (insoluble in hot *n*-heptane) were obtained using method 08.27 [14] of the 'Test Methods' Section of the Belgian Standard Tender Specifications [Ministère des Travaux Publics (1978)]. For penetration and ring and ball softening temperature, procedures 08.16 and 08.20 of that same Section were used.

### *Test results and interpretation*

The results are presented in Tables 17-3 to 17-5.

With this data and that found in other tests, it has been possible to establish highly significant linear relations between some bitumen characteristics as determined in the course of the aging process, more particularly between:

- R & B temperature and asphaltenes (A7) content;
- the reciprocal of penetration and this content;
- 1/pen and R & B; and
- absorbance at 1700 cm<sup>-1</sup> (A<sub>1700</sub>) and A7 or R & B.

TABLE 17-3  
Results of aging tests on bitumen 472

A. Normal test conditions										
<i>t</i> (h)	Asphaltenes A7 (%)			Pen (mm/10)			R & B (°C)			
<i>T</i> (°C):	70	80	90	70	80	90	70	80	90	
0	10.7	10.7	10.7	92	92	92	47.0	47.0	47.0	
2	–	10.8	10.9	–	82	76	–	49.0	47.5	
4	10.7	–	–	77	–	–	48.0	–	–	
8	–	–	11.5	–	–	66	–	–	51.0	
24	11.1	12.3	12.1	67	61	53	49.5	51.0	53.5	
48	12.5	12.7	14.2	58	51	44	52.0	53.0	56.0	
72	12.3	11.8	13.5	53	45	36	52.5	55.5	57.0	
96	–	13.6	13.9	–	41	33	–	56.5	58.5	
144	12.7	–	–	46	–	–	54.0	–	–	
168	–	14.7	16.7	–	36	25	–	58.0	63.5	
192	13.3	–	–	43	–	–	55.5	–	–	
240	14.6	–	–	40	–	–	56.0	–	–	

B. Other experimental parameters											
<i>t</i> (h)	Asphaltenes (%)				Pen (mm/10)			R & B (°C)			
<i>T</i> (°C):	100 1 r/m O <sub>2</sub>	100 5 r/m O <sub>2</sub>	100 1 r/m air	100 5 r/m air	100 1 r/m O <sub>2</sub>	100 5 r/m O <sub>2</sub>	100 5 r/m air	100 1 r/m O <sub>2</sub>	100 5 r/m O <sub>2</sub>	100 1 r/m air	100 5 r/m air
0	10.7	10.7	10.7	10.7	92	92	92	47.0	47.0	47.0	47.0
2	11.4	–	–	–	78	–	–	48.5	–	–	–
7	–	11.6	–	–	–	64	–	–	50.0	–	–
8	12.3	–	–	–	62	–	–	49.5	–	–	–
24	12.8	12.5	11.8	13.7	49	45	58	53.5	54.0	51.5	52.5
48	14.2	14.5	–	14.3	38	36	45	57.0	58.0	–	55.0
72	14.9	15.8	12.9	14.7	33	30	36	58.5	61.5	55.9	57.5
96	–	16.3	–	15.2	–	25	32	–	63.5	–	59.0
144	18.0	–	14.8	–	24	–	–	66.0	–	59.1	–
168	18.2	21.0	–	17.6	22	18	25	67.0	72.5	–	65.0
192	–	–	15.6	–	–	–	–	–	–	62.3	–
216	–	20.6	–	18.3	–	16	22	–	77.0	–	68.0
240	–	–	17.3	21.4	–	–	18	–	–	64.9	73.0
264	–	23.5	–	–	–	15	–	–	80.5	–	–
336	–	–	18.8	–	–	–	–	–	–	68.7	–
480	–	–	21.8	–	–	–	–	–	–	75.0	–

Examples have been presented and discussed in [11].  
Table 17-6 reviews the three indicators that considered the  $S_0$  values adopted and the overall reaction constants,  $K_T$ , calculated according to the procedure described in the previous section entitled *Procedure*, from the results obtained under the normal test

TABLE 17-4

Results of aging tests on bitumen 481

<i>t</i> (h)	Asphaltenes A7 (%)			Pen (mm/10)			R & B (°C)		
<i>T</i> (°C):	70	80	100	70	80	100	70	80	100
0	9.4	9.4	9.4	89	89	89	46.0	46.0	46.0
8	10.2	—	10.3	71	—	62	48.0	—	49.5
19	—	9.9	—	—	61	—	—	50.0	—
24	11.0	—	14.2	62	—	45	49.5	—	53.5
44	—	11.2	—	—	50	—	—	51.5	—
48	10.3	—	13.3	55	—	35	50.5	—	57.0
68	—	13.6	—	—	47	—	—	53.5	—
72	10.8	—	13.3	50	—	30	52.0	—	60.5
140	—	13.4	—	—	37	—	—	55.0	—
144	—	—	16.1	—	—	21	—	—	65.5
168	11.3	—	17.9	42	—	19	54.5	—	68.0
188	—	14.1	—	—	34	—	—	57.5	—
216	—	—	21.4	—	—	16	—	—	75.5
236	—	14.0	22.2	—	31	—	—	58.5	—
240	13.6	—	—	40	—	—	55.0	—	—
336	13.6	—	—	35	—	—	56.5	—	—
408	13.5	—	—	32	—	—	57.5	—	—
576	13.7	—	—	30	—	—	59.0	—	—

TABLE 17-5

Results of aging tests on bitumen 577

<i>t</i> (h)	Asphaltenes A7 (%)			Pen (mm/10)			R & B (°C)		
<i>T</i> (°C):	70	82.5	95	70	82.5	95	70	82.5	95
0	9.2	9.2	9.2	87	87	87	46.5	46.5	46.5
8	–	9.8	10.5	–	76	70	–	47.0	48.0
24	10.2	10.7	11.8	68	61	57	49.0	50.0	50.5
48	10.8	11.6	13.3	59	49	44	50.0	51.5	53.5
72	–	11.8	14.3	–	46	38	–	53.0	54.0
96	11.6	–	–	53	–	–	52.0	–	–
144	–	12.8	–	–	38	–	–	56.0	–
168	11.5	–	17.2	46	–	27	54.0	–	60.5
216	12.6	13.5	–	42	32	–	55.0	57.5	–
264	12.8	–	–	40	–	–	54.5	–	–
312	–	15.5	19.2	–	28	18	–	60.0	68.5
336	13.4	–	–	39	–	–	54.5	–	–

conditions (1 rev/min under a flow of oxygen). For example, Fig. 17-4 represents the test results for the development of the R & B temperature of bitumen 472. The curves correspond with the calculated values of the overall reaction constants; they perfectly fit

TABLE 17-6

Initial value  $S_0$  and mean overall reaction constant  $K_T$  according to Eqs. 17-5 and 17-6 — test at 1 rev/min under  $O_2$  flow

$T$ (°C)	$A7$ (% <sup>2</sup> h <sup>-1</sup> )			$R \ \& \ B$ (°C <sup>2</sup> h <sup>-1</sup> )			$1/\text{pen}^a$		
	472	481	577	472	481	577	472	481	577
70	0.0556	0.0408	0.0524	0.380	0.327	0.291	0.823	0.894	0.681
80	0.105	0.1095	—	0.847	0.673	—	1.73	1.78	—
82.5	—	—	0.112	—	—	0.634	—	—	1.82
90	0.196	—	—	1.59	—	—	4.34	—	—
95	—	—	0.346	—	—	1.425	—	—	5.17
100	0.357	0.473	—	2.35	3.22	—	6.38	10.1	—
$S_0$	10.4	9.4	9.1	46.8	46	46.8	92	89	90

<sup>a</sup>  $10^{-6}$  (10/mm)<sup>2</sup> h<sup>-1</sup>.

the experimental points from the tests at 70, 80 and 90°C.

On the other hand, Table 17-7 reviews the overall reaction constants calculated for the tests conducted under other conditions. Bitumens 569 and 577 are of the same origin and fairly similar in characteristics. The aging tests on bitumen 569 were performed in a Rotovapor, more or less according to the procedure described in DIN 52016 [2]. The test conditions adopted were: rotation rate of about 10 rev/min (it is, indeed, relatively difficult to keep this rate perfectly constant), oxygen (or air) flow of 4 to 5 l/h, 250 g of binder and 4 stainless steel balls [4].

Starting from the results in Table 17-7, the effects of the experimental parameters have been determined (as shown in Table 17-8) and then, according to the procedure

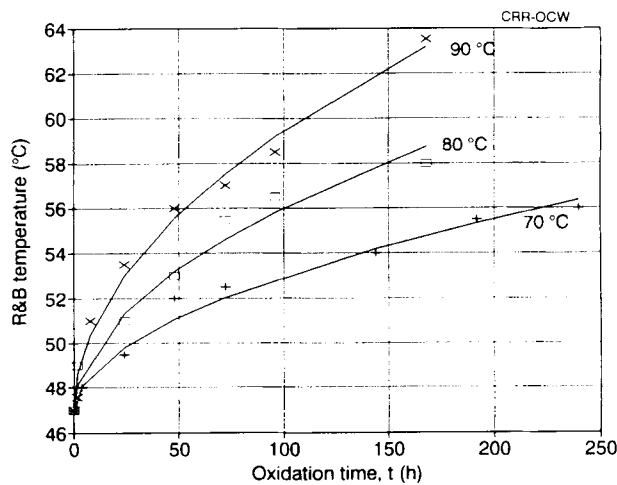


Fig. 17-4. Development of R & B temperature at different oxidation temperatures (curves calculated according to kinetic development).

TABLE 17-7

Overall reaction constant  $K$  according to Eqs. 17-5 and 17-6 — different test conditions

$T$ (°C)	Rotation rate (rev/min)	Gas	472			569		
			A7 % <sup>2</sup> h <sup>-1</sup>	R & B °C <sup>2</sup> h <sup>-1</sup>	1/pen <sup>b</sup>	A7 % <sup>2</sup> h <sup>-1</sup>	R & B °C <sup>2</sup> h <sup>-1</sup>	1/pen <sup>b</sup>
80	1	O <sub>2</sub>	0.105	0.847	1.73	—	—	—
80	10 <sup>a</sup>	O <sub>2</sub>	0.222	1.38	4.60	—	—	—
85	10 <sup>a</sup>	air	—	—	—	0.0589	0.527	1.24
85	10 <sup>a</sup>	O <sub>2</sub>	—	—	—	0.0955	0.858	2.38
90	1	O <sub>2</sub>	0.196	1.59	4.34	—	—	—
90	10 <sup>a</sup>	O <sub>2</sub>	0.491	3.35	8.92	—	—	—
100	1	air	0.214	1.42	—	—	—	—
100	1	O <sub>2</sub>	0.357	2.35	6.38	—	—	—
100	5	air	0.309	2.15	5.32	—	—	—
100	5	O <sub>2</sub>	0.547	3.85	11.0	—	—	—

<sup>a</sup> Aging test in a Rotovapor [4].<sup>b</sup> 10<sup>-6</sup> (10/mm)<sup>2</sup> h<sup>-1</sup>.

TABLE 17-8

Effect of test conditions

$T$ (°C)	Indicator	R <sub>1</sub>	R <sub>5</sub>	R <sub>10</sub>	$G(K_{\text{air}}/K_{\text{O}_2})$		
80	A7	1	—	2.11	—	—	—
	R & B	1	—	1.63	—	—	—
	1/pen	1	—	2.66	—	—	—
85	A7	—	—	—	—	0.617	—
	R & B	—	—	—	—	0.614	—
	1/pen	—	—	—	—	0.521	—
90	A7	1	—	2.50	—	—	—
	R & B	1	—	2.11	—	—	—
	1/pen	1	—	2.06	—	—	—
100 (O <sub>2</sub> )	A7	1	1.53	—	0.600	—	0.565
	R & B	1	1.64	—	0.604	—	0.558
	1/pen	1	1.72	—	—	—	0.484
100 (air)	A7	1	1.44	—	—	—	—
	R & B	1	1.51	—	—	—	—
Average		1	1.57	2.18	0.570		

previously stated in the section *Factors to be considered*, the correction factors from laboratory to field conditions were made. The mean values thus found are:

- $R_o = 0.88$  for the 'rotation rate' parameter,
- $G = 0.57$  for the 'gas' parameter.

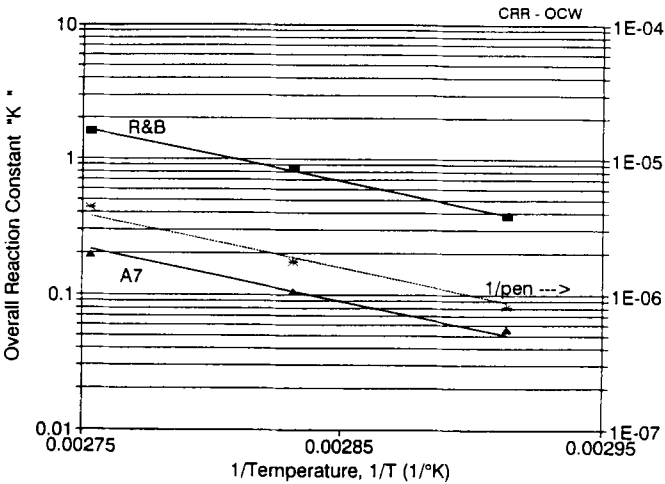


Fig. 17-5. Arrhenius plot for the aging tests on bitumen 472 (after common normalization).

Thus, the total correction factor ( $G \times R_o$ ) is 0.502 for the tests conducted under the 'standard' conditions (1 rev/min and oxygen flow).

The application of the procedure described in *Evaluation of activation energy* with the results gathered in Tables 17-3 and 17-5, which is illustrated by Fig. 17-5, resulted in the energy activation values presented in Table 17-9. The results obtained at 100°C were not taken into account since the exponent  $n$  (Eqs. 17-12 and 17-13), giving the best degree of correlation, proved to be either 2 or 3/2, depending on the indicator and the bitumen under consideration. The temperature of 100°C seems to fall into the range of transition between two different aging processes. This observation has already been reported in [3,4].

*Extrapolation to field conditions*

Table 17-9 also gives the values of the overall reaction constants extrapolated to the field conditions prevailing in the region of Brussels: surface of the pavement,

TABLE 17-9

Activation energy (on a common basis; tests at 100°C were not taken into account)

	472	481	577
$E$ (J/mole)	75,200	80,500	77,000
Standard error in $E$	4,300	9,500	4,300
$K$ on site <sup>a</sup> for			
A7 (% <sup>2</sup> h <sup>-1</sup> )	$2.67 \times 10^{-4}$	$1.73 \times 10^{-4}$	$2.39 \times 10^{-4}$
R & B (°C <sup>2</sup> h <sup>-1</sup> )	$2.05 \times 10^{-3}$	$1.21 \times 10^{-3}$	$1.21 \times 10^{-3}$
1/pen [(10/mm) <sup>2</sup> h <sup>-1</sup> ]	$4.69 \times 10^{-9}$	$3.26 \times 10^{-9}$	$3.51 \times 10^{-9}$

<sup>a</sup> Extrapolated and corrected ( $T_k = 19.5^\circ\text{C}$ : annual kinetic mean temperature for the region of Brussels).

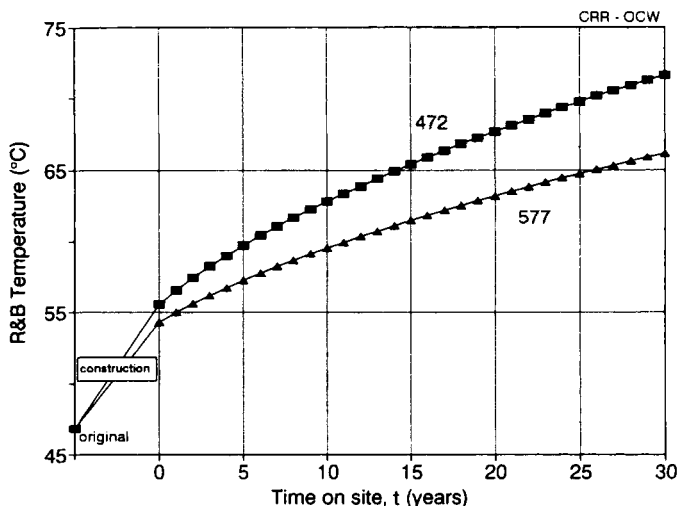


Fig. 17-6. Simulated field development of the R & B temperatures of bitumens 472 and 577.

static binder, annual value of kinetic mean temperature of 19.5°C (Table 17-1). For the three bitumens tested, the differences in overall reaction constants reached almost 40%. Fig. 17-6 simulates the development of R & B temperature that would be observed on site, for example, with bitumens 472 and 577 if they were exposed to exactly the same conditions of aging (also in construction). The pavement would have a markedly shorter life with bitumen 472; for example, an R & B temperature of 65°C would be reached after about 14 years for bitumen 472 and only after 26 years for bitumen 577.

The long-term in-service behavior of different bitumens thus seems to be predictable, at least in a relative way, from kinetic data yielded by accelerated tests in the laboratory. The important parameters are the overall reaction constant at various temperatures (between 70°C and approx. 95°C) and the activation energy of the reactions. If at a later stage the latter appears to be more or less equal for all bitumens or for a given type of bitumen, comparisons can be made by conducting an aging test at only one temperature (e.g., 85°C).

#### DISCUSSION OF A FEW RESULTS REPORTED IN THE LITERATURE

Tuffour, Ishai and Craus [15] have carried out tests using the RTFOT method at three different temperatures (120, 140 and 163°C), with exposure times ranging from 3 to 24 h. The results for the TS1 bitumen have been processed according to the method developed by BRRC.

The most suitable exponent  $n$  (Eqs. 17-12 and 17-13) for the three temperatures and for the three indicators used ( $A_7$ ,  $1/\text{pen}$  and  $\log(\eta_{60^\circ\text{C}})$ ) is  $3/2$ . This clearly shows that aging at temperatures above 100°C is another process. A possible explanation is that at higher temperatures one type of oxidation reaction is favored over another because



of a rather big difference in activation energy between the two reactions. To solve this problem, it is necessary to know the reaction mechanism(s) that actually govern(s) the binder aging process. IR spectrography and the analysis of generic composition by HPLC seem to be very promising tools in this respect [3,4,11,16].

The calculated mean activation energy is 65,000 ( $\pm 3200$ ) J/mole, which is markedly lower than for the tests conducted below 100°C. Assuming that the effect of the rotation rate of the containers follows a similar relation as that found from the results obtained at BRRC, the correction factor for 'rate',  $R$ , would be about 0.25 and the overall reaction constants extrapolated to  $T_k = 18.5^\circ\text{C}$  (annual value of kinetic mean temperature for  $E/R = 7800$ ) would be:

- for A7 content:  $6.5 \times 10^{-5} \text{ \%}^{3/2} \text{ h}^{-1}$ ,
- for 1/pen:  $1.6 \times 10^{-8} (10/\text{mm})^{3/2} \text{ h}^{-1}$ ,
- and for  $\log(\eta_{60^\circ\text{C}})$ :  $4.06 \times 10^{-6} (1)^{3/2} \text{ h}^{-1}$ .

These constants and exponent  $n = 3/2$  lead, for the assumptions made, to a simulation of field aging, which is relatively compatible with actual aging on site and comparable to that obtained in tests carried out with the 'BRRC' equipment. The assumption made for correction factor  $R$ , however, remains to be verified. As there is, indeed, no countercurrent mixing in tests such as RTFOT, this factor may very well have been overestimated ( $R$  is probably greater than 0.25) and, consequently, lead to an underestimation of aging in the simulation. Subject to this verification, tests conducted at temperatures above 100°C are very likely to result in simulating in-service aging at too high a rate.

This also shows that tests performed beyond 100°C are hardly suitable for simulating in-service aging. Tests of the RTFOT type conducted at different rotation rates would definitively confirm this view.

#### LABORATORY/FIELD COMPARISON

Two different ways to proceed may be adopted:

- Compare the overall reaction constants estimated for the binder on site with the laboratory test results.
- With due consideration of age in service, compare the variations in characteristics with those that can be estimated from the laboratory test results.

Data available on the binder used on a given site is generally scarce (except for controlled test sections). Moreover, this data is often prone to error as a result of the operations that are necessary to recover the binder from the mix. The margin of error in this data, and hence, in the results of the calculations will depend on the care taken in carrying out the work in the laboratory.

Ideally, the following data should be known on an in-service aged binder:

- $S_t$ : the value at time  $t$  of characteristic  $S$  of the binder recovered from the top slice (approx. 0.5 cm) of the pavement. The more different  $t$  values there are, the better.
- $S_i$ : the value of  $S$  at the beginning of in-service aging. This value is known if samples are taken during laying or the day after. If not, the value of  $S$  in the bulk of core

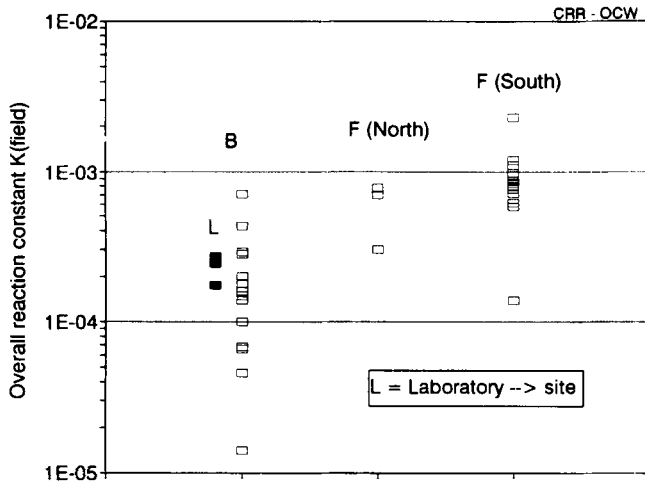


Fig. 17-7. Laboratory/field comparison for the overall reaction constant relating to development of asphaltene content.

samples (excluding the top slice) is a very good approximation of  $S_i$  in the case of a well-compacted dense mix (less than about 5% of voids).

- $S_0$ : the  $S$  value of the original bitumen. If it is unknown, an estimation of R & B temperature and penetration can be made from the tender specifications for the binder.

Using this data, it is possible to evaluate the overall field reaction constant for different indicators and to compare it with the laboratory results. Fig. 17-7 gives an example of this comparison of asphaltene content (A7), based on data published in the literature [3,9,10].

The second way to proceed is illustrated in Fig. 17-8, where the increase in R & B temperature, due to in-service aging, is plotted against the age of the asphalt pavement. The field development calculated for bitumens 472 and 577 is represented by two pecked lines.

In both cases, a good agreement is found between aging observed on site and aging estimated from the accelerated laboratory tests on the three 80/100 grade bitumens. As for the overall reaction constants (as shown in Fig. 17-7), their values increase in ascending order in Belgium, the North of France and the South of France. Such is also the case of mean air temperature and, consequently, kinetic mean temperature.

## CONCLUSIONS

(1) Any binder for bituminous road pavements is subject to two types of aging during its life: rapid aging in construction and slow aging in service. The standard tests (RTFOT and DIN 52016) simulate in-construction aging in an adequate way.

(2) On the other hand, to simulate the in-service aging of a bituminous binder in

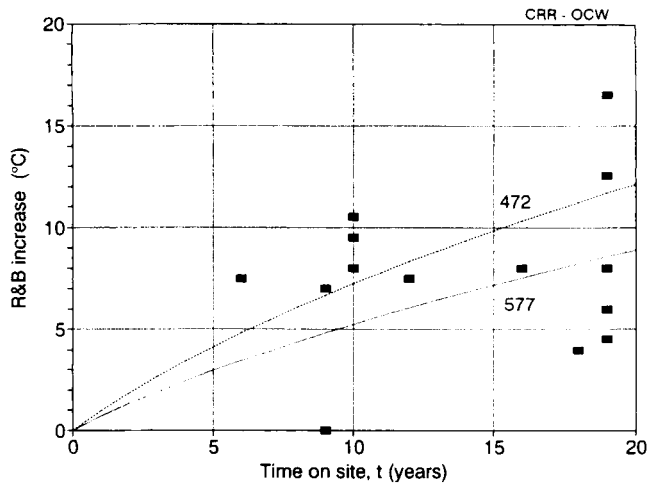


Fig. 17-8. Increase in R & B temperature with the years of service of the pavement.

the laboratory, accelerated tests must be conducted at a temperature below 100°C; at higher temperatures the reaction mechanism is rather different from that which occurs on site.

(3) The RCAT equipment developed at BRRC and the range of temperatures adopted (70°C to max. 95°C) seem appropriate for accelerated simulations of the in-service aging of bituminous binders. Its marketing is now in progress.

(4) The kinetic approach developed from the extent of reaction concept and involving technological characteristics as reaction indicators has proved feasible both in interpreting laboratory tests and in assessing field behavior. Below 100°C, generally, the kinetic model of diffusion most accurately fits the set of results obtained.

(5) The selected characteristics have proved suitable for kinetic studies of bitumen aging. R & B temperature is, however, to be preferred because of the wider range of values covered and the smaller error in its determination.

(6) In order to make the transition from laboratory data to field behavior, it is necessary to know the (annual value of) kinetic mean temperature to which the pavement layer under consideration has been or will be exposed. This temperature is (to be) evaluated from:

- (a) on the one hand, the activation energy of the reactions investigated; and
- (b) on the other, statistical data on the distribution of temperatures in road structures and/or the climatic conditions (air temperature, amplitude of daily variation, sun radiation, etc.) in the region concerned.

(7) The adopted procedure, based on a kinetic approach to the aging of bituminous binders, leads to an extremely satisfactory agreement between the behavior which can be predicted for a given region and that which is observed on binders in the field.

## REFERENCES

- [1] ASTM Method D2872-88. Standard method of test for effect of heat and air on a moving film of asphalt (Rolling Thin Film Oven Test).
- [2] DIN 52016. Prüfung bituminöser Bindemittel: Thermische Beanspruchung im rotierende Kolben.
- [3] Choquet, F.S., The search for an aging tests based on changes in the generic composition of bitumens. *Proc. International Symposium 'Chemistry of Bitumens'*, Rome, II: 787-812 (1991).
- [4] Choquet, F.S. and Verhasselt, A.F., Natural and accelerated ageing of bitumens — effects on the asphaltenes. *Symposium 'Asphaltene Particles in Fossil Fuel Exploration, Recovery, Refining and Production Processes'*, Las Vegas, July 13-17 (1992).
- [5] Oliver, J.W.H., Asphalt durability: from laboratory test to field implementation. *Fuel Science and Technology International, Special Issue on the American Chemical Society Symposium on 'Chemistry and Characterization of Asphalts'*, New York, 10 (4-6): 501-518 (1992).
- [6] Verhasselt, A.F., The UV/VIS characterization of bitumens and their generic fractions. *Proc. International Symposium 'Chemistry of Bitumens'*, Rome, I: 79-92 (1991).
- [7] De Backer, C., Personal paper. Centre de Recherches routières, Brussels (1979).
- [8] Brown, M.E. and Galwey, A., Arrhenius parameters for solid-state reactions from isothermal rate-time curves. *Anal. Chem.*, 61: 1136-1139 (1989).
- [9] Chipperfield, E.H., Duthie, J.L. and Girdler, R.B., Asphalt characteristics in relation to road performance. *Asphalt Paving Technol.*, 39: 575-613 (1970).
- [10] Farcas, F. and Such, C., Influence de la structure chimique des bitumes sur leur comportement rhéologique. Description des méthodes analytiques utilisées. *Journée d'études AFREM — Les Bitumes*, Saint-Rémy-lès-Chevreuse, 29-55 (1991).
- [11] Verhasselt, A.F. and Choquet, F.S., A new approach to studying the kinetics of bitumen ageing. *Proc. International Symposium 'Chemistry of Bitumens'*, Rome, II: 686-705 (1991).
- [12] Veverka, V. and De Backer, C., Aspects techniques du renforcement des chaussées. *Ve Conférence routière africaine de l'IRF, Formation technique et recherche*, Libreville, 151-160 (1983).
- [13] Institut royal météorologique de Belgique. Observations climatologiques. *Bulletin mensuel*, Brussels.
- [14] Ministère des Travaux publics (Belgium). *Fascicule Méthodes d'essais*, Ed. Fonds des Routes, Brussels (1978).
- [15] Tuffour, Y.A., Ishai, I. and Craus, J., Relating asphalt aging and durability to its compositional changes. *Asphalt Paving Technol.*, 58: 163-181 (1989).
- [16] Verhasselt, A.F., Liquid chromatography and IR and UV/VIS spectrophotometry: a pertinent triple way to the chemical characterization of bitumens. *Proc. Workshop 'The Chemical Components and Structure of Asphaltic Materials'*, Rome, 10-13 (1991).
- [17] Decoene, Y., Comportement dans le temps. *Les enrobés drainants — Demi-journée d'études*, Centre de Recherches routières, Brussels (1988).
- [18] Larsson, J.A. and Pardue, H., Linearized model for error-compensated kinetic determinations without prior knowledge of reaction order or rate constant. *Anal. Chem.*, 61: 1949-1954 (1989).
- [19] De Backer, C., Les températures dans les structures routières. *La Technique Routière*, XXV (2): 1-29 (1980).

This page intentionally left blank

## *Chapter 18*

### **OIL SHALES IN ASPHALT MIXES**

DRAGOMIR VITOROVIĆ and DUŠAN SVETEL

#### **INTRODUCTION**

Road paving asphalt mixes consist of minerals of various grain size and bitumen, which serves as a binder. The mineral constituents, representing the major part of the mixture, are composed of 2–22 mm rock aggregates, sand and a filler of the finest granular composition. The binder (bitumen) usually originates either from the soluble fractions of natural asphalts and asphaltic rocks or from specially treated distillation residues of asphaltic or paraffinic–asphaltic crude oils. Other asphaltic mixes, used for different purposes, such as water-proofing and insulation, mastic asphalt or ‘gussasphalt’ mixtures, also contain smaller or larger amounts of mineral constituents, including the filler [1].

The filler is generally defined as finely ground (powdered) rock fragments, the purpose of which is to fill cavities and pores to enlarge the specific surface area of the minerals. Moreover, the filler stabilizes the binder (bitumen), i.e., makes it more resistant to temperature changes. According to Rick [2], the bitumen in asphalt mixes is spread over the surface of the filler grains, so that almost every particle is coated with a thin layer of the binder. Thus, the necessary amount of bitumen is adsorbed on the filler surfaces in asphalt mixes.

The surface properties of the filler depend on the type of material used for its manufacture. From a practical point of view, the interaction between the binder and the filler is important, influencing the properties of the mixes. Consequently and because of the increasing requirements of the market, special attention has long been paid to investigate different kinds of fillers.

The road paving mixes and other asphaltic mixtures are expected to be resistant to heat, frost, atmosphere, light, wear, etc. The filler may influence all these properties. Consequently, the filler itself must have specific chemical and physical properties.

The most often used fillers are powdered limestones, marble or chalk, powdered shale, calcareous marlstone or contact-metamorphic rocks, as well as natural mixtures of bitumen and minerals. In addition to these mineral materials, organic fillers have also been used, including natural products, such as wool and plant fibers, and textile industry waste, as well as different kinds of powdered coals, ranging from peat to hard coals. Since the beginning of the nineteenth century and for a long period after that, natural rubber has also been used as a component in making asphalt mixes [3,4]. Karius and Dickinson [5], for example, investigated the effect of natural rubber and some South African coals on the characteristics of bituminous binders. Both types of fillers were

shown to improve the properties of the mixes, particularly those concerned with the change of viscosity upon heating and the decrease of brittleness at low temperatures. The synergetic effect of coals and polymers was found to be even better than the effect of individual additives. The amounts of added natural rubber and coal were 3% and up to 13%, respectively.

Synthetic polymers have also been blended with bitumen in order to improve its properties [3,4]. Polymer-modified bitumens, however, are not discussed here, because this special topic is outside the scope of this chapter.

#### OIL SHALES AS FILLER

Oil shales also belong to the organic matter containing fillers of natural origin. Very old patent literature reveals data on the usage of modified oil shales in asphalt mixtures. Thus, Mulholland [6] suggested that very rich United Kingdom oil shales could be used as a filler in manufacturing mixtures for roads and roofs (Fig. 18-1). Prior to usage, the oil shale was treated mechanically and chemically: it was crushed, powdered, sieved and finally 'cooked' in concentrated or diluted solutions of acids. On the other hand, Thuret and Hubert [7] used three kinds of materials for making road paving mixtures: solid oil shale distillation residue, raw oil shale, and bituminous limestone. Data on the properties of the mixtures obtained were not presented. The main goal was, as indicated, to improve the adhesion and cohesion of the bitumen by incorporating special fillers into the mixes.

Systematic investigation of raw oil shale as the filler in asphaltic mixtures was initiated by Stefanović and Vitorović [8,9] and Stefanović et al. [10]. The rationale in using oil shales as the filler in asphaltic mixes is based on two facts. On the one hand, oil shale kerogen is a substance of macromolecular nature which, containing heteroatoms such as oxygen, sulfur and nitrogen, in a sense resembles bitumen used as a binder in asphalt mixes. On the other hand, the addition of natural or synthetic polymers to asphalt mixes improves their properties. Therefore, these authors suggested that powdered raw oil shale could be used as a filler, expecting that the mineral fraction would have the role of the filler itself, and the native kerogen would serve to improve the interaction between the binder (bitumen) and the filler. Simultaneously, the kerogen, as a macromolecular material, should enhance the rheological properties of the binder-bitumen and, thus, of the asphaltic mixes [8].

The first experiments were carried out with oil shale from Aleksinac (Serbia, Yugoslavia), which is a Miocene–Oligocene lacustrine deposit. The sample contained ca. 26% organic matter (type I kerogen) and 65% ash. The oil shale was easily powdered in a ball mill to the filler grain size (over 90% passage through a 0.09-mm sieve). In addition to testing the properties of the oil shale itself, the first experiments involved examination of mixtures of bitumen and the oil shale filler, and in parallel, for the sake of comparison, of mixtures of bitumen with a standard limestone filler, which consisted of marble from Arandjelovac, Serbia. Both fillers were of the same grain size. However, the oil shale filler was of lower density, higher porosity and had a considerably higher specific surface area.




---

A.D. 1871, 18th OCTOBER. N° 2772.

---

**Composition for Roadways, Roofs, &c.**

---

*(Provisional Protection not allowed.)*

**PROVISIONAL SPECIFICATION** left by Frederick George Mulholland  
at the Office of the Commissioners of Patents, with his Petition,  
on the 18th October 1871.

I, **FREDERICK GEORGE MULHOLLAND**, of No. 21, Great St. Helen's,  
Bishopgate, in the City of London, Civil Engineer, do hereby declare  
the nature of the said Invention for "**IMPROVEMENTS IN THE PREPARATION  
OF MATERIALS AND MANUFACTURE THEREFROM OF COMPOSITIONS TO SUPERSEDE THE  
USE AND APPLICATION OF FOREIGN PRODUCTS FOR COATING, COVERING, OR LAYING  
ROADWAYS, FOOTPATHS, FLOORING, ROOFING, AND OTHER LIKE OR SIMILAR PUR-  
POSES,**" to be as follows :—

This Invention relates to the treatment both mechanically and  
chemically of the bituminous shales found in the United Kingdom, and  
under ordinary circumstances it is found in practice that mere crushing  
or rolling and subsequent screening is sufficient preparation for  
effectuating the above objects, but when obtained of peculiarly rich  
quality, that is, when impregnated to an unusual extent with bitumen,  
oil, or wax, a system of boiling is preferentially resorted to, with the  
addition of either strong or weak acid solutions as may be deemed or

Fig. 18-1. Composition for roadways, roofs, etc.

Several standard, as well as non-standard, tests of rheological properties were chosen as criteria for the quality evaluation of the asphalt mixes.

In preparing mixtures of oil shale filler and certain fixed amounts of bitumen, considerably smaller quantities of filler compared to the mixes with limestone filler were found to be sufficient to obtain satisfactory properties of the asphaltic mixes. On the other hand, the preparation of asphaltic concrete and 'gussasphalt' mixtures with



TABLE 18-1

Composition of the mixtures for asphaltic concrete and 'gussasphalt'

Constituent	Mixtures for asphaltic concrete			Mixtures for 'gussasphalt'		
	1	3	5	2	4	6
Filler, % of total mixture	7	7	4	23	23	13
Bitumen 50/75 or 65/25, % of total mixture	6.7	7.6	6.7	8.9	15.0	9.4

TABLE 18-2

Tensile strength of eight-sided prisms made of asphaltic concrete and 'gussasphalt' mixes (kg/cm<sup>2</sup>)

Mixtures	Temperature, °C				
	+21°	+10°	0	−10°	−20°
1 (limestone filler)	6.85	9.06	11.40	20.96	26.00
5 (oil shale filler)	8.90	15.83	24.80	34.20	32.40
2 (limestone filler)	17.50	35.40	35.20	36.90	36.70
6 (oil shale filler)	26.60	42.56	46.00	46.40	46.10

TABLE 18-3

Flexural strength of prisms made of asphaltic concrete and 'gussasphalt' mixes (kg/cm<sup>2</sup>)

Mixtures	Temperature, °C				
	+21°	+10°	0	−10°	−20°
1 (limestone filler)	25.70	33.45	54.70	79.40	62.90
5 (oil shale filler)	26.40	43.40	66.00	81.30	77.90
2 (limestone filler)	33.65	49.20	75.50	62.90	61.90
6 (oil shale filler)	55.00	73.30	90.12	98.20	91.80

identical amounts of limestone and oil shale filler required higher amounts of bitumen for the mixes with oil shale filler. Therefore, both types of mixes were prepared for testing, i.e., those with identical amounts of fillers, as well as those with the same amounts of bitumen (Table 18-1).

Investigation of the different mixes showed that mixtures with lower amounts of oil shale filler ([5,6], Table 18-1) did not substantially differ from the standard mixtures [8].

Results of non-standard tests were particularly interesting. The tensile and flexural strengths of the mixes containing oil shale filler were considerably higher than those of the mixtures prepared with standard limestone filler. This was observed over a wide temperature range (−20° to 21°C) with both the asphaltic concrete mixtures (mixtures 1 and 5, Tables 18-2 and 18-3), as well as the 'gussasphalt' mixtures (mixtures 2 and 6, Tables 18-2 and 18-3).

Investigations were then expanded to insulating and waterproofing mixtures [9].

TABLE 18-4

Properties of insulating and waterproofing mixtures with Aleksinac oil shale and limestone fillers

Content of filler, % of total weight	R and B softening point, °C		Softening point (Wilhelmi test), °C	
	Mixture of limestone filler	Mixture of oil shale filler	Mixture of limestone filler	Mixture of oil shale filler
20	45	47	57	61
30	45	49	57	62
40	47	51	60	67
50	49	75	62	83

These types of asphaltic mixtures also require filler. Its role is to increase their general stability and improve properties such as plasticity, strength and resistance towards heat, frost, atmosphere and sun. Insulating and waterproofing mixtures were prepared with both Aleksinac oil shale filler, and a standard limestone filler. To determine the optimal bitumen/filler ratio, the amount of filler in both cases was changed in the range of 20 to 50%. The properties of the obtained mixtures are shown in Table 18-4. Mixes with oil shale filler had substantially higher softening points. Hence, they were more resistant to heat, i.e., they had considerably lower tendency towards flowing.

All the improved properties demonstrated by the mixtures containing oil shale filler were of practical importance, particularly for building and construction.

In as much as the composition of oil shales generally varies widely, it was of interest to study the effect of organic matter content in the oil shale on the rheological properties of asphaltic mixtures [10]. For this purpose, three samples of Aleksinac oil shale having different organic matter contents were used for preparing three kinds of filler (I, II and III). The Fischer assay oil yields of the three samples were 6.0% (I), 9.2% (II) and 17.7% (III). The properties of the mixes with different oil shale fillers were again compared to standard mixes containing limestone filler. To eliminate the eventual effect of grain size, the granulometric compositions of the four fillers were adjusted to be approximately the same.

Three types of mixtures were prepared with all four fillers: asphaltic concrete, 'gussasphalt' and an insulating (waterproofing) mixture. Moreover, two series of each type of mixture with oil shale contained the same or lower quantities of filler compared to the limestone filler mixture.

The asphaltic concrete mixtures with filler I (the leanest oil shale) required the smallest quantity of bitumen, whereas mixtures with richer shale fillers (II and III) demanded higher amounts of bitumen (Table 18-5). Mixtures with filler I demonstrated superior properties in spite of the fact that they contained smaller amounts of bitumen; they were more stable according to the Marshall test [10] and more resistant towards pressure.

'Gussasphalt' mixtures made with the same amount of Aleksinac oil shale filler I required approximately the same quantity of bitumen as the mixture with standard limestone filler. The stability according to the Marshall test was superior and the tensile and flexural strengths were also better compared to the standard mixtures. On the other

TABLE 18-5

The proportion of binder (bitumen) in asphaltic concrete mixtures

	Filler content in the mixture (% of total weight)	Bitumen (BIT 40/200) in the asphaltic mixture (% of total weight)
<i>Calcareous filler</i>		
	11.05	5.80
<i>Larger contents of oil shale filler</i>		
I	11.35	5.30
II	10.31	6.10
III	10.40	7.50
<i>Smaller contents of oil shale filler</i>		
I	10.00	5.20–5.30
II	7.00	6.20–6.30
III	7.00	7.00

TABLE 18-6

Properties of waterproofing mixtures containing different proportions of various fillers

Type of filler	Mixtures with bitumen IB 85/40 Softening point according to Wilhelmi test, °C			Mixtures with bitumen BIT 40/200 R and B softening point, °C
Content of filler (%):	25	35	45	55
Limestone	100	102	104	45
Oil Shale I	103	106	110	49
Oil Shale II	106	112	115	54
Oil Shale III	110	118	124	59

hand, the corresponding mixture with oil shale filler III required a considerably higher amount of bitumen.

The testing of waterproofing mixes containing different amounts of the standard limestone and the three kinds of Aleksinac oil shale fillers (I, II, III) showed that the amount of organic matter in the oil shale filler considerably affected the properties of the mixtures. The greater the content of organic matter in the shale filler, the higher the softening point of the mixture (Table 18-6). For example, by adding 45% of oil shale filler I, the same quality was achieved as by adding 25% of oil shale filler III.

Consequently, the leaner oil shale fillers were shown not only to save bitumen but also to improve the properties of asphaltic mixtures. Nevertheless, any planned use of oil shale as a filler in asphaltic mixtures requires prior investigations to find the optimal contents of filler and bitumen, and organic matter content of oil shale, to achieve the best properties of asphaltic mixes.

Hence, the application of Aleksinac oil shale filler for making different asphaltic paving and waterproofing mixtures was shown to be of practical interest, particularly because of the considerably higher resistance of these mixtures to heat.

## INVESTIGATIONS OF OIL SHALE FILLERS

Ballie [11] described the possibilities of using different French oil shales as a filler in asphaltic mixtures. Since 1974, these oil shales have been examined as potential road-making materials. The investigations were aimed at the possibility of saving expensive bitumen. In addition to laboratory experiments, investigations were expanded to actual road paving. In the first experiment, oil shales from Autun (Saône-et-Loire) were used in the form of powder and sand. The content of organic matter (kerogen) in the oil shale samples varied from 8.9 to 11.5%. The specific surface area (BET) of the oil shale filler was found to be high, indicating a high porosity of the material. The affinity of the oil shale towards bitumen was excellent. The oil shale filler had a higher hardening effect than the common, standard filler. Various kinds of asphaltic mixtures were made and used for road paving.

It was shown that powdered oil shale filler led to a possible 0.5% saving of bitumen. On the other hand, mixtures with sand-size oil shale created difficulties in manufacturing and usage.

Recently, several factors concerning asphaltic mixtures have changed, i.e., not only the economic criteria (the price of bitumen has increased), but also the requirements on the composition of asphaltic mixtures and their properties have changed. A certain composition of asphaltic mixtures is required today so that forces caused by traffic load are transferred via contact points in the rocky skeleton, while the binder covers the rock fines. The size of the filler voids becomes important because it affects the ratio of the bound to unbound bitumen in the asphaltic mortar. The bitumen consumption is established. New standards for the fillers were introduced, as well as the new analytical methods.

These changes stimulated new investigations of oil shale fillers [12].

## PROPERTIES REQUIRED OF OIL SHALE FILLERS

The three most important properties of a filler are the granulometric composition (grain size distribution), the shape of the grains, and the volumetric content of Rigid voids. The latter should be as low as possible.

Furthermore, the plasticity index, which indicates the possible presence of swelling clays, should also be as low as possible. With the standard limestone filler, the plasticity index is generally under 4, whereas with volcanic rock fillers it is somewhat higher. A higher plasticity index may also be the result of too high a proportion of the finest grains in the filler.

The bitumen hardening index with limestone and dolomite fillers ranges from 1.8 to 2.40, whereas with fillers of volcanic origin, it is between 1.40 and 1.60. The filler density depends on the type and properties of the rock.

## GRANULOMETRIC COMPOSITION OF THE OIL SHALE FILLER

Investigations have clearly shown [13,14] that from a practical point of view the granulometric composition of the filler for standard asphaltic concrete mixtures is particularly important. In the case of oil shale, to obtain a filler of optimal grain size and other properties, it is necessary to pay special attention to the shale grinding conditions. Therefore, grinding experiments were carried out with a number of different oil shales in Serbia [13] in a ball mill of 30-kg capacity. The steel ball filling was 10 kg. The grinding time was varied over a wide range.

The oil shales grind quite easily. However, it was shown that two oil shale fillers of almost identical granular composition, determined by the usual filler standards, may have quite different compositions of the  $<63\text{-}\mu\text{m}$  fraction. As an example, the results of grain size determination by two methods, the sieving method and the areometric method, of two samples of oil shale fillers obtained from oil shale from Knjazevac, Serbia, are shown in Table 18-7. Sample A was obtained by grinding for  $7 + 3$  min, and sample B by grinding for  $8 + 3$  min. As shown in Table 18-7, according to the standard sieving method, both filler samples had almost identical granulometric compositions. However, the grains of  $<46\text{ }\mu\text{m}$  in size had a substantially different composition as determined by the non-standard areometric method.

As a consequence, the volume concentration of Rigden voids and other filler properties of the two samples were different. Also, bitumen consumption during the preparation of asphaltic mixtures depends on these characteristics. The composition of the  $<63\text{-}\mu\text{m}$  fraction of a filler is not standardized. Nevertheless, the results observed suggested that by grinding the oil shale filler, the usual sieving control was not sufficient. Areometric control of the  $<63\text{-}\mu\text{m}$  fraction was shown to be necessary. Moreover, grinding conditions should be chosen to give the optimal granular composition of this fraction, i.e., to the lowest possible content of the smallest particles.

TABLE 18-7

Granulometric composition of oil shale fillers, Knjazevac (Serbia)

Mesh ( $\mu\text{m}$ )	Sample A	Sample B
<i>wt% (sieve analysis)</i>		
-63	59.7	59.8
-90	71.0	72.6
-250	94.3	96.3
-710	100.0	100.0
<i>Areometric granulometric composition, %</i>		
-80.4	62.8	70.2
-46.4	37.0	51.5
-14.7	11.3	29.0
-7.3	6.4	17.7
-4.2	4.8	9.7
-1.5	3.2	4.8

TABLE 18-8

Properties of fillers obtained from Aleksinac oil shale after grinding for 60, 25 and 10 min

Property	Sample		
	I	II	III
Density (kg/dm <sup>3</sup> )	2.304	2.487	2.500
Plasticity index	28.8	9.3	5.0
Hardening index	1.134	1.380	1.400
Content of Rigden voids (% of bulk volume)	46.80	42.80	41.40

The dependence of the filler properties on the grinding time is illustrated in Table 18-8, giving the properties of three samples of Aleksinac oil shale fillers (I, II and III) obtained by grinding the same initial oil shale sample for 1 h, 25 min, and 10 min.

The volume concentration of Rigden voids of filler III was found to be almost in the range of voids of the standard calcareous filler. Other characteristics of filler III were also superior to those of fillers II and I.

#### INVESTIGATIONS OF OIL SHALE FILLER RELATED TO THE SPATIAL DESIGNING OF ASPHALTIC MIXTURES

For the spatial designing of asphaltic concrete type mixtures, an insight is necessary into the volume concentration of each component of the asphaltic mixture as a system, as well as bitumen mortar as a sub-system. In the case of asphaltic mortar, the so-called void concentration (filler intergranular pore space) after the interaction of the filler with bitumen is of prime importance [15,16]. Investigations have shown [14,16] that interaction between the filler and bitumen leads to the change of filler voids in the mixture of filler and bitumen. The interaction between filler and bitumen was studied by using the ENAX-RAMPEIN computer program [16,17], which enabled the determination of the void concentration after the spatial interaction of filler with bitumen [CŠPR(INT)] on the basis of the R and B softening point increase of the bitumen mortar ( $\Delta R$  and B) as a function of the filler content in the bitumen mortar (CP/BM):

$$\Delta R \text{ and } B = \frac{B \times CP/BM}{100 - CP/BM - C\check{S}PR(INT)}$$

The volume concentration of Rigden voids (CŠPR) is compared in Table 18-9 with the void concentration after the spatial interaction of filler with bitumen [CŠPR(INT)] of the Aleksinac oil shale fillers, the properties of which are shown in Table 18-8. The integral results of the corresponding values of oil shale fillers of various origin and properties are given in Table 18-10.

The results presented in Tables 18-9 and 18-10 demonstrate that the chemical and mineralogical compositions of the oil shale filler, as well as the grinding conditions, affect the volume concentration of voids before and after the interaction of bitumen with filler. The interaction varied depending on the kind of filler. The organic matter content

TABLE 18-9

Porosity of Aleksinac oil shale fillers I, II and III before and after interaction with bitumen

Porosity, %	Filler		
	I	II	III
CŠPR	46.80	42.80	41.40
CŠPR (INT)	43.16	44.80	40.82

TABLE 18-10

Properties of oil shale fillers of various origin in Serbia as well as their volumetric content of voids before and after interaction with bitumen

Property	Vranje		Knjazevac			Mionica		Bubanj potok
	1	2	3	4	5	6	7	8
Grinding time, min.	8 + 2	8 + 2	7 + 3	8 + 3	7 + 3	6 + 3	4.5 + 3	7 + 3
Content of organic matter (wt%)	5.6	1.8	6.1	6.1	7.2	3.3	3.3	4.6
Density (kg/dm <sup>3</sup> )	2.534	2.620	2.610	2.610	2.520	2.624	2.628	2.602
Plasticity index	11.0	11.6	0	0	0	10.4	13.7	16.0
Hardening index	1.289	1.380	1.637	1.662	1.585	1.141	1.067	1.210
Content of Rigid voids CŠPR (% of bulk volume)	42.23	42.43	34.23	35.28	33.59	42.40	37.00	43.93
CŠPR (INT)	45.30	38.82	33.85	40.38	36.83	50.77	50.96	49.77

did not substantially influence the void concentration after the interaction between the bitumen and filler.

#### SPATIAL DESIGN OF ASPHALTIC MIXTURES WITH OIL SHALE FILLER

The principles of spatial designing [18] are based on the qualitative composition of asphaltic mixtures, which are composed of seven components:

(1) The rock skeleton ( $C_{KS/AU}$ ) represents the fragments (grains > 0.09 mm in size); it is responsible for most of the resistance of the system towards deformation.

(2) The adsorbed bitumen ( $C_{BS(AD)/AU}$ ) is the fraction of bitumen adsorbed on the rocky skeleton grains in the pores; this part of the bitumen does not have the role of binder in the asphaltic system.

(3) The intergranular free bitumen ( $C_{BS(INT)/AU}$ ) represents the sticky bitumen film around the grains of the rock fragments skeleton.

(4) The bound bitumen ( $C_{BV/AU}$ ) represents the part of the bitumen which serves as the binder of filler particles.

(5) The filler ( $C_{P/AU}$ ) is the <0.09 mm in size grain fraction of the rock fragments.

(6) The closed voids are the part of the intergranular space of the rock fragments

skeleton filled with air that does not have contact with the surface of the sample.

(7) The open voids are part of the intergranular space of the rock fragments skeleton filled with air, water or ice, which has contact with the surface of the sample.

Investigations have shown [19] that an asphaltic layer, the composition of which fits Eq. 18-1, will not have a tendency to damage or show ruts and tracks, which are primarily formed at elevated temperatures.

$$C_{\$/AU} \geq \left(1 - \frac{C_{KS(POR)/AU}}{C_{KS(POR)_{max}/AU}}\right) \times 100 \quad (18-1)$$

where:  $C_{\$/AU}$  = volume concentration of voids in the asphaltic specimen, % of bulk volume;  $C_{KS(POR)/AU}$  = volume concentration of the rock fragments skeleton with pores in the asphaltic specimen;  $C_{KS(POR)_{max}/AU}$  = maximal volume concentration of the rock skeleton with pores, i.e., the concentration which provides the maximal possible number of contacts between the particles.

The asphaltic mixture incorporated into the layer of roadway structure does not have a high concentration of bitumen mortar, so that the strains in the roadway structure caused by traffic load are transferred via the grains of the rock fragments skeleton, provided they satisfy the prerequisites given in Eq. 18-1.

Cracks often appear in asphaltic mixtures at low temperatures. For an asphaltic mixture to be resistant at low temperatures, in addition to the prerequisites defined by Eq. 18-1, it is also necessary that Eq. 18-2 is satisfied.

$$C_{BS(INT)/AU} \geq \frac{C_{KS(POR)/AU}}{100} \sum_{i=1}^{i=n} P Z_{FiKS} D F_{FiKS} \quad (18-2)$$

where:  $P Z_{FiKS}$  = the specific surface area of the grains of a fraction of the rock fragments skeleton, of the range of grain size;  $D F_{FiKS}$  = the thickness of the bitumen film around the grains of rock fragments skeleton, the optimal value of which is a function of the grain size, temperature and strain-deformational conditions encountered during use.

Asphalts having properties which satisfy Eq. 18-2 are resistant to cracking. This means that in the asphaltic layer of the roadway structure, the thickness of the film around the rock fragments is sufficient to prevent cracking.

Based on these principles, asphaltic mixtures for the wearing course containing oil shale filler were spatially designed. At the same time, the possible use of oil shale filler in these mixes was examined. For this purpose the RAMPEIN DOKAZ computer program was used [20].

The properties of asphaltic mixtures containing the oil shale filler were compared to those containing the standard limestone filler for asphaltic concrete 0/16 mm, designed according to the Yugoslav standard [21]. This standard corresponds to the European standards for the same type of asphaltic mixtures. Following the results of the computer analysis, the necessary changes in the composition were made, in order to obtain the optimal spatial composition.

The composition of this mixture was as follows: rock fragments skeleton ( $C_{KS/AU}$ ), 81.19% by volume; adsorbed bitumen ( $C_{BS(AD)/AU}$ ), 1.49%; intergranular free bitumen ( $C_{BS(INT)/AU}$ ), 7.47%; bound bitumen ( $C_{BV/AU}$ ), 3.35%; and the filler ( $C_{P/AU}$ ), 6.51%.



TABLE 18-11

Granulometric composition of spatially designed asphaltic mixture with limestone filler

Mesh (mm)	Passage through sieve (wt%)
0.09	7.5
0.25	14.0
0.71	22.5
2.00	35.5
4.00	48.0
8.00	67.5
11.20	80.0
16.00	100.0

The specific surface area of the rock fines was  $9837 \text{ cm}^2/100 \text{ cm}^3$ , and the maximal content of the rock fragments skeleton with pores (with maximal possible number of contacts between the particles), 82.76% by volume. Expressed in weight percent, the content of bitumen was 5.0%. In formulating the asphaltic mixture, the thickness of the bitumen film for the 0.09 to 0.25 mm fraction of rocks was  $8 \text{ }\mu\text{m}$ , and that of the fraction up to 16 mm in size was  $200 \text{ }\mu\text{m}$ , suitable for the heaviest traffic load and unfavorable temperature conditions. The porosity of the standard limestone filler after interaction (CŠPR(INT)) was 34%.

The granulometric composition of the rock fragments in this standard asphaltic mixture with limestone filler is shown in Table 18-11. The formulation of asphaltic mixtures containing oil shale filler was initially based on the granulometric composition of the mixture containing the standard limestone filler. The same amounts of bitumen and filler were used as in the standard mixture. The mixture with oil shale filler was analyzed by the RAMPEIN DOKAZ computer program under the conditions used for the standard mixture. The input differed only by the values of the filler porosity and density. The porosity was determined after the interaction between bitumen and filler. These have been shown earlier in Tables 18-9 and 18-10.

The results showed that in the case of asphaltic mixtures containing oil shale filler, the concentrations of the bound, intergranular and adsorbed bitumens, as well as the content of filler, differed with the standard mixture. However, the analysis provided data for changing the composition of asphaltic mixture aimed to obtain a composition corresponding to the mixture containing calcareous filler, i.e., the ideal (optimal) composition.

The changes required for the mixtures presented in Tables 18-9 and 18-10 are given in Table 18-12. The changes depend mainly on two factors: the content of the finest grain fraction and the content of organic matter in the oil shale filler. However, in the case of several oil shale fillers, such as fillers 3, 4 and 5, the changes in composition may also depend on the chemical and mineralogical compositions of the oil shale filler.

Consequently, in addition to the selection of the oil shale sample of optimal composition, it is of primary importance to control the grinding of the shale, particularly to limit the content of the  $<63\text{-}\mu\text{m}$  fraction. Thus, as already mentioned, areometric control of the composition of the  $<63\text{-}\mu\text{m}$  fraction is suggested.

TABLE 18-12

Necessary corrections of the composition of asphaltic mixtures containing different oil shale fillers

	Asphaltic mixtures with oil shale filler										
	I	II	III	1	2	3	4	5	6	7	8
Required additional bitumen (% by weight)	0.4	0.5	0.3	0.5	0.2	0.0	0.0	0.2	0.7	0.7	0.7
Required reduction of filler (% by weight)	2.0	1.8	1.3	1.7	0.8	0.8	0.3	1.0	2.1	2.1	2.0

Also, it is necessary to study the interaction between the filler and the bitumen, because this may lead to a change in the volumetric content of Rigden voids. During the spatial design of asphaltic mixtures, special care should be paid to this fact, because the filler-bitumen sub-system (i.e., the bitumen mortar) plays a major role in the design of asphaltic concrete mixtures.

All investigations involving the spatial design of asphaltic mixtures, demonstrated the possibilities of using oil shale fillers as a component in asphaltic concrete. Moreover, it was shown that when attention was paid to the above-mentioned oil shale properties, as well as to the processing parameters, the bitumen content in asphaltic mixtures could be either the same or only 0.2 to 0.4% higher compared to the mixtures containing standard limestone filler. On the other hand, based on earlier evidence [8–10], it may be expected that asphalt layers with oil shale filler will be more durable, the ageing of the bitumen in these asphaltic mixtures less intensive and, finally, the fatigue of the roadway structure less pronounced. These effects may be due to some kind of interaction between the shale organic matter (kerogen) and the binder (bitumen) during the use of roads. Actual tests on roads should be made to confirm such predictions.

#### POTENTIAL USE OF OIL SHALE AS A FILLER IN SPECIAL ASPHALTIC MIXTURES AND BITUMINOUS AGGREGATES

Asphaltic concrete-type mixtures as described, are designed so that every grain of the rock fines is covered with a bitumen film of optimal thickness, whereas the granulometric composition of the rock fines is close to the Fuller parabola, leading to a minimum content of voids in the mixture of rock fines and an optimum content of voids in the asphaltic mixture. Recently, asphaltic mixtures not formulated according to the concrete properties have been used more often. A few examples are mentioned here.

The so-called discontinuous mixtures are those mixtures lacking some size fractions of the rock aggregate, e.g., the 2/4-mm or 4/8-mm fractions or both. Such mixtures in the rolled state have a higher porosity.

Skeletal asphaltic mixtures have a higher content of coarser fractions of rock aggregates.

In some roadway structures, particularly those with frequent and heavy traffic, drainage layers are incorporated, allowing the drainage of water from the surface of the road preventing aquaplaning of the vehicles. These type of mixtures have higher contents of coarser fractions of the rock aggregates and, therefore, high contents of voids.

In all the above-mentioned mixtures, the binder (bitumen) should have superior qualities compared to the standard bitumen. In addition, the trend is to incorporate the higher amounts of binder into such mixtures. To achieve this, various additives are added to the bitumen, such as different natural or synthetic polymers. Also, activated fillers or other kinds of fillers are used which bind larger amounts of bitumen in the asphaltic mixture.

Based on earlier experiments with oil shale filler [8–10], an oil shale filler should be superior compared to the limestone filler in the special-purpose mixtures.

Bituminous mixes, which contain around 50% by weight or more of hydrocarbon binder, the rest being filler, bituminous joint fillers on concrete roadways, waterproofing mixtures for different purposes, etc. might be of superior quality when a filler with a lower hardening index is used. This means that the effect of the filler on the rheological properties of the mixture of bitumen and filler is more pronounced, provided that the plasticity index is minimal. All this may be achieved with an oil shale filler, because a chemical or physicochemical interaction between the bitumen and the oil shale organic matter is expected during use. Such modified bitumen is expected to be more resistant and durable than the pure bitumen.

To be economical, an oil shale filler should have the same price as the standard limestone filler. According to experimental evidence, oil shale filler production (grinding) should be easier than the production of limestone filler, once the optimal grinding regime has been determined. During use, the asphaltic mixtures with an oil shale filler are not expected to unfavorably adsorb the lightest fractions of the bitumen. Also, the grains of calcareous origin will not selectively adsorb the bitumen. On the contrary, an interaction is expected between the bitumen or some of its fractions with the organic matter of the oil shale filler. This, on the other hand, should lead to improvement of the resistance towards ageing and fatigue, as well as some of the rheological properties of the mixture. Nevertheless, because the above-mentioned processes take time, final conclusions concerning all the potentials of oil shale filler require more experimentation and testing.

## REFERENCES

- [1] Traxler, R.N., Asphalts. In: R. Houwink (Editor), *Elastomers and Plastomers*. Elsevier, New York, 2nd Vol., 486 pp. (1949).
- [2] Rick, A.W., *Bitumen-Füllstoffgemische*. Berlin-Pankov (1949).
- [3] Zenke, G., Polymer modifizierte Strassenbaubitumen im Spiegel von Literatur-Ergebnisse — Versuch eines Resümes. *Die Asphaltstrasse* 1, 5–16 (1985); 4, 170–182 (1985).
- [4] Svetel, D., From bitumen and polymer to polymerbitumen (in Serbo-Croatian). In: S. Galjanić and A. Šolc (Editors), *Bitumen and Asphalt Mixture, Proc. JAZU Scientific Council for Petroleum, Refining and Application Division Ser. C*, 9, 1–14 (1990).
- [5] Karius, H. and Dickinson, E.J., Effect of coal and long chain polymers on the characteristics of bituminous road binders. *J. Appl. Chem.*, 9: 542 (1959).
- [6] Mulholland, F.G., *Composition for Roadways, Roofs, etc.* Brit. Patent No. 2772 (1871).
- [7] Thuret, Ch. and Hubert, O.A., *Perfectionnement à la confection des revêtements routiers bitumineux et goudronneux, nouveaux fillers pour la mise en oeuvre de ces perfectionnements et leur procédé de fabrication*. Fr. Patent No. 825.945 (1937).

- [8] Stefanović, Dj. and Vitorović, D., Application of Aleksinac oil shale as filler for bituminous mixtures, I. Paving mixtures (in Serbian). *Hem. Ind.*, 20: 678–683 (1966).
- [9] Stefanović, Dj. and Vitorović, D., Application of Aleksinac oil shale as filler for bituminous mixtures, II. Insulation and waterproofing mixtures (in Serbian). *Hem. Ind.*, 20: 683–685 (1966).
- [10] Stefanović, Dj., Vitorović, D., Granžan, M. and Svetel, D., Application of Aleksinac oil shale as filler for bituminous mixtures, III. The effect of the oil shale kerogen content on mixture properties (in Serbian). *Hem. Ind.*, 20: 1233–1239 (1966).
- [11] Ballie, M., Utilisation des schistes bitumineux sous formes de fines ou de sable dans les bétons bitumineux. *Bull. Liaison Labo. P. Ch.*, 109: 25–35 (1980).
- [12] Vitorović, D., Svetel, D., Pap, I., Milovanović, T. and Bajc, S., The potential for the application of bituminous shales from Aleksinac as a filler in asphalt mixtures (in Serbo-Croatian). *Gradjevinar (Zagreb)*, 36 (9): 125–132 (1984).
- [13] Vitorović, D., Svetel, D., Bajc, S. and Milovanović, T., Oil shale as filler for asphaltic mixtures. Study of grinding conditions (in Serbo-Croatian). *Hem. Ind.*, 43: 5–10 (1989).
- [14] Vitorović, D., Svetel, D., Bajc, S., Cvetković, O. and Milovanović, T., Bitumen consumption in the production of asphalt mixtures with oil shale as filler—Influence of the grinding and the organic matter content of the filler (in Serbo-Croatian). In: S. Galjanić and A. Šolc (Editors), *Bitumen and Asphalt Mixture, Proc. JAZU Scientific Council for Petroleum, Refining and Application Division, Ser. C*, 9, 331–335 (1990).
- [15] Ramljak, Z. and Pejnović, V., Yugoslav National Report. *RILEM, Third Int. Symp. Testing of Hydrocarbon Binders and Materials, Theme IV. Practical Mechanical Tests for the Design and Control of Asphaltic Mixes, Belgrade*, pp. 3–27 (1983).
- [16] Ramljak, Z. and Ladika, J., Dependence of properties of bitumen mortars on their composition (in Croatian). In: S. Galjanić and A. Šolc (Editors), *Bitumen and Asphalt Mixture, Proc. JAZU Scientific Council for Petroleum, Refining and Application Division, Ser. C*, 9, 195–199 (1990).
- [17] Ramljak, Z., *Computer program ENAX-RAMPEIN*. Zagreb (1990).
- [18] Ramljak, Z., *Program-apparatus package for spatial designing of asphaltic mixtures of optimal composition according to the RAMPEIN method* (in Croatian). Zagreb.
- [19] Ramljak, Z. and Pejnović, V., Dependence of permanent deformations on the spatial characteristics of asphaltic layer (in Croatian). *Ceste Mostovi (Roads Bridges)*, 23: 273 (1983).
- [20] Ramljak, Z., *Programme for the Computer DOKAZ — Checking the Optimality of the Composition of the Manufactured Asphaltic Mixture*. Zagreb (1984).
- [21] Yugoslav standard for manufacturing asphaltic concrete, technical conditions. *JUS U.E4.014*.

This page intentionally left blank

## *Chapter 19*

# **SULPHUR-MODIFIED ASPHALTS**

IRENA GAWEL

## **INTRODUCTION**

The idea of incorporating sulphur in asphalt is very old. The process of treating asphalt with sulphur was first disclosed by Day in 1866 [1] and subsequently by Dubbs [2] who subjected the two substances to high temperatures at which a chemical reaction took place between sulphur and asphalt, with the vigorous evolution of hydrogen sulphide. The first thorough studies of the treatment of different asphalts with sulphur at a comparatively low temperature were carried out in Texas in the 1930s. Benzowitz and Boe [3] reported the effect of sulphur on the bitumen binder and on the mixes, and although the properties of sulphur-containing asphalt mixes were better than those of conventional asphalt mixes, the differences in prices between sulphur and asphalt made the product uneconomical. In view of the increase in the asphalt price since the beginning of the 1970s, the product was studied again. The decrease in sulphur costs was attributable to the availability of large quantities of sulphur recovered from secondary sources, e.g., from sour gas, from the refining of fossil fuels, and from power-plant stack gases. The surplus sulphur recovered from these sources was one of the major reasons that interest in sulphur utilization in asphalt paving materials was rekindled. Of several potential uses for sulphur recovered from fuels, a sulphur–asphalt combination for pavements seemed the most promising.

The probability of more sulphur being recovered as a result of more restrictive environmental legislation resulted in developing a number of different processes for producing sulphur-extended asphalts (SEA). A variety of methods to incorporate sulphur in pavements have been proposed, tested and reported [4–27]

There were two reasons for considering the use of sulphur in asphalt mixes: (1) to improve the mix quality and (2) to reduce the cost. The latter depends mainly on the relative costs of sulphur and asphalt, but energy saving is also important. Since the 1980s, the prices of sulphur and asphalt have been such that conventional asphalt mixes are cheaper. However, the properties of sulphur-containing paving materials are generally superior to those of the conventional ones.

## **SULPHUR–ASPHALT INTERACTION**

The unique chemical and physical properties of elemental sulphur make it possible to use it in construction materials. Sulphur molecules in the solid state crystallize in the orthorhombic structures and are stable up to 95.5°C. At this temperature they pass into monoclinic crystals.

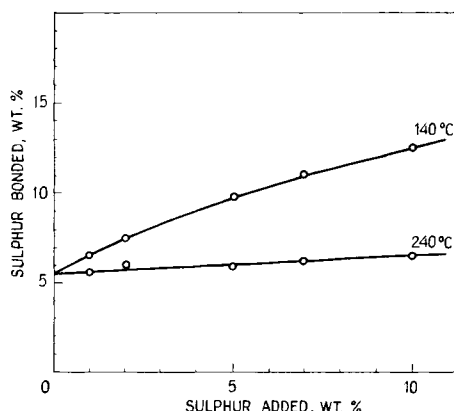


Fig. 19-1. Effect of temperature on the amount of chemically bonded sulphur [29].

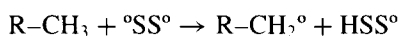
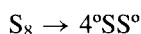
From the viewpoint of modification of asphalt with sulphur, the most interesting problem is the behaviour of sulphur in the liquid state. Molten sulphur is composed of eight-membered rings. At a temperature of above 130°C the rings undergo a partial decomposition. Sulphur atoms have a well-developed tendency to combine with one another to form an extremely complicated system of chain and/or ring molecules  $S_x$  where  $x$  varies from two to several hundred thousand atoms [28]. Depending on  $x$ , the physical and chemical properties of sulphur change considerably.

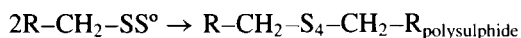
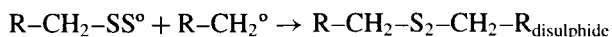
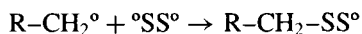
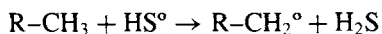
Sulphur in sulphur–asphalt blends has been found to occur in three different forms: (1) chemically bonded, (2) ‘dissolved’ in asphalt, and (3) crystalline sulphur which generally exists in the form of discrete tiny particles dispersed in asphalt.

#### *Chemically bonded sulphur*

Part of the sulphur added reacts chemically with asphalt. Big differences have been found as regards the percentage of the reacted sulphur. Petrossi et al. [29], Qarles van Ufford and Vlugter [30] and Gawel [26] reported higher values (Fig. 19-1) of bonded sulphur up to 85% at a temperature below 150°C, whereas Kennepohl and Miller [14] and Lee [31] calculated that only a few to 20% of the sulphur reacted with asphalt and entered into its molecule. The differences that have been observed were most likely caused by variations in the asphalt composition as well as by the reaction temperature and the contact time.

As has been confirmed by electron paramagnetic resonance [14,29], sulphur reacts with hydrocarbons competitively, by addition to give carbon–sulphur bonds, or by abstraction of hydrogen and subsequent hydrogen sulphide formation. On the basis of the results of complex investigations into the products of sulphur reactions with model hydrocarbons, the most likely mechanism of reaction between sulphur and asphalt has been presented [32,33]:





It has been suggested that the most reactive part of asphalt is the naphthene-aromatic fraction. At low sulphur-to-asphalt ratios, the prevalent reaction depends on temperature.

At the lower temperature range (120–150°C) sulphur introduced into asphalt enters the molecules. Naphthene-aromatics are partially transformed into polar-aromatics, mainly polysulphides. This can be assumed by considering the increase in the sulphur content of the polar-aromatic fraction corresponding to 4–5 sulphur atoms per molecule [29]. It has been observed that at lower temperatures sulphur reacts not only with hydrocarbons but also with other organic compounds, e.g., with indole to simultaneously form polysulphides [30].

Polysulphides undergo partial decomposition to form a polysulphide with a lower degree of polymerization and free sulphur. Subject to cleavage are not the newly formed bonds between sulphur and carbon atoms. Investigations with the use of sulphur isotopes have shown [30] that in  $\text{R-S-S}_x\text{-S-R}$  compounds only atoms designated as  $\text{S}_x$  can take part in decomposition reactions with the separation of elementary sulphur, whereas the atoms of sulphur connected directly with carbon do not take part in the reaction. The increase in the content of asphaltenes at temperatures of up to 150°C is negligible. Asphaltenes isolated from asphalt treated with sulphur at 130°C contain less sulphur than maltenes [30].

At temperatures above 180°C dehydrogenation with the emission of hydrogen sulphide takes place and only a negligible part of the introduced sulphur remains in the asphalt (Fig. 19-1). It has been found [30] that the raising of temperature by about 20°C causes approximately a fourfold increase in the dehydrogenation reaction rate. At temperatures of above 220°C the action of sulphur is analogous to that of oxygen in the air-blowing process. There are, however, some differences, i.e., the reaction sets in at a lower temperature than is the case with oxygen, and more sulphur is combined as compared with oxygen [34].

At elevated temperatures, polysulphide linkages which might have been formed first at lower temperatures, are broken to produce cyclic sulphides as well as complex cross-linking between separate molecules. The infrared analyses data of the various fractions of the sulphurized asphalts indicated the presence of sulphur in the cyclic tiophenic-type form [35]. With increasing temperature, naphthene-aromatics are transformed into asphaltenes through dehydrogenation and cyclization processes. For different asphalt samples treated with sulphur at a temperature of 240°C, a varied content of asphaltenes ranging from several percent [36] to 40% [35] is given. The amount of the asphaltenes formed is, to a great extent, dependent on the composition of original asphalt and on the quantity of sulphur being added. The increase in sulphur content leads to an increase in



the quantity of asphaltenes. It has been stated [36] that the lower the asphaltene content of unreacted asphalt, the higher the growth of the asphaltene content of the product at the same reaction temperature.

The change of the chemical structure of asphalt caused by introducing sulphur involves a change of its colloidal structure. The increase in the reaction temperature results in the increase in the asphaltenes/resins ratio, which causes their structure to be changed into the gel-structure. A comparison of the transmission electron photomicrographs of asphaltenes isolated from the asphalt treated by sulphur and from the initial asphalt has shown [37] a more pronounced degree of association of the sulphurized asphalt.

### *Dissolved sulphur*

Sulphur has a 20% or greater solubility in most asphalts in the temperature range of 130–150°C [9,15]. The 'dissolved' sulphur plays the role of the binder. Polysulphides that are formed as a result of the reactions at temperatures above 120°C partly dissolve unreacted sulphur [18]. The solubility of sulphur depends upon the type of asphalt as well as its origin. A slowly developing recrystallization of dissolved sulphur can be observed when a sulphur–asphalt mixture is being cooled to ambient temperatures. However, it is possible to prevent or to reduce the recrystallization by increasing the mixing time [30]. The relative amounts of dissolved and crystalline sulphur in the sulphur–asphalt binders, depending on the amount of sulphur added, are presented in Fig. 19-2.

### *Crystalline sulphur*

The excess sulphur that is not dissolved in asphalt exists in the crystalline state. The crystalline sulphur finely dispersed in asphalt acts as a filler or a structuring agent playing the role of the aggregate. Elemental sulphur disperses readily in asphalt, although the surface tensions of the two substances are quite different [38].

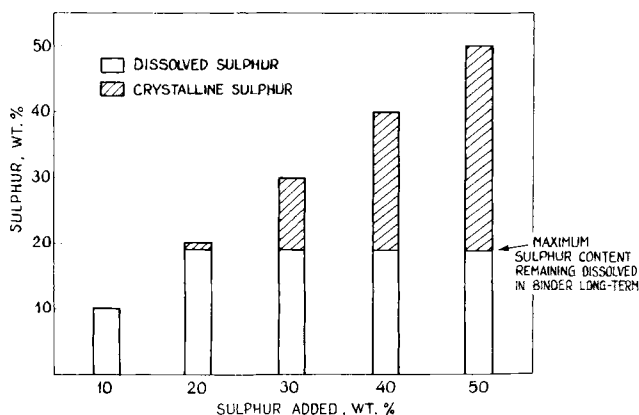


Fig. 19-2. Relative amounts of dissolved and crystalline sulphur in sulphur–asphalt blends [9].

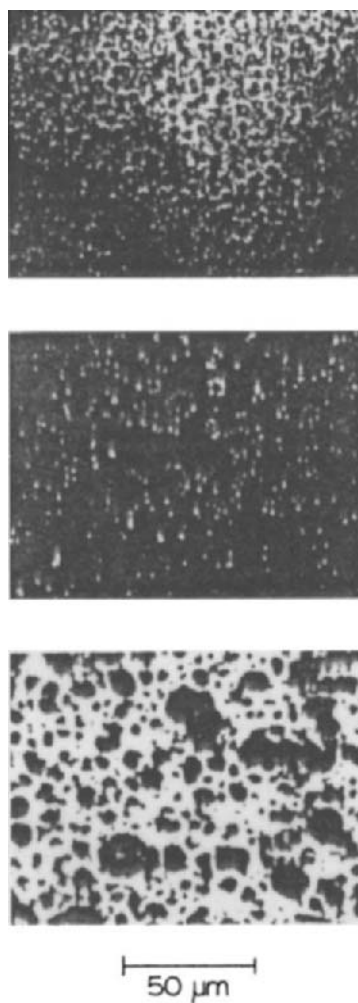


Fig. 19-3. Photomicrographs of sulphur–asphalt blends [39]. Top, sulphur to asphalt 10/90; middle, sulphur to asphalt 25/75; bottom, sulphur to asphalt 50/50.

The microscopic studies of sulphur–asphalt mixtures have shown [39] the apparent differences in the degree of the dispersion of crystalline sulphur, depending on the sulphur concentration. As shown in the photomicrographs (Fig. 19-3) in a blend of 10S/90A (wt%), sulphur particles with the diameters of approximately  $1\text{--}2\text{ }\mu\text{m}$  are homogeneously distributed throughout the asphalt. When the concentration of sulphur in the sulphur–asphalt blend increases to 25%, then some heterogeneity in its structure can be observed.

Sulphur occurs in the form of discrete particles as well as groups of many particles with an average size of  $6\text{ }\mu\text{m}$ . In the 50S/50A (wt%) blend, the heterogeneity of dispersion is quite evident.

## PREPARATION OF SULPHUR-ASPHALT MIXTURES

A sulphur-extended asphalt mix can be prepared in two ways: (1) the sulphur and asphalt can be mixed directly with the aggregate; and (2) the sulphur-asphalt binder can be prepared before being mixed with the aggregate.

In the first method sulphur may be introduced into asphalt in the pulverized or liquid form; however, the latter is preferred.

Preparation of the sulphur-asphalt binder consists of emulsifying sulphur into the asphalt [9,10]. The hot emulsion is mixed with the aggregate.

Both these methods of preparation have proved successful and produce a fine dispersion of sulphur throughout the asphalt. The evaluation of sulphur-asphalt paving mixes has shown no differences in the materials prepared no matter whether the emulsified or the direct substitution method was used [15]. However, the direct addition method is simpler.

The sulphur-asphalt emulsion is prepared by mixing liquid asphalt with molten sulphur to attain a fine sulphur dispersion of particles with several micrometers in diameter. Since the density of sulphur is approximately twice that of asphalt, a very fine droplet size of sulphur must be obtained. High shear during mixing is essential to obtain a good sulphur dispersion and a stable binder. Sulphur dispersion in asphalt can be obtained by means of different mechanical methods. The best results are achieved by mixing the components in a colloid mill. The freshly prepared sulphur-asphalt binder exhibits a similarity to most finely dispersed aqueous asphalt emulsions. Microscopic examinations of sulphur-asphalt emulsions have shown [9,37,40] a uniformly small size of the average particle immediately after preparation. After a period of time dependent on the sulphur to asphalt ratio, as well as on the mixing time, the coagulation becomes noticeable. The stability of dispersion can be improved by prolonging the mixing time as well as by using additives. The storage of the liquid binder leads to the settlement of sulphur particles and, therefore, the binder must be used immediately after being prepared. Another disadvantage of this method is the formation of hydrogen sulphide in the storage tank.

The direct addition of sulphur and asphalt to the aggregate has appeared to be more practical in the preparation of paving mixes than the use of the emulsification method. No special blending apparatus is required and the sulphur-asphalt-aggregate mixes can be prepared at the same mixing plant as those used for conventional blends.

Sulphur and asphalt may be added together to the mixer, or asphalt is poured into the hot aggregate and sulphur added subsequently. It is also possible to doze the filler lastly, i.e., after the binder [41], or to mix sulphur with the filler before they are added to the asphalt [42].

The total volume of the sulphur-asphalt binder in the mix is the same as that of the conventional asphaltic binder. Since the density of sulphur is twice that of asphalt, approximately double the weight of sulphur is required to replace an equal volume of asphalt.

The sulphur to asphalt ratio varies from about 0.1 to 4. The optimum sulphur concentration is dependent on its function in the mixture and the type of sulphur-asphalt-aggregate mixture. For a particular asphalt and a particular mixing temperature there is an optimum sulphur content.

The optimum sulphur content in sulphur-extended asphalt binders is found somewhere between 20 and 30 wt% [9,13]. Below the former, no hardening effect is obtained. Above the latter the improvement of mix workability is reduced.

Sulphur has also been used in substantial concentration in sulphur–asphalt–aggregate mixes in order to directly improve their mechanical properties. The sulphur to asphalt ratios from 1 : 1 to 4 : 1 were recommended in these materials [4–6]. To obtain the best results a sufficient amount of sulphur should be added so as to completely fill the void spaces between the aggregate.

Asphalts having a 40 to 300 penetration are preferred for preparation of sulphur–asphalt blends. The utilization of very hard asphalts should be avoided since, when used in sulphur-modified paving materials, they increase their tendency to crack at low temperatures. The higher the asphalt penetration the larger the optimum concentration of sulphur in the blend [43].

The mixing temperature should be maintained in the range of 127–150°C. The former temperature represents the sulphur melting point plus the tolerance to avoid its structuring effect; the latter one is the temperature above which sulphur undergoes an abrupt and appreciable increase in viscosity resulting in the deterioration of the workability of the paving mix. The temperature of 150°C should not be exceeded because of the formation of hydrogen sulphide and sulphur dioxide. It has been found that in order to attain the best workability and strength of mixtures containing a sulphur–asphalt binder with the typical 30% sulphur concentration, the mixing temperature should be maintained in the 130–140°C temperature range [18]. When a mixture with a higher sulphur to asphalt ratio is prepared, an approximate 150°C mixing temperature is preferred [6].

The mixing times range from about a dozen seconds to a few hours, depending on the method being used. McBee and Sullivan [15], who used a direct addition method for preparing paving materials with improved properties, have found that a two-minute mixing time is sufficient to obtain a beneficial result. The optimum mixing time to attain a fine sulphur dispersion in asphalt, with a diameter satisfying the requirements for particle size of emulsions, was 15–30 s after sulphur addition [17]. To obtain the best results, sulphur should be mixed intimately and uniformly with asphalt. A preparation at high sulphur-to-asphalt ratios requires continuous stirring even during casting so as to avoid segregation of sulphur.

#### TECHNOLOGICAL PROCESSES

A number of different industrial processes for manufacturing sulphur–asphalt–aggregate mixtures have been developed and tested.

There are two main approaches to the use of sulphur in asphalt mixes: sulphur-extended asphalt and sand–asphalt–sulphur mix techniques.

The former consists of using sulphur for a partial replacement (up to 50 wt%) of asphalt at the binder. In this technique, sulphur acts as an asphalt extender and modifies the rheological properties of the binder. The resultant binder may be utilized in all types of paving mixes, in lieu of pure asphalt.

The processes based on this technique have been developed by Société National Elf Aquitaine (SNEA), Gulf Canada, Sulphur Development Institute of Canada (SUDIC), U.S. Bureau of Mines and Esso Europe.

The latter idea is based on the utilization of sulphur in a way which makes it possible to use lower-quality aggregates, mainly the poorly graded sands. In this technique a much higher amount of sulphur is used and it functions both as an integral part of the binder and an extender of the significant portion of the aggregate. Hence, sulphur has a considerable effect on the mechanical properties of the mixes.

This approach was pioneered by Shell Canada and further developed in cooperation with the Texas Transportation Institute and the Federal Highway Administration.

One of the more extensively tested processes is that of the Société National Elf Aquitaine, which patented their procedure in France in 1973. According to this process, up to 50 wt% sulphur is finely dispersed within the asphalt [10]. The dispersion is accomplished in a patented mobile manufacturing unit which can be adapted for use with any of the existing hot-mix plants. The resultant binder is directly used to produce hot-mix paving mixtures with the use of a conventional mix plant and paving equipment. The emulsion can be stored at a temperature of 130°C for 10 h. After this time special stabilizing agents must be used.

The SNEA method was tested throughout the world in a variety of climates.

In the Gulf Canada up to 50 wt% of asphalt is replaced with molten sulphur as well [14]. The method produces sulphur in binder dispersion with sulphur particles having an average size of 4–5  $\mu\text{m}$ , without the use of additives [14]. A specially designed blending unit, the so-called sulphur–asphalt module (SAM), makes it possible to mix sulphur and asphalt automatically in the proper proportion and at the proper temperature, and to pump the blend to a pugmill where it is mixed with the aggregate. Except for a storage tank for sulphur, and SAM for sulphur–asphalt binder production, the conventional equipment can be used for mix production and paving procedure.

Since 1974, a number of field trials had been carried out with the use of the Gulf Canada technique, where both the good quality aggregates as well as the poorly graded ones were utilized.

The Sulphur Development of Canada process, called Pronk after its developer, makes use of an additive to promote dispersion of sulphur in asphalt and to stabilize the resulting binder [44–47]. As an additive polydimethylsiloxane was used. The SUDIC process used an in-line blending unit, whereas the former processes (SNEA and Gulf) utilized a high-shear rate to produce a sulphur–asphalt emulsion binder.

U.S. Bureau of Mines developed a simplified method to prepare and utilize the sulphur–asphalt binder [11,15,48]. According to this procedure, sulphur and asphalt were not premixed, but were introduced into a pugmill and mixed with the aggregate. This eliminates the need for a separate high-shear rate blender. In the year 1977, the Bureau of Mines constructed an experimental pavement.

An additional approach involved the use of sulphur in recycling old asphaltic pavement [49].

As early as 1960, Shell Canada hit upon the idea of incorporating sulphur into asphalt mixes, where sulphur was used in excess. When the sulphur weight content was equal to or higher than that of asphalt, the utilization of aggregates considered to

be unacceptable for pavement construction proved possible. The typical example was the sand–asphalt–sulphur mixes patented under the name ‘Thermopave’ [4,17,50,51]. The unique feature of the Thermopave process is that it permits manufacturing of high-quality paving materials with the use of poorly graded sands. Sulphur was well dispersed by the aggregate shearing action during mixing in the pugmill of a hot-mix plant. The liquid sulphur, in the Thermopave, increases the mix workability to a point where it is placed without roller compaction. The conventional hot-mix plant may be adapted by adding the liquid sulphur supply system; a specialized system is required, however, for transporting and placing the sand–asphalt–sulphur mixture.

Various features of the Thermopave process were patented in a number of countries.

#### EFFECT OF SULPHUR UPON THE PROPERTIES OF ASPHALT

The addition of sulphur to asphalt results in a change in the properties of the binder as well as in the mechanical properties of sulphur–asphalt–aggregate mixes. Sulphur can function both as an integral part of the binder and as a filler. At the low sulphur to asphalt ratio, sulphur replaces asphalt by modifying its rheological properties, whereas at the high sulphur to asphalt ratio, sulphur acts as a filler and a structuring agent having a considerable effect on the mechanical properties of the mixture.

The rheological properties of asphalt are modified mainly due to the change in the asphaltenes to resins ratio [31,32] which leads to the formation of a new binder with a pronounced gel-like structure [52]. The effect of sulphur on the properties of asphalt depends mainly on the sulphur concentration and the preparation conditions.

At the mixing temperature range (120–150°C) the following alteration of binder properties occur with the addition of sulphur in amounts which permit it to be ‘dissolved’.

The density of binder increases with the increasing amount of sulphur due to the higher density of elemental sulphur. This growth, however, is less than expected, with the sulphur content, up to 10 wt%, and it increases normally with the higher sulphur content [10].

The viscosity of sulphur-extended asphalt above the sulphur melting point is lower than that of asphalt (Fig. 19-4). The viscosity decreases with increase in the sulphur-in-binder content (Fig. 19-5) hitting a minimum with about 15 wt% of sulphur content [9,13]. Further addition of sulphur, however, increases the viscosity, surpassing the viscosity of the original asphalt at the sulphur level of approximately 56–60% [9,13]. These results are not in full agreement with those obtained by Garigues and Vincent [10] who found (for the same penetration grade asphalt at 130°C) that the phenomenon of viscosity reduction is inverted as soon as the sulphur content exceeds 25–30% by weight.

The penetration of sulphur–asphalt blends increases up to 10 wt% of sulphur-in-binder content (Fig. 19-6). With over 20–30% sulphur, penetration reverts to its initial value, and then decreases in an almost linear fashion [10,54]. There are, however, some discrepancies between the results obtained by different researchers in regard to the value at which the curve of the penetration dependence on the sulphur content in the binder attains a maximum. According Kennepohl et al. [9] and Alama [41], the penetration increases up to 40% of the sulphur content, and after reaching this value it decreases steadily.

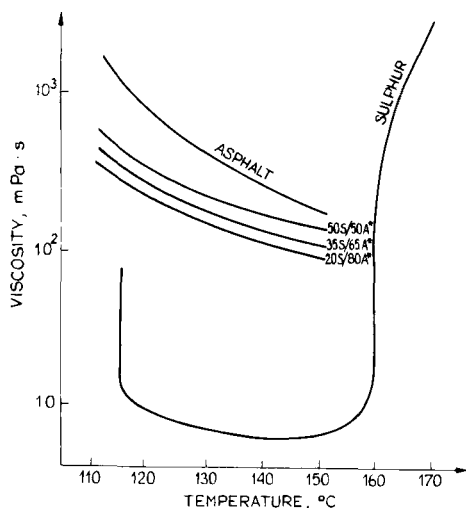


Fig. 19-4. Viscosities of asphalt, sulphur, and sulphur-asphalt blends [22]; \* sulphur-asphalt blend, wt%.

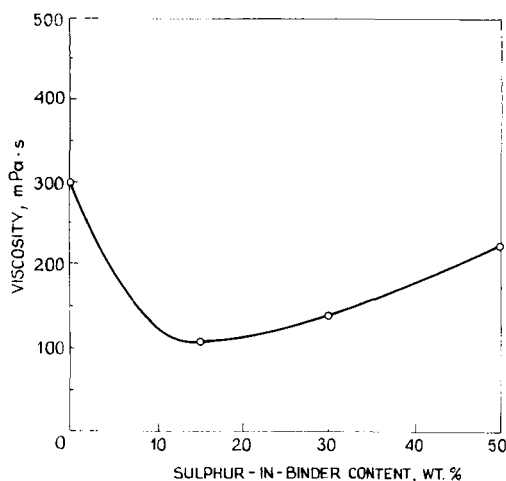


Fig. 19-5. Effect of sulphur content on binder viscosity (at 135°C).

The addition of sulphur results in a negligible increase of the penetration index, proportional to the amount of the sulphur introduced.

The ring-and-ball softening point hits its minimum with a 10% sulphur content (Fig. 19-7) and then increases slowly, exceeding the value for pure asphalt [9,10,31,41, 53,54].

The Fraass breaking point increases slightly with the increase of the sulphur content [9,29]. Some researchers, however, have observed the decrease in the breaking point of the sulphur-asphalt blend in the initial period after its preparation [41,55].

The change in binder ductility caused by introducing sulphur is dependent on the

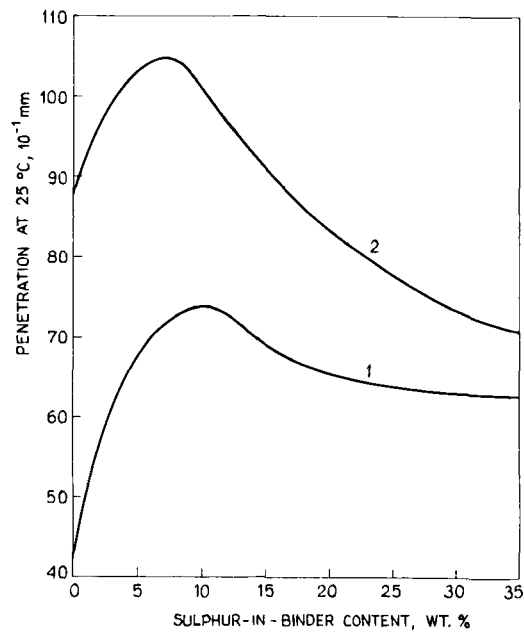


Fig. 19-6. Effect of sulphur content on binder penetration. Curve 1 = 40–50 pen. grade asphalt with sulphur [53]; curve 2 = 85–100 pen. grade asphalt with sulphur [10].

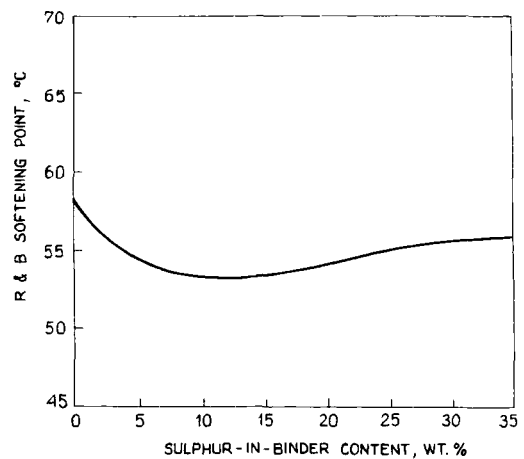


Fig. 19-7. Effect of sulphur content on the Ring and Ball softening point [53].

temperature and the penetration of pure asphalt. The addition of sulphur displaces the ductility maximum towards lower temperatures [54]. The introduction of sulphur into the asphalt results in an increase in its ductility at lower temperatures (0°C, 5°C) [29,43]. At a temperature of 25°C, a sulphur content of up to 5% increases the ductility, whereas



with further addition of sulphur, the ductility drops. On account of the ductility, the optimal content of sulphur in the binder is 15 wt% [31,43,54].

The treatment of asphalt strongly affects its surface characteristics. Views regarding the influence of sulphur addition on the adhesion of the binder to the aggregate are controversial. The study of the performance of sulphur–asphalt–sand mixes under the influence of water, with the use of three different kinds of sand has shown that the addition of sulphur improves adhesion [53]. Also Papirer and Fritschy [38] accepted the beneficial effect of sulphur on the adhesive properties of the binder. Alama and Wojdanowicz [43] have found, however, deterioration of the binder adhesion to different aggregates with an increased sulphur content.

The temperature conditioning has a conspicuous effect on the aging of sulphur–asphalt binders [55].

The penetration (at 25°C) of sulphur-modified asphalts conditioned at ambient temperature decreases with time to a greater extent than that of pure asphalt (Fig. 19-8), exceeding the value for asphalt in the time depending on the sulphur content. The reduction in penetration takes place within the first 20–30 days after the blend preparation, and thereafter the value of penetration remains constant [43,53,54].

The viscosity of sulphur-extended asphalt increases appreciably within five days after its preparation [39].

The softening point of sulphur–asphalt blend increases slightly with the increase in the conditioning time.

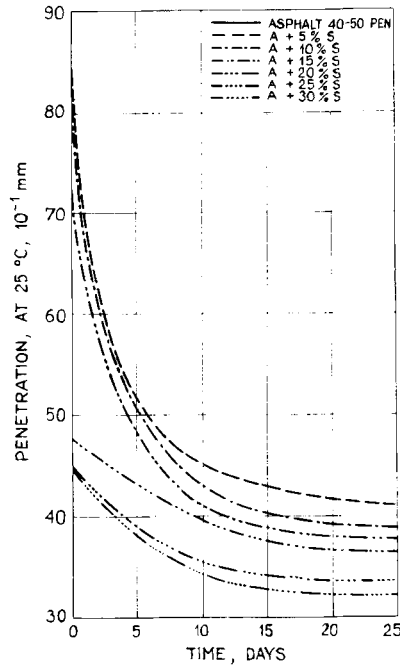


Fig. 19-8. Penetration changes with time [54].

When sulphur is mixed with asphalt at temperatures above 180°C, the changes of asphalt properties are similar to those occurring during the blowing process. The chemical reactions leading to an increase in asphaltene content result in the increase of hardness and brittleness of the asphalt. The penetration and ductility become lower, whereas the softening point and Fraass breaking point increase.

Sulphur has a favourable effect on the mechanical properties of sulphur–asphalt–aggregate mixes in terms of improvement in Marshall stability, increase of the resilient modulus, and decrease in the rutting tendency when compared with conventional asphalt concrete. The mixtures exhibit a high water resistance due to the presence of sulphur.

It has been shown by microscopic studies that when the mix cools, the sulphur solidifies in the void spaces between the binder-coated aggregate particles, conforming to the configuration of the void [51].

By conforming to the shape of the void, the sulphur causes a mechanical interaction between the particles, which results in a higher Marshall stability of the mixture [37].

The Marshall stabilities of the sulphur–asphalt–binder-based mixes are considerably higher than those made with asphalt only. The stability increases with an increase in sulphur content for all sulphur levels (Fig. 19-9). The amounts of sulphur substitution being larger than 50 wt% of the binder yield high stabilities of the mixes but these would have to be worked at higher compaction temperatures.

As has been pointed out by McBee and Sullivan [15], there are no apparent differences in Marshall stabilities of the sulphur–asphalt paving mixes prepared by both the direct addition and the emulsifying methods. Their stabilities after water-soaking are retained completely [9]. The stability improves slightly with age.

Despite the appreciable increase in the stability of the mixes with the sulphur content, the Marshall flow decreases slightly.

When reducing the void content the solid sulphur increases the stiffness of the material. At a sulphur level of greater than 25 wt%, the stiffness exhibits dependence on load. This dependence is more pronounced at relatively lower temperatures. The

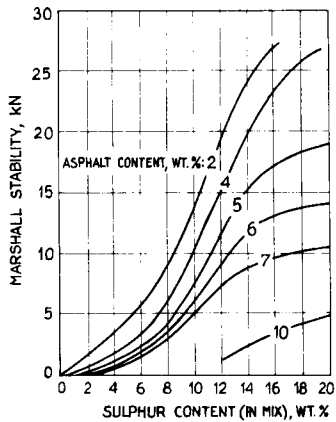


Fig. 19-9. Effect of sulphur content on mix stability [51]. Materials: 150–180 pen. asphalt, medium-coarse sand.

stiffness modulus of the sulphurized asphalt paving material can be even five times greater than that of asphaltic concrete at the intermediate rates of loading [7].

The splitting tensile strength of a mix increases with the increase of the sulphur content.

The fatigue life of sulphur-asphalt paving mixtures at low to moderate rates of loading is better than that of asphaltic concrete and it is relatively equal at high rates.

The properties of sulphur-asphalt-aggregate mixes alter within a period of 20–30 days after their preparation. The amount of sulphur having remained ‘undissolved’ crystallizes first and rapidly, causing an appreciable alteration in the mix properties. A further variation of the properties being observed till the end of the above-mentioned period may be attributed to the slow recrystallization of the ‘dissolved’ sulphur [13,30]. It appears that a one-month mix storage is a period needed for the stabilization of the mechanical properties. After the end of this period, sulphur hardens the mix without altering its viscoelastic behaviour [13].

#### ENVIRONMENTAL AND SAFETY ASPECTS

When mixed with asphalt at high temperatures, sulphur forms hydrogen sulphide and sulphur dioxide which can create a health hazard.

The hydrogen sulphide evolution is a function of the mixing temperature and time as well as of the sulphur concentration in the blend. The relationship between the hydrogen sulphide emission and both the mixing temperature and time are given in Fig. 19-10. As can be seen, hydrogen sulphide emission increases considerably with increasing temperature, and it is the most intensive during the first period of mixing [31,56]. The

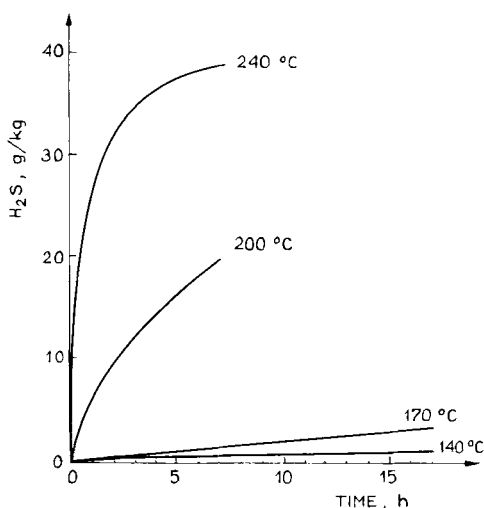


Fig. 19-10. Variation of hydrogen sulphide emission with temperature and reaction time. Blend composition: 95% of asphalt of 120–150 pen. grade and 5% sulphur [56].

rate of increase has been found to be higher at temperatures above 150°C, and a sulphur concentration above 1 wt% of the blend.

Since the evolution of gaseous effluents could be of crucial importance for the acceptance of sulphur–asphalt–binder-based materials in pavement construction, a number of experiments were carried out to estimate the environmental effects of these materials during and after construction [7,9–11,14,16,22,57,58].

There are upper limit levels for the concentrations of hydrogen sulphide and sulphur dioxide. In different countries various limits have been accepted; however, the maximum allowable concentrations for H<sub>2</sub>S and SO<sub>2</sub> have generally been settled at 20 ppm and 5 ppm, respectively. Although the H<sub>2</sub>S level of 20 ppm is not injurious to the health, it does irritate the eyes, and that is why the threshold limits for H<sub>2</sub>S at 10 ppm and for SO<sub>2</sub> at 5 ppm were suggested and accepted by the American Governmental Conference on Toxicology and Health [7,14].

The gaseous emissions were monitored in the sulphur–asphalt mixing equipment, at the hot-mix plant, and around the paving site. The results showed [7,10,14,16,22,57] that the concentrations of toxic gases in the areas most frequented by personnel were below the hazardous level. The only exceptions were the heated storage tanks as well as the sulphur-unloading hopper [16,57,58]. The hydrogen sulphide levels detected over the surface of the pavement just after it was laid were between 0 to 4 ppm [11,22].

Based on the results a conclusion may be drawn that no safety hazard exists during the pavement construction or after it. Although peak concentrations of hydrogen sulphide exceeding the critical level were encountered, they occurred for a short period of time only.

The emission of hydrogen sulphide and sulphur dioxide can be reduced with the use of appropriate additives as well as by installing constructional protection. Cupric oxide, sodium carbonate, aluminum oxide, and calcium chloride were found effective in reducing hydrogen sulphide emission [31]. The addition of 1% of these substances caused approximately a 50% reduction in hydrogen sulphide evolution. The hydrogen sulphide formation in the course of mixing sulphur with asphalt may be inhibited by the addition of a redox catalyst [59]. It has been found that the addition of lime flour (often used as a filler in paving mixes) to sulphur–asphalt blends in the mixing temperature range reduces the hydrogen sulphide evolution [58]. As it followed from other studies, the addition of Fe(II) and Fe(III) compounds to the sulphur–asphalt blend at a temperature of 140°–150°C caused a decrease in hydrogen sulphide emission by 50% and in the emission of sulphur dioxide by 75% [60].

For full environmental assessment of the effects of using sulphur in pavement, soil and water quality measurements were carried out before and after road construction [14]. The results indicated no change in the sulphur content or pH.

On account of the potential environmental and safety risks during the production of sulphur-extended asphalts and their utilization in pavement construction, no problems should appear unless the temperature of 140°C is exceeded. Below this temperature the formation of hydrogen sulphide and sulphur dioxide is negligible.

## APPLICATIONS

Among the possible applications of sulphur-modified asphalts, their utilization in pavements has proved to be the most attractive.

The first test road with a sulphur–asphalt mixture as the aggregate binder was built in Texas early in 1934. Further experimental pavements were laid in the 1970s in a number of European countries, as well as in the United States, Canada, and the Middle East. The performance of these pavements was tested under different climatic and traffic conditions.

The replacement of up to 52 wt% of asphalt with sulphur produces materials with properties equal or superior to those of conventional asphalt concrete [11]. In addition, the sulphur–asphalt-based mixes can be produced in the existing paving plants with only minor modifications. Also the conventional equipment is suitable for transporting, laying and compacting these materials.

The sulphur–asphalt–aggregate mixes have an excellent workability. The workability of a mix above the sulphur melting point increases with increasing amount of the binder (SEA). Properly designed mixes may be placed without roller-compaction.

From the viewpoint of the pavement performance many advantages result from the addition of sulphur.

(1) Sulphur-substituted asphalt mixes exhibit significantly higher fatigue lives than comparable conventional mixes.

(2) The behaviour of sulphur-containing pavements is more elastic compared with conventional pavements (at the same loading time) [61].

(3) The addition of sulphur makes it possible for softer asphalts to be used in order to reduce low-temperature cracking without the high-temperature deformation which occurs when virgin asphalt is used. It has been found that the use of sulphur-extended asphalt with 30% to 40 wt% of sulphur in paving mixes leads to the reduction in deformation approximately by a half [62]. Their notable resistance to plastic deformation at the service temperature prevents the rutting of the surface.

(4) Paving materials based on sulphur–asphalt and binder exhibit a better resistance to water as compared with conventional mixes.

The behaviour of the tested roads under traffic showed that the paving mixes of sulphur-extended asphalt kept those properties after several years of use [12,63].

The decreasing availability or lack of quality aggregates in a number of regions became a starting point of studies of the use of sulphur–asphalt binders for upgrading low-grade aggregates, including one-size sands. It has been found that sulphur–asphalt–sand mixes yield high-performance flexible pavements [4,6,7,12,15,51].

These paving materials meet the requirements for heavy-duty highways [15]. Sand–asphalt–sulphur mixes may be used in the construction of all types of pavements. They are also suitable for overlaying the existing road surfaces.

Depending on the composition of sulphur–asphalt–aggregate mixes, the pavement can be formed by the compacting or casting of the mix. It has been found that the casting technique should be employed instead of the commonly used compaction, in cases where mixes with high sulphur-to-asphalt ratios were used [6]. Casting of the sulphur–asphalt paving mixes permits a good-performance pavement to be obtained with the use of poorly graded sands. The hard-cast sulphur–asphalt paving mixes have

proved to be suitable for producing durable slabs which could be used for constructing footpath surfaces, industrial acid-resistant floors, etc. [64,65].

The features of sulphur-extended asphalts discussed in this chapter make these materials attractive for special applications.

One of the potential uses for sulphur–asphalt mixes is pavement patching. Sand–asphalt–sulphur mixes are particularly suitable as pavement patching materials because the mixes may be poured into the required place and levelled.

The apparent plastification of sulphur–asphalt mixes might find a practical application in the recycling of used-up asphaltic concrete [49]. The ability of sulphur to lower the viscosity of sulphur–asphalt mixtures below that of pure asphalt makes it possible to eliminate costly plasticizing agents used for improving the workability of recycled paving mixes.

The use of sulphur in asphalt–aggregate mixes permits the design of impervious materials being suitable for hydraulic applications.

The durability and the chemical resistance of sulphur-extended asphalts make it possible to consider their utilization as protective coatings. A typical application is the protection of concretes from acid solutions used in metal ore leaching plants [66]. It has been found that sulphur–asphalt–binder-based mixes with quartz aggregate or silica sand display a good resistance to the action of acids and salts, which would make it possible for these materials to be used as protective coatings for storage tanks designed for storing corrosive liquids, pipes for the flow of these liquids, as well as for the building of floors and pavements that are brought into contact with aggressive substances [48].

The sulphur-extended mixes have an improved resistance to being damaged by fuel spillage as compared with the conventional asphaltic concrete [67]. The increase of the sulphur content decreases the damaging action of fuels. The sulphur–asphalt paving materials may prove useful in areas where frequent spillage or dripping of fuels occurs, e.g., in constructing parking lots, airports, driveways, and pavements for filling stations.

Despite the numerous advantages offered by sulphur–asphalt paving mixes, they have also certain disadvantages which detract from their utility. Materials containing over 50 wt% of sulphur in the binder are temperature-sensitive and require final compaction above 120°C. Temperature control is important during preparation, handling, transporting and storing of the mix. Because of the increased workability of the mixes, careful mix handling is essential to avoid segregating the coarse aggregate from the finer mix components. Mixes with a high sulphur-to-asphalt ratio are difficult to compact with the use of the conventional rolling technique. In addition, the rolling of a mix under pressure results in the deterioration of the pavement performance due to a breakdown in the macrostructural bonding between the constituents as the mix cools [6,7].

## ECONOMIC ASPECTS

The potential economic benefits of the utilization of sulphur-substituted asphalts in paving mixes consist of: (1) saving of materials; and (2) a considerable improvement in the mechanical properties of paving mixes and, consequently, a substantially better performance of the pavement.

A saving of 20% asphalt can be reached by incorporating sulphur into an asphalt paving mix. The partial replacement of asphalt with sulphur is economical only in the case where the price of sulphur is, at the very least, half that of asphalt, because of the greater density of sulphur as well as the additional technological costs.

There may also be savings in aggregates, because the sulphur-asphalt binder allows conventional aggregates to be replaced by inexpensive low-quality aggregates, such as windblown sands or aggregates with a poor gradation.

The use of a sulphur-asphalt binder in paving mixes instead of normal asphalt might bring significant economic benefits on account of the properties which are superior to those of conventional asphalt mixes. The improved performance characteristics of sulphur-extended asphalt materials offer a promise of more durable pavements, and enable thinner road surfaces to be built, which would make it possible to conserve both asphalt and aggregate. It has been found that the thickness of the layer can be reduced by as much as 20% [8].

The evaluation of the economic aspects of using sulphur-extended asphalts involves also the saving of energy. The addition of sulphur reduces the binder viscosity and this significantly improves the workability of the mix. Therefore, the hot-mix paving materials can be prepared and compacted at lower temperatures, which results in lower energy consumption (30% saving of fuels [10]).

The economics of using sulphur in asphalt paving mixes varies in different parts of the world. The availability and the price of sulphur in relation to asphalt is the most important factor. The possibility of substituting high-quality and costly aggregates for local aggregate sands should also be taken into consideration when making an economic assessment. In areas with favourable economics, the use of sulphur-substituted asphalt in pavement construction might reduce the binder and aggregate costs.

Although at present the world prices of asphalt and sulphur take shape in such a way that the use of sulphur-extended asphalts in paving mixes is uneconomical, still the increasing amount of sulphur as a by-product (Table 19-1) may reverse these proportions.

With a stricter control of sulphur pollution sources, sulphur is expected to become more plentiful.

Since 1991 the sulphur consumption has declined, and although it is expected to slightly increase in the near future, still with the amount of sulphur continuing to rise as a by-product, the balance between produced sulphur and consumed sulphur will show an upward tendency (Table 19-2).

TABLE 19-1

Sulphur production (in million metric tons) [68,69]

	1988	1989	1990	1991	1992	1998	2020 <sup>a</sup>
Mined	14.3	14.3	13.6	10.3	8.2	3.7	0
Recovered	25.0	24.7	25.5	26.1	27.4	37.0	55.0
Total	39.3	39.1	39.1	36.4	35.6	40.7	55.0

<sup>a</sup> Estimated.

TABLE 19-2

Sulphur supply (in million metric tons) [68]

	Production	Consumption	Balance
<i>Actual</i>			
1989	39.1	39.9	-0.9
1990	39.1	39.4	-0.3
1991	36.4	36.8	-0.4
1992	35.6	34.8	+0.8
<i>Potential</i>			
1993	36.0	33.9	+2.1
1994	39.6	35.9	+3.7
1995	42.5	37.4	+5.1
1996	44.4	38.2	+6.2
2000	49.2	41.5	+7.7

Even though the use of pure sulphur in asphalt paving mixes is uneconomical, the utilization of industrial wastes with an appropriately high sulphur content in sulphur-asphalt mixes should be taken into consideration.

It has been found that wastes from coking plants (obtained by desulphurizing coke oven gas), with approximately 30% sulphur, may be applied as asphalt modifier producing material which performs well in paving mixes [25,26]. The method eliminates the evolution of sulphur dioxide, whereas the hydrogen sulphide emission was markedly lower than that observed during the preparation of sulphur-asphalt blends.

Another by-product that proved to be useful in asphalt paving mixes was the waste material which remained after flotation of sulphur ore [24,70] (containing approximately 40% sulphur). In this method, however, the gaseous emissions were slightly higher.

## REFERENCES

- [1] U.S. Patent, 58,615 (1866).
- [2] U.S. Patent, 468,867 (1892).
- [3] Benzowitz, J. and Boe, E.S., Effect of sulfur upon some of the properties of asphalt. *Proc. ASTM*, 38: 539 (1938).
- [4] Canadian Patent, 755,999 (1967).
- [5] German Patent, 1,295,463 (1970).
- [6] U.S. Patent, 3,738,853 (1973).
- [7] Saylak, D., Gallaway, B.M. and Ahmad, H., Beneficial use of sulfur in sulfur-asphalt, pavements. *New Uses of Sulfur. Adv. Chem. Ser.*, 140: 102 (1975).
- [8] Saylak, D. and Gallaway, B.M., The use of sulfur in sulfur-asphalt aggregate mixes. *Interam. Conf. Mater. Technol.*, Caracas, p. 636 (1975).
- [9] Kennepohl, G.J., Logan, A. and Bean, D.C., Conventional paving mixes with sulfur-asphalt binders. *Proc. Assoc. Asphalt Paving Technol.*, 44: 485 (1975).
- [10] Garrigues, G. and Vincent, P., Sulfur/asphalt binders for road construction. *New Uses of Sulfur. Adv. Chem. Ser.*, 140: 130 (1975).
- [11] McBee, W.C. and Sullivan, T.A., Direct substitution of sulfur for asphalt in paving materials. *Report of Investigations 8303*. U.S. Department of the Interior, Bureau of Mines (1978).



- [12] Harlin, J.P., Bitumen and sulphur in road technique. *Eurobitume Seminar*, London, p. 339 (1978).
- [13] Celard, B., Sulfur addition to asphalt paving mixes. *Eurobitume Seminar*, London, p. 318 (1978).
- [14] Kennepohl, G.J. and Miller, L.J., Sulfur-asphalt binder technology for pavements. *New Uses of Sulfur II. Adv. Chem. Ser.*, 165: 113 (1978).
- [15] McBee, W.C. and Sullivan, T.A., Sulfur utilization in asphalt paving materials. *New Uses of Sulfur II. Adv. Chem. Ser.*, 165: 135 (1978).
- [16] Prince, S.M., Construction and performance of a sulfur-asphalt road in Texas. *New Uses of Sulfur II. Adv. Chem. Ser.*, 165: 167 (1978).
- [17] Deme, I., Sulfur as an asphalt diluent and a mix filler. *New Uses of Sulfur II. Adv. Chem. Ser.*, 165: 172 (1978).
- [18] Love, G.D., Sulfur: potential pavement binder of the future. *Transp. Eng. J. ASCE*, 105: 525 (1979).
- [19] Celard, B., Schwefel-Asphalt. *Das Stationäre Mischwerk*, 3: 23 (1980).
- [20] Anon., Work Commences on RN 21 SNEA sulphur-extended-asphalt to undergo further road tests. *Sulphur*, 163: 34 (1982).
- [21] Polish Patent, 116,236 (1982).
- [22] Anon., Sulphur-extended asphalt load in London. *Sulphur*, 170: 30 (1984).
- [23] Akili, W., Properties and behaviour of sulphur-asphalt-sands for road bases in desert terrain. *Sulphur*, 181: 44 (1985).
- [24] Polish Patent, 133,599 (1986).
- [25] Polish Patent, 138,643 (1989).
- [26] Gawel, I., Modifikation der Bitumen durch Schwefelabfallprodukte der Kokerei- und Gasindustrie. *Strassen Tiefbau*, 43: 20 (1989).
- [27] Polish Patent, 149,755 (1990).
- [28] Schmidt, M., The scientific basis for practical applications of elemental sulfur. *Symp. Sulfur Utilization*, New Orleans (1977).
- [29] Petrossi, U., Bocca, P.L. and Pacor, P., Reactions and technological properties of sulfur-treated asphalt. *Ind. Eng. Chem. Prod. Res. Dev.*, 11: 214 (1972).
- [30] Qarles Van Ufford, J.J. and Vlughter, J.C., Schwefel und Bitumen. II. *Bremst. Chem.*, 46: 7 (1965).
- [31] Lee, D.Y., Modification of asphalt and asphalt paving mixtures by sulfur additives. *Ind. Eng. Chem. Prod. Res. Dev.*, 14: 171 (1975).
- [32] Rahimian, I., Reaktion zwischen Bitumen und Schwefel sowie Charakterisierung der entstehenden Verbindungen. 4. *Gemeinschaftstagung ÖGEW/DGMK*, Salzburg (1976).
- [33] Korn, J., Prinzel, H.W. and Pape, D., Zur Kenntnis der Reaktion zwischen Paraffinkohlenwasserstoffen und Schwefel. *Erdöl Kohle*, 19: 651 (1966).
- [34] Siegmann, M.C., Manufacture of asphaltic bitumen. In: J. Ph. Pfeiffer (Ed.), *The Properties of Asphaltic Bitumen*. Elsevier, New York, 143 (1950).
- [35] Tucker, J.R. and Schwyer, M.E., Distribution and reactions of sulfur in asphalt during air blowing and sulfurizing processes. *Ind. Eng. Chem. Prod. Res. Dev.*, 4: 51 (1965).
- [36] Oyekunle, L.O. and Onyehanere, L.N., Studies on Nigerian crudes. 3. Analysis of sulfurized asphalts. *Fuel Sci. Technol. Int.*, 9: 681 (1991).
- [37] Papirer, E., Fritschy, G. and Eckhardt, A., Structural modes of sulphur in sulphur-bitumen composites as studied by electron microscopy. *Fuel*, 59: 617 (1980).
- [38] Papirer, E. and Fritschy, G., Modification of the surface properties of bitumen and asphaltenes following treatment with sulfur at 140°C. *Fuel*, 60: 670 (1981).
- [39] Courval, G.J. and Akili, W., Sulfur asphalt binder properties by the sliding plate rheometer. *Asphalt Paving Technol.*, 51: 222 (1982).
- [40] Beaudoin, J.J. and Sereda, P.J., A two-continuous-phase sulphur-asphalt composite — development and characterization. *Can. J. Civ. Eng.*, 6: 406 (1979).
- [41] Alama, K., Siarka – zamiennik lepiszcza bitumicznego i składnik strukturalny w drogowych mieszkankach nawierzchniowych. *Prace Instytutu Badawczego Dróg i Mostów (Warsaw)*, 4: 23 (1987).
- [42] German Patent, 1,805,769 (1970).
- [43] Alama, K. and Wojdanowicz, G., Właściwości lepiszczy siarkowo-asfaltowych. *Prace Instytutu Badawczego Dróg i Mostów (Warsaw)*, 3: 42 (1981).

- [44] Anon., First sale made of sulfur-asphalt process. *Chem. Eng. news*, 56: 7 (1978).
- [45] Canadian Patent 1,045,265 (1978).
- [46] Pronk, F.E., Soderberg, A.F. and Frizzell, R.T., Sulphur modified asphalt concrete. *Annu. Conf. Can. Tech. Asphalt Assoc.*, Toronto, Ont. (1975).
- [47] Pronk sulphur asphalt paving job completed. *Sulphur*, 145: 31 (1979).
- [48] McBee, W.C. and Sullivan, T.A., Utilization of secondary sulfur in construction materials. *Proc. 5th Mineral Waste Utilization Symp.*, Chicago, p. 39 (1976).
- [49] Saylak, D., Lytton, R.L., Gallaway, B.M. and Pickett, D.E., Prediction of in-service performance of sulfur-asphalt pavement. *Symp. Sulfur Utilization*, New Orleans (1977).
- [50] Shane, G. and Burgess, R.A., The Thermopave process. *Symp. New Uses for Sulphur*, Madrid (1976).
- [51] Burgess, R.A. and Deme, J., Sulfur in asphalt-paving mixes. *New Uses of Sulphur. Adv. Chem. Ser.*, 140: 85 (1975).
- [52] Fritschy, G., Papirer, E. and Chambu, C., Sulfur modified bitumen: a new binder. *Rheol. Acta*, 20: 78 (1981).
- [53] Rubbio, G., Einfluss von Schwefelzusatz auf die Eigenschaften von Bitumen. *Bitumen*, 39: 142 (1977).
- [54] Stefańczyk, B., Wpływ siarki na różne rodzaje asfaltów. *Drogownictwo (Warsaw)*, 37: 142 (1982).
- [55] Qarles Van Ufford, J.J. and Vlugter, J.C., Schwefel und Bitumen I. *Brennst. Chem.*, 43: 173 (1962).
- [56] Kunath, H., Was bringt die Verwendung von Schwefel-Bitumen?. *Die Strasse*, 25: 374 (1985).
- [57] Anon., Sulphur extended asphalt. *Highway Heavy Construct.*, 8: 62 (1979).
- [58] Alama, K., Blasiak, I. and Dojka, M., Badania emisji gazowych związków siarki z mieszanek siarkowo-asfaltowych. *Prace Instytutu Badawczego Dróg i Mostów (Warsaw)*, 3: 105 (1981).
- [59] German Patent, 2,459,386 (1975).
- [60] Gawel, I., The selection of additives reducing the evolution of gaseous effluents during the preparation of sulphur-bitumen mixes. *Int. Conf. Catalysis and Adsorption in Environmental Protection*, Szklarska Poręba, Poland (1994).
- [61] Vincent, P., Sulphur in road construction technology. *Eurobitume Sem.*, London, p. 353 (1978).
- [62] Bissada, A., Al-Hashimi, K. and Abushihada, A., Prediction of pavement deformation in sulphur extended asphalt pavements using the shell creep test. *Proc. 1st Arabic Regional Conf. Sulphur, its Usages in Arabic World*, Safat, Kuwait, p. 241 (1982).
- [63] Cepas, A.S., The performance evaluation of sulfur extended asphalt base course on Edmonton's Victoria Trail. *Proc. Third Int. Conf. Sulphur-84*, Calgary, Alta., p. 518 (1984).
- [64] Polish Patent 160,656 (1993).
- [65] Gawel, I., Badania nad sposobem wytwarzania płtek z asfaltu twardo-lanego z lepiszczem modyfikowanym produktami oczyszczania gazu koksowniczego. *Report 614*, Technical University of Wrocław (1987).
- [66] Paulson, J.E., Simic, M., Cambell, R.W. and Ankers, J.W., Sulfur composites as protective coatings and construction materials. *New Uses of Sulfur II. Adv. Chem. Ser.*, 165: 215 (1978).
- [67] McBee, W.C. and Sullivan, T.A., Improved resistance of sulfur-asphalt paving formulations to attack by fuels. *Ind. Eng. Chem. Prod. Res. Dev.*, 16: 93 (1977).
- [68] Anon., Sulfur's price collapse to force market changes. *Oil Gas J.*, 91: 75 (1993).
- [69] Hyre, J., Doerv, L., d'Aquin, G.E. and Jenny, N.P., Facing the future. *Sulphur*, 258: 49 (1998).
- [70] Bojanowicz, A., Walter, Z. and Kazmierczak, R., Rozdrabnianie keku siarkowego dla celów drogowych. *Fizykochemiczne Problemy Mineralurgii (Wrocław)*, 17: 231 (1985).

This page intentionally left blank

## Chapter 20

# PRODUCTION AND RESEARCH DEVELOPMENT OF ASPHALTS IN CHINA

YAOHUA FAN, CHANGXIANG ZHANG, GUOJING DING and YUZHEN ZHANG

## INTRODUCTION

The production of crude oil in the People's Republic of China reached 161 million tons in 1998. The production of asphalt was 3.9 million tons, of which about 68.2% was paving asphalt, 26.8% roofing asphalt, 1% special-use asphalt, and 4% for other industrial uses.

Asphalt production developed quickly in China, from 20,000 tons in 1950 to 3.9 million tons in 1998. This is a 195-fold increase during the past 50 years.

Currently, China produces 5 categories, 23 types, and 55 specific asphaltic products for paving, roofing, waterproofing, hydrotechnologies, electrical insulating, and anticorrosion projects. The five categories of products are listed in Table 20-1.

TABLE 20-1

Products obtained from asphalt

Paving	Super traffic Heavy traffic Light traffic
Roofing	Architecture Hydro technologies Immersion-belt oil
Special uses	Lacquer Anticorrosive Accumulator Rubber Motor insulating Drilling Optic Cable Battery sealing Non-lead Electro-insulating Others
Emulsion	Non-ionic Anionic Cationic
Polymer modified	

The four largest oil fields in China are Daqing, Shengli, Renqiu, and Liaohe, which account for more than 80% of the country's total oil production. Most of the crude oils belong to paraffinic or intermediate bases. These crudes cannot produce quality paving asphalts by simple distillation. The asphalts obtained from these crudes are characterized by a high wax content, low asphaltene content, and low density.

The principal characteristics of Chinese paraffinic crudes are shown in Table 20-2, and the properties of asphalt from these crudes are presented in Table 20-3.

As the production of heavy oil (API degree < 15) increases, the raw materials used to make asphalt change. The heavy oil production in China reached 10 million tons by the end of 1991, which is more than 8% of the total oil production. The naphthenic oil is used for asphalt manufacturing.

The straight-run asphalts from heavy oil were used successfully in the construction of an express highway in China.

A comparison of properties between domestic and foreign asphalts is shown in Table 20-4, whereas the characteristics of Chinese heavy oils are presented in Table 20-5.

TABLE 20-2

Characteristics of Chinese paraffinic crudes

Sample:	Daqing	Shenli	Renqiu	Liaohe
API	33.1	28.0	27.9	28.7
Density (20°C) (g/ml)	0.8854	0.8829	0.8837	0.8793
Viscosity (50°C) (Cs)	20.2	42.8	43.4	17.4
Solidification point (°C)	30.0	28.0	34.0	21.0
Paraffine (%)	26.2	15.8	22.8	16.8
Asphaltene (%)	0.0	0.4	—	0.0
Resin (%)	3.9	—	2.57	11.9
Sulfur (%)	0.1	0.72	0.31	0.18

TABLE 20-3

Properties of asphalt from paraffinic crudes

Sample:	SL	SH	DSZ	DL	JS	DQ	MM
Penetration (25°C) (0.1 mm)	57	74	83	53	86	102	73
Solidification point (°C)	52.3	48.0	47.3	51	47.9	47.3	52.6
Ductility (25°C) (cm)	100	100	100	46	89	100	33
Ductility (15°C) (cm)	11	16	21	—	56	21	—
S.G. (25°C/25°C)	—	1.014	—	1.008	0.986	0.986	0.989
Boiling point (°C)	−13	−12	−13	−9.5	—	−16	−17
Wax content (%)	10.4	11.8	8.6	8.0	12.6	7.5	9.5
Saturate	17.8	44.5	40.5	13.0	8.2	42.7	28.5
Aromatic	37.2	32.0	43.5	31.0	—	—	—
Resin	31.7	33.6	48.1	55.0	48.2	47.7	31.6
Asphalt	12.8	10.0	48.1	<1.0	0.2	2.1	9.1

The results in Tables 20-4 and 20-5 suggest that the resources of asphalt in China are abundant. Quality asphalt can be obtained using a simple process. Thus, the asphalt industry in China can look forward to good prospects for the future.

For many years, the Heavy Oil Research Institute and Chemical Engineering Department of the University of Petroleum (China) have been investigating the relationship between the chemical composition and physical properties of asphalt. Researchers have

TABLE 20-4

Comparison of properties between domestic and foreign asphalts

	China				Japan	Albania	Singapore	
	SJS	HXL	KLMI	YSM			SHELL	EXXO
Penetration (25°C) (0.1 mm)	87	100	104	97	87	94	90	95
Ductility (15°C) (cm)	150+	150+	126	100	150+	150+	150+	100+
Solidification point (°C)	48.8	45.5	49.0	47.3	47.0	46.7	48.2	46.0
Solubility (TCE) (%)	99.7	99.9	99.9	99.4	99.9	99.7	99.2	99.1
F.P. (°C)	292	270	300+	259	300+	252	296	328
S.G. (25°C/25°C)	1.004	1.012	0.9703	1.005	1.024	1.051	1.029	1.037
TFOT:								
Loss on heating (%)	0.18	0.23	0.02	0.13	0.11	0.52	0.38	0.02
Ratio of penetration (%)	81	66.5	86	65	81	56	59	71
Ductility (25°C) (cm)	150+	150+	107	150+	150+	150+	150+	150+
Wax content (%)	2.91	2.78	3.10	1.38	4.38	0.04	2.40	1.88
Saturate (%)	35.69	30.72	46.68	31.99	34.25	18.46	36.56	—
Aromatic (%)	25.59	27.48	28.24	28.11	38.29	40.79	35.46	—
Resin (%)	29.12	20.49	22.74	18.94	10.82	14.14	7.95	—
Asphalt (%)	4.61	16.31	0.33	15.96	11.64	21.61	15.03	—

TABLE 20-5

Characteristics of Chinese heavy oil

Sample:	SJS	URH	HXL
Density (20°C) (g/ml)	0.9746	0.9609	0.9788
Solidification point (°C)	12	15	14
Viscosity (100°C) (cs)	266.2	1105.0	49.5
Asphaltene (%)	1.84	0.00	43.3
Resin (%)	22.8	24.7	43.3
Paraffine (%)	1.85	4.7	2.2
Sulfur (%)	0.18	0.38	0.26
Distillation:			
<200°C (%)	0.63	—	1.5
200–350°C (%)	13.10	—	18.4
350–480°C (%)	21.05	27.8	59
>480°C (%)	64.92	61.7	65.0
			(>425°C)

TABLE 20-6

Relationship between chemical composition and physical properties

Sample:	HXL	SJS	GD	SL	GS	KLMI	ZR	Japan
Penetration (25°C) (0.1 mm)	56	97	113	136	95	149	119	76
Solidification point (R&B) (°C)	50.0	43.7	45.0	42.5	48.0	42.0	43.1	45.1
Ductility (25°C) (cm)	100	100	100	82	100	100	48	100
Ductility (15°C) (cm)	100	100	100	—	78	100	36	100
Saturated (%)	17.1	17.1	13.7	17.6	22.62	28.2	14.3	15.5
Aromatic (%)	36.5	27.0	35.2	36.3	26.4	26.9	34.3	47.2
Resin (%)	43.8	53.5	44.1	40.7	50.8	44.8	51.3	27.7
Asphalt (C <sub>7</sub> ) (%)	2.6	2.4	7.0	5.4	0.2	<0.1	0.1	9.6
Asphalt (C <sub>5</sub> ) (%)	12.6	17.0	16.7	15.4	11.0	8.5	5.4	16.9
Saturated wax (%)	2.6	0.9	4.2	4.1	2.4	4.4	2.6	3.2
Aromatic wax (%)	2.8	2.1	4.1	6.7	4.4	2.7	10.0	2.2
Total wax (%)	5.4	3.0	8.3	10.8	6.8	7.1	12.6	5.4
H/C	1.48	1.49	1.51	1.55	1.58	1.61	1.60	1.47
$f_a^a$	0.29	0.29	0.28	0.24	0.22	0.21	0.21	0.30

<sup>a</sup> Fraction of aromatic carbon.

made excellent progress in this area. Table 20-6 is an example of their investigations.

According to the experience of Chinese refiners, good asphalt must have a low H/C (<1.49), and a high  $f_a$  (ratio of aromatic carbon/total carbon) (>0.28).

Currently, there are 27 sets of oxidation plants and 16 solvent deasphalting units in China. They can manufacture 4.4 million tons of asphalt per year from 20 types of crude oils. All existing technologies of asphalt production have been mastered in China. The technology of supercritical fluid extraction (SCFE), which can produce quality asphalts, has been developed independently, and a pilot plant with a yearly capacity of 15,000 tons of SCFE has been built and is operating successfully.

The Heavy Oil Research Institute of the University of Petroleum (China) is recognized as one of the main research centers of asphalt. It is not only adequately equipped, but also has pilot plant facilities.

#### DEVELOPMENT OF CHEMICAL COMPOSITION RESEARCH

Asphalt is an extremely complex material composed of hydrocarbons and heterocompounds. It is impossible to compare the separation of asphalt into individual hydrocarbons or non-hydrocarbons with the separation of light products. There are two types of separation widely used. (1) Group separation based on the polarity of compounds. Rostler and Sternberg [1] proposed that asphalt can be separated into five fractions by first precipitating asphaltene with pentane and then determining the fraction of the pentane soluble material that reacts with successively stronger sulfuric acid. In addition, Corbett [2] used heptane to precipitate asphaltene and then separate the soluble material on an aluminum oxide column with solvents of increasing polarity, thus

successfully obtaining the saturate, aromatic, resin, and asphaltene (SARA) fractions separately. (2) Fraction separation based on the molecular size of compounds, i.e., size exclusion chromatography (SEC) and gel permeation chromatography (GPC) make the evaluation of asphalt constituents simple and efficient.

The anti-aging performance is one of five important properties considered in the SHRP project. The thin-film oven test (TFOT) is often used to evaluate this property in the laboratory.

For several years, we have been trying to investigate the chemical composition and molecular structure of asphalt and relate these to its physical properties. A lot of information was obtained by SARA about the chemical composition and by GPC about the distribution of molecular weight of several asphalts widely used in road construction. The results showed that asphalt obtained from different sources has a varying chemical composition and molecular weight distribution; furthermore, there are some differences in the molecular weight distribution in the same compositional group obtained from different asphalts.

The supercritical fluid fractionation (SCFF) developed at our institute provides an efficient method to investigate the chemical behavior of asphalt. It is a new process to fractionate the mixture, including asphalt, mainly according to the molecular weight. Combining SCFF with SARA analysis, a two-dimensional separation (i.e., according to the molecular weight and polarity) is realized. Another advantage of SCFF is that a large amount of sample was obtained, so that further analyses could be carried out, i.e., TFOT, viscosity, etc. In this study, the shift of composition distribution before and after TFOT was used to explain the anti-aging performance of every constituent (as some differential point). The study scheme is outlined in Fig. 20-1.

SCFF is an extraction process with a reflux above the critical temperature and pressure of the solvent. The research results showed that the solubility of supercritical fluid increases with a temperature decrease and/or a pressure increase. In the extractive column, the extractive separation was obtained with some distillation effects as the temperature increased from the bottom to the top of the column. In this work, asphalt fractionation was carried out in a semi-continuous unit, which is designed for evaluating the vacuum residue and asphalts. About 1 kg of the sample can be fed into the unit, where the flow rate of solvent recycling is about 100 ml/min. The fractions can be obtained with a constant temperature gradient between the top and bottom of the extractive column by increasing the pressure. In this study, four typical asphalts (A, B, C, and D) were fractionated separately into 14–16 fractions using SCFF. At first, the asphalt fractionated into 12–14 fractions, with an isobutane fraction as the solvent by increasing the pressure from 4 to 12 MPa, with a constant temperature gradient of about 20°C between the bottom and top of the extraction column. The total yield of the fractions extracted was about 50% of the asphalt. The bottom fraction, called residue, was asphaltene and maltene precipitates with heptane.

The relationships between the operational pressure and the yield of A, B, C, and D asphalts are shown in Fig. 20-2. It suggests that increasing solubility with increasing pressure is different for various asphalts. The yield of asphalt A reaches 40% when the pressure is about 7 MPa, which means that the solubility of asphalt A in the isobutane fraction is significant. The increase in yield is only 10%, while the pressure



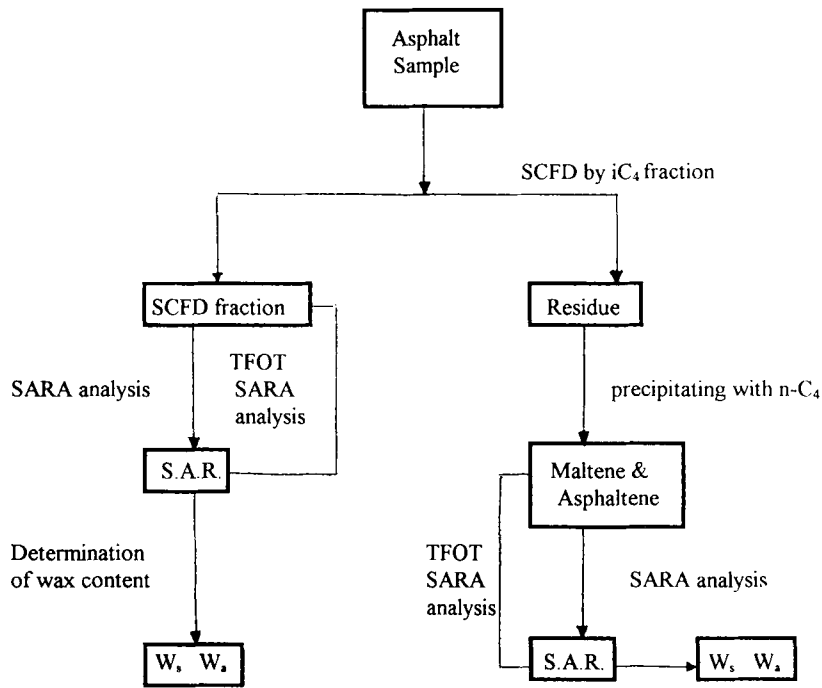


Fig. 20-1. Scheme of process;  $W_s$  = wax from saturates;  $W_a$  = wax from aromatics.

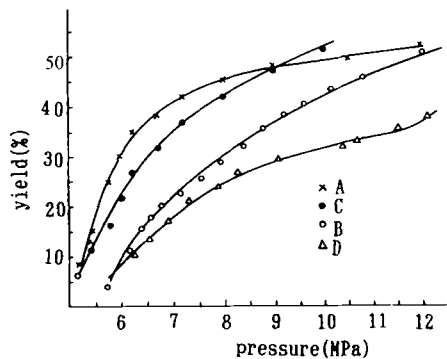


Fig. 20-2. Relationship between SCFF pressure and yield.

increases from 7 to 12 MPa. This indicates that the increase in yield is not considerable with increasing pressure. The heavier fractions of asphalt A have a larger molecular weight and/or higher polarity. The yield of asphalt C gradually changes with increasing pressure. The yield is lower than that of asphalt A at pressures below 8.8 MPa and is higher at pressures above 8.8 MPa. The polarity of the heavier fraction of asphalt C is relatively weak. Although asphalt B has a lower solubility under a lower pressure, the yield is 50% when the pressure reaches 12 MPa. Curve A almost intersects curve B at

about 12 MPa, which means that the polarity of the heavier fraction of A is similar to that of B. Asphalt D has a lower solubility in the testing pressure range, but drifts off the curve unlike A, B, and C. Evidently, the properties of the fractions of one asphalt can differ from those of the others.

The distribution of chemical composition (SARA) is shown in Fig. 20-3. Asphaltene does not appear in each one of the fractions of the four asphalts, which indicates that asphaltene is not soluble in isobutane fractions at an operational temperature and pressure. The portion of the curve over 50% is obtained according to the composition of the residue and the asphalt. The analyses of the residue are given in Table 20-7.

The results in Fig. 20-3 and Table 20-7 show that:

- (1) The saturates are present mainly in the extractive fractions of SCFF.
- (2) The distribution of saturates in asphalt A is similar to that in asphalt B, and the content of saturates is about 50% when the fraction yield is 15%. The saturates of asphalt C almost linearly decrease as its fraction yield increases.
- (3) The distribution of aromatics for asphalts showed that the heaviest aromatics of asphalt A would be fractionated when the fraction yield is about 90%, but those of B, C, and D would require a yield of about 80%. The asphaltene line would be represented by a horizontal line because it does not dissolve in the solvent and does not mix with the resin. The distance between the point of the heaviest aromatic and asphaltene line is different for various asphalts: about 6, 17, 17, and 2 for A, B, C, and D, respectively.

There is a certain similarity among the constituents of the same SCFF fraction in the same yield. The distance mentioned above may be used to study the properties of asphalt. The smaller the distance, the greater the amount of heavier aromatics compatible with resins. It is important to form a stable colloidal system where the asphaltene is in the center, surrounded by resins, aromatics, and saturates; thus, the properties of asphalt are improved.

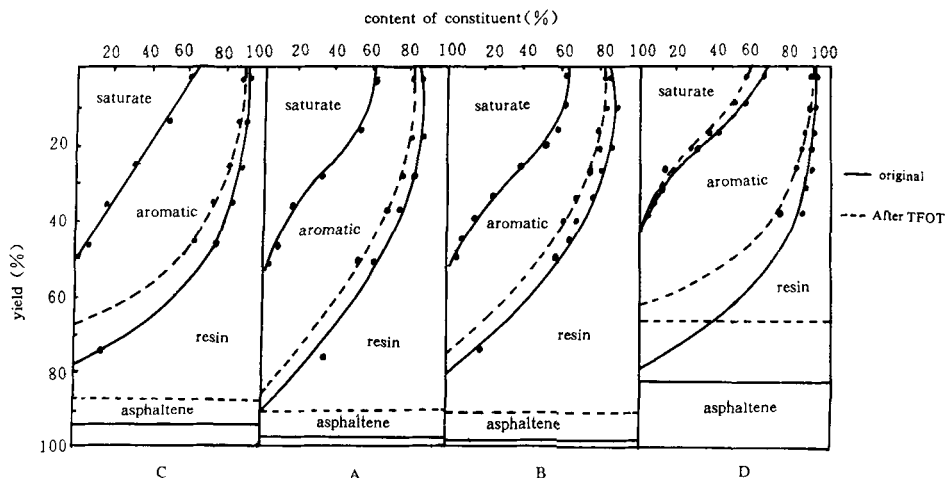


Fig. 20-3. Distribution of the constituents for four major asphalts.

TABLE 20-7

Analysis of four residues

Sample	Chemical composition (%) of the residue <sup>a</sup>				W <sub>s</sub>	W <sub>a</sub>	Chemical composition (%) of the composition of the asphalt			
	S	A	R	At			S	A	R	At
A	2.2	15.6	72.9	9.3	0.2	0.2	5.5	23.3	81.1	100.0
B	1.5	15.6	72.9	9.3	0.2	0.6	4.2	26.2	75.4	100.0
C	1.8	11.8	64.9	21.4	0.0	0.7	5.2	17.9	80.8	100.0
D	1.3	33.9	27.7	37.1	0.0	0.2	6.5	43.5	81.5	100.0

<sup>a</sup> S, A, R, At, W<sub>s</sub>, W<sub>a</sub> represent saturate, aromatic, resin, asphaltene, saturate wax, and aromatic wax, respectively.

The analysis results of SARA for each extractive fraction from SCFF, both before and after TFOT, show the absence of asphaltene. This means that the lighter resins (about 25% of the total resin) of the four asphalts or resins formed in the TFOT process are relatively stable and will not easily combine to form a heavier compound, i.e., asphaltene. The changes in chemical composition after TFOT for each fraction are shown in Fig. 20-3.

Information about the composition after TFOT for the saturates of asphalts A, B, and C is not provided in Fig. 20-3 because it differs only slightly. In asphalt D, the saturates in lighter fractions have decreased somewhat because of losing some of its lighter compounds. A loss of about 20% in weight occurs in the lightest fraction.

Aromatics content decreases in the TFOT process. The tendency of aromatics to decrease in asphalts A and B is similar, i.e., they have a similar amount of decrease in their light, middle, and heavy fractions. The aromatics in heavier fractions of asphalts C and D are largely changed to resins, i.e., these heavier aromatics are not stable under TFOT conditions, and easily transform to resins.

The area between the solid and dotted lines representing asphaltene is proportional to the amount of asphaltene formed from maltene to serve as a residue of SCFF in the TFOT process. The results in Fig. 20-3 show that the area of asphalt D is larger than that of the others.

As mentioned above, most of the asphalts in China were manufactured from paraffinic or intermediate crude oils. The problem faced by the paving engineers in China is the wax content. It is well known that the existence of wax affects the properties of asphalts considerably, but its level is different from the shape and size of crystalline wax if different types (saturates or aromatics) and different fractions (lighter or heavier) are present.

The distributions of W<sub>s</sub> (wax from saturates) and W<sub>a</sub> (wax from aromatics) are shown in Figs. 20-4 and 20-5, respectively. There is a significant difference for various asphalts not only in the amount of wax, but also in its distribution. Both the W<sub>a</sub> and W<sub>s</sub> of asphalt A are arranged in the fraction at a level of 20–50%. There is a higher saturate wax content in the lighter fraction of asphalt C, and a higher aromatic wax content in the middle fraction. The aromatic wax content of asphalt A is similar to that of B and D,

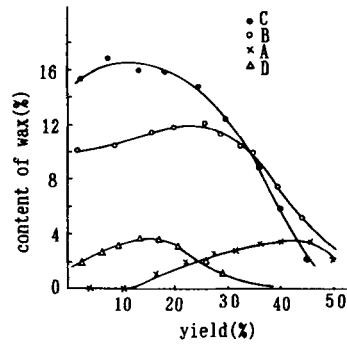


Fig. 20-4. Distribution of the saturate wax for four major asphalts.

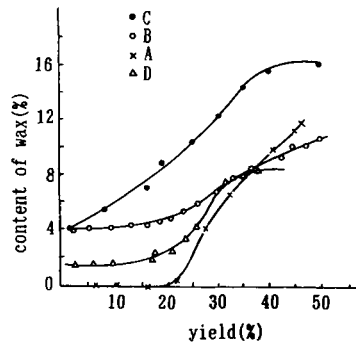


Fig. 20-5. Distribution of the aromatic wax for four major asphalts.

but its content of saturate wax and aromatic wax in the lighter fraction of asphalt A is lower than that of B and C.

The information about the wax type and its distribution obtained in this study can help us to scientifically understand the existence of wax and its effect on the asphalt properties in order to conduct the production of blending fractions and predict the properties of asphalts manufactured by the extraction–blending process.

The writers reached the following conclusions.

(1) Asphalt is a complex material. Two asphalts can have varying chemical composition and performance, even though they have the same specifications. It is far from perfect to characterize asphalt exactly using the SARA analysis.

(2) SCFF is a successful method for the separation and analysis of asphalt. It is a simple and flexible process that is easily reproduced and many samples can be obtained. Arbitrary fractions and constituents can be separated by SCFF and liquid–solid chromatography if necessary. The composition and performance of asphalt can be determined by the information obtained from this process.

(3) It is difficult to evaluate the quality of asphalt only through analyzing its constituents or its wax content. The kind of wax and its distribution, as well as the composition distribution, are important factors in the evaluation.

(4) The changes in group composition take place mainly in heavy aromatics, resin, and asphaltene during the TFOT process. Asphaltene is also formed from heavier resin.

(5) The changes for each fraction under the influence of heat and air were understood according to TFOT, and the relation between the chemical composition of asphalt and its performance in the field can be explained chemically.

#### INVESTIGATION OF ASPHALT AGING

Asphalt will deteriorate during service due to weathering. As a result, an increase of its softening point, a decrease of penetration, and a loss of ductility will be observed. These changes are typically those which cause failure of a paved road surface.

Many researchers have confirmed that asphalt aging may be influenced by various factors. The deterioration of asphalts begins when it undergoes mixing with mineral aggregates, due to a high temperature and contact with air. The physical properties of some asphalts change rapidly. TFOT can approximately simulate the extent to which asphalts age in mixing machines with air under high temperatures. The viscosity, softening point, penetration, ductility, etc., can be measured before and after TFOT. According to their changes, the anti-aging of property asphalts can be evaluated. Up to now, only the ratio of final to initial viscosity can express the tendencies of asphalt aging. The anti-aging of several Chinese asphalts was estimated with viscosity ratios and peak spreads of GPC by TFOT and the absorption of oxygen.

##### *Asphalt aging in TFOT*

Based on the results of our study, the tendency of asphalts to age in TFOT is identical with that of their service in paved roads. It has been shown that the durability of asphalts in roads is related to their aging index (AI), which is the viscosity ratio at 60°C or 135°C before and after TFOT. The larger the AI, the worse is the anti-aging of asphalt. The maximum AI has a limit of 5.

Table 20-8 shows the AI of several Chinese paving asphalts (penetration grade 90/120) aged in TFOT. The rankings of AI could be compared with those of the actual road service properties. It is interesting to note that the AI of the blown asphalt is higher than that of the straight one.

In order to observe how asphalts aged by temperature, they were tested at increasingly higher temperatures. The AI increased rapidly as the temperature rose. The mixing temperature, therefore, should be seriously controlled, and partial overheating should be prevented in asphalt mixing plants to avoid further deterioration of asphalts. This is very important in maintaining quality and extending service life.

A rapid method for predicting the anti-aging properties of asphalts was developed to measure the distribution of molecular weight before and after TFOT, using GPC to determine the relationship between changes of molecular weight and asphalt aging. The method uses the difference in peak spreading ( $\Delta R$ ) obtained from GPC diagrams of asphalts before and after TFOT to evaluate the asphalt anti-aging properties. The GPC of two asphalts before and after TFOT are shown in Figs. 20-6 and 20-7.

TABLE 20-8

Peak spreading and aging index of several asphalts before and after TFOT

Sample	M10%	M90%	$R$ (10%, 90%)	$\Delta R$	Viscosity, 60°C (Pa s)	AI
Gaosheng bef.	3600	570	6.316	141.0		
Gaosheng aft.	4700	600	7.833	1.517	386.5	2.74
Japanese bef.	2550	505	5.050	205.3		
Japanese aft.	2750	505	5.446	0.396	374.3	1.82
Shanjiasi bef.	2350	506	4.644	151.0		
Shanjiasi aft.	3000	570	5.262	0.619	269.2	1.78
Shengli bef.	2650	530	5.000	96.3		
Shengli aft.	3400	555	6.182	1.182	256.4	2.66
Goudong bef.	3200	550	5.818			
Goudong aft.	3300	560	5.893	0.075		

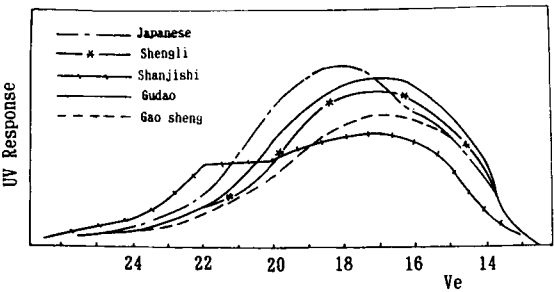


Fig. 20-6. GPC diagram of five asphalts.

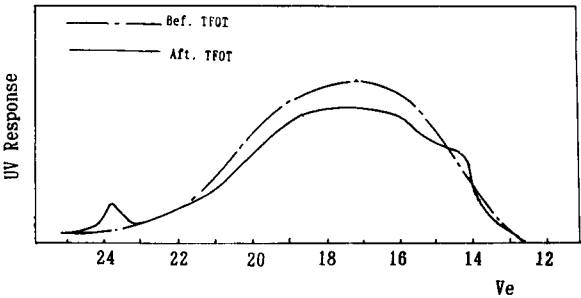


Fig. 20-7. GPC diagram of Shanjiasi asphalt.

For the purpose of quantitative description, the peak spreading  $R$  can be used as an index. According to GPC diagrams, the  $R$  (10%, 90% elute) values before and after TFOT can be calculated to obtain the difference:

$$\Delta R = R_{\text{aft}} - R_{\text{bef}}$$

where  $R = M10\%/M90\%$ , where M10% is the larger molecular weight of 10% eluent,

and M90% is the smaller molecular weight of 90% eluent. A smaller value of  $\Delta R$  leads to a stronger resistance to aging. Table 20-8 lists the peak spreading of several paving asphalts.

In the method mentioned above, we assume that the GPC diagram is a Gaussian distribution.

The results of the five asphalts are listed in Table 20-8. As can be seen,  $\Delta R$  is closely related to the AI. The relationship between  $\Delta R$  and the aging index is shown in Fig. 20-8.

The changes of molecular weight distribution of asphalts before and after TFOT can be determined quantitatively by GPC. It is time-saving and can be used as a routine test to predict the aging resistance of an asphalt.

#### *Durability of paving asphalts by absorption of oxygen*

The oxygen absorption of four Chinese asphalts was adopted to simulate the aging under service conditions.

The standard apparatus and experimental procedure were used. Different asphalts would absorb 0.7–2.6 (ml oxygen)/(g asphalt).

Oort [3] presented the kinetic model of oxygen absorption by asphalts. The reaction can be described by a first-order kinetic model:

$$r = k(G_m - G) \quad (20-1)$$

After integrating Eq. 20-1, Eq. 20-2 can be obtained:

$$G = G_m[1 - \exp(-kt)] \quad (20-2)$$

where,  $r$  = reaction rate, (ml oxygen)/[(g asphalt) h];  $k$  = apparent constant of reaction rate, 1/h;  $G_m$  = maximum concentration of reacted oxygen, (ml oxygen)/(g asphalt);  $G$  = concentration of reacted oxygen, (ml oxygen)/(g asphalt);  $t$  = reaction time, h. The results for four Chinese asphalts are shown in Table 20-9.

We plotted  $G$  vs.  $t$  as shown in Fig. 20-9. From this figure, it can be seen that the kinetics model describes the process of oxygen absorption quite well.

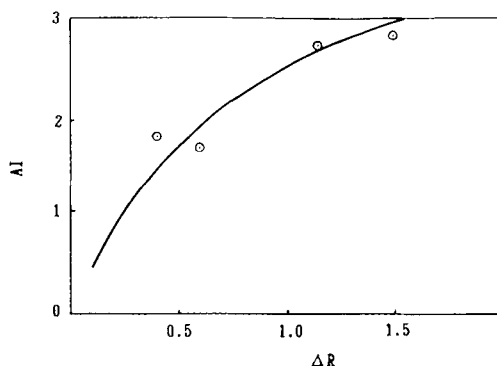


Fig. 20-8. Relationship between  $\Delta R$  and aging index.

TABLE 20-9

The kinetics parameters of four Chinese asphalts

	Renqiu	Daqing	Shanjiasi	Gudao
$G_m$ , (ml/g)	2.9	1.3	1.0	1.4
$k$ (30°C), (1/h)	0.0049	0.0083	0.0106	0.0071
$G_m$ , (ml/g)	2.8	1.9	2.0	2.6
$k$ (50°C), (1/h)	0.023	0.022	0.019	0.023
$R^a$	0.98	0.99	0.98	0.99
$G_m$ , (ml/g)	2.5	1.7	—	—
$k$ (70°C), (1/h)	0.039	0.042	—	—
$R$	0.99	0.99	—	—
Gudao				
Partial pressure of oxygen, (kPa)		1.84	6.16	8.92
$G_m$ , (ml/g)		1.2	1.5	2.6
$k$ (50°C), (1/h)		0.017	0.019	0.023
$R$		0.99	0.99	0.99

<sup>a</sup>  $R$  is relative coefficient.

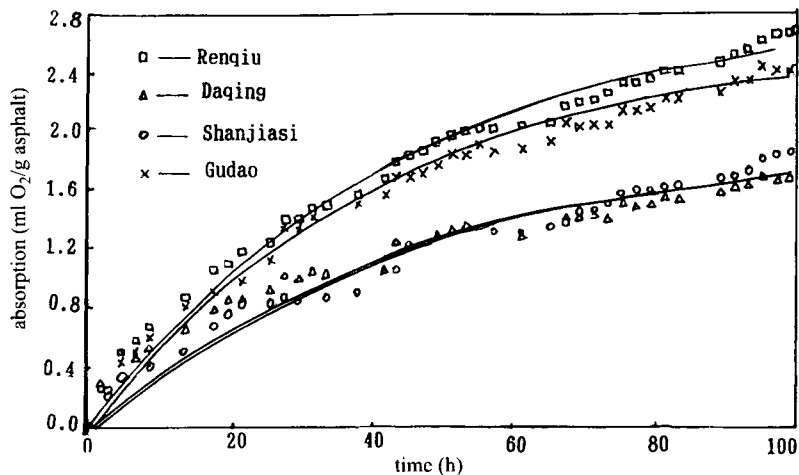


Fig. 20-9. Relationship between absorption of oxygen and time.

*Effect of absorbing oxygen on the physico-chemical properties of asphalts and their constituents*

The changes of the physico-chemical properties of several Chinese paving asphalts and their constituents, i.e., saturates, aromatics, resins and asphaltenes were investigated after they had been absorbing oxygen for 125 h at 50°C, 1 mm sample film thickness, and 0.133 MPa in darkness (Table 20-10).

The experimental results showed that the oxygen absorbed by the samples was



TABLE 20-10

Effect of air distributor

Air distributor	$d = 1 \text{ mm}$	No. 4 micropole glass plate
Temperature ( $^{\circ}\text{C}$ )	300	300
Rate of air ( $\text{l h}^{-1} \text{ kg}^{-1}$ )	240	40
Time (h)	10	4
Properties of product:		
Softening point ( $^{\circ}\text{C}$ )	114	104
Penetration (0.1 mm)	24	24

mainly changed into O-H, S=O and C=O groups. The colloidal stability of the asphalts deteriorated after oxygen absorption, and the molecular weight, as shown by the GPC peak spread, leaned toward higher values. The results of the kinetics study demonstrated that the rate of conversion of resins into asphaltenes is greater than for those of other constituents.

#### ADVANCES IN MANUFACTURE OF ASPHALTS

There are four ways of producing asphalt, i.e., distillation, oxidation, solvent deasphalting (SDA), and blending. The distillation process is more economical and the most convenient way to produce asphalt for road pavement. The method of oxidation is an effective means of raising the softening point of the asphalts when the PI value of asphalt can be raised. The SDA process was widely used in producing asphalt and feedstock for upgrading from petroleum residua. This method can be improved by using supercritical solvent extraction. In this section, we emphasize air blowing and SCFF processes, which have been developed at our institute.

##### *Continuous asphalt blowing*

Residue oxidation is a traditional method for producing asphalts that have high softening points. Generally, the continuous oxidation plant is available for the production of certain special asphalts. The conditions of oxidation are as follows: oxidation temperature, 260–290 $^{\circ}\text{C}$ ; air flow rate, 100–150 ( $\text{m}^3 \text{ air}$ )/[( $\text{m}^3 \text{ asphalt}$ ) h]; residence time (in reactor), 8 h. According to these, the softening point of asphalt can be raised from 46 $^{\circ}$  to 110 $^{\circ}\text{C}$ .

Oxidation reactions of asphalt act in accordance with chain reaction mechanisms. The kinetics of the reaction can be described by a first-order reaction. The average reaction heat for different origin residues ranges from 4.2 to 4.6  $\text{kJ kg}^{-1} \text{ K}^{-1}$ .

The main technological problems of asphalt blowing are the following three points.

##### *(1) Air distribution*

The oxidation rate of air blowing at a certain temperature is directly proportional to the contact surface between asphalt and air. The oxygen molecules penetrate into

asphalt by diffusion, then the oxidation reaction occurs. We will say that the change of concentration of oxygen molecules along the length ( $dx$ ) is  $dc$ . The amount of diffusion can be written as:

$$G = -DF \frac{dc}{dx} \tau$$

where,  $D$  = coefficient of diffusion;  $F$  = contact surface;  $\tau$  = time;  $F$  is a function of the air rate, air nozzle type and size, surface tension of the liquid, density of the two phases, etc.

The results of the studies showed that the residence time can be changed to a great extent by using different air distributors. The details are listed in Table 20-10. Due to the modification of air distribution, the conditions of diffusion of oxygen can be improved. Experience at a refinery sets the height of the reaction zone at only 6 m. The efficiency of air utilization can be modified by using six sieve plates set in the reactor. The oxygen content in the waste gas decreases from 12–14% to 7–9%.

### (2) Controlling reaction temperature

For the purpose of removing the reaction heat, several methods can be adopted: decreasing the temperature of feedstock, spraying cooling water on top of the reactor, installing a steam generator, etc. In China, the first and second methods have been applied.

The typical asphalt blowing plants are shown in Table 20-11.

### (3) Treatment of waste gas

Waste gas contains large amounts of nitrogen (85–90%), carbon dioxide, oxygen, and light hydrocarbons. Besides these, there are some harmful components, such as organic nitrides, sulfides, and oxides, of which especially 3,4-benzopyrene exists in the waste gas.

In China, incinerators have been used to treat the waste gases and they are often combined with feedstock heaters. The waste gas passes through the oxygen-rich zone of the heater (where temperature  $> 650^{\circ}\text{C}$ , and residence time  $> 1$  s). As a result, the content of 3,4-benzopyrene decreases from 179–393 to 1–1.8  $\mu\text{g}/(100 \text{ m}^3)$ .

To avoid water condensation, the temperature of the waste gas must be kept over its dew point before being placed in the incinerator.

## Supercritical solvent extraction of petroleum residue

The solvent deasphalting process is an effective method for upgrading of heavy residue. Asphaltenes, resins, and/or heavy aromatics, which exist in the residue, can be separated. However, due to the lower yield of DAO and the lower mass transfer rate

TABLE 20-11

Reactor data of three asphalt blowing plant

Refinery	Feedstock (ton/h)	Height of liquid, $L$ (m)	Reactor diameter, $D$ (m)	$L/D$
1	21–26	13.8–14.6	3.4	4.04–4.29
2	25–40	14	3.6	0.88
3	1.5–3.0	10.0–12.5	1.44	6.94–8.68

using propane as a solvent, its use in heavy residue upgrading is limited. During the past two decades, more consideration has been given to the use of supercritical fluid (SCF) as a solvent (e.g.,  $C_4$ ,  $C_5$  fraction or  $n$ - $C_5$ ) for separating heavy residue in order to yield more DAO for FCC or hydrocracking and to provide the residue for blending asphalt.

Since 1980, a series of studies have been done on SCF phase equilibrium, phase behavior, and continuous SCF extraction using  $C_4$  or  $C_5$  fractions to treat petroleum residua. On the basis of the above results, a pilot plant with a yearly capacity of 15,000 ton residue was set up and put into operation successfully. The operation results showed that the SCFE process using  $C_5$  fraction as a solvent could get about 50% DAO with a low heavy-metal content and Conradson carbon residue from Gudao and Shanjiasi residua. Its lower energy consumption (1315 MJ/t), smaller equipment size, and simple flow sheet showed that the process has a good prospect.

Based on the results of our previous study,  $C_5$  fraction is preferred as a solvent for SCFE. This is because (a)  $C_5$  fraction is plentiful in refineries and oil fields, (b) the dissolving power of the SCF  $C_5$  fraction is higher than that of  $C_3$  and  $C_4$  fractions for residue extraction and the yield and quality of DAO can be controlled by changing temperature and pressure, (c)  $C_5$  fraction (SCF) has a higher  $T_c$ , so that mass transfer can be improved, and (d)  $C_5$  fraction can be used at a higher temperature (the temperature of the recycled solvent is below  $T_c$  by 10–15°C). Compared with other solvents, the heat exchange area can be reduced significantly with  $C_5$  fraction.

#### (1) Study on operation conditions

Using  $n$ - $C_5$  as a solvent, its normal pentane content is over 99% mol. The properties of the feedstocks are shown in Table 20-12.

The laboratory SCFE schematic diagram is designed in correspondence with one- or two-stage operations. The effect of temperature and pressure on the DAO yield and quality are shown in Fig. 20-10. From the figures, it can be seen that the yield of DAO increases when the temperature decreases or the pressure increases. Fig. 20-11 illustrates the relation of the DAO yield with its quality.

The yield of DAO and process selectivity is enhanced as the S/O ratio increases. The yield of DAO and process selectivity does not change with an increase of the S/O ratio when S/O reaches a limit.

TABLE 20-12

Properties of feedstocks

	Gudao	Shanjiasi
Density (15°C) (ml/g)	0.9941	0.9887
CCR (wt%)	16.2	15.2
Ni (ppm)	47.5	59.5
Viscosity (Pa.s):		
60°C	23.4	53.9
135°C	0.172	0.345
Softening point (°C)	44.5	46.5

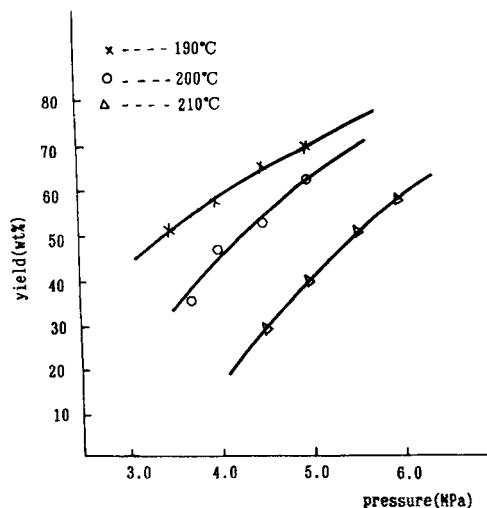


Fig. 20-10. Changes of DAO yield with pressure and temperature in the system of Gudao residue  $n$ -C<sub>5</sub> fraction.

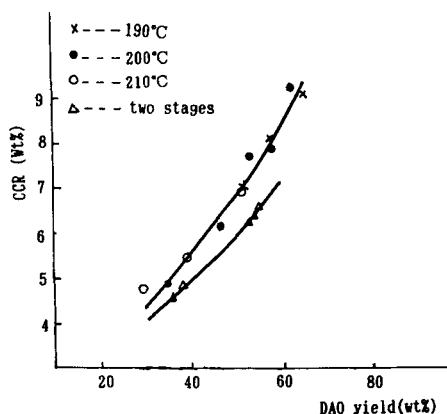


Fig. 20-11. Relationship of Conradson carbon residue (CCR) with the yield of DAO in the system of Gudao residue  $n$ -C<sub>5</sub> fraction.

## (2) Investigation of application fundamentals

Currently, the thermodynamics of residue SCFE are rarely reported. Heavy solvent is frequently used. In designing an extraction process, the knowledge of phase behavior and phase equilibrium is indispensable. By using a PVT apparatus with a long window, the phase behavior of Daqing residue in a C<sub>4</sub> system with differing S/O values can be observed.

On the basis of the results of phase equilibrium study, a mathematical model of SCF extraction was established to predict the solubility of C<sub>5</sub> fraction-residue systems. The

calculated results of solubilities and concentrations of heavy and light phases agreed well with experimental data.

### (3) Pilot plant

A vacuum residue supercritical fluid extraction pilot plant with an annual capacity of 15,000 tons was designed in 1986 and into operation in May of 1988. The results of successful plant operation proved that the process has a number of advantages. The flow diagram is shown in Fig. 20-12.

The vacuum residue charge, mixed with the heated C<sub>5</sub> fraction solvent recycled from storage (S202), is fed to the first stage separator (T201), in which temperature and pressure are kept above the supercritical point. In the first separator, asphaltene and some heavy resins settle to the bottom and are transferred to the solvent stripper, while the heated overhead effluent from T201 maintains a suitable temperature for entering separator T202. Due to increasing temperature, the solubility of resins and heavy aromatics decreases. As a result, resins can be drawn out from the bottom of separator T202.

The top effluent from T202, after raising the temperature and depressurizing to a limit, then enters separator T203, in which the DAO can be drawn out with a small amount of solvent and transferred to the stripper, where almost over 86% of the solvent is recovered.

The features of the pilot plant are as follows.

(1) The temperature and pressure of the extraction section are above the critical point of the solvent, so that a change in DAO yield and quality can be flexibly reached by means of changing the temperature and pressure.

(2) Because SCF has good mass transfer behavior, the solvent mixes with vacuum residue in a mixer without a special structure and then enters the separator at suitable temperature and pressure conditions.

(3) Using the supercritical solvent recovery technique, more than 80% of the solvent can be recovered without vaporization.

(4) All of the heaters (F201, F202, and F203) used in the plant are vertical cylindrical furnaces. Vertical tubes are adopted to avoid coke formation. In this case, the change of effluent flow direction would disturb the liquid phase, which is rich in asphaltenes and resins.

(5) About 5–15 wt% of the resin fraction can be obtained from the resin separator (T202) through heating the overhead effluent of T201. Polar aromatics and heavy metals are concentrated in the resin fraction, so that the quality of DAO can be improved. Table 20-13 lists the utilities requirement. Table 20-14 shows the properties of the DAO product obtained and the bitumens after blending with vacuum residue.

From Table 20-14, one can see that the DAO has a lower content of metals and a lower Conradson carbon residue; therefore, it can be used as FCC feedstock or hydrocracking feedstock. The blending bitumens have a good ductility and serve well as road paving asphalt.

The capital and operation costs of this process are far lower than that of the conventional propane deasphalting process. The features mentioned above illustrate that its low energy consumption, small equipment size, and simple flow sheet offer a good prospect for economical application.

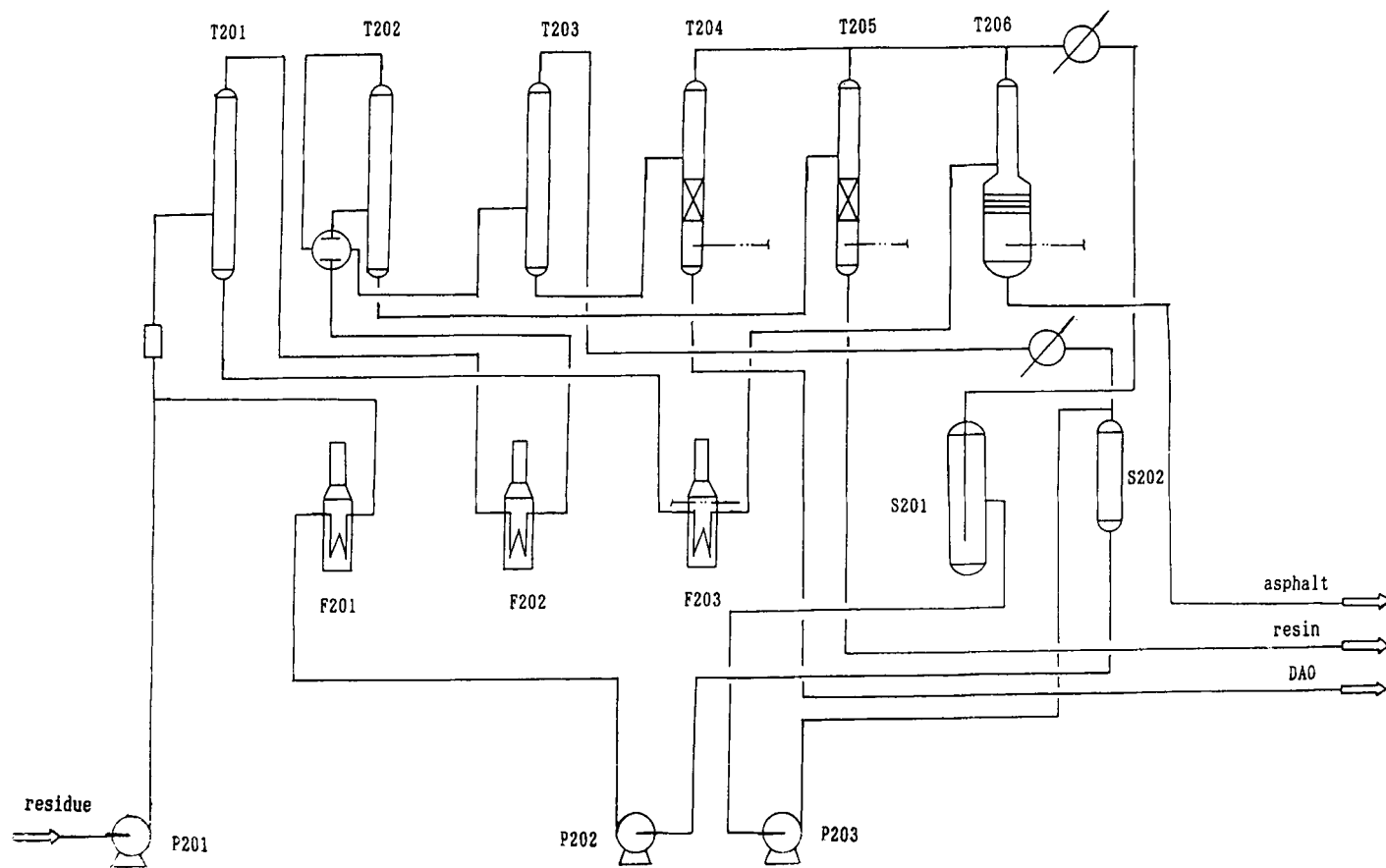


Fig. 20-12. Flow diagram of residue supercritical solvent extraction.

TABLE 20-13

## Utilities requirement

	Per ton stock	Per hour
Steam <sup>a</sup> (kg)	50.9	109.5
Cooling water (t)	16.88	36.3
Power (kW)	16.3	35
Fuel (kg)	21.7	46.7

<sup>a</sup> From steam regenerator of this plant.

TABLE 20-14

## Properties of DAO and resin products

	Shanjiasi Resin	DAO	Gudao DAO
Yield (wt%)	14.8	38.1	36
Density (20°C) (g/ml)	0.9642	0.9462	0.9529
CCR (wt%)	9.8	4.2	5.2
Ni (ppm)	26.5	9.9	9.4
Viscosity (60°C) (Pa s)	3.45	0.576	0.746
MW	760	—	722

## REFERENCES

- [1] Rostler, F.S. and Sternberg, H.W., *Ind. Eng. Chem.*, 41: 598 (1949).
- [2] Corbett, L.W., *Anal. Chem.*, 41: 576 (1969).
- [3] Oort, W.P.V., Durability of asphalt. *Ind. Eng. Chem.*, 48 (7): 1196–1201 (1956).

## Chapter 21

# WAX PRECIPITATION FROM PETROLEUM FLUIDS: A REVIEW

C. LIRA-GALEANA and A. HAMMAMI

## INTRODUCTION

Petroleum reservoir fluids are complex mixtures of hydrocarbons whose composition and properties are not known in detail [1–6]. The light fraction of these fluids contains associated gases and low molecular weight hydrocarbons (i.e., CO<sub>2</sub>, H<sub>2</sub>S, N<sub>2</sub>, C<sub>1</sub>, C<sub>2</sub>, C<sub>3</sub>, *n*-C<sub>4</sub>, *i*-C<sub>4</sub>), while the rest of the oil contains a wide variety of paraffinic, naphthenic and aromatic compounds whose molecular weights range from approximately 100 to 2000 [6]. When the temperature falls, the heavy hydrocarbon components within this interval can crystallize and precipitate in the form of a solid mass, known as *wax*, which can deposit in the pipe walls or processing equipment. This precipitation has operative as well as economic implications of significant value to the petroleum industry.

While the molecular and thermodynamic behavior of the light fraction of these fluids are known with a good degree of accuracy, a clearly different situation exists in the case of the heavier hydrocarbon fractions, whose complexity and crude-oil dependant properties make generalized behaviour still lacking. In spite of this, however, significant experimental findings and semi-simplified modeling descriptors have been reported in the past few years.

This chapter presents a review of the experimental techniques and theoretical tools for the study of wax precipitation in petroleum fluids. We first present a review on the analytical techniques for characterizing waxy crudes and their solid deposits. Starting with some operative definitions for the main hydrocarbon fractions of the crude, the experimental protocols to separate and further analyze the composition and properties of the wax are presented and discussed.

In the second section, the modern experimental methods for studying the phase behavior of waxy crudes are presented. Since the basic quantity that characterizes the formation of waxes is called *the cloud point* (or initial crystallization temperature), special emphasis is paid to the most recent analytical techniques to measure the cloud points in dead or live-oil systems. These techniques make it possible to define the geometric projection in which the wax crystallizes and precipitates at a given pressure, temperature or petroleum composition (i.e., phase diagram).

Lastly, this chapter presents a review on the most significant thermodynamic tools to model wax precipitation. The reviewed methods range from ideal solution approaches to models that consider solid–solid immiscibility in the precipitated wax. Comparisons of the above-mentioned models with experimental information are presented. The chapter concludes with an inventory of research issues aimed at a better understanding of the precipitation of wax in the near future.



## CHARACTERIZATION AND PROPERTIES OF WAX COMPONENTS IN PETROLEUM FLUIDS

Most crude oils consist of various fractions of heavy hydrocarbons, which are known to precipitate as paraffin deposits due to either an evaporation of volatile light ends, which otherwise act as naturally-occurring solvents, or a drop in the system temperature [7]. Accumulation of these solids in transport pipes and process equipment is an old and expensive problem in the petroleum industry. This problem is expected to increase in the future as existing reserves are depleted and offshore explorations continue to grow.

In field operations, asphaltenes and residual oil components often co-precipitate with the waxes, and result in a varying appearance (color) and texture of the precipitated solids. As expected, waxes from condensates and wet gases tend to be cleaner and lighter in color than those from heavier crudes. The predominately waxy character of the precipitated solids can only be defined based on the analysis of the deposit and the remedial techniques that can be used to re-dissolve such a precipitate. In general, only small amounts of aromatic components co-precipitate with waxes and the resulting solid material usually melts by applying heat.

In order to avoid and/or establish a remedial action plan for this problem, it has become necessary to develop adequate analytical protocols to separate and characterize waxy crudes and wax/asphaltene co-precipitates. Prior to addressing the details of waxy crude characterizations and related analytical protocols, however, it is useful to provide a brief review of petroleum fluid chemistry.

*Petroleum chemistry and composition*

Petroleum fluids are mixtures of naturally-occurring hydrocarbons which may range from dry natural gas to extremely viscous heavy oil and bitumen depending upon their composition and the conditions of pressure and temperature to which they are subjected. Operating temperature and pressure in petroleum industry can range from near ambient to extremes as high as 20,000 psia ( $\approx 1380$  bar) and 600°F ( $\approx 320^\circ\text{C}$ ). Fluid composition and properties can also vary significantly depending on production/injection operations, ambient conditions, geological factors, and numerous other variables. In addition to hydrocarbon fluids, most produced fluids contain significant amounts of water and other inorganic minerals derived from fluid-rock interactions in the petroleum reservoir.

In general, petroleum constituents are classified under two major groups: the well-defined and volatile  $C_7-$  fraction and the poorly defined and relatively non-volatile  $C_7+$  fraction. The  $C_7-$  fraction consists of all pure hydrocarbon components (and non-hydrocarbons) with carbon numbers up to  $C_5$ . These include all isomers in each carbon number range; the physical properties of each of the pure component species are well understood and recorded in the literature [8]. The  $C_7+$  fraction, on the other hand, is far more complex due to the multiple isomer combinations available to hydrocarbons with increasing chain length [9]. This group of components can be classified into four major fractions denoted as saturates, aromatics, resins, and asphaltenes. Examples of each of these classes of chemicals are defined below; their chemical structures are shown in Figs. 21-1 and 21-2.

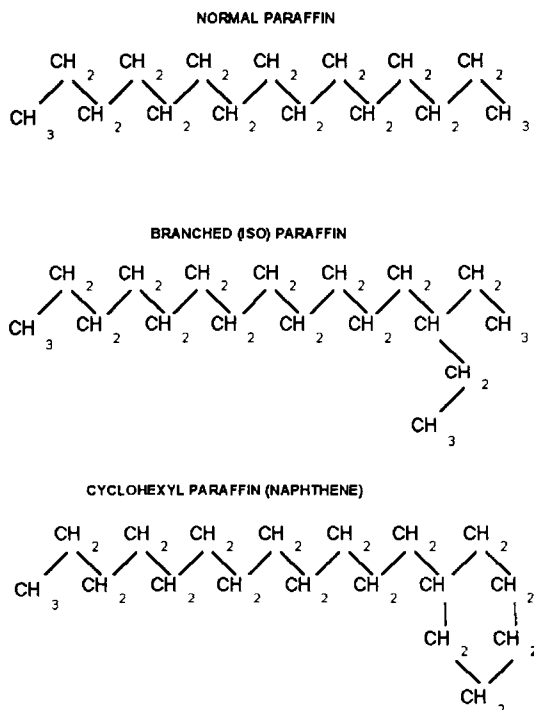


Fig. 21-1. Typical components of the saturates fraction.

### Saturates

Saturates consist of normal alkanes (*n*-paraffins), branched alkanes (*iso*-paraffins) and cyclo-alkanes (naphthenes). The *n*-paraffins and the *iso*-paraffins are flexible hydrocarbon molecules and, hence, tend to cluster together and precipitate from crude oil as wax solids. Being branched molecules, however, the *iso*-paraffins tend to delay the formation of wax nuclei and usually form unstable wax solids. Naphthenes are stiff and bulky in nature; they tend to disturb and/or disrupt the wax nucleation and/or growth processes.

### Aromatics

Aromatics consist of hydrocarbons which are chemically and physically very different from paraffins and naphthenes. They contain at least one ring structure similar to benzene. The corresponding atoms are connected by aromatic double bonds, hence the name aromatics. Aromatics are known as good solvents for paraffin waxes.

### Resins

Resins are typically composed of a highly polar end group, which often contains heteroatoms such as oxygen, sulfur and nitrogen, as well as long, nonpolar paraffinic groups. The resins are attracted to the asphaltene micelles through their end group. This attraction is a result of both hydrogens bonding through the heteroatoms and

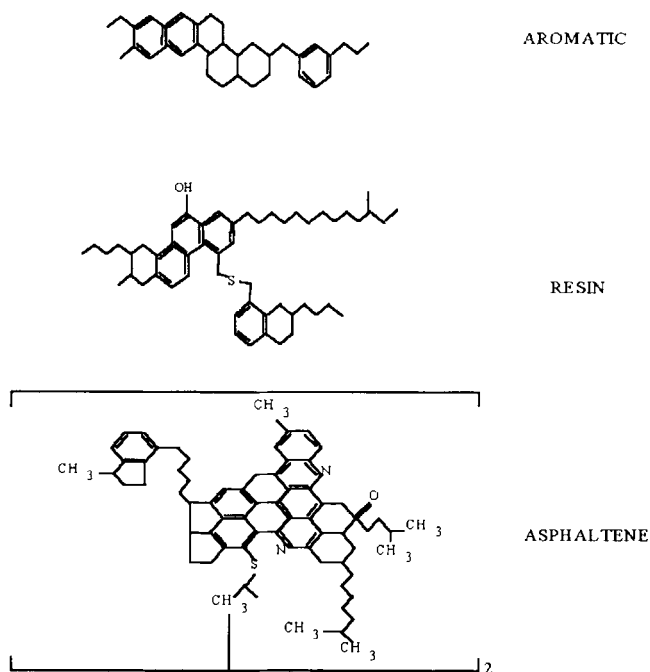


Fig. 21-2. Hypothetical structures of aromatic, resin, and asphaltene molecules.

dipole–dipole interactions arising from the high polarities of the resin and asphaltene molecules. The long paraffinic component of the resin molecule acts as a tail, making the transition to the relatively non-polar bulk of the oil where individual molecules also exist in true solution [10]. Resins can be converted to asphaltenes by oxidation. Resins are assumed to be dissolved in the petroleum fluid. Pure resins are heavy liquids or sticky (amorphous) solids and are as volatile as hydrocarbons of the same size.

### *Asphaltenes*

Asphaltenes are usually comprised of condensed aromatic and naphthenic molecules with molecular weights ranging from several hundred to several thousands. They also consist of polar molecules containing much of the heteroatom (N, O, S) and metal (Ni and V) content of heavy oils. It is often assumed that asphaltenes do not dissolve in petroleum, but are dispersed/suspended in the fluid as colloids (evidence of this is mixed). Pure asphaltenes are black dry powders and are nonvolatile; they tend to crack before boiling.

It is emphasized that the solid materials precipitating from hydrocarbon systems in a field operation will rarely be comprised of components derived from one of the above general component groups. On the contrary, hydrocarbon precipitates are most often mixtures of components from different fractions. In many instances, the identification of the field problem as wax or asphaltene related is difficult to make, because the wax and

asphaltene components of a crude oil often co-precipitate. Accordingly, the definition of whether a deposit is wax or asphaltene must be based on the analytic, physical, and phase behavior properties of the deposit.

### *Analytical methods*

Analytical methods are available for the separation and characterization of asphaltenes in heavy crudes and bitumens, and waxes in waxy crudes. As discussed previously, both of these component types can give rise to production, transportation and processing problems related to the crudes or their products. Good data characterizing the asphaltenes in terms of their content and stability, and waxes in terms of their content and carbon number distribution, are usually required to help solve these problems. Increasingly, both asphaltenes and waxes are being found in the same crudes, and the established methods for their separation are often not applicable [11]. This chapter provides a review of some of the existing characterization methods, describes new separation techniques, and discusses their applicability to different crude types.

#### *Modified UOP 46-64 method for wax content determination*

This method involves dissolving 2 g of oil sample (or wax deposit) in toluene, and the solution is clarified using Fuller's Earth. As such, all polar materials including asphaltenes are removed, dried, and quantified. The toluene is evaporated and the clarified (de-asphalted) oil is re-dissolved in an acetone–petroleum naphtha mixture. This solution is then chilled to  $-17^{\circ}\text{C}/0^{\circ}\text{F}$  and filtered through a cold filter funnel, with the wax collected on an asbestos mat in the funnel. The wax is subsequently washed from the mat into a weighed flask, using hot petroleum naphtha. Finally, the naphtha is evaporated and the precipitated wax is weighed.

The number of steps required to separate the wax fraction makes one suspicious of the accuracy and precision of the UOP method. When samples, containing large amounts of polars/asphaltenes and trace quantities of waxes, are subjected to the UOP 46-64 test, the ratio of Fuller's Earth to wax recovered is very large; therefore, a small loss of Fuller's Earth can result in significant errors in the wax recovery value.

#### *UOP asphaltene content (n-pentane insoluble material)*

The UOP 614-80 method involves dissolving 5 g of oil in 5 ml of chloroform in a glass flask. While swirling the mixture, 200 ml of *n*-pentane is added slowly. The resulting mixture is then agitated for five minutes and eventually stored in the dark for two hours to precipitate asphaltenes (with occasional shaking). The content of the flask is then filtered, using a sintered glass crucible having a nominal pore retention of 10–15  $\mu\text{m}$ . An additional volume of *n*-pentane is used to rinse the flask and is poured on the filter cake until the wash becomes colorless (approximately 50 ml). The resulting filtrate is re-filtered through a 0.45- $\mu\text{m}$  filter. Both precipitates are thereafter washed with methylene chloride to dissolve the asphaltenes. The washings are stopped when the filtrates appear colorless. Finally, the methylene chloride is evaporated and the dissolved asphaltenes are dried and cooled before weighing.

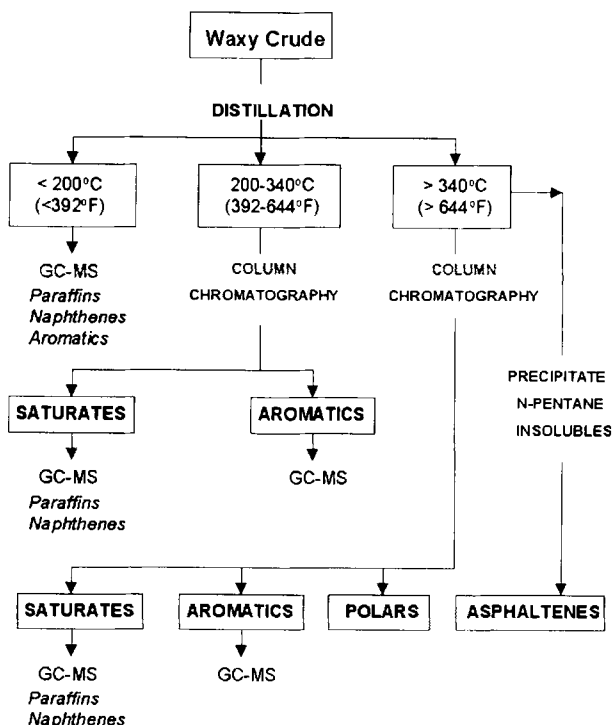


Fig. 21-3. Fractionation protocol for waxy crude characterization.

#### *Detailed PNA analysis of waxes and waxy crudes*

Several other analytical tools, such as high performance liquid chromatography (HPLC), super critical fluid chromatography (SFC) with flame ionization detection (FID), and gas chromatography coupled with mass spectrometry (GC-MS), can be used to determine the paraffin-naphthene-aromatic (PNA) contents of crude oil distillation fractions. These methods are quite expensive but provide additional useful data for characterizing heavy fractions in a reservoir fluid. Typical measurement procedures are discussed below and are augmented by referring to the flowchart of Fig. 21-3. These analytical protocols have been developed by Alex et al. [12] to generate the required input data for the wax model formulated by Majeed et al. [13].

*Preparation of distillation cuts.* Initially, the crude oil is fractionated into three distillation cuts, namely naphtha (<200°C/392°F), middle distillate (200–340°C/392–644°F) and residue (>340°C/644°F), using a spinning band distillation system. The middle distillate and residue cuts are further separated by a silica-alumina (Si-Al) column chromatographic method. Both cuts are separated into saturates, aromatics and polars fractions. The respective eluents used in this separation procedure are as follows: 150 ml *n*-pentane for saturates, 300 ml toluene/*n*-pentane (30:70 v/v) for aromatics, and 300 ml methylene chloride/methanol (50:50 v/v) for polars. The asphaltenes in the residue

TABLE 21-1

Sample analysis of a naphtha cut

Saturates (percent of total IBP-200°C)		Aromatics (percent of total IBP-200°C)	
Open chain	35.3	Monoaromatics	15.0
1-ring	40.5	Diaromatics	<0.1
2-ring	5.7	Polyaromatics	nd <sup>a</sup>
3-ring	3.3		
Total	85		15

Saturates by carbon (percent of total IBP-200°C)		Aromatics by type (percent of total IBP-200°C)	
C5	1.4	Alkylbenzenes	14.7
C6	7.3	Benzocycloparaffins	0.2
C7	19.8	Benzodicycloparaffins	0.1
C8	19.6	Naphthalenes	<0.1
C9	17.7	Naphthocycloparaffins	nd <sup>a</sup>
C10	12.3	Fluorenes	nd <sup>a</sup>
C11	5.7	Phenanthracenes/anthracene	nd <sup>a</sup>
C12	1.2		

<sup>a</sup> nd = not detected.

cut of the waxy crude are first precipitated with *n*-pentane and the resulting maltenes are separated by the Si-Al method.

*Characterization of the distillation cuts by mass spectrometry. Naphtha:* The whole naphtha cut is analyzed by supercritical fluid chromatography-mass spectrometry (SFC-MS) with N<sub>2</sub>O chemical ionization (CI). Typical breakdown, in terms of paraffins (open chain), naphthenes (1-, 2- and 3-ring) and aromatics (mono-, di- and polyaromatic), is given in Table 21-1. A further distribution of carbon numbers for saturates (semi-quantitative) and aromatic types (alkylbenzenes, etc.) is also given.

*Middle distillate:* The separate saturate and aromatic fractions of the middle distillate cut are analyzed by GC-MS with N<sub>2</sub>O CI. Typical breakdown, in terms of paraffins (open chain), naphthenes (number of rings) and aromatics (types), as well as the saturates carbon number distribution, is given in Table 21-2.

The results should only be considered qualitative since constant response factors for all carbon numbers for saturates and aromatics are usually assumed, and contributions to mass spectral peaks by fragmentation are ignored.

*Residue:* The separate saturate and aromatic fractions from the residue are analyzed by GC-MS with N<sub>2</sub>O CI. As with the middle distillate, the typical breakdown in terms of paraffins (open chain), naphthenes (number of rings) and aromatics (types), as well as the saturates carbon number distribution is given in Table 21-3.

The accuracy of the carbon number data for the residue fractions is limited by two factors. Both the previously mentioned fragmentation ion problem and the large degree of overlap between carbon number groups in the mass spectra add to the uncertainty

TABLE 21-2

Sample analysis of a middle distillate cut

Saturates (percent of total 200–340°C saturates fraction)		Aromatics (percent of total 200–340°C aromatics fraction)	
Open chain	28.7	Alkylbenzenes	25.5
1-ring	34.5	Benzocycloparaffins	17.8
2-ring	23.6	Benzodicycloparaffins	13.8
3-ring	10.2	Naphthalenes	27.3
4-ring	3.0	Naphthocycloparaffins	9.0
		Fluorenes	4.0
		Phenanthracenes/anthracene	2.6

Saturates by carbon # (percent of total 200–340°C saturates fraction)	
C11	0.7
C12	6.8
C13	13.7
C14	13.9
C15	12.7
C16	11.1
C17	9.3
C18	8.1
C19	7.2
C20	6.1
C21	4.7
C22	3.2
C23	1.7
C24	0.8

in generating quantitative data. It is also noted that the GC–MS results for the residue fractions showed that only a portion of the samples are sufficiently volatile to elute from the GC column and enter the MS sample introduction system. A serious problem with the MS technique in characterizing high carbon numbers is their nominal cut-off at approximately C<sub>40</sub> [12].

*Modified protocol for waxy deposits.* The waxy crude protocol described above (as shown in Fig. 21-3) has been shown to have serious limitations when applied to waxy deposits [12]. For instance, the separations of *n*-pentane insolubles from the residue fractions of waxy deposits often yield ‘waxy’ asphaltenes, probably containing mixtures of high molecular weight asphaltic material and *n*-paraffins. More importantly, attempts to further separate the residues of waxy deposits into saturates, aromatics and polars by Si–Al chromatography have been hampered by problems with column loading and irreversibly bound polar materials. Therefore, the modification shown in Fig. 21-4 has been developed for the residue cut.

In this procedure, the UOP method is adopted to separate the heavy (long) *n*-paraffins from both the polars plus asphaltenes fraction and the oil residue. The polars plus

TABLE 21-3

Sample analysis of a residue cut

Saturates (percent of total >644°F saturates fraction)		Aromatics (percent of total >644°F aromatics fraction)	
Open chain	20.3	Alkylbenzenes	18.3
1-ring	27.3	Benzocycloparaffins	14.9
2-ring	24.6	Benzodicycloparaffins	14.4
3-ring	16.7	Naphthalenes	19.5
4-ring	9.0	Naphthocycloparaffins	13.7
5-ring	1.8	Fluorenes	11.3
6-ring	0.3	Phenanthracenes/anthracene	7.91

Saturates by carbon # (percent of total >644°F saturates fraction)	
C21	0.3
C22	5.6
C23	12.4
C24	17.9
C25	19.0
C26	16.4
C27	12.4
C28	8.0
C29	4.8
C30	2.2
C31	0.7
C32	0.3

asphaltenes, which are attached to Fuller's Earth, are quantified by weight only. The de-waxed and de-asphalted oil (maltene), on the other hand, is fractionated by the Si-Al chromatography into saturates, aromatics and polars, with the two fractions subjected to SFC, GS and MS analyses. The separated acetone wax (essentially *n*-paraffins) is dissolved in CS<sub>2</sub> and analyzed for carbon number distribution up to C-90+ using high temperature gas chromatography (HTGC).

*Sample results.* Table 21-4 shows the overall component type distributions of two waxy crudes and a wax deposit as determined by the above protocols [12]. For the residue fraction from the wax deposit sample, the paraffin values are the sum of those obtained from the weight of precipitated *n*-paraffins plus those from the MS data of the oil (maltene) portion. The reproducibility of these results is found to be on the order of 10%.

As can be seen, waxy crude 2 has a significantly more waxy character than 1, as evidenced by the higher paraffin content and relatively lower naphthenes, aromatics and polars of the former. The waxy deposit, on the other hand, has the highest paraffin, polar, and asphaltene content, but the lowest amounts of naphthenes and aromatics. This finding is consistent with the expected composition of a deposited wax sample.



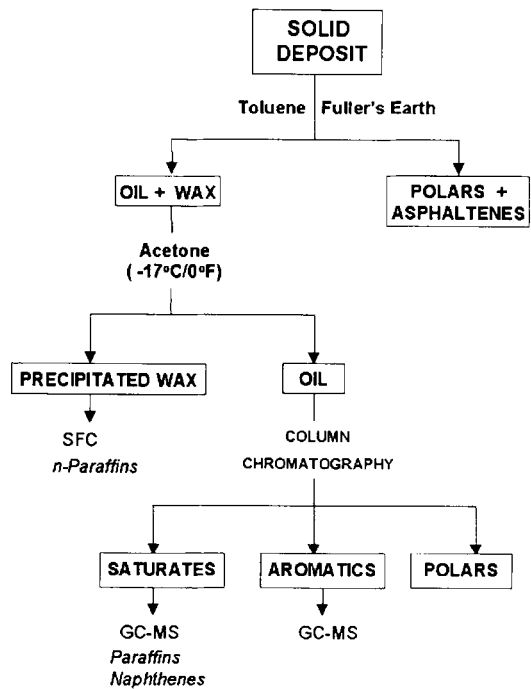


Fig. 21-4. Modification protocol for deposited wax samples.

TABLE 21-4

Component type distributions for waxy crudes and a wax deposit [12]

Weight percent of whole sample						
	Distillation cut yields	Paraffins	Naphthenes	Aromatics	Polars	Asphaltenes
<i>Naphtha</i>						
Waxy crude 1	17.4	5.7	8.6	3.1		
Waxy crude 2	11.5	5.0	4.2	2.3		
Wax deposit	12.7	8.4	3.3	1.0		
<i>Mid-dist.</i>						
Waxy crude 1	28.4	5.3	15.3	7.8		
Waxy crude 2	24.1	14.0	4.6	5.5		
Wax deposit	13.8	4.7	5.4	3.7		
<i>Residue</i>						
Waxy crude 1	54.2	6.0	19.4	17.5	10.8	0.5
Waxy crude 2	64.4	31.9	20.2	9.7	1.7	0.9
Wax deposit	73.5	40.0	7.4	9.4		16.7 (Pol + Asp)
<i>Total</i>						
Waxy crude 1	100.0	17.0	43.3	28.4	10.8	0.5
Waxy crude 2	100.0	50.9	29.0	17.5	1.7	0.9
Wax deposit	100.0	53.1	16.1	14.1		16.7 (Pol + Asp)

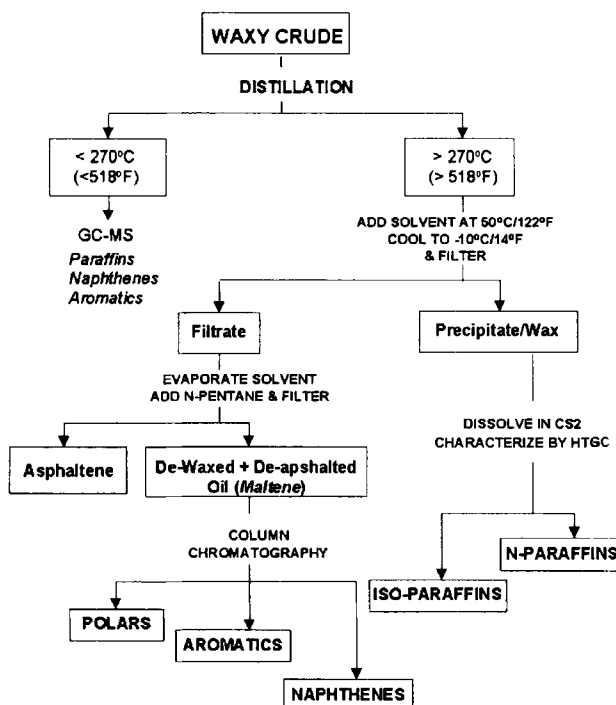


Fig. 21-5. Refined fractionation protocol for conventional waxy crude characterization.

#### *Refined PNA analysis for waxes and waxy crudes*

Recognizing the semi-quantitative nature of the data generated using the protocol of Fig. 21-3 for waxy crude oils and the relatively high cost associated with the inherent analytical procedures, much improved and efficient characterization schemes have recently been established [11]. These techniques consist of the steps shown in the flowcharts of Figs. 21-5 and 21-6 for conventional and heavy waxy crudes/deposits, respectively.

**Conventional waxy crudes protocol.** In Fig. 21-5, the crude oil is initially fractionated into two cuts through distillation at 270°C/518°F (i.e., the boiling point of C<sub>15</sub>). The residue (>270°C) fraction is then dissolved in a special solvent at 50°C; the mixture is cooled and eventually filtered at -10°C/14°F. The special solvent allows only paraffins (*n*-paraffins and *iso*-paraffins) to crystallize at a low temperature. The precipitate (wax) is then weighed, dissolved in CS<sub>2</sub> and analyzed by high temperature gas chromatography (HTGC) to C-90+. The assignment of the weight percent data to the appropriate *n*-paraffin and *iso*-paraffins will be based on the measured retention times of the calibration standard *n*-alkanes. The weight percent of *iso*-paraffins for a given carbon number will correspond to the sum of the area percent values of the peaks between two consecutive (neighboring) *n*-alkanes.

Meanwhile, the solvent is evaporated from the de-waxed residue (i.e., filtrate) and 40 volumes of pentane is subsequently added to precipitate asphaltenes. Following the

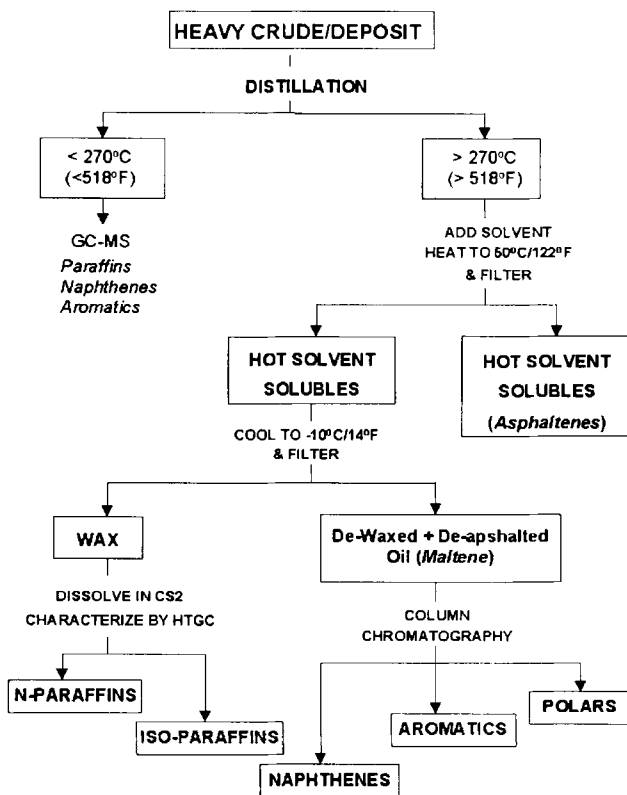


Fig. 21-6. Refined fractionation protocol for heavy crude/deposit characterization.

filtration of the asphaltenes, the filtrate is once more heated to evaporate excess  $C_5$ . The remaining de-waxed and de-asphalted residue (maltene) is separated into saturates (essentially naphthenes), resins and aromatics using a packed column filled with silica and alumina. The silica section of the column strips out the polars (i.e., resins). The alumina section removes the aromatics and, hence, only the saturates can pass through. The saturate fraction recovered is observed to be white and opaque just like candle wax; whereas the aromatic fraction appears to be brownish and the resins exhibit a very dark color.

*Heavy waxy crudes/deposits protocol.* Upon application of the conventional waxy crude protocol of Fig. 21-5 to extremely waxy and asphaltic fluids/deposits, it is found that the separated waxes are not homogeneous in color or texture. In other words, the solids recovered in this manner are rather co-precipitates of wax and asphaltenes. A modified protocol has been developed to overcome this problem [11].

In the protocol of Fig. 21-6, the crude oil is initially fractionated into two cuts by distillation at 270°C/518°F (i.e., the boiling point of  $C_{15}$ ). The residue (>270°C) fraction is then dissolved in a special (proprietary) solvent at 50°C/122°F; the solution is

filtered hot (i.e.,  $\approx 50^{\circ}\text{C}$ ) to remove undissolved asphaltenes. Following this, the filtrate (i.e., de-asphalted oil) is cooled and eventually filtered at  $-10^{\circ}\text{C}/14^{\circ}\text{F}$ . The resulting precipitate (essentially *n*-paraffin waxy mixture) is then weighed; the wax content is determined. The special solvent allows only open chain paraffins (i.e., *n*-paraffins and *iso*-paraffins) to crystallize at low temperature. The precipitate is then weighed, dissolved in  $\text{CS}_2$  and analyzed by high temperature gas chromatography (HTGC) to C-90+. The assignment of the weight percent data to the appropriate *n*-paraffin and *iso*-paraffins is based on the measured retention times of the calibration standard *n*-alkanes. The weight percent of *iso*-paraffins for a given carbon number corresponds to the sum of the area percent values of the peaks between two consecutive (neighboring) *n*-alkanes.

Meanwhile, the remaining de-waxed and de-asphalted residue (maltene) is separated into saturates (essentially naphthenes), polars/resins and aromatics using a packed column filled with silica and alumina.

*Sample results.* Table 21-5 shows the overall component type distributions of three waxy crudes (viz. one light, one intermediate and one heavy) as determined by the above protocols (i.e., Figs. 21-5 and 21-6). As can be seen, crude A has the largest  $\text{C}_{15}-$  fraction; and hence, is the lightest. Crude C is the heaviest sample for it has the lowest  $\text{C}_{15}-$  fraction.

The asphaltene contents of crude A and B determined according to the protocol of Fig. 21-5 are less than or equal to those obtained by UOP asphaltene method. These results suggest that the addition of *n*-pentane to stock tank oils at room temperature will likely cause the heavy *n*-paraffins to crystallize and/or co-precipitate with asphaltenes. In much the same way, the wax contents of the three crudes, determined according to the protocol of Fig. 21-5, are systematically and consistently lower than UOP measured values. This finding also suggests that the UOP wax method does not guarantee proper separation of waxes from asphaltenes.

In the case of heavy crude C, the UOP method yielded a significantly larger wax fraction than the protocol of Fig. 21-6. The UOP asphaltene fraction was also relatively higher than that measured using a hot solvent. The hot solvent insolubles were found to be soluble in toluene; therefore, they are termed asphaltenes. These asphaltenes contained less than 5% paraffins, and hence, the separation protocol was deemed to be adequate.

## EXPERIMENTAL METHODS FOR WAX PRECIPITATION FROM PETROLEUM FLUIDS

Paraffin wax is the major constituent of most solid deposits from crude oils. The detrimental effects of wax precipitation are encountered in all facets of crude oil production, transportation, heat transfer and processing in many of the world's oil-producing regions, especially offshore fields. These problems are expected to increase in the future as existing reserves are being depleted and offshore explorations continue to grow. Due to the relative difficulty and expense associated with operating asphaltic and/or waxy reservoirs, it has become necessary to understand the natures

TABLE 21-5

Wax contents and characteristics of three waxy crudes as determined by UOP and refined analytical protocols

	Crude A (conventional)	Crude B (medium)	Crude C (heavy)
<i>UOP methods</i>			
Wax content (wt%)	5.7	11.7	45.7
Polars + asphaltenes (wt%)	0.0	0.9	n.d. <sup>a</sup>
Asphaltene content (wt%)	0.2	4.4	11.0
<i>Protocol of Fig. 21-9</i>			
C15- fraction	49	33	20
C15+ fraction	51	67	80
Solvent wax (wt%)	3.1	7.6	38.6
<i>n</i> -Pentane asphaltenes (wt%)	0.2	0.1	—
<i>n</i> -paraffins (>C15)	1.0	2.7	—
<i>Iso</i> -paraffins (>C15)	2.1	6.9	—
Naphthenes (>C15)	35.3	28.8	—
Aromatics (>C15)	5.8	19.3	—
Polars/resins (>C15)	3.1	11.2	—
<i>Protocol of Fig. 21-10</i>			
C15- fraction	—	—	20
C15+ fraction	—	—	80
Hot solvent wax (wt%)	—	—	28.0
Hot solvent asphaltenes (wt%)	—	—	8.8
<i>n</i> -paraffins (>C15)	—	—	24.3
<i>Iso</i> -paraffins (>C15)	—	—	3.8
Naphthenes (>C15)	—	—	14.2
Aromatics (>C15)	—	—	17.6
Polars/resins (>C15)	—	—	11.4

<sup>a</sup> Not detected.

of petroleum waxes and the fundamental variables that affect their depositions during production and/or processing [12].

Waxes are essentially mixtures of long-chain hydrocarbons (*n*-paraffins) with carbon chain lengths ranging from C<sub>15</sub>–C<sub>20</sub> to C<sub>75</sub><sup>+</sup> [10,14,15,47]. They are crystalline in nature and tend to crystallize/precipitate from crude oils at and below their melting/dissolution temperatures. Crystallization is the process where an ordered solid structure is produced from a disordered phase, such as a melt or dilute solution (e.g., crude oil). It usually involves two distinct stages, nucleation and growth, which may be considered separately [16,17].

As the temperature of the liquid solution or melt is lowered to its *wax appearance temperature* (WAT), the energy of molecular motion becomes increasingly hindered, and the randomly tangled molecules in the melt tend to move closer together and form clusters of adjacently aligned chains. The paraffin molecules continue to attach and detach to and from these ordered sites until the clusters reach a critical size and become stable. This process is termed nucleation and the clusters are called

nuclei. These nuclei are only stable below the *wax dissolution temperature* (WDT) as they are disrupted by thermal motion above this temperature. Once the nuclei are formed and the temperature is kept at or below the WAT (also known as cloud point temperature), additional molecules are laid down successively on the nucleation sites and become part of the growing lamellar structure. This mechanism is called the growth process.

Nucleation can be either homogeneous, meaning that the sample is pure and the nucleation sites are time dependent, or heterogeneous, which implies that all nucleation sites are activated instantaneously. The latter type is the most common in crude oils where impurities such as asphaltenes, formation fines, clay and corrosion products act as nucleating materials for wax crystals [14].

Although cloud and pour point (crude gelling) temperatures are specific thermodynamic properties for waxy crude oils, their relative positions/boundaries within  $P$ - $T$  diagrams as well as the rate (and amount) of wax deposition and accumulation between them are dependent upon a number of factors which include [18]:

- oil composition;
- temperature/cooling rate;
- pressure;
- paraffin concentration;
- molecular mass of paraffin molecules;
- occurrence of nucleating materials such as asphaltenes, formation fines and corrosion products;
- water-oil ratio;
- shear environment.

In open literature [10,19–24], most of the laboratory measurements of the so-called cloud points are made on stock tank oil (STO) samples. These measurements are sensitive to the thermal history as well as the experimental technique used in the laboratory, such as the standard ASTM D2500-88 or IP 219/82 methods, differential scanning calorimetry (DSC), cross polar microscopy (CPM), light transmittance (LT), viscometry, and cold finger (CF), to name a few. As such, the true definitions depend on the measurement principles of the equipment and techniques/procedures being employed [25]. This chapter provides a review for the most common measurement techniques of wax formation from crude oils.

### *Measurements of cloud/pour point temperatures of dead oils*

#### *ASTM cloud point methods*

There are two standard methods used for the determination of the onset temperature of wax crystallization in STO:

- ASTM D2500 (IP 219) for measuring cloud point of petroleum oils;
- ASTM D3117 for measuring ‘wax appearance point’ of distillate fuels.

Briefly, both methods rely on the visual observation of oil cloudiness at the bottom of a 1½-in.-diameter glass jar. The glass jar is mounted in a larger metal cylinder submerged in a cooling bath. The oil temperature is read under quiescent conditions (i.e., no agitation) using a glass thermometer resting against the bottom of the jar.

In addition to the perceived inaccuracies inherent in the ASTM procedures [22], this method often fails when testing dark crude oils (e.g., black oils).

#### *ASTM pour point method (ASTM D97)*

Similar to cloud point measurements, the ASTM D97 method for pour point temperature determination involves the visual examination of the STO sample during cooling. At each temperature step (3°C/5.4°F decrement), the ASTM sample vial is *poured or tipped* to determine if the oil has any mobility. The pour point temperature is usually identified as the temperature at which the STO gels. The precision of this crude test is reported to be  $\pm 3^\circ\text{C}$ .

#### *WAT using cold finger (CF)*

The CF method for measuring the cloud point temperature of dead oils is another simple (or crude) technique. It involves the submergence of a temperature controlled rod in a gently heated oil sample. Below the WDT, petroleum wax will start to accumulate on the metal rod surface; however, a significant quantity of wax must precipitate before visual determination is possible. Consequently, the CF technique is subjective and usually yields the lowest, or least conservative, estimate of the WAT.

#### *WAT using standard viscometry*

Viscometry enables the detection of a gradual change of rheological properties of an oil as wax precipitates. Fig. 21-7 is a schematic of a conventional parallel plates

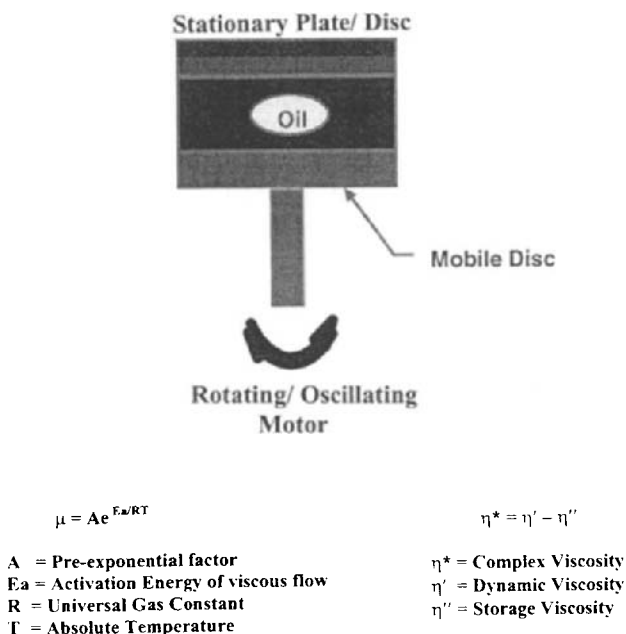


Fig. 21-7. Schematic of the rheometric mechanical spectrometer (RMS) 800.

viscometer. The viscosity of the crude is measured at a fixed temperature by applying a constant shear rate on the oil. At temperatures higher than the onset of wax precipitation, almost all crude oils, with the exception of extremely asphaltene-rich oils, behave like a Newtonian fluid, i.e., the viscosity is a single-valued function of temperature in laminar flow. Mathematically, the variation of the viscosity with temperature within the Newtonian range, is most often adequately described by a simple exponential Arrhenius or Guzman–Andrade type equation:

$$\mu = Ae^{E_a/RT} \quad (21-1)$$

where  $\mu$  is the Newtonian dynamic viscosity,  $E_a$  is the activation energy of viscous flow,  $A$  is a pre-exponential factor largely dependent on the entropy of activation of flow,  $R$  is the universal gas constant, and  $T$  is the absolute temperature.  $A$  and  $E_a$  are usually constant over limited temperature ranges. For temperatures lower than the onset of wax precipitation, the waxy oils behave like non-Newtonian fluid; hence,  $\mu$  must be replaced with the apparent or shear rate dependent viscosity  $\eta$ . The parameters  $A$  and  $E_a$  are also functions of shear stress or rate of shear.

If the crude oil viscosity follows Eq. 21-1, i.e., behaves like Newtonian fluid, for as long as wax does not precipitate, a plot of  $\ln(\mu)$  against  $1/T$  should yield a straight line within such a Newtonian range. As illustrated in Fig. 21-8, the WAT is identified as the temperature corresponding to the break in the curve in the semi-log plot. However, this technique is not recommended because of the following reasons:

- The WAT is usually shear rate dependent.
- At a fixed shear rate, a number of viscosity tests at different temperatures (six total) are required, namely three below and three above the WAT.
- This method can be costly and time consuming without a prior knowledge of the WAT.
- Often, the viscometry data is misinterpreted.
- A more serious problem is the fact that sufficient wax must crystallize before the rheological properties of the crude change enough for a WPT to be detected.
- Not designed for live oil measurements.

#### *Cloud and pour points using complex viscometry*

Complex viscometry tests are completed using a mechanical spectrometer, model 800 (RMS 800). The RMS 800 is a comprehensive rheological instrument. Its operation consists of applying a dynamic shear on a liquid (or liquid–solid) specimen, at a controlled frequency and strain, and then measuring the resulting torque generated by the fluid's resistance to this motion. The torque is then interpreted in terms of fluid viscosity. In all cases, dynamic shear is created by a pair of parallel disks, 50 mm in diameter, in which one is driven at a known frequency and the other is responsive to the stress in the liquid contained between the two plates (see Fig. 21-7).

For each trial, a sample of fluid is charged on the disk at 60°C/140°F; the thickness of the sample is maintained between 1.0 and 1.2 mm. To initiate a run, the sample is cooled by enclosing the disks within a cooling jacket and the complex viscosity ( $\eta^*$ ) is recorded as a function of temperature. A small frequency (1 rad/sec) and strain are used in all cases to ensure that any developing structure is not disturbed. The complex



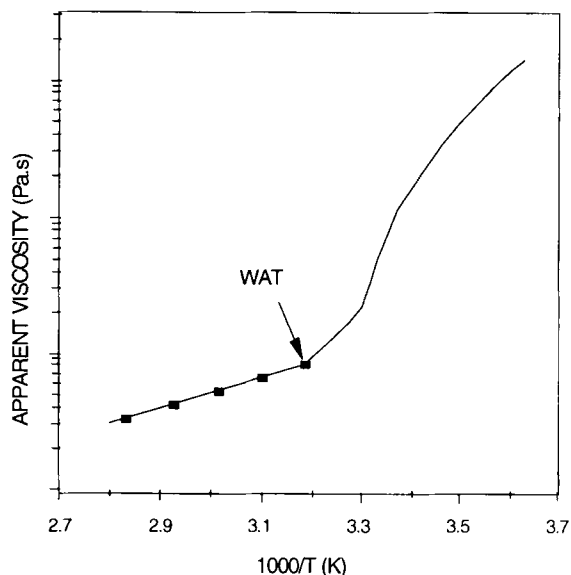


Fig. 21-8. Identification of cloud point temperature by conventional viscometry.

viscosity,  $\eta^*$ , is defined as:

$$\eta^* = \eta' - i\eta'' \quad (21-2)$$

where  $i$  is a complex number and  $\eta'$  and  $\eta''$  represent the dynamic viscosity and elastic or storage viscosity, respectively. From complex viscosity measurements, it is possible to determine dead oil pour points accurately as well as cloud points depending on the overall wax content of the source crude [26]. An example of a complex viscosity plot is given in Fig. 21-9 where the WAT is identified as the break in the plot of  $\log(\eta')$  vs. temperature. A typical plot of complex viscosity against temperature for pour point determination of STO is provided elsewhere [27]. The main disadvantages of this technique are:

- Often, the identification of the WAT is subjective (see Fig. 21-9).
- A sufficient wax must crystallize before the rheological properties of the crude change enough for a WPT to be detected by complex viscometry.
- Not designed for live oil measurements.

#### WAT using differential scanning calorimeter (DSC)

The measurement principle of *differential scanning calorimetry* (DSC) is based on the measurement of the difference in the heat flows to the sample crucible and reference crucible (see Fig. 21-10). These heat flows are directly proportional to the temperature difference between the furnace and crucible, but inversely proportional to the thermal resistance of the system.

The DSC has been widely used for the determination of wax appearance and/or dissolution temperatures (WAT or WDT) in petroleum products [24]. The method is based on the detection of the latent heat of fusion released during crystallization, giving

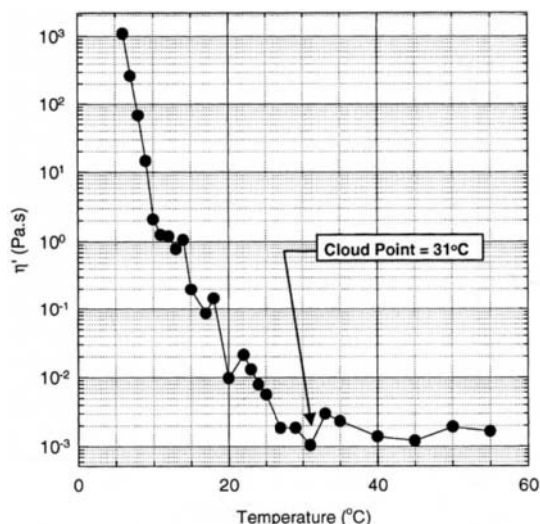


Fig. 21-9. Identification of cloud point temperature by complex viscometry.

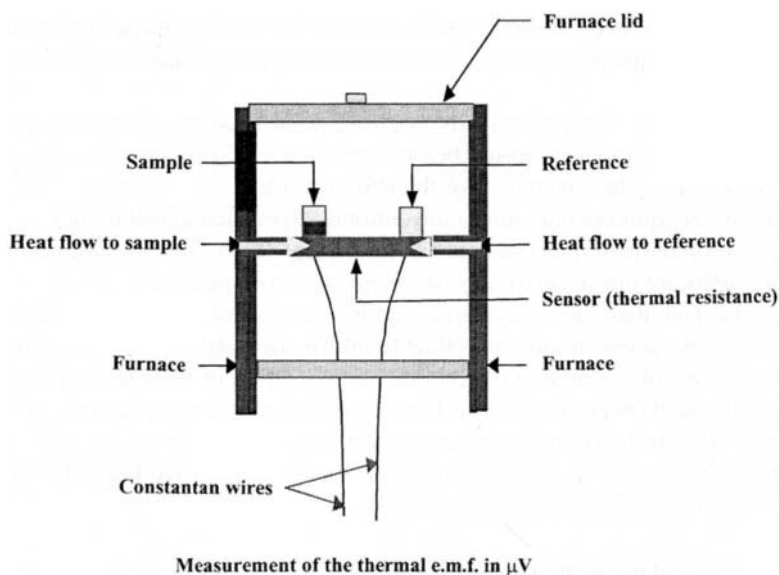


Fig. 21-10. Schematic representation of the DSC measuring cell.

rise to an exothermic peak on cooling. While this exothermic peak provides information on the wax content of the sample, it is sometimes difficult to establish the onset of the heat flow shift in fluids with low wax contents. Fig. 21-11 shows a typical cooling DSC thermogram for a waxy crude oil. The main disadvantages of the DSC are:

- A source of uncertainty in the determination if either WAT or WDT is the baseline

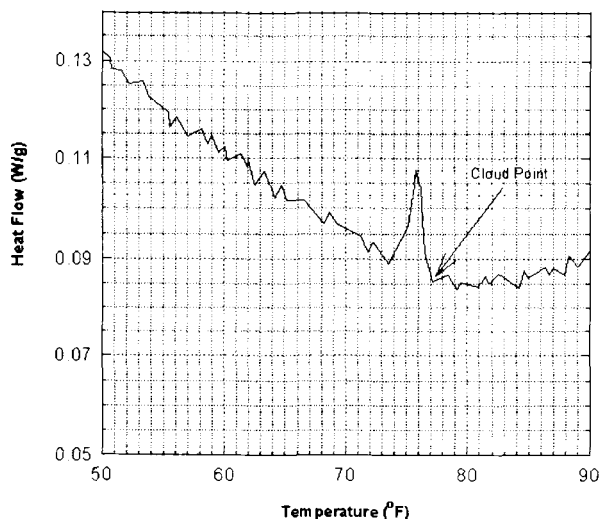


Fig. 21-11. DSC crystallization trace for a light waxy crude oil.

determination. The decision as to where to draw the baseline in the high temperature region, and consequently to establish the exact onset temperature is sometimes highly subjective;

- For extremely low wax content oils, a cloud point may go completely undetected (i.e., no crystallization peak would be observed in the DSC trace).

On the other hand, the advantages of the DSC include.

- Being relatively quicker than most conventional experimental techniques.
- Needs very small quantities (i.e., only a few milligrams) of testing sample.
- Measurements are not sensitive to system operation or operator.
- Despite the fact that thermodynamic equilibrium is not usually established, DSC provides a tremendous amount of valuable information about phase transitions of the samples and enables a relatively accurate quantification of their related energies and physico-chemical properties such as heat capacities and heats of fusion.
- Can be used to study live oils (high pressure DSC cells available).
- Can characterize the wax fraction and components which have been shown recently to correlate well with a GC analysis [19,23].

#### *WAT using cross polarized microscopy (CPM)*

As shown in Fig. 21-12, the CPM consists of a light source, an IR-filter, a polarizer, a temperature controlled (programmable) hot stage, an analyzer, a video camera, a VCR, a video monitor and a PC. The hot stage is mounted on the stage of the microscope and connected to a liquid nitrogen tank to control the rate of cooling of the STO sample. Therefore, the CPM allows for visual determination of the WAT (or cloud point) as well as providing a record of the crystal growth and morphology. Typically, crystal sizes in the order of 1  $\mu\text{m}$  are detectable at the WAT.

The use of CPM for the study of wax crystallization is based on the fact that

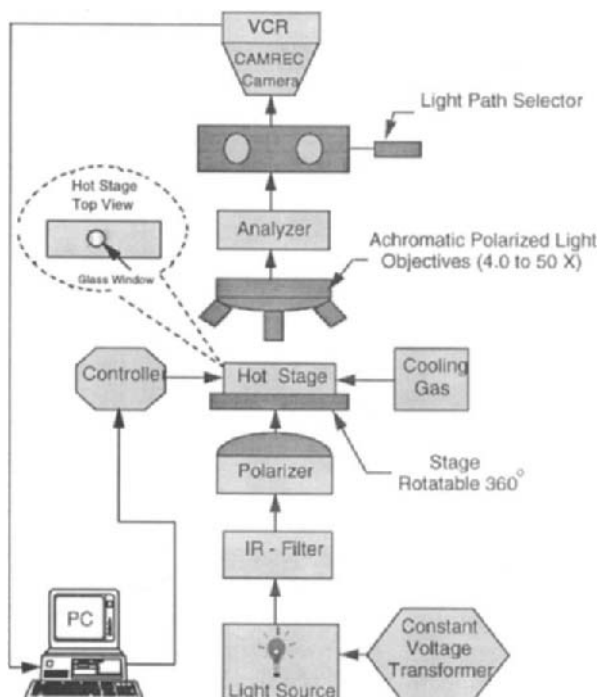


Fig. 21-12. Schematic of cross polarized microscope.

all crystalline materials rotate the plane of polarization of transmitted polarized light. Hence, by crossing two prisms on opposite sides of the oil sample, all light is initially blocked and the entire field of view appears black. On cooling, the crystallizing material appears as bright spots against this black background. This technique usually provides the most conservative (or highest) value of the crude oil cloud point temperature [20,23–25].

The measurement procedure involves preheating the STO in a water bath to 60°C/140°F for 30 min so as to melt the waxes and homogenize the sample. Next, the corresponding sample container is hand-rocked prior to transferring one drop of the oil to a special glass slide and covering it with a cover slip. The glass slide containing the oil sample is inserted in the CPM hot stage and the field of view is brought into focus. The temperature of the programmable hot stage is then increased at a constant rate of 1°C/min from ambient temperature to 10°C above the WDT. The WDT is defined as the temperature at which the last trace of wax disappears from the field of view upon heating. Next, the sample is allowed to equilibrate at the maximum temperature (i.e., 10°C above WDT) for two minutes. Finally, the sample is cooled at 1°C/min from the equilibration temperature to 0°C. The entire run is videotaped simultaneously. The corresponding WAT is identified (off-line) as the temperature at which the first detectable bright spots (i.e., wax crystal size in the order of 1  $\mu\text{m}$ ) emerge in the view of a black field (see Fig. 21-13).

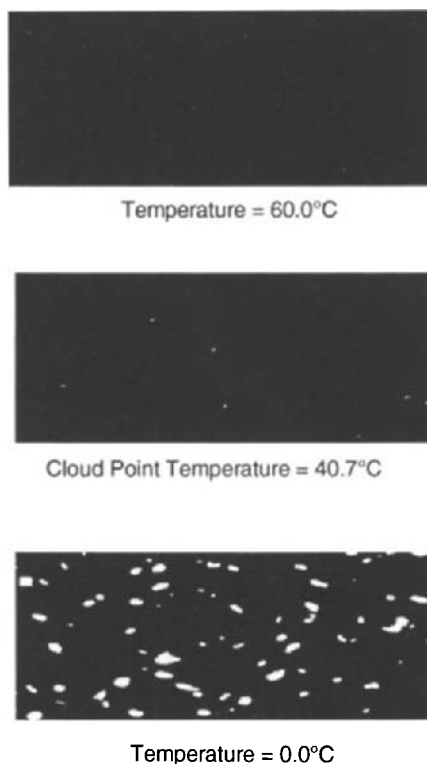


Fig. 21-13. CPM photomicrographs of a waxy STO taken at different temperatures (cooling rate =  $1^{\circ}\text{C}/\text{min}$ ).

The greatest advantage in the use of CPM is the ability to visually detect and establish the presence of very small ( $\approx 1\text{ }\mu\text{m}$  in size) wax crystals (i.e., at the nucleation stage). It has been established that CPM is the most sensitive of the available techniques for the measurement of wax crystallization temperatures for dead oils [20,23,25].

#### *Cold filter*

This measurement technique is based on the movement of dead (or live) oils through a temperature controlled flow-loop (Hsu and Brubaker [28], personal communication). As the system temperature is reduced below the WDT of the waxy crude, crystallized paraffins collect in a filter causing an increased pressure drop across its width. This procedure seems more practically founded than those presented previously in that a flowing situation is more representative of true field conditions. However, somewhat extensive experimentation (evaluation of filters, temperature control, pressure transducers, verification of wax precipitation and collection only at filter and not in lines, etc.) may be required to perfect this procedure.

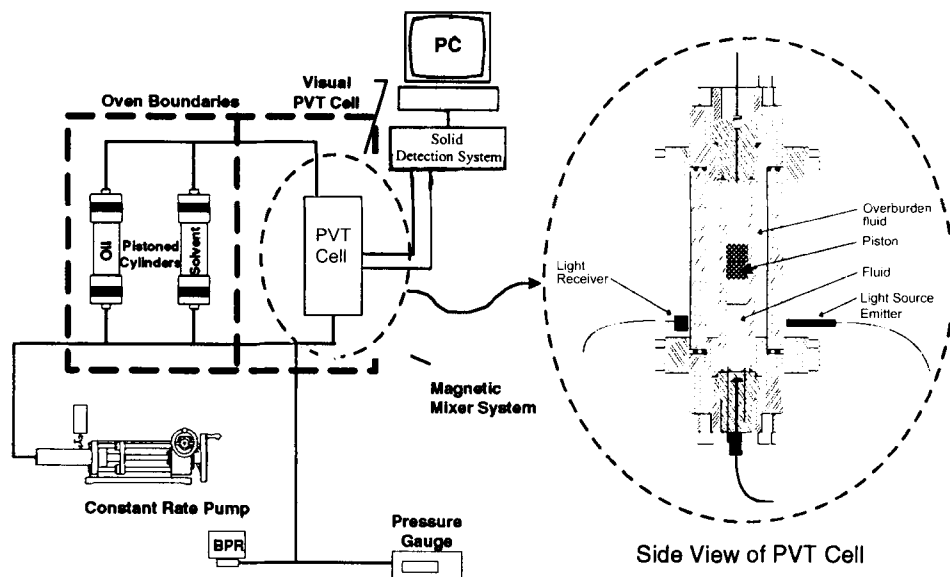


Fig. 21-14. Schematic of the solids detection system.

### *Measurements of cloud/pour point temperatures of live oils*

Wax precipitation during petroleum production and/or processing, e.g., in well tubings, flowlines and/or process equipment, normally proceeds under elevated temperature and pressure conditions. Therefore, the effects of pressure, temperature and composition on live oil wax formation are critical. It has been established that the presence of light ends in crude oils tends to depress the WAT [29,30]; therefore, dead oil cloud points are usually observed to be higher than those measured for the corresponding live oils. It is conceivable that the following high pressure techniques allow for dead oil cloud point measurements as well.

### *WAT using light transmittance*

The schematic of a light transmittance technique is shown in Fig. 21-14 [18]. The apparatus consists of two divisions, source components and detector components. Source components include a power source, a fiber bundle encased in a protective steel sheath, and a collimating lens that distributes the laser into a beam of exacting dimensions. Detection components consist of a collimator that focuses the transmitted beam onto a receiver fiber bundle (again sheathed in steel) and a light power meter.

The source and detector components are mounted on a high temperature, high pressure visual PVT cell. The main body of the cell consists of a pistoned glass cylinder eight inches long with an internal diameter of 1.25 inches. The effective working volume of the tube is approximately  $130 \text{ cm}^3$ . The glass cylinder is housed inside a steel shell with vertical tempered glass plates to permit visual observation of the internal tube and its contents. The volume and pressure of the fluid under investigation are controlled by a

variable volume displacement pump. The same displacement fluid is connected to the outer steel shell to maintain a balanced differential pressure on the cylinder. Equilibration of the fluid under investigation is achieved by means of a specially designed magnetically coupled impeller mixer. The entire PVT cell is mounted inside a temperature controlled oven. The cell temperature is measured with a platinum RTD. The temperature is read and controlled on a digital temperature indicator/controller and is accurate to within  $\pm 0.2^\circ\text{F}$ . Pressure is measured with a calibrated digital Heise pressure gauge.

A specially designed end cap mounted in the bottom of the cell allows for the charging and sampling of the reservoir fluid. The maximum operating pressure and temperature for the SDS are 15,000 psi and  $360^\circ\text{F}$ , respectively. The entire system is controlled by a proprietary software package that accomplishes two significant objectives. First of all, a computerized pump is used to maintain the system pressure and to inject solvents/chemicals for wax remediation studies. Secondly, the software (in real time) records and presents the system temperature, pressure, solvent volume, time and most importantly, the power of transmitted light (PTL) from the detector.

The experimental procedure for the measurement of WAT using the apparatus shown in Fig. 21-14 is relatively straightforward. A sample of the live oil (or live oil + solvent mixture) is isobarically charged into the PVT cell at reservoir temperature. After an initial equilibration period, the system is cooled, at approximately  $1^\circ\text{F}$  per minute, down to  $0^\circ\text{C}/32^\circ\text{F}$  while recording the PTL signal. The temperature at which the PTL signal begins to markedly drop to noise level is interpreted as being the live fluid WAT (see Fig. 21-15). This technique is suitable for detecting wax as well as asphaltene onsets of

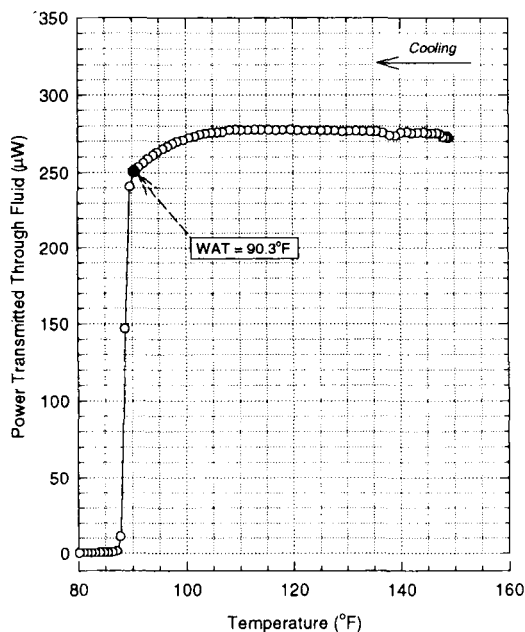


Fig. 21-15. WAT of live crude oil at 469 psia [18].

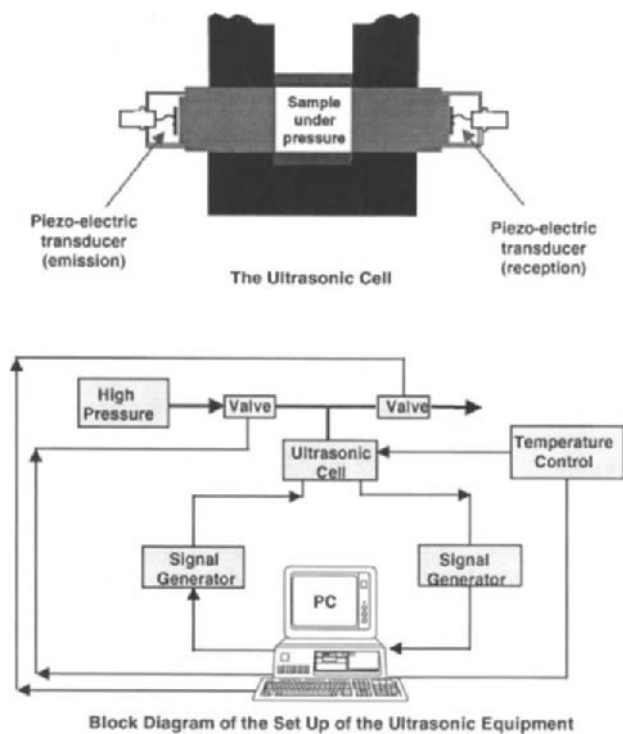


Fig. 21-16. Schematic of the ultrasound apparatus for measuring cloud points [29].

precipitation from both dead and live crude oils concurrently with the measurement of fluid property data (i.e., vapor–liquid equilibrium data).

#### *WAT using ultrasonics*

The ultrasonic test system consists of a signal generator, which delivers short electrical bursts to a transmitting transducer, and a digital oscilloscope, which converts the signal received at a second transducer into numeric data [29,31]. A schematic of the ultrasonic cell is shown in Fig. 21-16. The measurement principle of the ultrasonic system is based on the following considerations:

The velocity of an ultrasonic wave through a medium depends on the density and elasticity of the medium. Therefore, a noticeable variation of the ultrasonic velocity (change in slope of the transit time versus temperature) is expected to occur at the WAT (i.e., the emergence of the solid phase) during a cooling experiment of a crude oil sample, see Fig. 21-17. In addition, specific phenomena leading to a strong attenuation of ultrasonic waves are known to occur in two-phase media. The main dissipation mechanism is due to heat exchange between the liquid and solid phases which are not subjected to the sample cyclic variation of temperature-induced acoustic pressure. This phenomenon depends strongly on the acoustic frequency and on the shape and dimension of the solid particles. Fig. 21-17 shows a typical plot of the variation of the



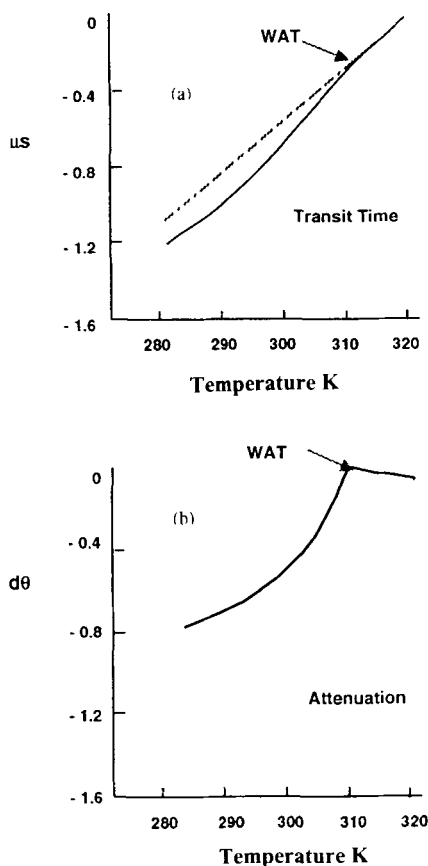


Fig. 21-17. Variation of the transit time and amplitude during cooling [29].

amplitude of the ultrasonic signal with temperature. The WAT is identified as the brake in the curve which corresponds to the start of the attenuation.

At this time and aside from the relatively large volume ( $>70 \text{ cm}^3$ ) of sample crude required for cloud point measurement using the ultrasonic cell, little is known about the limitations of this technique. In principle, however, this technique is suitable for detecting wax as well as asphaltene onsets of precipitation from both dead and live crude oils.

#### *Bulk deposition measurements*

Since the previous live oil methods do not provide accurate data on the actual quantities of solid formation, the use of a bulk deposition apparatus is rather vital. A schematic is shown in Fig. 21-18 [32]. This technique operates over a similar range of temperatures and pressures as the onset apparatus and facilitates the isolation of a wax sample for qualitative and quantitative analysis.

Briefly, the apparatus consists of two stainless steel high-pressure cylinders (1 liter capacity) equipped with floating pistons. The cylinders are suitably connected to each

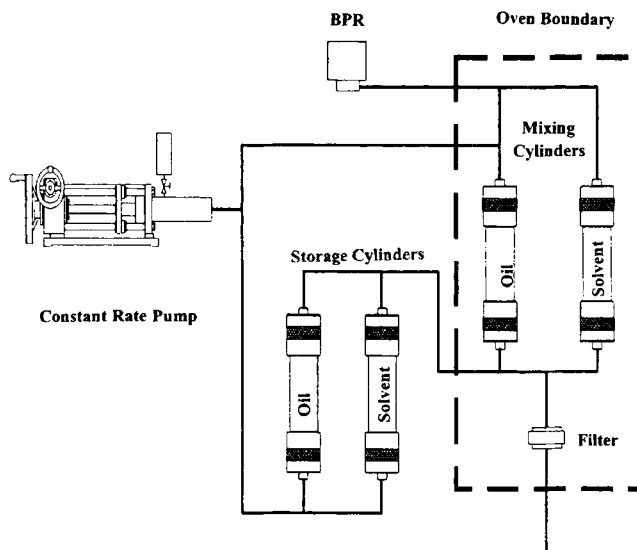


Fig. 21-18. Schematic of the bulk solid deposition apparatus.

other and a Millipore filter is placed in-line such that the contents of both cylinders can be displaced through it. A mineral oil hydraulic fluid and a motorized high-pressure displacement pump is used to displace the cell contents from one cell to the other for mixing and through the filter for separation and analysis. The entire apparatus (excluding the displacement pump) is enclosed in a constant temperature controlled air-bath.

Typically, a live oil (or even dead oil) is charged to one of the high-pressure cells, where it is initially equilibrated at the specified thermodynamic conditions. The system temperature, pressure or composition is then altered to the specified final value at which time both the crude oil and precipitated solids are ejected from the cylinder. These solids are collected in a high-pressure filter where they are separated from the rest of the sample for further analysis as described in the previous section.

Obviously, this technique is laborious and time consuming; therefore, expensive. The main advantage of this procedure is the detailed characterization data that becomes available from the analysis of the precipitated solids. Combined with a detailed PNA characterization of the source crude oil [12], comprehensive thermodynamic and kinetic models describing the precipitation become possible [13].

#### *Standardized measurement techniques: WAT under flow conditions*

Crude oils below their melting point display complex rheology, and at least eight parameters affecting their flow behavior have been identified [33]. Of these, the most important variables are the thermal history (i.e., the initial pre-treatment temperature and the cooling/heating rate) and the shear rate [28,34]. Many standardized measurement equipments have been designed to duplicate downhole, production and pipeline shear, pressure and temperature histories in order to obtain representative rheological field data. Typical pipeline apparatus is described elsewhere [28].

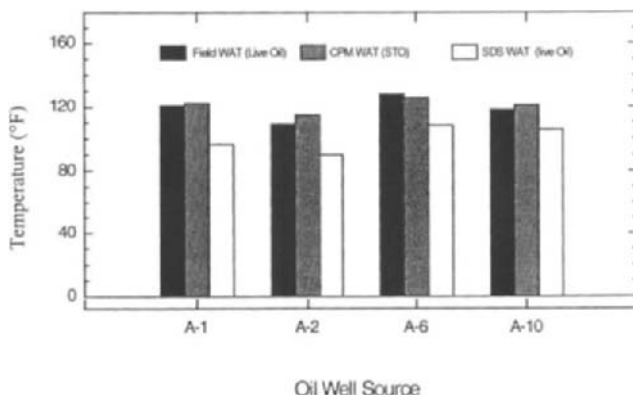


Fig. 21-19. Comparison of laboratory results to field data [18].

### *Comparisons of laboratory paraffin wax deposition data with observed field results*

The onsets of paraffin wax deposition temperatures as measured by cross polar microscopy (CPM) and light transmittance for the various samples are plotted in Fig. 21-18. The corresponding field wax deposition temperatures were surveyed from wells producing at relatively low flow rates (practically in the laminar regime). These results are also plotted in Fig. 21-18 for comparison. Based on the findings of Erickson et al. [20], Fig. 21-19 provides yet more proof that CPM results agree fairly well with surveyed field wax deposition data.

The fact that CPM onsets of wax crystallization temperatures of the dead oils match the field wax deposition temperatures of these same live oils is plausible for wells operating in laminar flow regimes. The general consensus is that shear environment can either delay or induce wax deposition depending on the regime (i.e., turbulent vs. laminar) of flow and/or agitation. In high shear environments (i.e., turbulent regime), the ability of wax constituents to congeal and reach a pour point or to plug a tube is diminished as the nucleation process is disrupted [28], whereas, in a low shear environment (i.e., laminar regime and/or closer to equilibrium/static condition), the flexible paraffinic molecules tend to be aligned adjacent to one another in the direction of flow and, thus, inducing/speeding the nucleation/clustering process [18]. Hence, the severity of flowline plugging is usually observed to diminish in high-shear environments. This effect can counteract and/or negate that of the light ends, which tend to depress the onset of wax crystallization temperature.

From this section, one can conclude that the increasing frequency of solid deposition problems in oilfield operations has led to various developments of experimental techniques for the measurement of WAT. For dead oils, it has been established that cross polar microscopy (CPM) yields the most conservative measurements of the so-called cloud points and with certain modifications, may provide for live oil WAT. In terms of live oil measurements, the SDS seems to offer reasonable solid formation data.

Lastly, it is emphasized that the reproducibility of laboratory results is contingent upon a number of factors including experimental procedure, thermal history/homogeneity of the tested sample, and the experience of the interpreter/engineer. In order to reduce (as much as possible) the extent of and/or eliminate the subjectivity from the final results, it is important that a systematic and/or a standardized methodology be implemented in identifying the onset of wax crystallization for a given technique.

## REVIEW OF METHODS TO MODEL WAX PRECIPITATION IN PETROLEUM FLUIDS

Efficient design of oil production processes requires an adequate prediction of the thermodynamic conditions in which wax can precipitate from crude oil as a function of pressure, temperature and petroleum composition. To date, various thermodynamic models that employ activity coefficients ( $\gamma_i$ ) and/or equations of state (EOS) have been proposed in the literature. These models have been applied to the calculation of the solubility of heavy hydrocarbons in both synthetic and real petroleum fluids at low and high pressures. The proposed models are distinguishable in the way that the equilibrium relationships for the precipitated solid phase are formulated. A common parameter in these models is the evaluation of the solid-phase component fugacities,  $f_{is}$ , whose treatment differs from one application to another.

There are some factors that have hampered the development and application of rigorous theories for thermodynamic prediction of wax equilibria in a wide range of conditions. For instance, current analytical restrictions in the characterization of the heavy fraction of crude oils as well as the unavailability of vapor–liquid–solid (VLS) equilibrium data in wide pressure and temperature intervals are some of the limitations. While recent experimental techniques for measuring the onset of wax crystallization using spectrometry and microscopy are now available, it has not yet been possible to develop a purely predictive computational tool for the thermodynamic prediction of oil–wax equilibria with a more direct application in the design and optimization of the reservoir/oilwell/production facilities system.

The main purpose of this section is to provide a review of the thermodynamic models for wax precipitation proposed in the literature. First, the thermodynamic basis of liquid–wax equilibria in multicomponent mixtures is presented. The form of the various models proposed in the literature is derived and discussed. The features and performance of the most representative ideal-solution theory based models, the activity-coefficient based models, and models that employ equations of state are presented.

Lastly, the features of an EOS-based vapor–liquid–multisolid wax thermodynamic model, which considers that the precipitated wax is composed of a number of pure solid phases, is presented. Application of this model to petroleum fluids at low and high pressures is illustrated. By no means is this review intended to provide the details on the development of each of the models discussed. Instead, it provides a comprehensive description of the characteristics and performance of the most representative models proposed so far. The main trends of research in this area are also presented.

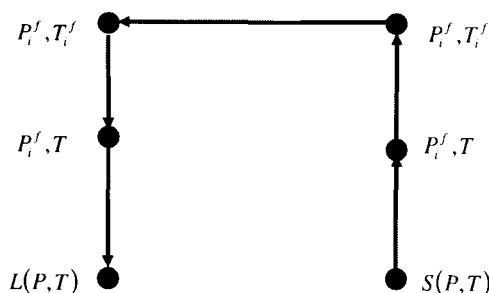


Fig. 21-20. Thermodynamic path used to obtain the Gibbs free energy of transition at the melting point.

### Thermodynamic basis of oil–wax equilibria

A brief description of the thermodynamic principles of oil–wax equilibria in multi-component mixtures is presented in this section.

The precipitation of wax in petroleum is a reversible crystallization process [35]. This process can be described in terms of the Gibbs free energy change between the liquid and solid phases in equilibrium,  $\Delta\mu_i$ . Fig. 21-20 shows a thermodynamic path to obtain the Gibbs free energy of transition between the liquid and solid phases for a pure component  $i$  at temperature  $T$  and pressure  $P$ .

Let us assume that  $\mu_{\text{pure } i}^S(P, T)$  represents the pure-component chemical potential of the solid phase at pressure  $P$  and temperature  $T$ , and that  $\mu_{\text{pure } i}^L(P, T)$  represents the pure-component chemical potential of the liquid phase at the same conditions. The change  $\Delta\mu_{\text{pure } i} = \mu_{\text{pure } i}^L(P, T) - \mu_{\text{pure } i}^S(P, T)$  can be obtained from the expression:

$$\Delta\mu_i = \Delta h_i - T \Delta s_i \quad (21-3)$$

in which  $\Delta h_i$  and  $\Delta s_i$  are the transition enthalpy and entropy of component  $i$ , respectively. These properties are defined by means of the expression:

$$\begin{aligned} \Delta h_i = & \int_T^{T_i^f} C p_i^S dT + \Delta h_i^f + \int_{T_i^f}^T C p_i^L dT \\ & + \int_P^{P_i^f} \Delta v_i dP - T \int_P^{P_i^f} \frac{\partial}{\partial T} (\Delta v_i)_P dP \end{aligned} \quad (21-4)$$

If negligible temperature effects on the pure component heat capacities,  $C p_i$ , are considered, we obtain:

$$\Delta h_i = \Delta h_i^f + \Delta C p_i (T - T_i^f) + \int_P^{P_i^f} \Delta v_i dP - T \int_P^{P_i^f} \frac{\partial}{\partial T} (\Delta v_i)_P dP \quad (21-5)$$

where  $\Delta C p_i = C p_{\text{pure } i}^L - C p_{\text{pure } i}^S$  the heat capacity of transition, and  $\Delta v_i = v_{\text{pure } i}^L - v_{\text{pure } i}^S$ .

Similarly, for the melting entropy:

$$\Delta s_i = \frac{\Delta h_i^f}{T_i^f} + \Delta C p_i \ln \frac{T}{T_i^f} - \int_P^{P_i^f} \frac{\partial}{\partial T} (\Delta v_i)_P dP \quad (21-6)$$

Combining Eqs. 21-3–6, one obtains:

$$\frac{\mu_i^L(P, T) - \mu_i^S(P, T)}{RT} = \frac{\Delta h_i^f}{RT_i^f} \left[ \frac{T_i^f}{T} - 1 \right] - \frac{\Delta C p_i}{R} \left[ \frac{T_i^f}{T} - 1 \right] + \frac{\Delta C p_i}{R} \ln \frac{T_i^f}{T} + \int_{P_i^f}^P \Delta v_i dP \quad (21-7)$$

At equilibrium of the liquid and solid solutions, for every component  $i$ :

$$\mu_i^L(P, T, \underline{x}^L) = \mu_i^S(P, T, \underline{x}^S) \quad (21-8)$$

where  $\underline{x}$  is the composition (mole fraction) vector.

By expressing Eq. 21-8 in terms of fugacities, one obtains:

$$\ln \left( \frac{f_i^S f_{\text{pure } i}^L}{f_i^L f_{\text{pure } i}^S} \right) = \left( \frac{\mu_i^L - \mu_i^S}{RT} \right)_{\text{pure } i} \quad (21-9)$$

Eq. 21-9 is the starting point to derive expressions to calculate liquid–solid equilibrium by imposing different assumptions in the calculation of  $f_i^L$  and  $f_i^S$ , the fugacities of component  $i$  in the liquid and solid solutions. For instance, by expressing  $f_i^S$  and  $f_i^L$  in Eq. 21-9 by means of the expressions [36]:

$$f_i^S = \gamma_i^S x_i^S f_{\text{pure } i}^S \int_0^P \frac{v_i}{RT} dP, \quad f_i^L = \gamma_i^L x_i^L f_{\text{pure } i}^L \exp \int_0^P \frac{v_i^L}{RT} dP \quad (21-10)$$

Eq. 21-9 turns out to be:

$$\frac{x_i^L}{x_i^S} = \frac{\gamma_i^L}{\gamma_i^S} \exp \left[ -\frac{\Delta h_i^f}{RT_i^f} \left( \frac{T_i^f}{T} - 1 \right) + \frac{\Delta C p_i}{R} \left( \frac{T_i^f}{T} - 1 \right) - \frac{\Delta C p_i}{R} \ln \frac{T_i^f}{T} - \int_{P_i^f}^P \frac{\Delta v_i}{RT} dP \right]_{\text{pure } i} \quad (21-11)$$

Eq. 21-11 relates the composition of component  $i$  in the solid phase with respect to its composition in the liquid phase by means of purely caloric and volumetric properties, as well as by the use of liquid and solid-phase activity coefficients.

Reddy [37] used Eq. 21-11 as a starting point and considered the second, third and fourth terms of the exponential argument in Eq. 21-11 to be negligible. He also assumed that the non-idealities of the liquid and solid solutions were marginal, i.e., the ratio of activity coefficients  $\gamma_i^S/\gamma_i^L$  in Eq. 21-11 is equal to 1. These assumptions allowed him to express the mole fraction of a heavy component  $i$  in the liquid phase by means of:

$$x_i^L = \exp \left[ \frac{\Delta h_i^f}{T} \left( \frac{1}{T_i^f} - \frac{1}{T} \right) \right] \quad \text{or} \quad \ln x_i^L = \left[ \frac{\Delta h_i^f}{R} \left( \frac{1}{T_i^f} - \frac{1}{T} \right) \right] \quad (21-12)$$

where, to further simplify the picture, Reddy assumed that the composition of component  $i$  in the solid phase is 1 (i.e.,  $x_i^S = 1$ ). Eq. 21-12 is best known as the equation of *ideal solubility*.

In his method, Reddy introduced the concept of ‘solubility-equivalent-to-a-paraffin of reference’, in which the distribution of ‘soluble-equivalent’ components is expressed

TABLE 21-6  
Predicted and experimentally measured cloud points of test fuels [37]

Fuel	Cloud point (°C)	
	Predicted	Measured
SNA	-7.8	-9.0
SNB	-1.0	-2.0
SNC	0.5	0.0
PA	11.4	11.0
PB	-3.0	-3.0
PC	-3.4	-5.0
PD	-3.5	-5.0
PE	-3.2	-7.0
PF	-8.3	-10.0
PG	-12.8	-12.0
PH	-11.8	-12.0

in terms of a key paraffinic component, whose solubility behavior is known in advance. Reddy used Eq. 21-12 for a binary paraffin-equivalent/solvent system, and determined the cloud point temperature and amounts of precipitated wax at atmospheric pressure.

Table 21-6 shows a comparison of the experimental cloud points and those calculated by Reddy for various diesel fuels. Close agreement with the experimental values is observed. Fig. 21-21 shows the results obtained in the calculation of wax amounts for one of the diesel fuels shown in Table 21-6. For wax amounts, an overprediction, up to

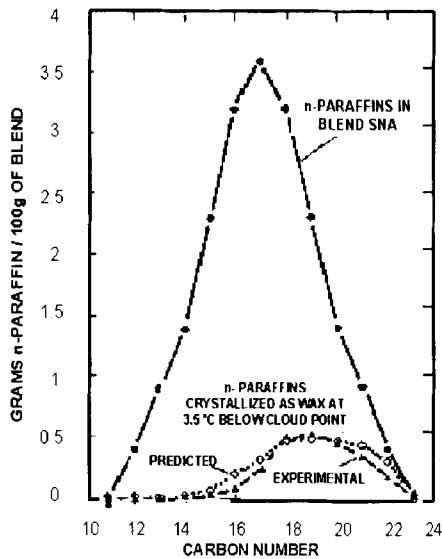


Fig. 21-21. Experimental and calculated wax amounts for a diesel fuel at -11.3°C and 1 bar [37].

around 100% for all components whose carbon-atom numbers are far from that of the 'base-paraffin', is observed.

Reddy's method requires one solubility datum of a single hydrocarbon constituent of the precipitated wax (in the case of Reddy, wax deposits were referred to *n*-eicosane,  $nC_{20}$ ). The method seems to provide reasonable results of paraffin deposition for petroleum fractions with a well-defined component distribution (i.e., diesel fuels, petroleum naphthas, etc.). For petroleum reservoir fluids, however, the large and diverse chemical nature of the constituents of the crude may preclude a direct and practical application of this method. The method does not consider the effect of pressure in the solubility of heavy hydrocarbon species and, thus, its application to live-oil and light petroleum fluids seems to be limited.

Weingarten and Euchner [38], reported the application of Eq. 21-12 to monitor wax precipitation in reservoir fluids. These authors wrote Eq. 21-12 in the following form:

$$\ln \Gamma_w = \ln n - \ln \Gamma_l = \frac{\Delta h_f}{R} \left( \frac{1}{T_f} - \frac{1}{T} \right) \quad (21-13)$$

where  $\Gamma_l$  is the number of moles of liquid remaining after liberation of gas from one mole of reservoir fluid, and  $n$  is the number of moles of the wax in one mole of deposit.

Solving Eq. 21-13 for temperature  $T$ , the authors rewrote Eq. 21-13 as:

$$T = \ln n - \frac{A_i}{B_i + \ln \Gamma_l} \quad (21-14)$$

where  $A_1 = \Delta h_f$ , the heat of fusion of the wax, and  $B_1 = \frac{\Delta h_f}{T_f} - \ln n$ . The constants  $A_1$  and  $B_1$  in these equations were obtained from cloud point data of the oil under investigation. Fig. 21-22 shows the results for a typical crude oil.

Industrial applications of Eq. 21-12 have also been reported by Frezzotti et al. [39] in the study of the solubility of  $\epsilon$ -caprolactama and its oligomers, with only qualitative agreement.

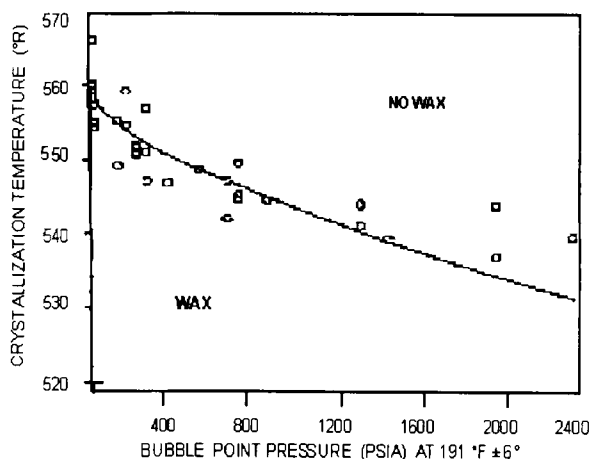


Fig. 21-22. Variation of cloud point temperature with saturation pressure using the ideal solution (Eq. 21-13) [38].



Although Eq. 21-12 constitutes one simple method to analyze the equilibrium solubility in model systems and binary mixtures, its extrapolation to petroleum and other polydisperse fluid systems is only limited to qualitative results. Furthermore, it is no longer possible to implicitly include the effects of pressure and composition in the calculations. As in the methods of Reddy [37] and that of Weingarten and Euchner [38], the approaches based on ideal-solubility, while simple, require special modifications, and do not offer theoretical foundation.

Won [40], in order to consider the effects of pressure and composition, applied Eq. 21-12 by including the calculation of activity coefficients for the solid and the liquid phase. In this way, Won wrote Eq. 21-12 as:

$$\frac{x_i^S}{x_i^L} = K_i^{sl} = \frac{\gamma_i^L(T, \underline{x}^L)}{\gamma_i^S(T, \underline{x}^S)} \exp \left[ -\frac{\Delta h_i^f}{RT} \left( 1 - \frac{T}{T_i^f} \right) \right] \quad (21-15)$$

where both the effects of the heat capacities and volume expansion at the melting point were neglected. Won used a modified form of the regular solution theory of Scatchard [52] and Hildebrand [53] to calculate the activity coefficients, i.e.:

$$\ln \gamma_i = \frac{v_i(\bar{\delta} - \delta_i)^2}{RT} \quad (21-16)$$

in which  $\bar{\delta}$  and  $\delta_i$  are the solubility parameters of the mixture and pure component  $i$ , and  $v_i$  is the molar volume of the component. Won developed correlations to estimate the values of  $T_i^f$ ,  $\Delta h_i^f$ , and  $v_i$  using the molecular weight of the particular hydrocarbon as an independent variable. Using the activity coefficients,  $\gamma_i^S$  and  $\gamma_i^L$ , the expression for  $K_i^{SL}$  transformed to:

$$K_i^{SL} = \frac{x_i^S}{x_i^L} = \frac{\gamma_i^L}{\gamma_i^S} \exp \left[ \frac{\Delta h_i^f}{RT} \left( 1 - \frac{T}{T_i^f} \right) + \frac{v_i}{RT} \left[ (\bar{\delta} - \delta_i)_l^2 - (\bar{\delta} - \delta_i)_s^2 \right] \right] \quad (21-17)$$

On the other hand, Won used an EOS (Soave [54]) to calculate the vapor-liquid equilibrium. The liquid-vapor  $K$ -value was calculated in the usual way:

$$K_i^{VL} = \frac{y_i}{x_i} = \frac{\hat{\phi}_i^L}{\hat{\phi}_i^V} \quad (21-18)$$

where  $\hat{\phi}_i^V$  and  $\hat{\phi}_i^L$  are the fugacity coefficients of the vapor and liquid phase for the component  $i$ , respectively, and  $x_i$  and  $y_i$  are the compositions of the component in the liquid and vapor phases, respectively.

The *flash* equations for the multicomponent, vapor-liquid-solid-equilibrium calculation were written by Won as:

$$g_1 \left( \frac{V}{F}, \frac{S}{F} \right) = \sum_{i=1}^n \frac{z_i (K_i^{VL} - 1)}{1 + \frac{V}{F} (K_i^{VL} - 1) + \frac{S}{F} (K_i^{SL} - 1)} = 0 \quad (21-19)$$

$$g_2 \left( \frac{V}{F}, \frac{S}{F} \right) = \sum_{i=1}^n \frac{z_i (K_i^{SL} - 1)}{1 + \frac{V}{F} (K_i^{VL} - 1) + \frac{S}{F} (K_i^{SL} - 1)} = 0$$

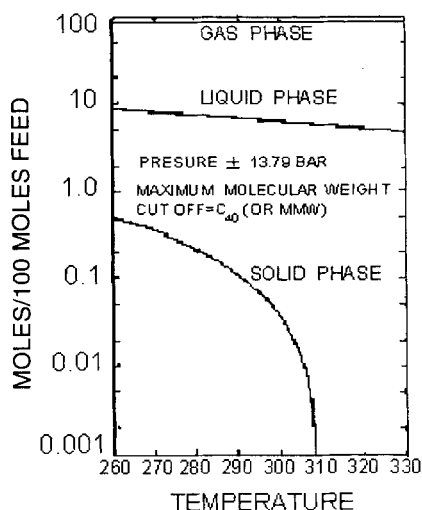


Fig. 21-23. Effect of temperature on wax precipitation for a synthetic 41-component mixture at 13.8 bar [40].

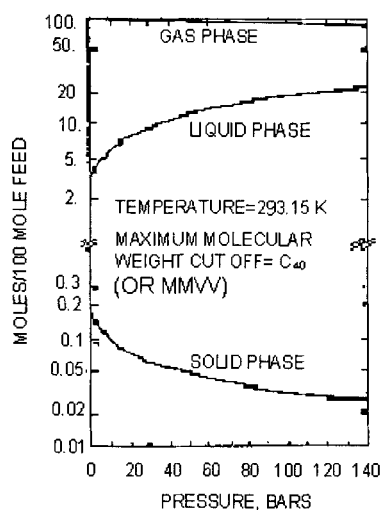


Fig. 21-24. Effect of pressure on wax precipitation for a synthetic 41-component mixture at 293 K [40].

The aforementioned equations were solved by a Newton–Raphson method, thus finding the values for the fractions of the feed that coexist as vapor and solid,  $\frac{V}{F}$  and  $\frac{S}{F}$ , respectively, and for the equilibrium compositions in all the three phases.

Figs. 21-23 and 21-24 present the results obtained by Won in illustrating the effects of temperature and pressure on the distribution of phases for a synthetic 41-component hydrocarbon system.

Won's approach was the first work that considered the non-idealities of the liquid

and solid solutions by means of use of activity coefficients. In the same way, he was the first author to incorporate a formal multicomponent description of wax precipitation. His method, however, included two different descriptions to compute the properties of the liquid phase (i.e., an equation of state to calculate  $\hat{\phi}_i^L$  in Eq. 21-18, and a solution model to calculate  $\gamma_i^L$  in Eqs. 21-15 to 21-17). Such a description provides different values for the molar volumes of the liquid phase. Notwithstanding this fact, this model became the starting point to a *new era* of model development, as will be seen in the following methods.

In 1988, Hansen et al. [21] introduced a model to predict the formation of waxes in crude oil. Similar to Won [40], Hansen et al. did not consider the inclusion of the second, third and fourth terms in Eq. 21-11, but unlike Won, Hansen et al. considered that the solid solution was ideal (i.e.,  $\gamma_i^S = 1$ ). For the liquid phase, Hansen et al. introduced an activity coefficient model derived from a polymer solution theory of Flory [41], which introduced a binary interaction parameter. The final expression for the activity coefficient,  $\gamma$ , was given by:

$$\ln \gamma_i^L = -\ln x_a + \ln v_a + 1 - v_a - \sum_{i \neq a} \frac{\psi_a}{\psi_i} v_i + \sum_{j \neq a} v_i x_{aj} \sum_{k \neq a} v_k - \sum_{j \neq a} \sum_{i < k} \frac{\psi_a}{\psi_i} v_i v_j x_{ij} \quad (21-20)$$

where  $\psi_i$  is the number of carbon atoms of the component  $i$  (Hansen et al. [21] considered a maximum of 80 components in the calculation).  $v_a$  is the volumetric fraction of the component  $i$ , given by the expression:

$$v_i = \frac{\psi_i \Omega_i}{\sum_j \psi_j \Omega_j} \quad \text{where } \Omega = \text{component volume} \quad (21-21)$$

Hansen et al. considered the inclusion of one term due to the subcooling of the precipitated wax, in terms of surface tension of the waxy phase. The authors, however, did not identify whether the quality of the predictions seemed to be affected by this contribution.

As for the treatment assumed in the characterization of pseudocomponents, Hansen et al. further subdivided each component into its paraffinic (P), naphthenic (N) and aromatic (A) hydrocarbon fractions, giving a total up to 160 components in one typical calculation, in addition to the complicated form of  $\gamma$  given by Eq. 21-20. This gives an idea of the computed times involved, even though the authors assure that, in accordance with their sensibility analysis, a maximum of 40 pseudocomponents (20 paraffins and naphthenes + 20 aromatics) gave satisfactory results.

Due to the publication of an extensive quantity of data on the precipitation of waxes (i.e., cloud points and quantities of precipitated wax) by W.B. Pedersen et al. in 1991 [42], it has since been possible to make a more complete analysis of the quality of the thermodynamic models of wax precipitation. K.S. Pedersen et al. [43] presented a model to calculate the precipitation of waxes in petroleum mixtures in which a modification to the model by Won [40] was presented. K.S. Pedersen et al. [43] modified Won's model, including (1) one linear dependency of the heat capacities of liquid–solid transition with

the temperature and the molecular weight of the hydrocarbon considered, which has the following form:

$$\Delta C p_i = p_1 MW_i + p_2 MW_i T \quad (21-22)$$

where  $p_1$  and  $p_2$  are parameters independent of component  $i$ ; (2) as for the solubility parameters of the solid and liquid phase for component  $i$ , the following functions were proposed:

$$\begin{aligned} \delta_i^L &= 7.41 + p_3 (\ln C_N - \ln 7) \\ \delta_i^S &= 8.50 + p_4 (\ln C_N - \ln 7) \end{aligned} \quad (21-23)$$

where  $p_3$  and  $p_4$  are fitting parameters; and (3) the following dependency for the enthalpy of fusion of the component  $i$ :

$$\Delta h_i^f = \Delta h_{i_{\text{won}}}^f p_5 \quad (21-24)$$

The liquid–solid  $K$ -value was given by the expression:

$$\begin{aligned} K_i^{\text{SL}} = \frac{x_i^S}{x_i^L} = \frac{\gamma_i^L(p_3)}{\gamma_i^S(p_4)} \exp \left[ \frac{\Delta h_{i_{\text{won}}}^f p_5}{RT} \left( 1 - \frac{T}{T_i^f} \right) \right. \\ \left. - \frac{p_1 MW_i}{R} \left( \frac{T_i^f}{T} - 1 - \ln \frac{T_i^f}{T} \right) - \frac{p_2 MW_i}{2R} \left( \frac{(T_i^f)^2}{T} - T - 2T_i^f \right) \right] \end{aligned} \quad (21-25)$$

To test the model with the experimental data on cloud points and quantity of precipitated wax reported by W.B. Pedersen et al. [42], K.S. Pedersen et al. [43] used the same multiphase procedure proposed by Won [40] (i.e., Eq. 21-19). A simultaneous regression for the above five model parameters was applied. The final parameter values obtained from the data of 17 North Sea stabilized crude oils were:

$$\begin{aligned} p_1 &= 0.3033 \text{ (Cal/g - K)} \\ p_2 &= -4.635 \times 10^{-4} \text{ (Cal/g - K}^2\text{)} \\ p_3 &= 0.5914 \text{ (Cal/cm}^3\text{)}^{1/2} \\ p_4 &= 5.763 \text{ (Cal/cm}^3\text{)}^{1/2} \\ p_5 &= 0.5148 \end{aligned} \quad (21-26)$$

Figs. 21-25 and 21-26 show the results of the application of this model in oils 1 and 11 as shown in Table 21-7. The amounts of precipitated wax are for the interval of 321 to 230 K. In discussing the results, K.S. Pedersen et al. [43] suggested that the inclusion of the effect of heat capacities of the components is significant in the calculated results. As in the work of Hansen et al. [21], K.S. Pedersen et al. [43] included a P, N and A description of pseudocomponents. Figs. 21-25 and 21-26 show that, in spite of the inclusion of a considerable number of fitting parameters in this model, the calculations did not follow the trend of the experimental results reported. In the results of the Figs. 21-25 and 21-26, as those for the 17 crude oils studied, an overestimation of the amounts of precipitated wax can be observed. These results suggest that, even though there was some improvement in the quality of the results in relation to the preceding models, there was still much room for improvement.

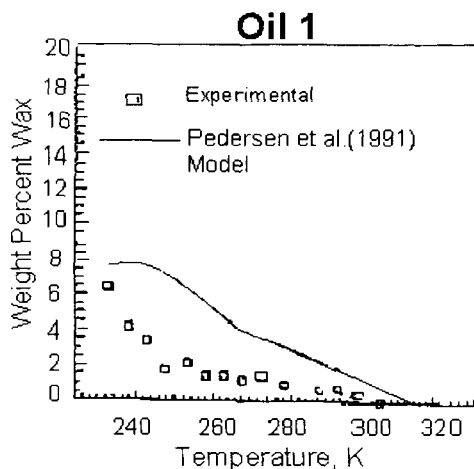


Fig. 21-25. Calculated and experimental results of wax precipitation for a North Sea crude oil at 1 bar [43].

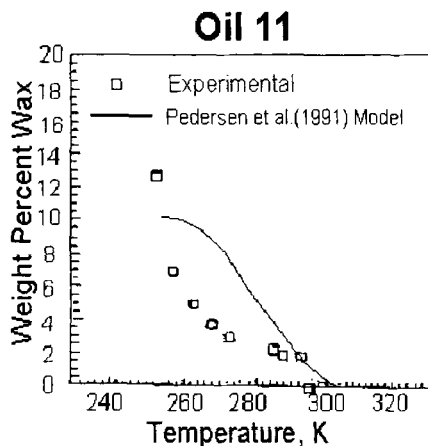


Fig. 21-26. Calculated and experimental results of wax precipitation for a North Sea crude oil at 1 bar [43].

In 1993, Erickson et al. [20] proposed a thermodynamic model that used the ideal solution, Eq. 21-12, with the consideration that the precipitated solid phase of crude oil is formed by *n*-paraffins and other paraffins (*cyclo*- and *iso*-paraffins). Thus, these authors used the expression Eq. 21-12 considering that the solid phase was a multicomponent mixture, instead of the pure-component nature for the solid that was involved in the derivation of Eq. 21-12. In this form, the liquid–solid equilibrium ratio was written as:

$$K_i^{SL} = \frac{x_i^S}{x_i^L} = \exp \left[ \frac{\Delta h_i^f}{RT} \left( 1 - \frac{T}{T_i^f} \right) \right] \quad (21-27)$$

As for the evaluation of  $T_i^f$ , Erickson et al. [20] distinguished between normal

TABLE 21-7

Compositions and properties of oil mixtures [42]

Carbon no.	I		II	
	Mol %	Mol wt.	Mol %	Mol wt.
C <sub>1</sub>	1.139			
C <sub>2</sub>	0.507		0.100	
C <sub>3</sub>	0.481		0.118	
<i>i</i> -C <sub>4</sub>	0.563		0.106	
C <sub>4</sub>	0.634		0.099	
<i>i</i> -C <sub>5</sub>	1.113		0.162	
C <sub>5</sub>	0.515		0.038	
C <sub>6</sub>	2.003		0.458	
C <sub>7</sub>	5.478	90.9	2.194	90.8
C <sub>8</sub>	8.756	105.0	2.847	106.5
C <sub>9</sub>	7.222	117.7	1.932	122.3
C <sub>10</sub>	5.414	132.0	5.750	135.0
C <sub>11</sub>	5.323	148.0	4.874	149.0
C <sub>12</sub>	4.571	159.0	5.660	162.0
C <sub>13</sub>	5.289	172.0	6.607	176.0
C <sub>14</sub>	4.720	185.0	6.149	189.0
C <sub>15</sub>	4.445	197.0	5.551	202.0
C <sub>16</sub>	3.559	209.0	5.321	213.0
C <sub>17</sub>	3.642	227.0	5.022	230.0
C <sub>18</sub>	3.104	243.0	4.016	244.0
C <sub>19</sub>	2.717	254.0	4.176	256.0
C <sub>20</sub> <sup>a</sup>	2.597	262.0	38.8+	473.0
C <sub>21</sub>	1.936	281.0		
C <sub>22</sub>	2.039	293.0		
C <sub>23</sub>	1.661	307.0		
C <sub>24</sub>	1.616	320.0		
C <sub>25</sub>	1.421	333.0		
C <sub>26</sub>	1.233	346.0		
C <sub>27</sub>	1.426	361.0		
C <sub>28</sub>	1.343	374.0		
C <sub>29</sub>	1.300	381.0		
C <sub>30</sub> <sup>+</sup>	13.23	624.0		
Sp.Gr.+	0.953		0.963	

<sup>a</sup> C<sub>20</sub> or C<sub>20</sub>+

paraffins and other paraffins by:

$$T_{i\text{ non-normal}}^f = T_{i\text{ normal}}^f(\text{Won}) - \left(90 - \frac{80C_i}{100C_i}\right) \tag{21-28}$$

In addition, the authors proposed the following dependency of the enthalpy of fusion of all hydrocarbons:

$$\Delta h_i^f = 1.14\Delta h_i^f(\text{Won}) \tag{21-29}$$

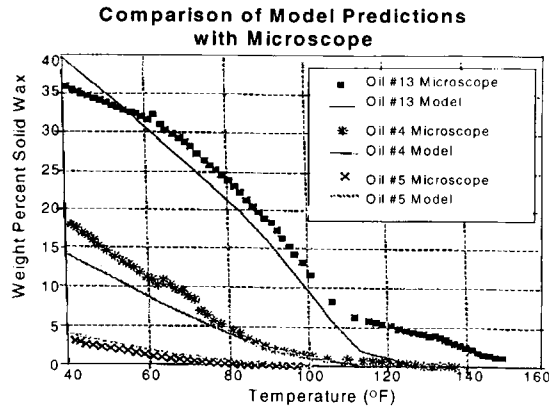


Fig. 21-27. Calculated and experimental wax amounts for three oils [20].

in which:

$$\Delta h_i^f(\text{Won}) = 0.1426 MW_i T_i^f(\text{Won})$$

$$T_i^f(\text{Won}) = 374.5 + 0.02617 MW_i - \frac{20172}{MW_i} (\text{K}) \quad (21-30)$$

The use of (a) different expressions to estimate the melting temperatures of normal and other paraffins, (b) a PNA-pseudocomponent description in the model, in addition to (c) use of the method for *stage-equilibrium* calculation in which, according to the authors, once solids form, they are not mixed with additional solids that precipitate at lower temperatures, appears to be responsible for the good results obtained by the authors. Neither the concept of staged-equilibria, however, was explained in detail, nor the form in which the mentioned concept modifies the mass balance expressions (Eq. 21-19) is shown. Nevertheless, Fig. 21-27 shows the results of this model. According to the authors, parameter 1.14, as embedded in Eq. 21-29, is the only fitting parameter.

In 1994, Erickson et al. modified his previous model by incorporating an EOS to calculate  $f_i^L$  in Eq. 21-9:

$$f_i^L = \hat{\Phi}_i^L(P, T, \underline{x}^L) x_i^L P \quad (21-31)$$

where  $\hat{\Phi}_i^L$  is the fugacity coefficient. This resulted in a new expression to calculate  $K_i^{\text{SL}}$  in a different form than the one given by Eq. 21-27, i.e.:

$$K_i^{\text{SL}} = \frac{x_i^S}{x_i^L} = \frac{\hat{\Phi}_i^L(P, T, \underline{x}^L)}{\Phi_{\text{pure } i}(P, T)} \exp \left[ \frac{\Delta h_i^f}{RT} \left( 1 - \frac{T}{T_i^f} \right) \right] \quad (21-32)$$

where it was considered that the non-idealities of the solid phase were negligible (i.e.,  $\gamma_i^S = 1$ ).

These authors also considered that the melting points of the components of the system varied with pressure in a systematic form. A non-cubic EOS was used, with binary interaction parameters taken from binary solid solubilities of highly asymmetric hydrocarbon systems, also calculated with the same model. The authors showed the

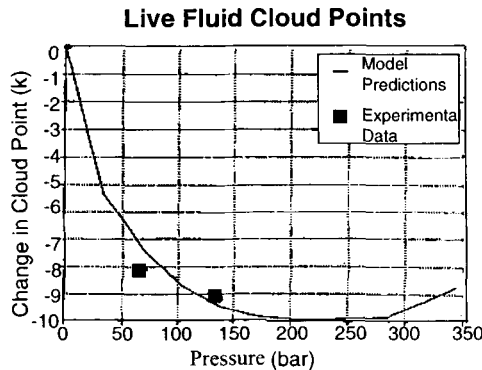


Fig. 21-28. Comparison of experimental and calculated cloud points with pressure for a live-oil fluid.

efficiency of the resulting method by reproducing the effect of pressure in the cloud points of dead and live oils at elevated pressure. In general, the results were satisfactory. Fig. 21-28 shows the obtained results compared with the experimental values of cloud points of a live-oil sample.

As one will notice in the last three models, the calculation methods of wax precipitation showed a tendency towards improvement in the description of the 'interactions' in the condensed phases. Poor attention, however, had been paid to the study of the physics of the precipitation process itself.

In 1993, K.S. Pedersen et al. [44] proposed an EOS-based model in which only a few of the total components of the crude were allowed to participate in the solid phase (solid solution). K.S. Pedersen et al. proposed to describe both the liquid and solid solutions by means of the Soave EOS. K.S. Pedersen et al. used the following expression to calculate the fugacities:

$$f_i^L = \hat{\phi}_i^L (P, T, \underline{x}^L) x_i^L P \quad (21-33)$$

where  $\hat{\phi}_i^L$  is the fugacity coefficient. For the solid phase, K.S. Pedersen et al. proposed an ideal expression to compute the fugacity of component  $i$  in the ideal solid solution as:

$$f_i^S = x_i^S f_{\text{pure } i}^S \quad (21-34)$$

since:

$$\ln \left( \frac{f_i^S}{f_i^L} \right)_{\text{pure } i} = - \left[ \frac{\Delta h_i^f}{RT} \left( 1 - \frac{T}{T_i^f} \right) \right] \quad (21-35)$$

then, by the definition of fugacity coefficient, one derives:

$$\phi_i^S = \left( \frac{f_{\text{pure } i}^S}{P} \right) \exp \left[ - \frac{\Delta h_i^f}{RT} \left( 1 - \frac{T}{T_i^f} \right) \right] \quad (21-36)$$

from which  $f_i^S$ , the fugacity of pure  $i$  in the solid solution, becomes  $f_i^S = x_i^S \phi_i^S P$ . To find the fraction of component  $i$  that goes to the solid solution, K.S. Pedersen et al. used



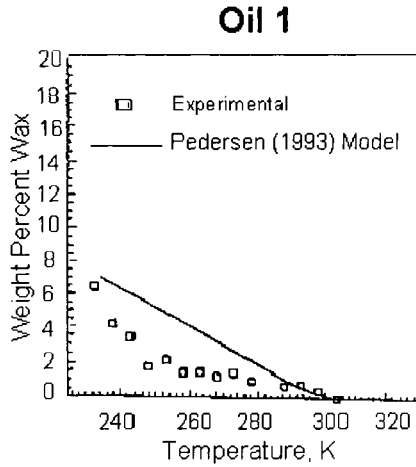


Fig. 21-29. Calculated and experimental results of wax precipitation for a North Sea crude oil at 1 bar [44].

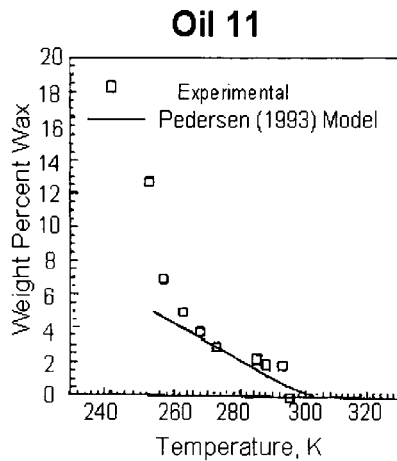


Fig. 21-30. Calculated and experimental results of wax precipitation for a North Sea crude oil at 1 bar [44].

the following empirical equation:

$$z_i^S = z_i^{\text{tot}} \left[ 1 - (A + B MW_i) \left( \frac{\rho_i - \rho_i^p}{\rho_i^p} \right)^C \right] \quad (21-37)$$

where  $z_i^S$  and  $z_i^{\text{tot}}$  are the mole fractions of component  $i$  in the solid (solution) phase and in the whole crude oil, respectively, and parameters  $A$ ,  $B$  and  $C$  were determined by matching experimental and calculated results with the model. Figs. 21-29 and 21-30 show the behavior of this model in the reproduction of experimental precipitation data of oils 1 and 11 shown in Table 21-7. As can be seen, while this model improved the calculation of wax amounts compared to all previous models, its results did not follow the trend of the experimental precipitation curve.

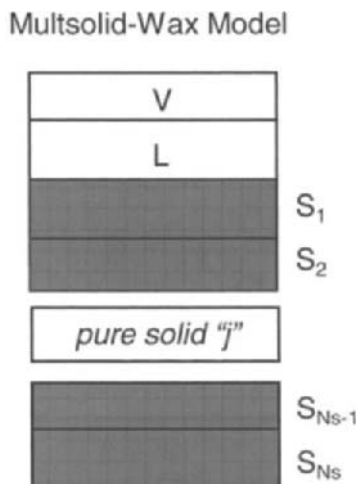


Fig. 21-31. Multisolid-phase model for wax precipitation.

In general, it can be seen that, until 1995, the various models proposed in the literature frequently showed a poor agreement with the experimental data. The overestimation of wax precipitation below the cloud point temperature was the major weakness of most models proposed. It can also be said that, until 1995, all the proposed techniques considered that the totality of the components that precipitate from petroleum do so in a *solid solution* state.

Lira-Galeana et al. [45], using the experimentally-supported assumption that precipitated wax consists of several solid phases (Snyder et al. [46–48]), proposed a thermodynamic model in which the precipitation of wax produces a solid mass that contains mutually immiscible precipitating components. Based on these observations, these authors proposed the multisolid-wax model shown schematically in Fig. 21-31, in which  $S_1$ ,  $S_2$ ,  $S_{N_s-1}$  are immiscible solid phases 1, 2, ..., etc., whose total number is  $N_s$ . Fig. 21-32 shows a plot of precipitated wax vs. temperature. Below the initial solidification temperature of the mixture (i.e., cloud point), the precipitation of wax consists of a consecutive precipitation process of pure components, each of these is completely immiscible with the other solids in the solid state. At a given temperature level, the total precipitated wax is given by the sum of the contributions of all solid phases that exist in equilibrium at that temperature. Lira-Galeana et al. established that the precipitating components are those which satisfy the following test of thermodynamic stability:

$$f_i(P, T, \underline{z}) - f_{\text{pure } i}^S(P, T) \geq 0; \quad (i = 1, 2, \dots, N) \quad (21-38)$$

The crude oil components that fulfill the above equation will precipitate, while those which do not will only coexist in the liquid and vapor phases. Lira-Galeana et al. [45] used the Peng-Robinson [49] EOS to calculate  $f_i$ . If  $N_s$  is the number of components that satisfy Eq. 21-38 then the vapor–liquid–multisolid wax equilibrium problem is

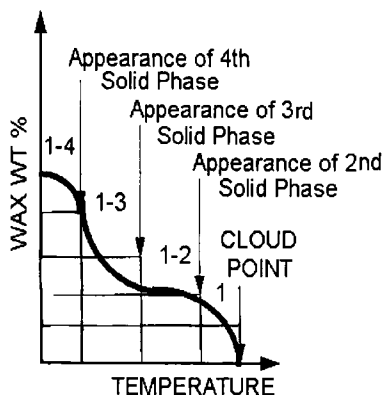


Fig. 21-32. Precipitation of multiple pure solids.

established by satisfying:

$$f_i^V = f_i^L = f_{\text{pure } i}^S; \quad (i = N - (N_S - 1), \dots, N) \quad (21-39)$$

$$f_i^V = f_i^L; \quad (i = 1, 2, \dots, N - N_S)$$

For a system of  $N$  components with  $N_S$  precipitating species, the total number of material balance and phase-equilibrium equations to solve is  $N_S + 2N - 1$ . Further details are given in Lira-Galeana et al. [45].

Figs. 21-33 and 21-34 show the results in the prediction of wax precipitation for oils 1 and 11 of Table 21-7. As can be seen, the multisolid-phase model presents satisfactory results according to the experimental data. In these results, no parameter adjustment was made.

An additional result obtained with this model is that the nature of the components that constitute petroleum wax was found to fall in the range of  $C_{25}$  to approximately  $C_{100}$ . 100. This result is in agreement with the experimental information on the carbon-atom distribution in waxes reported by Bishop and Philp [50].

The multisolid-wax model proposed by Lira-Galeana et al. suggested that the pseudocomponent breakdown to be used with the EOS can actually be considered as a matching parameter. This is independent, however, of the form in which the pseudocomponent properties (i.e., critical properties, acentric factors, etc.) are defined. This characterization procedure differs radically from conventional characterization procedures for heavy hydrocarbons (in which increasing the number of pseudocomponents is only expected to improve the calculation results). Thus, there is an optimum number of pseudocomponents that provide the best representation of the experimental data.

Fig. 21-35 shows the predicted wax deposition envelope (WDE) for a synthetic 9-component mixture whose composition and EOS properties are shown in Table 21-8. The predicted bubble point and cloud point curves intersect each other at the three-phase V-L-S bubble point pressure of the system. Table 21-9 shows the calculated phase compositions predicted at 265 K and 100 bar, where a 4-phase vapor-liquid-solid 1-solid 2 system is present.

In a recent application of this model, Pan et al. [51] compared experimental and

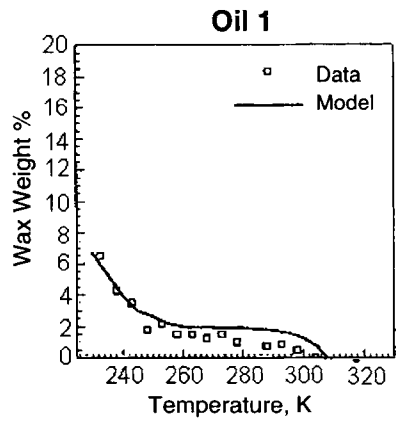


Fig. 21-33. Prediction of wax precipitation amounts for oil-1 [45].

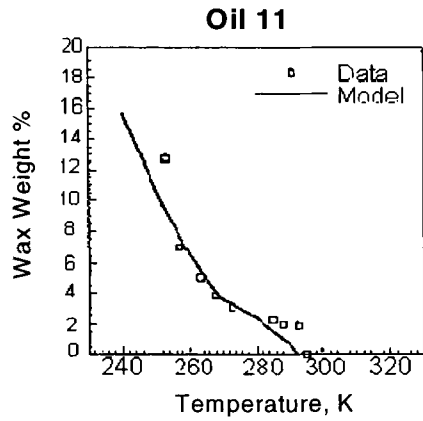


Fig. 21-34. Prediction of wax precipitation amounts for oil-11 [45].

TABLE 21-8

Composition and EOS properties of a synthetic hydrocarbon mixture

Component	Mole %	Mol. wt	$P_c$ (bar)	$T_c$ (K)	Acentric factor, $\omega$	$T_i^f$ (K)	Heat of fusion $\Delta H_i^f$ (cal/mol)
C <sub>1</sub>	51.471	16.0	46.0	190.5	0.012	90.0	225.0
C <sub>2</sub>	7.353	30.1	48.7	305.3	0.099	90.0	698.6
C <sub>3</sub>	5.882	44.1	42.5	369.8	0.152	86.0	861.3
C <sub>4</sub> s	4.412	58.1	37.9	425.2	0.199	138.0	905.0
C <sub>5</sub> s	4.412	72.5	33.8	469.8	0.251	97.0	996.0
C <sub>6</sub> s	5.882	86.2	30.4	507.9	0.299	143.0	1750.0
PC-1	8.824	142.0	25.1	614.7	0.590	228.7	4631.5
PC-2	7.353	282.0	14.3	763.1	1.091	295.6	11886.5
PC-3	4.412	338.0	12.1	799.2	1.279	306.0	14747.6

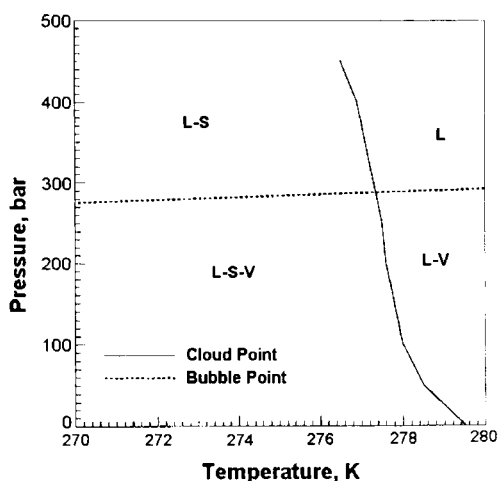


Fig. 21-35. Calculated wax deposition envelope for a synthetic 9-component mixture.

TABLE 21-9

Distribution of fluid and solid phases in equilibrium for a synthetic hydrocarbon mixture at 100 bar and 265 K

Component	Feed phase (mole %)	Vapor phase (mole %)	Liquid phase (mole %)	Solid phase-1 (mole %)	Solid phase-2 (mole %)
C <sub>1</sub>	51.471	90.39	38.81	0.00	0.00
C <sub>2</sub>	7.353	5.926	9.018	0.00	0.00
C <sub>3</sub>	5.882	2.305	8.425	0.00	0.00
C <sub>4</sub> s	4.412	0.776	6.792	0.00	0.00
C <sub>5</sub> s	4.412	0.358	7.000	0.00	0.00
C <sub>6</sub> s	5.882	0.223	9.461	0.00	0.00
PC-1	8.824	0.009	14.353	0.00	0.00
PC-2	7.353	$1.01 \times 10^{-6}$	5.087	0.00	100.00
PC-3	4.412	$1 \times 10^{-8}$	1.049	100.00	0.00

calculated cloud point temperatures as a function of pressure for three oil fluids ranging from 23 to approximately 32 components. Instead of using a pseudocomponent description for the C<sub>10</sub>+ fractions of these oils, Pan et al. divided each one of the C<sub>10</sub>+ pseudocomponents into their P, N, and A constituents, resulting in a more detailed characterization. Figs. 21-36–21-38 show the calculated and experimental results at temperatures ranging from 230 to around 270 K, as a function of pressure. A single fitting parameter within the EOS was employed. The results show a very good agreement with the experimental information.

Other applications of the approach developed by Lira-Galeana et al., including realistic gas-condensate fluids exhibiting retrograde behavior on the amount of precipitated wax (similar to the retrograde phenomenon in gas–liquid systems) have been recently reported by Nichita et al. [55].

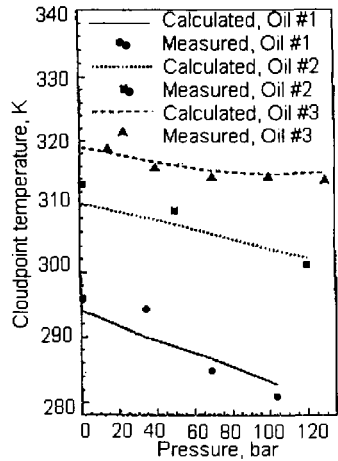


Fig. 21-36. Calculated and experimental cloud points [51].

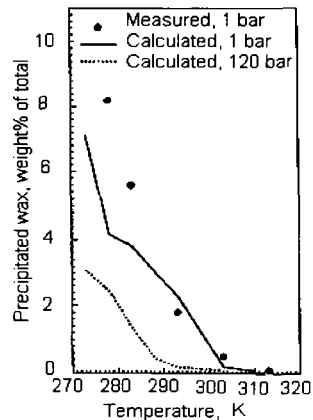


Fig. 21-37. Calculated and experimental amounts of wax and predictions to higher pressures [51].

To conclude this section, in spite of the progress made in the field of wax precipitation modeling, the current state of achievement can still be considered to be modest, and accurate predictions in realistic reservoir fluids are still limited to the availability of experimental information. Table 21-10 shows a comparison of the methods discussed in this chapter and presents their advantages and primary limitations. Ideal solution models, when modified properly, can only provide a qualitative description over wide pressure and temperature ranges. However, these models are the simplest models to use. The solid solution models that employ the so-called *gamma (L,S)-phi (V)* approach are more accurate than the ideal approaches, but their performance has shown to depend on the availability of wax precipitation data over the pressure and temperature ranges of interest [56–59]. These models are based on the use of the *solid-solution* approach and require a detailed characterization of the reservoir fluid under investigation.

TABLE 21-10

Benefit–cost–limitation relationships for models reviewed

Group references	Benefit	Cost	Limitation
1. Ideal solution [37–39]	Computational simplicity	Solubility data of each of the fluid's species required. Special ad-hoc assumptions needed	It provides only <i>qualitative</i> description of LSE
2. Ideal solution + EOS (solid solution) [20,21]	Simplest method for VLSE	Requires detailed chemical analysis of the heavy fraction. Two model parameters required	Predictions limited to the availability of experimental data
3. Activity coefficients + EOS (solid solution) [21,40,56–59]	Non-idealities of the condensed phases considered	Requires up to five regression parameters to provide reasonable estimates of LSE	Incorrect theoretical treatment to simultaneous VLE and LSE
4. EOS (solid solution) [20,44]	Thermodynamic consistency assured	Three model parameters that define precipitation components (solid solution) required	Predictions limited to the availability of experimental data
5. EOS (Multisolid-phase approach) [45,51,55]	Same as for group 4	One model parameter required	–

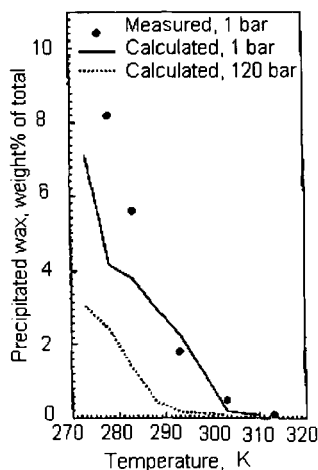


Fig. 21-38. Calculated and experimental wax amounts and predictions to higher pressures [51].

Due to the fact that wax precipitation is a multisolid-phase process, the multisolid phase treatment of wax equilibria has proven to be a consistent and simple method to use, and provides an adequate description of wax precipitation in a wide range of conditions. Since asphaltene and wax can precipitate together in oilwells and processing equipment, efforts should be made in developing models for the thermodynamic prediction of wax/asphaltene equilibria. Both experimental and theoretical studies regarding the interaction and properties of the above two fractions of crude oil need to be addressed in the near future.

## REFERENCES

- [1] Bowman, C.F., Distillation of an undefined number of components. *Ind. Eng. Chem.*, 73: 17 (1983).
- [2] Taylor, P. and Edmister, W.C., Flash distillation of a natural gasoline. *Pet. Ref.*, 58 (1): 35 (1952).
- [3] Khelen, J. and Ratzch, J.M., Continuous thermodynamics of complex mixtures. *Fluid Phase Equilibria*, 32 (5): 17 (1981).
- [4] Whitson, C.H., Characterizing hydrocarbon plus fraction. *J. Pet. Tech.*, April, 53 (1983).
- [5] Wilhelm, A. and Teja, A.S., Continuous thermodynamics using a bivariate distribution function and an equation of state. *AIChE J.*, 65, 4: 1235 (1987).
- [6] Boduszinski, M.M., Composition of heavy petroleum 1, Molecular weight, hydrogen deficiency, and heteroatom concentration as a function of atmospheric equivalent, Boiling point up to 1400°F (760°C). *Energy Fuels*, 1: 2 (1987).
- [7] Svetgof, J., Paraffin problem can be resolved with chemicals. *Oil & Gas J.*, 79, Feb. 27 (1984).
- [8] McCain, W.D., Jr., *The Properties of Petroleum Fluids*, Chap. 1. PennWell Publishing Co., OK (1990).
- [9] Altgelt, K.H. and Gow, T.H., *Chromatography in Petroleum Analysis*. Marcel Dekker, Inc., New York, 224 (1979).
- [10] Hunt, A., Uncertainties remain in predicting paraffin deposition. *Oil & Gas J.*, 94 (31): 96–103 (1996).
- [11] Fuhr, B.J., Holloway, L. and Hammami, A., Analytical considerations related to asphaltenes and waxes in the same crudes. In: *5th North American Chemical Congress*, Cancun, Nov. 11–15 (1997).
- [12] Alex, R.F., Fuhr, B.J., Rawluk, M. and Kalra, H., Characterization of waxy crudes and waxes. *Symposium on Modern Analytical Techniques for the Analysis of Petroleum*. Presented before the



- division of Petroleum Chemistry, Inc., American Chemical Society, New York, August 25–30 (1991).
- [13] Majeed, A.I., Bringedal, B. and Overå, S., Model calculates wax deposition for N. Sea oils. *Oil & Gas J.*, June: 63 (1990).
  - [14] Allen, T.O. and Roberts, A.P., *Production Operations: Well Completions, Workover, and Stimulation*. Oil and Gas Consultants International, Inc., Second edition, 2: 11–19 (1989).
  - [15] Srivastava, S.P., Handoo, J., Argawal, K.M. and Joshi, G.C., Phase-transition studies in *n*-alkanes and petroleum related waxes — a review. *J. Phys. Chem. Solids*, 54: 639 (1993).
  - [16] Wunderlich, B., *Macromolecular Physics*, Volume 2. Academic Press, New York (1976).
  - [17] Hammami, A., *Thermal Behavior and Non-isothermal Crystallization Kinetics of Normal Alkanes and their Waxy Mixtures under Quiescent Conditions*. PhD dissertation, University of Calgary (1994).
  - [18] Hammami, A. and Raines, M.A., Paraffin deposition from crude oils: comparison of laboratory results to field data, SPE 38776. In: *1997 SPE Annual Technical Conference and Exhibition*, San Antonio, Texas, October 5–8 (1997).
  - [19] Claudy, P., Létoffé, J.M., Chagué, B. and Orrit, J., Crude oils and their distillates: characterization by differential scanning calorimetry. *Fuel*, 67: 58 (1988).
  - [20] Erickson, D.D., Niesen, V.G. and Brown, T.S., Thermodynamic measurement and prediction of paraffin precipitation in crude oil, SPE 26604. In: *68th Annual Technical Conference and Exhibition of the Society of Petroleum Engineers*, Houston, TX, October 3–6 (1993).
  - [21] Hansen, J.H., Fredenslund, A., Pedersen, K.S. and Rønningsen, H.P., A thermodynamic model for predicting wax formation in crude oils. *AIChE J.*, 34: 1937 (1988).
  - [22] Kruka, V.R., Cadena, E.R. and Long, R.E., Cloud-point determination for crude oils. *JPT*, August: 681 (1995).
  - [23] Létoffé, J.M., Claudy, P., Garcin, M. and Volle, J.L., Crude oils: characterization of waxes precipitated on cooling by d.s.c. and thermomicroscopy. *Fuel*, 74: 810 (1995).
  - [24] Rønningsen, H.P., Bjørndal, B., Hansen, A.B. and Pedersen, W.B., Wax precipitation from North Sea crude oils I. Crystallization and dissolution temperatures and Newtonian and non-Newtonian flow properties. *Energy Fuels*, 5: 895 (1991).
  - [25] Ferworn, K.A., Hammami, A. and Nighswander, J.A., Review of experimental techniques for the measurement of petroleum solid deposition. In: *ISCOP*, Rio de Janeiro, Brazil, November (1995).
  - [26] Ferworn, K.A. and Hammami, A., Final report. *DeepStar IIA CTR 902 Project: Round Robin Tests of Paraffin Inhibitor Section Methods* (1995).
  - [27] Ferworn, K.A., Hammami, A. and Ellis, H., Control of wax deposition: An experimental investigation of crystal morphology and an evaluation of various chemical solvents, SPE 37240. In: *1997 SPE International Symposium on Oilfield Chemistry*, Houston, TX, February 18–21 (1997).
  - [28] Hsu, J.J.C. and Brubaker, J.P., Wax deposition of waxy live crudes under turbulent flow conditions, SPE 28480. In: *SPE 69th Annual Technical Conference and Exhibition*, New Orleans, LA, September 25–28 (1994).
  - [29] Meray, V.R., Volle, J., Schranz, C.J.P., Le Marechal, P. and Behar, E., Influence of light ends on the onset crystallization temperature of waxy crudes within the frame of multiphase transport, SPE 26540. In: *68th Annual Technical Conference and Exhibition of the Society of Petroleum Engineers*, Houston, TX, October 3–6 (1993).
  - [30] Brown, T.S., Niesen, V.G. and Erickson, D.D., The effects of light ends and high pressure on paraffin formation, SPE 28505. *Proc. of the 69th SPE Annual Technical Conference and Exhibition of the Society of Petroleum Engineers*, New Orleans, LA, Sept. 25–28, (1994).
  - [31] de Boer, R.B., Leerlooyer, K., Eigner, M.R.P. and van Bergen, A.R.D., Screening of crude oils for asphalt precipitation: theory, practice and the selection of inhibitors. *SPE Prod. Facil.*, 2: 55 (1995).
  - [32] Hammami, A., Chang-Yen, D., Nighswander, J.A. and Stange, A., An experimental study of the effect of paraffinic solvents on the onset and bulk precipitation of asphaltenes. *Fuel Sci. Tech. Intern.*, 13 (9): 1167–1184 (1995).
  - [33] Cawkwell, M.G. and Charles, M.E., *J. Pipelines*, 7: 251 (1989).
  - [34] Hsu, J.J.C. and Brubaker, J.P., Wax deposition measurement and scale-up modeling for waxy live crudes under turbulent flow conditions, SPE 29976. In: *International Meeting on Petroleum Engineering*, Beijing, PR China, November 14–17 (1995).

- [35] Broadhurst, M.G., An analysis of the solid phase behavior of the normal paraffins. *J. Res. Nat. Bureau of Stds.*, A. Vol 66A No. 3, 241, May–June (1962).
- [36] Prausnitz, J.M., Lichtenthaler, R.N. and Azevedo, E.G., *Molecular Thermodynamics of Fluid Phase Equilibria*, Chap. 9. Prentice-Hall, Englewood Cliffs, NJ (1986).
- [37] Reddy, S.R., A thermodynamic model for prediction n-paraffin crystallization in diesel fuels. *Fuel*, 65: 1648 (1986).
- [38] Weingarten, J.S. and Euchner, J.A., Methods for predicting wax precipitation and deposition. *SPE-Production Engineering*, 121, Feb. (1988).
- [39] Frezzotti, D., Bonifaci, L., Cavalea, G., Malaguti, E. and Ravanetti, G.P., Solid–liquid equilibrium studies on  $\epsilon$ -caprolactam-oligomers systems. *Fluid Phase Equilibrium*, 83: 399 (1993).
- [40] Won, K.W., Thermodynamics for solid solution–liquid–vapor equilibrium, Wax phase formation from heavy hydrocarbon mixtures. *Fluid Phase Equilibrium*, 30: 265 (1986).
- [41] Flory, P.J., *Principles of Polymer Chemistry*. Cornell Univ. Press, Ithaca, NY (1953).
- [42] Pedersen, W.B., Hausen, A.B., Larsen, E., Nielsen, A.B. and Rønningsen, H.P., Wax precipitation from North Sea crude oils 2, Solid phase content as function of temperature determined by pulsed NMR. *Energy Fuels*, 5: 908 (1991).
- [43] Pedersen, K.S., Skovbarg, P. and Rønningsen, H.P., Wax precipitation from North Sea crude oils 4, Thermodynamic modeling. *Energy Fuels*, 5: 924 (1991).
- [44] Pedersen, K.S., Prediction of cloud point temperatures and amount of wax precipitation, SPE 27629. *Soc. Pet. Engrs.*, Richardson, TX (1993).
- [45] Lira-Galeana, C., Firoozabadi, A. and Prausnitz, J.M., Thermodynamics of wax precipitation in petroleum mixtures. *AIChE J.*, 42 1: 239 (1996).
- [46] Snyder, R.G., Goh, M.C., Srivatsaroy, V.J.P., Strauss, H.L. and Dorset, D.L., Measurement of the growth kinetics of microdomains in binary  $n$ -alkane solid solutions by infrared spectroscopy. *J. Phys. Chem.*, 96: 10008 (1992).
- [47] Snyder, R.G., Conti, G., Strauss, H. and Dorset, D.L., Thermally-induced mixing in partially microphase segregated binary  $n$ -alkane crystals. *J. Phys. Chem.*, 97: 7342 (1993).
- [48] Snyder, R.G., Srivatsavoy, V.J.P., Cates, D.A., Strauss, H.L., White, J.W. and Dorset, D.L., Hydrogen/deuterium isotope effects in microscope separation in unstable crystalline mixtures of binary  $n$ -alkanes. *J. Phys. Chem.*, 98: 674 (1994).
- [49] Peng, D.Y. and Robinson, D.B., A new two-constant equation of state. *Ind. Eng. Chem. Fund.*, 15: 59 (1976).
- [50] Bishop, A. and Philp, P., *Prediction of Potential Wax Deposition Problems during Petroleum Production*. Internal Report, Organic Geochemistry Group, Univ. of Oklahoma, Norman, OK (1994).
- [51] Pan, H., Firoozabadi, A. and Fotland, P., Pressure and composition effect on wax precipitation: experimental data and model results, SPE 36740. In: *1996 SPE Annual Technical Conference and Exhibition of the Society of Petroleum Engineers*, Denver, CO, Oct. 6–9 (1996).
- [52] Scatchard, G., *Chem. Rev.*, 7: 44 (1949).
- [53] Hildebrand, J.H. and Scott, R.L., *The Solubility of Non-Electrolytes*. Reinhold, New York, 3rd Ed. (1950).
- [54] Soave, J., Equilibrium constants from a modified Redlich–Kwong equation of state. *Chem. Eng. Sci.*, 27: 1197 (1972).
- [55] Nichita, D.V., Goval, L and Firoozabadi, A., Wax precipitation in gas condensate mixtures SPE 56488. In: *1999 SPE Annual Technical Conference and Exhibition of the Society of Petroleum Engineers*, Houston, TX, Oct. 3–6 (1999).
- [56] Coutinho, J.A.P., Knudsen, K., Andersen, S.I. and Stenby, E.H., A local composition model for paraffinic solid solutions. *Chem. Eng. Sci.* 51: 3273–3282 (1996).
- [57] Coutinho, J.A.P. and Stenby, E.H., Predictive local composition models for solid–liquid and solid–solid equilibrium in  $n$ -alkenes: Wilson equation for multicomponent systems. *Ind. Eng. Chem. Res.*, 35: 918–925 (1996).
- [58] Coutinho, J.A.P., Predictive local composition models: NRTL and UNIQUAC and their application to model solid–liquid equilibrium of  $n$ -alkenes: *Fluid Phase Equilibria*, 158: 447–457 (1999).
- [59] Lindeloff, N., Andersen, S.I., Stenby, E.H. and Heideman, R.A., Phase boundary calculations in

systems involving more than two phases, with application to hydrocarbon mixtures. *Ind. Eng. Chem. Res.* 38: 1107–1113 (1999).

## Subject Index

- Abiogenic, 25
- Acidaffins, 368, 369
- Activated anionic resin, 371
- Activated cationic resin, 371
- Activation energy, 133, 136, 137, 138, 139, 140, 141, 142, 143, 460, 468, 477
  - –, evaluation of, 481, 492
  - –, of reactions, 493
- Adhesion of bitumen, 500
- Adhesion member, 198
- Adsorption, 2, 243
  - , ESR, 243
- Adsorption intensity, 261
- Adsorption liquid chromatography, 206
- Agglomeration, 322, 327, 329
  - , electrochemically induced, 319
  - , ionic induced, 319
  - , peptized asphaltenes, 321
- Aggregates, 328, 447, 476, 499
  - asphalt mixtures, 363
- Aggregation, 4, 336
  - , fractal kinetics, 2
  - , intermolecular, 336
- Aging, 196, 393, 475, 488, 489, 491
  - , asphalt, 546
  - –, kinetic approach, 475
  - index, 196
  - –, bitumen, 196
  - , oxidative, 393
  - tests, 488, 489, 491
  - –, bitumen, 488, 489, 491
- Albertite, 17, 402
- Aliphatic chain, 59
- Aliphatics, 111, 130
- Alkanes, 16, 30
  - , biochemical degradation of, 13
  - , cyclic, 14
  - iso, 14
  - , normal, 14
  - , subjected to sulfuration, 23
- Alkylaromatic, 130, 141
- Alkylhydroaromatic, 130
- Alkylnaphthenic, 130
- Aluminosilicates, 140
- Amphilitic substances, 4
- Amphiphile, 103
  - , oil-soluble, 336
- Amphiphilic resins, 322
- Anionic emulsion, 537
- Anisotropic, 40
- Anthracene, 69
- Anthracite, 247
- Anthraxolite, 17, 402
- Anti-foulants, 3
- Antioxidants, 455, 457, 458, 459, 460, 465, 466
  - activity, 457
  - chain-breaking, 466
  - , concentration of, 466
  - , in resins, 460
  - , phenolics, 465
  - properties, 459
- Antistripping additives, 388
- API gravity, 152
- Aquaconversion, 151
- Arachidonic acid, 20
- Aromatic, 14, 65, 69, 250, 251, 309, 365
  - asphaltene, 14
  - carbon, 65
  - clusters, 250, 251
  - condensation index, 345
  - core, 69
  - – configuration, 69
  - hydrocarbons, 14
  - intermediate oil, 14
  - naphthenic, 14
  - radicals, 247
  - ring system, 365
  - , tricyclic, 309
- Aromaticity, 13, 23, 143, 168, 184, 188, 192, 234, 239, 240, 246, 336, 344, 345, 347
  - factor, 220

- oil, 3
- parameter, 192
- Aromatics, 103, 113, 114, 140
  - electrophilic hydroxylation of, 23
  - hydrogenated fused-ring, 16
  - hydroxylation, 23
  - – by percarbonate, 24
  - – by sodium salts of perborate, 24
  - nitration of, 24
  - perhydro-peri-fused, 19
  - polar, 140
  - separation of, 283
- Aromatization, 25, 32, 93, 254, 256
  - of naphthenics, 256
- Arrhenius
  - equation, 477
  - expression, 132
  - parameters, 75
  - plot, 52, 53, 460
  - – for bitumen aging test, 492
- Asphalmastic, 8
- Asphalt
  - analysis, 309
  - – elution solvent system, 309
  - blowing, 550
  - building stones, 8
  - Chinese paraffinic crudes, 538
  - concrete, 502, 503, 504, 512
  - mixtures, aggregate, 363, 508, 510, 511
  - –, composition of, 511
  - –, design of, 511
  - –, granulometric composition, 510
  - –, spatial design, 508, 511
- Asphaltic concrete, 528
- Asphaltite, 11, 13
- Asphaltoids, 17
- Asphaltos, 8
- Asymptotic simulation, 97
- Athabasca bitumen, 111
- Autoxidation, 452, 458
  
- Bacteria, 20, 22
  - anaerobic sulfate-reducing, 20
- Bauxite, 165
- Bimodal, 92
- Binders, 176, 177, 179
  - aging, 203
  - bituminous, 499
  - – aging, 476, 485
  - characterization of, 174
  - complex organic
  - gluing ability, 221
  - organic, 173, 174, 178, 206
  - plasticity, 214
  - polymer-bitumen, 196, 211, 214
  - viscosity, 214
- Bingham flow limit, 200
- Bingham yield strength, 225
- Biogenic, 25
- Biomarker, geological, 25
- Biomarkers, 30
- Biosynthesis, 21
  - of endoperoxide, 21
  - of prostaglandin derivatives, 21
- Biradical, 262
- Bitumen, 2, 129, 132, 144, 173, 176, 180, 181, 187, 192, 193, 192, 197
  - aging, 203, 475, 477
  - –, kinetic approach, 475
  - –, theoretical approach, 477
  - albertite, 402
  - anthraxolite, 402
  - authigenic, 402, 403, 415, 417, 418, 431
  - autochthonous, 438, 439
  - biological markers, 418, 422
  - biomarkers maturity parameters of, 431, 435
  - brittleness, 202
  - classification of, 17
  - degradation of, 421
  - emplacement, 438
  - epigenetic reservoir, 402, 403, 416, 417, 419, 439, 440
  - ESR spectra, 257
  - extraction, 38
  - genetic classification of, 402
  - genetic types, 401
  - gilsonite, 402
  - glass pitch, 402
  - grahamite, 402
  - group chemical compositions, 199
  - heterochthonous, 417, 438
  - impsomite, 402
  - indigenous, 403
  - magmatic thermal alteration, 402, 404
  - maturity, 404, 410
  - – parameters, 412, 413
  - mezometa impsomite, 402

- model characteristics, 189
- model parameters, 216, 217
- morphological structure, 410
- occurrence of, 412
- physicochemical characteristics, 183
- pyrobitumen, 402
- reflectance, 405, 406, 408, 416, 417, 431, 440
- rheological characteristics, 197, 200, 202, 203, 183
- rheological properties, 184, 187
- softening temperature, 202
- solubility, 405
- standard characteristics, 198
- structure of, 447
- supergene, 403, 404
- surficial degradation, 402, 403
- thermal evolution, 414
- thermal maturation, 407
- thermal simulation, 405, 411
- thixotropic properties of, 195
- wurtzite, 402
- X-ray diffraction patterns, 409
- Bohr magneton, 230
- Boltzmann's constant, 261
- Bragg angle, 409
- Branching, 454
- Brittle point, 183, 207
- Brittleness, 500
  - of asphalt, 527
  - of bitumen, 202
- Bubble point, 338
  
- Calcareous marlstone, 499
- Calcination, 352
- Carbenes, 167, 348
- Carboids, 17, 167, 348
  - solubility in benzene, 11
- Carbon, 7, 8, 13, 65, 66, 88, 89, 302, 319, 330, 564, 565
  - , aromatic, 65
  - atoms, 13
  - derived from natural gas combustion, 8
  - , methylene, 65
  - , naphthenic, 65
  - number, 88, 89, 319, 330, 564, 565
  - , peripheral, 65, 66
  - , aromatic, 66
  - , naphthenic, 66
  - , petroleum derived, 7
  - residue, 302
  - , saturated, 65
  - , total, 65
- Carbonization, 26, 243
- Casting of sulphur-asphalt paving mixes, 530
- Catagenesis, 235, 237, 243, 466
- Cavitation, 30
- Characterization, asphaltene, 1, 336
- Characterization, asphalts, 4
- Chelates, 53
- Chelation, 32, 40
- Chemical composition, of asphalt, 364
- Chemical functionality, 384
- Chemical bonding, 310
- China, heavy oil, 539
- Chinese asphalts, kinetics parameters of, 549
- Chlorins, 32
- Chlorophylls, 32
- Chromatotron, 306
  - characterization of asphalt by, 313
  - for asphalt composition, 310
  - schematic diagram, 311
  - time saving method, 315
- Classification
  - , asphalts, 4
  - , crude oils, 13
- Cloud point, 3, 557, 573, 574, 575, 576, 578, 579, 581, 588, 597, 599, 603
  - – variation w/saturation pressure, 589
- Coagulation, 328
- Coal
  - desulfurization, 30
  - liquefaction, 238
  - liquid, 22, 65
- Coalescence, 327
- Coalification, 235, 243
- Coefficient of dispersion, 373
- Coefficient of correlation, 182, 185
- Coefficient of elasticity, 186, 188
- Cohesion, kinetics, 196, 203
- Cohesive energy, 103, 105, 115, 118
- Coke, 59, 62, 63, 129, 132, 134, 135, 136, 137, 138, 139, 140, 141, 145, 150, 161, 166
  - formation, chemistry of, 2
- Coking characteristics, 140
- Coking kinetics, 131
- Cold filter, 578

- Colloidal, 305, 319, 335, 338, 550
  - asphalt system, 305
  - , existence of asphaltenes, 335
  - materials, 391
  - models, 338
  - stability, asphalts, 550
  - system, 319
- Color index, 243, 244, 270
- Color intensity, 243, 269
- Compatibility, 388, 389, 390
- Complex flow, degree of, 392
- Compression strength, 213, 223, 224
- Compression test, 215
- Computer Assisted Structure Elucidation (CASE), 104, 105, 107
- Condensation, 111, 121
  - index, 184, 342, 344, 348, 349
- Contact interactions, 230
- Condensity, degree of, 191
- Convection, 321
- Coorongite, 17
- Copolymer, 19
- Corrin, 32
- Covalent bonding, 379
- Cracking, 1, 129, 131, 132, 136, 140, 150, 383, 385
  - , of asphaltene, 134
  - , of heavy oil, 132
  - , thermal, 130
- Cretaceous, geologic age, 33
- Critical concentration, 175
- Critical Micelle Concentration (CMC), 329
- Cross Polar Microscopy (CPM), 571, 576, 577, 578, 584
- Cross-linking, 19
- Crystallization, 575, 576, 577
- Cumulative Probability Distribution (CPD), 68, 71
- Cyclic structures, 23
- Deactivated catalysts, 165
- Deactivating, 458
- Deactivation, 59
- Dealkylation, 86, 89, 92, 95, 265
- Deasphaltation, 402, 403
- Deasphalting, 4, 151
- Deasphaltization, 180, 220
- Decarboxylation, 32
- Decomposition, 454
  - , kerogen, 20, 38
- Deficiencies, hydrogen, 348
- Deformability, 214, 223
- Deformation, 176
  - scale, 197
- Degasification, 265
- Degradation, 66
- Dehydrogenation, 75, 97, 98, 349, 462, 470, 517
- Delocalization, 458
- Demetallization, 153, 154, 461
- Density, 13, 110, 115, 118, 121, 175, 176, 184, 195, 216
- Depeptization, asphaltenes, 462
- Depolymerization, 25, 26, 66, 86, 92, 95
- Deposit formation, asphaltenic, 336
- Deposition, asphaltene, 4, 336
- Destabilization, 461
- Desulfurization, 153, 163
- Diagenesis, 23, 402, 466
- Diamondoids, behavior, 2
- Diaromatics, 341
- Dicyclic aromatics, 309
- Differential Scanning Calorimetry (DSC), 460, 571, 574, 575, 576
- Differential Thermal Analysis (DTA), 468
- Diffusion, 164
- Dimerization, 46, 53
- Dipolar interactions, 230, 233
  - , spin–spin, 233
- Dipole–dipole, charge transfer, 336
- Dispersants, polymeric, 336
- Dispersibility, 388
- Dispersion, 173, 305, 373, 374
- Dissolution, asphalt fractions, 312
- Distillable, 133, 135, 136
- Distillation, 11
- Disturbance, structure, 200
- Disulfide linkage, 20, 22
- Dolomitization, 438
- Dubbs, thermal cracking process, 335
- Ductility, 4, 198, 212
- Durability
  - , asphalt, 4, 363, 364, 372, 378, 385
  - , parameter, 373
- Ebullating-bed reactors, 156, 157, 159
- Elastic modulus
- Elasticity, 212, 214

- coefficient, 200, 207
- index, 183
- Elastomers, 214
- Electrokinetic phenomena, 2
- Electromagnetic irradiation, 1
- Electron density, 230
- Electron Paramagnetic Resonance (EPR), 229, 516
- Electron spin, 229, 253
  - density, 253
  - resonance, 229
  - splitting, 231
  - transfer, 457, 458
  - –, initiated oxidation, 459
- Electrophilic, 23
  - hydroxylation, 25
- Electrostatic forces, 310
- Element content, 182
- Elemental analyses, 112, 365
- Eluted fraction, 371
- Embrittlement, 363, 385
- Emulsifying agent, 388
- Emulsion, 7, 103, 123, 537
- Energy levels, 230
- Energy minimization, 115
- Enhanced oil recovery, 1, 30
- Enmers, 321
- Enthalpy, 110, 119, 122, 123
- Eocene, geologic age, 33
- Equilibrium algorithms, 2
- Equations of state, rdf-based mixing rules, 2
- Equilibrium, 379
  - elastic modulus, 183, 200
- ESR, 233, 247, 259, 261, 265, 267, 272
- Exchange, interaction, 233
- Excitation energy, 261
- Exinite, 264
  
- Fatigue life, sulphur-asphalt blend, 528
- Fillers
  - , limestones, 500, 501, 502, 503, 505
  - , oil shales, 500, 502, 503, 505, 508, 511, 512
- FI-MS, 305
- Fission, 135
- Fixation, 305
- Fixed-bed reactors, 152, 153
- Flame Ionization Detection (FID), 313
- Flexural, 502
  
- Flocculation, 3, 111, 328
  - dynamic flow limit, 207
- Fractals, 2, 30
- Fractionation, 366, 371
  - protocol, heavy oil, 568
- Free radicals, 130, 152, 238, 239, 244, 251, 257, 262, 377, 410, 454, 458
  - densities, 265
  - mechanisms, auto-oxidation, 459
  - oxidation, 465
- Frequency factor, 137, 138, 140, 142, 143
- Frost resistance, 214
- FT-IR, 305
- Fuel processing, 238
- Fullerene, 26
- Functional groups, 336, 369, 375
  - in asphalt, 363
  - , heavy oil, 449
- Functionalities, 342
- Functionality analysis, 379
- Fusains, 248, 250, 265
- Fusinization, 248
  
- Gamma distribution, 68
- Gas chromatography, of oil fraction, 3
- Gas condensates, 3
- Gas Phase Hydrogenation (GPH), 159
- Gas phase minimization, 115, 118
- Gaussian distribution, 32
- GC, 305
  - column oxidation, 386
- GC/FT-IR, 305
- GC-MS, 108, 131, 305, 418, 419, 420, 422, 563
- Gel Permeation Chromatography (GPC), 284, 295, 366, 541
- Geochemistry, organic, 23
- Geolipids, 401
- Geologic age, 167
- Geomacromolecules, 104, 105, 106
- Gibbs free energy, 586
- Gilsonite, 17, 402
  - asphaltenes, 242
  - solubility, carbon sulfide, 12
- Glass pitch, 402
- Glycine, 25
- GPC diagram, 547
- Grahamites, 17, 402
  - solubility, carbon disulfide, 12



- Graphite, 16, 18, 26, 244, 248
- Graphitization, 53
- Gussasphalt, 499, 501, 502, 503
- Gypsum, 8
  - cementation, 438
- Halogenated radicals, 255
- Hardening, 391, 392, 393
  - index, 387, 505, 507, 508
  - rate, asphalt, 387
- Hardness, asphalt, 527
- Heat exchanger, 59
- Hematite, 165
- Hempel distillation, 12
- Heterogeneity, 137
- Heteroatomic antioxidants, 455
- Heteroatomic organic compounds, 103
- Heteroatoms, 240, 247, 252, 253, 265, 267, 365, 366, 445
  - functionality, 382
- Hetrocyclic compounds, 23
- High Pressure Liquid Chromatography (HPLC), 3, 305, 419, 447, 487, 494, 562
- Homologs, fused-ring saturated, 16
- Homolysis, 238
- Homopolymer, 19
- Hückel Rule, aromaticity, 69
- Humic substances, 17, 18
- Hydrolysis, 355, 366
- Hydroconversion, 149, 164
- Hydrocracking, 138, 139, 160, 161, 167, 267
- Hydrodemetallization, 154, 164
- Hydrodesulfurization, 154
- Hydrodynamic radius, 179, 218
- Hydrogen bonding, 53, 310, 336, 379, 462
- Hydrogenation, 152
- Hydrogenolysis, 144
- Hydrotreating, 152, 161, 164
- Hydrovisbreaking, 150, 151, 154
- Hydroxylation, 23
- Hyperfine interactions, 230
  - coupling constant, 230
  - tensor, 231
- Hyperstructure, 107
- Ichthamnol, 20
- Ichthyoleum, 20, 22
- Impsonite, 402
- Incineration, 163
- Indene, 23
- Indicators, 479
- Infrared Radiation (IR), 108, 111, 284, 287, 476, 494
  - – absorption, 461
  - – spectra for asphaltenes, 345
  - – spectroscopy, 351, 353, 355, 357
- Ingramite, 17
- Inhibition, 336
  - kinetics, 465
- Inhibitors, 457, 465
  - concentration, 465
- Initiation, 453
- In-situ combustion, 445
- In-situ recovery, heavy oil, 445
- Instability, crude oil, 340
- Interfacial phenomena, 319, 322
- Intermolecular forces, 310
- Internal energy, 110
- Internal pressure, 370
- Ion Exchange Chromatography (IEC), 370
- Isomers, 106
- Isothermal compressibility, 110
- Isotropic parameters, 40, 44
- Jacobson rearrangement, 25
- Kata-condensed system, asphaltenes, 22
- Kerogen, 20, 38, 107
  - , cross-linked asphaltene, 19
  - , genesis, 259
  - , isolation from minerals, 38
  - , macromolecular material, 500
  - maturation, 257
  - oxidation, 30, 38
- Kinetics, 130, 135
  - analysis, 61
  - , asphalt oxidation, 467
  - , asphaltene cracking, 129
  - behavior, 59
  - , bond breaking, 82
  - constant, 138
  - energy, 382
  - molecular model systems, 74
  - models, 3, 59
  - parameters, 60, 140, 142
  - , reaction probabilities, 82
  - review of some concepts, 476

- Lacquers, 175
- Lewis acid-catalyzed, sulfur insertion, 23
- Ligand complexes, 32
- Light Transmittance (LT), 571
- Limestone fillers, 4, 499, 500, 501, 502, 503, 505, 508, 511, 512
- Limonite, 165
- Lineshape, 233
- Linewidth, 232, 243, 245, 249, 250, 261, 262
- Lipophilic, 319
  - resins, 320
- Lipophobic, 319
- Liquefaction, 268
  - , coal, 271
- Liquid chromatography, oil fraction, 3
- Liquid Phase Hydrogenation (LPH), 159
- London, 310
- Lower Miocene, geologic age, 33
- Low-Temperature Carbonization (LTC), 159
- Lumped solubility, 141
- Lyophilicity, 180, 184
  - index, 216
- Macerals, 236
- Macroscopic, models, 327
- Magnetic field, 229, 230, 231
- Magnetic moment, 229
- Magnetic nuclei, 230
- Magnetite, 165
- Maltene, 59, 60, 63, 137, 138, 139, 144, 197, 368, 374, 446, 447, 459, 460
- Manjack, 17
- Markov chain, 76, 79, 82
- Markovian trials, 76
- Mastics, 175, 225
- Maturation, 23
  - degree, 36
  - index, 167
- Mechanical entrapment, 2
- Mesomorphic, 167
- Mesophase
  - formation, 262
  - pitches, 262
- Metamorphism, 237
  - , thermal, 404
- Methane Sulfonic Acid (MSA), 32
- Methanization, 466
- Methylene carbon, 65
- Mezometa impsomite, 402
- Micellar, 2, 320
  - configuration, 320
  - theory, 2
- Micelles, 30, 103, 104, 305, 320, 447
- Micellization, 103, 335
- Microbubbles, 1, 2
- Microcat-RC (MRC) process, 158
- Microscopic models, 327
- Microwave, 230
  - dielectric coefficient, 409
- Migration, bitumen, 401
- Mild Resid Hydrocracking (MRH), 160
- Mineral wax, 17
- Model isomer, 116, 121, 122
- Modeling, asphaltene, 73
- Molar volume, 118, 119, 122
- Molecular Dynamics (MD), 104, 105, 108, 109
  - – simulation, 110, 115, 118
- Molecular Mechanics (MM), 104, 105
- Monoaromatics, 341
- Monocrystal, 206
- Monocyclic aromatics, 309
- Monomers, 17, 63
- Monte Carlo simulation, 59, 61, 73, 75, 79, 80, 99, 104, 107, 108, 109
  - – –, algorithms, 76, 78
  - – –, asphaltene reaction, 76, 82
  - – –, asphaltene structures, 82
  - – –, pyrolysis, 87
  - – –, reaction model, 62
- Morphology, 576
- Multipolymer, 19
- Multivariate analysis, 191, 192, 193, 216
  - –, regression, 184, 187
- Naphtha bitumens, solubility, 11
- Naphthenoaromatic, 111
- Naphthenic, 14, 65, 111
  - carbon, 65
  - oils, 14
  - ring system, 365
- Naphthenics, 16, 19, 130
  - , pericondensed, 19
- Neural network statistics, 2
- Neutralization, 355
- Newtonian flow, 382, 390
- Newtonian viscosity, 175, 180, 183, 194, 200, 204

- Newton's equation of motion, 109
- Nickel, 64
- compounds, 12
  - laterites, 165
- Non-Newtonian, 372, 390, 392
- flow, 390, 392
- Nonpolar solvents, 310
- Nonporphyrins, 31, 32, 49
- model compounds, 42
- Nuclear Magnetic Resonance (NMR), 3, 108, 111, 229, 305, 336, 342, 365
- , oil fraction, 3
- Nuclear magneton, 231
- Nucleation, 319, 322
- Nuclei, 201, 202, 205, 206, 211, 215
- , bi-disperse, 201, 202, 205, 206, 211, 215
  - , coalesced, 202
  - , dispersed-phase particles, 177, 196
  - , monodispersed, 205, 206, 211, 215
  - , polydispersed, 211, 215
- Oil shales, 4, 499, 500, 502, 503, 505, 506, 508
- –, fillers, 500, 502, 503, 505, 506, 508
  - –, granulometric composition, 506
  - –, asphalt mixes, 499
- Oil–wax equilibria, thermodynamics, 586
- Olefin, 88, 89, 92
- , carbons distribution, 89
  - function, 19
- Olefinic, 87
- Oligomer, 18, 63
- Oligomeric, 59, 85
- Oligomerization, 53
- Organic, 3, 242, 244
- diversity, 3
  - free radicals, 244
  - radicals, 242
- Organ concretes, 213, 214, 215
- characterization, 215
  - , frost resistance, 215
  - , physicochemical characteristics, 213
  - , shear resistance, 215
- Organometallics, 2, 305
- Osmometry, 336
- Oxidation, 445, 461, 462, 463, 465, 466, 475, 479
- , Athabasca asphaltenes, 461
  - , asphalt, 445, 462, 463, 465, 466
  - , bitumen, 479
  - , cumene, 465, 466
  - , free radicals, 465
  - , low-temperature, 445
  - , oils and resins, 462
  - , radical chain, 466
  - reactions, 475
- Oxidative, 374, 387, 388, 450, 459
- aging, 387, 388
  - degradation, 450, 459
- Ozokerite, 11, 17
- Paraffins, 2, 13, 87, 88, 90, 92, 340, 538, 571
- , carbons distribution, 89
  - , China, 538
  - concentration, 571
  - , cyclo-, 340
  - , linear, 340
  - , waxes, 2
- Parameter of aromaticity, 192
- Paraphenic oils, 14
- Partitioning, 366, 368
- Pavements, 530, 531, 537, 548
- , asphalt in China, 537
  - , highways, 530
  - , high-performance flexible, 530
  - patching, 531
  - durability, 548
- Penetration index, 195, 198, 524
- Peptization, 30, 321, 373, 372, 462
- Peptizing agents, 305
- Percolation, theory, 2
- Perhydroflorene, 23
- Period, stress relaxation, 183
- Peripheral aromatic carbon, 65
- Peroxide, 454, 456
- decomposer, 456
  - , decomposition, 454
- Petrolenes, 16, 239, 373, 386, 388
- fractions, 386, 388
- Petroporphyrins, 31, 34, 35, 36
- , demetallated fractions, 35
  - , mass relations, 36
  - , molecular weight distribution, 34
- Petroporphyrins, 32, 38, 49
- , DPEP type, 32, 33, 34, 35, 36, 38, 39
  - , etio, 31, 32, 34, 35, 36, 38, 39
  - , MS studies, 39
- Phase, 4, 182

- , equilibrium, 4
- , separation, 4
- , volume, 182
- Phenanthrene, 69
- Phenol interaction coefficient, 384, 385
- Physicochemical characteristics
  - , asphaltenes, 181, 182
- Phyterals, 236
- Pitch, 9, 11
- Plastic flow, 435
- Plastic viscosity, 195
- Plasticity index, 507, 508
- Plastometer, 197
- Pleistocene, geologic age, 33
- Pliocene, geologic age, 33
- Plugging, reservoirs, 103, 124
- PNA ratio, 323
- Point of inflection, 175
- Polar, 305, 307, 382, 383, 385, 386, 387
  - components, 386
  - –, effects on viscosity, 386
  - –, aging characteristics, 386
  - , compounds, 307
  - functional groups, 383
  - functionality, 387
  - groups, 385
  - interactions, 382
  - molecules, 305
- Polarity, 103, 305
  - , asphaltene, 169
- Polyaromatic, 243, 311
  - base, 243
  - compounds, 311
- Polycondensation, 26, 238
- Polyconjugated structures, 167
- Polycyclic Aromatic Hydrocarbons (PAHs), 26, 104, 120, 309, 458
- Polycyclic core, 63, 69
- Polydisperse
  - monomer–polymer solution, 2
  - organic binders, 170
  - statistical mechanics, 2
- Polyethylene, linear conjugated, 18
- Polymethane, 18
- Polymerization, 17, 25, 64, 68, 69, 97, 138, 238, 256, 261, 262, 462, 470, 517
- Polymers, 17, 19, 175, 235, 458
  - , cross-linked, 235
  - rheology, 197
  - , saturated, 458
- Polymerization, 138
- Polynuclear Aromatics (PNA), 26, 111, 129, 319
- Polystyrene, 19
- Polysulfide linkage, 19, 20, 22
- Pore size distribution, 164
- Porosity, aggregates, 213, 476
- Porphyrins, 18, 25, 30, 31, 32, 46, 445
  - , biosynthesis, 25
  - , DPEP type, 31
  - , etio-type, 38
  - , kerogen, 30
  - , lunar rocks, 30
  - , model compounds, 46
  - , oils, 30
  - , quantification, 40
  - , structure, 31
  - –, crude oils, 31
- Pour point, 3, 572, 573, 579
  - , dynamic, 3
  - , static, 3
- Preasphaltene, 15, 17, 268
- Precipitation, 2, 3, 319, 327
  - , asphaltene, 103, 104, 123, 129, 336
  - wax, 557
- Precipitator, 181, 192
- Precursors, 25
- Probability distribution function (pdfs), 3
- Prooxidants, 465
- Propagation, 2, 454
- Proportionality factor, 241
- Prostacyclin, 22
- Prostaglandin, precursor, 22
- Proton Magnetic Resonance (PMR), 229
- Pseudo-activation energy, 145
- Pseudocomponents, 323
  - , aromatic, 323
  - , paraffin, 323
- Pseudo-frequency factor, 145
- PVT, 323, 579, 580
  - analysis, 323
  - cell, 579, 580
- Pyrite, 165
- Pyrobitumen, 402
- Pyrolysis, 23, 74, 75, 81, 82, 96, 111, 142, 143, 144, 149, 262, 264
  - , asphaltene, 60, 84
  - , coals, 30

- , maximum temperature, 410
- , simulation, 86, 91, 94, 97

## Quantum mechanics, 2

## Radicals, 229, 238

- , anions, 229
- , cations, 229

## Ragusa, Italy, 17

## Range of serviceability, 188

## Rate constant, 137, 141, 145

## Reaction, 79, 84

- probability distribution, 79
- trajectory, 84

## Reactors, 152, 153, 155, 156

- , ebullating-bed, 156
- , fixed-bed, 152, 153
- , mobile fixed bed, 155
- , slurry, 159

## Recrystallization, 42

- , carbonate, 438

## Recycling, 388

- , emulsification, 388
- , pavement mixture, 388

## Refraction coefficient, 197

## Refractive index, crude oils, 13

## Regression, 184, 185, 252

- analyses, 252
- coefficients, 184, 185, 252

## Relative elasticity coefficient, 184

## Relaxation period, 200, 207, 253

## Renormalization, 2

## Resid model, compound, 61

## Resilience, 189, 192

- coefficients, 189
- index, 192

## Resins, 2, 11, 12, 15, 103, 104, 129, 139, 145, 173, 175

- attraction to asphaltene micelles, 559
- behavior, 2
- , neutral, 11
- , separation, 283
- subtraction from organics, 15
- , thermal reactions, 2

## Resolidification, 262

## Retardation, 458

## Retarder, 457, 458

## Reticulation, degree, 115

## Reverse micelle, 319, 326, 327

## Rheological

- characteristics of bitumens, 180, 184, 187, 197, 297

## –, Petroleum–Bitumen–Resin (PBR), 207

- properties, 180, 184, 187, 573

## – –, crude oil, 573

## – –, model bitumens, 180

## Rheology, 173, 181

## Road paving, mixes, 499, 500, 501, 505

## Roofing asphalt, China, 537

## Rotating Cylinder Aging Test (RCAT), 485, 486

## Rozel Point, 17, 33

- –, tar asphaltene, 22

- –, tar sand, 20

## Ru ion reaction, 130

## SARA, 315, 339, 340, 344, 541, 542, 544, 545

- analysis, 541, 542, 544, 545

- distributions for crude oils, 340

- , fractions characterization, 339

- , group-type analysis

- procedure, 315

- , survey, 344

## Saturates, 103, 129, 140, 292, 305

- distributions by GC, 341

- fraction, 559

- fractionation, 139

- , typical components, 559

## Sealants, 173

## Sedimentary, organic matter, 401, 402

- – –, genetic classification, 402

## Seepage, liquid asphalt, 8

## Shale oil, 22, 65

## Shear, 197

- rate, 197

- stress, 197

## Siderite, 165

## Silica gel, 206

## Size Exclusion Chromatography (SEC), 541

## Size Exclusion Liquid Chromatography (SELC), 342, 366, 367, 370

## Slurry reactors, 159, 160, 163, 164, 166

## Softening, 183, 207, 503, 504

- point, 183, 207, 503, 504

- temperature, 202

- –, bitumen, 202

## Solidification, 404

- Solubility, 59, 118, 119, 120, 121, 123, 310, 312, 321, 324, 325, 326
  - , asphaltene, 11
  - , common solvents, 312
  - fraction, 59
  - fractionation, 348
  - parameters, 118, 119, 120, 121, 123, 310, 324, 325
  - –, alkanes, 325
  - –, asphaltenes, 324
  - –, aromatic hydrocarbons, 325
  - –, petroleum fluids, 325
  - , solvent mixtures, 312
  - , theory, 321, 326
- Solubilization, 321
  - , asphaltenes, 326, 327
- Solution theory, 330
- Solvency, 388
- Solvent, 15, 59, 63, 550
  - , aromatic, 59, 63
  - Deasphalting (SDA), 550
  - extraction, 59
  - –, protocol, 59
  - fractionation, 15
  - paraffinic, 59
- Sonochemical treatment, 30
- Specific heat, 110
- Specific surface area, 500, 505, 509, 510
- Spectroscopic splitting factor, 230
- Spectrum content, 248, 249, 250
- Spin, 230, 231, 232, 234, 239, 240, 244, 245, 257, 261, 263, 264, 265, 266, 267, 270
  - angular moment, 230
  - concentration, 231, 232, 234, 239, 240, 244, 245, 257, 261, 263, 264, 265, 266, 267, 270
  - delocalization, 254
  - intensity, 269
  - quantum number, 230
  - stabilization, 262
- Spin-lattice, 233, 242
  - interaction, 233
  - relaxation time, 242
- Splitting interactions, 230
- Spot test, 311
- Stabilization, asphaltene, 342
- Static, 3, 207
  - limit, 207
  - pour point, 3
- Statistical mechanics, 2
- Steric, 2, 123, 391, 458
  - hardening, 391
  - protection, 458
  - stabilization, 123
  - theory, 2
- Stochastic, 3, 69, 70, 80, 96, 108
  - algorithm, 70
  - –, asphaltene structures, 70
  - , construction, 96
  - modeling, 3
  - reaction, 96
  - sampling, 69
  - simulation, 80
  - –, fixed time, 80
  - –, variable time step, 80
  - structure, 108
  - –, generation, 108
- Stoichiometric coefficients, 75, 82
- Strain energy, 119
- Stress relaxation, period, 183, 188
- Structural, 63, 130
  - hierarchy, 63
  - –, asphaltene, 63
  - parameters, 130
  - –, asphaltenes, 130
- Structure, 188, 195, 200, 207
  - disturbance, 200, 207
  - –, degree, 200, 207
  - distortion, 188
  - –, degree, 188
  - failure, 195
  - –, degree, 195
- Student's test, 190
- Styrene, 19
- Sulfur, 2, 4, 23, 169, 515, 516, 518, 519, 520, 523, 524, 525, 526
  - , asphalt, 4, 515, 516, 518, 519, 520, 521, 523
  - –, blend, 516, 518, 519
  - –, binder, 520, 521
  - –, dispersion, 520
  - –, emulsion, 520
  - –, binder, 522
  - –, interaction, 515
  - –, mixes, 4
  - –, mixtures preparation, 520
  - –, paving mixtures, 520, 521
  - –, properties, 523

- , behavior, 2
- , binder, 526
- , adhesion, 526
- , ductility, 524, 525, 526
- , penetration, 525
- , stability, 527
- , viscosity, 524
- , chemically bonded, 516
- content, 169
- conversion, 23
- , crystalline, 518
- , dissolved, 518
- , softening point, 525
- Sulphurized asphalt, 518, 528, 530, 531, 532
  - , economic aspects, 531, 532
  - pavement, 530, 531
  - –, applications, 530
  - –, patching, 531
  - , paving material, 528, 530
  - , protective coating, 531
- Supercritical Fluid Chromatography (SFC), 305, 562
- Supercritical Fluid Extraction (SCFE), 540
- Supercritical Solvent Extraction (SSE), 551, 555
- Surfactants, 30
- Swelling, 213
- Syn crude, 150
- Synergic effects, 500
  - , coal, 500
  - , polymers, 500
- Synergistic, 393
- Tabbyite, 17
- Tar, 9, 11
  - asphaltenes, 20
  - , porphyrin content, 20
  - characterization, 30
  - sand, 22, 65
  - , degradation, 22
- Tenderness characteristics, 387
- Tensile strength, 502
- Termination, 452
- Ternary diagram, 13, 240, 241
- Terpolymer, 19
- Terrigenous, 404
- Tetragonal ligand, 25
- Tetramerization, 53
- Tetramatics, 341
- Thermal, 16, 105, 110, 122, 261, 335
  - cracking process, 335
  - diffusion, 16
  - expansion, 110
  - coefficient, 105, 122
  - reversibility, 261
- Thermoboxane, 22
- Thermodynamic
  - lumping, 96
  - properties, 103, 124
  - , asphaltenes, 103, 124
  - stability, 600
- Thermodynamics, 2, 110
- Thermogravimetric Analysis (TGA), 460
- Thin-Film Oven Test (TFOT), 541, 546
- Thin-Layer Chromatography (TLC), 3, 305, 315
  - , asphalt, 306, 309
  - –, analysis, 306
  - –, separation, 309
  - –FID, 312, 313, 315
  - – matrix, 316
  - –, quantitative analysis, 306
  - , jet fuel identification, 306
  - , protocol procedures, 307
  - scanner, 314
- Thixotropic, 364, 391
  - effects, 364
  - flow, 391
  - properties of bitumens, 195
- Tiophenics, 341
- Total carbon, 65
- Transalkylation, 111
- Transport phenomena, 2
- Triaromatics, 341
- Tricyclic aromatics, 309
- Ultrasonics, 1, 581
- UNITAR, 11
- Upgrading, asphaltenes, 129
- Upper Cretaceous, geologic age, 33
- UV, 108, 111, 310
- Vacuum residue, 281, 290, 299, 301, 335
- Van der Waals force, 204, 310
- Vanadium, 31, 32, 64, 242, 321, 446, 451
  - , asphaltenes, 40, 46, 49, 50, 53
  - , bound form (ANISO), 51
  - compounds, 12

- , crude oils, 42
- deposition, 166
- , free form (ISO), 51
- model compounds, 30
- , nonporphyrins, 42
- removal, 166
- Vanadyl, 42, 43, 50
- compound, 42, 43, 50
- –, modeling, 50
- –, square pyramidal, 46, 48
- Vapor Pressure Osmometry (VPO), 64, 108, 111, 336
- Veba Combi Cracking process, 159
- Vesicles, 30
- Visbreaker, 242, 243
- Viscometry, 572, 573, 574, 575
- Viscosity, 150, 152
- , bitumen, 129
- , crude oil, 1
- , dynamic, 573
- , intrinsic, 389
- , quasi-Newtonian, 447
- , saturates, 382
- , specific, 389, 390
- , sulfur-extended asphalt, 524, 526
- Vitrains, 244, 265
- Vitrinite, 264, 405, 406, 408
- , reflectance, 406, 408
- , thermal simulation, 405
- Vitrinization, 244
- Void concentration, 507
- Volatile yield, 405
- Volumetric coefficient, 178
- Voluminosity coefficient, 182, 201, 219, 220
- Wax, 4, 557, 558, 600, 602, 651, 570
  - appearance temperature, 570, 571, 572, 573, 574, 575, 579, 580, 581, 583, 584
  - –, under flow conditions, 583
  - components, 558
  - content, 570
  - , asphalts, 4
  - content determination, 561
  - deposition envelope (WDE), 600, 602
  - precipitation, 557, 591, 594
  - – amount, 601
  - – modeling, 585
  - –, multisolid-wax model, 599
- Waxy, 562, 564, 566, 567
  - crude, 567
  - –, fractionation protocol, 567
  - deposits, 564
  - –, modification protocol, 566
- Wetability, 103, 123
  - reversal, 123
- Workability, 183, 212, 530
  - interval, 212
  - , sulphur–asphalt–aggregate mixes, 530
- Wurtzilite, 17
- Wurtzite, 402
- X-ray diffraction, 285
- Yield strength, dynamic, 204, 211
- Yield limit, dynamic, 183, 188
- Zeta potential, 3
- Zone elution method, quantification, TLC, 315



This page intentionally left blank